UNITED STATES DEPARTMENT OF THE INTERIOR

GEOLOGICAL SURVEY

PROCEEDINGS OF

WORKSHOP XLIV

GEOLOGICAL, GEOPHYSICAL, AND TECTONIC SETTING OF THE CASCADE RANGE

01-04 December 1988

Sponsored by

U.S. GEOLOGICAL SURVEY

GEOTHERMAL RESEARCH PROGRAM

OPEN-FILE REPORT 89-178

MENLO PARK, CALIFORNIA

1989

TABLE OF CONTENTS

ACKNOWLEDGMENTS

This volume presents nearly all of the contributions presented at a Redbook Conference on the geological, geophysical, and tectonic setting of the Cascade Range, held in Monterey, California, 01-04 December 1988. The conference was sponsored by the U.S. Geological Survey and financed by the USGS Geothermal Research Program. We are indeed grateful for the consistent and enthusiastic support of the Coordinator of the Geothermal Research Program, Robert L. Christiansen.

Absolutely indispensable to the success of this Redbook Conference was Wanda Seiders, who was responsible for arranging all the logistics and travel. She, her staff (Barbara Charonnat and Muriel Jacobson), and the Doubletree Inn in Monterey put on a near-perfect performance that was key to the success of the conference. Our thanks to them also for the production of this volume. Finally, our thanks to Mary Ann Mikus, responsible for much of the pre-conference correspondence and for reformatting some of the contributions.

L.J. Patrick Muffler
Craig S. Weaver
David D. Blackwell

LIST OF PARTICIPANTS

Charles R. Bacon
Branch of Igneous & Geothermal Processes
U.S. Geological Survey
345 Middlefield Rd., MS 910
Menlo Park, CA 94025

Marvin H. Beeson
Geology Department
Portland State University
P.O. Box 751
Portland, OR 97207

David D. Blackwell
Department of Geological Sciences
Southern Methodist University
Dallas, TX 75275-0395

Richard J. Blakely
Branch of Geophysics
U.S. Geological Survey
345 Middlefield Road, MS 989
Menlo Park, CA 94025

Thomas D. Bullen
Branch of Igneous & Geothermal Processes
U.S. Geological Survey
345 Middlefield Road, MS 910
Menlo Park, CA 94025

Robert L. Christiansen
Branch of Igneous & Geothermal Processes
U.S. Geological Survey
345 Middlefield Road, MS 910
Menlo Park, CA 94025

Michael A. Clynne
Branch of Igneous & Geothermal Processes
U.S. Geological Survey
345 Middlefield Rd., MS 910
Menlo Park, CA 94025

Michael L. Cummings
Department of Geology
Portland State University
P.O. Box 751
Portland, OR 97207

Julie M. Donnelly-Nolan
Branch of Igneous & Geothermal Processes
U.S. Geological Survey
345 Middlefield Rd., MS 910
Menlo Park, CA 94025

Carol Finn
Branch of Geophysics
U.S. Geological Survey
Box 25046, Federal Center, MS 964
Denver, CO 80225

Robert O. Fournier
Branch of Igneous & Geothermal Processes
U.S. Geological Survey
345 Middlefield Rd., MS 910
Menlo Park, CA 94025

M. Charles Gilbert
Geosciences Program/BES/ER-15
Department of Energy, G-236/GTN
Washington, DC 20545

Marianne Guffanti
Branch of Igneous & Geothermal Processes
U.S. Geological Survey
National Center, MS 922
Reston, VA 22092

Wes Hildreth
Branch of Igneous & Geothermal Processes
U.S. Geological Survey
345 Middlefield Rd., MS 910
Menlo Park, CA 94025

Scott S. Hughes
Oregon State University
Radiation Center A100
Corvallis, OR 97331-5903

Steve E. Ingebritsen
Water Resources Division
U.S. Geological Survey
345 Middlefield Rd., MS 439
Menlo Park, CA 94025

Douglas M. Johnson
National Science Foundation
1800 G St., NW, Room 602
Washington, DC 20550

Hiroki Kamata
Geological Survey of Japan
1-1-3 Higashi, Tsukuba, Ibaraki
305 Japan

William P. Leeman
Earth Sciences Division
National Science Foundation
1800 G St., NW, Room 602
Washington, DC 20550

Trevor J. Lewis
Pacific Geoscience Centre
Geological Survey of Canada
PO Box 6000, Sidney, B.C.
V8L-4B2 Canada

Robert H. Mariner
Water Resources Division
U.S. Geological Survey
345 Middlefield Rd., MS 434
Menlo Park, CA 94025

L.J. Patrick Muffler
Branch of Igneous & Geothermal Processes
U.S. Geological Survey
345 Middlefield Road, MS 910
Menlo Park, CA 94025

William M. Phillips
Washington Division of Geology and Earth Resources
M.S. PY-12
Olympia, WA 98504

George R. Priest
Department of Geology and Mineral Industries
910 State Office Bldg.
1400 S.W. 5th Ave.
Portland, OR 97201

John Rasmussen
Department of Geological Sciences
University of Oregon
Eugene, OR 97403

David R. Sherrod
Branch of Western Mineral Resources
U.S. Geological Survey
345 Middlefield Road, MS 941
Menlo Park, CA 94025

Gary A. Smith
Department of Geology
University of New Mexico
Albuquerque, NM 87131

James G. Smith
Branch of Western Mineral Resources
U.S. Geological Survey
345 Middlefield Road, MS 901
Menlo Park, CA 94025

W. D. Stanley
Branch of Geopysics
U.S. Geological Survey
Box 25046, Federal Center, MS 964
Denver, CO 80225

Edward M. Taylor
Department of Geology
Oregon State University
Corvallis, OR 97331

Philip E. Wannamaker
Earth Science Laboratory
Univ. of Utah Research Institute
391 Chipeta Way, Suite C
Salt Lake City, UT 84108

Craig Weaver
Branch of Seismology
U.S. Geological Survey
Geophysics Program, AK-50
University of Washington
Seattle, WA 98195

Ray E. Wells
Branch of Western Regional Geology
U.S. Geological Survey
345 Middlefield Road, MS 975
Menlo Park, CA 94025

Robert L. Wesson
Office of Earthquakes, Volcanoes, and Engineering
U.S. Geological Survey,
National Center MS 905
Reston, VA 22092

Redbook Conference on the Geological, Geophysical, and Tectonic Setting of the Cascade Range

L.J. Patrick Muffler[1], Craig S. Weaver[2], and David D. Blackwell[3]

The Cascade Range is an active volcanic arc that is formed by the continuing subduction of the Juan de Fuca plate system beneath North America. Understanding of the Cascade Range and its tectonic setting is not only of broad scientific interest, but also is important for the assessment of geothermal resources and the evaluation of volcanic and seismic hazards.

The past decade has seen increasing attention to the study of the Cascade Range by a wide range of disciplines; these studies have been conducted at scales ranging from individual volcanic centers to the entire range. Integration of these studies into a comprehensive regional understanding, however, has lagged. In part this is because much of the work initiated over the past decade was original to the Cascade Range, and individual investigators tended to concentrate on reduction and analysis of their own data rather than seeking collaboration. Furthermore, research efforts in the Cascades have tended to be isolated by artificial disciplinary barriers separating geologists, geophysicists, geochemists, and hydrologists.

The need for understanding the regional aspects of the Cascade Range is particularly important to the USGS Geothermal Research Program. Although identified geothermal resources in the Cascade Range are modest, substantial undiscovered geothermal resources have been inferred, owing primarily to the favorable volcanic and tectonic setting but also to the high regional heat flow known to exist along the Cascade Range. Consequently, a multiyear, multidisciplinary program of studies to refine the geothermal resource estimates of the Cascade Range is a major objective of the USGS Geothermal Research Program. By far the smallest and easiest part of this effort is a new inventory of known hydrothermal convection systems. Much larger and far more difficult is the estimation of the geothermal resources yet to be discovered. Since the forseeable economic climate appears unlikely to allow the drilling of numerous deep holes, the magnitude of the undiscovered geothermal resources can be addressed only by supplementing the sparce available drill-hole information with a comprehensive analysis of the tectonic, geophysical, volcanic, and hydrologic setting of the Cascade Range.

As a first step in the integration of a wide spectrum of regional geological, geophysical, and geochemical investigations into a comprehensive understanding of the Cascade Range, the USGS Geothermal Research Program sponsored a Conference on the Geological, Geophysical, and Tectonic Setting of the Cascade Range, in Monterey, California, on 01-04 December 1988. The geographic scope of the conference was the Cascade Range as a whole, from

---

[1] U.S. Geological Survey, MS 910, 345 Middlefield Road, Menlo Park, CA 94025

[2] U.S. Geological Survey, Geophysical Program, AK-50, University of Washington, Seattle, WA 98195

[3] Department of Geology, Southern Methodist University, Dallas, TX 75275

Northern California through Oregon and Washington to British Columbia. The intellectual scope was as broad and interdisciplinary as possible, with participants representing the fields of geology, heat flow, seismology, igneous petrology, hydrology, electromagnetic geophysics, magnetics, water geochemistry, gravity, paleomagnetism, and tectonics. The conference was organized around three major themes:

- Variations in tectonics, geophysical signature, and magmatism along the length of the Cascade volcanic arc.
- Relationship of the Cascade Range to the subduction tectonics to the west and to the continental tectonics to the east.
- Controls on the location, composition, and rates of magmatism in the Cascade Range.

The 35 attendees were almost equally divided between USGS scientists and scientists from other research institutions, including universities, other federal agencies, state agencies, Canada, and Japan.

This Redbook contains nearly all the presentations made at the 01-04 December 1988 Conference in Monterey. We do not intend or imply that it is the final word on the Cascade Range. Instead, its purpose is to release promptly the material presented at the December 01-04 Conference to other concerned investigators and to the public. Accordingly, we have not attempted to edit the contributions, even lightly. It is our plan, however, that each of the authors will revise his/her Redbook contribution in view of the other contributions and that the resultant papers will form the nucleus of a reviewed and edited special section of the Journal of Geophysical Research, hopefully to be published within the year.

UNITED STATES DEPARTMENT OF THE INTERIOR

GEOLOGICAL SURVEY

WORKSHOP XLIV

GEOLOGICAL, GEOPHYSICAL, AND TECTONIC SETTING OF THE CASCADE RANGE

01-04 December 1988

Sponsored by

U.S. GEOLOGICAL SURVEY

GEOTHERMAL RESEARCH PROGRAM

Editors

L.J. Patrick Muffler
U.S. Geological Survey
Menlo Park, California 94025

Craig S. Weaver
U.S. Geological Survey
University of Washington
Seattle, Washington 98195

David D. Blackwell
Southern Methodist University
Dallas, Texas 75275-0395

OPEN-FILE REPORT 89-178

Compiled by
Muriel Jacobson

MENLO PARK, CALIFORNIA

1989

PALEOMAGNETIC ROTATIONS AND THE CENOZOIC TECTONICS OF THE CASCADE ARC, WASHINGTON, OREGON, AND CALIFORNIA

by Ray E. Wells

U.S. Geological Survey
345 Middlefield Road, MS 975
Menlo Park, California, 94025

ABSTRACT

Paleomagnetic results from Cenozoic (62-12 Ma) volcanic rocks of the Cascade arc and adjacent areas indicate that moderate to large clockwise rotations are an important component of the tectonic history of the arc. High quality paleomagnetic evidence from Eocene to Miocene rocks indicates that the arc and forearc regions have undergone distributed dextral shear rotation that increases westward toward the coast. Oblique subduction of the Juan de Fuca plate is the likely driving force for the simple shear rotation, which is accommodated in the upper crust by strike-slip faulting. The Mount St. Helens seismic zone is an active manifestation of the process of simple shear rotation. Dextral shear probably obscures a subequal contribution to arc and forearc rotation that is driven by intraarc or backarc extension. This rotation is suggested by the average southward increase in continental margin rotations into the region outboard of the Basin and Range. The apparent eastward migration of the volcanic front for successively younger arc volcanic rocks in the rotated arc terrane implies that the frontal arc has been migrating westward in front of a zone of extension since Eocene time. The westward migration of bimodal Basin and Range volcanism since 16 Ma may be tracking westward rotation of the frontal arc and growth of the Basin and Range in its wake.

INTRODUCTION

The Pacific Northwest has been a zone of convergence between North America and oceanic plates of the Pacific basin throughout much of Cenozoic time (Atwater, 1970; Engebretson and others, 1985). Abundant, high quality paleomagnetic results from 62-12 m.y. (million year) old rocks of the forearc, arc, and backarc indicate that large clockwise rotations (15-80°) have occurred in western Oregon and Washington, and that rotations increase with age and with proximity to the coast (Figure 1). For any given time interval, forearc strata are rotated the most, arc rocks have intermediate rotations, and backarc rocks are rotated the least. The rate of clockwise rotation has been about 1.3°/m.y. for most of Cenozoic time, with no indication of a hiatus (Beck and Plumley 1980; Bates and others 1981).

Several plate tectonic models have been proposed to explain the clockwise rotations, including: 1) rotation of an oceanic Coast Range microplate during its oblique collision with North America in Eocene time (Simpson and Cox, 1977; Magill and others, 1981); 2) dextral shear rotation of the continental margin throughout Cenozoic time, driven by northward-moving oceanic plates to the west (Beck, 1980; Wells and others, 1984; Engebretson and others, 1985); and 3) late Cenozoic microplate rotation of the arc and forearc in front of intracontinental extension in the Basin and Range region (Magill and Cox, 1980; Magill and others, 1981). Dextral shear and extension were probably the most important contributors to tectonic rotation (Figure 2). Collision

rotation was small because most of the rotation can be shown to postdate onlap of continental shelf sedimentary units onto the Coast Range oceanic basement (Wells and Heller 1988).

Volcanic rocks of the Cascade arc are part of the rotated terrane, according to the paleomagnetic studies. On average, Oligocene and lower Miocene rocks of the Western Cascades (30-20 Ma) are rotated clockwise about 18-30° and middle Miocene rocks (15-12 Ma) about 12-15° (Beck and Burr, 1979; Bates and others, 1981; Magill and Cox, 1981; Beck and others, 1986; Wells and others, in press). Both rigid plate and small block rotation mechanisms have been proposed to explain the paleomagnetic results. The purpose of this paper is to review the relevant paleomagnetic data in light of recent advances in our understanding of Cascade arc structure and volcanic history. The tectonic implications for Cascade arc development may be substantial. For example, rigid plate rotation of the arc and forearc region implies major extension behind the arc front (i.e. - within and behind the arc) and westward migration of the arc front with time. Volcanic sequences on the migrating plate should have equivalent but less rotated sequences left as remnant arcs behind the active volcanic arc, if analogies with western Pacific arcs are valid (Karig, 1971; see also Hamilton, 1988 for recent review). Alternatively, simple dextral shear rotation in the arc requires no linkage between rotation and extension, but it does imply the existence of mesoscale structures to accommodate small block rotations.

This paper will present evidence for both dextral shear and extension-driven rotation in the arc and will suggest first order correlations between rotation domains, regional Cascade structure and position of the volcanic front through time.

DEXTRAL SHEAR IN THE ARC

Paleomagnetic Evidence

The widespread, originally flat lying flows of the Miocene Columbia River Basalt Group provide an excellent structural datum across the arc and are useful for studying post-middle Miocene Cascade deformation (Beeson, this volume; Sherrod and Pickthorn, this volume). At least 20 flows travelled down an ancestral Columbia River drainage, across the Cascade arc and into the forearc. Several flows made it to the Pacific Ocean. Some flows, such as the Pomona Member and the flows of Ginkgo, have distinctive lithologic, chemical, and paleomagnetic signatures that permit tracking of individual flows over great distances. These flows are ideal rotational-strain markers and allow paleomagnetic traverses within a single flow to be made normal to the convergent margin.

Paleomagnetic results from closely spaced sites in the flows of Ginkgo and in the Pomona Member show a progressive westward increase in tectonic rotation from the relatively stable central Plateau to the coast, a distance in excess of 200 km (Figure 3). Sheriff (1984), Reidel and others (1984), and Wells and Heller (1988) interpreted these trends as good evidence for post-12 Ma dextral shear distributed across the forearc and arc on some intermediate scale. Rotating blocks are larger than a paleomagnetic site (10^2 m), but must be considerably smaller than the width of the rotated region (10^2 km), because differential rotations can be measured over distances of less than 10 km. Wells and England (1988) have examined post-15 Ma deformation of the Pacific Northwest convergent margin in the context of simple continuum mechanical models. They successfully modelled the observed pattern of rotations by applying a north-directed simple dextral shear to the western edge of a thin, viscous sheet behaving according to a power law rheology. The model implies that rotation in the Pacific Northwest is a surface manifestation of non-linear viscous flow in the lithosphere above an obliquely subducting oceanic plate.

Similar trends of decreasing rotation inboard from the coast can be seen in paleomagnetic results from older arc and forearc volcanic sequences when plotted against longitude (Figure 3). Both Oregon and Washington data are plotted together because results from any one latitudinal region are scarce. Some bias is introduced by this because Oregon is slightly west of Washington. Each rotation value represents the average of many paleomagnetic sites collected throughout a formation and so tends to average out local structural perturbations. However, plotting results

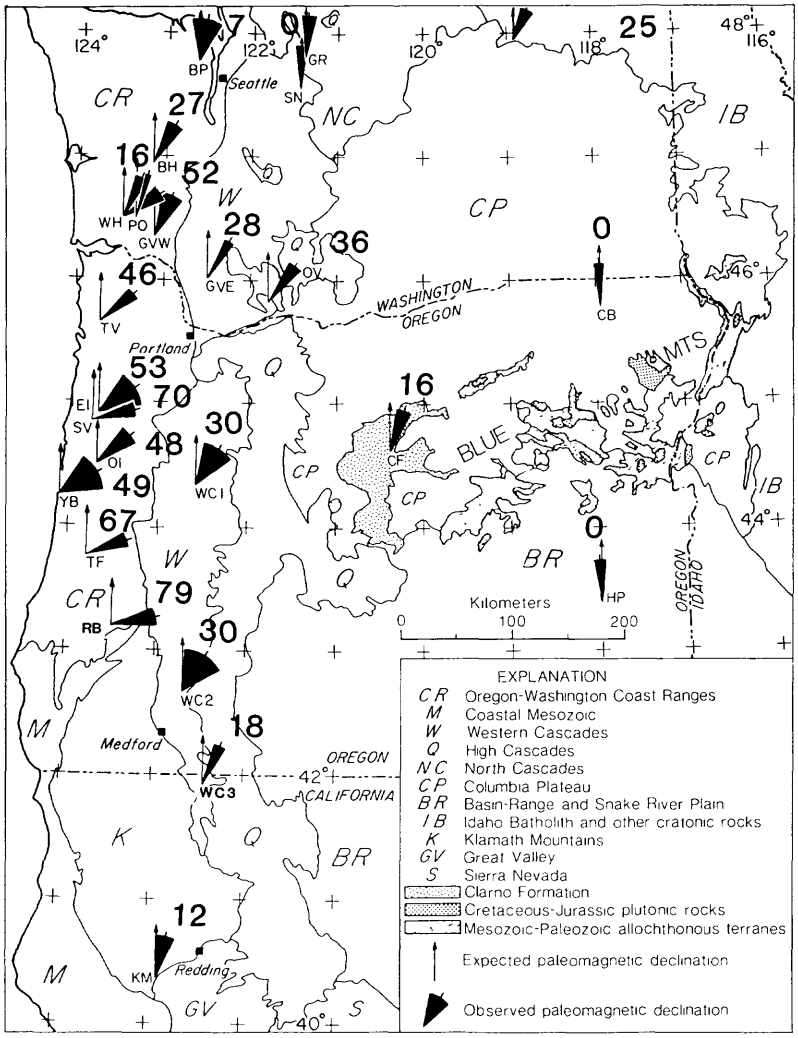

Figure 1. Tectonic rotations of rock units, in degrees, slightly modified from Grommé and others (1986); shaded sectors indicate 95% confidence limits on rotations. WASHINGTON: BP - Eocene volcanic rocks at Bremerton-Port Ludlow (Beck and Engebretson, 1982); BH - Eocene Crescent Formation, Black Hills (Globerman and others, 1982); WH - Eocene Crescent Formation, Willapa Hills (Wells and Coe, 1985); GV - upper Eocene Goble Volcanics (Beck and Burr, 1979; Wells and Coe, 1985); PO - Miocene Pomona Member, Saddle Mountains Basalt (Magill and others, 1982) OV - upper Eocene and Oligocene Ohanapecosh Formation of Bates and others (1981); SN - Miocene Snoqualmie and Grotto batholiths (Beske and others, 1973); SP - Eocene Sanpoil Volcanics (Fox and Beck, 1985). OREGON: TV - Eocene Tillamook Volcanics (Magill and others, 1981); EI - Eocene intrusions (Beck and Plumley, 1980); OI - Oligocene intrusions (Beck and Plumley, 1980); SV - Eocene Siletz River Volcanics (Simpson and Cox, 1977); TF - Eocene Tyee Formation (Simpson and Cox, 1977); RB - Paleocene basalt at Roseburg (Wells and others, 1985); YB - upper Eocene Yachats Basalt (Simpson and Cox, 1977); WC1, WC2 - Oligocene and Miocene volcanic rocks of the western Cascade Range (Magill and Cox, 1980); CF - Eocene and Oligocene Clarno Formation (Grommé and others, 1986); CB - Miocene Columbia River Basalt Group and Steens Basalt (SB) (Mankinen and others, 1987); CALIFORNIA: KM - Upper Cretaceous Hornbrook Formation (Mankinen and Irwin, 1982); SN - Late Cretaceous Sierra Nevada batholith (Frei and others, 1984). WC3 - Oligocene and Miocene volcanic rocks of the western Cascade Range (Beck and others, 1986).

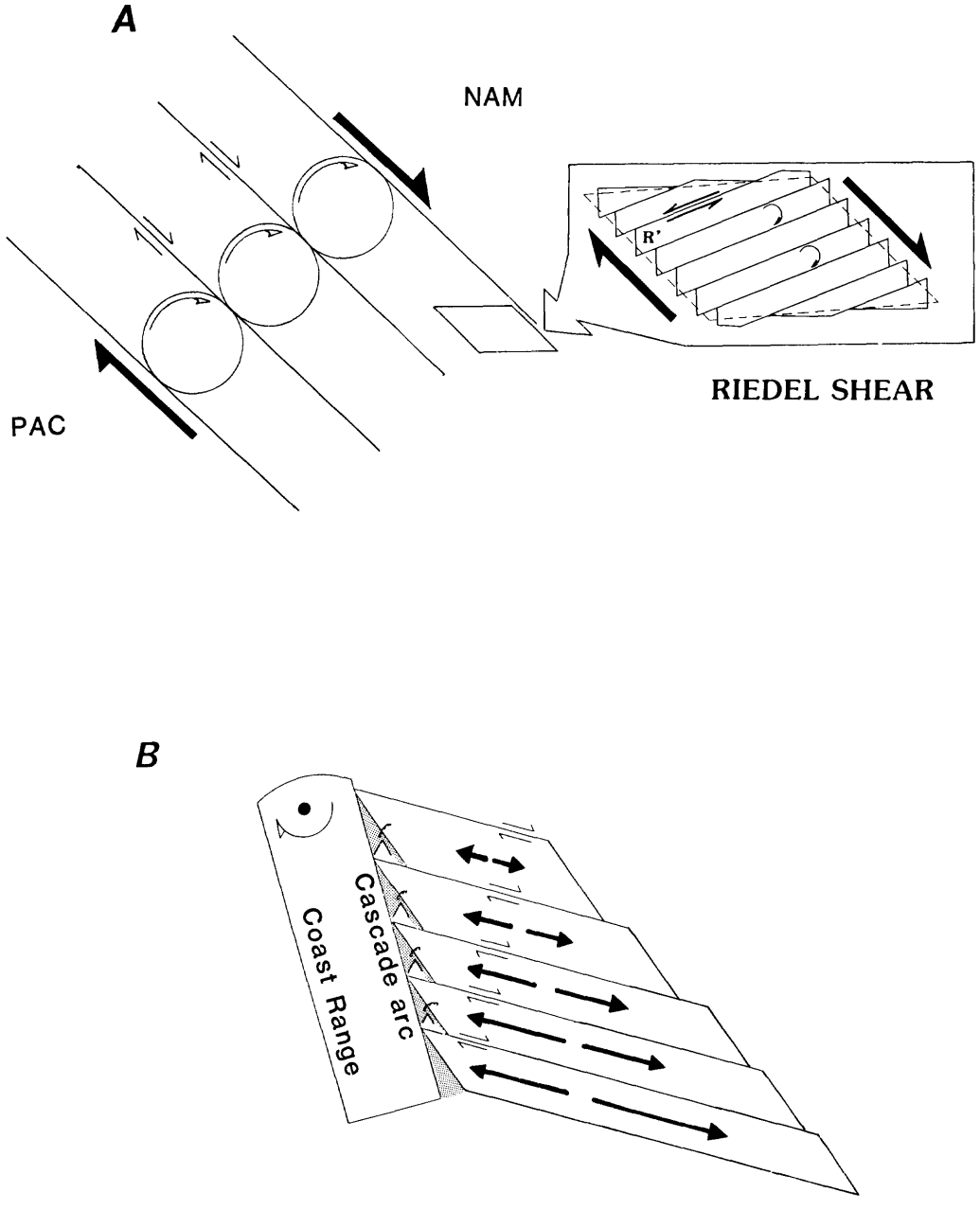

Figure 2. a) Schematic model of dextral shear rotation along western North America (Beck, 1980). Circles may be considered representations of the vorticity in a viscously deforming lithosphere (eg. McKenzie and Jackson, 1983), rather than the actual shape of rotating blocks. Fault patterns that accommodate the rotation in the upper crust may be some variant of that shown in the inset (see Garfunkel and Ron, 1985). b). Rigid plate rotation of western Oregon and Washington in front of an extending region, with extension decreasing to the north. Active arc acts as a tectonic boundary between extended terrane and rotating block. Modified from Magill and others (1982).

together from units in a 10-15 m.y. time window adds some uncertainty to the trends because differntial rotation could have occurred during the long interval.. Nevertheless, the same progressive increase in rotation toward the coast is seen in all of the older sequences, indicating that regional dextral shear has been an important rotation mechanism throughout Cenozoic time.

Structural and Seismological Evidence

Combined paleomagnetic and structural studies in the Coast Range of southwest Washington have demonstrated that small basement structural blocks are bounded by faults and have undergone differential clockwise rotations of between 20 to 65° (Wells and Coe, 1985).Wells and Coe also noted that horizontal slickensides are ubiquitous on exposed fault surfaces throughout the forearc region, and that fault patterns locally appear to be Riedel shears, which can accommodate clockwise rotation in regions of dextral shear (Figure 2). Similar domains of rotation and fault patterns may exist in the Cascade arc, but the difficulties of correlation in Cascade volcanic stratigraphy and the lack of detailed mapping may preclude recognition of structures accommodating local rotation. Lineament analysis of the Oregon Cascade arc suggests numerous, potential faults for accommodating rotations, but few of the linear features have been related to actual faults (Venkatakrishnan and others, 1980). In most of the western Cascades, the dip of strata is gentle, and evidence for substantial faulting is rare (eg., Smith and others, 1982). However, dike trends in the western Cascades are unusual and trend northwest (Sherrod, 1986; Sherrod and Pickthorn, this volume), seemingly at odds with north-trending normal faults along the present day High Cascades. Perhaps they represent intrusions into faults, which had strike-slip displacement, and therefore could have accommodated some dextral-shear rotation.

In southwest Washington, the pattern of seismicity following the eruption of Mount St. Helens in 1980 indicates that significant dextral slip can occur in the Cascade arc. Weaver and Smith (1983) have defined a 90 km-long St. Helens seismic zone that trends northwest and passes beneath Mount St. Helens. Dextral slip on the zone is indicated by first motion studies of the Elk Lake earthquake swarm of 1981 and the northwest trend of the aftershocks. Weaver and Smith (1983) suggested that consistency between the northeast trending P axes of the earthquakes, the contraction direction based on geodetic measurements (071°),and the plate convergence direction (050°) implies locking of the forearc region to the obliquely subducting oceanic plate. This is exactly what is required to drive clockwise rotations in the upper plate. The dextral shear-driven paleomagnetic rotations might be considered the long-term integral of the coupling between the obliquely subducting oceanic plate and the overlying arc and forearc regions.

ARC ROTATION BY INTRACONTINENTAL EXTENSION

Several workers have suggested that Cenozoic extension in the Basin and Range province has contributed substantially to clockwise rotation of western Oregon and Washington (Simpson and Cox, 1977; Magill and Cox, 1981; Magill and others, 1981, 1982). In this model, the thermally elevated Basin and Range region would exert a ridge-push force against the southern part of the Cascade arc and forearc in Oregon, and cause it to rotate clockwise around a fixed point north of the expanding region. A similar mechanism has been invoked to explain rotation of Japan during Miocene opening of the Japan Sea. Otofuji and others (1985) have shown that clockwise rotation of southern Honshu and counterclockwise rotation of northern Honshu can be explained by fan-shaped spreading in the Sea of Japan and resultant pivoting of the arc in front of the expanding region. This intracontinental rifting may be analogous to Cenozoic rifting in the Pacific Northwest.

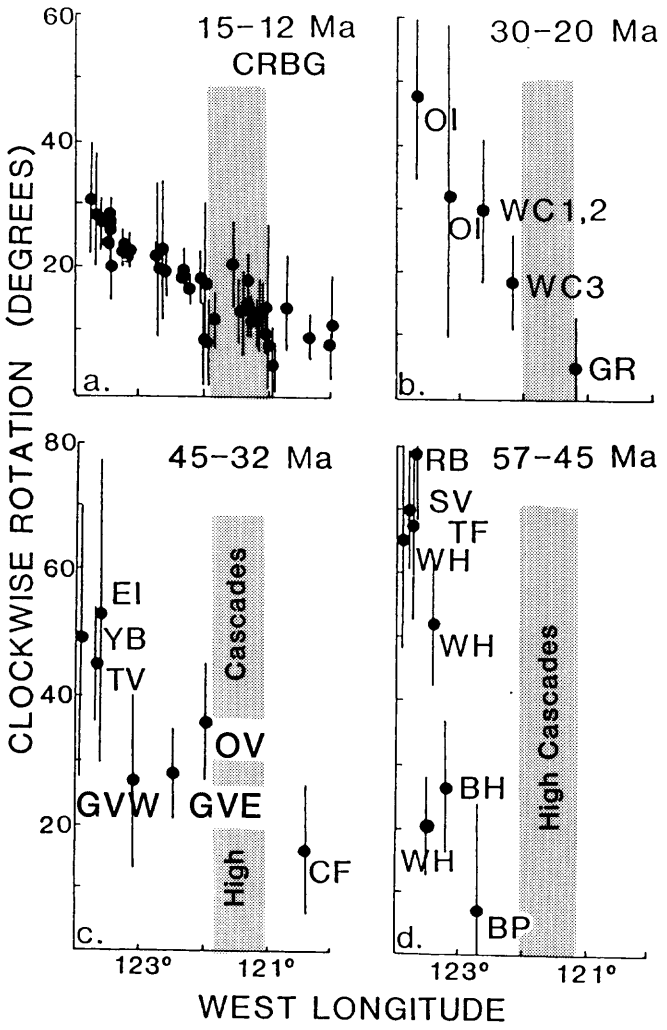

Figure 3. East-west profiles of rotation against longitude for Pacific Northwest units grouped by age; unit symbols as in Figure 1 except CRBG which is Miocene Columbia River Basalt Group. Shaded area represents location of High Cascade axis. Figure slightly modified from Wells (1988).

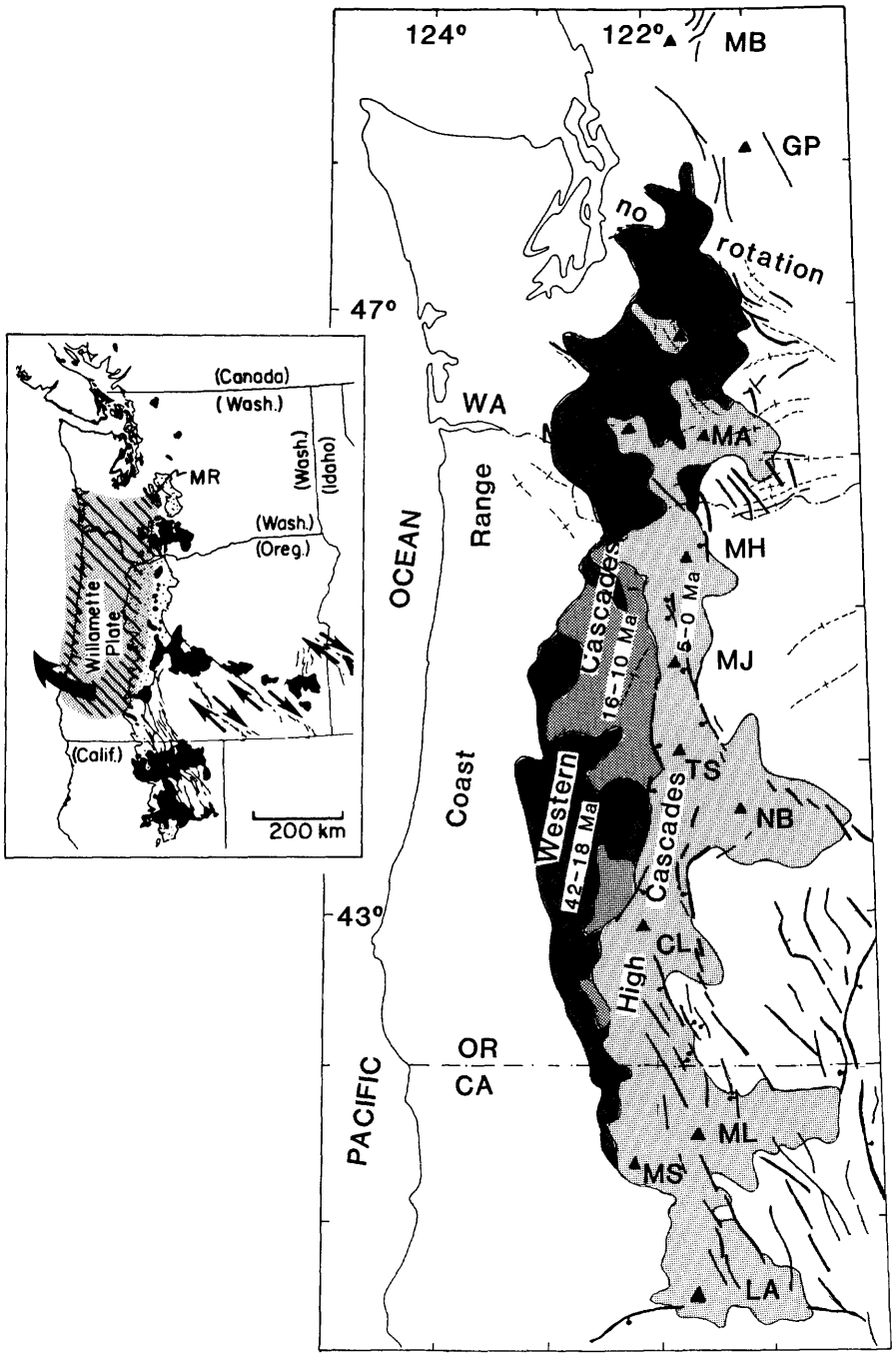

Figure 4. Simplified map of Cascade structure, modified from King and Beikman (1974), Sherrod (1986), and Smith (in press). Heavy solid lines are faults, ball on down thrown side; light dashed lines are fold axes. Rotated regions lie outboard of extensional arc, and northern boundary of rotated region is a zone of strong deformation, possibly marking pivot zone of rotating "Willamette plate." Inset shows presumed outline of rotated plate. Triangles represent major Quaternary volcanoes: MB = Mt. Baker, GP = Glacier Peak, MR = Mt. Rainier, SH = Mt. St. Helens, MA = Mt. Adams, MH = Mt. Hood, MJ = Mt. Jefferson, TS = Three Sisters, NB = Newberry Crater, CL = Crater Lake, MS = Mt. Shasta, LA = Mt. Lassen, ML = Medicine Lake.

Paleomagnetic Evidence

Direct paleomagnetic evidence supporting rotation in front of an expanding Basin and Range province is obscured by the effects of superimposed dextral shear, as discussed earlier. Ideally, an east-west paleomagnetic traverse across the convergent margin should show a stepwise drop in rotation at the trailing edge of the outboard, rotating plate. The paleomagnetic data is permissive of a stepwise decrease in rotation near the Cascade axis, but the "tectonic overprint" of dextral shear does not allow recovery of a unique extensional component of rotation from east-west traverses (Figure 3). Although rotation due to extension is not resolvable on east-west profiles, the southward increase in rotation from western Washington into Oregon may be related to Basin and Range extension. On average, late Eocene and Oligocene units of western Oregon are rotated about 20° more than equivalent units in western Washington. The only substantial difference in plate geometry between Oregon and Washington is the existence of the Basin and Range province inboard of the Oregon segment of the convergent margin. The greater rotation of the Oregon segment probably reflects a component of Basin and Range extension.

Rotation Domains and Arc Structure

Magill and others (1982) proposed that the High Cascade arc is the present eastern boundary of the coastal rotating block, which they called the Willamette plate (Figure 4). They envisioned the High Cascades to be the zone of accommodation between the rotating plate and the extending backarc region (Figure 2). Discontinuous axial grabens along the High Cascades, which seem to merge eastward with Basin and Range structures, and the abundance of basalt and basaltic andesite along the High Cascade axis define the western limit of the extended terrane. The northern extent of the rotated region seems to correlate rather well with the northern limit of extension and young (0-5 Ma) basaltic volcanism in the Cascade arc (Figure 4). North of Mount Rainier, Tertiary rocks of the Cascade Range are essentially unrotated (Beck, 1980), and the structure of the arc is quite different. Pre-Tertiary crust is widely exposed and volcanic rocks are volumetrically insignificant (Ludke and Smith, 1982). The boundary between rotated and unrotated areas is essentially coincident with the boundary between a compressional arc segment to the north and an extenional arc segment to the south. It is marked by abundant folds in Eocene to Miocene volcanic and sedimentary sequences and by transverse faults, roughly parallel to the Olympic-Wallowa lineament (Figure 4; see Smith, in press for a recent compilation). This structural "knot" may mark compression and shearing around the pivot point at the northern edge of the rotating Willamette plate.

At the southern end of the arc, clockwise rotation in Oligocene rocks of the Western Cascades appears to be less than the 30° observed in equivalent rocks of Oregon and Washington. Paleomagnetic results of Beck and others (1986) indicate about 18° of rotation for volcanics (33-23 Ma) exposed along the Klamath River near Copco Reservoir. The outcrop pattern of Western Cascade volcanic rocks in northern California trends about 335°, about 20° west of the present western Cascade trend in Oregon, and suggests that bending of the arc may have occurred.

Tectonic Rotation and Migration of the Volcanic Front

The present-day axis of Cascade volcanism lies east of the volcanic front that was active during Oligocene and Miocene time (e g. Peck and others, 1964). One might ask whether this represents eastward migration of the volcanic front or westward migration of the rifted arc in front of a zone of interarc extension (Figure 5). The southwest trend of Miocene plutons in the Western Cascades along with paleomagnetic evidence for clockwise rotation in the Western Cascades suggest to me that westward migration of the rifted arc is most likely. In fact, the clockwise shift of the Western Cascade pluton alignment with respect to the present volcanic axis is about 15°, close to observed rotations for Miocene rocks in the Western Cascades (Beck and others, 1986, Wells and others, in press and unpublished data).

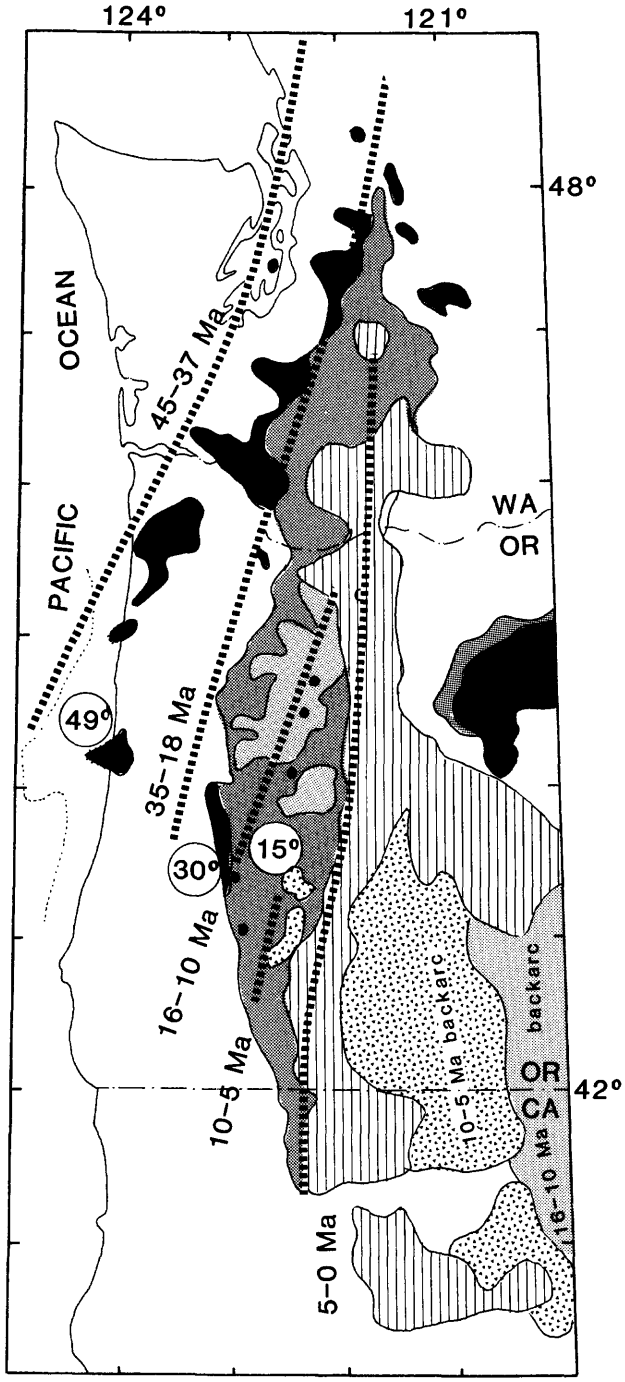

Figure 5. Distribution of Cenozoic volcanic belts of the Pacific Northwest convergent margin, grouped according to age (modified from Guffanti and Weaver, 1988; Smith, in press; King and Beikman, 1974; and Wells and others, 1984). Line indicates approximate location of volcanic front for each belt, number in circle indicates paleomagnetically-determined clockwise rotation of volcanic belt in degrees. Dots in western Cascades of Oregon are mid-Tertiary plutons.

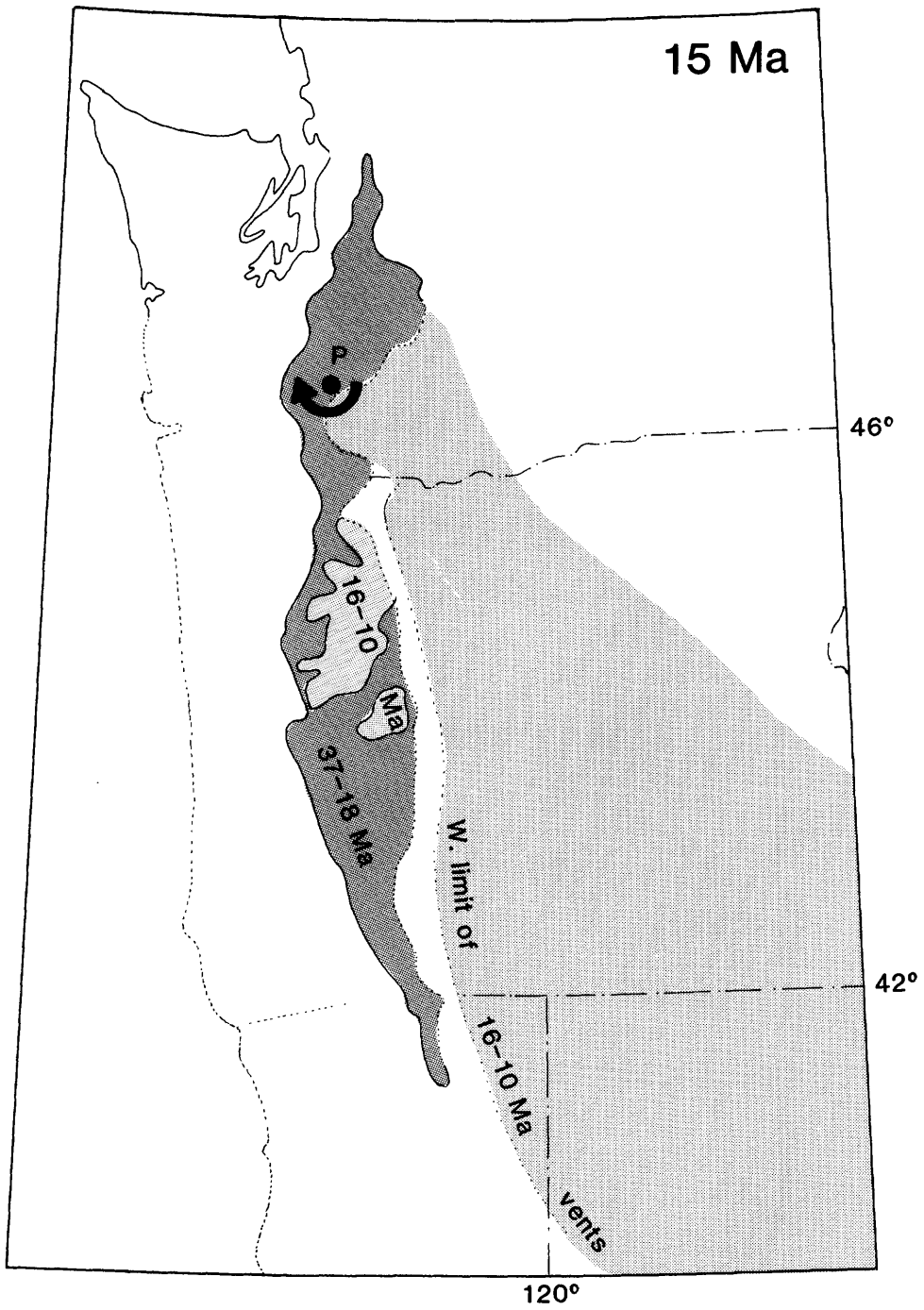

Figure 6. 15 Ma reconstruction of Cascade arc and northwest Basin and Range based on paleomagnetic data (modified from Wells and Heller, 1988 and Guffanti and Weaver, 1988). Miocene arc restores neatly up against western limit of 10-16 Ma volcanism (shaded) defined by Guffanti and Weaver (1988), after removing 12° of rigid plate rotation about pivot point "P". Closeness of fit does not allow for pre-15 Ma crust beneath the High Cascades, although space would be available if accounting was made for post-15 Ma Basin and Range extension to the east.

The volcanic front, or western limit of flows and intrusions, is shifted progressively westward for early Oligocene volcanic rocks and also for Eocene arc volcanic rocks. (Figure 5). If we include contemporaneous Coast Range forearc(?) volcanic rocks (which interfinger with arc-derived detritus) in our determination of the volcanic front, then we obtain a sequence of westward-stepping, progressively more clockwise rotated magmatic belts that merge northward into the unrotated terrane of the north Cascades (Figure 5). This pattern implies that the frontal arc has been migrating westward since Eocene time, with its trailing edge successively off-lapped by younger volcanic sequences, each of which is split by successive episodes of intraarc rifting. The rotating frontal arc would always have been the western limit of extension, similar to what we see today in the southern Cascade arc.

This geometry of a migrating extensional front implies that remnant arc volcanic rocks should be distributed across eastern Oregon in the wake of the rotating terrane. The westward migration of Basin and Range volcanism since 16 Ma (MacLeod and others, 1976, McKee and others, 1983, Guffanti and Weaver, 1988) may, in fact, be tracking the westward migration of the arc (Figure 5). Reconstructions of the rotated arc at 15 Ma closely approach the western limit of 10-16 Ma volcanism indicated by Guffanti and Weaver (1988) and suggest a relationship between westward migrating backarc volcanism and clockwise rotation of the frontal arc (Figure 6). A similar argument might be made for the Eocene and Oligocene volcanic rocks of the present back-arc region, but the distribution of these rocks is poorly known beneath the cover of younger volcanic rocks. However, a broad isostatic residual gravity low behind the southern arc (Blakely and Jachens, this volume) may represent these older volcanic accumulations.

SUMMARY

Paleomagnetic results from Cenozoic volcanic rocks of the Cascade arc and surrounding regions indicate that clockwise tectonic rotations are an important part of the tectonic evolution of the arc. Quality paleomagnetic evidence indicates that the forearc and arc have undergone dextral shear rotations which become larger to the west. These rotations are apparently driven by oblique subduction of the Juan de Fuca plate and are accommodated in the upper crust by local faulting, similar to the St. Helens seismic zone.

These dextral shear rotations probably mask coastal rotation driven by intraarc or backarc extension, which is suggested by the average southward increase of coastal rotations into areas outboard of the Basin and Range. The progressive westward-stepping volcanic front in successively older rocks of the rotated arc terrane implies that the frontal arc block has been migrating westward in front of a zone of extension since Eocene time. The westward migration of Basin and Range volcanism may be tracking the rotation of the frontal arc.

REFERENCES

Atwater, T., 1970, Implications of plate tectonics for the Cenozoic evolution of western North America: Geological Society of America Bulletin, v. 81, p. 3513-3536.

Bates, R.B., Beck, M.E., Jr., and Burmester, R.F., 1981, Tectonic rotations in the Cascade range of southern Washington: Geology, v. 9, p. 184-189.

Beck, M.E., Jr., 1980, Paleomagnetic record of plate-margin tectonic processes along the western edge of North America: Journal of Geophysical Research, v. 85, p. 7115-7131.

Beck, M.E., Jr., and Burr, C.D., 1979, Paleomagnetism and tectonic significance of the Goble Volcanic Series, southwestern Washington: Geology, v. 7, p. 175-179.

Beck, M.E., Jr., and Engebretson, D.C., 1982, Paleomagnetism of small basalt exposures in the west Puget Sound area, Washington, and speculations on the accretionary origin of the Olympic Mountains: Journal of Geophysical Research, v. 87, p. 3755-3760.

Beck, M.E., Jr., and Plumley, P.W., 1980, Paleomagnetism of intrusive rocks in the Coast Range of Oregon: Microplate rotation in middle Tertiary time: Geology, v. 8, p. 573-577.

Beck, M.E., Jr., Burmester, R.F., Craig, D.E., Grommé, C.S., and Wells, R.E., 1986, Paleomagnetism of middle Tertiary volcanic rocks from the Western Cascade series, Northern California: Timing and scale of rotation in the southern Cascades and Klamath Mountains: Journal of Geophysical Research, v. 91, p. 8219-8230.

Beeson, M.H., 1989, The Columbia River Basalt Group in the Cascade Range: a middle Miocene reference datum for structural analysis: this volume.

Beske, S.J., Beck, M.E., Jr., and Noson, L., 1973, Paleomagnetism of the Miocene Grotto and Snoqualmie Batholiths, central Cascades, Washington: Journal of Geophysical Research, v. 78, p. 2601-2608.

Blakely, R.J., and Jachens, R.C., 1989, Volcanism, isotatic residual gravity, and regional tectonic setting of the Cascade volcanic province: this volume.

Engebretson, D.C., Cox, A., and Gordon, R.G., 1985, Relative motions between oceanic and continental plates in the Pacific Basin: Geological Society of America Special Paper 206, 59 p.

Fox, K.F., and Beck, M.E., Jr., 1985, Paleomagnetic results for Eocene volcanic rocks from northeastern Washington and the Tertiary tectonics of the Pacific Northwest: Tectonics, v. 4, p. 323-341.

Frei, L.S., Magill, J.R., and Cox, A., 1984, Paleomagnetic results from the central Sierra Nevada: Constraints on reconstructions of the western United States: Tectonics, v. 3, p. 157-178.

Garfunkel, Z., and Ron, H., 1985, Block rotation and deformation by strike-slip faults 2. The properties of a type of macroscopic discontinuous deformation: Journal of Geophysical Research, v. 90, p. 8589-8602.

Globerman, B.R., Beck, M.E., Jr., and Duncan, R.A., 1982, Paleomagnetism and tectonic significance of Eocene basalts from the Black Hills, Washington Coast Range: Geological Society of America Bulletin, v. 93, p. 1151-1159.

Grommé, C.S., Beck, M.E., Wells, R.E., and Engebretson, D.C., 1986, Paleomagnetism of the Tertiary Clarno Formation of central Oregon and its significance for the tectonic history of the Pacific Northwest: Journal of Geophysical Research, v. 91, p. 14089-14103.

Guffanti, M., and Weaver, C.S., 1988, Distribution of late Cenozoic volcanic vents in the Cascade Range (U.S.A.): volcanic arc segmentation and regional tectonic considerations: Journal of Geophysical Research, v. 93, p. 6513-6529.

Hamilton, W.B., 1988, Plate tectonics and island arcs: Geological Society of America Bulletin, v. 100, p. 1503-1527.

Karig, D.E., 1971, Origin and development of marginal basins in the western Pacific: Journal of Geophysical Research, v. 76, p. 2542-2561.

King, P.B., and Beikman, H.M., 1974, Geologic map of the United States, scale 1:2,500,000: U.S. Geological Survey, Washington, D.C.

Luedke, R.G., and Smith, R.L., 1982, Map showing distribution, composition, and age of late Cenozoic volcanic centers in Oregon and Washington: U.S. Geological Survey Miscellaneous Investigation Series Map I-1091-D, map scale 1:1,000,000.

MacLeod, N.S., Walker, G.W., and McKee, E.H., 1976, Geothermal significance of eastward increase in age of Upper Cenozoic rhyolitic domes in southeastern Oregon: United Nations Symposium on the Development and Use of Geothermal Resources, v. 1, p. 465-474.

Magill, J.R., and Cox, A., 1980, Tectonic rotation of the Oregon western Cascades: Oregon Department of Geology and Mineral Industries Special Paper 10, 67 p.

Magill, J.R., and Cox, A.V., 1981, Post-Oligocene tectonic rotation of the Oregon western Cascade Range and the Klamath Mountains: Geology, v. 9, p. 127-131.

Magill, J.R., Cox, A., and Duncan, R., 1981, Tillamook Volcanic Series: Further evidence for tectonic rotation of the Oregon Coast Range: Journal of Geophysical Research, v. 86, p. 2953-2970.

Magill, J.R., Wells, R.E., Simpson, R.W., and Cox, A.V., 1982, Post 12 m.y. rotation of southwest Washington: Journal of Geophysical Research, v. 87, p. 3761-3776.

Mankinen, E.A., and Irwin, W.P., 1982, Paleomagnetic study of some Cretaceous and Tertiary sedimentary rocks of the Klamath Mountains province, Califonia: Geology, v. 10, p. 82-87.

Mankinen, E.A., Larson, E.E., Grommé, C.S., Prevot, M., and Coe, R.S., 1987, The Steens Mountain (Oregon) geomagnetic polarity transition 3. Its regional significance: Journal of Geophysical Research, v. 92, p. 8057-8076.

McKee, E.H., Duffield, W.A., and Stern, R.J., 1983, Late Miocene and early Pliocene basaltic rocks and their implications for crustal structure, northeastern California and south-central Oregon: Geological Society of America Bulletin, v. 94, p. 292-304.

McKenzie, D., and Jackson, J., 1983, The relationship between strain rates, crustal thickening, paleomagnetism, finite strain and fault movements within a deforming zone: Earth and Planetary Science Letters, v. 65, p. 182-202.

Otofuji, Y., Matsuda, T., and Nohda, S., 1985, Opening mode of the Japan Sea inferred from paleomagnetism of the Japan arc: Nature, v. 317, p. 603-604.

Peck, D.L., Griggs, A.B., Schlicker, H.G., Wells, F.G., and Dole, H.M., 1964, Geology of the central and northern parts of the Western Cascade Range in Oregon: U.S. Geological Survey Professional Paper 449, 56 p., map scale 1:250,000.

Reidel, S.P., Scott, G.R., Bazard, D.R., Cross, R.W., and Dick, B., 1984, Post-12 million year clockwise rotation in the central Columbia Plateau, Washington and Oregon: Tectonics, v. 3, p. 251-274.

Sheriff, S.D., 1984, Paleomagnetic evidence for spatially distributed post-Miocene rotation of western Washington and Oregon: Tectonics, v. 3, p. 397-408.

Sherrod, D.R., 1986, Geology, petrology, and volcanic history of a portion of the Cascade Range between latitudes 43-44°, central Oregon, U.S.A.: Santa Barbara, California, University of California, Ph.D., 320 p.

Sherrod, D.R., and Pickthorn, L.B.G., 1989, Some notes on the Neogene structural evolution of the Cascade Range in Oregon: this volume.

Simpson, R.W., and Cox, A., 1977, Paleomagnetic evidence for tectonic rotation of the Oregon Coast Range: Geology, v. 5, p. 585-589.

Smith, J.G., 1989, Geologic map of upper Eocene to Holocene volcanic and related rocks in the Cascade Range, Washington: U.S. Geological Survey Miscellaneous Investigations Map I, scale 1:500,000, in press.

Smith, J.G., Page, N.J., Johnson, M.G., Moring, B.C., and Gray, F., 1982, Preliminary geologic map of the Medford 1° x 2° quadrangle, Oregon and California: U.S. Geological Survey Open-File Report 82-955, map scale 1:250,000.

Venkatakrishnan, R., Bond, J.G., and Kauffman, J.D., 1980, Geological linears of the northern part of the Cascade Range, Oregon: Oregon Department of Geology and Mineral Industries Special Paper 12, 25 p.

Weaver,C.S., and Smith, S.W., 1983, Regional tectonic and earthquake hazard implications of a crustal fault zone in southwestern Washington: Journal of Geophysical Research, v. 88, p. 10,371-10,383.

Wells, R.E., 1988, Mechanisms of Cenozoic tectonic rotation, Pacific Northwest convergent margin, U.S.A.: in Kiessel, C., and Laj, C., eds., Paleomagnetic rotations and continental deformation, NATO Advanced Study Institute Volume, Kluwer Publishing Co., in press.

Wells, R.E., and England, P.C., 1988, Continuum model of rotations recorded in Miocene flows of the Columbia River Basalt Group, Oregon and Washington: Eos, Transactions, American Geophysical Union, v. 69, p. 1456.

Wells, R.E., Simpson, R.W., Bentley, R.D., Beeson, M.H., Mangan, M.T., and Wright, T.L., 1989, Correlation of Miocene flows of the Columbia River Basalt Group from the central Columbia River Plateau to the coast of Oregon and Washington: Geological Society of America Special Paper, in press.

Wells, R.E., and Coe, R.S., 1985, Paleomagnetism and geology of Eocene volcanic rocks of southwest Washington, Implications for mechanisms of rotation: Journal of Geophysical Research, v. 90, p. 1925-1947.

Wells, R.E., and Heller, P.L., 1988, The relative contribution of accretion, shear, and extension to Cenozoic tectonic rotation in the Pacific Northwest: Geological Society of America Bulletin, v. 100, 325-338.

Wells, R.E., Engebretson, D.C., Snavely, P.D., Jr., and Coe, R.S., 1984, Cenozoic plate motions and the volcano-tectonic evolution of western Oregon and Washington: Tectonics, v. 3, no. 2, p. 275-294.

Volcanism, Isostatic Residual Gravity, and Regional Tectonic Setting of the Cascade Volcanic Province

RICHARD J. BLAKELY AND ROBERT C. JACHENS

U. S. Geological Survey, Menlo Park, California

ABSTRACT

A technique to automatically locate boundaries between crustal blocks of disparate densities was applied to upward-continued isostatic residual gravity data. The boundary analysis delineates a narrow gravitational trough that extends the length of the Quaternary volcanic arc from Lassen Peak in northern California to Mount Baker in northern Washington. Gravitational highs interrupt the trough at two localities: a northwest-trending high in southern Washington and a northeast-trending high between Mount Shasta and Lassen Peak. The latter anomaly is one of a set of northeast-trending anomalies that, within the Quaternary arc, appear related to volcanic segmentation proposed previously on the basis of spatial and compositional distributions of volcanoes. These northeast-trending anomalies extend hundreds of kilometers northeast of the Quaternary arc, are caused by sources in the upper crust, and in some cases are related to exposed pre-Tertiary rocks. Segmentation models invoke geometric characteristics of the subducting plate as the primary factor controlling location and chemistry of volcanism, and these northeast-trending gravity sources also may be a product of disturbance of the upper crust by the subduction process. More likely, the gravity sources may reflect upper crustal structures, possibly relicts from earlier accretionary events or more recent crustal deformation, that have actively influenced the spatial location of more recent volcanism. Much of the Pliocene and Quaternary volcanism of the Cascade arc has concentrated on or near contacts between crustal blocks of disparate density. These contacts may promote the ascension of magma to the earth's surface.

INTRODUCTION

Volcanism associated with orogenic belts has been a part of the Pacific Northwest since at least the Mesozoic era, but the narrow Cascade volcanic arc of today, extending from northern California to British Columbia, is a relatively modern feature of the continental margin. The Cascade volcanic province is often divided into two parts on the basis of age and volcanic style. Calc-alkaline volcanic rocks of the Western Cascade Range (Figure 1) erupted from late Eocene to Miocene time in a broad zone across much of western Oregon and Washington. The volcanic arc narrowed markedly during Pliocene and Quaternary time to form the distinctive High Cascade volcanoes of today (Figure 1). The Quaternary arc, generally less than 75 km wide, extends over 1100 km from southeast of Lassen Peak in northern California to Mount Garibaldi in British Columbia. The Cascade volcanic province is clearly a consequence of subduction of the Juan de Fuca, Gorda, and Explorer plates beneath North America, although various aspects of subduction are not well displayed: there is no pronounced trench offshore, no clearly defined Benioff zone along most of the arc, and relatively little volcanism during historic time [*McBirney and White*, 1982].

Various authors have proposed plate-plate interactions to explain geological and geophysical variations along the length of the Cascade Range. *Rogers* [1985], for example, suggested that regional tectonism changes from slightly compressional in Washington to slightly extensional in Oregon because of the orientation of the convergent margin. *Weaver and Michaelson* [1985] divided the northern Cascades into three segments based on distribution of earthquakes and Cenozoic volcanism. More recently, *Guffanti and Weaver* [1988] have studied the spatial, temporal, and compositional distribution of volcanoes and proposed a five-segment model for the Cascade Range.

The application of gravity measurements to the Cascade volcanic province has had a long history [e.g., *Pakiser*, 1964; *LaFehr*, 1965; *Blank*, 1968; *Thiruvathukal et al.*, 1970; *Couch et al.*, 1981, 1982; *Williams and Finn*, 1985; *Blakely et al.*, 1985]. Variation in density between volcanic ejecta, flows, and underlying

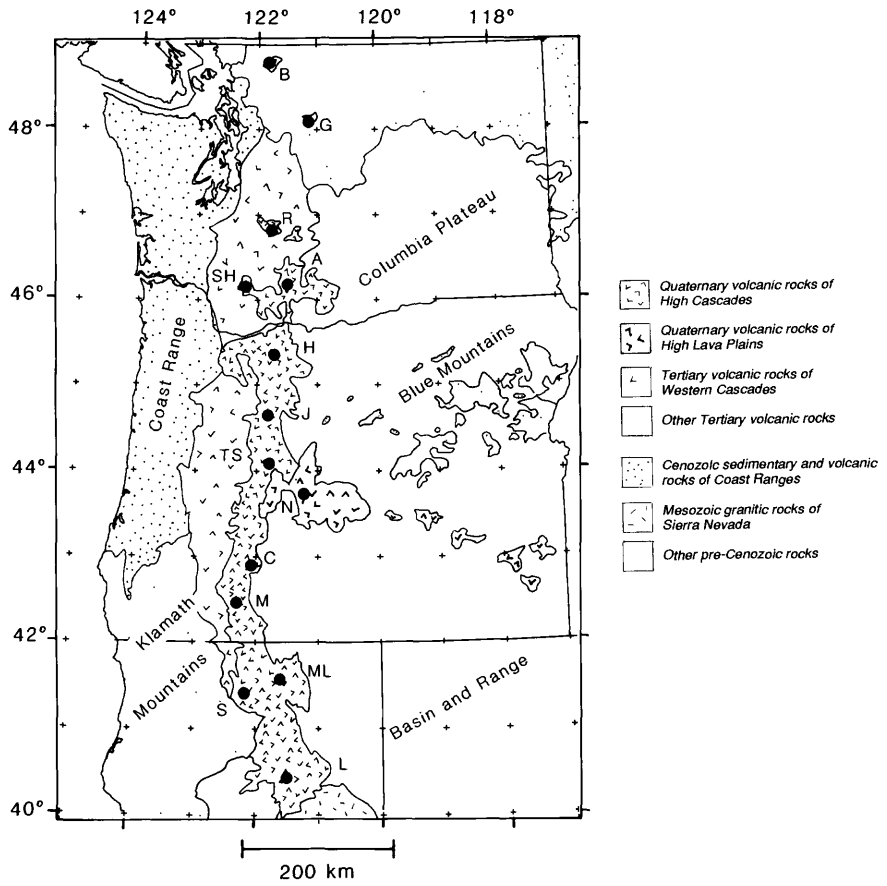

Fig. 1. Generalized geologic map of the Cascade volcanic province and surrounding areas of the Pacific Northwest. Modified from *Walker and King* [1969], *Weissenborn* [1969], and *Grommé et al.* [1986]. Letters refer to major volcanoes: B, Mount Baker; G, Glacier Peak; R, Mount Rainier; SH, Mount St. Helens; A, Mount Adams; H, Mount Hood; J, Mount Jefferson; TS, Three Sisters; N, Newberry Crater; C, Crater Lake; M, Mount McLoughlin; S, Mount Shasta; ML, Medicine Lake; L, Lassen Peak.

basement rocks causes distinctive regional gravity anomalies that can be used to learn about the distribution of mass in and beneath the volcanic terrane. Specifically, aspects of the structure of underlying basement rocks, the petrology and lithology within the volcanic terrane, and the tectonic setting of the entire province can be inferred from gravity data. Such studies are most powerful when used concomitantly with other geophysical, geological, and geochemical information.

The Cascade volcanic province contains many regional structural features of sufficient size to be detected by gravity techniques. *Thayer* [1936], for example, proposed that an eastward-facing, north-trending scarp, which he termed the "Cascade fault," forms the structural boundary between the Western and High Cascades in Oregon. Movement along the Cascade fault raised the older Western Cascades at least 600 m relative to the eastern block and was followed by initiation of High Cascade volcanism to the east which largely buried the surface expression of the fault. *Allen* [1966] proposed a second north-trending fault, down-dropped to the west, parallel to and ≈30 km east of the Cascade fault. The resulting inferred graben includes Mount Hood, Mount Jefferson, Three Sisters, and Crater Lake; south of Crater Lake, the trend of the graben swings southeast to exclude Mount McLoughlin [*Allen*, 1966]. *Couch et al.* [1981, 1982] examined residual gravity data from the Cascade Range and found a narrow, north-trending gravitational minimum that extends from

the Columbia River to nearly the Oregon-California border. They proposed that this minimum delineates a major fracture or brecciated zone. The gravitational minimum is generally coincident with the graben of *Allen* [1966], but it lies west of Mount Jefferson and Three Sisters.

Blackwell et al. [1982] noted a correlation between Bouguer gravity gradients and high conductive heat flow gradients roughly 35 km west of the Three Sisters at latitude 44°N. They interpreted the correspondence between Bouguer anomalies and heat flow in this region to reflect a north-south zone of hot, partially molten material at a depth of about 10 km beneath the High Cascades and extending west to the location of high heat-flow and gravity gradients. However, part of the Bouguer gradient in this region is caused by proximity to the continental edge and by the presence of deep crustal masses that compensate the topographic edifice of the Cascade Range. Bouguer anomaly values do show a slight correlation with measured heat flow values, but residual values, calculated by subtracting a regional field from the Bouguer anomaly, are not statistically correlated [*Ingebritsen et al.*, this volume].

Ingebritsen et al. [this volume] suggested that anomalous heat flow in the Western Cascade Range near latitude 44°N. is caused by a narrow, spatially variable intrusive zone, and that the heat flow anomaly expands laterally at shallow depths due to ground-water flow. The Quaternary Cascade arc has virtually no conductive near-surface heat flow, whereas older rocks display anomalously high conductive and advective heat flow. The analysis of *Ingebritsen et al.* [this volume] indicated that anomalous near-surface heat flow arises from ground-water circulation that sweeps heat advectively from the young rocks to the old. Any deeper thermal anomaly is essentially confined to the Quaternary arc; laterally extensive magmatic sources of the type envisioned by *Blackwell et al.* [1982] are not required.

The gravity field of the Pacific Northwest reflects significant crustal structures that have influenced the location of modern-day volcanic activity. It was noted earlier [*Blakely et al.*, 1985] that major volcanoes south of Mount Jefferson are located along the margins of regional gravity depressions. The gravity depressions were interpreted as reflecting structural depressions; volcanoes are focused near the edges of these depressions presumably because bounding faults and fractures have promoted ascension of magma to the surface. In this paper, we investigate the spatial relation between Pliocene and Quaternary volcanism and regional gravity data throughout the Cascade volcanic province in the United States and compare that relationship with arc segmentation and heat-flow observations.

Method

The gravity method is well-established as a tool to delineate regional geologic features. In this paper, we are interested particularly in regional aspects of the middle and upper crust and, therefore, want to eliminate long-wavelength anomalies related to isostatic compensation of topographic loads and short-wavelength anomalies caused by local density variations. These problems are treated by an isostatic correction and by upward continuation, respectively.

Isostatic Residual

The Bouguer anomaly includes long-wavelength components caused by deep sources that isostatically support topographic loads. These regional anomalies are especially prominent in mountainous regions and in regions near continental borders and tend to obscure anomalies caused by lithotectonic variations in the crust. Regional anomalies can be removed by subtracting long-wavelength surfaces estimated from the Bouguer anomaly. Regional fields are often calculated by polynomial fitting [*Coons et al.*, 1967] or by wavelength filtering [*Kane and Godson*, 1985] of the Bouguer anomaly, but these techniques suffer from the fact that they eliminate all wavelengths longer than some threshold, whether or not they are related to topographic features. In particular, long-wavelength anomalies due entirely to lateral variations in crustal density will be eliminated by these techniques.

An isostatic correction is our prefered method for eliminating regional anomalies in the western United States [*Simpson et al.*, 1983, 1986]. Digital topographic models are used to calculate the shape of the crust-mantle interface consistent with the Airy-Heiskanen model for local isostatic compensation; the gravitational effect of this interface is calculated and subtracted from the Bouguer anomaly to produce an isostatic residual anomaly. The isostatic residual data used in this paper were calculated from the Gravity Anomaly Map of the United States [*Godson and Scheibe*, 1982; *Society of Exploration Geophysicists*, 1982]. These same data

were used previously to prepare an isostatic residual map for the conterminous United States [*Simpson et al.*, 1986, plate 1].

The Airy model assumes purely local isostatic compensation, which may not be entirely appropriate for areas of regional stress and distributed tectonic and thermal phenomena like the Pacific Northwest. Although the Airy model is undoubtedly oversimplified, the isostatic correction that it provides is very long in wavelength [*Simpson et al.*, 1986, Figure 6], and minor differences provided by other models will not greatly affect our conclusions. Moreover, *McNutt* [1980] studied the isostatic response of continental lithosphere to topographic loads and concluded that local compensation dominates regional compensation in the western U. S.

Upward Continuation

Figure 2 shows isostatic residual gravity anomalies continued upward to 10 km above the earth. Upward continuation is a transformation of anomalies measured at one level into those that would be observed at a higher level. Upward continuation tends to smooth all wavelengths, but shortest wavelengths are attenuated more rapidly than long wavelengths [*Blakely*, 1977]. Because anomalies increase in wavelength with increasing dimensions of and increasing distance from the source, upward continuation emphasizes anomalies due to regional, deep structures at the expense of smaller, shallower sources.

Consider, for example, an anomaly caused by a spherical mass located at depth z below the survey elevation. Upward continuation by height Δz attenuates the anomaly by a factor

$$A = \left[\frac{z}{z + \Delta z}\right]^2$$

and A is clearly dependent on the depth z of the mass. Upward continuation by 10 km attenuates the anomaly of a 1-km-deep sphere by a factor of 0.008 but attenuates the anomaly of an identical sphere at 10 km depth by only 0.250. A similar relation holds for more complicated masses: upward continuation attenuates anomalies due to shallow sources more than anomalies due to deep sources.

Upward continuation requires no assumptions about the distribution of crustal densities beneath the survey area. However, assumptions are required about the manner in which crustal density continues beyond the limits of the gravity survey; incorrect assumptions can cause large errors in anomalies located near the edge of the survey. Our starting grid covers the entire conterminous United States. Therefore, we were able to extend our "survey" well beyond the limits shown in Figure 2, perform the upward continuation, and then trim the survey back to the limits of Figure 2, virtually eliminating the possibility of errors near the edges of our survey.

Boundary Analysis

A technique [*Blakely and Simpson*, 1986] for automatically locating the edges of gravity sources was applied to the upward-continued isostatic residual gravity data. The method is a two-step procedure. First, the magnitude of maximum horizontal gradient is calculated. Anomaly gradients tend to be steepest over the edges of gravity sources. Consequently, the horizontal-gradient calculation transforms gravity anomalies into maxima that approximately overlie boundaries between regions with disparate density [*Cordell*, 1979]. Second, maxima in the horizontal gradient are automatically located and plotted [*Blakely and Simpson*, 1986], which results in sinuous sequences of dots that represent density boundaries. Figure 3 shows the application of this technique to the residual gravity data of Figure 2.

VOLCANOES

The distribution of volcanic vents can be a better indicator of regional volcanism than either the lateral extent of eruptive products or the distribution of major stratovolcanoes or composite centers [*Smith and Luedke*, 1984]. Vent location, composition, and age were digitized by *Guffanti and Weaver* [1988] from maps compiled by *Luedke and Smith* [1981, 1982]. Figure 4 shows the distribution of volcanoes in the Cascade Range calculated from digital vent locations.

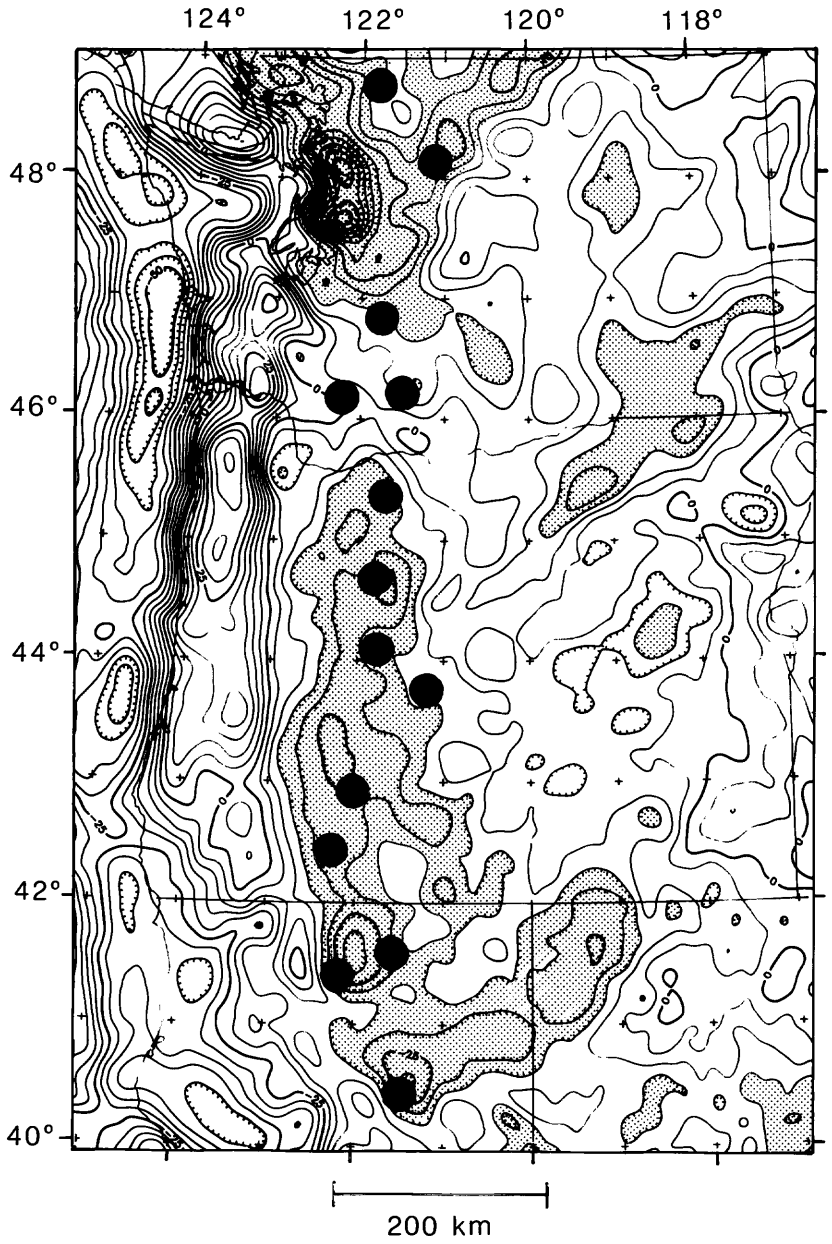

Fig. 2. Isostatic residual gravity continued upward 10 km. Contour interval 5 mGal. Hachures directed toward gravitational minima. Stipple pattern indicates <-25 mGal. Dots indicate major volcanoes; see Figure 1 for labels.

Guffanti and Weaver [1988] discussed in detail the spatial, temporal, and compositional distribution of Cascade vents and divided them into five segments shown in Figure 4: (1) the isolated stratovolcanoes of northern Washington, (2) the wide zone of dominantly basaltic vents from Mount Rainier to Mount Hood, (3) the narrow zone of andesitic vents from south of Mount Hood to the Oregon-California border, (4) the broad zone that includes Mount Shasta and Medicine Lake volcano, and (5) the spatially isolated Lassen Peak area. The west-northwest-trending belt of vents of the High Lava Plains (Figure 1) forms a sixth

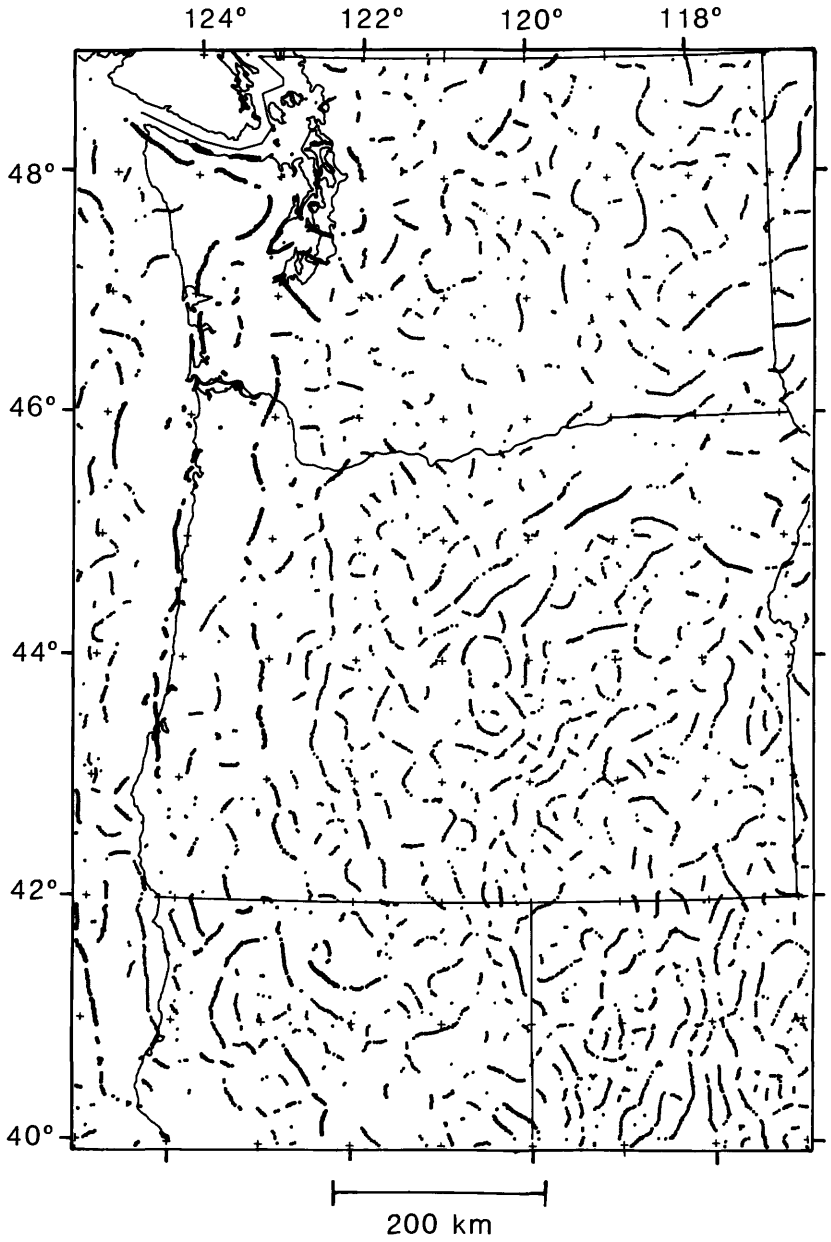

Fig. 3. Automatically calculated boundaries between mass densities. Size of circle proportional to steepness of horizontal gradient.

segment outside of the Cascade arc. The relationship between isostatic residual gravity (Figure 2), volcanic vents (Figure 4), and proposed segmentation will be discussed subsequently.

Discussion

A prominent gravitational depression is visible along most of the Cascade Range (Figure 2). The trough extends from the Lassen Peak area to the Washington-Oregon border where it is interrupted by a northwest-trending gravity ridge in southern Washington. The trough continues in northern Washington, although

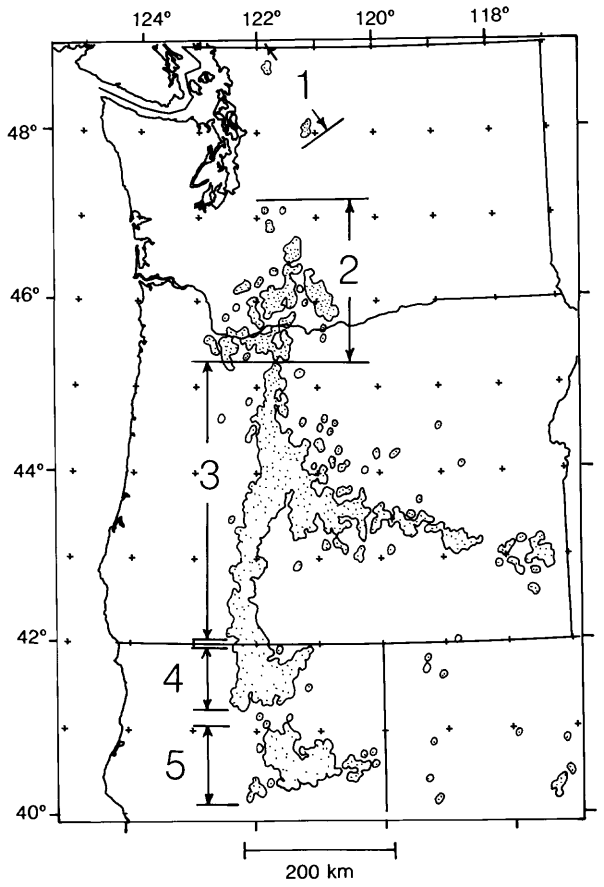

Fig. 4. Location of volcanoes younger than 5 Ma. Vents were tallied in overlapping cells 0.5 degrees on each side. Stippled area encloses cells with at least one vent. Numbers refer to segments discussed by *Guffanti and Weaver* [1988].

its relationship with the Cascade arc is less obvious. A less pronounced gravity ridge trends northeast and separates the Lassen Peak gravity low from the trough that extends from Mount Shasta to the Washington-Oregon border. With the exception of two groups of volcanoes, all Pliocene and younger vents (Figure 4) lie within or on the edge of the gravitational depression (Figure 2). The exceptions are the cluster of vents in southern Washington and extreme northern Oregon, including Mount St. Helens and Mount Adams, and the chain of vents of the High Lava Plains of central Oregon.

The gravitational depressions of the Cascade arc are bounded on the west by one of the largest positive anomalies in North America [*Simpson et al.*, 1986]. This positive anomaly is caused in part by mafic igneous rocks of the Coast Ranges in Oregon and Washington [e.g., *Finn*, this volume] and by mafic and ultramafic rocks of the Klamath Mountains in southern Oregon and northern California [e.g., *Griscom*, 1980] (Figure 1), but part of the anomaly may be caused by isostatic effects. An isostatic residual gravity map for the whole of North America [*Simpson et al.*, 1988] shows a broad positive anomaly west of the trench (and west of Figure 2) that corresponds with a fore-trench bulge in bathymetric data. This offshore anomaly may indicate loading and flexing of the Juan de Fuca plate by the North American plate. Similar but larger bulges are seen at other subduction zones, such as south of the Aleutian Islands [*Watts et al.*, 1976] and west of Central America. If the offshore anomaly is caused by loading and flexing of the Juan de Fuca plate, then the plate probably has sufficient strength to support the overriding North American plate to some extent, thereby contributing to the large positive anomaly over the Coast Ranges.

A broad region with generally subdued anomalies lies east of the gravitational depression. The region is interspersed with a series of northeast-trending anomalies. *Riddihough et al.* [1986] interpreted the most prominent of these northeast-trending anomalies, the steep gradient trending northeast from central Oregon to extreme southeastern Washington (Figure 2), as reflecting a buried connection between pre-Tertiary rocks in the Blue Mountains with similar rocks in the Klamath Mountains; its present northeast orientation is presumably the result of clockwise rotation of a Jurassic-age, north-south transform fault or continental margin.

The gravitational depression over the Cascade volcanic province is not an artifact of the data reduction. A density of 2.67 g/cm^3 was assumed for all rocks above sea level in order to compute both the Bouguer and isostatic correction, and this density may be too high for typical Cascade volcanic rocks [*Williams and Finn*, 1985]. We recomputed the upward-continued, isostatic residual map using densities of 2.43 and 2.28 g/cm^3. The latter density is unreasonably small, but provides a limiting case. The regional depression was preserved in both cases, and we conclude that the gravitational trough is not a result of our selection of an improper density for the Cascade Range.

Spatial Relation of Density Boundaries and Volcanism

Figure 5 shows our interpretation of isostatic residual gravity data in the northwestern United States. Boundaries between areas of disparate density were interpreted from Figures 2 and 3 with particular attention to north-trending features associated with the Cascade arc and northeast-trending features subparallel to the Blue Mountain-Klamath Mountain lineament [*Riddihough et al.*, 1986].

The long, north-south boundary (Figure 5, location a) in western Oregon, southern Washington, and northern California lies near the western limit of the Western Cascades. It reflects the difference in density between the volcanic rocks of the Western Cascades and the more mafic igneous rocks of the Coast Ranges and Klamath Mountains.

The Quaternary arc in Oregon and northern California (Figure 5) sinuates within and along the edge of the gravity trough. From 43°30' to 45°N., Quaternary volcanism has concentrated very close to the eastern edge of the trough. South of 43°30'N., Quaternary volcanism has concentrated near the center of the trough. Moreover, nearly all major volcanic centers lie very near a gravitational boundary. Mount St. Helens, Mount Adams, Mount Hood, Mount Jefferson, Three Sisters, Crater Lake, Medicine Lake volcano, Mount Shasta, and Lassen Peak all lie within 10 km of a density boundary. Mount Rainier and Mount Baker lie approximately 20 km from a boundary. Newberry Crater is the only major volcanic center of the Quaternary arc that is not near a density boundary. Gravity anomalies in the Cascade volcanic province reflect geologic boundaries between blocks of disparate density; apparently these boundaries are foci for the ascension of magma to the surface within the Quaternary arc [*Blakely et al.*, 1985].

Segmentation

Guffanti and Weaver [1988] proposed on the basis of spatial, temporal, and compositional distribution of volcanoes that the Cascade arc is divided into five segments (Figure 4). As summarized in Figure 6, the gravity data are consistent with much of their interpretation. The best agreement between gravity data and their proposed segmentation occurs in the Mount Shasta and Lassen Peak area. The residual gravity low over Lassen Peak is part of a more regional northeast-trending depression (Figure 6, region A). Within the Quaternary arc, the southern boundary of region A agrees precisely with the southern limit of segment 5 (Figure 4; Figure 5, location b), but the gravity boundary extends nearly 400 km northeast of Lassen Peak, across the northwestern corner of Nevada and nearly into southeastern Oregon. It extends northeast well beyond the majority of young vents, although basaltic vents appear associated with the gravity boundary as far east as the Nevada-California border. The gradients of the anomaly indicate that its source is in the upper crust. In Nevada, this abrupt gradient has been interpreted by *McKee et al.* [1989] as the northwestern limit of pre-Cenozoic basement rocks.

A northeast-trending gravity high (Figure 6, region B) separates the gravitational depressions over Mount Shasta and Lassen Peak. Within the Quaternary arc, the gravity high corresponds closely with the boundary between segments 4 and 5 (Figure 4; Figure 5, location c), but the gravity high extends over 400 km northeast of Mount Shasta. The steepness of the gravity gradients indicate that the source is located in the upper crust [*Griscom*, 1980; *Blakely et al.*, 1985]. Moreover, *Zucca et al.* [1986] interpreted a shallow

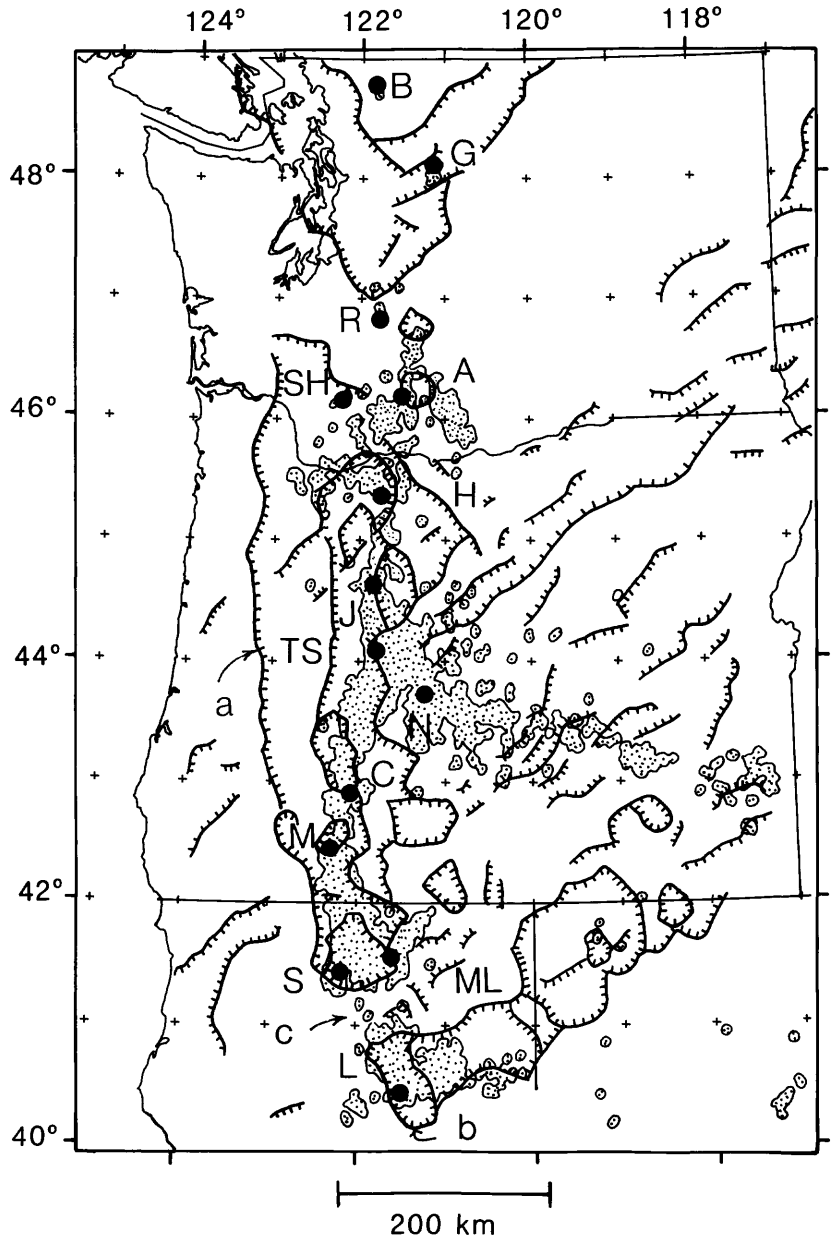

Fig. 5. Interpretation of boundary analysis. Bold, hachured lines indicate boundaries between regions of disparate density as interpreted from Figures 2 and 3. Stippled area indicates lateral extent of young volcanic vents (Figure 4). Capital letters and associated dots are major volcanoes; see Figure 1 for volcano names. Lowercase letters indicate features discussed in text.

"basement" high from seismic refraction data in the vicinity of Medicine Lake which corresponds spatially with region B (Figure 6). The basement high is approximately 40 km wide in the north-south direction and is buried approximately 1 km below sea level; the basement has a seismic velocity of 6.2-km/sec.

Similar to region A, the gravity depression over Mount Shasta (Figure 6, region C) continues at least 400 km to the northeast. The northern limit of region C within the Quaternary arc corresponds only roughly

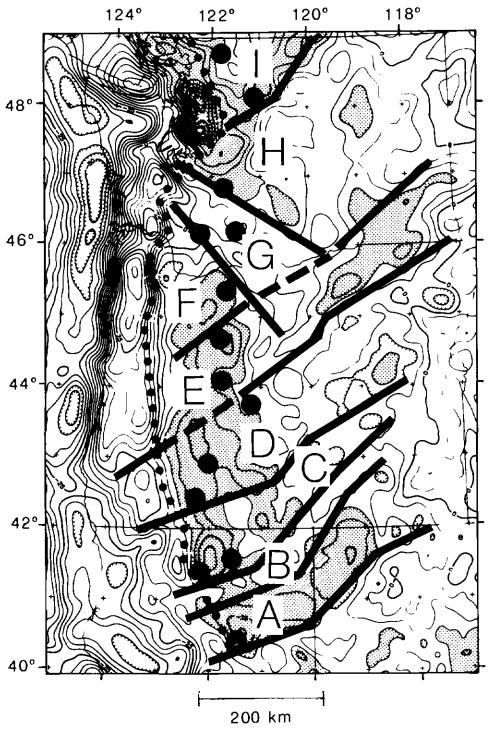

Fig. 6. Relation between gravity boundaries and segmentation. Contour and stippling same as Figure 2. Bold lines are structural contacts interpreted from Figures 2, 3, and 5. Dotted line is the eastern edge gravitational expression of the Klamath Mountains, Coast Range, and Puget Sound. Large dots indicate major volcanoes; see Figure 1 for labels.

with the boundary between segments 3 and 4 (Figure 4). *Guffanti and Weaver* [1988] considered segment 3 to continue from the California-Oregon border to just south of Mount Hood. The gravity data suggest that other segments (Figure 6, regions D and E) may exist north and south of the Three Sisters on strike with the gravity lineations over the Blue Mountains, as suggested by *Riddihough et al.* [1986].

A northwest-trending gravity high (Figure 6, region G) is located within segment 2, includes most of the vents of segment 2, and separates the Oregon-California gravity depressions from similar depressions in Washington. Region G is enigmatic for several reasons. It is the most pronounced high in an otherwise reasonably continuous gravity trough that extends the full length of the Cascade Range in the United States. It includes the only vents of the Cascade arc that do not lie within or near the edge of a gravitational depression. It trends northwest, whereas most gravitational features crossing the Cascade arc trend northeast. Nearly all large-magnitude earthquakes of the Cascade arc have occurred within this enigmatic gravity feature [*Weaver*, this volume].

The relation between volcanic activity and gravity anomalies is confused in northern Washington partly because of the very pronounced minimum over the Puget Sound area. This minimum probably is caused by thick accretionary deposits related to subduction of the Juan de Fuca plate [*Simpson et al.*, 1986]. *Stuart* [1961] estimated the thickness of the sedimentary deposits to be greater than 12 km assuming a density

contrast with surrounding Eocene volcanic rocks of 0.2 g/cm^3. In spite of the complex gravity anomalies in this region, the southern boundary of segment 1 (Figure 4) corresponds closely with the southern boundary of region I (Figure 6).

Northeast-trending gravity anomalies in eastern Oregon, southeastern Washington, northeastern California, and northwestern Nevada appear related to segmentation of the Cascade arc proposed by *Guffanti and Weaver* [1988]. Segmentation at other convergent margins [e.g., *Carr et al.*, 1973, 1974] is defined by longitudinal changes in distribution of epicenters, dip of the Benioff zone, and distribution of andesitic volcanoes. These longitudinal changes are explained by fundamental structures of the descending lithosphere, such as tear faults that affect the dip of the subducting slab and shift the axis of volcanism perpendicular to the trench. The Cascade arc, however, has very little seismicity and no pronounced Benioff zone, and *Guffanti and Weaver* [1988] relied primarily on the spatial and compositional distribution of volcanoes to define Cascade segmentation.

The relation between northeast-trending gravity anomalies and Cascade segmentation, and the fact that the anomalies are approximately parallel to motion of the Farallon plate relative to North America [*Engebretson et al.*, 1985], suggest that the sources of these anomalies are also related to presently subducting lithosphere. Several factors argue against this explanation. First, many of the gravity gradients are too steep to be caused by sources in the lower crust or below, and at least some of the gravity boundaries are caused in part by structural features that crop out. For example, the southern boundary of region A (Figure 6) is the northern limit of exposed pre-Tertiary basement [*McKee et al.*, 1989], and *Riddihough et al.* [1986] interpreted the gravity anomaly that trends northeast from central Oregon to extreme southeastern Washington (Figure 2) to be caused in part by exposed pre-Cenozoic rocks of the Blue Mountains. Seismic refraction data indicate that region B is caused by sources within a few kilometers of the earth's surface. It is difficult to imagine a causal connection between the emplacement of these upper crustal rocks and present-day subduction of the oceanic plate.

Second, geologic and paleomagnetic evidence indicates that rocks associated with the northeast-trending gravity anomalies have been in their present orientation since the early part of the Tertiary. The Blue Mountains province is an accreted island arc terrane of pre-Tertiary age [*Hamilton*, 1978; *Dickinson and Thayer*, 1978]. Upper Jurassic to Lower Cretaceous granitic and high-temperature metamorphic rocks within the Blue Mountains province have rotated 60° ±29° clockwise relative to the stable craton [*Wilson and Cox*, 1980]. However, andesitic and volcaniclastic rocks of the nearby Clarno Formation, mostly of Eocene age, have rotated only 16° ±10° clockwise [*Gromme et al.*, 1986], and the Columbia River Basalt Group of middle Miocene age has not rotated significantly [*Choinere and Swanson*, 1979; *Hooper et al.*, 1979; *Rietman*, 1966; *Watkins and Baksi*, 1974]. Rotation of the Blue Mountains province, therefore, was largely completed prior to eruptions of the Clarno Formation and entirely completed by the end of Columbia River Basalt eruptions [*Gromme et al.*, 1986].

Hence, the northeast-trending gravity anomalies are not related to modern-day subduction of the Farallon plate, and their relationship with Cascade segmentation may be coincidental. Alternatively, segmentation of the Quaternary arc may be influenced by the upper-crustal, pre-Tertiary structures that cause the northeast-trending anomalies. These structures predate the Quaternary volcanism and may extend beneath the Quaternary arc. As discussed previously, the location of volcanism appears partially controlled by crustal structures that are reflected in gravity data, and Cascade segmentation may be influenced by similar effects.

Gravity and Heat Flow

Blackwell et al. [1982] noted a correlation between Bouguer gravity and heat flow gradients located roughly 35 km west of Three Sisters volcanoes at about 44°N. They interpreted the correlation to reflect a widespread, mid-crustal magmatic heat source at this location, elongated north-south and extending west well into the Western Cascade Range. *Ingebritsen et al.* [this volume] disagreed on the basis of a detailed heat-budget analysis and interpreted the near-surface heat flow to reflect advective transfer of heat from a narrow magmatic source no wider than the Quaternary arc itself.

Figure 5 (location d) shows a density boundary located roughly 40 km west of Three Sisters at 44°N., which seems to support the interpretation of *Blackwell et al.* [1982]. Other explanations for the density boundary are possible, however. For example, the density boundary may reflect a geologic contact rather than a thermal discontinuity. The juxtaposition of rocks of disparate density along a north-south fault, as

described in the same location by *Sherrod* [1986], may account for the gravitational gradient near 44°N.

Conclusions

Gradients in isostatic residual gravity data define boundaries between crustal blocks of disparate density that are related to the volcanic development of the Cascade Range. Our results are consistent with previous ideas about segmentation of the Cascade arc [*Guffanti and Weaver*, 1988], but deciphering the causal relationship between crustal density and segmentation is not straightforward.

Segmentation models commonly invoke geometric characteristics of the subducting plate as the primary factor controlling location and chemistry of upper-crustal volcanism. Like volcanoes, the gravitational boundaries are upper crustal in origin, and perhaps they also are a product of disturbance of the crust by the subduction process. More likely, the density boundaries may reflect upper-crustal structures that predate the Cascade arc and have influenced the spatial location of volcanism. The array of linear anomalies extending hundreds of kilometers northeast of the Cascade Range supports the latter hypothesis. At least one of these anomalies, extending northeast from central Oregon to southeastern Washington (Figure 2), appears related to segmentation within the Cascade arc but is caused by exposed pre-Tertiary rocks of the Blue Mountains province far from the arc. These rocks were in their present orientation by the middle Miocene and are not related to modern-day subduction of the Farallon plate. Moreover much of the Pliocene and Quaternary volcanism has concentrated on or near the contact between crustal blocks of disparate density. Apparently, these contacts promote the ascension of magma to the earth's surface.

Acknowledgments

We are grateful to Andy Griscom, Dave Sherrod, Jim Smith, Jim Case, Tom Hildenbrand, and Marianne Guffanti for helpful comments and discussions. We also thank Marianne Guffanti and Craig Weaver for providing us with digital vent locations. This research was funded by the U. S. Geological Survey Geothermal Research Program.

References

Allen, J. E. The Cascade Range volcano-tectonic depression of Oregon, in *Transactions of the Lunar Geological Field Conference, Bend, Oregon, August 1965*, 98pp. State of Oregon Department of Geological and Mineral Industries, Portland, 1966.

Blackwell, D. D., R. G. Bowen, D. A. Hull, J. Riccio, and J. L. Steele, Heat flow, arc volcanism, and subduction in northern Oregon, *J. Geophys. Res., 87*, 8735-8754, 1982.

Blakely, R. J., Documentation for subroutine REDUC3, an algorithm for the linear filtering of gridded magnetic data, *U. S. Geol. Surv. Open-File Report 77-784*, 27 p., 1977.

Blakely, R. J., R. C. Jachens, R. W. Simpson, and R. W. Couch, Tectonic setting of the southern Cascade Range as interpreted from its magnetic and gravity fields, *Geol. Soc. Am. Bull., 96*, 43-48, 1985.

Blakely, R. J. and R. W. Simpson, Approximating edges of source bodies from magnetic or gravity anomalies, *Geophysics, 51*, 1494-1498, 1986.

Blank, H. R., Aeromagnetic and gravity surveys of the Crater Lake region, Oregon, *in* Dole, H. M., ed., *Andesite Conference Guidebook*, Oregon Department of Geology and Mineral Industries Bulletin 62, 42-52, 1968.

Carr, M. J., R. E. Stoiber, and C. L. Drake, Discontinuities in the deep seismic zones under the Japanese arcs: *Geol. Soc. Am. Bull., 84*, 2917-2930, 1973.

Carr, M. J., R. E. Stoiber, and C. L. Drake, The segmented nature of some continental margins, *in* Burke, C. A., and C. L. Drake, eds., *The Geology of Continental Margins*, Springer-Verlag, New York, 105-114, 1974.

Choinere, S. A., and D. A. Swanson, Magnetostratigraphy and correlation of Miocene basalts of the northern Oregon coast and Columbia plateau, southeast Washington, *Am. J. Sci., 279*, 755-777, 1979.

Coons, R. L., G. P. Woollard, and G. Hershey, Structural significance and analysis of mid-continent gravity high, *Bull. Am. Assoc. Petrol. Geol., 51*, 2381-2399, 1967.

Cordell, L., Gravimetric expression of graben faulting in Santa Fe country and the Española basin, New Mexico, *in* R. V. Ingersoll, ed., *Guidebook to Santa Fe country*, New Mexico Geol. Soc. Guidebook, 30th Field Conference, 59-64, 1979.

Couch, R. W., M. Gemperle, G. Connard, and G. S. Pitts, Structural and thermal implications of gravity and aeromagnetic measurements made in the Cascade volcanic arc, *Society of Exploration Geophysicists Annual International Meeting*, Los Angeles, California, 14, 1981.

Couch, R. W., G. S. Pitts, M. Gemperle, D. E. Braman, and C. A. Veen, Gravity anomalies in the Cascade Range in Oregon: structural and thermal implications, Oregon Department of Geology and Mineral Industries Open-File Report 0-82-9, 66 p., 1982.

Dickinson, W. R., and T. P. Thayer, Paleogeographic and paleotectonic implications of Mesozoic stratigraphy and structure in the John Day inlier of central Oregon, *in* Howell, D. G., and K. A. McDougall, eds., *Mesozoic Paleogeography of the Western United States*, Society of Economic Paleotologists and Mineralogists, Los Angeles, Calif., 147-161, 1978.

Engebretson, D. C., A. Cox, and R. G. Gordon, Relative motions between oceanic and continental plates in the Pacific basin, *Geol. Soc. Am. Sp. Pub. 206*, 59 p., 1985.

Finn, C., Structure of the Washington margin, *U. S. Geol. Surv. Open-File Rep.*, this volume.

Godson, R. H., and D. M. Scheibe, Description of magnetic tape containing conterminous U. S. gravity data in gridded format, *Rep. PB82-254798*, magnetic tape with description, 5 pp., Natl. Tech. Inf. Serv., Springfield, Va., 1982.

Griscom, A., Klamath Mountains province, *in* H. W. Oliver, ed., *Interpretation of the gravity map of California and its continental margin*, Calif. Div. Mines and Geol. Bull. 205, 34-36, 1980.

Guffanti, M., and C. S. Weaver, Distribution of late Cenozoic volcanic vents in the Cascade Range: volcanic arc segmentation and regional tectonic considerations, *J. Geophys. Res., 93*, 6513-6529, 1988.

Grommé, C. S., M. E. Beck, Jr., R. E. Wells, and D. C. Engebretson, Paleomagnetism of the Tertiary Clarno Formation of central Oregon and its significance for the tectonic history of the Pacific Northwest, *J. Geophys. Res., 91*, 14,089-14,103, 1986.

Hamilton, W., Mesozoic tectonics of the western United States, *in* Howell, D. G., and K. A. McDougall, eds., *Mesozoic Paleogeography of the Western United States*, Society of Economic Paleotologists and Mineralogists, Los Angeles, Calif., 33-70, 1978.

Hooper, P. R., C. R. Knowles, and N. D. Watkins, Magnetostratigraphy of the Imnaha and Grande Ronde basalts in the southeast part of the Columbia Plateau, *Am. J. Sci, 279*, 737-754, 1979.

Ingebritsen, S. E., D. R. Sherrod, and R. H. Mariner, Heat flow and hydrothermal circulation in the Cascade Range, north-central Oregon, *U. S. Geol. Surv. Open-File Rep.*, this volume.

Kane, M. F., and R. H. Godson, Features of a pair of long-wavelength (>250 km) and short-wavelength (<250 km) Bouguer gravity maps of the United States, *in* W. J. Hinze, ed., *The Utility of Regional Gravity and Magnetic Anomaly Maps*, Society of Exploration Geophysicists, Tulsa, Oklahoma, 46-61, 1985.

LaFehr, T. R., Gravity, isostacy, and crustal structure in the southern Cascade Range, *J. Geophys. Res., 70*, 5581-5597, 1965.

Luedke, R. G., and R. L. Smith, Map showing distribution, composition, and age of late Cenozoic volcanic centers in California and Nevada, scale 1:1,000,000, *U. S. Geol. Surv. Misc. Invest. Ser., Map I-1091-C*, 1981.

Luedke, R. G., and R. L. Smith, Map showing distribution, composition, and age of late Cenozoic volcanic centers in Oregon and Washington, scale 1:1,000,000, *U. S. Geol. Surv. Misc. Invest. Ser., Map I-1091-D*, 1982.

McBirney, A. R., and White, C. M., The Cascade Province, *in* Thorpe, R. S., ed., *Andesites*, J. Wiley and Sons, 115-135, 1982.

McKee, E. H., R. C. Jachens, and R. J. Blakely, Major crustal differences between the NW part of the Great Basin and other parts of the province, *Geology and Ore Deposits of the Great Basin*, Geol. Soc. Nev., in press, 1989.

McNutt, M., Implications of regional gravity for state of stress in the earth's crust and upper mantle, *J. Geophys. Res., 85*, 6377-6396, 1980.

Pakiser, L. C., Gravity, volcanism, and crustal structure in the southern Cascade Range, California, *Geol. Soc. Am. Bull., 75*, 611-620, 1964.

Riddihough, R., C. Finn, and R. Couch, Klamath-Blue Mountain lineament, Oregon: *Geology, 14*, 528-531, 1986.

Rietman, J. D., Remanent magnetism of the Late Yakima basalt, Washington State, Ph.D. thesis, 114 p., Stanford Univ., Stanford, Calif., 1966.

Rogers, G. C., Variation in Cascade volcanism with margin orientation, *Geology, 13*, 495-498, 1985.

Sherrod, D. R., Geology, petrology, and volcanic history of a portion of the Cascade Range between latitudes 43°-44°N., central Oregon, U. S. A., Ph.D. dissertation, University of California, Santa Barbara, California, 320 p., 1986.

Simpson, R. W., T. G. Hildenbrand, R. C. Jachens, and D. F. Barnes, Geologic implications of a new isostatic residual gravity map of North America, *Geol. Soc. Am. Abstracts with Programs*, A325, 1988.

Simpson, R. W., R. C. Jachens, and R. J. Blakely, AIRYROOT: A Fortran program for calculating the gravitational attraction of an Airy isostatic root out to 166.7 km, *U. S. Geol. Surv. Open File Rep., 83-883*, 66 pp., 1983.

Simpson, R. W., R. C. Jachens, R. J. Blakely, and R. W. Saltus, A new isostatic residual gravity map of the conterminous United States with a discussion on the significance of isostatic residual anomalies, *J. Geophys. Res., 91*, 8348-8372, 1986.

Smith, R. L., and R. G. Luedke, Potentially active volcanic lineaments and loci in western conterminous United States, in *Explosive Volcanism: Inception, Evolution, Hazards*, pp. 47-66, National Academy Press, Washington, D. C., 1984.

Society of Exploration Geophysicists, Gravity anomaly map of the United States (exclusive of Alaska and Hawaii), scale 1:2,500,000, Tulsa, Okla., 1982.

Stuart, D. J., Gravity study of crustal structure in western Washington, *U. S. Geol. Surv. Prof. Pap., 424-C*, C273-C276, 1961.

Thayer, T. P., Structure of the north Santiam River section of the Cascade Mountains in Oregon, *J. Geol., 44*, 701-716, 1936.

Thiruvathukal, J. V., J. W. Berg, and D. F. Heinrichs, Regional gravity of Oregon, *Geol. Soc. Am. Bull., 81*, 725-738, 1970.

Watkins, N. D., and A. K. Baksi, Magnetostratigraphy and oroclinal folding of the Columbia River, Steens, and Owyhee basalts in Oregon, Washington, and Idaho, *Am. J. Sci., 274*, 148-189, 1974.

Watts, A. B. M. Talwani, and J. R. Cochran, Gravity field of the northwest Pacific ocean basin and its margin, *in* Sutton, G. H., M. H. Manghani, and R. Moberly, eds., *The Geophysics of the Pacific Ocean Basin and Its Margin*, American Geophysical Union Monograph 19, 17-34, 1976.

Walker, G. W., and P. B. King, Geologic map of Oregon, *U. S. Geol. Surv. Misc. Geol. Inv. Map I-595*, scale 1:2,000,000, 1969.

Weaver, C. S., Seismotectonic fabric of the Cascade Range, *U. S. Geol. Surv. Open-File Rep.*, this volume.

Weaver, C. S., and C. A. Michaelson, Seismicity and volcanism in the Pacific Northwest: Evidence for the segmentation of the Juan de Fuca plate, *Geophys. Res. Lett., 12*, 215-218, 1985.

Weissenborn, A. E., Geologic map of Washington, *U. S. Geol. Surv. Misc. Geol. Inv. Map I-583*, scale 1:2,000,000, 1969.

Williams, D. L., and C. Finn, Analysis of gravity data in volcanic terrain and gravity anomalies and subvolcanic intrusions in the Cascade Range, U. S. A., and at other selected volcanoes, *in* W. J. Hinze, ed., *The Utility of Regional Gravity and Magnetic Anomaly Maps*, Society of Exploration Geophysicists, Tulsa, Oklahoma, 361-374, 1985.

Wilson, D., and A. Cox, Paleomagnetic evidence for tectonic rotation of Jurassic plutons in Blue Mountains, eastern Oregon, *J. Geophys. Res., 85*, 3681-3689, 1980.

Zucca, J. J., G. S. Fuis, B. Milkereit, W. D. Mooney, and R. D. Catchings, Crustal structure of northeastern California, *J. Geophys. Res., 91*, 7359-7382, 1986.

DETAILS OF CRUSTAL STRUCTURE IN THE CASCADE RANGE AND SURROUNDING REGIONS FROM SEISMIC AND MAGNETOTELLURIC DATA

William D. Stanley, *Gary S. Fuis, and *Walter D. Mooney
Box 25046, MS964, Denver Federal Center, Denver , CO
*345 Middlefield Road, Menlo Park, California

ABSTRACT

Several long seismic and magnetotelluric profiles have been completed across the Cascade Range and surrounding geologic provinces in California, Oregon and Washington in recent years. These measurements have been made along coincident transects in some locations and independent interpretations made from the two data sets. Joint geologic interpretation of the two data sets provide constraints on the nature of the crust not available from either data set alone. Joint analysis of coincident MT and seismic refraction data from northern California along a transect crossing the Klamath Mountains, High Cascades, and Modoc Plateau indicates that (1) in the Klamath Mountains, complex layering caused by stacked oceanic plates and subduction complexes is reflected as both velocity, and to a lesser extent, resistivity variations; (2) the structure of Medicine Lake volcano appears as an intrusive buildup and (3) a low velocity layer interpreted to dip upwards to the east under the Modoc Plateau coincides with the top of a deep crustal conductor. Magnetotelluric and seismic refraction determined structure of the Newberry volcano is very similar to that of Medicine lake, except that the volcano occurs near of thickening of the 6.4-6.5 km/s seismic layer and on the east side of a structural trough indicated on the MT data. A long north-south seismic refraction profile along the axis of the high Cascades in Oregon indicates a constant depth to the 6.5 km/s velocity layer and several orthogonal, east-west MT profiles indicate a pervasive deep crustal conductor occurring in the top of this velocity unit. This relationship of the crustal conductor and the 6.4-6.5 km/s velocity unit was observed for all of the coincident data in northern California and Oregon in the region from the High Cascades volcanoes eastward. Magnetotelluric surveys in Washington reveal that accretionary structures in the southern Cascades may control seismicity and volcanism. Comparison of seismic refraction and magnetotelluric data from the Columbia Plateau reveal that large depths to the deep crustal conductor may be due to mafic lower crustal rocks delineated by the seismic model. Analysis of various mechanisms for producing the deep crustal conductor in the Cascades region leads to a model with additive conductivity enhancing factors of metamorphic based carbon-mineral, partial melt, and hydrous films in a region of the crust where ductile behavior occurs at the top of the 6.4-6.5 km/s velocity layer.

INTRODUCTION

Crustal scale seismic refraction and magnetotelluric (MT) data have been obtained along several transects as part of a comprehensive study of the Cascade Range volcanoes under the U.S.G.S. Geothermal Research, Department of Energy and other programs. In this paper we discuss newly developed refinements of structural models for the Cascades and surrounding regions made possible by utilizing combined geologic interpretation of the MT and seismic data, and in some instances, gravity and magnetic data. The objectives for this combined study

of regional geophysical data from the Cascade Range and surrounding regions are to:

(1) Summarize pertinent velocity and and geoelectrical information from the region
(2) Illustrate combined contraints on crustal physical properties
(3) Address the key question of the significance of a deep crustal conductor as it relates to mid-crustal temperatures
(4) Relate types of structures interpreted from the geophysical data in the Cascades to those in surrounding regions and to observed seismicity and location of volcanic centers

Examples of the combined geophysical survey data available include a long east-west transect in northern California (GG', fig. 1) with coincident seismic and MT data which is the most complementary measurement profile using these two techniques. A long north-south refraction experiment in the Oregon Cascades from Crater Lake to Mt. Hood crosses several east-west MT profiles. A previously interpreted, detailed refraction experiment across the Newberry volcano region (Catchings and Mooney, 1988) has been combined with MT and other electromagnetic sounding data (Fitterman and others, 1988) for refinement of crustal structures in eastern Oregon. MT surveys by Stanley and others (1987) in the southern Washington Cascades-Columbia Plateau are combined in the present paper with refraction studies of the Columbia Plateau by Catchings and Mooney (1988), of the Coast Range of Washington by Taber (1986), and gravity-magnetic modelling of the Coast Range of Washington by Finn (1988) to derive a broad structural profile through Washington. Several MT models of the Klamath Mountains of northern California, Coast Range of Oregon and Washington, and of Vancouver Island are compared and an accretionary model for the suture zone between the Coast Range and Cascades is developed. A main focus of the paper is development petrological model for the occurrence of a deep crustal conductor that occurs within a 6.4-6.5 km/s seismic layer in the Cascades and its significance to heat flow and seismicity.

CASCADE RANGE SETTING

The Cascades Range of northern California, Oregon, and Washington includes a belt of mostly Miocene volcanic centers (McBirney, 1978) known as the western Cascades (WC) and another north-south alignment of Quaternary volcanos known as the High Cascades. The core rocks of the North Cascades are composed of crystalline and high grade metamorphic rocks that were amalgamated through accretionary processes in early Mesozoic time (Misch, 1966). The Quaternary volcano belt has been formed by subduction processes as the Juan de Fuca plate is consumed beneath North America. The Western Cascades and High Cascades were formed in the later stages of four volcanic and plutonic episodes that swept across the present Pacific Northwest (fig. 2). At about 70 Ma, magmatism was centered in the region of the Idaho batholith, then migrated eastward across Montana and subsequently swept back to Idaho by 50 Ma (Heller and others, 1987). During the latter part of this interval the northwest trending Challis volcanic belt formed prior to migration of the volcanic activity into Oregon (where volcanic units of the mixed sedimentary-volcanic Clarno Formation were erupted at about 45 Ma). Similar volcaniclastic units of the John Day Formation were laid down in present Oregon over the interval 35-20 Ma. In northern Washington, the westward shift of the arc began earlier than in Oregon and comagmatic plutonism in the North Cascades has been documented. Arc magmatism has been restricted to the Cascade Range of Washington-Oregon-California for the past 35 Ma. The apparent wider sweep of magmatism in Oregon than in Washington has been interpreted by Heller and others (1987) as due mostly to greater amounts of subsequent extensional movement in Oregon (fig. 2). In the backarc region, Micoene to Recent volcanic flows of basaltic to rhyolite composition cover the High Lava Plains (HLP, fig. 1) and Basin and Range portions of eastern Oregon; and also in the backarc, Miocene basalts fill an apparent rifted oceanic basin in the Columbia Plateau (CP).

Most of the Quaternary volcanoes occur on a nearly north-south line from Lassen Peak in northern California to Mt. Hood in Oregon. In Washington, the pattern of volcanoes is more complex, being not nearly so linear as in Oregon and California; in addition, Quaternary

volcanic flows are limited to the area near the main stratovolcanoes. Other volcanic centers associated with the High Cascades are located to the east of the main trend of volcanoes; for instance, Medicine Lake (ML) and Newberry (NB) volcanoes are located some tens of km east of the main chain. Guffanti and Weaver (1988) have plotted spatial-temporal distributions of approximately 4000 volcanic vents formed since 16 Ma in the Cascades. Guffanti and Weaver (1988) interpret that Basin and Range volcanism migrated west to the Cascade arc from 5-10 Ma in a process they term "impingement". These authors also interpret that:

(1) Basaltic volcanism east of Cascade Range continued in the past 5 Ma in the northeastern California Modoc Plateau where impingement is not yet complete.

(2) In central Oregon where the High Lava Plains intersect the Cascade arc, impingement approximately coincides in time with the commencement of extension-related volcanism and development of a graben in the High Cascades between Three Sisters and Mount Jefferson.

Guffanti and Weaver (1988) divide the Quaternary volcano belt into six segments. Segments one and two include the northern Washington and southern Washington volcanoes which are separated by a gap of 90 km. They correlate the Washington volcanoes with a segment of the subducting Juan de Fuca plate which has the least average dip over the length of the magmatic arc. The narrow, NS trending belt of predominantly andesitic vents in Oregon constitutes a third segment, which Guffanti and Weaver point out is adjacent to the seismically quiet portion of the subduction zone. They interpret the narrowness of the volcano belt in Oregon as indicating steep dip in the subducting plate. Guffanti and Weaver group Mount Shasta and other extreme northern California volcanoes in segment four and the southernmost Cascades volcanoes near Lassen Peak as segment five and suggest that these segments are distinctive in differing ages of the Juan de Fuca and Gorda North plates, amounts of subcrustal seismicity and plate geometry. Stanley (1982b) argued that east-west MT profiles from the Cascades indicated largely thrust type structures in Washington on segments one and two and partially in segments 4 and 5, whereas segment 3 in Oregon is characterized by extensional structures. Segment 6 encompasses the northwest-southeast belt of vents of the High Lava Plains in Oregon.

The development of the Pacific Northwest during the period prior to formation of the magmatic arc is poorly understood, but Dickinson and Thayer (1978) have defined a Mesozoic arc-trench system preserved in the present Blue Mountains region of Oregon (fig. 2). Nilson (1985) has theorized the existence of a late Cretaceous sedimentary basin on the flank of the Klamath Mountains province (fig. 2). The Klamath Mountains province consist of a system of complex, thrusted accretionary units of Paleozoic and Mesozoic age (Irwin, 1977). Hamilton (1969) interprets that the Sierra Nevada and Idaho batholith were once connected, but have been separated by Basin and Range extension. Later stages of this extension are indicated in figure 2. A marine sedimentary basin (SWCC, fig. 2) is interpreted by Stanley and others (1987) to have developed prior to accretion of a major seamount complex (Siletzia). This marine sedimentary system is believed to include the MacIntosh, Raging River (Buckovic, 1979), and other formations found in the Puget and Chehalis basins (fig. 2). A system of syn- and post-accretion sedimentary basins (Tyee Fm., etc) developed in the present Coast Range region of Oregon and Washington. Fritts and Fisk (1985) interpret that an incipient rift developed in the present Columbia Plateau (fig. 2, upper) in late Cretaceous, eventually leading to a thermally subsiding basin that filled with voluminous Miocene flood basalts.

HEAT FLOW, MAGMA PRODUCTION AND GEOTHERMAL RESOURCES

The Cascades Range contains voluminous Quaternary volcanic rocks and it is hypothesized that a large geothermal resource may reside beneath the surface of these volcanic flows (Muffler, 1987). Heat flow values in the Oregon High Cascades from Mount Jefferson to Crater Lake typically exceed 100 mw/m^2 (Blackwell and Steele, 1984) at the western margin of the High Cascades and remain high throughout most of southeastern Oregon and northeastern California. Heat flow in the Washington Cascades volcanoes is not as high as that in the remainder of the High Cascades to the south. The temperature gradients over

most of the high heat flow area in Oregon are greater than 50°C/km. Blackwell and others (1982) have modelled the heat flow data in Oregon, south of Mt. Jefferson (fig. 1), with a tabular magma accumulation at depths of 7-10 km. The depth to the Curie isotherm (about 570° C) in approximately the same area is estimated to be 9 km (Connard and others, 1983). In contrast to Blackwell and others (1982) model of an extensive magma accumulation underneath the Cascades, detailed study of earthquakes at Mount St. Helens by Scandone and Malone (1985) and Shemeta and Weaver (1986) suggest that magmatic bodies associated with the Cascades volcanoes may be small. Weaver and his co-workers argue that only a thin conduit of 100 m diameter may comprise the magmatic plumbing at Mt. St. Helens. Below a depth of 8 km they estimate the possible magma storage to be less than 2 km in diameter and less than 4-5 km in vertical extent. If these assumptions were applied to the central Oregon Cascades, they would be in conflict with Blackwell's models which calls for large volumes of molten rock at depths of 7-10 km.

Stanley (1982,1983,1984) discussed the role of partial melting in producing a deep crustal conductor at a depth of 12-20 km in the Cascades, but did not present any firm conclusions. This conductor occurs over much of Oregon and northern California east of the boundary of the western and High Cascades. It is important to determine, if possible, the relationship of this deep crustal conductor to heat flow and magma occurrences, and consequently, the geothermal resources of the Cascades. We will attempt to place further constraints on its nature in this paper.

INTERPRETATION OF MT AND SEISMIC DATA

The seismic refraction profiles have been interpreted by a combination of ray-tracing and synthetic seismogram methods as described in Catchings and Mooney (1988), Zucca and others (1986), and Mooney (1988). MT soundings were interpreted using combinations of one-dimensional (layered) and two-dimensional geoelectrical models derived with iterative forward and generalized inversion computer programs. We will not discuss the derivation of the models in detail in this paper, but instead focus upon the possible geologic constraints placed upon the crust in the Cascades by the two different geophysical data sets. We show that, in some instances, the direct comparison of the two data sets and integration of gravity and magnetic data allow valuable refinement of the individual models. This integration has been somewhat completed for the Newberry volcano study (Fitterman and others, 1988), but even there an optimum model that satisfies all of the data sets has not been derived.

The ability to interpret lithology from the MT and seismic data sets is dependent upon our understanding of the electrical and acoustic properties of rocks under the temperatures and pressures encountered in the Cascade Range and surrounding region. A short discussion of rock properties is essential to provide a background for statements concerning lithological correlations of various MT and seismic models in this paper. Regarding electrical properties, it is well known that electrical resistivity varies over an extremely large dynamic range, with common rock resistivities ranging from 1 ohm-m to 10,000 ohm-m. Commonly rock forming minerals at surface pressures and temperatures are normally very resistive, with the exception of metallic minerals and graphitic carbon, which are very low in resistivity. For most rocks, resistivity is controlled by fluids in pore spaces or intergranular coatings in an ionic conduction process rather than solid electronic conduction through the mineral matrix. This ionic controlled resistivity is a function of salinity of the pore fluids, temperature, and pressure and is important for sedimentary and other rocks with connected porosities of greater than a few tenths of percent. The effect of temperature is to increase ionic mobility and decrease resistivity and is at a maximum at temperatures around 200-250°C. As porous rocks are buried to depths greater than a few km, porosities are decreased due to lithostatic loading until they normally become highly resistive. This process is complicated in shales, however, because ionic conduction in shales occurs in trapped water in layered clays and zeolites; as a result, the resistivity of shales will be low (1-20 ohm-m) and more constant as normal porosity decreases. As shales are metamorphosed, both porosity and layered clays are destroyed, but resistivities can be maintained at a low value due to formation of carbonaceous or iron

mineral films along fissile planes in the metashales. Intrusive rocks have minor porosity and thus are normally very resistive, typically in the range of 500-20,000 ohm-m. Fracture porosity and intense alteration of intrusive rocks can lower their resistivity well below this range in some instances. Volcanic rocks normally can have significant porosity, but also have very high resistivities when unaltered and pore waters are very fresh, as tends to be the case with volcanic rocks. As volcanic rocks increase in age, the formation of layered clays and zeolites dramatically increase their resistivity so that typical values for tuffaceous rich (tuff alters very fast) flows and volcaniclastic rocks of Tertiary age in the Cascades is less than 20 ohm-m. Metamorphism of crustal rocks beyond zeolite facies generally increases resistivities; although, as mentioned for shales, low resistivities may be maintained until any carbonaceous or metallic minerals films are destroyed. As temperatures and pressures increase, melting or anatexis of the rocks may occur and this leads to decrease in resistivity of the rocks by up to two orders of magnitude due to ionic conduction in the melt.

Seismic compressional velocities in crustal rocks vary over a much narrower range than do resistivities, typically ranging from 2-8 km/s for the crust, with a narrow range of 4-7.5 km/s observed for basement and deep crustal rocks in the Cascade region. Velocity for Tertiary sedimentary rocks in the area are in the low end of this range, normally 3 km/s or less. Compressional velocities for volcanic rocks are highly variable, but are believed to fall in the range from 3-5 km/s in the Cascade region. The velocity of intrusive rocks is influenced by the proportion of quartz to mafic minerals in the rocks, with felsic rocks such as granite having velocities of 5-6 km/s and intermediate to mafic intrusive rocks ranging higher than 6.3 km/s. The average velocity of crustal rocks is generally accepted to be 6 km/s. The compressional velocity of crustal rocks generally increases with depth along with a well defined relationship to density (Birch, 1961) and decreases with temperature. The increase in density with depth may be offset starting a some depth by the increase in temperature. This temperature controlled negative velocity gradient has been cited as the possible cause of some interpreted low velocity zones in the crust (Meissner, 1983). Development of mid-crustal zones of hydrofractures from release of high-pressure metamorphic water may also cause lowered velocities. For instance, Hall and Ali (1985) state that 0.5% fracture porosity can cause compressional velocities to be lowered by 10%.

Because of the different controls over resistivity and compressional velocities, we do not expect complete agreement between the MT and seismic refraction models that we studied. However, in general the two data sets derive similar models for shallow crustal features and coincide to a certain extent for some mid-crustal features. It is the analysis of the coincidence or variance in the models and attendent scrutiny of constraints on lithology that make the exercise we attempt in this paper significant. However, this analysis represents only a first step and does not include a re-evaluation of the uniqueness of the individual models. We will not discuss at length the uncertainty of the individual models, but it should be pointed out that the MT models normally have the minimum number of model parameters required to fit the data. The seismic models discussed normally have a large number, typically eight, which may not be a minimum parameter set. In some instances, we discuss the seismic interpretations in a simplified manner by combining model layers. The uncertainties for a given depth or resistivity or seismic velocity cannot be satifactorally quantified, but are typically large with a typical lower limit of possibly 20%, except for special situations such as for very accurately determined surficial layers or extremely thick, uniform subsurface units. Accuracies in the MT models are influenced by data quality, selection of strike direction, static shifts (Sternberg and others, 1988) and limited geometry of the model among other factors. Refraction models are similarly limited by data quality, accuracy of event arrival picks, style of record correlation (Mooney, 1988), effects of low-velocity layers, multiples, and other factors. The possibilities for extracting optimum models from combined MT and seismic refraction-reflection models have not been commonly exploited and to this date we have not accomplished much along these lines for the data discussed in this paper.

CHARACTERISTIC STRUCTURES OF THE OREGON CASCADES

We begin with a discussion of the Oregon Cascades because the overall pattern of

structure in this part of the volcanic belt is somewhat simpler than that in northern California and Washington. Interpretation of four east-west (fig. 1) MT profiles (Stanley,1982;1984) indicated that the geoelectrical structure of the Oregon Cascades could be approximated with a four layer sequence consisting of (from the surface down):

(1)A resistive layer (150-1500 ohm-m) of .5 to 2 km thickness representing Quaternary volcanic flows.
(2) A conductive layer (4-30 ohm-m) of 1 to 4 km thickness that is made up of Tertiary felsic volcanic flows, ash sheets, sedimentary rocks and volcaniclastics. Locally, such as on the margins of the Blue Mountains, this conductive unit may include some Cretaceous sedimentary rocks.
(3) A resistive layer (>100 ohm-m) that represents the upper part of the crust; comprised of pre-Tertiary accreted crustal units and intrusive materials from subduction related magmatic activity.
(4) A conductive zone (2-20 ohm-m) at depths of 12-25 km; this zone has been generally thought to represent a combined effect of temperatures greater than 500°C and small percentages of free water. Other possibilities for the causes of this conductive zone will be discussed at length in this paper.

An example of a typical one-dimensional MT model section was derived for profile DD' (fig. 1) across the Cascades as shown in Figure 3a. A two-dimensional model that better fits the low-frequency parts of the MT data is shown in figure 3b. In these models layer no. 2 thickens beneath the axis of the High Cascades. The increased thickness of layer no. 2 near the axis of the High Cascades is expressed on other profiles in Oregon and northern California and may be indicative of subsidence initiated by outpouring of the Quaternary volcanic pile. Alternately, the thickening of layer no. 2 may be an outward stepping structural graben caused by continued extension of the crust. The High Cascades volcanoes are interpreted to be located within a shallow graben by McBirney (1978), but Smith and Taylor (1983) prefer to limit the graben to the central Oregon Cascades. Extension is very much in evidence in the Oregon Cascades, with many north-south trending normal faults associated with the central graben, as well as northwest trending normal faults that extend into the Cascades from the Basin and Range province.

The deep crustal conductor (DCC, layer no. 4) on this section occurs at depths of about 12-15 km. Temperature gradients in this part of Oregon are approximately 55°C/km (Blackwell and Steele, 1983); even though these gradients cannot be extrapolated through the crust, conservative calculations of deep geotherms along the lines followed by Lachenbruch and Sass (1978) for the Basin and Range indicate that temperatures should be well over 500°C at depths of 15 km. It certainly would be reasonable to expect that the low resistivities could be caused by partial melting at these depths. The rise in the deep crustal conductor under soundings 4 and 5 on profile DD' is believed to be real, although the westward pinchout of layer 2 on this section and others makes for equivocal models.

A more detailed look at the local structure where the conductor is shallower is provided by profiles completed in the Breitenbush Hot Springs area (fig. 5), which is near the contact between the High and Western Cascades. Breitenbush Hot Springs is one of several hot springs areas that are located on the approximate contact between the High and Western Cascades. A geothermal exploration well (Sunedco Hole, fig. 5) indicated that temperatures of 130° C are found at a depth of 1700 m. The Breitenbush Hot Springs area has been proposed as a deep continental drilling site (Priest and others, 1987). On the one-dimensional interpretation of MT profiles BR1 and BR2 (fig. 6) a shallow zone with resistivities of 2-20 ohm-m (mostly <6 ohm-m) represents a highly altered section of Oligocene-Miocene volcanics that may have been a Holocene hydrothermal system. The resistive area west of sounding 7 on profile BR2 is thought to be a Tertiary pluton. The depth to the deep crustal conductor is from 7 to 18 km beneath this area and although the variations along this profile may not be significant due to the limitations in the modelling process, the predominately shallow depths to the conductor

are. A detailed MT profile from the Oregon coast to the High Cascades (location denoted by "EM" in fig. 1) has been completed as part of a large electromagnetic survey funded by the National Science Foundation (EMSLAB Group, 1988). This eastern end of the EMSLAB profile approximately overlaps our Breitenbush MT profiles and the central part of MT profile DD'. Wannamaker and others (1989) describe a two-dimensional model for the EMSLAB MT profile which indicates a deep crustal conductor under the Cascades similar that determined from our data. Under the Western and High Cascades this conductor is presented in the Wannamaker and others (1989) model as a horizontal feature at depths of 25 km beneath the Western Cascades and about 10 km underneath the High Cascades. These two regions for the deep crustal conductor are joined by a rise of the conductor top surface to as shallow as 5 km in the Breitenbush area. Wannamaker and others (1989) doubt that this deep crustal conductor underneath the Cascades results primarily from silicate melt in large volume, but rather from hydrothermal fluids and the cumulative alteration attending repeated intrusion and crystallization.

Interpretation of the north-south refraction profile in Oregon (fig. 1) by Leaver and others (1986) provided a velocity structure with eight major layers (fig. 4). It should be noted that the velocity in each layer is not constant, but the velocity function consists of a linear gradient within each individual layer. The first layer, with a thickness of 1.3 km and velocity of 2.9-3.0 km/s corresponds approximately to the MT model layer no. 1 interpreted to be made up of Quaternary volcanic flows. Seismic layer no. 2 extends to about 3.4 km depth with a velocity of 4.7-4.8 km/s. We assume that this layer represents the Tertiary sedimentary and volcanic rocks beneath the surface Quaternary flows and corresponds approximately to MT model layer no. 2 (fig. 3a). Seismic layers no. 3 and 4 encompass velocities of 6.0-6.1 and 6.3-6.4 km/s and depths down to 11 km. These units approximately correspond to MT model layer no. 3 and are thought to represent pre-Tertiary sedimentary and metamorphic crust.

Probable lithology for this pre-Tertiary crust in the region of MT profile DD' may be Jurassic metasedimentary rocks and accreted-arc, metavolcanic rocks similar to those found in the Blue Mountains of Oregon (fig. 1). The western extent of the fossil subduction zone in the Blue Mountains is not known, but if the crust beneath the central part of profile DD' has not been totally distended and reconstructed, it is reasonable to assume that accreted units similar to those found in the Blue and Klamath Mountains may form the upper part of the sub-volcanic basement. If the crust had been totally rifted apart and reconstructed, this probably would have involved a rise of mafic material from the mantle, causing large gravity and velocity highs as demonstrated by Catchings and Mooney (1988) for the Columbia Plateau and other rifted areas. The extended crust of the Cascades may have been modified in a manner similar to that in the Basin and Range where Lachenbruch and Sass (1978) proposed crustal adjustment by magmatic underplating and possible dike injection. Cretaceous sedimentary rocks probably do not make up a large part of this basement, because MT soundings and well-logs (Sternberg and others, 1988) in the Blue Mountains show that these Cretaceous units are quite conductive (10-40 ohm-m). Also, acoustic velocities of the Cretaceous shales and sandstones would be expected to be lower than those observed in seismic layers no. 3 and 4. This zone undoubtedly also contains Tertiary and Quaternary intrusive rocks, but the overall extent of such intrusive bodies cannot be determined from the MT and seismic data.

The next major unit on the seismic model, layer no. 5, has a velocity of 6.5-6.6 km/s and extends from 11 km to 27 km depth. Layer no. 5 represents the mid-crust beneath the Cascades and the MT data indicate that DCC occurs within the upper part of this seismic unit. A seismic layer of 7-7.1 km/s (layer no. 6) forms the lower crust on the model from Leaver and others (1986) at depths of 27-44 km. The Moho is represented by the strong velocity gradient layer (layer no. 7) at depths of 44-46 km, underlain by mantle velocities of greater than 7.7 km/s. Regional earthquake travel times were used by Leaver and others (1986) to refine the mantle velocities and crustal thickness.

CRUSTAL STRUCTURE EAST OF HIGH CASCADES

Detailed geoelectrical and seismic studies have been done in the area of Newberry

volcano (fig. 7) in east central Oregon (Fitterman and others, 1988; Catchings and Mooney, 1988). The seismic refraction profile extended from just west of Newberry volcano to east of the Brother's Fault zone that bounds the Blue Mountains on the south side. The Brother's Fault is a possible strike slip fault system (Lawrence, 1976) that forms the northern boundary of Basin and Range structures in Oregon. MT profile EE' crosses the High Cascades and ends just east of Newberry volcano. Measurements across the western end of the profile were made at widely spaced intervals, but more detailed surveys were conducted around Newberry volcano. The MT surveys at Newberry were combined with other geoelectrical soundings made using time domain electromagnetic (TDEM) and direct current (DC) methods as described in Fitterman and others (1988). MT profile EE' (fig. 7) did not extend into the High Lava Plains east of Newberry as did the refraction experiment, but another MT profile, FF, did extend well into the Basin and Range. Newberry volcano appears to represent the eastern edge of Cascades volcanism and is at the leading edge of a propagating volcanic-extensional front (fig. 7) trending southeast to northwest from the Basin and Range (Macleod and others, 1976).

The interpretation of the western part of MT profile EE' (fig. 8b) indicates a well developed structural trough along the axis of the High Cascades volcanoes similar to that on profile DD'(fig. 3). Blakely and others (1985) have noted an expression of this trough in upward continued gravity data. It would be worthwhile to jointly invert the MT and gravity data to remove the effect of the trough on the gravity field in order to investigate deeper anomalies, but we have not done this yet. Newberry volcano forms a resistive high on the pre-Tertiary basement with a relief of about 2 km. In general, the same generic four-layer model discussed above for the central Oregon Cascades fits the local Newberry data with minor modifications. Lake sediments and volcanic fill in the central part of the volcanic crater require a more conductive first layer of about 80-180 ohm-m in the MT-TDEM model (fig. 9). Excellent constraints are provided on the resistivity of the first and second MT model layers in the Newberry volcano because of extensive TDEM and DC soundings. The geoelectrical structure in the upper 2-3 km from the MT and TDEM soundings are compared with the surface of the subvolcanic structure (5.6 km/s layer) as determined from the seismic refraction profile (fig. 8a) of Catchings and Mooney (1988) in figure 9. Agreement between the two EM methods is excellent, especially in light of the fact that there was no attempt made to jointly interpret the two data sets. The sub-volcanic basement surface as determined independently from the MT and seismic refraction data shows some major discrepancies. The basement high on the seismic refraction model is much narrower and shallower than on the MT interpretation. Modelling of the gravity data (Williams and Finn, 1985) seems to support the width and depth of the basement high from the MT model over the narrow structure interpreted from the refraction data. The gravity data appear to mimic the MT derived basement surface except for the minor minimum on the gravity profile underneath the center of the Newberry caldera. This gravity minimum is probably caused by the low density fill and lake sediments in the crater (Williams and Finn, 1985) as also evidenced by the low resistivities in the MT and TDEM first layer.

The resistive first layer in the MT and TDEM models corresponds to unaltered Quaternary volcanic flows as discussed in Fitterman and others (1988). The base of this resistive upper layer is largely controlled by a zone of layered clay formation below the water table and not by a basic lithological boundary. Thus, the electrical boundary should not necesarily be the same as a layer boundary on the seismic model. This is in fact the case, since the first major seismic layer (fig. 8a) is interpreted to be almost 2 km thick and has a velocity of 4.1 km/s. A slightly higher velocity layer (4.7 km/s) was used for the second unit on the seismic model. This unit is comparable to 4.7-4.8 km/s velocities used in the central Oregon refraction model by Leaver and others (1986). The base of the 4.7 km/s layer on the Newberry refraction profile approximately corresponds to the base of the 5-20 ohm-m MT model layer (layer no. 2). The presence of conductive Cretaceous sandstones and shales on the southern flank of the Blue Mountains mentioned earlier suggests that part of the 4.7 km/s and 5-20 ohm-m units could contain such sedimentary rocks, especially to the east of Newberry,; however, there is no conclusive evidence in the MT or seismic data to confirm this possibility.

A thin 1.60 km/s layer is noted at the surface in the refraction model and Catchings and Mooney correlated this unit primarily with lake beds in the Newberry area and alluvium elsewhere.

The seismic refraction model (fig. 8a) for Newberry includes units of 5.6-6.2 km/s that comprise the pre-Tertiary upper crust and correspond roughly to units of 100-750 ohm-m in the MT model (layers no. 3). As was discussed for the central Oregon Cascades, these units are possibly Jurassic and older subduction complex sedimentary rocks, ophiolites, and accreted arcs of the fossil subduction zone found in the Blue Mountains.

A mid-crustal layer of 6.5 km/s thickens under Newberry volcano in the preferred seismic model. A lower crustal unit of 7.4 km/s is underlain by upper mantle velocities of 8.15 km/s at a depth of 37 km. Catchings and Mooney suggest that the interpreted thickening of the 7.4 layer is related to the extensional formation of a basin just east of Newberry volcano. They envision that magmatic underplating may have played a role in maintaining relatively thick (37 km) crust despite large amount of crustal extension in the region of Newberry.

The regional MT model for profile EE' (fig. 8b) indicates that the deep crustal conductor occurs at depths of about 15-17 km west of Newberry. Soundings in the near vicinity of Newberry were difficult to interpret regarding depths to this conductor because of the resistive structure directly under Newberry at depths of 2-4 km. For soundings just west of Newberry, the depths to the deep conductor appears to be somewhat shallower, or about 12-15 km. Comparison of depths to the DCC on both EE' and FF' suggests that a median value for its depth is about 15 km, with some deepening on the eastern end of FF' in the Oregon Basin and Range. Regardless of sounding to sounding variations that may largely reflect model limitations, the conductor appears to occur in the mid-crust about where velocities of 6.5 km/s have been interpreted, in a manner analogous to the central Oregon High Cascades. None of the MT data for profiles EE' and FF" were taken with long enough recording times to see through the deep conductor, but selected soundings on the west end of profile DD' did sense the bottom of the conductive layer. If a resistivity of 1-3 ohm-m is assumed for the conductor, the thickness must be at least 5 km; higher resistivites will permit proportionately thicker conductors. It is our assumption that the conductor occurs largely within the 6.4-6.5 seismic layer for geologic reasons that we will subsequently discuss.

NORTHERN CALIFORNIA SEISMIC AND MT PROFILE

The most satisfactory profile for combined interpretation of crustal refraction and MT data across the Cascades is the joint MT-seismic profile in northern California (GG', fig. 1) that extends east-west from the Klamath Mountains province, across the High Cascades and Modoc Plateau and onto the Basin and Range (fig. 10). The main east-west seismic refraction profile was interpreted by constructing velocity models using perpendicular, crossing profiles that roughly parallel the geologic strike as discussed in Zucca and others (1986).

Klamath Mountains Section

In contrast to the profiles discussed above that were completely located on volcanic terranes, the northern California MT-seismic profiles start on complex, accreted units of the Klamath Mountains. The Klamath Mountains province is composed of several lithotectonic belts that are largely bounded by thrust faults. From west to east these belts are: a western Jurassic, western Paleozoic and Triassic belt (Irwin, 1966, 1981), a central metamorphic belt, and an eastern belt of sedimentary and volcanic rocks of forearc and arc affinities ranging in age from Middle Jurassic to Ordovician. A large sheet of ultramafic rocks (Trinity ultramafic body) crops out over a broad area in the east-central Klamath Mountains. Mt. Shasta appears to be located on the suture joining the Klamath province to the pre-accretion continental margin. The age of accretion is not known but late Cretaceous basin sediments of the Hornbrook Formation (Nilson, 1985) lap on the northern edge of the Klamath Mountains, thus accretion must have occurred prior to late Cretaceous.

The preferred seismic refraction model for the Klamath section of profile GG' (Zucca and others, 1986) consists of 8 layers as indicated in figure 11c. The authors used three low

velocity layers in the model (layers 3,5, and 7) in an attempt to reproduce large amplitude secondary arrivals and oather more subtle parts of the travel-time curves in synthetic seismograms. The 7.0 km/s unit was derived from an unreversed segment of the travel time curve and was interpreted to be loosely constrained because phases beyond the critical point were poorly observed. On the Klamath crossing line, only the reflection from this basal unit was clearly observed.

The MT model for the Klamath Mountains region indicates a 190 ohm-m unit that correlates with outcrops of the Trinity ultramfic body. The base of the ultramafic unit on the refraction was interpreted by Fuis and others (1987) to be the bottom of the 6.5 km/s layer. Fuis and others correlated magnetic models for the Trinity ultramafic body computed by Griscom (1977) with the seismic refraction model and Blakely and others (1985) interpret the aeromagnetic data to indicate that the ultramfic units extend underneath Mt. Shasta. The velocity model (fig. 11d) beneath the Trinity ultramafic sheet was interpreted by Fuis and others in the following manner with the aid of laboratory measurements of sample velocities:

- o the 6.7 km/s layer was correlated with the central metamorphic belt
- o a low velocity zone beneath the 6.7 km/s unit is correlated with the Stuart Fork Formation (Davis and others, 1980) and with the upper sedimentary and volcanic sequence of the North Fork terrane of Ando and others (1983)
- o the velocity step to 7.0 km/s was tentatively correlated with the ophiolitic basement of the North Fork terrane or the Hayfork Bally meta-andesite

The MT model for the Klamaths is somewhat simpler for the section beneath the Trinity ultramafics. The 20-60 ohm-m units have a resistivity range possibly suggestive of metasedimentary rocks containing mildly carbonaceous and/or pyritic foliation plane coatings, thus we correlate this unit with the metasedimentary part of the Stuart Fork Formation. These rocks have been intruded by a Mesozoic pluton where resistivities of 1100 ohm-m are indicated. This pluton was not directly observed on the seismic data, but postulated by Fuis and others (1987) from nearby outcrops on either side of the seismic line. The 300 ohm-m unit just east of the pluton may be comprised of thermally metamorphosed Stuart Fork Formation units which outcrop near the sounding location. Units of 110-200 ohm-m west of the pluton and at depth beneath the Trinity ultramafics are correlated with hornblende and mica schists (Salmon Group) and the ophiolitic part of the North Fork terrane. The 600 ohm-m unit just west of Mt. Shasta may represent a minor intrusive body associated with the suture zone between the Klamath province and the pre-accretion margin.

Of major interest for the Klamath section of the MT-seismic profile is the conductive layer that forms the base of the MT model (fig. 11a). Data recording was not long enough to enable detection of the base of this conductor, but if a median for the range of 10-20 ohm-m is used for the intrinsic resistivity of the conductor, then it's minimum thickness must be about 10 km. Deep, east-dipping conductors have been found below the central Oregon Coast Range in the EMSLAB MT study (EMSLAB group, 1987), under the Coast Range of Washington by Stanley and others (1987), and under Vancouver Island by the Canadian Lithoprobe group (Clowes, 1987). In the Oregon, Washington, and Vancouver Island occurrences of this dipping conductor the rocks are interpreted to be Tertiary subduction complex rocks that have been thrust beneath the oceanic basalts and other units in the coastal ranges region. Blake and Jones (1986) suggest that late Cretaceous sedimentary rocks of the western Franciscan Formation have been thrust beneath the Klamath Mountains province in their study area to the southwest of the MT-seismic profile. We believe that this tectonic model is the most probable one for the east-dipping conductor beneath the main part of the Klamath Mountains. The seismic model involves a poorly constrained 7.0 km/s layer in about the position of the conductor in the central and eastern part of the Klamath profile section. However, it must be noted that a low velocity layer of 6.6 km/s was placed above this basal unit. Strong wide-angle reflections in the true-amplitude record section indicated the need for the 6.6 km/s low velocity zone in the refraction model, but the model is extremely equivocal with regard to the velocity and thickness of this layer and the actual depth to the basal 7.0 km/s layer. We propose that the original interpretation by Zucca and others (1986) for the refraction data

could be modified by simulation of the east-dipping conductor on the MT model; this would be accomplished by increasing the thickness of the 6.6 km/s low-velocity layer and and requiring the 7.0 km/s interface to dip to the east. This augmentation of the refraction model would better fit the MT and geologic model.

Cascades and Modoc Plateau Sections

The section of the MT-seismic profile across the volcanic terranes of the Cascades and Modoc Plateau (fig. 11a) is much simpler than that from the Klamath Mountains. Quaternary volcanic flows are represented by the thin, resistive (<1 km thick, >100 ohm-m) surface layer on the MT data. The refraction model (fig. 11c) utilizes velocities of 3.5 km/s for both the Quaternary volcanic flows and underlying, assumed Tertiary volcanic and sedimentary rocks. A highly variable surficial layer on the refraction model is believed to be lake sediments and alluvium. A 5-20 ohm-m second layer on the MT model and a 3.5-5.4 km/s layer on the refraction model appear to be largely the same geologic unit. These units on the MT and seismic models are believed to be geologically similar to MT and seismic layers for the central Oregon Cascades, Newberry, and eastern Oregon Basin and Range and High Lava Plains discussed above. Namely, this geologic unit probably consists of extensive Tertiary volcanic flows, ash falls, ash laden sedimentary rocks, and other volcaniclastics; however, minor amounts of Cretaceous sedimentary strata may be found in this model horizon.

The high resistivity bump at Medicine Lake volcano (fig. 11a) is also indicated on the refraction model (5.7 km/s). We interpret that this resistive, high velocity structural feature underneath Medicine Lake is an intrusive buildup very similar to that under Newberry volcano in Oregon. Williams and Finn (1985) have made a similar interpretation based upon gravity and magnetic models.

The sub-volcanic upper crust underneath the Cascades and Modoc Plateau is represented on the refraction model by a 6.1-6.3 km/s layer extending to depths of 6-14 km. The mid-crust is denoted by a 6.4 km/s layer above a fixed depth (25 km) 7.0 km/s layer. This final layer is based upon a 7.0 km/s moveout observed in the record sections, but because this event was not observed on a reversed record, its velocity and dip are uncertain. Additional late arrivals were postulated to represent mantle at depths of either 36 or 45 km, but the possibility that these arrivals were multiples of a shallower event could not be ruled out.

East of Medicine Lake the upper and mid-crustal velocities were interpreted by Zucca and others (1986) to be separated by a thin (1.5 km) low velocity layer (6.0 km/s) that dips to the west. This low velocity layer must be considered as highly conjectural in regard to velocity or thickness, although its existence is strongly suggested by wide-angle reflections. However, it is interesting to note that the deep crustal MT conductor also dips westward underneath the Modoc Plateau. The conductor occurs approximately within the top of the mid-crustal seismic layer (6.4 km/s); this is consistent with the position of the conductor in relation to refraction models in central and eastern Oregon.

Fuis and others point (1987) out the similarity of the velocity-depth curve for the Modoc line to those from the Sierra Nevada and Gabilan Range. Velocities below a depth of about 3-4 km were demonstrated to be quite similar, but a low-velocity zone such as that at a depth of 6-14 km on the Modoc Plateau model was not used to fit the Sierran or Gabilan Range data. Strong similarities also exist between the Modoc model and Basin and Range velocity models, but thicker low-velocity layers were selected for the Basin and Range models. Fuis and others prefer the geologic interpretation that the Modoc Plateau is underlain by granitic and metamorphic rocks similar to those of the Sierra Nevada and Gabilan Ranges. Surface exposures of granitic rocks in the Sierra and Gabilan Ranges have velocities of 6.0-6.2 km/s. However, the rocks in the upper crustal unit under the Modoc Plateau may not be Sierran granites, because the main trend of the Sierran batholith occurs well to the east of the Modoc Plateau (Smith and others, 1971).

Zucca and others (1986) interpret that the 6.4 km/s layer is composed of either intermediate composition crystalline rocks or metamorphic rocks of amphibolite or granulite facies. Velocities compiled for samples of these metamorphic rocks (Christensen, 1982) ranges

between 6.4 and 7.0 at pressures of 4-6 Kbar (12-18 km). By considering the significant reduction in velocity due to increased temperatures, this range for the Modoc Plateau would likely be approximately 6.3-6.9 km/s which would be compatible with the refraction model. The authors discount the possibility that the Modoc Plateau is underlain by a rift filled with new crust as proposed by Blake and Jones (1977) and Hamilton (1978) because such rifts are normally compensated by shallow, high velocity mafic rocks. MT surveys in rift areas such as the Snake River Plain, show that the deep crustal conductor occurs deeper than 20 km where the crust has been reconstructed through mafic compensation (Stanley, 1982). Other rifts, such as the Rio Grande Rift (Jiracek, 1983) have both shallow conductors and seismic low velocity layers in addition to high velocity lower crustal regions. Thus, the general picture with rifts regarding MT and seismic models is not uniform. It seems clear that there is no strong evidence in the geophysics for a rift under the Modoc Plateau; however, there is good support, both in the geology and geophysics, for the strong overprint of Basin and Range structures on the Modoc Plateau. We suggest that the west to east rise in the deep crustal conductor is evidence for this increased thermal input. High heat flow values in the Modoc Plateau (Mace and others, 1985), a shallow MT deep conductor, and large density of northwest trending normal faults all suggest that the crust beneath the Modoc Plateau is highly extensional.

Zucca and others (1986) and Fuis and others (1987) suggest that the Modoc Plateau may be a composite of the roots of several magmatic arcs. Hamilton (1988) has reviewed the deep crustal lithology of exposed island arc crust and finds that examples from west-central Idaho and the North Cascades consist of upper and mid-crustal zones of crosscutting mafic and intermediate plutons above isotopically primitive amphibolitic, tonalitic, and trondjemitic gneisses, with the amphibolites becoming increasing garnetiferous or pryroxene-bearing with depth. A classical exposed 40 km exposed section of island arc crust in Pakistan is interpreted by Hamilton to contain stocks and small batholiths in the upper and middle crust that grade from low greenschist through lower and upper amphibolite to garnet amphibolite facies. The lower crust of this section consists of mafic granulites and mafic plutonic rocks. In light of this crustal characterization we suggest in figure 11d that the 6.1-6.3 km/s zone in the Modoc Plateau consists of crosscutting plutons rocks of intermediate composition, the 6.4 km/s layer represents amphibolitic gneisses at temperatures above 500^{o}C, and the 7.0 km/s lower crustal section consists of mafic granulites and mafic plutonic rocks. With the increased temperatures under the Modoc Plateau water would be released from amphibolites, possibly fluxing partial melts and creating other changes in the rock matrix at depths coincident with the deep crustal conductor and the dipping low velocity zone. We will discuss this petrologic model in detail later.

STRUCTURE OF THE WASHINGTON CASCADES

Extensive magnetotelluric surveys have been completed in the southern Washington Cascades as described in Stanley and others (1987). Stanley (1984) also provided a deep electrical model for the northern Columbia Plateau. Although Catching and Mooney (1988) have studied the central Columbia Plateau (fig. 12) with refraction profiling, no active refraction or reflection profiles have been completed across the Washington Cascades. Taber (1983) studied the Olympic Peninsula and part of the Coast Range with earthquake travel-time analyses and Taber and Lewis (1986) studied the Washington continental margin east of Gray's Harbor with a refraction profile that used offshore shots and onshore quarry blasts. Finn (1988) constructed detailed gravity and magnetic models for a long profile through southern Washington along Taber and Lewis' refraction line and Stanley's (1984) MT profile through the southern Cascades and Columbia Plateau.

Stanley and others (1987) found that a conductivity anomaly first detected by Law and others (1982) consisted of an east dipping conductive package they termed the southern Washington Cascades conductor (SWCC) shown in figure 14a. The extent of this conductivity anomaly is indicated in the contour map of fig. 12 along with significant magnetic anomalies that were used to postulate a geologic model for the MT results. The conductive package was

interpreted to be a possible late-Cretaceous to early-Eocene forearc basin-accretionary prism system (fig. 2) that was sutured against and under the pre-Eocene North American continent by accretion of a major seamount complex, Siletzia (partially outlined by magnetic highs (S) and (T) in figure 12). Other possibilities for the conductive rocks were considered, including altered volcanic flows, thick continental sedimentary rocks, and graphitic/pyritic rich pre-Mesozoic rocks. However, based upon correlation of shallower parts of the conductor with outcrops of Eocene marine and transitional marine rocks, the lithology preferred for the MT model is that of a marine sedimentary rock complex in the suture zone. Important relationships of the conductive SWCC units with strike-slip seismicity and possible influence over the location of Mt. St. Helens were also discussed.

Other features indicated in the MT model for profile AA' are an intrusive body (Goat Rocks pluton) east of Mt. Rainier, the Chehalis Basin, and details of the northern part of the Columbia Plateau. On the Columbia Plateau the MT model indicates up to 3.3 km of surface basalts of the Columbia River Basalt Group (CRBG) overlying about 3 km of conductive units interpreted to be comprised largely of Tertiary continental sediments rich in tuffaceous clasts. Seismic refraction profiling by Catchings and Mooney (1988) provides other details about the deep crust and mantle underneath the Columbia Plateau. Key features of their model for the Columbia Plateau region are shown in figure 13a. Catchings and Mooney used their 260 km long NE-SW trending profile (fig. 1) to interpret that the central part of the CP is covered by 3-6 km of flows of the CRBG. The CRBG was interpreted to cover a variable accumulation of sedimentary rocks assigned to a model low-velocity layer (5.0 km/s) up to 5 km thick. The remainder of their seismic model included an upper crustal layer of 6.1-6.3 and an assumed mafic, mid-crustal layer of 6.8 km/s. A high velocity (7.5 km/s) layer forms the lower crust starting at depths of 25 km underneath the deepest part of the central basin of the CP, the Pasco Basin. Catchings and Mooney interpret their model to represent evidence for continental rifting that was compensated for by a lower crustal rift pillow.

The deep conductive zone that dips to the east under the western Columbia Plateau may not be directly associated with the SWCC, but instead may be caused by the same petrological factors or physical processes behind the deep crustal conductor in the Oregon-California High Cascades and in the eastern Oregon-northeastern California Basin and Range and Modoc Plateau. It is tempting, however, from a simplistic, plate-tectonic standpoint to connect the two conductors (SWCC and western CP). Note, however, that no deep conductor occurs in the lower crustal 6.8 km/s layer as it does in the 6.4-6.5 km/s lower crustal units in Oregon and California. This indicates lithologies, temperatures, or other physical conditions under the Columbia Plateau that are different from the Cascades in Oregon and California.

In addition to profile AA', profile CC' (fig. 12) provided important information on structures in the western Washington area. A two-dimensional model of data from CC' is indicated in figure 14 reproduced from Stanley and others (1987). On this profile SWCC units were interpreted to be a highly compressed version of similar rocks on profile AA'. In addition. Siletzia rocks were observed to be underlain by conductive units interpreted to be an underplated Tertiary subduction complex like that in the Olympic Mountains and mapped under Vancouver Island by the Lithoprobe experiments (Clowes and others, 1987).

The geophysical data along the transect AA' allow us to construct an geological section for our interpretation (fig. 13b). This transect coincides with DNAG transect C-3 (Cowan and Potter, 1987). In this geological schematic we show Siletzia, as the major component of the Coast Range, being underplated by post-Eocene subduction complex units. This interpretation is somewhat a composite of the west end of MT profiles AA' and CC' and unpublished MT data. Gravity and magnetic modelling of this section of the profile by Finn (1988) shows that the section directly beneath conductive rocks must have relatively high densities (>2.9), indicating the underplated unit is highly metamorphosed and may consist of a minor component of sedimentary units, but mostly of dense and possibly altered ophiolites.

In the Cascades the SWCC forms a major part of the upper crust, possibly underlain by oceanic crust and overlain by thick, post accretion volcanic flows that covered the region starting at 40-25 Ma (figure 2). Seismicity that defines the SHZ zone of Weaver and Smith

(1983) and source magmas for Mount St. Helens are interpreted to be coincident with the suture between Siletzia and the SWCC. Narrow magma bodies are indicated ascending along the SHZ at the western boundary of this suture in a manner envisioned by Scandone and Malone (1985). Mount Rainier is interpreted to have developed on the pre-Eocene suture between the SWCC complex and older units of the continent.

STRUCTURE OF THE COAST RANGE IN OREGON AND WASHINGTON

The Coast Ranges in Oregon and Washington are largely comprised of Tertiary forearc sedimentary rocks underlain by Eocene basalts of Siletzia (fig. 2). In addition to the long MT profile across the Cascades and Columbia Plateau in Washington discussed above, Stanley and others (1987) discuss the comparison of their profile CC' (which crosses part of the Olympic Peninsula and Coast Range) with Canadian Lithoprobe program MT models from Vancouver Island. Figure 15 shows (A) the Lithoprobe MT model from Vancouver Island (Clowes, 1987); (B)a composite MT model from this paper across the Washington Coast Range; (C) the MT model of the Coast Range in central Oregon from the EMSLAB experiment (EMSLAB Group, 1988); and the MT model for the Klamath Mountains from this paper. In this schematic we have shown only details down to an interpreted deep conductor. The inferred edge of Wrangellia in (A) and Siletzia in (C) from aeromagnetic data are also indicated. The Lithoprobe model utitlizes constraints provided by deep reflection data across Vancouver Island; the structure beneath Vancouver Island is envisioned to be somewhat analogous to that of the Klamath Mountains with a stack of lithotectonic plates that decrease in age with depth. A late Paleozoic-early Mesozoic oceanic plateau, Wrangellia (Jones and others, 1984) is underlain by subthrust Metchosin basalts (part of Siletzia terrane), core rocks of the Olympic Mountains subduction complex, and other underplated oceanic sedimentary and plate rocks. It should be noted that the scales on the figure are somewhat variable, but the similarity in structure for the various models is very evident, with a reasonably consistent style for the conductive part of the subthrust units. However, thrusting of possible late Cretaceous (western Franciscan) rocks under the Klamath block and Olympic subduction complex rocks (Tertiary) under the north edge of Siletzia appears to be occurring at somewhat shallower depths than the thrusting of sedimentary rocks beneath the main core of Siletzia in Oregon and beneath combined Siletzia-Wrangellia terrane on Vancouver Island. This may be due to a larger depth of shearing underneath thicker parts of Siletzia in Oregon and Wrangellia than underneath the thinner Klamaths and northern part of Siletzia just south of the Olympic Peninsula. Monger (1988) has postulated that both continental plateau and island arc complexes are generally sheared along horizontal planes during accretion. In other words, generally only the upper parts of accreted units may be welded to the continent, whereas the lower surfaces may actually be subducted. This could easily be envisioned for a stack of relatively thin accretionary plates such as that found in the Klamath Mountains. Massive oceanic rift-seamount complexes like those in the core of Siletzia and the huge Wrangellia terrane (oceanic plateau) may have sheared at larger depths, maintaining a greater thickness of primary accreted material.

LOCATION OF EOCENE SUTURE IN THE CASCADES

The Eocene suture which is interpreted to be located in the area of the SWCC in Washington has not been located elsewhere along the Cascades to the south. The suture between the Klamath Mountains and continental crust underneath the Cascades in northern California is clearly located near Mt. Shasta as indicated in the MT and seismic profiles through this region. However, this suturing took place prior to late Cretaceous and may be steeply dipping as suggested by the seismic refraction model and interpretation of Blakely and others (1985) that Trinity ultramafic rocks extend underneath Mt. Shasta. Consideration has been given as to where the suture zone between Siletzia and pre-Eocene crust occurs in Oregon. The very simplistic structures indicated in east-west MT profiles across the High Cascades provide that the suture zone probably does not occur in the region of the Quaternary volcanoes. The more probable occurrence of the suture is within the Tertiary arc

which is defined by the Western Cascades volcanic field. The eastern edge of Siletzia basalts in central Oregon can be somewhat discerned in aeromagnetic and gravity data and we suggest that the suture occurs about as indicated in figure 15; the Tertiary volcanoes may have filled this suture in central Oregon. Downwarps evidenced in the Chehalis and Willamette Basins may be a result of compressive deformation of the leading edge of Siletzia during final accretionary closure. Coastal Basins such as the Tyee, Astoria, and Grays Harbor Basin formed on the west side of the central core of Siletzia.

NATURE OF THE MID-CRUST IN THE CASCADES

The seismic and MT interpretations discussed above allow us to speculate about the nature of the mid-crust in the Cascades. As we have mentioned previously, knowledge of the lithology and physical state of the rocks at depths of 10-25 km is crucial to accurate assessment of geothermal, seismicity, and volcanic hazards potentials. The one phenomenon that is essential to understand in this regard is the presence of a deep electrical conductor within the region. It has been demonstrated that this conductor is generally located within the mid-crust at depths of 12-20 km where seismic velocities are 6.4-6.5 km/s and higher. However, there are some noteable variations in the depth. These variations are not considered to include the underthrusting conductor found in the Coast Range-Klamath Mountains-Vancouver Island models. The important departures of depths to the DCC from a general value of 12-20 km in the Cascades and surrounding region are:

(1) very shallow DCC on the western margin of the High Cascades, near the contact with the western Cascades
(2) shallowing of the DCC under the Modoc Plateau in correlation with the determined dip of a low velocity zone at the top of the mid-crustal velocity layer of 6.4-6.5 km/s
(3) large depths to a DCC under the Columbia Plateau

Previous models for the DCC in the western U.S. have mainly involved the effects of either free water and temperatures of over 500^{o}C or of simply partial melt fractions. Stanley (1977) discussed the role of temperature and water in terms of the conductor in the Snake River Plain; Wannamaker (1987) calculated possible percentages of fluxed melt in the Basin and Range and its role in the conductor; Jiracek (1983) advocated a trapped zone of free water beneath a brittle-ductile transition in the Rio Grande rift to explain a deep crustal conductor underneath the rift, in opposition to the interpretation by Hermance and Pedersen (1980) that the deep rift conductor was caused by magma. Stanley (1988) has advanced arguments for some deep crustal conductors in low heat flow areas being caused by carbon/metallic mineral films in metamorphosed shales. Duba (1985,1988), pointed out the role of a carbon in the crust and mantle as a possible factor in deep MT conductors. Stanley and others (1988b) interpret regional conductors in the Alaska Range that extend from depths of as shallow as 3 km to over 20 km to be massive sections of underplated Mesozoic flysch with 3-5% high grade carbonaceous material in fissile plane coatings.

Clowes and others (1987) interpret the east-dipping conductor under Vancouver Island to be the result of saline fluids filling the pore spaces of interbedded sediments and basalts of the upper oceanic crustal layers that have been underplated. The effect of saline or other pore waters begins to decrease at upper crustal depths and temperatures above about 250^{o} C due to mixed phase fluid development. At mid-crustal depths (12-15 km) any free water becomes significant if temperatures are greater than 500^{o} C because of its ability flux granitic melts. The development of mid-crustal magma and its ability to stope upwards through the crust and remain molten is highly dependent on the amount of water in the melt.

Recent work on mid-lower crustal rocks illustrate the fact that large amounts of water accompany metamorphic events. Russian workers (Feldman, 1976) have postulated the role of trapped mid-crustal zone of water in development of deep crustal conductors. The formation of granulites is accompanied by considerable amounts of hydrous fluid, possibly in equilibrium with carbon dioxide and methane (Fyfe and others, 1978). Hoisch (1985) used occurences of

wollastonite (calcite+quartz=wollastonite+CO_2) in the Big Maria Mountains of Southern Califronia to demonstrate that huge volumes of water have flowed through the mid-crust as these rocks were metamorphosed at temperatures of 360-600^{o}C. Free water in the Cascades may have originated in the generation of granulites from amphibolite grade metamorphic rocks in the lower crust as they were heated in the Quaternary by Cascades arc magmatism and Basin and Range thermal overprinting.

Fournier (this volume;written comm., 1988) has discussed the role of crustal fluids and high pore pressures in the deep crust. He points out that release of fluids from deep crustal rocks may hydrofracture, or disaggregate (Fyfe and others, 1978) host rocks when the released fluid pressure, P_f, is greater than the confining pressure, P_s plus the tensile strength of the rock (usually much smaller than the lithostatic pressure in the deep crust). He points out that release of high pressure fluids may lead to several key effects:

- o When least principal stress is horizontal, the released fluids act to hydrofracture the deep crustal rocks along horizontal planes that concentrate the fluids..
- o If rocks overlying a zone of fluid release are semipermeable, then reverse osmosis due to steep pressure gradients may cause the residual fluid to become more saline with time, contributing to an increase in electrical conductance. Non-dehydrating rocks above reacting ones can form the impermeable or semipermeable zone (Fyfe and others, 1978).
- o The effect of thin horizontal films of high pore-pressure fluids in hydrofractured laminations would be exhibited at the shallowest depth where competent rocks are being subjected to compressive stress and especially pronounced where heating to temperatures in excess of 350-400^{o} C has occurred.

Fyfe and others (1978) provide a comprehensive analysis of the role of high pressure fluids in propagating fractures through the crust and details on the characteristic pulses of water generated in metamorphic dehydrations. They point out that a basic amphibolite contains water in hornblendes and biotite, with hornblende frequently making up 50% of the rocks volume and containing 2% weight water; thus a typical amphibolite could release 1% of its total weight in dehydration water. The higher grade amphibolite facies dehydrate into granulite facies producing the anhydrous minerals garnet-plagioclase-pyroxene. Partial melting frequently occurs before complete dehydration, and because of the great affinity of water for a silicate melt-phase, the hydrous fluids may be effectively tranported to higher levels of the crust as the silicate magmas stope upward. Fluids and gases not soaked up by the silicate magmas work their way upward through vertical microfractures and by grain boundary migration until an impermeable zone is reached or until the pressure of the fluids is significantly greater than the lithostatic pressure, P_l. If P_l is the maximum stress component, then the fluids will disaggregate or hydrofracture the rocks horizontally until enough volume is created to accomodate the released fluids and gases. The overlying impermeable zone may simply be the non-dehydrating metamorphic rocks, a change in lithology, or the ductile transition as envisioned by Eaton (1980) and Jiracek and others (1983), since mylonitic texturing is normally found at this level. The impermeable zone will be effective in limiting the vertical migration of fluids until the expanding width of the horizontal fractures effectively creates a network of vertical fractures. In addition, upwardward stoping magmas may disrupt the impermeable zone and purge the ponded water. Such horizontal fractures may contain a mixture of hydrous fluids, partial melts, and mobilized graphitic or metallic mineral films. It is possible to envision how this process could create a highly conductive zone in the deep crust.

We suggest that the petrological processes outlined above explain the deep conductor in the Cascades and has important implications to tectonic problems, such as limiting brittle behavior in the crust. Normal brittle to ductile transitions in deep crustal rocks are produced by the effect of pressure and temperature, but a horizontal network of microfractures would simulate ductile behavior and effectively depth-limit seismicity due to extensional stress. Seismicity in active tectonic regions typically has a sharp depth limit. For instance, earthquakes in the Basin and Range of Nevada (Eaton, 1980), in Haicheng, China and Greece

(Meissner, 1986) have a depth cutoff at about 15 km (Eaton, 1980)l; in the Rio Grande rift (where heat flow is similar to that of the High Cascades), the cutoff is about 13 km (Sanford and others, 1979); in the Coso, California geothermal area the cutoff is about 7 km (Meissner, 1986); and in the Yellowstone, Wyoming area it is only about 4-5 km (R. B. Smith, personal comm). Earthquakes in the Oregon Cascades are very rare, but more frequent in the northern California Cascades. A regional depth limit for events in the latter area is about 15 km (written comm., C. S. Weaver, 1988). In the Columbia Plateau, seismicity extends to somewhat larger depths of about 20-25 km. The depth limits for seismicity in northern California and the Columbia Plateau are very crudely equivalent to the depth of the DCC, thus a brittle-ductile transition could conceivably cap a zone of horizontal hydrofractures in the region discussed in this paper.

These concepts are portrayed in the cartoon of figure 16. Ideas from Lachenbruch and Sass (1978) and Hamilton (1988) on mafic underplating of the crust are utilized. Hamilton (1988, oral comm.) suggests that mafic magmas pond at the base of the crust and partially fill extensional gaps, but mainly generate silic magma that actually transport the heat upward through the crust. In our model, this heat dehydrates amphibolite grade metamorphic rocks, fluxes additional silicate melts, and releases water internal and external to the melts at higher crustal levels. When an impermeable zone is encountered and $P_l<P_f$, then a system of horizontal fractures is formed that may fill with fluids, including partial melt, and may be coated with mobilized graphitic carbon and sulfide minerals. The metamorphic scaling for this cartoon comes from considering the temperature profile and facies data of figure 17 modified from Fyfe and others (1978). We selected a specific temperature profile shown by the dashed line that coincides with the 50°C/km profile down to the point where the wet granite solidus curve is intersected (13 km, 650°C) and was assumed to be nearly isothermal with a gradient of about 10°C/km where the granitic partial melts and liberated fluids transfer the heat upwards (depths of 13-21 km). Finally, the temperature profile was selected to be 20°C/km in the granulitic, dehydrated zone from 24-40 km. Below 35 km temperatures approaching 1000°C are interpreted to exist and mafic magmas fill extensional zones in the deep crust. Mafic partial melts and underplating mafic intrusions may floor the crust as envisioned by Hamilton (1988).

The process indicated in figure 16 may sweep upward with time as a heating cycle advances in accreted terranes such as that of the Cascades region. For steeper temperature gradients than assumed in this figure, the zone of partial melting and horizontal fracture development will occur shallower and the vertical sequence of metamorphic facies will be depth compressed. This effect may be the cause of shallowing of the deep crustal conductor in the Modoc Plateau and along the boundary of the High Cascades and Western Cascades where thermal inputs from the base of the crust may be considerably higher than in the remainder of the region. Late-stage mafic intrusions at Medicine Lake and Newberry volcano may be occurring in largely dehydrated upper and mid-crust, thus the crustal conductor is not conspicuously shallow near these volcanoes. In the Columbia Plateau the larger depth to the crustal conductor may be related to both the lower heat flow in the Plateau and the probability that the deep crust in this region consists of mafic rocks. Mafic rocks have a higher temperature of formation of partial melt in the presence of water than more silicic rocks. In addition, the lower crust under the Plateau may not have bound metamorphic water, limiting the water of dehydration available for upward migration.

SIGNIFICANCE OF DEEP CONDUCTOR MODEL TO GEOTHERMAL REGIME

We hypothesize that the DCC mapped at average depths of 12-15 km in the Cascades is related to a zone of hydrous fluid and partial melt in horizontal hydrofractures beneath an impermeable layer. The partial melt component is called for by probable high temperatures at this depth. Waff (1974) and Shankland and Waff (1977) have developed a theoretical model to simulate the effect of melt distributions on electrical resistivity. Hermance and Pedersen (1980) have extended these author's analysis by modifying a well known relationship (Archies Law) for pore fluid conduction to include the effect of a melt component. Such analyses show that

connected melt components amounting to about 2% of the rock produce resistivities of about 20 ohm-m and 25% connected melt produces resistivities of about 2 ohm-m, representing the approximate range of resistivities interpreted for the DCC in the Cascade MT interpretations. Of course, with the presence of free water in horizontal fractures, as well as partial melt, the actual percentage of melt could be much smaller. These assumptions imply that the volume of magma present as partial melt in the Cascades is very limited above a depth of 12-15 km. Although it could be argued that the extensive mid-crustal magmatic heat source proposed by Blackwell and Steele (1983,1985) is compatible with the MT data if placed somewhat deeper than they interpret, such an extensive magma accumulation would not be compatible with the seismic refraction data; a significant low-velocity zone would be required for such a feature. Interpretation of the long refraction profile of Leaver and others (1986) indicated in figure 4 indicates that such a low velocity region is not required by the data. The velocity and resistivity structure hypothesized in the model of figure 15 implies some crustal petrological control over the DCC; this assumption diminishes the possibility that the DCC is caused by a large scale magma accumulation.

An excellent analogy for the MT, refraction, and heat flow results from the Cascades can be found in the Rio Grande rift of New Mexico and Colorado. Heat flow in the rift is comparable to that in the Oregon Cascades, exceeding 100 mw/m^2. Excellent shear wave and compressional seismic reflection and refraction data are available from the central New Mexico part of the rift, where mid-crustal magma has been postulated by Sanford and others (1979). The postulated magma accumulation occurs at a depth of about 20 km as evidenced in COCORP P-wave reflection data as a series of bright reflections. These reflections occur very near the so-called Conrad discontinuity where velocities increase from about 5.8 to 6.5 km/s. Analysis of shear wave reflection data from microearthquakes by Rinehart and others (1979) indicate that the postulated magma body is contained just beneath the brittle uppermost crust (above the 6.5 km/s layer) and consists of very low fractions of partial melt. This analysis closely corresponds to our hypothesized petrologic model for the Cascades. In fact, both the high reflectivity and shear wave reflection data from the Rio Grande rift could be explained by a zone of hydrofracturing with a combination of hydrous fluids and partial melt. Similar zones of mid-crustal high reflectivity have been correlated with trapped metamorphic water (for instance,in the Alps, Pfiffner and others, 1988). MT interpretations in the Rio Grande rift by Jiracek (1983) and Hermance and Pedersen (1980) show somewhat divergent depths (10-20 km) to a deep crustal conductor because of very complicated resistivity structures in the thick, conductive rift clastics at the surface, but it is possible that the DCC in the Rio Grande rift coincides with the zone of high reflectivity at the top of the 6.5 km/s layer.

This discussion of the Rio Grande rift geophysics tends to support our interpretation of limited amounts of partial melt suggested by the petrologic model of figure 16. Future studies in the Cascades should focus upon obtaining high quality compressional and shear velocity information to study the mid-crust. Microearthquakes are rare in the Oregon Cascades, but attempts should be made to study the shear wave information from any events available and specific wide-angle reflection-refraction studies should be done to study the mid-crust. Such seismic geophysics and additional high-resolution electromagnetic studies combined with better heat flow sampling are necessary to determine the nature of the deep crust in the Cascades and the extent of geothermal resources. These studies could be employed most effectively to study the region of the High Cascades-Western Cascades boundary in Oregon where the DCC becomes shallow.

SUMMARY AND CONCLUSIONS

Our review of MT and seismic profiles in the Cascades and surrounding regions has been employed to develop new geologic models based upon the combined information. The MT data show a well defined structural trough in the central Oregon Cascades as thickening of layer no. 2 of a generic four-layer model that effectively simulates most of the Oregon and California High Cascades, High Lava Plains, and Basin and Range. MT data in the central Oregon High Cascades shows that a deep crustal conductor normally found at depths of 12-15

km in the Cascades become somewhat shallower in the region near the boundary of the High Cascades and western Cascades. This was demonstrated with detailed profiles in the Breitenbush Hot Springs area. In the central Oregon Cascades and elsewhere in Oregon and northern California, the deep crustal conductor occurs in the upper part of a seismic layer of 6.4-6.5 km/s velocities. Coincident MT and seismic refraction models for Newberry crater in east-central Oregon indicate an intrusive buildup with clear indication on both sets of data, as well as on gravity data.

Comparison of MT and seismic refraction models for a long, east-west profile in northern California reveals complex structures in the Klamath Mountains with equally complex resistivity, velocity, gravity, and magnetic signatures. Mount Shasta is interpreted to be located near a suture zone between the Klamath Mountains complex and pre-accretion crust beneath the Cascades. The Modoc Plateau is interpreted to be a highly extensional zone with high sub-crustal heat input, but not a major rift zone with completely reconstructed crust.

Previously interpreted MT profiles through southern Washington and the Columbia Plateau of eastern Washington were discussed along with interpretations of a Columbia Plateau seismic refraction model. A combined geological model based upon these geophysical data and magnetic and gravity data were interpreted to indicate a direct correlation of seismicity and volcanism with the suture zone between a major seamount system (Siletzia) and an forearc-accretionary prism complex (SWCC) against the pre-Eocene continental margin.

Comparison of mapped deep electrical structures in the Coast Ranges-Klamath Mountains-Vancouver Island regions of the Pacific Northwest shows similar styles of underplating occurring in these regions and the possible location of the main Eocene suture resulting from accretion of Siletzia. This suture may have acted to localize Oligocene-Miocene volcanism in Oregon and Quaternary volcanism in the Mount St. Helens region, while the suture between the Klamath Mountains and the pre-accretion margin constrained the location of Mount Shasta in northern California.

Several mechanisms for producing the regional deep crustal conductor in the Cascades and elsewhere were discussed and concepts proposed by Fournier (1988) and Fyfe and others (1978) on the role of high-pressure fluids in hydrofracturing the mid-crust were entertained. It was interpreted that an additive effective in the reduction of resistivities may be produced in the area of the deep conductor, with graphitic-metallic mineral films in metamorphic rocks enhanced by hydrous and partial melt fluids contained in horizontal fracture planes. This zone is interpreted to represent the lower limit of normal fault penetration and an effective lower depth limit to seismicity. Anomalous shallow depth to the deep conductor appears to correlate with areas of highest heat flow in the central Oregon Cascades, but we believe the geophysical interpretations do not favor a large accumulation of magma at depths of 7-10 km as postulated by Blackwell and Steele (1983,1985) to explain the heat flow data.

ACKNOWLEDGMENTS

We wish to thank Craig Weaver for supplying seismicity information for comparison with the other geophysical data and for fruitful discussions on the role of the SWCC in seismicity and volcanism in the southern Washington Cascades. In addition to primary support from the U.S.G.S. Geothermal Program, funding for much of the MT work in the southern Washington region was provided by the Department of Energy, Morgantown Energy Technology Center, administered by W. J. Gwilliam and partial funding for detailed electrical geophysical studies at Newberry volcano was provided by the Department of Energy, Geothermal Division, administered by Marshall Reed. Steve Ingebritsen, Water Resources Division, was instrumental in arranging support for some of the detailed investigations in the Breitenbush Hot Springs area.

REFERENCES

Achauer, U., L. Greene, J. R. Evans, and H. M. Iyer, 1988, High-resolution tomography of compressional wave velocity structure at Newberry volcano, Oregon: J. Geophys. Res., 93, no. B9.

Ando, C. J., W. P. Irwin, D. L. Jones, and J. B. Saleeby, 1983, The ophiolitic North Fork terrane in the Salmon River region, central Kalamth Mountains, California: Geol. Soc. Amer. Bull., 94, 236-252.

Berg, J. W., Jr., L. Trembly, J.D. A. Emiliam, J. R. Hutt, J. M. King, L. T. Long, W. R. McKnight, S. K. Sarmah, R. Souders, J. V. Thiruvathukal, and D. A. Vossler, 1966, Crustal refraction profile, Oregon Coast Range: Seismol. Soc. Amer. Bull., v. 56, p. 13567-1362.

Birch, F., 1960, The velocity of compressional rocks to 10 kilobars, Part 1:Jour. Geophy. Res., 65, 1083-1102.

Birch, F., 1961, The velocity of compressional rocks to 10 kilobars, Part 2: Jour. Geophy. Res., 66, 2199-2224.

Blackwell, D.D., Bowen, R.G., Hull, D. A., Riccio, J., and Steele, J. A., 1982, Heat flow, arc volcanism, and subduction in northern Oregon: J. Geophys. Res., v. 87, p. 8735-8754.

Blackwell, D. D., and Steele, J. L.,1983, A summary of heat flow studies in the Cascade Range: Transactions of the Geothermal Resources Council, v. 7, p. 233-236.

Blackwell, D. d., and Steele, J. L., 1985, Heat flow of the Cascade Range: in Guffanti, M., and Muffler, L. J. P. (eds.), Proceedings of the workshop on geothermal resources of the Cascade Range, U.S. Geological Survey Open-File Report 85-521, p. 20-23.

Blake, M. C. and D. L. Jones, 1977, Plate tectonic history of the Yolla Bolly junction, northern California: (abs) 73rd Annual Meeting, Cordilleran Sect., Geol. Soc. Am., Los Angeles, California.

Blake, M. Clark, Jr. and D. L. Jones, 1986, Franciscan assemblage of Northern California: Unconventional Gas Recovery Program Peer Review, Dept. of Energy, Bethesda, Maryland, 279 p.Brooks, H. C., 1979, Plate tectonics and the geologic history of the Blue Mountains: Oregon Geology, v. 41, p. 71-80.

Blakely, R. j., R. C. Jachens, R. W. Simpson, and R. W. Couch, 1985, Tectonic setting of the southern Cascade Range as interpreted from its magnetic and gravity fields: Geol. Soc. Am. Bull., v. 96, p. 43-48.

Carmichael, R. S., 1982a, Magnetic properties of minerals and rocks: in Carmichael, R. S., ed., Handbook of physical properties of rocks: Boca Raton, Florida, Chemical Rubber Company Press, Inc., p. 229-288.

Catchings, R. D., and W. D. Mooney, 1988, Crustal structure of the Columbia Plateau: evidence for continental rifting: J. Geophys. Res., v. 93, p. 459-474.

Catchings, R. D., and W. D. Mooney, 1988, Crustal structure of east-central Oregon: relationship between Newberry volcano and regional crustal structure: J. Geophys. Res., v. 93, p. 10081-10094.

Clowes, R. M., Brandon, M.T., Green, A.G., Yorath, C. J., Brown, A., Sutherland, Kanasewich, E. R., and Spencer, C., 1987, LITHOPROBE, southern Vancouver Island: Cenozoic subduction complex imaged by deep seismic reflections: Canadian Jour. Earth Sci., v. 24, p. 31-51.

Clowes, R. M., 1987, LITHOPROBE: Exploring the subduction zone of western Canada: The Leading Edge, Soc. Expl. Geophs., v. 6, no. 6, p. 12-19.

Connard, G., R. Couch, and M. Gemperle, 1983, Analysis of aeromagnetic measurements from the Cascade Range in central Oregon: Geophysics, v. 48, p. 376-390.

Cowan, D. S., and C. J. Potter, 1986, Continental-Oceanic Transect B-3: Juan de Fuca Plate to Montana Thrust Belt: Continental Oceanic Transic Ser., Geol. Soc. Am., Boulder, Colo.

Christensen, N. I., 1978, Ophiolites, seismic velocites and oceanic crustal structure: Tectonophysics, 47, 131-157.

Christensen, N. I., 1982, Seismic velocites: in Handbook of Physical Properties of Rocks,

Volume II, ed. R. S. Carmichael, p. 2-227, CRC Press., Boca Raton, Florida, 345 p.
Davis, G. A., and P. W. Lipman, 1962, Revised structural sequence of pre-Cretaceous metamorphic rocks in the southern Klamath Mountains, California: Geol. Soc. Am. Bull., 73, 1547-1552.
Davis, G. A., C. JH. Ando, P. H. Cashman, and L. Goulland, 1980, Geologic cross section of the central Klamath Mountains, California: Summary, part 1, Geol. Soc. Am. Bull., 91, 139-142.
Dickinson, W. R., 1976, Sedimentary basins developed during evolution of Mesozoic-Cenozoic arc-trench system in western North America: Can. J. Earth Sci., 13, 1268-1283.
Dickinson, W. R., and T. P. Thayer, 1978, Paleogeographic and paleotectonic implication of Mesozoic stratigraphy and structure in the John Day inlier of central Oregon: in Mesozoic Paleogeography of the Western United States, Pacific Coast Paleogeography Symp. 2, edited by D. G. Howell and K. A. McDougall, 147-161, Pacific Section, Socie5ty of Economists, Paleontologists, and Mineralogists, Los Angeles, Calif.
Duba, A. G., and T. J. Shankland, 1982, Free carbon and electrical conductivity in the Earth's mantle: Geophys. Res. Let., 9, 1271-1274.
Duba, A. G., E. Huenges, G. Nover, G. Will and H. Jodecke, 1988, Impedance of black shale from Munsterland 1 borehole: an anomalously good conductor: in press, Geophysical Journal.
Eaton, G. P., 1980, Geophysical and geological characteristics of the crust of the Basin and Range province: in Studies in Geophysics-Continental Tectonics, National Academy of Science. Washington, D.C. pp. 96-113.
EMSLAB Group, 1988, The EMSLAB electromagnetic sounding experiment:EOS, Transaction of the Amer. Geophys. Uniion, v. 69, p. 89-99.
Feldman, I. S., 1976, On the nature of conductive layers in the Earth's crust and upper mantle: in Geoelectric and Geothermal Studies, A. Adam, editor, published by Akademiai Kiado, Budapest, 752 p.
Finn, Carol A., 1988, Structure of the Washington convergent margin, implications for other subduction zones and for continental growth processes: Ph.D. thesis, Univ. of Colorado, Boulder, Colo., 143 p.
Fitterman, D. V., W. D. Stanley, and R. J. Bisdorf, 1988, Electrical structure of Newberry volcano: J. Geophys. Res., 93, p. 10120-1031.
Fournier, R. O., 1988, A proposed methodology for estimating convective and conductive heat fluxes from the Cascades province and adjacent regions using seismic and electrical resistivity data: this conference.
Fritts, S. G. and L. H. Fisk, 1985, Tectonic model for formation of Columbia basin: implications for oil, gas potential of North Central Oregon: Oil and Gas Journal, Aug. 26, p. 84-88.
Fuis, G. S., J. J. Zucca, W. D. Mooney, and B. Milkereit, 1987, A geologic interpretation of seismic-refraction results in northeastern California: Geol. Soc. Am. Bull, 98, 53-65.
Fyfe, W. S., N. J. Price, and A. B. Thompson, 1978, Fluids in the Earth's crust: Elsevier, New York, Amsterdam, 388 p.
Griscom, A., 1977, Aeromagnetic and gravity interpretation of the Trinity ophiolite complex, northern California: Geol. Soc. Am. Abstr. Progr., 9, 426-427.
Guffanti, M. and C. S. Weaver, 1988, Distribution of late Cenozoic volcanic vents in the Cascade Range (USA): volcanic arc segmentation and regional tectonic consideration: in press, Jour. Geophys. Res.
Hamilton, W. B., 1988, Plate tectonics and island arcs: Bull. Geol. Soc. Am., v. 100, p. 1503-1527.
Hamilton, W. B., 1969, Mesozoic California and the underflow of Pacific mantle: Geol. Soc. Amer. Bull., v. 80, p.2409-2430.
Hamilton, W. B., and Meyers, W. B., Cenozoic tectonics of the western United States: Reviews of Geophysics: v. 4, p. 509-550.
Hamilton, W., 1978, Mesozoic tectonics of the western United States: in Mesozoic Paleogeography of the Western United States, Pac. Coast Paleog. Symp. 2, edited by D. G.

Howell and K. McDougall, 33-70, Soc. Ecom. Pal. Min., Pacific Coast Sect., Bakersfield, California.
Hammond, P. E., 1979, A tectonic model of the evolution of the Cascade Range: in Cenozoic Paleogeography of the Western United States, Pacific Coast Paleogeography Symp. 3, edited by J. M. Armentrout and M. R. Cole, 219-237, Society of Economists, Paleontologists, and Mineralogists, Bakersfield, California.
Heller, P. L., R. W. Tabor, and C. A. Suczek, 1987, Paleogeographic evolution of the United States Pacific Northwest during Paleogene time: Can. Jour. Earth Sci., 24, 1652-1667.
Hermance, J. F., and Jens Pedersen, 1980, Deep structure of the Rio Grande Rift: A magnetotelluric interpretation: Jour. Geophys. Res., 85, B7, p. 3899-3912.
Hoisch, T. D., 1985, Metamorphism in the Big Maria Mountains, Southeastern California: Ph.D. Thesis, University of Southern California, Los Angeles, California, 264 p.
Hotz, P. E., 1971, Plutonic rocks of the Klamath Mountains, California and Oregon: U.S. Geol. Surv. Prof. Pap. 684-B, 20 pp.
Ingebritsen, S. E., D. R. Sherrod, and R. H. Mariner, 1988, Heat flow and hydrothermal circulation in the Cascade Range, north-central Oregon: this conference.
Irwin, W. P., 1966, Geology of the Klamath Mountains province: in Geology of Northern California, edited by E. H. Bailey, Bull. Calif. Div. Mines Geol., 190, 19-38.
Irwin, W. P., 1981, Tectonic accretion of the Klamath Mountains: in The Geotectonic Development of California, Rubey Vol. 1, edited by W. G. Ernst, 30-49, Prentice Hall, Englewood Cliffs, N. J.
Jiracek, G. R., E. P. Gustafson, and P. S. Mitchell, 1983, Magnetotelluric results opposing magma origin of crustal conductor in the Rio Grande Rift: Tectonophysics, v. 94, p. 299-326.
Lachenbruch, A. H., and J. H. Sass, 1978, Models of an extending lithosphere and heat flow in the Basin and Range province: Geol. Soc. Am. Memoir 152, p. 209-249.
LaFehr, T. R., 1965, Gravity, isostasy, and crustal structure in the southern Cascade Range: J. Geophys. Res., 70, 5581-5597.
Law, L. K., D. R. Auld, and J. R. Booker, 1980, A geomagnetic variation anomaly coincident with the Cascade volcanic belt: J. Geophys. Res., 85, 5297-5302.
Lawrence, R. D., 1976, Strike-slip faulting terminates the Basin and Range province in Oregon: Geol. Soc. Amer. Bull., v. 87, p. 486-850.
Leaver, D. S., Mooney, W. D., and W. M. Kohler, 1986, A seismic refraction study of the Oregon Cascades: J. Geophys. Res., v. 89, p. 3121-3134.
Mace, C. W., Sass, J. W., Lachenbruch, A. H., and R. J., Monroe, 1982, Preliminary heat flow of the California Cascades: U.S. Geol. Surv. Open File Rept. 82-150.
Macdonald, G. A., 1966, Geology of the Cascades Range and Modoc Plateau: in Bailey, E. H., ed., Geology of Northern California, Calif. Div. of Mines and Geol. Bull.,190, 65-96.
MacLeod, N. S., and E. A. Sammel, 1982, Newberry Volcano, Oregon: a Cascade Range geothermal prospect: Oregon Geology, 44, 123-131.
Macleod, N. S., G. W. Walker, and E. H. McKee, 1976, Geothermal significance of eastward increase in age of upper Cenozoic rhyolitic domes in southeast Oregon: Proc. U. N. Symp. Dev. Use Geotherm. Resour. 2nd, 1, 455-474.
MacLeod, N. S., and D. R. Sherrod, 1988, Geologic evidence for a magma chamber beneath Newberry volcano, Oregon: Jour. Geophys. Res., 93, 10067-10079.
McBirney, H. R., Volcanic evolution of the Cascade Range: Earth Planet. Sci. Lett., 6, 1437-1456.
Magill, J. R., R. E. Well.s, Simpson, R. W., and Cox, A. V., 1982, Post 12 million rotation of southwest Washington: J. Geophys. Res., 87, 3761-3776.
McBirney, A. R., 1978, Volcanic evolution of the Cascade Range: Earth and Planetary Sciences Ann. Rev., 6, 437-456.
McClain, K., 1981 A geophysical study of accretionary processes on the Washington continental margin: Ph.D. thesis, University of Washington, Seattle, 141 pp.
Misch, P., Tectonic evolution of the northern Cascades of Washington State: Can. Inst. Min.

and Met., 8, 101-148.
Monger, J. W. H., 1988, Accretionary complexes: structures forming Cordilleran crust: (abs) Geol. Soc. Am. Annual Meeting, Program with Abstracts, p. A183.
Mooney, W. D., 1988, Seismic methods for determining earthquake source parameters and lithospheric structure: in press, Geol. Soc. Am. Memoir., W. D. Mooney and L. C. Pakiser, eds.
Morrison, J., and J. W. Valley, 1988, Post-granulite facies fluid infiltration in the Adirondack Mountains: Geology, 16, 513-516.
Muffler, L. J. P., 1987, Geothermal studies of the U.S. Geological Survey in the Cascade Range: Geoth. Res. Coun., Transactions, 11, 281-283.
Nilson, Tor H., 1984, Tectonics and sedimentation of the upper Cretaceous Hornbrook Formation, Oregon and California: in Tectonics and Sedimentation along the California Margin, Crouch, J. K. and Bachman, S. B., eds., Pacific Section, S.E.P.M., 38, 101-118.
Olhoeft, G. R., 1981, Electrical properties of granite with implications for the lower crust: J. Geophys. Res., 86, 931-936.
Pffifner, O. A., W. Frei, P. Finckh, and P. Valasek, 1988, Deep seismic reflection profiling in the Swiss Alps: Explosion seismology results for line NFP 20-EAST: Geology, v. 16, p. 987-990.
Potter, C. J., Sandford, W. E., Yoos, T. R., Prussen, E. L., Keach, W., Oliver, J. E., Kaufman, S., and Brown, L. D., 1986, COCORP deep seismic reflection travers of the interior of the North American cordillera, Washington and Idaho: Implications for orogenic evolution: Tectonics, 5, 1007-1025.
Priest, G. R., 1986, A program for scientific drilling in the Cascades, Northern California, Oregon, and Washington: Administrative Report, Dept. of Geology and Mineral Ind., Portland, Oregon, 15 p.
Riddihough, R., C. Finn, and R. Couch, Klamath-Blue Mountain lineament, Oregon: Geology, 14, 528-531.
Rinehart, E. J., A. R. Sanford, and R. M. Ward, 1979, Geographic extent and shape of an extensive magma body at midcrustal depths in the Rio Grande rift near Socorro, New Mexico: in Rio Grande Rift: Tectonics and Magmatism, edited by R. E. Riecker, pp. 237-252.
Sanford, A. R., Olsen, K. H., and L. H. Jaksha, 1979, Seismicity of the Rio Grande rift: in R. E. Riecker (Editor), Rio Grande Rift: Tectonics and Magmatism, American Geophysical Union. Washington, D.C., pp. 145-168.
Scandone, Jr., and Malone, S. D., 1985, Magma supply, magma discharge, and readjustment of the feeding system of Mount St. Helens during 1980: Jour. Volcanoes and Geothermal Resources, 22, 239-262.
Shemeta, J. E., and Weaver, C. S., 1986, Seismicity accompanying the May 18, 1980 eruption of Mount St. Helens, Washington: in Mount St. Helens: Five Years Later, edited by S. A. C. Keller, Eastern Washington University Press, Cheney, Washington, 44-58.
Sherrod, D. R., 1987, New compilation map of the Cascade Range in Oregon: Geothermal Res. Coun. Trans., 11, 305-307.
Simpson, R. W., and Cox, A., 1977, Paleomagnetic evidence for tectonic rotations of the Oregon Coast Range: Geology, 5, 585-589.
Smith, G. A., and Taylor, E. M., 1983, The central Oregon High Cascade graben: what?, where?, and when?: Transactions of the Geothermal Resource Council, 7, 275-279.
Smith, J. G., E. H. McKee, D. B. Tatlock, and R. F. Marvin, 1971, Mesozoic granitic rocks in northwestern Nevada-a link between the Sierra Nevada and Idaho batholiths: Geol. Soc. Am. Bull., 82, 2933-2944.
Snavely, P. D., Jr.,1988 Tertiary geologic framework, neotectonics, and petroleum potential of the Oregon-Washington continental margin: in Geology and Resource Potential of the Continental Margin of Western North American and Adjacent Ocean Basins-Beaufort Sea to Baja California, edited by D. S. Scholl, A. Grantz, and J. G. Vedder, Circum-Pacific Council for Energy and Mineral Resources Earth Science Series, 6, 305-335.

Stanley, W. D., 1982, Magnetotelluric soundings on the Idaho National Engineering Laboratory facility, Idaho: Jour. Geophys. Res., 87, no. B4, 2683-2691.
Stanley, W. D., 1982b, A regional magnetotelluric survey of the Cascade Mountains regions: U.S. Geol. Surv. Open File Rept., 82-126, 198 p.
Stanley, W. D., 1983, Regional electrical structures in the Cascades and their significance in geothermal and volcano hazards assessment: EOS Trans., AGU, 64, 887.
Stanley, W. D., 1984, Tectonic study of the Cascade Range and Columbia Plateau in Washington based upon magnetotelluric soundings: J. Geophys. Res., 89, 4447-4460.
Stanley, W. D., Finn, C., and Plesha, J. L., 1987, Tectonics and conductivity structures in the southern Washington Cascades: J. Geophys. Res., 92, 10179-10193.
Stanley, W. D., 1988, Comparison of geoelectrical/tectonic models from Mesozoic orogenic regions of the United States and Europe: are black shales a source of conductivity anomalies: in press, Physics of the Earth and Planetary Interiors, Elsevier, Amsterdam.
Stanley, W. D., V. F. Labson, Bela Csejtey, Jr., W. J. Nokleberg, and C. L. Long, 1988b, Evidence for accretion and thin-skinned tectonics in the Alaska Range, Alaska: (abs) Program and Abstracts, Annual Meeting, Geological Society of America, Denver, Colo.
Sternberg, B. K., J. C. Washburne, and L. Pellerin, 1988, Correction for the static shift in magnetotellurics using transient electromagnetic soundings: Geophysics, v. 53, p. 1459-1468.
Taber, J. J., 1983, Crust and upper mantle structure of the Olympic Peninsula: Ph.D. Thesis, University of Washington, Seattle, 159 pp.
Taber, J. J. and Lewis, B. T. R., 1986, Crustal structure of the Washington continental margin from refraction data: Bull. Seism. Soc. Amer., 83, p. 1805-1816.
Thiruvathukal, J. V., Berg, J. R., and D. F. Heinrichs, 1970, Regional gravity of Oregon: Geol. Soc. Am. Bull., 81, 725-738.
Wannamaker, P. E., 1986, Electrical conductivity of water-undersaturated crustal melting: Jour. Geophys. Res., 91, 6321-6328.
Wannamaker, P. G., J. R. Booker, A. G. Jones, A. D. Chave, J. H. Filloux, H. S. Waff, and L. K. Law, 1989, Conductivity cross-section through the Juan de Fuca subduction system and its tectonic implications: this volume
Weaver, C. S., and Smith, S. W., 1983, Regional tectonic and earthquake hazard implications of a crustal fault zone in southwestern Washington: J. Geophys. Res., 88, 10371-10383.
Weaver, C. S., and Baker, G. E., 1988, Geometry of the Juan de Fuca plate beneath Washington and northern Oregon from seismicity: Bull. Seism. Soc. Amer., 78, 264-275.
Wells, R. E., D. C. Engebretson, P. D. Snavely, Jr., and R. S. Coe, 1984, Cenozoic plate motions and the volcano-tectonic evolution of western Oregon and Washington: Tectonics, 3, no. 2, 275-294.
Williams, D. L., Hull, D. A., Ackermann, H. D., and Beeson, M. H., 1982, The Mt. Hood region: volcanic history, structure, and geothermal energy potential: J. Geophys. Res., 87, 2767-2781.
Williams, D. L., and C. A. Finn, 1985, Analysis of gravity data in volcanic terranes and gravity anomalies and sub-volcanic intrusions in the Cascade Range, USA and at other selected volcanoes: in Utility of Gravity and Magnetic Maps, ed. W. Hinze, Soc. Expl. Geophys., p. 361-374.
Zablocki, C. J., 1964, Electrical properties of serpentinite from Mayaguez, Puerto Rico: in C. A. Burk (editor), A Study of Serpentinite-The AMSOC Core Hole near Mayaguez, Puerto Rico, NAS-NRC, pub. 1188, p. 107-117.
Zucca, J. J., Fuis, G. S., Milkeriet, B., Mooney, W. D., and Catchings, R., 1986, Crustal structure of northern California from seismic refraction data: J. Geophys. Res., 91, 7359-7382.

FIGURE CAPTIONS

Figure 1-Geological index map of Cascades Range and surrounding region showing location of MT (long-short dashed) and seismic (diagonal dashed) profiles. Geological base modified from Wells and others (1986). EM=EMSLAB MT profile; VI=Vancouver Island, BK=Mount Baker, GL=Glacier Peak, S=Seattle, PB=Puget Basin, GH=Grays Harbor Basin, Sp=Spokane, RN=Mount Rainier, SH=Mount St. Helens, AD=Mount Adams, WB=Willamette Basin, HD=Mount Hood, JF=Mount Jefferson, NB=Newberry volcano, TY=Tyee Basin, CL=Crater Lake, MD=Modoc Plateau, ML=Medicine Lake volcano, SA=Mount Shasta, HN=Hornbrook Formation, HLP=High Lava Plains.

Figure 2-Paleogene tectonic reconstruction modified from Heller and others (1987). SCF=Straight Creek Fault, ID=Idaho Batholith, KM=Klamath Mountains, GH=Grays Harbor Basin, WB=Willamette Basin, PL=Puget Lowland basin, BM=Blue Mountains, FA=Farallon Plate, NA=North American Plate, KU=Kula Plate, HN=Hornbrook Formation, MC=MacIntosh-Raging River marine Eocene Formations, SWCC=southern Washington Cascades conductor. Major extension vectors are indicated by bold arrows. Contours represent successive volcanic fronts.

Figure 3-(a)Layered MT model for profile DD' (fig. 1). Triangles are MT sounding locations. (b)Two-dimensional model for profile DD' which was constructed to fit low frequency part of MT data sensitive to deep crustal conductor.

Figure 4-Interpretation of seismic refraction profile between Mt. Hood and Crater Lake in the Oregon Cascades (fig. 1). Numbers in the model are interpreted velocities in kilometers/second (km/s). The position of the top of the MT deep crustal conductor is indicated by the dot pattern. In the lower part of the figure the seismic refraction model is plotted along with a generic MT model which is the basis for starting models for most of the Oregon and California Cascades region. It should be noted that the layers are not constant velocity, but represent linear gradients within each layer.

Figure 5-Index for central and northern Oregon Cascades showing the location of MT profile BB", DD', BR1, and BR2, DOE-Chevron drill hole (4000 feet TD), SUNEDCO drill hole (9500 feet TD), and several hot springs.

Figure 6-MT models for Breitenbush Hot Springs profiles BR1 and BR2.

Figure 7-Oregon index map modified from MacLeod and others (1988). Location of Oregon MT (diagonal dashed) and seismic (bold dashed) profiles are shown, along with the location of the Klamath Blue-Mountain lineament of Riddihough and others (1984). The isochrons for a propagating volcanic front that migrated from the Basin and Range northwestward to the area of Newberry volcano is reproduced from MacLeod and others (1988).

Figure 8-(a) seismic refraction model for Newberry-Brother fault zone profile; (b) MT layered model for profile EE' (c) MT layered model for profile FF' (fig. 7).

Figure 9-Detailed MT and TDEM layered models of Newberry, surface of seismic model 5.6 km/s layer (bold dashed line), and gravity data (lower figure) from Williams and Finn (1984). Numbers in electrical model are resistivities in ohm-m, dashed line is top of MT layer no. 2 (conductor), and solid line in approximately the same depth range is TDEM determined top of conductive layer. Numbers directly below these two lines are resistivities of upper part of the conductive layer determined from the TDEM inversions and numbers just above the line represent the MT electrical basement surface are resistivities of the conductive, second layer from the MT inversions.

Figure 10-Geological index map for northern California MT and seismic profiles GG' (fig. 1) reproduced from Fuis and others (1987). Numbers correspond to shotpoint locations and triangles are location of MT soundings.

Figure 11-(A) Layered model for MT profile GG' (fig. 10); numbers in model are resistivities in ohm-m (B) Observed (solid) and calculated (dashed) gravity data reproduced from Fuis and others (1987) based upon density blocks added to refraction model and assignment of densities to seismic velocity units (C) seismic refraction model from Zucca and others (1986); numbers in model are velocities in km/s; cross-hatched regions are low-velocity section interpreted from seismic data; layer boundaries dashed where uncertain; dot pattern for Modoc Plateau section represent approximate position of deep crustal conductor from MT model (D) geologic interpretation of combined MT and seismic data.

Figure 12-Index map of Washington showing location of MT profiles AA' and CC', as well as the seismic profile of Catchings and Mooney (1988). Other details include earthquake epicenters supplied by C. S. Weaver, conductance contours and magnetic anomalies from Stanley and others, (1987).

Figure 13- (A) MT model for profile AA' (fig. 12) modified from Stanley and others (1987) including more recent data in the Chehalis Basin and the refraction model for the Pasco Basin portion of the refraction model from Catchings and Mooney (1988) across the Columbia Plateau. (B) Interpretive geological cross-section for profile AA' transect, but including a composite with the western end of the profile CC' model (fig. 14). SHZ=St. Helens seismic zone defined by Weaver and Smith (1983).

Figure 14-Two-dimensional interpretation of MT profile CC' reproduced from Stanley and others (1987).

Figure 15-Schematic of MT models for (A) Lithoprobe experiment (modified from Clowes (1987) (B) western Washington from this paper and Stanley and others (1987) (C) EMSLAB experiment modified from EMSLAB Group (1988) (D) Klamath Mountains MT model from this paper

Figure 16-Cartoon illustrating a crustal framework for the deep crustal conductor involving dehydration of amphibolite grade metamorphic rocks and a localized zone of horizontal hydrofracturing or disaggregation. Earthquakes in the brittle part of the crust are indicated by the symbols in the upper 12 km. Velocities from the northern California seismic model (figure 11) are indicated along the left portion of the figure and proposed lithology along the right margin. The metamorphic-temperature profiles assumed are indicated in figure 17.

Figure 17-Approximate location of metamorphic mineral facies based upon experimental data for different temperature-depth profiles reproduced from Fyfe and others (1978). The temperature profile assumed in our figure 16 is shown by the heavy dashed line.

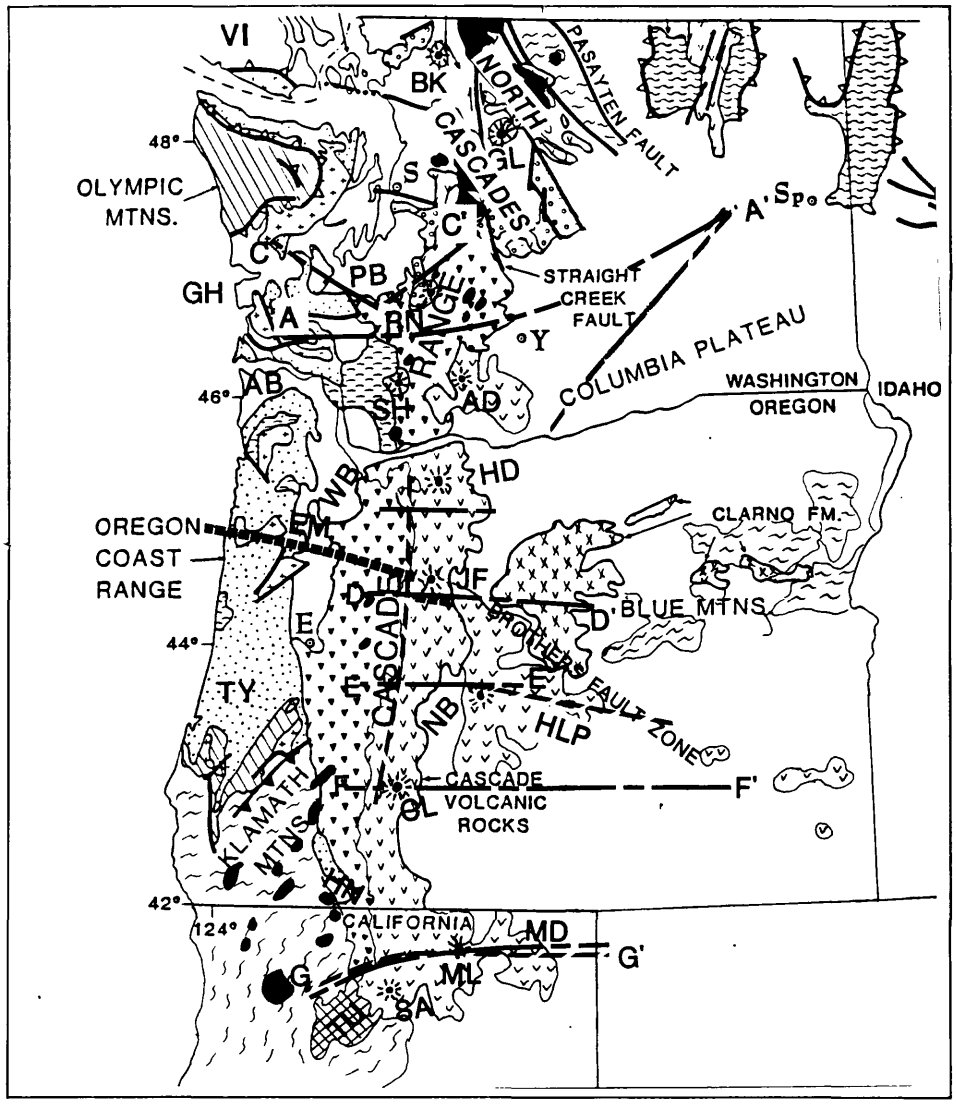

continental sedimentary rocks

post-accretion forearc sedimentary rocks

Quaternary volcanics High Cascades

Oligocene-Miocene volcanic rocks (Western Cascades)

John Day-Clarno Fm.

Tertiary subduction complex

forearc volcanic rocks

Coast Range seamounts (Siletzia)

Pre-Tertiary rocks

Trinity ultramafics

intrusive body

volcano

Figure 1-Geological index map of Cascades Range and surrounding region showing location of MT (long-short dashed) and seismic (diagonal dashed) profiles. Geological base modified from Wells and others (1986). EM=EMSLAB MT profile; VI=Vancouver Island, BK=Mount Baker, GL=Glacier Peak, S=Seattle, PB=Puget Basin, GH=Grays Harbor Basin, Sp=Spokane, RN=Mount Rainier, SH=Mount St. Helens, AD=Mount Adams, WB=Willamette Basin, HD=Mount Hood, JF=Mount Jefferson, NB=Newberry volcano, TY=Tyee Basin, CL=Crater Lake, MD=Modoc Plateau, ML=Medicine Lake volcano, SA=Mount Shasta, HN=Hornbrook

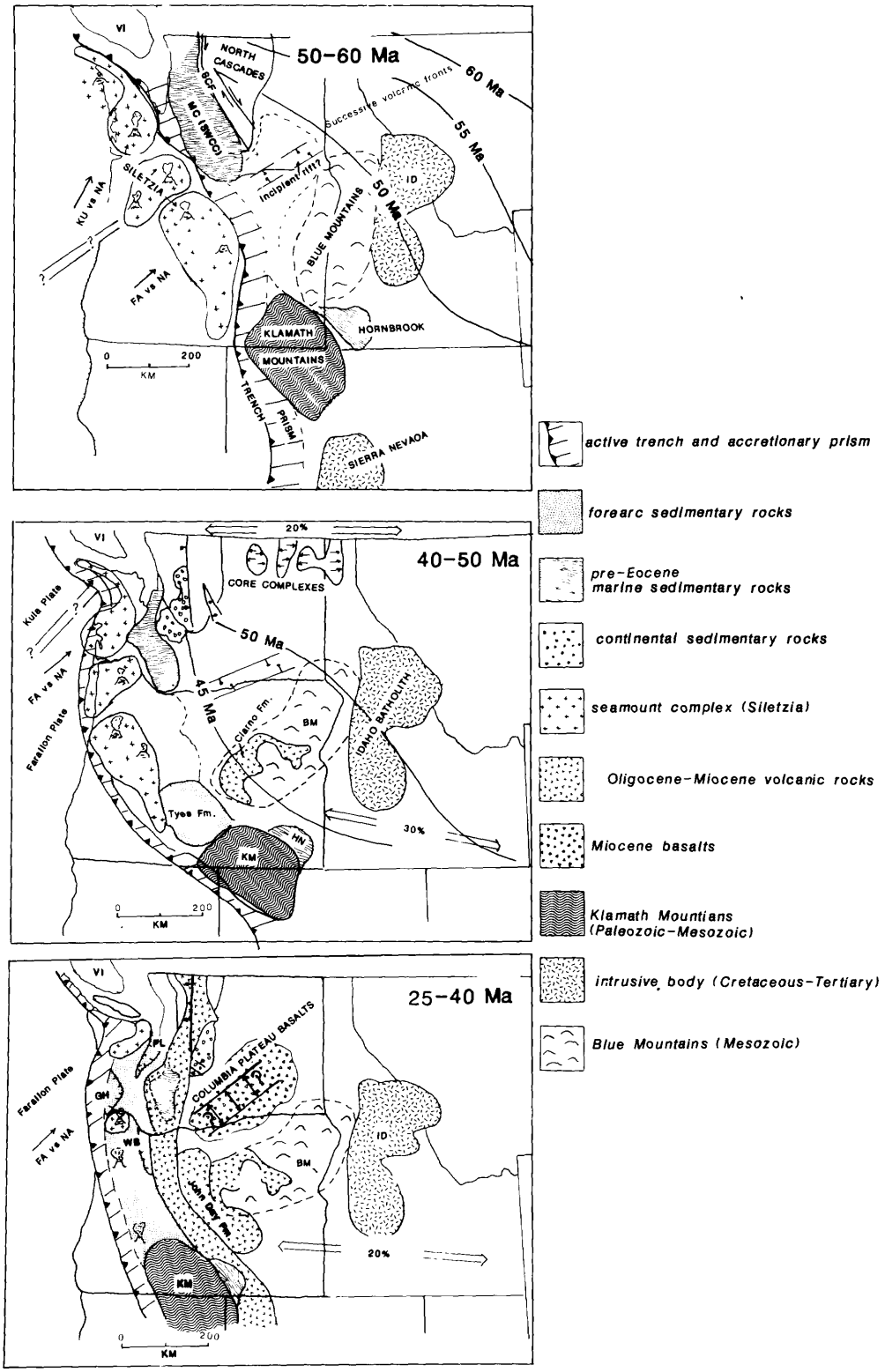

Figure 2-Paleogene tectonic reconstruction modified from Heller and others (1987). SCF=Straight Creek Fault, ID=Idaho Batholith, KM=Klamath Mountains, GH=Grays Harbor Basin, WB=Willamette Basin, PL=Puget Lowland basin, BM=Blue Mountains, FA=Farallon Plate, NA=North American Plate, KU=Kula Plate, HN=Hornbrook Formation, MC=MacIntosh-Raging River marine Eocene Formations, SWCC=southern Washington Cascades conductor. Major extension vectors are indicated by bold arrows. Contours represent successive volcanic fronts.

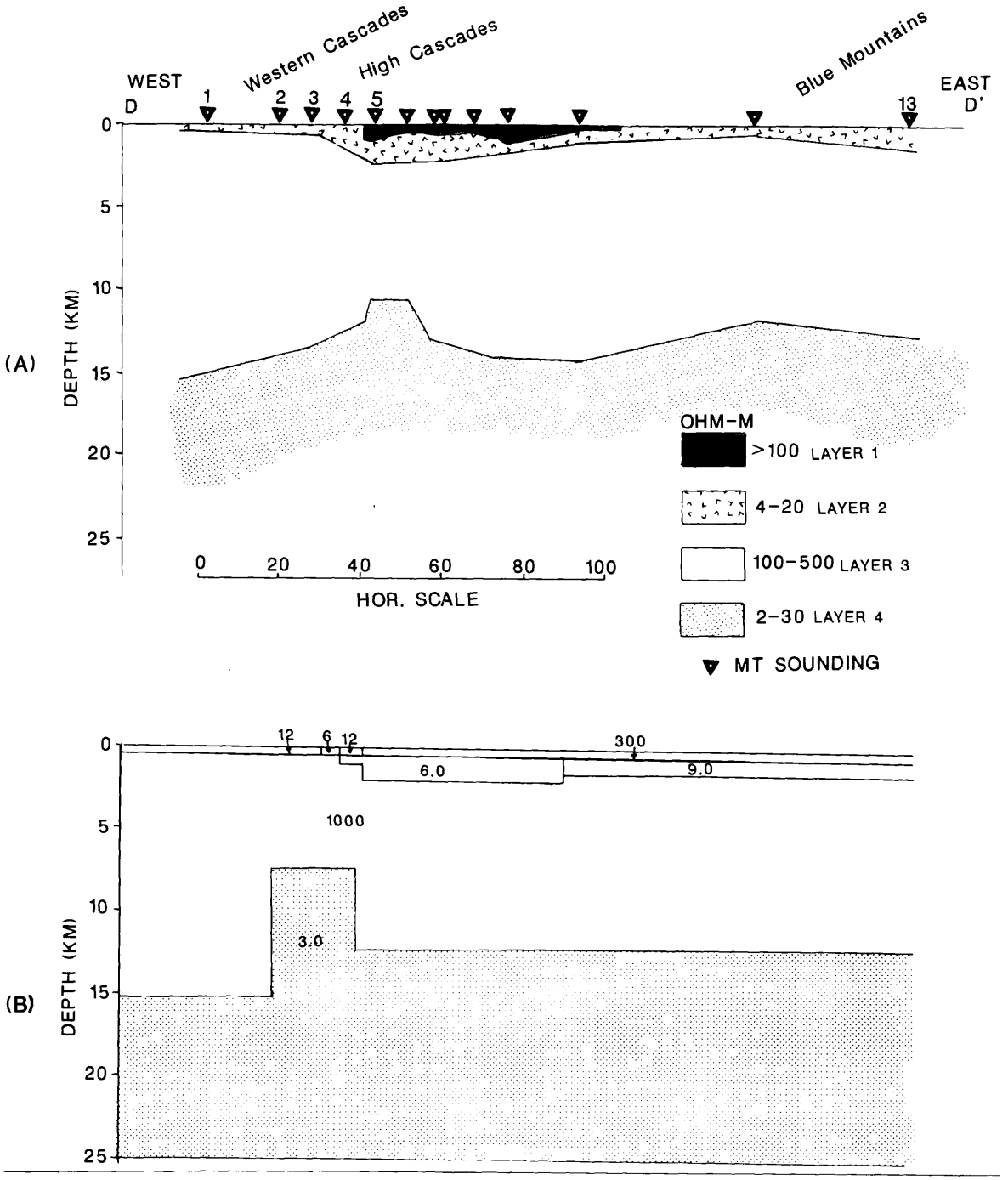

Figure 3-(a)Layered MT model for profile DD' (fig. 1). Triangles are MT sounding locations. (b)Two-dimensional model for profile DD' which was constructed to fit low frequency part of MT data sensitive to deep crustal conductor.

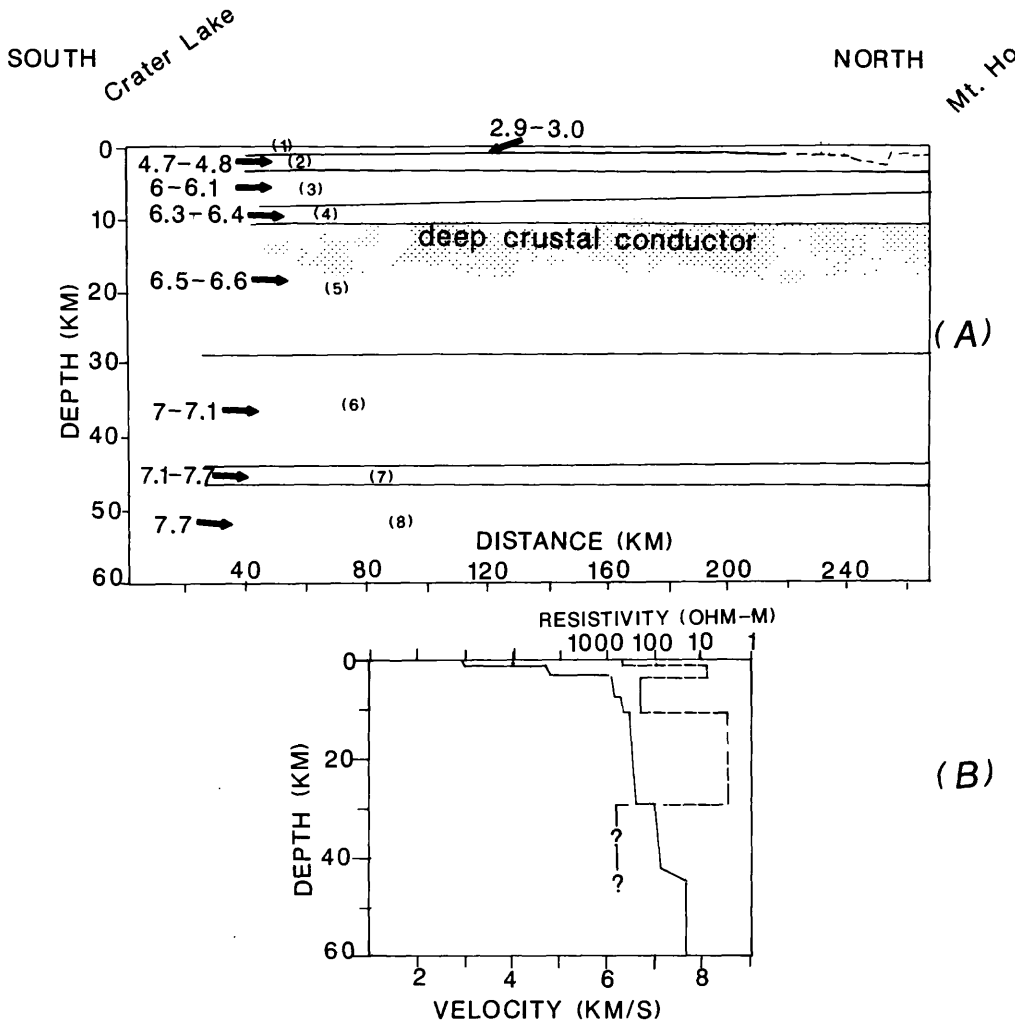

Figure 4-Interpretation of seismic refraction profile between Mt. Hood and Crater Lake in the Oregon Cascades (fig. 1). Numbers in the model are interpreted velocities in kilometers/second (km/s). The position of the top of the MT deep crustal conductor is indicated by the dot pattern. In the lower part of the figure the seismic refraction model is plotted along with a generic MT model which is the basis for starting models for most of the Oregon and California Cascades region. It should be noted that the layers are not constant velocity, but represent linear gradients within each layer.

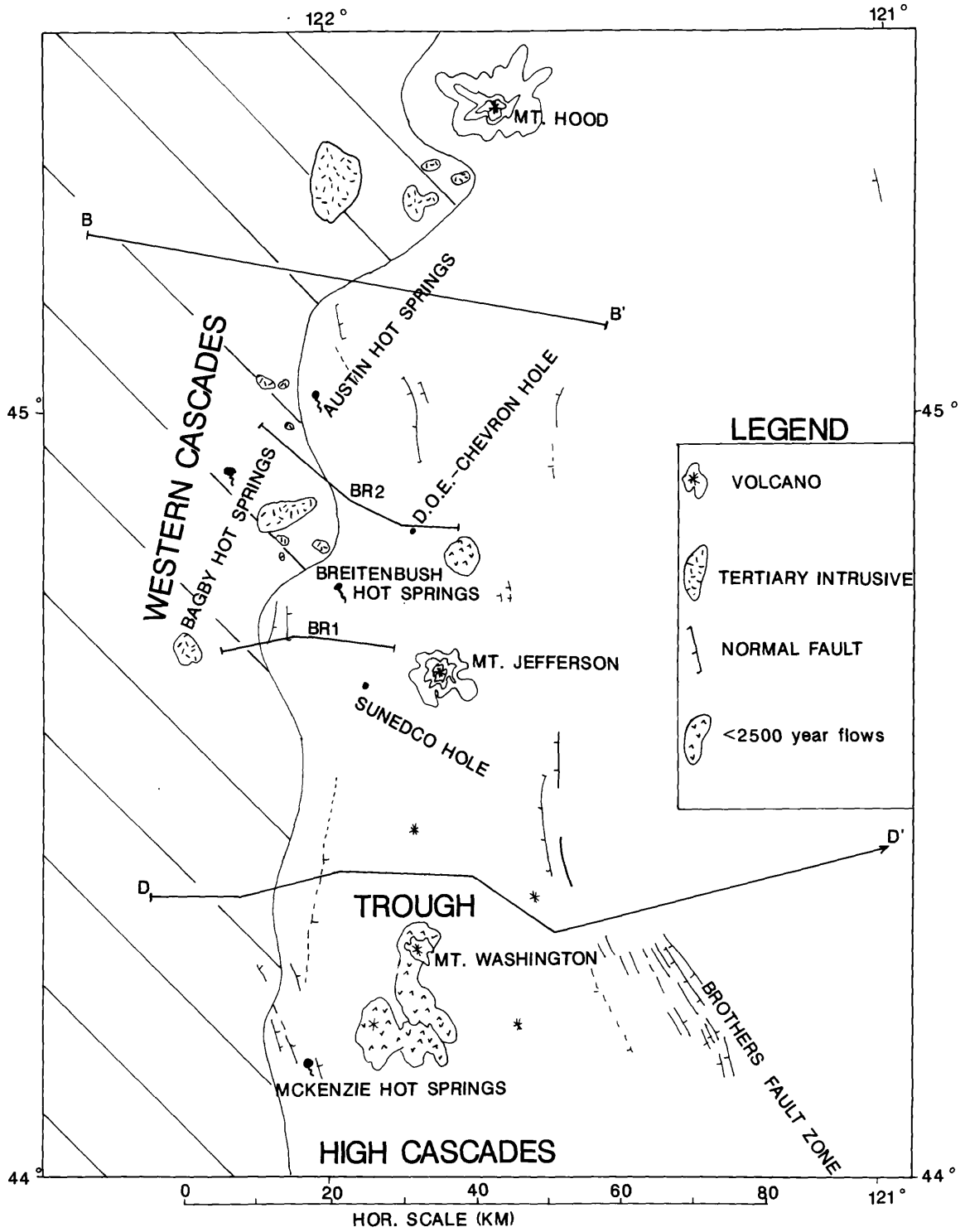

Figure 5-Index for central and northern Oregon Cascades showing the location of MT profile BB", DD', BR1, and BR2, DOE-Chevron drill hole (4000 feet TD), SUNEDCO drill hole (9500 feet TD), and several hot springs.

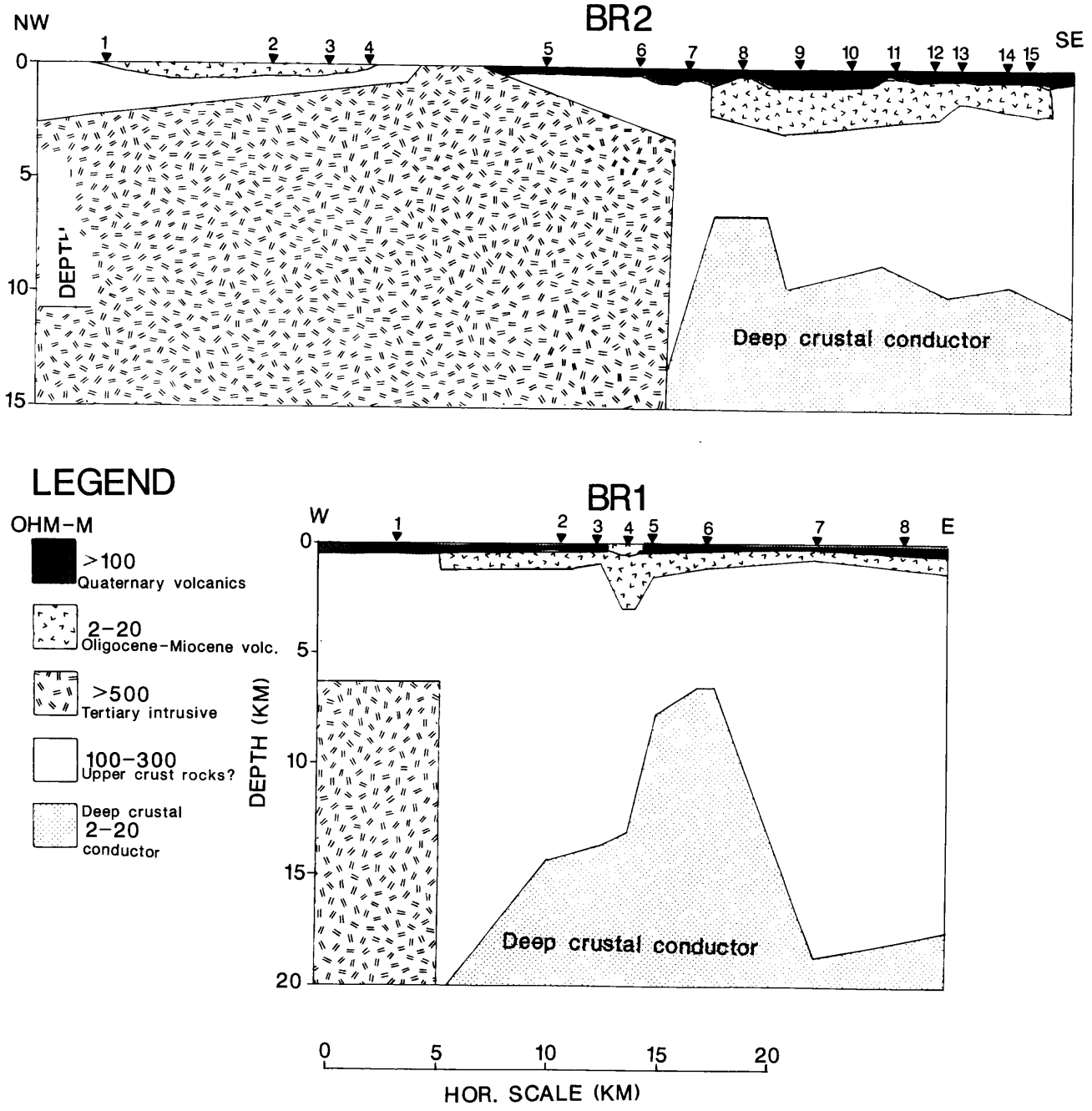

Figure 6-MT models for Breitenbush Hot Springs profiles BR1 and BR2.

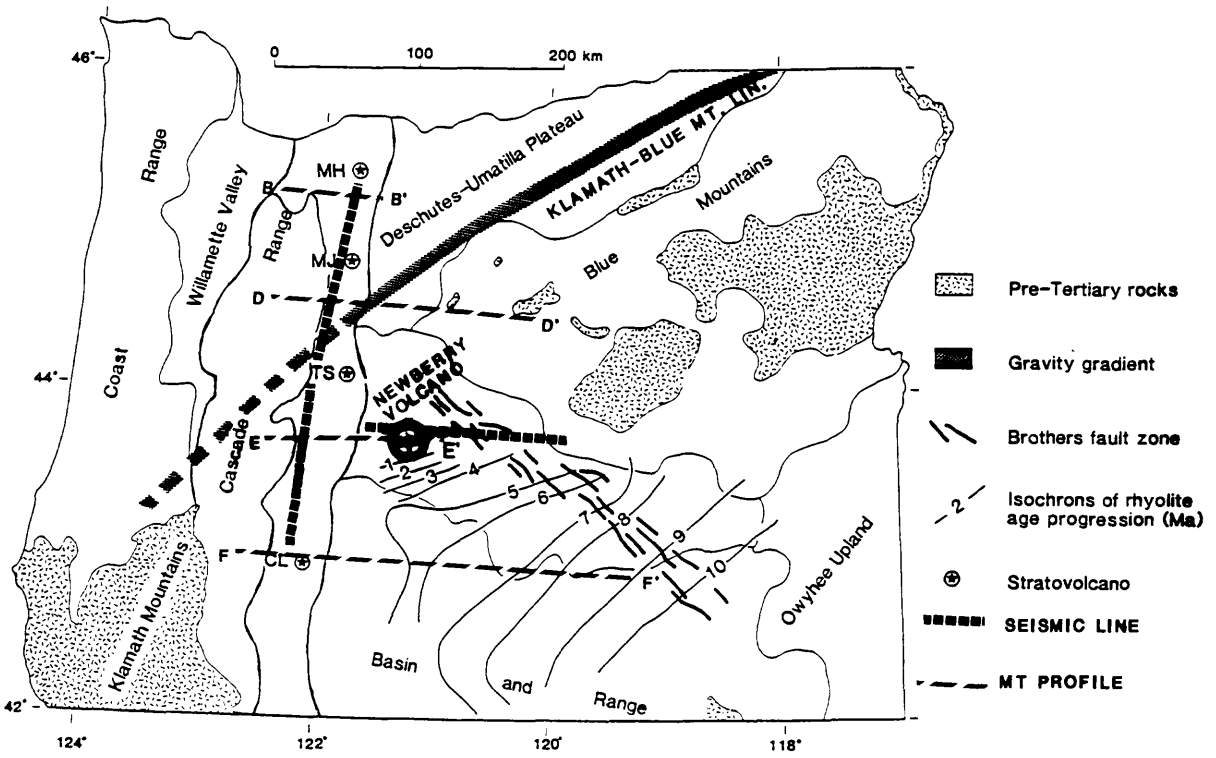

Figure 7-Oregon index map modified from MacLeod and others (1988). Location of Oregon MT (diagonal dashed) and seismic (bold dashed) profiles are shown, along with the location of the Klamath Blue-Mountain lineament of Riddihough and others (1984). The isochrons for a propagating volcanic front that migrated from the Basin and Range northwestward to the area of Newberry volcano is reproduced from MacLeod and others (1988).

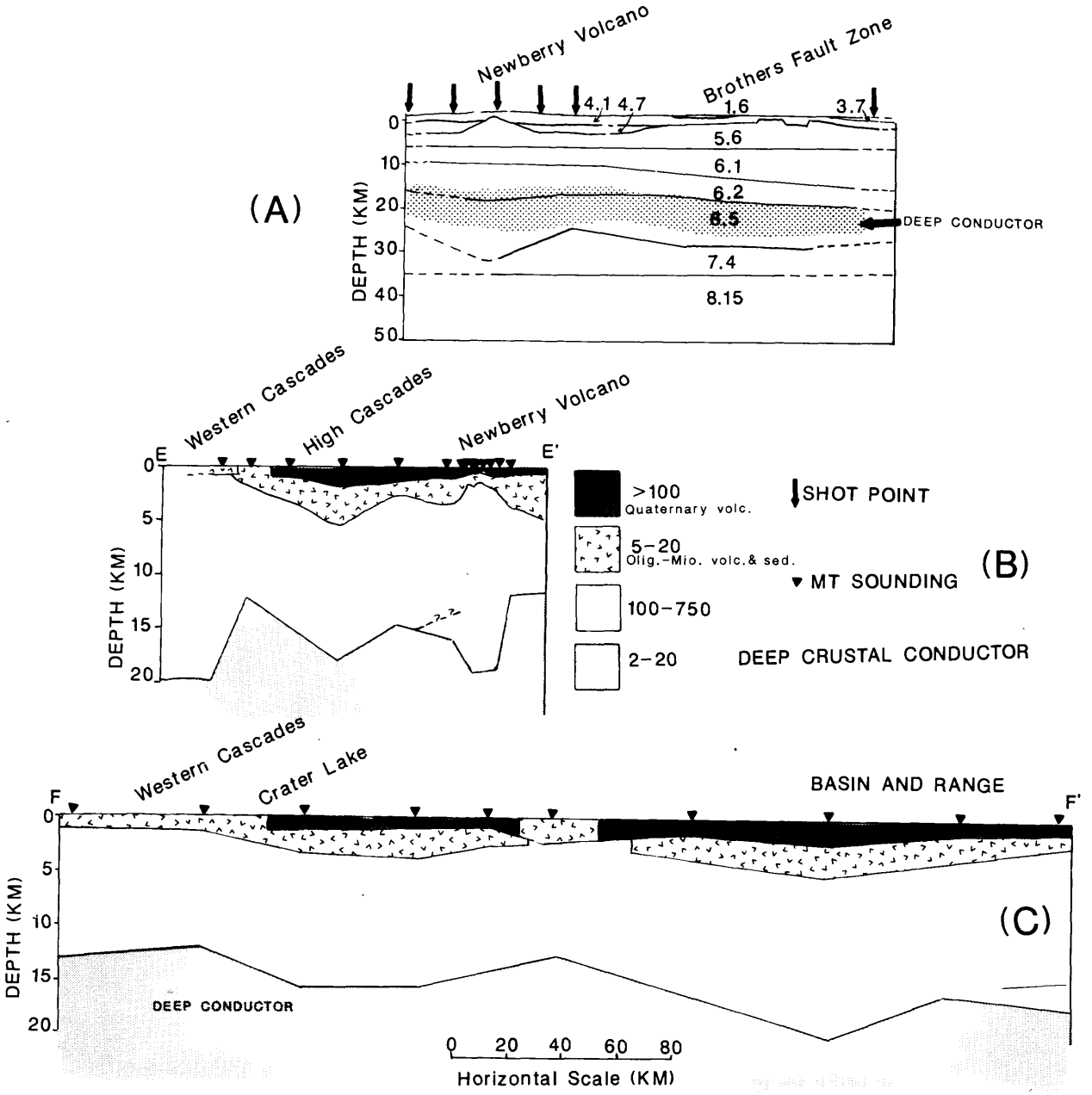

Figure 8-(a) seismic refraction model for Newberry-Brother fault zone profile; (b) MT layered model for profile EE' (c) MT layered model for profile FF' (fig. 7).

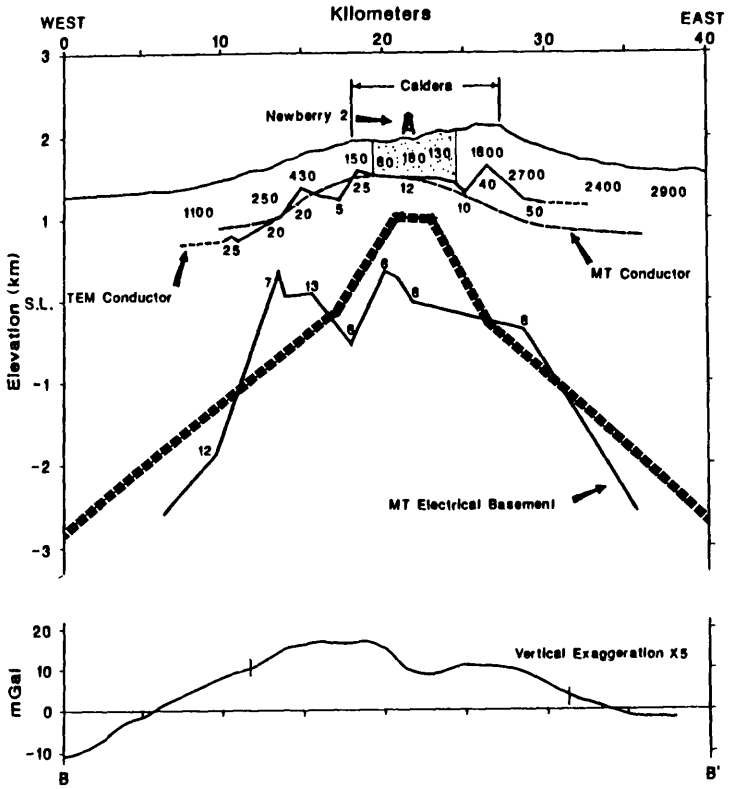

Figure 9-Detailed MT and TDEM layered models of Newberry, surface of seismic model 5.6 km/s layer (bold dashed line), and gravity data (lower figure) from Williams and Finn (1984). Numbers in electrical model are resistivities in ohm-m, dashed line is top of MT layer no. 2 (conductor), and solid line in approximately the same depth range is TDEM determined top of conductive layer. Numbers directly below these two lines are resistivities of upper part of the conductive layer determined from the TDEM inversions and numbers just above the line represent the MT electrical basement surface are resistivities of the conductive, second layer from the MT inversions.

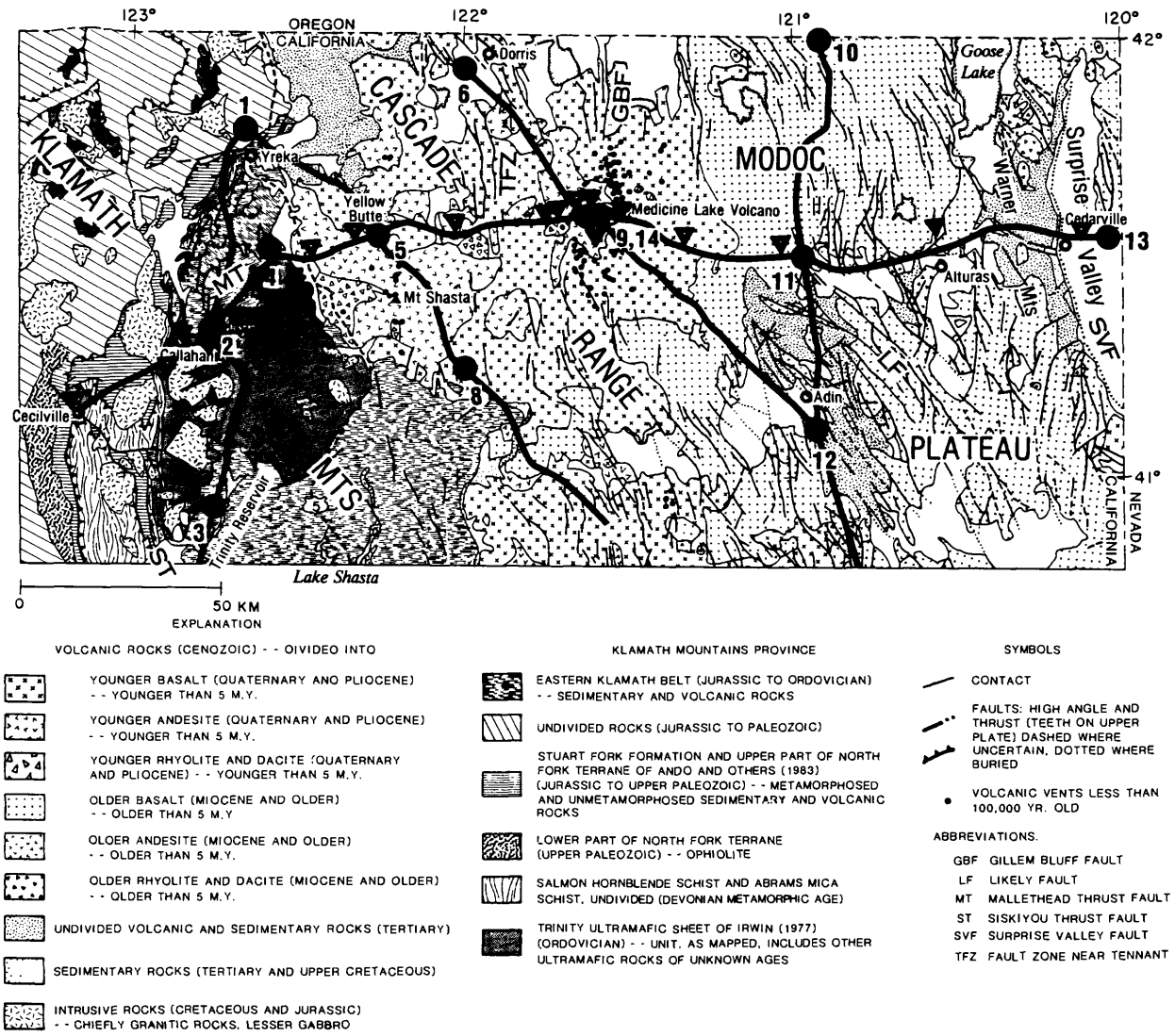

Figure 10-Geological index map for northern California MT and seismic profiles GG' (fig. 1) reproduced from Fuis and others (1987). Numbers correspond to shotpoint locations and triangles are location of MT soundings.

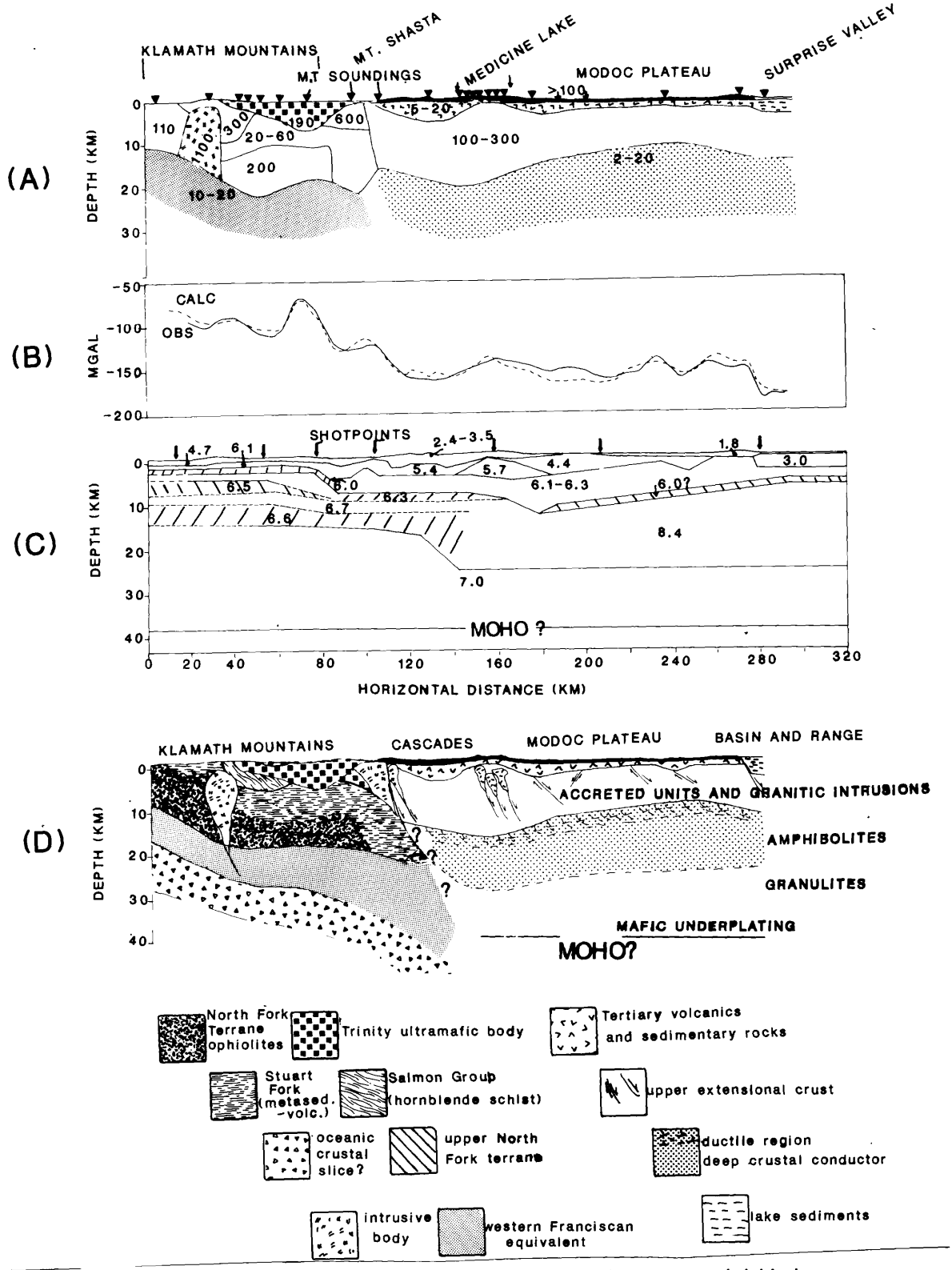

Figure 11-(A) Layered model for MT profile GG' (fig. 10); numbers in model are resistivities in ohm-m (B) Observed (solid) and calculated (dashed) gravity data reproduced from Fuis and others (1987) based upon density blocks added to refraction model and assignment of densities to seismic velocity units (C) seismic refraction model from Zucca and others (1986); numbers in model are velocities in km/s; cross-hatched regions are low-velocity section interpreted from seismic data; layer boundaries dashed where uncertain.

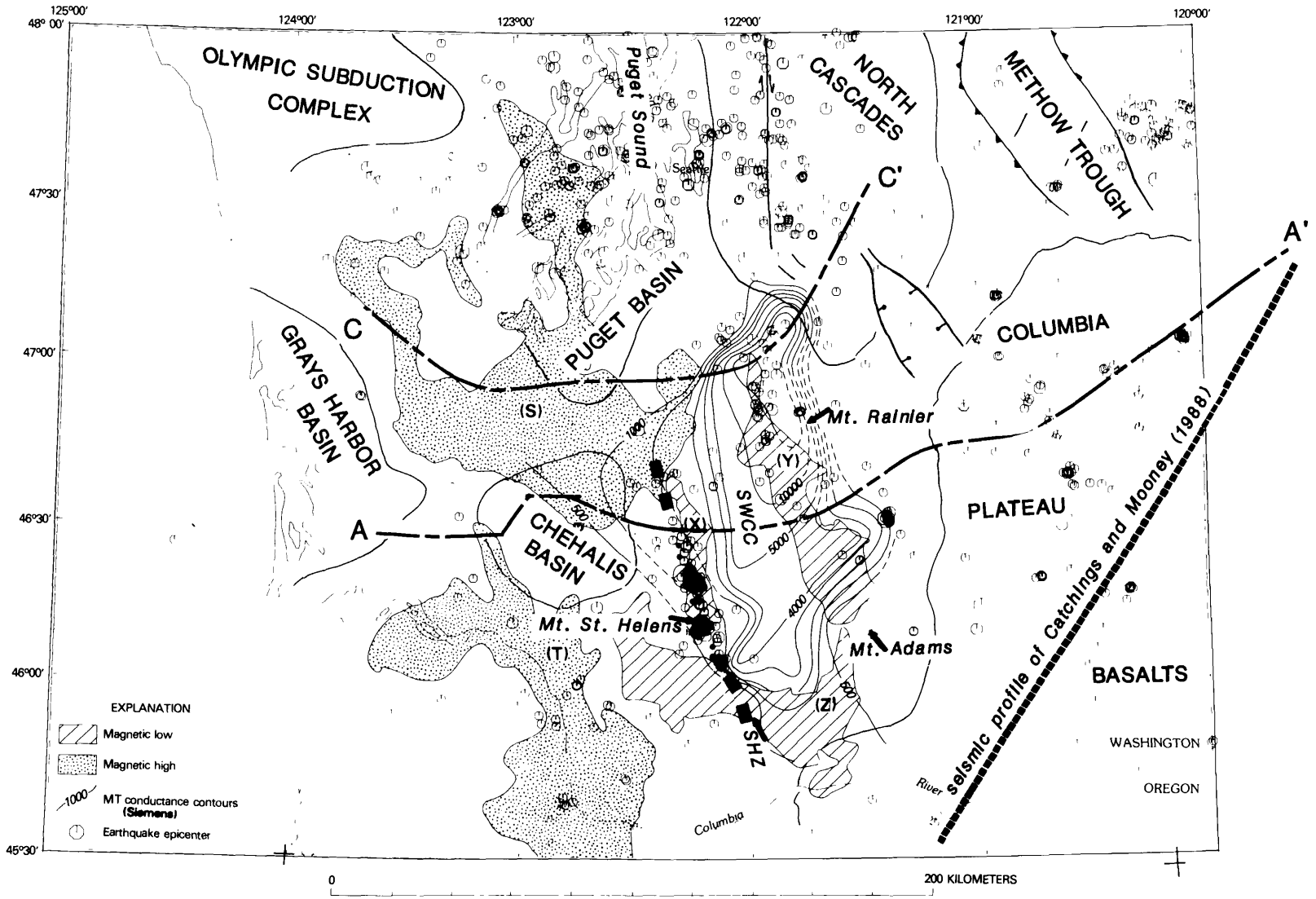

Figure 12-Index map of Washington showing location of MT profiles AA' and CC', as well as the seismic profile of Catchings and Mooney (1988). Other details include earthquake epicenters supplied by C. S. Weaver, conductance contours and magnetic anomalies from Stanley and others, (1987).

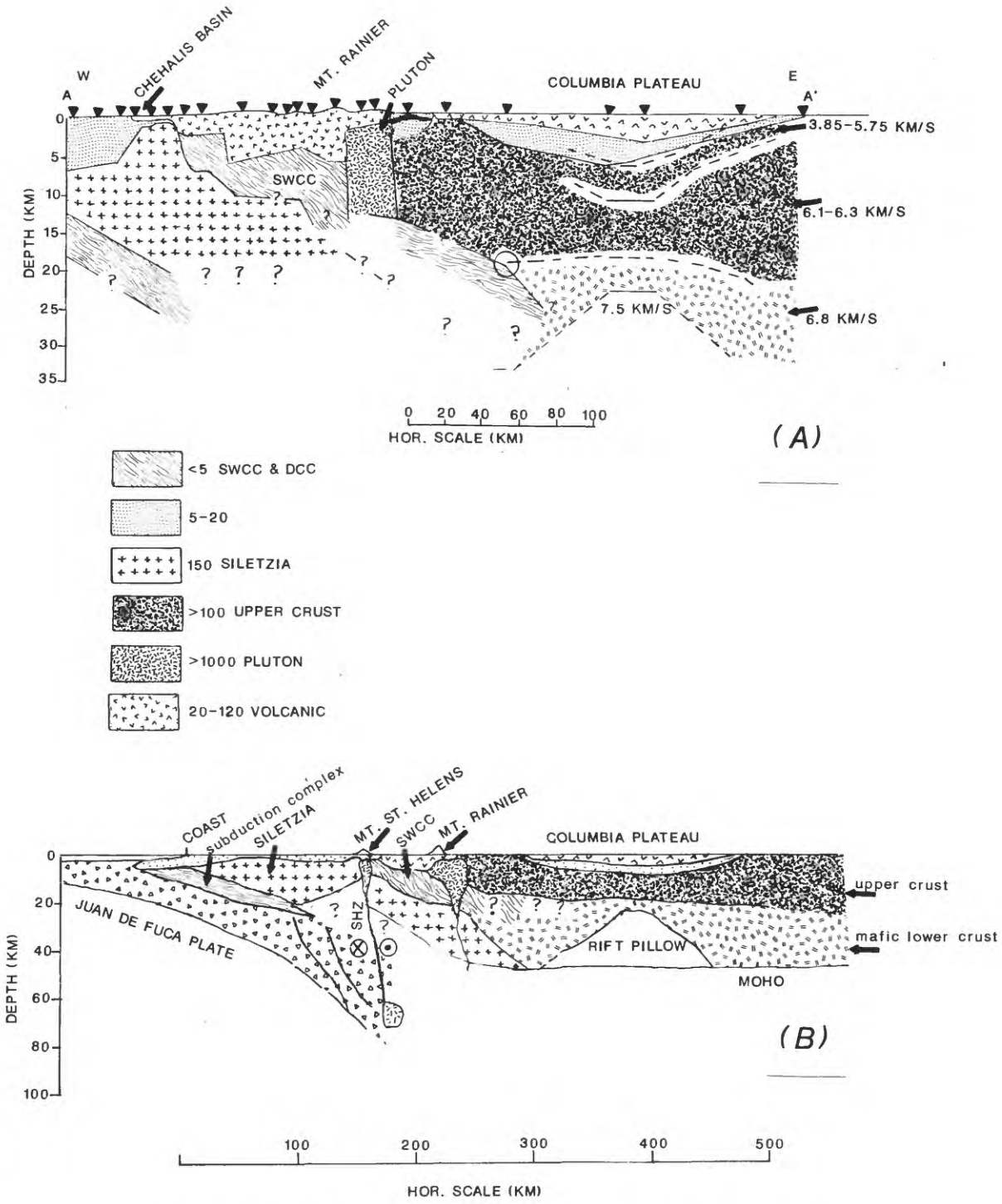

Figure 13- (A) MT model for profile AA' (fig. 12) modified from Stanley and others (1987) including more recent data in the Chehalis Basin and the refraction model for the Pasco Basin portion of the refraction model from Catchings and Mooney (1988) across the Columbia Plateau. (B) Interpretive geological cross-section for profile AA' transect, but including a composite with the western end of the profile CC' model (fig. 14). SHZ=St. Helens seismic zone defined by Weaver and Smith (1983).

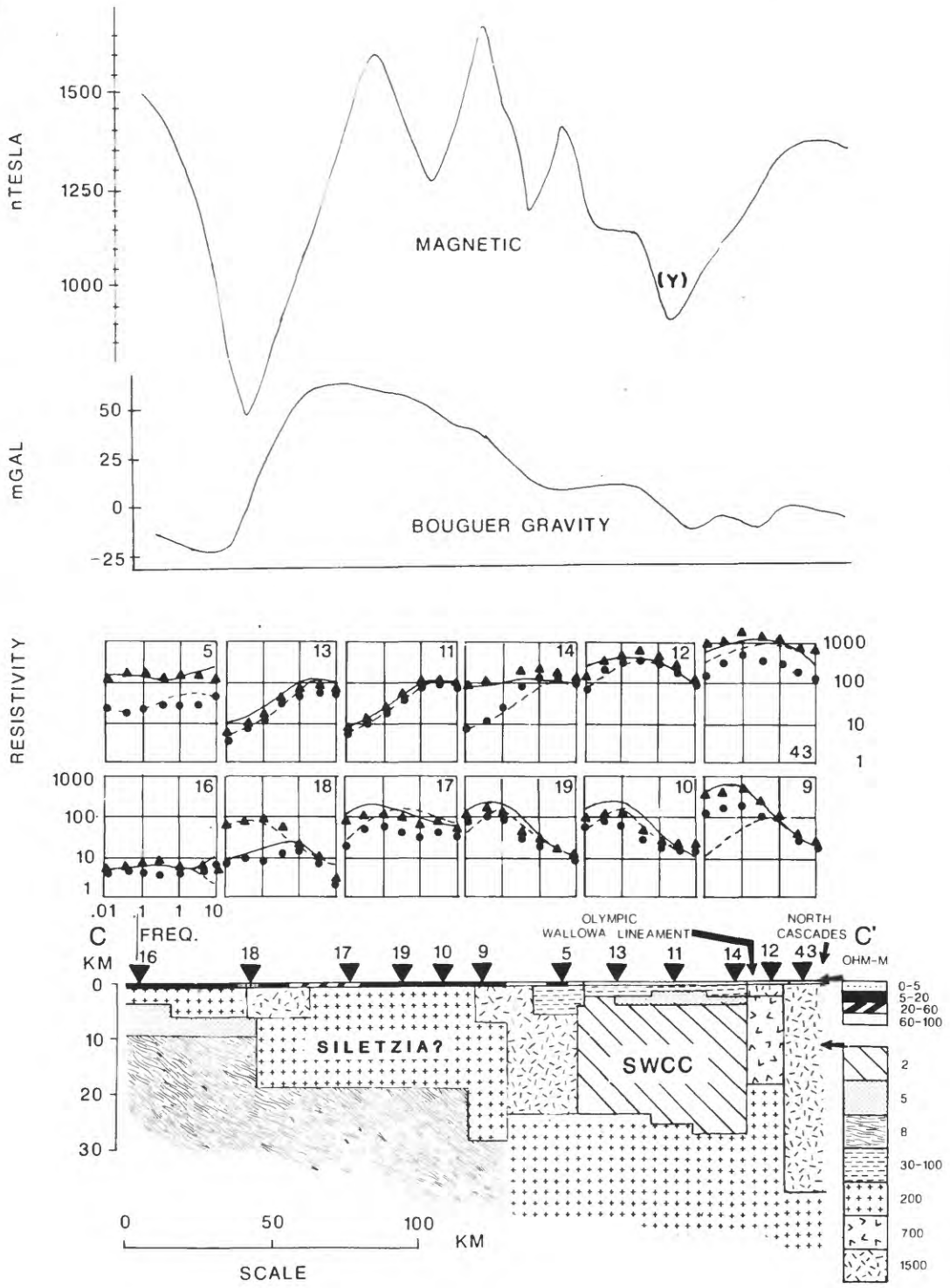

Figure 14-Two-dimensional interpretation of MT profile CC' reproduced from Stanley and others (1987).

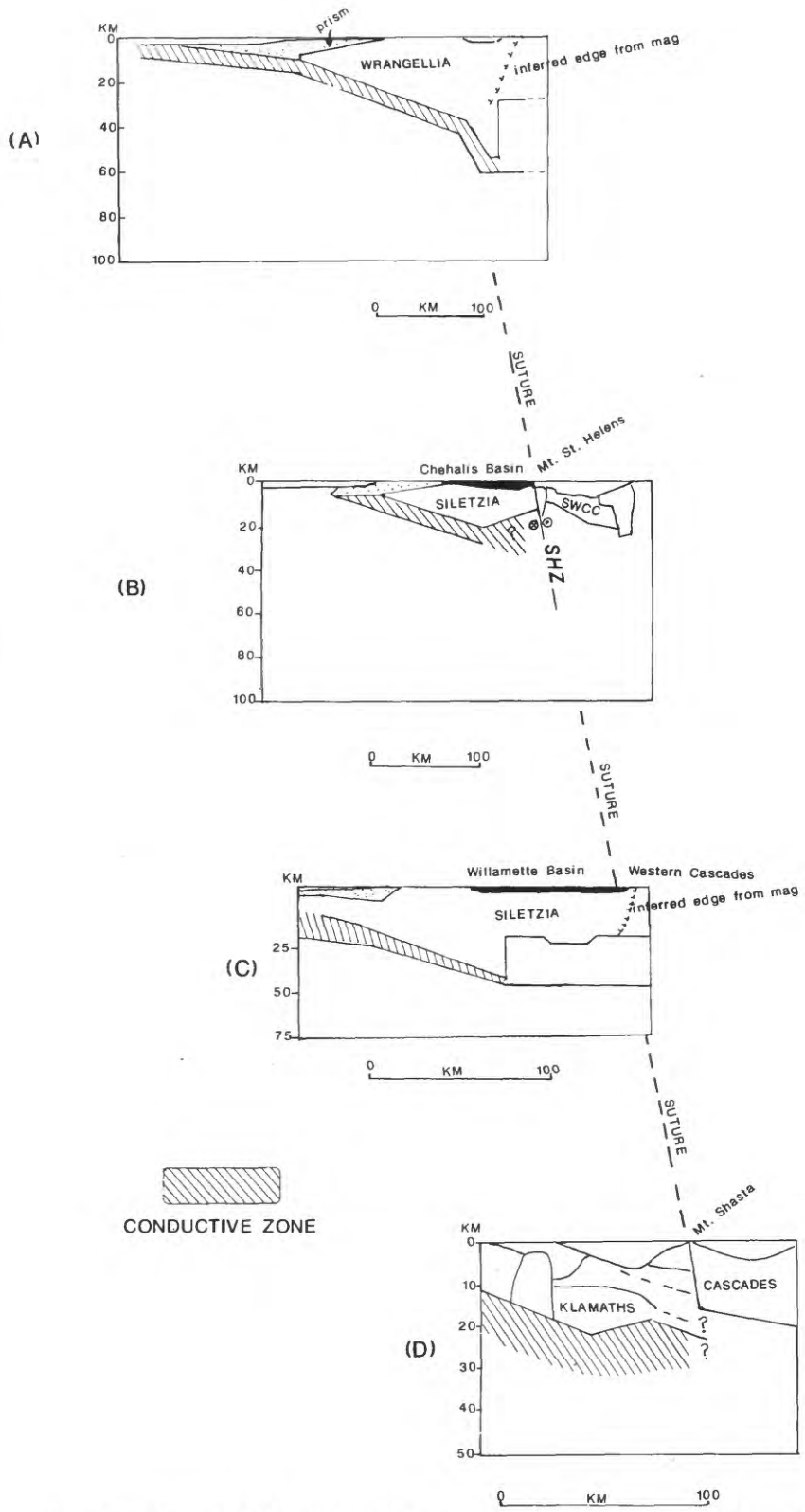

Figure 15-Schematic of MT models for (A) Lithoprobe experiment (modified from Clowes (1987) (B) western Washington from this paper and Stanley and others (1987) (C) EMSLAB experiment modified from EMSLAB Group (1988) (D) Klamath Mountains MT model from this paper

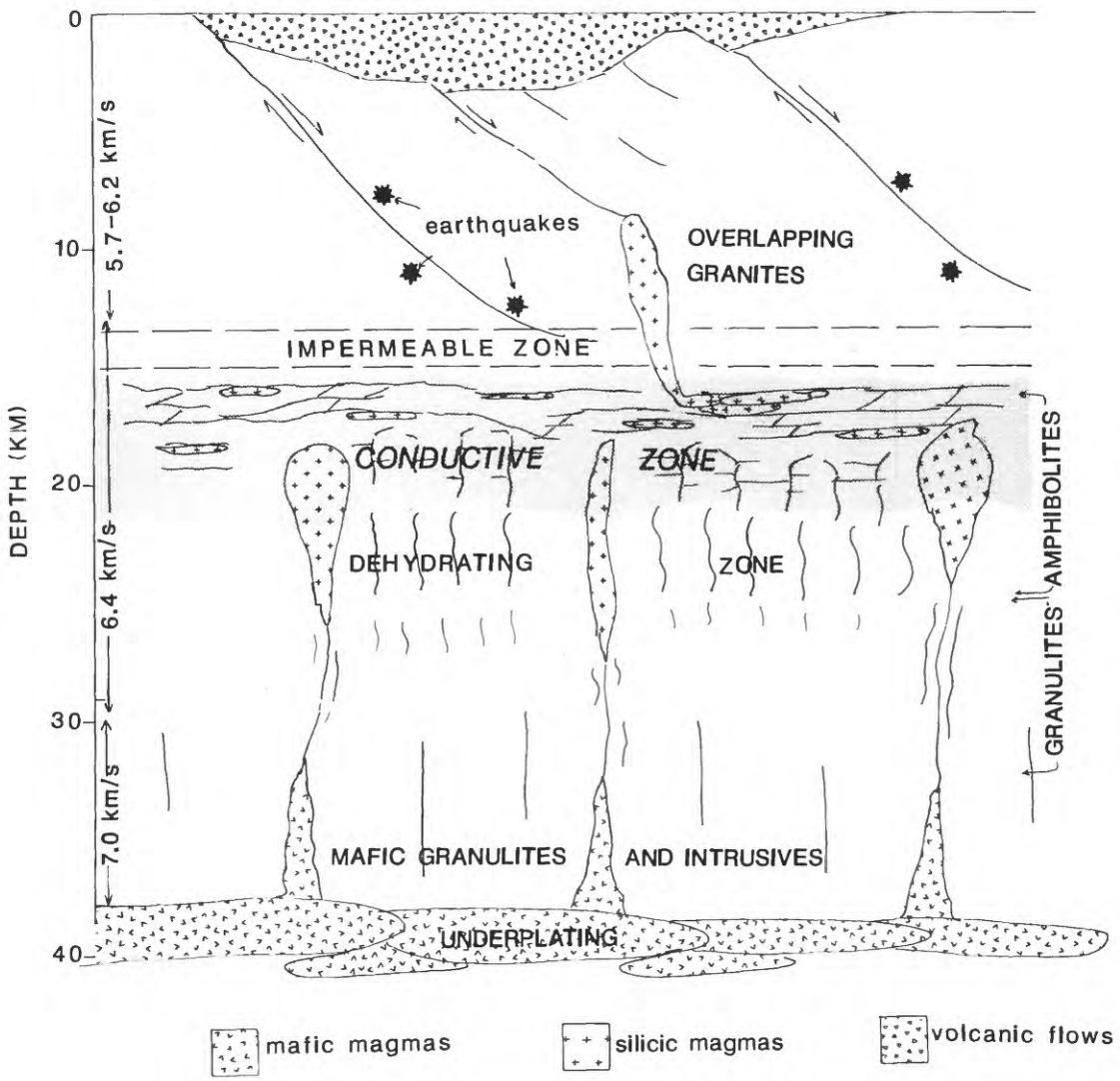

Figure 16-Cartoon illustrating a crustal framework for the deep crustal conductor involving dehydration of amphibolite grade metamorphic rocks and a localized zone of horizontal hydrofracturing or disaggregation. Earthquakes in the brittle part of the crust are indicated by the symbols in the upper 12 km. Velocities from the northern California seismic model (figure 11) are indicated along the left portion of the figure and proposed lithology along the right margin. The metamorphic-temperature profiles assumed are indicated in figure 17.

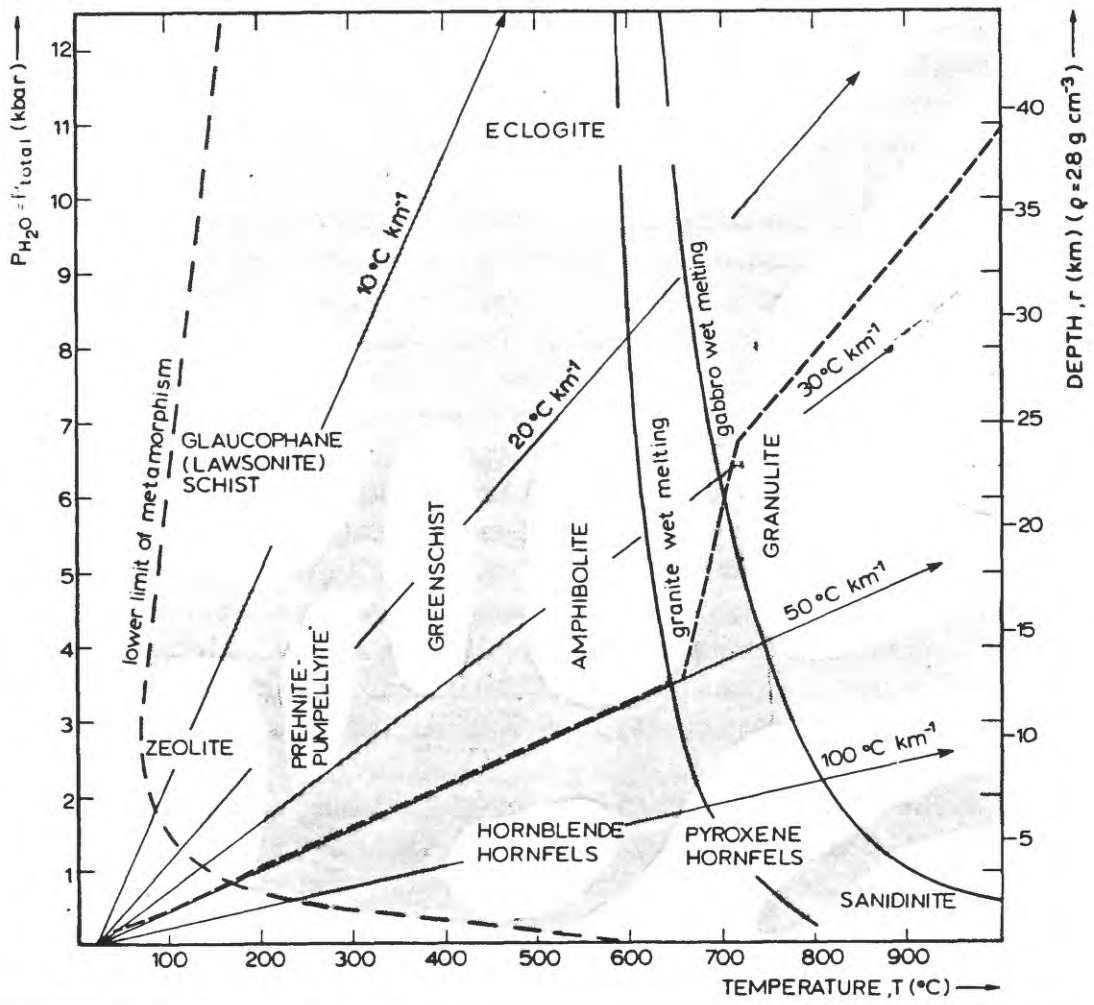

Figure 17-Approximate location of metamorphic mineral facies based upon experimental data for different temperature-depth profiles reproduced from Fyfe and others (1978). The temperature profile assumed in our figure 16 is shown by the heavy dashed line.

SEISMICITY OF THE CASCADE RANGE AND ADJACENT AREAS

Craig S. Weaver
U.S. Geological Survey
Geophysics Program AK-50
Univeristy of Washington
Seattle, Washington 98195
(206) 442-0627

INTRODUCTION

The Cascade Range of the Pacific Northwest represents a unique opportunity to examine the relation of regional seismicity to volcano-tectonic processes because, compared to most subduction-related volcanic arcs, relatively good seismic network coverage exists for much of the arc. Throughout the entire range, seismic network coverage since 1960 has been sufficient to allow a nearly complete catalog of earthquakes greater than magnitude 4 to be compiled; much of the range has been monitored down to magnitude 2.5 since 1975. Further, in Washington seismicity has been monitored east of the Cascade Range since 1969, allowing the variations in earthquake activity to be mapped from the frontal arc region into the backarc.

In this paper I have taken advantage of recent compilations and reviews of the seismicity distribution of Washington, Oregon and northern California. For Washington and Oregon, Yelin [submitted] reviewed helicorder records to produce a comprehensive list of earthquakes greater than magnitude 3.5; this catalog is thought to be complete since 1960 at the magnitude 4 level for all of Oregon and Washington. Three papers in the Decade of North American Geology volume, *Neotectonics of North America,* provide a thorough introduction to the seismicity of the region: Ludwin et al. [1989] summarized the general pattern of earthquakes in Washington and Oregon, and Uhrhammer [1989] and Hill et el. [1989] provided discussions of the seismicity of northern California.

I have drawn the seismicity catalogs for this paper for the Oregon and Washington portion of the Cascade Range from that used by Ludwin et al. [1989]. The data for northern California is taken from the catalogs maintained by the USGS in Menlo Park. I have combined these data sets to focus on the seismicity of the Cascade Range and the relation between the volcanic arc and surrounding geological provinces.

This range-wide focus results in three conclusions. First, there are variations in the seismicity within the range that suggest that the range can be divided into five segments. These segments are nearly congruent with the five segments of Guffanti and Weaver [1988] who subdivided the range based on the distribution and composition of late Cenozoic volcanic vents. Second, the distribution of earthquakes in the Cascade Range tends to mimic the distribution of earthquakes in the backarc regions that are adjacent to the arc; there is apparently little influence of subduction tectonics on the distribution of crustal earthquakes within most of the range. The only exception to this observation is in the South Cascades of Washington, where the distribution of earthquakes is continuous from the frontal arc region to the backarc. Third, seismicity outlines a major crustal block in the southern Washington Cascade Range, and I interpret this block as the linking element between a potential for arc volcanism that arises from the subducting plate geometry and regional crustal tectonics. I conclude by suggesting that the subduction potential, crustal tectonics and crustal blocks may form the fabric for volcanism everywhere within the Cascade Range, and speculate on this

fabric in Oregon and northern California where there is much less seismicity than in southern Washington.

VARIATIONS OF THE SUBDUCTION AND GEOLOGICAL SETTING

The volcanic arc of the Cascade Range is generally accepted as being related to the subduction of the Juan de Fuca plate beneath North America. Throughout most of the Cenozoic, the Pacific Northwest has been a zone of convergence [Atwater, 1970], but geological mapping within the Cascade Range indicates that volcanism has been discontinuous through this time. The current Cascade Range began developing within the last 8 Ma, after a hiatus of volcanism of several million years that extended over most of the current range [McBirney, 1978; Luedke and Smith, 1981; 1982; Smith and Luedke, 1984].

Because most volcanic arcs occur over the area where subducting plates reach a depth of 100-150 km [e.g., Gill, 1981], the position of arc volcanism is related to the geometry of the subducting plate. The geometry of the Juan de Fuca plate system is complicated by the tendency of the main Juan de Fuca plate to develop smaller subplates (i.e., the Explorer and Gorda plates) with independent motions and by the change in the orientation of the margin off the Washington coast (Figure 1). These complications are partly reflected in the geometry of the plate beneath the position of the Cascade arc. Benioff zone earthquakes have not been detected everywhere within the subducting plate, so the position of the plate at a depth of 60 km has been inferred only beneath Washington, northernmost Oregon, and a portion of northern California (Figure 1). The most prominent feature in the Juan de Fuca plate geometry is the upward arch beneath the Puget Sound basin, landward of the change in margin orientation [see Weaver and Baker, 1988). North of this arching, the Juan de Fuca plate dips to the northeast, whereas to the south, the plate dips east-southeast beneath southwestern Washington (Figure 1,2). Because of the relation between plate depth and arc volcanism, a major change in plate geometry is expected in the area lacking Benioff zone earthquakes near the Oregon-California border. There projecting the known position of the plate at a depth of 60 km northward leads to an improbably shallow depth of the plate beneath Mount Shasta.

To the west, most of the Cascade Range is bounded by sedimentary and marine volcanic complexes of Miocene to Eocene age that have been accreted to the North American continent [Cady, 1975; Snavely, 1988]. These older rocks have been covered by Quaternary sediments in the Puget Sound basin and the Willamette trough [Tabor, 1972; Cady, 1975]. Beneath southwestern Washington and northernmost Oregon, geological mapping and regional electrical conductivity studies indicate that these complexes form an east-dipping sequence that continues beneath the western margin of the Cascade Range [Stanley et al., 1987]. In central Oregon, both recent mapping in the Western Cascades and the conductivity structure suggest that the Tertiary units here are nearly flat-lying and continue eastward beneath at least the western flank of the Cascade Range [Sherrod, 1987; W. D. Stanley, personal communication, 1988]. In northern California the western margin of the Cascade Range is bounded by the pre-Cenozoic Klamath Mountains province that includes the early Paleozoic Trinity ultramafic sheet. The Klamath Mountain complex forms an east-dipping imbricate sequence that abuts directly the modern Cascade Range in the vicinity of Mount Shasta (Figure 1). Pre-Cenozoic rocks are also mapped south of Lassen Peak as both the largely sedimentary Great Valley sequence and the granitic rocks of the Sierra Nevada (Figure 1).

East of the Cascade Range, a series of high lava plateaus bounds the range from Lassen Peak as far north as the Three Sisters-Mount Jefferson area. During the late Cenozoic, these plateaus have been characterized by extensional tectonics, with the development of north-south striking normal faults and largely basaltic volcanism

[Christiansen and McKee, 1978]. North of the Brothers fault zone, the tectonic style east of the Cascades changes in the Columbia Plateau, which contains extensive Miocene volcanism of the Columbia River basalt group, but little geological evidence of post-Miocene extensional tectonics. Finally, the most striking break in the geology of the Cascade Range is that between the pre-Eocene complex of the North Cascades of Washington and the rest of the range to the south, where most of the basement rocks of the Cascade arc are covered by late Cenozoic volcanics. The North Cascades are adjacent to the largely pre-Cenozoic Okanogan Highlands, although this region experience extensive reworking of the crust by both compressional and extensional processes as late as the Eocene [Potter and others, 1986; Sanford and others, 1988].

Within this larger structural fabric, and approximately above the position where the subducting Juan de Fuca plate system reaches a depth of about 100 km, are the late Cenozoic volcanic vents (approximately younger than 5 Ma) of the Cascade arc (Figure 2). Between Mount Shasta and Mount Hood these vents define a narrow belt approximately 30-50 km in width except where the basaltic volcanism along the High Lava Plains joins the volcanic arc (Figure 2). On both the north and south ends of the narrow belt, the distribution of vents changes. To the north between Mount Hood and Mount Rainier, the zone of vents broadens to about 150 km but the distribution of vents is less dense. In the pre-Eocene rocks of the North Cascades the distribution of volcanic vents is limited, confined to the vicinity of the stratovolcanoes Mount Baker and Glacier Peak. To the south in California, the area of vents widens near both Mount Shasta and Lassen Peak compared to the very linear distribution in Oregon, and the Lassen area is spatially separated from the continuous distribution to the north. Based on this distribution, Guffanti and Weaver [1988] suggested that the range could be divided into the five segments shown in Figure 2.

Despite the variations of the volcanic vent distribution and the changes in the geological setting of the backarc region, a recent estimate of crustal thickness (Figure 3) concluded that the crust beneath the Cascade Range is everywhere thick, on the order of 40-46 km [Mooney and Weaver, 1989]. Beneath the North Cascades relatively sparse seismic refraction date suggests a crustal thickness of about 40 km [Rohay, 1982]; beneath the western Oregon Cascades a reversed refraction line found crustal thicknesses between 40 and 46 km [Leaver et al., 1984]. Detailed crustal studies in the Mount Shasta and Medicine Lake area did not observe mantle arrivals on the refraction lines, but Zucca et al. [1986] concluded that the crust must be about 40 km thick based on the lower crustal velocity structure that was resolved and the constraint of no observed Pn arrivals.

RANGE-WIDE PERSPECTIVES OF SEISMICITY

The most striking aspect of the distribution of all known earthquakes detected since 1960 that are greater than magnitude 4 is the concentration of these events in western Washington and off the northern California coast (Figure 4). As noted by Ludwin et al. [1989], in Washington most of the events of magnitude 4 and greater in the Puget Sound region are within the subducting Juan de Fuca plate, whereas in southern Washington all of these events are within the crust. As is evident in Figure 4 all of the crustal earthquakes greater than magnitude 5 in the Cascade Range are located in southern Washington. The only other crustal earthquakes greater than magnitude 5 have been in the Basin and Range province of southeastern Oregon (Figure 4), where a swarm of earthquakes occurred in 1968. Clearly along most of the Cascade arc few earthquakes greater than magnitude 4 have been detected.

The earthquakes plotted in Figure 4 were not screened for the quality of the location, and many of the events occurring before 1970 have very poor depth control. Therefore, in Figure 5 I have screened the events in Figure 4 with the criteria that

hypocentral errors be less than 5 km, at least 6 stations were used in the solutions, and that the RMS of the traveltime residuals be less than 0.35 seconds. These standards are also applied to all subsequent data sets in this paper; most hypocenters have statistics much better than these minimum criteria. In addition to the magnitude 4 and greater events that meet the quality standards, I have added events greater than magnitude 2.5 recorded since 1975 that meet the above criteria and plotted the resulting catolog in Figure 5. In Figure 5 earthquakes greater than 30 km deep are plotted as squares; nearly all of these deeper events are within the Juan de Fuca or Gorda plates beneath North America. The exceptions are obscurred by the shallower events in the central Puget Sound basin.

Adding the well-located but smaller magnitude events sharpens the variations in the distribution of seismicity along the strike of the Cascade Range. Once again, the onshore activity is clearly greatest in western Washington. However, there are important details. First, the North Cascades are seismically quite, with all of the well-located earthquakes being west of the stratovolcanoes Mount Baker and Glacier Peak (Figure 5). The crustal events (circles in Figure 5) are confined to the region between the Olympic Mountains and the stratovolcanoes in the North Cascades. These crustal events have a sharp cutoff that strikes nearly west-east in southern Puget Sound (Figure 5). Second, in southern Washington the St. Helens zone (SHZ) described by Weaver and Smith [1983] is prominent. Although there is an hiatus of activity east of the SHZ, it is apparent that seismicity continues a in broad zone from the area immediately west of the SHZ into the Columbia Plateau of southeastern Washington (Figure 5). Third, most seismicity ends just south of Mount Hood. Although the portion of the range from Mount Hood south to Mount Shasta has only been monitored continouous for two years (1980-1982), very few earthquakes at any magnitude were observed [Kollman, 1984]. In 1987 the University of Washington re-installed a sparse monitoring network on the eastern flank of the central Oregon Cascade Range between Mount Jefferson and Newberry Volcano and during the past year very few earthquakes have been detected within this area. Fourth, the number of earthquakes increases near the California border, and the number of events increases again near Lassen Peak (Figure 5).

It is apparent from comparing Figures 2 and 5 that there are similarities between the apparent divisions in the seismicity distribution and the segmentation of the Cascade Range based on the distribution and composition of volcanic vents. Segment 1 of the vent distribution consists of the region north of Glacier Peak, and this is the region where the range is seismically quite. Segment 2 was defined between Mount Rainier and Mount Hood, and this is the most seismicallly active area within the range. The seismically quite portion of the range in Oregon south of Mount Hood is congruent with segment 3. Finally, the relatively sparse seismicity near the Mount Shasta area encompases segment 4 and the somewhat higher apparent rate of seismicty near Lassen Peak corresponds to segment 5 of the vent distribution model.

The relation between the seismicity in the subducting Gorda and Juan de Fuca plates and the volcanic arc can best be observed by plotting cross sections drawn perpendicular to the strike of the volcanic arc. Because there are few earthquakes located within the subducting de Fuca plate, most studies of the plate geometry include events of smaller magnitude than 2.5. In the next three figures I have added events located since 1980 that are greater than magnitude 1.5 and at depths below 30 km and events that are greater than magnitude 2.0 at depths above 30 km. These additions are restricted to Washington and northernmost Oregon and northern California where the seismic network is dense enough to allow these smaller magnitude events to be routinely located. In both areas the details of the seismicity pattern remain essentially the same as that shown in Figure 5.

In Washington, there are again few earthquakes in the North Cascades; virtually all of the crustal events are west of the stratovolcanoes (Figure 6). The west-east cutoff in crustal events is more pronounced in southern Puget Sound and earthquakes within the Juan de Fuca plate (squares in Figure 6) are more widely distributed beneath the Coast Range than with the smaller magnitude cutoff used in Figure 5. Again, very few earthquakes locate east of the SHZ, but by including the smaller magnitude crustal events the continuous nature of the activity across the southern Washington Cascade Range is more apparent. Similarly, there are few changes in the distribution in northern California (Figure 7). Crustal earthquake activity is largely confined to the eastern Great Valley and Lassen Peak. In the Klamath Mountains the shallow earthquakes (circles) have hypocentral solutions that satisfy the selection criteria outlined above, but are not judged to be as well constrained as the crustal events closer to Lassen Peak where the seismic network is more dense.

The orientation and extent of each cross-section shown in Figure 8 is indicated on Figures 6 and 7. Beneath Washington a comparison of hypocentral depths with seismic refraction models of the continental margin indicates that the Benioff zone earthquakes fall below the Moho of the subducting plate [Taber and Smith, 1985]. I have used this observation to sketch the position of the Moho for the subducting plates.

There are both differences and similarities between the cross sections plotted here and previously published sections. Figure 8a differs from previous cross sections drawn for the region [e.g., Weaver and Baker, 1988; Ludwin et al., 1989] in that it is perpendicular to the volcanic front and excludes the more dense distribution of crustal earthquakes in central Puget Sound. Figure 8b reproduces a portion of a longer section shown by Mooney and Weaver [1989], whereas Figure 8c has not been plotted previously. Finally, Figure 8d is similar to a section plotted by Mooney and Weaver [1989], but is narrower in width than similarly oriented sections by Cockerham [1983] and Walter [1986].

The two sections across Washington (Figure 8a & b) have well-defined Benioff zones, extending from the coast landward to the western edge of the Cascade Range. Although no Benioff zone earthquakes have yet been located beneath the position of the large stratovolcanoes, projecting the dip of the located earthquakes downward results in an estimate of the plate depth of about 100 km. It is clear from the sparsity of hypocenters beneath northern Oregon (Figure 8c) that not enough Benioff zone events have been located to unambiguously define the subducting plate geometry. Beneath northern California the deep activity again defines a Benioff zone that appears to increase dip near the coast (Figure 8d). However, the details of this distribution are much less clear than those in Washington, probably because of a sparser seismic network and large uncertainties in the velocity model.

The crustal earthquake distribution shows large differences among the four sections. In northern Washington the crustal activity begins at the eastern edge of the Olympic Mountains, and most of the westerly earthquakes are in the mid crust, between 20-30 km (Figure 8a). Eastward toward the Cascade Range hypocentral depths shallow, largely confined to the more normal crustal range of near surface (a few kilometers) down to about 20 km. Everywhere except in the center of the Puget Sound basin, the maximum seismogenic depth is about half the crustal thickness.

In southern Washington the crustal earthquakes are concentrated near Mount St. Helens; because of the angle of the projection (see Figure 6) the SHZ is elongated across the section. West of Mount St. Helens there are some deeper crustal events, at depths similar to those found in the western Puget Sound basin. East of Mount St. Helens the earthquakes arch upward, with only shallow events (<10 km) recorded beneath the central Cascade Range. Further east in the Columbia Plateau earthquakes are scattered as deep as about 20 km (Figure 8b).

Although there are few events in northern Oregon, the developing pattern is similar to southern Washington. Deep crustal events (15-25 km) are located near Portland, and the maximum earthquake depth apparently shallows beneath the Cascade Range to less than 20 km. Events as deep as 20 are located east of the Cascade Range in the adjacent Columbia Plateau.

The distribution of crustal events in northern California is similar to that of northern Washington. Crustal events are largely confined between the middle of the Great Valley and the volcanic arc (Figure 8d). Across this active region the maximum seismogenic depth is about half the estimated crustal thickness.

CRUSTAL BLOCKS IN THE SOUTHERN WASHINGTON CASCADES

From the above discussion, it is clear that the southern Washington Cascade Range is the most seismically active portion of the range. In addition, it is also the only portion of the range where major arc-related stratovolcanoes are well displaced east of the central axis of largely mafic volcanism that extends from Mount Shasta to Glacier Peak (Figure 2). Not only are the stratovolcanoes Mount Rainier and Mount St. Helens 25 and 60 km to the west of the central trend of major cones, but the distribution of basaltic vents broadens as well (Figure 2). This broadened distribution of basaltic vents has an abrupt northwestern boundary between Mount Adams and Mount Rainier (Figure 2); few late Cenozoic basaltic vents exist north of this lineation.

It is very likely that the enhanced seismicity, the distribution of major volcanic centers, and the northern limit to basaltic volcanism are all the result of the presence of a major crustal block in the southern Washington Cascades. Regional conductivity studies [Stanley, 1984; Stanley et al., 1987] have identified a major conductivity high, referred to as the Southern Washington Cascade Conductor (SWCC) that is approximately bounded by Mount Rainier, Mount Adams, Goat Rocks, and Mount St. Helens (Figure 9). Aeromagnetic lows follow the strike of the eastern and western edges of the conductivity anomaly, and approximately bound the southern edge [Stanley, 1984; Stanley et al., 1987]. The SHZ is coincident with the western edge of the conductivity anamoly and the western aeromagnetic low.

In addition to the earthquakes along the SHZ, all earthquakes greater than magnitude 4.0 that have reliable locations (Figures 5 & 7) in the southern Cascade Range of Washington and all three earthquakes greater than magnitude 5 since 1960 have occurred along the interpreted boundary of the conductor. Thus virtually all of the seismic moment released since 1960 in the southern Washington Cascades has been at or near the boundary of the SWCC. Earthquake focal mechanisms for the events greater than magnitude 5 are nearly pure strike-slip solutions, and the preferred fault plane for each of these mechanisms strikes approximately parallel to the local direction of the conductor boundary (Figure 9). I interpret these seismicity observations as indicating that the SWCC acts as a coherent crustal block, concentrating regional seismic activity along the boundaries. The concentration of all of the larger magnitude earthquakes along the boundaries of the conductor indicates that regional shear is being accommodated nearly completely there, as opposed to within the block where only a few smaller magnitude events are located (compare Figures 5, 7 & 9).

Although previous studies [Weaver and Malone, 1987; Stanley et al., 1987] have emphasized the relation between the SHZ and the SWCC, it is apparent that the relation between the SWCC and the SHZ is essentially observed throughout the entire area bounded by the major volcanic centers. The crustal block represented by the conductor apparently has such coherent boundaries with the surrounding crust that the volcanic centers at Mount Adams, Goat Rocks, Mount Rainier, and Mount St. Helens have been firmly anchored to the surrounding tectonic framework, presumably by the style of localized crustal extension described for Mount St. Helens [Weaver et al.,

1987]. At the same time, the coherency of the block has allowed only a few scattered basaltic vents to reach the surface within the body itself.

The preferred interpretation of Stanley et al. [1987] for the SWCC is that it represents a marine forearc basin that has been highly compressed as the Coast Range block to the west has been forced eastward by convergence at the subduction zone. Although somewhat uncertain, as the body responsible for the conductivity anomaly is not exposed at the surface, the interpretation of a compression-dominated basin may explain why the SWCC has been able to form such a sharp boundary to basaltic volcanism.

The details of how structural and tectonic elements combine to control volcanism along the edges of the conductor have previously been described for Mount St. Helens [Weaver and Malone, 1987; Weaver et al., 1987]. The volcano is located at the intersection of a series of northeast-striking volcanic vents of late Quaternary age and older linements. Both sets of features are approximately parallel with the inferred northeast direction of the regional maximum principal stress [Weaver and Smith, 1983]. These structural trends continue beneath Mount St. Helens, where they are defined by earthquake hypocenters that are interpreted as being on a northeast-striking fault [Weaver et al., 1987]. The actual location of Mount St. Helens occurs where these structural trends intersect the SHZ; there the SHZ shows a small dextral offset that has a geometry favorable for local crustal extension.

The congruence of the geophysical and geological observations in the southern Washington Cascade Range presents a particularly impressive case for the importance of crustal blocks and faults interacting with contemporary regional tectonic stresses to control Quaternary volcanism. As is apparent from the distribution of late Cenozoic vents (Figure 2), volcanism has occurred over a wide area of southern Washington, but I propose that longevity at a particular volcanic center is related to the ability of the crust to localize (anchor) crustal extension. The data available from Mount St. Helens indicates that this firm anchoring will occur only if a favorable fault (or block boundary) geometry exists that will allow the development of local crustal extension. If, as has been argued for southwestern Washington, the crust is dominated by horizontal compression, then it may be difficult for new volcanic centers to initiate, leading to the long-lived centers apparent today in the southern Washington Cascades.

DISCUSSION

The presence of a relatively well-identified crustal block in the southern Washington Cascade Range suggests that there is a three-way relation (Figure 10) that forms the fabric for arc volcanism. First there is the potential for arc volcanism that arises simply from the position of the Juan de Fuca plate. From the cross section for southern Washington (Figure 8b), it is clear that the western limit of the volcanic vents, including Mounts Rainier and St. Helens, is near the position where the minimum depth of arc-related volcanism, ultimately derived from the presence of the descending plate, would be expected. The second element is the driving stresses for regional crustal tectonics. In southern Washington Weaver and Smith [1983] have suggested that the region is subject to a maximum horizontal compressive stress that is directed northeast. They suggested that the origin of this stress was the Juan de Fuca-North American plate interface. The third, and critical linking element, that controls the location of major stratovolcanoes, limits the basaltic volcanism, and provides the boundaries for regional shearing, is the crustal block identified as the SWCC.

I have schematically shown these interactions in Figure 10. For simplicity, I have used arrows to show the link between the three variables, designated "S, T, and B" for subduction, crustal tectonics, and crustal blocks, respectively. Ideally, the weight of the lines linking the "S, T and B" corners would be varied to reflect changing

interactions along the volcanic arc.

In southwestern Washington, there is clearly a strong influence of subduction on both the T and B variables. As noted above, subduction is viewed as the cause of the regional tectonic stress (T). Subduction is responsible for accreting the former forearc basin to the North American continent and for compressing the basin in its current position, thus the strong influence of S on B. Finally, the interaction between the SWCC and regional tectonics is documented by the earthquakes along the boundaries of the block and the anchoring of the major stratovolcanoes, thus the strong T-S link shown in Figure 10.

This simple scheme may thus be useful in attempting to explain the differences in the Cascade Range that the recent segmentation model of Guffanti and Weaver [1988] has described. Of course, application of the "S-T-B" relation described throughout the range will involve being able to define the blocks using data other than seismicity. In the North Cascades of Washington, for instance, there is very little seismicity. Thus, I suggest that here the appropriate block may be the limit of the pre-Cenozoic rocks; with the late Cenozoic centers then occurring *within* rather than on the *boundaries* of the block. The lack of seismicity within the North Cascades suggests that the contemporary subduction tectonics has little influence on this block, thus an "S-T-B" diagram might have a weaker link between "S" and "T" than that shown for the southern Washington Cascades.

In Oregon and northern California, it is possible that the matrix of density boundaries inferred by Blakely et al. [1883] could be associated with the block idea suggested here. As in the North Cascades, there appears to be only a spatial link between "S" and "T" in the Oregon and northern California portion of the range. On the other hand, if the density boundaries correlate with actual normal faults (buried by subsequent volcanism), then the T-B connection may be quite strong, as these faults likely would represent the widespread extensional processes found in the backarc region.

REFERENCES

Atwater, T., Implications of plate tectonics for the Cenozoic tectonic evolution of western North America, *Bull. Geol. Soc. Amer. 81,* 3513-3536, 1970.

Blakely, R. J., R. C. Jachens, R. W. Simpson, and R. W. Couch, Tectonic setting of the southern Cascade Rang as interpreted from its gravity and magnetic fields, *Geol. Soc. Am. Bull., 96,* 43-48, 1985.

Cady, W. M., Tectonic setting of the Tertiary volcanic rocks of the Olympic Peninsula, Washington, *U.S. Geol. Survey J. Research 3,* 573-582, 1975.

Christiansen, R. L., and E. H. McKee, Late Cenozoic volcanic and tectonic evolution of the Great Basin and Columbia Intermountane regions, *Mem. Geol. Soc. Am., 152,* 283-311, 1978.

Cockerham, R. S., Evidence for a 180-km long subducted plate beneath Northern California, *Bull. Seismol. Soc. Amer.,74,* 569-576, 1984.

Gill, J. B., *Orogenic Andesites and Plate Tectonics,* 390 pp., Springer-Verlag, New York, 1981.

Guffanti, M., and C. S. Weaver, Distribution of late Cenozoic volcanic vents in the Cascade Range: Volcanic arc segmentation and regional tectonic considerations, *J. Geophys. Res., 93,* 6513-6529, 1988.

Hill, D. P., J. P. Eaton, W. L. Ellsworth, R. S. Cockerham, F. W. Lester, and E. J. Corbett, The seismotectonic fabric of central California, in E. R. Engdahl, ed., *Neotectonics of North America,* Geol. Soc. Amer., Boulder, Co., (in press), 1989.

Kollman, A., Oregon seismicity, August 1980-October 1982, *U.S. Geol. Surv., Open-File Rept. 84-832,* 33 pp., 1984.

Leaver, D. S., Mooney, W. D., and W. M. Kohler, A seismic refraction study of the Oregon Cascades, *J. Geophys. Res., 89,* 3121-3134, 1984.

Luedke, R. G., and Smith, R. L., Map showing distribution, composition, and age of late Cenozoic volcanic centers in California and Nevada, scale 1:1,000,000, *U.S. Geol. Surv. Misc. Invest. Ser., Map I-1091-C,* 1981.

Luedke, R. G., and Smith, R. L., Map showing distribution, composition, and age of late Cenozoic volcanic centers in Oregon and Washington, scale 1:1,000,000, *U.S. Geol. Surv. Misc. Invest. Ser., Map I-1091-D,* 1982.

Ludwin, R. S., C. S. Weaver and R. S. Crosson, Seismicity of Washington and Oregon, in E. R. Engdahl, ed., *Neotectonics of North America,* Geol. Soc. Amer., Boulder, Co., (in press), 1989.

McBirney, A. R., Volcanic evolution of the Cascade Range, *Earth Planetary Sciences Annual Review,6,* 437-456, 1978.

Mooney, W. D., and C. S. Weaver, Regional crustal structure and tectonics of the Pacific Coastal states: California, Oregon, and Washington, in Pakiser, L. C., and W. D. Mooney, Ed., *The Geophyscial Framework of the Continental United States, Geol. Soc. Amer. Memoir,* (in press), 1989.

Potter, C. J., Sanford, W. E., Yoos, T. R., Prussen, E. L., Keach, W., Oliver, J. E., Kaufman, S., and Brown, L. D., COCORP deep seismic reflection traverse of the interior of the North American cordillera, Washington and Idaho: Implications for orogenic evolution, *Tectonics,5,* 1007-1025, 1986.

Rohay, A., Crust and mantle structure of the North Cascades Range, Washington, Ph. D. dissertation, University of Washington, Seattle, 163 pp., 1982.

Sanford, W. E., Potter, D. J., and Oliver, J. E., Detailed three-dimensional structure of the deep crust based on COCORP data in the Cordillera interior, north-central Washington, *Geol. Soc. Amer. Bull.,100,* 60-71, 1988.

Sherrod, D. R., New complilation map of the Cascade Range in Oregon, *Trans. Geotherm. Resour. Counc., 11,* 305-307, 1987.

Smith, R. L., and R. G. Luedke, Potentially active volcanic lineaments and loci in

western conterminous United States, in *Explosive Volcanism: Inception, Evolution, Hazards,* pp. 47-66, National Academy Press, Washington, D.C., 1984.
Snavely, P.D., Jr., Tertiary geologic framework, neotectonics, and petroleum potential of the Oregon-Washington continental margin: *in,* Geology and resource potential of the continental margin of western North America and adjacent ocean basins - Beaufort Sea to Baja California, Scholl, D.S., Grantz, A., and Vedder, J.G., editors, *Circum-Pacific Council for Energy and Mineral Resources Earth Science Series,* 6, 305-335, 1988.
Stanley, W. D., Tectonic study of the Cascade Range and Columbia Plateau in Washington State based upon magnetotelluric soundings, *J. Geophys. Res.,89,* 4447-4460, 1984.
Stanley, W. D., C. Finn and J. L. Plesha, Tectonics and conductivity structures in the southern Washington Cascades, *J. Geophys. Res.,92,* 10,179-10,193, 1987.
Taber, J. J. and S. W. Smith, Seismicity and focal mechanisms associated with the subduction of the Juan de Fuca plate beneath the Olympic Peninsula, Washington, *Bull. Seismol. Soc. Amer., 75,* 237-249, 1985.
Tabor, R. W., Age of Olympic metamorphism, Washington: K-Ar dating of low-grade metamorphic rocks, *Geol. Soc. Amer. Bull., 83,* 1805-1816, 1972.
Uhrhammer, R. A., Seismicity of northern California, in E. R. Engdahl, ed., *Neotectonics of North America,* Geol. Soc. Amer., Boulder, Co., (in press), 1989.
Walter, S. R., Intermediate-focus earthquakes associated with Gorda plate subduction in northern California, *Bull. Seis. Soc. Am., 76,* 583-588, 1986.
Weaver, C. S. and S. W. Smith, Regional tectonic and earthquake hazard implications of a crustal fault zone in southwestern Washington, *J. Geophys. Res., 88,* 10,371-10,383, 1983.
Weaver, C. S., and Malone, S. D., Overview of the tectonic setting and recent studies of eruptions of Mount St. Helens, Washington, *J. Geophys. Res.,92,* 10,149-10,155, 1987.
Weaver, C. S., W. C. Grant, and J. E. Shemeta, Local crustal extension at Mount St. Helens, Washington, *J. Geophys. Res., 92,* 10,170-10,178, 1987.
Weaver, C. S., and Baker, G. E., Geometry of the Juan de Fuca plate beneath Washington and northern Oregon from seismicity, *Bull. Seism. Soc. Amer.78,* 264-275, 1988.
Zucca, J. J., Fuis, G. S., Milkeriet, B., Mooney, W. D., and Catchings, R., Crustal structure of northern California from seismic-refraction data, *J. Geophys. Res.,91,* 7359-7382, 1986.

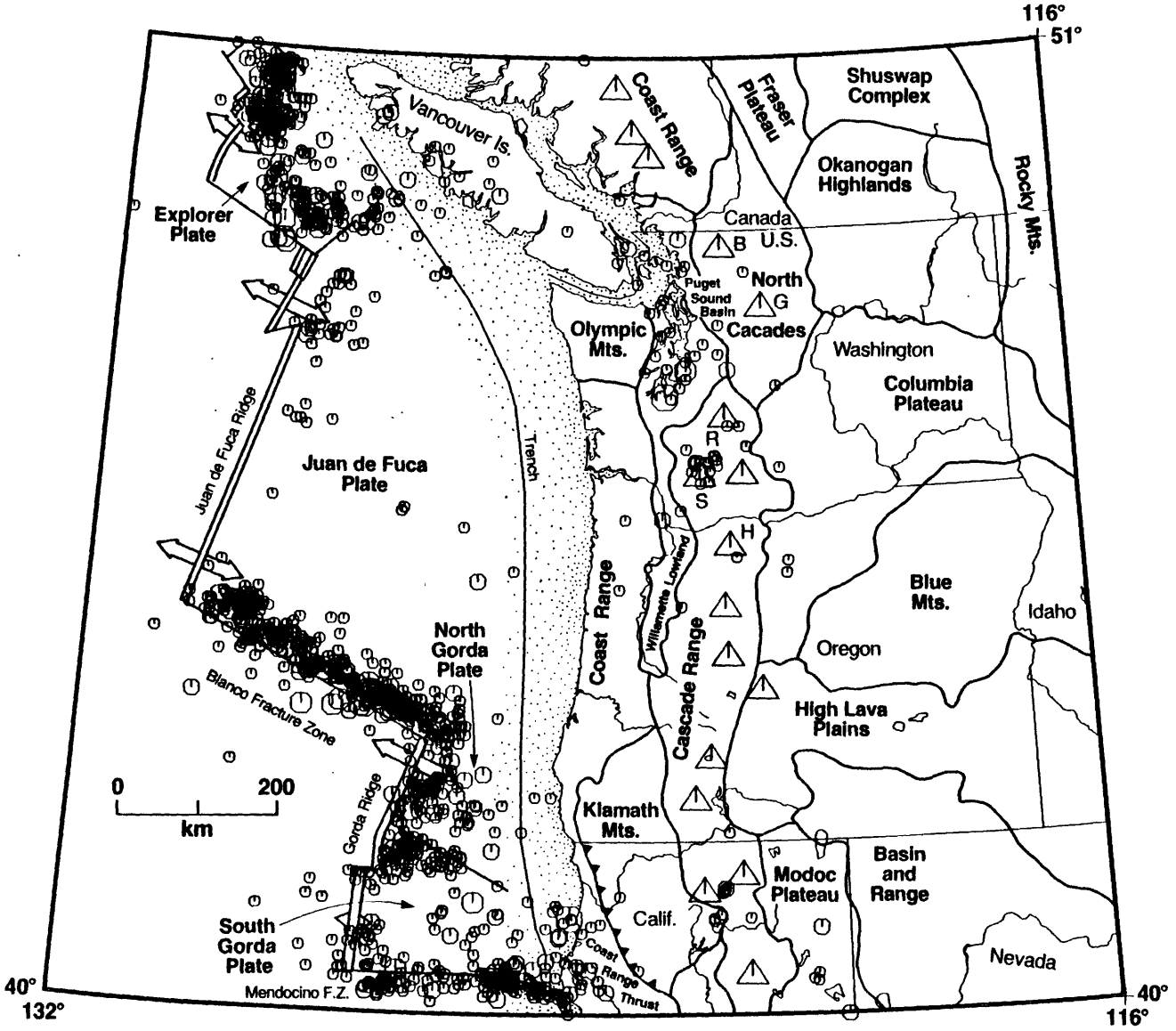

Figure 1: Plate tectonic setting and geological provinces of the Pacific Northwest. Earthquakes are from NOAA catalog, greater than magnitude 4, through 1985, plus the 1949 south Puget Sound event. Large triangles are the Quaternary Cascade volcanoes.

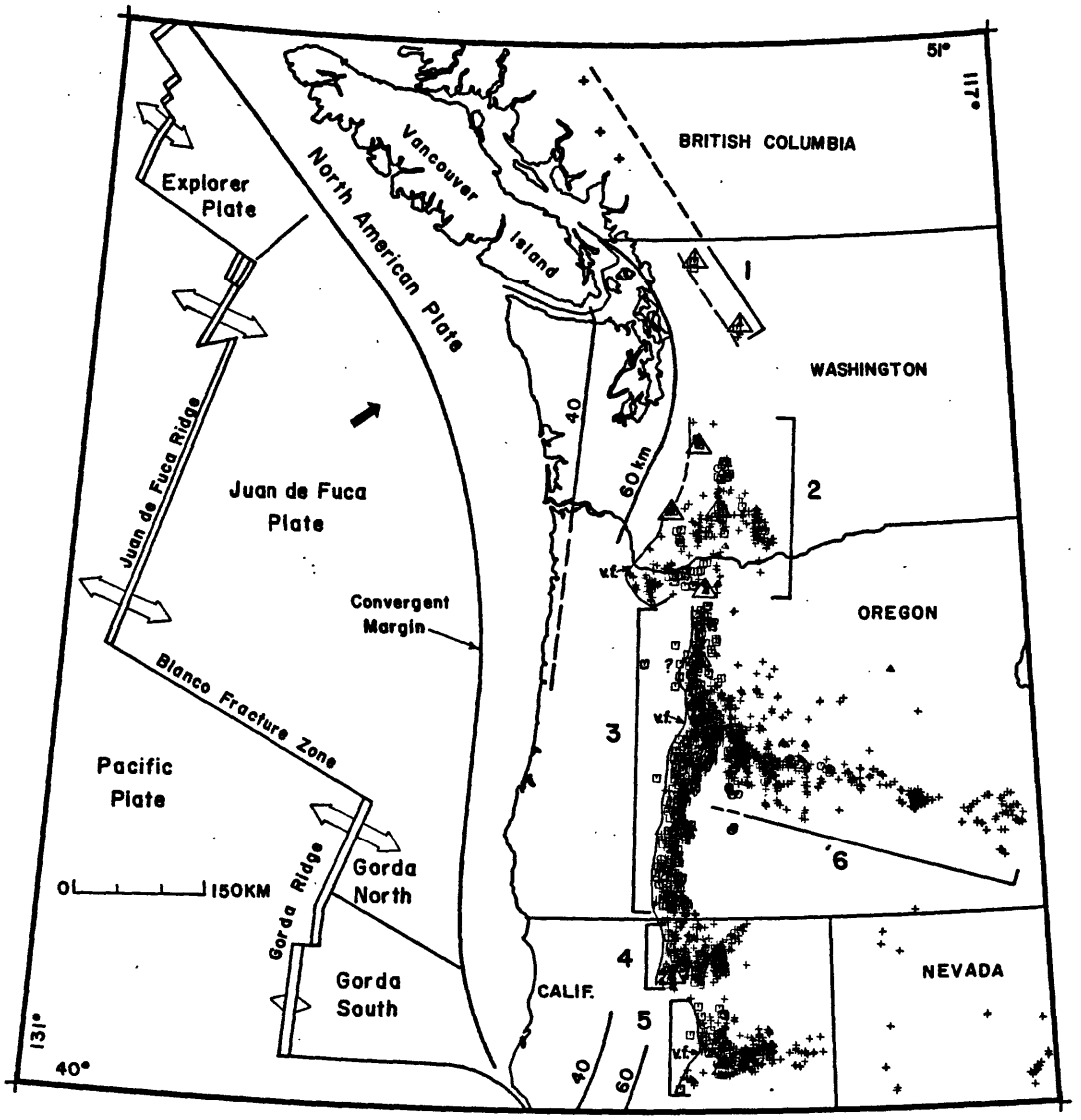

Figure 2: Late Cenozoic volcanic vent distribution. Small symbols are vents, large triangles are major stratovolcanoes. Crosses in British Columbia are major stratovolcanoes, but vent data is incomplete. The position of the Juan de Fuca and Gorda plates at depth is indicated by the 40 and 60 km lines. Numbers refer to segments. [from Guffanti and Weaver, 1988]

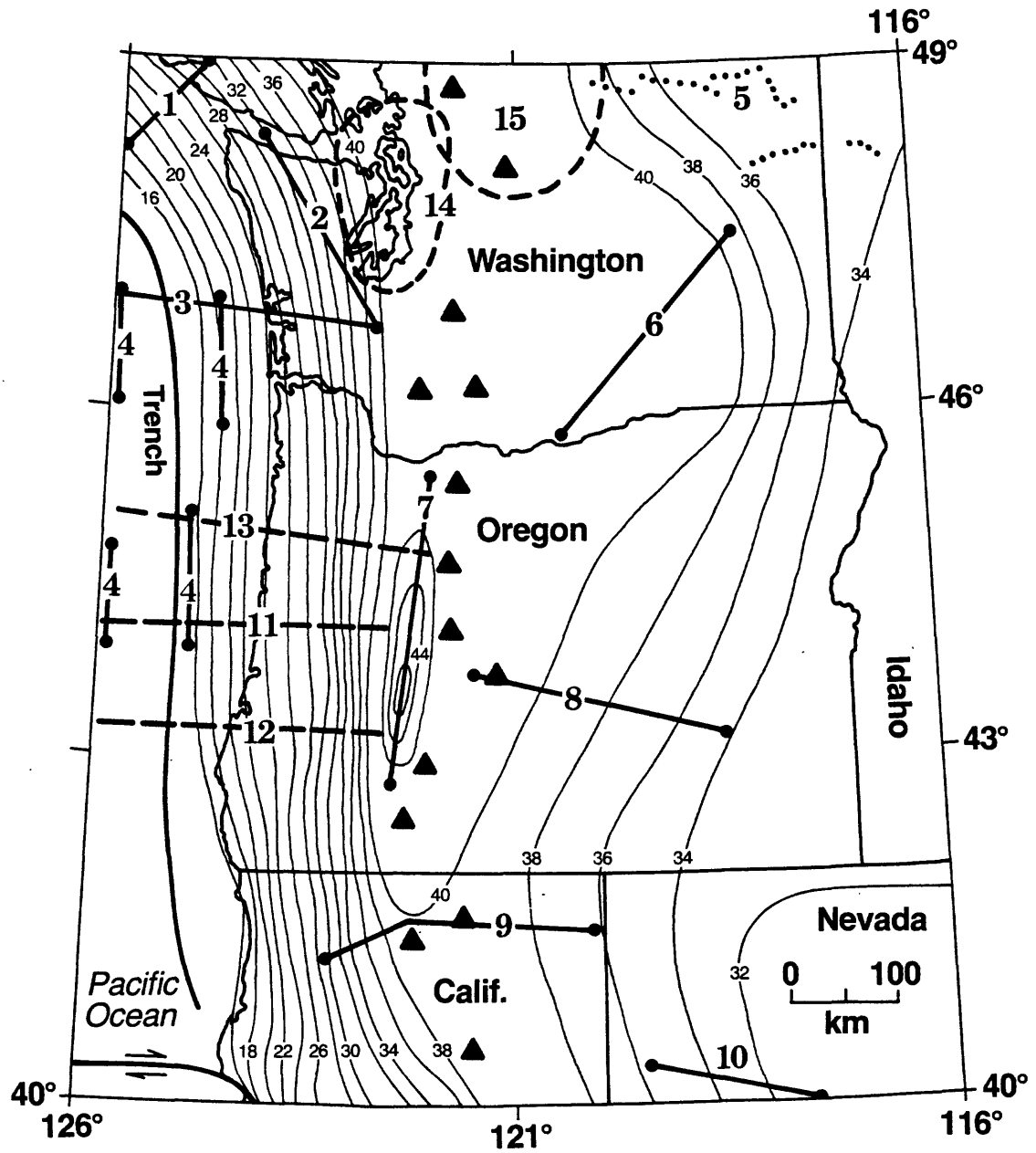

Figure 3: Estimate of crustal thickness in the Pacific Northwest. Heavy bold lines indicate position of reversed refraction profiles, dotted lines are land reflection, dashed lines are either electromagnetic or gravity profiles. Dashed contours in Washington are seismic array studies. Line references are given in Mooney and Weaver, Table 2 [1989, in press]. Figure from Mooney and Weaver, 1989.

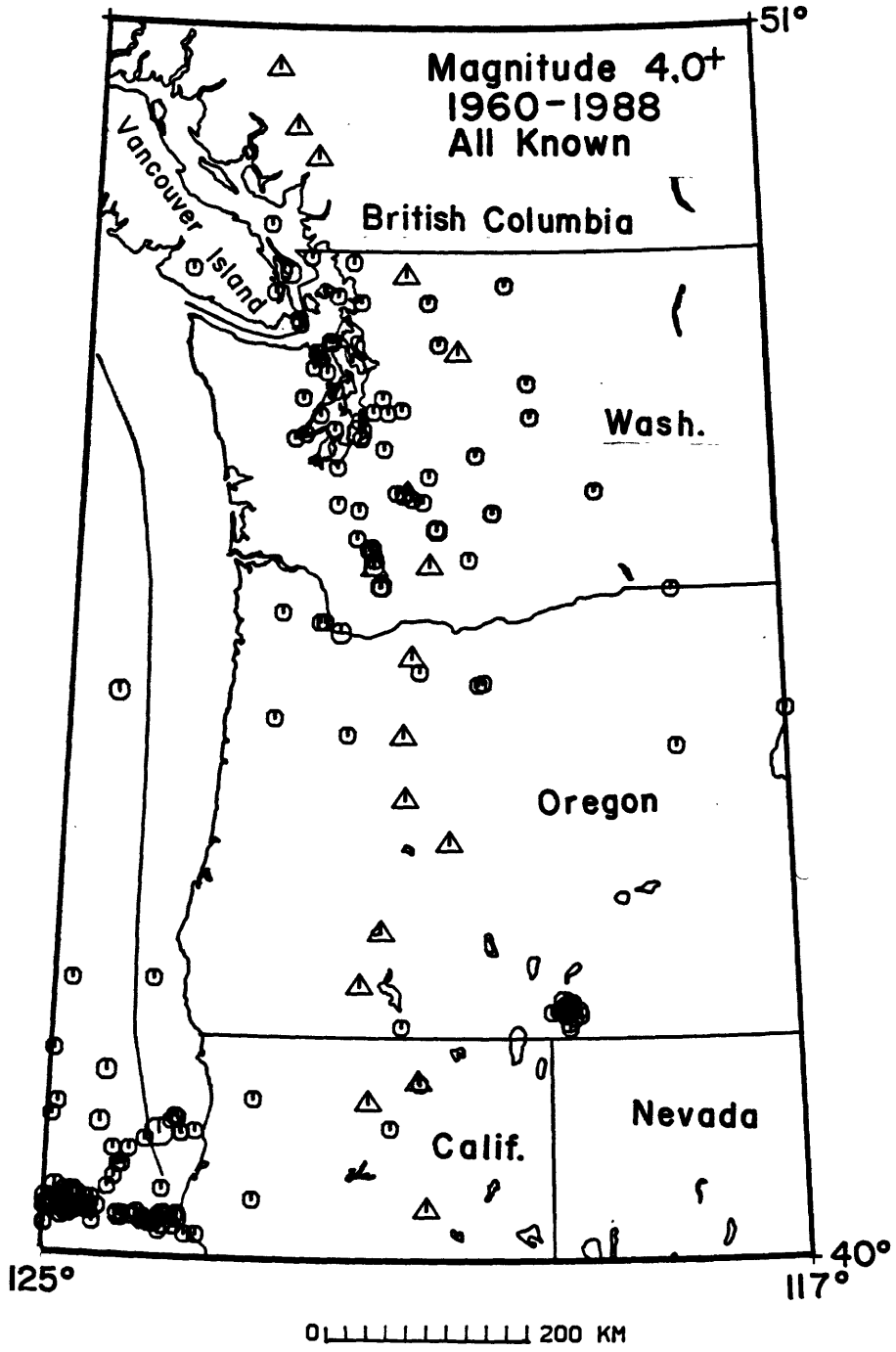

Figure 4: All known magnitude 4 and greater earthquakes since 1960.

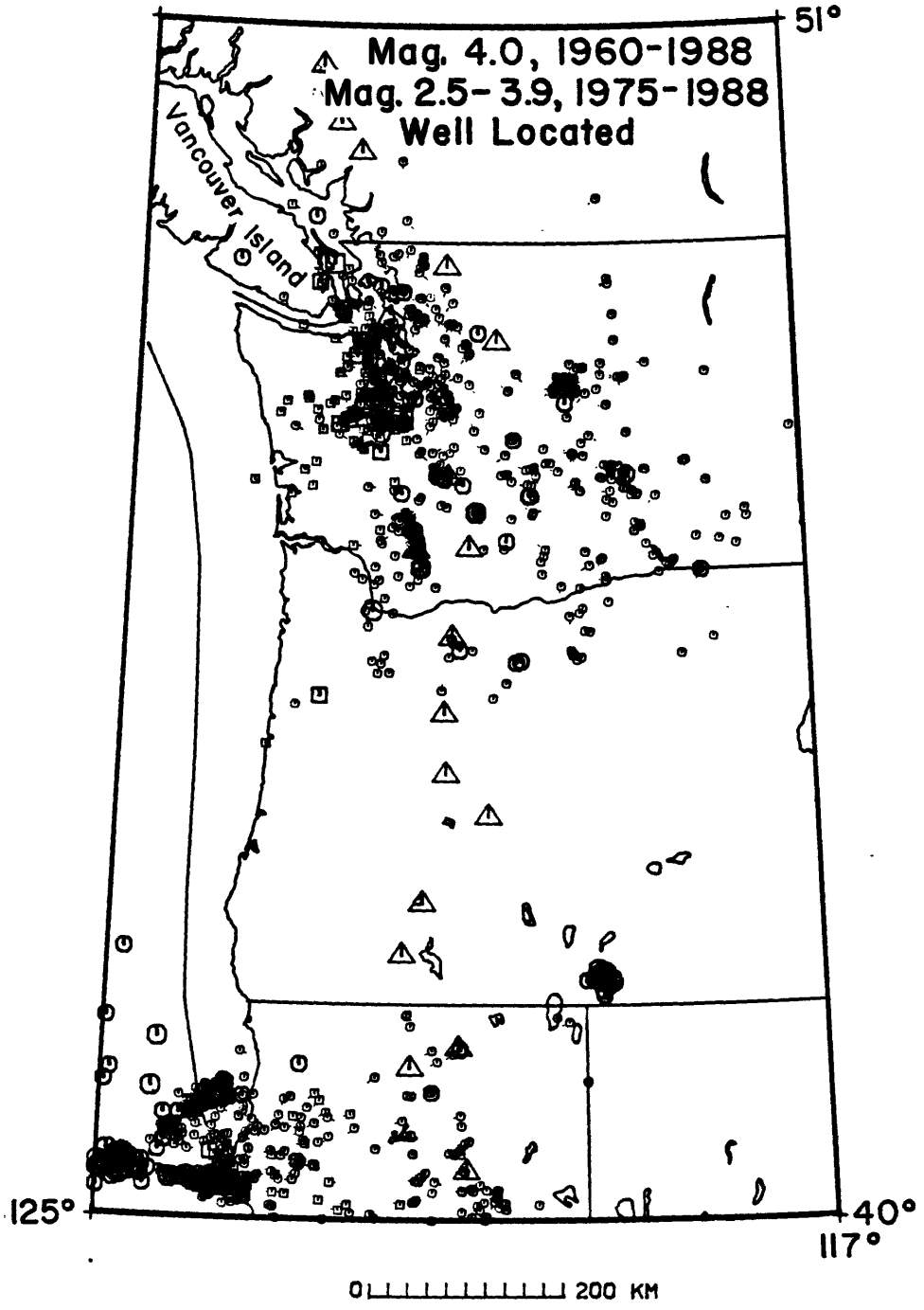

Figure 5: Well located earthquakes. Magnitudes and dates as given in figure. Small symbols are less than magnitude 4, larger symbols greater than 4. Squares are below 30 km depth, circles above 30 km.

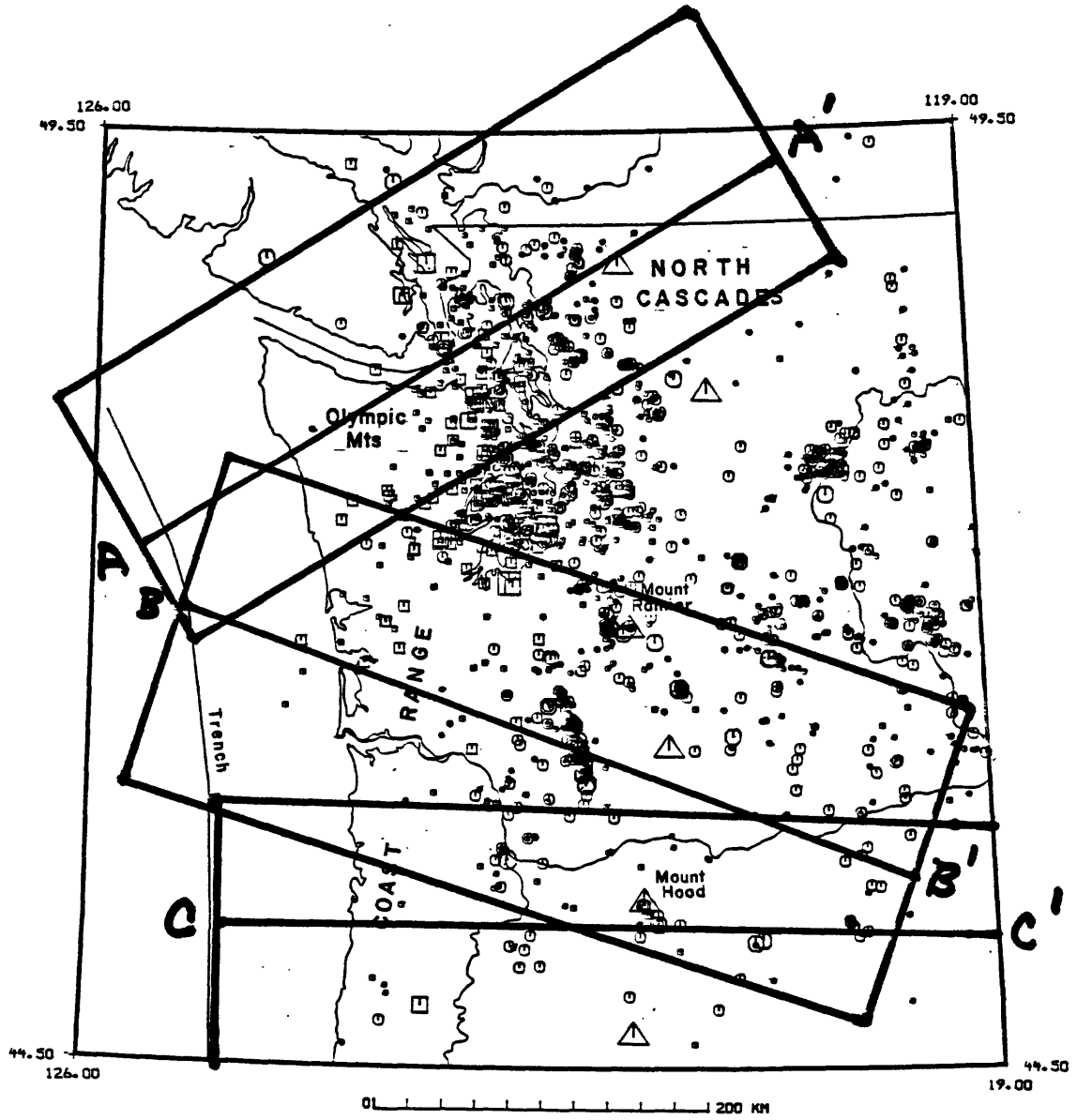

Figure 6: Location of areas and orientation of cross-sections plotted in Figure 8.

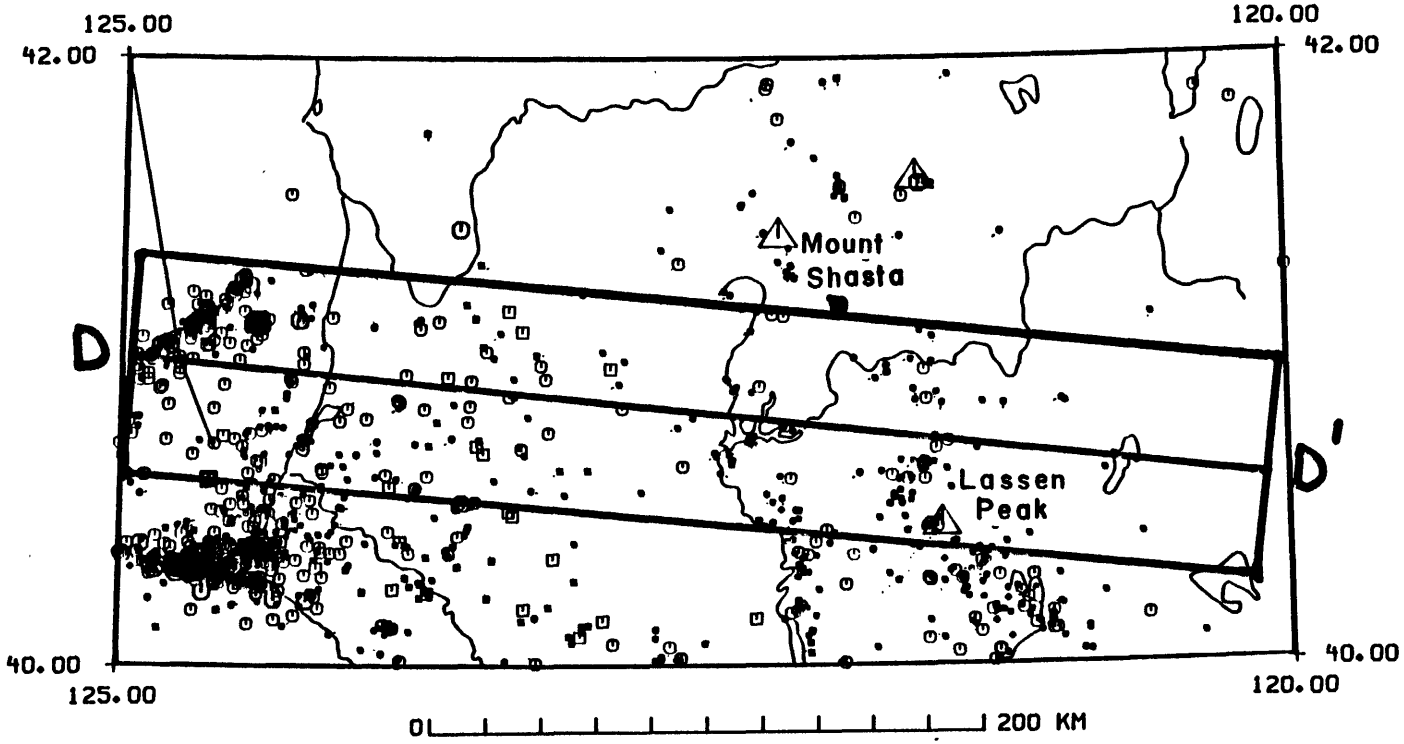

Figure 7: Location of northern California cross-section plotted in Figure 8. Squares are earthquakes below 30 km, circles are earthquakes above 30 km.

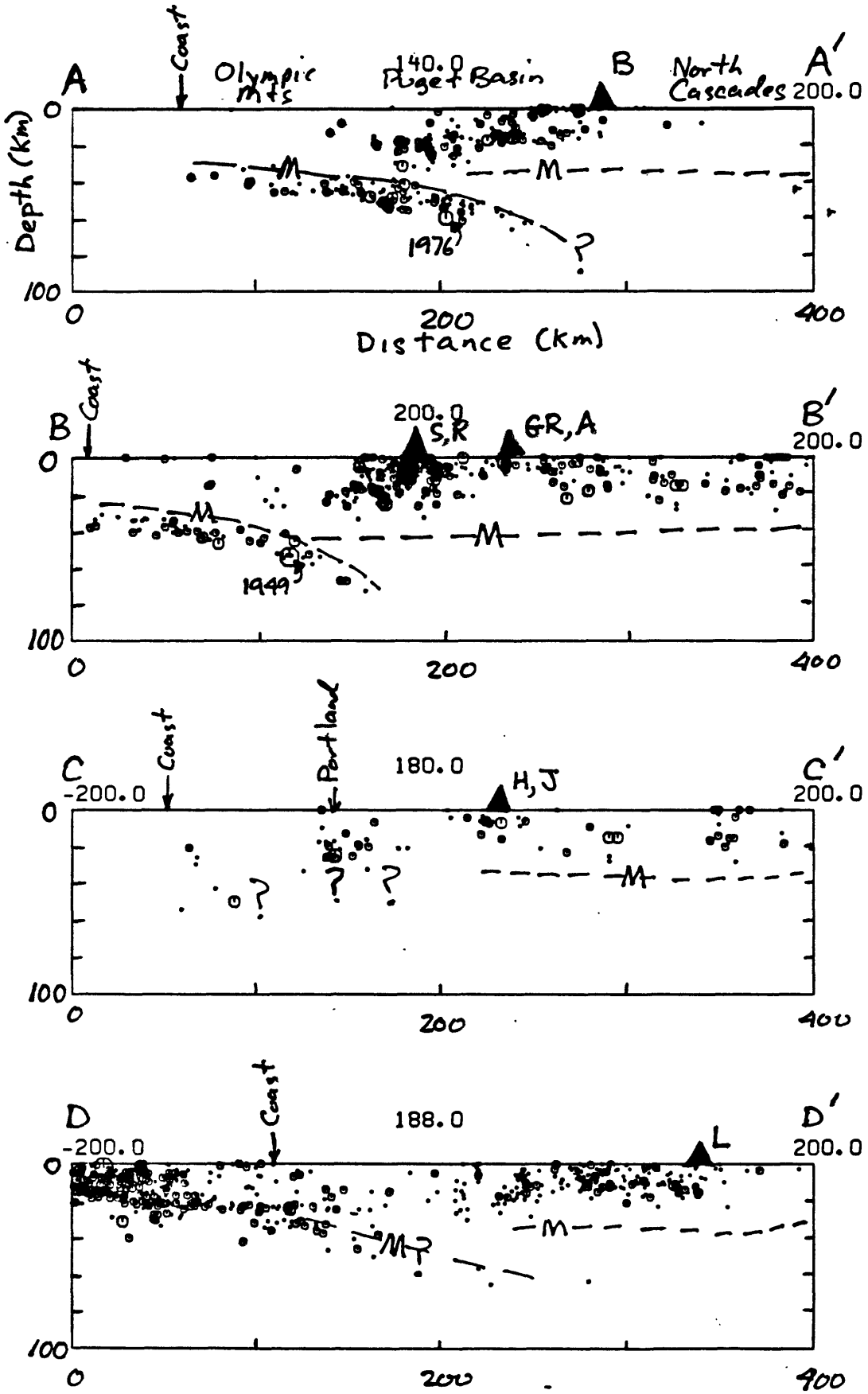

Figure 8: Cross-section plots, all 1:1. Section locations and orientation given in Figures 6 & 7. Moho depth from Figure 3 is indicated by the dashed lines.

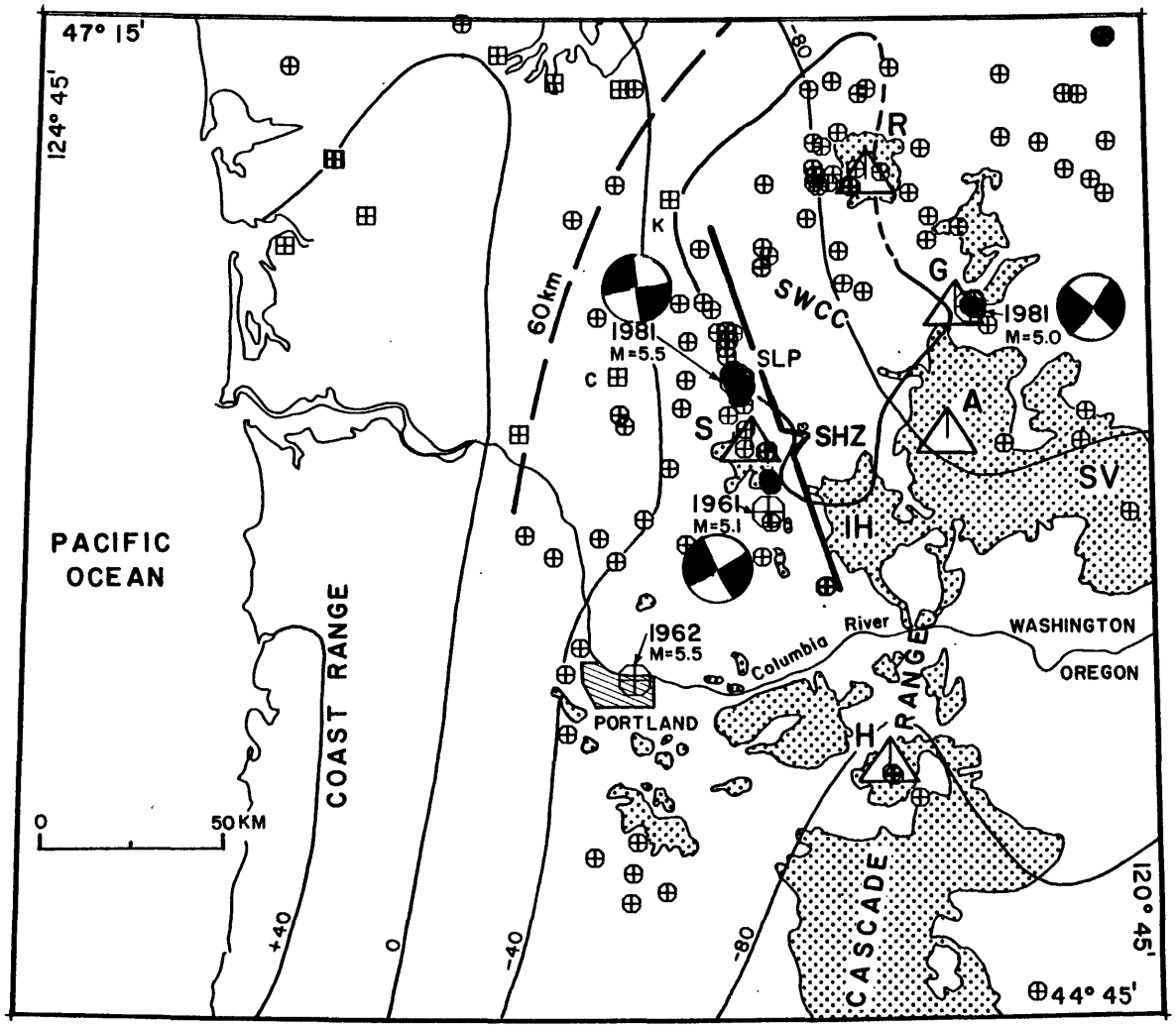

Figure 9: Seismicity and location of Southern Washington Cascade Conductor (SWCC). Conductor boundary from Stanley et al., 1987. Focal mechanism for the three magnitude 5+ events from summary provided by Ludwin et al. [1989]. Stipled area indicates extent of volcanics plotted in Figure 2.

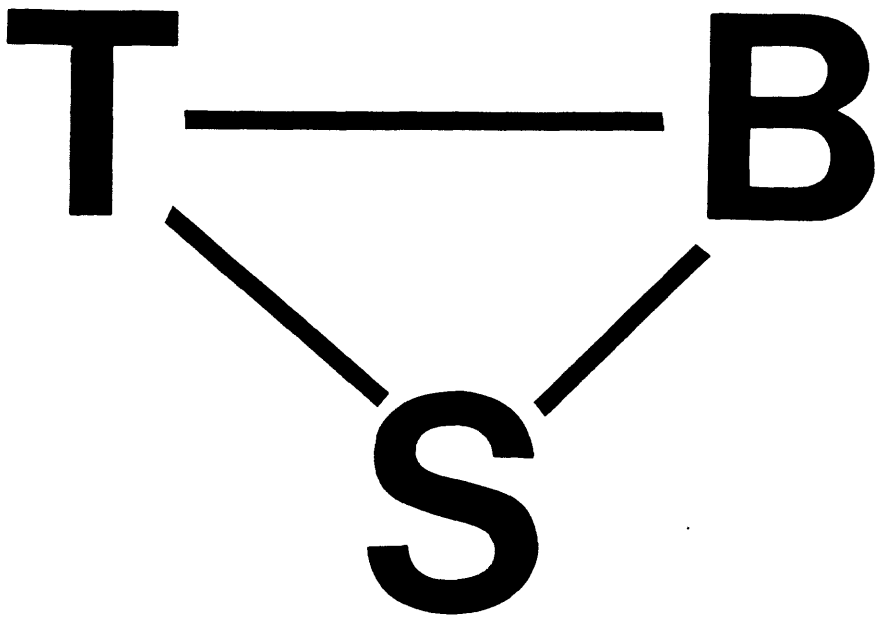

Figure 10: S-B-T triangular relation described in text. T represents crustal tectonics, B crustal blocks, and S subduction. Links between the three elements may vary as noted in text.

Quaternary extrusion rates from the Cascade Range, northwestern United States and British Columbia

David R. Sherrod and James G. Smith
U.S. Geological Survey, Menlo Park, California 94025

ABSTRACT

The Quaternary extrusion rate and style of eruption for the Cascade Range of the Pacific Northwest changes abruptly along the length of the volcanic arc. The Quaternary rate north of Mount Rainier is about 0.21 $km^3/km/m.y.$; in southern Washington and northern

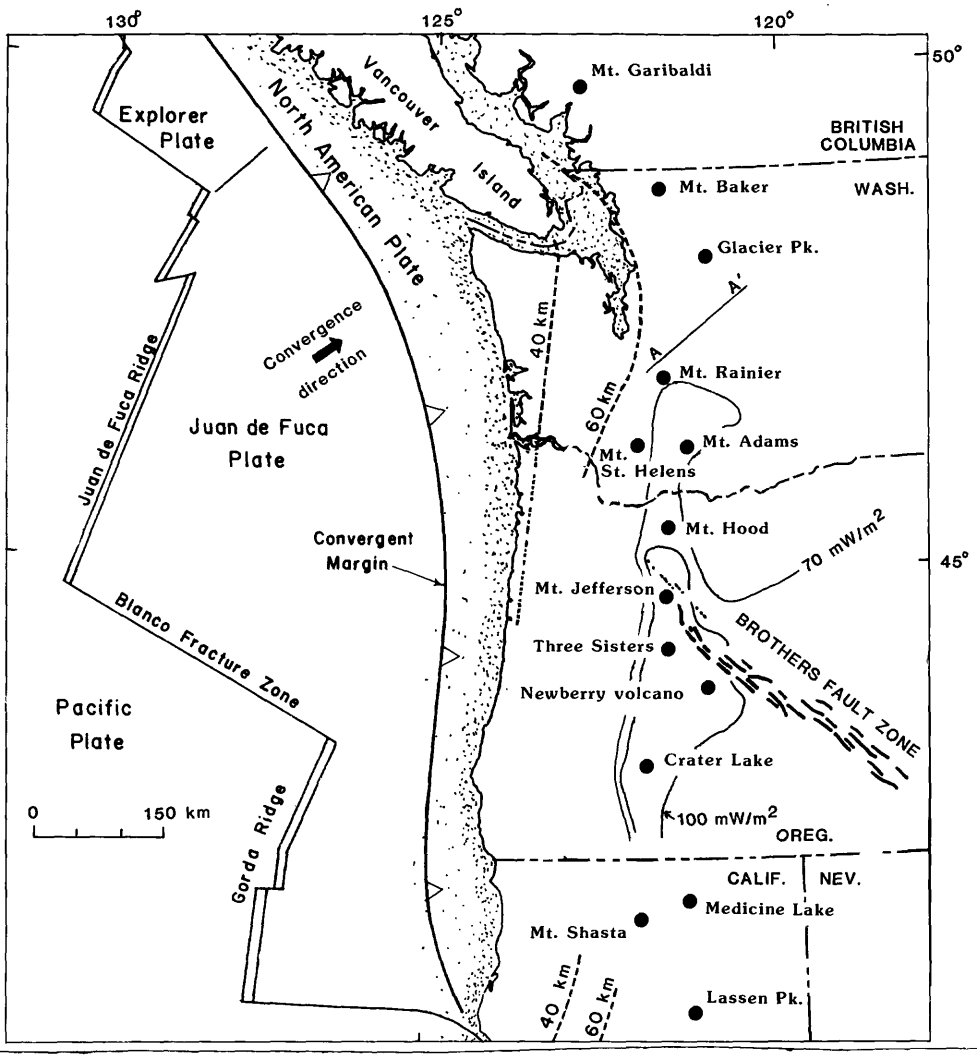

Figure 1. General setting of the Quaternary Cascade volcanic arc in western North America, modified from Guffanti and Weaver (1988). Dots locate major Quaternary volcanoes. Arrow on the Juan de Fuca plate indicates direction of present-day convergence between the Juan de Fuca and North American plates. Dashed lines are depth contours drawn on top of the Juan de Fuca plate under part of the Coast ranges as located by Weaver and Baker (1988); shown dotted where inferred. Line with saw teeth shows location of subduction zone marking the boundary between the Juan de Fuca and North American plates; sawteeth on upper plate. Line A-A' from Weaver and Michaelson (1985) divides the arc in Washington state into two segments. Heat-flow contours of 70 and 100 mW/m^2 from Blackwell and others (1989). Brothers fault zone from Walker and King (1969); its postulated extension shown dotted through Cascade Range (from Sherrod and Conrey, 1988).

Oregon as far south as Mount Hood, the rate is about 1.6 km^3/km/m.y. In contrast, the rate is 3 to 6 km^3/km/m.y. in central Oregon and 3.0 km^3/km/m.y. in northern California. For central Oregon, short- and long-term Quaternary extrusion rates have not varied significantly over intervals as short as 0.25 m.y.

Volcanic style changes at different latitudes than rate. Volcanic style at the ends of the arc is characterized by volcanism focused near isolated intermediate to silicic central volcanoes. These central volcanoes are ~30 percent of the total volcanic production along the arc. Mafic volcanic fields partly ring some central volcanoes, more so in the south than in the north, but they contribute less volume than central volcanoes along a corresponding length of arc. In contrast, diffuse volcanism characterizes the middle of the arc, a 260-km-long segment in central Oregon stretching from north of Mount Jefferson to south of Mount Mazama. Numerous overlapping mafic shields and a few central volcanoes have built a broad ridge.

Quaternary extrusion rate correlates closely with regional heat flow. That part of the arc in Washington and Oregon where extrusion rate is greater than 1.6 km^3/km/m.y. lies within the 70-mW/m^2 regional heat-flow contour. Different extrusion rates likely indicate zones of differing heat input. Contrasting volcanic style may signify diffuse versus focused heat sources or crustal changes in permeability to ascending magma along the arc. Both extrusion rate and volcanic style may be significant in the search for exploitable geothermal energy.

INTRODUCTION

In igneous-related geothermal systems, the rate of upper crustal magmatism is an important component of the shallow-level heat budget. Although the balance between volcanism and intrusion is difficult to assess, the extrusion rate may be a first-order approximation of the overall rate of magmatism.

Until the middle 1980's, reliable estimates of volume, timing, and extrusion rate for the Cascade Range volcanic arc of the United States could not be made for lack of sufficient isotopic ages and detailed geologic maps from which to draw the necessary stratigraphic and structural details. Our rate calculations are based on volumes measured while constructing 1:250,000- and 1:500,000-scale geologic compilation maps of the Cenozoic volcanic rocks of the Cascade Range in Washington, Oregon, and California (Smith, 1987, in press-a, in press-b; Sherrod, 1987; Sherrod and Smith, 1989). These maps are not merely reworkings of previously published data but instead rely largely on newly published and unpublished mapping and radiometric determinations completed since 1980.

We report here some surprising conclusions about the rates and volumes of Quaternary volcanism in the Cascade volcanic arc. In comparing different parts of the volcanic arc from British Columbia to California, we find that the extrusion rate changes abruptly along the arc's length, diminishing by an order of magnitude northward from Mount Rainier across a zone that matches an apparent seismic boundary suggested by Weaver and Michaelson (1985). Consequently, arc segments north and south of this boundary may have different resource potential for igneous-related geothermal energy.

GEOLOGIC SETTING

The Cascade volcanic arc reaches from British Columbia to northern California. It parallels the Pacific coastline and convergent margin between the North American and Juan de Fuca plates (fig. 1). In northern Washington and British Columbia, the arc lies 300 to 400 km east of the margin and is built largely upon lower Eocene and preTertiary sedimentary and crystalline rocks. In northern California, Oregon, and southern Washington, the Quaternary Cascade arc lies 250 to 300 km east of the convergent margin and is built upon upper Eocene and younger volcanogenic rocks.

In Washington, the most important components of Quaternary Cascade volcanism are the Indian Heaven and southern part of the Simcoe volcanic fields and six composite stratovolcanoes (Mount Baker, Glacier Peak, Mount Rainier, Goat Rocks, Mount Adams, and Mount St. Helens). In the Oregon part of the arc, Quaternary volcanic rocks form a continuous outcrop belt (High Cascades) that extends from Crater Lake northward to near Mount Hood (fig. 2). The northern and southern parts of Oregon have only a few small, discrete volcanic centers. In California, Quaternary volcanic rocks are areally extensive in a roughly triangular area whose corners are formed by Mount Shasta, Medicine Lake volcano, and Lassen Peak.

In the following discussion, the extrusion rate is normalized to cubic kilometers per kilometer of arc length per million years (km^3/km/m.y.). Except for low-density air-fall tephra, we did not adjust volumes of different eruptive products to dense-rock-equivalent magma; all volumes are shown as 1 or 2 significant figures. Thus the calculated extrusion rates are only approximate. However, as even these approximate rates differ by close to an order of magnitude for different segments of the arc, we predict our conclusions will not be modified greatly as more detailed mapping,

geochronology, and refined volume calculations become available.

Quaternary volcanism in northern Washington and southern British Columbia: Volume and extrusion rate

Quaternary volcanogenic rocks are not volumetrically abundant in this segment of the Cascade Range, which contains Mount Baker, Glacier Peak, Mount Garibaldi, and a few basalt flows and cinder cones between Glacier Peak and Mount Rainier. All known Quaternary volcanic rocks were erupted less than 1 Ma; volcanic rocks 1 to 2 Ma are unknown (table 1). This distribution suggests that volcanic production in this arc segment is episodic over intervals less than one million years. Volumes for some volcanoes are published. For others we estimated volumes by conventional methods, either subdividing the volcano into approximate regular geometric solids or using a planimeter to measure areas at successive elevations (Church, 1981).

The present cone of Mount Baker and underlying Pleistocene volcanoes erupted 72 km^3 of mainly andesite flows during the last 700 ka. The summit forms an impressive snow-covered peak over 3,200 m high, but the volcano is perched on a high bedrock ridge and thus its volume is much less than its summit elevation would suggest. A few flank flows, volcanic debris flows and tephra layers contribute less than 2 km^3 to the total volume. The next stratovolcano south along the arc, Glacier Peak, also sits on a bedrock ridge. The main cone, comprising dacite domes and short flows, contains only 6 km^3 of lava (Tabor and Crowder, 1969; R.L. Christiansen, U.S. Geological Survey, written commun., 1987). However, vigorous explosive activity resulted in deposition of about 20 km^3 of downstream debris- and pyroclastic-flow deposits (Beget, 1982) and about 3.4 km^3 of downwind tephra (reduced to an equivalent volume of dacite magma) (Porter, 1978).

A few cinder cones and short basalt flows between Glacier Peak and Mount Rainier account for 1.3 km^3 at most. The Mount Garibaldi volcanic field in southern British Columbia has a volume of approximately 26 km^3 (Mathews, 1958).

The Quaternary extrusion rate for the Cascade arc in northern Washington and southern British Columbia is ~0.21 km^3/km/m.y. (volume = 130 km^3; length from Mount Garibaldi to line A-A' (see figure 1) of Weaver and Michaelson (1985) = 310 km). Because all known volcanic deposits in this segment are younger than 1 Ma, the rate for the last million years is twice the Quaternary rate or ~0.42 km^3/km/m.y.

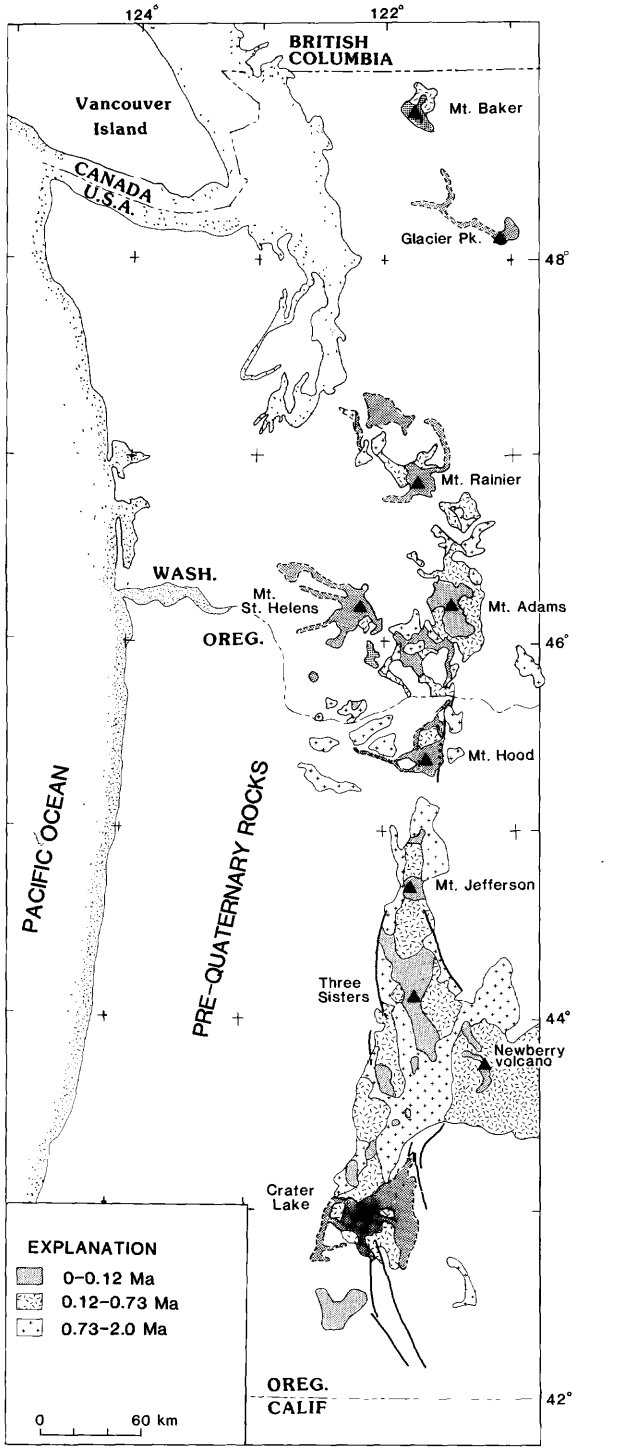

Figure 2. Generalized geologic map showing extent of Quaternary volcanic deposits in the Cascade Range of Washington and Oregon, generalized from Smith (in press a) and Sherrod and Smith (1989). Dashed contacts indicate downstream or distal debris-flow and pyroclastic-flow deposits from Glacier Peak and Mounts Rainier, St. Helens, Hood and Mazama.

Table 1. Amount of material extruded in Washington and southern British Columbia during the Quaternary period. Only tephra corrected to an equivalent volume of magma. Dash indicates no volcanic activity. All volumes and totals rounded to two significant figures.

	Volcano or field name	Volume (km^3)	
		0 to 1 Ma	1 to 2 Ma
1.	Mount Garibaldi, B.C.	26	—
2.	Mount Baker	72	—
3.	Glacier Peak	29	—
4.	Mafic flows between Glacier Peak and Mount Rainier	1.3	—
	total for northern Washington segment	130	—
5.	Mount Adams	210	—
6.	Small volcanoes north and south of Mount Adams	10	4.9
7.	Mount Rainier	140	—
8.	Goat Rocks volcano	10	30
9.	Hornblende andesite near Goat Rocks	15	—
10.	Basaltic shields north of Goat Rocks	20	—
11.	Mount St. Helens	79	—
12.	Indian Heaven volcanic field	34	27
13.	Small volcanoes in southern Washington	7	3.8
14.	Mount Hood	50	
15.	Small volcanoes in northern Oregon	5	5
	total for southern Washington-northern Oregon segment	580	71

Quaternary volcanism in southern Washington and northern Oregon: Volume and extrusion rate

Quaternary volcanism in southern Washington and northern Oregon contrasts in style and timing with volcanism in segments of the range to the north and south. Mafic and intermediate Quaternary volcanic vents are common. Andesitic and dacitic activity is concentrated at five stratovolcanoes: Mount Adams, Mount Rainier, Mount St. Helens, Goat Rocks, and Mount Hood. Goat Rocks is the only stratovolcano with rocks older than 1 Ma. Quaternary basaltic activity is found primarily in the Tumac Mountain area (20 km southeast of Mount Rainier), the Indian Heaven volcanic field, basaltic fields peripheral to Mount Adams, and in numerous, small isolated volcanoes located in the area between Vancouver, Wash., Mount St. Helens, Indian Heaven, and Mount Hood. Many vents in these areas erupted 1 to 2 Ma. However, in contrast to central Oregon, Quaternary volcanism in southern Washington and northern Oregon is limited to these centers and does not form a continuous outcrop belt of volcanic rocks (fig. 2).

Mount Adams, with a volume of about 210 km^3, is the most voluminous Quaternary stratovolcano in Washington. Widespread tephra layers and debris-flow deposits are not common in the volcano's history (Hildreth and others, 1983;Vallance, 1986), and 99 percent of the volume is contained in the main cone. Mount Adams is flanked on the north and south by several smaller basalt and andesite volcanoes. Their total volume is about 15 km^3 (Hammond and Korosec, 1983; and also our volume calculations).

Mount Rainier (140 km^3) is the second most voluminous stratovolcano in Washington. The volume of the main cone is about 86 km^3; large intracanyon lava flows that extend beyond the main cone contribute about 40 km^3; volcanic sedimentary deposits (Holocene

and Pleistocene) contribute about 14 km^3 (Smith, in press a). Tephra contributes less than 0.3 km^3.

Volcanism in the Goat Rocks area includes the largely eroded Goat Rocks stratovolcano, small-volume hornblende andesite volcanoes, and basaltic shields located between Goat Rocks and Tumac Mountain (Clayton, 1983). Goat Rocks volcano was active from 3 to 0.7 Ma, with probably two-thirds of its activity taking place in the Quaternary. It erupted approximately 40 km^3 during the Quaternary (Clayton, 1983, his table 2) of which we estimate 30 km^3 erupted between 1 and 2 million years ago. Hornblende andesite volcanoes north of Goat Rocks are all less than 2 Ma and erupted about 15 km^3 of lava (Clayton 1983, his table 2). Several basaltic shields between Goat Rocks volcano and Tumac mountain are less than 1 Ma and erupted 20 km^3 of lava and tuff (Clayton, 1983, his table 1).

Mount St. Helens (79 km^3), which began erupting only about 40 ka, is the youngest, most active, and most explosive stratovolcano in the Washington Cascade Range (Crandell and Mullineaux, 1978). The main cone contains about 25 km^3. Flank flows beyond the main cone total less than 0.5 km^3. Extensive debris and pyroclastic flows, which choke the surrounding valleys, account for 6 to 8 km^3 (Crandell and Mullineaux, 1973). There are no published volumes of tephra layers erupted before May, 1980. However, Sarna-Wojcicki and others (1981) compared volume and thickness at arbitary distances from vents for modern ash-fall deposits and constructed an empirical curve for estimating volume from thickness known at a given distance. Their results for May 18th deposits from Mount St. Helens agree well for volume calculated from the curve and from isopach maps. Using this curve, they calculated the volume of Mount St. Helens tephra layer Y_n: 4.5-5 km^3. Since Y_n forms 45 percent (by thickness) of tephra set Y (all thickness measurements made 8 to 10 km downwind and reported in Mullineaux, 1986), then tephra set Y is 10-11 km^3, which agrees well with the estimate made by Crandell and Mullineaux (1973). Applying this technique to the 1.46-m total thickness of Mount St. Helens tephra at 8-10 km from source (Mullineaux, 1986), we calculate 73 km^3 of uncompacted tephra or 47 km^3 of dense-rock-equivalent dacite.

Mount Hood (50 km^3) is a Quaternary volcano built chiefly of andesite (Wise, 1969). Dacite is limited to the products of the last 15,000 yrs (Crandell, 1980). Its cone overlaps a few basaltic andesite shields.

The Indian Heaven volcanic field, located between Mount Adams and Mount St. Helens, forms the largest volume of Quaternary mafic volcanic rocks in Washington (Church and others, 1983). Hammond (unpublished data) estimated its volume at just over 70 km^3, of which 34 km^3 has erupted in the last 1 Ma (P.E. Hammond, Portland State University, written commun., 1985).

More than 30 small-volume volcanoes, mostly basalt and basaltic andesite, have been mapped between Vancouver, Wash., Mount St. Helens, the Indian Heaven volcanic field, and Mount Hood (Phillips, 1987a and b; Korosec, 1987a and b; Sherrod and Smith, 1989; Smith in press a). The largest volcano contains less than 3 km^3 and all these volcanoes add only some 20 km^3 to the total volume in southern Washington and northern Oregon.

The Quaternary extrusion rate for the Cascade arc in southern Washington and northern Oregon is about 1.6 km^3/km/m.y. (volume = ~648 km^3; length from line A-A' of Weaver and Michaelson (1985) to Mount Hood = 200 km). The extrusion rate for just the last million years is higher, 2.9 km^3/km/m.y., because the major stratovolcanoes are relatively young. The rate for 0 to 1 Ma in this segment is approximately equal to the rate in central Oregon, but the Quaternary rate is less.

Quaternary volcanism in central Oregon: Volume and extrusion rate

In central Oregon, the volcanic arc has built a broad ridge that extends for 260 km from north of Mount Jefferson to south of Crater Lake (fig. 2). Basaltic andesite and basalt generally predominate; they were erupted from cinder cones and shield volcanoes, some as large as 15 km^3. Andesite, dacite, and rhyolite are concentrated near the composite volcanoes Mount Jefferson (14 km^3), Three Sisters-Broken Top (36 km^3), and Mount Mazama (130 km^3).

For the central Oregon High Cascades from Mount Jefferson to Crater Lake, we calculated long- and short-term extrusion rates by different methods. We calculated the long-term rate by drawing numerous cross sections that represent the thickest and thinnest parts of the volcanic arc. Each cross section was assigned a width of one kilometer to obtain a representative cross sectional volume. For stratigraphic and structural reasons, the base of the modern Cascade arc includes rocks as old as 3.5 Ma (Sherrod, 1986). The long-term extrusion rate ranges from 3 to 6 km^3/km/m.y. (table 2).

We calculated short-term extrusion rates for the intervals 0.73 to 0.25 Ma and 0.25 to 0 Ma in the central Oregon Cascade Range by using the conventional geometric method of cones, frustums, and prisms because the rocks are sufficiently well exposed, mapped and dated (Sherrod, 1986; Taylor and others, 1987). The

Table 2. Extrusion rate for upper Pliocene and Quaternary volcanic rocks, Cascade Range of central Oregon

Age	Volume per km	Extrusion rate $km^3/km/m.y.$
3.5-0 Ma	10 to 20 km^3	3 to 6
0.73-0.25 Ma	1.8	3.8
0.25-0 Ma	1.0	4.0
7500-0 yrs ago	0.01	1.3

rate is constant at about 4 $km^3/km/m.y.$ for those two time intervals, which indicates no discernible lessening of volcanic rate (table 2). Within the error of the method, we consider the long- and short-term rates to be the same.

Rates over shorter intervals are difficult to assess, however, because single eruptive events can bias the very short-term rate. Between latitudes 43°-44° N, a very short-term rate of 1.3 $km^3/km/m.y.$ was calculated for rocks younger than Mazama ash, a widespread air-fall tephra deposited during climatic eruptions at Crater Lake (3 km south of lat. 43° N) about 6845±50 ^{14}C yrs ago (7500 calendar years ago) (Bacon, 1983). We put no significance in this low rate because we believe that the time interval is too short to be statistically meaningful. Indeed, the Holocene extrusion rate exceeds 50 $km^3/km/m.y.$ when Crater Lake-related volcanic rocks (south of latitude 43°) are combined with High Cascades lava erupted between latitudes 43°-44° N. This conclusion echoes that of Sample and Karig (1982), who found from their study of the Mariana arc that "pulses of igneous activity at individual centers . . . can dominate the extrusion rates for periods of perhaps 100,000 years."

The Quaternary extrusion rate diminishes slightly in northern and southern Oregon. North of Mount Jefferson, Quaternary volcanic rocks are mostly older than 0.73 Ma, and even these rocks pinch out south of Mount Hood (fig. 2). Similarly the rate falls off south of Crater Lake in southern Oregon as the style of arc volcanism changes from numerous small-volume basaltic andesite shields to two large-volume stratocones: Mount Shasta and Lassen Peak. Cones in the Mount McLoughlin area of southern Oregon contain less than 40 km^3 of lava and near-vent tephra (Mount McLoughlin, 13 km^3; Pelican Butte, 20 km^3; Browns Mountain, 5 km^3). Eruptions farther south comprise a few cinder cones and small-volume lava flows too small to show at the scale of figure 2.

Quaternary volcanism in northern California: Volume and extrusion rate

Volume calculations for California are not as detailed as for other parts of the arc because existing mapping is not as detailed. However, the two volcanic centers of Mount Shasta and Lassen Peak dominate this section of the arc.

Mount Shasta's cone has a volume of about 350 km^3, all of which erupted in the last 0.73 Ma. Its associated 300-ka landslide adds an additional 45 km^3 (Crandell, in press) to the total. Smaller Quaternary volcanoes that ring Mount Shasta on 3 sides account for another 121 km^3; approximately 70 km^3 erupted 1 to 2 Ma and 51 km^3 erupted 0 to 1 Ma. The Lassen Peak volcanic center contains approximately 200 km^3 of lava, all erupted in the last 0.73 Ma (M.A. Clynne, U.S. Geological Survey, oral commun., 1988). Extensive areas of calc-alkaline Quaternary volcanic rocks, indistinguishable from volcanic rocks elsewhere in the Cascade Range, crop out between Lassen Peak and Susanville, Calif. A conservative estimate of their volume is about 350 km^3.

Using the above volumes, the Quaternary extrusion rate for the Cascade arc in California is about 3.0 $km^3/km/m.y.$ (volume = 1066 km^3; length from latitude 42° to Susanville, Calif. = 180 km).

DISCUSSION

Along-arc variation in extrusion rate

The extrusion rate diminishes by a factor of 5-15 north of Mount Rainier. This geographic division coincides with a seismically defined boundary between segments of the Cascade arc (Weaver and Michaelson, 1985). Weaver and Michaelson, who reported on pre-

sent-day seismicity patterns in northern Oregon and Washington, drew their boundary parallel to the direction of convergence between the Juan de Fuca and North American plates. Guffanti and Weaver (1988) recognized the same segment boundary on the basis of vent distribution; substantially fewer vents are located north of Mount Rainier. The abrupt change in extrusion rate indicates that the segment boundary may have significance beyond the location of earthquake hypocenters.

This boundary also separates areas of contrasting heat flow (Duffield, 1983). Heat flow ranges from 50 to 70 mW/m^2 north of Mount Rainier; regional heat flow is greater than about 100 mW/m^2 in the Cascade arc of central and southern Oregon (fig.1; Blackwell and others, 1989).

Along-arc variation in style of volcanism

Figure 3 shows extruded volume versus arc length for the Cascade Range. The contributions from the major composite volcanoes form pronounced spikes on the volume-latitude plot (e.g., Mounts Adams and Rainier in Washington), whereas the volume of the numerous basalt and basaltic andesite shields in the central Oregon part of the arc is distributed over a wide latitude. Thus, the volume-latitude plot shows a change in volcanic style from large, localized centers in southern Washington and northern Oregon to a broad, extensive accumulation of lava flows in central Oregon and back to localized centers in California.

In northern Oregon, the transition in volcanic style occurs between Mounts Jefferson and Hood, and roughly coincides with the projection of the Brothers fault zone, which may pass through the Cascade Range north of Mount Jefferson (Smith, 1986; Sherrod and Conrey, 1988) (fig. 1). The Brothers fault zone (Walker, 1969) accommodates differential extension and faulting between the Blue Mountains province to the north and the Basin-Range province to the south (Lawrence, 1976; Walker and Nolf, 1981). Presumably the change in style of Quaternary volcanism in the Cascade Range results from relatively greater deviatoric stress that promotes extension south of Mount Hood. In such an environment, magma would be expected to rise rapidly along dikes, with less chance of differentiating to intermediate and silicic compositions (Hildreth, 1981).

A similar transition from extensive volcanic platform to localized large stratocones occurs south of Crater Lake. In this location, however, there is no evidence for a structural boundary east of the arc that separates regions of contrasting extensional deformation, as is the case across the Brothers fault zone farther north. Guffanti and Weaver (1988) postulated a segment boundary at about the Oregon-California boundary on

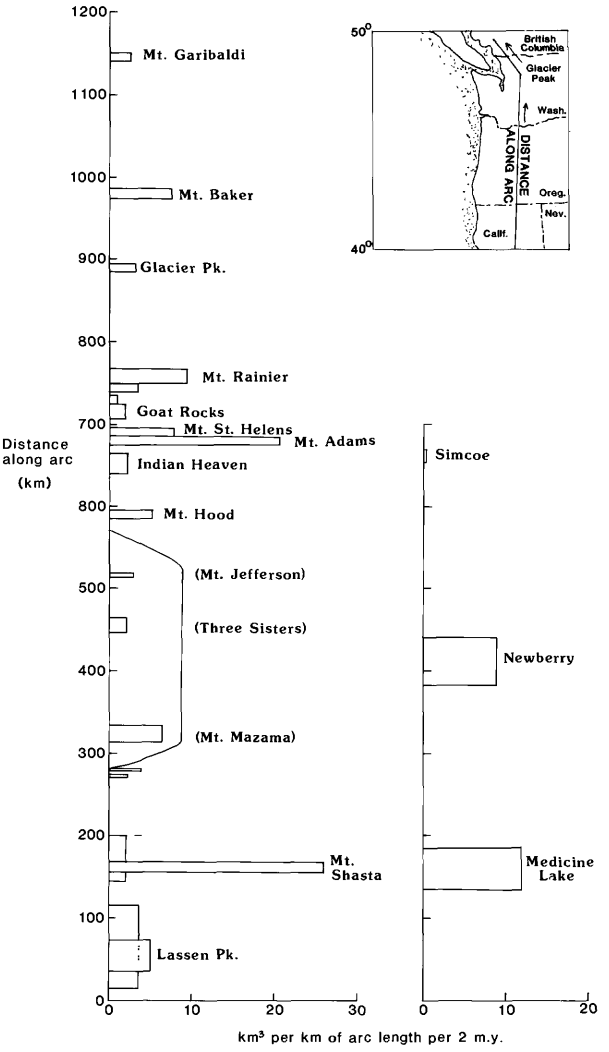

Figure 3. Graph showing extrusion rate per km per 2 m.y. (Quaternary) for Cascade arc from Lassen Pk to Mount Garibaldi. Vertical axis is distance along arc, measured north from lat 40°N (0 km) to Glacier Peak (890 km) and northwest from Glacier Peak to Mount Garibaldi (see inset). Medicine Lake, Newberry, and Simcoe volcanoes shown with separate vertical axis (same horizontal axis) because they are east of the main arc. Boxes for individual volcanoes drawn so that base of box equals basal diameter of volcano along arc length, and area of box equals Quaternary volume. Mount Jefferson, Three Sisters-Broken Top, and Mount Mazama labeled parenthetically because their volume is part of the continuous belt of Quaternary volcanic rocks in the High Cascades of central Oregon; their volumetric contribution is shown.

Table 3. Comparison of extrusion and convergence rates from volcanic arcs.

Arc	Extrusion rate $km^3/km/m.y.$	Convergence rate cm/yr
Lesser Antilles	3 to 5	2 to 3.7
Cascade Range (Jefferson to Shasta)	3 to 6	2 to 3
Marianas	12	
Central America	31	8.1

the basis of a changing ratio of andesitic and basaltic vents as defined by Luedke and Smith (1981, 1982). This putative compositional change has no basis in published chemical analyses, but results from the arbitrary age and composition categorization of rocks by Luedke and Smith.

The Quaternary volcanoes of Medicine Lake (≈ 600 km^3, Donnelly-Nolan, 1985) and Newberry (≈ 450 km^3, MacLeod and Sherrod, 1988) are two large shield-like volcanic landforms east of the Cascade Range. Though not included in this calculation of extrusion rates, each of their volumes exceeds the volume erupted along an equivalent length of the axis of the Cascade Range to the west. The Simcoe volcanic field, which lies east of the Cascade Range in Washington, is dominantly basaltic in composition and Pliocene in age (Anderson, 1987a, b); it contains about 5.2 km^3 of lava estimated to be 1 to 2 Ma (Smith, in press a; our volume calculations). The genetic relation of these volcanoes to the Cascade Range is unknown.

In our opinion, the contrasting style of Quaternary volcanism along the Cascade arc led previous workers to an erroneous conclusion concerning changes of volume and rate. McBirney and White (1982) suggested that the total volume of Cascade Quaternary rock in Washington and California is small compared to Oregon. According to our calculations, however, the southern Washington and northern California volumes are only slightly smaller than the central Oregon volume, and the difference may further diminish with more detailed calculations. Clearly, the large stratocones of Mounts Adams and Rainier in Washington (347 km^3 combined volume) or Mount Shasta in California (395 km^3) contain as much Quaternary volcanic rock as 30 to 70 km of arc length in central Oregon.

Rates at other arcs

For comparison, extrusion rates from the Cascade and other volcanic arcs are listed in table 3. Wadge (1984) suggested that convergence rate at a plate boundary might be broadly correlated with volcanic vigor, and the Cascade data generally support this contention. Within the Cascade arc, however, the geometry seems contradictory: extrusion rate is lowest where convergence presumably should be highest—that part of the arc oriented normal to the convergence direction (north of Mount Rainier). One explanation is that relatively greater crustal contraction in the Cascade arc of northern Washington and British Columbia accounts for the lesser amount of volcanism (Rogers, 1985; Weaver and Michaelson, 1985). If so, the crustal stress regime of the overriding plate becomes a first-order control on extrusion rate (though perhaps not intrusion rate), at least in arcs with low convergence rates.

ACKNOWLEDGMENTS

This work results partly from regional mapping and compilation done in conjunction with the U.S. Geological Survey's Geothermal Research Program. We thank C. Dan Miller for his review of the manuscript.

REFERENCES CITED

Anderson, J.L., 1987a, Geologic map of the Klickitat 15-minute quadrangle, Washington: Washington Department of Natural Resources, Division of Geology and Earth Resources Open File Report 87–14, scale 1:38,400, 1 sheet, plus 13 p.

Anderson, J.L., 1987b, Geologic map of the Goldendale 15' quadrangle, Washington: Washington Department of Natural Resources, Division of Geology and Earth Resources Geological Open File Report 87–15, scale 1:38,400, 1 sheet, plus 9 p.

Beget, J.E., 1982b, Recent volcanic activity at Glacier Peak: Science, v. 215, no. 4538, v. 215, p. 1389-1390.

Bacon, C.R., 1983, Eruptive history of Mount Mazama, Cascade Range, U.S.A.: Journal of Volcanology and Geothermal Research, v. 18, p. 57-115.

Blackwell, D.D., Bowen, R.G., Hull, D.A., Riccio, Joseph, and Steele, J.L., 1982a, Heat flow, arc volcanism, and subduction in northern Oregon: Journal of Geophysical Research, v. 87, no. B10, p. 8735-8754.

Blackwell, D.D., Priest, G., Black, G., Schuster, E., and Korosec, M., 1982b, Heat flow, gravity, and magmatism in the Cascade Range of the Pacific Northwest: Eos (Transactions, American Geophysical Union), v. 63, no. 45, p. 1091.

Blackwell, D.D., Steele, J.L., Frohme, M.K., Murphy, C.F., Priest, G.R., and Black, G.L., 1989, Heat flow in the Oregon Cascade Range and its correlation with regional gravity, magnetic, and geologic patterns, *in* Muffler, L.J.P., Blackwell, D.D., and Weaver, C. S., eds., Geology, geophysics, and tectonic setting of the Cascade Range: U.S. Geological Survey Open-File Report (this volume).

Church, H.K., 1981, Excavation Handbook: New York, McGraw-Hill, 1 volume.

Church, S.E., Hammond, P.E., and Barnes, D.J., 1983, Mineral resource potential of the Indian Heaven Roadless Area, Skamania County, Washington: U.S. Geological Survey Open-File Report 83-467, 9 p.

Clayton, G.A., 1983, Geology of the White Pass area, south-central Cascade Range, Washington: Seattle, University of Washington, M.S. thesis, 212 p.

Crandell, D.R., in press, Gigantic debris avalanche of Pleistocene age from ancestral Mount Shasta volcano California, and debris-avalanche hazard zonation: U.S. Geological Survey Bulletin.

Crandell, D.R., and Mullineaux, D.R., 1973, Pine Creek volcanic assemblage at Mount St. Helens, Washington: U.S. Geological Survey Bulletin 1383-A, 23 p.

Crandell, D.R., and Mullineaux, D.R., 1978, Potential hazards from future eruptions of Mount St. Helens volcano, Washington: U.S. Geological Survey Bulletin 1383-C, 25 p.

Donnelly-Nolan. J.M., 1985, Geothermal potential of Medicine Lake volcano, in Guffanti, Marianne, and Muffler, L.J.P., eds., Proceedings of the workshop on geothermal resources of the Cascade Range: U.S. Geological Survey Open-File Report 85-521, p. 34-36.

Duffield, W.A., 1983, Geologic framework for geothermal energy in the Cascade Range: Geothermal Resources Council Transactions, v. 7, p. 243-246.

Guffanti, Marianne, and Weaver, C.S., 1988, Distribution of late Cenozoic volcanic vents in the Cascade Range: volcanic arc segmentation and regional tectonic considerations: Journal of Geophysical Research, v. 93, no. B6, p. 6513-6529.

Hammond, P.E., and Korosec, M.A., 1983, Geochemical analyses, age dates, and flow-volume estimates for Quaternary volcanic rocks, southern Cascade Mountains, Washington: Washington Department of Natural Resources, Division of Geology and Earth Resources Open-File Report 83-13, scale 1:125,000, 1 sheet, plus 36 p.

Hildreth, Wes, 1981, Gradients in silicic magma chambers: Implications for lithospheric magmatism: Journal of Geophysical Research, v. 86, no. B11, p. 10,153-10,192.

Hildreth, Wes, and Fierstein, Judy, 1983, Mount Adams volcano and its 30 "parasites" [abs.]: Geological Society of America Abstracts with Programs, v. 15, no. 5, p. 331.

Korosec, M.A., 1987a, Geologic map of the Mount Adams [1° by 30'] quadrangle, Washington: Washington Department of Natural Resources, Division of Geology and Earth Resources Open File Report 87-5, scale 1:100,000, 1 sheet, plus 41 p.

Korosec, M.A., 1987b, Geologic map of the Hood River [1° by 30'] quadrangle, Washington and Oregon: Washington Department of Natural Resources, Division of Geology and Earth Resources Open File Report 87-6, scale 1:100,000, 1 sheet, plus 42 p.

Lawrence, R.D., 1976, Strike-slip faulting terminates the Basin and Range province in Oregon: Geological Society of America Bulletin, v. 87, no.6, p. 846-850.

Luedke, R.G., and Smith, R.L., 1981, Map showing distribution, composition, and age of late Cenozoic volcanic centers in California and Nevada: U.S. Geological Survey Miscellaneous Investigations Map I-1091-C, scale 1:1,000,000.

———1982, Map showing distribution, composition, and age of late Cenozoic volcanic centers in Washington and Oregon: U.S. Geological Survey Miscellaneous Investigations Map I-1091-D, scale 1:1,000,000.

MacLeod, N.S., and Sherrod, D.R., 1988, Geologic evidence for a magma chamber beneath Newberry volcano, Oregon: Journal of Geophysical Research, v. 93, no. B9, p. 10,067-10,079.

Mathews, W.H., 1958, Geology of the Mount Garibaldi map area, Southwestern British Columbia, Canada. Part II: Geomorphology and Quaternary volcanic rocks: Geological Society of America Bulletin, v. 69, no. 2, p. 179-198.

McBirney, A.R., and White, C.M., 1982, The Cascade Province, in Thorpe, R.S., ed., *Andesites: Orogenic andesites and related rocks*: New York, John Wiley and Sons, p. 115-135.

Mullineaux, D.R., 1986, Summary of pre-1980 tephra-fall deposits erupted from Mount St. Helens, Washington: Bulletin of Volcanology, v. 48, no. 1, p. 17-20.

Phillips, W.M., 1987a, Geologic map of the Mount St. Helens [1° by 30'] quadrangle, Washington: Washington Department of Natural Resources, Division of Geology and Earth Resources Open File Report 87-4, 59 p.

Phillips, W.M., 1987b, Geologic map of the Vancouver [1° by 30'] quadrangle, Washington: Washington Department of Natural Resources, Division of Geology and Earth Resources Open File Report 87-10, scale 1:100,000, 1 sheet plus 32 p.

Porter, S.C., 1978, Glacier Peak tephra in the north Cascade Range, Washington: Stratigraphy, distribution, and relationship to late glacial events: Quaternary Research v. 10, p. 30-41.

Rogers, G.C., 1985, Variation in Cascade volcanism with margin orientation: Geology, v. 13, no. 7, p. 495-498.

Sample, J.C., and Karig, D.E., 1982, A volcanic production rate for the Mariana Island arc: Journal of Volcanology and Geothermal Research, v. 13, p. 73-82.

Sarna-Wojcicki, A.M., Shipley, Susan, Waitt, R.B., Dzurisin, Daniel, and Wood, S.H., 1981, Areal distribution, thickness, mass, volume, and grain size of air-fall ash from the six major eruptions of 1980, *in* Lipman, P.W, and Mullineaux, D.R., eds., The 1980 eruptions of Mount St. Helens, Washington: U.S. Geological Survey Professional Paper 1250, p. 577-600.

Sherrod, D.R., 1986, Geology, petrology, and volcanic history of a portion of the Cascade Range between latitudes 43°- 44° N., central Oregon, U.S.A.: Santa Barbara, University of California, Ph.D. dissertation, 320 p.

———1987, New compilation map of the Cascade Range in Oregon: Geothermal Resources Council Transactions, v. 11, p. 305-307.

Sherrod, D.R., and Conrey, R.M., 1988, Geologic setting of the Breitenbush-Austin Hot Springs area, Cascade Range, north-central Oregon, *in* Sherrod, D.R., ed., Geology and geothermal resources of the Breitenbush-Austin Hot Springs area, Clackamas and Marion Counties, Oregon: Oregon Department of Geology and Mineral Industries Open-File Report O-88-5, p. 1-14.

Sherrod, D.R., and Smith, J.G., 1989, Preliminary map of upper Eocene to Holocene volcanic and related rocks of the Cascade Range, Oregon: U.S. Geological Survey Open-File Report 89-14, scale 1:500,000.

Smith, G.A., 1986, Stratigraphy, sedimentology, and petrology of Neogene rocks in the Deschutes basin, central Oregon: A record of continental-margin volcanism and its influence on fluvial sedimentation in an arc-adjacent basin: Richland, Washington, Rockwell Hanford Operations Publication RHO-BW-SA-555 P, variously paged.

Smith, J.G., 1987, New compilation geological map of the Cascade Range in Washington: Geothermal Resources Council Transactions, v. 40, p. 309-314.

Smith, J.G., in press a, Geologic map of Upper Eocene to Holocene volcanic and related rocks in the Cascade Range, Washington: U.S. Geological Survey Miscellaneous Investigations Map, scale 1:500,000.

Smith, J.G., in press b, Geologic map of Upper Eocene to Holocene volcanic and related rocks in the Yakima 1° by 2° quadrangle, south-central Washington: U.S. Geological Survey Miscellaneous Investigations Map, scale 1:250,000.

Tabor, R.W., and Crowder, D.F., 1969b, On batholiths and volcanoes—Intrusion and eruption of Late Cenozoic magmas in the Glacier Peak area, North Cascades, Washington: U.S. Geological Survey Professional Paper 604, 67 p.

Taylor, E.M., MacLeod, N.S., Sherrod, D.R., and Walker, G.W., 1987, Geologic map of the Three Sisters Wilderness, Deschutes, Lane, and Linn Counties, Oregon: U.S. Geological Survey Miscellaneous Field Studies map MF-1952, scale 1:63,360.

Vallance, J.W., 1986, Late Quaternary volcanic stratigraphy of the southwestern flank of Mount Adams volcano, Washington: Boulder, University of Colorado, Ph.D dissertation, 120 pages.

Wadge, 1984, Comparison of volcanic production rates and subduction rates in the Lesser Antilles and Central America: Geology, v. 12, no. 9, p. 555-558.

Walker, G.W., 1969, Geology of the High Lava Plains province, *in* A.E. Weissenborn, ed., Mineral and Water Resources of Oregon: Oregon Department of Geology and Mineral Industries Bulletin 64, p. 77-79.

Walker, G.W., and Nolf, Bruce, 1981, High Lava Plains, Brothers fault zone to Harney Basin, Oregon, *in* Johnston, D.A., and Donnelly-Nolan, Julie, eds., Guides to some volcanic terranes in Washington, Idaho, Oregon, and northern California: U.S. Geological Survey Circular 838, p. 105-118.

Weaver, C.S., and Baker, G.E., 1987, Geometry of the Juan de Fuca plate beneath Washington from seismicity: Bulletin of the Seismological Society of America, v. 78, no. 1, p. 264-275.

Weaver, C.S., and Michaelson, C.A., 1985, Seismicity and volcanism in the Pacific Northwest: evidence for the segmentation of the Juan de Fuca plate: Geophysical Research Letters, v. 12, no. 4, p. 215-218.

Wise, W.S., 1969, Geology and petrology of the Mt. Hood area: A study of High Cascade volcanism: Geological Society of America Bulletin, v. 80, no. 6, p. 969-1006.

THERMAL STRUCTURE OF THE NORTHERN (CANADIAN) CASCADES

T. J. Lewis, W. H. Bentkowski, E. E. Davis, R. D. Hyndman, J. G. Souther[1] and J. A. Wright[2]

Geological Survey of Canada
Pacific Geoscience Centre, Box 6000, SIDNEY, B.C. V8L 4B2

In southwestern British Columbia the heat flux above the presently subducting Juan de Fuca plate varies from 25 to several hundred mW m^{-2}. Heat is absorbed in the warming of the descending lithosphere and in the dehydration of the oceanic crust, producing a small, decreasing heat flux above the descending oceanic crust and a very thick, cool continental crust as the volcanic arc is approached. An abrupt transition from low values to 70-80 mW m^{-2} occurs 30 km seaward of the Garibaldi Volcanic Belt, similar to the contrast measured in Oregon (Blackwell et al, 1982). The very large, local variations in heat flux within this belt are postulated to be the result of advective cooling of intruded magmas. Although some water flows are driven through the crystalline rock by the large hydrologic heads caused by the rugged topography, our limited data suggest that they do not transport significant amounts of heat compared to the observed conductive heat flow. Marine measurements from a southern fjord were used to define the large transition in heat flux ocurring over a 20-km width above the subducting Juan de Fuca plate. The apparent heat source at a depth of 10 km is thought to be circulating hot water, heated while cooling deeper magmas. The transition in heat flux may not be as abrupt south of the Coast Plutonic Complex. Low radioactive heat generation is measured on surface samples and postulated at depth. East of the Coast Plutonic Complex is a heat-flow province with a high reduced heat flow of 58 mW m^{-2}.

INTRODUCTION

The rugged Cordillera has been created by various dynamic processes that are dominated by past and present plate tectonic motions and interactions. A summary of the models proposed for the Canadian Cordillera together with the geological record and geophysical data that support them is given by Gabrielse and Yorath (DNAG volume: Geology of Canada Series: Cordilleran Orogen, Canada, in prep.). Recent investigations of the convergent continental margin of southwestern Canada, phase I of the LITHOPROBE multidisciplinary geoscience program [e.g., Clowes et al., 1984; Geological Association of Canada, 1985] included the geology [e.g., Yorath et al., 1985a] and an interpretation of the multichannel seismic reflection profile on land and the offshore continuation [Clowes et al., 1987; Yorath et al., 1985b] shown in Figure 1. Studies across the Vancouver Island margin also included seismic refraction, magnetotelluric, seismicity, heat flow, gravity, and magnetic surveys, as well as paleomagnetic, geochronological, and isotope studies.

[1]100 West Pender Street, Vancouver, B. C. V6B 1R8
[2]Memorial University of Newfoundland, St. John's, Newfoundland, A1C 5S7

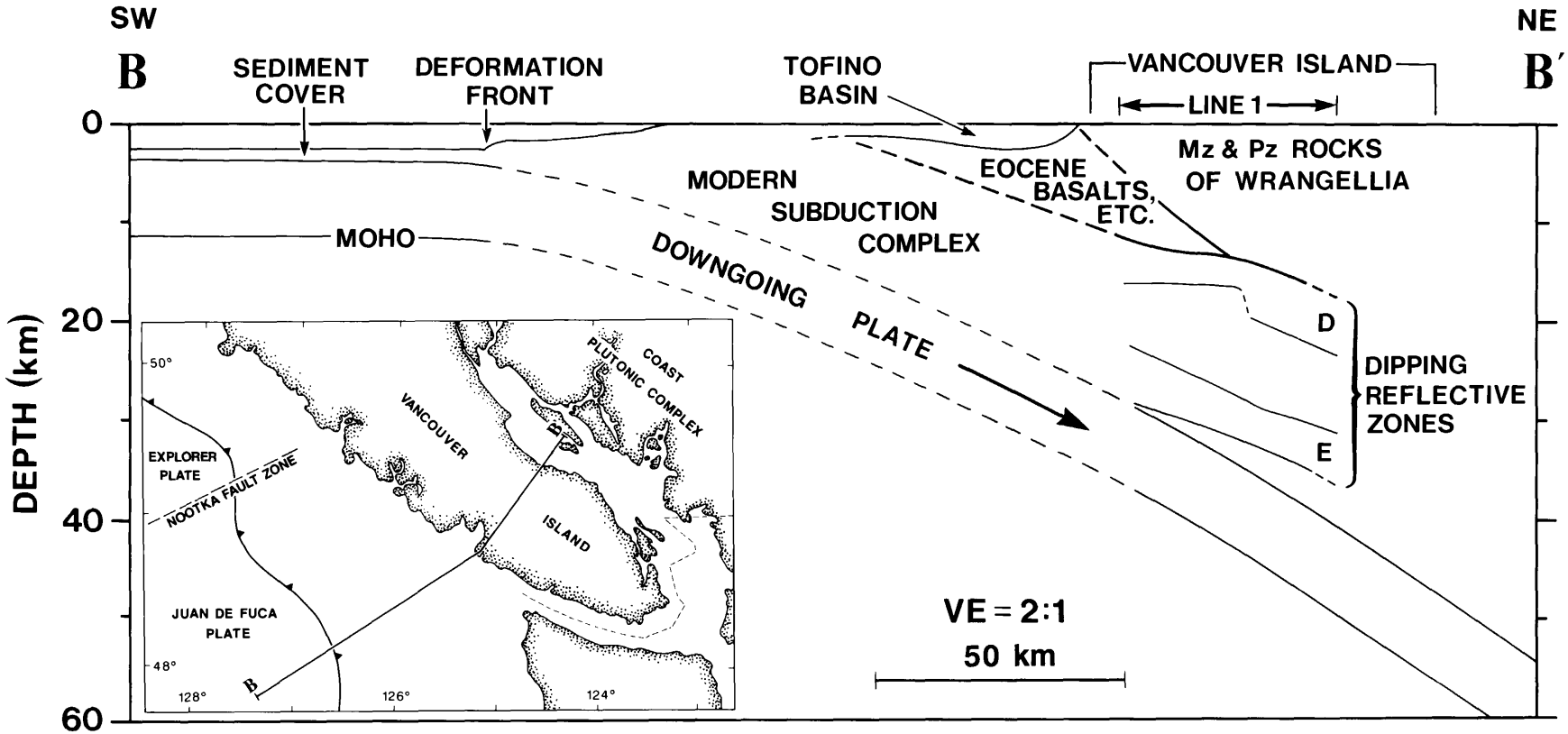

Fig. 1. Cross section summarizing the geology and seismic reflectors under Vancouver Island, Lithoprobe phase I, and offshore [from Clowes et al., 1987].

This paper presents some details of the heat flow measurements in the Coast Plutonic Complex and summarizes the conclusions coming from the heat flow studies.

The Juan de Fuca plate, a remnant of the Farallon plate, has been subducting beneath the present margin of western North America since at least 45 Ma [Riddihough, 1982]. The plate is bounded on the west by the Juan de Fuca ridge and on the east by a subduction zone extending from northern California to northern Vancouver Island. As the size of the Juan de Fuca plate decreased, during the past 10 Ma there was some reduction in the spreading rate and clockwise rotation of the ridge-plate system. At approximately 3.5 Ma the northern part of the Juan de Fuca plate was detached along the northeast trending Nootka fault zone that intersects central Vancouver Island, forming the Explorer plate.

The part of the American plate lying above the subducting Juan de Fuca plate is a collage of several allochthonous terranes accreted to ancestral North America during the late Mesozoic and Tertiary, the largest being Wrangellia. The small Eocene Crescent terrane (e.g., the Metchosin volcanics) that appears to be a slice of oceanic crust is exposed on southernmost Vancouver Island [e.g. R. D. Hyndman et al., manuscript in preparation, 1988]. To the southwest and beneath these Eocene basalts are the sedimentary "Core Rocks", the modern accretionary prism dating from about 42 Ma to the present. Small early Tertiary intrusions on Vancouver Island range mostly from quartz diorite to quartz monzonite.

The southern mainland adjacent to Vancouver Island is underlain by granitic and metamorphic rocks of the Coast Plutonic Complex, a belt of mainly quartz diorite and granodiorite plutons, migmatite, and roof pendants. Rapid uplift has allowed accelerated erosion and dissection of the complex into a region of rugged mountains. Neogene volcanics related directly to subduction of the Juan de Fuca plate include the young Garibaldi Volcanic Belt, defined by several moderately dissected Plio-Pleistocene composite volcanoes including Garibaldi, Cayley, and Meager mountains. The belt is a northern extension of the High Cascades in the United States (Figure 2).

A combination of models based on seismic refraction [Ellis et al., 1983; McMechan and Spence, 1983; Spence et al., 1985] and results from two offshore seismic reflection profiles [Snavely and Wagner, 1981; R. D. Hyndman et al., manuscript in preparation, 1988] and the Lithoprobe Phase I profiles on Vancouver Island [Clowes et al., 1987] as well as seismicity studies [Crosson, 1983; Rogers, 1985] image clearly the subducting oceanic crust. Its dip steepens from 3° at the base of the continental slope to 15°, at a distance of 35 km landward. Above the oceanic crust are zones of reflectors, D and E in Figure 1, that were interpreted as regions of decollement and underplating beneath Vancouver Island [Clowes et al., 1987], although more recent interpretations suggest that any such underplating must have been pre-Eocene. An accreted slice of Eocene basalt may also be present. Recently studied earthquakes [Rogers, 1985, also personal communication, 1986] define a Benioff-Wadati zone within the upper part of the subducting oceanic plate to depths of 65 km under Georgia Strait. Models based on magnetotelluric data [Kurtz et al., 1986] are consistent with an electrical conductor under western Vancouver Island dipping approximately 10° eastward at or below the top of the E zone seismic reflectors. The electrical conductivity of this 6-km-thick layer, attributed to conductive fluid in the pore spaces, is comparable to those obtained in oceanic layers 1 and 2. Kurtz et al. also found that a large conductive region was required east of their sites in order to model their long-period results.

Berry and Forsyth [1975] were unable to resolve the crustal seismic velocity structure beneath the Coast Plutonic Complex using refraction profiles. Models to explain observed magnetic anomalies [Coles and Currie, 1977] include a cold, deep crust under the western edge of the Coast Plutonic Complex, with a fairly high magnetite content to a depth of 40 km. Gravity models to fit observed profiles extending 500 km northeast from the trench seaward of Vancouver Island [e.g., Riddihough, 1979] include a subducted oceanic crust overlain by a wedge of high-density material underneath the western Coast Plutonic

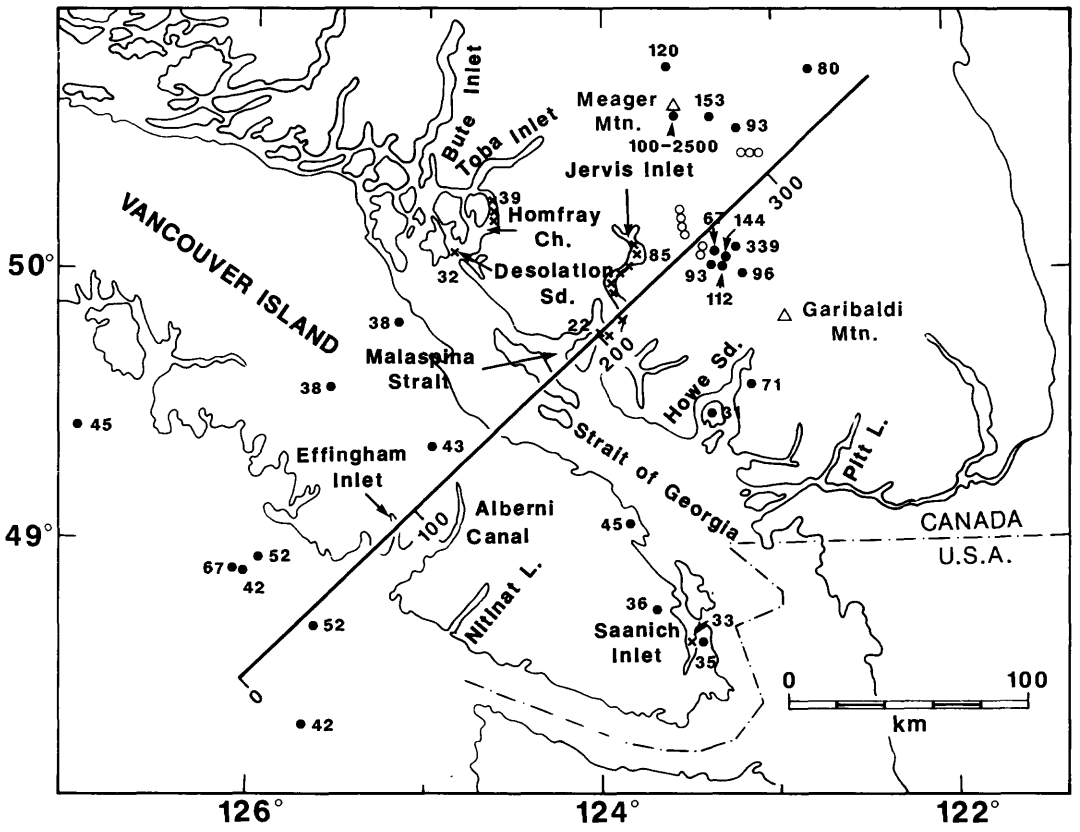

Fig. 2. Location map of Vancouver Island and the British Columbia mainland, showing the position of the profile used for this study and the heat fluxes in mW m^{-2}. Open circles indicate shallow holes; crosses indicate marine measurement sites.

Complex. Farther inland under much of the Intermontane Belt, a seismic low-velocity layer is close to the base of the crust [Wickens, 1971; Berry and Forsyth, 1975]. Magnetic anomalies in that region are relatively subdued compared to the Coast Plutonic Complex anomalies [Haines et al., 1971], and geomagnetic depth sounding [e.g., Caner et al., 1971] reveals an electrically conductive (low Z) region. All of these latter data are consistent with a very warm crust.

The regional heat flux above many convergent margins is characterized by low values between the trench and volcanic front and high values behind the front [e.g., Watanabe et al., 1977]. On the western margin of North America the transition from low to high heat flux in Oregon occurs over a distance of 20 km, along the boundary between the young, high Cascades, and the older Cascades to the west [Blackwell et al., 1982]. In Mexico, Ziagos et al. [1985] defined a zone of low heat flux, lying between the coastline and the Trans-Mexico volcanic belt where the heat flux increases to greater than 80 mW m^{-2}. Their modeling suggested low-angle subduction. In southwestern British Columbia Hyndman [1976], using marine measuring techniques, first showed that a heat flux transition existed at the heads of the fjords. Additional heat flux data [Lewis and Jessop, 1981; Reader and Fairbank, 1983; Lewis et al., 1985] supported such a pattern. A heat flow province with a very high reduced heat flux lies inland of the Coast Plutonic Complex [Lewis et al., 1985]. This province is a northern extension of the Cordilleran Thermal Anomaly Zone [Blackwell, 1969]. The Intermontane Belt, the western part of this province in Canada, has a well determined average heat flux of 75 mW m^{-2} [Davis and Lewis, 1984].

MEASUREMENTS AND CORRECTIONS

Heat Flow

The heat flow data come from five offshore wells drilled on the continental shelf, from 30 boreholes collared on land within 100 km of the profile modelled, and from marine heat flow probe measurements in the soft bottom sediments over a period of years in Homfray Channel, Desolation Sound, and Jervis and Saanich fjords. Since these measurements were quite complex, mostly they are summarized here. Extensive details are given in Lewis et al (1988). However, some details for measurements made in the Coast Plutonic Complex are given, for comparison with other measurements in the Cascades reported in this volume.

Bottom-hole temperatures from the offshore wells and thermal conductivities measured on drill cuttings were combined to obtain the heat flux on the shelf. Seismic velocity data were available, but since the offshore wells were overpressured, they were not used to estimate the porosity. The in situ porosity, needed to obtain the formation thermal conductivity, was obtained indirectly from resistivity logs and from porosity measurements on drilling chips. The accuracy of these heat fluxes is relatively low.

Standard logging of boreholes on land and measurements of thermal conductivity on cores or cuttings produced good quality heat flow data. Severe topography at most sites required large refraction corrections, which were calculated using a two-dimensional finite element grid [Lee and Henyey, 1974]. Previously published results on the mainland [Lewis et al., 1985, Lewis and Jessop, 1981] were included on the profile of Figure 2, and topographic corrections were recalculated for the latter sites (303 and 304).

In areas of steep topography, thermal disturbances produced by groundwater flows can be a particular problem. Where cracks, faults, joints and/or fissures in the crystalline rock are interconnected with the surface, they form routes for water to flow from higher to lower elevations. However, since only a minority of the deep boreholes intersected small water flows and since the water table is always near the surface at higher elevations, most heat flow is by conduction. Within the average depth interval of 434 m in five boreholes in the Coast Plutonic Complex, 90% of the the heat flowed conductively to the surface. However, undetected water flowing beneath any borehole can alter the conducted heat flux measured in the borehole. A constant heat flux over deeper depth intervals or agreement between closely spaced holes increases the probability of the measured value representing the heat flux at depth.

The heat flux in areas of subdued topography within the Canadian Cordillera has been successfully determined in many shallow (<100 m) holes [Bentkowski and Lewis, 1983, 1985; Davis and Lewis, 1984]. However, abundant rainfall and steep topography in the western Coast Plutonic Complex make shallow, ungrouted holes less reliable. Variation in heat flux among shallow holes less than a kilometer apart was assumed to be caused by water flow near, but not necessarily penetrated by a hole. Eight of 15 shallow holes showed no evidence of internal water flow. The mean heat flux, uncorrected for topography, is 86 +/- 15 mW m^{-2}, but heat flux between nearest neighbors varies from 3 to 37%, close to the maximum uncertainty in measurement expected for short holes where conductivities were measured on chip samples. The poor agreement among the eight holes and the obvious water flows in the other seven suggest that such shallow holes are of doubtful value in rugged topography. Results from the shallow holes were thus not included in the analysis.

Five deeper boreholes, drilled to assess the potential for geothermal energy near young volcanic centers of the Garibaldi Volcanic Belt yielded more consistent results (Figure 3). The high heat flux in four holes near Mount Cayley (Figure 2) suggests the presence of residual crustal heat from shallow intrusions [Souther, 1980] where electromagnetic sounding indicated zones of very low electrical resistivity [Shore, 1981]. Changes in heat flux with respect to depth, 56 mW m^{-2} at site 344 and -51 mW m^{-2} at site 339 (Figure 3), are caused by water flowing upward at the first site and downward at the second, along dipping planes intersected by the holes. The vertical components of fluid flow are 15 and -21 g s^{-1} per meter width of

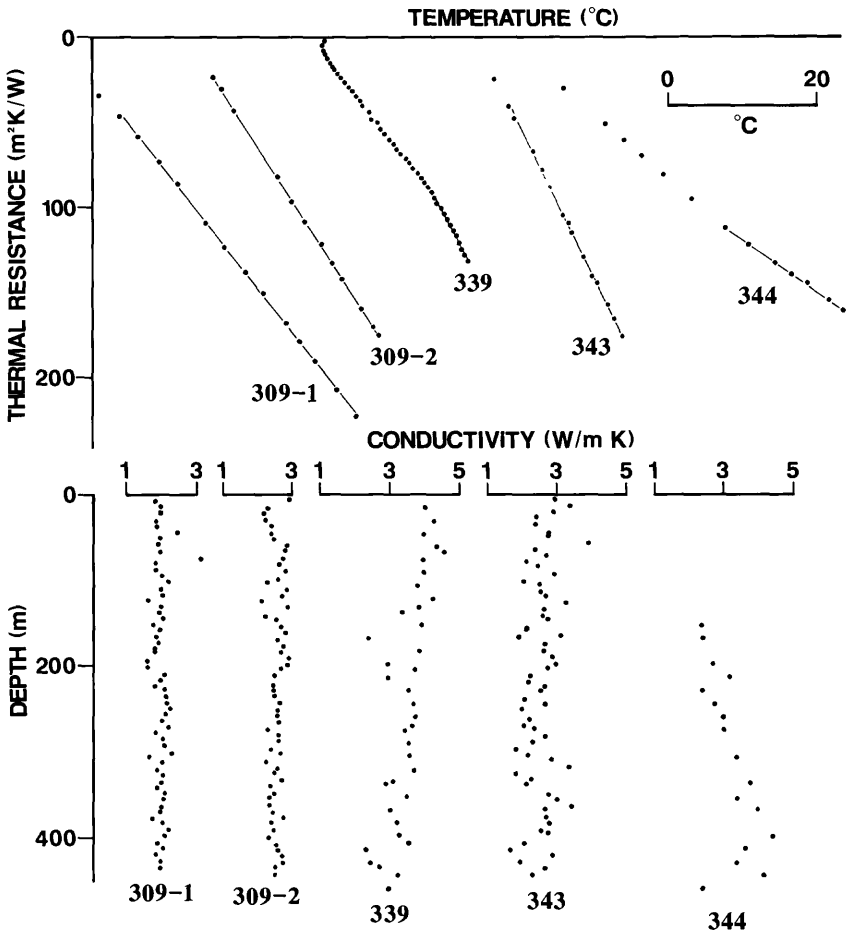

Fig. 3. Bullard plots of temperature versus the thermal resistance for five boreholes in the Garibaldi Volcanic Belt (high heat fluxes) and measured thermal conductivity as a function of depth. The changes in heat flux (slope of the Bullard plots) for boreholes 339 and 344 indicate very old water flows.

plane [Lewis and Beck, 1977]. The reliability of the heat flux at these two sites is less than at the other three locations due to these inferred water flows.

Good quality marine data were obtained with probe penetrations from 3 to 12 m into the fjord sediments and in situ thermal conductivity measurements to 7 m depth. Since the bottom water temperatures (BWTs) of these fjords change aperiodically, repeat cruises were made to obtain a series of temperature profiles at individual sites. An interactive computer program with graphics was used to model the propagation of thermal disturbances into the sediments. Calculated sediment temperatures from trying likely water temperature histories at each site for a range of equilibrium gradients were compared to data obtained over periods of up to 5 years. Although BWTs were not recorded between cruises, some older data show that there were no large changes up to 20 years previous to the cruises. Attempts to find the best fitting model(s) suggested a 10 mK m^{-1} resolution for the gradient. The refraction caused by rugged topography and the insulating sediments was modeled with two-dimensional finite element models.

Comparison of Land and Marine Measurements

The heat flux measured in Saanich Inlet by marine methods is within 6% of the heat flux

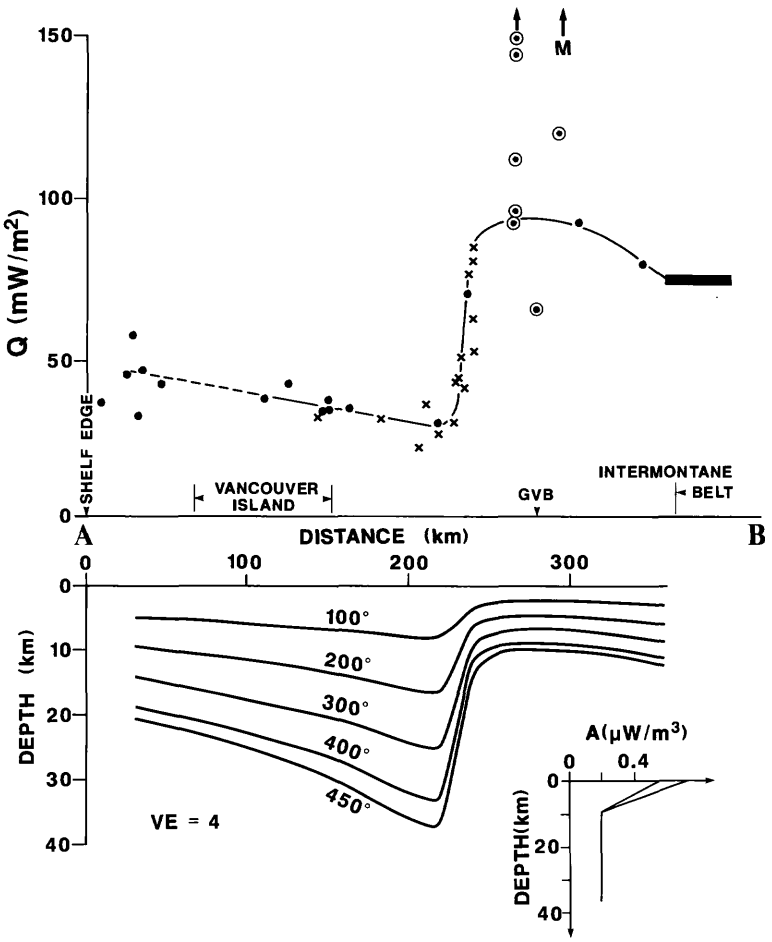

Fig. 4. Heat flux along the profile of Figure 2, corrected only for topography and sediment refraction. Marine results, indicated by crosses, are also corrected for BWT changes. Circled dots are values from the Garibaldi Volcanic Belt (GVB), where some much higher heat fluxes have been measured, including many near Meager Mountain, indicated by an "M." The Intermontane values come from Davis and Lewis [1984]. Isotherms underneath the profile of Figure 2, calculated assuming conductive heat flow and using the heat generation distributions and heat flux profile shown.

without glacial correction measured in the 400-m borehole on the Saanich Penninsula less than 5 km away. Two very different values of heat flux measured on land near Howe Sound (Figure 2), one uncorrected for glacial effects and the other not requiring such a correction [Lewis et al., 1985], were projected 60 km onto the heat flux profile (Figure 4). They projected onto the transition, agreeing with the marine determinations made in Jervis Inlet. If the profile were oriented differently, agreement would not be as good. A previous measurement in Powell Lake 45 km northwest of the profile [Hyndman, 1976] agrees with the value of heat flux required to model the diffusion of salt water from the bottom of this former fjord [Sanderson et al., 1986]. This general agreement supports the accuracy of the inlet measurements and corrections and the absence of unrecognized long-term changes in BWT, and it favors a minimal effect near sea level from lower surface temperatures during glacial periods.

Heat Generation

Unweathered surface samples and borehole samples from Vancouver Island and the Coast Plutonic Complex as well as drill cuttings from the continental shelf were collected to ascertain crustal rates of radioactive heat generation. The amounts of uranium, thorium, and potassium were determined by gamma ray spectroscopy, using the method of Lewis [1974] with a smaller (330 g), constant sample mass and an assumed constant sample absorption.

The radioactive heat generation in the crust along all of this profile is low. The heat generation of shelf sediments [Lewis, 1987] represented by 71 samples from the six offshore wells averages 0.60 μW m^{-3}. Such a low value is consistent with the low values of the source rocks on Vancouver Island and in the Coast Plutonic Complex. The average heat generation in all igneous rocks on Vancouver Island is not much greater than that of the volcanic rocks. The more acidic crystalline rocks have slightly higher values, but average values from all locations on the island are less than 1.2 μW m^{-3}, and the average value for all plutonic rocks is 0.60 μW m^{-3}.

Nearly all of the exposed Coast Plutonic Complex along the profile has K/Ar ages greater than 80 Ma and has not been geochemically altered by crustal differentiation associated with the present episode of subduction. Heat generation is low, the highest average value, 1.3 μW m^{-3}, coming from the most acidic of the common rock types, quartz monzonite [Lewis, 1976; Lewis and Bentkowski, 1988]. The areally averaged heat generation is 0.79 μW m^{-3}. There is

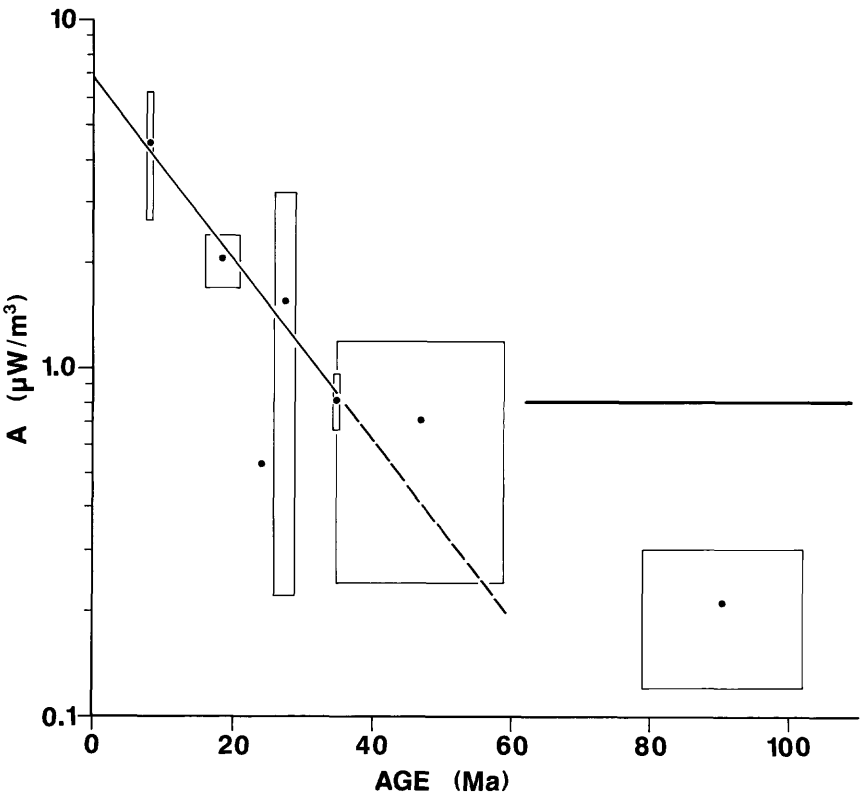

Fig. 5. Measured surficial heat production, A, of plutons as a function of K/Ar age. Limits come from the ranges in ages and the S.D.s of the heat generation. The line at 0.8 μW m^{-3} represents the Coast Plutonic Complex. The line fitting the data comes from an assumed vertical distribution of heat generation within the plutons at the time of their formation and subsequent uplift and erosion at a constant rate.

little variation in heat generation with distance along the profile among 68 representative samples.

A small, epizonal, high level pluton near Meager Mountain (Salal Creek Pluton), the only young exposed intrusive near the profile (Figure 2), has the highest heat production. The Chilliwack composite batholith, chemically similar to Cenozoic andesites of Oregon and Washington, lies at the extreme northern limit of the Cascades 150 km southeast of the profile. The heat generation within it varies with the age of emplacement of successive phases [Richards and White, 1970]. These data support a model proposed by Lachenbruch [1968] in which volumes of magma are successively emplaced into a crust undergoing constant uplift and erosion. If the individual phases have the same original heat generation which decreases with depth, then the value at the present surface is a function of emplacement age. Variation of heat generation with depth in plutons depends on the constitution of and conditions in the magma and crust during emplacement [Lee et al., 1984; Webb et al., 1984], the amount of water in the magma being an important consideration.

Subduction at present may be creating a systematic heat flow versus heat generation relation as bodies are intruded into relatively unenriched crust of the Coast Plutonic Complex. The crust formed has a heat generation which varies with age due to continuous uplift and erosion. If the same exponential distribution of heat generation A with depth z is assumed for each pluton at the time of emplacement [Lachenbruch, 1968], then $A = A_0 e^{-z/b}$ where b is the characteristic depth [Birch et al., 1968; Lachenbruch, 1968]. Also, if constant rates of uplift and erosion are assumed over this entire period, then the depth z now exposed at the surface is related to the age t by the uplift and erosion rate, c: $z = c\ t$. For an uplift rate of 0.3 km/Ma, the depth parameter b for the straight line in Figure 5 representing the present observed heat generation is 8 km, similar to values from established heat flow provinces.

In the Pemberton area where the Salal Creek pluton is located, Parrish [1983] modeled uplift rates of 0.3 km/Ma over the last 10 m.y., using fission track ages of apatite samples from various elevations. However, in the middle Cenozoic from 15 to 30 Ma, uplift rates in most of the Coast Plutonic Complex were low. All of the bodies except the Salal Creek pluton are located at the northern end of the Cascades that may have had continuous uplift from 15 to 30 Ma. Alternatively, since the age range of these plutons is large (Figure 5), their tectonic origins and evolutions may differ.

ANALYSIS AND DISCUSSION

Pattern of Heat Flux and Crustal Temperatures

Along the profile from the continental shelf to the Garibaldi Volcanic Belt, the heat flux, constrained by data within 150 km of the cross section, is remarkably well defined (Figure 4). It decreases from 50 mW m^{-2} on the continental shelf to a minimum of 25 mW m^{-2} in the lower part of Jervis Inlet, 30 km seaward of the Garibaldi Volcanic Belt. Further east it rapidly increases to values of 60-80 mW m^{-2} over a distance of 20 km. Within the Garibaldi Volcanic Belt the heat flux is high, and local variations are large. Variable heat flux within this recently active belt is due to hydrothermal cooling of shallow intrusive bodies [Lewis and Souther, 1978; Reader and Fairbank, 1983]. Past the eastern end of the profile, the western edge of the Intermontane Belt, the heat flux remains 75 mW m^{-2} for 60 km further east [Davis and Lewis, 1984]. Two features of regional significance are the linear decrease in heat flux over 200 km from the shelf across Vancouver Island to the most westerly part of the mainland and the very abrupt increase in heat flux 30 km seaward of the volcanic belt.

Crustal temperatures (Figure 4) were calculated with a one-dimensional conductive model using the heat flux plotted in Figure 4 and the average measured surface heat productions for Vancouver Island and the Coast Plutonic Complex. The assumed thermal conductivity, a function of temperature, T(°C), is $k = 2.4 / (1.0 + 0.001\ T)$ [Cermak, 1971], and the assumed heat generation below 10 km is 0.2 μW m^{-3}. The calculated temperatures are sensitive to the

values of conductivity and heat generation at depth which are poorly known. A thermal conductivity of 3.0 W m^{-1} K^{-1} at 0°C and a minimum heat generation of 0.3 μW m^{-3} produce a temperature of 450°C at a maximum depth of 60 km near the top of the subducting oceanic plate, 220 km along the profile. Crustal heat generation above the underthrusting oceanic plate can produce the entire observed heat flux near the eastern side of Vancouver Island if the minimum heat generation is 0.4 μW m^{-3}. With higher values, heat generated in the crust by radioactivity must flow downward into the cooler, descending oceanic plate.

Dipping Isotherms and Seismic Reflectors Under Vancouver Island

The computed isotherms under Vancouver Island (Figure 4), dip gently landward at angles increasing with temperature, reaching 7° at 450°C. This dip is similar to the 8°-12° dip of the E zone containing strong seismic reflectors approximately 30 km beneath Vancouver Island [Clowes et al., 1987; R. D. Hyndman et al., manuscript in preparation, 1988]. Thus the boundaries of the E seismic reflectors are approximately isothermal (Figure 6). A calculation using heat flux values only measured on land and corrected for maximum glacial effects produces shallower isotherms. Clowes et al. [1987] interpret two reflective zones (Figure 1) as accreted marine sediments and the layer in between as either a piece of underplated oceanic lithosphere or imbricated slices from the top of the subducting oceanic crust. However, recent offshore seismic data suggest that most of the incoming sediment is scraped off at the deformation front. The reflective bands may represent water driven off the downgoing plate trapped at metamorphic fronts [Hyndman, 1988]. Two possible reasons for the E layer reflectors being nearly isothermal are that water flow keeps the temperature nearly constant, and that metamorphic reactions buffer the temperature. Such water movement is likely because the magnetotelluric data suggest that the seismic reflectors probably delineate highly porous layers that may be permeable. Water has been observed flowing from sediments on the continental slopes off Oregon, Japan and Barbados [Ocean Drilling Project Leg 110 Scientific Party, 1987], indicating that upward fluid expulsion is common in the shallow parts of subduction zones.

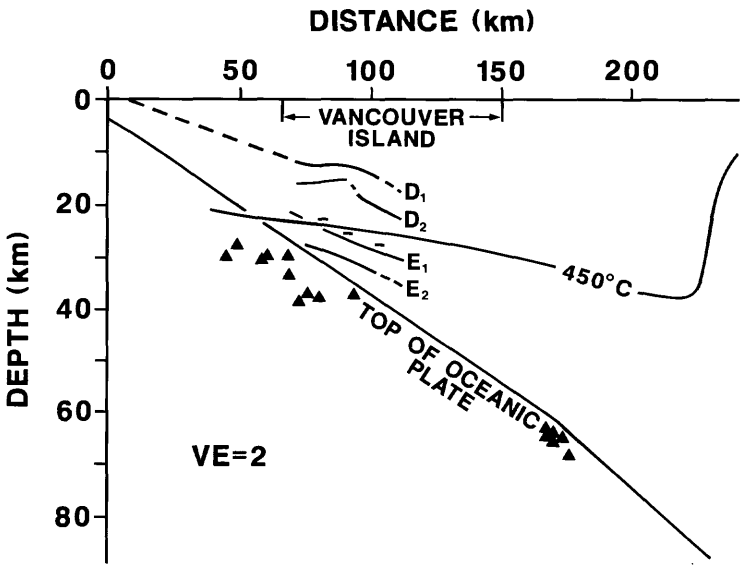

Fig. 6. The subducting oceanic crust with locations of earthquakes indicated by triangles, the zones of seismic reflectors bounded by D1 and D2, and E1 and E2, the high electrical conductivity layer indicated by short horizontal lines near E1, and the 450°C isotherm from this study.

Both free water in the subducted crust and sediments and bound (metamorphic) water in the oceanic crust are possible sources of water. West of Vancouver Island, 2-3 km of sediments with an average porosity of 5% converge with the North American plate at an average velocity of 40 mm yr^{-1}. But it is estimated that less than 6 mW m^{-2} extra heat is brought to the surface over the first 50 km of this profile by the vertical component of water coming up from completely dewatered sediments.

More water is available from dehydration of the oceanic crust at deeper depths. Anderson et al. [1976] estimated water contents by weight of 2-5% for layer 2B (2 km thickness) and 1-6% for layer 3A (2.6 km thickness). Alt et al. [1986] measured approximately 2% bound water in a kilometer-thick section of the oceanic crust using samples from Deep Sea Drilling Project Hole 504B. The rate of water flow updip from this source is 0.2-0.9 cm^3 s^{-1} per meter of cross section. Tatsumi [1986] showed that most dehydration of the basaltic layer terminates at pressures less than 25 kbar, giving a lower depth limit. Therefore crustal dehydration along this profile can produce water between 18 and 60 km depth. The heat flux contained in this water bringing heat nearer to the surface is estimated to be an average of 4 mW m^{-2} across Vancouver Island. However, the amount of heat absorbed by the dehydration reaction itself may be much larger, as discussed below.

Thermal Budget for the Subducting Lithosphere

The measured surficial heat flux above the subduction complex is much smaller than that expected from a young oceanic lithosphere [Parsons and Sclater, 1977; Lister, 1977]. The upper boundary temperature of the oceanic crust approaching the trench increases to 200°C beneath 2.5 km of sediments [Yorath et al., 1985b], and during subduction it increases to 450°C. The temperature difference across the oceanic lithosphere and therefore the heat flux within it are thus reduced to 64% assuming a simple steady state model. The difference between this heat flux from the subducting oceanic lithosphere and that measured (minus the heat production) represents heat that must be accounted for by other processes: warming the top of the oceanic lithosphere and dehydrating the crust. The heat associated with water transport was already shown to be small, and frictional heating along faults is not considered here.

Heating the subducting oceanic lithosphere landward of the trench to change the upper boundary from 200° to 450°C (excluding dehydration) requires $7x10^{12}$ J m^{-2} if the base is held at 1250°C, assuming reasonable geothermal parameters. A transient model of a plate of constant thickness (20 km) moving at a constant speed of 4 cm yr^{-1} was used to represent the oceanic lithosphere during two phases: during a first, 5-m.y. period of sedimentation the upper surface temperature increases linearly from 0° to 200°C, and during a second, 2-m.y. period, from 200° to 450°C. Above the moving plate, the fixed continental crust and modern subduction complex were assumed to have a constant temperature distribution with respect to time. The heat needed to warm the 20-km-thick plate is supplied by conduction, mostly while the plate travels from the trench to the west coast of Vancouver Island, corresponding to the model's second phase. The temperature gradient within the oceanic plate is lowest under western Vancouver Island after 7 m.y. (9 Ma plate), when the heat flux through the top of the lithosphere into the oceanic crust is 45 m Wm^{-2}.

Anderson et al. [1976] estimated that $2x10^5$ J is required to dehydrate each kilogram of oceanic crust. In our model the total heat required to dehydrate the oceanic crust, a maximum of about $3x10^{12}$ J m^{-2}, is conducted upward through the oceanic lithosphere to the dehydration zone where the temperature remains at approximately 450°C. Between 80 and 220 km along the profile, $8x10^{12}$ J m^{-2} of heat is conducted upward through the oceanic lithosphere to the oceanic crust, an amount nearly equal to the total surficial heat flux observed between the trench (0 km) and the heat flux transition at 220 km. We postulate that heat is being "redistributed" seaward by water produced by dehydration of the oceanic crust flowing updip and being mostly absorbed in hydrating parts of the overlying continental lithosohere. For example, a flow of 0.9 cm^3 s^{-1} of water crossing under the western edge of Vancouver Island across a meter width of the subduction complex could produce in hydration reactions most of

the 50 mW m^{-2} observed on the shelf. Such processes and the contribution from dewatering the sediments could explain the large variation in heat flux observed on the continental shelf.

Landward of the first 80 km along the profile, the top of the subducting plate defined by seismicity and seismic refraction becomes deeper than the calculated 450°C isotherm (Figure 6). If the rigid top of the oceanic plate remains near 450°C, there is a relatively cool wedge between it and the seismic reflective zone. In this model the wedge is kept nearly isothermal by water produced by dehydration at its base and absorbed at its top in hydration of the overlying material. This model effectively limits mechanical strength within the wedge, which is aseismic. The model is also in agreement with the low temperature-high pressure metamorphic grades observed for some exhumed subduction complexes and a magnetotelluric model [Kurtz et al., 1986] requiring high electrical conductivity in this region.

A different model [Cloos, 1985; Wang and Shi, 1984] proposes that convection is transporting heat to the surface within the sedimentary wedge next to the trench beneath the continental shelf. Our model can include this process, but the amount of water available is not sufficient to produce the observed heat flux on the continental shelf (see also Reck [1987]). Also, the heat generation within sediments of the Canadian Pacific shelf [Lewis, 1987] is much less than the amount required in the model by Wang and Shi [1984], so another process such as hydration is needed to provide additional heat above the subducting plate.

The Abrupt Transition and Apparent Uplift

The abrupt transition in heat flux from approximately 25-80 mW m^{-2} (Figure 4) is a thermal signature very similar to the transition Blackwell et al. [1982] measured in a very different crust in Oregon: a sharp increase over a distance of 20 km, 30 km seaward of the current volcanic axis. The abruptness of the transition requires a heat source within 10 km of the surface. The time constant to establish or smooth out such a transition if it is not actively maintained is only about 3 Ma, and consequently, abrupt heat flux transitions occur only above active zones of melting and intrusion. A pronounced decrease in the Bouger gravity anomaly is associated with the increase in heat flux, although it occurs over a broader zone. Blackwell et al. [1982] proposed that the source of heat under Oregon was magma or a series of small subvolcanic chambers. East of the transition, 230 km along the profile shown in Figure 4, a purely conductive regime is unlikely at depths greater than 10 km. All important dehydration reactions are completed in the subducted Juan de Fuca plate at about 110 km depth. Thus the temperature rises, melting occurs, and magma moves upward.

The location of an abrupt heat flux transition 30 km seaward of the volcanic centers may be a general relation for the boundary of magma-heated crust above a subduction zone (Figure 7). A transition from low to high heat flux occurs along many convergent margins between the trench and volcanic front, including the Kuril Trench, northeast Japan, Bonin Trench and off Oregon [Yamano, 1985]. Along the Bonin and Kuril trenches [Yamano, 1985] and in Oregon [Blackwell et al., 1982] the transition is seaward of the most recent volcanic front. Although the heat flow data for northeast Japan indicate a transition occurring at the volcanic front [Yamano, 1985], an aseismic zone commences seaward of the front [Tatsumi et al., 1983], and Hashida [1985] has reported a low seismic attenuation zone occupying the Pacific side of the volcanic front, the large contrast in attenuation suggesting very large temperature gradients. Hsui et al. [1983] calculated that melting occurs in a subducting oceanic crust 30 km downdip from the asthenosphere wedge corner.

An alternative model for producing the sharp transition in heat flux must be considered. Differential uplift and erosion in the Coast Plutonic Complex must increase the heat flux, and a sharp transition could be produced between two crustal blocks having differing amounts of uplift and erosion. But to increase the heat flux by 100% requires a difference in constant uplift and erosion [Jaeger, 1965, p. 13] of 1 mm yr^{-1} for 10 m.y. (total relative change in elevation of 10 km). Parrish [1983] studied apparent uplift rates in the coast mountains using fission track dating of zircons and apatites. Implicit in the use of such dates to determine the actual uplift for closely spaced sample locations at varying altitudes is an erosional history. Using the present heat flux to calculate the depth of the 105° and 175°C isotherms in the

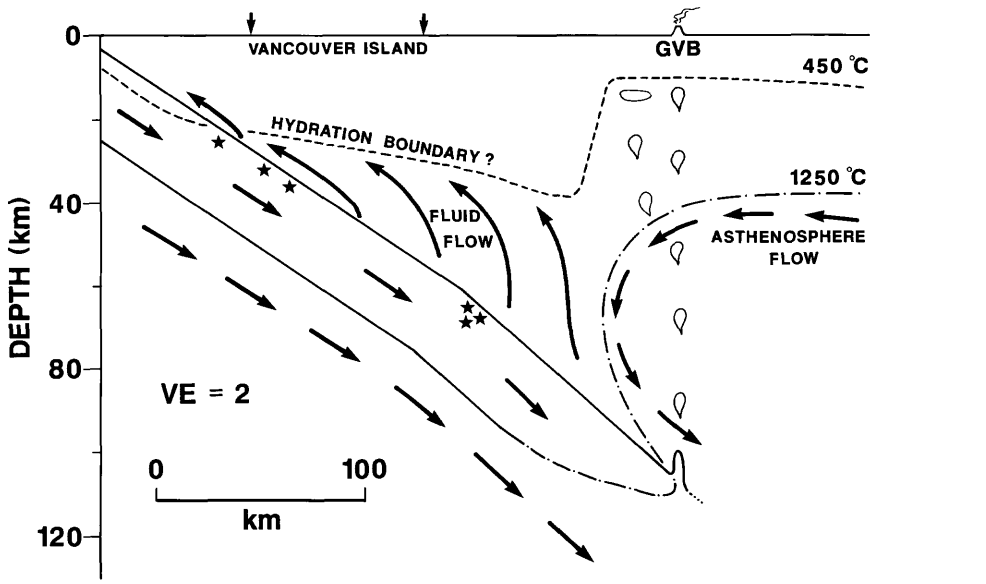

Fig. 7. A model of the subducting oceanic crust being consumed, showing water flow updip from the dehydration of the oceanic crust. Asterisks indicate earthquake focii.

Pemberton area yields results 50% shallower than those calculated by Parrish [1983] and hence either smaller apparent uplift rates or shorter periods of apparent uplift since 10 Ma. There is no geological evidence for such a large amount of uplift over the 20 km width, although based on analysis of the envelopes of peaks, Culbert [1971] did suggest such a boundary at the heads of the fjords. A certain amount of differential uplift is inevitable due to the thermal contrast along this profile, and there is evidence of large amounts of uplift and erosion for the Coast Plutonic Complex compared to Chilcotin lavas to the east and Nanaimo sandstones to the west. We conclude that the differential uplift amplifies the heat flow transition but does not cause it.

Agreement With Other Geophysical Constraints

The presence of Wadati-Benioff earthquakes within the oceanic mantle east of Vancouver Island at depths of 60-70 km (G. Rogers, personal communication, 1985) indicates that temperatures at these depths are near or less than 700°C (Figure 6) because a certain crustal strength is required to support the buildup of the required elastic strain. Without the buffering provided by the postulated endothermic reactions, the young, hot oceanic crust would be heated up much more quickly. The aseismic wedge above the subducting plate below a depth of 30 km can be explained by boundary conditions which prevent the transmission of large stresses to the wedge or by aseismic slip along zones of seismic reflectors having little strength, and not producing significant frictional heat, but we propose that the higher temperatures allow creep.

The wedge-shaped, nearly isothermal region bounded on the bottom by the subducting oceanic plate and at the top by an isotherm of approximately 450°C is consistent with other restraints. Magnetotelluric studies [Kurtz et al., 1986] located a highly conductive zone coincident with the top of the E seismic reflectors and the 450°C isotherm (Figure 6). Gravity models [e.g., Riddihough, 1979] require a dense, thick crust where this relatively cool wedge is located. A magnetic model [Coles and Currie, 1977] for the western edge of the Coast Plutonic Complex requires both a cool thick crust and an enhanced magnetization. E. Irving (personal communication, 1987) suggested that enhanced thermal remanent magnetization (TRM) could occur in the wedge, and where unaltered rocks are metamorphosed to greenschist facies at the

heat flux transition, the TRM would be destroyed, producing the large magnetic gradient. This suggests that the landward, thickest part of the wedge is composed partly of unaltered rock.

Thermal Structure North and South of the Profile

Although the thermal structure of the corridor across the south central Vancouver Island subduction zone shown in Figure 4 is remarkably two-dimensional, there are substantial variations farther to the north and south. In Oregon there is a similar rapid change to higher heat flux inland, but in Washington [e.g., Blackwell and Steele, 1983] and probably in the Fraser Valley of southern British Columbia [Lewis et al., 1985; Bentkowski and Lewis, 1988] the heat flux transition is not so abrupt. Although heat flux data are sparse, gravity, geomagnetic, and seismicity data also indicate a different structure to the south under Washington.

The mean heat flux at five sites on northern Vancouver Island [Lewis et al., 1985; Bentkowski and Lewis, 1984] is 65.6 ± 3.9 mW m^{-2}, significantly higher than the average value of 39.4 mW m^{-2} from the eight sites on central and southern Vancouver Island. The northern edge of the oceanic plate subducted between 4 and 10 Ma [Riddihough, 1977, 1984] lies just to the south of the northern sites, near the late Tertiary Alert Bay Volcanic Belt [Armstrong et al., 1985]. The more normal surficial heat flux and more subdued topography of northern Vancouver Island might be the result of the much lower convergence rate under the northern island [Hyndman et al., 1979b]. The low heat generation measured in surficial samples and values expected for the upper crust lead to an abnormally large heat flux from the lower crust, equivalent to the south central British Columbia heat flow province [Lewis et al., 1985]. Under the northern part of the island the 650°C isotherm is estimated to be less than 20 km deep, and no earthquakes occur at any greater depths. Reheating of the crust of northern Vancouver Island may account for the observed differential uplift to the north in this region [Dragert, 1987].

SUMMARY

A combination of borehole measurements, data from offshore wells and marine probe measurements define a smooth trend of decreasing heat flow from the edge of the continental shelf to near the volcanic zone. The heat flux above the subducting Juan de Fuca plate decreases approximately linearly landward from 50 mW m^{-2} west of Vancouver Island to 25 mW m^{-2} near the Garibaldi Volcanic Belt where an abrupt transition to 80 mW m^{-2} occurs over a distance of 20 km. This transition 30 km seaward of the volcanic zone was defined by closely spaced marine measurements in Jervis Inlet. Within the Garibaldi Volcanic Belt the heat flux varies locally from 80 to several hundred mW m^{-2}, reflecting the advective distribution of heat from cooling magmatic bodies. Large corrections were made for the refractive effects of topography and sediment prisms and for bottom water temperature variations. There was good agreement between these corrected results from marine and borehole measurements if the large glacial corrections to borehole measurements were omitted. Glacial corrections were not used for the calculation of crustal temperatures. Computed crustal isotherms dip from offshore toward the mainland, the 450°C isotherm reaching a maximum depth of 38 km under the western edge of the mainland. East of the heat flux transition this isotherm lies at only 10 km depth. Although there is permeability in the crystalline massifs of the Coast Plutonic Complex along connected cracks, joints, or fractures with large spacing, in general, most heat is moved by conduction.

The subduction zone thermal regime is thought to be controlled by the heating of the descending oceanic plate, heat absorbed during dehydration of the oceanic crust, water flowing updip in the subduction complex, and heat regenerated from hydration reactions. Between the subducting oceanic crust and the 450°C isotherm, a large, nearly isothermal wedge is postulated. This thermal structure is consistent with results from gravity, magnetic, and

magnetotelluric models. The seismic reflectors in this relatively cool, aseismic wedge may be zones where fluids flow updip and metamorphic reactions occur, reducing the shear strength of the wedge.

The abrupt heat flux transition appears to require the intrusion of magmas into the crust beneath the Coast Plutonic Complex 30 km seaward of the volcanic belt. The contrast in crustal temperature must result in uplift and erosion of the central and eastern Coast Plutonic Complex, amplifying the heat flux.

Acknowledgments. We thank the officers and crews of CSS Vector, CSS Parizeau and CFAV Endeavour for their competent help in acquiring the marine data, and Falconbridge Copper (D. Lefebure, H. Gibson) and Novacorp (P. Proudlock) for their cooperation in allowing us to use boreholes drilled for exploration purposes. We thank A. Wilkinson, K. Kotorynski, R. Adams, and T. Leslie for making the conductivity measurements on discs and drill cuttings and A. Beck, D. Blackwell, D. Chapman, L. Law, P. Morgan, R. Riddihough, and R. von Herzen for helpful reviews of versions of this manuscript. Geological Survey of Canada Contribution #47788.

REFERENCES

Alt, J. C., J. Honnorez, C. Laverne, and R. Emmermann, Hydrothermal alteration of a 1 km section through the upper oceanic crust, Deep Sea Drilling Project hole 504B: Mineralogy, chemistry and evolution of seawater-basalt interactions, *J. Geophys. Res.*, *91*, 10,309-10,335, 1986.

Anderson, R. N., S. Uyeda, and A. Miyashiro, Geophysical and geochemical constraints at converging plate boundaries, Part I, Dehydration in the downgoing slab, *Geophys. J. R. Astron. Soc.*, *44*, 333-357, 1976.

Armstrong, R. L., J. E. Muller, J. E. Harakal, and K. Muehlenbachs, The Neogene Alert Bay Volcanic Belt of northern Vancouver Island, *J. Volcanol. Geotherm. Res.*, *26*, 75-97, 1985.

Bentkowski, W. H., and T. J. Lewis, Preliminary results of shallow drilling in the Garabaldi Volcanic Belt, British Columbia, 1982, Earth Phys. Branch, *Open File Rep. 83-23*, 38 pp., Energy, Mines and Resour., Ottawa, Ont., 1983.

Bentkowski, W. H., and T. J. Lewis, Preliminary results from shallow drilling in the Alert Bay Volcanic Belt, 1982, *Open File Rep. 84-2*, 16 pp., Earth Phys. Branch, Energy, Mines and Resour., Ottawa, Ont., 1984.

Bentkowski, W. H., and T. J. Lewis, Preliminary results from shallow drilling in the Anahim Volcanic Belt, B. C., *Open File Rep. 85-9*, 19 pp., Earth Phys. Branch, Energy, Mines and Resour., Ottawa, Ont., 1985.

Bentkowski, W. H., and T. J. Lewis, Thermal measurements in the Fraser Valley, British Columbia, *Open File Rep. 1743*, Geol. Surv. of Can., Ottawa, Ont., 1988.

Berry, M. J., and D. A. Forsyth, Structure of the Canadian Cordillera from seismic refraction and other data, *Can. J. Earth Sci.*, *12*, 182-208, 1975.

Birch, F., R. F. Roy, and E. R. Decker, Heat flow and thermal history in New England and New York, in *Studies of Appalachian Geology: Northern and Maritime*, edited by E. Zen, W. S. White, J. B. Hadley, and J. B. Thompson, pp. 437-451, Wiley-Interscience, New York, 1968.

Blackwell, D. D., Heat flow determinations in the northwestern United States, *J. Geophys. Res.*, *74*, 992-1007, 1969.

Blackwell, D. D., R. G. Bowen, D. A. Hull, J. Riccio, and J. L. Steele, Heat flow, arc volcanism, and subduction in northern Oregon, *J. Geophys. Res.*, *87*, 8735-8754, 1982.

Blackwell, D. D. and J. L. Steele, A summary of heat flow studies in the Cascade Range, *Trans. Geotherm. Resour. Counc.*, *7*, 233-236, 1983.

Caner, B., D. R. Auld, H. Dragert, and P. A. Camfield, Geomagnetic depth sounding and crustal structure in western Canada, *J. Geophys. Res.*, *76*, 7181-7201, 1971.

Cermak, V., Underground temperature and inferred climatic temperature of the past millenium, *Paleogeogr. Paleoclimatol. Paleoecol.*, *10*, 1-19, 1971.

Cloos, M., Thermal evolution of convergent plate margins: Thermal modeling and reevaluation of isotopic Ar-ages for blueschists in the Franciscan Complex of California, *Tectonics*, *4*, 421-433, 1985.

Clowes, R. M., A. G. Green, C. J. Yorath, E. R. Kanasewich, G. F. West, and G. D. Garland, Lithoprobe-A national program for studying the third dimension of geology, *J. Can. Soc. Explor. Geophys.*, *20*, 23-39, 1984.

Clowes, R.M., M. T. Brandon, A. G. Green, C. J. Yorath, A. Sutherland Brown, E. R. Kanasewich, and C. Spencer, Lithoprobe-southern Vancouver Island: Cenozoic subduction complex imaged by deep seismic reflections, *Can. J. Earth Sci.*, *24*, 31-51, 1987.

Coles, R. L., and R. G. Currie, Magnetic anomalies and rock magnetizations in the southern Coast Mountains, British Columbia: Possible relation to subduction, *Can. J. Earth Sci.*, *14*, 1753-1770, 1977.

Crosson, R. S., Review of seismicity in the Puget Sound region from 1970 through 1978, Proceedings Workshop XIV, Earthquake Hazards of the Puget Sound region, Washington, edited by J. C. Yount and R. S. Crosson, *U.S. Geol. Surv. Open File Rep.*, *83-19*, 6-18, 1983.

Culbert, R. R., A study of tectonic processes and certain geochemical abnormalities in the Coast Mountains of British Columbia, Ph. D. thesis, Dep. of Geophys., Univ. of B. C., Vancouver, 1971.

Davis, E. E., and T. J. Lewis, Heat flow in a back-arc environment: Intermontane and Omineca Crystalline belts, southern Canadian Cordillera, *Can. J. Earth Sci.*, *21*, 715-726, 1984.

Dragert, H., The fall (and rise) of central Vancouver Island: 1930-1985, *Can. J. Earth Sci.*, *24*, 689-697, 1987.

Ellis, R. M., et al., The Vancouver Island Seismic Project: A CO-CRUST onshore-offshore study of a convergent margin. *Can. J. Earth Sci.*, *20*, 719-741, 1983.

Geological Association of Canada, Pacific Section, A symposium on the deep structure of southern Vancouver Island: Results of LITHOPROBE phase I, Programme and Abstracts, 30 pp., Victoria, B. C., 1985.

Haines, G. V., W. Hannaford, and R. P. Riddihough, Magnetic anomalies over British Columbia and the adjacent Pacific Ocean, *Can. J. Earth Sci.*, *8*, 387-391, 1971.

Hashida, T., 3D seismic attenuation structure and its implication to the thermal structure beneath the Japanese Islands, paper presented at Twenty-third IASPEI Assembly, Int. Assoc. of Seismol. and Phys. of the Earth's Inter., Tokyo, 1985.

Hsui, A. T., B. D. Marsh, and M. N. Toksoz, On melting of the subducted oceanic crust: Effects of subduction induced mantle flow, *Tectonophysics*, *99*, 207-220, 1983.

Hyndman, R. D., Heat flow measurements in the inlets of southwestern British Columbia, *J. Geophys. Res.*, *81*, 337-349, 1976.

Hyndman, R. D., Dipping seismic reflectors, electrically conductive zones, and trapped water in the crust over a subducting plate, *J. Geophys. Res.*, *93*, 13391-13405, 1988.

Hyndman, R. D., R. P. Riddihough, and R. Herzer, The Nootka fault zone-A new plate boundary off western Canada, *Geophys. J. R. Astron. Soc.*, *58*, 667-683, 1979b.

Jaeger, J. C., Application of the theory of heat conduction to geothermal measurements, in *Terrestrial Heat Flow*, *Geophys. Monogr. Ser.*, vol. 8, edited by W. H. K. Lee, pp. 7-23, AGU, Washington, D.C., 1965.

Kurtz, R.D., J. M. DeLaurier, and J. C. Gupta, A magnetotelluric sounding across the subducting Juan de Fuca plate, *Nature*, *321*, 596-599, 1986.

Lachenbruch, A. H., Preliminary geothermal model of the Sierra Nevada, *J. Geophys. Res.*, *73*, 6977-6989, 1968.

Lee, M.K., J. Wheildon, P. C. Webb, G. C. Brown, K. E. Rollin, C. N. Crook, I. F. Smith, G. King, and A. Thomas-Betts, Hot dry rocks prospects in Caledonian granites:

Evaluation of the results from the BGS-IC-OU research programme (1981-1984), report, 83 pp, Br. Geol. Surv., Keyworth, U.K., 1984.
Lee, T.-C., and T. L. Henyey, Heat-flow refraction across dissimilar media, *Geophys. J. R. Astron. Soc.*, *39*, 319-333, 1974.
Lewis, J. F., and A. M. Jessop, Heat flow in the Garibaldi Volcanic Belt, a possible Canadian geothermal energy resource area, *Can. J. Earth Sci.*, *18*, 366-375, 1981.
Lewis, T. J., Heat production measurement in rocks using a gamma-ray spectrometer with a solid state detector, *Can. J. Earth Sci.*, *11*, 526-532, 1974.
Lewis, T. J., Heat generation in the Coast Range Complex and other areas of British Columbia, *Can. J. Earth Sci.*, *13*, 1634-1642, 1976.
Lewis, T. J., Measuring the thermal conductivity and heat generation of sedimentary units, in Proceedings of Third Canadian/American Conference on Hydrogeology, Banff, 1986, National Water Well Assoc., Dublin, OH, 1987.
Lewis, T. J., and A. E. Beck, Analysis of heat-flow data--Detailed observations in many holes in a small area, *Tectonophysics*, *41*, 41-59, 1977.
Lewis, T. J., and W. H. Bentkowski, Potassium, uranium and thorium concentrations of crustal rocks: A data file, , *Open File Rep. 1744*, Geol. Surv. of Can., Energy, Mines and Resour. Can., Ottawa, Ont., 1988.
Lewis, T. J., W. H. Bentkowski, E. E. Davis, R. D. Hyndman, J. G. Souther, and J. A. Wright, Subduction of the Juan de Fuca plate: Thermal consequences, *J. Geophys. Res.*, (in press), 1988.
Lewis, T.J., and J. G. Souther, Meager Mountain, B. C., A possible geothermal energy resource, *Geotherm. Ser.*, *9*, Energy, Mines and Resour., Ottawa, Ont., 1978.
Lewis, T.J., A. M. Jessop, and A. S. Judge, Heat flux measurements in southwestern British Columbia: The thermal consequences of plate tectonics, *Can. J. Earth Sci.*, *22*, 1262-1273, 1985.
Lister, C. R. B., Estimates for heat flow and deep rock properties based on a boundary layer model, *Tectonophysics*, *41*, 157-171, 1977.
McMechan, G. A., and G. A. Spence, P-wave velocity structure of the Earth's crust beneath Vancouver Island, *Can. J. Earth Sci.*, *20*, 742-752, 1983. Ocean Drilling Project Leg 110 Scientific Party, Expulsion of fluids from depth along a subduction-zone decollement horizon, *Nature*, *326*, 785-788, 1987.
Parsons, B., and J. G. Sclater, Analysis of the variation of ocean floor bathymetry and heat flow with age, *J. Geophys. Res.*, *82*, 803-827, 1977.
Parrish, R. R., Cenozoic thermal evolution and tectonics of the Coast Mountains of British Columbia, 1, Fission track dating, apparent uplift rates, and patterns of uplift, *Tectonics*, *2*, 601-631, 1983.
Reader, J. F., and B. D. Fairbank, Heat flow in the vicinity of the Meager Volcanic Complex, southwestern British Columbia, *Trans. Geotherm. Res. Counc.*, *7*, 535-539, 1983.
Reck, B. H., Implications of measured thermal gradients for water movement through the northeast Japan accretionary prism, *J. Geophys. Res.*, *92*, 3683-3690, 1987.
Richards, T., and W. H. White, K-Ar ages of the plutonic rocks between Hope, British Columbia and the 49th parallel, *Can. J. Earth Sci.*, *7*, 1203-1207, 1970.
Riddihough, R. P., A model for recent plate interactions off Canada's west coast, *Can. J. Earth Sci.*, *14*, 384-396, 1977.
Riddihough, R. P., Gravity and structure of an active margin-British Columbia and Washington, *Can. J. Earth Sci.*, *16*, 350-363, 1979.
Riddihough, R. P., One hundred million years of plate tectonics in western Canada, *Geosci. Can.*, *9*, 28-34, 1982.
Riddihough, R. P., Recent movements of the Juan de Fuca plate system, *J. Geophys. Res.*, *89*, 6980-6994, 1984.
Rogers, G. C., The seismicity of the Vancouver Island Lithoprobe corridor (abstract) in *A Symposium on the Deep Structure of Southern Vancouver Island: Results of Lithoprobe*

Phase 1, Programme and Abstracts, p. 28, Geological Association of Canada, Pacific Section, Victoria, B. C., 1985.

Sanderson, B., K. Perry, and T. Pedersen, Vertical diffusion in Meromictic Powell Lake, British Columbia, *J. Geophys. Res.*, *91*, 7647-7655, 1986.

Shore, G. A., Resistivity survey in the vicinity of Mt. Cayley, August, 1980, *Open File Rep. 1017*, Geol. Surv. of Can., Ottawa, Ont., 1981.

Snavely, P. D., Jr., and H. C. Wagner, Geologic cross section across the continental margin off Cape Flattery, Washington, and Vancouver Island, British Columbia, *U.S. Geol. Surv. Open File Rep., 81-978*, 1981.

Souther, J. G., Geothermal reconnaissance in the central Garibaldi Belt, British Columbia, in *Current Research, Pap. 80-1A*, pp. 1-11, Geological Survey of Canada, Ottawa, Ont., 1980.

Spence, G. D., R. M. Clowes, and R. M. Ellis, Seismic structure across the active subduction zone of western Canada, *J. Geophys. Res.*, *90*, 6754-6772, 1985.

Tatsumi, Y., Formation of the volcanic front in subduction zones, *Geophys. Res. Lett.*, *13*, 717-720, 1986.

Tatsumi, Y., M. Sakuyama, H. Fukuyama, and I. Kushiro, Generation of arc basalt magmas and thermal structure of the mantle wedge in subduction zones, *J. Geoghys. Res.*, *88*, 5815-5825, 1983.

Wang, C.-Y., and Y.-L. Shi, On the thermal structure of subduction complexes: A preliminary study, *J. Geophys. Res.*, *89*, 7709-7718, 1984.

Watanabe, T., M. G. Langseth, and R. N. Anderson, Heat flow in back-arc basins of the western Pacific, in *Island Arcs, Deep Sea Trenches, and Back-Arc Basins, Maurice Ewing Ser., vol. 1*, edited by M. Talwani, and W. C. Pitman III, pp. 137-161, AGU, Washington, D.C., 1977.

Webb, P.C., A. G. Tindle, S. D. Barritt, G. C. Brown, and J. F. Miller, Radiothermal granites of the United Kingdom: comparison of fractionation patterns and variation of heat production for selected granites, in *High Heat Production (HHP) Granites, Hydrothermal Circulation and Ore Genesis*, pp. 409-424, Institution of Mining and Metallurgy, London, England, 1984.

Wickens, A. J., Variations in lithospheric thickness in Canada, *Can. J. Earth Sci.*, *8*, 1154-1162, 1971.

Yamano, M., Heat flow studies of the Circum-Pacific subduction zones, Ph. D. thesis, Univ. of Tokyo, 1985.

Yorath, C.J., R. M. Clowes, A. G. Green, A. Sutherland-Brown, M. T. Brandon, N. W. D. Massey, C. Spencer, E. R. Kanasewich, and R. D. Hyndman, Lithoprobe-phase 1: Southern Vancouver Island: Preliminary analyses of reflection seismic profiles and surface geological studies, in *Current Research, Pap. 85-1*, pp. 543-554, Geological Survey of Canada, Ottawa, Ont., 1985a.

Yorath, C. J., A. G. Green, R. M. Clowes, A. Sutherland-Brown, M. T. Brandon, E. R. Kanasewich, R. D. Hyndman, and C. Spencer, Lithoprobe, southern Vancouver Island: Seismic reflection sees through Wrangellia to the Juan de Fuca plate, *Geology*, *13*, 759-762, 1985b.

Ziagos, J. P., D. D. Blackwell, and F. Mooser, Heat flow in southern Mexico and the thermal effects of subduction, *J. Geophys. Res.*, *90*, 5410-5420, 1985.

HEAT FLOW AND HYDROTHERMAL CIRCULATION IN THE CASCADE RANGE, NORTH-CENTRAL OREGON

S.E. Ingebritsen, D.R. Sherrod, and R.H. Mariner
U.S. Geological Survey, Menlo Park, California

ABSTRACT

In north-central Oregon young volcanic rocks of the Cascade Range comprise a large area of near-zero near-surface conductive heat flow. Ground-water circulation sweeps sufficient heat out of areas where rocks younger than 6 Ma are exposed to account for the anomalously high conductive heat flow measured in older rocks at lower elevations. Previous studies proposed an extensive mid-crustal magmatic heat source to explain a sparser set of heat flow observations. Our analysis suggests that high heat flow in areas where rocks older than 6 Ma are exposed may be a relatively shallow phenomenon caused by regional ground-water flow. Any deeper anomaly may be relatively narrow, spatially variable, and essentially confined to the Quaternary (<2 Ma) arc. The total heat flow anomaly can be explained by magmatic intrusion at a rate of 9-33 km^3/km arc length/m.y.

INTRODUCTION

Quaternary volcanoes of the Cascade Range form a 1200-km-long volcanic arc that extends from southern British Columbia to northern California. The arc is related to subduction of the Juan de Fuca plate beneath North America. Detailed geologic mapping, measurements of advective heat discharge, and numerous conductive heat flow measurements are available for a 135-km-long section of the Cascade Range in north-central Oregon. This unique data set allows us to estimate fluxes of heat and mass (thermal fluid and magma) and to document the role of ground-water movement in redistributing heat in the upper crust.

In the study area (approximately latitude 44°00′ to 45°15′ N), the High Cascades physiographic subprovince is a broad constructional ridge of upper Pliocene and Quaternary (<3.3 Ma) volcanic rocks surmounted by several

Quaternary stratovolcanoes. The High Cascades are flanked to the west and east by Oligocene to lower Pliocene volcanic rocks of the Western Cascades and Deschutes basin, respectively. Western Cascades rocks underlie the High Cascades and are deeply eroded where exposed, commonly hydrothermally altered, and generally less permeable than the younger rocks. In this paper we use Western Cascades and High Cascades as location terms, but emphasize two age divisions that are more useful for our purposes (Fig. 1). We distinguish the Quaternary (<2 Ma) arc, or area of Quaternary vents, because pre-Quaternary magmatic heat sources will generally have cooled to near ambient temperatures. We also distinguish uppermost Miocene, Pliocene, and Quaternary (<6 Ma) rocks, because their areal extent is roughly coincident with an extensive area of near-zero near-surface conductive heat flow. Our geologic data rely on a detailed compilation map prepared as part of the U.S. Geological Survey's Geothermal Research Program, on which the Oligocene and younger (<37 Ma) volcanic rocks are divided into 40 units, on the basis of age and composition (Sherrod and Smith, 1989).

HYDROTHERMAL CIRCULATION

Most of the thermal springs in the study area discharge in deep valleys up to 15 km west of the Quaternary arc in the Western Cascades. One set of thermal springs discharges from Oligocene or Miocene rocks 18 km east of the Quaternary arc (Fig. 2). No thermal springs occur in the Quaternary rocks.

With two exceptions, the thermal waters are Na-Cl or Na-Ca-Cl waters. Br/Cl ratios that are the same as sea water and the high concentrations of Na and Cl (Table 1) suggest that the thermal waters may have circulated through rocks deposited in a marine environment. Na-Ca-Cl thermal waters are typical of rift zones around the world, but in North America occur primarily in the Salton Trough and in the Columbia embayment of Hamilton and Myers (1966) in the Pacific Northwest.

The high Cl content of the thermal waters makes Cl a useful natural tracer, because surface waters in the Cascade Range of Oregon average only about 0.5 mg/L Cl. The discharge of groups of thermal springs can be calculated by measuring the increased Cl load of streams passing through hot spring areas (see, e.g., Ellis and Wilson, 1955). These measurements (Table

1) have a reproducibility of ±10-15 percent or better, depending on the flow rate of the stream relative to the flow rate of the hot springs and on the Cl concentration in the thermal water.

The product of the measured hot spring discharge, an appropriate density and heat capacity, and the difference between a chemical geothermometer temperature (Table 1) and a reference temperature ($Q\rho C(T_g - 5^oC)$) gives a measure of the heat transported advectively by the hot spring systems (Fig. 2). The total advective heat transport by thermal water in the study area is 159 MW, which represents a significant fraction of the regional heat budget. For comparison, the Quaternary magma extrusion rate of 3-6 km^3/km arc length/m.y. (Sherrod, 1986) represents an average heat release of 65-130 MW within the study area, assuming a basaltic magma with typical properties (initial temperature 1200°C, latent heat of crystallization 420 J/g, specific heat 1.25 J/g/°C, and density 2.65 g/cm^3; see, e.g., Jaeger, 1964; Harris and others, 1970).

The isotopic composition of the thermal waters in the Western Cascades indicates that they were recharged at relatively high elevations in the Quaternary arc, assuming that the isotopic composition of precipitation has not changed significantly since recharge took place (i.e., that the thermal waters were recharged during the Holocene). The thermal waters are much more depleted isotopically than local meteoric waters in the Western Cascades. Their isotopic composition best matches that of meteoric waters at elevations of 1300-1900 m near the Cascade crest (Fig. 3). The hot springs are at elevations of 500-700 m. Thus an elevation difference on the order of 600-1400 m drives the thermal circulation systems.

The available data suggest that thermal waters recharged near the Cascade crest circulate to depth and flow laterally for distances of 10-20 km (Fig. 2) before discharging at relatively low elevations in the Western Cascades. Gravitationally driven thermal fluid circulation transports significant amounts of heat from the Quaternary arc into rocks older than 6 Ma, and must profoundly affect the pattern of near-surface conductive heat flow. Gravitationally driven flow of lower-temperature ground water must also transfer heat from the younger rocks to older rocks at lower elevations, but this effect is very difficult to measure.

CONDUCTIVE HEAT FLOW

A large conductive heat flow data set is available for the study area. We have augmented the extensive published data set (Blackwell and others, 1982; Black and others, 1983; Steele and others, 1982; Blackwell and Baker, 1988b) by logging open holes and by analyzing data collected by the state and private companies that were previously unpublished or published only as temperature-depth profiles (Table 2). The data show that the Quaternary arc and adjacent 2-6 Ma volcanic rocks comprise a large area of near-zero near-surface conductive heat flow, due to downward and lateral flow of cold ground water. Temperature profiles from the Quaternary arc (Fig. 4) typically show little or no temperature increase to depths of 200 meters or more.

In contrast, near-surface conductive heat flow is anomalously high in rocks older than 6 Ma exposed at lower elevations in the Western Cascades, as Figure 5 shows for the Breitenbush Hot Springs area (see Figure 2 for approximate location). A similar pattern of low-to-vanishing conductive heat flow in permeable volcanic highlands and relatively high heat flow in older, less permeable rocks at lower elevations has been observed in the Cascade Range of northern California (Mase and others, 1982).

On the basis of temperature profiles from the Mt. Hood area (Steele and others, 1982), Newberry Volcano (Swanberg and others, 1988), and the current study area, the thickness of the nearly-isothermal zone in the younger rocks generally ranges from 150-1000 m. In the present study area only two drill holes collared in Quaternary rocks are deep enough to measure conductive heat flow beneath the nearly-isothermal zone. A 587-m-deep well (EWEB-TM) at lat. 44°32′42" N, long. 121°57′48" W (T. 12 S., R. 7 E., Sec. 9) provides a value of 95 mW/m^2, and a 1465-m-deep well (CTGH-1) at lat. 44°51′02" N, long. 121°49′54" W (T. 8 S., R. 8 E., Sec. 28) provides a value of about 109 mW/m^2. Detailed data for these wells are given in Ingebritsen and others (1988).

The temperature profiles in the Breitenbush area (Fig. 5) suggest that the high conductive heat flow measured in rocks older than 6 Ma may be a relatively shallow phenomenon. Seventeen shallow holes (<500 m deep) show

high gradients generally corresponding to heat flows >110 mW/m^2. However, a similar gradient in the upper part of the deepest hole (SUNEDCO 58-28) changes abruptly below a zone of thermal fluid circulation at ~800 m depth, suggesting that the gradients in the shallow holes are also controlled by ground-water flow.

HEAT BUDGET

The role of advective heat transfer in mountainous terrain is widely recognized, and the physics of the process has been described in numerical modeling studies (e.g., Smith and Chapman, 1983; Forster, 1987). The data set from this study area offers an opportunity to examine the process on a more specific level. We use a heat budget approach to compare the magnitude of the heat deficit in the rocks younger than 6 Ma with that of the anomalous heat discharge in the adjacent older rocks, and to estimate the magmatic heat input required to account for the total heat flow anomaly. The regional heat flow map used in our analysis is shown as Figure 6, and the components of the budget are summarized in Table 3. The conductive components of the budget are defined relative to assumed "background" heat flow values, and are obtained by measuring areas on Figure 6 with a planimeter. In general, heat flow in a given area is taken as the average of adjacent contours (e.g., 70 mW/m^2 between the 60 mW/m^2 and 80 mW/m^2 contours). We assign values of 140 mW/m^2 within the 120 mW/m^2 contours and 60 mW/m^2 outside the 80 mW/m^2 contours east of the Quaternary arc.

Important assumptions in the heat budget are as follows:

(1) The "background" conductive heat flow beneath the isothermal zone in the Quaternary arc is 100 mW/m^2. This value is typical of areas of Quaternary volcanism (see, e.g., Hasabe and others, 1970) and is consistent with the two measurements in the study area.

(2) The "background" conductive heat flow in Tertiary terrane is 60 mW/m^2. Values over 60 mW/m^2 are the result of tectonic, magmatic, radiogenic, or hydrologic sources.

(3) The heat output of the hot springs represents the anomalous advective heat discharge from rocks older than 6 Ma. This is a minimum value because it does not include lower-temperature advective discharge, which is difficult to measure.

Assumptions (2) and (3) require some additional explanation. The global mean continental heat flow is about 60 mW/m^2 (Jessop and others, 1976). The mean heat flow for Tertiary tectonic provinces is higher than 60 mW/m^2, with a large scatter. The "background" heat flow for a given setting is determined by the competing effects of sinks (subducting slabs in this case) and sources (e.g., radioactivity). One could as easily assume a background value of 50 or 70 mW/m^2 in Tertiary terrane (J.H. Sass, written communication, 1988). Thus (as beneath the Quaternary arc) the appropriate background heat flow is subject to considerable uncertainty. However, our results are not particulary sensitive to the exact value assumed. For example, a background value of 50 mW/m^2 in Tertiary terrane west of the Quaternary arc would increase the conductive anomaly from 137 (Table 3) to 178 MW.

The values for hot spring heat output used in the budget (assumption 3) are based on discharge temperatures (T_d) rather than the geothermometer temperatures (T_g) used for Figure 2. Two lines of evidence suggest that the difference between T_g and T_d is due to conductive cooling. First, there is a strong correlation between hot spring discharge rates and discharge temperatures (Table 1). Second, tritium data (unpublished) indicate that the thermal waters do not cool by mixing with shallow, relatively tritium-rich ground water. Since the difference between T_g and T_d results primarily from conductive cooling, this increment of heat presumably appears as part of the conductive anomaly. In the Western Cascades, the thermal power represented by the difference between the T_g and T_d (67 MW) is equal to about half of the conductive anomaly (compare the values in Figure 2 and Table 3).

The area of near-zero near-surface conductive heat flow in this part of the Cascade Range generally coincides with the areal extent of permeable volcanic rocks younger than 6 Ma. On the basis of our assumptions regarding background heat flow, about 460 MW of heat are swept out of these younger

rocks between latitudes 44°00′ and 45°15′ N by ground-water circulation. This amount is roughly balanced by 350 MW of anomalous heat discharge in the rocks older than 6 Ma (Table 3). Apparently, sufficient heat is removed advectively from the rocks younger than 6 Ma to explain the anomalous heat discharge measured on the flanks of the Cascade Range.

The difference between the heat deficit in the younger rocks and the anomaly in the older rocks (about 110 MW) may occur as lower-temperature advective discharge, which was not determined directly. The difference between the heat deficit in the younger rocks and the heat (T_g) transported advectively by the hot spring systems (460-160 = 300 MW) is an estimate of the heat removed from the younger rocks by lower-temperature ground-water flow or by yet-unidentified thermal fluids.

Since the anomalous heat discharge in the older (>6 Ma) rocks can be explained in terms of advection from the younger rocks, we need invoke magmatic heat input only to explain an increment of about 40 mW/m^2 (100 mW/m^2 - 60 mW/m^2) in the background conductive heat flow beneath the Quaternary arc (an area of 3990 km^3). This requires an intrusion rate of 9-33 km^3/km arc length/m.y., again assuming a basaltic magma with an initial temperature of 1200°C, a latent heat of crystallization of 420 J/g, specific heat of 1.25 J/g/°C, and a density of 2.65 g/cm^3. The lower intrusion rate assumes 900°C of magmatic cooling; the higher rate that heat is supplied by latent heat only, with no cooling. For intermediate amounts of cooling, inferred intrusion rates scale linearly between these values. Because the magmatic extrusion rate has been 3-6 km^3/km arc length/m.y. during the Quaternary (Sherrod, 1986), our analysis suggests an intrusion/extrusion ratio of 1.5-11. Greater rates of magmatic heat input would be expected to cause larger anomalies on the flanks of the Cascades than those observed at present.

The assumption of a uniform, average heat flow value of 100 mW/m^2 below the isothermal zone in the Quaternary arc is certainly an over-simplification. The distribution of anomalous heat discharge in the Western Cascades relative to Quaternary dacitic and rhyolitic volcanoes (Fig. 6) suggests that lateral flow of heated ground water into the Western Cascades may originate from heat sources localized near Quaternary silicic magmatic

centers, as originally suggested by R.L. Smith and H.R. Shaw in the early 1970's. The areas of silicic volcanism are presumably areas with relatively high intrusion rates, high intrusion/ extrusion ratios, and (by inference) relatively high "background" heat flow (Hildreth, 1981).

CONCEPTUAL MODELS

Our conceptual model of the thermal structure of the north-central Oregon Cascades is shown as Figure 7a. Other workers (e.g., Blackwell and others, 1982; Blackwell and Steele, 1983; 1985) have preferred to explain the near-surface heat flow observations in terms of an extensive mid-crustal magmatic heat source underlying both the Quaternary arc and adjacent older rocks (Fig. 7b). More recently, Blackwell and Steele (1987) and Blackwell and Baker (1988a; 1988b) have suggested that the thermal effects of hydrothermal circulation are locally superimposed on the effects of this extensive mid-crustal heat source. On the basis of our current understanding of the hydrothermal systems and the energy-balance considerations discussed above, we prefer to explain the near-surface observations in terms of a narrower, spatially variable deep heat flow anomaly that expands laterally at relatively shallow depths because of ground-water flow. The actual thermal structure will undoubtedly prove more complex than either of the simple models shown in Figure 7.

Our preferred model (Figure 7a) is similar to two of the models for the Western Cascade hot springs presented by Blackwell and others (1982, Fig. 10, models 2 and 3), except that we suggest significant spatial variability in the "heat source." Blackwell and others (1982) preferred their model 1 (represented in our Figure 7b) because of the "close correspondence of the heat flow and [Bouguer] gravity anomalies" (Blackwell and others, 1982, p. 8749; see also their Figure 8). They "prefer the model that relates the gravity and heat flow data to a (large) zone of low-density (partially molten) material in the upper part of the crust (10 $\pm$ 2 km) beneath the High Cascade Range and extending about 10 km west of the High Cascade Range boundary" (Blackwell and others, 1982, p. 8750).

Because of its critical importance to other workers' choice of thermal models, we have looked at the gravity data from the study area in some

detail. Figure 8 shows the relationship between gravity and heat flow values. As noted by Blackwell and others (1982) there is a negative correlation between Bouguer gravity and heat flow west of the Cascade crest. However, on a regional basis there is no significant correlation between wavelength-filtered residual gravity and heat flow or between isostatic residual gravity and heat flow. Locally, there is a persistent correlation in the vicinity of Mount Hood that can be at least partially explained as a relict of strong correlations between elevation and heat flow and elevation and gravity.

The wavelength-separated residual gravity was derived by spectral separation at a wavelength of approximately 90 km, yielding residual anomalies due to sources at depths less than approximately 20 km (Couch and others, 1982a). The isostatic residual data have been processed to remove topography-induced regional trends and to enhance gravity anomalies related to crustal geologic features (Simpson and others, 1986). Any correlation between gravity and heat flow that is due to a hot, partially molten body at shallow- to mid-crustal levels should persist through, or even be enhanced by such data processing. The fact that there is no significant correlation between heat flow and residual gravity suggests that the relationship between heat flow and Bouguer gravity may be due to density contrasts at greater depths.

SUMMARY

Sufficient heat is swept out of rocks younger than 6 Ma by ground-water circulation to explain the anomalous advective and conductive heat flow measured in adjacent older rocks. The high conductive heat flow measured in the older rocks, if caused by regional ground-water flow, is a shallow phenomenon (in comparison to the mid-crustal heat source model). The lateral flow of thermal water into the Western Cascades may originate from areas of silicic volcanism in the Quaternary arc; if so, there is probably significant spatial variability in heat flow below the nearly-isothermal zone in the Quaternary arc. The total heat-flow anomaly can be explained by Quaternary magmatic intrusion at a rate of 9-33 km^3/km arc length/m.y., which corresponds to an intrusion/extrusion ratio of 1.5-11. Compared to the

mid-crustal heat source model (Fig. 7), our model suggests a more limited geothermal resource base, but a better-defined exploration target.

ACKNOWLEDGMENTS

We would like to thank numerous colleagues at the U.S. Geological Survey for helpful discussions on this topic; the advice and comments of R.J. Blakely, T.E.C. Keith, A.H. Lachenbruch, L.J.P. Muffler, J.H. Sass, and M.L. Sorey were particularly helpful. Diane Cassidy derived the data shown in Figure 8. The compilation of geologic map data relied in part on generous contributions from R.M. Conrey (Washington State University) and E.M. Taylor (Oregon State University). David Jones and Sandy Peters drafted the figures.

REFERENCES CITED

Black, G.L., Blackwell, D.D., and Steele, J.L., 1983, Heat flow in the Oregon Cascades in Priest, G.R., and Vogt, B.F. (eds.), Geology and geothermal resources of the central Oregon Cascade Range: Oregon Department of Geology and Mineral Industries Special Paper 15, p. 69-76.

Blackwell, D.D., and Baker, S.L., 1988a, Thermal analysis of the Breitenbush geothermal system: Geothermal Resources Council Transactions, v. 12, p. 221-227.

Blackwell, D.D., and Baker, S.L., 1988b, Thermal analysis of the Austin and Breitenbush geothermal systems, Western Cascades, Oregon in Sherrod, D.R. (ed.), Geology and geothermal resources of the Breitenbush-Austin Hot Springs area, Clackamas and Marion Counties, Oregon: Oregon Department of Geology and Mineral Industries Open-File Report O-88-5, p. 47-62.

Blackwell, D.D., Bowen, R.G., Hull, D.A., Riccio, J., and Steele, J.L., 1982, Heat flow, arc volcanism, and subduction in northern Oregon: Journal of Geophysical Research, v. 87, p. 8735-8754.

Blackwell, D.D., and Steele, J.L., 1983, A summary of heat flow studies in the Cascade Range: Geothermal Resources Council Transactions, v. 7, p. 233-236.

Blackwell, D.D., and Steele, J.L., 1985, Heat flow of the Cascade Range in Guffanti, M., and Muffler, L.J.P. (eds.), Proceedings of the workshop on geothermal resources of the Cascade Range, U.S. Geological Survey Open-File Report 85-521, p. 20-23.

Blackwell, D.D., and Steele, J.L., 1987, Geothermal data from deep holes in the Oregon Cascade Range: Geothermal Resources Council Transactions, v. 11, p. 317-322.

Couch, R.W., Pitts, G.S., Gemperle, M., Braman, D.E., and Veen, C.A., 1982a, Gravity anomalies in the Cascade Range in Oregon: structural and thermal implications: Oregon Department of Geology and Mineral Industries Open-File Report O-82-9, 66 p.

Couch, R.W., Pitts, G.S., Gemperle, M., Veen, C.A., and Braman, D.E., 1982b, Residual gravity maps, northern, central, and southern Oregon Cascade Range: Oregon Department of Geology and Mineral Industries Geological Map Series GMS-26, 3 sheets.

Ellis, A.J., and Mahon, W.A.J., 1977, Chemistry and geothermal systems: New York, Academic Press, 392 p.

Ellis, A.J., and Wilson, S.H., 1955, The heat from the Wairakei-Taupo thermal region calculated from the chloride output: New Zealand Journal of Science and Technology, v. 36, p. 622-631.
Forster, C.B., 1987, Interaction of groundwater flow systems and thermal regimes in mountainous terrain: a numerical study: Ph.D. thesis, University of British Columbia, 202 p.
Fournier, R.O., 1981, Application of water geochemistry to geothermal exploration and reservoir engineering in Rybach, L., and Muffler, L.J.P. (eds.), Geothermal systems: principles and case histories: Chichester, J. Wiley and Sons, p. 109-144.
Godson, R.H., and Scheibe, D.M., 1982, Description of magnetic tape containing conterminous U.S. gravity data in gridded format: National Technical Information Service Report PB-254798, 5 p.
Hamilton, W., and Myers, W.B., 1966, Cenozoic tectonics of the western United States: Reviews of Geophysics and Space Physics, v. 4, p. 509-549.
Harland, W.B., Cox, A.V., Llewellyn, P.G., Pickton, C.A.G., Smith, A.G., Walters, R., 1982, A geologic time scale: Cambridge, Press Syndicate of the University of Cambridge, 131 p.
Harris, P.G., Kennedy, W.Q., and Scarfe, C.M., 1970, Volcanism versus plutonism - the effect of chemical composition in Newall, G., and Rast, N. (eds.), Mechanism of igneous intrusion: Geological Journal Special Issue 2, p. 187-200.
Hasabe, K., Fujii, N., and Uyeda, S., 1970, Thermal processes under island arcs: Tectonophysics, v. 10, p. 335-355.
Hildreth, W., 1981, Gradients in silicic magma chambers: implications for lithospheric magmatism: Journal of Geophysical Research, v. 86, p. 10,153-10,192.
Ingebritsen, S.E., Mariner, R.H., Cassidy, D.E., White, L.D., and Shepherd, L.D., 1988, Heat-flow and water-chemistry data from the Cascade Range and adjacent areas in north-central Oregon: U.S. Geological Survey Open-File Report 88-702, 205 p.
Jaeger, J.C., 1964, Thermal effects of intrusions: Reviews of Geophysics, v. 2, p. 443-466.
Jessop, A.M., Hobart, M.A., and Schlater, J.G., 1976, The world heat flow data collection - 1975: Geothermal Service of Canada Geothermal Series Number 5, 125 p.
Mase, C.W., Sass, J.H., Lachenbruch, A.H., and Munroe, R.J., 1982, Preliminary heat-flow investigations of the California Cascades: U.S. Geological Survey Open-File Report 82-150, 240 p.
Priest, G.R., 1985, Geothermal exploration in Oregon, 1984: Oregon Geology, v. 47, p. 63-66.
Sherrod, D.R., 1986, Geology, petrology, and volcanic history of a portion of the Cascade Range between latitudes 43°-44° N, central Oregon, U.S.A.: Ph.D. thesis, University of California Santa Barbara, 320 p.
Sherrod, D.R., and Smith, J.G., 1988, Preliminary map of the upper Eocene to Holocene volcanic and related rocks of the Cascade Range, Oregon: U.S. Geological Survey Open-File Report 89-14, map scale 1:500,000.
Simpson, R.W., Jachens, R.C., Blakely, R.J., and Saltus, R.W., 1986, A new isostatic residual gravity map of the conterminous United States with a discussion of the significance of isostatic residual anomalies: Journal of Geophysical Research, v. 91, p. 8348-8372.
Smith, L., and Chapman, D.S., 1983, On the thermal effects of groundwater flow 1. regional scale systems: Journal of Geophysical Research, v. 88, p. 593-608.

Smith, R.L., and Shaw, H.R., 1978, Igneous-related geothermal systems in Muffler, L.J.P. (ed.), Assessment of the geothermal resources of the United States: U.S. Geological Survey Circular 790, p. 12-17.

Steele, J.L., Blackwell, D.D., and Robison, J.H., 1982, Heat flow in the vicinity of the Mount Hood volcano, Oregon in Priest, G.R., and Vogt, B.F. (eds.), Geology and geothermal resources of the Mount Hood area, Oregon: Oregon Department of Geology and Mineral Industries Special Paper 14, p. 31-42.

Swanberg, C.A., Walkey, W.C., and Combs, J., 1988, Core hole drilling and the "rain curtain" phenomenon at Newberry Volcano, Oregon: Journal of Geophysical Research, v. 93, p. 10,163-10,173.

Table 1. Geochemical and discharge data for hot springs in the study area. Hot spring locations are shown in Figure 2.

Name	Q [a/] (L/s)	T_d [b/] (°C)	T_g [c/] (°C)	pH	Ca	Mg	Na	K	HCO_3	Cl	Br	SO_4	SiO_2
					(mg/L)								
Austin	120	86	186	7.4	35	0.10	305	6.4	36	390	1.4	130	81
Bagby	1	58	52	9.4	3.3	<0.05	53	0.7	69	14	-	42	74
Breitenbush	12	84	174	7.0	95	1.1	745	31	137	1200	5.0	140	163
Bigelow	[d/]	59	155	7.8	195	0.53	675	15	22	1250	8.7	140	73
Belknap	18 [d/]	73	152	7.6	210	0.34	660	15	20	1200	5.4	150	91
Foley	9	79	100	8.0	510	0.08	555	8.7	20	1350	-	510	63
unnamed on Rider Creek	5	46	135	8.5	215	0.07	405	6.1	21	790	2.4	240	47
Kahneeta	69	83	137	8.1	13	0.05	400	11	603	240	-	31	78

a/ Discharge based on chloride-flux measurements, except for Bagby Hot Spring, where discharge was measured directly

b/ Discharge temperature

c/ Chemical geothermometer temperatures based on anhydrite saturation, except for Kahneeta and Bagby, which are based on the silica (quartz) and cation geothermometers. The solubility of $CaSO_4$ provides a geothermometer which indicates maximum temperature, since few geothermal waters are saturated with gypsum or anhydrite (Ellis and Mahon, 1977). Anhydrite saturation values for the Na-Cl and Na-Ca-Cl waters that discharge in the Western Cascades correlate well with calcite saturation and sulfate-water isotope temperatures (R.H. Mariner, T.S. Presser, and W.C. Evans, written commun, 1988). The temperatures listed for Kahneeta and Bagby are averages of the quartz and cation geothermometers. These and other geothermometers are discussed by Fournier (1981)

d/ Combined discharge of Bigelow and Belknap Hot Springs

Table 2. Conductive heat flow data set.

	Temperature-depth profiles used for heat flow estimates	Advectively disturbed temperature-depth profiles[a/]	Total number of profiles
Blackwell and others (1982) or Steele and others (1982) or Black and others (1983) or Blackwell and Baker (1988b)	88	13	101
This study[b/]	142	111	253

a/ In rocks <6 Ma these are generally near-isothermal temperature-depth profiles, i.e., sites with near-zero near-surface conductive heat flow. In rocks >6 Ma these are generally nonisothermal profiles that are advectively disturbed to the extent that it is not possible to estimate conductive heat flow

b/ Data presented by Ingebritsen and others (1988)

Table 3. Components of the heat budget.

Heat deficit represented by near-zero conductive heat discharge in <6 Ma rocks:

Quaternary arc	-399 MW
2-6 Ma rocks west of Quaternary arc	-18 MW
2-6 Ma rocks east of Quaternary arc	-40 MW
	-457 MW

Anomalous heat discharge in >6 Ma rocks:

Conductive anomaly in the Western Cascades[*/]	137 MW
Advective anomaly in the Western Cascades[*/]	55 MW
Conductive anomaly in the Deschutes Basin[*/]	133 MW
Advective anomaly in the Deschutes Basin[*/]	22 MW
	347 MW

*/ Based on hot spring discharge temperatures. The difference between the geothermometer and discharge temperatures (Table 1) is primarily due to conductive heat loss and represents a significant fraction of the conductive anomaly. Tritium data and the strong correlation between hot spring discharge rates and discharge temperatures (Table 1) indicate that conductive cooling, rather than mixing with cool water, controls the discharge temperatures

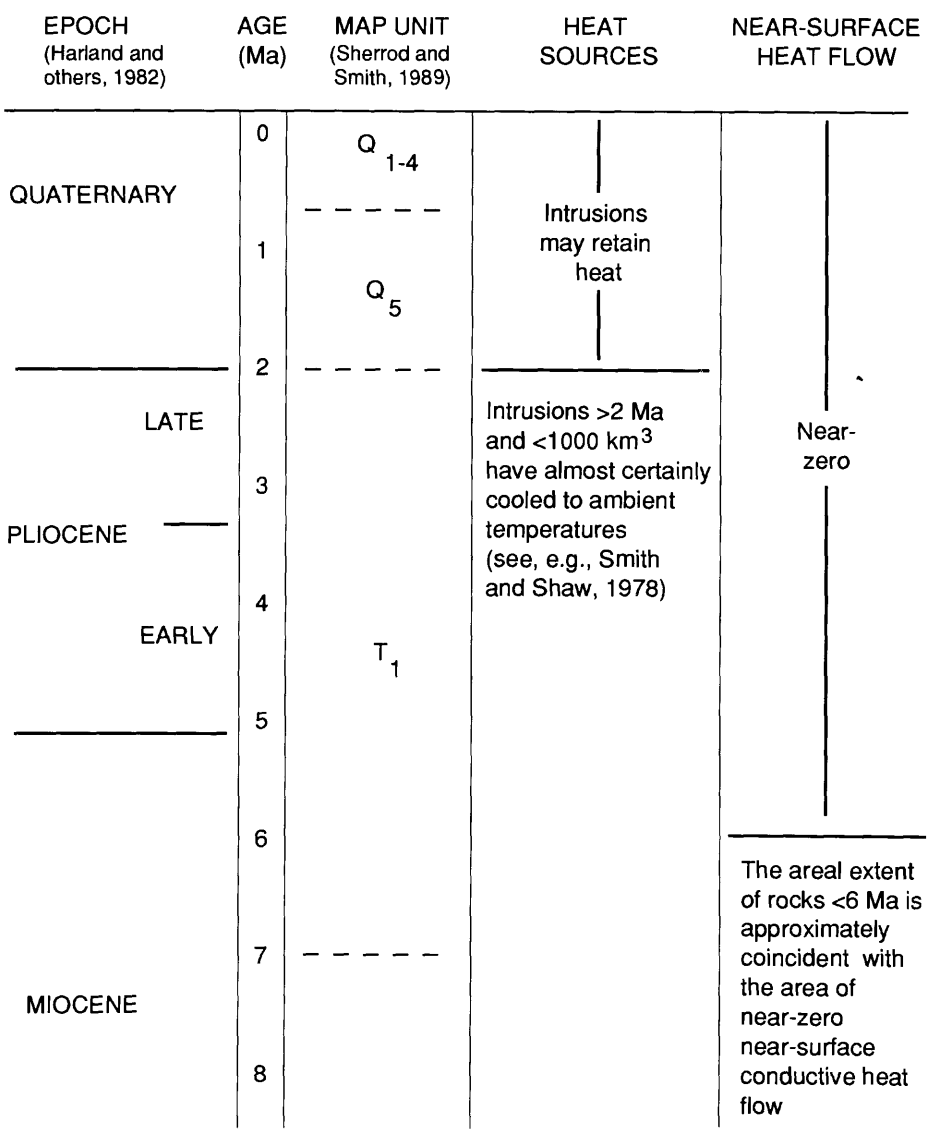

Figure 1. Geologic time scale showing the age divisions emphasized in this paper.

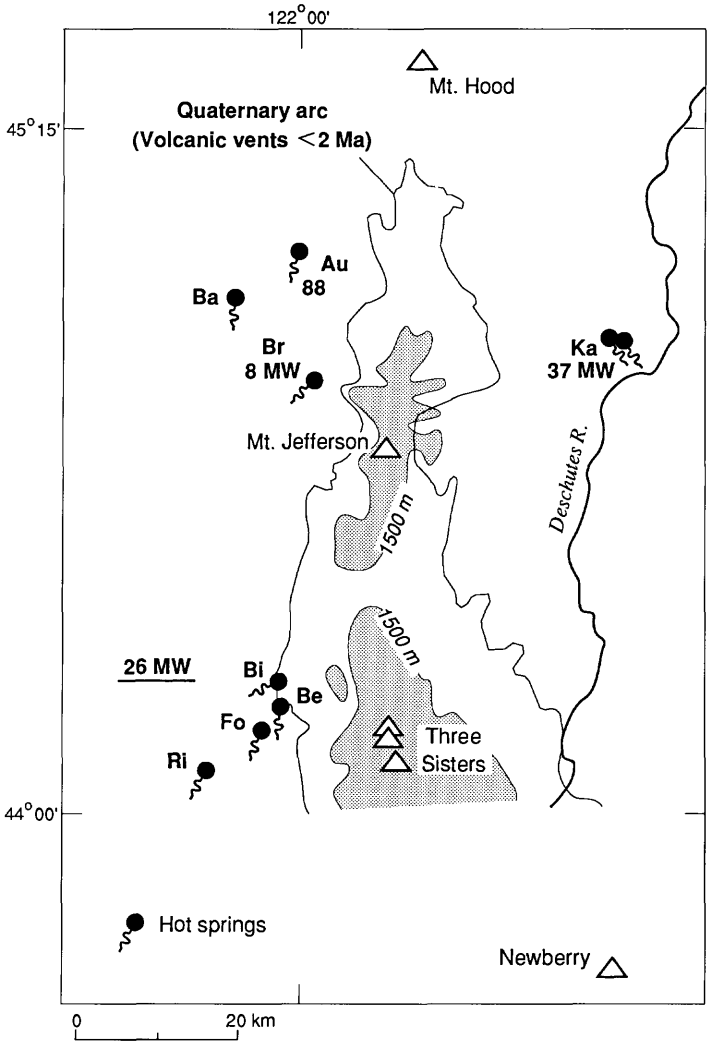

Figure 2. Map showing the location of hot springs, the Quaternary arc, prominent volcanoes, the 1500-m-elevation contour, and the amount of heat transported advectively by the hot spring systems. The total for the southerly group of hot springs (~26 MW) is 1.5x the value obtained from the individual spring groups (Table 1), due to diffuse input of thermal water into the surface drainage. (Hot springs: Au, Austin; Ba, Bagby; Br, Breitenbush; Bi, Bigelow; Be, Belknap; Fo, Foley; Ri, unnamed spring on Rider Creek; Ka, Kahneeta).

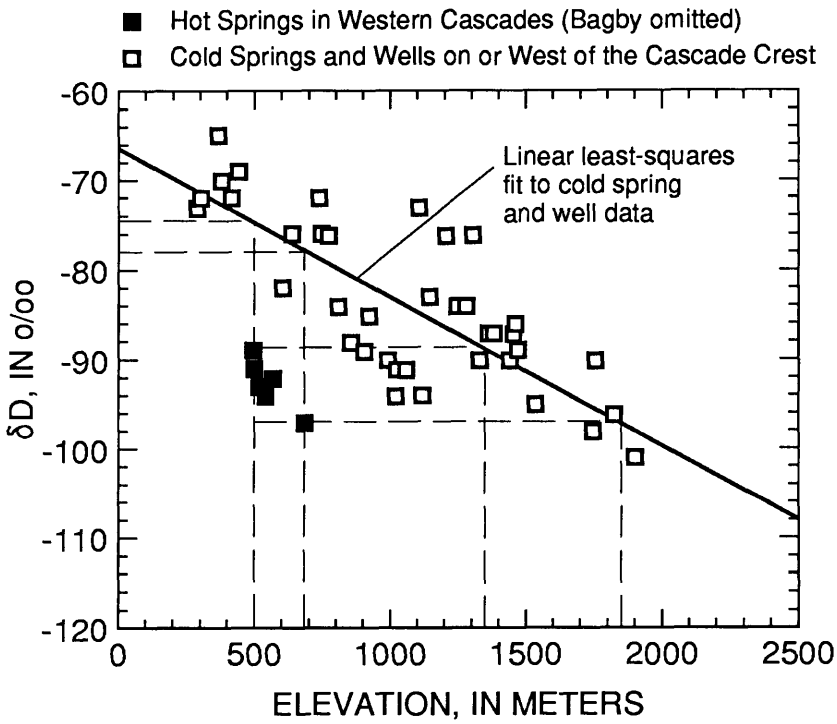

Figure 3. Relationship between deuterium content and elevation for waters on or west of the Cascade crest. Deuterium content (δD) is expressed as D/H ratios in per mil (o/oo) relative to SMOW (Standard Mean Ocean Water). The nonthermal samples are from low-salinity springs and wells in zero- or first-order (unchanneled or headwater) basins, and represent local meteoric water. Because there is little oxygen shift in the thermal waters, $\delta^{18}O$ shows a similar pattern.

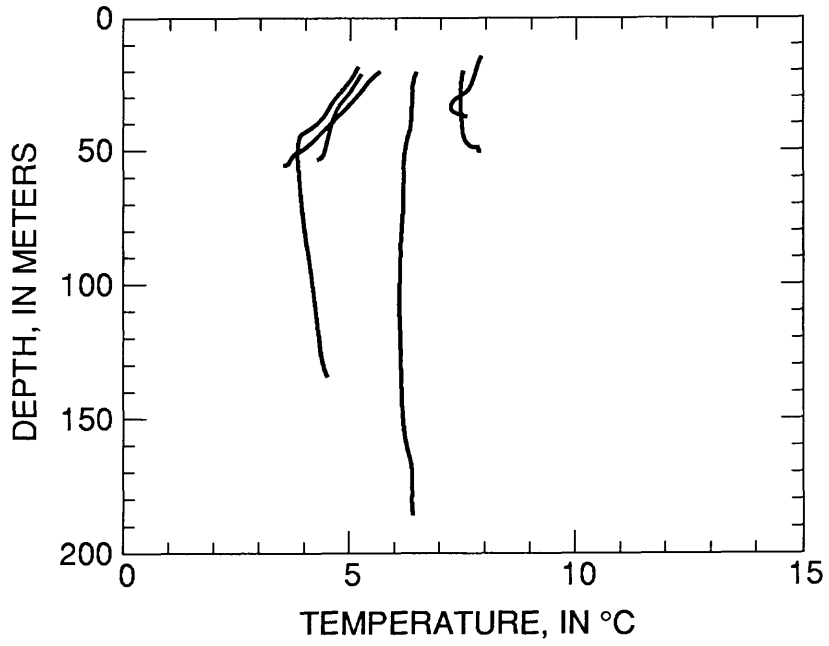

Figure 4. Typical temperature-depth profiles from the Quaternary arc. Data were originally presented in open-file reports released by the Oregon Department of Geology and Mineral Industries.

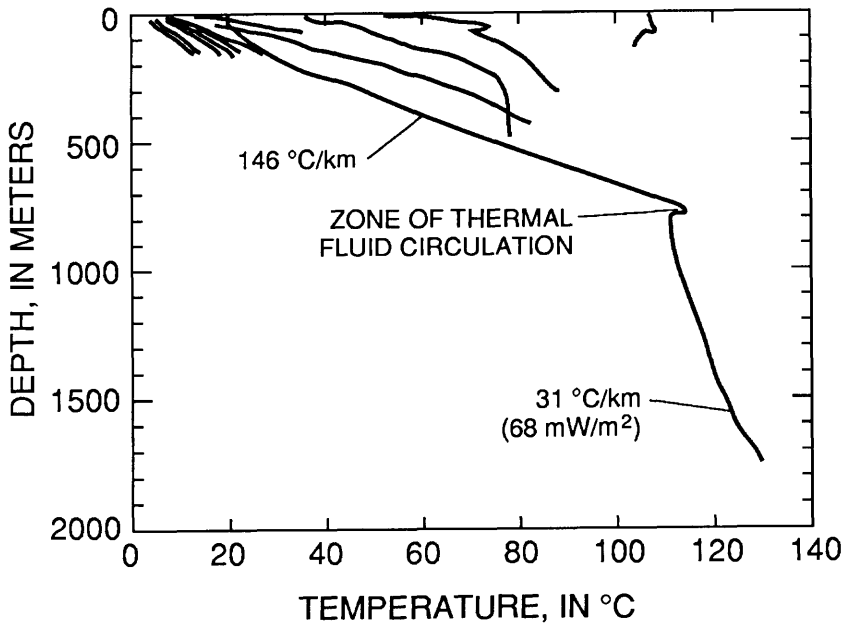

Figure 5. Temperature-depth profiles from drill holes collared in >6 Ma rocks in the Breitenbush Hot Springs area. The deeper hole was completed to 2457 m, but was only logged to 1715 m. The bottom-hole (2457 m) temperature was >141°C (Priest, 1985). The gradient measured over the 1465-1715 m interval (31°C/km) projects to a bottom-hole temperature of 152°C. Data were originally presented in open-file reports released by the Oregon Department of Geology and Mineral Industries or in Ingebritsen and others (1988).

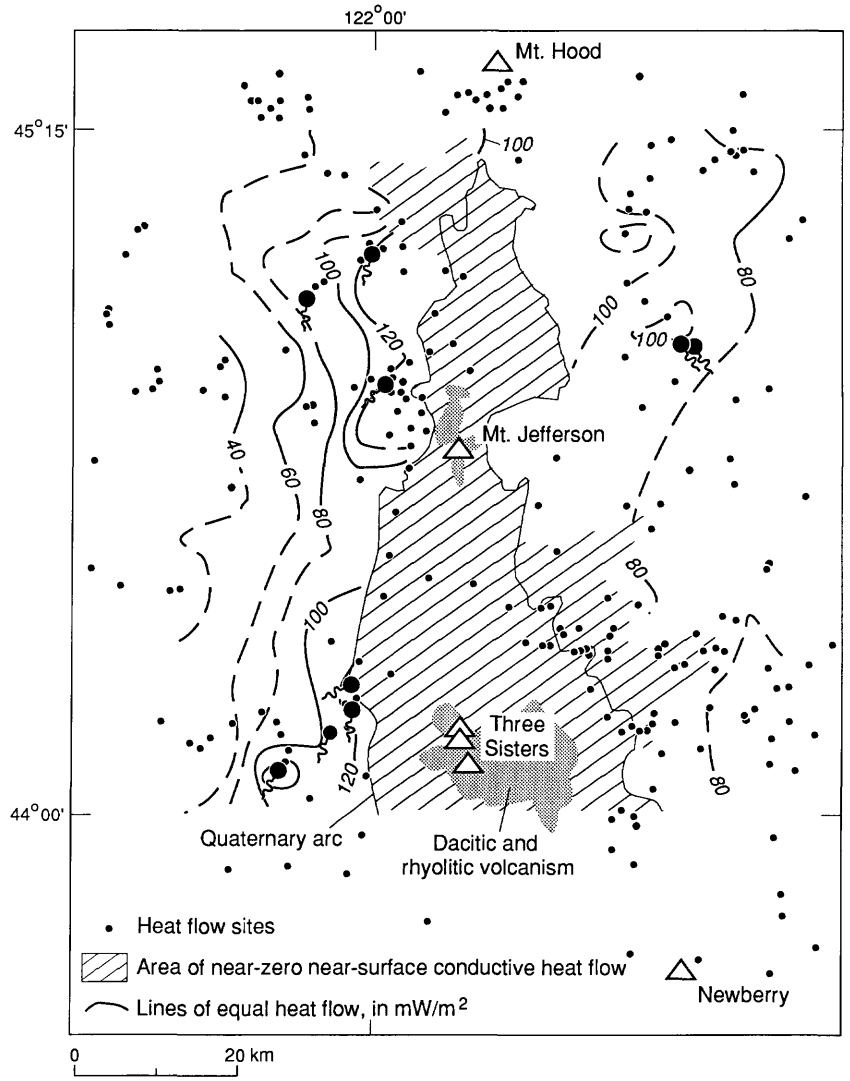

Figure 6. Map showing lines of equal heat flow, in mW/m^2. Area of near-zero near-surface conductive heat flow in rocks <6 Ma is diagonally hatched. This area is estimated conservatively; we have included all of the <2 Ma rocks, but only included 2-6 Ma rocks in areas where temperature profiles confirm near-isothermal conditions. Areas of silicic volcanism in the Quaternary arc are shown with a gray pattern. Dots are sites where temperature profiles have been measured. Names of hot springs are shown on Figure 2.

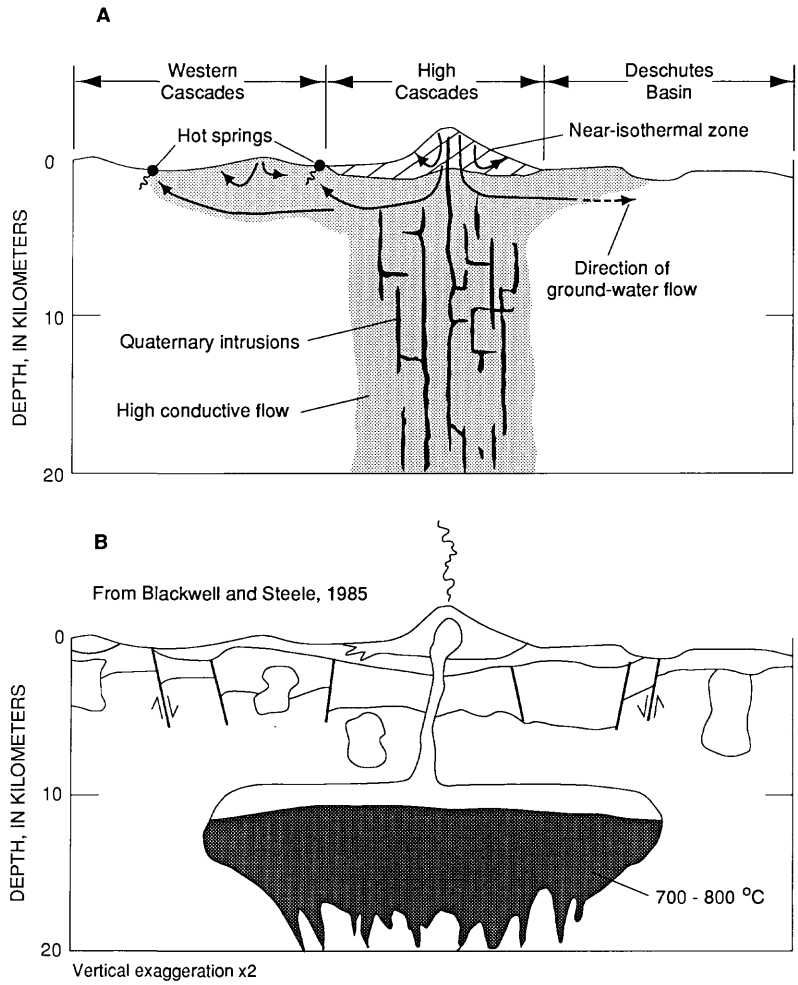

Figure 7. (a) Our conceptual model of the thermal structure of the north-central Oregon Cascades, showing magmatic heat sources confined to the Quaternary arc, and (b) the extensive mid-crustal magmatic heat source proposed in earlier studies (e.g. Blackwell and others, 1982; Blackwell and Steele, 1983; 1985).

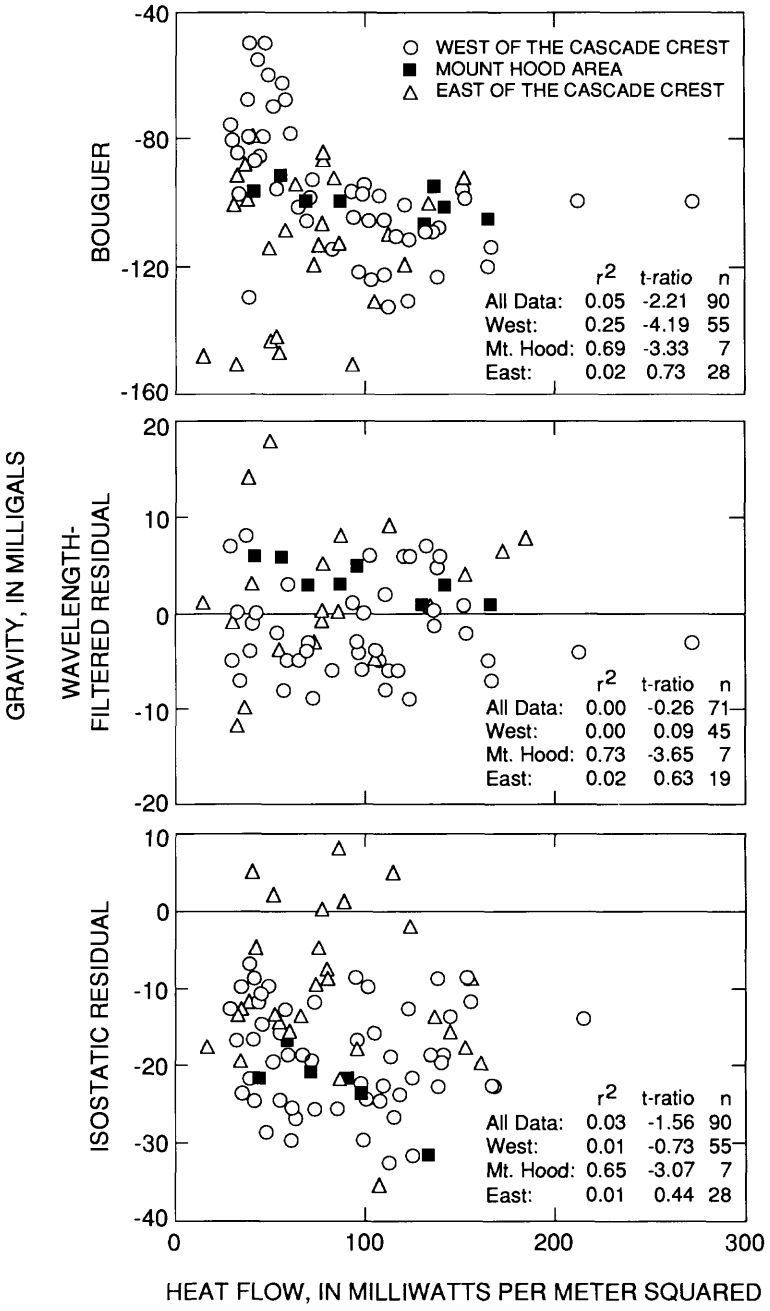

Figure 8. Relationship between heat flow and gravity data. The r^2 and t-ratio values are for linear regressions of gravity on heat flow. Heat flow data from the study area were compiled by Ingebritsen and others (1988); only the better-quality estimates are used here. Bouguer gravity data are from Godson and Scheibe (1982), wavelength-filtered residual data from Couch and others (1982b), and isostatic residual data from Simpson and others (1986).

Heat Flow in the Oregon Cascade Range and its Correlation with Regional Gravity, Magnetic, and Geologic Patterns

David D. Blackwell and John L. Steele (Department of Geological Sciences, Southern Methodist University, Dallas, Texas 75275), Michael K. Frohme (CERI, Memphis State University, Memphis, Tennessee 38152), Charles F. Murphy (21602 Park Villa, Katy, TX 77450), George R. Priest and Gerry L. Black (Department of Geology and Mineral Industries, 905 State Office Building, Portland, Oregon 97201)

ABSTRACT

New heat flow data for the Oregon Cascades are presented and discussed. Heat flow measurements from several deep wells (as deep as 2500 m) are mentioned as well as extensive new data from industry exploration efforts in the Austin/Breitenbush hot springs areas and the Santiam Pass/Foley hot springs areas. The regional heat flow pattern is similar to that discussed previously. The heat flow is about 100 mWm^{-2} in the High Cascades and at the western edge of the Western Cascades. It is about 40 to 50 mWm^{-2} to the west in the outer arc block of the subduction zone. In the high heat flow zone the heat flow is low in young volcanic rocks due to the high permeability of the rocks and the resultant rapid groundwater flow. There are perturbations to the heat flow in the vicinity of the hot springs where values are typically up to twice the background. The remainder of the area appears to be dominated by conductive heat transfer at least to 2 - 2.5 km depth.

The gravity field in the Cascades is closely related to the heat flow pattern. It is proposed in this paper that the relationship is causal and earlier 2-D modeling is extended to 3-D. Consideration of the effects of a midcrustal density anomaly, such as might be associated with a region of partial melting, has two major consequences. The first of these is that a Western Cascade/High Cascade boundary graben is not required - as opposed to a High Cascade wide feature proposed on the basis of geological studies. Secondly, a prominant northeast/southwest striking regional Bonguer gravity anomaly associated with the south edge of the Columbia Plateaus becomes continuous with a similar feature along the north side of the Klamath Mountains. Apparently this zone is a major crustal feature upon which the gravity effect related to the thermal pattern is superimposed.

INTRODUCTION

It has become clear in the last 10 years that the coastal provinces of the Pacific Northwest of the United States represent a more typical subduction zone terrain than was initially thought. The 1980 eruptions of Mt. St. Helens demonstrated the active volcanism already emphasized by the fact that almost all of the Cascade strato-volcanoes have been active in the last two hundred years. Detailed seismic studies have identified clear evidence of a subducting slab under Oregon and Washington (Weaver and Malone, 1987; Weaver and Baker, 1988). In addition evidence has accumulated that large subduction zone type earthquakes may also be charactistic of the Pacific Northwest, although perhaps on a time scale more extended than those in areas with faster subduction rates (Atwater, 1987; Heaton and Hartzell, 1987).

The thermal pattern in the Pacific Northwest is clearly that of a subduction zone (Blackwell, 1971, 1978, Blackwell et al., 1978, 1982; Hyndman, 1976, and Lewis et al., 1985, 1989). The object of this paper is to summarize thermal results that have become available since the detailed discussion of Blackwell et al. (1982a) for the Oregon Cascade Range and adjoining provinces, including the outer arc, volcanic arc, and back arc provinces. This discussion builds on the results of that study and reference to that paper should be made for the background and interpretations on which this paper is based.

Subsequent to the detailed presentation of the thermal data from north-central Oregon, broad area studies in the United States have been reported for Washington (Blackwell et al., 1985), for the California Cascade Range (Mase et al., 1982), range-wide data have been summarized by Blackwell and Steele (1983a), and some new data for the Oregon part of the Cascade Range have been discussed by Black et al. (1983a). In addition several local area studies have increased understanding of the regional data and because the objective of this paper is to discuss the regional character of the thermal measurements, it is necessary to describe some of these local studies.

A detailed study of the Mt. Hood volcano was described by Steele et al. (1982) and Blackwell et al. (1982b). These holes range in depth to 1.8 km. In general the upper parts of the holes are disturbed by groundwater flow as is typical of volcanic terraines. However, most of the holes are deep enough to penetrate below this disturbing effect, which typically extends to 200 m or more. The heat flow values below the shallow disturbances indicate an systematic increase toward the volcanic center, from regional values of 70-80 mWm^{-2} to over 120 mWm^{-2} within 5 km of the center of the volcano. The shape of the anomaly is consistant with a modest subvolcanic magma chamber larger than a volcanic neck, but of smaller extent and shallower than the regional heat flow anomaly. This anomaly is shown on the heat flow map in Figure 1.

Further to the south extensive industry data have been described in the vicinity of Breitenbush and Austin hot springs (44°40'N to 45°N, Blackwell and Baker, 1988a, 1988b). These data include a well 2.5 km deep drilled near Breitenbush hot springs (Sunedco Fed 58-28). The results of this exploration augment the regional data base and are included in Figure 1. Temperature-depth data from the deep well are shown in Figure 4.

Even further to the south industry data are also available for the McKenzie River-Belnap/Foley hot springs area (44°20'N to 44°30'N). These data will be discussed in a subsequent portion of this paper.

Williams and Von Herzen (1983) attempted to make heat flow measurements in Crater Lake using oceanic techniques. Their penetrations were very small, however, and interpretations of heat flow values were made based on penetrations of a few centimeters. These interpreted values show major variations of heat flow. Subsequently a hole was drilled as part of an exploration project along the western border of the park which encountered temperatures of over 100°C with a depth of about 400 m (see Blackwell and Steele, 1987). A controversy has developed about the implications of the geothermal systems and drilling on Crater Lake (Sammuel and Benson, 1987 for example).

Near the California border Black et al. (1983b) described preliminary values for a number of heat flow sites made the vicinity of Ashland, Oregon at and around a small geothermal system there. These measurements are presented in final form in this paper (Figure 1). The Ashland area is part of the Western Cascade regional background except in the vicinity of the geothermal anomaly where heat flow values are approximately twice the regional background.

Mase et al. (1982) presented extensive data from the California portion of the Cascade Range and in ajoining provinces. Most of their holes in the Cascade Range were water wells that did not penetrate below the groundwater circulation effects, consequently they provide little thermal information along the axis of the Cascade Range. The results do document the low heat flow characteristic of an outer arc block in the Klamath Mountains. Beall (1981) presented temperatures from a well at the southern border of Mt. Lassen National Park which indicated extremely high temperatures and active fluid flow in a geothermal aquifer. This area has since been incorporated within the National Park.

Extensive studies have been carried out at Newberry volcano, near the intersection of the Brothers fault zone/Walker Lane and the Cascade Range. A hole was drilled in 1980 that encountered temperatures as high as 265°C in the crater (Sammuel, 1981). Subsequent reports of additional drilling and discussion of the thermal data, and of models, are presented by Blackwell and Steele (1983b, 1987), Swanberg et al. (1988), Sammuel et al. (1988) and others. The most extensive recent discussion of the data is by Sammuel et al. (1988), and further references to the various studies can be found in that paper and in the companion papers describing USGS research at Newberry volcano.

HEAT FLOW MAP

A number of heat flow studies have been completed in the time period since the original discussion by Blackwell et al. (1982a). References have been made to most of the published papers in the introductory section. All of the data have been compiled onto a single map for the southern Washington and Oregon Cascades. This map is shown in Figure 1. All data shown on the map are classified as C or better quality, using the classification as described by Blackwell et al. (1982a). All points shown are holes for which there are samples or reasonable estimates of thermal conductivity. The depth of the holes ranges from about 100 m to 2.5 km for the Sunedco Federal 58-28 at Breitenbush hot springs. Terrain corrections have been made to all the data plotted in the figure. The heat flow data in southern Washington discussed by Blackwell et al. (1985) are shown to complete the anomaly. There are still large data gaps in the southern Oregon Cascade Range and the pattern there is preliminary. There are a number of reliable heat flow determinations in the Klamath Mountains and at the south end of the Willamette Valley adjacent to the Cascades indicating typical values for the outer-arc low-heat-flow province. The heat flow pattern east of the Cascades around Klamath Falls is very complicated, but the average is certainly high, on the order of 80 to 100 mWm^{-2} (see Sass and Sammel, 1976; Sammel, 1980). The drill hole east of Crater Lake shown in Figure 1 has temperatures in excess of 100°C at 400 m as shown in Figure 4 below (Blackwell and Steele, 1987). Most of the other data have been previously discussed, including the data around Mt. Hood, in the

Breitenbush-Austin hot springs region just north and south of 44°N, and at Newberry volcano. There is little new heat flow data in the outer arc block so the measurements there are still as described by Blackwell et al. (1982a), as is also the case for the Oregon provinces east of the Cascades. The new data presented here do not change the heat flow contours described by Blackwell et al. (1982a) in a significant way although they add to the details of the pattern.

The only area of new data which has not been extensively discussed in the literature is the area between Santiam Junction and Belnap/Foley hot springs, approximately 44° 30' to 44° 20'N (Figure 2). Shown in Figure 2 are locations of drill holes, geothermal gradients and heat flow values. Most of these holes were drilled for geothermal exporation and thermal conductivity samples were not available for measurement, therefore the thermal conductivities were estimated from lithology. Since there are a number of nearby holes with thermal conductivity as described by Blackwell et al. (1982a), and since the thermal conductivity in the Cascades rocks does not vary much, these estimates probably result in reasonably reliable values of heat flow. As shown in Figure 2 the heat flow pattern is complicated. It is zero to negative on the east side, increases to quite high values in the center of the map, and then decreases west of the map to values of less than 60 mWm^{-2}. This same regional pattern is observed elsewhere in the Cascades.

The geology of the area is shown in a very simplified form in Figure 2. The western part of map is underlain by Pliocene and older volcanic rocks, whereas the eastern part of the map is occupied by predominantly Quaternary volcanic rocks with much of it composed of a series of basalt flows that are about 3000 years old (Taylor, 1968). Drill holes 150 m deep in these very young rocks give isothermal gradients due to the rapid lateral flow of groundwater. At slightly greater depths, in slightly older rocks, the lower permeability decreases fluid flow velocity and ubiquity, and the pattern changes significantly.

Two histogram sets are shown in Figure 3 to illustrate the characteristics of the gradient distributions along the boundary of the High and Western Cascades. In Figure 3a a gradient histogram is shown for the wells in Figure 2. In Figure 3b a histogram is shown for the wells in the vicinity of Breitenbush hot springs (Blackwell and Baker, 1988a, 1988b). In the case of the Santiam Pass-Belnap/Foley springs area the ages of rocks cut in the holes are shown in three catagories, older than 2 Ma, less than 2 Ma at low elevation, and less than 2 Ma at high elevation. The mean gradients for the third set of data are negative, whereas the mean gradients for the second set of data are on the order of 25°C/km with the exception of gradients exceeding 100°C/km in 2 wells that are probably associated with the flow of warm water. Temperature gradients in volcanic rocks older than 2 Ma range from 50 to 82°C/km and the mean gradient in this group of wells is 67±4°C/km (N=10).

In one hole (13S/7E-32DC, Blackwell et al., 1982a) the geothermal gradients range from 26°C/km depth to 112°C/km between 15-200 m. The shape of the temperature-depth curve clearly indicates lateral flow of warm water in a confined aquifer through an area characterized by recharge. An adjacent 150 m well has a gradient of 100°C/km (13S/6E-25AC) the highest gradient in the boundary province not near a known geothermal anomaly. So in the northern

part of the map there is probably lateral flow of warm water at relatively shallow depth.

Also shown in Figure 3 are data from Breitenbush hot springs. All of these wells, with one exception, were drilled in rocks older 2 Ma and all have gradients in excess of 50°C/km. In this case the wells are coded based to whether or not they occur in the geothermal anomaly associated with the hot springs. Clearly the cutoff point is arbitrary because the heat flow anomaly blends with the background. If the gradients definitely associated with the thermal anomaly are not included, the average geothermal gradient is 72±4°C/km (N=9).

These two areas are both ones characterized by the presence of high heat flow associated with a geothermal anomaly superimposed on typical background values. These results can be compared to the histogram shown in Figure 3 of Blackwell et al. (1982a, geothermal gradient of the High/Western Cascade boundary province) which shows a very similar distribution (66±4°C/km). As a farther investigation of the distribution of gradients a correlation of geothermal gradient with elevation was investigated. In general no correlation between elevation and gradient was found and high gradients are observed in high elevation as well as low elevation with the converse also being true. These results suggest that regional hydrology cannot be invoked to explain the distribution of gradients and heat flow values in the Western Cascades. This point is farther illustrated by the Wolf Meadow hole, one of the farther west holes showing high gradient in the area shown in Figure 2. This hole has a collar elevation of over 999 m and a geothermal gradient of 73°C/km. It is well to the west of the set of down-to-the-east Cascade graben bounding faults along the McKenzie River and it is very difficult to understand how regional groundwater circulation could explain such a high value of gradient, at such high elevation, so far west of the bounding structures associated with the more porous, young volcanic rocks in the High Cascades.

The gradient patterns shown in Figure 3 have been previously reported by Blackwell et al. (1982a) where it was clearly realized from the drilling that the shallow hydrology and shallow thermal conditions were related to age, i.e. maximum depth of burial (maximum temperature reached) of the rocks. The effect of alteration on decreasing permeability and supressing groundwater flow is very clear in the Breitenbush area (Blackwell and Baker, 1988a, 1988b). The degree of success of drilling 150 m holes in the Cascades is a testimony to the careful selection of sites based on age and alteration criteria by the DOGAMI geologists in charge of siting the wells. Other studies which have been more constrained by a need to have data from certain locations and/or characterized by lack of attention to the local geology, have had significantly lower rates of success in 150 m exploration holes.

This fluid flow phenomenon has been referred to as the "rain curtain" and discussed in detail for two Newberry volcanic holes by Swanberg et al., 1988. Deep temperature gradient holes in the Cascades are shown in Figure 4. All holes in excess of 1 km are plotted, excluding data from the Newberry volcano. This figure shows that isothermal sections occur to depths ranging between 100 and approximately 400 m at various sites within the Cascades. It also shows that, on the basis of present data, consistently high geothermal gradients (in excess of 50°C/km) are observed below the zone of shallow groundwater circulation suggesting that there is often an abrupt transition between rocks

which have high permeability and rapid fluid through flow and rocks where the average permeability is quite low and fluid flow is greatly supressed except along particularily favorable stratigraphic regions (such as between 800 and 820 m in Sunedco 58-28) or along fractures or fault zones.

Also shown in this figure are temperature-depth curves from the well at the edge of Crater Lake Park (CE-CL-1) and a deep exporation hole drilled by an exploration company approximately mid-way between Mount Shasta and Medicine Lake (ML-88-12) at high elevation in the region of zero to negative surface geothermal gradients based on shallow hole data (Mase et al., 1982). This hole shows the characteristics of most of the holes in the High Cascades of low gradient to some depth (on the order of 400 m here) and high gradients below that depth. The temperature log is not equilibrium as indicated by hooks in the curve, however the mean gradient between 500 m and 1.2 km is 100°C/km and a depth of 1.2 km the temperature is over 105°C.

GRAVITY INTERPRETATION

Blackwell et al. (1982a) presented a simplified 2-D interpretation of the gravity field in the Cascades and discussed features that may correlate with the heat flow anomaly. Couch et al. (1982a, 1982b) have recently published extensive measurements that are suitable for detailed 3-D analysis. Thus an areal study of the gravity field was carried out as part of this study in order to examine the plausability of the 2-D interpretation.

In the analysis of gravity data, one is usually concerned with those data that represent either the large-scale, long wavelength features (regional), or the small-scale short wavelength features (residual). In either case, it is necessary to determine the regional trends in the data, so that they may be analyzed or removed, depending upon the features of interest. Many different methods have been used to estimate such regional trends including low-order polynomial surface fitting and various filtering methods in the frequency domain. These filtering methods, usually based on Fourier transform applications, are currently the most common means of determining regional trends. A typical approach with this method is to determine the shortest wavelength for which isostatic compensation occurs. This wavelength can then be used to define the break between regional and residual trends. Statistical methods relating the gravity signal to that of topography (Dorman and Lewis, 1970; Aiken and Anders, 1981) have been used in an attempt to better estimate this cutoff wavelength, and in turn, the regional trends defined by the data. Murphey (1982) proposed a similar statistical method that defines the regional trends as those components of the transformed (Fourier) data which show a linear relationship between gravity and topography.

The last of these methods is utilized in the analysis of gravity data from the Cascades Range in Oregon. This analysis combines the gravity, topographic, and heat flow data (Blackwell et al., 1982a and this paper), in conjunction with previous interpretations of magnetic and gravity data (Connard et al., 1983; Blakely et al., 1985) into a possible regional interpretation of the observed features in all of the data.

Geological Setting The study area for the gravity analysis is located between 121° W and 122° 30'W, longitude, and between 42° and 45° 30'N latitude. This area contains portions of several physiographic provinces including

the Western Cascades, the High Cascades, and small parts of the High Lava Plains, the Basin and Range, and the Deschutes-Umatilla Plateau.

There are many mapped faults, fault zones, and structural lineaments in and around the Cascades that present possible constraints on interpretations to the observed gravity data. Major normal faults (down to the west) exist on the eastern edge of the High Cascades Range (Green Ridge Fault, Walker Rim), while minor normal faults (down to the east), lineaments, and hot springs, exist on the western edge. It has been suggested (Peck et al., 1964; Allen, 1965) that the entire High Cascades Range occupies a broad north-south trending graben. This structural depression contains all of the major stratovolcanoes except Mt. McLoughlin, where the western bounding faults change from a north-south trend, to a more northwest-southeast trend, possibly associated with the mechanism causing the Mt. McLoughlin zone.

Data Reduction The data for this project have come from a number of sources. A magnetic tape of gravity data collected by the Geophysics group at Oregon State University was available, containing location, observed gravity, free-air and simple Bouguer anomalies, and terrain corrections. Due to the rapid changes in elevation associated with mountainous terrain, the terrain corrections may be somewhat inaccurate. The data were reduced to Complete Bouguer Anomaly values using an assumed crustal density of 2.67 gm/cc. There may be some question as to whether or not this reduction density is valid, but the features in question, to be discussed later, have been shown to exist for reduction densities of 2.43 gm/cc, and 2.28 gm/cc as well (Blakely et al., 1985). The original data locations are shown by Couch et al. (1982a, 1982b) The gravity data were interpolated to an evenly spaced grid using a standard interpolation routine (Shepard, 1968). After preparing contour maps of the original gravity data, spurious data points, usually representing incorrect terrain corrections, were located and removed. The data were regridded, yielding Bonguer gravity map shown in Figure 5a. Digital topographic data were reduced to the same grid as the gravity data. A smoothed topographic contour map is shown in Figure 5b.

Before transforming the data sets, the standard techniques to avoid "ringing" and edge effects were applied: mean removal, tapering, and padding the data set. Next, both the gravity and the topographic data sets were transformed into the frequency domain using a 2-dimensional arbitrary radix Fast Fourier Transform. Converting the data into the frequency domain allows for simple determination of the regional trends in whatever spectral analysis technique is desired.

Process and Analysis Technique As stated earlier, the topographic coherency method proposed by Murphey (1982) is used in order to define the regional trends in the data as well as conventional band pass filtering. The topographic coherency method is based on several principles. One of the standard corrections applied to the data is the assumption that the topography is a load upon the lithosphere. Now, if the topography is already in isostatic compensation, these corrections are applied incorrectly, so that the gravity should "mirror" the corresponding topography. Therefore, by comparing the shapes of both the gravity and the topography signals, one can assign a correlation coefficient between corresponding frequencies in the two data sets. This coefficient will take on values from 0 to 1, where 1 represents a linear relationship. The actual equation is:

$$\text{Coherency Coefficient} = \frac{[(A^*)*B]}{[|A|^2]*[|B|^2]}$$

With A,B = elements of the transformed data matrices

A^* = complex conjugate of the element

$[\cdot\cdot]$ = averaging by pyramidal window

Applying this equation to the data sets creates a matrix which indicates how well each wavenumber pair (Kx,Ky) in the gravity signal agrees with its corresponding pair in the topography, or equivalently, how well the gravity can be predicted from the topography (Murphey, 1982). At this point, the regional trends can be defined as those wavenumber pairs that have a coherency greater than a certain "cutoff coherency". This cutoff value is determined by inspecting the coherency plot for the classical long-wavelength gravity to topography linear relationship as described by Nettleton (1976).

Application to the Cascades Range Visual analysis of the gravity data reveals a change in Bouguer gravity of more than 50 mgals, decreasing from west to east, onto the High Cascades platform. The most rapid decrease in Bouguer gravity occurs 10-15 km west of the Western Cascades - High Cascades boundary, and corresponds directly to the increase in heat flow (Blackwell et al., 1982a, Figure 8). There are several explanations that could account for the rapid change in gravity. The first possibility is that the mechanism responsible for the rapid change in gravity is also responsible for the change in the heat flow data (the interpretation favored by Blackwell et al., 1982a). The second possibility is that the gravity gradient corresponds to the proposed Cascades graben, with low density young volcanics to the east (Couch, 1979; Couch et al., 1982b). A third possibility is that the correlation is accidental, and the gravity is explained by a change in the density structure in the crust across the Western Cascades - High Cascades boundary. Because of the close correlation of the gravity and heat flow data across the transition zone, and the lack of major changes in geologic structure, Blackwell et al. (1982a) argued for the first possibility as a reasonable explaination for the observed data.

Separation of regional trends was done in the frequency domain by standard low-pass techniques and by the coherency method. The regional gravity, as determined by those features of wavelength > 89.25 km., is given in Figure 5c. The value of 89.25 km. was determined by inspecting maps of the regional trends created using different cutoff wavelengths and choosing the most representative value. This cutoff wavelength is also used by Couch (1979; Couch et al., 1982b) define the regional trends. The regional trends as determined for a coherency limit of 0.80 are given in Figure 5d, although correlations were also prepared for coherency limits of .75, and .85. Note that the coherency-derived regional contains high frequency components, due to the assumption that the regional trend is defined by all those wavelengths showing a strong linear relationship between gravity and topography. A regional difference map was constructed by subtracting the conventional band-pass regional from the coherency derived regional (the regional trend as defined by the coherency cutoff of .80 was used). This difference map, given in Figure 6a, reveals parallel, north-south trending linear highs and lows.

Removal of the regional trends defines the residual map. The residual map for the coherency limit of 0.80, leaving only those features not showing a strong relationship between gravity and topography, is given in Figure 6b. The residual map derived by the conventional band pass method is shown in Figure 6c for comparison.

Motivation for Heat Flow Model A predominant feature in the residual maps is the linear trend of negative residual anomalies along the western edge of the study area. Comparson of the trend of the anomalies to the heat flow data shows that the residual lows almost directly coincide with the 80 mWm^{-2} contour in the heat flow data. In comparing the regional data, there is an even more striking resemblence between the heat flow and gravity data sets. The regional anomaly pattern in the northern half of the study area (Figures 5c and 5d) mimics the heat flow contours. In order to determine if the heat flow and gravity data could be related to the same source mechanism, a 3-D density difference model was calculated from the heat flow data.

Blackwell et al. (1982a) derived a density vs depth structure (2-D) by removing characteristic background temperatures from the data, and multiplying the temperature differences by the coefficient of thermal expansion. Using average surface gradients and heat flow, known thermal conductivities and heat production rates, and presumed radioactivity distributions with depth, temperatures were calculated as a function of depth. Subtracting these temperatures from the downward continued heat flow data (calculated using the method of Brott et al., 1981) resulted in the temperature differences, which were converted into density difference Model A (Blackwell et al., 1982a, Figure 2). In order to fit the observed gravity more accurately, the density contrast between 6 and 10 km, was increased to 0.15 gm/cc, giving model B (Blackwell et al., 1982a, Figure 2). A density contrast of this magnitude, however, can not be explained by thermal expansion alone, so a phase change such as partial melting would be needed to account for the contrast. The choice of 0.15 gm/cc is not arbitrary, as common volcanic rocks tend to exhibit a density change of about 6% (0.15 gm/cc) at or near the melting point (Murase and McBirney, 1973). A third model that would correspond to a slightly deeper melt zone than model B was also derived (Blackwell et al., 1982a, Figure 2, Model C).

Leaver et al. (1984) analyzed seismic refraction data along a north-south line extending from Mt Hood to Crater Lake. The crustal models interpreted from this data show surprisingly little structural variation along the entire length of the survey. This lack of variation in the north-south direction would seem to imply that the problem may be more of a two- dimensional problem than a true three dimensional problem. Based on this assumption, the 2-D density differences were extended into three dimensions as finite length rectangular prisms. Model B was used to represent the highest temperature region, directly under the High Cascades axis, while model C, somewhat cooler, was used to the north and to the east to model thermally caused density contrasts between the Basin and Range province and the low heat flow block. Where thermal data are sparce, the region of shallow Curie point isotherms identified from aeromagnetic data (Connard et. al., 1983) was used to constrain the prism boundaries.

The effects of thermal model upon the gravity field are illustrated as calculated using a 3-D Talwani approach (Talwani and Ewing, 1960) in Figure 7.

In order to determine to what extent the thermal structure affects the gravity, the calculated gravity was subtracted from the original Complete Bouguer Anomaly values. The "heat flow corrected" data were then transformed again, and the coherency and band pass regional separation methods were reapplied to the data. The corrected regional trends are shown in Figures 8a for the coherency method, and Figure 8b for the standard bandpass method, with 89.25 km cutoff wavelength.

Gravity-Heat Flow Correlation Recently, analyses of the Cascades Range have been done using gravity data (Couch et al., 1982a, 1982b), or magnetic data (Couch et al, 1985; Connard et al., 1983). Blakely et al. (1985) combined available gravity and magnetic data in interpreting the tectonic setting of the southern Cascades. In these cases, the surface heat flow data was not considered of major importance in the interpretation of the gravity data. However, in view of the close correspondance of the thermal and magnetic data it seems appropriate to investigate the correlation of the gravity and heat flow data.

A visual inspection of the regional gravity (Figures 5b and 5c) and the contoured heat flow data (Figure 1) reveals a striking similarity. The shapes of the contours are remarkably similar in the northern half of the study area, which seems to imply that the same source mechanism might explain some features observed in both data sets, especially in the area between 43 N latitude and 45 30' N latitude. Removing the gravity that would be observed over this structure due to change in density with temperature due to thermal expansion and possible phase changes reveals several interesting features.

The difference between the temperature - corrected regional (Figures 8a and 8b) and the non-corrected regional trends (Figures 5c and 5d) is remarkable. In the corrected regional, almost all traces of the north-south trend present in the original data have been removed. Now, the major directional trends have become northeast-southwest across the center of the study area, and northwest-southeast in the southern half. The Bouguer gravity values increase by about 50 mgals across the center of the map, from south to north. Outside the map area, to the northeast, there is a similar northeast-southwest trend with a regional gravity contrast of 50 mgals (Riddihough et al., 1986). Comparison of the map area in Figure 8 to Oregon-wide data shows that when the gravity-thermal correlation is applied the trend continues across the map area.

In addition to the gradient across the center of the map, the removal of these "heat flow effects" accentuates a Basin and Range type gravity signal (highs and lows trending northwest-southeast) in the southeastern part of the study area. The wavelength of the observed features is typical for Basin and Range type regional trends. Furthermore, the majority of the linear trend of negative anomalies in the western edge of the study area has been accounted for by the removal of the heat flow corrected regional trends from the data (Figure 6d).

Gravity Explained by Cascade Graben In examining the gravity data for the Cascades, Couch et al. (1982a, 1982b) and Blakely et al. (1985) interpreted a narrow north-south trending minimum as the signature of the proposed buried graben of Allen (1965). This graben includes most major stratovolcanoes (Mt. Hood, Mt Jefferson, Three Sisters, Crater Lake), although it swings southwest

to exclude Mt. McLoughlin. All the major stratovolcanoes also lie along the western edge of the gravity low, whose position agrees approximately with the proposed graben, although Mt. McLoughlin is included in the gravity low (Blakely et al., 1985). The interpreters have proposed that the volcanoes have formed along perimeter faults associated with subsidence of volumes of low-density material. The perimeter faults would provide the magma with easier access to the surface, thus explaining the observed gravity and the geologic features. The gravity gradient observed in the western edge of the study area is proposed to be due to the density contrast across a fault at depth. Couch et al. (1982a,1982b) show that for the rock types and densities found throughout the section, the required displacement across this fault would be on the order of 1.2 to 1.5 km. The surface heat flow data, and the presence of numerous hot springs attest to the known geothermal potential of the area, but these thermal effects are proposed to be local events, and would have little effect upon the gravity data.

A graben model similar to the one proposed by Couch et al. (1982a, 1982b) was constructed. The boundaries of this model were aligned to match the surface gravity as well as possible, while the density contrast (0.40 gm/cc) was chosen to give a signal amplitude of approximately 25 mgal. The gravity generated by this model was removed in the fashion previously described. The bandpassed gravity is given in Figure 8c. The effect of this model is most obvious in the southwest part of the study area. In looking at the coherency defined regional trends, the high frequency signal due to the graben density structure is immediately obvious. The predominant trends are north-south, due to the strong influence of the shallow density contrast.

The interpretation presented by Blackwell et al. (1982a) was that the High Cascades are underlain by magma staging chambers, thus allowing for the accumulation of lower density, partially molten material. This model provides the source mechanism(s) that would explain the features seen in the gravity, magnetic, and heat flow data. The heat flow and gravity can be accounted for by considering the magma chamber(s) to occupy the low density/high temperature region (in model B, Figures 8a and 8b) from 6 to 10 km in depth. The partially molten rock could also provide the temperatures needed for the Curie point isotherms at depths of 6 - 10 km. The location of Mt. McLoughlin would now associated with the magma, and therefore the gravity low. The structural features seen, such as the northwest trending lineaments and fault zones could be caused by extension of the Basin and Range province. Thus the fact that Mt. McLoughlin does not occupy the graben, while coinciding with the gravity low, implies that the graben structure would not be a controlling factor in the gravity signal, but merely an effect of the extension of the Basin and Range.

Crust-Mantle Model In order to compare the possible interpretations involving the upper crust, a third, deep source model, a model was examined. A deeply buried source (40 km) having the same shape as the heat flow model previously discussed was used. The gravity effect due to this source was calculated and removed form the original data. The corrected regional trends are shown in Figure 8d. Since the signal due to the deep source is broad, its effect is seen over the whole map area, thus the shapes are not noticeably changed. These alternative models present different ways of trying to explain the observed gravity signal, yet they do not seem to reveal as much information (in terms of influence from outside the map area) as the heat flow model does.

Conclusions of Gravity Analysis The fact that the heat flow contours agree with the regional trends in the gravity is evidence that: 1) the heat flow transition is related to regional crustal effects, rather than surficial groundwater circulation, and 2) that the regional gravity and heat flow data might be controlled and defined by the same mechanism.

Although the results of the study are not conclusive, they are suggestive, and the basic conclusions regarding the relationship of the thermal effects to the gravity data should remain. Several features explained by this relationship have been proposed. First, the removal of the "heat flow generated effects" upon the gravity results in outside trends in the gravity being projected through the study area. Next, this removal also suppresses the linear trend of negative residual anomalies that correlate directly with the heat flow data. Finally, the strong correlation between regional gravity and heat flow contours is possible evidence of one source mechanism for both data sets. Due to the evidence presented, we do not believe that the thermal effects upon the gravity data seen in the Cascades can be neglected in any full-scale interpretation.

DISCUSSION

It is argued in this paper that the regional thermal, gravity and magnetic data point toward a major heat source in the upper crust beneath High Cascades in northern Oregon. This heat source is required by the heat flow and Curie point depth data and is consistent with the gravity data. In fact taking into account the heat source and its possible effect on the gravity field results in an interpreted regional gravity field which is more consistant with regional patterns outside the Cascades. Figures 9 and 10 are prepared as a summary of the various geophysical data in the Cascades. Figure 10 shows in summary cross-section form the results of seismic, thermal, magnetic and electric investigations. Leaver et al. (1984) presented data from a north-south refraction profile along the Western Cascades near the boundary of the High Cascades. Catchings and Mooney (1988) have discussed the extensive refraction data set that deals with the vicinity of the Newberry volcano, immediately east of the High Cascades and Zucca et al. (1986) have studied the Medicine Lake area. No data is available for the area in between Newberry and the Western Cascades except along the line of a reflection profile that does not furnish any additional information on deep crustal structure (Keach, 1987). In the Western Cascades the crust is in excess of 40 km thick, whereas in the High Lava Plains it is approximately 35 km thick. The High Lava Plains has a velocity structure and crustal thickness more typical of the Basin Range province because it has approximately equal portions of velocity below and above 6.5 km/sec. On the other hand the Western Cascades crust has a velocity distribution more typical of an island arc because velocities below 6.5 km/sec make up only 25% of the total crustal thickness. Unfortunately the data do not allow resolution of where the change in crustal type occurs across the High Cascades.

The areomagnetic data discussed by Connard et al. (1983) are in remarkable agreement with the heat flow data. Areas of shallow Curie point based on a spectral analyses of the magnetic data are shown in Figure 9 as overlays on the contoured heat flow map. Connard et al. (1983) pointed out the remarkable coincedence between the areas of shallow Curie point and the heat flow anomaly in the Western Cascades/High Cascades. These results are shown diagramatically

in Figure 10 as bands giving the variation of depth to the Curie point in the particular cross sectional location of the High Cascades near the intersection with the High Lava Plains. Finally Stanley (1982) has presented a pliminary interpretation of electrical resistivity information for the Oregon Cascades. He located the boundary of a major upwarp of the crustal conductor and pointed out that it coincided with the major gravity gradient between the Western Cascades and High Cascades which, as has been illustrated previously, also coincides with the heat flow boundary. The results from the profile across central Oregon are shown as the dotted line, which represents the boundary between areas of resistivity between areas of 30 and 1000 Ω-m above and 3 to 40 Ω-m below (Figure 10).

Blackwell et al. (1982a) interpreted the heat source to represent a major staging magma chamber or magma reservior underlying most of the High Cascades and at temperatures near the melting for silicic rocks. So upper crustal rocks that are in contact with the heat source there could be at least partially melted. Physical conditions at this depth would be pressures on the order of 3 kbars and temperatures on the order 600-800°C. Interpretation of the results from the southern Washington Cascades suggest a similar depth to heat source but indicate a temperature of only 400-500°C for that heat source (Blackwell et al., 1985). There should be little or no partial melt available on a regional basis there, although small pockets are not resolvable as individual bodies because of the sparse regional heat flow data.

In the case of the Oregon crust it is inticing to think of the location of the magma chamber as related to the density change indicated by the seismic refraction data from higher densities associated with relocaties of 6.4-6.5 km/sec to densities associated with upper crustal velocities of 6.0-6.1 km/sec at a depth of about 10 km. The significant density change might localize residence of magmas if they do not have significant hydraulic head to reach the surface. However, in the Washington Cascades such an interpretation is not as viable because the upper crust is more silicic and the major crustal density change occurs well below the depth the top of the heat source. Therefore, in the case of the Washington Cascades at least the major factor may be the rapid decrease in temperature above depths of 10 km associated with the bottom of the upper crustal radioactive layer. Some unknown structural discontinuity might also provide the localizing effect.

The composition of material in the magma chamber is not resolved at the present time. The gravity data have been interpreted to suggest that the magma chamber represents a more or less continuous body of partially melted silicic material. However, there are other interpretations of the gravity data and the area might also be characterized by discontinuous, unconnected pockets of magma that only appear as a continuous heat source at the surface on the order of 10 km away. Also not known is whether there might be a more or less continuous gabbroic magma chamber underlying the heat source or wheather pockets of gabbroic magma in the lower crust, or perphaps concentrated at the crust/mantle contact (Hildreth and Moorbath, 1988) are generating secondary magmas by partical melting and by fractional crystalization which subsequently move up and form the upper crustal heat source identified by the heat flow data.

In earlier discussions of heat flow data Blackwell et al. (1978, 1982a) discussed in detail the possible groundwater circulation patterns which might

generate the heat flow anomally along the Western Cascades/High Cascades boundary and also might generate the geothermal systems associated with the Western Cascades. Recently Ingebritsen et al. (1988) have resurrected the idea that high heat flow along the Western Cascades/High Cascades boundary is related to groundwater circulation and not to a mid-crustal heat source. They prefer to interpret any heat source as being confined more narrowly to the axis of the High Cascades. However, as shown in Figure 9, when the heat flow anomaly is compared to the areas of volcanic sources over the past 1 m.y. as described by Guffanti and Weaver (1988), there is a close correlation between the width of the source zone and the width of the extrusive heat flow anomaly, particularly if it is taken into account that the heat flow anomaly is somewhat wider at the surface than the actual source would be at depth. Since the thermal process over a depth and/or distance range of 10 km is averaging over several million years, the concidence of the data sets is consistent with the interpretation of an upper crustal heat source. One implication is that the present day surface position of the stratavolcanos, which represent the most charactristic features of the arcs, are not related to long term intrusive features. Thus over a longer period of time than the life of one stratavolcano (probably on the order of a few hundred thousand years), the positions are such volcanos will probably migrate back and forth over the width of this upper crustal staging chamber. In the Cascades the width of this zone appears to be on the order of 50-60 km. Based on this interpretation, for example, the width on the volcanic arc at Mt. St. Helens and Mt. Adams is related to the source width and indicates the width of the upper crustal chamber along the axis of the Cascades.

ACKNOWLEDGEMENT

Most of the studies described in this paper have been supported by USDOE. Collection and interpretation of the Cascade thermal data in particular has been supported by USDOE Grant No DG-FG07-86ID12623 to SMU. Edward Western and John Knox were responsible for permission to use extensive SUNEDCO exploration results in the Breitenbush and Santiam Pass areas.

REFERENCES

Aiken, C.L.V., and M.E. Ander, A regional strategy for geothermal with emphasis on gravity and magnetotellurics, J. Vol. Geophys. Res., 9, 1-27, 1981.

Allen, J.E., The Cascades Range volcano-tectonic depression of Oregon, in Transactions of the Lunar Geological Field Conference, Bend, Oregon, August, 1965, 98 pp., Oregon Dept. Geol. Mineral Industries, Portland, 1966.

Atwater, B.F., Evidence for great Holocene earthquakes along the outer coast of Washington State, Science, 236, 942-944, 1987.

Beall, J., A hydrologic model based on deep test data from the Walker "O" No. 1 well, Terminal Geyser, California, Trans. Geothermal Resources Council, 5, 153-156, 1981.

Black, G.L., D.D. Blackwell, and J.L. Steele, Heat flow in the Oregon Cascades, p 69-76, in Geology and geothermal resources of the central Oregon Cascade Range, ed. G.R. Preist and B.F. Vogt, Ore. Dept. Geol. and Mineral Industries Spec. Paper 15, 1983a.

Black, G.L., G.R. Priest, and N.M. Woller, Temperature data and drilling history of the Sandia National Laboratories Well at Newberry caldera, Oregon Geol., 46, 7-9, 1984.

Black, G.L., N.M. Woller, and M.L. Ferns, Geologic map of the Crescent Mountain area, Linn County, Oregon, Ore. Dept. Geol. Mineral Industries Geol. Map Series - 47, 1987.

Black, G.L., M. Elliott, J.D'Alluva, and B. Purdom, Results of a geothermal resource assessment of the Ashland, Oregon, area, Jackson County, Oregon Geology, 45, 51-55, 1983b.

Blackwell, D.D., and S.L. Baker, Thermal analysis of the Breitenbush geothermal system, Geothermal. Resources Council Trans, 12 221-227, 1988a.

Blackwell, D.D., and S.L. Baker, Thermal analysis of the Austin and Breitenbush geothermal systems, Western Cascades, pp 44-62, in Geology and Geothermal Resources of the Breitenbush-Austin hot spring area, Clackmas and Marion Counties, Oregon, ed. D.R. Sherrod, Ore. Dept. Geol. Mineral Industries Open File Rept. 0-88-5, 1988b.

Blackwell, D.D., R.G. Bowen, D.A. Hull, J. Riccio, and J. L. Steele, Heat Flow, Arc Volcanism, and Subduction in Northern Oregon, J. Geophys. Res., 87, 8735-8754, 1982.

Blackwell, D.D., C.F. Murphey, and J.L. Steele, Heat flow and geophysical log analysis for OMF-7A geothermal test well, Mt. Hood, Oregon, pp 47-56, in Ore. Dept. Geol. Mineral Industries Special Paper 14, 100 pp, 1982.

Blackwell, D.D., and J.L. Steele, A summary of heat flow studies in the Cascade Range, Geothermal Resources Council Trans., 7, 233-236, 1983a.

Blackwell, D.D., and J. L. Steele, Thermal model of the Newberry Volcano, Oregon, in Survey of potential geothermal exploration sites at Newberry Volcano Deschutes County, Oregon, Open File Rep. 9-83-3, pp. 83-113, Oregon Dep. of Geol. Miner. Ind., Portland, 1983b.

Blackwell, D.D., and J.L. Steele, Geothermal data from deep holes in the Oregon Cascade Range, Trans. Geothermal Resource Council, 11, 317-322, 1987.

Blackwell, D.D., J.L. Steele, and S.A. Kelley, Heat flow and geothermal studies in the State of Washington, US DOE Rept. ID/12307-1, 77pp, 1985.

Blakely, R.J., R.C. Jachens, R.W. Simpson, and R.W. Couch, Tectonic setting of the southern Cascade Range as interpreted from its magnetic and gravity fields, Geol. Soc. Am. Bull., 96, 43-48, 1985.

Brott, C.A., D.D. Blackwell, and P. Morgan, Continuation of heat flow data; a method to construct isotherms in geothermal areas, Geophysics, 46, 1732-1744, 1981.

Catchings, R.D., and W.D. Mooney, Crustal structure of the Columbia Plateau: Evidence for continental rifting, J. Geophys. Res., 93, 459-474, 1988.

Catchings, R.D., and W.D. Mooney, Crustal structure of east central Oregon: Relation between Newberry volcano and regional crustal structure, J. Geophys. Res., 93, 10081-10094, 1988.

Connard, G., R.W. Couch, and M. Gemperle, Analysis of aeromagnetic measurements from the Cascade Range in central Oregon, Geophysics, 48, 376-390, 1983.

Couch, R.W., Geophysical investigations of the Cascades Range in central Oregon, Final Report, Grant 14-08-001-G-393, 95 pp., U.S. Geol. Surv., Reston, Va., 1979.

Couch, R.W., M. Gemperle, and R. Peterson, Total-field aeromagnetic anomaly maps, Cascade Mountain Range, northern Oregon: Ore. Dept. Geol. Mineral Industries Geological Map Series GMS-40, scale 1:250,000, 1985.

Couch, R.W., G.S. Pitts, M. Gemperle, D.E. Braman, and C.A. Veen, Gravity anomalies in the Cascade Range in Oregon: Structural and thermal implications: Ore. Dept. Geol. Mineral Industries Open-File Rept. 0-82-9, 66 p, 1982a.

Couch, R.W., G.S. Pitts, M. Gemperle, C.A. Veen, and D.E. Braman, Residual gravity maps of the northern, central, and southern Cascade Range, Oregon: Ore. Dept. of Geol. Mineral Industries Geol. Map Series GMS-26, scale 1:250,000, 1982b.

Dorman, L.M., and B.T.R. Lewis, Experimental Isostasy 1. Theory of the determination of the earth's isostatic response to a concentrated load, J. Geophys. Res., 75, 3357-3365, 1970.

Ferguson, W.E., Jr., A simple derivation of Glassman's general N Fast Fourier Transform, Mathematics Research Center, University of Wisconsin, Technical Summary Report no. 2029, 17 pp., 1979.

Frei, L.S., Additional paleomagnetic results from the Sierra Nevada: Further constraints on Basin and Range extension and northward displacement in the Western United States, Geol. Soc. Am. Bull., 97, 840-849, 1986.

Furlong, K.P., and D.M. Fountain, Continental crustal underplating: Thermal consequences and seismic-petrologic consequences, J. Geophys. Res., 91, 8255-8294, 1986.

Gromme, C.S., M.E. Beck, Jr., R.E. Wells, and D.C. Engebretson, J. Geophys. Res., 91, 14089-14103, 1986.

Guffanti, M., and C.S. Weaver, Distribution of late Cenozoic volcanic vents in the Cascade Range (USA): Volcanic arc segmentation and regional tectonic considerations, J. Geophys. Res., 93, 6513-6529, 1988.

Heaton, T.H., and S.H. Hartzell, Earthquake hazards of the Cascadia subduction zone, Science, 236, 162-168, 1987.

Hildreth, W., and S. Moorbath, Crustal contributions to arc magmatism in the Andes of Central Chile, Contrib. Mineral. Petrol., 98, 455-489, 1988.

Hughes, S.S., and E. M. Taylor, Geochemistry, petrogenesis, and tectonic implications of central High Cascade mafic platform lavas, Geol. Soc. Am. Bull., 97, 1024-1036, 1986.

Hyndman, R.D., Heat flow measurements in the inlets of southwestern British Columbia, J. Geophys. Res., 81, 337-349, 1976.

Ingebritsen, S.E., D.R. Sherrod, and R.H. Mariner, Heat flow and hydrothermal circulation in the Cascade Range, this volume, 1988.

Leaver, D.S., W.D. Mooney, and W.M. Kohler, A seismic refraction study of the Oregon Cascades, J. Geophys. Res., 89, 3121-3134, 1984.

Lewis, T.J., A.H. Jessop, and A.J. Judge, Heat flux measurements in south-western British Columbia; The thermal consequences of plate tectonics, Can. J. Earth. Sci., 22, 1261-1273, 1985.

Lewis, T.J., W.H. Bentkowski, E.E. Davis, R.D. Hyndman, J.G. Souther, and J.A. Wright, Subduction of the Juan de Fuca plate: thermal consequences, J. Geophys. Res., in press, 1989.

Mase, C.W., J.H. Sass, A.H. Cachenbrush, and R.J. Munroe, Preliminary heat-flow investigations of the California Cascades, U.S. Geol. Surv. Open-File Rept. 82-150, 240 p, 1982.

Murphey, C.F., An investigation of the Cascade Range of Oregon through the use of gravity, topography, and heat flow, M.S. Thesis, Southern Methodist University, Dallas, Tex., 1982.

Murase, T., and A.R. McBirney, Properties of some common igneous rocks and their melts at high temperatures, Geol. Soc. Am. Bull., 84, 3563-3592, 1973.

Nettleton, L.L., Gravity and Magnetics in Oil Prospecting, McGraw-Hill, Inc., p. 160-163, 1976.

Peck, D.L., A.B. Griggs, H.G. Schliker, and H.M. Dole, Geology of the central and northern parts of the Western Cascade Range in Oregon, U.S. Geol. Surv. Prof. Paper 449, 56 pp., 1964.

Priest, G.R., N.M. Woller, and G.L. Black, Overview of the central Oregon Cascade Range, in Special Paper 15, Geology and Geothermal Resources of the central Oregon Cascade Range, Oregon Dept. Geol. Mineral Industries, Portland, 1983.

Riddihough, R., C. Finn, and R. Couch, Klamath-Blue Mountain lineament, Oregon, Geology, 14, 528-531, 1986.

Rogers, G.C., Variation in Cascade volcanism with margin orientation, Geology, 13, 495-498, 1985.

Sammel, E.A., Hydrogeologic appraisal of the Klamath Falls geothermal area, Oregon, U.S. Geol. Surv. Prof. Paper 1044-G, 1980.

Sammel, E.A., Results of test drilling at Newberry volcano, Oregon, and some implications for geothermal prospects in the Cascades, Geothermal Resources Council Bull., 10(11), 3-8, 1981.

Sammel, E.A., and S. Benson, An analysis of the hydrologic effects of proposed test drilling in the Winema National Forest near Crater Lake, Oregon, Trans. Geothermal Resources Council, 11, 293-303, 1987.

Sammel, E.A, S.E. Ingebritsen, and R.H. Mariner, The hydrothermal system at Newberry volcano, Oregon. J. Geophys. Res., 93, 10149-10162, 1988.

Sass, J.H., and E.A. Sammel, Heat flow data and their relation to observed geothermal phenomena near Klamath Falls, Oregon, J. Geophys. Res., 81, 4863-4868, 1988.

Shepard, D., A 2-D interpolation function for computer mapping of irregularly spaced data, Geography and Properties of Surface Series no. 15, Harvard University, 1968.

Smith, G.A., L.W. Snee, and E.M. Taylor, Stratigraphic, sedimentologic, and petrologic record of late Miocene subsidence of the Central Oregon High Cascades, Geology, 15, 389-392, 1987.

Stanley, W.D., A regional magnetotelluric survey of the Cascade Range region, northwestern United States, U.S. Geol. Surv. Open-file Rept. 82-126, 387 pp, 1982.

Steele, J.L., D.D. Blackwell, and J.H. Robison, p 31-42, Heat flow in the vicinity of the Mt. Hood volcano, Oregon, in Geology and Geothermal Resources of the Mt. Hood area, Oregon, ed. G.R. Priest and B.F. Vogt, Ore. Dept. Geol. Mineral Industries Special Paper 14, 100 pp, 1982.

Summer, N.S., and K.L. Verosub, Maturation anomalies in sediments underlying thick volcanic strata, Oregon: Evidence for a thermal event, Geology, 15, 30-33, 1987.

Swanberg, C.A., and J. Combs, Geothermal drilling in the Cascade Range: Preliminary results from a 1387-m core hole, Newberry volcano, Oregon, EOS, 67, 578-580, 1986.

Swanberg, C.A., W.C. Walkey, and J. Combs, Core hole drilling and the "Rain Curtain" phenomenon at Newberry Volcano, Oregon, J. Geophys. Res., 93, 10163-10173, 1988.

Taylor, E.M., Roadside geology, Santiam and McKenzie Pass Highways, Oregon, pp 3-34, Andesite Conference Guidebook, ed. H.M. Dole, Ore. Dept. Geol. Mineral Industries Bull., 62, 107 pp, 1968.

Verplanck, E.P., and R.A. Duncan, Temporal variation in plate convergence and eruption rates in the Western Cascades, Oregon, Tectonics, 6, 197-209, 1987.

Walker, G.E., Geology of the High Lava Plain province, Oregon Dept. Geol. Min. Ind. Bull., 64, 77-79, 1969.

Weaver,C.S., G.E. Baker, Geometry of the Juan de Fuca plate beneath Washington from seismicity and the 1949 South Puget Sound earthquake, Bull. Seismol. Soc. Am., 78, 264-275, 1988.

Weaver, C.S., and S.D. Malone, Overview of the tectonic setting and recent studies of eruptions of Mt. St. Helens, Washington, J. Geophys. Res., 92, 10149-10155, 1987.

Williams, D.L., and R.P. Von Herzen, On the terrestrial heat flow and physical limnology of Crater Lake, Oregon, J. Geophys. Res., 88, 1094-1104, 1983.

Zucca, J.J., G.S. Fuis, B. Milkereit, W.D. Mooney, and R.D. Catchings, Crustal structure of northeastern California, J. Geophys. Res., 91, 7359-7382, 1986.

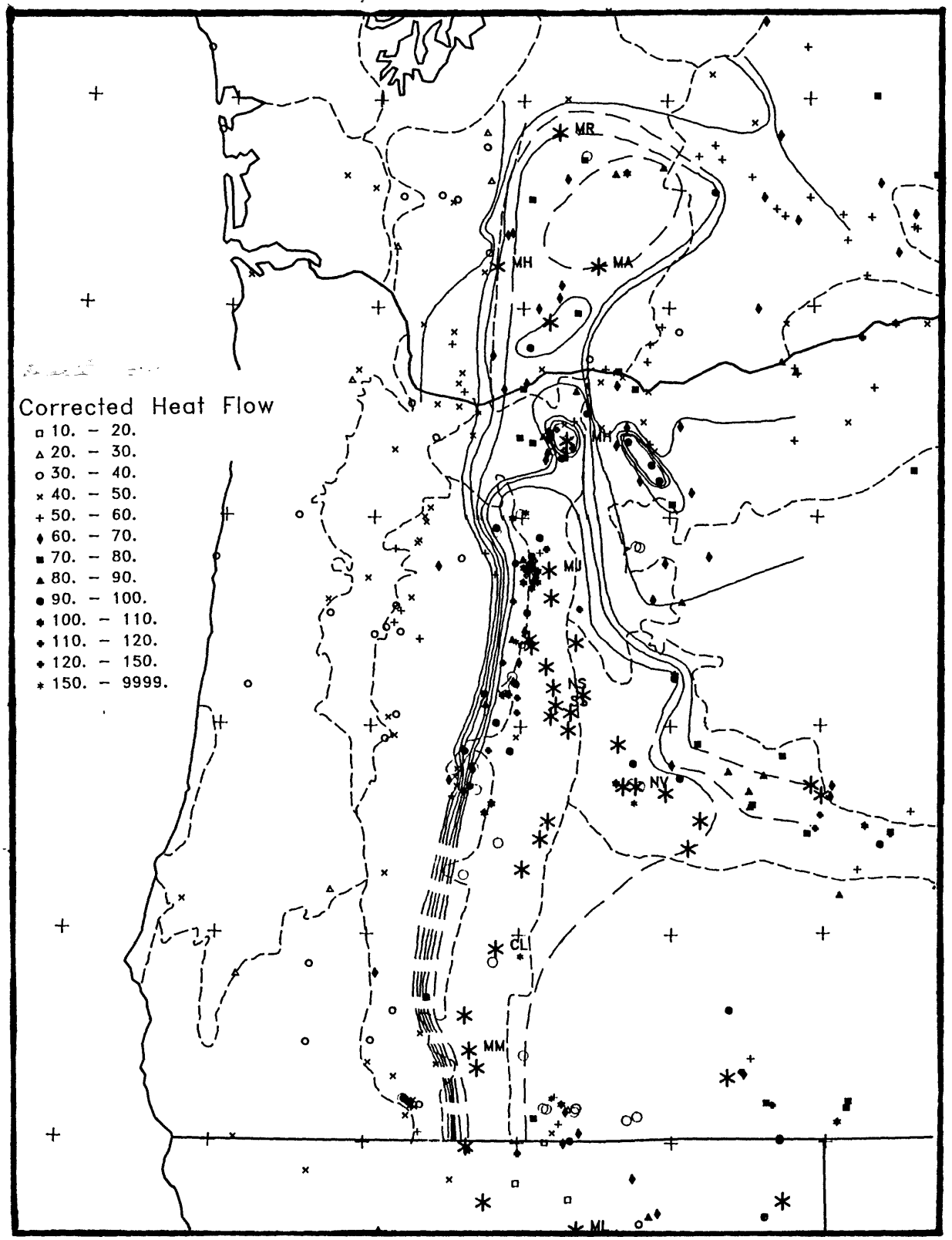

Figure 1. Heat flow map of western Oregon and southwestern Washington. Large open circles are hot springs, intermediate and large asterisks are Holocene volcanic centers and dashed lines are physiographic province boundaries. Heat flow symbols are: open triangle, 20-30; open circle, 30-40; x, 40-50; +, 50-60; diamond, 60-70; square, 70-80; triangle, 80-90; dot, 90-100; star, 100-110; cross, 110-120; asterisk, >120 mWm^{-2}.

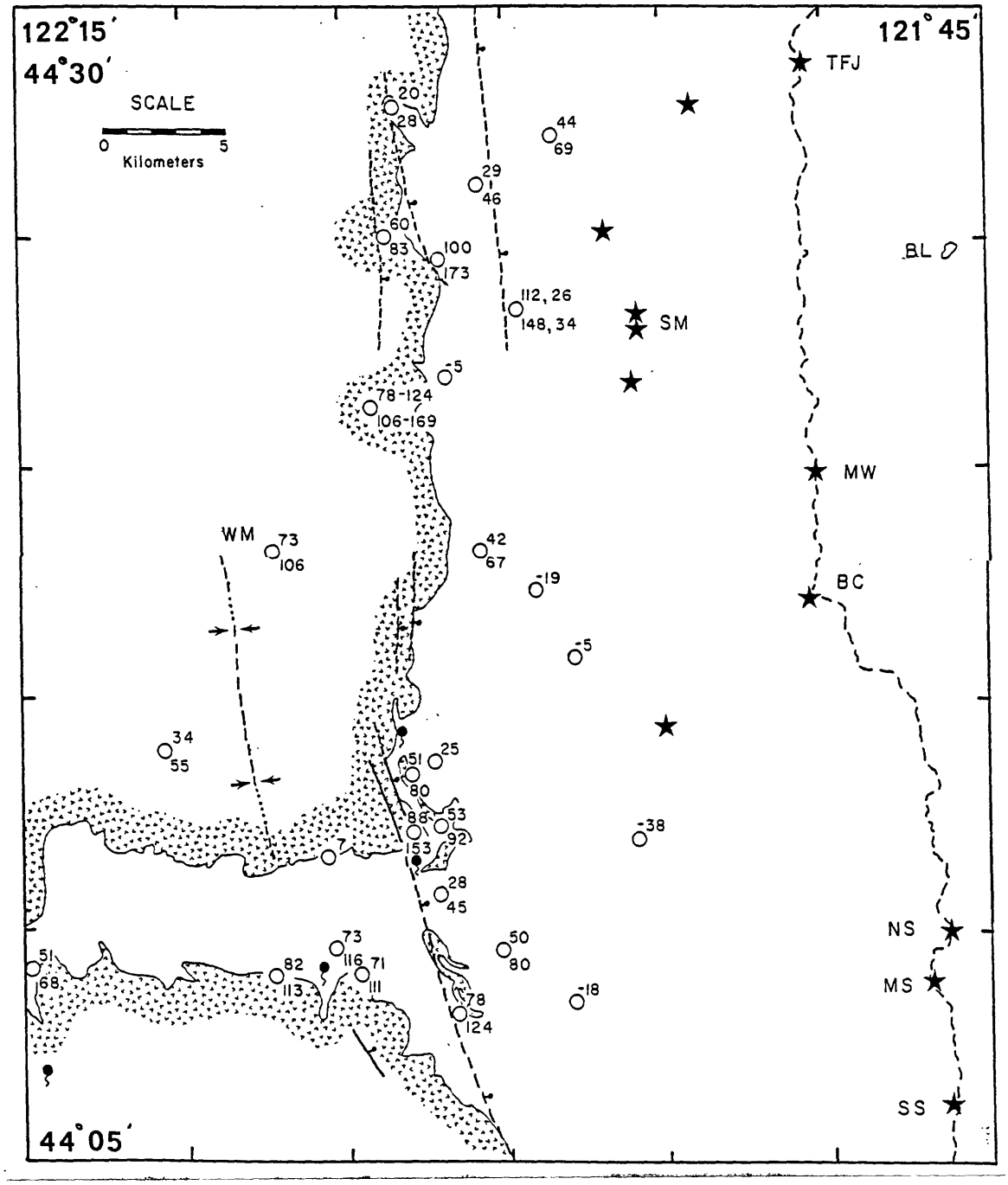

Figure 2. Geothermal gradient (°C/km, upper value) and heat flow values (mWm^{-2}) for sites in Santiam Pass - Belnap/Foley area. Major volcanic centers are shown as stars, Cascade crest is dashed line. Major west edge bounding faults of Cascade graben are shown. Boundary of rocks older than Quaternary shown by pattern (Black et al., 1987). Abbreviations are TFJ, Three Finger Jack; BL, Blue Lake; MW, Mt. Washington; BC, Belnap Crater; NS, MS, SS; Sisters; SM, Sand Mountain; WM, Wolf Meadow Lake.

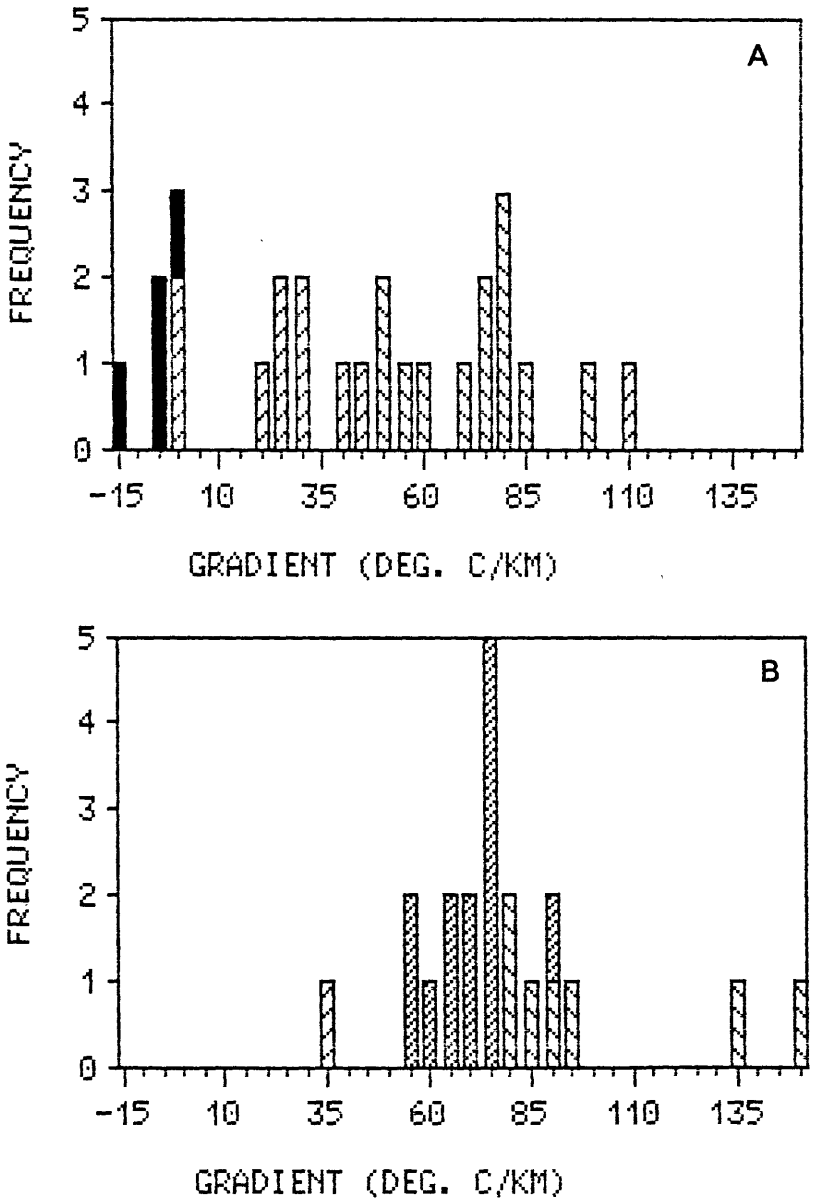

Figure 3a. Histograms of geothermal gradient for Santiam Pass - Belnap/Foley area. Gradients in Holocene rocks are solid blocks, in Late Pliocene and Quaternary rocks are left sloping lines, and in Western Cascade rocks are right sloping lines.

Figure 3b. Histograms of geothermal gradient for Breitenbush area. Gradients outside the geothermal system are indicated by the left sloping pattern and those inside the geothermal system are indicated by the right sloping pattern. One hole in Quaternary rock is indicated by sparse left sloping pattern.

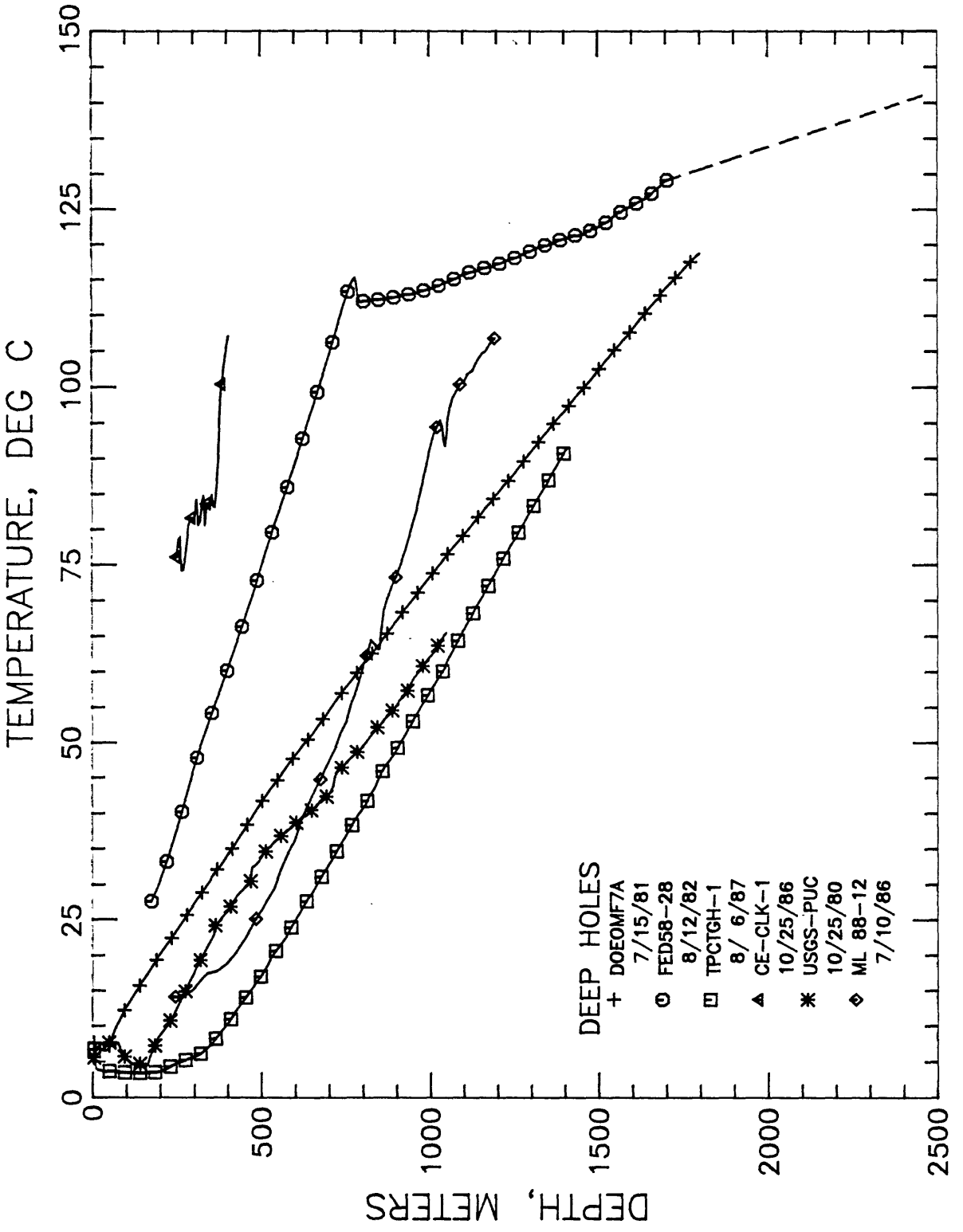

Figure 4. Temperature-depth curves for deep wells in the Cascade Range. Township and range locations and dates of logging are given.

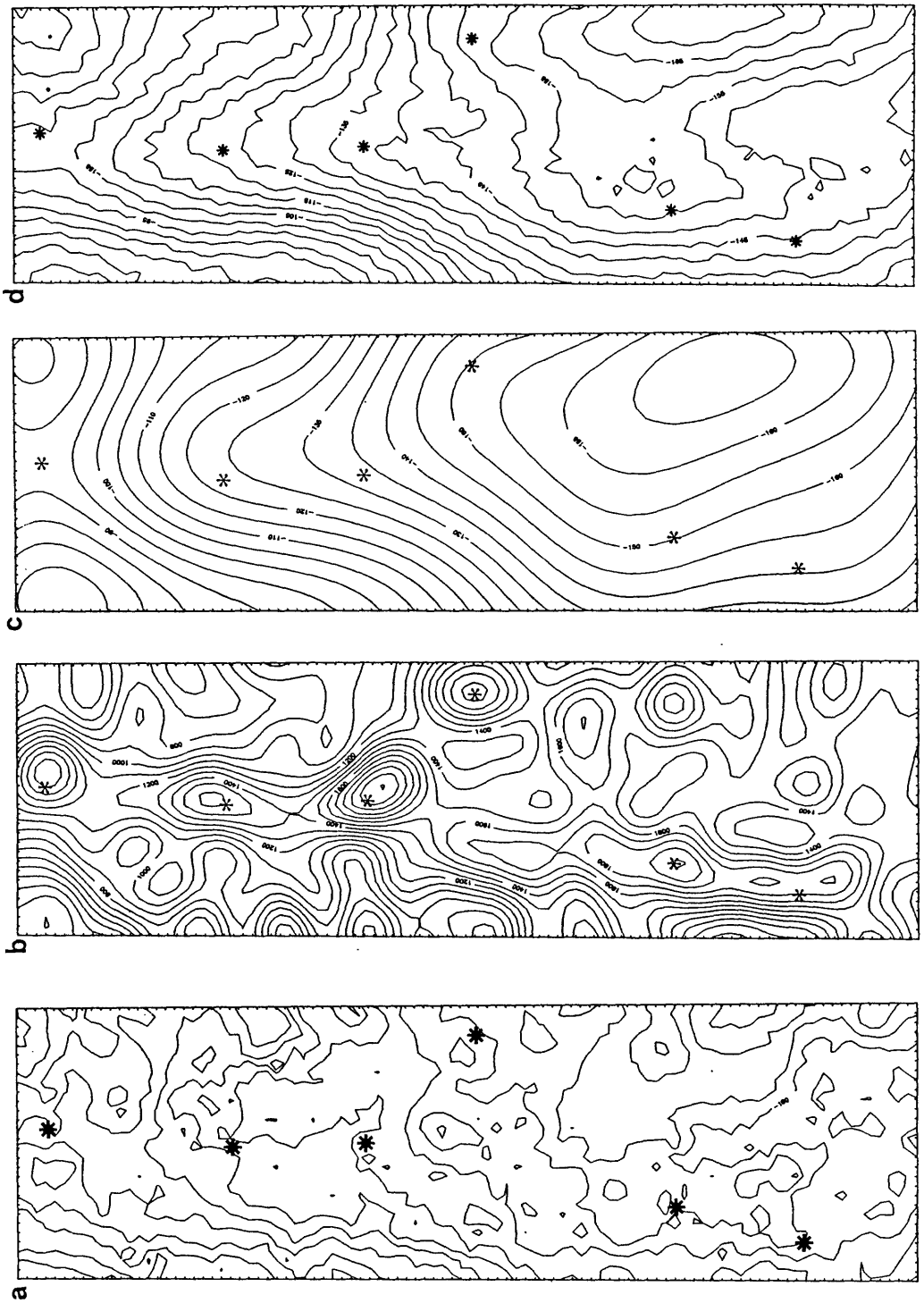

Figure 5a. Complete Bouguer Anomaly map of area 121°-122°30'W, 42°-45°30'N. Contour interval 10 mgal. In these maps and those in Figures 6, 7 and 8 the asterisks are, from north to south, Mt. Hood, Mt. Jefferson, the Sisters, Newberry volcano, Crater Lake, Mt. McLoughlin.

5b. Regional topography (89.25 km band pass). Contour interval is 100 m.

5c. Wave length filtered regional Bouguer gravity anomaly (89.25 km band pass). Contour interval 5 mgal.

5d. Topography filtered regional Bouguer gravity anomaly (0.80 coherency). Contour interval 5 mgal.

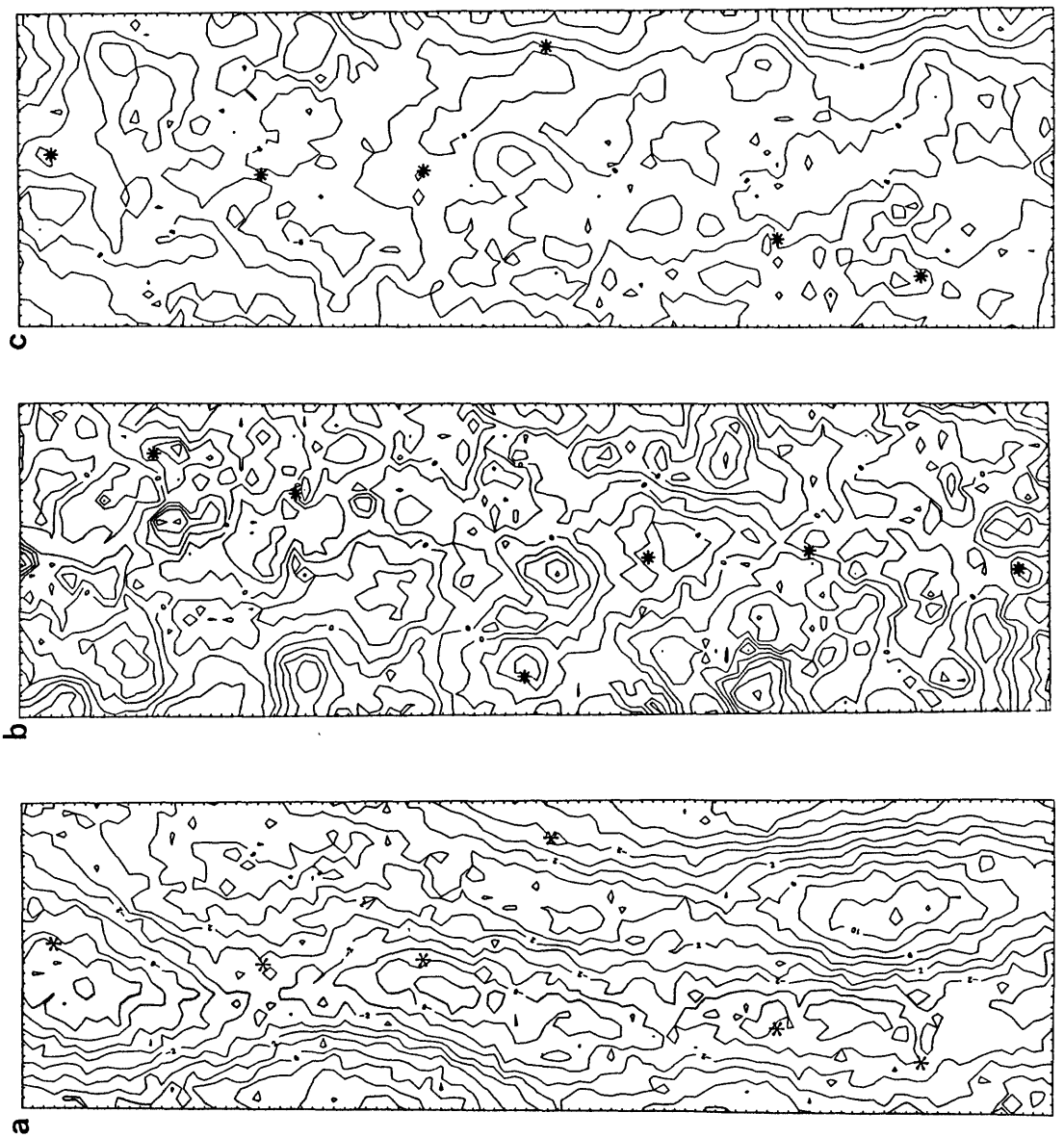

Figure 6. Residual Bouguer gravity maps.

6a. Difference map between band passed regional Bouguer gravity and coherency based regional Bouguer gravity. Contour interval 2 mgal.

6b. Residual gravity anomaly from coherency based (0.8) regional anomaly.

6c. Residual gravity anomaly from "heat flow corrected" coherency based (0.8) regional anomaly from band passed regional anomaly.

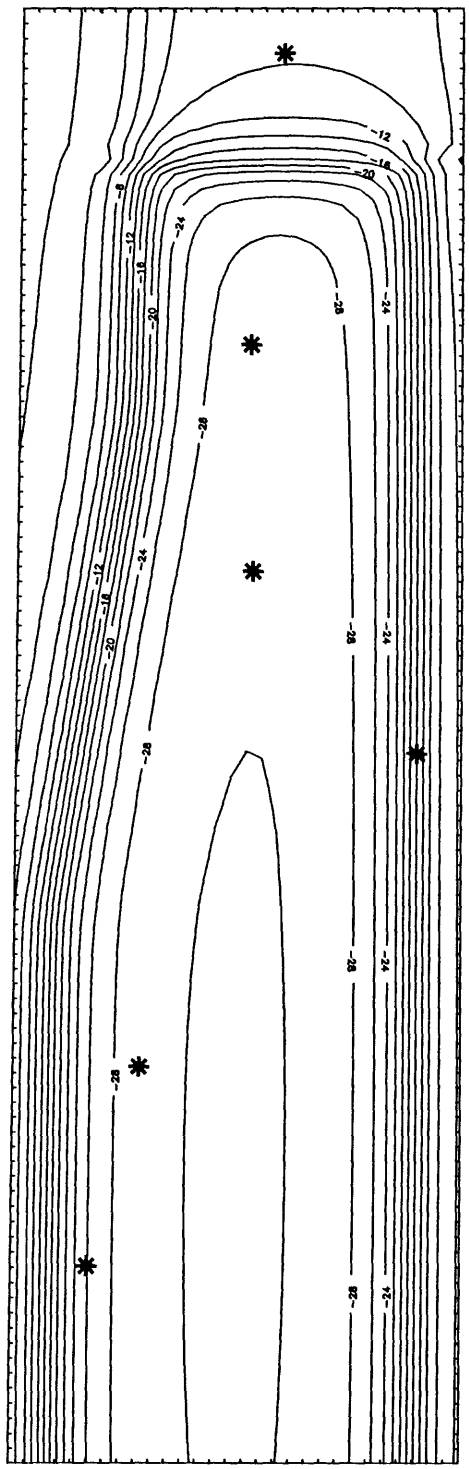

Figure 7. Gravity anomaly predicted from heat flow (model B of Blackwell et al., 1982a).

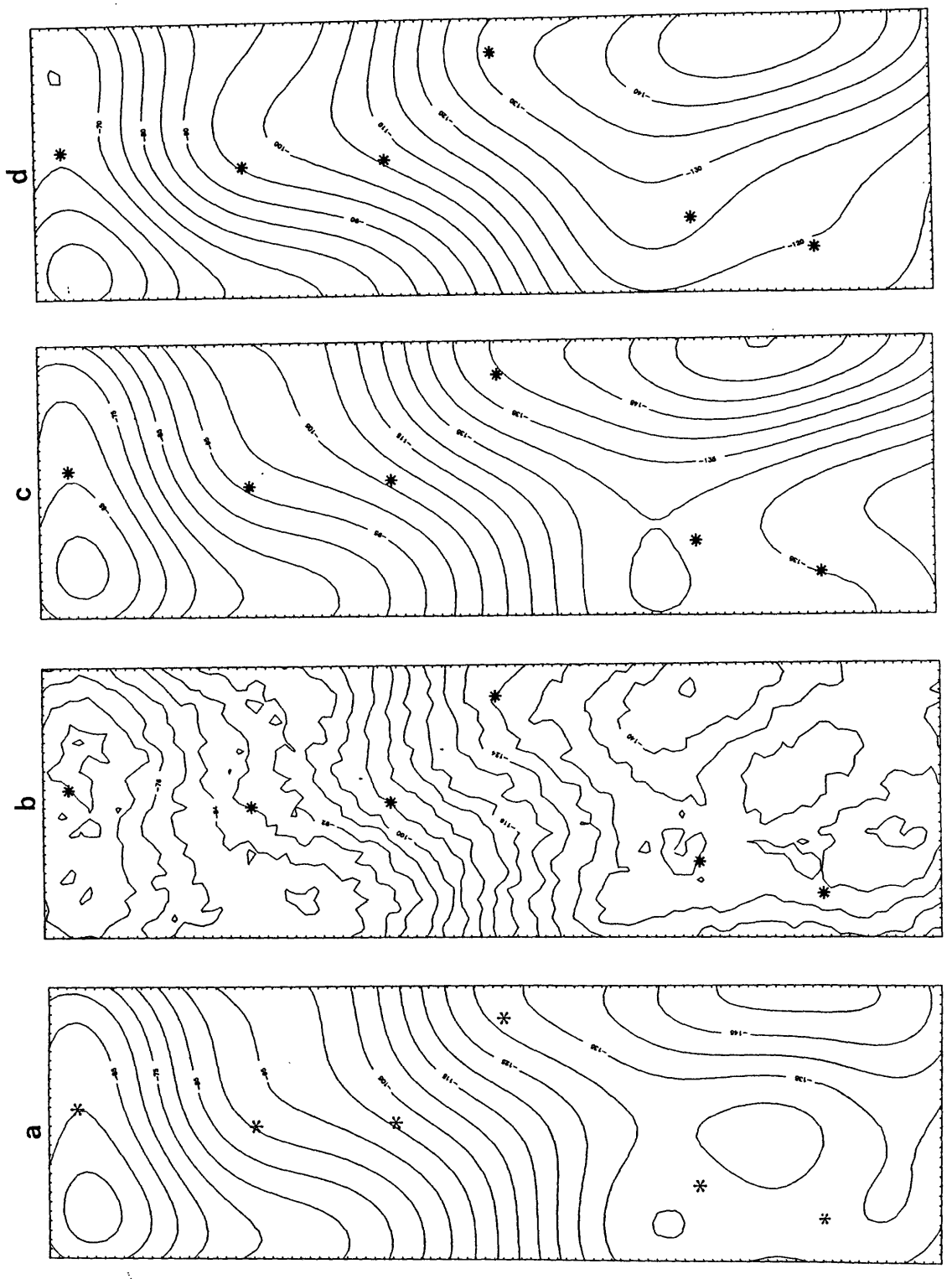

Figure 8. Heat flow corrected gravity anomaly maps.
8a. Band passed regional corrected for crustal heat source effect (model B).
8b. Coherency regional (0.8) corrected for crustal heat source effect.
8c. Band passed regional corrected for graben effect.
8d. Band passed regional corrected for crust/mantle effect.

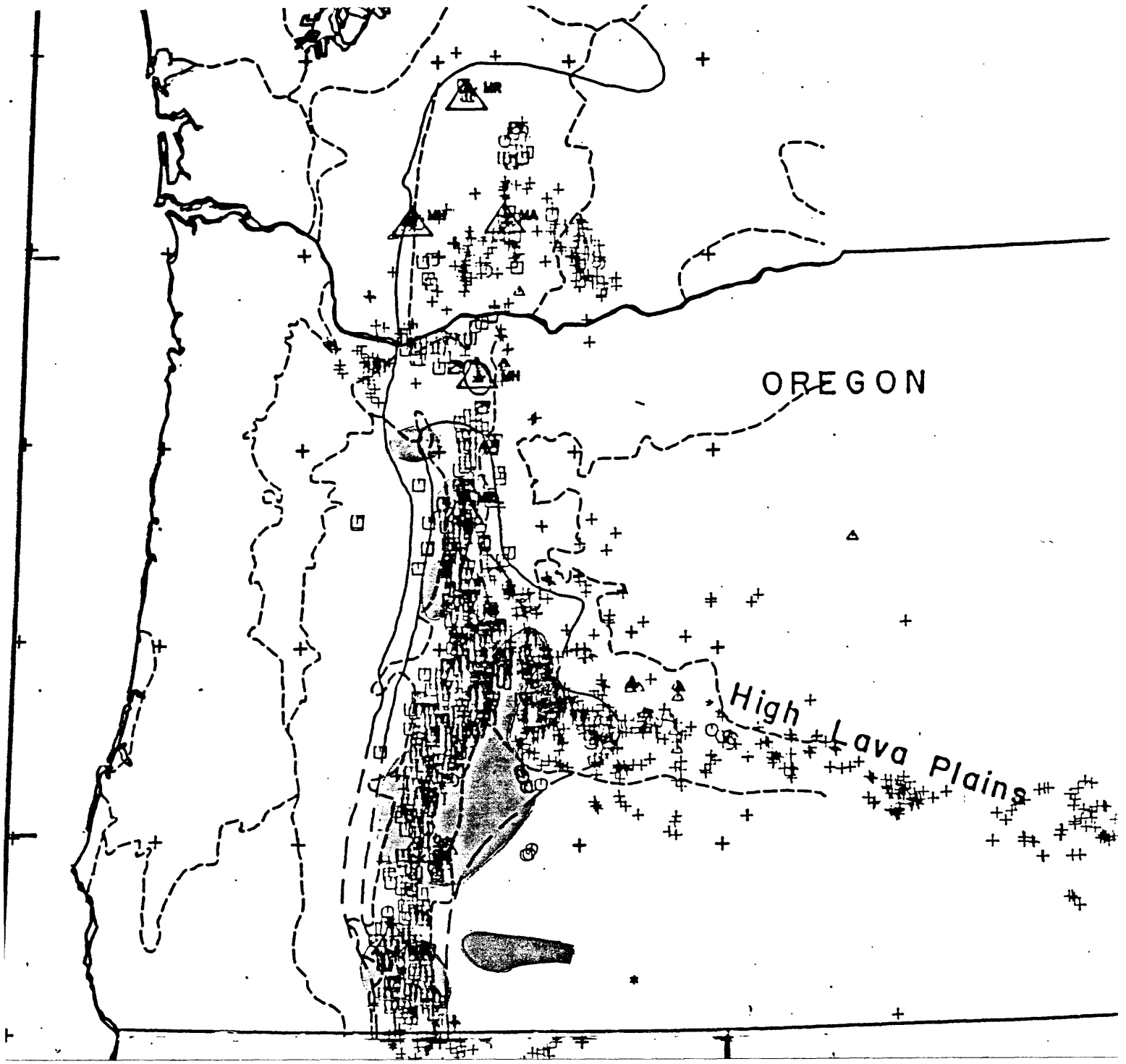

Figure 9. Comparison of heat flow, volcanic source sites (Guffanti and Weaver, 1988), and shallow Curie point areas (Connard et al., 1983), in Cascades.

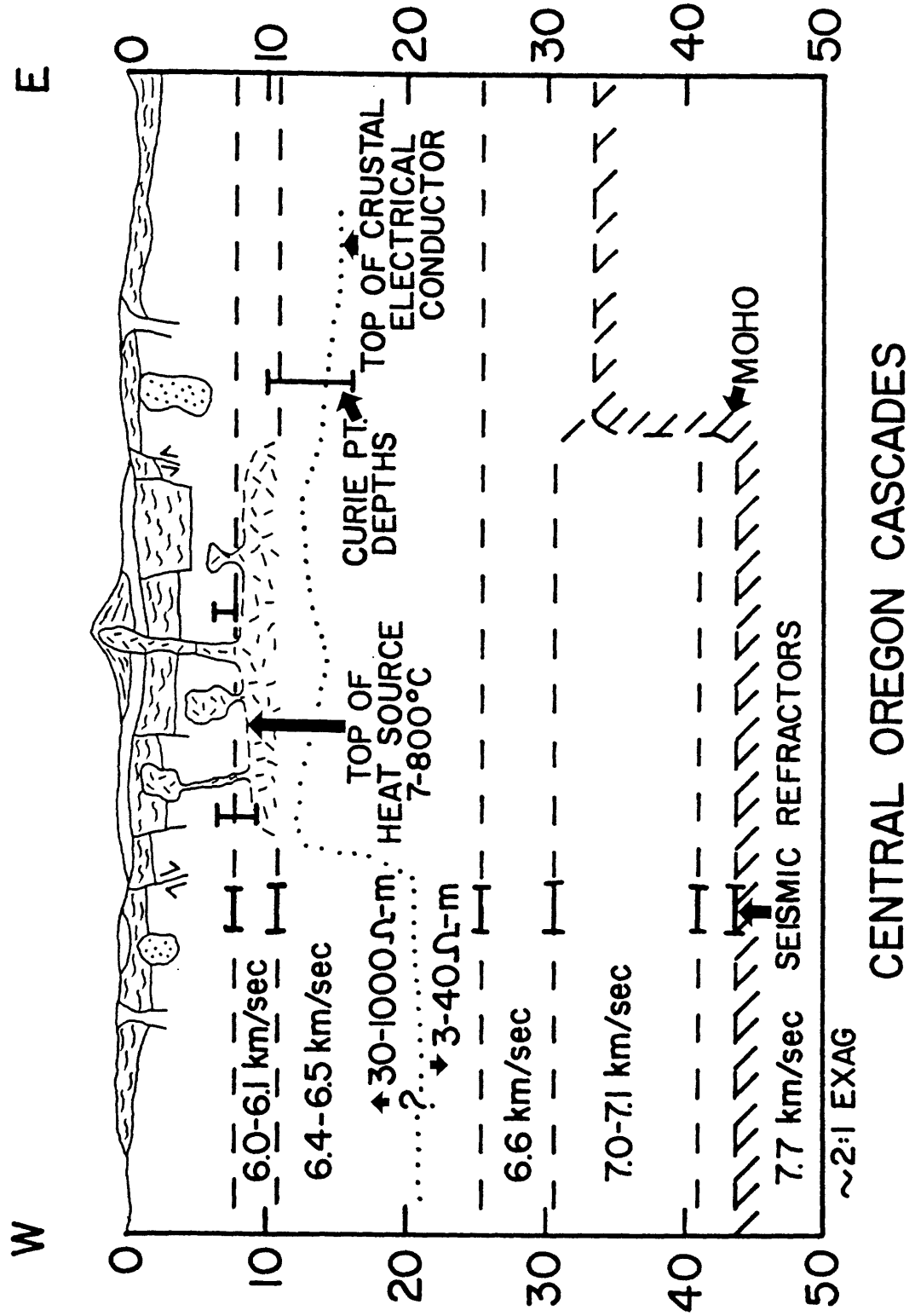

Figure 10. Generalized cross section of the northern Oregon Cascade Range summerizing geophysical results. Dotted line is the upper boundary of the lower crustal electrical conductor.

Maximum Depths of Earthquakes as an Aid in Evaluating Convective and Conductive Heat Fluxes from the Cascade Province and Adjacent Regions

Robert O. Fournier
U.S. Geological Survey, Menlo Park, CA 94025

ABSTRACT

Heat-flow measurements are usually employed to deduce the thermal structure of the upper crust. The interpretation of heat-flow measurements in the Cascade province, however, is complicated because high topographic relief and abundant precipitation may lead to deep circulation of meteoric water that decreases heat flow in some places and increases it in others. The distribution of earthquake hypocenters provides information that may be of value in assessing possible effects of meteoric water circulation upon heat flow. The depth of earthquake activity in the upper crust is limited by a transition from brittle to plastic behavior of rock, the rate of strain, and the attainment of very high pore-fluid pressures. This paper examines the effect of temperature on chemical and mechanical processes that decrease permeability and increase plasticity to such an extent that lithostatic pore-fluid pressures are attained.

Deep holes drilled into hydrothermally altered sediments near The Geysers, California, into metasediments at Larderello, Italy, and into basalt at Nesjavellir, Iceland, all encountered a rapid increase in pore-fluid pressure from hydrostatic (or less than hydrostatic) to much greater than hydrostatic at about 400°C. At 400°C the plastic strength of "wet" quartz becomes relatively low, and quartz-rich rocks will deform at relatively high strain rates when pore-fluid pressures are less than lithostatic. Where normal strain rates prevail in the crust at temperatures above about 350°-400°C, deformation is dominantly by plastic flow and differential stresses are very low. At these conditions silica-rich rocks deform in response to the force exerted by their own weight, decreasing pore volumes and increasing pore-fluid pressure. Plastic flow is likely to generate pore-fluid pressure/rock-pressure ratios close to 0.9 within a few months at 400°C. Pore-fluid pressure/rock-pressure ratios will be further increased by pressure solution effects, and steeper pressure gradients in vertical, fluid-filled channels compared to those in the surrounding rock are likely to boost pore-fluid pressures the rest of the way to lithostatic shortly thereafter. The information obtained from drilling into basalt at Nesjavellir, Iceland, suggests that even in mafic rocks, which are much less plastic at a given temperature than quartz-rich rocks, chemical processes may decrease permeability to such an extent at about 400°C that very high pore-fluid pressures are attained beneath impermeable caps. The main conclusions are that (1) lithostatic pore-fluid pressures generally are attained at about 400°C irrespective of rock type at depths less than about 10-12 km, and possibly as low as 350°C in quartz-rich rocks at depths of about 12-20 km, (2) fluids become stabilized in regions of interconnected horizontal permeability that are separated by thin impermeable regions, (3) where water and CO_2 are most abundant, thin, roughly horizontal lenses of fluid develop that lift or float the overlying rock, and (4) the base of seismic activity corresponds approximately with the 400°C isotherm in the mid to upper crust because rock has essentially no effective strength where pore-fluid pressure is equal to the lithostatic load.

INTRODUCTION

The thermal structure of the crust beneath the Cascade Range and adjacent regions has been deduced mainly from studies of measured conductive heat flow [Blackwell and Steele, 1983, 1985; Blackwell et al., 1982, 1989; Lewis, in press], augmented by calculated depths to the Curie point temperature using aeromagnetic data [Connard et al., 1983]. Interpretations of the heat-flow measurements, however, are uncertain in this region of high topographic relief and high precipitation because deep circulation of meteoric water may decrease the apparent conductive heat flux in some places and increase it in others. For example, Ingebritsen et al. [1989] suggest that, in north-central Oregon, meteoric recharge results in near-zero near-surface conductive heat flow in the Pliocene and Quaternary volcanic rocks of the Cascade Range, and discharge of heated groundwaters in adjacent pre-Pliocene rocks results in relatively high advective and conductive heat discharge. In contrast, Blackwell et al. (1982) concluded that groundwater circulation has a local effect upon heat-flow measurements at and near the crest of the Cascades but has little effect upon heat-flow measurements in adjacent pre-Pliocene rocks

Calculated depths and assumed temperatures of Curie points have a high degree of uncertainty. The calculated Curie point depth is affected by the particular mathematical model and geologic assumptions that are employed, and the Curie point temperature is markedly affected by variable amounts of titanium and other impurities that are commonly present in iron-bearing oxides. An example of widely ranging estimated Curie temperatures within a volcanic arc setting is given by Okubo et al. (in press), who compared calculated Curie point depths and heat-flow values within Japanese island arcs and concluded that the Curie temperature is generally about 250°C on the forearc side and about 435°C on the backarc side.

Intrusions of magma to shallow levels beneath centers of volcanic activity within the Cascades have locally perturbed the regional thermal structure, and greatly complicate efforts to assess the total heat flux from the region. Iyer [1984] has summarized geophysical methods of assessing the locations, shapes, and sizes of magma chambers beneath regions of Quaternary volcanism. Most of these methods rely on a dramatic decrease in density and seismic velocity and an increase in seismic attenuation and electrical conductivity at the onset of partial melting in rocks. However, small bodies of magma may be overlooked because their detection requires relatively closely spaced geophysical observations, and larger bodies of hot, crystalline igneous rocks that have been intruded to a relatively shallow level may go undetected by geophysical methods designed to find molten or partly molten material.

Seismicity results when stresses within the crust build up to the point where brittle fracturing occurs. However, whether a given rock responds to an applied stress by brittle fracture or plastic flow depends in great part on temperature and pressure. This has prompted several investigators to use earthquake hypocenters and temperature-depth profiles, calculated from near-surface heat-flow data, to estimate depths and temperatures of the brittle-ductile transition [Meissner and Strehlau, 1982; Sibson, 1982, 1983; Smith and Bruhn, 1984; Kusznir and Park, 1986]. There is disagreement about the appropriateness of the use of "brittle-ductile" to describe the mechanisms involved in the rock deformation, and Rutter (1986) suggests that the term "brittle-plastic" be used in order not to confuse ductile deformation that might result either from cataclastic or plastic flow mechanisms.

It is the purpose of this presentation to suggest that in some places information may be obtained about the thermal structure of the crust, and about the depth and size of shallow intrusive rocks that are still hotter than about 400°C, given seismic focal depth information and assumptions about the general brittle-plastic behavior of rocks at high temperatures in the crust. There are, however, complicating factors. The brittle-plastic behavior of rocks is influenced by mineral composition, pore-fluid pressure, and rate of strain, as well as by temperature and pressure. Each of these factors will be discussed in the succeeding sections. A major limitation of the methodology that will be proposed is the low frequency of earthquake activity within the Oregon Cascade Range. However, earthquakes do occur frequently throughout much of the state of Washington [Crosson and Owens, 1987; Weaver, 1989], so the methodology should be applicable there.

THE BRITTLE-PLASTIC TRANSITION

Effects of Temperature, Pressure, and Rock Type

The brittle strength of a given rock type is controlled mainly by lithostatic pressure and increases bilinearly with depth, while plastic strength decreases exponentially with increasing temperature and, therefore, decreases with depth because of the geothermal gradient [Goetze and Evans, 1979; Brace and Kohlstedt, 1980; Meissner and Strehlau, 1982; Sibson, 1983; Smith and Bruhn, 1984; Kusznir and Park, 1986]. For given temperature and stress conditions, experimentally determined strain rates tend to be greater for more silica-rich minerals than for less silica-rich minerals, and rocks are less strong under wet conditions than dry [Kusznir and Park, 1986]. It is commonly assumed that quartz (probably wet) controls plastic deformation in the upper crust while olivine (probably dry) is the controlling mineral in the mantle [Smith and Bruhn, 1984; Kusznir and Park, 1986]. Kusznir and Park [1986] suggested that plagioclase controls plastic deformation in the lower crust.

Figure 1 shows calculated shear and tensile stresses in the crust required to deform quartzite in dry conditions (curves ABC and ADE), and wet conditions with hydrostatic pore-fluid pressure, P_h, (curves AFG and AHJ) in a region where the strain rate is 10^{-15} s^{-1} and the conductive heat flow is 71 mWm^{-2}. Similar figures showing maximum stress profiles for specific minerals have been constructed by others [Brace and Kohlstedt, 1980; Meissner and Strehlau, 1982]. Fractures are thought to be present throughout the brittle upper crust, and frictional sliding will occur on those fractures before the stress reaches a level great enough to cause brittle fracture of the mass as a whole [Brace and Kohlstedt, 1980]. Therefore, for dry conditions the maximum stress from A to B (or A to D for tensile stress) in Figure 1 is constrained by frictional resistance that is about the same for all geologic materials, except certain clays [Byerlee, 1968; Brace and Kohlstedt, 1980].

Going from shallower to deeper levels in the crust, the maximum possible stress first increases as an almost linear function of depth because rock gets stronger with increasing confining pressure (e.g., line segment AB or AD in Fig. 1 for dry conditions), and then decreases where the effect of increased temperature (resulting in exponentially increased plasticity) becomes more important than the effect of increased pressure (line segment BC or DE). The shear stresses required for plastic deformation of dry and wet quartz are given by experimentally determined equations of Koch et al. [1980], as quoted by Kusznir and Park [1986]. The point at which the maximum stress is attained (e.g., point F for a wet shear-stress environment, or point H for a

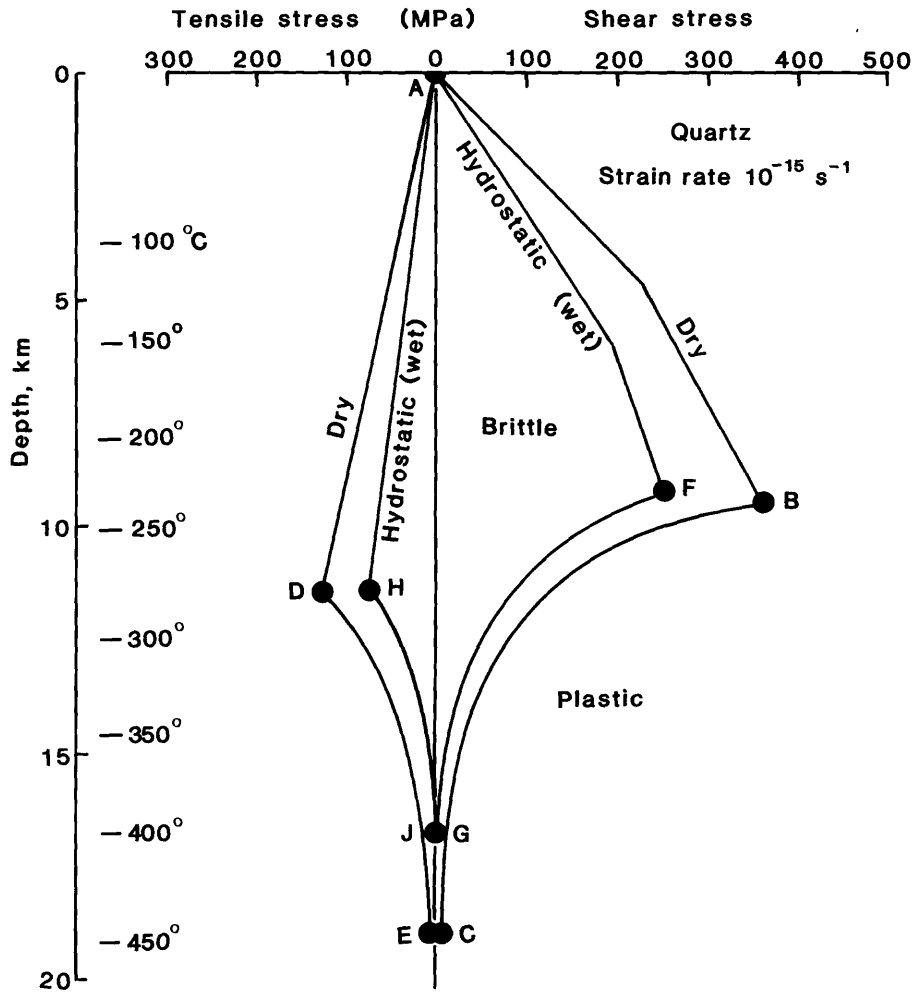

Figure 1. Maximum shear stress for brittle/plastic behavior (quartz rheology) of the crust with no pore-fluid pressure (dry), and hydrostatic (wet) conditions with pore-fluid pressure/rock pressure = 0.36. Temperatures at given depths are assumed to be fixed by conductive transfer of heat at about 71 mWm^{-2}. See text for discussion.

wet tensile-stress environment) has commonly been called the brittle-ductile or brittle-plastic transition [Sibson, 1983; Scholz, 1988]. Below the brittle-plastic transition point it is likely that there is a transition region in which deformation occurs by a mixture of brittle and plastic processes even for the simplest monomineralic systems [Paterson, 1978]. Scholz [1988] emphasizes that in multimineralic rocks different minerals will exhibit brittle-plastic transition points at different pressure-temperature conditions, and Sibson [1982, 1983] and Smith and Bruhn [1984] refer to a region of quasi-plastic deformation below the brittle-plastic transition.

In general, plots of frequency of seismic events versus depth look similar in shape to the stress-depth diagram shown in Figure 1 [Meissner and Strehlau, 1982; Sibson, 1982, 1983], and the depth at which the maximum number of hypocenters occur has been interpreted to be the brittle-plastic transition [Meissner and Strehlau, 1982; Sibson, 1982, 1983]. However, deep hydrothermal circulation that may affect the depth-temperature profile and major changes in rock composition with depth may change the shape of the theoretical stress-depth diagram and affect the depth-frequency relations of seismic events. Also, recently several investigators have stressed the possible importance of a rate and state variable friction law in which a change from velocity weakening to velocity strengthening with increasing temperature determines the lower limit of the seismogenic crust [Hobbs et al., 1986; Shimamoto and Logan, 1986; Tse and Rice, 1986; Scholz, 1988]. Velocity weakening occurs when $\partial\tau^{SS}/\partial V < 0$, where τ^{SS} is the steady-state frictional stress and V is velocity, and velocity strengthening occurs when $\partial\tau^{SS}/\partial V > 0$ [Hobbs et al., 1986]. Whether the base of seismic activity is controlled mainly by the transition from brittle to plastic behavior of rock, or by the transition from velocity weakening to velocity strengthening, increasing temperature is a major contributing factor. Note, however, that velocity weakening and velocity hardening considerations lose their importance where interconnected pore-fluid pressure, P_f, is equal to the least principal stress and rock has no effective strength.

The general correspondence in shape of plots of maximum stress versus depth and frequency of earthquake hypocenters with depth [Meissner and Strehlau, 1982] suggests that a transition from brittle to plastic behavior of rock with increasing temperature and pressure is an important factor in controlling seismic activity, and especially in controlling the depth of maximum seismic activity. To the extent that the brittle-plastic transition for quartz-rich rocks occurs within a narrow temperature range, its position in the crust (determined by the depth at which the maximum of earthquake hypocenters occur) may be used as a temperature marker. Note, however, that for similar rock type, strain rate, and heat-flow conditions, the transition will occur at a slightly greater depth (and greater temperature) in a region where rocks are subjected to tensile stress compared to regions of shear stress (point H is about 2 km deeper than point F in Fig. 1). Also, the maximum possible stress is strongly affected by P_f. In Figure 1 note the decrease of about 1.1 kbar in maximum possible shear stress in going from dry conditions (point B) to hydrostatic "wet" conditions (point F). Where the fluid phase is interconnected between pores, increasing P_f to values greater than hydrostatic moves line AF (or line AH) to even lower maximum possible stress values, and when P_f equals the pressure exerted by the lithostatic load, rock generally has zero effective strength and cannot sustain differential stress.

Several investigators have calculated likely depths to the brittle-plastic transition for various assumed conditions of heat flow, P_f, and rock composition [Goetze and Evans, 1979; Brace and Kohlstedt, 1980; Meissner and Strehlau, 1982; Sibson, 1982, 1983; Smith and Bruhn, 1984], and most investigators calibrated their results with earthquake focal depth information in regions of known heat flow. Kusznir and Park [1986] used experimentally determined strengths of quartz to calculate depths to the brittle-plastic transition as a function of heat flow for compressional and tensional conditions, and 1 million years after application of a force to the lithosphere. Their results for compressional conditions are shown in Figure 2, curve A. Figure 2 also shows isotherms obtained from generalized conductive tempera-

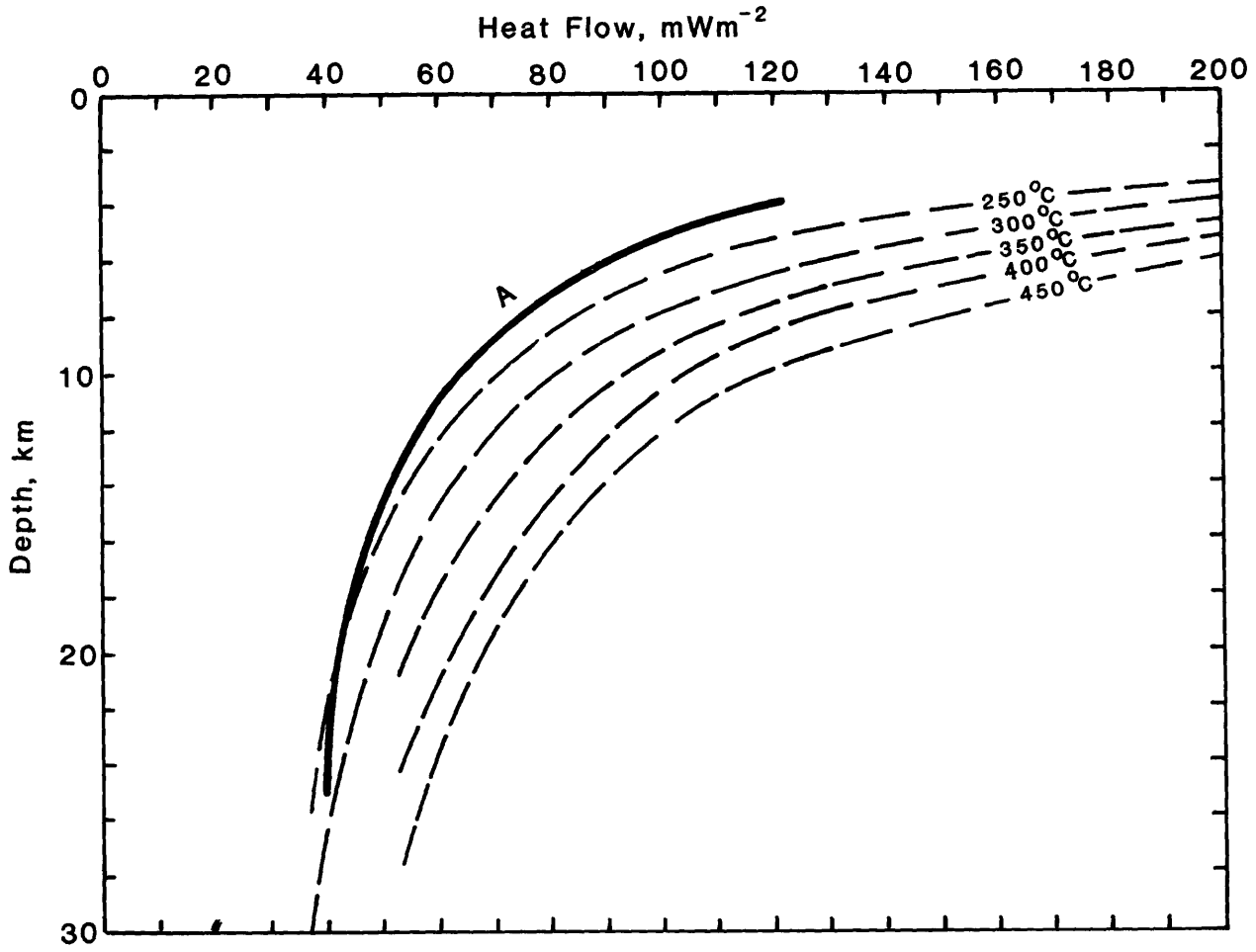

Figure 2. Approximate depth-temperature relations for different values of conductive heat flow (data from Lachenbruch and Sass, 1978). Curve A shows the approximate depth at which wet quartz will withstand maximum shear stress 1 million years after application of a force to the lithosphere (from calculations by Kusznir and Park, 1986).

ture profiles for a variety of heat-flow conditions, taken from Lachenbruch and Sass [1978]. Curve A corresponds closely with the 250°C isotherm at depths greater than about 13 km, and is significantly above that isotherm at shallower depths. Smith and Bruhn [1984] suggest that approximately 80% of earthquakes in a given thermal/tectonic region occur above the brittle-plastic transition, and note that the overriding evidence from geologic and petrologic observations suggests that quasi-plastic creep initiates at about 300°C for quartz-rich rocks. This criterion (80% of earthquakes above the 300°C isotherm) should be checked in additional regions where depth-temperature profiles are not likely to be affected by deep circulation of meteoric waters.

Two major limitations of the above approach to determining the depth and temperature of the brittle-plastic transition are uncertainties in earthquake focal depth determinations and uncertainties in calculated depth-temperature profiles resulting from variations in thermal conductivities and deep convective flow of fluids that may increase or decrease the apparent near-surface heat flux.

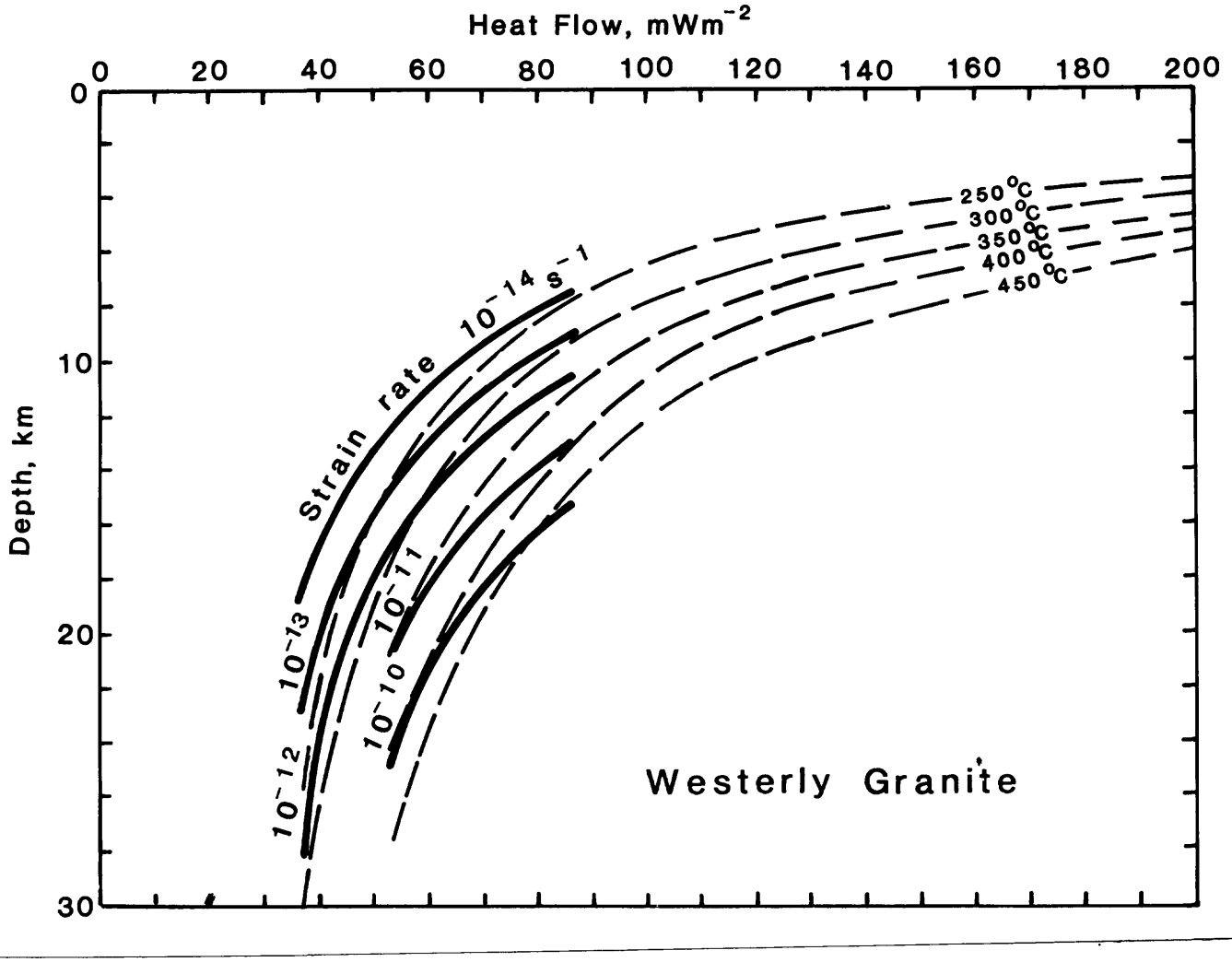

Figure 3. Depths at which maximum shear stress may be attained within "wet" Westerly granite at various strain rates (solid lines) as a function of the geotherm, for conditions of normal faulting (from calculations by Sibson 1983). Dashed lines show isotherms from Lachenbruch and Sass (1978).

Effects of Strain Rate

A rock at a given depth and temperature and with a particular P_f may respond to a particular stress either by brittle fracture or plastic deformation, depending on the rate at which strain occurs in response to the applied stress. It is likely that rocks near their melting points and even viscous magmas may undergo brittle fracture at very high strain rates and/or where magma fluid pressures approximate the lithostatic load [Shaw, 1980]. Holes drilled into hot rock in search of geothermal resources commonly intersect fractures filled with fluids at hydrostatic pressure at temperatures of 300°-350°C, indicating that strain rates commonly are appropriate for fractures to form and persist at these temperatures. In contrast, the lack of normal "tectonic" earthquakes (with most energy concentrated between 5 and 10 Hz) within the upper crust, where temperatures are thought to be in the 400°-500°C range, suggests that strain rates generally are such that siliceous rocks behave in a plastic manner above about 400°C.

Sibson (1983) calculated depths at which maximum stress may be attained within "wet" Westerly granite for conditions of thrust, strike-slip, and normal faulting, at various assumed strain rates and heat flows. His results for normal faulting at strain rates of 10^{-10} s^{-1} to 10^{-14} s^{-1} have been recast in a depth versus heat flow diagram (Fig. 3) in which calculated isotherms also are displayed. The curves showing depths at which maximum stress may be attained cut across isotherms at low angles, reaching higher temperatures at shallower depths.

Pfiffner and Ramsay [1982] suggest that strain rates of 10^{-14} s^{-1} to 10^{-15} s^{-1} are characteristic of regional deformation in orogenic belts, and Smith and Bauer [1982] calculated strain rates of 10^{-13} s^{-1} to 10^{-16} s^{-1} for contemporary earthquake-contributed strain in the Basin-Range across Nevada and Utah. Kusznir and Park [1986] noted that typical strain rates for significant tectonic deformation should be in the range 10^{-15} s^{-1} to 10^{-16} s^{-1}, and Sibson [1977] suggested that ductile shearing that produces mylonitic rocks occurs at strain rates of 10^{-10} s^{-1} to 10^{-12} s^{-1}. Figure 4 shows the calculated effects of changing the rate of strain from 10^{-13} s^{-1} to 10^{-16} s^{-1} on the plastic and shear strengths of "wet" quartz [Koch et al., 1980] for heat-flow conditions of 71 mWm^{-2}. At a strain rate of 10^{-16} s^{-1} the maximum shear stress is attained at a depth of about 8.2 km, and at a strain rate of 10^{-14} s^{-1} it is attained at a depth of about 10.4 km. Thus, it appears that the strain rate must be known to within about an order of magnitude when using the depth of maximum earthquake activity (indicative of the depth of maximum shear stress) to estimate the temperature of the brittle-plastic transition.

Figure 5 shows strain rates at which plastic deformation of "wet" quartz will occur for given temperature and stress conditions. For hydrostatic P_f, the difference in pressure exerted by the lithostatic load and a hydrostatic column of fluid is about 51 MPa at a depth of 3 km, and 170 MPa at 10 km (assuming an average difference in density of 1.7 g cm^{-3} for rock at lithostatic pressure compared to fluid at hydrostatic pressure). The stippled rectangle in Figure 5 shows approximate strain rates at which fluid-filled pores at temperatures of 350°C to 450°C and hydrostatic pressure will be deformed by plastic flow in response to the force exerted by the weight of a 3 to 10 km vertical column of overlying rock. A minimum depth of 3 km was chosen because 350°C temperatures at hydrostatic pressures have been encountered at this depth in presently active hydrothermal systems [Cappetti et al., 1985; Elders and Sass, 1988], and 10 km is probably a maximum likely depth for sustained circulation of fluids at hydrostatic pressure. The strain rates within the stippled rectangle in Figure 5 are in the same range as suggested by Sibson [1983] for ductile deformation of mylonitic rocks. At 400°C and a depth of 5 km the strain rate of plastic flow of quartz in response to the force exerted by the overlying rock is about 10^{-12} s^{-1}. This strain rate is equivalent to a reduction in length of about 0.003% per year. The extent, if any, to which P_f will increase as a result of plastic flow of rock will depend mainly on the rate at which fluid is able to flow out of the rock in response to the pores squeezing shut, as discussed by Bredehoeft and Hanshaw [1968].

PORE-FLUID PRESSURES IN THE CRUST

The Transition from Hydrostatic to Anomalously High Pore-Fluid Pressure

The maximum depth of circulation of fluid at hydrostatic pressure is controlled by permeability that may fluctuate with time. Processes that tend to maintain or increase permeability deep in the crust are faulting, hydraulic

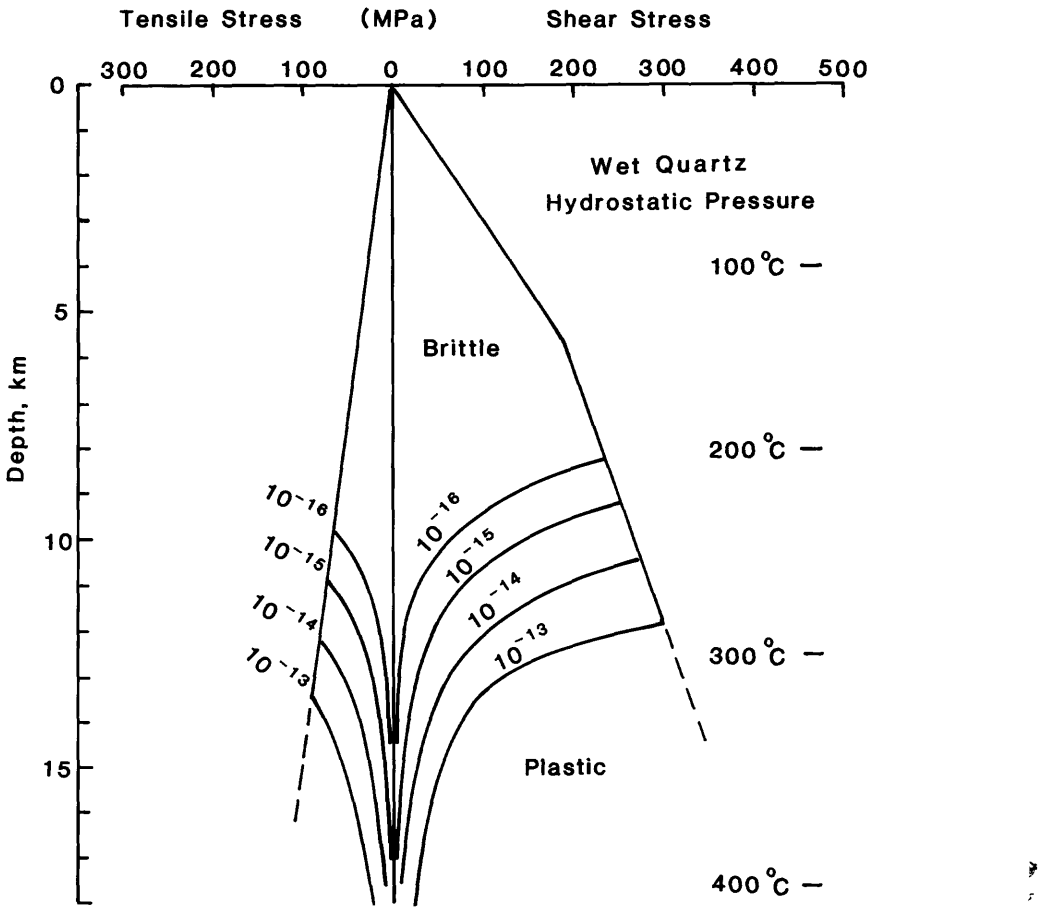

Figure 4. Effect of changing the strain rate from 10^{-13} s^{-1} to 10^{-16} s^{-1} on the plastic strength and maximum stress of wet quartz in a region where the conductive heat flow is about 71 mWm^{-2} and the pore-fluid pressure/ rock-pressure ratio is 0.36. See text for discussion.

fracturing, thermal cracking, mineral dissolution, and sudden formation and expansion of steam and other gases related to movement and/or crystallization of magma. Processes that tend to decrease permeability are plastic flow, precipitation of minerals, formation of clay by hydrothermal alteration processes, and thermal expansion of rock. Deposition of minerals and plastic flow of rock probably are the most important porosity reduction processes, although the formation of clay and other hydrous mineral alteration products may be very important locally.

Values of P_f will become greater than P_h where the rate of porosity reduction and/or the rate of addition of liquid and gas to the system is greater than the rate at which fluid may escape from the system [Bredehoeft and Hanshaw, 1968]. Specific mechanisms for achieving anomalously high P_f ($P_f > P_h$) have been reviewed by Hanshaw and Zen [1965] and Bredehoeft and Hanshaw [1968]. These include mechanisms suggested by Hubbert and Rubey [1959], namely (1) aquifer head, (2) tectonic compression, and (3) rapid loading and compaction of sediments. Others have suggested (4) "fossil"

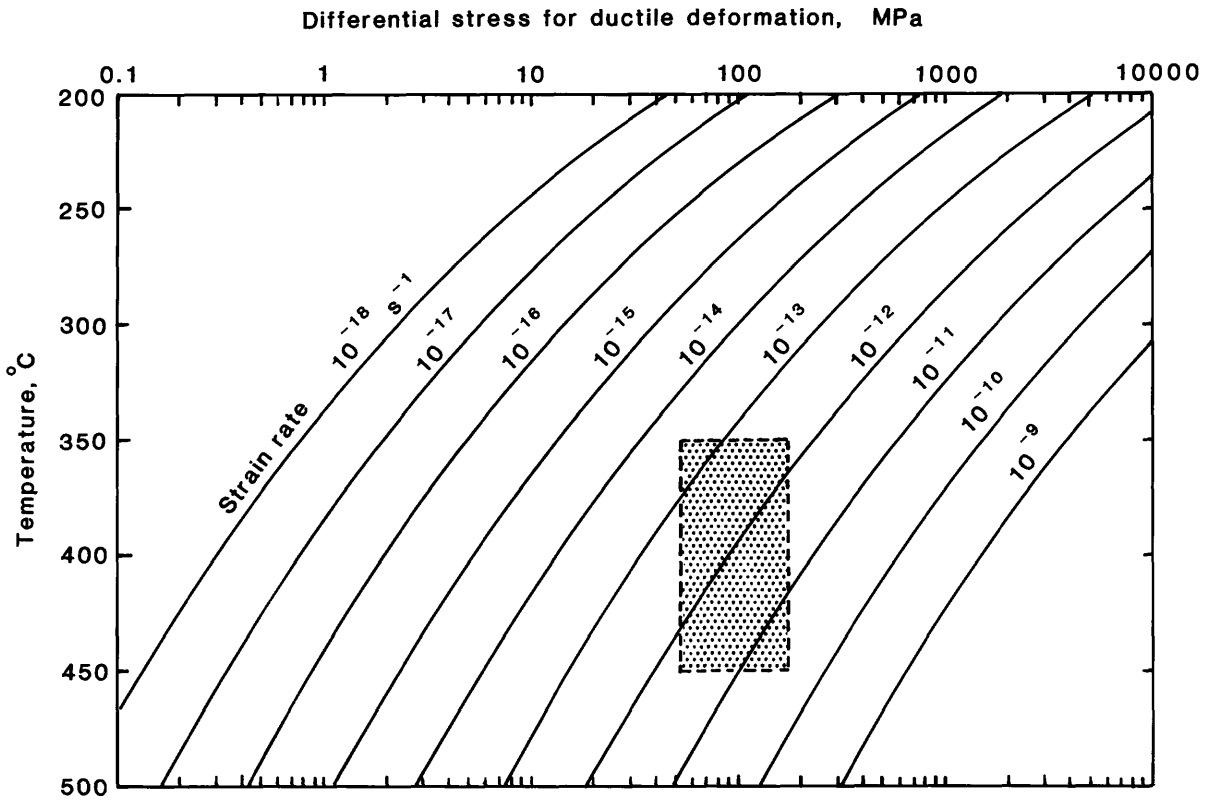

Figure 5. Strain rates at which wet quartz will undergo plastic deformation in response to differential stress as a function of temperature. The stippled region shows the approximate differential stress resulting from the pressure difference between hydrostatic and lithostatic loads at depths ranging from about 3 to 10 km, and temperatures of 350°-450°C.

pressure corresponding to a previous greater depth of burial [Watts, 1948], (5) water derived from magmatic intrusions [Platt, 1962], (5) infiltration of gas [Aliyev, cited in Tkhostov, 1963], (6) solution or precipitation of minerals with consequent change in pore volume [Levorsen, 1954], (7) phase changes that liberate water [Heard and Rubey, 1966; Powers, 1967], or transform heavy hydrocarbons to lighter fractions [Chaney, 1949], (8) volume expansion of fluids upon heating [Levorsen, 1954], (9) osmotic membrane phenomena [Hanshaw and Zen, 1965], and (10) mineral plasticity at high temperature [Brace, 1968].

Movement of fluid inclusions toward regions of higher temperature by dissolving material from the high-temperature (generally bottom) side and depositing material upon the lower-temperature (generally top) side is another mechanism for moving aqueous liquids into the crust against a pressure gradient. This mechanism may be very effective at the base of circulation of some hydrothermal systems where high gradients of temperature and pressure exist and temperatures are in excess of 350°C (see later discussion of high pore-fluid pressures in geothermal exploration wells). Fluid inclusions form where extraction of heat by circulating water at hydrostatic pressure results in thermal cracking of minerals, and pockets of liquid become trapped by subsequent water-mineral reactions that "heal" the

cracks. This healing occurs relatively quickly as a result of dissolution of high energy surfaces and depositing on lower energy surfaces. Once formed, these fluid inclusions may migrate toward the hotter part of the system, as described above.

Measurements in hundreds of wells in deep sedimentary basins show that P_f commonly becomes greater than P_h at a depth of about 2-3 km, and may equal the lithostatic load at depths as shallow as 5-6 km. Only a few deep wells have been drilled entirely or mostly in crystalline rocks in regions with normal geothermal gradients, and little information is available about the variation of P_f with depth in that environment. Brace [1980] reviewed direct and indirect estimates of crustal permeability and concluded that P_f is not likely to exceed P_h to depths of at least 10 km in regions where crystalline rocks extend to the surface. Other investigators have measured $^{18}O/^{16}O$ ratios in igneous rocks that crystallized deep in the crust and concluded that surface-derived aqueous fluids must convect to about 10-20 km in crystalline rocks [Taylor, 1977; Norton and Taylor, 1979].

It was shown previously (Fig. 5) that "wet" quartz at hydrostatic P_f will deform by plastic flow at relatively high strain rates (10^{-12} s^{-1} to 10^{-13} s^{-1}) at temperatures above about 400°C at a depth of 3 km, and above about 350°C at a depth of 10 km. Figure 3 shows that at depths of 15-20 km Westerly granite will deform at a strain rate of about 10^{-12} s^{-1} to 10^{-11} s^{-1} at 350°C and 10^{-11} s^{-1} to 10^{-10} s^{-1} at 400°C. Strain rates, in general, appear to increase by about an order of magnitude for each 50°C increase in temperature. From a rock strength point of view it appears that the depth of circulation of meteoric fluids at hydrostatic pressure is likely to be controlled mainly by the temperature of the surrounding rock, deeper in regions with relatively low heat flows, and shallower in regions of high heat flow. Deep circulation of surface-derived fluids is particularly likely to occur along steep normal faults in actively extending areas. There, repeated brittle fracturing in response to tensional stress may renew permeability frequently enough to maintain convective flow at depths of 10-15 km, where temperatures are 300°-350°C.

Just as a shale horizon within sandstone may prevent upflow of fluids in a compacting sedimentary basin (resulting in increased P_f beneath the shale), precipitation of minerals at one horizon within the channels of fluid upflow may cause fluid pressures to increase throughout a large volume of permeable rock below the permeability barrier. Many authors [Levorsen, 1954; Fyfe et al. 1978; Walder and Nur, 1984] have stressed the importance of porosity reduction caused by chemical solution and redeposition processes that occur at constant temperature in response to differences between P_f and P_r. Etheridge et al. [1983] suggest that an impermeable cap is a natural consequence of prograde metamorphism, and that this cap forms initially at the interface between hot, rising metamorphic fluid and cooler meteoric fluid. Jones [1987] and Hyndman [1988] stress the importance of hydration reactions and deposition of minerals, in general, that occur as a result of a reduction in temperature of an upward flowing fluid, producing impermeable layers that trap the fluid horizon below. The importance of temperature and pressure changes in causing deposition of quartz from convecting hydrothermal solutions at temperatures above 350°C has been discussed by many authors [Kennedy, 1950; Fournier, 1983a].

The variation in quartz solubility with changing temperature and pressure is shown in Figure 6 for pure water as solvent (Fig. 6a) and in 20 wt% NaCl solution (Fig. 6b). NaCl markedly decreases the effect of pressure at constant temperature on the solubility of quartz, but does not eliminate this

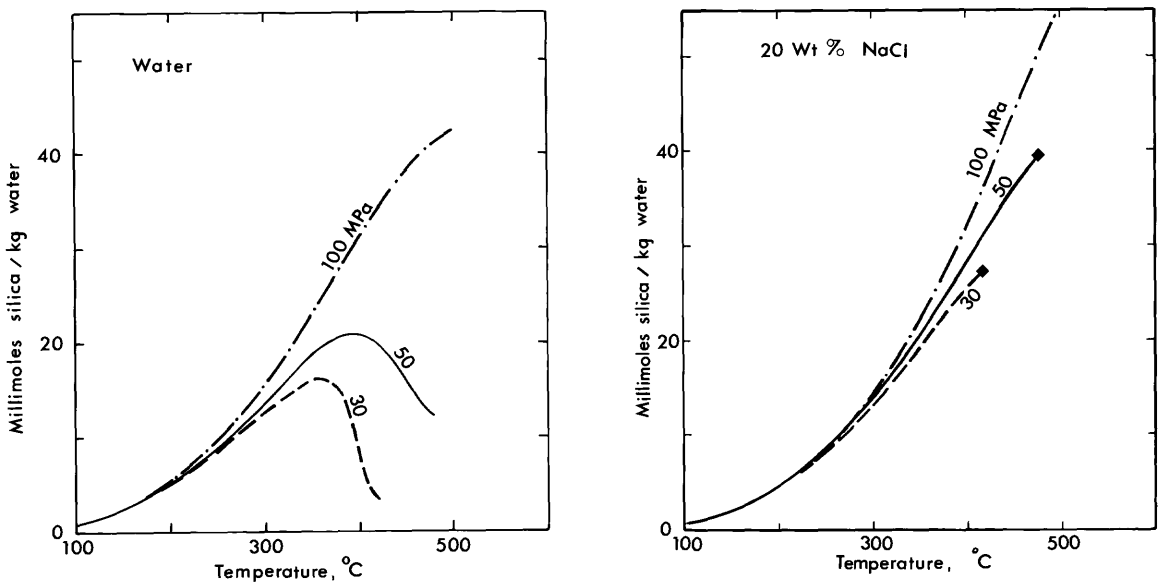

Figure 6. Solubility of quartz as a function of temperature at 30, 50, and 100 MPa. (a) With pure water as solvent and (b) with 20 wt% NaCl as solvent (from Fournier, 1983a).

effect for conditions that are likely to prevail in the upper crust. The solubility data suggest that (1) $P_f > P_h$ might be generated at relatively shallow depths in crystalline rocks below permeability barriers created by chemical processes, and (2) deep circulation of surface-derived fluids into the crust might be episodic, being initiated when and where tectonic stresses or hydraulic fracturing result in the development of new fractures or the reopening of old fractures, and being terminated when chemical processes create a new permeability barrier that inhibits upward flow [Angevine et al., 1982; Walder and Nur, 1984].

Hydraulic Fracturing as a Control on Pore-Fluid Pressures

According to the Griffith theory of fracture [Griffith, 1921, 1925], solids are filled with minute cracks, and when differential stress of a certain magnitude exists, high tensile stress will occur near the ends of such cracks, even when all the principal stresses are compressive. Failure occurs by growth of cracks in response to this tension. Hydraulic fracturing occurs in the earth's crust when P_f exceeds the least principal stress plus the tensile strength of the rock [Hubbert and Willis, 1957; Secor, 1965, 1969]. Although the theoretical tensile strength of a rock-forming mineral is generally close to 10^5 bar, the tensile strength at grain boundaries may be much lower, and the actual tensile strength of rock in hydraulic failure situations (measured at temperatures less than 300°C in drilled holes) is generally a relatively small number because the rocks already contain a multitude of tiny cracks [Brace, 1964, Secor, 1969, Fyfe et al., 1978].

Where the least principal stress lies in approximately a horizontal plane, perpendicular to the lithostatic load, hydraulic fracturing can provide a means of efficiently transporting fluid upward through near-

vertical fractures in rock that was initially relatively impermeable. Hydraulic fracturing at high angles to the earth's surface is likely to be the general case in the upper crust, particularly in extensional terrains. In contrast, where the least principal stress is in the direction of the lithostatic load, as in some compressional terrains, hydraulic fracturing is in horizontal planes and will tend to lift the overlying rock, without providing new channels for upward flow of fluids. Therefore, chemical and physical processes that tend to increase P_f by decreasing porosity and/or by increasing the volume of fluid (by chemical reactions that liberate liquids or gas from solids or by osmotic diffusion) will also tend to expel fluid upward in the crust when and where P_f exceeds the least principal stress and $P_h < P_f < P_r$. These same chemical and physical processes will allow fluid to become concentrated in roughly horizontal layers or lenses in the crust where the least principal stress is parallel to the lithostatic load.

High Pore-Fluid Pressures in Geothermal Exploration Wells at about 400°C

Pore-fluid pressures significantly greater than hydrostatic have been encountered in three deep geothermal energy exploration wells drilled in crystalline rocks: (1) in the Wilson No. 1 well near The Geysers, California (T. M. Evans, personal communication, 1988); (2) in the San Pompeo 2 deep well at Larderello, Italy [Cavarretta et al., 1983; Cappetti et al., 1985; Cathelineau et al., 1986], and (3) in Well NJ-11 at Nesjavellir, Iceland (unpublished manuscript of Benedikt Steingrimsson, 1988). In each of these wells there was a rapid transition from low to high P_f when temperatures exceeding about 400°C were attained. The temperatures and P_f at the bottoms of each of the above wells were much higher than anticipated, and instruments were not available that could accurately measure the extreme conditions. For safety reasons two of the wells (The Geysers and Larderello) were quickly sealed and abandoned, and the Nesjavellir well was partly filled with gravel and cement so that steam and hot water at manageable temperatures and pressures could be produced from relatively shallow zones.

The Nesjavellir geothermal field is a part of the Hengill geothermal area, one of the largest geothermal areas in Iceland. It is in a basaltic terrain within a young fissure swarm. Deep magnetotelluric soundings show a low resistivity layer (apparently indicative of partial melt) that rises to within about 8 km of the surface beneath the Hengill region [Eysteinsson and Hermance, 1985]. The NJ-11 well is close to a fissure that has erupted lava at least twice in post-glacial time, the latest eruption occurring about 2000 years ago. An approximate depth-temperature profile for Nesjavellir well NJ-11 is shown in Figure 7. The relatively small increase in temperature with depth from about 0.5 km to 2 km indicates significant convective flow of fluids at hydrostatic pressure within this depth interval. There is an abrupt increase in the temperature gradient below about 2 km, indicative of a high flux of heat by conduction across relatively impermeable rock. Depth-temperature data are not available to evaluate the possibility of a vertical component of convective flow of fluid at high pressure at temperatures above 400°C. The pressure and temperature results obtained in the NJ-11 well are considered to be very significant because they show that very high pore-fluid pressures can be attained in basaltic rocks at about 400°C. The high pressure probably is the result of entrapment of fluids beneath a chemically sealed impermeable cap and differential water/rock pressure gradients that develop in a vertical column beneath the cap in response to the gravitational field (discussed later).

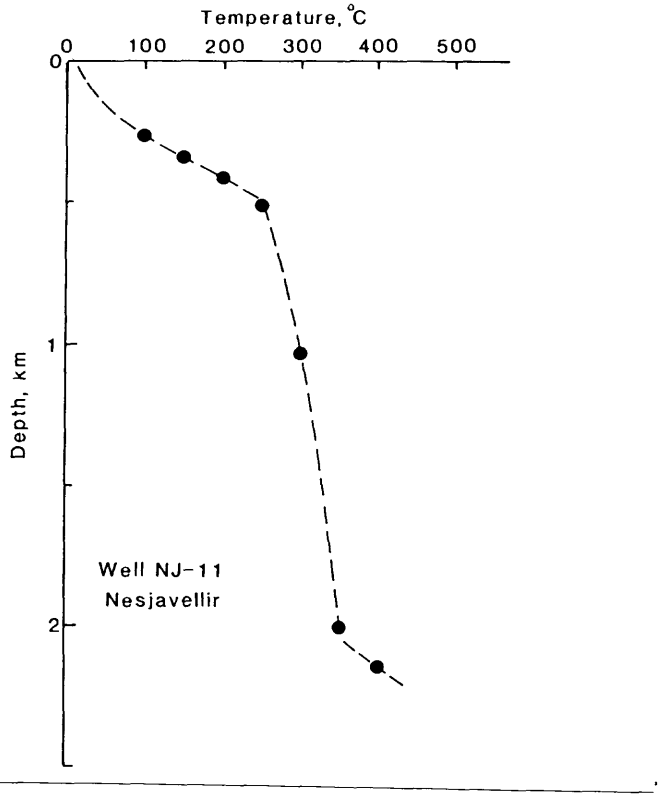

Figure 7. Approximate depth-temperature relations encountered by the NJ-11 well at Nesjavillir, Iceland (constructed using isotherms shown on a cross section in an unpublished manuscript of Benedikt Steingrimsson).

The Geysers geothermal field is within The Geysers-Clear Lake volcanic field that ranges in age from 10,000 to 2 million years. A large, negative gravity anomaly is centered beneath Mount Hannah, a few kilometers northeast of the current main geothermal production area [Isherwood, 1976]. In addition there are magnetic and seismic anomalies in the same region [Iyer, 1984]. These anomalies, taken together, can be modeled as resulting from a spherical magma body centered at a depth of 13.5 km with a radius of 6.9 km [Iyer, 1984]. The Wilson No. 1 well is located about 1.7 km northwest of Mount Hannah. The following information about this well was supplied to the author by T. M. Evans (personal communication, 1988). It was drilled to a total depth of 3673 m into hydrothermally altered sediments, and there were steam entries at 242°C (calculated 34.6 bars P_f) in the depth interval 2800-3000 m. While drilling, P_f remained much below hydrostatic (typical of vapor-dominated systems in which steam fills open fractures and liquid plus steam fills pores in the adjacent rock) until a depth of about 3500 m was attained. Below about 3500 m a thick zone of highly indurated rock was penetrated, rich in quartz and tourmaline. Below that zone of hydrothermal quartz-tourmaline mineralization very high values of P_f were encountered, sufficient to collapse casing in the well. An attempt was made to measure the temperature at a depth of 3368 m (about 300 m above the bottom of the well), but the instrument failed at 345°C before the actual temperature was attained. However, on the basis of isotopic and fluid-inclusion data the assemblage quartz-tourmaline is thought by many investigators to form in the 400°-600°C range [Taylor, 1974; Grant et al., 1980; Scherkenbach et al., 1985] and a minimum temperature of

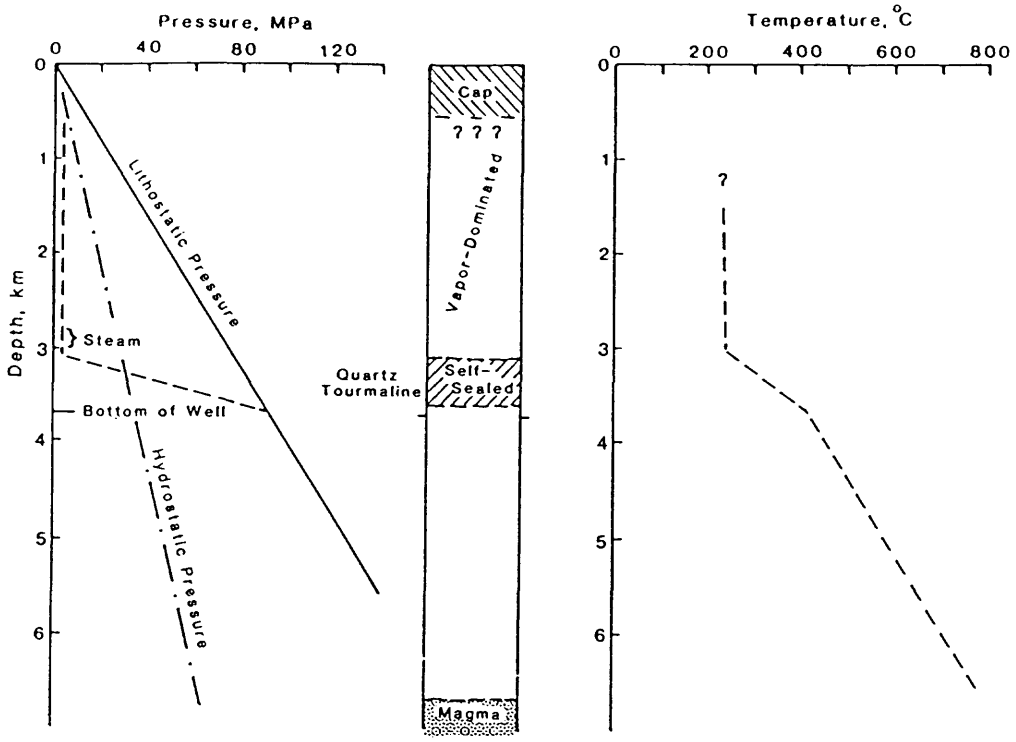

Figure 8. Approximate depth-temperature relations encountered by the Wilson No. 1 well near The Geysers, California (constructed using information supplied by T. M. Evans, personal communication, 1988).

400°C is likely at the bottom of the well. Figure 8 shows probable predrilling temperature and pressure profiles for the Wilson No. 1 well, deduced from the available data.

The conditions encountered in the San Pompeo 2 deep well at Larderello were very similar to those encountered in the Wilson No. 1 well at The Geysers. It was drilled through a sequence of hydrothermally altered sediments into phyllite and quartzite, and bottomed in mica schist. A vapor-dominated, under-pressured, geothermal system is present throughout a large vertical extent in the upper part of the section. Self-sealed impermeable rock was found in the depth interval 2200-2900 m, and quartz-tourmaline mineralization with biotite and labradorite was found in a sample from 2900 m [Bertini et al., 1985; Cathelineau et al. 1986]. Below 2900 m very high values of P_f were encountered, and according to Cappetti et al. [1985], reservoir pressure and temperature could not be measured in the bottom of the well because violent explosions caused the formation to cave in each time the drill bit reached this level. After the last violent blowout only 2560 m of the well were accessible. Attempts to determine the bottom pressure by extrapolation of pressure build-up measurements (made at the wellhead and at a depth of 2560 m) were unsuccessful because of leakages in the surface equipment and in the casing. A temperature of 394°C was measured at 2560 m after the pressure build-up test [Cappetti et al., 1985].

In each of the above wells there appear to have been very steep temperature and pressure gradients across self-sealed zones that formed at about 350°-400°C. This is the temperature range in which the solubility of quartz is greatly influenced by changes both in temperature and in pressure

[Kennedy, 1950; Fournier, 1983a], and also is the temperature range in which strain rates for plastic deformation of quartz in response to the weight of overlying rock become relatively high. Also, at temperatures above 350°C the kinetics of solution and deposition of silica are very rapid [Rimstidt and Barnes, 1980]. Beneath the self-sealed zones pressures may have been as high as lithostatic, but the definitive measurements could not be made. The generation of high P_f beneath self-sealed zones in the vicinity of shallow heat sources has been postulated by various authors including Phillips [1973], Henley and McNabb [1978], and Fournier [1983a, 1983b]. It now appears that abnormally high P_f values in rocks at temperatures in excess of 400°C may be the rule, rather than the exception. However, the magnitude of P_f deep in these active hydrothermal systems remains to be determined.

POSTULATED LITHOSTATIC PORE-FLUID PRESSURES ABOVE 400°C

Mechanisms for Generating and Maintaining Lithostatic Pore-Fluid Pressures

The information presented in Figures 1-4 shows that plastic deformation greatly limits the stress that may accumulate in rocks at temperatures above about 350°-450°C, and that strain rates of 10^{-13} s^{-1} to 10^{-10} s^{-1} (about 0.0003% to 0.3% per year) are attained where hydrostatic conditions prevail at depths of 5 to 10 km in this same temperature range. Therefore, plastic flow resulting from rock settling under the force exerted by its own weight can be expected to decrease the volumes of pore spaces (including fractures) by significant amounts within months at about 400°C, and P_f will increase where a lack of permeability prevents escape of fluids from the system. The strain rate, however, will decrease as the difference between P_r and P_f decreases, and strain rates of 10^{-14} s^{-1} to 10^{-16} s^{-1} are likely to prevail after relatively short periods of time (months to a few years). Thus, plastic flow alone can be expected to generate fluid-pressure/rock-pressure ratios close to 0.9 in a few months, but ratios closer to unity may require exponentially longer periods of time. Other effects, however, such as pressure solution, addition of fluids to the system by chemical reactions or diffusion, and differential fluid/rock pressure gradients in a vertical column may shorten the time that it takes to generate $P_f \simeq P_r$.

It was noted previously that in brittle rocks the maximum P_f that can be attained is limited by the onset of hydraulic fracturing that occurs when P_f exceeds the least principal stress plus the tensile strength of the rock. For strain rates of 10^{-14} s^{-1} to 10^{-16} s^{-1} at about 400°C, plastic flow limits the accumulation of differential stress in the crust so that the least principal stress is likely to be within about 2 to 13 MPa of the maximum principal stress (Fig. 5) (assuming pre-existing fluid-filled fractures and zero tensile strength). Therefore, for usual rates of tectonic deformation the P_f/P_r ratio may reach at least 0.90-0.985 at a depth of 5 km, and 0.95-0.993 at 10 km without hydraulic fracturing. However, there are questions that remain to be answered about whether the Griffith theory of tensile fracturing [Griffith, 1921, 1925] generally applies at high temperatures in those parts of the crust where deformation takes place dominantly by plastic deformation that may involve twinning and translation gliding [Secor, 1969]. There is a good possibility that hydraulic fracturing will not occur where rock deforms by plastic flow in response to the downward force exerted by its own weight, where differential stress is very small, and where dissolving of highly stressed material and redeposition on less stressed surfaces has annealed the regions around the ends of fluid-filled cracks, markedly decreasing the high

tensile stress that normally exists there. I suggest that this is generally the case for aqueous fluids in silicic rocks in the upper crust at temperatures above about 400°C, and that P_f generally is fixed by the lithostatic load, not by hydraulic fracturing at less than the lithostatic load. Under these conditions fluids added to the system by chemical reactions or diffusion make room for themselves by lifting or "floating" the overlying rock. This lifting of overlying rock is likely to occur mainly at grain boundaries so that tensile strength is a less important factor.

Concepts about porosity, permeability, and trapped water in deep crustal rocks have been discussed recently by Etheridge et al. [1983, 1984] and Hyndman [1988]. In this regard, important information has come from (1) a transmission electron microscope (TEM) study of grain boundaries in a range of metamorphic rocks of simple mineralogy [White and White, 1981], (2) an experimental study of the dihedral angle for aqueous fluids in crustal rocks [Watson and Brenan, 1987], and (3) many observations and experiments describing the distribution and geometry of melts within partially molten rocks [von Bargen and Waff, 1986, and references therein]. The main conclusion of all the above studies is that when only a very small amount of liquid is present in a rock, that liquid is located mainly in pores with tapered edges at grain boundary corners, and there is little, if any interconnected porosity. When the amount of liquid increases above some critical value, grain boundary tubes come into being and provide good interconnected porosity and relatively high electrical conductivity. The amount of liquid necessary to initiate interconnected porosity is strongly dependent on the dihedral or wetting angle and curvature of the liquid-solid interface at grain corners, with more liquid being required for larger dihedral angles.

Waff [1980] considered the effects of the gravitational field on liquid distribution in partial melts within the upper mantle. According to his model, for a situation in which the fluid phase is continuously connected over a finite vertical column, the fluid pressure will increase relative to lithostatic pressure in the solid phase with increasing elevation z above the base of the partially molten zone. The differential pressure ΔP existing between the two is given by

$$\Delta P = gz(\rho_r - \rho_f) + \Delta P_o, \qquad (1)$$

where g is the acceleration due to gravity, ρ_r is the average bulk density of the surrounding rock, ρ_f is the density of the fluid, and ΔP_o is the difference in liquid and crystalline phase pressures existing at the base of the partially molten zone where the effect of the gravity field is negligible. Furthermore, according to Waff [1980], if mechanical equilibrium is to be achieved or maintained, the pressure differential existing across liquid-solid interfaces must be exactly balanced by the effect of interfacial surface tension. An increase in surface tension requires an increase in the wetting angle, and this, in turn, forces closure of fluid pathways when ΔP exceeds a critical value that is dependent on vertical distance above the base of the zone of interconnected permeability. Thus, interconnected vertical permeability may be self limited to some particular height with horizontal regions of interconnected permeability separated from each other by relatively thin, horizontal, impermeable layers. For the above model to work, textural equilibrium must be maintained, the wetting angle of the dominant crystalline phases must be less than 60°, and the liquid fraction must not exceed a critical value (probably 5-22 volume percent for partly molten rock). Increase in the liquid fraction above a particular critical value will result in interconnected permeability irrespective of the wetting angle.

Equation (1) applies to water-rock systems (with or without CO_2) as well as to partial melts. It provides a mechanism for boosting P_f to lithostatic at the top of an interconnected permeable zone while deeper in the system P_f is less than lithostatic and strain rates remain relatively high as a result of differential pressure. For the situation in which there is interconnected permeability and P_f equals the lithostatic load, I suggest that the mechanically most stable response to an increase in volume of the fluid phase (by upward squeezing of fluid from below or locally derived by metamorphic reactions that release water and carbon dioxide) is likely to be a lifting or "floating" of the overlying rock and formation of discontinuous horizontal tension veins. Upward movement of fluid out of the system is likely to be very slow, possibly mainly by infrequent breakthrough from one "water-sill" to another, as suggested by Fyfe et al. [1978].

Permissive Evidence from Geothermal and Metamorphic Environments

Results obtained from wells drilled into very hot geothermal systems, cited above, show that chemical processes very effectively create permeability barriers in crystalline rocks that separate high-pressure fluids at about 400°C from fluids at lower temperatures and much lower pressures. However, whether or not pore pressures increase to the point of actually equaling the lithostatic load under these conditions remains open to question. A major concern is the role that hydraulic fracturing may play in limiting P_f to values significantly less than the lithostatic load where there are steep temperature and pressure gradients.

The textures and mineralogy of metamorphic rocks and associated veins that appear to have formed at temperatures above about 400°C seem to favor P_f values significantly above hydrostatic, and petrologists commonly have concluded that P_f is lithostatic deep in the crust [Etheridge, 1983, 1984; Crawford and Hollister, 1986; Wood and Walther, 1986]. There has been considerable discussion about the quantity of fluid that has flowed through a given metamorphic rock and whether a single-pass or multiple-pass process is required to explain the isotopic and chemical changes that have occurred during metamorphism [see reviews by Ferry, 1986; Wood and Walther, 1986]. Wood and Walther [1986] concluded that a single-pass model readily produces high fluid-rock ratios in rocks that do not produce large amounts of fluid and that are the dominant components of the metamorphic sequence. In contrast, Etheridge et al. [1983] advocated a multiple-pass process in which large-scale fluid convection is responsible for chemical transport of silica and other constituents. However, most of the evidence cited by Etheridge et al. [1983] for a multiple-pass process seems to apply mainly to low metamorphic grade rocks (<400°C).

Weber [1986] correlated metamorphic grade and crustal rheology and concluded that the orogenic continental crust during prograde metamorphism consists of three layers of contrasting bulk rheology: a lower layer of "dry" granulite-facies rock able to carry bulk flow stresses in the range of 50 to 100 MPa or more depending on composition and temperature; a middle, relatively "wet" layer of migmatites and amphibolite-facies rocks of very low mechanical strength; and an upper layer of low-grade and very low-grade metamorphic rocks, the so-called "brittle" crust. The temperature of transition from greenschist-facies to amphibolite-facies rocks increases with increasing fugacity of water [Turner, 1981], and at a depth of about 10 km and water pressure equal to the pressure exerted by the lithostatic load, this transition takes place at about 400°C. Again, the evidence for lithostatic P_f is

permissive, but not conclusive. However, consideration must be given to why the middle crust appears to remain relatively wet and very weak.

Relatively high P_f values should build up relatively quickly by plastic flow in the crust where temperatures are in excess of 400°C, as previously discussed. The fact that this environment appears to remain relatively "wet" suggests to me that hydraulic fractures at steep angles to the earth's surface generally do not form there. If they did form to any great extent, fluid would be expelled upward relatively efficiently, and the middle crust would soon become relatively dry.

Geophysical Consequences

From the point of view of this paper, a major consequence of P_f becoming equal to P_r is a decrease in the effective strength of rock to essentially zero where there are fractures or interconnected, fluid-filled pores, and a corresponding change from seismic to aseismic conditions. I suggest that P_f near or equal to P_r generally occurs in the upper crust at temperatures above about 350°–400°C, but may occur at lower temperatures in deep sedimentary basins and in crystalline rock subjected to thrust faulting. Within the Cascade Range, the base of earthquake activity probably marks the 400°C isotherm to depths of about 10–12 km in tensional and strike-slip tectonic environments. At greater depths the transition from seismic to aseismic conditions is likely to take place at lower temperatures for quartz-rich rocks and at higher temperatures for dry mafic rocks. Also, when determining the depth to the 400°C isotherm, "long-period" (LP) earthquakes, in which most of the recorded energy is concentrated between 2 and 4 Hz, should be excluded because they are likely to be the result of poorly understood short-term local stresses resulting from magma movement.

Many geophysicists have speculated that high P_f in some places deep in the crust may account for extremely high electrical conductivity [Shankland and Ander, 1983; Gough, 1986; Jones, 1987; Hyndman, 1988], for increased seismic reflectivity [Walder and Nur, 1984; Gough, 1986; Hall, 1986; Jones, 1987; Matthews, 1986; Matthews and Cheadle, 1986; Hyndman, 1988], and for relatively low seismic velocities [Berry and Mair, 1977]. Calculations by Walder and Nur [1984] indicate that the P_f required to account for seismic low-velocity zones in the crust at >6–8 km depth would be close to P_r. South of the Canadian border the electrical structure beneath the Cascades and adjacent regions has been determined by Stanley [1982, 1983, 1984] and Stanley et al. [1987, 1989] and their models show that a deep crustal conductor is found in a region of the crust where plastic behavior occurs at the top of a 6.4–6.5 km s^{-1} velocity layer [Stanley et al., 1989].

Perhaps the most compelling correlation of geophysical response with the onset of high pore-fluid pressures in the crust at temperatures of about 400°C comes from investigations north of the Canadian border where seismic and electrical data have been acquired across Cascadia and the Juan de Fuca subduction zone by the LITHOPROBE program. Hyndman [1988] reviewed all the available geophysical data and showed that there is a dipping band of seismic reflectors in the continental crust above the oceanic plate that also appears to be electrically conductive. Using detailed heat-flow data of Lewis et al. [1988] and Hyndman [1988] showed that the dipping bands are nearly isothermal at a temperature of 400°–500°C, and concluded that free water generated by dehydration reactions of the downgoing oceanic plate migrates upward until reduced temperature results in hydration reactions and mineral precipitation that forms an impermeable barrier.

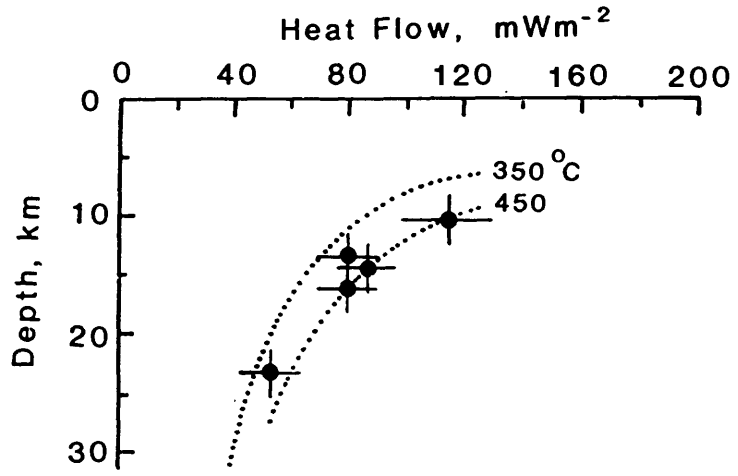

Figure 9. Depths to the reflective lower crust (dots with error bars) as a function of heat flow (from Klemperer, 1987), and in respect to the 350°C and 450°C isotherms.

Adam [1976, 1987] found a correlation between the depths to tops of high-conductivity lower crustal layers and heat flow with an inferred temperature of about 350°-400°C. Klemperer [1987] correlated the depth to the seismically reflective lower crust with heat flow, and a comparison of his results with calculated depths to 350° and 450°C isotherms (Fig. 9) indicate that, in regions of noncompressive stress, the lower crust becomes seismically reflective at about 400°C. Again, the above electrical and seismic reflector results corresponds approximately with the region where P_f is likely to become equal to P_r, and also corresponds approximately with the transition from greenschist-facies to amphibolite-facies rocks in a region of "wet" crust. In contrast, in the interiors of compressional orogens the reflective lower crust is not always recognizable as a separate entity because reflective zones are visible throughout the crust [Klemperer, 1987]. This latter environment also corresponds to regions where high P_f may result in hydraulic fractures roughly parallel to the earth's surface.

There are various reasons why rocks in the crust may exhibit extremely high electrical conductivity, relatively low seismic velocities, and increased seismic reflectivity, and different explanations may apply in different places. However, these geophysical phenomena commonly seem to become manifest at depths where rock temperatures are likely to be about 400°C and where, I believe, P_f should be about equal to P_r. Thus, high P_f may be a contributing factor that is partly or wholly responsible in some places for the development of these geophysical properties.

EVALUATION OF HEAT FLOW

The earthquake methodology suggested here for evaluating heat flux should apply only to "tectonic" seismic events in which most energy is concentrated between 5 and 10 Hz. The methodology is based mainly on the assumption that, in seismically active regions where the stress field is noncompressive, the transition from seismic to aseismic conditions in the upper crust generally takes place at about 400°C for most rock types and possibly as low as about 350°C for quartz-rich rocks at depths greater than about 12-20 km. In arriving at these temperatures, great emphasis was placed on determining the

likely conditions in the crust at which P_f is likely to become equal to P_r because differential stress cannot accumulate where this situation exists. Thus, effects of rock type on the maximum amount of stress that can accumulate at a given depth, temperature, and strain rate are nullified. Earthquakes will occur only where there has been accumulation of differential stress in the crust. In compressional terrains, P_f equal to P_r may be attained at temperatures much lower than 350°C, and this should be kept in mind when using the seismic to aseismic boundary to estimate subsurface temperature conditions. Also, the utility and accuracy of using depths of earthquakes to determine the depth to the 350° or 400°C isotherm is highly dependent on the occurrence of enough earthquakes in the particular region to outline the base of seismic activity, and on the accuracy with which focal depths of those seismic events can be determined.

Knowledge of the approximate depth to the 350° isotherm (at seismic/aseismic depths of about 12-20 km) or 400°C isotherm (at seismic/aseismic depths of less than 10-12 km) allows one to construct a theoretical temperature-depth profile, and then to estimate the heat flow, assuming reasonable values for the thermal conductivity. Figure 2 can be used to obtain a first approximation of the expected heat flow for a given region where there has been no transfer of thermal energy by convective flow of fluids. Measured heat flows that are lower than those estimated by the above method may be low because the heat-flow measurements were made in a region of downward percolation or recharge of meteoric water. Similarly, measured heat flows that are higher than those estimated by the above method may be high because the heat-flow measurements were made in a region of discharge of heated fluids.

It would be very advantageous to be able to use earthquake hypocenter information or other geophysical methods to estimate with confidence the depth to an isotherm at a lower temperature than 350°-400°C. Unfortunately, there appear to be too many uncertainties at this time to use the depth at which the maximum number of seismic events occur as a reliable temperature marker. However, the suggestion of Smith and Bruhn [1984] that 80% of earthquakes in quartz-rich rocks occur above the 300°C isotherm deserves further consideration. If this proves to be generally true, the estimated depth to the 300°C isotherm, in respect to its depth calculated using the 350° or 400°C isotherm and a conductive heat-flow model, may give a rough indication of whether or not significant convective flow is occurring. For example, an estimated depth to the 300°C isotherm very close to the estimated depth of the 400°C isotherm would be indicative of a very high flux of thermal energy by conduction to an overlying cooler system. The overlying system may or may not be hydrothermal; relatively recent intrusion of magmatic material into cooler overlying rock might lead to a steep thermal gradient with little or no associated hydrothermal activity because the system is too young for extensive hydrothermal activity to have developed. Comparison of the measured heat flow in the region with a calculated conductive heat-flow model, based on the depth to the 300°C isotherm, might provide information about the likely presence of a convecting hydrothermal system at depth. A 300°C isotherm that is at too high a level compared to its expected depth in respect to the 400°C isotherm would be indicative of a large, high-temperature, convecting hydrothermal system.

In some places the 400°C isotherm might be depressed to lower than expected depths (based on regional heat flow and geologic considerations) because of a much higher than average rate of "mining" of heat from the system by deep convective flow of meteoric fluids. In particular, this is likely to

be the situation where meteoric waters flow into hot rock along major faults which keep reopening channels of fluid flow that have become clogged by mineral deposition. In other places the 400°C isotherm may be at a very shallow level, the result of a shallow magmatic intrusion.

Iyer [1984] mentioned that zones of seismic quiescence may be indicative of magma chambers. To the extent that the magma has recently been intruded into rock having a temperature less than 400°C, zones of seismic quiescence may indeed be indicative of the location of the magma chamber. In general, however, shallow zones of seismic quiescence beneath young volcanic structures should be viewed as regions where temperatures are likely to be above 400°C, and other geophysical methods should be employed to look for possibly smaller volumes of magma within the seismically quiescent block of ground.

CONCLUSIONS

It is likely that in any given region there will be a maximum number of earthquake hypocenters at the depth of the brittle-plastic transition. However, the temperature of this transition is affected by the local stress field, the strain rate, the composition of the rock, and the pore-fluid pressure at the depth in question. Therefore, although the depth to this transition can be determined with some degree of accuracy, it appears at this time to be of limited use for estimating depths to a specific temperature. However, the generality that only about 20% of earthquakes in siliceous rocks in the upper crust occur at temperatures above 300°C should be investigated further. It appears that within the upper crust where pore-fluids are present, conditions generally change from seismic to aseismic at about 400°C. This is because chemical processes that decrease permeability, metamorphic reactions that release water and CO_2, and plastic flow of rock that increases pore-fluid pressures, all appear to act relatively quickly at about 400°C, and fluid becomes trapped in regions where there is interconnected horizontal permeability but little vertical permeability. The net effect is a general increase in P_f until it becomes equal to P_r, with a corresponding decrease in the effective strength of rock to zero. The main conclusion of this presentation is that the surface separating seismic from aseismic conditions generally marks the approximate depth to the 400°C isotherm for most rock types and possibly the approximate depth to the 350°C isotherm for quartz-rich rocks at depths of about 12-20 km. This information allows calculation of a depth-temperature profile, and estimation of heat flow, assuming a reasonable average thermal conductivity and heat production for the rocks in the region. This estimated heat flow can then be compared with measured heat flows to determine whether the measured values appear to be greatly affected by convective flow of fluids in the crust.

The "earthquake method" of estimating depths to the 400°C isotherm is limited to regions in which there is a significant amount of natural seismic activity, and by the accuracy with which hypocenters can be located. However, it offers a way of evaluating possible effects of deep convective flow that otherwise could be determined only by very deep drilling in many places. It also provides additional information that may be of use in assessing the amount of heat likely to be stored in various parts of the crust down to any chosen depth or temperature.

REFERENCES

Adam, A., Quantitative connection between regional heat flow and depth of conductive layers in the earth's crust and upper mantle, Acta Geod. Geophys. Montanistica, 11, 503-509, 1976.

Adam, A., Are there two types of conductivity anomalies (CA) caused by fluid in the earth's crust?, Phys. Earth Planet. Inter., 45, 209-215, 1987.

Angevine, C. L., D. L. Turcotte, and M. D. Furnish, Pressure solution lithification as a mechanism for the stick-slip behavior of faults; Tectonics, 1, 151-160, 1982.

Berry, M. J., and J. A. Mair, The nature of the earth's crust in Canada, in The earth's crust: Its nature and physical properties, edited by J. H. Heacock, Geophys. Monogr. Ser., AGU, 20, 319-348, 1977.

Bertini, G., G. Gianelli, E. Pandeli, and M. Puxeddu, Distribution of hydrothermal minerals in Larderello-Travale and Mt. Amiata geothermal fields (Italy), Geoth. Resourc. Counc. Trans., 9, 262-266, 1985.

Blackwell, D. D., and J. L. Steele, A summary of heat flow studies in the Cascade Range, Geoth. Resourc. Counc. Trans., 7, 233-236, 1983.

Blackwell, D. D., and J. L. Steele, Heat flow of the Cascade Range, in Proceedings of the Workshop on Geothermal Resources of the Cascade Range, edited by M. Guffanti, and L. J. P. Muffler, US Geol. Surv. Open-File Rep. 85-521, 20-23, 1985.

Blackwell, D. D., R. G. Bowen, D. A. Hull, J. Riccio, and J. L. Steele, Heat flow, arc volcanism and subduction in northern Oregon, J. Geophys. Res., 87, 8735-8754, 1982.

Blackwell, D. D., J. L. Steele, and M. K. Frohme, Heat flow in the Oregon Cascade Range and its correlation with regional gravity, magnetic and geologic patterns, US Geol. Surv. Open-File Rep., 1989, this volume.

Brace, W. F., Brittle fracture of rocks, in State of Stress in the Earth's Crust, edited by W. R. Judd, pp. 110-178, Elsevier, New York, 1964.

Brace, W. F., The mechanical effects of pore pressure on the fracturing of rocks, in Research in Tectonics, edited by A. J. Baer and D. K. Norris, Geological Survey of Canada Paper 68-52, 113-124, 1968.

Brace, W. F., Permeability of crystalline and argillaceous rocks, Int. J. Rock Mech. Min. Sci. Geomech. Abs. 17, 241-251, 1980.

Brace, W. F., and D. L. Kohlstedt, Limits on lithospheric stress imposed by laboratory experiments, J. Geophys. Res., 85, 6248-6252, 1980.

Bredehoeft, J. D., and B. B. Hanshaw, On the maintenance of anomalous fluid pressures: I. Thick sedimentary sequences, Geol. Soc. Am., 79, 1095-1104, 1968.

Byerlee, J. D., Brittle-ductile transition in rocks, J. Geophys. Res., 73, 4741-4750, 1968.

Cappetti, G., R. Celati, U. Cigni, P. Squarci, G. Stefani, and L. Taffi, Development of deep exploration in the geothermal areas of Tuscany, Italy, in 1985 International Symposium on Geothermal Energy, International Volume, edited by C. Stone, Geoth. Resourc. Counc. Trans., 303-309, 1985.

Cathelineau, M., C. Marignac, and M. Puxeddu, Early stage of hydrothermal metamorphism at temperatures of 325°-600°C in the deepest part of the Larderello geothermal field (Italy), in Fifth International Symposium on Water-Rock Interaction, Reykjavik, Iceland, Extended Abstracts, pp. 100-103, 1986.

Cavarretta, G., G. Gianelli, and M. Puxeddu, Hydrothermal and contact metamor-phism in the Larderello geothermal field (Italy), in Fourth International Symposium on Water-Rock Interaction, Misasa, Japan, Extended Abstracts, pp. 82-84, 1983.

Chaney, P. E., Abnormal pressures and lost circulation, in Drilling and Production Practice, pp. 145-148, Am. Petrol. Inst., 1949.

Connard, G., R. Couch, and M. Gemperle, Analysis of aeromagnetic measurements from the Cascade Range in Central Oregon, Geophysics, 48, 376-390, 1983.

Crawford, M. L., and Hollister, L. S., Metamorphic fluids: The evidence from fluid inclusions, in Fluid-rock interactions during metamorphism, edited by J. V. Walter and B. J. Wood, pp. 1-35, Springer-Verlag, New York, 1986.

Crosson, R. S., and T. J. Owens, Slab geometry of the Cascadia subduction zone beneath Washington from earthquake hypocenters and teleseismic converted waves, Geophys. Res. Lett., 14, 824-827, 1987.

Elders, W. A., and Sass, J. H., The Salton Sea scientific drilling project, J. Geophys. Res., 93, 12953-12968, 1988.

Etheridge, M. A., V. J. Wall, and R. H. Vernon, The role of the fluid phase during regional metamorphism and deformation, J. Metamorph. Geol., 1, 205-226, 1983.

Etheridge, M. A., V. J. Wall, S. F. Cox, and R. H. Vernon, High fluid pressure during regional metamorphism and deformation: Implications for mass transport and deformation mechanisms, J. Geophys. Res., 89, 4344-4358, 1984.

Eysteinsson, H., and J. F. Hermance, Magnetotelluric measurements across the eastern neovolcanic zone in south Iceland, J. Geophys. Res., 90, 10093-10103, 1985.

Ferry, J. M., Reaction progress: A monitor of fluid-rock interaction during metamorphic and hydrothermal events, in Fluid-rock interactions during metamorphism, edited by J. V. Walter and B. J. Wood, pp. 60-88, Springer-Verlag, New York, 1986.

Fournier, R. O., Self-sealing and brecciation resulting from quartz deposition within hydrothermal systems, in Fourth International Symposium on Water- Rock Interaction, Misasa, Japan, Extended Abstracts, pp. 137-140, 1983a.

Fournier, R. O., Active hydrothermal systems as analogues of fossil systems, in The role of heat in the development of energy and mineral resources in the northern Basin and Range province, Geoth. Resourc. Counc. Spec. Rep. No. 13, 263-284, 1983b.

Fyfe, W. S., N. J. Price, and A. B. Thompson, Fluids in the Earth's Crust, Elsevier, Amsterdam, 1978.

Goetze, C., and B. Evans, Stress and temperature in bending lithosphere as constrained by experimental rock mechanics, Geophys. J. R. Astron. Soc., 59, 463-478, 1979.

Gough, D. I., Seismic reflectors, conductivity, water and stress in the continental crust, Nature, 323, 143-144, 1986.

Grant, J. N., C. Halls, S. M. F. Sheppard, and W. Avila, Evolution of the porphyry tin deposits of Bolivia, Min. Geol. Spec. Iss. 8, 151-173, 1980.

Griffith, A. A., The phenomena of rupture and flow in solids, R. Soc. London Philos. Trans., Ser. A, 221, 163-198, 1921.

Griffith, A. A., The theory of rupture, Cong. Appl. Mech., 1st, Delft, 1924, Proc., pp. 55-63, 1925.

Hall, J., Nature of the lower continental crust: Evidence from BIPS work on the Caledonides, in Reflection Seismology: The continental Crust, Geodynam. Ser., v. 14, edited by M. Barazangi and L. Brown, pp. 223-231, AGU, Washington, D.C., 1986.

Hanshaw, B. B., and E-an Zen, Osmotic equilibrium and overthrust faulting, Geol. Soc. Am. Bull., 76, 1379-1386, 1965.

Heard, H. C., and W. W. Rubey, Tectonic implications of gypsum dehydration, Geol. Soc. Am. Bull., 77, 741-760, 1966.

Henley, R. W., and A. McNabb, Magmatic vapor plumes and ground-water interaction in porphyry copper emplacement, Econ. Geol., 73, 1-20, 1978.

Hobbs, B. E., A. Ord, and C. Teyssier, Earthquakes in the ductile regeim?, Pure Appl. Geophys., 124, 309-336, 1986.

Hubbert, M. K., and W. W. Rubey, Role of fluid pressure in mechanics of over-thrust faulting, I. Mechanics of fluid-filled porous solids and its application to overthrust faulting, Geol. Soc. Am. Bull., 70, 115-166, 1959.

Hubbert, M. K., and D. G. Willis, Mechanics of hydraulic fracturing, J. Petrol. Tech., Petrol. Trans., 210, 153-166, 1957.

Hyndman, R. D., Dipping seismic reflectors, electrically conductive zones, and trapped water in the crust over a subducting plate, J. Geophys. Res., 93, 13391-13405, 1988.

Ingebritsen, S. E., D. R. Sherrod, and R. H. Mariner, Heat Flow and hydrothermal circulation in the Cascade Range, north-central Oregon, US Geol. Surv. Open-File Rep.; 1989, this volume.

Isherwood, W. F., Gravity and magnetic studies of The Geysers-Clear Lake geothermal region, California, USA, in Proceedings Second United Nations Symposium on the Development and Use of Geothermal Resources, San Francisco, 1975, US Govt. Printing Office, Washington, DC, 2, 1065-1073, 1976.

Iyer, H. M., Geophysical evidence for the locations, shapes and sizes, and internal structures of magma chambers beneath regions of Quaternary volcanism, Philos. Trans. R. Soc. London, Ser. A, 310, 473-510, 1984.

Jones, A., MT and reflection: An essential combination, Geophys. J. R. Astron. Soc., 89, 7-18, 1987.

Kennedy, G. C., A portion of the system silica-water, Econ. Geol., 45, 629-653, 1950.

Klemperer, S. L., A relation between continental heat flow and seismic reflectivity of the lower crust, J. Geophys. 61, 1-11, 1987.

Koch, P. H., J. M. Christie, and R. P. George, Flow law of "wet" quartzite in the α-quartz field (abstract), Eos Trans. AGU, 61, 376, 1980.

Kusznir, N. J., and R. G. Park, Continental lithosphere strength: The critical role of lower crustal deformation, in The nature of the lower continental crust, edited by J. B. Dawson, D. A. Carswell, J. Hall, and K. H. Wedepohl, Geol. Soc. London Spec. Pub. 24, 79-93, 1986.

Lachenbruch, A. H., and J. H. Sass, Models of an extending lithosphere and heat flow in the Basin and Range province, Geol. Soc. Am. Memoir 152, 209-249, 1978.

Lewis, T. J., Thermal structure of the southern coast plutonic complex and the northern (Canadian) Cascades, Geol. Survey Canada Contrib. (in press).

Lewis, T. J., W. H. Bentkowski, E. E. Davis, R. W. Hyndman, J. G. Souther, and J. A. Wright, Subduction of the Juan de Fuca plate: Thermal consequences, J. Geophys. Res., 93, 15207-15225, 1988.

Levorsen, A. I., Geology of Petroleum, 703 pp., W. H. Freeman, San Francisco, 1954.

Matthews, D. H., Seismic reflections from the lower crust around Britton, in The nature of the lower continental crust, edited by J. B. Dawson, D. A. Carswell, J. Hall, and K. H. Wedepohl, Geol. Soc. London Spec. Pub. 24, 11-22, 1986.

Matthews, D. H., and M. J. Cheadle, Deep reflections from the Caledonides and Variscides west of Britain and comparison with the Himalayas, in Reflection Seismology: The continental Crust, Geodynam. Ser., v. 14, edited by M. Barazangi and L. Brown, pp. 5-19, AGU, Washington, D.C., 1986.

Meissner, R., and J. Strehlau, Limits of stresses in continental crusts and their relation to the depth-frequency distribution of shallow earthquakes, Tectonics, 1, 73-89, 1982.

Norton, D., and H. P. Taylor, Jr., Quantitative simulation of the hydrothermal systems of crystallizing magmas on the basis of transport theory and isotope data, J. Petrol., 20, 421-486, 1979.

Okubo, Y., H. Tsu, and K. Ogawa, Estimation of Curie point temperature and geothermal structure of island arcs of Japan, Tectonophysics (in press).

Paterson, M. S., Experimental Rock Deformation - the Brittle Field, 254 pp., Springer-Verlag, New York, 1978.

Pfiffner, O. A., and J. G. Ramsay, Constraint on geological strain rates: Arguments from finite strain rates of naturally deformed rocks, J. Geophys. Res., 87, 311-321, 1982.

Phillips, W. J., Mechanical effects of retrograde boiling and its probable importance in the formation of some porphyry ore deposits, Am. Inst. Min. Metal. Eng. Trans., sec. B, 82, B90-B98, 1973.

Platt, L. B., Fluid pressure in thrust faulting, a corrollary, Am. J. Sci., 260, 107-114, 1962.

Powers, M. C., Fluid-release mechanisms in compacting marine mudrocks and their importance in oil exploration, Am. Assoc. Petrol. Geol. Bull., 51, 1240-1254, 1967.

Rimstidt, J. D., and H. L. Barnes, The Kinetics of silica-water reactions, Geochim. Cosmochim. Acta, 44, 1683-1699, 1980.

Rutter, E. H., On the nomenclature of mode of failure transitions in rocks, Tectonophysics, 122, 381-387, 1986.

Scherkenbach, D. A., F. J. Sawkins, and W. E. Seyfried, Jr., Geologic, fluid inclusion, and geochemical studies of the mineralized breccias at Cumobabi, Sonora, Mexico, Econ. Geol., 80, 1566-1592, 1985.

Scholz, C. H., The brittle-plastic transition and depth of seismic faulting, Geologische Rundschau, 77, 319-328, 1988.

Secor, D. T., Role of fluid pressure in jointing, Am. J. Sci., 263, 633-646, 1965.

Secor, D. T., Mechanics of natural extension fracturing at depth in the earth's crust, in Research in Tectonics, edited by A. J. Baer, and D. K. Norris, Canada Geol. Surv. Pap. 68-52, 3-48, 1969.

Shankland, T. J., and M. E. Ander, Electrical conductivity, temperatures and fluids in the lower crust, J. Geophys. Res., 88, 9475-9484, 1983.

Shaw, H. R., The fracture mechanism of magma transport from the mantle to the surface, in Physics of Magmatic Processes, edited by R. B. Hargraves, pp. 204-264, Princeton Univ. Press, 1980.

Shimamoto, T., and J. M. Logan, Velocity-dependent behavior of simulated halite shear zones: an analog for silicates, in Earthquake source mechanisms, edited by S. Das, J. Boatwright, and C. Scholz, AGU Geophys. Mono. 37, Washington D.C., 49-64, 1986.

Sibson, R. H., Fault rocks and fault mechanisms, J. Geol. Soc. London, 133, 191-214, 1977.
Sibson, R. H., Fault zone models, heat flow, and the depth distribution of earthquakes in continental crust of the United States, Bull. Seismological Soc. Am., 72, 151-163, 1982.
Sibson, R. H., Continental fault structure and shallow earthquake source, J. Geol. Soc. London, 140, 741-767, 1983.
Smith, R. B., and M. S. Bauer, Seismotectonic deformation of intraplate areas in the Western United States (abstract), Eos Trans. AGU, 63, 1024, 1982.
Smith, R. B., and R. L. Bruhn, Intraplate expansional tectonics of the Eastern Basin-Range: Inferences on structural style from seismic reflection data, regional tectonics, and thermal-mechanical models of brittle-ductile deformation, J. Geophys. Res., 89, 5733-5762, 1984.
Stanley, W. D., A regional magnetotelluric survey of the Cascade Mountains regions, US Geol. Surv. Open-File Rep. 82-126, 198 p., 1982.
Stanley, W. D., Regional electrical structures in the Cascades and their significance in geothermal and volcano hazards assessment (abstract), EOS Trans. AGU, 64, 887, 1983.
Stanley, W. D., Tectonic study of Cascade Range and Columbia Plateau in Washington State based upon magnetotelluric soundings, J. Geophys. Res., 89, 4447-4460, 1984.
Stanley, W. D., C. A. Finn, and J. L. Plesha, Tectonics and conductivity structures in the southern Washington Cascades, J. Geophys. Res., 92, 10179-10193, 1987.
Stanley, W. D., G. S. Fuis, W. D. Mooney, and C. A. Finn, Details of structure in the Cascade Range and surrounding regions from seismic and magnetotelluric data, US Geol. Surv. Open-File Rep., 1989, this volume.
Taylor, H. B., The application of oxygen and hydrogen isotopes studies to problems of hydrothermal alteration and ore deposition, Econ. Geol., 69, 843-883, 1974.
Taylor, H. P., Jr., Water/rock interaction and the origin of H_2O in granitic batholiths, J. Geol. Soc. London, 33, 509-558, 1977.
Tkhostov, B. A., Initial Rock Pressures in Oil and Gas Deposits, 118 pp., MacMillan, New York, 1963.
Tse, S. T., and J. R. Rice, Crustal earthquake instability in relation to the depth variation of frictional slip properties, J. Geophys. Res., 91, 9452-9472, 1986.
Turner, F. J., Metamorphic Petrology (2d ed.), McGraw-Hill, New York, 1981.
von Bargen, N. and H. S. Waff, Permeabilities, interfacial areas and curvatures of partially molten systems: Results of numerical computations of equilibrium microstructures, J. Geophys. Res., 91, 9261-9276, 1986.
Waff, H. S., Effects of the gravitational field on liquid distribution in partial melts within the upper mantle, J. Geophys. Res., 85, 1815-1825, 1980.
Walder, J., and A. Nur, Porosity reduction and crustal pore-pressure development, J. Geophys. Res., 89, 11539-11548, 1984.
Watson, E. B., and J. M. Brenan, Fluids in the lithosphere, 1, Experimentally-determined wetting characteristics of CO_2-H_2O fluids and their implications for fluid transport, host-rock physical properties, and fluid inclusion formation, Earth Planet. Sci. Lett., 85, 497-515, 1987.
Watts, E. V., Some aspects of high pressures in the D-7 zone of the Ventura Avenue field, Am. Inst. Min. Metall. Eng. Trans., 174, 191-205, 1948.

Weaver, Craig, Seismotectonic fabric of the Cascade Range, US Geol. Surv. Open-File Rep., 1989, this volume.
Weber, K., Metamorphism and crustal rheology-implications for the structural development of the continental crust during prograde metamorphism, in The nature of the lower continental crust, edited by J. B. Dawson, D. A. Carswell, J. Hall, and K. H. Wedepohl, Geol. Soc. London Spec. Pub. 24, 93-106, 1986.
White, J. C., and S. H. White, On the structure of grain boundaries in tectonics, Tectonophysics, 78, 613-628, 1981.
Wood B. J. and J. V. Walther, Fluid flow during metamorphism and its implication for fluid-rock ratios, in Fluid-rock interactions during metamorphism, edited by J. V. Walter and B. J. Wood, pp. 89-108, Springer-Verlag, New York, 1986.

EOCENE TRANSITION FROM OCEANIC TO ARC VOLCANISM, SOUTHWEST WASHINGTON

William M. Phillips and Timothy J. Walsh
Division of Geology and Earth Resources
Department of Natural Resources,
Olympia, Washington

Randy A. Hagen
Donald Herzog and Associates, Inc.
Santa Rosa, California

ABSTRACT

Southwest Washington contains an unusually complete section of Paleogene volcanic rocks relative to the remainder of the Pacific Northwest. Four distinct suites of volcanic rocks are recognized on the basis of major and trace element data, isotopic and biostratigraphic age, and inferred eruptive setting:

1. middle Eocene (48-50 Ma) oceanic tholeiitic basalt of the Washington coast ranges (Crescent Formation);
2. middle to upper Eocene (55-38 Ma), dominantly bimodal (basalt-rhyolite) volcanic rocks associated with nonmarine transtensional basin development;
3. tholeiitic basalts (volcanic rocks of Grays River) highly enriched in K- and Ti-group elements that were erupted in a middle to upper Eocene (44-38 Ma) marginal marine and deltaic forearc setting;
4. transitional tholeiitic to calcalkaline andesites and basaltic-andesites of the upper Eocene to Oligocene (42 to 25 Ma) Cascade arc.

Units with less certain affinities are also present in southwest Washington. These include the sills near the top of the Crescent Formation and basalt and tuffs at Fort Columbia. The sills are geochemically correlative with oceanic tholeiites of the Crescent and do not appear related to forearc volcanism. The Fort Columbia sequence contains high-K and Ti-group elemental concentrations similar to the forearc suite.

INTRODUCTION

Recent stratigraphic and tectonic syntheses of the Pacific Northwest [Armentrout, 1987; Heller et al., 1987; Wells et al., 1984; Ewing, 1980] describe a Paleogene volcanic history dominated by two complex events. First, from about 62 to 48 Ma, tholeiitic basalts of the Washington-Oregon coast ranges were erupted in a marginal oceanic setting and accreted by 50 to 48 Ma to North America. Second, beginning about 60 Ma and culminating at about 35 Ma, the focus of calcalkaline volcanism shifted from the diffuse Challis arc of central Idaho and adjacent northern Washington, British Columbia, Wyoming, and Montana into the Cascade arc of western Washington and Oregon.

The relationship between these two events is unclear and of great interest in terms of unraveling the Paleogene tectonic and stratigraphic history of the region. Economic concerns are also present as the Pacific Northwest Eocene section hosts much of the regions' mineral and fossil fuel resources. These include large gold deposits in central and northeast Washington, coal in western Washington, and natural gas in northwest Oregon.

In this report, we explore via major and trace element geochemistry the evolution from coast range volcanism and accretion to Cascade arc magmatism in a key area of the Pacific Northwest. Geologic mapping [compiled in Walsh et al., 1987] demonstrates that southwest Washington contains among the most complete records of Paleogene sedimentation and volcanism in the Pacific Northwest. Based upon reconnaissance sampling, we characterize geochemically the Paleogene volcanic units and suggest regional correlations using geochemistry, physical stratigraphy, biostratigraphy, and isotopic age data. One of our central goals is to correct a major miscorrelation between previously defined volcanic units in southwest Washington. Accordingly, we suggest criteria to classify Paleogene volcanic rocks into four major geochemical and petrologic groups. These empirical criteria should prove useful in applications such as subsurface correlations based upon geochemical analysis of well cuttings.

The geologic time scale used in this report is basically that used for the "Correlation of Stratigraphic Units of North America (COSUNA)" project of the American Association of Petroleum Geologists [Salvador, 1985]. We have added regional faunal zonations [Armentrout et al., 1983], and set the Eocene-Oligocene boundary at 35.7 Ma [Montanari et al., 1985] and within the Refugian benthic foraminiferal stage [Prothero and Armentrout, 1985]. All volcanic rock names follow International Union of Geological Sciences (IUGS) guidelines [Le Bas et al., 1986] and are designated using the total alkali-silica (TAS) diagram. Classification of alkaline vs. subalkaline is based upon the TAS diagram and IUGS guidelines. Tholeiitic vs. calcalkaline classification is based upon the FeO^*/MgO vs. SiO_2 diagram [Miyashiro, 1974; Gill, 1981].

REGIONAL PALEOGENE VOLCANIC UNITS

Paleogene volcanic units of the Pacific Northwest (Figure 1) are divisible into 5 groups on the basis of time, location, general geochemical characteristics, and inferred eruptive setting. Our southwest Washington study area contains four of the six groups. From west to east and oldest to youngest the groups are:

1) early to middle Eocene (62 to 48 Ma) oceanic tholeiitic basalt of the Washington-Oregon coast ranges;

2) calcalkaline to alkaline nonmarine units of the early to middle Eocene (55 to 48 Ma) Challis magmatic arc of northeast Washington and adjacent Idaho and British Columbia;

Figure 1. Index map showing Paleogene volcanic rocks of the Pacific Northwest; A. 62-48 Ma; B. 48-36 Ma; C. 36-25 Ma. Geology after Walsh et al. [1987], Wells et al. [1983], and Washington Public Power Supply System [1981]. Unit names and major references emphasizing geochemical, petrologic, and stratigraphic data are as follows:

1. Roseburg Formation; Baldwin [1974]
2. Siletz River Volcanics; Baldwin, 1964; Snavely et al. [1968]
3. Crescent Formation; southwest Washington, this report Wells [1981]; Black Hills, Globerman et al. [1982]; Olympic Peninsula, Tabor and Cady [1978], Glassley, [1974, 1976], Cady [1975], Lyttle and Clarke [1975, 1976], Muller et al. [1983]
4. Metchosin Igneous Complex; Massey [1986], Muller [1977, 1980], Muller et al. [1983]
5. Silver Pass Volcanic Member of the Swauk Formation; Tabor et al. [1984, 1982b], Ort et al. [1983]
6. O'Brien Creek Formation, Sanpoil Volcanics, Klondike Mountain Formation; Pearson and Obradovich [1977], Stoffel [In Press]
7. Springbrook, Marron, Marama, White Lake, and Skaha Formations; Church [1973]; Island Mountain Volcanics; White [1986]
8. Yachats Basalt; Snavely and MacLeod [1974]
9. Basalts of Cascade Head, Wells et al. [1983]
10. Tillamook Volcanics; Wells et al. [1983], Rarey [1986]; Mumford [1988]; Niem and Niem [1985]
11. Grays River volcanics; this report, Walsh [1987], Phillips [1987a], Wells [1981], Wells and Coe [1985]
12. Fisher and Colestin Formations; Peck et al. [1964]; Vokes et al. [1951]
13. Clarno Formation; Rogers and Ragland [1980], Noblett [1981], Rogers and Novitsky-Evans [1977]
14. Northcraft Formation; this report, Hagen [1987], Schasse [1987a], Snavely et al. [1958]
15. Basalt of Summit Creek; this report; Vance et al. [1987]
16. Naches Formation, Taneum Formation; Ort et al. [1983], Tabor et al. [1984, 1982b], Frizzell et al. [1984]
17. Tukwila Formation; Vine [1968]; Walsh [1984]
18. Teanaway Formation, Basalt of Frost Mountain; Ort et al. [1983], Tabor et al. [1984, 1982b]
19. Tuffs and volcanics within the Chumstick Formation; McClincy [1986], Margolis [1988]; Gresens [1983]
20. Mt. Persis volcanics; Tabor et al. [1982a]
21. Barlow Pass volcanics; Ort et al. [1983]; Vance [1957]
22. Rhyolite interbedded with Chuckanut Formation; Cruver [1981]; Whetten et al. [1986]
23. Hannegan and Skagit volcanics; Staatz et al. [1972]
24. Little Butte Volcanics; Lux [1981, 1982], Sherrod and Smith [In Press]
25. John Day Formation; Robinson [1975]
26. Goble Volcanics; this report, Phillips [1987a], Beck and Burr [1984], Wilkinson et al. [1946]
27. Ohanapecosh Formation and undivided Oligocene equivalents; Korosec [1987a,b], Schasse [1987b], Fiske et al. [1963]
28. Hatchet Mountain Formation; this report, Phillips [1987a], Roberts [1958]
29. Huckleberry Mountain volcanics; Frizzell et al. [1984]
30. Skamania Volcanics and undivided Oligocene equivalents; Phillips et al. [1987b]
31. Undivided Oligocene volcanic rocks of the Mount St. Helens area; Evarts et al. [1986]

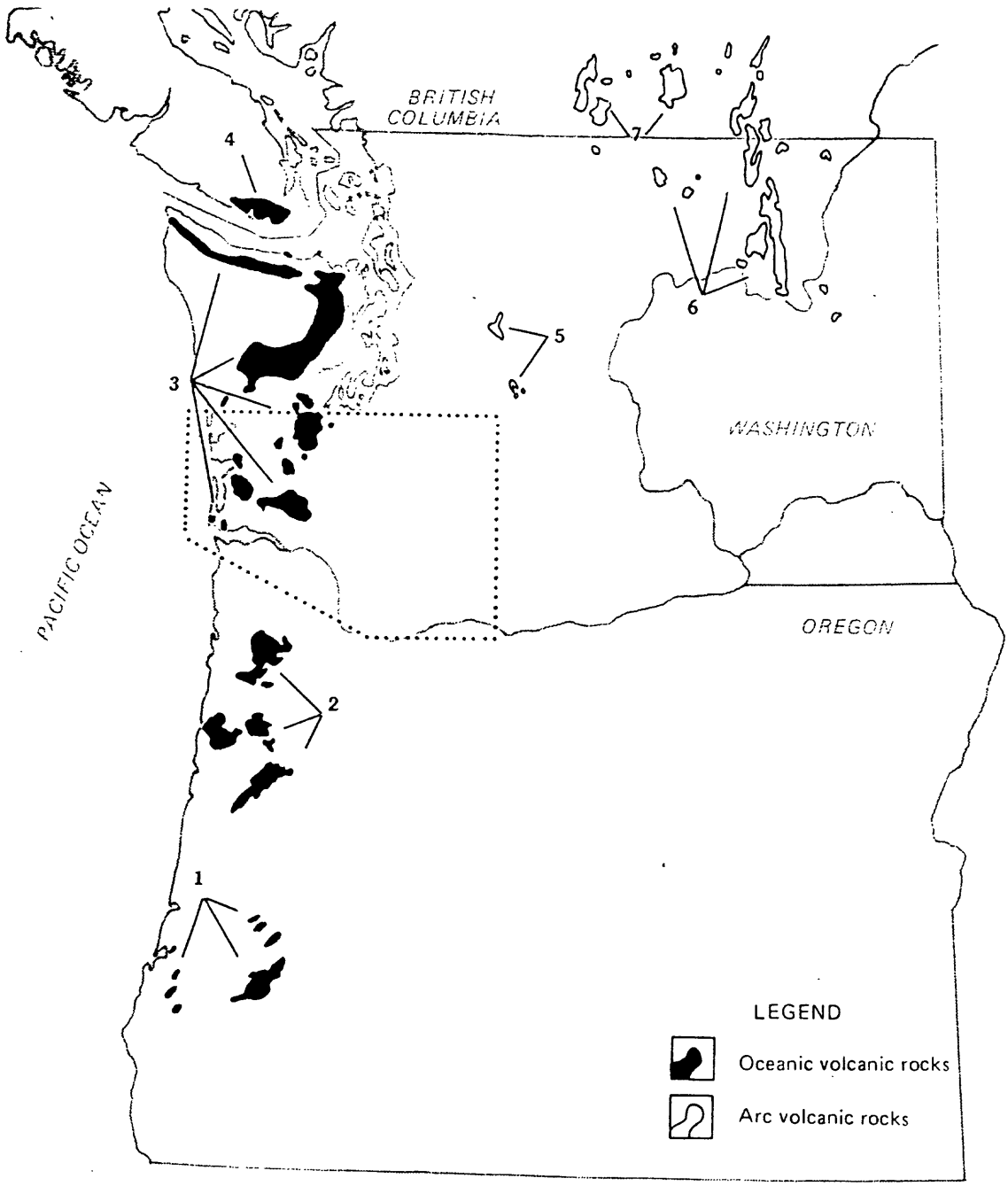

A. 62-48 Ma

Figure 1, continued

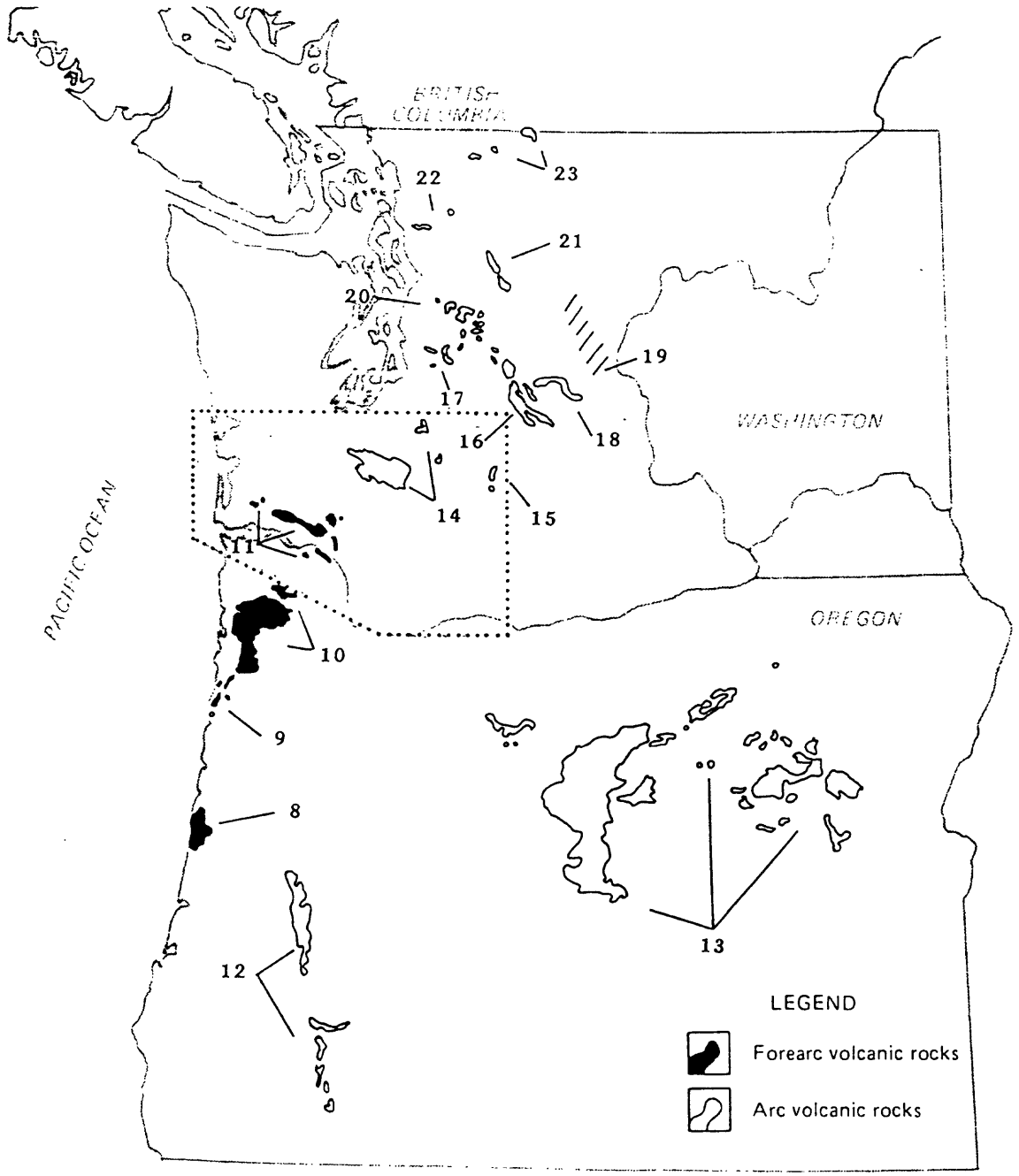

B. 48-36 Ma

Figure 1, continued

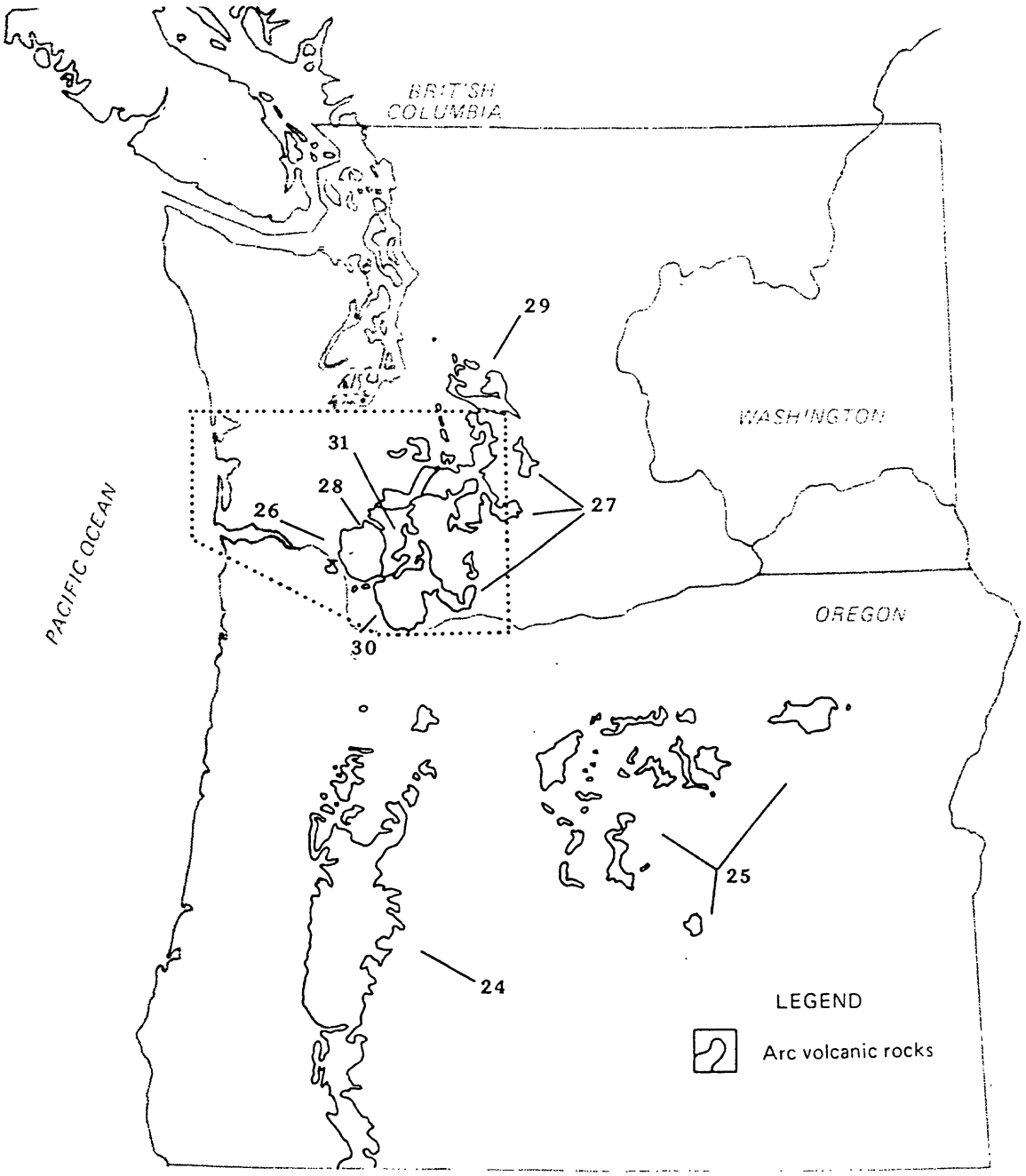

C. 36-25 Ma

Figure 1, continued

3) tholeiitic to alkaline lavas of the middle to upper Eocene (48-38 Ma) marine forearc of western Oregon and southwest Washington;

4) diverse, often bimodal (rhyolite-basalt) calcalkaline units of central and northern Washington; associated with middle to late Eocene (48-36 Ma) nonmarine transtensional basins and/or the west-migrating Challis magmatic arc;

5) transitional (tholeiitic to calcalkaline) andesites of the late Eocene Cascade to Oligocene (42-25 Ma) Cascade arc of western Washington and Oregon; also includes somewhat older transitional andesites of north-central Oregon;

The numerous stratigraphic terms applied to these volcanic rocks and associated sedimentary units are provided in Figure 1 together with major petrologic, geochemical, and geochronological references.

Coeval and probably correlative intrusive igneous rocks are present for many of groups but are not discussed here. In particular, extensive plutonic suites in northeast Washington and the North Cascades of Washington have been recognized to be closely associated with the Challis arc (group 2) and Cascade arc (group 5) units, respectively.

SOUTHWEST WASHINGTON REGIONAL GEOLOGIC SETTING

The Paleogene stratigraphic framework of southwest Washington consists of three unconformity-bounded sequences, labeled S_1, S_2, and S_3 in Figure 2 [Armentrout, 1987]. Sequence 1 consists of lower to middle Eocene oceanic coast range basalts and associated sedimentary rocks. A major regional unconformity (U_1 in Figure 2) separates the coast range sequence from middle to upper Eocene forearc strata of sequence 2. As discussed below, the unconformity may reflect accretion of a coast range seamount terrane to North America in the early middle Eocene (48-50 Ma). Potassic tholeiitic basalts are contained within the forearc sequence. Sequence 3 contains strata derived from or strongly influenced by development of the Cascade arc. The bounding unconformity, U_2 of Figure 2, is not present at or near basin depocenters [Armentrout, 1987].

The three unconformity-bounded sequences undergo many complex facies and structural transitions to the east. An east-west cross-section across southwest Washington (Figure 3) illustrates these transitions. The eastern portion of the study area contains basement of Cretaceous to Jurassic strata and coast range units are entirely absent. Time correlatives of sequence 1 and 2 units consist of nonmarine fluvial rocks deposited in transtensional basins. The contact between the Cretaceous-Jurassic units and Eocene coast range lithologies is not exposed. Two geometries appear reasonable for this suture: a vertical transcurrent boundary (Johnson [1984]) or a low-angle contact with coast range units under-thrust beneath the pre-Tertiary continental margin [Cowan and Potter et al., 1986]. Volcanic units of the Cascade arc (sequence 3) thicken to the east and dominate the geology of the eastern portion of the study area.

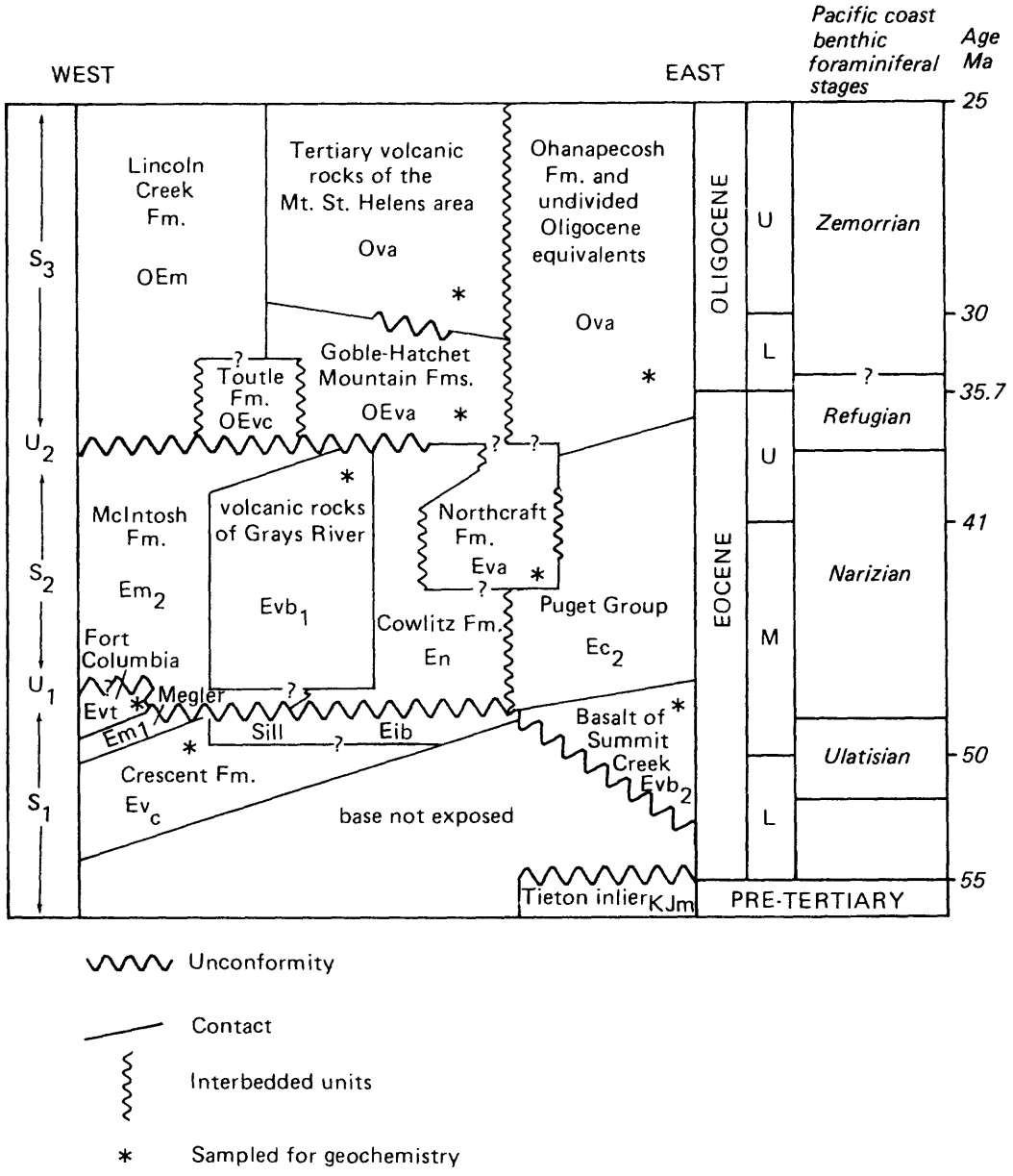

Figure 2. Stratigraphic relationships for the Paleogene of southwest Washington [after Walsh et al., 1987]. Symbols after the unit names are also used in the geologic cross-section of Figure 3.

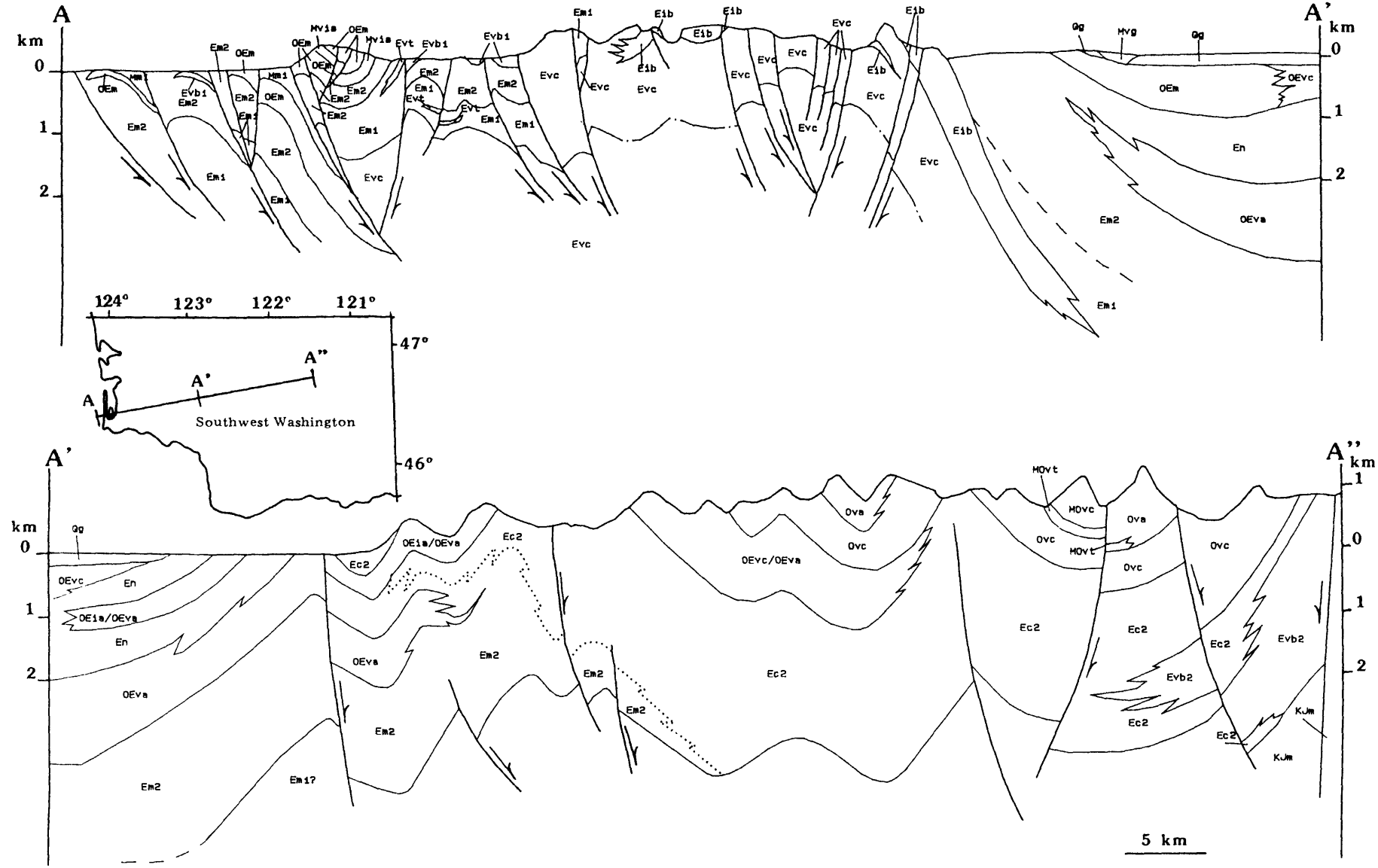

Figure 3. Geologic cross-section of southwest Washington (modified from an unpublished cross-section by W. S. Lingley and T. J. Walsh). Base map for the cross-section is Walsh et al. [1987].

Qg	Quaternary gravel
Mm_1	Lower to middle Miocene marine sedimentary rocks (Astoria Fm)
OEm	Upper Eocene through Oligocene marine sedimentary rocks (Lincoln Ck Fm)
Em_2	Middle and upper Eocene marine sedimentary rocks (McIntosh Fm and equivalents)
En	Middle and upper Eocene near shore and deltaic sediment (Skookumchuck and Cowlitz Fms)
EC_2	Middle and upper Eocene continental sediments (Puget Group and equivalents)
Em_1	Lower and middle Eocene (sandstone at Meglar and equivalents)
KJm	Jura-Cretaceous sediments (Russell Ranch Fm)
MVg	Miocene Grande Ronde Basalt
Mvis	Miocene Invasive Saddle Mountains Basalt (Pommona flow)
MOvt	Uppermost Oligocene to Miocene tuff
MOvc	Uppermost Oligocene to Miocene volcaniclastics
Ova	Oligocene andesite flows
Ovc	Oligocene volcaniclastics (Ohanapecosh Fm and equivalents)
OEvc	Upper Eocene to Oligocene volcaniclastics (Toutle Fm, Northcraft and equivalents)
OEva	Upper Eocene to Oligocene andesite flows (Northcraft Fm and equivalents)
OEia/OEva	Upper Eocene to Oligocene intrusive and extrusive andesites
Evb_1	Middle to upper Eocene basalt flows, (volcanic rocks of Grays River)
Evb_2	Middle to upper Eocene basalt flows, (basalt of Summit Creek)
Evt	Middle Eocene basalt lapilli breccia and flows at Fort Columbia
Evc	Lower and middle Eocene basalt flows and breccia (Crescent Fm)

Figure 3, continued.

Oceanic Tholeiitic Basalt of the Coast Range (62-48 Ma)

Extremely thick sequences of pillow basalts and breccias overlain by much thinner, regionally discontinuous, shallow-water to subaerial basalt flows characterize the basement of the Washington-Oregon coast ranges and the southern portion of Vancouver Island. Sedimentary rock interbedded with the volcanics yield foraminifera referred to the Ulatisian and Penutian stages (lower to middle Eocene). K-Ar and $^{40}Ar/^{39}Ar$ age estimates [Duncan, 1982] demonstrate that the basalts are youngest (circa 48 Ma) in southwest Washington and become progressively older both north and south, reaching a maximum of about 60-62 Ma in southwestern Oregon and Vancouver Island. On Vancouver Island [Massey, 1986] and near Bremerton, Washington [Clark, 1987], partial ophiolite sequences have been documented.

In southwest Washington, the coast range sequence is represented by the Crescent Formation. The Crescent is divided into two units [Wells, 1979; 1981]. Unit 1 is a pillow basalt complex with interbedded volcaniclastic sandstones and basaltic debris flows. Pillows are typically altered to brown-green or black chlorite and clay mixtures. Fresh samples of pillow basalts for geochemical analyses are difficult to obtain. Fracture fillings of zeolites and calcite are ubiquitous.

Overlying Unit 1 are massive to platy, dense to vesicular flows of Unit 2 which are interpreted to have been subaerially erupted. Lavas of unit 2 are interbedded locally with conglomerate of possible fluvial origin. Flows are both porphyritic (plagioclase-clinopyroxene-olivine-phyric) and aphyric.

The lower subaqueous and upper subaerial divisions of the southwest Washington Crescent are characteristic of the lower to middle Eocene Coast Range units. The correlative Siletz River Volcanics of Oregon [Snavely et al., 1968], the Olympic Peninsula Crescent [Tabor and Cady, 1978], and the Metchosin Volcanics of Vancouver Island [Muller, 1977] all possess similar lithofacies associations.

The pioneering work of Snavely et al. [1965, 1968] in the Siletz River Volcanics of the Oregon Coast Range (Figure 1a, map unit 2) has greatly influenced concepts of Coast Range chemical and physical stratigraphy. The Siletz River sequence is similar to some oceanic intraplate volcanic assemblages, such as those observed in the Hawaiian Islands, where tholeiitic units very similar to mid-ocean ridge basalts (MORB) are overlain by alkaline subaerial flows. Later workers exploring the petrologic and geochemical relationships of correlative rocks (Figure 1a, map units 3 and 4) in southwest Washington, on the Olympic Peninsula of northwestern Washington, and on Vancouver Island, describe similar physical stratigraphies. However, regional geochemical evidence for shallow-water to subaerial alkalic flows capping deep-water tholeiitic pillow-basalts is much less compelling. Truly alkalic, lower to middle Eocene Coast Range basalt sequences in the sense of IUGS nomenclature have not yet been documented outside of the Siletz River Volcanics of Oregon.

Geochemical data from the coast ranges indicate that

subalkaline, tholeiitic basalts dominate the sequence. These basalts are geochemically compatible with a mid-ocean ridge basalt (MORB) origin. As previously noted, the largely subaerial upper Siletz River Volcanics [Snavely et al., 1968] that contain alkalic basalt, trachybasalt, tephrite, and phonotephrite are very much the exception in the coast ranges. Glassley [1974, 1976] reported somewhat similar, but far less alkaline units in the eastern Olympic Peninsula, and believed them associated with dominantly subaerial flows. This correlation was disputed by other workers [Cady, 1975; Lyttle and Clarke, 1975, 1976], however.

Efforts to use minor and trace element geochemistry to identify the petrotectonic setting of Coast Range basalts have produced mixed results. Inferred eruptive settings range from island arc [Lyttle and Clarke, 1975, 1976], MORB [Glassley, 1974], oceanic-intraplate (seamount) [Cady, 1975; Glassley, 1976], and ridge-island (Icelandic) [Muller, 1980].

The base of the coast range sequence is not generally exposed and accurate estimates of the unit's thickness are difficult to obtain throughout the region. Where estimated, the sequence is extremely thick [9 to 16 km; Tabor and Cady, 1978; Muller, 1977; Massey, 1986]. In some instances unrecognized faulting may have repeated pillow basalt assemblages. However, the great thickness of the Coast Range units is also suggestive of seamount volcanism, whether in an intraplate setting or associated with a spreading ridge. Seamounts produce crust far thicker than average oceanic crust.

Tectonic models for the Coast Range volcanic sequence are summarized by Wells et al. [1984]. Most are mobilistic models requiring docking of an allochthonous coast range seamount terrane (termed the Crescent Terrane by Silberling and Jones [1984]) by about 50 to 48 Ma. Paleomagnetic data documenting large clockwise rotations for much of the coast ranges have tended to support accretionary tectonic hypotheses until recently when Wells and Heller [1988] demonstrated that a combination of dextral shear and Basin and Range extension could readily explain most of the rotation.

Because the Kula-Farallon spreading ridge traversed the latitude of the Pacific Northwest in the Paleogene [Lonsdale, 1988; Engebretson et al., 1985], spreading ridge-subduction zone or spreading ridge-transform interactions may have been fairly common. In order to explain the observed isotopic age pattern, Duncan [1982] proposed that the coast range sequence formed on a spreading ridge centered over a hot spot. The Yellowstone hotspot was invoked for the required mantle melting anomaly. Wells et al. [1984] and Lonsdale [1988] note difficulties with this model, specifically with hot-spot seamounts becoming older to the south on a northeast moving plate. Wells et al. [1984] proposed a revised hot-spot/ridge model in which complex ridge reorganizations and "leaky transforms" occurring near the subduction zone produce the Coast Ranges.

Alternatively, Snavely [1987] and Wells et al. [1984] propose rifting of the North American continental margin and extrusion of the Coast Range sequence in a marginal rift basin.

Convergence between oceanic plates and North America was most oblique between about 55 and 43 Ma [Lonsdale, 1988]. A tectonic setting conducive to northward transport of microplates, oblique continental margin rifting, and transtensional basin development in the continental interior may have been present at this time.

The feldspathic sandstone of Megler [Wells, 1979] and its equivalents, the lower McIntosh of Wagner [1967] and unit A of Wolfe and McKee [1968], unconformably overlie the Crescent Formation in southwest Washington, yet seem contained within unconformity-bounded sequence 1. Basalts and basaltic lapilli breccia at Fort Columbia [Wells, in press], that we have sampled geochemically, also appear correlative with the Megler section. These sediments contains a Ulatisian fauna [Rau in Armentrout, 1987] suggesting little hiatus from the Crescent section. The Megler is, in part, a facies E turbidite sandstone and siltstone [Mutti and Ricci-Lucchi, 1978] deposited in a fan fed by rivers originating in northern Washington or the Idaho batholith [Heller et al., 1985; Heller, 1983]. We interpret that the Megler and correlative Fort Columbia basalts were deposited over the topography of Crescent-age seamounts, resulting in the observed unconformity.

Sills at the top of the Crescent Formation

Thick gabbroic sills are present at the top of the Crescent Formation in southwest Washington. The sills consist of fine- to medium-grained, massive to columnar-jointed, uralitized plagioclase-pyroxene gabbro with a porphyritic, coarsely subophitic texture [Rau, 1986]. Age of the sills is uncertain as K-Ar results are equivocal [R. E. Wells, U. S. Geological Survey, oral communication, 1985]. However, in the northern portion of the study area, the sills cut the Narizian Humptulips Formation. Field relationships suggest that the sill emplacement was controlled by faults within the Crescent and that the sills exploited the regional unconformity (U_1 in Figure 2) between Ulatisian and Narizian strata [Rau, 1986].

Transtensional (?) Volcanic Rocks (55-38 Ma)

Central Washington is characterized by early to middle Eocene depocenters bounded by faults with strike-slip and dip-slip motions. Sedimentary facies within these basins implies development within a strike-slip setting. Examples include the early to middle Eocene Swauk Formation [Taylor et al., 1988], Chumstick Formation [Gresens, 1983], and the Naches Formation [Tabor et al., 1984]. Associated volcanic rocks are calcalkaline and locally bimodal [Ort et al., 1983]. The basins and associated volcanism may represent westward stepping of Challis arc magmatism from northeast Washington into central Washington and Oregon (Armstrong, 1978; Vance, 1977, 1979; Ewing, 1980; Wells et al., 1984). Alternatively, widespread extension of the continental margin due to right-lateral motion between North American and oceanic plates may have generated extensional volcanism in both marginal oceanic basins [Snavely, 1987; Wells et al., 1984] and

within the continental margin.

In this report, we provide geochemical data from the basalt of Summit Creek [Vance et al., 1987]. The Summit Creek unit consists of about 2000 m of dense, sparsely phyric subaerial basalt flows with lesser hornblende andesite [Ellingson, 1959], silicic tuff, argillite, and feldspathic and volcaniclastic sandstone. Fission track and U-Pb data suggest an age of from 55 to 45 Ma [Vance et al., 1987]. The basalt of Summit Creek conformably underlies feldspathic sandstone correlative to the Puget Group. Conformably above the Puget Group are volcanic rocks of the early Cascade arc assigned to the Ohanapecosh Formation. Silicic ash flows are contained with both the Puget Group and the basal Ohanapecosh. The association of basalt and high-silica volcanics, together with hydrous mineral phases (hornblende) contrasts sharply with Oligocene Cascade arc units.

Forearc Volcanic Rocks (48-38 Ma)

Unconformably overlying the Crescent Formation are middle to late Eocene marginal marine and nonmarine deltaic sedimentary rocks assigned to the McIntosh, Cowlitz, and Skookumchuck formations, and to the Puget Group. Mafic volcanic rocks interbedded with the Cowlitz are assigned to the informally named volcanic rocks of Grays River, which we have sampled extensively for geochemistry.

The Cowlitz-McIntosh-Skookumchuck sedimentary sequence consists of marine to estuarine feldspathic and lithic sandstones, tuffaceous siltstones, coal deposits, and interbedded basaltic tuff. These units are gradational eastward with the nonmarine deposits of the Puget Group (Figure 3). The four units form a major deltaic lithofacies association of a major river system or systems [Buckovic, 1979]. The dominant lithologies of feldspathic sandstones reflect distant eastern source terranes, possibly in present-day northeast Washington or central Idaho [Heller et al., 1987]. Foraminifera contained within the Cowlitz-McIntosh-Skookumchuck sequence are assigned to the Narizian Stage [Rau, 1981; Wells, 1981].

Basin geometries were probably inherited from the accreted Crescent terrane [Heller et al., 1987]. In southwest Washington, three major depocenters are recognized, Centralia, Grays Harbor, and Astoria. The Centralia basin represents deltaic and estuarine to bathyal deposition in a tidally dominated marginal basin restricted to the west by topographically high blocks of Crescent and Grays River volcanic rocks. The Narizian section in the Astoria and Grays Harbor Basins is dominated by siltstone and mudstone, although locally derived basaltic conglomerate and sandstone are present in the Astoria Basin (Niem and Niem, 1985).

Each of the basins contains over 3 km of middle to upper Eocene forearc deposits. Rapid depositional rates characterize many of the middle to late Eocene forearc basins of western Washington and Oregon [Heller et al., 1987; Turner et al., 1983]. Strike-slip faulting is an important ingredient in the coeval basin formation of central Washington [Taylor et al., 1988; Tabor et al., 1984] and may have influenced the more westerly forearc

[e.g. Johnson, 1984].

Interbedded with the forearc sedimentary rocks are two distinctly different assemblages of volcanic rocks. On the east side of the study area, the type-Northcraft Formation [Snavely et al., 1958] is sandwiched between the McIntosh and Skookumchuck formations. These rocks, which have Cascade arc affinities, are discussed below.

The volcanic rocks of Grays River [Phillips, 1987a, 1987c; Walsh, 1987] lie between the Cowlitz Formation and the upper Narizian siltstone beds of Skamokawa Creek [Wells, 1981]. These basalt lava flows and mafic tuffs were referred to the Goble Volcanics by Livingston [1966] following the work of Henriksen [1956]; however, they are not correlative with that unit [Phillips and Kaler, 1985; Phillips, 1987a]. Later workers [Wells, 1981; Wells and Coe, 1985; Wells and Heller, 1988] have continued with this usage or referred to the "western Goble Volcanics of Livingston [1966]". Not shown in Figure 2 are minor accumulations of mafic pyroclastic rocks and basalt flows associated with the McIntosh Formation [Pe Ell volcanic member of the Cowlitz Formation of Henriksen, 1956] that we have sampled for geochemistry.

The volcanic rocks of Grays River consist of augite-plagioclase phyric basalt flows with lesser mafic tuff and lithic sandstone. The sequence was erupted in a southwest-deepening marginal marine setting. On the east, subaerial lava flows are interbedded with arkose and coal of the Cowlitz Formation. To the west, pillow basalt and aquagene tuffs become more common, and the unit is sandwiched between deep-water marine facies of the McIntosh Formation and the siltstone of Skamokawa Creek [Wells, 1981; Wolfe and McKee, 1972]. Most Grays River lava flows contain sparse medium-grained olivine, clinopyroxene, and plagioclase phenocrysts, or are aphyric. Green, vitreous augite phenocrysts are often abundant in Grays River lavas and volcaniclastic rocks.

Earliest (42-38 Ma) Cascade Arc Volcanic Rocks

The middle to upper Eocene forearc sequence described above also contains volcanic rocks with continental magmatic arc affinities. In southwest Washington, these subaerial flows of pyroxene basaltic andesites and andesites are assigned to the Northcraft Formation. Though the Northcraft is at least partially time-correlative with the transtensional basin volcanic rocks of central Washington, the unit lacks the bimodal character and hydrous mineral phases of those rocks. Geochemical data presented below indicates that the Northcraft is extremely similar to younger upper Eocene and Oligocene flow-dominated sequences of the Cascade arc. Together with the Clarno Formation of Oregon (Figure 1, map unit 13), the Northcraft represents volcanic arc distinct from the diffuse transtensional or Challis arc activity of the preceding 10 Ma. While stratigraphic and petrologic relationships for most volcanic units of this time are poorly known, Hagen [1987] has recently mapped much of the Northcraft in detail.

The type-Northcraft [Snavely et al., 1958] is sandwiched between the marine McIntosh Formation and the coal-bearing, near-

shore marine to fluvial Skookumchuck Formation. The 200-300 m type-section thins to the west and north; to the east, the Northcraft is as much as 4300 m thick [Hagen, 1987]. Stratigraphic relationships to the east and south are unclear because of interfingering of the unit with very similar flows of the Goble Volcanics-Hatchet Mountain Formation and unnamed Oligocene volcanic rocks [Schasse, 1987a; Phillips, 1987a; Hagen, 1987].

Beginning about 42-40 Ma [Hagen, 1987], basaltic andesites of the Northcraft were erupted through deposits of the Puget deltaic system and soon developed subaerial shield volcanoes. Constructional volcanic topography diverted Puget deltaic deposits away from volcanic centers. Occasionally, fluvial sedimentation outpaced volcanism and complex interbedding of andesites and feldspathic sedimentary rocks occurred. Volcanic centers appear to be most numerous in the eastern portion of the Northcraft outcrop area. Here, deposits of the Skookumchuck Formation or correlative Puget Group are absent, and Northcraft flows are in contact with somewhat younger Oligocene or latest Eocene units.

The first volcanic rocks erupted were augite-olivine basalt and basaltic andesite. Vent structures consisting of breccia pipes have been mapped by Hagen [1987] for these lavas. These products were gas-poor and produced little tephra. Basic dikes and sills were also emplaced into shallow levels of the shield volcanoes.

Later products of the Northcraft shield structures include slightly more differentiated, augite-hypersthene andesite dikes, associated breccia pipes, and lava flows. Volcaniclastic detritus possibly representing laharic activity is also present in minor quantities. Locally, unusual hornblende-phyric andesite dikes are present. These dikes appear to be late-stage features of Northcraft volcanism closely associated with intrusive centers [Hagen, 1987].

Volcanic Rocks of the Cascade Arc (36-25 Ma)

Volcanic and volcaniclastic sedimentary rocks of the Goble Volcanics, Hatchet Mountain Formation, Toutle Formation, and Lincoln Creek Formation overlie the forearc sequence with variable contact relationships. These units are products of the latest Eocene to Oligocene Cascade arc. At depocenters within basins, the Cascade and forearc sequences are often interbedded (see for example, Wilkinson et al., 1946]; at basin margins or over intrabasinal highs, unconformities are the rule. [Armentrout, 1987].

In stark contrast to underlying strata, sedimentary units of the Cascade sequence completely lack feldspathic sandstones of extrabasinal origin. The Toutle Formation [Roberts, 1958; May, 1980] consists of fluvial, lacustrine, and shallow-water marine volcaniclastic deposits and a few interbedded lava flows. The unit is the largely nonmarine equivalent of the marine basaltic sandstone member of the Lincoln Creek Formation. The Lincoln Creek consists of tuffaceous siltstone and sandstone deposited in a marine forearc setting. Molluscan and foraminiferal faunas both

indicate an age range from latest Eocene (Refugian Foraminiferal Stage) to latest Oligocene [Armentrout, 1987].

Arc rocks of the Goble Volcanics [Wilkinson et al., 1946] and the equivalent Hatchet Mountain Formation [Roberts, 1958] are probable sources for many of the volcaniclastic deposits within the Toutle and Lincoln Creek formations. Published K-Ar ages on these rocks range from about 45 to 33 Ma [Beck and Burr, 1979; Armentrout et al., 1980]; however, acid-treated whole rock and plagioclase dates of about 37 to 34 Ma [Phillips et al., 1986] are compatible with biostratigraphic data.

The Goble-Hatchet Mountain units are divisible into two regionally extensive, informally designated members [Phillips, 1987a; Walsh et al., 1987]. The base of the section is marked by 50 to 180 m of light-colored (andesitic?) pyroclastic and volcaniclastic sedimentary rocks that are intercalated with micaceous feldspathic sandstones of the Cowlitz Formation. This member is probably partly equivalent to the Toutle Formation.

Most of the Goble-Hatchet Mountain unit consists of porphyritic pyroxene basaltic-andesite and andesite lava flows. Most flows are thin (1-4 m) and lenticular; top and bottom contacts are typically wavy, with thin (5-50 cm) reddish siltstone or sandstone layers separating cooling units. Zeolite minerals characteristically fill vugs and fractures in flows. Flows are usually plagioclase-augite phyric with a trachytic groundmass. Augite-hypersthene andesite is also present, together with lesser olivine basalt and pyroxene dacite. The unit is about 1500 m thick in the type section [Wilkinson et al., 1946].

Overlying the Goble Volcanics are several km of Oligocene to lower Miocene unnamed volcanic rocks that are well-exposed in the blast and blow-down regions of the May, 1980 Mount St. Helens eruptions. While pyroxene basaltic-andesite and andesite flows and hypabyssal dikes and sills are the most common lithology, this section also contains a much greater concentration of pyroxene dacite and andesitic pyroclastic rocks [Evarts et al., 1987].

As much as 3 km of well-bedded, dominantly pyroclastic and volcaniclastic strata of the Ohanapecosh Formation and unnamed correlatives make up the Southern Washington Cascades [Vance et al., 1987]. Flow units are relatively rare in the Ohanapecosh; where present, they consist of altered pyroxene basaltic-andesite and andesite. Unlike most Oligocene Cascade rocks, rhyolites are present in minor quantities within the Ohanapecosh. The correlative John Day Formation of Oregon (Figure 1C, map unit 25) contains a similar abundance of pyroclastic units. Together the two units may represent deposition in an Oligocene back-arc system.

GEOCHEMICAL DATA

All the analyses reported here are by x-ray fluorescence (XRF) and were performed at Washington State University. Analyses consist of 10 major and minor oxides and a suite of 9 to 13 alkaline earth and transition trace elements. Volatiles were not determined and the analyses are normalized to 100 weight percent. Iron (FeO*) was determined as total iron expressed as FeO. Where Fe_2O_3 and FeO ratios are required to calculate CIPW norms, we used

TABLE 1. Statistical summary of geochemical data for Eocene and Oligocene volcanic rocks. Numbers in parentheses indicate number of analyses used in calculating statistics

	Crescent Formation (16/14)				Sill at top of the Crescent Formation (6/3)				Grays River volcanics (44/20)				Northcraft Formation (32/22)			
ELEMENT	MEAN	S.D.	MIN	MAX	MEAN	S.D.	MIN	MAX	MEAN	S.D.	MIN	MAX	MEAN	S.D.	MIN	MAX
SiO_2 %	49.16	1.02	47.74	52.10	49.42	0.38	49.19	50.26	50.62	1.59	47.78	55.69	56.67	3.45	51.19	66.47
Al_2O_3 %	14.65	0.78	13.22	16.46	15.49	1.02	14.34	16.80	14.95	0.81	13.29	17.54	17.74	1.15	15.45	19.63
TiO_2 %	2.60	0.28	2.12	3.18	2.05	0.17	1.81	2.23	3.24	0.35	2.22	3.89	1.21	0.26	0.77	1.84
FeO* %	12.29	0.96	10.28	13.95	11.56	0.66	10.26	12.15	12.34	0.79	10.42	14.15	8.05	1.06	4.58	10.26
MnO %	0.22	0.04	0.17	0.33	0.20	0.03	0.14	0.23	0.21	0.04	0.15	0.34	0.14	0.03	0.06	0.22
CaO %	11.16	1.07	8.75	12.67	11.77	0.80	10.46	12.95	9.60	1.06	6.35	11.43	8.02	1.74	2.74	10.68
MgO %	6.34	0.86	3.84	7.52	6.35	0.79	5.50	7.76	4.80	0.95	3.19	7.14	3.86	1.23	0.74	7.97
K_2O %	0.31	0.24	-0.11	0.83	0.24	0.09	0.12	0.38	0.79	0.31	0.19	1.62	0.68	0.41	0.12	1.65
Na_2O %	2.95	0.87	1.99	5.28	2.70	0.30	2.34	3.21	2.90	0.38	2.31	4.17	3.38	0.41	2.84	5.11
P_2O_5 %	0.32	0.13	0.20	0.77	0.22	0.02	0.18	0.24	0.55	0.14	0.27	0.93	0.25	0.06	0.14	0.35
Ni ppm	55	22	3	107	48	10	40	62	40	40	0	167	39	30	0	160
Cr ppm	129	77	11	279	156	29	127	196	70	82	2	375	48	55	0	271
Sc ppm	37	5	26	44	42	3	39	46	28	3	21	33	23	4	15	29
V ppm	343	55	163	400	377	8	365	383	295	46	194	367	180	45	117	305
Ba ppm	92	68	20	276	35	7	29	45	238	63	151	389	205	88	96	418
Rb ppm	5	3	1	11	4	2	1	6	16	7	4	30	13	13	0	58
Sr ppm	285	102	180	606	212	20	190	238	469	45	397	545	455	106	345	886
Zr ppm	183	42	135	301	140	4	135	145	254	45	184	359	158	38	101	225
Y ppm	34	7	25	47	31	1	30	32	37	5	29	49	19	4	14	29
Nb ppm	25.6	13.0	11.0	57.8	13.9	1.6	11.8	15.6	46.7	12.9	33.0	77.0	15.5	0.5	15.0	16.0
Ga ppm	21	2	18	23	21	1	19	22	24	2	20	28	23	1	22	23
Cu ppm	154	76	22	254	208	25	178	239	59	31	16	121	138	75	63	213
Zn ppm	112	15	89	137	103	1	102	104	128	13	109	168	105	8	97	113
$K_2O_{57.5}$	0.36	0.27	-0.13	0.92	0.28	0.11	0.14	0.44	0.89	0.33	0.22	1.77	0.67	0.38	0.13	1.63
$F/M_{57.5}$	2.31	0.35	1.73	2.95	2.14	0.20	1.82	2.41	3.02	0.50	2.11	4.04	2.32	0.71	1.21	5.35

S.D. One standard deviation
FeO* Total iron expressed as FeO
$K_2O_{57.5}$ K_2O % at 57.5 % SiO_2
$F/M_{57.5}$ FeO*/MgO at 57.5 % SiO_2

TABLE 1, continued

	Basalt of Summit Creek (6/2)				Goble-Hatchet Mountain (58/3)				Oligocene volcanic rocks, undivided (30/0)			
ELEMENT	MEAN	S.D.	MIN	MAX	MEAN	S.D.	MIN	MAX	MEAN	S.D.	MIN	MAX
SiO_2 %	53.65	6.72	47.27	66.01	56.55	3.26	49.78	66.27	57.44	3.52	50.00	64.65
Al_2O_3 %	16.35	0.53	15.69	16.97	17.00	1.12	13.86	20.82	16.72	0.70	15.35	18.27
TiO_2 %	1.49	0.64	0.57	2.48	1.44	0.35	0.79	2.19	1.32	0.24	0.77	1.92
FeO* %	9.83	3.32	4.10	14.18	8.61	1.50	3.71	12.45	8.88	1.47	5.86	13.10
MnO %	0.18	0.05	0.07	0.23	0.15	0.03	0.07	0.22	0.15	0.03	0.09	0.21
CaO %	8.95	2.82	4.11	12.66	7.98	1.58	4.50	12.19	7.59	1.60	4.31	10.50
MgO %	5.52	1.99	1.88	7.86	3.94	1.28	1.08	8.33	3.88	1.38	1.29	7.70
K_2O %	0.33	0.62	0.00	1.71	0.86	0.49	0.14	2.65	0.89	0.54	0.24	2.27
Na_2O %	3.50	0.66	2.69	4.56	3.18	0.37	2.53	4.43	2.90	0.26	2.44	3.45
P_2O_5 %	0.19	0.07	0.10	0.30	0.29	0.09	0.15	0.52	0.22	0.05	0.11	0.32
Ni ppm	62	10	52	72	68	29	43	109	n.d.	n.d.	n.d.	n.d.
Cr ppm	171	102	69	273	117	45	62	173	n.d.	n.d.	n.d.	n.d.
Sc ppm	37	3	34	39	27	3	23	30	n.d.	n.d.	n.d.	n.d.
V ppm	305	3	302	307	179	44	117	218	n.d.	n.d.	n.d.	n.d.
Ba ppm	97	30	67	127	160	89	94	286	n.d.	n.d.	n.d.	n.d.
Rb ppm	2	0	2	2	15	12	3	32	n.d.	n.d.	n.d.	n.d.
Sr ppm	301	122	179	423	391	10	379	403	n.d.	n.d.	n.d.	n.d.
Zr ppm	126	26	100	151	135	52	88	207	n.d.	n.d.	n.d.	n.d.
Y ppm	33	6	27	39	20	3	17	25	n.d.	n.d.	n.d.	n.d.
Nb ppm	12	4	8	15	9	3	5	13	n.d.	n.d.	n.d.	n.d.
Ga ppm	21	2	19	23	18	2	16	20	n.d.	n.d.	n.d.	n.d.
Cu ppm	130	34	96	163	251	105	135	389	n.d.	n.d.	n.d.	n.d.
Zn ppm	100	21	79	121	165	51	108	231	n.d.	n.d.	n.d.	n.d.
$K_2O_{57.5}$	0.30	0.54	0.00	1.49	0.86	0.43	0.15	2.30	0.87	0.47	0.25	2.02
$F/M_{57.5}$	2.02	0.51	1.46	3.05	2.39	0.62	1.23	3.87	2.51	0.75	1.34	5.06

S.D. One standard deviation
FeO* Total iron expressed as FeO
$K_2O_{57.5}$ K_2O % at 57.5 % SiO_2
$F/M_{57.5}$ FeO*/MgO at 57.5 % SiO_2

the method of Irvine and Baragar [1971] to set the Fe_2O_3/FeO partition. The Appendix to this report contains major and minor oxide values and sample locations (Table A1), trace element data (Table A2), and estimates of analytical and instrumental precision for the XRF analyses (Table A3). The geochemical data are summarized in Table 1.

Crescent Formation

The Crescent Formation was sampled in a traverse across the Willapa Hills of southwest Washington. Beginning near the town of Pe Ell and continuing south to the mouth of the Columbia at Fort Columbia, 11 samples in Unit 1 of the Crescent, 1 sample from Unit 2, and 3 samples of sills near the top of the Crescent were collected and analyzed.

All analyses are tholeiitic on the FeO*/MgO vs. SiO_2 diagram [Figure 4]. On the Alkali (Na_2O+K_2O) vs. FeO* vs. MgO (AFM) diagram (not shown), two samples with anomalously high Na_2O values from southernmost Crescent exposures at Fort Canby and in the Chinook 7.5' quad fall within the calcalkaline field. On the TAS diagram (Figure 5), all but these samples cluster tightly in the subalkaline basalt field. All samples are quartz-normative or olivine-normative; no alkalic basalt (nepheline-normative) was analyzed.

Comparison with other Coast Range analyses indicates that the southwest Washington samples from pillows of Unit 1 are similar to the lower Siletz River Volcanics [Snavely et al., 1968] and the lower Crescent of the Olympic Peninsula (Glassley, 1974; Lyttle and Clarke, 1975]. The sole sample from subaerial Unit 2 is not distinctive save for slightly higher total alkalies. Figure 6 is a Harker-type variation diagram that summarizes major and minor oxide values for the southwest Washington Crescent Formation.

Rock/MORB diagrams [Pearce, 1982] permit rapid visual appraisal of trace element patterns. The "average" MORB values of Pearce [1982] are supplemented by those of Engel et al. [1965]. The Rock/MORB plot for the southwest Washington Crescent Formation (Figure 7] demonstrates that K-group elements (K_2O, Rb, Ba, Sr) possess substantial within group variation but overall are enriched 2 to 5 times MORB. These elements are probably mobile during alteration or zeolite facies metamorphism. Ti-group elements (TiO_2, Zr, Nb) are incompatible (concentrated in the melt fraction) until crystallization of magnetite and often are relatively immobile during alteration. All of these elements are enriched relative to MORB, especially Nb. Variation between samples is quite small. The compatible elements (Ni, Cr, Sc, V) are preferentially incorporated into ferromagnesian phases compared to coexisting melt. Ni and Cr are strongly depleted relative to MORB, perhaps as result of olivine or clinopyroxene fractionation mechanisms. Sc and V contents are MORB-like. Cu values are quite "noisy" but overall are elevated relative to MORB. Native copper is present in trace amounts in drill core from the Black Hills Crescent and the Metchosin Volcanics of southern Vancouver Island host copper deposits [Muller, 1977]. Y

Grays River volcanics

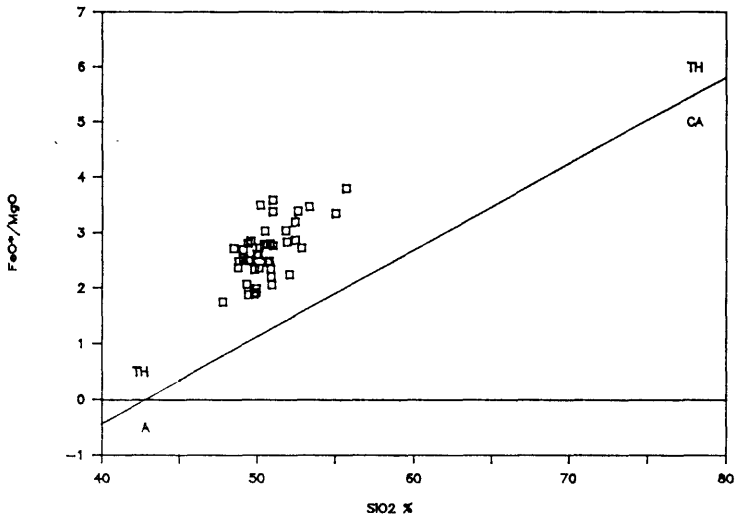

Crescent Formation

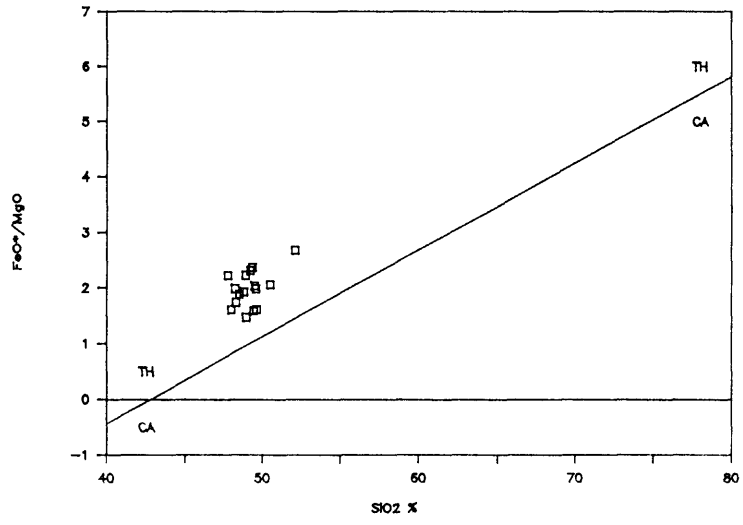

Northcraft Formation

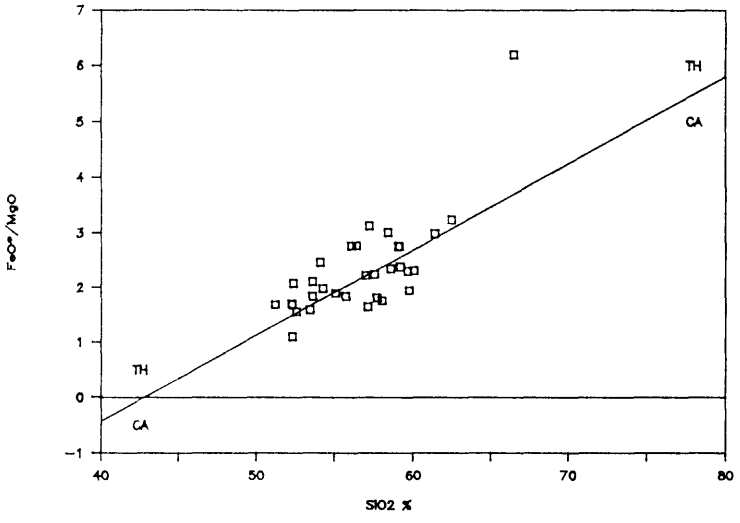

Sill at top of the Crescent Formation

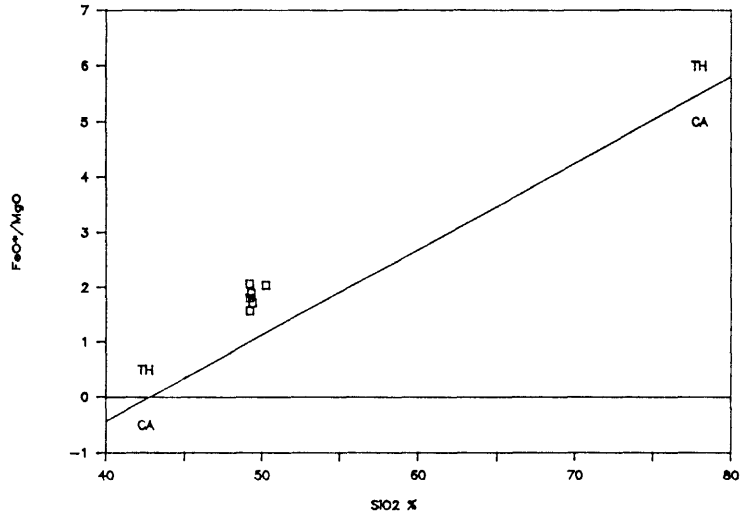

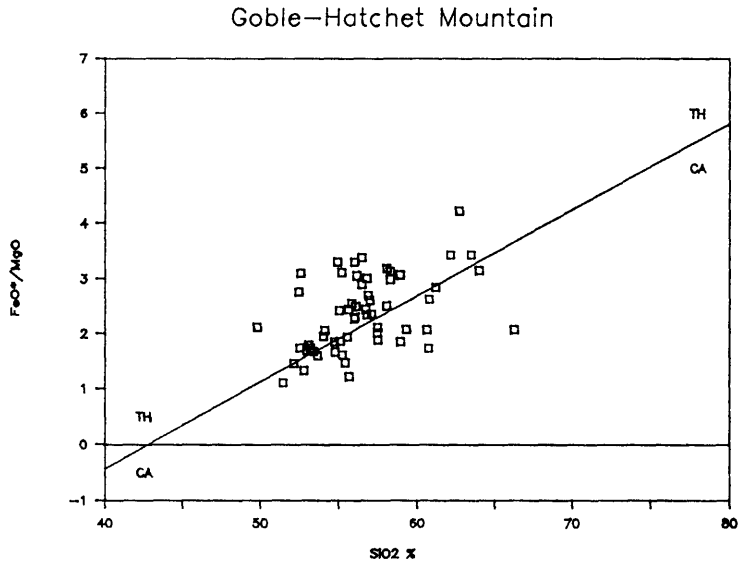

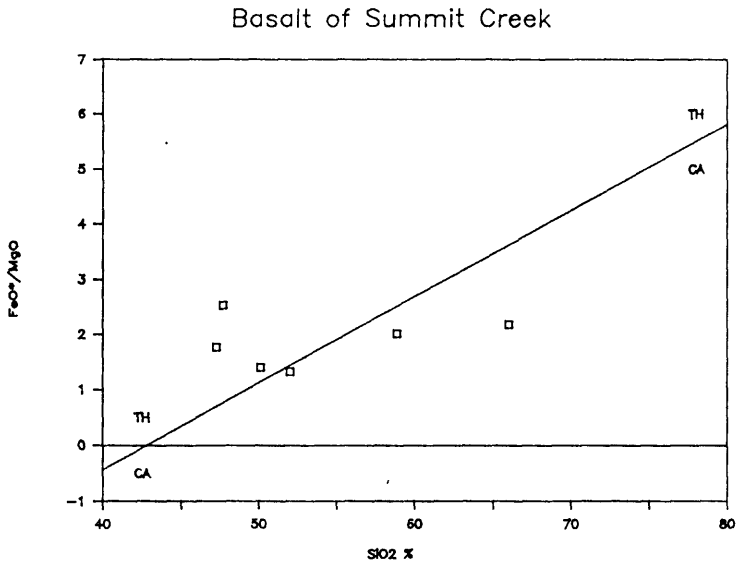

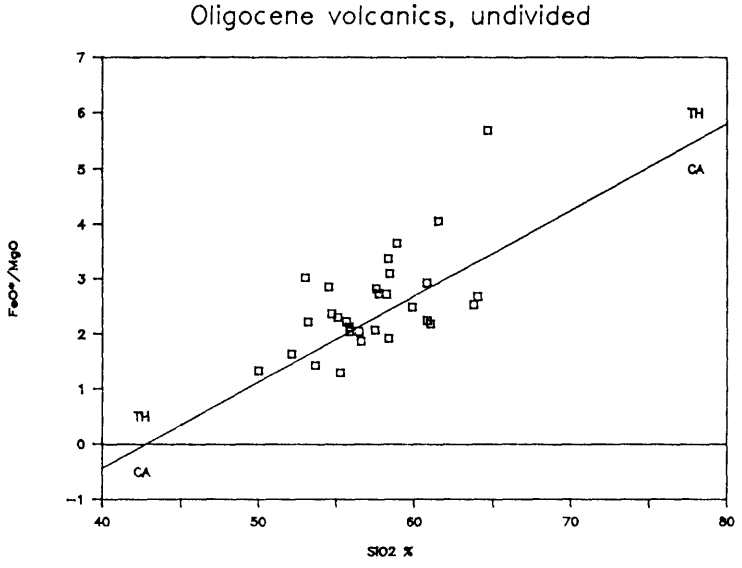

Figure 4. FeO*/MgO vs. SiO2 diagrams for Paleogene volcanic rocks of southwest Washington. Fields after Miyashiro [1974]; TH = tholeiitic; CA = calcalkalic.

Grays River volcanics

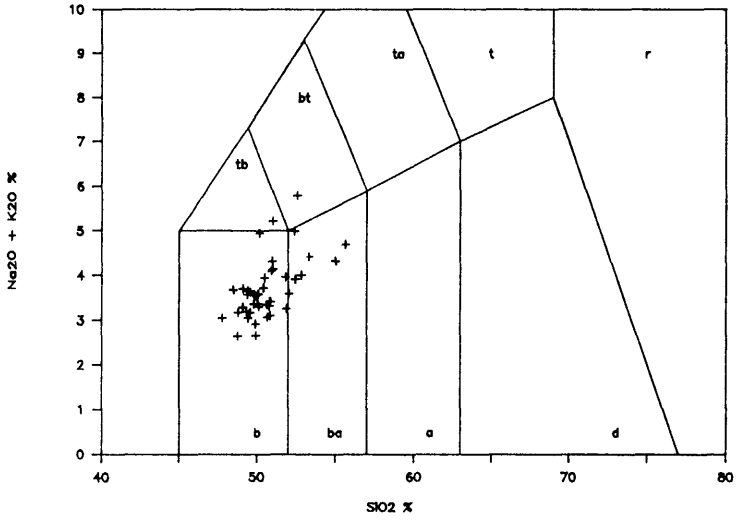

Crescent Formation

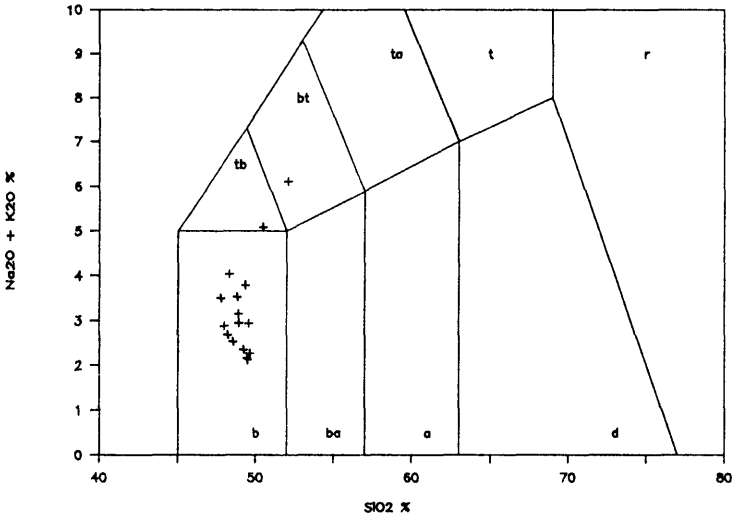

Northcraft Formation

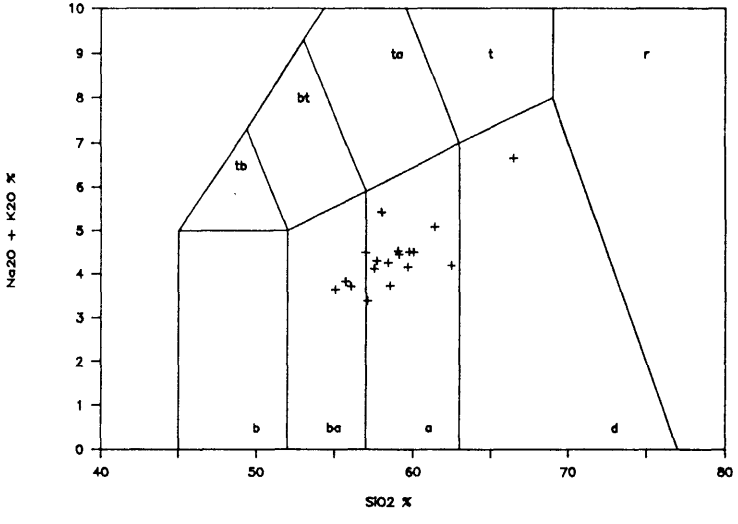

Sill at top of the Crescent Formation

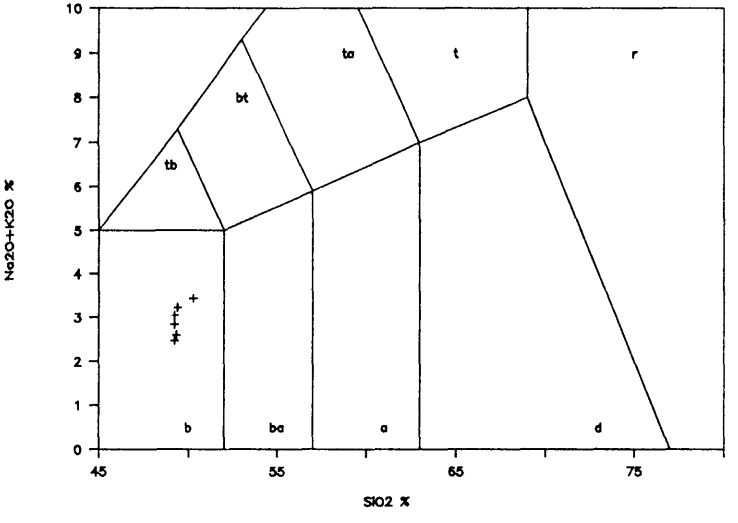

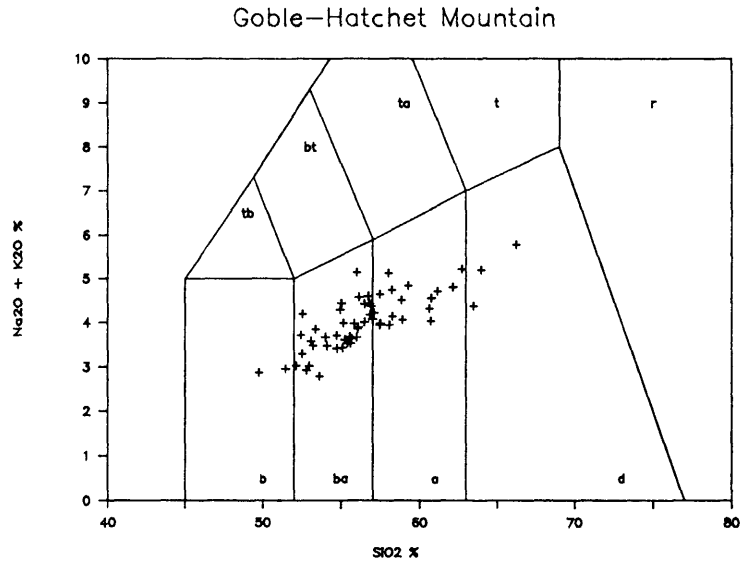

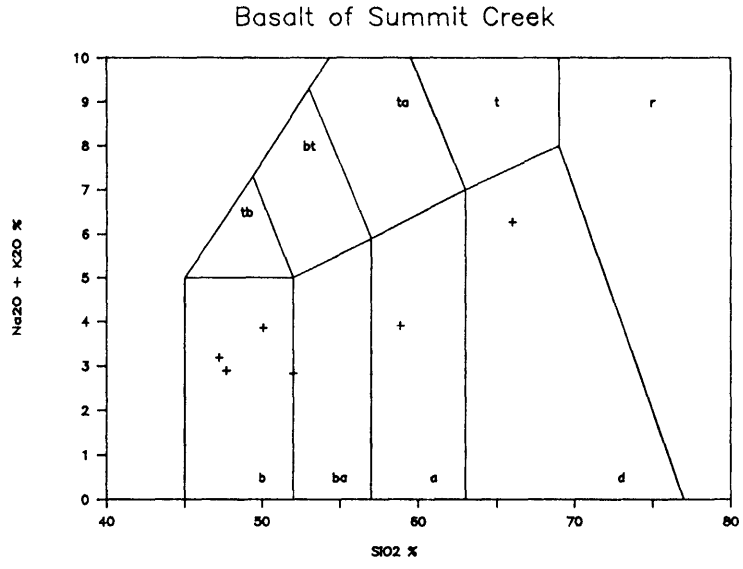

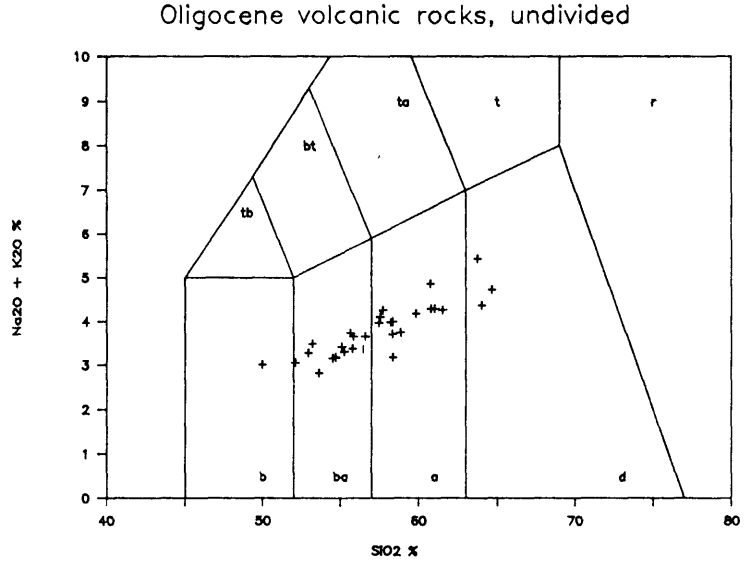

Figure 5. Total alkali vs. SiO2 (TAS) diagrams for Paleogene volcanic rocks of southwest Washington. Fields after Le Bas et al. [1986]; b = basalt; ba = basaltic-andesite; a = andesite; d = dacite; r = rhyolite; tb = trachybasalt; bt = basaltic-trachyandesite; ta = trachyandesite; t = trachyte.

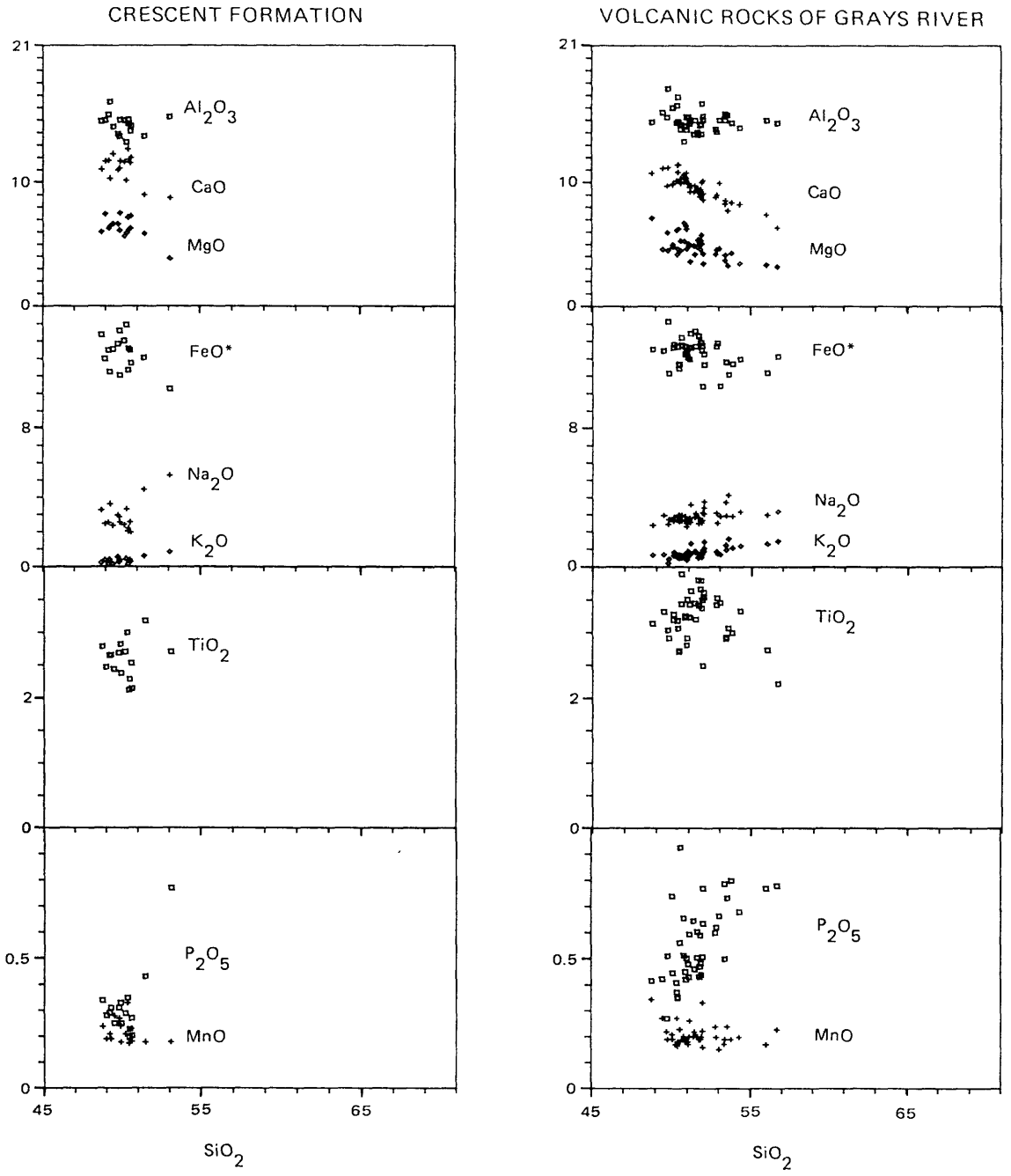

Figure 6. Harker variation diagrams for Paleogene volcanic rocks of southwest Washington.

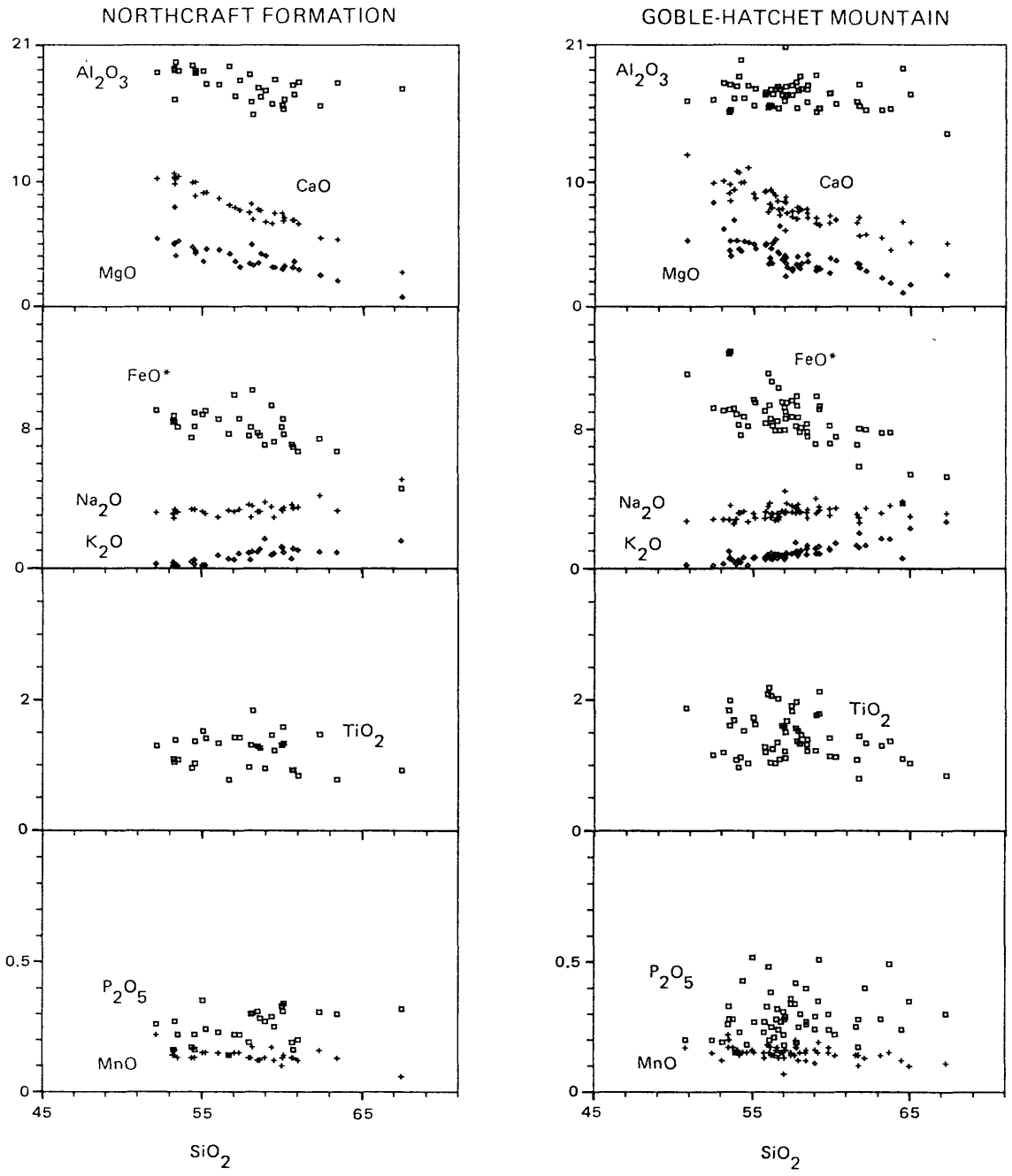

Figure 6, continued

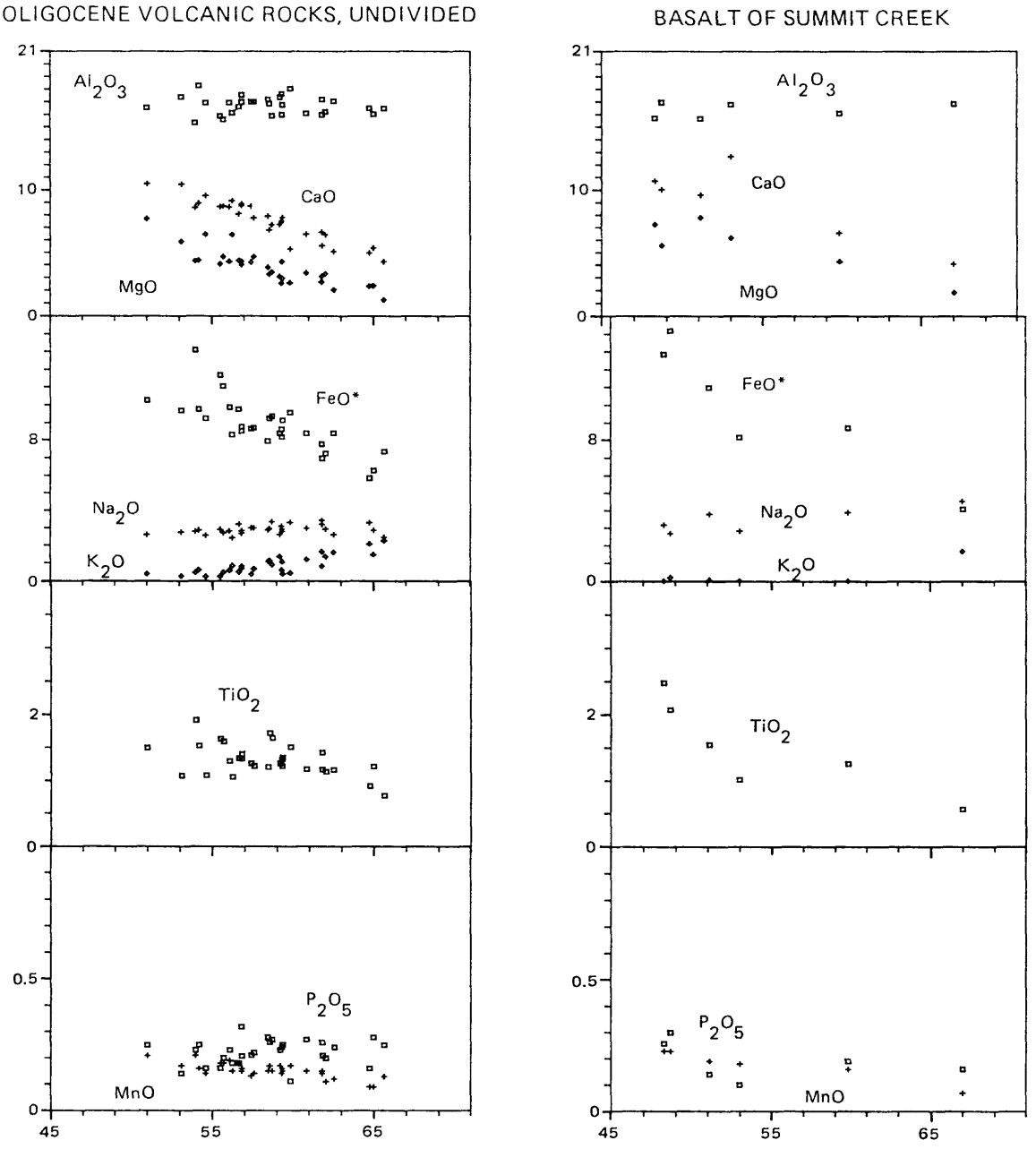

Figure 6, continued

SILL AT TOP OF THE CRESCENT FORMATION

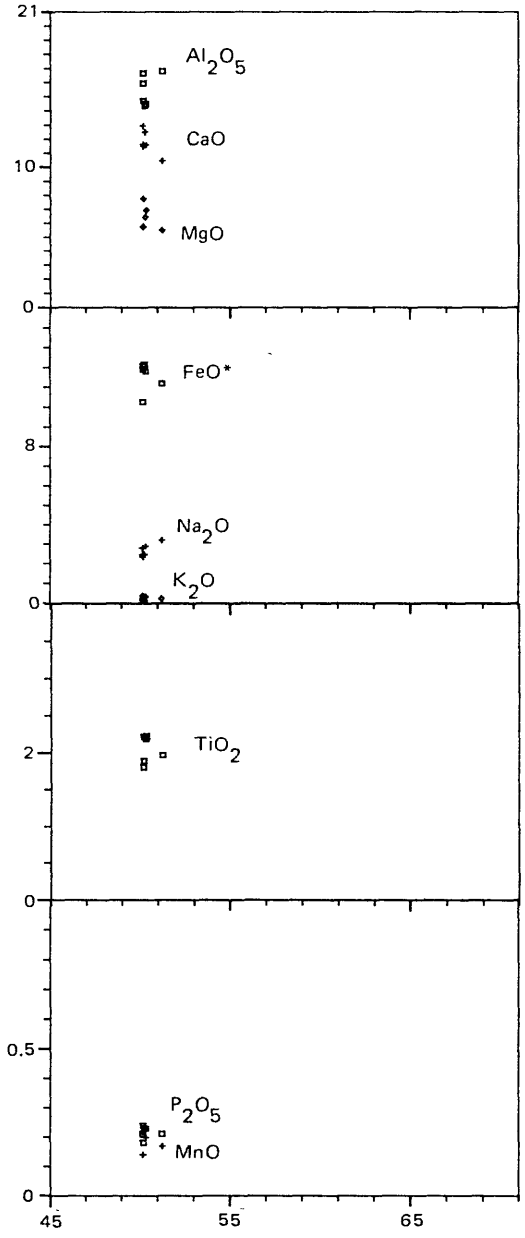

Figure 6, continued

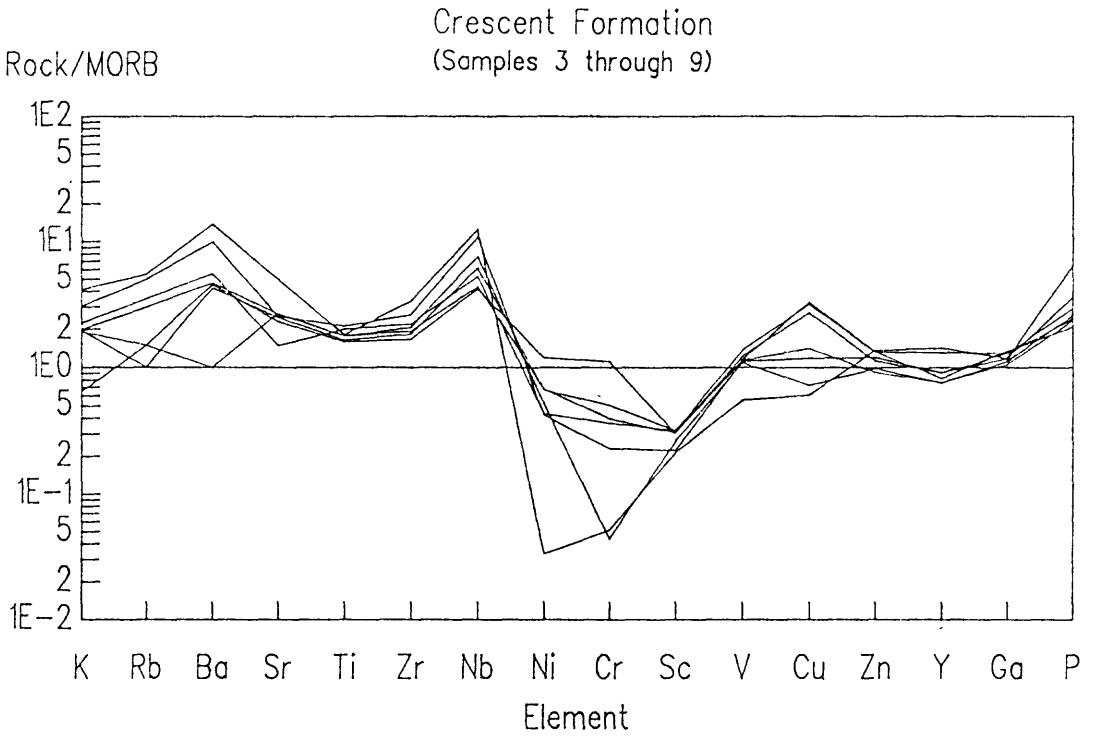

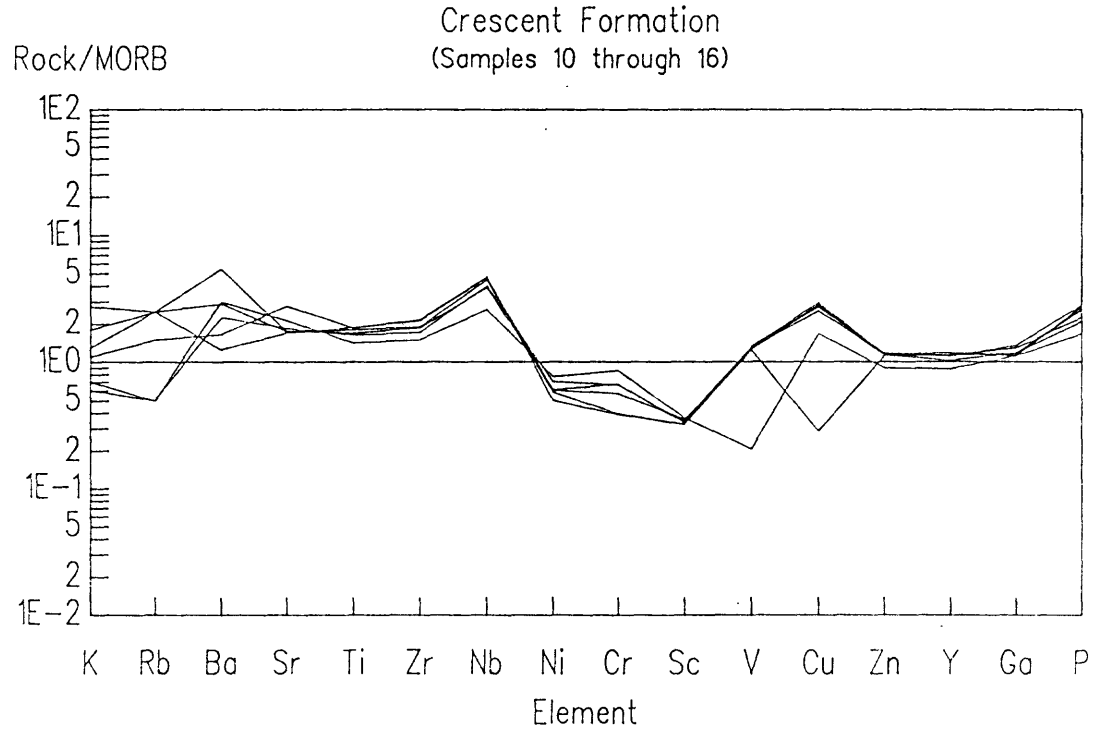

Figure 7. Rock/MORB plots for Paleogene volcanic rocks of southwest Washington. MORB values from Pearce [1982] and Engel et al. [1965]; K20 = 0.20 %; Rb = 2 ppm; Ba = 20 ppm; TiO2 = 1.40 %; Zr = 90 ppm; P205 = 0.12 %; Nb = 4.6 ppm; Sr = 121 ppm; Ni = 90 ppm; Y = 33 ppm; Sc = 40.6 ppm; Cr = 251 ppm; Cu = 77 ppm; Ga = 17 ppm; V = 292 ppm; Zn is set to the arbritary value of 100 ppm.

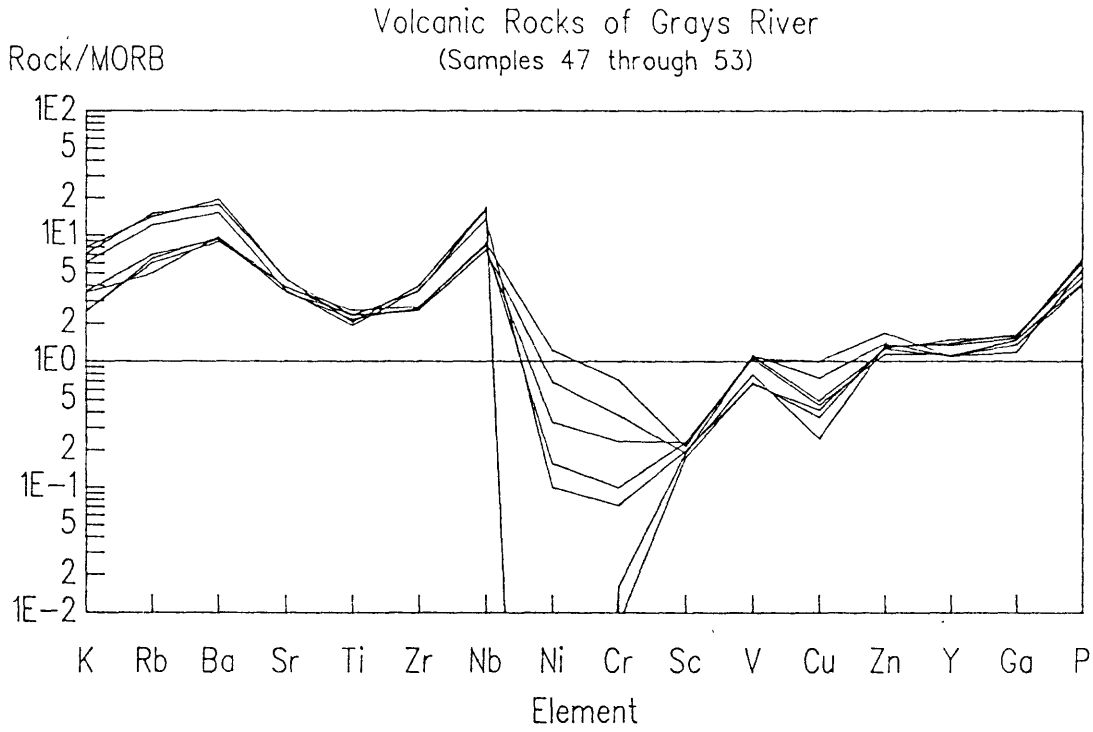

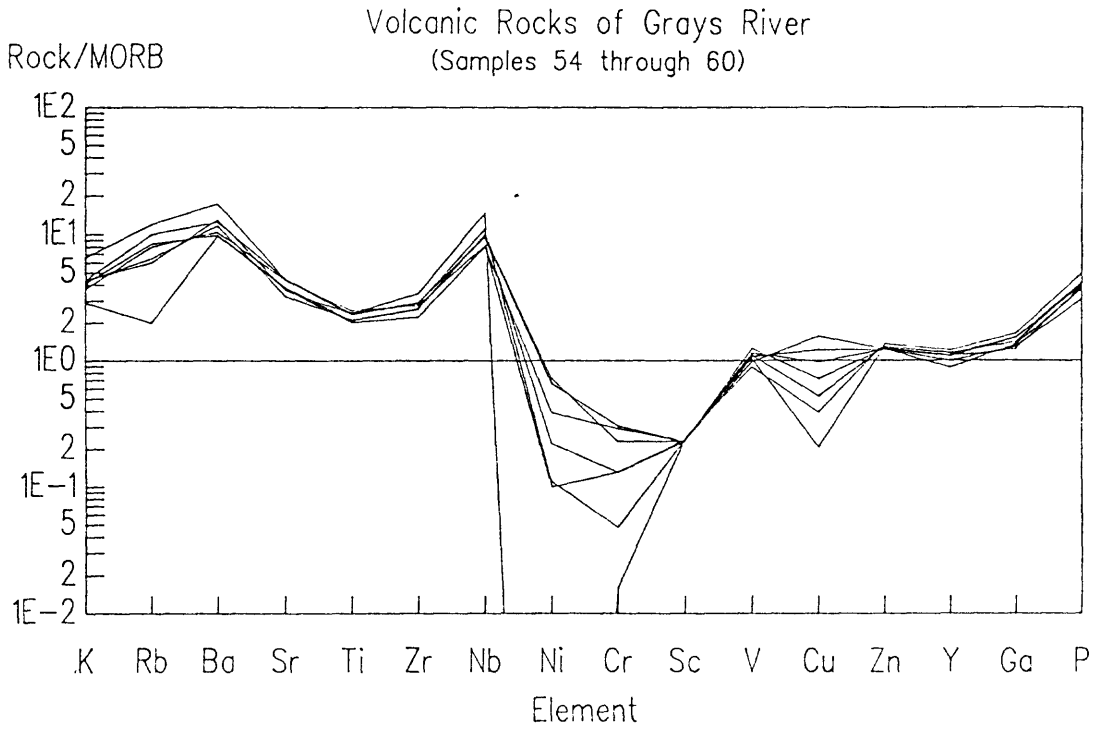

Figure 7, continued

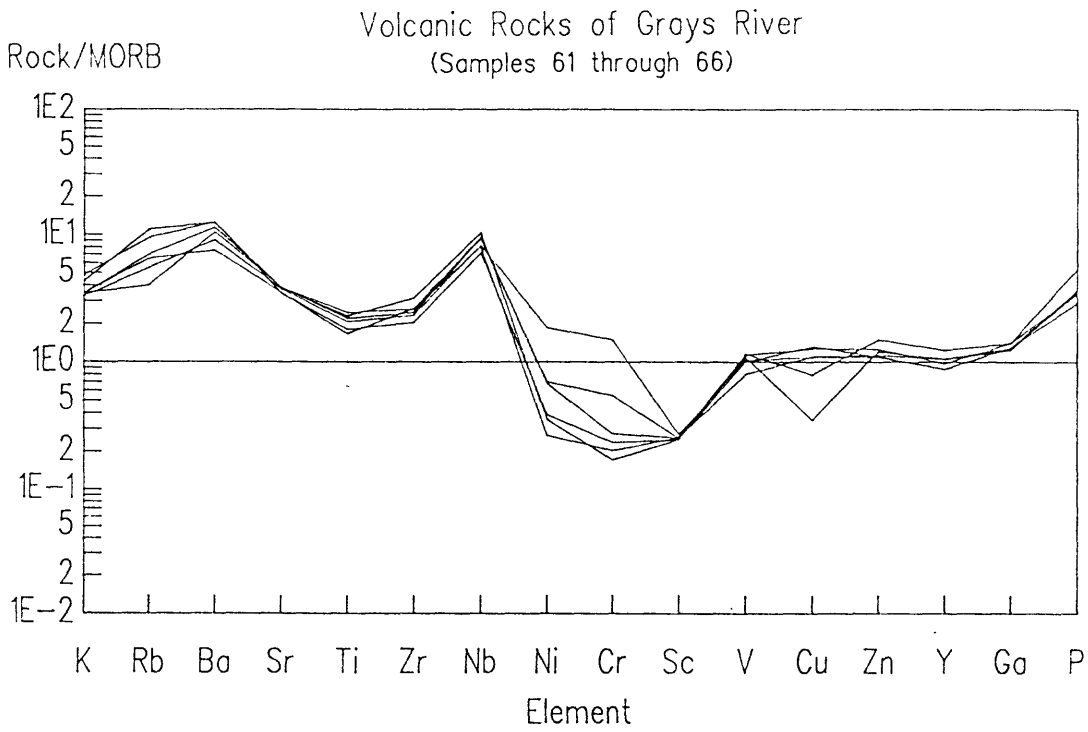

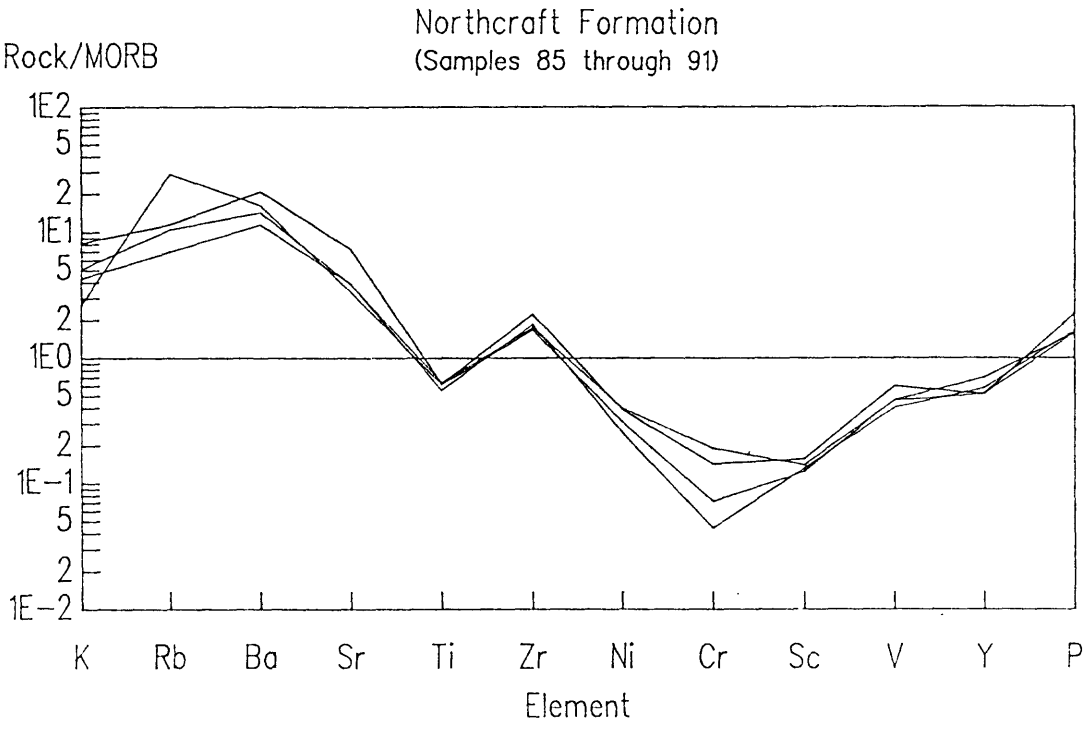

Figure 7, continued

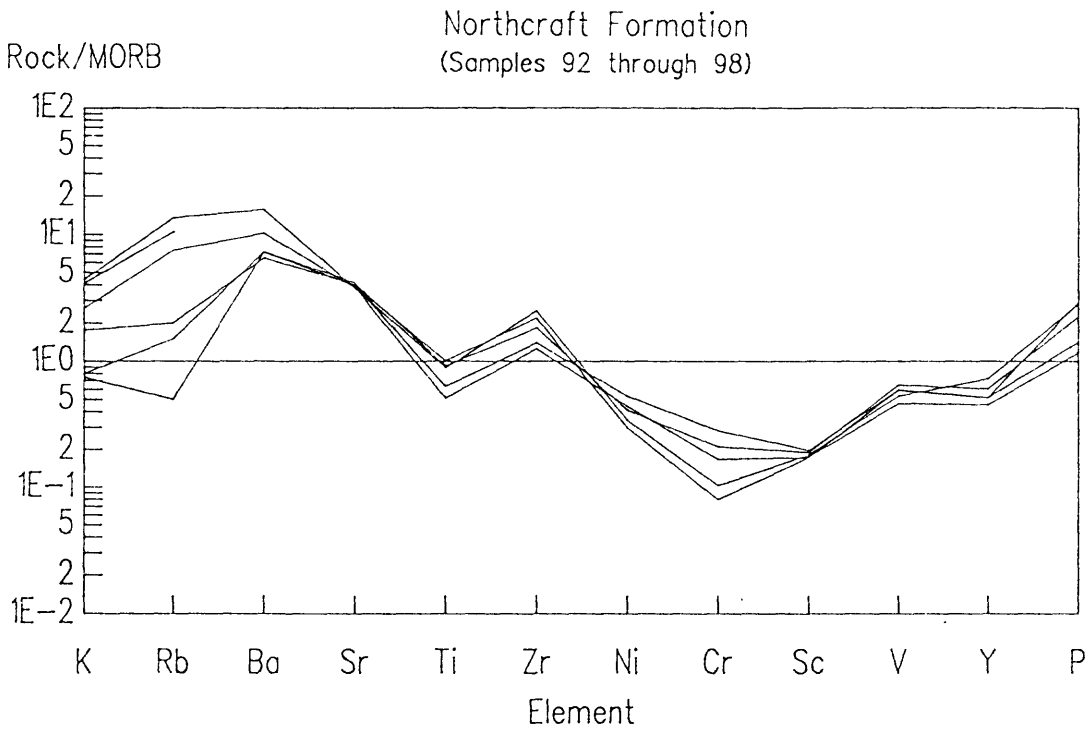

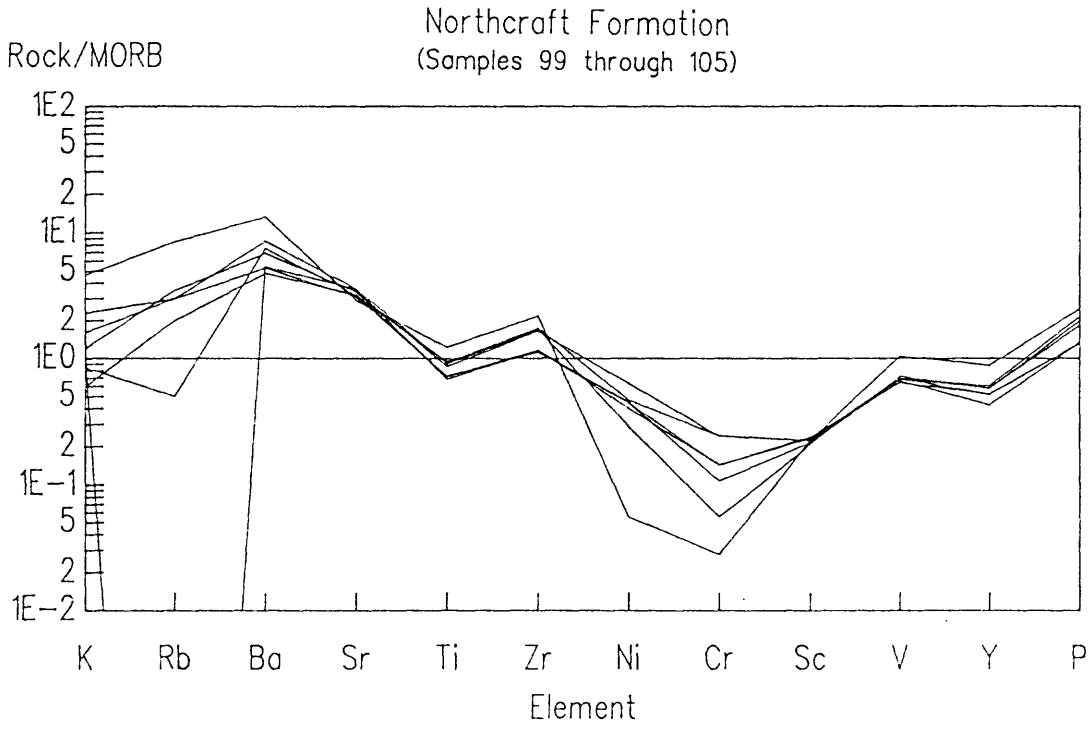

Figure 7, continued

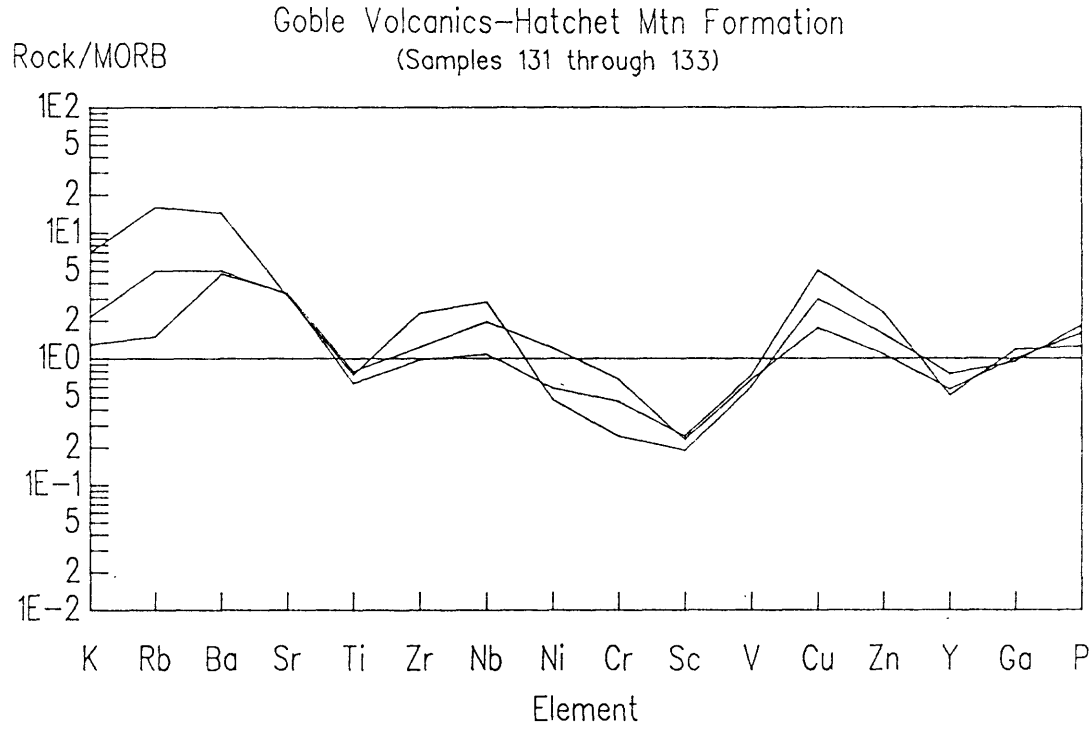

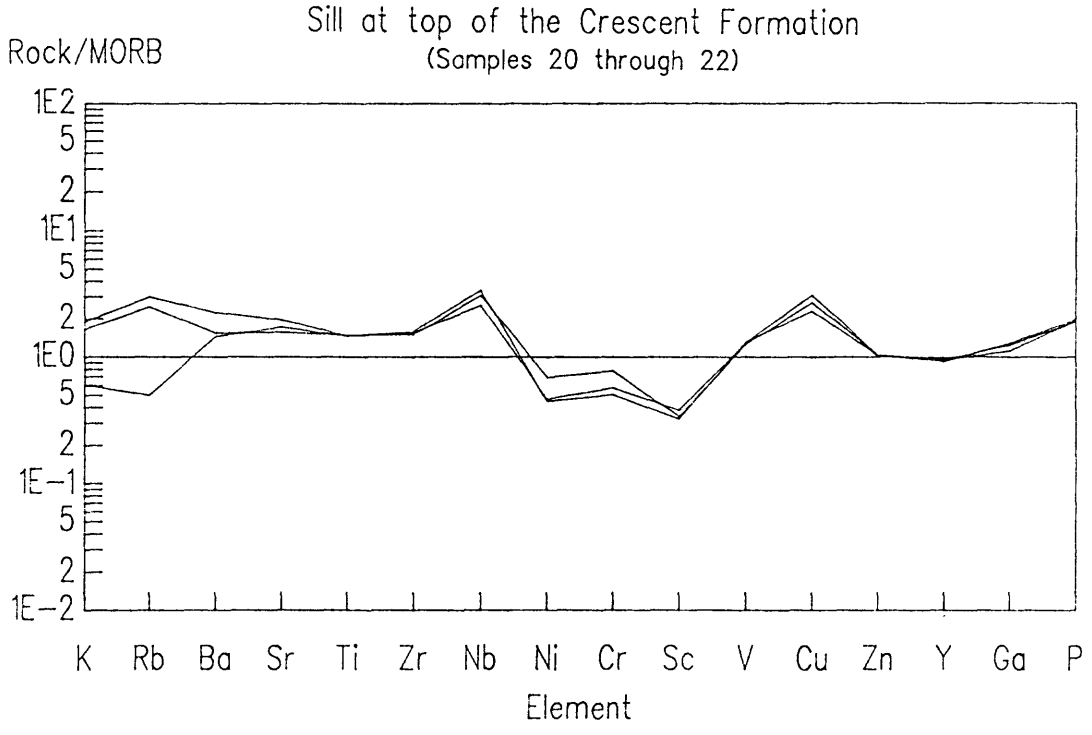

Figure 7, continued

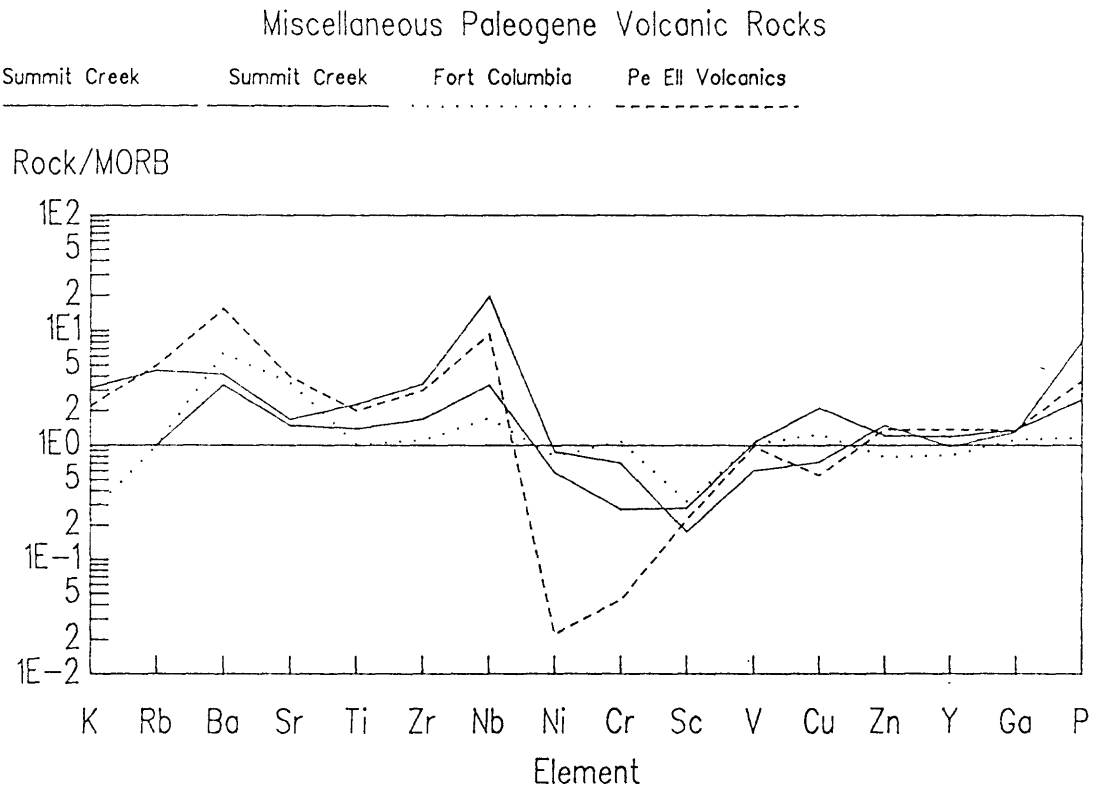

Figure 7, continued

behaves like heavy rare earth element (HREE) and has nearly constant values close to MORB. Ga contents are also stable and similar to MORB. However, P_2O_5 is enriched relative to MORB and shows significant within-group variation.

Volcanic rocks of Grays River

A series of 12 lava flow samples that cross the entire outcrop area of the Grays River unit were collected along logging roads in the vicinity of Grays River Divide in township 10 north, range 6 west. In this area, the Narizian siltstone beds of Skamakowa Creek [Wells, 1981] lie above the flows while Narizian Cowlitz and/or correlative McIntosh strata lie beneath. These analyses are augmented by samples from the Olequa Creek type-section of the Cowlitz Formation [Henriksen, 1956; Weaver, 1937]. Here individual flows 3 to 10 m thick are interbedded with feldspathic sandstone and coal of the Cowlitz.

All sampled flows are olivine- and quartz-normative subalkaline basalts on the TAS diagram (Figure 5). All are tholeiitic on FeO^*/MgO diagram (Figure 4) and the AFM diagram. Major and minor oxide ranges are summarized on the Harker diagram of Figure 6. The Rock/MORB plot (Figure 7) depicts trace element ranges.

The volcanics of Grays River possess highly distinctive and stable K-group element variation. K_2O, Rb, Ba, and Sr all show consistent enrichment relative to MORB of 3 to 10 times. The Ti-group of TiO_2, Zr, and Nb show similar trends with very stable values shown by a narrow envelope between minimum and maximum values. Ti and Zr have 2x enrichment relative to MORB while Nb has 10x enrichment. Ni and Cr are strongly depleted although the dataset is very "noisy." Sc, V have values similar to MORB. Cu is notably lower than the high-Cu group of Crescent samples. Y and Ga contents are similar to MORB while P_2O_5 is elevated relative to MORB.

Sills near the top of the Crescent Formation

The sills at or near the top of the Crescent have an uncertain age and relationship to surrounding volcanic units [Wells, 1981]. They clearly cut much of Unit 1 of the Crescent. In general, it is not known if they cut younger Narizian rocks of the Cowlitz-McIntosh-Skookumchuck sequence. The sills could be associated with late Crescent volcanism (i.e. Unit 2) or could be feeders for volcanic rocks of Grays River Divide.

On the TAS and FeO^*/MgO vs. SiO_2 diagrams (Figures 4 and 5), the sills plot within both the southwest Washington Crescent field and the Grays River field. Trace elements for the sills are reasonably similar to Crescent. Ni, Cr, Sc, Rb, Y, Ga, and Zn agree with mean Crescent values within 1 standard deviation (Table 1). Ba contents of the sills are similar to the low Ba (<50 ppm) population of Crescent. However, though represented in the range of Crescent values, the relatively immobile elements Ti, Zr, and Nb vary in all instances from average Crescent. Concentrations of Y, Ga, and Cu are similar between the two units. No correlation

exists between the sills and the single analyzed subaerial Crescent Unit 2 flow. Major elements also do not fit the sills exactly.

Geochemically, the sills are dissimilar to sampled Grays River flows. Relative to Grays River units, the sills are depleted in K-type elements and Ti-group (as in most of the Crescent). The sills are enriched relative to Grays River in compatible elements (although both posses similar average Ni contents). Chalcophiles show contrasting behavior with Cu greater in sills than Grays River and Zn slightly less to almost equal. Major oxides have elevated CaO and MgO, and depleted P_2O_5 relative to Grays River, just as the Crescent flows do. SiO_2, Al_2O_3, MnO, and FeO* contents are about the same in the sills as both the Crescent Formation and the volcanic rocks of Grays River Divide.

In summary, chemical trends of the sills are highly similar to trends observed in the Crescent Formation. Exact correlation between the sills and Crescent volcanism cannot be made but the correlation is strengthened by the dissimilarity of the sills to Grays River units.

Flows at Fort Columbia

The single sample of a flow at Fort Columbia (Sample 67 of Table A1 and A2) is almost a basaltic-andesite on the TAS diagram (Figure 5) and falls into the tholeiitic field on the FeO*/Mgo vs. SiO_2 diagram (Figure 4). Elevated Ti-group and K-group elements are elevated relative to Crescent while compatible elements (Ni, Cr, Sc, V) are depleted. The sample has chemistry distinct from the Crescent trends. Conversely, the sample shares average Grays River Ti-group values. K-group elements (which respond readily to alteration) fall outside of Grays River group means, except for Sr. Contents of Mgo, CaO and P_2O_5 are all well within Grays River average values. The flow appears to be an early (pre-accretion of coast range?) example of Grays River-type chemistries.

Northcraft Formation

Samples from the Northcraft Formation form a transitional, subalkaline tholeiitic to calcalkaline assemblage (Figure 4). Most Northcraft samples are andesite, with lesser basaltic-andesite, and a dacite (Figure 5). Unlike the Crescent and Grays River suites, major elements for the Northcraft (Figure 6) display strong correlation with silica values.

The Northcraft is chemically similar to the other sampled arc units. K-group elements ar strongly enriched on the Rock/MORB plots (Figure 7), as is Cu. Ti-group elements and P_2O_5 are significantly lower in concentration that in coeval forearc volcanic rocks of the Grays River unit. Also in contrast to Grays River, the Northcraft shows only mild compatable element depletion.

Goble Volcanics and Hatchet Mountain Formation

All Goble-Hatchet Mountain analyses are subalkaline. Out of

28 analyses, 3 classify as basalts, 19 as basaltic-andesites, and 6 as andesites. On the TAS diagram (Figure 5), Goble analyses form a trend that is approximately parallel to the slope of the trachyandesite/basaltic-andesite and andesite field boundary. This suggests a differentiation trend although field data are not complete enough to confirm this. The analyses classify as both tholeiitic and calcalkaline on AFM and FeO*/MgO diagrams (Figure 4). Major and minor oxide values are depicted in the Harker diagrams of Figure 6.

The unit is easily distinguished from Grays River or Crescent Formation on SiO_2 content alone. Compared to Grays River, Goble has higher Al_2O_3 and Na_2O contents and lower TiO_2, FeO*, MnO, CaO, MgO, K_2O, and P_2O_5. It is especially interesting to compare K_2O at similar values of SiO_2. With SiO_2 at values close to the Grays River mean of 50.15%, K2O in the Goble ranges between 0.33% and 0.15% while Grays River has K_2O=0.82%. Trace element data for 3 Goble-Hatchet Mountain are shown on the Rock/MORB plot of Figure 7. The same enrichment in K-type elements relative to MORB occurs as in the Crescent and Grays River suites. Note the sharp depletion in Ti relative to MORB (and also relative to Crescent and Grays River). Interestingly, Zr and Nb are slightly enriched compared to MORB (but not as much as Grays River and Crescent). Compatible elements show patterns (noisy) much like Grays River and Crescent. Cu is very enriched relative to the Grays River with values similar or higher than the Cu enrichment present in the Crescent.

Northcraft and Goble-Hatchet Mountain element concentrations are very similar. The two units should be considered a single geochemical suite that spans a time of approximately 42 to 34 Ma.

Oligocene volcanic rocks of the Cascade Range

The sample Oligocene units are essentially indistinguishable from Northcraft and Goble-Hatchet Mountain on a chemical and petrological basis.

Basalt of Summit Creek

Analyses from the basalt of Summit Creek classify as subalkaline basalt, andesite, and dacite (Figure 4), and are both tholeiitic and calkalkaline (Figure 5). Major elements (Figure 6) tend to vary with SiO_2. Trace elements (Figure 7) are overall most similar to the Cascade arc patterns seen in the Northcraft, Goble-Hatchet Mountain and Oligocene units. These include moderate to low K-group enrichment and mild compatable element depletion. The Summit Creek section appear to possess higher values for Ti-group elements and P_2O_5 than Cascade arc rocks.

REGIONAL CORRELATIONS

Relationship between Crescent Formation and volcanic rocks of Grays River

Both the Crescent Formation and the Grays River flows are tholeiitic with overlapping major oxides ranges. Specifically, SiO_2, Al_2O_3, FeO*, MnO, and Na_2O contents are not distinctive between the two units. However, Grays River flows are distinctly higher in K_2O, P_2O_5, and Ti-group elements, and somewhat lower in MgO and CaO values. Plots utilizing Ti-group elements are successful in discriminating between 8 out of 12 Crescent analyses. Unfortunately, high Ti-group Crescent flows are present as well as several low Ti-group Grays River analyses. These analyses may represent mismapped Grays River flows; exposure conditions are generally poor in the Willapa Hills while faulting is very complex (Figure 3). However, the analyses may also signal that chemistries of the Grays River type are present in limited quantities within the Crescent. This conclusion is similar in many respects to those reached by Cady [1975] and Lyttle and Clarke [1975, 1976] for data presented by Glassley [1974, 1976]. Additional criteria such as stratigraphic position, associated biostratigraphic data, and mineralogic qualities (the Crescent often is associated with glossy black chlorite while the Grays River commonly possesses pilotaxitic texture) are required to definitively classify the units.

The younging of the Crescent and Siletz River formations towards southwest Washington [Duncan, 1982] suggests very that Crescent- and Grays River-type volcanism may overlap in southwest Washington. The basalt at Fort Columbia could represent an initial transition from Crescent to Grays River chemistries. If the sandstone of Megler and basalt of Fort Columbia are pre-accretion, then the change to Grays River chemistry probably has nothing to do with accretionary tectonics. If the Megler and Fort Columbia units are syn- or post-accretion, then transition to Grays River-type chemistries might reasonably be supposed to relate to accretionary events.

Relationship between volcanic rocks of Grays River, the Tillamook Volcanics and other forearc volcanic rocks of Oregon

The volcanic rocks of Grays River are chemically, mineralogically, and texturally similar to the Tillamook Volcanics of northwest Oregon. K-Ar ages from both sequences are similar, yielding ages of around 46-41 Ma [McElwee and Duncan, 1984], although the analytical errors are substantial. The Tillamook Volcanics are both underlain and overlain by sedimentary rocks yielding Narizian benthic foraminifers (Niem and Niem, 1985). The volcanic rocks of Grays River are also generally sandwiched between Narizian rocks, but locally are interbedded with rocks yielding a Refugian fauna [Livingston, 1966], suggesting that they in part may be younger.

Chemically, the forearc volcanic rocks of Oregon are in general much more differentiated than the Grays River unit. The

Tillamook contains numerous reported analyses of basaltic-andesite, andesite, and trachyandesite [Rarey, 1986; Mumford, 1988], and Wells et al. [1983] report dacitic ash flow tuffs. Regionally, the forearc sequence appears to become both more alkaline and younger to the south [McElwee et al., 1985a]. Based upon trace element and isotopic data, McElwee et al. [1985a, 1985b] suggest that the forearc volcanic units were derived from partial melting of an oceanic-island type mantle, followed by fractional crystallization of olivine, clinopyroxene, plagioclase, and oxide phases.

We agree with Wells and Heller (1988) that correlative Eocene sections are found on both sides of Columbia River and that the two regions did not experience separate tectonic and stratigraphic histories as suggested in some microplate rotation models [see for example, Frei et al., 1984]. However, detailed comparison of northwest Oregon and southwest Washington lithologies suggests that the Grays River and Tillamook are not identical and were probably not erupted from same volcanic center.

Sill at the top of the Crescent Formation

The sill are chemically similar to the Crescent Formation and dissimilar to the Grays River unit. Based upon geochemistry, they appear to be related to a late phase of Crescent volcanism, perhaps one without an extrusive equivalent.

Relationship of the volcanic rocks of Grays River to the Goble Volcanics-Hatchet Mountain Formation

The Cascade arc rocks of the Goble Volcanics should be clearly separated from the forearc volcanics of the Grays River unit. Extent of the Grays River is shown on Phillips [1987a] and Walsh [1987].

Relationship of the Goble Volcanics-Hatchet Mountain Formation to the Northcraft Formation and to other early Cascade arc volcanics

Chemically and texturally, the Northcraft and Goble appear virtually indistinguishable. However, the type Northcraft is probably 2 to 3 Ma older than most of the Goble. Both represent arc-front, flow-dominated volcanism associated with initiation of the Cascade arc. Both are not "island-arc tholeiites" by the definition of Jakes and Gill (1970), but are flow-dominated, "transitional tholeiitic-calcalkaline" similar to other early Cascade arc products like the Clarno Volcanics [Rogers and Novitsky-Evans, 1977; Rogers and Ragland, 1980], or older portions of the Little Butte Volcanics [Lux, 1981, 1982]. Based upon the analysis of Evarts et al. [1987], transitional calcalkaline-tholeiitic flow-dominated volcanism continued in the southern Washington Cascades well into the Oligocene.

Extension behind the arc-front volcanoes of Northcraft and Goble generated a regionally extensive forearc basin. The dominantly pyroclastic and volcaniclastic Ohanapecosh Formation

[Fiske et al., 1963; Vance et al., 1987] and the John Day Formation were deposited in the back-arc setting together with rare bimodal assemblages of rhyodacites and basalts.

Acknowledgments

Discussion with R. E. Wells and P. D. Snavely, Jr. were instrumental in helping us recognize the break between Goble and Grays River volcanism. We thank C. Cushman, K. L. Kaler, and M. J. McClincy for able assistance in the field. Our colleagues at the Division of Geology, R. L. Logan, M. A. Korosec, and H. W. Schasse collected some of the Northcraft, Ohanapecosh, and Crescent samples and provided many hours of stimulating discussion and review of our ideas. The cross-section of Figure 3 is a joint product of W. S. Lingley and Walsh.

REFERENCES

Armentrout, J. M., Cenozoic stratigraphy, unconformity-bounded sequences, and tectonic history of southwestern Washington, in Selected papers on the geology of Washington, edited by J. E. Schuster, Bull. 77, 291-320, Wash. Div. Geol. and Earth Resources, Olympia, Wash, 1987.

Armentrout, J. M., K. A. McDougall, P. T. Jefferis, and E. Nesbitt, Geologic field trip guide for the Cenozoic stratigraphy and late Eocene paleoecology of southwestern Washington, in Geologic field trips in western Oregon and southwestern Washington, Bull. 101, 79-120, Ore. Dept. Geol. Min. Industries, Portland, Ore, 1980.

Armentrout, J. M., D. A. Hull, J. D. Beaulieu, W. W. Rau, Correlation of Cenozoic stratigraphic units of western Oregon and Washington, Oil and Gas Invest. 7, 90 pp., Ore. Dept. Geol. Min. Industries, Portland, Ore, 1983.

Armstrong, R. L., Cenozoic igneous history of the U. S. Cordillera from lat. 42° to 49° N., in Cenozoic tectonics and regional geophysics of the western cordillera, edited by R. P. Smith and G. P. Eaton, Geol. Soc. Amer. Memoir, 152, 265-282, 1978.

Baldwin, E. M., Geology of the Dallas and Valsetz quadrangles, Oregon, Bull. 35 (Rev. ed.), 56 pp., Ore. Dept. Geol. Min. Industries, Portland, Ore, 1964.

Baldwin, E. M., Eocene stratigraphy of southwestern Oregon, Bull. 83, 40 pp., Ore. Dept. Geol. Min. Industries, Portland, Ore, 1974.

Beck, M. E., Jr. and C. D. Burr, Paleomagnetism and significance of the Goble volcanic series, southwestern Washington, Geology, 7, 4, 175-179, 1979.

Buckovic, W. A., The Eocene deltaic system of west-central Washington, in Cenozoic paleogeography of the western United States, Pacific Coast Paleogeography Symposium 3, edited by J. E. Armentrout, M. R. Cole, Harry Ter Best, Jr, pp 147-163, Society of Economic Paleontologists and Mineralogists, Pacific Section, Los Angeles, Calif., 1979.

Cady, W. M., Tectonic setting of the Tertiary volcanic rocks of the Olympic Peninsula, Washington, Geol. Surv. J. Res., 3, 5, 573-582, U.S. Geol. Surv., Reston, Va, 1975.

Church, B. N., Geology of the White Lake basin, Bull. 61, 120 pp., British Columbia Dept. Mines and Petrol. Resources, Victoria, B.C., 1973.

Clark, K. P., Stratigraphy and geochemistry of the Crescent Formation basalts and related rocks near Bremerton, Washington (abstract), Eos Trans. AGU, 68, 52, 1814, 1987.

Cowan, D. S., C. J. Potter, M. T. Brandon, D. M. Fountain, D. W. Hyndman, S. Y. Johnson, B. T. R. Lewis, K, J. McClain, and D. A. Swanson, B-3 Juan de Fuca spreading ridge to Montana thrust belt, scale 1:500,000, Geol. Soc. Amer. Centennial Continent/Ocean Transect 9, 1986.

Cruver, S. K., The geology and mineralogy of bentonites and associated rocks of the Chuckanut Formation, Mt. Higgins area, North Cascades, Washington, M.S. thesis, 105 pp., Western Washington Univ., Bellingham, 1981.

Duncan, R. A., A captured island chain in the coast range of Oregon and Washington, J. Geophys. Res., 87, 10,827-10,837, 1982.

Ellingson, J. A., 1959, General geology of the Cowlitz Pass area, central Cascade Mountains, Washington, M.S. thesis, 60 pp., Univ. Washington, Seattle, 1959.

Engebretson, D. C., Allan Cox, and R. C. Gordon, Relative motions between oceanic and continental plates in the Pacific Basin, Geol. Soc. Amer. Spec. Paper 206, 59 pp., Geol. Soc. Amer., Boulder, Colo, 1985.

Engel, A. E. J., C. G. Engel, and R. G. Havens. Chemical characteristics of oceanic basalts and the upper mantle, Geol. Soc. Amer. Bull., 76, 719-734, 1965.

Evarts, R. C., R, P. Ashley, and J. G. Smith, Geology of the Mount St. Helens area--Record of discontinuous volcanic and plutonic activity in the Cascade arc of southern Washington, J. Geophys. Res., 92, B10, 10,155-10,169, 1987.

Ewing, T. E., Paleogene tectonic evolution of the Pacific Northwest, J. Geol., 88, 6, 619-638, 1980.

Fiske, R. S., C. A. Hopson, and A. C. Waters, Geologic map and sections of Mount Rainier National Park, Washington, Geol. Surv. Prof. Paper, 444, 93 pp., U.S. Geol. Surv., Reston, Va, 1963.

Frei, L. S., Jr., J. R. Magill, and Allan Cox, Paleomagnetic results from the central Sierra Nevada: Constraints on reconstructions of the Western United States, Tectonics, 3, 2, 157-177, 1984.

Frizzell, V. A., Jr., R. W. Tabor, D. B. Booth, K. M. Ort, and R. B. Waitt, Jr., Preliminary geologic map of the Snoqualmie Pass 1:100,000 quadrangle, Washington, scale 1:100,000, Open-File Map OF-84-693, U.S. Geol. Surv., Reston, Va, 1984.

Gill, J. B., Orogenic Andesites and Plate Tectonics, 385 pp., Springer-Verlag, N. Y. , N. Y., 1981.

Glassley, W. E., Geochemistry and tectonics of the Crescent volcanic rocks, Olympic Peninsula, Washington, Geol. Soc. Amer. Bull. 85, 5, 785-794, 1974.

Glassley, W. E., New analyses of Eocene basalt from the Olympic Peninsula, Washington: Discussion, Geol. Soc. Amer. Bull., 87, 8, 1200-1201, 1976.

Globerman, B. R., M. E. Beck Jr., and R. A. Duncan, Paleomagnetism and tectonic significance of Eocene basalts from the Black Hills, Washington Coast Range, Geol. Soc. Amer. Bull., 93, 11, 1151-1159, 1982.

Gresens, R. L., geology of the Wenatchee and Monitor quadrangles, Chelan and Douglas Counties, Washington, Bull., 75, 75 pp., Wash. Div. Geol. and Earth Resources, Olympia, Wash, 1983.

Hagen, R. A., The geology and petrology of the Northcraft Formation, Lewis County, Washington, M.S. thesis, Univ. Oregon, Eugene, 252 pp., 1987.

Heller, P. L., Sedimentary response to Eocene tectonic rotation in western Oregon, Ph.D. dissertation, 321 pp., Univ. Ariz., Tucson, 1983.

Heller, P. L., Z. E. Peterman, J. R. O'Neil, and Muhammad Shafiqullah, Isotopic provenance of sandstones from the Eocene Tyee Formation, Oregon Coast Range, Geol. Soc. Amer. Bull., 96, 6, 770-780, 1985.

Heller, P. L., R. W. Tabor, and C. A. Suczek, Paleogeographic evolution of the United States Pacific Northwest during Paleogene time, Can. J. Earth Sci., 24, 1652-1667, 1987.

Henriksen, D. H., Eocene stratigraphy of the lower Cowlitz River-eastern Willapa Hills area, southwestern Washington, Bull. 43, 122 pp., Wash. Div. Geol. and Earth Resources, Olympia, Wash, 1956.

Irvine, T. N. and W. R. Baragar, A guide to the chemical classification of the common igneous rocks, Can. J. Earth Sci., 8, 523-548, 1971.

Jakes, P. and J. B. Gill, Rare earth elements and the island arc tholeiitic series, Earth and Planetary Sci. Lett., 9, 17-28, 1970.

Johnson, S. Y., Evidence for a margin-truncating transcurrent fault (pre-late Eocene) in western Washington, Geology, 12, 538-541, 1984.

Korosec, M. A., Geologic map of the Mount Adams quadrangle, Washington, scale 1:100,000, Open-File Report 87-5, Wash. Div. Geol. and Earth Resources, Olympia, Wash, 1987a.

Korosec, M. A., Geologic map of the Hood River quadrangle, Washington, scale 1:100,000, Open-File Report 87-6, Wash. Div. Geol. and Earth Resources, Olympia, Wash, 1987b.

Le Bas, M. J., Le Maitre, R. W., Streckeisen, A., Zanettin, B, A chemical classification of volcanic rocks based on the total alkali-silica diagram, Jour. Petrol., 27, 745-75-, 1986.

Livingston, V. E., Jr., Geology and mineral measures of the Kelso-Cathlamet area, Cowlitz and Wahkiakum Counties, Washington, Bull. 54, 110 pp., Wash. Div. Geol. and Earth Resources, Olympia, Wash, 1966.

Lonsdale, Peter, Paleogene history of the Kula plate: Offshore evidence and onshore implications, Geol. Soc. Amer. Bull., 100, 5, 733-754, 1988.

Lux, D. R., Geochronology, geochemistry and petrogenesis of basaltic rocks from the Western Cascades, Oregon, Ph.D. thesis, 171 pp., Ohio State Univ., Columbus, 1981.

Lux, D. R., K-Ar and ^{40}Ar-^{39}Ar ages of mid-Tertiary volcanic rocks from the Western Cascade Range, Oregon, Isochron/West, 33, 27-32, 1982.

Lyttle, N. A. and D. B. Clarke, New analyses of Eocene basalt from the Olympic Peninsula, Washington, Geol. Soc. Amer. Bull., 86, 3, 421-427, 1975.

Lyttle, N. A. and D. B. Clarke, New analyses of Eocene basalt from the Olympic Peninsula, Washington: Reply, Geol. Soc. Amer. Bull., 87, 8, 1201-1204, 1976.

McClincy, M. J., Tephrostratigraphy of the middle Eocene Chumstick Formation, Cascade Range, Douglas County, Washington, M.S. thesis, 125 p., Portland State Univ., Portland, 1986.

McElwee, K. R., R. A. Duncan, Punctuated volcanism in Oregon's Coast Range (abstract), EOS Trans. AGU, 65, 17, 330, 1984.

McElwee, K. R., R. A. Duncan, W. P. Leeman, Geochemistry of upper Eocene volcanic rocks, Coast Range, Oregon and Washington (abstract), EOS Trans. AGU, 66, 3, 23, 1985a.

McElwee, K. R., R. A. Duncan, W. P. Leeman, Petrogenesis of Middle Tertiary forearc volcanic rocks, Oregon and Washington Coast Range (abstract), EOS Trans. AGU, 66, 46, 1112, 1985b.

Margolis, Jacob, Structure and hydrothermal alteration associated with epithermal Au-Ag mineralization, Wenatchee Heights, Washington, M.S. thesis, 90 pp., Univ. Washington, Seattle, 1988.

Massey, N. W. D., Metchosin Igneous Complex, southern Vancouver Island: Ophiolite stratigraphy developed in an emergent island setting, Geology, 14, 602-605, 1986.

May, D. J., The paleoecology and depositional environment of the late Eocene-early Oligocene Toutle Formation, M.S. thesis, 110 pp., University of Washington, Seattle, 1980.

Miyashiro, A., Volcanic rock series in island arcs and active continental margins, Am. J. Sci., 274, 321-355, 1974.

Montanari, Alessandro, Robert Drake, D. M. Bice, Walter Alvarez, G. H. Curtis, B. D. Turrin, and D. J. DePaolo, Radiometric time scale for the upper Eocene and Oligocene based on K/Ar and Rb/Sr dating of volcanic biotites from the pelagic sequence of Gubbio, Italy, Geology, 13, 9, 596-599, 1985.

Muller, J. E., Metchosin volcanics and Sooke intrusions of southern Vancouver Island, Geol. Surv. Can. Report of Activities, Part A, Paper 77-1a, 287-294, 1977.

Muller, J. E., Chemistry and origin of the Eocene Metchosin Volcanics, Vancouver Island, British Columbia, Can. J. Earth Sci., 17, 199-209, 1980.

Muller, J. E., P. D. Snavely, Jr., and R. W. Tabor, The Tertiary Olympic Terrane, southwest Vancouver Island and northwest Washington Field Trip Guidebook, Trip 12, 59 pp., Geol. Soc. Canada, Victoria Section, Victoria, B. C., 1983.

Mumford, D. F., Geology of the Elsie-lower Nehalem River area, south-central Clatsop and northern Tillamook counties, northwestern Oregon, M.S. thesis, 392 pp., Oregon State Univ., Corvallis, 1988.

Mutti, E., and F. Ricci Lucchi, Turbidites of the northern Appenines: introduction to facies analysis, Internat. Geology Rev.,v. 20, no.2, translated by Tor Nilsen, 1978.

Niem, A. R. and W. A. Niem, Oil and gas investigation of the Astoria Basin, Clatsop and northernmost Tillamook Counties, northwest Oregon, scale 1:100,000, OGI-14, Ore. Dept. Geol. Min. Industries, Portland, Ore, 1985.

Noblett, J. B., Subduction-related origin of the volcanic rocks of the Eocene Clarno Formation near Cherry Creek, Oregon, Oregon Geology, 43, 91-98, 1981.

Ort, K. M., R. W. Tabor, and V. A. Frizzell, Jr., Chemical analyses of selected Tertiary and Quaternary volcanic rocks, Cascade Range, Washington, Open-File Report 83-1, 14 pp., U.S. Geol. Surv., Reston, Va, 1983.

Pearce, J. A., Trace element characteristics of lavas from destructive plate boundaries, in Andesites, orogenic andesites and related rocks, edited by R. S. Thorpe, 525-548, J. Wiley and Sons, Chichester, 1982.

Pearson, R. C. and J. D. Obradovich, Eocene rocks in northeastern Washington--radiometric ages and correlations, Geol. Surv. Bull. 1433, U.S. Geol. Surv., Reston, Va, 41 pp., 1977.

Peck, D. L., A. B. Griggs, H. G. Schlicker, F. G. Wells, and H. M. Dole, Geology of the central and northern parts of the western Cascade Range in Oregon, Geol. Surv. Prof. Paper 449, 56 pp., U.S. Geol. Surv., Reston, Va, 1964.

Phillips, W. M., Geologic map of the Mount St. Helens quadrangle, Washington and Oregon, Open-File Report 87-4, 59 p., Wash. Div. Geol. and Earth Resources, Olympia, Wash., 1987a.

Phillips, W. M., Geologic map of the Vancouver quadrangle, Washington and Oregon, Open-File Report 87-10, 27 p., Wash. Div. Geol. and Earth Resources, Olympia, Wash., 1987b.

Phillips, W. M., Geochemistry and areal extent of the Grays River volcanic rocks, southwest Washington and adjacent Oregon (abstract), Eos Trans. AGU, 68, 52, 1815, 1987c.

Phillips, W. M. and K. L. Kaler, Chemical variation in upper Eocene volcanic rocks, southwestern Washington (abstract), Geol. Soc. Amer. Abs. with Programs, 17, 6, 400, 1985.

Phillips, W. M., M. A. Korosec, H. W. Schasse, J. L. Anderson, and R. A. Hagen, K-Ar ages of volcanic rocks in southwest Washington, Isochron/West, 47, 18-24, 1986.

Prothero, D. R. and J. M. Armentrout, Magnetostratigraphic correlation of the Lincoln Creek Formation, Washington--Implications for the age of the Eocene/Oligocene boundary, Geology, 13, 3, 208-211, 1985.

Rarey, P. J., Geology of the Hamlet-north fork of the Nehalem River area, southern Clatsop and northernmost Tillamook Counties, northwest Oregon, M.S. thesis, 426 pp., Oregon State Univ., Corvallis, 1986.

Rau, W. W., Pacific Northwest Tertiary benthic foraminiferal biostratigraphic framework: An overview, in Pacific Northwest Cenozoic biostratigraphy, edited by J. M. Armentrout, Geol. Soc. Amer. Spec. Paper 184, 67-84, 1981.

Rau, W. W., Geologic map of the Humptulips quadrangle and adjacent areas, Grays Harbor County, Washington, scale 1:62,500, Geol. Map GM-33, Wash. Div. Geol. and Earth Resources, Olympia, Wash, 1986.

Roberts, A. E., Geology and coal resources of the Toledo-Castle Rock district, Cowlitz and Lewis Counties, Washington, Geol. Surv. Bull. 1062, 71 pp., U.S. Geol. Surv., Reston, Va, 1958.

Robinson, P. T.,Reconnaissance geologic map of the John Day Formation in the southwestern part of the Blue Mountains and adjacent areas, north-central Oregon, Misc. Invest. Map I-872, U.S. Geol. Surv., Reston, Va, 1975.

Rogers, J. J. W. and J. M. Novitsky-Evans, The Clarno Formation of central Oregon, U. S. A.: Volcanism on a thin continental margin, Earth and Plan. Sci. Let., 34, 56-66, 1977.

Rogers, J. J. W. and P. C. Ragland, Trace elements in continental-margin magmatism: Part I. Trace elements in the Clarno Formation of central Oregon and the nature of the continental margin on which eruption occurred, Geol. Soc. Amer. Bull., 91, pt. II, card 1, 1217-1292, 1980.

Salvador, Amos, Chronostratigraphic and geochronometric scales in COSUNA stratigraphic correlation charts of the United States, Amer. Assoc. Petrol. Geol. Bull., 69, 2, 181-189, 1985.

Schasse, H. W., Geologic map of the Centralia quadrangle, Washington, Open-File Report 87-11, 28 pp., Wash. Div. Geol. and Earth Resources, Olympia, Wash, 1987a.

Schasse, H. W., Geologic map of the Mount Rainier quadrangle, Washington, Open-File Report 87-16, 43 p., Wash. Div. Geol. and Earth Resources, Olympia, Wash, 1987b.

Sherrod, D. R. and J. G. Smith, Preliminary map of upper Eocene to Holocene volcanic and related rocks of the Cascade Range, Oregon, Open-File Report, U.S. Geol. Surv., Reston, Va, in press.

Silberling, N. J., and D. L. Jones, Lithotectonic terrane maps of the North American Cordillera, Open-File Report 84-523, U.S. Geol. Surv., Reston, Va, 1984.

Snavely, P. D., Jr., Tertiary geologic framework, neotectonics, and petroleum potential of the Oregon-Washington continental margin, in Geology and resource potential of the continental margin of western North America and adjacent Ocean Basins: Beaufort Sea to Baja California, edited by D. W., Scholl, Grantz, A., and Vedder, J. G., Circum-Pacific Council for Energy and Mineral Resources Earth Science Series, 6, 305-335, 1987.

Snavely, P. D., Jr., R. D., Brown, Jr., A. E. Roberts, and W. W. Rau, Geology and coal resources of the Centralia-Chehalis district, Washington, Geol. Bull. 1053, 159 pp., U.S. Geol. Surv., Reston, Va, 1958.

Snavely, P. D., Jr., H. C. Wagner, and N. S. MacLeod, Preliminary data on compositional variations of Tertiary volcanic rocks in the central part of the Oregon Coast Range, Ore Bin, 27, 6, 101-117, 1965.

Snavely, P. D., Jr., N. S. MacLeod, and H. C. Wagner, Tholeiitic and alkalic basalts of the Eocene Siletz River Volcanics, Oregon Coast Range, Am. J. Sci., 266, 6, 454-481, 1968.

Staatz, M. H. , R. W. Tabor, P. L. Weiss, J. F. Robertson, R. M. Van Noy, and E. C. Pattee, Geology and mineral resources of the northern part of the North Cascades National Park, Washington, Geol. Surv. Bull. 1359, 132 pp., U.S. Geol. Surv., Reston, Va, 1972.

Stoffel, K. S., Geologic map of the Republic 1:100,000-scale quadrangle, Washington, Open-File Report, Was. Div. Geol. and Earth Resources, Olympia, WA, In press.

Tabor, R. W. and W. M. Cady, Geologic map of the Olympic Peninsula, Washington, scale 1:125,000, Misc. Invest. Map I-994, U.S. Geol. Surv., Reston, Va, 1978.

Tabor, R. W., V. A. Frizzell, Jr., D. B. Booth, J. T. Whetten, R. B. Waitt, Jr., and R. E. Zartman, Preliminary geologic map of the Skykomish River 1:100,000 quadrangle, Washington, scale 1:100,000, 25 pp., Open-File Map OF-82-747, U.S. Geol. Surv., Reston, Va, 1982a.

Tabor, R. W., R. B. Waitt, Jr., V. A. Frizzell, Jr., D. A. Swanson, G. R. Byerly, and R. D. Bentley, Geologic map of the Wenatchee 1:100,000 quadrangle, central Washington, scale 1:100,000, Misc. Invest. Map I-1311, U.S. Geol. Surv., Reston, Va, 1982b.

Tabor, R. W., V. A. Frizzell, Jr., J. A. Vance, and C. W. Naeser, Ages and stratigraphy of lower and middle Tertiary sedimentary and volcanic rocks of the central Cascades, Washington: Application to the tectonic history of the Straight Creek Fault, Geol. Soc. Amer. Bull., 95, 26-44, 1984.

Taylor, S. B., S. Y. Johnson, G. T. Fraser, and J. W. Roberts, Sedimentation and tectonics of the lower and middle Eocene Swauk Formation in eastern Swauk Basin, central Cascades, central Washington, Can. J. Earth Sci., 25, 1020-1036, 1988.

Turner, D. L., V. A. Frizzell, Jr., D. M. Triplehorn, and C. W. Naeser, Radiometric dating of ash partings in coal of the Eocene Puget Group, Washington: Implications for paleobotanical stages, Geology, 11, 9, 527-531, 1983.

Vance, J. A., The geology of the Sauk River area in the northern Cascades of Washington, Ph.D. thesis, 312 pp., Univ. of Washington, Seattle, 1957.

Vance, J. A., Early and middle Cenozoic magmatism and tectonics, Cascade Mountains, Washington, EOS Trans. AGU, 58, 12, 1247, 1977.

Vance, J. A., Early and middle Cenozoic arc magmatism and tectonics in Washington state, Geol. Soc. Amer. Abstracts with Programs, 11, 132, 1979.

Vance, J. A., G. A. Clayton, J. M. Mattinson, and C. W. Naeser, Early and middle Cenozoic stratigraphy of the Mount Rainier-Tieton River area, southern Washington Cascades, in Selected Papers on the Geology of Washington, edited by J. E. Schuster, pp.269-290, Bulletin 77, Wash. Div. Geol. and Earth Resources, Olympia, Wash, 1987.

Vine, J. D., Geology and coal resources of the Cumberland, Hobart, and Maple Valley quadrangles, King County, Washington, Profess. Paper, 624, 67 p., U. S. Geol. Surv., Reston, Va., 1969.

Vokes, H. E., P. D. Snavely, Jr., and D. A. Myers, Geology of the southern and southwestern border area of the Willamette Valley, Oregon, Oil and Gas Invest. Map OM-110, U.S. Geol. Surv., Reston, Va, 1951.

Wagner, H. C., Preliminary geologic map of the Raymond quadrangle, Pacific County, Washington, scale 1:62,500, Open-file Map OF 67-265, U.S. Geol. Surv., Reston, Va., 1967.

Walsh, T. J. Geology and coal resources of central King County, Washington, 23 pp., Open-File Report 84-3, Wash. Div. Geol. and Earth Resources, Olympia, Wash, 1984.

Walsh, T. J. Geologic map of the Astoria and Ilwaco quadrangles, Washington and Oregon, scale 1:100,000, 28 pp., Open-File Report 87-2, Wash. Div. Geol. and Earth Resources, Olympia, Wash, 1987.

Walsh, T. J , M. A. Korosec, W. M. Phillips, R. L. Logan, and H. W. Schasse, Geologic map of Washington-southwest quadrant, scale 1:250,000, 28 pp., Geologic Map GM-34, Wash. Div. Geol. Earth Resources, Olympia, Wash., 1987.

Washington Public Power Supply System, Regional geologic map, fig. 2.5-2, Supply System Nuclear Project No. 3 Final Safety Analysis Report Vol. 2, 1981.

Weaver, C. E., Tertiary stratigraphy of western Washington and northwestern Oregon, Univ. Wash. Pub. in Geol., 4, 266 pp., 1937.

Wells, R. E., Geologic map of the Cape Disappointment-Naselle River area, Pacific County, Washington, scale 1:48,000, Open-File Report 79-389, U.S. Geol. Surv., Reston, Va, 1979.

Wells, R. E., Geologic map of the eastern Willapa Hills, Cowlitz, Lewis, Pacific, and Wahkiakum Counties, Washington, scale 1:62,500, Open-File Report 81-874, U.S. Geol. Surv., Reston, Va, 1981.

Wells, R. E., Geologic map of the Cape Disappointment-Naselle River area, Pacific and Wahkiakum Counties, Washington, Misc. Invest. Map I-1832, U.S. Geol. Surv., Reston, Va., in press.

Wells, R. E. and R. S. Coe, Paleomagnetism and geology of Eocene volcanic rocks of southwest Washington: Implications for mechanisms of tectonic rotation, J. Geophys. Res., 90, B2, 1925-1947, 1985.

Wells, R. E., D. C. Engebretson, P. D. Snavely, Jr., and R. S. Coe, Cenozoic plate motions and the volcano-tectonic environment of western Oregon and Washington, Tectonics, 3, 275-294, 1984.

Wells, R. E. and P. L. Heller, The relative contribution of accretion, shear, and extension to Cenozoic tectonic rotation in the Pacific Northwest, Geol. Soc. Amer. Bull., 100, 3, 325-338, 1988.

Wells, R. E., A. R. Niem, N. S. MacLeod, P. D. Snavely, Jr., and W. A. Niem, Preliminary geologic map of the west half of the Vancouver (Wa.-Ore.) 1 by 2 degree quadrangle, Oregon, scale 1:250,000, Open-File Map OF-83-591, U.S. Geol. Surv., Reston, Va, 1983.

Whetten, J. T., P. I. Carroll, H. D. Gower, E. H. Brown, and F. Pessl, Jr., Bedrock geologic map of the Port Townsend 30- by 60-minute quadrangle, Puget Sound region, Washington, scale 1:100,000, Misc. Invest. Map-1198-G, U.S. Geol. Surv., Reston, Va, 1988.

White, P. J., Geology of the Island Mountain area, Okanogan County, Washington, M.S. thesis, 80 pp., Univ. Washington, Seattle, 1986.

Wilkinson, W. D., W. D. Lowry, and E. M. Baldwin, Geology of the St. Helens quadrangle, Oregon, Bull. 31, 39 pp., Ore. Dept. Geol. Min. Industries, Portland, Ore, 1946.

Wolfe, E. W. and E. H. McKee, Geology of the Grays River quadrangle, Wahkiakum and Pacific Counties, Washington, scale 1:62,500, Geologic Map GM-4, Wash. Div. Geol. and Earth Resources, Olympia, Wash, 1968.

Wolfe, E. W. and E. H. McKee, Sedimentary and igneous rocks of the Grays River quadrangle, Washington, Geol. Surv. Bull. 1335, 70 pp, U.S. Geol. Surv., Reston, Va, 1972.

William M. Phillips and Timothy J. Walsh, Department of Natural Resources, Division of Geology and Earth Resources, M.S. PY-12, Olympia, WA 98504

Randy A. Hagen, Donald Herzog and Associates, Inc., 3000 Cleveland Ave., Suite 200, Santa Rosa, CA 95403

APPENDIX

Tables A1 and A2 on the following pages provide major and trace element data for Paleogene volcanic rocks of southwest Washington. Table A3 gives analytical and instrumental precision estimates for the analyses.

TABLE A1. Whole-rock geochemical analyses (wt. %) for Eocene and Oligocene volcanic rocks of southwestern Washington. Analyses by XRF, Department of Geology, Washington State University. All analyses normalized to 100% on a volatile-free basis with total iron (FeO*) expressed as FeO

Sample	Field Number	Sub-section	Sec	Twp	Rge	SiO_2	Al_2O_3	TiO_2	FeO*	MnO	CaO	MgO	K_2O	Na_2O	P_2O_5
	Crescent Formation														
1	RL19N5W2752	SE/4 SW/4	27	19	05W	49.20	14.96	2.71	13.02	0.21	11.62	5.64	-0.08	2.43	0.29
2	RL19N5W2727	CEN. NW/4	27	19	05W	49.48	15.05	2.29	12.58	0.19	11.85	6.19	-0.11	2.22	0.23
3	BP0630881	SE/4 NE/4	8	09	11W	52.10	15.25	2.71	10.28	0.18	8.75	3.84	0.83	5.28	0.77
4	BP0630886	NW/4 NE/4	16	09	10W	50.47	13.70	3.18	12.06	0.18	9.02	5.87	0.61	4.48	0.43
5	BP06298811	NW/4 NW/4	10	11	05W	48.29	16.46	2.66	11.24	0.19	10.33	6.48	0.40	3.64	0.31
6	BP06298813	SE/4 NE/4	15	11	05W	48.21	15.44	2.65	12.49	0.21	11.75	6.29	0.13	2.55	0.29
7	BP06298814	NE/4 NE/4	23	11	05W	48.94	15.02	2.38	11.06	0.18	11.70	7.52	0.38	2.57	0.25
8	BP0629885	SW/4 NW/4	14	12	05W	49.34	13.22	3.00	13.95	0.33	10.13	5.89	0.45	3.34	0.35
9	BP06298812	SW/4 NW/4	10	10	05W	47.99	14.99	2.47	12.00	0.19	11.72	7.47	0.39	2.49	0.28
10	BP0629889	NE/4 NE/4	33	12	05W	47.74	14.93	2.79	13.37	0.24	11.08	6.01	0.22	3.28	0.34
11	BP0629887	SW/4 SE/4	22	12	05W	48.90	13.68	2.83	13.61	0.24	11.12	6.12	0.26	2.89	0.33
12	BP0629884A	NE/4 NW/4	15	12	05W	48.80	13.90	2.69	12.85	0.27	10.99	6.67	0.55	2.98	0.31
13	JLVANDH3608	SW/4 NW/4	22	16	04W	49.63	14.54	2.14	11.75	0.18	11.99	7.28	0.27	1.99	0.20
14	BP06298810	SE/CORNER	33	12	05W	48.50	14.49	2.44	12.54	0.28	12.30	6.67	0.14	2.38	0.25
15	BP0629883	SW/4 SW/4	10	12	05W	49.59	14.11	2.53	12.48	0.23	11.56	6.29	0.36	2.58	0.27
16	BP0320863	NW/4 NE/4	3	16N	05W	49.45	14.72	2.12	11.33	0.17	12.67	7.16	0.12	2.04	0.20
	Sill at top of the Crescent Formation														
17	W-18-17**	NW/4 SW/4	17	11	04W	49.19	16.66	1.81	10.26	0.14	12.95	5.72	0.24	2.81	0.21
18	WR1**	SW/4 NE/4	28	21	08W	50.26	16.80	1.97	11.19	0.17	10.46	5.50	0.23	3.21	0.21
19	WR2**	NW/4 NW/4	36	21	08W	49.21	14.72	1.89	12.07	0.22	11.48	7.76	0.13	2.34	0.18
20	BP0629886	NE/4 NW/4	23	12	05W	49.20	15.95	2.22	11.91	0.22	11.64	5.78	0.38	2.46	0.24
21	BP0629888	SE/4 SW/4	7	12	05W	49.37	14.46	2.23	11.80	0.20	11.57	6.92	0.33	2.90	0.23
22	BP0629882	SW/4 SW/4	3	12	05W	49.31	14.34	2.19	12.15	0.23	12.51	6.43	0.12	2.48	0.23
	Grays River volcanics														
23	BP0529851	NW/4 NW/4	27	08	02W	48.74	15.25	3.04	14.15	0.22	9.72	5.98	0.19	2.45	0.27
24	BP0523856	SE/4 NW/4	26	10	04W	52.83	14.79	3.00	11.71	0.19	8.38	4.30	1.08	2.92	0.80
25	KK0626853	NW/4 NW/4	28	08	03W	49.90	14.56	2.81	12.47	0.18	10.45	6.51	0.35	2.31	0.45
26	BP0425851	SW/4 SE/4	19	09	02W	49.80	14.51	3.26	12.26	0.20	10.62	5.26	0.66	2.92	0.51
27	BP1204842	NW/4 NE/4	11	10	03W	49.31	14.77	3.18	12.68	0.17	10.14	6.14	0.48	2.71	0.41
28	BP0523859	NW/4 NW/4	13	09	04W	51.00	15.34	3.54	11.71	0.16	9.10	4.23	1.07	3.07	0.77
29	BP0710844	CENTER	9	10	02W	49.55	14.25	3.44	13.23	0.23	10.29	5.29	0.50	2.67	0.56
30	BP0523853	SE/4 SW/4	22	10	04W	49.08	15.96	3.28	12.62	0.21	9.85	4.97	0.65	2.64	0.74
31	BP0801851	SE/4 SE/4	3	10	06W	51.80	14.29	3.42	12.71	0.24	8.80	4.18	0.85	3.11	0.60
32	BP0109851	NW/4 SW/4	24	10	05W	53.33	14.38	3.33	11.98	0.20	8.24	3.45	1.20	3.21	0.68
33	BP0115853	NE/4	30	10	02W	49.42	14.90	2.73	11.70	0.18	11.43	6.24	0.45	2.59	0.35
34	BP0523855	NE/4 SW/4	21	10	04W	50.06	15.23	3.24	12.67	0.18	9.87	4.88	0.65	2.72	0.48
35	BP0523857	SW/4 NE/4	35	10	04W	48.78	17.54	2.92	11.17	0.19	11.21	4.50	0.42	2.75	0.51
36	BP0108851	SE/4 SW/4	25	08	03W	49.92	14.24	2.92	12.37	0.19	10.77	6.24	0.42	2.50	0.42
37	BP05238510	SE/4 SE/4	2	09	04W	50.13	14.73	3.23	13.45	0.20	9.59	4.94	0.72	2.58	0.43
38	BP1205842	SW/4 NW/4	1	10	03W	50.07	15.29	3.43	11.97	0.17	9.94	5.07	0.76	2.82	0.48
39	BP0523852	SE/4 NE/4	16	09	03W	55.69	14.75	2.22	12.12	0.23	6.35	3.19	1.47	3.21	0.78
40	TW0404851	NW/4 SW/4	6	07	04W	49.58	14.63	3.89	12.78	0.18	9.91	4.48	0.62	3.01	0.93
41	KK0626852	NW/4 SE/4	28	08	03W	51.87	14.06	3.53	12.90	0.20	9.00	4.55	0.72	2.54	0.62
42	BP0115851	CENTER	7	10	02W	52.05	15.01	3.46	10.44	0.15	9.96	4.65	0.68	2.90	0.66

** Sample from Rau, 1986

TABLE A1, continued

Sample	Field Number	Sub-section	Sec	Twp	Rge	SiO_2	Al_2O_3	TiO_2	FeO*	MnO	CaO	MgO	K_2O	Na_2O	P_2O_5
	Grays River volcanics, continued														
43	BP0710843	NE/4 NW/4	16	10	02W	50.85	14.64	3.38	12.48	0.19	9.44	5.33	0.54	2.56	0.59
44	BP0523858	NW/4 NE/4	35	10	04W	52.43	15.54	2.93	11.83	0.19	8.55	4.13	0.96	2.95	0.50
45	KK0626851	NW/4 NW/4	34	08	03W	50.66	13.84	3.41	13.30	0.20	9.52	5.39	0.57	2.50	0.60
46	BP0523854	NE/4 SW/4	21	10	04W	55.01	15.00	2.74	11.21	0.17	7.44	3.35	1.31	3.01	0.77
47	BP0412873	NW/4 NW/4	9	10	06W	52.58	15.44	3.07	11.10	0.24	7.77	3.27	1.62	4.17	0.73
48	BP0412876	SE/4 SE/4	4	10	06W	51.00	14.98	3.54	12.27	0.33	8.60	3.42	1.43	3.78	0.64
49	BP1205841	NW/4	9	10	02W	50.88	13.91	3.50	12.76	0.19	9.06	5.80	0.71	2.70	0.48
50	BP0412872	NE/4 SE/4	8	10	06W	52.40	15.00	2.91	11.79	0.17	8.26	3.69	1.23	3.75	0.79
51	BP0116851	NW/4	9	10	02W	49.79	13.29	3.23	12.72	0.19	10.03	6.74	0.69	2.67	0.65
52	BP0710844	CENTER	9	10	02W	49.56	14.25	3.44	13.23	0.23	10.29	5.29	0.50	2.67	0.56
53	BP0604851	CENTER SE/4	27	10	02W	50.63	14.03	3.80	13.34	0.20	9.36	4.78	0.49	2.86	0.51
54	BP0115852	NW/4	30	10	02W	49.96	15.29	3.51	12.06	0.18	10.32	4.63	0.88	2.67	0.50
55	BP0412871	NE/4 SE/4	8	10	06W	49.09	16.00	3.20	12.81	0.19	9.79	4.76	0.83	2.87	0.45
56	BP0412879	NW/4 NW/4	26	11	06W	50.47	15.02	3.20	12.72	0.22	9.76	4.20	0.85	3.09	0.46
57	BP0412874	SE/4 NW/4	10	10	06W	49.36	16.16	3.06	11.63	0.27	11.42	4.15	0.59	2.99	0.37
58	BP0412877	NW/4 SW/4	34	11	06W	50.99	15.09	3.62	11.65	0.22	10.14	3.44	0.88	3.42	0.51
59	BP0412875	NW/4 NW/4	10	10	06W	50.15	14.95	3.64	12.62	0.26	9.24	3.61	1.33	3.61	0.59
60	BP0710841	NE/4 NW/4	21	10	02W	50.82	14.67	3.80	12.95	0.19	9.09	4.61	0.74	2.68	0.47
61	BP0131851	NW/4 NW/4	17	07	02W	50.41	13.86	3.45	13.59	0.20	9.23	4.88	0.86	2.87	0.64
62	BP04128710	SW/4 SW/4	23	11	06W	49.40	16.86	2.70	11.42	0.16	10.85	4.60	0.69	2.97	0.35
63	BP0710842	CENTER	16	10	02W	50.78	14.64	3.67	12.92	0.19	8.86	5.19	0.69	2.63	0.43
64	BP04128711	SE/4 NE/4	27	11	06W	50.92	16.35	2.50	10.42	0.20	10.01	5.07	0.96	3.14	0.44
65	BP0412878	SE/4 NE/4	27	11	06W	48.46	15.64	3.32	12.46	0.27	11.16	4.59	0.69	2.98	0.42
66	BP04128712	SW/4 SW/4	34	11	06W	47.78	14.84	3.14	12.53	0.34	10.74	7.14	0.66	2.39	0.42
	Basalt at Fort Columbia														
67	BP0630883	SE/4 NW/4	21	09	10W	52.68	15.17	3.00	11.29	0.29	8.66	4.68	0.44	3.34	0.44
	Pe Ell Volcanic Member of the Cowlitz Formation of Henriksen [1976]														
68	BP0629881	NE/4 NW/4	4	12	05W	43.17	10.66	3.40	18.12	0.24	10.26	12.13	0.63	0.40	0.98
	Basalt of Summit Creek														
69	WLE030878005	SE/4	13	14	11E	58.82	16.08	1.26	8.70	0.16	6.57	4.31	0.00	3.90	0.19
70	WLE040878032	NW/4	7	14	11E	47.27	15.73	2.48	12.85	0.23	10.73	7.26	0.00	3.19	0.26
71	WLE060878001	SE/W	1	14	10E	52.00	16.80	1.02	8.20	0.18	12.66	6.22	0.00	2.83	0.10
72	WLE020878001	CENTER	13	14	10E	66.01	16.83	0.57	4.10	0.07	4.11	1.88	1.71	4.56	0.16
73	MK8882	NE/4 NW/4	8	14	11E	47.69	16.97	2.08	14.18	0.23	10.06	5.60	0.20	2.69	0.30
74	MK8881	SW/4 SW/4	7	14	11E	50.11	15.69	1.55	10.99	0.19	9.60	7.86	0.05	3.81	0.14
	Northcraft Formation														
75	HS0117851B	SE/4 NW/4	33	13	04E	57.09	16.45	1.31	8.12	0.13	8.26	4.95	0.45	2.93	0.30
76	HS0117854	CENTER	17	13	03E	58.56	18.22	1.22	7.27	0.12	7.51	3.10	0.82	2.91	0.25
77	HS0116854	CENTER	30	13	04E	55.06	17.81	1.34	8.57	0.15	8.67	4.54	0.71	2.93	0.23
78	CC0730853	NE/4 NE/4	18	13	03E	62.46	17.97	0.78	6.73	0.13	5.37	2.08	0.89	3.30	0.30
79	HS0117851A	SE/4 NW/4	33	13	04E	57.52	17.57	1.29	7.79	0.12	7.81	3.48	0.90	3.21	0.31
80	HS0116851	NW/4 NE/4	3	15	01W	59.10	15.86	1.59	8.57	0.13	6.88	3.11	1.17	3.28	0.31
81	HS1018835	NE/4 NW/4	7	18	06E	66.47	17.50	0.92	4.58	0.06	2.74	0.74	1.55	5.11	0.32
82	HS0116853	SW/4 NW/4	12	13	01E	56.06	16.88	1.43	9.98	0.15	7.96	3.61	0.47	3.24	0.22
83	HS0409851B	NW/4 NW/4	17	16	01E	58.40	16.27	1.47	9.36	0.17	6.65	3.11	0.73	3.53	0.29
84	CC0814852	NE/4 SW/4	13	14	04E	57.67	16.82	1.26	7.61	0.12	7.71	4.22	1.08	3.22	0.28
85	RH146-23	NW/4 SE/4	15	14	04E	59.67	17.78	0.92	7.11	0.13	6.94	3.09	0.53	3.63	0.19

TABLE A1, continued

Sample	Field Number	Sub-section	Sec	Twp	Rge	SiO_2	Al_2O_3	TiO_2	FeO*	MnO	CaO	MgO	K_2O	Na_2O	P_2O_5
	Northcraft Formation, continued														
86	RH163-16	CENTER	5	14	04E	60.05	18.03	0.83	6.71	0.12	6.64	2.91	1.02	3.48	0.20
87	RH172-25	SW/4 NW/4	13	14	03E	56.97	18.63	0.96	7.62	0.13	7.57	3.43	0.86	3.63	0.19
88	RH185-28B	SW/4 NW/4	32	14	03E	57.98	17.33	0.94	7.08	0.13	6.79	4.04	1.65	3.77	0.27
89	BP0330862	SW/CORNER	6	15	01E	61.39	16.15	1.47	7.45	0.16	5.49	2.49	0.91	4.17	0.31
90	RH185-80	SE/4 SE/4	33	14	03E	59.76	17.02	0.92	6.97	0.13	6.95	3.59	1.10	3.41	0.16
91	RH172-7B	SE/4 NW/4	23	14	03E	59.03	16.13	1.31	8.12	0.10	7.50	2.95	1.19	3.33	0.33
92	RH187-45	SW/4 NW/4	8	14	03E	54.08	18.92	1.53	8.84	0.15	9.16	3.59	0.15	3.23	0.35
93	RH170-34	NE/4 NW/4	9	14	03E	55.71	19.28	0.77	7.72	0.14	8.18	4.22	0.52	3.30	0.14
94	RH161-50A	NE/4 SE/4	13	14	03E	59.16	16.62	1.33	7.68	0.14	7.14	3.23	0.88	3.46	0.34
95	RH172-1A	NW/4 NW/4	24	14	03E	52.35	19.63	1.39	8.41	0.16	10.23	4.06	0.16	3.34	0.27
96	RH161-25	NE/4 NE/4	19	14	04E	53.41	19.37	0.95	7.52	0.13	9.97	4.75	0.35	3.37	0.17
97	RH148-3A	NE/4 NE/4	4	13	04E	56.37	18.19	1.43	8.61	0.15	7.74	3.11	0.82	3.36	0.22
98	RH187-13A	NE/4 SW/4	16	14	03E	52.53	18.91	1.08	8.12	0.13	10.45	5.24	0.13	3.19	0.22
99	RH170-2	SW/4 SW/4	11	14	03E	53.59	18.73	1.37	8.95	0.17	8.88	4.25	0.46	3.37	0.22
100	RH172-26	SW/4 NE/4	14	14	03E	53.59	18.94	1.02	8.14	0.13	10.00	4.45	0.21	3.36	0.16
101	BP0330861	NE/4 NW/4	18	15	01E	57.19	15.45	1.84	10.26	0.17	6.99	3.28	0.93	3.57	0.30
102	RH172-19	SW/4 NE/4	14	14	03E	51.19	18.80	1.30	9.08	0.22	10.29	5.42	0.24	3.20	0.26
103	RH172-20	SW/4 SE/4	15	14	03E	54.27	17.86	1.42	9.06	0.15	9.14	4.58	0.17	3.11	0.24
104	RH159-2	NW/4 NE/4	32	14	04E	52.25	19.09	1.09	8.41	0.14	10.68	4.96	0.12	3.09	0.16
105	RH170-30	NE/4 SE/4	9	14	03E	52.30	16.61	1.04	8.77	0.14	9.84	7.97	0.31	2.84	0.16
106	RH174-19	SW/4 SE/4	25	14	03E	52.26	18.96	1.08	8.52	0.14	10.37	5.07	0.32	3.11	0.16
	Goble Volcanics of Wilkinson et al.[1946]														
107	KKDI12	NW/4 NE/4	26	06	01W	58.06	15.62	1.77	9.93	0.16	7.10	3.12	0.81	3.14	0.29
108	BP0713841	S/2	2	05	01W	56.80	15.94	1.37	9.36	0.17	7.99	4.00	0.78	3.40	0.19
109	BP0402851	SE/4 NW/4	18	07	01W	54.94	15.99	2.09	11.19	0.18	7.59	3.39	0.76	3.53	0.33
110	BP0227853	CENTER	15	08	01W	55.54	17.67	1.35	8.48	0.16	8.47	4.37	0.55	3.13	0.28
111	BP0706842A	NE/4 SE/4	13	08	01W	52.79	16.68	1.69	9.19	0.17	9.38	6.91	0.39	2.53	0.28
112	BP0802845	SW/4 SE/4	35	07	01W	56.88	17.34	1.53	8.69	0.17	7.60	3.23	0.71	3.66	0.19
113	BP0227851	NE/4 SE/4	21	08	01W	55.83	16.98	1.61	9.57	0.15	7.86	3.75	0.72	3.26	0.27
114	BP0404851	CEN. NW/4	6	07	01W	56.47	16.98	1.91	9.66	0.15	7.20	2.86	0.83	3.59	0.34
115	BP0802841	CENTER	32	07	01W	54.78	17.20	1.20	8.35	0.13	9.31	5.03	0.50	3.21	0.27
116	BP0402852	SW/4 NE/4	18	07	01W	56.07	17.66	1.51	8.61	0.16	8.34	3.45	0.74	3.16	0.28
117	BP0402855	SE/4 SE/4	8	07	01W	52.48	15.62	1.84	12.30	0.22	9.08	4.46	0.96	2.76	0.26
118	BP0802846	SW/4	6	06	01E	56.14	17.01	1.68	9.53	0.16	7.49	3.12	0.86	3.72	0.29
119	BP0610852	SW/4 NE/4	26	07	02W	57.45	16.41	1.32	8.32	0.15	7.85	4.13	0.77	3.18	0.40
120	BP0712842	NW/4 SW/4	30	07	01W	54.02	16.14	1.73	9.71	0.16	9.06	4.97	0.57	3.10	0.52
121	KKDI8	NE/4 SE/4	34	06	01W	62.18	15.74	1.30	7.78	0.14	5.49	2.27	1.65	3.16	0.28
122	BP0403851	SW/4 NW/4	37	06	01W	55.11	17.42	1.04	8.61	0.15	9.39	4.62	0.54	2.90	0.20
123	BP0814851	SW/4 SE/4	15	08	03E	55.99	16.51	1.58	9.25	0.15	8.45	4.08	0.50	3.17	0.31
124	BP0802842	NW/4 SW/4	33	07	01W	55.23	17.04	1.25	8.21	0.14	9.17	5.10	0.51	3.11	0.25
125	KKDI10	NE/4 SW/4	12	06	01W	55.40	17.44	1.03	7.92	0.14	8.92	5.38	0.81	2.73	0.21
126	BP0814852	SW/4	15	08	03E	58.28	15.92	2.13	9.33	0.19	6.51	2.98	0.82	3.31	0.51
127	BP0711847	NW/4 NW/4	30	07	01W	53.41	16.73	1.53	8.72	0.15	9.97	5.20	0.60	3.24	0.43
128	BP0404852	SE/4 NE/4	19	07	01W	51.48	16.59	1.16	9.21	0.15	9.91	8.33	0.15	2.81	0.20
129	KKDI9	NE/4 SW/4	12	06	01W	54.74	17.00	1.28	9.06	0.15	9.20	4.91	0.58	2.84	0.23
130	BP0712845	SW/4 SW/4	8	06	01W	56.06	16.91	1.11	9.02	0.13	8.80	3.92	0.59	3.27	0.18
131	BP0610851	SW/4 SE/4	15	07	02W	52.13	17.94	1.20	9.06	0.12	10.11	6.22	0.26	2.77	0.19
132	BP0712844A	E/2 SE/4	7	06	01W	53.09	18.46	0.96	8.23	0.16	10.77	4.58	0.43	3.15	0.15
	Hatchet Mountain Formation														
133	BP1004842	SW/4 SE/4	16	10	01W	59.31	16.24	1.12	7.55	0.14	6.95	3.63	1.40	3.43	0.22
134	KK0628851	SE/4 SE/4	1	11	03E	58.93	17.13	1.14	7.16	0.17	7.30	3.86	1.04	3.02	0.24

TABLE A1, continued

Sample	Field Number	Sub-section	Sec	Twp	Rge	SiO_2	Al_2O_3	TiO_2	FeO*	MnO	CaO	MgO	K_2O	Na_2O	P_2O_5
	Hatchet Mountain Formation, continued														
135	KK0703852	NE/4 NE/4	8	11	04E	57.48	17.41	1.22	7.85	0.12	7.49	4.16	1.12	2.86	0.27
136	BP1004841	SE/4	36	10	02W	52.56	15.78	1.99	12.45	0.20	8.51	4.02	0.58	3.61	0.28
137	KK0627852A	NW/4 NW/4	9	11	03E	58.91	17.08	1.43	8.22	0.15	6.71	2.68	1.11	3.40	0.30
138	BP0117855C	SW/4	13	09	02W	53.67	17.73	1.02	8.18	0.15	11.16	5.12	0.14	2.65	0.18
139	KK0619853	SE/4 NW/4	30	11	03E	60.78	16.08	1.45	8.02	0.14	5.63	3.06	1.98	2.57	0.28
140	BP0710846A	N/2	25	11	02W	55.03	16.16	2.19	9.39	0.18	8.25	3.88	0.70	3.74	0.48
141	BP0706845	NE/4	11	10	01E	57.49	17.77	1.40	7.57	0.16	7.13	3.58	1.29	3.35	0.26
142	KK0628855	SW/4 NW/4	4	11	04E	60.63	16.40	1.08	7.08	0.14	6.69	3.41	1.26	3.06	0.25
143	BP0117855A	SW/4	13	09	02W	49.78	16.50	1.87	11.15	0.17	12.19	5.26	0.18	2.69	0.20
144	KK0705852	NE/4 NW/4	32	11	03E	57.08	17.47	1.47	8.09	0.15	7.78	3.43	1.01	3.21	0.30
145	BP0117854	NE/4 SW/4	13	09	02W	52.95	17.69	1.08	8.86	0.15	10.84	5.25	0.23	2.79	0.15
	Oligocene-Eocene volcanic rocks, undivided														
146	HS0117856	CENTER	3	12	04E	55.60	15.91	2.02	10.37	0.17	7.81	4.25	0.77	2.76	0.32
147	MK85611	SW/4 NE/4	21	12	05E	63.51	19.11	1.10	3.71	0.12	6.76	1.08	0.57	3.80	0.24
148	HS0515853	NE/4 NE/4	17	12	05E	61.18	15.75	1.34	7.96	0.13	5.72	2.80	1.28	3.44	0.40
149	TW0619850	SE/4 SE/4	7	15	05E	64.00	17.02	1.03	5.40	0.10	5.15	1.72	2.27	2.94	0.35
150	HS0514851	NW/CORNER	29	12N	02E	55.16	16.10	2.06	10.73	0.17	7.94	3.45	0.87	3.12	0.38
151	HS06198510	CENTER	3	16	05E	55.68	17.44	1.09	7.94	0.13	7.35	6.48	0.72	2.92	0.24
152	HS1220843	NW/4 SW/4	10	12	03E	53.21	19.81	1.12	7.66	0.14	9.94	4.41	0.32	3.16	0.23
153	BP0710851	NE/4 NE/4	27	12	04E	54.12	17.49	1.63	9.53	0.15	8.69	4.63	0.61	2.87	0.27
154	HS0515852	SE/4 NW/4	5	12	05E	62.74	15.87	1.37	7.81	0.15	4.50	1.85	1.65	3.57	0.49
155	CC0712852	CENTER	11	16	05E	66.27	13.86	0.84	5.27	0.11	5.02	2.54	2.65	3.14	0.30
156	TW061885B	SW/4 NW/4	35	16	05E	60.76	17.79	0.79	5.85	0.10	7.12	3.38	1.16	2.87	0.17
157	HS0823841	CENTER	21	12	05E	56.02	20.82	1.22	7.96	0.07	6.12	2.41	0.72	4.43	0.22
158	HS1002841	NE/4 SW/4	12	12	03E	58.03	18.57	1.23	7.15	0.11	6.67	2.85	1.13	4.01	0.24
159	HS1220842	SW/4 SW/4	7	12	03E	56.79	15.93	1.97	9.91	0.20	7.06	3.30	0.98	3.45	0.42
160	HS1220844	CENTER	4	11	03E	58.24	15.93	1.79	9.15	0.15	6.59	3.07	1.23	3.51	0.35
161	HS0514852B	NW/4 NW/4	9	12	03E	52.52	17.82	1.61	9.13	0.17	9.86	5.24	0.53	2.77	0.33
162	HS0618858	NE/4 SW/4	2	16	05E	56.98	18.48	1.33	7.84	0.12	7.91	3.01	0.88	3.20	0.25
163	HS0117859	NE/4 NE/4	7	12	04E	56.73	18.02	1.57	8.19	0.14	7.06	3.36	1.44	3.16	0.34
164	HS0514853	CENTER	10	12	03E	56.47	17.77	1.83	8.71	0.14	7.68	3.01	0.82	3.19	0.36
	Oligocene volcanic rocks, undivided														
165	MK98415	SW/4 NW/4	12	11	08E	56.42	17.02	1.27	8.64	0.13	8.71	4.23	0.36	3.00	0.21
166	MK8558	NW/4 SW/4	21	04	08E	55.66	16.61	1.35	9.78	0.18	8.12	4.39	0.50	3.24	0.18
167	MK85524	NW/4 SW/4	21	05	07E	58.39	16.76	1.36	9.15	0.15	7.81	2.95	0.38	2.79	0.25
168	MK98422	NW/4 NW/4	11	11	09E	56.59	17.00	1.23	8.72	0.14	7.77	4.67	0.66	3.00	0.22
169	BP0814854	NW/4	24	08	03E	58.35	16.00	1.22	8.19	0.16	7.55	4.28	1.06	2.93	0.25
170	BP0604853	SW/4 NW/4	15	10	02E	59.85	16.12	1.18	8.40	0.15	6.49	3.37	1.21	2.97	0.27
171	MK8586	SW/4 SW/4	35	07	06E	53.19	18.27	1.54	9.77	0.16	8.94	4.39	0.61	2.87	0.25
172	MK162831	NW/4 SE/4	2	10	04E	64.01	16.03	1.22	6.29	0.09	5.37	2.35	1.49	2.88	0.28
173	MK85531	SW/4 SW/4	6	05	07E	58.21	17.37	1.27	8.41	0.17	7.26	3.09	1.37	2.62	0.23
174	MK232831	NW/4 SE/4	2	10	04E	55.83	16.96	1.41	8.77	0.15	8.74	4.28	0.82	2.84	0.21
175	MK98416	NW/4 SW/4	7	11	09E	58.33	17.64	1.33	8.63	0.14	7.42	2.56	0.60	3.11	0.24
176	MK85675	SW/4 NW/4	29	11	04E	63.75	16.51	0.92	5.86	0.09	4.95	2.32	2.11	3.32	0.16
177	MK8584	NE/4 SE/4	25	06	06E	55.09	16.96	1.31	9.87	0.19	8.64	4.28	0.59	2.83	0.23
178	MK8589	SE/4	4	09	02E	61.03	16.22	1.14	7.26	0.11	6.43	3.32	1.36	2.93	0.20
179	MK85526	SW/4 NE/4	6	05	07E	61.55	17.08	1.16	8.42	0.12	5.09	2.08	1.65	2.61	0.24
180	MK85525	N/2 SW/4	17	05	07E	55.83	17.54	1.34	8.52	0.16	8.91	4.01	0.68	2.69	0.32
181	MK85544	NW/4 NE/4	5	04	08E	54.71	15.61	1.60	11.08	0.18	8.75	4.69	0.48	2.69	0.20
182	BP0117861	SW/4	43	06	01E	57.73	15.90	1.65	9.37	0.15	7.24	3.43	0.90	3.36	0.27
183	BP0814856	SE/4 NE/4	7	08	04E	53.63	16.92	1.08	9.24	0.14	9.53	6.47	0.24	2.58	0.16
184	BP0619851	CENTER	10	10	04E	55.25	16.13	1.06	8.32	0.15	9.16	6.45	0.86	2.44	0.18

TABLE A1, continued

Sample	Field Number	Sub-section	Sec	Twp	Rge	SiO_2	Al_2O_3	TiO_2	FeO*	MnO	CaO	MgO	K_2O	Na_2O	P_2O_5
	Oligocene volcanic rocks, undivided, continued														
185	MK85610	SE/4 NE/4	21	12	05E	57.47	17.20	1.21	7.95	0.15	7.92	3.83	1.08	2.89	0.28
186	MK382831	NW/4 SE/4	2	10	04E	60.81	17.19	1.17	6.98	0.14	5.54	3.11	1.65	3.21	0.21
187	BP0117853	SE/CORNER	43	05	01E	60.80	15.99	1.43	7.78	0.15	6.65	2.66	0.84	3.45	0.26
188	KK0904855	NE/4 SE/4	3	03	04E	54.51	15.89	1.64	11.69	0.18	8.68	4.09	0.24	2.92	0.16
189	MK85532	NW/4 NW/4	17	05	07E	64.65	16.50	0.77	7.37	0.13	4.31	1.29	2.27	2.46	0.25
190	MK85723	SW/4 NW/4	21	12	08E	58.86	18.05	1.52	9.60	0.17	5.30	2.63	0.43	3.32	0.11
191	BP1003842	CENTER	35	10	01E	50.00	16.56	1.50	10.26	0.21	10.50	7.70	0.40	2.61	0.25
192	BP0816851	SW/4 NW/4	7	05	05E	52.11	17.39	1.07	9.70	0.17	10.44	5.92	0.30	2.75	0.14
193	BP0317861	CENTER	32	05	01E	57.56	16.86	1.72	9.24	0.17	6.80	3.28	1.14	2.97	0.26
194	MM0903851	SW/4	28	02	04E	52.98	15.35	1.92	13.10	0.21	8.60	4.34	0.46	2.81	0.23

TABLE A2. Trace element data (ppm) for Eocene and Oligocene volcanic rocks. All analyses by XRF, Department of Geology, Washington State University. See Table A1 for location of samples and major oxide analyses

Sample	Field Number	NI	CR	SC	V	BA	RB	SR	ZR	Y	NB	GA	CU	ZN
	Crescent Formation													
3	BP0630881	3	13	26	163	276	11	606	301	47	57.8	20	47	137
4	BP0630886	38	58	27	326	200	10	308	234	30	50.2	20	91	120
5	BP06298811	47	11	32	318	94	6	320	186	25	35.2	19	56	98
6	BP06298813	61	100	37	360	20	3	326	174	30	20.1	22	208	112
7	BP06298814	107	279	37	334	91	3	278	150	27	19.2	23	254	133
8	BP0629885	39	92	39	400	111	7	180	199	43	24.2	22	242	132
9	BP06298812	60	127	39	333	85	2	300	164	25	28.4	18	109	91
10	BP0629889	45	97	39	392	33	3	336	196	37	21.8	23	210	113
11	BP0629887	52	99	39	362	25	5	205	191	39	21.6	19	218	117
12	BP0629884A	55	168	40	374	109	5	210	172	37	20.6	20	195	113
13	JLVANDH3608	72	243	41	345	74	6	231	137	29	11.0	20	140	89
14	BP06298810	63	167	41	363	45	1	223	154	34	18.5	20	22	112
15	BP0629883	54	142	43	384	58	5	209	167	37	17.9	22	229	116
16	BP0320863	69	215	44	346	60	1	257	135	29	12.0	19	129	89
	Sill at top of the Crescent Formation													
20	BP0629886	40	127	39	382	45	6	238	145	30	15.6	22	239	104
21	BP0629888	62	196	41	365	31	5	190	135	31	14.2	19	208	104
22	BP0629882	42	144	46	383	29	1	209	140	32	11.8	21	178	102
	Grays River volcanics													
47	BP0412873	0	2	21	200	389	28	545	359	44	77.0	26	28	133
48	BP0412876	0	4	23	232	353	30	539	323	46	74.0	28	19	131
49	BP1205841	62	95	23	320	185	14	431	230	36	35.0	23	38	125
50	BP0412872	9	18	24	194	304	24	441	332	49	62.0	27	32	127
51	BP0116851	110	180	26	328	193	10	423	239	36	40.0	20	57	139
52	BP0710844	30	59	28	305	176	12	470	227	37	35.0	25	35	114
53	BP0604851	14	25	28	311	193	13	468	245	36	38.0	25	77	168
54	BP0115852	59	77	28	367	251	20	539	264	36	44.0	26	55	125
55	BP0412871	65	58	28	286	197	17	469	232	29	46.0	23	121	123
56	BP0412879	20	33	28	336	234	13	397	234	36	46.0	21	75	123
57	BP0412874	35	73	28	315	196	4	452	201	33	37.0	22	94	122
58	BP0412877	10	12	29	323	262	12	442	259	38	51.0	24	40	129
59	BP0412875	0	4	29	260	347	24	544	309	40	68.0	28	30	136
60	BP0710841	9	33	29	305	209	16	530	248	38	38.0	26	16	129
61	BP0131851	32	43	30	339	250	22	458	284	41	48.0	24	61	150
62	BP04128710	35	59	30	292	151	13	422	184	29	33.0	22	102	110
63	BP0710842	24	51	31	321	228	14	467	234	35	37.0	22	27	121
64	BP04128711	63	137	31	234	250	19	418	237	35	44.0	21	85	113
65	BP0412878	61	69	31	334	210	8	468	220	32	43.0	24	98	127
66	BP04128712	167	375	33	302	182	11	451	209	29	38.0	22	84	109
	Basalt at Fort Columbia													
67	BP0630883	2	11	27	284	308	10	479	271	45	43.2	23	42	137
	Pe Ell Volcanics Member of the Cowlitz Formation of Henriksen [1956]													
68	BP0629881	79	176	21	175	83	9	202	307	32	90.7	22	55	149

TABLE A2, continued

Sample	Field Number	NI	CR	SC	V	BA	RB	SR	ZR	Y	NB	GA	CU	ZN
	Basalt of Summit Creek													
73	MK8882	52	69	34	307	67	2	179	151	39	15.4	23	163	121
74	MK8881	72	273	39	302	127	2	423	100	27	7.9	19	96	79
	Northcraft Formation													
85	RH146-23	28	18	15	135	324	58	408	150	23	n.d.	n.d.	n.d	n.d.
86	RH163-16	23	11	16	117	286	21	472	168	19	n.d.	n.d.	n.d.	n.d.
87	RH172-25	36	48	17	134	229	14	471	157	17	n.d.	n.d.	n.d.	n.d.
88	RH185-28B	35	36	19	174	418	23	886	201	17	n.d.	n.d.	n.d.	n.d.
89	BP0330862	0	0	19	141	236	19	390	179	28	16.0	22	63	97
90	RH185-80	40	58	19	134	249	18	516	203	16	n.d.	n.d.	n.d.	n.d.
91	RH172-7B	29	27	21	147	280	21	397	221	22	n.d.	n.d.	n.d.	n.d.
92	RH187-45	27	20	21	173	146	1	474	197	17	n.d.	n.d.	n.d.	n.d.
93	RH170-34	40	42	21	136	205	15	458	113	15	n.d.	n.d.	n.d.	n.d.
94	RH161-50A	31	26	22	156	314	27	457	225	24	n.d.	n.d.	n.d.	n.d.
95	RH172-1A	37	53	23	190	146	3	505	165	20	n.d.	n.d.	n.d.	n.d.
96	RH161-25	48	71	24	174	130	4	483	126	17	n.d.	n.d.	n.d.	n.d.
97	RH148-3A	10	13	25	281	289	21	465	160	22	n.d.	n.d.	n.d.	n.d.
98	RH187-13A	68	110	25	187	110	1	487	139	14	n.d.	n.d.	n.d.	n.d.
99	RH170-2	26	14	25	211	172	6	438	153	19	n.d.	n.d.	n.d.	n.d.
100	RH172-26	40	27	26	191	109	n.d.	434	105	14	n.d.	n.d.	n.d.	n.d.
101	BP0330861	5	7	27	305	266	17	351	197	29	15.0	23	213	113
102	RH172-19	57	61	27	200	138	7	415	148	20	n.d.	n.d.	n.d.	n.d.
103	RH172-20	42	61	27	201	151	1	388	158	19	n.d.	n.d.	n.d.	n.d.
104	RH159-2	36	36	28	199	96	4	390	106	17	n.d.	n.d.	n.d.	n.d.
105	RH170-30	160	271	28	184	107	5	345	102	16	n.d.	n.d.	n.d.	n.d.
106	RH174-19	40	36	29	186	106	6	375	101	17	n.d.	n.d.	n.d.	n.d.
	Goble Volcanics of Wilkinson et al.[1946]													
131	BP0610851	109	173	28	201	94	3	403	111	19	9.0	17	135	108
132	BP0712844A	53	116	30	218	100	10	390	88	17	5.0	20	389	231
	Hatchet Mountain Formation													
133	BP1004842	43	62	23	117	286	32	379	207	25	13.0	16	230	156

n.d. Element not determined

TABLE A3. Instrumental and total analytical precision for major oxide and trace element XRF analyses (P. R. Hooper and D. Johnson, Washington State University, written communication, 1987)

Element	Instrumental** Precision		Total Analytical** Precision	
	1#	2##	1#	2##
SiO_2 %	0.650	0.26	0.660	0.070
Al_2O_3 %	0.310	0.08	0.410	0.06
TiO_2 %	0.040	0.028	0.050	0.010
FeO* %	0.300	0.44	0.350	0.06
MnO %	0.003	0.004	0.010	<0.002
CaO %	0.100	0.06	0.220	0.02
MgO %	0.180	0.06	0.150	0.02
K_2O %	0.020	0.02	0.030	<0.02
Na_2O %	0.150	0.10	0.160	0.04
P_2O_5 %	0.010	0.008	0.014	0.0032
Ni ppm	n.d.	2.0	n.d.	1.3
Cr ppm	n.d.	5.3	n.d.	5.7
Sc ppm	n.d.	2.7	n.d.	4.2
V ppm	n.d.	10.0	n.d.	6.4
Ba ppm	n.d.	16.2	n.d.	18.3
Rb ppm	n.d.	1.3	n.d.	0.9
Sr ppm	n.d.	4.0	n.d.	1.4
Zr ppm	n.d.	2.1	n.d.	0.9
Y ppm	n.d.	1.2	n.d.	0.9
Nb ppm	n.d.	0.8	n.d.	0.7
Ga ppm	n.d.	1.3	n.d.	0.9
Cu ppm	n.d.	2.3	n.d.	5.0
Zn ppm	n.d.	5.7	n.d.	2.6

* Total iron as FeO
** Two standard deviations from the mean
# Analyses made prior to 1987 on Philips spectrometer
Analyses made on Rigaku spectrometer; replicate analyses of international standard BCRP-84 used in calculating statistics

THE COLUMBIA RIVER BASALT GROUP IN THE CASCADE RANGE: A MIDDLE MIOCENE REFERENCE DATUM FOR STRUCTURAL ANALYSIS

Marvin H. Beeson and Terry L. Tolan

Geology Department, Portland State University, Portland, Oregon

Abstract. Flows of the Columbia River Basalt Group (CRBG) encroached upon the Cascade Range in northern Oregon via a northeast-trending topographic low, the Columbia Trans-Arc Lowland, that extended across the volcanic arc in Miocene time. The first CRBG flows that crossed the Cascade Range, approximately 16 Ma ago, recorded the width of this low from the present-day Columbia River Gorge southward 60 km to the Clackamas River area. For the next million years the succeeding CRBG flows filled developing synclinal lows and generally built up a nearly horizontal layer of areally extensive flows approximately 600 m thick. This thick sequence of CRBG flows forms a datum that is useful for evaluating deformatation of the northern Oregon Cascade Range. At ~15.2 Ma, ~14.5 Ma, and ~12 Ma intracanyon flows of the Ginkgo basalt of the Frenchman Springs Member, the Rosalia basalt of the Priest Rapids Member, and the Pomona Member respectively, recorded ancestral Columbia River channels that extended across the Cascade Range.

The distributional patterns of individual CRBG units and structures recorded in the CRBG place the following constraints on Neogene tectonics of the northern Oregon Cascade Range:

1) A northeast-trending topographic low of regional extent, the Columbia Trans-Arc Lowland, transected the Miocene northern Oregon Cascade Range. The Columbia Trans-Arc Lowland existed prior to the eruption of the CRBG and served to funnel CRBG flows across the Miocene Cascade Range. The lowland was apparently devoid of active volcanic centers from before 17 to ~14.5 Ma. After 15 Ma, volcanic centers began to emerge in the southern and central parts of the lowland.

2) Folds and associated faults of the Yakima Fold Belt extend from the western Columbia Plateau far into the Cascade Range. These structures began to develop, under a N-S stress regime, by ~16 Ma and continued to grow till at least 8 Ma. Evidence for post-8 Ma growth on these structures is sketchy and poorly constrained.

3) The Portland Hills - Clackamas River structural zone is a northwest-trending dextral wrench fault zone that had developed prior to the incursion of CRBG flows (~16 Ma). This structural zone appears to mark the western termination of the Yakima Fold Belt. Other similarly trending, dextral strike-slip faults are common in the northern Oregon Cascades, but did not affect the distribution of CRBG flows and therefore developed in post-CRBG time.

4) Mount Hood is located near the axis of a major Yakima Fold syncline in the CRBG. This same location was the site of major andesitic volcanic activity related to the Rhododendron Formation.

Erosional and depositional features of the ancestral

Columbia River provide another set of reference data for structural analysis that is unique to the northern Oregon Cascade Range. The ancestral Columbia River is assumed to have maintained a channel that was very close to sea level, except when interrupted by catastrophic volcanic or landslide events. Channels preserved by intracanyon flows and sediment deposited by the ancestral Columbia River indicate an extended history of subsidence until approximately 2 to 3 Ma ago when rapid uplift of the northern Oregon Cascade Range occurred causing the Columbia River to incise its present gorge. Total uplift is approximately 700 to 1000 m.

The CRBG is a unique reference layer in the Cascade Range that allows a relatively detailed structural history of this part of the range to be developed. However, the northern Oregon Cascade Range may be more important for its uniqueness than for its similarity with the rest of the volcanic arc.

INTRODUCTION

The flood basalt flows of the Columbia River Basalt Group (CRBG) that were erupted from fissure systems in northeastern Oregon, eastern Washington, and western Idaho covered approximately 160,000 km^2 of Oregon, Washington, and Idaho during the Miocene Epoch (17 - 6 Ma)[Tolan et al., in press]. During the peak period of CRBG eruptive activity (16 to 14 Ma) voluminous flows (>1,000 km^3) were commonly produced. These voluminous flows (termed "Great Flows" by Tolan et al., in press] extended into western Oregon and Washington through a topographic lowland in the Cascade Range [Beeson et al., in press](Figure 1). These huge flows are thought to have flowed westward toward the Pacific Coast at very low gradients (~1 m/km) [Anderson and Vogt, 1987] and to a first approximation can be considered to have initially formed a horizontal surface across the Cascade Range.

The CRBG in the northern Oregon Cascade Range is unique as a reference datum for evaluating the Neogene deformational history of the Cascade Range. We know of no other rock layer in the Cascade Range that is either as continuous across the range or known to be as originally horizontal as the CRBG. Advancing CRBG flows naturally followed topographic lows that existed as a result of structural deformation or that were produced by erosion and flowed around or overwhelmed topographic highs produced by tectonic deformation or constructional volcanism. CRBG flows thereby preserved a record of the pre-emplacement topography and ground conditions. The emplacement of each voluminous CRBG flow tended to inundate and bury existing topography and essentially create an areally extensive, relatively flat plain. The areally extensive and relatively flat CRBG flow tops provided a series of reference surfaces to determine later folding, faulting, or uplift. Therefore, the CRBG is a reference datum that can be used in determining the nature, age, and history of major structural features in the northern Oregon Cascade Range. In addition, it also provides data on the age relationships of Cascadian volcanism and the

regional tectonic evolution of this area.

STRATIGRAPHIC SETTING

A brief description of each stratigraphic unit present in the northern Oregon Cascade Range (Figure 2) area is given in Table 1. For a more complete discussion of each of these units see papers referenced in Table 1.

Most of the exposed pre-CRBG units in the northern Oregon Cascade Range were basically produced by Cascadian arc volcanism. These pre-CRBG formations are shown on Figure 2 and briefly described in Table 1.

The CRBG is the most distinctive and extensive formation in the northern Oregon Cascade Range, but is not directly related genetically to the Cascadian volcanic arc. The CRBG flows were erupted from fissures in the eastern part of the Columbia Plateau and are only present in the Cascade Range (Figure 3) because of gravity flow through a lowland that extended across the arc (Figure 1). Only the Prineville basalt (Figure 3), interfingered with the Grande Ronde Basalt, was probably erupted adjacent to the east side of the Cascade Range. The CRBG is also the only stratigraphic unit exposed in the Cascade Range that has been divided into a number of readily identifiable layers (see Table 2) making it most suitable for use in detailed structural analysis [Tolan et al., in press; Beeson et al., 1985, in press].

The units lying stratigraphically above the CRBG (Figure 2 and Table 1) are products of Cascadian volcanism or are deposits of the ancestral Columbia River that has a long history (more than 15 m.y.) of flowing across the Cascade arc. The ancestral Columbia River sediments (Troutdale Formation (Figure 2 and Table 1) in the Cascade Range and Portland Basin) are helpful in analyzing the structural history of the Cascade Range because they were deposited by the ancestral Columbia River when it was graded to near sealevel.

THE STRUCTURAL HISTORY OF THE CASCADE RANGE IN NORTHERN OREGON

Structural Setting - 17 to 12 Ma

The CRBG flows crossed the Cascade Range in Northern Oregon because it was a topographic low in the volcanic arc. We think this low, the Columbia Trans-Arc Lowland [Beeson et al., in press] was structural in origin. The width of this lowland across the Cascades is approximately 60 km, as defined by the CRBG distribution (Figure 1) from the present-day Columbia River Gorge southward to the Clackamas River. The lowland seems to extend beyond the Cascade Range both east (toward the Pasco Basin) and west (slightly offset dextrally along the northwest-trending Portland Hills - Clackamas River structural zone). These extensions are based on much greater than normal CRBG thicknesses along these zones. There is even a low in the Coast Range at the southwest extension of the Columbia Trans-Arc Lowland that probably allowed early CRBG flows (Figure 3) to

flow to the central Oregon coast.

It seems that the Columbia Trans-Arc Lowland was a regional structure that exerted considerable control on the distribution of CRBG flows from the Columbia Plateau to the Oregon Coast (Figure 3). Its origin was probably not related to the development of the Cascade volcanic arc, but conversely was a regional structure that affected the development and growth of the volcanic arc in this area.

When the first CRBG flows approached the Cascade Range, approximately 16.5 Ma ago, there were no active volcanic centers in the Columbia Trans-Arc Lowland [Beeson and Moran, 1979b; Vogt, 1981; Tolan, 1982; Priest et al., 1982]. During this period, it appears that volcanic activity occurred only south of, or much farther north of this lowland [Anderson, 1978; Hammond, 1979; Smith, 1987]. However by about 14.5 Ma, volcanic centers began to emerge within the southern portion of the lowland [Anderson, 1978; Priest, 1982; Hammond, 1979; Tolan and Beeson, 1984]. It is interesting to note that this apparent hiatus in volcanic activity within the lowland corresponds to the same period that the entire lowland was experiencing its greatest rates of subsidence. We suspect that this hiatus in Cascadian volcanic activity began prior to the emplacement of the CRBG flows since they appear to rest unconformably on volcanic rocks where seen along the northern margin of the lowland [Swanson et al., 1979a, 1981; Tolan, 1980, unpublished mapping; Anderson, 1987]. Isotopic age determinations that have been reported on some of these older Cascadian rocks suggest that they are late Oligocene to early Miocene in age [Phillips et al., 1986]. This information would incidate that the eruptive hiatus, in at least the northern portion of the lowland, certainly lasted much longer than just two m.y. - perhaps it lasted as long as 7 m.y.

It is important that there was a hiatus in Cascadian volcanic activity during the period when the earliest CRBG flows advanced through this lowland. The very fact that no major accumulations of volcaniclastic debris/sediment, as well as major constructional volcanic edifices, are found within this area means that the advancing CRBG flows encountered a relatively obstacle-free pathway through the Miocene Cascade Range.

Within the Columbia Trans-Arc Lowland, the CRBG and younger units are deformed by a series of regional structures (Figure 4). Table 3 lists some of the major structural features that occur in this region and briefly describes their chief characteristics.

Mapping of individual CRBG units through the Cascade Range shows that the thickness and distribution of most of these units were influenced by developing northeast-trending folds that represent a western extension of the Yakima Fold Belt (Figure 4 and Table 3). Where data are available, most units show thinning over the anticlines. Two major synclines, the Mount Hood and the Bull Run (Figure 4), exerted considerable control on the path of CRBG flows (Figure 3) and on the positions where the ancestral Columbia River developed canyons (Figure 4) that

later channeled CRBG flows through the Cascades.

The Portland Hills - Clackamas River structural zone (Table 3) is a northwest-trending zone characterized by dip-slip and dextral strike-slip faults that greatly affected the distribution of CRBG flows. Several CRBG units (some R_2 Grande Ronde units, the Prineville Basalt, and all but one Sand Hollow flow; Figure 3) did not make it past this zone and into the Willamette Valley area. The total CRBG thickness decreases from ~550 m to ~150 m across this structural zone.

Structural Development - 12 Ma to present

The Yakima Fold Belt folds that showed evidence of developing during the CRBG incursion continued to grow in post-CRBG time. Two major synclines, the Mount Hood and the Bull Run synclines (Figure 4), accumulated volcaniclastic and epiclastic sediments of the Rhododendron Formation (Figure 2 and Table 1) that give us an indication of the amount of structural relief that developed from about 15 Ma to 10 Ma. The Mount Hood syncline, in particular, contains at least 1000 m of Rhododendron rocks while the adjacent Bull Run anticline, to the north, accumulated none and is capped by younger lava flows. The Bull Run syncline contains less than one-third the thickness of Rhododendron Formation that the Mount Hood syncline does. In order for these sediments to accumulate, the synclinal lows must have been subsiding so that the sediment was deposited close to sea level. Continued growth of the Yakima Fold Belt structures in the Cascade Range resulted in the development of large thrust faults associated with the anticlines. A major thrust fault was mapped on the Bull Run anticline [Vogt, 1981; Figure 5]. Thrust faults have also been found in the Salmon River area [Burck, 1986] and in Eagle Creek drainage [Beeson et al., 1985, in press] south of the Columbia River Gorge.

The northwest-trending dextral-slip faults also continued to be active in post-CRBG time. The Portland Hills - Clackamas River structural zone (Figure 4 and Table 3) presently displays en echelon faults in the Clackamas River area and faulted anticlines and a pull-apart basin in the Portland area (Figure 4 and Table 3).

In addition to those structures that continued their development, some new structures became evident in post-CRBG time. These structures seem to have developed in the last several million years and may be genetically related to each other. The largest of these structures is the uplift or upwarp of the Cascade Range that has tilted the CRBG away from the axis of the range in both directions, and has also resulted in pre-CRBG rocks being exposed along the Columbia River Gorge in the center of the range. Apparently associated with the broad upwarping of the Cascade Range was north-south faulting and graben formation along much of the axis of the Cascades in northern Oregon. The Hood River fault zone (Figure 4) is the eastern part of such a graben that has has displaced or deformed young lava flows (<3.7 Ma). Other near N-S trending fractures were the sites of magma intrusions forming basaltic dikes.

DISCUSSION AND CONCLUSIONS

The CRBG has recorded considerable deformation of the northern Oregon Cascade Range in the past 16 Ma. The nature and timing of this deformation is fairly complex and not yet completely understood, but some generalizations can be made.

First, the CRBG occurs in the Cascade Range because there was a wide, topographic low (the Columbia Trans-Arc Lowland) that transected the range. This low does not seem to be directly related to the volcanic arc, but rather was an existing regional cross structure (Figure 1 and Table 3) that the Cascade Range was superimposed upon. There were no active volcanic centers within the lowland from ~16.5 to ~14.5 Ma. The duration of this hiatus in Cascadian volcanic activity was at least 2 m.y., but evidence suggests that it may have begun 5 m.y. prior to the incursion of the CRBG. After 14.5 Ma, volcanic centers began to emerge within the southern and central part of the lowland.

During the CRBG emplacement and for 4 or 5 m.y. thereafter, the dominant deformation is consistent with stress applied from the north and south or in a dextral wrench couple. This same stress field has apparently existed for at least the last 17 m.y. [Davis, 1981]. Yakima Fold Belt structures (Figure 4 and Table 3) developed under this stress regime within the Columbia Trans-Arc Lowland. Northwest-trending, dextral fault systems, like the Portland Hills - Clackamas River structural zone, were also active at the same time. Significant north-south shortening must have occurred across the Columbia Trans-Arc Lowland during this time, perhaps as much as 10%.

Cascadian volcanic activity seems to have been largely absent from northern Oregon until after most of the CRBG flows had been emplaced. Rhododendron volcaniclastic sediments, and minor lava flows, may be interbedded with the uppermost CRBG flows under Mount Hood [Priest et al., 1982] and culminated approximately 8 to 10 Ma ago with the intrusion of Laurel Hill Pluton in the vicinity of Mount Hood [Priest et al., 1982; Keith et al., 1985]. Volcanic activity has occurred fairly steadily in the site of Mount Hood syncline from CRBG time to the present [Priest, 1982; Priest et al., 1982].

The last major deformational event in the northern Oregon Cascades was the upwarping of the northern Oregon Cascade Range in the past 2 to 3 Ma. This uplift is apparent from the attitude of the CRBG on both flanks of the Cascades and from the position of Columbia River-deposited Troutdale sediments and also the younger basaltic lavas that have formed hyaloclastite deposits by interaction with the river (Figure 6). High Cascades basaltic lavas were erupted from north-south dikes reflecting an apparent east-west extension of the area.

We have reviewed our CRBG and other data in an attempt to evaluate the history of vertical movements in the northern Oregon Cascade Range in the past 16 million years. The data are complicated by the fact that the CRBG has been strongly folded by north-south compression (Yakima Fold Belt structures) and the present elevation of a mappable unit is a result of regional

vertical movement plus local deformation. Nevertheless, a general idea can be obtained of the broader, regional vertical movements from these data. Several lines of evidence indicate that the Cascade Range in northern Oregon was generally subsiding up until the last 2 or 3 m.y., when it began to rapidly uplift.

The chronology of vertical movement is as follows:

1) The presence of the Columbia Trans-Arc Lowland suggests that the northern Oregon Miocene Cascades was subsiding when the CRBG flows first crossed this area.

2) Although the emplacement of approximately 1500 to 550 m of CRBG across the Cascades represents a buildup of the land, isostatic adjustments would result in depression of the crust (subsidence).

3) When the Rosalia intracanyon flow (Figure 2 and Table 2) filled up the ancestral Columbia River channel, the canyon was up to 300 m deep based on the thickness of the Priest Rapids intracanyon flow in the Bull Run Watershed and at Crown Point. If the CRBG were 600 m-thick and the base of the canyon close to sea level, then nearly 300 m of subsidence had occurred from 16 to 14.5 Ma.

4) The Pomona intracanyon flow (12 Ma)(Figure 2 and Table 2) also filled a canyon that was cut at least to present-day sea level in the western Columbia River Gorge at Bridal Veil (Figure 6). Gravel deposits beneath the Pomona intracanyon flow at Mitchell Point [Anderson and Vogt, 1987] indicates subsidence had depressed the bottom of that channel to near, or below, sea level by that time.

5) After the Pomona flow partially filled the Bridal Veil channel, the ancestral Columbia River first re-incised and then aggraded its channel (Fig 6). By 10 Ma, two Rhododendron lahars were emplaced in this channel (Figure 7). Aggradation continued until this channel was finally covered by high-Alumina basalts and basaltic andesites of the High Cascade Lavas (Figure 2, Table 1). We assume that a stream the size of the ancestral Columbia River could only deposit an accumulation of sediments if it had cut its channel to near sea level.

6) Uplift of the northern Oregon Cascade Range is indicated by sediments of the Troutdale Formation (deposited by the ancestral Columbia River while near sea level) and the Rhododendron Formation (also probably deposited near sea level) that are now exposed approximately 1000 m above sea level. High Cascade Lavas on Benson Plateau (south of Bonneville Dam) that formed hyaloclastite by interaction with the ancestral Columbia River are also now almost 1000 m above sea level. The oldest radiometric date on lava flows of this type is 3.67 Ma on those involved with the pillow complex west of Hood River, Oregon [James L. Anderson, 1986, personal communication]. Most other dates on Boring Lavas group at from 1 to 3 Ma.

The magnitude of the uplift in northern Oregon in the past 2 or 3 Ma is about 1000 m based on these observations. In addition, the top of the Rosalia intracanyon flow is approximately 670 m higher in the center of the Cascade Range at Bull Run (Figure 4) than it is near Moiser, Oregon on the

eastern flank of the range. Since the Priest Rapids intracanyon flow was largely confined to a syncline the effects of local uplift/subsidence due to folding are relatively minor. If we use the Rosalia flow as a reference horizon, it suggests the center of the Cascades has been uplifted approximately 700 m. Therefore the uplift recorded by the Rosalia flow reflects regional, Cascadian uplift. By the same reasoning and approach, the uplift recorded by the Troutdale Formation in the Cascade Range is almost 1000 m. However, the Troutdale Formation has been uplifted almost 250 m in the Portland Basin area to the west of the Cascades, leaving approximately 750 m of net uplift. Therefore, the uplift of the Cascade Range may be superimposed on a more extensive regional uplift perhaps related to the North American plate overriding the very young and buoyant Juan de Fuca plate.

Thus, the magnitude of Cascadian uplift can be deduced from the CRBG, but the timing is based on the younger deposits of Troutdale Formation and High Cascades/Boring Lavas. However, there are other evidences that corroberate a late uplift of the Cascade Range in northern Oregon that relates to the incision of the Columbia River into its present gorge. Recent radiometric dates on the Wind Mountain and Shellrock Mountain plutons show that they were emplaced around 5 or 6 Ma [Beeson and Tolan, 1985 unpublished data; Phillips et al., 1986]. Their emplacement certainly preceded the incision of the Columbia River Gorge that deeply exposed them. Also, a very recent date on Bonney Rock, a diabasic intrusion at Bonneville Dam, Oregon, shows that it was emplaced approximately 3 Ma ago. Therefore, some or all of the incision of the Columbia River Gorge was post 3 Ma. The Columbia River probably first occupied its present location when forced from the Bridal Veil channel 2 or 3 Ma ago [Tolan and Beeson, 1984].

In conclusion, the CRBG aids greatly in understanding the tectonic history of the northern Oregon Cascade Range. We have thus far made no attempt to compare the structural history of this portion of the Cascades to adjacent segments and do not suggest that the history of the northern Oregon Cascade Range should apply to the Cascade Range in general. The CRBG exists in this part of the Cascade Range because of a unique structural low, the Columbia Trans-Arc Lowland [Beeson et al., in press], that extended across the volcanic arc in middle Miocene time. The structural history of this part of the Cascades may therefore not be representative of the Cascade Range as a whole, but the differences that may exist should also be important to the understanding of the nature and history of the Cascade Range.

REFERENCES

Anderson, J.L., The stratigraphy and structure of the Columbia River basalt in the Clackamas River drainage, M.S. thesis, Portland State Univ., Portland, Oreg., 1978.

Anderson, J.L., Pomona Member of the Columbia River Basalt Group: an intracanyon flow in the Columbia River Gorge, Oregon, Oreg. Geol., 42, 195-199, 1980.

Anderson, J.L., The structure and ages of deformation of a portion of the southwest Columbia Plateau, Washington and Oregon, Ph.D. dissertation, Univ. of S. Calif., Los Angles, 1987.

Anderson, J.L. and Vogt, B.F., Intracanyon flows on the Columbia River Basalt Group in the southwest part of the Columbia Plateau and adjacent Cascade Range of Oregon and Washington, in Selected papers on the geology of Washington, Bull. 77, edited by J.E. Schuster, pp. 249-267, Wash. State Div. of Geol. and Earth Res.. Olympia, Wash., 1987.

Beeson, M.H., Johnson, A.G., and Moran, M.R., Portland environmental geology - fault identification, Open file report submitted to the U.S. Geological Survey, 1975.

Beeson, M.H., and Moran, M.R., Columbia River Basalt Group stratigraphy in western Oregon, Oreg. Geol., 41, 11-14, 1979a.

Beeson, M.H., and Moran, M.R., Stratigraphy and structure of the Columbia River Basalt Group in the Cascade Range, Oregon, in Geothermal resource assessment of Mount Hood, Oreg. Open-File Rept. O-79-8, edited by J.F. Riccio, pp. 5-77, Dept. of Geol. and Min. Ind., Portland, Oregon, 1979b.

Beeson, M.H., Moran, M.R., Anderson, J.L., and Vogt, B.F., The relationship of the Columbia River Basalt Group to the geothermal potential of Mount Hood area, Oregon, in Geology and geothermal resources of the Mount Hood area, Special Paper 14, edited by G.R. Priest and B.F. Vogt, pp. 43-46, Oreg. Dept. of Geol. and Min. Ind., Portland, Oreg., 1982.

Beeson, M.H., Fecht, K.R., Reidel, S.P., and Tolan, T.L., Regional correlations within the Frenchman Springs Member of the Columbia River Basalt Group: new insights into the middle Miocene tectonics of northwestern Oregon, Oreg. Geol., 47, 87-96, 1985.

Beeson, M.H., Tolan, T.L., and Anderson, J.L., The Columbia River Basalt Group in western Oregon: geologic structures and other factors that controlled flow emplacement patterns, in Volcanism and Tectonism of the Columbia River Basalt Province, Geol. Soc. Am. Special Paper, edited by S.P. Reidel and P.R. Hooper, in press.

Beeson, M.H., Tolan, T.L., Duncan, R.A., and Johnson, A.G., The Waverly Heights Formation: Late Eocene-age basalt flows in the Portland, Oregon, area, in prep.

Burck, M.S., The stratigraphy and structure of the Columbia River Basalt Group in the Salmon River area, Oregon, M.S. thesis, Portland State Univ., Portland, Oreg., 1986.

Carlin, R.A., A Geochemical study of the Eagle Creek Formation in the Columbia River Gorge, Oregon, M.S. thesis, Portland State Univ., Portland, Oreg., 1988.
Davis, G.A., Late Cenozoic tectonics of the Pacific Northwest with special reference to the Columbia Platuea, WPPSS Nucl. Proj. 2, Subappendix 2.5N, FSAR, Amend. 18, 49pp., 1981.
Hammond, P.E., A tectonic model for evolution of the Cascade Range, in Cenozoic paleogegraphy of the western United States, edited by J.M. Armentrout, M.R. Cole, and H. Terbest, Jr., pp. 219-237, Pacific Section, Society of Economic Paleontologists and Mineralogists, Los Angles, Calif., 1979.
Hammond, P.E., Reconnaissance geologic map and cross sections of southern Washington Cascade Range, Portland State Univ. publication, Portland, Oreg. 31 pp., 1980.
Hoffman, C.W., A stratigraphic and geochemical investigation of ferruginous bauxite deposits in the Salem Hills, Marion County, Oregon, M.S. thesis, Portland State University, Portland, Oregon, 1981.
Keith, T.E.C., Donnelly-Nolan, J.M., Markman, J.L., and Beeson, M.H., K-Ar ages of rocks in the Mount Hood area, Oregon, Isochron/West, 42, 12-16, 1985.
Phillips, W.M., Korosec, M.A., Schasse, H.W., Anderson, J.L., and Hagen, R.A., K-Ar ages of volcanic rocks in southwest Washington, Isochron/West, 47, 18-24, 1986.
Priest, G.R., Overview of the geology and geothermal resources of the Mount Hood area, Oregon, in Geology and geothermal resources of the Mount Hood area, Oregon, Special Paper 14, edited by G.R. Priest and B.F. Vogt, pp. 6-15. Oreg. Dept. of Geol. and Min. Ind., Portland, Oreg., 1982.
Priest, G.R., Beeson, M.H., Gannett, M.W., and Berri, D.A., Geology, geochemistry, and geothermal resources of the Old Maid Flat area, Oregon, in Geology and geothermal resources of the Mount Hood area, Oregon, Special Paper 14, edited by G.R. Priest and B.F. Vogt, pp. 43-46, Oreg. Dept. of Geol. and Min. Ind., Portland, Oreg., 1982.
Reidel, S.P. and Fecht, K.R., Wanapum and Saddle Mountains Basalt of the Cold Creek Syncline area, in Subsurface geology of the Cold Creek Syncline, RHO-BWI-ST-14, edited by C.W. Myers and S.W. Price, pp. 3.1-3.45, Rockwell Hanford Operations, Richland, Wash., 1981.
Reidel, S.P., Tolan, T.L., Hooper, P.R., Beeson, M.H., Fecht, K.R., Bentley, R.D., and Anderson, J.L., The Grande Ronde Basalt, Columbia River Basalt Group: stratigraphic descriptions and correlations in Washington, Oregon, and Idaho, in Volcanism and Tectonism of the Columbia River Basalt Province, edited by S.P. Reidel and P.R. Hooper, Geol. Soc. Am. Special Paper, in press.
Smith, G.A., Stratigraphy and sedimentology, and petrology of Neogene rocks in the Deschutes Basin, central Oregon: a record of continental-margin volcanism and its influence on fluvial sedimentation in an arc-adjacent basin, Rockwell Hanford Operations Report RHO-SA-555P, Richland, Wash., 260 pp., 1986.

Smith, G.A., Sedimentology of volcanism-induced aggradation in fluvial basins: examples from the Pacific Northwest, U.S.A., in Recent Developments in Fluvial Sedimentology, Special Publications 39, edited by F.G. Ethridge, R.M. Flores, and M.A. Harvey, pp. 217-228, Soc. of Economic Paleontologists and Mineralogists, Los Angles, Calif., 1987.

Snavely, P.S., Jr., MacLeod, N.S., and Wagner, H.C., Miocene tholeiitic basalts of coastal Oregon and Washington and their relations to coeval basalt of the Columbia Plateau, Geol. Soc. Am. Bull., 84, 387-424, 1973,.

Swanson, D.A., Anderson J.L., Bentley, R.D., Byerly, G.R., Camp, V.E., Gardner, J.N., and Wright, T.L., Reconnaissance geologic map of the Columbia River Basalt Group in eastern Washington and northern Idaho, U.S. Geological Survey Open-File Report 79-1363, scale 1:250,000, 1979a.

Swanson, D.A., Wright, T.L., Hooper, P.R., and Bentley, R.D., 1979, Revisions in stratigraphic nomenclature of the Columbia River Basalt Group: U.S. Geological Survey Bulletin 1457-G. 59 p.

Swanson, D.A., Anderson, J.L., Camp, V.E., Hooper, P.R., Taubeneck, W.H., and Wright, T.L., Reconnaissance geologic map of the Columbia River Basalt Group, northern Oregon and western Idaho, U.S. Geological Survey Open-File Report 81-797, scale 1:250,000, 1981.

Swanson, R.D., A stratigraphic-geochemical study of the Troutdale Formation and Sandy River Mudstone in the Portland Basin and lower Columbia River Gorge, M.S. Thesis, Portland State Univ., Portland, Oreg., 1986.

Tolan, T.L., The stratigraphic relationships of the Columbia River Basalt Group in the lower Columbia River Gorge of Oregon and Washington, M.S. thesis, Portland State Univ., Portland, Oreg., 1982.

Tolan, T.L., and Beeson, M.H., Intracanyon flows of the Columbia River Basalt Group in the lower Columbia River Gorge and their relationship to the Troutdale Formation, Geol. Soc. Am. Bull., 95, 463-477, 1984.

Tolan, T.L., Beeson, M.H., and Vogt, B.F., Exploring the Neogene history of the Columbia River: Discussion and geologic field trip guide to the Columbia River Gorge, Part I, Discussion, Oreg. Geol., 46, 87-97, 1984a.

Tolan, T.L., Beeson, M.H., and Vogt, B.F., Exploring the Neogene history of the Columbia River: Discussion and geologic field trip guide to the Columbia River Gorge, Part II, Road log and comments, Oreg. Geol., 46, 103-112, 1984b.

Tolan, T.L., Reidel, S.P., Beeson, M.H., Fecht, K.R., Anderson, J.L., and Swanson, D.A., Revisions to the estimates of the areal extent and volume of the Columbia River Basalt Group, in Volcanism and Tectonism of the Columbia River Basalt Province, edited by S.P. Reidel and P.R. Hooper, Geol. Soc. Am. Special Paper, in press.

Trimble, D.E., Geology of Portland, Oregon and adjacent areas, U.S. Geol. Sur. Bull. 1119, 119 pp., 1963.

Vance, J.A., Clayton, G.A., Mattinson, J.M., and Naeser, C.W., Early and middle Cenozoic stratigraphy of the Mount Rainier-Tieton River area, southern Washington Cascades, in Selected papers on the geology of Washington, Bulletin 77, edited by J.E. Schuster, pp. 269-290, Wash. State Div. Geol. and Earth Res., Olympia, Wash., 1987.

Vogt, B.F., The stratigraphy and structure of the Columbia River Basalt Group in the Bull Run Watershed, Oregon, M.S. thesis, Portland State Univ., Portland, Oreg., 1981.

Walsh, T.J., Korosec, M.A., Phillips, W.M., Logan, R,L., and Schasse, H.W., Geologic map of Washington-southwest quadrant, Geologic Map GM-34, Wash. Div. Geol. and Earth Res., Olympia, Wash., 28 pp., scale 1:250,000, 1987.

Wise, W.S., Cenozoic volcanism in the Cascade Mountains of southern Washington, Bulletin No. 60, Wash. State Div. Mines and Geol., 45 pp., 1970.

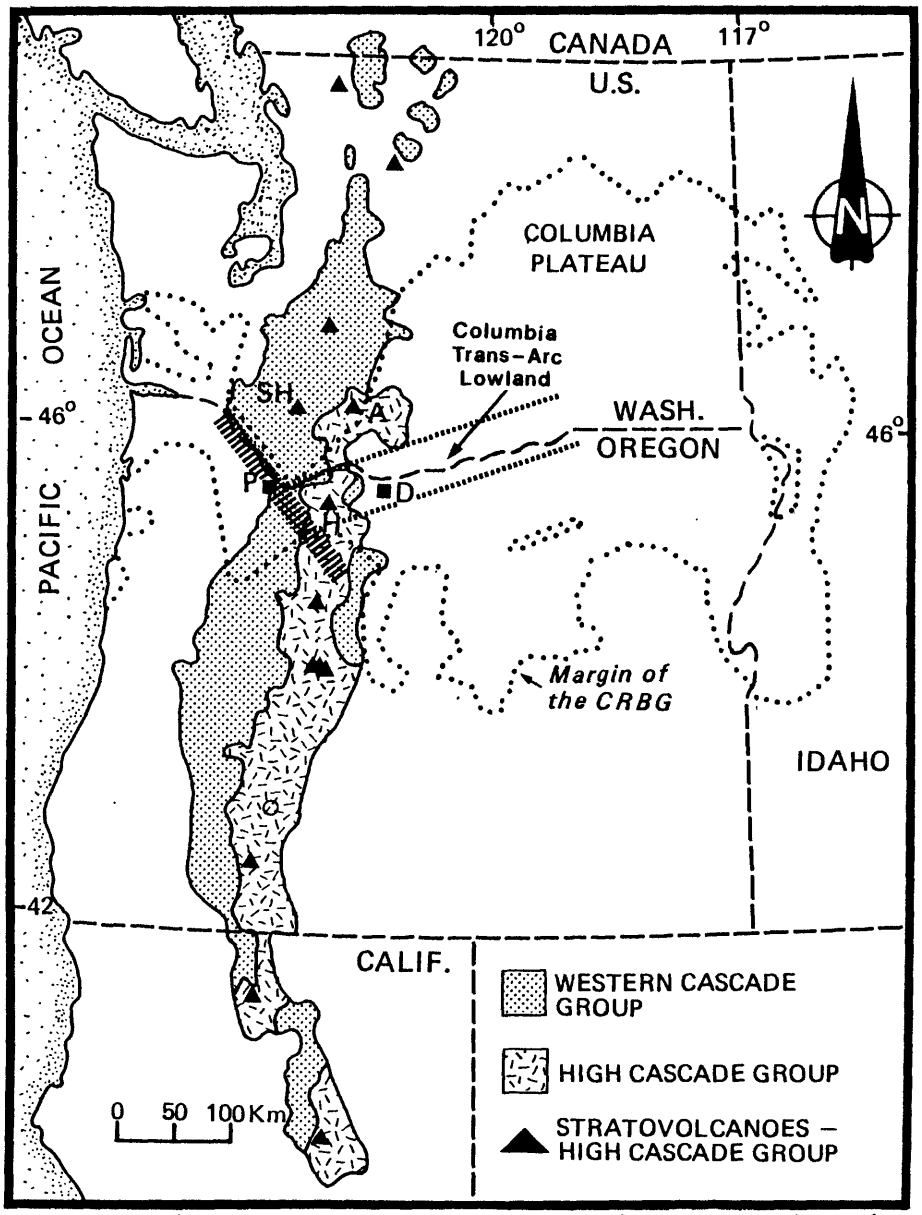

Fig. 1. Generalized sketch map showing the distribution of Western Cacade, High Cascade, and Columbia River Basalt Groups as modified after Hammond [1979] and Tolan et al. [in press]. The northern Oregon Cascade Range is transected by two major regional structures that predate the CRBG: 1) the northeast-trending Columbia Trans-Arc Lowland, and 2) the northwest-trending Portland Hills - Clackamas River structural zone (heavy hachured line). The Columbia Trans-Arc Lowland was a paleo-low that transected the Miocene Cascade Range and allowed CRBG to enter western Oregon and Washington. The Portland Hills - Clackamas River structural zone is a broad, dextral wrench fault system that bounds the lowland on the west, but some evidence suggests that the Columbia Trans-Arc Lowland extended farther to the southwest [Beeson et al., in press]. P, Portland; D, The Dalles; H, Mount Hood; A, Mount Adams, SH, Mount St. Helens.

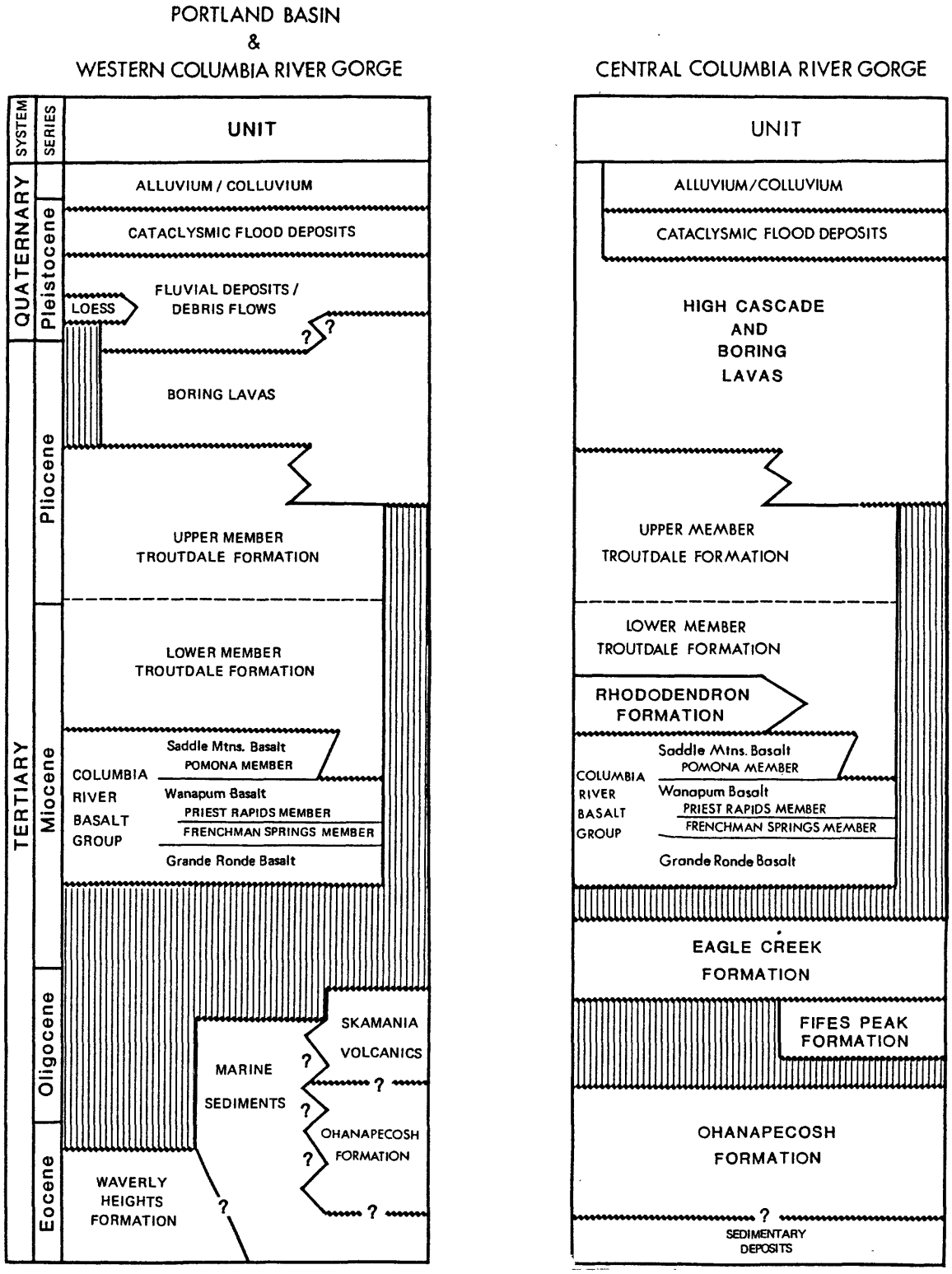

Fig. 2. Generalized stratigraphy of the Portland Basin - Columbia River Gorge area. See Table 1 for descriptions of units.

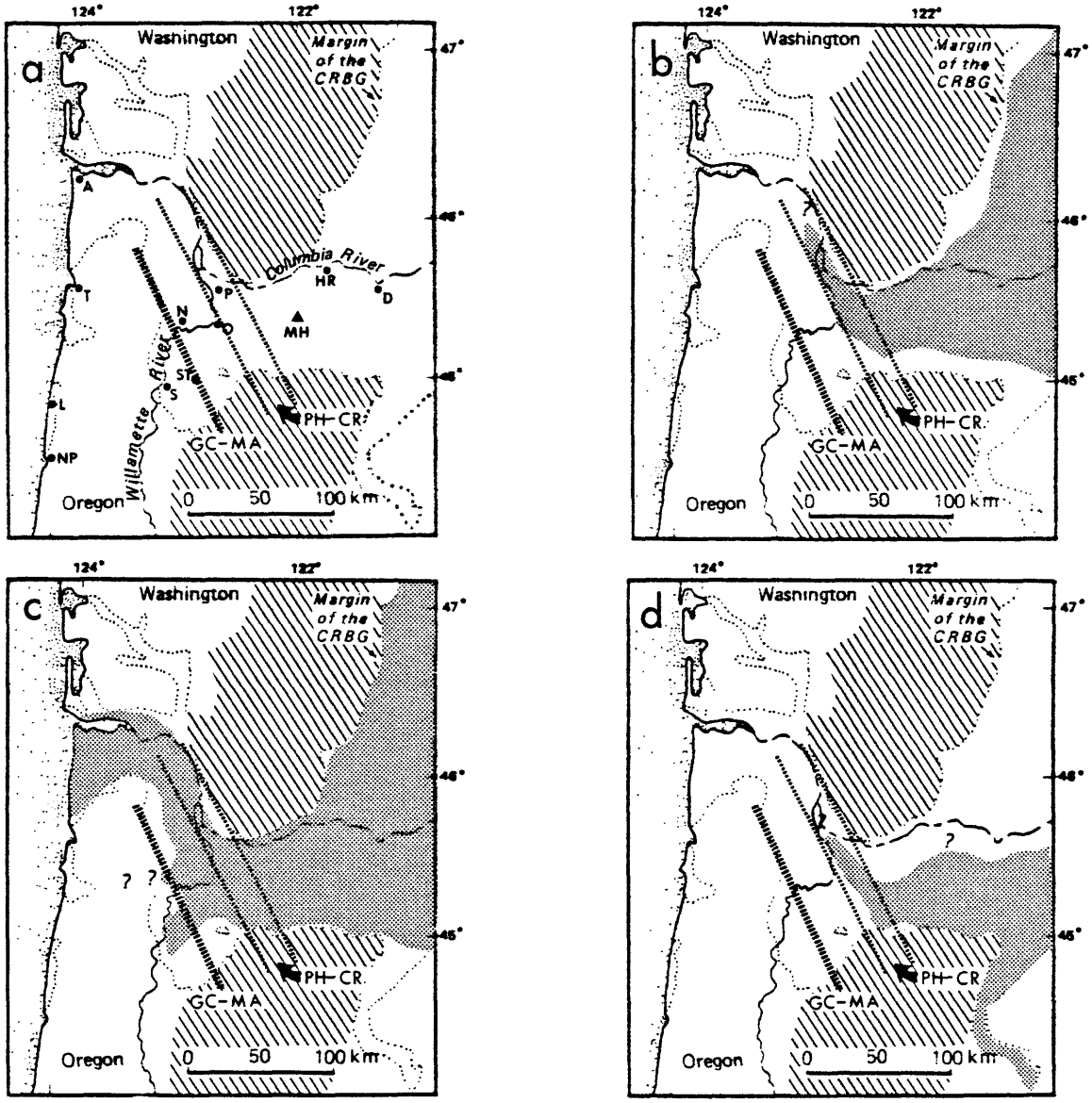

Fig. 3. Distribution maps of CRBG units in western Oregon and Washington. a) Base map showing cities and geographic features for location reference. P, Portland; D, The Dalles; HR, Hood River; O, Oregon City; N, Newberg; ST, Silverton; S, Salem; NP, Newport; L, Lincoln City; T, Tillamook; A, Astoria; MH, Mount Hood; GC-MA, Gales Creek - Mount Angel structural zone; PH-CR, Portland Hills - Clackamas River structural zone. b) N_1 Grande Ronde Basalt. c) R_2 Grande Ronde Basalt. d) Prineville basalt. e) N_2 Grande Ronde Basalt. Dashed lines show inferred path across Coast Range. f) Basalt of Ginkgo. Dashed line shows inferred path across Coast Range. g) Basalt of Silver Falls. Only one of three flows that entered the Willamette Valley area crosses the GC-MA structural zone. h) Basalt of Sand Hollow. Only one of five flows crosses the PH-CR structural zone in the southern lobe. i) Basalt of Sentinel Gap. j) Basalt of Lyons Ferry. k) Priest Rapids Member. l) Pomona Member.

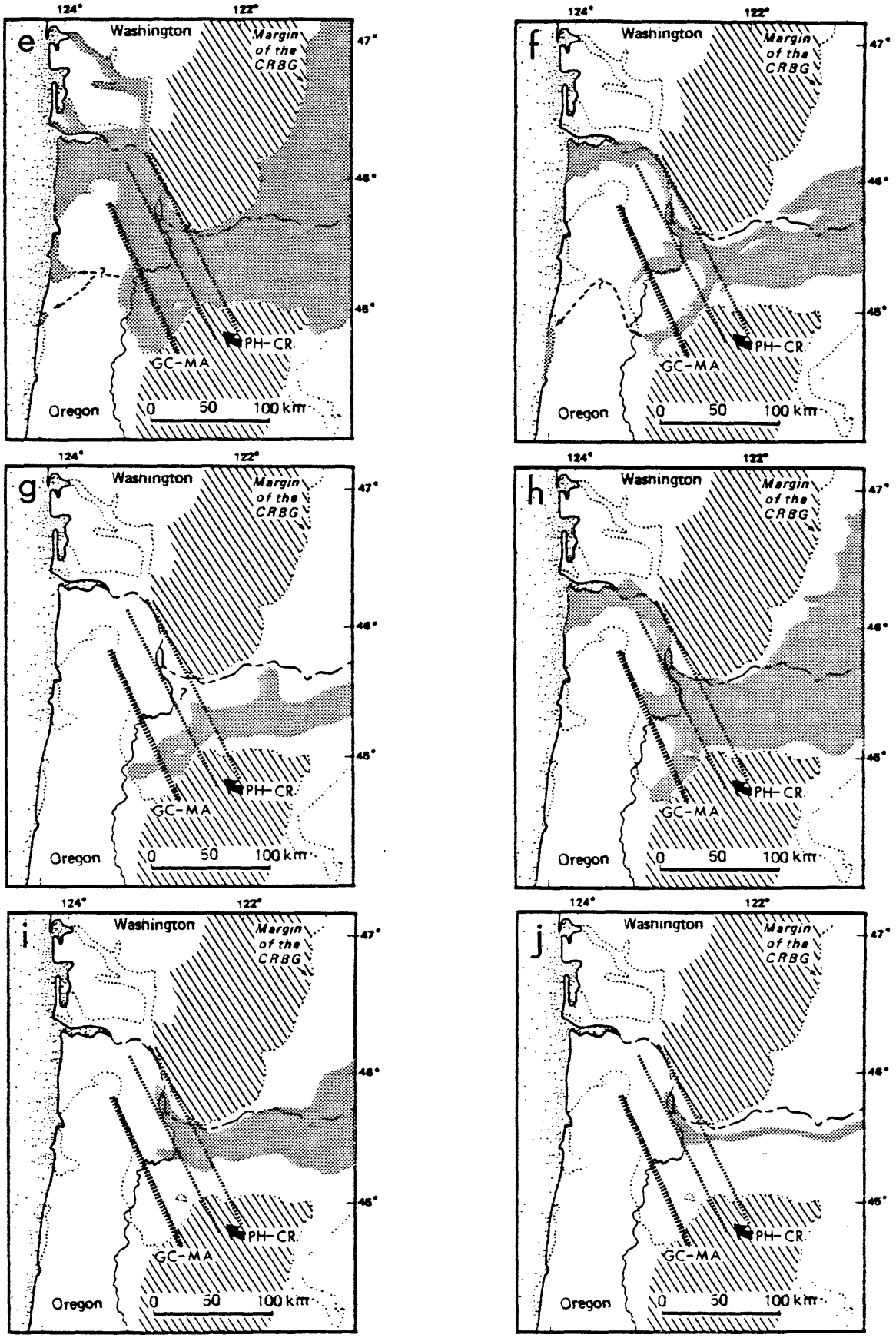
e
f
g
h
i
j
124°
122°
Washington
Margin of the CRBG
47°
46°
45°
PH-CR
GC-MA
Oregon
0 50 100 km

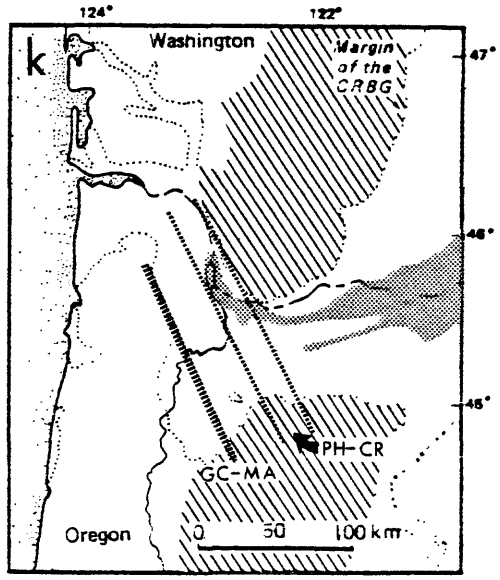
k
124°
122°
Washington
Margin of the CRBG
47°
46°
45°
PH-CR
GC-MA
Oregon
0 50 100 km

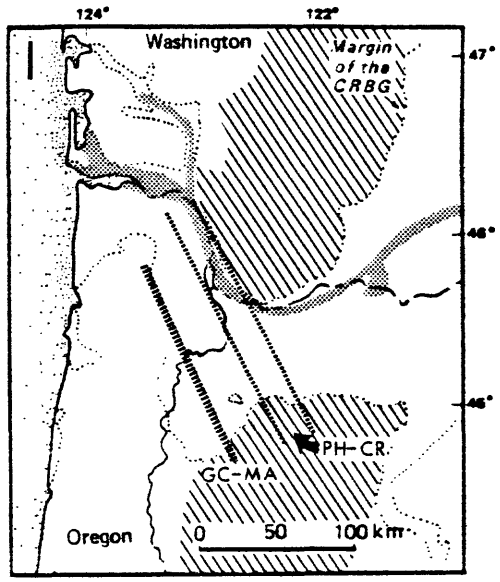
l
124°
122°
Washington
Margin of the CRBG
47°
46°
45°
PH-CR
GC-MA
Oregon
0 50 100 km

Fig. 4. Map showing selected structural features and pathways of CRBG intracanyon flows in western Oregon and southern Washington. Numbers adjacent to selected structural features correspond to those in Table 3. Other structures shown but not described in Table 3 include: A = Tygh Ridge (Yakima fold); B = Columbia Hills (Yakima fold); C = Maupin Fault; D = Bingen Anticline (Yakima fold); E = Horse Heaven Hills (Yakima fold); F = Mosier Syncline; G = Hood River Fault zone; H = Eola Hills homocline; I = Salem Hills homocline; J = Dundee Hills Homocline; and K = Chehalem Mountains homocline.

CRBG intracanyon flows followed the channel of the ancestral Columbia River. Oldest ancestral Columbia River Channel delineated by the ~15.2 Ma Ginkgo flow (heavy dots; Table 2) which overwhelmed the channel forcing the river northward [Beeson et al., 1985]. The next ancestral Columbia River channel is delineated by the ~14.5 Ma Rosalia flow (heavy dashes; Table 2) which also overwhelmed the channel and again forced the river to relocate northward [Tolan and Beeson, 1984]. The last channel of the ancestral Columbia River is delineated by the ~12 Ma Pomona flow. This CRBG flow did not overwhelm and destroy the river canyon and allowed the ancestral Columbia River to reoccupy this canyon in post-Pomona time [Tolan and Beeson, 1984]. Sources used in compilation of structure include unpublished mapping by the authors, Anderson [1978; 1987], Anderson [in Swanson et al., 1981], Vogt [1981], Walsh et al. [1987], and Burck [1986].

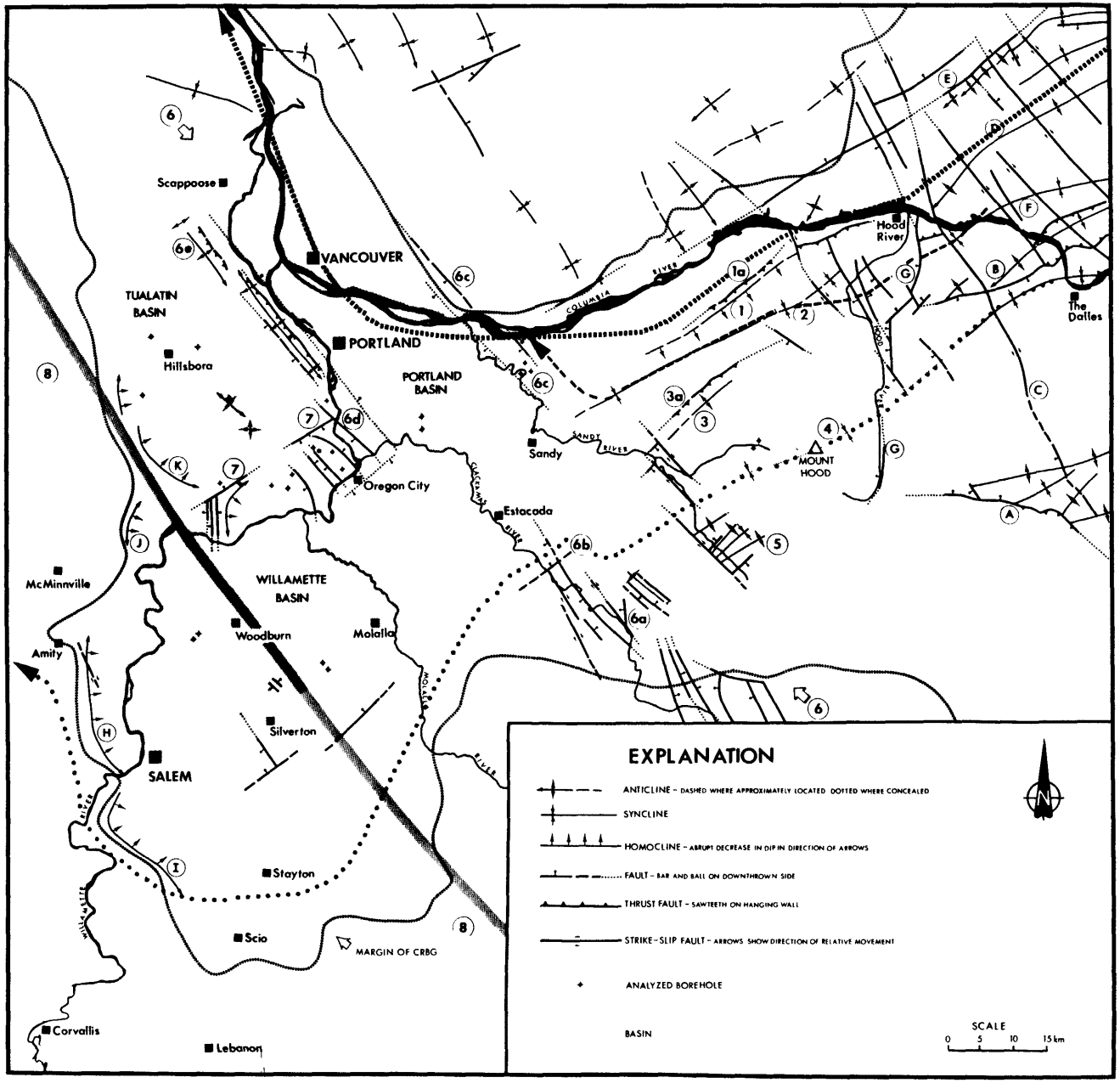
Scappoose
VANCOUVER
PORTLAND
TUALATIN BASIN
Hillsboro
PORTLAND BASIN
Oregon City
Sandy
Estacada
Hood River
The Dalles
MOUNT HOOD
WILLAMETTE BASIN
McMinnville
Woodburn
Molalla
Amity
Silverton
SALEM
Stayton
Scio
MARGIN OF CRBG
Corvallis
Lebanon
COLUMBIA RIVER
SANDY RIVER
SALMON RIVER
MOLALLA RIVER
EXPLANATION
ANTICLINE - DASHED WHERE APPROXIMATELY LOCATED DOTTED WHERE CONCEALED
SYNCLINE
HOMOCLINE - ABRUPT DECREASE IN DIP IN DIRECTION OF ARROWS
FAULT - BAR AND BALL ON DOWNTHROWN SIDE
THRUST FAULT - SAWTEETH ON HANGING WALL
STRIKE-SLIP FAULT - ARROWS SHOW DIRECTION OF RELATIVE MOVEMENT
ANALYZED BOREHOLE
BASIN
SCALE
0 5 10 15 km

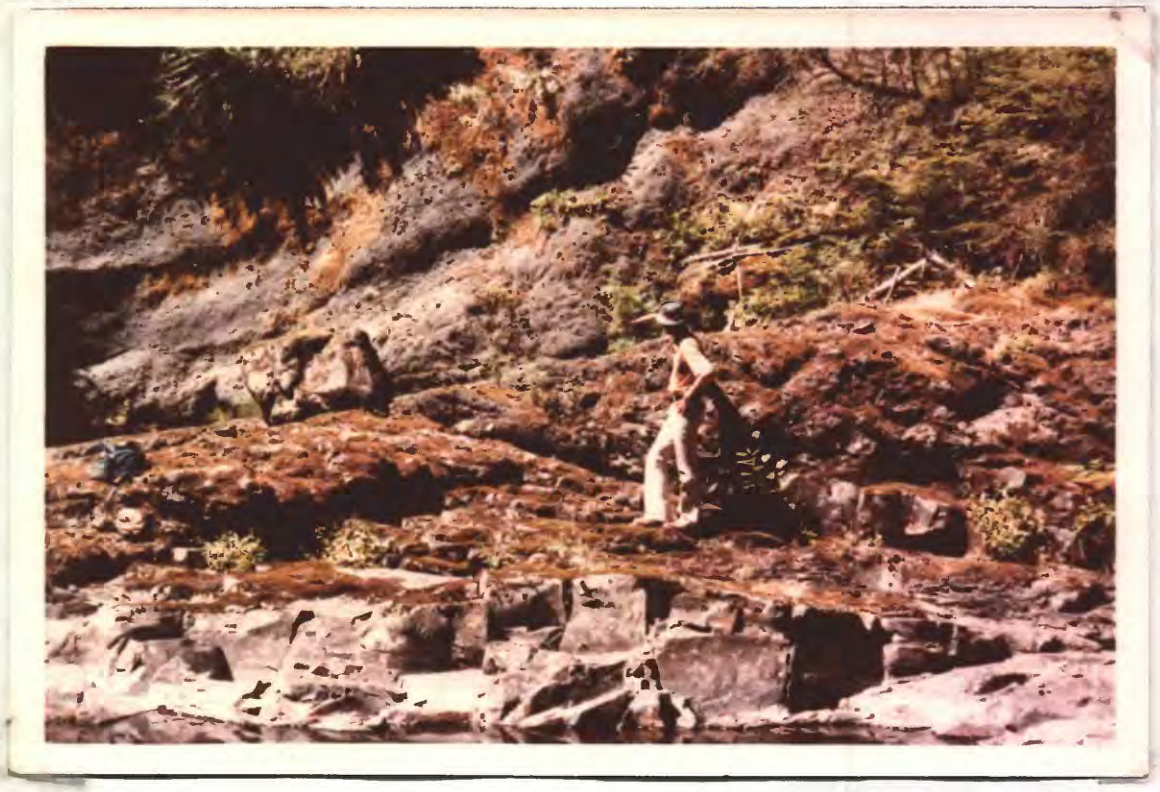

Fig. 5. Bull Run thrust fault on the northwest limb of Bull Run Anticline. Above the thrust plane (at hand level) is more than 60 m of finely crushed fault breccia. Note that the footwall (columnar basalt) displays only a thin zone of coarse brecciation. Forelimb thrust faults, like this one, are characteristic of Yakima Fold Belt anticlines (See Table 3).

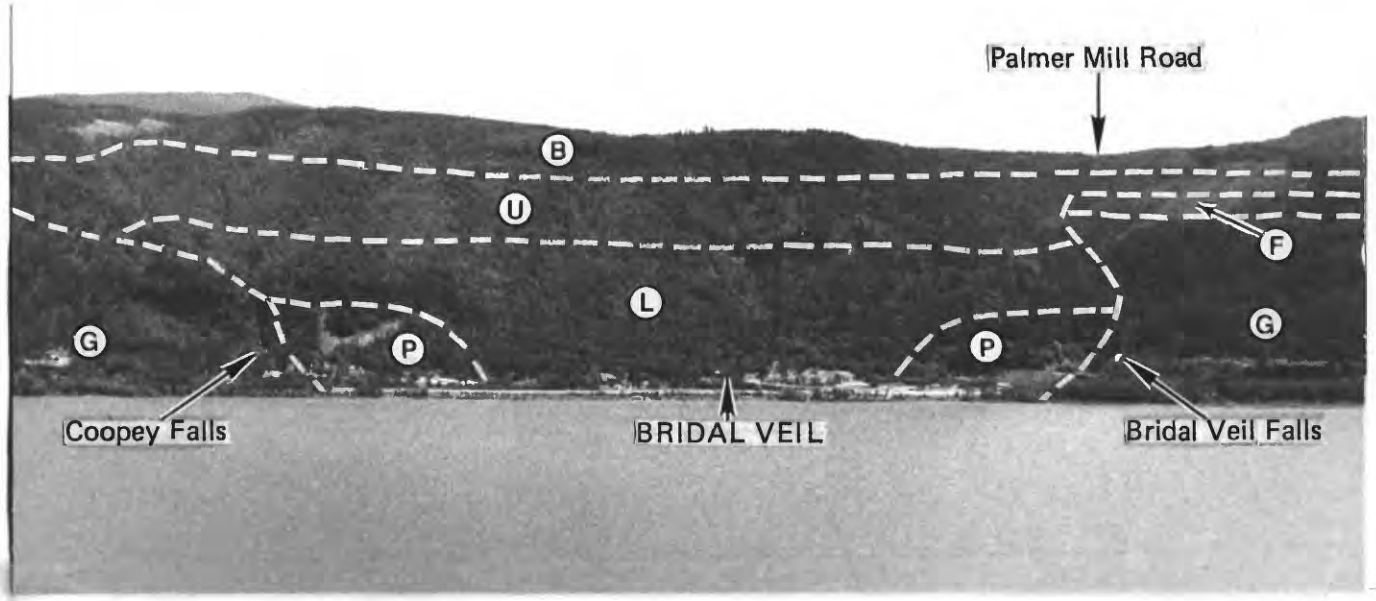

Fig. 6. View of a natural cross section through the Bridal Veil channel at Bridal Veil, Oregon. Here, the ancestral Columbia River incised a canyon into Frenchman Springs (F) and Grande Ronde (G) flows that was more than 245 m deep. Remnants of the Pomona Member intracanyon flow (P) indicate that it only partly filled the Bridal Veil channel about 12 Ma. In post-Pomona time, the ancestral Columbia River began again to deposit lower member Troutdale (L) sands and gravels. The onset of High Cascade volcanism 6 to 4 Ma is reflected in the composition of the upper member Troutdale (U) sediments. The contact between the upper and lower members is gradational and shown in a generalized manner. The total thickness of the Troutdale sediments exposed here exceeds 335 m. The High Cascade flows (B) also capped this channel and prevented the ancestral Columbia River from reoccupying this former course when the Cascades were uplifted. From Tolan et al (1984a, b).

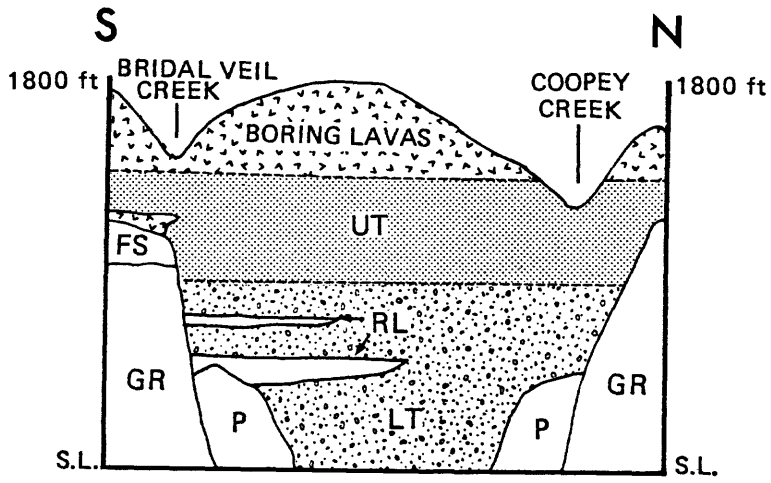

Fig. 7. Generalized cross section through the Bridal Veil channel at Bridal Veil, Oregon. Sgtratigraphic units: GR = Grande Ronde Basalt, FS = Frenchman Springs Member of the Wanapum Basalt, P = Pomona Member of the Saddle Mountains Basalt, RL = Rhododendron lahars, LT = lower Troutdale member, UT = upper Troutdale member. From Tolan and Beeson [1984, P.474].

Table 1. Bedrock Units, Northern Oregon Cascade Range (Columbia Trans-Arc Lowland).

UNIT	AGE	THICKNESS	DESCRIPTION	SELECTED REFERENCES
High Cascade/ Boring Lavas	0.2 to ~6 Ma	3 to >100 m	Chiefly olivine/plagioclase phyric, high-Al basalt and basaltic andesite flows erupted from shield volcanoes, cinder cones, and fissures. In the western portion of the Columbia River Gorge and Portland-Vancouver area, these rocks are called Boring Lavas.	Trimble (1963); Hammond (1979; 1980); Tolan and Beeson (1984)
Troutdale Fm. Upper Member	~2 to ~6 Ma	0 to >200 m	Fluvial conglomerates, vitric sandstones and siltstones deposited by the ancestral Columbia River. Vitric sandstone represents transported and reworked basaltic hyaloclastic debris created when High Cascade Lavas entered the ancestral Columbia River.	Tolan and Beeson (1984) Swanson (1986)
Lower Member	~6 to 13 Ma	0 to >300 m	Fluvial, quartzite-bearing conglomerates, arkosic sandstones and siltstones deposited by the ancestral Columbia River.	Tolan and Beeson (1984) Swanson (1986)
Rhododendron Fm.	~7 to 14 Ma	0 to >1000 m	Chiefly andesitic to dacitic debris flows, mudflows, and hyperconcentrated flood-flow deposits produced by Cascadian volcanism. East of the Cascades these are the Dalles Fm.	Hammond (1979) Priest et al. (1982) Tolan and Beeson (1984)
CRBG	12 to ~16 Ma	0 to 1500 m	See Table 2	Tolan and Beeson (1987); Beeson et al. (1985, in press).
Eagle Creek Fm.	~17 to 23? Ma	150 to >350 m	Chiefly andesitic to dacitic debris flows, mudflows, hyperconcentrated flood-flow deposits, and fluvial conglomerates.	Wise (1970); Hammond (1979); Carlin (1988).
Fifes Peak Fm.	~20 to ~27 Ma	>100 m	Chiefly porphyritic andesite flows with interstratified pyroclastic and volcaniclastic and sediments.	Hammond (1979, 1980); Vance et al. (1987)
Skamania Volcanics	25? to >30? Ma	0 to >300 m	Basaltic, andesitic, and dacitic lava flows and minor interstratified pyroclastic and volcaniclastic sediments.	Tolan (1982) Tolan and Beeson (1984) Phillips et al. (1986).
Ohanapecosh Fm.	30? to ~38 Ma	>1000 m	Basaltic to rhyolitic lava flows, debris flows, tuffs, and volcaniclastic rocks which display a variable degree of alteration. Believed to represent earliest deposits of Cascade volcanism and are intercalated with marine sediments north of the Columbia River Gorge (Wise, 1970). Includes Weigle Fm. of Wise (1961).	Wise (1970); Hammond (1979; 1980)
Waverly Heights Fm.	~40 Ma	>200 m	Subaerial basaltic lava flows believed to represent part of an accreted oceanic island.	Beeson et al. (in prep)

FORMATION	SADDLE MTNS. BASALT	WANAPUM BASALT	
MEMBER	POMONA	PRIEST RAPIDS	
UNIT		BASALT OF LOLO	BASALT OF ROSALIA
NO. OF FLOWS	1	1	1
COMPOSITION	$\bar{X}$ 1σ N	$\bar{X}$ 1σ N	$\bar{X}$ 1σ N
^ SiO_2	52.37 0.25 5	49.87 0.53 19	50.10 0.41 10
Al_2O_3	15.70 0.29 5	15.28 0.30 19	14.04 0.16 10
TiO_2	1.63 0.01 5	3.15 0.09 19	3.55 0.09 10
FeO	10.45 0.16 5	12.20 0.45 19	14.92 0.21 10
MnO	0.18 0.01 5	0.24 0.01 19	0.25 0.02 10
CaO	10.36 0.11 5	9.00 0.63 19	8.34 0.10 10
MgO	6.79 0.24 5	5.18 0.31 19	4.42 0.19 10
K_2O	0.57 0.04 5	0.98 0.11 19	1.19 0.11 10
Na_2O	1.51 0.35 5	2.45 0.17 19	2.32 0.28 10
P_2O_5	0.23 0.01 5	0.66 0.02 19	0.68 0.02 10
Cr +	NA	93 7 6	15 7 14
Ba +	NA	514 20 5	580 34 14
MAGNETIC POLARITY	REVERSED	REVERSED	REVERSED
LITHOLOGY	Sparsely phyric to phyric with tabular plagioclase phenocrysts that are commonly <0.3 cm in size. Clots of olivine, ranging from <0.1 to 0.3 cm, also common. Groundmass is commonly fine- to medium-grained.	Sparsely phyric with tabular and blocky plagioclase phenocrysts that range from to 0.5 cm in size. Groundmass commonly medium- to coarse-grained.	Rarely phyric with tabular plagioclase phenocrysts <0.2 cm in size. Groundmass commonly fine-grained (intracanyon exposures) to coarse-grained (non-intracanyon exposures).
COMMENTS	Intracanyon flow - except in coastal region. AGE: 12 MA	Confined to the Dalles-Mount Hood syncline. AGE: 14.5 MA	Intracanyon flow.
REFERENCES	Tolan and Beeson (1984); Anderson (1980); Anderson and Vogt (1987); Swanson and others (1979); Snavely and others (1973).	Swanson and others (1979); Reidel and Fecht (1981).	Tolan and Beeson (1984); Anderson and Vogt (1987); Swanson and others (1979); Reidel and Fecht (1981).

+ Values in ppm.
^ Major oxide values in wt.%.

Table 2.

FORMATION	WANAPUM BASALT		
MEMBER	FRENCHMAN SPRINGS		
UNIT	BASALT OF LYONS FERRY	BASALT OF SENTINEL GAP HIGH TiO_2 TYPE	BASALT OF SENTINEL GAP INTERMEDIATE TiO_2 TYPE
NO. OF FLOWS	1	1	1
COMPOSITION	$\bar{X}$ 1σ N	$\bar{X}$ 1σ N	$\bar{X}$ 1σ N
^ SiO_2	52.04 0.52 7	51.92 0.63 19	51.86 0.34 20
Al_2O_3	14.32 0.34 7	14.45 0.36 19	14.20 0.32 20
TiO	3.02 0.04 7	3.02 0.10 19	3.06 0.06 20
FeO	13.80 0.46 7	14.02 0.46 19	14.12 0.38 20
MnO	0.20 0.01 7	0.23 0.03 19	0.22 0.01 20
CaO	7.91 0.24 7	7.82 0.29 19	7.89 0.23 20
MgO	4.38 0.20 7	3.91 0.24 19	4.28 0.20 20
K_2O	1.24 0.08 7	1.41 0.16 19	1.35 0.11 20
Na_2O	2.40 0.18 7	2.43 0.42 19	2.28 0.25 20
P_2O_5	0.49 0.01 7	0.58 0.02 19	0.54 0.01 20
+ Cr	20.7 3.2 21	14.8 1.9 21	17.5 2.4 16
+ Ba	NA	NA	NA
MAGNETIC POLARITY	NORMAL	NORMAL	NORMAL
LITHOLOGY	Rarely to sparsely phyric with plagioclase phenocrysts that range from 0.5 to 1 cm in size. Groundmass medium-grained and microphyric with equant and acicular plagioclase microphenocrysts.	Rarely phyric with plagioclase phenocrysts commonly < 1 cm in size. Groundmass is fine-grained and abundantly microphyric with tabular and acicular plagioclase microphenocrysts.	Rarely to sparsely phyric with plagioclase phenocrysts that range from 0.3 to 2 cm in size. Groundmass is fine- to medium-grained and is microphyric with equant and acicular plagioclase microphenocryts.
COMMENTS			
REFERENCES	Beeson and others (1985).	Beeson and others (1985).	Beeson and others (1985).

+ Values in ppm.

^ Major oxide values in wt.%.

FORMATION	WANAPUM BASALT		
MEMBER	FRENCHMAN SPRINGS		
UNIT	BASALT OF SAND HOLLOW INTERMEDIATE P_2O_5 TYPE	BASALT OF SAND HOLLOW LOW P_2O_5 TYPE	BASALT OF SILVER FALLS
NO. OF FLOWS	2	3	3
COMPOSITION	$\bar{X}$ 1σ N	$\bar{X}$ 1σ N	$\bar{X}$ 1σ N
^ SiO_2	51.60 0.63 35	51.82 0.49 55	51.46 0.63 24
Al_2O_3	14.43 0.31 35	14.58 0.33 55	14.65 0.43 24
TiO	2.98 0.06 35	2.91 0.07 55	3.09 0.11 24
FeO	13.81 0.63 35	13.79 0.51 55	14.21 0.52 24
MnO	0.22 0.03 35	0.22 0.02 55	0.23 0.03 24
CaO	8.20 0.23 35	8.18 0.26 55	8.01 0.30 24
MgO	4.31 0.27 35	4.42 0.26 55	4.12 0.24 24
K_2O	1.29 0.14 35	1.19 0.14 55	1.19 0.17 24
Na_2O	2.44 0.21 35	2.20 0.37 55	2.31 0.47 24
P_2O_5	0.52 0.01 35	0.48 0.02 55	0.53 0.01 24
+ Cr	36.8 3.1 34	36.5 4.5 38	16.4 2.3 17
+ Ba	NA	NA	NA
MAGNETIC POLARITY	NORMAL	NORMAL	NORMAL/EXCURSIONAL
LITHOLOGY	Sparsely phyric with plagioclase phenocrysts/glomerocrysts that range from 0.3 to 2 cm in size. Groundmass is fine- to medium-grained and is sparsely microphyric with acicular plagioclase microphenocrysts.	Sparsely to abundantly phyric with plagioclase phenocrysts/glomerocrysts that commonly range from 0.3 to 3 cm in size. Groundmass is fine- to coarse-grained and is sparsely microphyric with tabular plagioclase microphenocrysts.	Sparsely to abundantly phyric with plagioclase phenocrysts /glomerocrysts that commonly range from 0.3 to 1.5 cm in size. Groundmass is medium- to coarse-grained and is abundantly microphyric with equant and acicular plagioclase microphenocrysts.
COMMENTS		Uneven lateral and vertical distribution of plagioclase phenocrysts/glomerocrysts is common. AGE: 15.3 Ma	
REFERENCES	Beeson and others (1985).	Beeson and others (1985).	Beeson and others (1985).

+ Values in ppm.

^ Major oxide values in wt.%.

FORMATION	WANAPUM BASALT	GRANDE RONDE BASALT	
MEMBER	FRENCHMAN SPRINGS		
UNIT	BASALT OF GINKGO	SENTINEL BLUFFS	SLACK CANYON
NO. OF FLOWS	3	5	2
COMPOSITION	$\bar{X}$ 1σ N	$\bar{X}$ 1σ N	$\bar{X}$ 1σ N
^SiO_2	51.55 0.55 38	53.99 0.67 63	53.58 0.44 6
Al_2O_3	14.38 0.31 38	15.26 0.36 63	15.26 0.08 6
TiO	3.08 0.10 38	1.97 0.10 63	1.80 0.03 6
FeO	14.19 0.37 38	11.05 0.60 63	11.49 0.28 6
MnO	0.23 0.02 38	0.21 0.03 63	0.20 0.02 6
CaO	8.03 0.28 38	8.54 0.33 63	8.81 0.21 6
MgO	4.66 0.21 38	4.66 0.26 63	5.25 0.08 6
K_2O	1.23 0.16 38	1.10 0.21 63	0.95 0.06 6
Na_2O	2.34 0.31 38	2.39 0.35 63	2.19 0.46 6
P_2O_5	0.58 0.02 38	0.30 0.02 63	0.26 0.01 6
+Cr	13.9 2.4 23	43 3 18	NA
+Ba	NA	480 31 17	NA
MAGNETIC POLARITY	EXCURSIONAL	NORMAL (N_2)	NORMAL (N_2)
LITHOLOGY	Abundantly phyric with plagioclase phenocrysts/glomerocrysts. Glomerocrysts commonly range from 0.3 to 2 cm in size. Groundmass is medium-grained and is sparsely microphyric with acicular and tabular plagioclase microphenocrysts.	Rarely to sparsely phyric with plagioclase phenocrysts that commonly range from 0.2 to 0.7 cm in size. Groundmass is fine- to medium-grained and microphyric with tabular and acicular plagioclase microphenocrysts.	Sparsely phyric with tabular plagioclase phenocrysts ranging from 0.2 to 0.5 cm in size. Groundmass is medium-grained and microphyric with acicular plagioclase microphenocrysts.
COMMENTS	Occurs as both sheet and intracanyon flows in western Oregon.	Typically only 2 flows found in Willamette Valley and coastal areas. This unit formerly called "N_2 high MgO flows". AGE: 15.6 MA	Formerly designated as "N_2 high MgO flows" in this region.
REFERENCES	[illegible] and others (1985).	Tolan (1982); Anderson (1978); Reidel and others (in press).	Reidel and others (in press).

+ Values in ppm.
^ Major oxide values in wt.%.

FORMATION	GRANDE RONDE BASALT		
MEMBER			
UNIT	WINTER WATER	UMTANUM	ORTLEY
NO. OF FLOWS	2	2	6
COMPOSITION	$\bar{X}$ 1σ N	$\bar{X}$ 1σ N	$\bar{X}$ 1σ N
^ SiO_2	55.40 1.02 16	56.35 0.87 13	55.92 0.60 36
Al_2O_3	15.04 0.46 16	15.19 0.47 13	15.15 0.19 36
TiO_2	2.07 0.09 16	2.20 0.06 13	2.02 0.05 36
FeO	13.59 1.21 16	10.79 1.21 13	10.85 1.74 36
MnO	0.20 0.02 16	0.19 0.02 13	0.20 0.01 36
CaO	7.16 0.29 16	7.03 0.34 13	7.06 0.18 36
MgO	3.71 0.28 16	3.35 0.18 13	3.61 0.12 36
K_2O	1.59 0.44 16	1.56 0.44 13	1.77 0.17 36
Na_2O	2.52 0.42 16	2.77 0.28 13	2.61 0.37 36
P_2O_5	0.31 0.03 16	0.34 0.01 13	0.31 0.02 36
+ Cr	NA	NA	NA
+ Ba	NA	NA	NA
MAGNETIC POLARITY	NORMAL (N_2)	NORMAL (N_2)	NORMAL (N_2)
LITHOLOGY	Sparsely to abundantly phyric with plagioclase phenocrysts/glomerocrysts that range from 0.1 to 0.3 cm in size. Groundmass is fine- to medium-grained and sparsely microphyric with acicular plagioclase microphenocrysts.	Aphyric to rarely plagioclase phyric. Groundmass is commonly glassy to fine-grained and is microphyric with acicular plagioclase microphenocrysts.	Aphyric to rarely plagioclase phyric. Groundmass commonly fine-grained and is not plagioclase microphyric.
COMMENTS	Usually the uppermost N_2 low MgO flows in this region.	Formerly designated as "N_2 low MgO flows" in this region.	Formerly designated as "N_2 low MgO flows" in this region.
REFERENCES	Hoffman (1981); Tolan (1982); Reidel and others (in press)	Reidel and others (in press)	Reidel and others (in press)

+ Values in ppm.

^ Major oxide values in wt.%.

FORMATION	GRANDE RONDE BASALT		
MEMBER			
UNIT	GROUSE CREEK	WAPSHILLA RIDGE	CHINA CREEK
NO. OF FLOWS	3	8	3
COMPOSITION	$\bar{X}$ 1σ N	$\bar{X}$ 1σ N	$\bar{X}$ 1σ N
^ SiO_2	56.00 0.67 22	54.96 0.52 22	54.88 0.64 8
Al_2O_3	15.27 0.28 22	14.89 0.23 22	15.54 0.24 8
TiO_2	2.04 0.03 22	2.37 0.08 22	1.87 0.12 8
FeO	10.45 2.37 22	12.20 0.45 22	11.59 0.45 8
MnO	0.19 0.02 22	0.20 0.01 22	0.20 0.01 8
CaO	7.04 0.23 22	6.93 0.23 22	7.98 0.23 8
MgO	3.70 0.20 22	3.51 0.24 22	4.58 0.26 8
K_2O	1.79 0.24 22	1.80 0.14 22	1.07 0.14 8
Na_2O	2.56 0.30 22	2.52 0.30 22	2.01 0.24 8
P_2O	0.30 0.02 22	0.36 0.02 22	0.29 0.03 8
+ Cr	NA	NA	NA
+ Ba	NA	NA	NA
MAGNETIC POLARITY	REVERSED (R_2)	REVERSED (R_2)	NORMAL (N_1)
LITHOLOGY	Aphyric to rarely plagioclase phyric. Groundmass is commonly glassy to fine-grained and not plagioclase microphyric.	Rarely to very sparsely phyric with plagioclase phenocrysts that are commonly <0.4 cm in size. Groundmass is commonly fine-grained and abundantly microphyric with acicular plagioclase microphenocrysts.	Sparsely phyric with plagioclase phenocrysts that are commonly <0.5 cm in size. Groundmass is fine- to medium-grained and is microphyric with tabular and acicular plagioclase microphenocrysts.
COMMENTS	Virtually identical to Ortley unit flows except Grouse Creek flows have reversed paleomagnetic polarity. AGE: 16.2 MA	Formerly designated as "R_2 low MgO flows" in this region.	Distinguished from Sentinel Bluffs flows by its stratigraphic position and lower CaO contents. Interfingers with Downey Gulch flows.
REFERENCES	Reidel and others (in press)	Reidel and others (in press)	Reidel and others (in press)

+ Values in ppm.

^ Major oxide values in wt.%.

FORMATION	GRANDE RONDE BASALT		
MEMBER			
UNIT	DOWNEY GULCH	CENTER CREEK	TEEPEE BUTTE
NO. OF FLOWS	5	3	4
COMPOSITION	$\bar{X}$ 1σ N	$\bar{X}$ N	$\bar{X}$ 1σ N
^ SiO_2	55.66 0.50 8	56.12 - 3	54.87 0.40 11
Al_2O_3	15.13 0.16 8	14.88 - 3	15.64 0.19 11
TiO_2	2.16 0.07 8	2.27 - 3	1.89 0.08 11
FeO	12.28 0.37 8	12.60 - 3	11.44 0.24 11
MnO	0.20 0.01 8	0.20 - 3	0.20 0.01 11
CaO	6.94 0.41 8	6.52 - 3	8.08 0.22 11
MgO	3.60 0.28 8	3.17 - 3	4.55 0.18 11
K_2O	1.50 0.20 8	1.90 - 3	0.88 0.19 11
Na_2O	2.20 0.20 8	2.00 - 3	2.20 0.15 11
P_2O_5	0.32 0.04 8	0.35 - 3	0.26 0.01 11
+ Cr	NA	NA	NA
+ Ba	NA	NA	NA
MAGNETIC POLARITY	NORMAL (N_1)	REVERSED (R_1)	REVERSED (R_1)
LITHOLOGY	Aphyric to very sparsely phyric with plagioclase phenocrysts commonly <0.3 cm in size. Groundmass is commonly fine-grained and microphyric to abundantly microphyric with acicular plagioclase microphenocrysts.	Aphyric. Groundmass is very fine- to fine-grained and microphyric with acicular plagioclase microphenocrysts.	Sparsely phyric to phyric with plagioclase phenocrysts that commonly range from 0.2 to 0.5 cm in size. Groundmass in fine-grained and not plagioclase microphyric.
COMMENTS		Flows only exposed in the vicinity of Dog Mountain in the Columbia River Gorge.	AGE: 16.5 MA
REFERENCES	Reidel and others (in press) Anderson (1987)	Anderson (1987); Reidel and others (in press)	Reidel and others (in press)

+ Values in ppm.

^ Major oxide values in wt.%.

FORMATION	PRINEVILLE BASALT	
MEMBER		
UNIT	LOW TiO_2, MgO AND HIGH K_2O TYPE	HIGH MgO-TiO_2 TYPE
NO. OF FLOWS	2	1
COMPOSITION	$\bar{X}$ N	$\bar{X}$ N
^ SiO_2	55.27 - 2	53.01 - 1
Al_2O_3	15.66 - 2	15.20 - 1
TiO_2	2.46 - 2	2.76 - 1
FeO	9.77 - 2	12.06 - 1
MnO	0.23 - 2	0.20 - 1
CaO	6.07 - 2	7.83 - 1
MgO	3.23 - 2	3.60 - 1
K_2O	3.28 - 2	1.73 - 1
Na_2O	2.67 - 2	2.18 - 1
P_2O_5	1.17 - 2	1.23 - 1
+ Cr	NA	NA
+ Ba	2099 - 1	2168 - 1
MAGNETIC POLARITY	NORMAL (N_2)	REVERSED (R_2)
LITHOLOGY	Rarely plagioclase phyric with tabular phenocrysts commonly <0.5 cm in size. Groundmass is fine- to medium-grained and not plagioclase microphyric.	Rarely plagioclase phyric with tabular phenocrysts commonly <0.5 cm in size. Groundmass is fine- to medium-grained and not plagioclase microphyric.
COMMENTS	Flows found interfingered with Ortley flows east of the Cascade Range in northern Oregon.	Flows found interfingered Grouse Creek flows east of the Cascade Range in northern Oregon.
REFERENCES	(General) Beeson and Moran (1979); Anderson (1978); Swanson and others (1979); Smith (1986); Burch(1986).	

+ Values in ppm.

^ Major oxide values in wt.%.

Table 3. Characteristics of selected structural features within western Oregon.

PRIMARY STRUCTURE	SECONDARY STRUCTURE	FIGURE AND MAP NUMBER	FOLD CHARACTERISTICS			FAULT CHARACTERISTICS			AGES OF DEFORMATION* (M.Y.) 16 12 8 4 0	COMMENTS	REFERENCES
			LENGTH (KM)	AXIAL TREND	GEOMETRY	LENGTH (KM)	STRIKE/ DIP	TYPE OF DISPLACEMENT			
COLUMBIA TRANS-ARC LOWLAND		FIGURE 1							————————?	Major regional structure. Provided pathway for CRBG flows into W.OR/WA. N60°-80°E trend. 60 km-wide gap in Miocene Cascade Range. Inferred length 250 km - extends east into the Columbia Plateau to Pasco Basin. Lowland subsided during Miocene time; thickness of CRBG emplaced exceeds 1.2 km.	Beeson and Moran (1979); Beeson and others (1985); Anderson (1987).
EAGLE CREEK HOMOCLINE (Yakima Fold Belt Structure)		FIGURE 4 NUMBER 1	>24	N50° - 60° E	Dips to the SE; dips decrease from 25° at crest to <5° at base.				———————??	Homocline remnant (SE limb) of NW-vergent Yakima Fold Belt anticline. NW limb of anticline eroded away by ancestral Columbia River. Inferred fold amplitude >550 m - estimated from top of Grande Ronde Basalt (Sentinel Bluffs unit).	Beeson and others (1985); also see Anderson (1980, 1987).
	EAGLE CREEK THRUST FAULT	FIGURE 4 NUMBER 1A				>24	N 45 - 50° E/ 29° SE	Thrust fault. Minimum vertical stratigraphic offset: 300 m. Amount of shorting: unknown.	? — NO DATA	Probably foreliab thrust fault. Thrust fault places N_1 Grande Ronde Basalt over younger R_2 Grande Ronde Basalt. Fault zone similar in appearance to Bull Run thrust fault.	
BULL RUN SYNCLINE (Yakima Fold Belt Structure)		FIGURE 4 NUMBER 2	>68	N 60° E	Broad, asymmetric syncline formed between the Eagle Creek homocline and Bull Run anticline.				?————————?	Probably the extension of the Mosier syncline. Syncline filled in post-CRBG time by Cascadian volcaniclastic sediment and lava flows.	Vogt (1981); Beeson and others (1982, 1985).
BULL RUN ANTICLINE (Yakima Fold Belt Structure)		FIGURE 4 NUMBER 3	>40	N50° - 60° E	Asymmetric, open box fold; NW limb dips 12° to 15°; SE limb dips <8°. Thrust fault along base of NW limb. Fold amplitude 420 m.				?————————??	Probably the extension of the Columbia Hills anticline. Fold growth during Grande Ronde time produced enough topographic relief to prevent emplacement of Winter Water and Ortley flows (N_2 Grande Ronde Basalt) on this anticline.	Vogt (1981); Beeson and others (1985); Anderson and Vogt (1987).
	BULL RUN THRUST FAULT	FIGURE 4 NUMBER 3A				>20	N 60°E/ 12° SE	Foreliab thrust fault. Minimum vertical stratigraphic offset: 180 m.	? — NO DATA	Fault breccia zone exceeds 160 m in thickness. Fault breccia primarily confined to hanging wall block.	Vogt (1981); Beeson and Moran (1979).
MOUNT HOOD SYNCLINE (Yakima Fold Belt Structure)		FIGURE 4 NUMBER 4	>70	N 50° E	Broad syncline formed between Bull Run anticline and Salmon River anticline.				?————————?	Extension of the Dalles-Umatilla syncline.	Beeson and others (1985).

* Solid line indicates good to excellent control on ages; dashed line indicates less certain or circumstantial control on ages; question marks indicate inferred ages.

PRIMARY STRUCTURE	SECONDARY STRUCTURE	FIGURE AND MAP NUMBER	FOLD CHARACTERISTICS			FAULT CHARACTERISTICS			AGES OF DEFORMATION (M.Y.) 16 12 8 4 0	COMMENTS	REFERENCES
			LENGTH (KM)	AXIAL TREND	GEOMETRY	LENGTH (KM)	STRIKE/ DIP	TYPE OF DISPLACEMENT			
SALMON RIVER STRUCTURES (Yakima Fold Belt Structure)		FIGURE 4 NUMBER 5	VARIABLE 5 TO >15	VARIABLE N50°- 80° E	Series of open, asymmetric anticlines separated by synclines. NW limb of anticlines typically faulted. Faults range from high-angle reverse to thrust.				?——— ? ?		Burck (1986).
PORTLAND HILLS-CLACKAMAS RIVER STRUCTURAL ZONE		FIGURE 4 NUMBER 6							———	Major NW-trending structural feature consisting of faults and folds generated in response to dextral transcurrent movement. PH-CR structural zone varies from 15 to >40 km in width and can be traced for >160 km.	Beeson and others (1975, 1982, 1985); Anderson (1978).
	RELATED FAULTS IN THE UPPER CLACKAMAS RIVER AREA	FIGURE 4 NUMBER 6A				VARIABLE <5 TO >20	TYPICALLY N 20° - 50° W/ NEARLY VERTICAL TO VERTICAL	Dextral strike-slip, oblique-slip and dip-slip faults. Stratigraphic offset varies, ranging from <5 to > 150 m. Amount of lateral offset difficult to quantify due to the lack of adequate piercing points.	?———??	Dextral wrench faults produced a series of horsts and grabens, with only minor folds.	Anderson (1978); Beeson and others (1985).
	PROMONTORY PARK FAULT (Yakima Fold Belt Structure)	FIGURE 4 NUMBER 6B				>7	N 70° E/ NO DATA	High-angle reverse fault. Vertical stratigraphic offset >100 m.	NO DATA	Inferred to be the westward extension of the Salmon River anticline.	Anderson (1978).
	PORTLAND BASIN	FIGURE 4							———	Pull-apart basin. Length of basin >65 km; width >25 km. Evidence suggests basin existed prior to emplacement of CRB6 flows. Basin continued to subside in post-CRB6 time and was filled with sediments. Post-CRB6 sediments up to 450 m thick in some parts of the basin.	Beeson and others (1985).
	SANDY RIVER FAULT ZONE	FIGURE 4 NUMBER 6C				>20	N 45° W/ NO DATA	Consists of many faults with both dip-slip and dextral strike-slip movement. Faults generally produce a step-down pattern to the SW. Amount of vertical stratigraphic on faults variable, but across the zone > 400 m.	———	Defines eastern Portland basin margin. Data on this structure obtained from boreholes and geophysical surveys. Associated faults exposed in the Corbett, OR area.	
	VARIOUS HORSTS AND GRABENS	FIGURE 4 NUMBER 6D				VARIABLE 5 TO >10	VARIABLE N 10° - 45° W/ VERTICAL TO LOW ANGLE	Dip-slip and dextral strike-slip. Amount of vertical stratigraphic offset varies from 250 to >350 m. Amount of lateral offset unknown.	———?	Defines part of the western margin of the Portland basin.	
	PORTLAND HILLS UPLIFT	FIGURE 4 NUMBER 6E	>40	N 30° - 45° W	Several en echelon, asymmetric, faulted anticlines.	VARIABLE 10 TO >40	N30° - 45° W/ VERTICAL TO LOW ANGLE	Dip-slip and dextral strike-slip. Vertical stratigraphic offset on thrust fault <120 m. Vertical stratigraphic offset on faults on NE and SW limbs of uplift estimated to be 200 m and > 100 m, respectively.	———?	Defines a portion of the western margin of the Portland basin. Uplift probably a "flower structure" created by transpressive deformation.	

STRUCTURE OF THE CONVERGENT WASHINGTON MARGIN

CAROL FINN

U. S. Geological Survey
MS 964, P.O. Box 25046
Denver Federal Center
Denver, CO 80225

ABSTRACT

Along the boundary between the Juan de Fuca and North American plates in southwest Washington Free-Air and Bouguer gravity maps both show the characteristic gravity signature observed over other active subduction zones. A low is over the trench and is due primarily to the bathymetric expression of the trench. A gravity high is centered over the Washington Coast Range. Interpretations of the high are more varied than for the low. Some studies relate the high to an increase in density of the subducting plate as it undergoes phase changes. Others attribute it to thin crust.

Detailed gravity modeling of the Bouguer gravity high in southwestrn Washington, constrained by magnetotelluric and seismic refraction data, suggests that its source is the density contrast between the dense basalts of the Coast Range and the adjacent sedimentary and volcanic rocks. Shallow mantle may contribute to the gravity high but is not required by the data. High density material in the subducting plate causes a longer wavelength and smaller amplitude gravity high that does not mimic the observed high.

INTRODUCTION

Free-Air gravity anomalies generally correlate positively with terrain and bathymetry (in addition to subsurface density contrasts). Although this correlation has been recognized over convergent margins (Eg. Watts and Talwani, 1975) confusion exists over how certain topographic and bathymetric features relate to Free-Air anomalies. For example, the Free-Air gravity signature of active subduction zones has been described as a low-high couple with the low over the trench and the high arcward of the trench (Eg. Grow, 1973, Riddihough, 1979). The Free-Air gravity map of the world (Bowin and others, 1982) shows that the large high part of the low-high couple is associated with different features from subduction zone to subduction zone indicating that the description of the subduction zone gravity signature as a low-high couple is incomplete. Therefore I will use a different terminology described in detail in Finn (in prep.). Figure 1 represents an ocean/continent subduction zone and indicates various morphological features and associated Free-Air gravity anomalies that will be used throughout this paper. Figure 2 shows a Free-Air gravity profile across southern Washington.

Another controversy over the sources of gravity anomalies over subduction zones is the relative contributions of deep vs. shallow sources. The identification of the "characteristic low-high gravity couple" over most convergent margins led many to believe that its source had to be related to the subducting plate, not to shallow features in the overriding plate (because of the wide variation in the geology from margin to margin). Gravity models, for example, Grow (1973), Grow and Bowin (1975), Segawa and Tomoda (1976) and Molnar (1977) suggest that much of the convergent margin gravity signature can be explained by density increases in the subducting plate due to shallow phases changes and by the density contrast between the

subducting plate and the surrounding asthenosphere. Others (Eg. Talwani and others, 1961; Watts and Talwani, 1975; Couch and Woodcock, 1981; Chapman and Talwani, 1982) suggest that density contrasts in the upper 60 km are the primary causes of the observed gravity anomalies.

In the Pacific northwest (Fig. 3), some early gravity studies (Eg. Stewart, 1961; Couch, 1969; Dehlinger and others, 1968) attribute the high amplitude forearc gravity high to high densities in the Coast Range crust and/or to high density, shallow mantle, without addressing the possibility of density changes within the subducting plate. Later studies (eg. Riddihough, 1979; Couch and Riddihough, in press) generally attribute the high to shallow mantle in the overriding North American plate and to density changes within the subducting Juan de Fuca plate.

These previous papers show mostly general features of the margin. In this study I attempt to delineate the structure of the overriding North American plate in southwest Washington in order to separate its effect from that of the subducting Juan de Fuca plate in the observed gravity anomalies. Part of this study is an update of Dehlinger and Couch's (1968) and Riddihough's (1979) gravity models of the southwest Washington margin.

This paper is organized into several main parts. The first is a description of the geology of the Washington margin. Gravity and magnetic maps are then discussed qualitatively. The next part describes the data and method used to construct a detailed 2 dimensional model that synthesizes much of the geophysical, geochemical and geological data from southwest Washington. Various hypotheses about the sources of the gravity anomalies are tested by the modeling procedure.

Features peculiar to the Washington margin are also discussed as well as the problems in relating its gravity signature and sources to other convergent margins.

Geology

In the Cascadia basin offshore (Fig. 3), an average of 500 m of marine sediments is underlain by 5 km thickness of marine basalts with a Moho at about 10 km. The continental shelf and slope consist of as much as 13 km of marine and continental sediments some of which are highly deformed (Shor and others, 1968; McClain, 1981).

The continental geology (Fig. 3) of southwest Washington and surrounding areas can be divided into four major provinces that emphasize the geologic framework established during the Late Eocene initiation of the present-day convergent margin (Atwater, 1968). The provinces are as follows:

(1) The Coast Range Province is composed of Paleocene to middle Eocene mostly submarine basalts inferred to be a seamount complex on oceanic crust that was accreted to the continent by the middle Eocene (Wells and others, 1984). These basalts, the Crescent Formation in Washington, the Siletz River Volcanics in Oregon and the Metchosin Formation in Vancouver Island will collectively be referred to as Coast Range basalts throughout the rest of this paper.

(2) The Puget-Willamette Valley is a discontinuous valley extending from Puget Sound to southern Oregon that is a forearc basin (Dickinson, 1976). In southwest Washington the province consists of the Chehalis basin that is filled with continental and marine sediments as well as volcaniclastic rocks (Armentrout and Suek, 1985).

(3) The Cascade Range Province is a magmatic arc related to subduction of the Juan de Fuca plate. In southwest Washington, Mt. St. Helens, Mt. Rainier, Mt. Adams and Goat Rocks Volcano are considered to be part of this range. Voluminous flows from other volcanic centers cover large areas in the region.

(4) The Columbia Plateau is a large plateau consisting of flood basalts. It has been postulated that the widespread volcanism there is associated with continental rifting (Catchings and Mooney, 1988).

Gravity and Magnetic Data

Digital gravity data (Finn, 1984) were used to compile the gravity map of the study area (complete Bouguer on land, Free-Air over the ocean) shown in Fig. 4 (Finn and others, 1984). The data were reduced at a density of 2.67 g/cm^3, roughly the average density of terrain in the area.

The gravity field offshore is relatively flat except for a Free-Air forearc gravity high superimposed on a low associated with the sediment-filled trench (Fig. 4) and geometry of the oceanic crust as it subducts. The high is due to the density contrast between dense deformed sediments within the trench and adjacent less dense sediments (Couch and Bramen, 1979; McClain, 1981).

Major Bouguer-gravity highs (Fig. 4) on the onshore part of the study area are associated with the Columbia Plateau, the Coast Range, and Vancouver Island. The Columbia Plateau has thick sections of wide-spread Miocene flood basalts. The gravity high may be the result of the high density of these basalts (Cady and Fox, 1984) as well as to high density lower crust (Catchings and Mooney, 1988). The Coast Range and Vancouver Island are composed of oceanic terranes that were accreted to the continent in late Mesozoic and early Cenozoic time (Davis and others, 1978; Dickinson, 1979). Both areas are composed of thick sections of relatively high-density basalt that contribute to the observed gravity high outlined in Fig. 4.

The major high topographic areas (the Olympic Mountains and the Cascade Range, Fig. 4) have associated Bouguer-gravity lows (Fig. 4) which probably reflect rocks that provide isostatic compensation of the mountains.

Positive magnetic anomalies are usually caused by normally magnetized rocks, more magnetic than the surrounding ones. Negative magnetic anomalies can be caused by reversely magnetized rocks or rocks with lower intensities than the surrounding ones. Most of the surficial rocks in the study area are normally magnetized (see, for ex., Wells, this issue; Wells and Coe, 1985; Bates and others, 1982; Beck, 1980).

The magnetic data used to make Fig. 5 was extracted from a grid used to compile the North American magnetic map (Comm. for the Mag. Anom. Map of North Amer., 1987). Individual aeromagnetic surveys were digitized at a scale of 1:1,000,000 and hand merged. No analytic continuation was done. This is one of the first complete aeromagnetic maps of the region.

On the west end of Fig. 5, the magnetic stripes associated with reversed and normal portions of seafloor can be observed. As the Juan de Fuca plate begins to subduct beneath the continental shelf and slope (Fig. 5) these anomalies disappear, forming a magnetic quiet zone. This quiet zone is characteristic of many trenches in the Pacific and is probably due to the increased distance of the magnetic Juan de Fuca plate from the magnetometer (Grow, 1972). The flatness of the magnetic field is also evidence that the continental slope and shelf are composed non-magnetic rocks, such as sediments, rather than containing large pieces of oceanic crust (McClain, 1981).

Magnetic highs (Fig. 5) are associated with exposed sections of the Coast Range basalts. The magnetic high outlined on Fig. 5 extends partially over the Puget lowland which is mostly covered by sediments and volcanic rocks. The high is not closely correlated with surface volcanic rocks and must have a buried source. It does however correlate with the unexposed portions of the Coast Range basalts in southern Vancouver Island (as delineated by seismic reflection data (Clowes and others, 1987) and in southern Washington (as delineated by magnetotelluric data (Stanley and others, 1987)), suggesting that the basalts are the source of the high. The steep gradients of the magnetic high also suggest that its source is shallow.

Magnetic highs in southwest Washington are also caused by the magnetic terrain of Mt. St. Helens and Mt. Adams, an intrusion underlying Goat Rocks Volcano (Fig. 5) (Willams and Finn, 1987) and Miocene andesite and basalt flows (see Walsh and others, 1987). An aeromagnetic low surrounds these magnetic highs. It is associated with anticlinal structures that thin the surficial magnetic volcanic rocks and bring sediments within 1 km of the surface (Stanley and others, 1987).

THE STARTING MODEL

The primary gravity and magnetic anomalies whose sources that I want to determine are those over the trench, Coast Range, Puget-Willamette Valley and Cascade Range. In order to determine the sources of the gravity and magnetic anomalies computer modeling is useful. For the best possible model, the gravity and magnetic data should be constrained with other data. Usually these constraints give information on the depths and lateral extents of bodies. Initial densities and magnetizations can be assigned based on average values given in the literature for certain rock types (e.g. Telford and others, 1976), and rock density and magnetization measurements. Densities can also be obtained from well data or can be inferred from seismic wave velocities. The relation between seismic wave velocities and density is approximately linear, however, densities can vary by as much as $\pm$ 0.2 g/cm^3 for a single velocity (Nafe and Drake, 1957). Magnetizations can also be measured.

The validity of the final model completely depends on the validity of the assumptions made when constructing the starting model. Many parameters can be changed to create a completely different model that fits the data. This is one of the problems when modeling any kind of regional geophysical data; the final model often fits ones preconceived ideas.

In the following section I describe the data and the assumptions made when interpreting the data that I use to construct the starting 2-dimensional structural model from which a final model based on gravity and magnetic data, shown in Fig. 7, is derived. The location of the gravity and magnetic profile to be modeled is shown in Figs. 4, 5 and 6.

On depth, dip and structure of Juan de Fuca plate

The offshore crustal structure of the starting model was constrained primarily by seismic refraction data (Shor and others, 1968; McClain and Taber, 1984; McClain, 1981). Fig. 6 shows the location of the data profiles. The interpretation of these data was done using the first arrivals. The data quality were fairly high and the assumption that the oceanic crust can be approximated as homogeneous plane layers is fairly reasonable for the regional model considered here.

The thickness and structure of the thick pile of sediments that compose the continental shelf and slope are constrained by the same seismic refraction data (Shor and others, 1968; McClain, 1981; McClain and Taber, 1984). The refraction model shows rocks with velocities ranging from 2 km/s at the top to about 5.4 km/s at about 9 km depth that may be related to sediments and to offscraped oceanic crust (McClain, 1981).

The magnetic field (Fig. 5) over the continental shelf and slope is flat. I did not model the magnetic stripes on the sea floor because the depth to the oceanic crust under the continental slope and shelf is great enough that the crust does not contribute much to the observed magnetic anomaly. Instead, I assigned it a constant value of magnetization (5 A/m) typical of oceanic crust (eg. Grow, 1973). The flatness of the magnetic field over the continental slope and shelf is consistent with the magnetic signature of sedimentary rocks. Small pieces of oceanic crust (like those observed on land in the Hoh melange (Rau, 1973)) could be incorporated into the continental slope and shelf rocks without causing a large magnetic anomaly.

The thickness of the oceanic lithosphere can be determined from its age (eg. Turcotte and Schubert, 1982). For the oceanic crust of the Juan de Fuca plate, which is about 8 m.y. old as it starts to subduct (Connard and others, 1984), the calculated lithospheric thickness is about 35 km.

The density of the upper mantle of the Juan de Fuca plate (Fig. 7) is consistent with the observed seismic refraction velocities (Shor and others, 1968; McClain, 1981; McClain and Taber, 1984). However the seismic refraction velocites and samples only reflect the density of the top of the upper mantle. The seismic data indicate that the mantle has a lower velocity

(thus density) on the west end of the profile near the Juan de Fuca ridge than on the west under the trench so that section was assigned a lower density than the eastern section.

The assigned single density of the asthenosphere is based on theoretical petrological studies (Ahrens and Schubert, 1975; Grow, 1973; Grow and Bowin, 1976) of the density variation of inferred asthenospheric materials with depth and temperature. Lateral variations in asthenospheric densities, particularly under magmatic arcs (where the density would decrease because of high temperatures there), have been proposed (Grow, 1973) but are unknown.

The density structure of the Juan de Fuca plate beneath the Coast Range is not well determined. Grow (1973), Grow and Bowin (1976), Ahrens and Schubert (1975) suggest that the subducting oceanic crust changes phase from basalt to eclogite and the subducting oceanic mantle changes phase from plagioclase to garnet peridotite between depths of 30 to 60 km in subducting slabs. These phase changes result in large density increases (from 2.9 to 3.58 g/cm3 from the eclogite change and from 3.26 to 3.38 for the garnet peridotite change). In normal mantle these phase changes are estimated to occur deeper than about 60 km depth. The proposed shallowing of the phase changes is postulated to occur because the subducting slab is colder than surrounding mantle at the same depth (pressures).

The position and dip of the Juan de Fuca plate under the North American plate was determined from seismic refraction (Fig. 6) (Taber, 1983; Taber and Lewis, 1986), and earthquake hypocenter data (Weaver and Baker, 1988; Crosson and Owens, 1987), teleseismic P delays (Michaelson and Weaver, 1986) and P to S converted phases (Langston, 1977).

A seismic refraction model (Taber and Lewis, 1986) shows that the increase in dip of the Juan de Fuca plate from 0.6 ^{o} under the Cascadia Basin (Shor and others, 1968; McClain, 1981; McClain and Taber, 1984) to about 9 ^{o} $\pm$ 2 ^{o} occurs about 110 $\pm$ 5 km offshore and continues at this dip to just below the longitude of Puget Sound. The offshore refraction surveys produced records with clear first arrivals so that the offshore dip estimates are probably correct (Taber and Lewis, 1986).

The estimate for the dip of the Juan de Fuca plate under the North American plate are probably not as good as that of offshore. The first arrivals in the refraction surveys from what is assumed to be the Moho of the Juan de Fuca plate are often not clear (Taber and Lewis, 1986). The velocity structure of the overriding plate in the Coast Ranges (where most of the seismic refraction recording stations were located) is not well known, which affects depth and velocity estimates of the Juan de Fuca plate.

The earthquakes in Washington can be divided into two groups on the basis of their depths. Cross-sections show a broad distribution of well-located earthquakes (detected by an extensive regional seismometer network) in the crust of the North American plate from depths of 0 - 20 km, separated by a zone of virtually no earthquake activity from a coherent dipping planar distribution of earthquakes inferred to be within the Juan de Fuca plate (Crosson, 1976, 1983). Crosson and Owens (1987) and Weaver and Baker (1988) use the distribution of earthquake hypocenters inferred to be within the Juan de Fuca plate to define its proposed south east dip of about 11^{o} - 20^{o} ($\pm$ 2^{o}). Along the east-west strike of the profile (Fig. 6) this translates to a dip of 11^{o} (Weaver and Baker, 1988) near the coast increasing to 20-25^{o} (Weaver and Baker, 1988; Crosson and Owens, 1987) at the longitude of central Puget Sound. Not many earthquakes constrain these estimates. For the starting model, the Juan de Fuca plate dips 11 ^{o}, from the offshore part of the model to the longitude of Puget sound where the dip increases to 25 ^{o} until reaching a depth of about 40 km.

The next problem was to determine the depth of the Juan de Fuca plate. Taber and Lewis (1986) model the first arrivals observed in the refraction data to be from the subducting plate. The observed earthquakes may occur within the Juan de Fuca plate crust and/or mantle. This means that, given the 5 km thickness of the oceanic crust extrapolated from the offshore results (and assumed not to have changed), the top of the Juan de Fuca plate can only be estimated within $\pm$ 5 km. I split the difference and put the top of the Juan de Fuca plate 2 km above the plane defined by the earthquakes.

The dip of the Juan de Fuca plate east of the longitude of Puget Sound is constrained by teleseismic P-wave residuals (Michaelson and Weaver, 1986; Rasmussen and Humphreys, 1988)

which indicate a plate dipping greater than 45 ^{o} probably closer to 60 ^{o}; its maximum dip is not constrained by the data. The dip cannot be much shallower than this and fit the teleseismic data. I used a 45 ^{o} dip for the starting model. The location of the increase in dip of the plate to 45^{o} is not well constrained. However, I constrained the 45^{o} dipping section of the Juan de Fuca plate to reach a depth of about 100 km under the Goat Rocks Volcano, roughly the depth of most plates over which magmatic arcs usually occur (Dickinson, 1970). The thickness of the plate is not constrained because the block size used in the teleseismic velocity model is 50 km, about the thickness of the plate (Michaelson and Weaver, 1986).

On Continental Crust Structure and Thickness

Most of the crustal structure of the area from the eastern boundary of Coast Range basalts to the western edge of the Columbia Plateau was constrained by a 2-d magnetotelluric model from the southern profile shown in Fig. 6. Most of the depth estimates are probably good to about 20% (Stanley, oral comm., 1988; Stanley, 1984; Stanley and others, this issue). Although, Mt data from the northern profile marked in Fig. 6 and seismic refraction data from Vancouver Island (Fig. 6) suggest that the Coast Range basalts range in thickness from 10 -25 km, the thickness of the Coast Range basalts is unknown along the modeled profile.

The seismic refraction data in the area (Taber and Lewis, 1985) (Fig. 6) do not detect a Moho in the North American plate under the Coast Range, but their data are not good enough to clearly define it. If the structure of the Coast Range resembles that found under southern Vancouver Island (Clowes and others, 1987) and Oregon (Wannamaker and others, this issue) then the Coast Range basalts would be underlain by a subduction complex consisting of underthrust sediments and offscraped oceanic crust with no continental mantle. I used densities compatible with both mantle material and a subduction complex in the starting model.

The Moho depth under Goat Rocks Volcano was obtained from extrapolating the 40 km depth obtained from a refraction survey of the Oregon Cascades to Washington (Leaver and others, 1984). I extended the 40 km Moho depth west to the eastern edge of the Coast Range basalts, but no information on the actual depth is known there.

The crustal structure and Moho depth in the Columbia Plateau was obtained from seismic refraction data (Fig. 6) (Catchings and Mooney, 1988). The shallow crustal structure (upper 10 km) matches that determined from MT data (Stanley, 1984) and corraborated from drilling (Stanley, 1984). The lower crustal structure and Moho depth are not as well known. Densities were inferred from the seismic velocities (Nafe and Drake, 1957; Catchings and Mooney, 1988).

The thicknesses of the mantle and Juan de Fuca plate under the Cascade Range and Columbia Plateau are completely unknown. The thickness of the lithosphere, based on thermal arguments is proposed to be between 80 and 100 km thick (see for ex. Turcotte and Schubert, 1982). I assigned a thickness of 90 km.

In all cases magnetizations of modeled bodies are assumed to be in the present Earth's field direction of inclination 69^{o}, declination of 19^{o} and intensity of 55,670 gammas (Peddie, 1987). This assumption is reasonable because the age of the rocks in the area with potentially high remanence (the volcanic rocks) are post Eocene (For ex., Walsh and others, 1987). Cox and Doell (1960) proposed that post-Eocene rocks have magnetization vectors effectively colinear with the Earth' present field direction. The total magnetization vectors (induced + remanent) for the Eocene Coast Range basalts were measured to have directions roughly aligned with the present Earth's field.

Structures lying deeper than about 20 - 25 km were assumed to be non-magnetic. The short wavelength of the observed magnetic anomalies indicates that their sources are shallow.

Modeling Results

Part of the purpose of constructing the starting model is to synthesize the geophysical, geological and geochemical data from the region. The next step is to determine where this starting model does not match the gravity and magnetic data. In order to determine the structures, densities and magnetizations that produce gravity and magnetic anomalies corresponding to the observed gravity and magnetic anomalies and satisfies the constraints I used a 2 1/2 dimensional gravity and magnetic modeling program (Webring, 1985). The program uses profiles of gravity and magnetic observations (locations on Figs. 3 and 4) and the starting model consisting of body corners, density and magnetization contrasts based on the constraints. The program then adjusts the starting model so that its gravitational and magnetic attraction fits the profiles of observed data. The evolution of the final model is controlled by only allowing a few parameters to vary in each modelling attempt and allowing those parameters to vary only within a specified range. Where the structures are well constrained (like that of the Juan de Fuca plate, for example) I did not allow the body corners to move. The magnetizations and densities were allowed to vary within a geologically reasonable range. The preferred final model is shown in Fig. 7 with its calculated and observed gravity and magnetic profiles.

The primary purpose of modeling the gravity and magnetic data is to test the various hypotheses about the sources of the gravity anomalies over over the continental slope and shelf and the Coast Range. Therefore, I only modeled the magnetic data over this general area.

The observed gravity profile (Fig. 7) over the oceanic plate west of the continental slope is flat. The modeled densities of the oceanic sediments and oceanic crust were allowed to vary in the modeling process but are consistent with expected values based on drilling in oceanic crust and the seismic velocities (Shor and others, 1968). A gravity low starting west of the continental slope and continuing east over the continental shelf is due primarily to the density contrast between the sediments and water in the continental slope and shelf and the continent to the east and the shallower oceanic crust to the west. Superimposed on the gravity low is a high partially related to the density contrast between rocks within the trench (2.4-2.7 g/cm^3) and lower density sediments (1.9 g/cm^3) in the Cascadia Basin. McClain (1981) modeled the gravity high also to be due to dense rocks within the trench that he interpreted to be deformed sediments, offscraped oceanic crust or both. His modeled density of 2.8 g/cm^3 is probably too high to be sediments; he did not discuss the implications of this high density. The density of 2.7 g/cm^3 obtained in my modeling is more reasonable but equivocal.

Densities of the Hoh melange (Rau, 1973) that may represent the typical material in the trench were measured in an well offshore of the Olympic Mtns. to range from 2.4 g/cm^3 to 2.55 g/cm^3 with porosities ranging from 10-20% at about a 1 km depth (Pan American well P0141, W. M. Phillips, oral comm., 1988). An increase to 2.7 g/cc would not be unreasonable at greater depths. Densities for mudstones with little or no porosity have been measured to be as high as 2.7 g/cm^3 (Hamilton, 1978). Additions of pieces of oceanic crust would also contribute to the high density material required in the trench.

If densities appropriate for phase changes in the subducting Juan de Fuca plate (from 30 -60 km depth) of 3.58 g/cm^3 for oceanic crust converted to eclogite and of 3.38 g/cm^3 for oceanic mantle converted from plagioclase to garnet peridotite are included in the model (Fig. 7), densities of 2.85 g/cm^3 for the Coast Range basalts and 3.05 or 3.28 g/cm^3 for the material beneath the Coast Range basalts are obtained. Densities of 2.92 g/cm^3 for the Coast Range basalts and 3.07 or 3.28 g/cm^3 for the underlying material are obtained without densities consistent with phase changes (Fig. 7). All of these values are geologically reasonable, leading to the conclusion that densities consistent with shallow phase changes are not required by the gravity modeling.

In the final model (Fig. 7) the 3.3 g/cm^3 density of the mantle of the Juan de Fuca plate for the offshore part of the plate continues under the Coast Range to a depth of about 40 km, increases to 3.32, and then to 3.33 g/cm^3, the 0.05 g/cm^3 density contrast suggested by

Riddihough (1979), Grow (1973) and Grow and Bowin (1975) to be between the subducting plate and surrounding asthenosphere.

The modeled magnetization for the Coast Range basalts is 6 A/m, within the range of about 2 - 8 A/m measured for Pacific seamounts (McNutt, 1986).

The upper crustal section (upper 20 km) in the Cascade Range section of the model (Fig. 7) is described in detail in Stanley and others (1987). The densities and magnetizations in the upper crustal parts of the model, although not well constrained, are compatible with the geologic structures inferred from the MT modeling. Part of the upper 1-4 km consists of Cenozoic basaltic flows and andesitic volcaniclastic rocks and flows with densities ranging from 2.5 to 2.6 g/cm^3 and magnetizations from 2.7 to 5.4 A/m. Sediments are believed to occur beneath the surficial volcanic rocks. The eastern half of the Cascade Range volcanic rocks are underlain by thin slivers of Jurassic/Cretaceous marine sediments of the Russell Ranch formation (Swanson and Clayton, 1983; Williams and Finn, 1987) and Tertiary plutonic rocks (Stanley and others, 1987; this issue; Smith, in press; Sherrod and Smith, this issue). West of the Goat Rocks Volcano, thick (2-5 km) Oligocene volcanic flows may be underlain by 5 to 10 km of proposed marine sediments (called the SWCC sediments) that may have been part of a forearc basin that developed prior to the Eocene jump in subduction (Stanley and others, 1987; 1988). Part of the gravity low over the Cascade Range (Fig. 7) is caused by the low densities of these rocks relative to those in the Coast Range and Columbia Plateau.

The magnetic high over the Cascade Range (Fig. 7) is caused by the surficial volcanic rocks. Thinning of the volcanic rocks over anticlinal structures that bring the less magnetic interpreted forearc basin sediments within 1 km of the surface (Stanley and others, 1988) is though to cause the magnetic lows on the both sides of the high .

The nature of the middle Cascade Range crust is unknown; its density is consistent with seismic velocities measured in the Oregon Cascade Range (Leaver and others, 1984) and can range in value from 2.7-2.93 g/cm^3 (the 2.93 value is used in the final model). It may be composed of oceanic crust that was once the leading edge of the North American continent before accretion of the Coast Range basalts. The sediments interpreted to be part of the older forearc basin could have been deposited on top of this crust. A density of 2.93 g/cm^3 is compatible with this model. A lower density of 2.7 g/cm^3 is considered average for middle crustal continental rocks. Either density fits the observed data. The composition of the lower crust is completely unknown so the modeled density of 3.08 g/cm^3, consistent with the seismic refraction results from Oregon was used (Leaver and others, 1984) in the final model. The middle and lower crusts are considered to be nonmagnetic.

The density of the Cascade Range mantle is modeled to be 3.3 g/cm^3, consistent with the 7.9 km/s velocities determined in the Oregon Cascades (Leaver and others, 1984) and at the same longitude in Puget sound (Crosson, 1976). The lateral extent of this density is unknown; I continued it west to its intersection with the Juan de Fuca plate, and east to the Cascade Range/Columbia Plateau boundary (Fig. 7). Part of the gravity low over the Cascade Range is related to the density contrast between this lower density mantle and the higher densities of the Juan de Fuca plate and the Columbia Plateau mantle. High densities are required in the model in this section so I somewhat arbitrarily forced the modeling program to put it in the Juan de Fuca plate, rather than in the Cascade Range mantle.

The densities in the Columbia Plateau section of the model (Fig. 7) were modified only slightly from the starting model. They are consistent with the seismic refraction velocities (Catchings and Mooney, 1988) and the geologic interpretation from the MT data (Stanley, 1984). The upper 10 km of the model consists of basalt flows with interbedded sediments. A compositional "rift pillow" may exist in the lower crust where higher seismic velocities than for normal continental crust are observed. Much of the observed gravity high (Fig. 7) is caused by the contrast between the dense rift pillow and the surrounding lower crust.

The measured Columbia Plateau upper mantle velocity is 8.4 km/s, higher than the 7.9 km/s measured in Puget Sound at this longitude (Crosson, 1976) and under the Oregon Cascades (Leaver and others, 1984). Therefore, the upper mantle densities are higher under the Plateau than under the Cascade Range section of the model. Some of the observed gravity high over

the Columbia Plateau is caused by this contrast. The density contrast between the deep part of the Juan de Fuca plate (0.05 g/cm^3) and the surrounding asthenosphere does not have a large effect on the observed gravity anomaly. This will be discussed later.

DISCUSSION

Sources of the Trench and Coast Range Gravity Anomalies

One of the questions addressed by the final model is what is the source of the trench gravity low and forearc gravity high? Grow (1973) in the Aleutian Islands and Grow and Bowin (1975) in Chile suggest that the forearc gravity high there is primarily due to density increases caused by shallow phase changes in the subducting slab and that these density increases also contribute to the trench gravity low. This does not seem to be true in the Coast Range.

The gravity high over the Coast Range (Fig. 7) correlates closely with the magnetic high (Fig. 7) whose source is mostly likely the Coast Range basalts (outlined in Figs. 4 and 5). It is unlikely that the source of the magnetic high is in the subducting Juan de Fuca plate; the plate does not cause a magnetic anomaly over the continental shelf and slope where it is shallower than it is under the Coast Range. The final model (Fig. 7) indicates that the Coast Range basalts can account for most of the gravity high and the magnetic high, also showing that the location of eastern edge of the Coast Range basalts delineated by the magnetic data is compatible with the gravity data. The fact that the gravity and magnetic highs are coincident is the strongest evidence for the Coast Range basalts as the source of the gravity high.

One of Grow and Bowin's (1975) arguments for shallow phase changes in the subducting Nazca plate was to eliminate the need for shallow mantle or other high density material in the outer trench wall, like that required in Chile gravity models by Hayes (1966). The density increases in the subducting plate due to the postulated shallow phase changes caused a broad enough gravity anomaly to extend over the trench. Shallow mantle nor high density material are not required in the Washington model regardless of the density of the subducted part of the Juan de Fuca plate. High densities are required of the sediments within the trench, however. I wondered whether these were required because I did not include shallow mantle in the outer trench wall. The apex of the gravity low due to the density contrast of these sediments and the continental rocks is east of that due to the kind of shallow mantle referred to Grow and Bowin's (1975) study. For shallow mantle to replace the need for high density sediments within the trench it would have had to be located under the western edge of the Coast Range, not under the outer trench wall.

Fig. 8 shows a 50 km thick version of the model shown in Fig. 8. Few densities had to be changed in this model to give a reasonable fit of the calculated to the observed anomaly, demonstrating that the shallow structures are the main sources of the observed gravity anomalies. The large, lateral density and magnetization contrasts, as between trench sediments and the accreted Coast Range basalts and between the basalts and the Cascade Range rocks, make gravity and magnetic data a powerful tool in delineating shallow tectonic boundaries in the Pacific Northwest. Furthermore, as demonstrated in earlier sections, these types of boundaries are present in many subduction zones. The combination of gravity and magnetic data can help to delineate accreted terrane boundaries and to determine whether fore arc ridges are underlain by oceanic crust or completely composed of melange.

The Composition of the Rocks below the Coast Range Basalts

Previous gravity models of the Washington margin (eg. Dehlinger and others, 1968; Riddihough, 1979) include shallow (about 16 km depth) high density mantle under the Coast Range basalts. This Moho depth was obtained from a short, unreversed seismic refraction survey in the Oregon Coast Range (Berg and others, 1966). This 16 km Moho depth estimate is probably wrong. Only one data point constrains it. No Moho was observed under the Olympic Mountains and northern part of the Coast Range in more recent seismic refraction surveys (Taber, 1983; Taber and Lewis, 1985). However, as shown in Fig. 7, the gravity data can be modeled with densities appropriate for mantle. The mantle would be nonmagnetic; a subduction complex may or may not be.

Shallow mantle is compatible with the proposed ocean island origin for the Coast Range. Mantle depths of about 18 km are found under the Hawaiian Islands (eg. Zucca and others, 1982). Berg and others' (1966) 8.2 km/s velocity estimate for the Oregon Coast Range is compatible with oceanic mantle velocites.

Other, more convincing evidence, suggests that the rocks under the Coast Range basalts belong to a subduction complex. Magnetotelluric data from the northern profile marked in Fig. 6 start in the Olympic Peninsula and extend south and then east across the Coast and Cascade Ranges (see Stanley and others, 1987). These data show a conductive layer beneath the Olympic Mountains and the Coast Range that probably corresponds to the marine sediments and ophiolites of the Olympic Peninsula, not to mantle. The thickness of this layer is not constrained, but does indicate that at least some marine sediments underlie the Coast Range basalts at depths greater than 18 km (Stanley and others, 1987; this issue). The presence of the marine sediments under the basalts indicates that the original mantle of the oceanic island complex that composes the Coast Range is no longer present. It is unlikely that a new mantle has formed at the shallow depths of the modeled bottom of the Coast Range basalts (less than 25 km in Fig. 7), suggesting that a subduction complex, rather than mantle underlies the Coast Range basalts. MT results from the Oregon Coast Range show a conductive layer interpreted to be due to a subduction complex (Wannamaker and others, this issue)

Studies of the waveforms of earthquakes in Victoria, British Columbia (Fig. 6) (Langston, 1981), Puget Sound (Fig. 6) (Langston and Blum, 1977) and Corvallis, Oregon (Langston, 1977, 1981) show evidence of a thick (about 15 km) low velocity zone above the subducted Juan de Fuca plate. The base of this proposed low velocity zone is at depths of 45 to 50 (+5) km under Victoria (Fig. 6) and Corvallis (Langston, 1981) and at 56 (+ 5) km under Puget Sound (Langston and Blum, 1977), depths consistent with the Moho of the Juan de Fuca plate from other studies. This thick low velocity zone would more likely correspond to subducted oceanic crust in the Juan de Fuca plate overlain by a subduction complex than to the crust overlain by mantle.

The subduction complex might resemble that proposed to underlie Vancouver Island (Clowes and others, 1987) (Fig. 6), based on seismic reflection and refraction data. The Metchosin basalts of Vancouver Island, correlative with the Coast Range basalts, may be underlain by as much as 10 km of the marine sediments exposed in the Olympic Mtns. Approximately 15 - 20 km of oceanic crustal rocks are proposed to underplate the sediments. Another 5 km of sediments are proposed to lie beneath the underplated oceanic crust and on topo of the subducting Juan de Fuca plate.

A multi-density model corresponding to this subduction model could fit the observed data. Because no constraints on the density of the material underlying the Coast Range basalts, I used a simple 2 density model. However, the gravity model does require that the proposed subduction complex be denser than the trench sediments, indicating that material denser (like offscraped oceanic crust) than sediments must also be incorporated within it. The modeled density of 3.07 g/cm^3 for the subduction complex is consistent with the 7.7 km/s seismic

velocity obtained from the Vancouver Island refraction survey (Spence and others, 1986) interpreted to consist mostly of offscraped oceanic crust (Clowes and others, 1987).

Relation of the Coast Range Basalts to Crustal Seismicity

In southwest Washington crustal seismicity falls along the eastern edge of the Coast Range basalts, surrounding the SWCC rocks to the east (Stanley and others, 1987; Weaver, this issue). North of this seismic activity is a gap until just south of Puget Sound where crustal seismicity does occur. There the seismicity occurs within the Coast Range basalts from the surface to depths of about 18 km (Weaver, this issue) where the bottom of the basalts is postulated. From central Puget Sound to the north the Coast Range basalts seem to be breaking up; they do not to be as coherent a block as they are to the south (Figs. 4 and 5). Accordingly, the crustal seismicity also decreases in occurance from the areas to the south. This may suggest that the difference in structure accounts for the latitudinal change in seismicity pattern.

Comparison of the Washington Gravity Model to Other Subduction Zone Models

Some features peculiar to the Washington margin make it difficult to compare it to other subduction zones. The Juan de Fuca plate is younger and therefore thinner and hotter than most other subducting plates (see Jarrard, 1986). Any density increases due to shallow phase changes in such a thin plate would cause much smaller gravity anomalies (about 60 mGals) than for a thicker plate such as the Nazca plate (128 mGals, Grow and Bowin, 1975). The deep part of the subducting Juan de Fuca plate (density = 3.3 g/cm^3, in Fig. 7), with its 0.05 g/cm^3 density contrast with the surrounding asthenosphere causes a gravity anomaly with an amplitude of about 24 mGals, smaller than the 60 mGal amplitude of the subducting plate underthe Aleutians (Grow, 1972) and Chile (Grow and Bowin, 1976). They do have similar wavelengths, about 300 km.

Because the Juan de Fuca plate is probably hotter than other plates the shallow phase changes proposed for the colder Nazca plate under the Chile margin may be occurring deeper in the Juan de Fuca plate (Riddihough, 1979) so that the main density contrast related to the subducting Juan de Fuca plate would be between the deep part (>60 km) of the subducting slab and the asthenosphere, rather than at shallower (30-60 km) levels.

CONCLUSIONS

The process of continental growth by accretion of terranes and arc magmatism are illustrated by the results of the model presented here. Parts of the following plate tectonic reconstruction of the Washington margin have been proposed by Dickinson (1976), Armentrout and Suek (1985) and Stanley and others (1987; 1988).

By the late Cretaceous to the early Eocene, the continental edge was in present-day eastern Washington. Forearc basin-type sediments could have been deposited on a piece of oceanic crust that may have been attached to the continent (like in present-day Sumatra (Hamilton, 1979) that was being underthrust by the Farallon plate (Dickinson, 1979), or on top of older forearc basin sediments (Fig. 9).

The geophysical signature of the margin at this time may have been analogous to the present-day Sumatran system. The marine sediments in the forearc basin between the forearc ridge (Hamilton, 1979) and Sumatra and Java are electrically conductive, and are probably non-magnetic as in the central Aleutians (Grow, 1973). The Bouguer anomalies over Sumatra are positive (Green and others, 1979), typical of oceanic values.

By the late Eocene, the ocean island terrane proposed for the origin of the Coast Range basalts (Duncan, 1982; Wells and others, 1984), was accreted to the continent, compressing the forearc basement against the continent. The subduction zone may have been clogged by the accreted terrane, forcing it to jump to the west (Dickinson, 1979; Armentrout and Suek, 1985) (Fig. 9).

The proposed westward shift of the subduction zone eventually resulted in a westward shift of arc volcanism (Dickinson, 1976). The volcanism associated with the present-day magmatic arc, the Cascade Range, started in the Miocene (McBirney, 1968) and continues in the present (Fig. 9). This volcanism is now intruding the older forearc basin and "continentalizing" it. The geophysical signatures of the proposed marine forearc basin (Stanley and others, 1987) is transitional between oceanic and continental. The electrical resistivities are appropriate for marine sediments. The proposed magnetizations are consistent with marine sediments altered by hydrothermal activity.

The seismic velocity structure of the Oregon Cascades crust (Leaver and others, 1984) is higher than that of the mature continent of the Sierra Nevada and is consistent with that of developing island arcs (Hamilton, pers. comm., 1988). This may be further evidence that the area of the Cascades is still evolving from oceanic structure to continental.

The estimated crustal thickness for the Cascades in Oregon (Leaver and others, 1984) and California (Zucca and others, 1986) is about 40 km; the value for southern Washington is probably similar. This is less than the 48 km thick crust estimated for the Sierra Nevada (Eaton, 1966). Because of arc volcanism, the crust has thickened and a Moho developed. It is unclear how far west the Moho in the North American plate extends, ie., whether it continues under the western edge of the Coast Range basalts. If no continental Moho exists under the Coast Range, that implies that arc volcanism is a requirement for its development. If a continental Moho is present then pressure/temperature conditions may be sufficient to form it. Reliable seismic refraction and/or deep reflection data are needed to resolve this question.

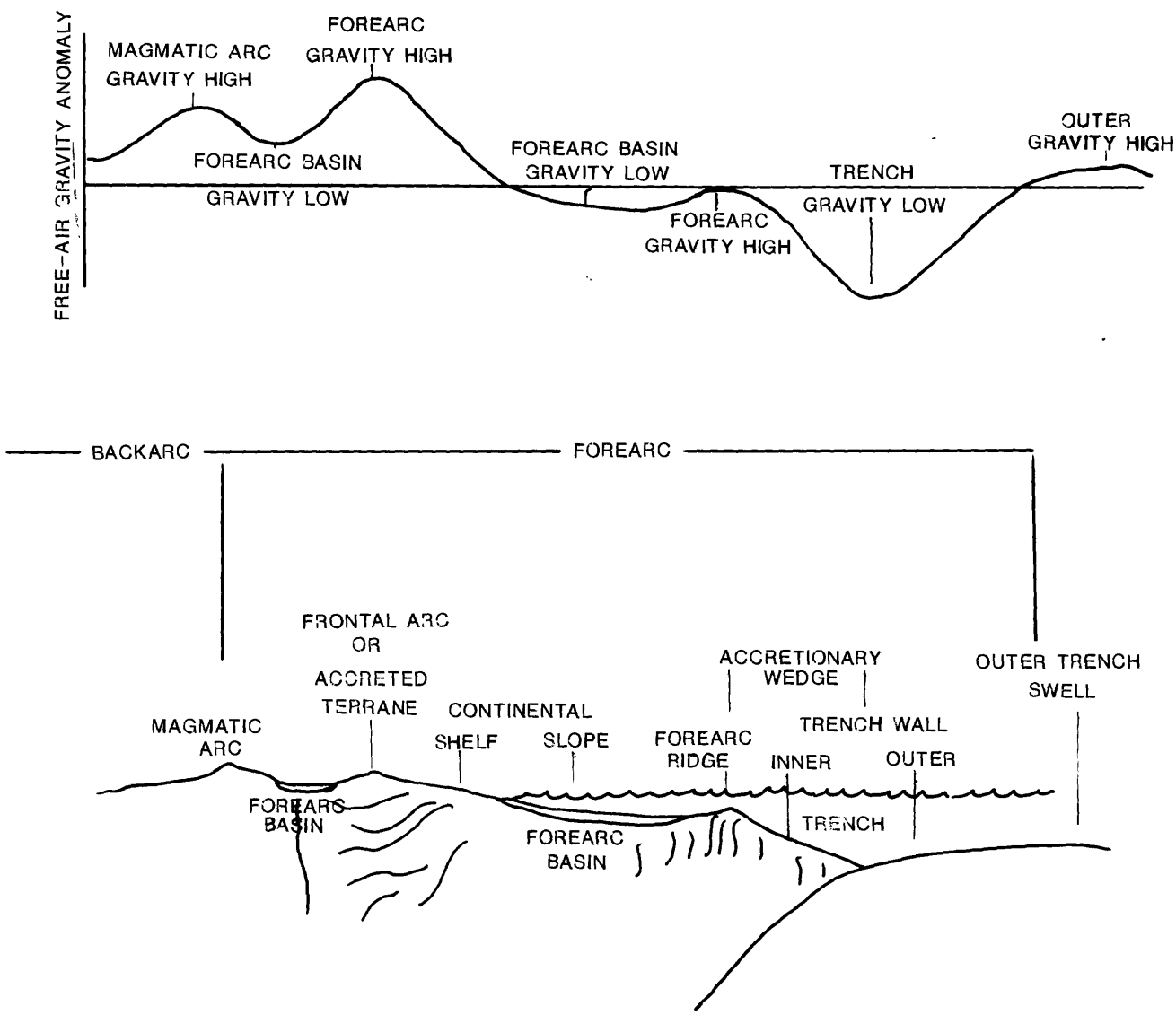

Figure 1 Morphology of subduction zones with the terminology used in this paper (after Honza, 1981; Karig and Sharman, 1975). The top of the figure shows the type of Free-Air gravity anomaly typically associated with the morphologic feature below it. Also indicated is the gravity terminolgy used in the test.

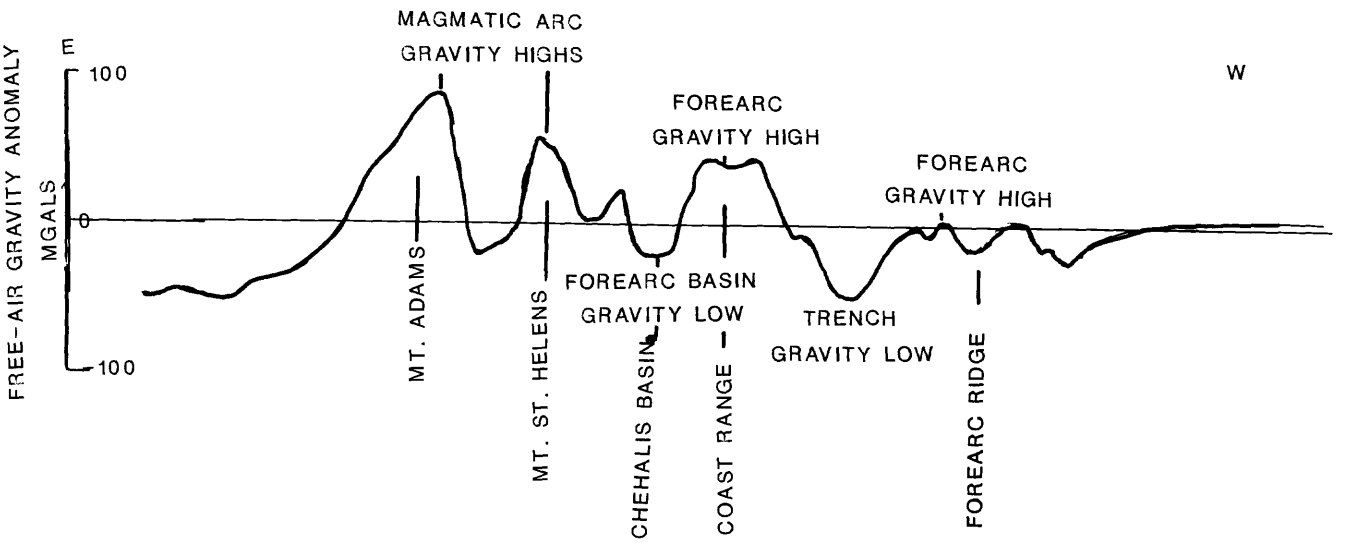

Figure 2. Free-Air gravity profile across southern Washington.

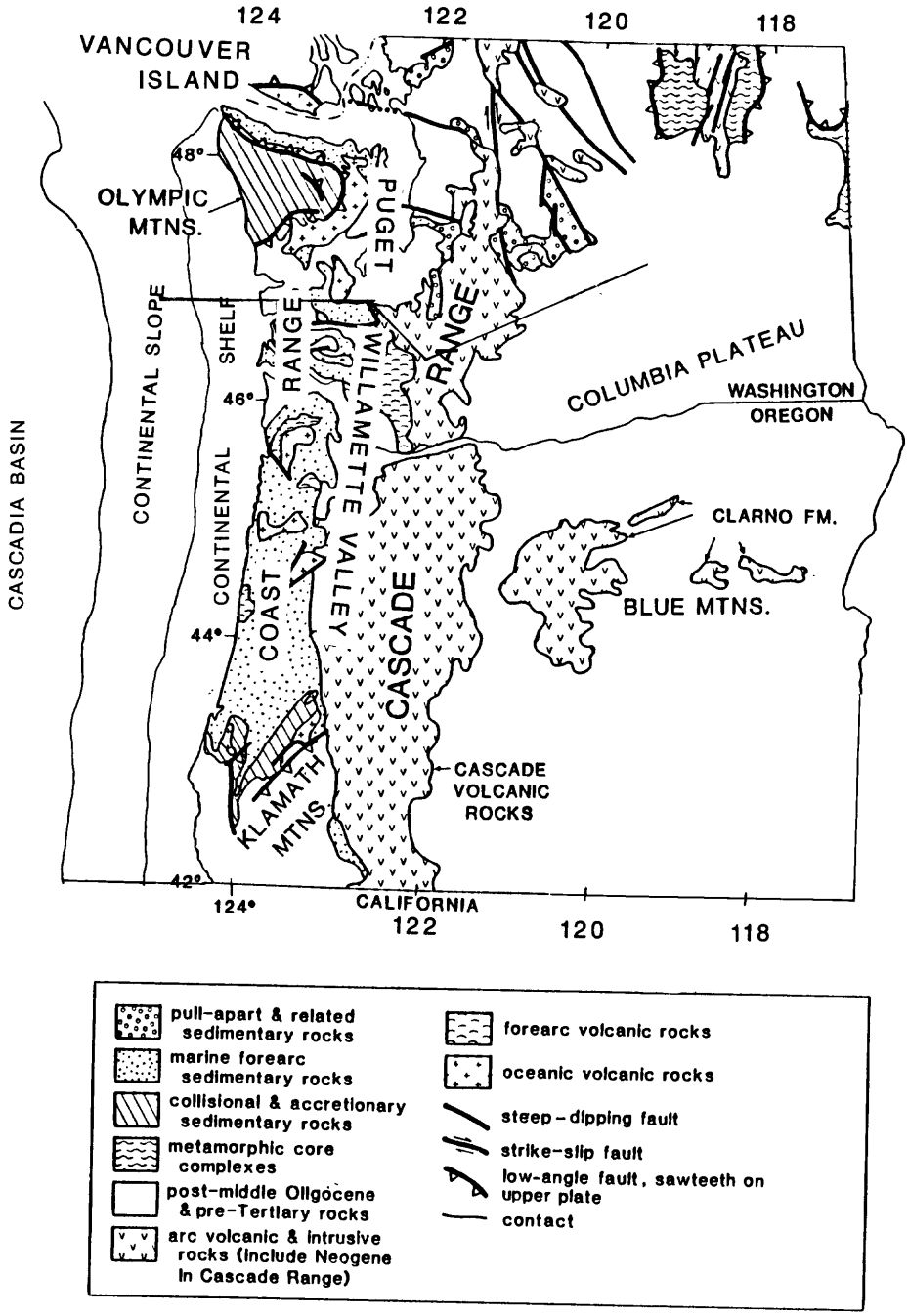

Figure 3. Generalized geologic map of Washington and Oregon (after Heller and others, 1987). The location of the modeled gravity profile modeled is indicated by the line.

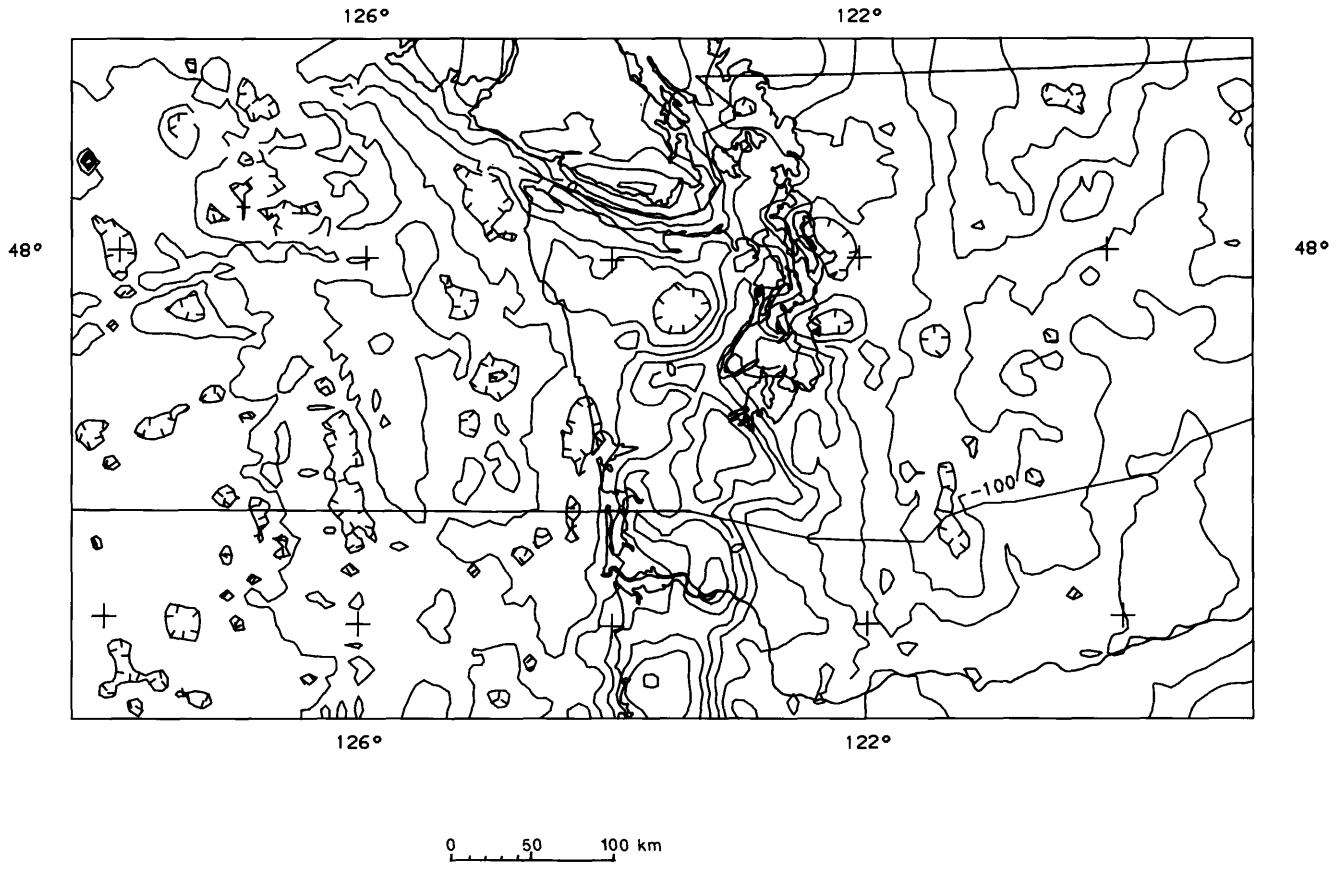

Figure 4. Grey-shade map of the complete Bouguer anomaly in MGals with Bouguer reduction density of 2.67 g/cm^3. The solid line marks the location of the modeled profile. The triangles mark the major Cascade volcanoes. The proposed boundaries of the Coast Range basalts are outlined.

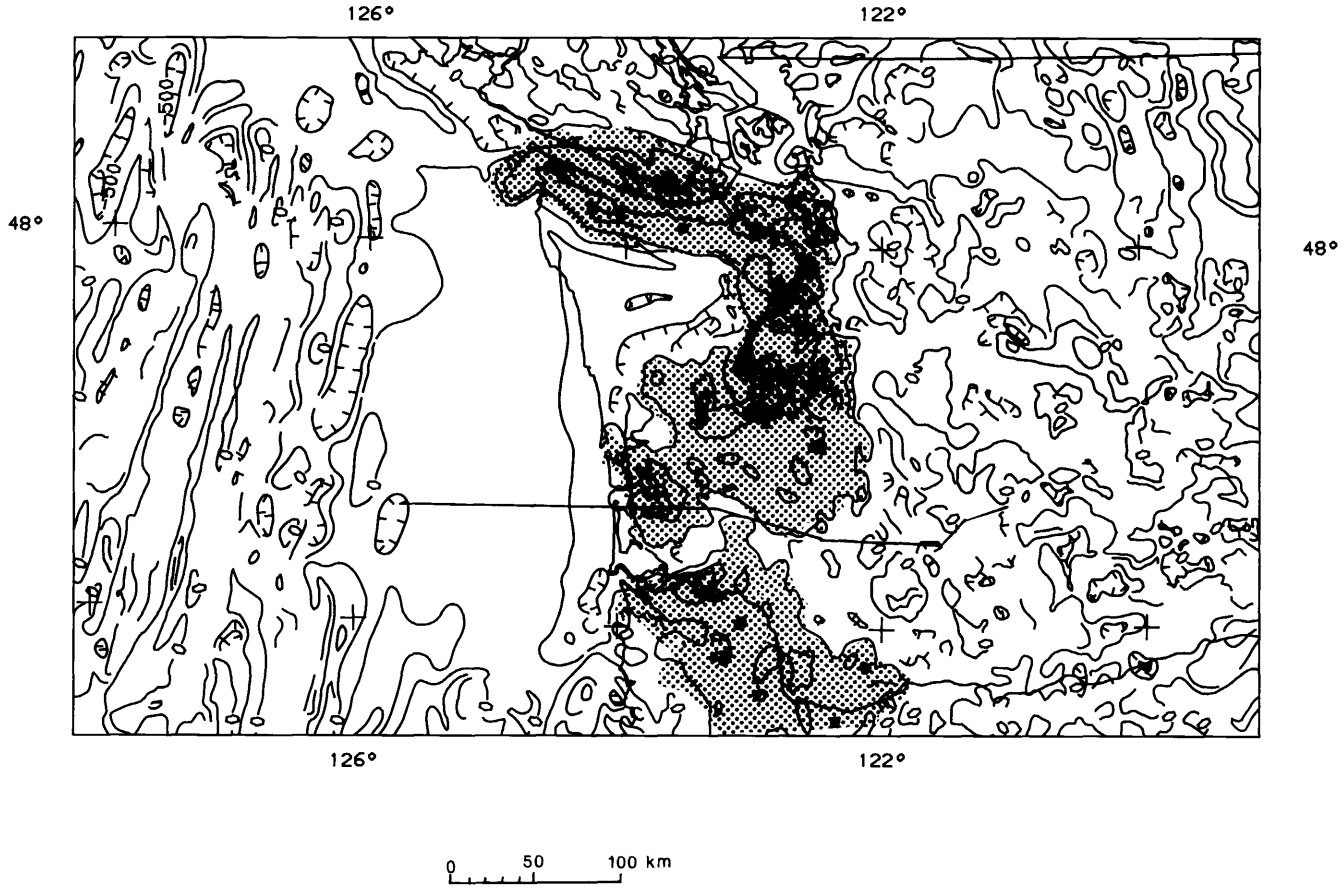

Figure 5. Grey-shade map of the aeromagnetic anomaly in nTesla (from Comm. for the mag. anom. map of North Am., 1987). The solid line marks the location of the modeled profile. The triangles mark the major Cascade volcanoes. The proposed boundaries of the Coast Range basalts are outlined.

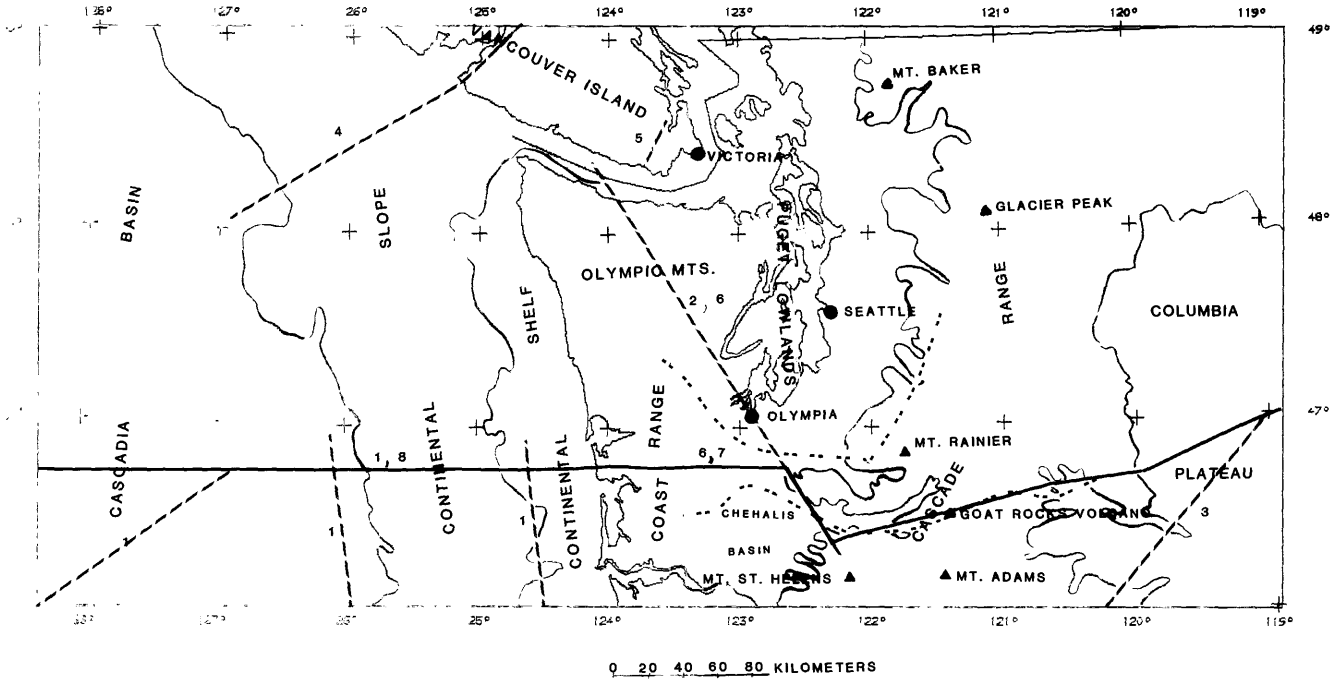

Figure 6. Major physiographic provinces in western Washington. The solid line marks the location of the modeled gravity and magnetic profile. The double dashed lines are magnetotelluric profiles (Stanley and others, 1987). The single dashed lines mark the locations of seismic refraction profiles. The numbers for these profiles denote the following references: 1. Shor and others (1968), 2. Taber and Smith (1986), 3. Catchings and Mooney (1988), 4. Spence and others (1985), 5. Clowes and others (1987), 6. Taber (1983), 7. Taber and Lewis (1986), 8. McClain and Taber (1984); McClain (1981).

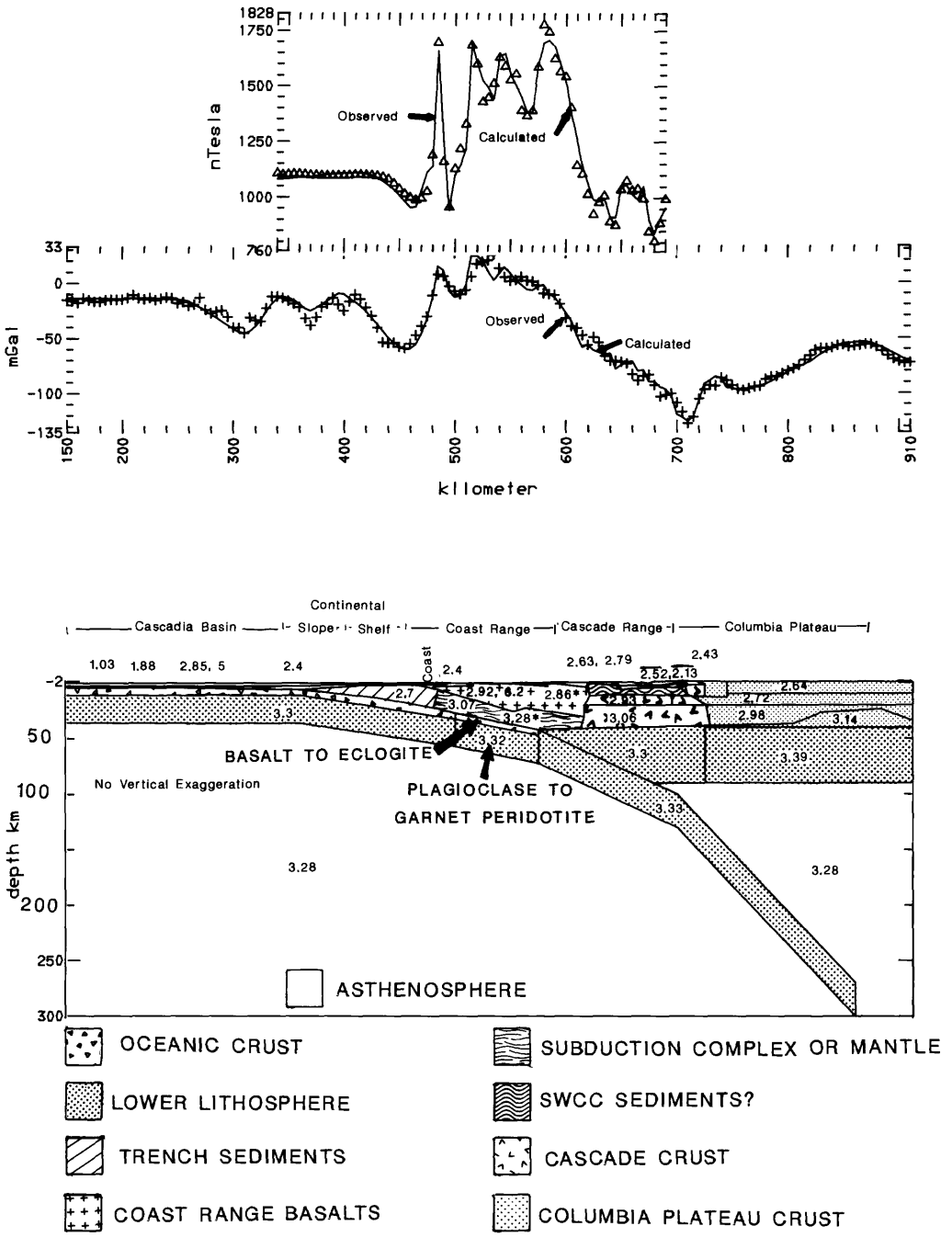

Figure 7. Final model. Results of the gravity and magnetic modeling for the profiles located on Figs. 4 and 5. For each profile, the calculated (line) and observed (crosses for gravity; triangles for magnetic) anomalies (from Figs. 4 and 5) are shown. Densities (in g/cm^3) for each body are listed first. The starred densities represent those required if shallow mantle underlies the Coast Range basalts; unstarred values are for a subduction complex beneath the basalts. Magnetizations (in A/m), if other than zero are listed second, after the comma. Average values (bar on top) are given for the upper 5 km of Cascades Range rocks. Details for the Cascade Range section are given in Stanley and others (1987). All magnetizations are assumed to be in the present Earth's field direction of 56000 nTesla, with an inclination of about 69^o and declination of about 20^o.

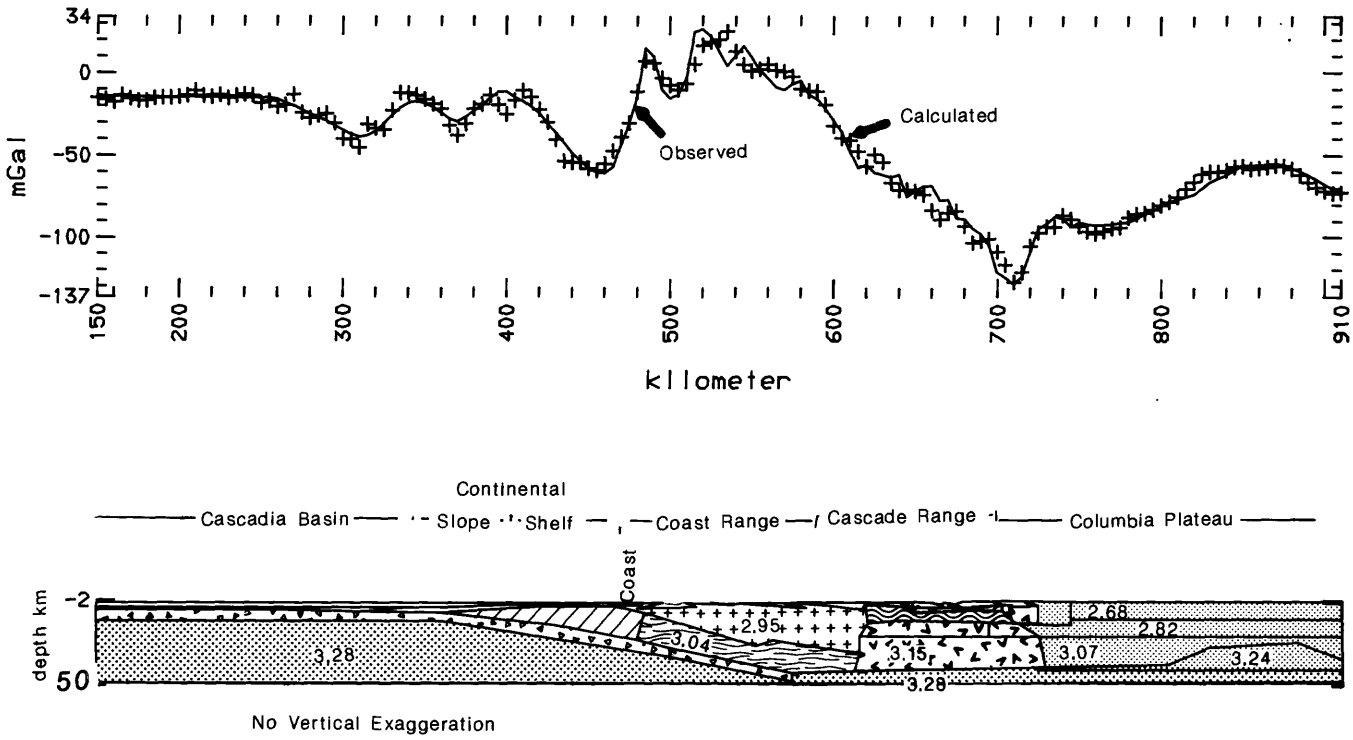

Figure 8. 50 km thick model. The same as the final model (Fig. 7) except for the base being at 50 km. The density values (in g/cm^3), where different from Fig. 7, are indicated. The magnetizations are the same as for Fig. 7.

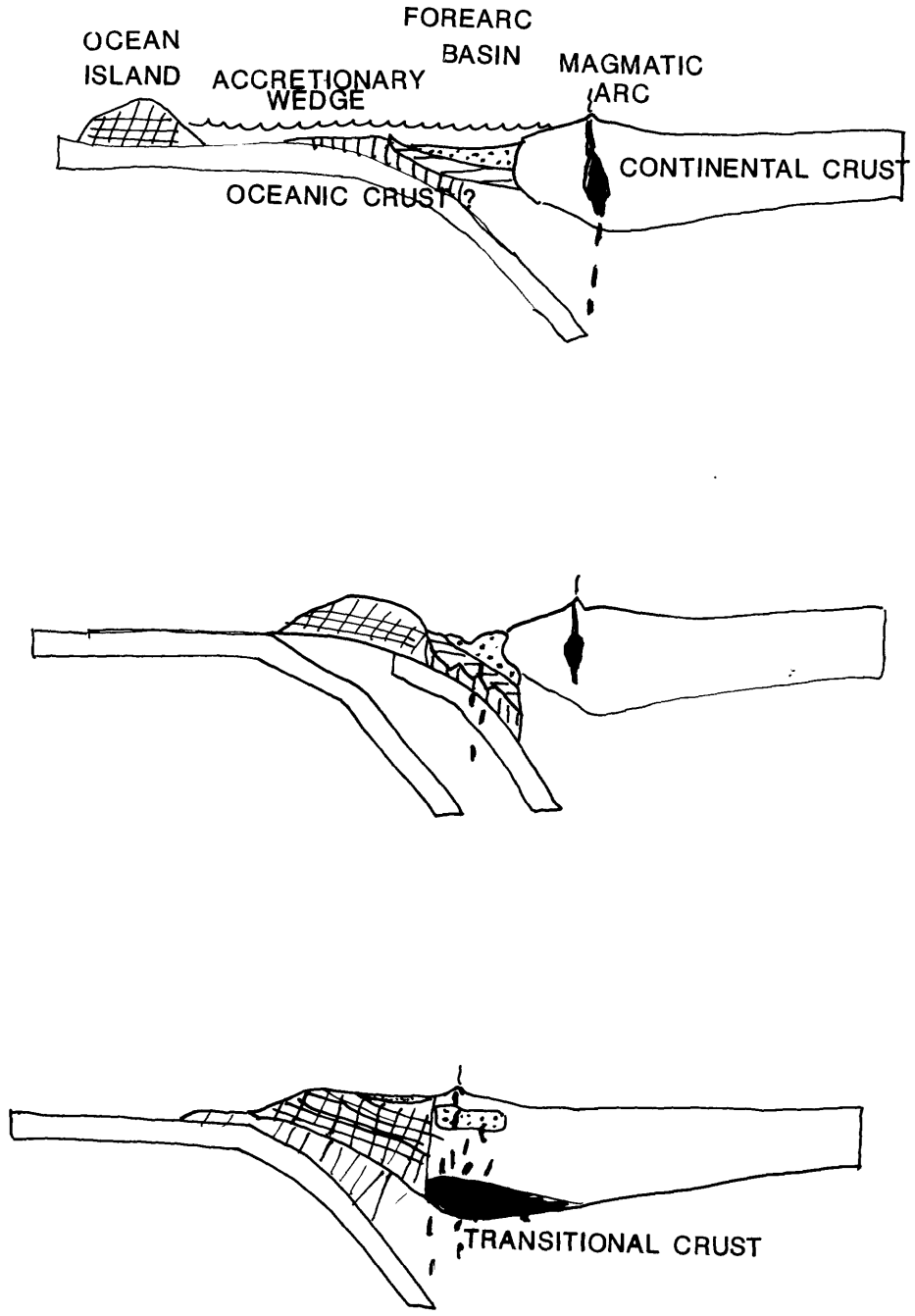

Figure 9. Schematic diagram of structures and proposed to represent the continental growth of the Washington margin. A) Pre-ocean island accretion. Melange wedge is subducting under oceanic crust (?) that underlies a forearc basin. B) Accretion of the ocean island causes the subduction zone and associated arc magmatism to shift to the west. The forearc basin is also accreted to the continent and begins to be intruded by subduction related magmatism (from Stanley and others, 1988). C) Present-day. The previously oceanic crust and basin of the forearc region, now termed transitional, is almost completely "continentalized" by arc magmatism.

REFERENCES

Ahrens, T. J. and Schubert, G., 1975, Gabbro-eclogite reaction rate and its geophysical significance: Revs. Geophys. and Space Phys., v. 13, p. 383-400.

Armentrout, J. M., and D. H. Suek, 1985, Hydrocarbon exploration in western Oregon and Washington: American Association of Petroleum Geologists Bulletin, v. 69, p. 627-643.

Atwater, T., 1970, Implications of plate tectonics for the Cenozoic tectonic evolution of western north America: Geol. Soc. Amer. Bull., v. 81, p. 3715-3722.

Bates, T. G., Beck, M. E.,Jr., Burmester, R. F., 1982, Tectonic rotations in the Cascade Range of southern Washington: Geology, v. 9, p.184-189.

Beck, M. E., Jr., 1980, Paleomagnetic record of plate-margin processes along the western edge of North America: Jour. Geophys. Res., v. 84, p. 7115-7131.

Berg, J.W., Jr., Trembly, L., Emilia, D.A., Hutt, J.R., King, J.M., Long, L.T., McKnight, W. R., Sarmah, S. K., Souders, R., Thiruvathukal, J. V., and Vossler, D.A., 1966, Crustal refraction profile, Oregon Coast Range: Bull. Seis. Soc. Amer., v. 56, p.1357-1362.

Bowin, C. Warsi, W., and Milligan , J., 1982, Free-Air gravity anomaly map of the world: Geol. Soc. Amer. Map and Chart Series MC-45, scale 1:22,000,000 at the Equator.

Cady, J. W. and Fox, Jr., K. F., 1984, Geophysical interpretation of the gneiss terrane of northern Washington and southern British Columbia, and its implications for uranium exploration: U. G. Geol. Surv. Prof. Paper 1260, 29 pp.

Catchings, R. D., and W. D. Mooney, 1988, Crustal structure of the Columbia Plateau: Evidence for continental rifting: Jour. Geophys. Res., v. 93, p. 459-474.

Chapman, M. E. and Talwani, M., 1982, Geoid anomalies over deep sea trenches: Geophys. J. R. Astr. Soc., v. 68, p. 349-369.

Clowes, R. M., Brandon, M.T., A. G. Green, C.J. Yorath, A. Sutherland-Brown, E.R. Kanasewich, and C. Spencer, 1987, LITHOPROBE- Southern Vancouver Island: Can. Jour. of Earth Sci., v. 24, p. 31-51.

Committee for the Magnetic Anomaly Map of North America, 1987, Magnetic anomaly map of North America: Boulder, CO, Geological Society of America, 4 sheets, scale 1:5,000,000.

Connard, G., R. W. Couch, G. Ness, and S. Troseth, 1984, Magnetic anomaly identifications: in Kulm, L.D. and others (eds.) Western North American continental margin and adjacent ocean floor off Oregon and Washington, Atlas 1, Ocean Margin Drilling Program Regional Atlas Series: Marine Science International, Sheet 5.

Couch, R. W., 1969, Gravity and structures of the crust and subcrust west of Washington and British Columbia: Ph. D. dissertation, Oregon State Univ., Corvallis.

Couch, R. W., and Braman, D., 1979, Geology of the continental margin near Florence, Oregon: Oregon Geology, v. 41, p. 171-179.

Couch, R. W. and S. Woodcock, 1981, Gravity and structure of the Continental margins of southwestern Mexico and nothwestern Guatemala: Jour. Geophy. Res., v. 86, p. 1829-1940.

Couch, R. W. and Riddihough, R. P., in press, The coastal Structure of the western continental margin of North America: in The Geophysical Framework of the Continental United States, (eds. L.C. Pakiser and W. D. Mooney), Geological Soc. of America Memoir.

Cox, A. and Doell, R. R., 1960, Review of paleomagnetism: Geol. Soc. Amer. Bull., v. 71, p. 645-768.

Crosson, R. S., 1976, Crustal structure modelling of earthquake data. 1. Simultaneous least squares estimation of hypocenter velocity parameters, 2. Velocity structure of the Puget Sound region: Journal of Geophysical Research, v. 81, p. 3036-3047.

Crosson, R. S., 1983, Review of seismicity in the Puget Sound region from 1970-1978: Proceedings of USGS Workshop XIV, Earthquake Hazards of the Puget Sound Region, Washington, p. 6-18.

Crosson, R. S. and T. J. Owens, 1987, Slab geometry of the Cascadia subduction zone beneath Washington from earthquake hypocenters and teleseismic converted waves: Geophys. Res. Lett., v. 14, p. 824-827.

Davis, G, Monger, J., and Burchfiel, B., 1978, Mesozoic construction of the Cordilleran "collage," central British Columbia to central California: in Mesozoic Paleogeography of the Western United States, Pacific Coast Paleogeography Symposium 2, Howell, D. and McDougall, K., eds., Los Angeles, p. 1-32.

Dehlinger, P., Couch, R. W., and Gemperle, M., 1968, Continental and oceanic structure from the Oregon coast westward across the Juan de Fuca Ridge: Can. Jour. of Earth Science, v. 5, p. 1079-1090.

Dickinson, W. R., 1970, Relations of andesites, granites, and derivative sandstones to arc-trench tectonics: Rev. Geophys. and Space Phys., v. 8, p. 813-860.

Dickinson, W. R., 1976, Sedimentary basins developed during evolution of Mesozoic-Cenozoic arc-trench system in western North America: Canadian Journal of Earth Sciences, v. 13, p. 1268-1283.

Dickinson, W.R., 1979, Cenozoic plate tectonic setting of the cordilleran region in the United States: in Cenozoic paleogeography of the western United States: Soc. of Econ. Paleontologists and Mineralogists, Pac. Sect., Pac. Coast Paleogeography Sym. 3, 1979, p. 1-13.

Duncan, Robert A., 1982, A captured island chain in the Coast Range of Oregon and Washington: Jour. Geophys. Res., v. 87, no. B13, p. 10827-10837.

Finn, Carol, 1984, Description of magnetic tape containing Washington State gravity anomaly data: U.S. Department of Commerce National Technical Information Service Report, no. USGS-GD-85-001.

Finn, Carol, Phillips, W. M., and Williams, D. L., 1984, Gravity maps of the State of Washington and adjacent areas (scale 1:250,000): U.S. Geological Survey Open-File Report 84-416, 18 sheets.

Green, R., Adkins, J. S., Harrington, H. J., and Untung, M., 1979, Bouguer gravity anomaly map of Indonesia, with marginal text: Univ. New England, Armindale, Australia, scale 1:5,000,000.

Grow, J., 1972, A geophysical study of the central Aleutian Arc: Phd. thesis, Scripps, U.C. San Diego, California, 132 pp.

Grow J., 1973, Crustal and mantle structure of the central Aleutian arch: Geol. Soc. Amer. Bull., v. 84, 2169-2192.

Grow, J., and Bowin, C., 1975, Evidence for high density crust and mantle beneath the Chile trench due to the descending lithosphere: Jour. Geophys. Res., v. 80, p. 1449-1458.

Hamilton, E. L., 1978, Sound velocity-density relations in sea-floor sediments and rocks: Jour. Acoustical Soc. Amer., v. 63, p. 366-377.

Hamilton, Warren, 1979, Tectonics of the Indonesian region: U. S. Geol. Surv. Prof. Paper 1078, 345 p.

Hayes, D. E., 1966, A geophysical investigation of the Peru-Chile trench, Marine Geology, v. 4, p. 309-351.

Hayes, D. E., 1978, A geophysical atlas of the east and southeast Asian seas: Geol. Soc. of Amer. Map and Chart Series, MC-25, 6 maps, scale 1:6,442,194 at latitude 0^{o}.

Heller, P. L., Tabor, R. W., and Suczek, C. A., 1987, Paleogeographic evolution of the United States Pacific Northwest during Paleogene time: Can. Jour. Earth Sci., v. 24, p. 1652-1667.

Jarrard, R. D., 1986, Relations amoung subduction parameters: Revs. Geophys., v. 24, p. 217-284.

Langston, C. A., 1977, Corvallis, Oregon, crustal and upper mantle receiver structure from teleseismic P and S waves: Bull. Seis. Soc. Amer., v. 67, p. 713-724.

Langston, C. A., 1981, Evidence for the subducting lithosphere under southern Vancouver Island and western Oregon from teleseismic P wave conversions: Jour. Geophys. Res., v. 86, p. 3857-3866.

Langston, C. A. and Blum, D. E., 1977, The April 29, 1965, Puget Sound earthquake and the crustal and upper mantle structure of western Washington, Bull. Seis. Soc. Amer., v. 67, p. 693-711.

Leaver, D. S., Mooney, W.D., and Kohler, W.M., 1984, A seismic refraction study of the Oregon Cascades: Jour. Geophys. Res., v. 89, p. 3121-3134.

McClain, K. J., 1981, A geophysical study of accretionary processes on the Washington continental margin: Ph.D. thesis, Univ. of Wa., Seattle.

McClain, K. J. and Taber, J.J., 1984, Regional Seismic Refraction: in Kulm, L.D. and others (eds.) Western North American continental margin and adjacent ocean floor off Oregon and Washington, Atlas 1, Ocean Margin Drilling Program Regional Atlas Series: Marine Science International, Sheet 9.

McNutt, M. K., 1986, Nonuniform magnetization of seamounts: A least squares approach: Journ. Geophys. Res., v. 91, p. 3686-3700.

Michaelson, C. A. and Weaver, C. S., 1986, Upper mantle structure from teleseismic P-wave arrivals in Washington and northern Oregon: Jour. Geophys. Res., v. 91, p. 2077-2094.

Molnar, P., 1977, Gravity anomalies and the origin of the Puerto Rico trench: Geophys. J. R. astr. Soc., v. 51, p. 701-708.

Mooney, W. D., in press, Seismic methods for determining earthquake source parameters and lithospheric structure: in The Geophysical Framework of the Continental United States, (eds. L.C. Pakiser and W. D. Mooney), Geological Soc. of America Memoir.

Nafe, J. E. and Drake, C. L., 1957, Variation with depth in shallow and deep water marine sediments of porosity, density and the velocities of compressional and shear waves: Geophysics, v. 22, p. 523-552.

Peddie, N. W., 1987, The 1985 magnetic model for the United States (abstract): EOS, Transactions of the Amer. Geophys. Union, v. 68, n. 20, p. 530.

Rasmussen, J. and Humphreys, E., 1988, Tomographic image of the Juan de Fuca plate beneath Washington and western Oregon using teleseismic P-wave travel times: Geophys. Res. Lett., v. 15, p. 1417-1420.

Rau, W., 1973, Geology of the Washington coast between Point Grenville and the Hoh River: Washington Div. Geol. and Earth Res. Bull., v. 66, 58 pp.

Riddihough, R. P., 1979, Gravity and structure of an active margin-British Columbia and Washington: Canadian Journal of Earth Sciences, v. 16, p. 350-363.

Segawa, J. and Tomoda, Y., 1976, Gravity measurements near Japan and study of the upper mantle beneath the oceanic trench--Marginal sea transitional zones: in The Geophysics of the Pacific Ocean Basin and its Margin, Geophys. Mono. Ser., v. 19, (G. H. Sutton, M. H. Manghnani and R. Moberly, (eds.), AGU, Washignton, D. C., p. 35-52.

Sherrod, D. R. and Smith, J. G., 1989, Quaternary extrusion rates from the Cascade Range, northwestern United States and British Columbia: U. S. Geol. Survey Open-File Report, this issue.

Shor, G. G., Dehlinger, P., Kirk, H. K., and French, W. S., 1968, Seismic refraction studies off Oregon and northern California: J. Geophys. Res., v. 73, p. 2175-2194.

Smith, D. R. and Leeman, W. P., 1987, Petrogenesis of Mount St. Helens dacitic magmas: Jour. Geophys. Res., v. 92, p. 10,313-10,334.

Smith, J. G., in press, Geologic map of Upper Eocene to Holocene volcanic and related rocks in the Cascade Range, Washington: U. S. Geological Survey Misc. Field Studies Map I.

Spence, G. D., Clowes, R. M. and Ellis, R. M., Seismic structure across the active subduction zone of western Canada: Jour. Geophys. Res., v. 90, p. 6754-6772.

Stanley, W. D., 1984, Tectonic study of Cascade Range and Columbia Plateau in Washington State based upon magnetotelluric soundings: Journal of Geophysical Research, v. 89, no. B6, p. 4447-4460.

Stanley, W. D., Fuis, G. S., and Mooney, W.D., this issue, Details of crustal structure in the Cascade Range and surrounding regions from seismic and magnetotelluric data.

Stanley, W. D., C. A. Finn and J. L. Plesha, 1987, Tectonics and conductivity structures in the southern Washington Cascades: Jour. Geophys. Res., v. 92, p. 10,179-10,193.

Stanley, W. D., Heran, W. and Finn, C. A., 1988, A major Eocene suture in the southwestern Washington Cascades: Are hydrocarbon source rocks buried beneath volcanic flows? (abstract): 1988 McKelvey Forum on Energy Resources.

Swanson, D. A. and Clayton, G. A. 1983, Generalized geologic map of the Goat Rocks Wilderness and roadless areas (6036, parts A, C, and D), Lewis and Yakima counties, WA: U. S. Geol. Surv. Open-File Report, no. 83-357.

Taber, J.J., 1983, Crustal structure and seismicity of the Washington continental margin, Ph. D. thesis, Univ. Washington, Seattle.

Taber, J.J. and B. T. R. Lewis, 1986,Crustal structure of the Washington continental margin from refraction data: Bull. Seism. Soc. Amer., v. 76, p. 1011-1024.

Talwani, M., Worzel, J. L., and Ewing, M., 1961, Gravity anomalies across the Tonga trench: Jour. Geophys. Res., v. 66, p. 1265-1278.

Telford, W. M., Geldart, L. P., Sheriff, R. E., and Keys, D. A., 1976: Applied Geophysics, Cambridge University Press, Camgridge, England, 860 pp.

Turcotte, D. L. and Schubert, G., 1982, Geodynamics, Applications of Continuum Physics to Geological Problems, John Wiley and sons, p. 164-165.

Walsh, T. J. M. A. Korosec, W. M. Phillips, R. L. Logan, and H. W. Schasse, 1987, Geologic map of Washington-southwest quadrant: Geologic Map g-34, WA Div. Geol. and Earth Res., 2 sheets, scale 1:250,000.

Wannamaker, P. E., Booker, J. R., Jones, A. G., Chave, A. D., Filloux, J. H., Waff, H. S., and Law, L. K., this issue, Conductivity cross-section through the Juan de Fuca subduction system and its tectonic implications.

Watts, A. B. and Talwani, M., 1974, Gravity anomalies seaward of deep-sea trenches and their tectonic implications: Geophys. J. R. Astr. Soc., v. 36, p. 57-90.

Watts, A. B. and Talwani, M., 1975, Gravity effects of downgoing lithospheric slabs beneath island arcs: Geol. Soc. of Amer. Bull., v. 86, p. 1-4.

Weaver, C. S., this issue, Seismicity of the Cascade Range and adjacent areas.

Weaver, C. S. and Baker, G. E., 1988, Geometry of the Juan de Fuca plate beneath Washington and northern Oregon from seismicity: Bull. Seis. Soc. Amer., v. 78, p. 264-275.

Webring, M., 1985, SAKI: A FORTRAN program for generalized inversion of gravity and magnetic profiles: U. S. Geological Survey Open File Report no. 85-112, 104 p.

Wells, R. E., this issue, Paleomagnetic rotations and the Cenozoic tectonics of the Cascade Arc.

Wells, R. E., D. C. Engebretson, P. D. Snavely, Jr., and R. S. Coe, 1984, Cenozoic plate motions and athe volcano-tectonic evolution of western Oregon and Washington: Tectonics, v. 3, no. 2, p. 275-294.

Wells, R. E. and Coe, R. S., 1985, Paleomagnetism and geology of Eocene volcanic rocks of southwest Washington, implications for mechanisms of tectonic rotation: Jour. Geophys. Res., v. 90, p. 1925-1948.

Williams, D.L. and Finn, Carol, 1987, Evidence for a shallow pluton beneath Goat Rocks Wilderness, Washington from gravity and magnetic data: Jour. Geophys. Res., v. 92, p. 4867-4880.

Zucca, J. J., Hill, D. P., and Kovach, R. L., 1982, Crustal structure of Mauna Loa Volcano, Hawaii, from seismic refraction and gravity data: Bull. Seism. Soc. Amer., v. 72, p. 1535-1550.

Zucca, J. J., Fuis, G. S., Milkereit, B., Mooney, W. D. and Catchings, R. D., 1985, Crustal structure of northeastern California: Jour. Geophys. Res., v. 91, p. 7359-7382.

Compositional Diversity of Late Cenozoic Basalts in a Transect Across the Southern Washington Cascades: Implications for Subduction Zone Magmatism

William P. Leeman[1,], Diane R. Smith[2], Wes Hildreth[3]*
*Zen Palacz[4,**], and Nick Rogers[4]*

[1]Keith-Wiess Geological Laboratories, Rice University, Houston, TX 77251
[2]Geology Department, Trinity University, San Antonio, TX 78284
[3]U.S. Geological Survey, 345 Middlefield Rd., Menlo Park, CA 90425
[4]Department of Earth Sciences, Open University, Milton Keynes, MK7 6AA, U.K.

**Presently at Earth Sciences Division, National Science Foundation, Washington, D.C. 20550*
***Presently at VG Isotopes Ltd., Ion Path, Road 3,Winsford, Cheshire CW7 3BX, U.K.*

Abstract

Major volcanoes of the Southern Washington Cascades (**SWC**) include the large Quaternary stratocones of Mount St. Helens (MSH) and Mount Adams (MA) and several interspersed but less imposing mafic volcanic fields (most notably the Indian Heaven (IH) field between MSH and MA, and the largely Pliocene Simcoe Mountain (SIM) volcanic field). There are significant differences among these volcanoes in terms of their composition and evolutionary history. The MSH and MA stratocones consist mainly of andesitic to rhyodacitic lavas and pyroclastics with minor basalt flows. MA is flanked by a large basaltic rift system and has numerous peripheral basaltic vents on its lower flanks. SIM has a poorly exposed andesite to rhyolite core, but largely consists of basaltic lavas erupted from numerous widely dispersed vents; it has the morphology of a shield volcano. The interspersed lava fields are dominantly basaltic with minor andesite. Distribution of mafic lavas across the **SWC** is related to north-northwest trending faults and fissure zones that indicate a significant component of east-west extension within the area. Although there is some overlap in eruptive history, these volcanoes are generally *older* (MSH [<40 Ka], IH [<0.3 Ma], MA [<0.5 Ma], SIM [1-4 Ma]) and more alkalic toward the east.

A variety of compositionally distinct mafic magma types has been identified in the **SWC**: low LILE tholeiitic basalts (Th), moderate LILE calcalkalic basalts (Ca), transitional basalts between these two (Tr), LILE enriched mildly alkalic basalts (Alk), and basaltic andesites (Ba). Compositions of basaltic lavas vary both within individual centers as well as across the **SWC** traverse: MSH (Tr, Ca, Ba); IH (Th, Tr, Ca, Ba); MA (Th, Tr, Ca, Ba); SIM (Alk). SIM is distinct from the other centers in both age and composition; a few of its lavas contain small ultramafic xenoliths. Evolved lavas at MSH, MA, and SIM also differ significantly in terms of their trace element patterns, most notably showing differences in styles of enrichment of REE and HFSE with increasing differentiation. MSH dacites appear to be mainly anatectic crustal melts, whereas those at MA are typical of magmatic differentiation series. **SWC** stratovolcanoes may

represent different evolutionary stages within an evolving arc segment in which magmatism has propagated westward with time.

The role of crustal contamination in modifying Cascade basaltic magmas is considered to be small, whereas associated andesitic and dacitic magmas have evolved by open system processes; some (e.g., MSH dacites) represent crustal anatectic melts formed in response to stagnation of hot basaltic magmas near the crust-mantle boundary. The primitive nature of the erupted basalts and the fact that they are relatively common in the **SWC** sector both imply that such magmas had little residence time in the crust. The fact that the basaltic magmas either show no correlation between isotopic and trace element components, or show trends quite distinct from those of the evolved lavas, suggests that their compositional variability is attributable to sub-crustal processes. The majority of samples studied are indistinguishable from oceanic island basalts (OIB) in terms of trace element and isotopic compositions. The absence of LILE enrichment and HFSE depletion distinguishes most **SWC** basalts from typical volcanic arc magmas. Because such compositional features are generally attributed to the role of fluids released by dehydration of subducted oceanic lithosphere, and to the effects of sediment subduction, we conclude that these features are not essential in producing the **SWC** basalts. We infer that these basalts formed by variable degree melting of a mixed mantle source consisting mainly of heterogeneously distributed OIB- and MORB-source domains. Relatively minor occurrences of HFSE-depleted arc-like basalts may reflect the presence of a small proportion of slab-metasomatized sub-arc mantle (possibly remnants of older accreted island arc terranes or of the Paleogene arc). The juxtaposition of such different mantle domains within the lithospheric mantle is viewed as a consequence of (1) tectonic mixing associated with accretion of oceanic and island arc terranes along the Pacific margin of North America prior to Neogene time, and (2) a seaward jump in the locus of subduction at about 40 Ma.

Finally, the Cascades arc is unusual in that the subducting oceanic plate is very young and hot. Because slab dehydration occurs outboard of the volcanic front, the role of aqueous fluids in generating arc magmas and in influencing their compositions is very diminished compared to the situation at most convergent margins. Furthermore, with low fluid flux conditions, basalt generation is presumably triggered by other processes that increase the temperature of the mantle wedge (e.g., convective mantle flow, shear heating, etc.).

Introduction

The Cascade Range is a conspicuous continental volcanic arc situated along the Pacific Northwest margin of North America. It has been a site of vigorous magmatic activity in response to oblique subduction of the Farallon/Juan de Fuca plate during approximately the last 40 Ma (cf. Lux, 1982; Verplanck and Duncan, 1987). In many respects, the Cascade Range has been considered to be a more or less typical subduction-related arc (e.g., McBirney, 1978; McBirney and White, 1982), although petrogenetic studies have largely focused on the more topographically imposing young stratovolcanoes of the High Cascades. We have undertaken petrologic studies of major central volcanoes and associated basaltic lava fields within an east-west transect across the southern Washington Cascades to document the spatial distribution of magma types in this portion of the arc. This region is an area of transition (Weaver and Malone, 1987) which separates the isolated central volcanoes to the north (e.g., Mts. Rainier, Baker, Glacier Peak) from the broad volcanic plateau of the Oregon Cascades to the south which has a widespread and nearly continuous volcanic cover from both large stratovolcanoes (e.g., Mts. Hood, Jefferson, Washington, the Three Sisters) and numerous monogenetic vents (cf. Luedke and Smith, 1982). Although magmatic activity in the vicinity of the Southern Washington Cascades (**SWC**) traverse dates back to about 30 Ma (cf. Evarts et al., 1987), this paper concentrates on magmatic activity within this part of the Cascades during the past few Ma (mainly Pleistocene to Recent), and principally on petrogenesis of the basaltic lavas and implications for subcrustal magmatic processes related to Cascades subduction.

Tectonic setting of the SWC

The Cascades subduction zone is somewhat atypical compared to other convergent margins (Duncan and Kulm, in press). There are no deep (>100 km) earthquakes associated with the present Juan de Fuca subduction, although a subducting slab has been imaged to greater depths by seismic tomography (Rasmussen and Humphries, 1988). Because the Juan de Fuca spreading ridge is exceptionally close to the subduction zone, the subducting plate is relatively thin and warm; this factor may explain the paucity of deep earthquakes and may influence the dip angle of the subducting plate as well as the rate of subduction. There is no topographically expressed trench along the convergent margin, possibly because the trench has been filled with terrigenous sediments owing to high rates of sedimentation along the Pacific Northwest margin. Convergence of the Juan de Fuca and North American plates presently occurs at a slow rate (approximately 4 cm/yr), and at an oblique angle (about N 50° E) to the continental margin (Riddihough, 1984; Rogers, 1985); both of these parameters have varied significantly with time (Rea and Duncan, 1986; Verplanck and Duncan, 1987). Teleseismic imaging of the subducting Juan de Fuca plate suggests that it is segmented and dipping relatively steeply (>45°) beneath the Oregon-Washington Cascades (Weaver and Michaelson, 1985; Michaelson and Weaver, 1986). Because of the oblique subduction, the regional stress field is not oriented symmetrically with respect to the subduction zone. Rather, the greatest principal stress corresponds to roughly north-south horizontal compression and the least principal stress to approximately east-west horizontal extension (Zoback and Zoback, 1980; G.A. Smith, 1982; Kim et al., 1986). Evidence for east-west extension elsewhere in the Cascade arc includes (1) earthquake fault-plane solutions (e.g., Klein, 1979), and (2) geological features such as abundance of basaltic lavas, north-south orientation of chains of cinder cones, and major normal faults (McBirney, 1978; Hammond, 1979; McKee et al., 1983; Priest, 1983; Bacon, 1985; Smith et al., 1987; Guffanti and Weaver, 1988). The Oregon High Cascades are actually situated within a N-S trending graben (Taylor, 1989). A belt of elevated heat flow coincident with this structure presumably reflects shallow magma intrusion and hydrothermal circulation concentrated within an axial extensional zone (Blackwell et al., 1982).

Geologic setting of the SWC and sample distribution

General geologic features of the **SWC** are shown in **Figure 1**. The large central volcanoes of Mt. St. Helens and Mt. Adams, and the shield-like Simcoe Mt. volcano define an easterly trend some 100 km in width. The underlying basement consists mainly of Cenozoic volcanic and sedimentary rocks. Each of these volcanoes comprises a variety of magma types ranging from basalt to rhyodacite (Hoblitt et al., 1980; Hildreth and Fierstein, 1985; Ort et al., 1983). Distributed between them are the Indian Heaven and numerous smaller lava fields, small shield volcanoes, and monogenetic vents comprising mainly basaltic lavas (e.g., Hammond and Korosec, 1983). Many of the latter vents are distributed in roughly N-S to NNW-trending alignments that presumably are perpendicular to the direction of least principle horizontal stress (e.g., Nakamura, 1977); in some cases these vents define NNW trending fissure systems. Loci of the large stratovolcanoes straddle such structures, and most notably Mts. St. Helens (C.S. Weaver et al., 1987) and Hood (Williams et al., 1982) appear to be situated above zones of local crustal extension along active NW trending strike-slip zones.

Mount St. Helens has been intermittently active during the last 36,000 years, during which time it produced predominantly dacitic magmas (Smith and Leeman, 1987). In the last 2000 years its eruptive products have become more diverse, ranging from basalt to rhyodacite. However, true basaltic lavas were produced only during the Castle Creek eruptive period (2200-1700 yrs. B.P.; Hoblitt et al., 1980). Somewhat older (about 690,000 to 30,000 yrs B.P., Hammond and Korosec, 1983) basaltic to andesitic lavas erupted from smaller vents in the vicinity (e.g., Marble Mountain, West Crater, Soda Peak, Trout Creek Hill, and the Wind River drainage); some of these vents lie along the NW-trending St. Helens seismic zone (C.S. Weaver et al., 1987). The Indian Heaven and King Mountain-Mount Adams volcanic fields are associated with northerly to

NNW-trending structures (fissures or normal fault zones) that are delineated by alignments of vents. Lavas of the Indian Heaven area are younger than 670,000 yrs. B.P. (Hammond and Korosec, 1983); these rocks are predominantly primitive basalts, although a few basaltic andesites and andesites are present. Most eruptive products of Mount Adams (a composite stratovolcano) are younger than about 450,000 yrs. B.P. (Hildreth and Fierstein, 1985); they range in composition from basalt to rhyodacite, although the basalts typically erupted from monogenetic or shield vents distributed on the flanks of the stratovolcano. Due south of Mount Adams, and east of Mt. Hood, the NNE-trending Hood River fault zone in northern Oregon is associated with a small field of Plio-Pleistocene basaltic lavas. East of Mount Adams, the Plio-Pleistocene Simcoe volcano is a large shield-like structure with exposures of dacites and rhyolites in its dissected core (Sheppard, 1967). However, its surrounding flanks are blanketed by basaltic lavas which erupted from numerous fissures, cinder cones, and small shield vents that define either N-S or NNW-trending alignments. Available K-Ar ages indicate that nearly all Simcoe lavas are older than 1 Ma; most range between 2-4 Ma (Farooqui et al., 1981; Luedke and Smith, 1982; Phillips et al., 1986). Although only approximate estimates of magma volumes are available for this sector of the Cascades arc (cf. Sherrod and Smith, 1989), it is clear that basaltic lavas are common except within the large stratovolcanoes, and even there basaltic lavas occur in significant volumes (cf. Hammond and Korosec, 1983). For comparison, basaltic rocks are also abundant in the southern Cascades (Luedke and Smith, 1982; McKee et al., 1983; Hughes and Taylor, 1986; Walker and Naslund, 1986), and it is estimated that they comprise as much as 85% by volume of the Oregon Cascades (McBirney and White, 1982). Although basaltic magmatism is characteristic of the entire traverse, such lavas are more voluminous toward the east. It is unclear whether this relation reflects fundamental differences in the supply of basaltic magma across the transect, or the possibility that eruption efficiency of mafic magmas is somehow proportional to the lifetime of the eruptive centers.

The main objective of this paper is to provide a concise overview of spatial variations in magma composition based on representative samples collected from all of the localities discussed. Detailed studies of petrology, mineralogy, and of the magmatic evolution of the individual eruptive centers have been (e.g., Smith and Leeman, 1987) or will be presented elsewhere. **Table 1** briefly summarizes the distribution of magma types recognized at the major SWC volcanic centers; criteria for subdividing the basaltic variants are discussed below. Those from the Simcoe field are notably distinct in that they commonly carry conspicuous phenocrysts of plagioclase, olivine, and occasionally clinopyroxene; in addition, small xenoliths of spinel lherzolite and diverse crustal lithologies were found in some of these lavas. Basalts from the other localities also tend to be porphyritic (plagioclase and olivine), but their phenocrysts are relatively small (usually less than a few mm in length). Hydrous phenocrysts are typically absent from the mafic lavas. The only known exception is the notable occurrence of rare, partially resorbed amphibole phenocrysts in one basaltic lava from the Indian Heaven field. Andesitic and dacitic lavas and pyroclastic deposits dominate the main stratovolcanoes. These are typically porphyritic with ubiquitous plagioclase phenocrysts and assorted combinations of mafic phenocrysts including clino- and orthopyroxene, amphibole (hornblende and/or cummingtonite), Fe-Ti oxides and olivine. Biotite and K-feldspar occur in some rhyodacites and rhyolites (e.g., SIM).

Analytical Methods

Major element compositions were determined for more than 150 whole-rock samples using a combination of x-ray fluorescence spectrometry and inductively-coupled plasma optical emission spectroscopy. Many of these rocks were also analyzed for trace element contents using the aforementioned methods along with instrumental neutron activation spectrometry. All analytical methods used are described in Smith and Leeman (1987), and error estimates for each element are given therein. Briefly, on the basis of replicate analyses, accuracy and precision of major element contents are estimated to range between 1-2%, and those of most trace elements between 2-10% of the amount reported. For elements determined by more than one method, either averages or results

by the most precise method are reported. Analyses of representative (mainly basaltic) lavas are given in **Table 2**; these are reported on a 'dry' basis recalculated to 100%.

Isotopic compositions of Sr, Nd, and Pb were measured using VG Isotopes 54E and Finnigan-MAT 251 mass spectrometers at the Open University, U.K. Ratios are normalized to correct for mass fractionation as follows: $^{86}Sr/^{88}Sr = 0.1194$, $^{146}Nd/^{144}Nd = 0.7219$. Pb isotope ratios were corrected for ca. 0.1% fractionation per amu based on replicates of the NBS-981 common lead standard. Accuracy of the reported ratios is about ± 0.00003 (0.004%) or better for $^{87}Sr/^{86}Sr$, ± 0.00002 (0.003%) or better for $^{143}Nd/^{144}Nd$, and ± 0.02 (.1%) or better for all lead isotope ratios; internal precision of the analyses is usually better than these estimates. $^{87}Sr/^{86}Sr$ ratios are reported relative to values of 0.70800 and 0.71028 for the Eimer & Amend and NBS-987 standards, respectively; analyses of BCR-1 during the course of this study averaged 0.70500. $^{143}Nd/^{144}Nd$ ratios are reported relative to values of 0.51182 and 0.51264 for La Jolla Nd oxide and BCR-1, respectively. Oxygen isotopic analyses were measured on whole-rock and plagioclase separates at Menlo Park (MA), University of Wisconsin (IH), the Geological Survey of Japan (MSH) and Southern Methodist University (SIM). $\delta^{18}O$ ratios are reported relative to SMOW with values of 9.6 per mil for the NBS-28 quartz standard; duplicate analyses indicate precision of ca. ± 0.1 per mil. Results of the isotopic analyses are shown in figures and representative analyses are given in **Table 2**. For comparison, only a few Pb, Nd, and Sr isotopic analyses have been published previously for **SWC** volcanoes (Church and Tilton, 1973; Church, 1976; Halliday et al., 1983); a survey of ore Pb data (Church et al., 1986) includes samples from the **SWC**.

Geochemistry of lavas from the SWC

Perhaps the most important observation of this study is the relatively wide range in compositions of basaltic lavas erupted within a relatively small region within the Cascade arc. Not only are there differences among the various eruptive centers sampled, but there are significant variations within single eruptive centers. The wide compositional spectrum of roughly contemporaneous basaltic magmas reveals that petrogenetic processes are more complex than might be expected, and that not all of these magmas were derived from common source materials. Secondly, most of the young Cascades basalts studied differ from those in other volcanic arcs; in many respects they more closely resemble oceanic (or within-plate) basalts despite their obvious association with an active subduction complex.

Major element compositions and definitions of basalt types

Approximately 150 major element analyses are compared in **Figure 2**, which shows the discriminant diagrams of Miyashiro (1973) and Gill (1981). The AFM (Alkalies-FeO*-MgO) diagram (not shown) of Irvine and Baragar (1971) was used to subdivide the mafic lavas into tholeiitic and calcalkalic magma series. Although most samples studied are broadly calcalkalic, tholeiitic basalts occur at IH and MA, and transitional basalts occur at MSH. **Figure 3** shows that basalts from MSH, IH, and MA have relatively high Mg#s (100 • molar MgO/[MgO+FeO*]; note that these are *minimal* values as some fraction of the iron actually occurs as Fe_2O_3); in particular, some from IH resemble high-Mg Aleutian basalts (Mg#s ca. 70; cf. Gust and Perfit, 1987). The basalts (and andesites) have relatively high alumina contents (typically between 16-18%). It can be noted in this diagram that the basaltic lavas with Mg# greater than 55 conform rather closely to an idealized olivine + clinopyroxene fractionation trend. In fact, many of these basalts do contain phenocrystic olivine and clinopyroxene along with plagioclase, implying evolution at relatively high pressure (> ca. 8 kbar; Gust and Perfit, 1987). However, alkali contents vary considerably in **SWC** basalts (0.2 to 1.5% K_2O; **Figure 2b**). The SIM basalts stand out in terms of their comparatively high alkali contents (0.6 to 2.4% K_2O); they comprise alkalic and subalkalic groups (cf. **Figure 2a**) the most potassic of which is characterized by normative nepheline. Most other **SWC** basalts are hypersthene normative.

Evolved lavas from MSH, MA, and SIM volcanoes consist of medium- to high-K andesites, dacites, and rhyolites. Volcanic rocks from each center define coherent compositional trends on silica variation diagrams (cf. **Figure 2**), but a few MSH dacites (oxidized pumices) have conspicuously high alumina (**Figure 3**) and relatively low silica contents. In terms of most other major and trace element constituents and their mineralogy, these rocks are indistinguishable from other MSH dacites. Smith and Leeman (1987) suggested that these features may reflect alteration processes (as opposed to accumulation of plagioclase phenocrysts, for example). In general, the alkalinity of each magma suite increases eastward with distance from the subduction zone, as does the maximum silica enrichment attained. However, there is considerable variability among IH and MA mafic lavas which range from low-K tholeiitic to calcalkalic basalts.

Representative analyses in **Table 2** illustrate the magmatic variants so far recognized. For most basaltic rocks, analyses are selectively tabulated to emphasize the compositional differences among magma types having comparable MgO contents (ca. 6%). Close inspection shows that the major and trace element compositions do not covary in any simple fashion. For MSH, mafic lavas are restricted mainly to the Castle Creek eruptive period (between 1.7-2.2 Ka; Hoblitt et al., 1980). Table 2 includes the 'transitional' Cave Basalt (DS-27) from the south flank, and a calcalkalic basalt (DS-6) and basaltic andesite (DS-72) from the (now obliterated) northern flank. Analyses of more evolved rocks are given by Hoblitt et al. (1980), Halliday et al. (1983), and by Smith and Leeman (1987). The dominantly basaltic IH field has been described by Hammond (1980) and Hammond and Korosec (1983) who mapped and named many of the flow units. Analyses are given for a low-K tholeiitic basalt (DS15A-80) from the Ice Caves flow, a calcalkalic basalt (DS3B-80) from the Big Lava Bed flow, a basaltic andesite with relic amphibole (DS23B-81) from Berry Mountain, and an olivine andesite (DS-63) of the Forlorn Lakes map unit which is the most evolved sample known from the IH field. Analyses for Mount Adams include several basalts (83-49, a low-K tholeiite from the Cispus River drainage on the north flank; 82-31 and 82-26, calcalkalic basalts from the King Mountain vent on the south flank) and the Holocene Aiken andesite flow (82-24). Samples from the SIM field include ca. 1-4 Ma basalts from peripheral vents from the west (L83-97), southeast (L83-94), and south (L83-67, Maryhill flow), and a dacite (L84-65) and rhyolite (L84-67) from the eroded core of the volcano near Indian Rocks. Major element analyses of additional SIM lavas are given by Ort et al. (1983).

Trace element compositions

Representative trace element patterns for **SWC** mafic lavas are shown in **Figure 4**, as normalized to the 'primordial mantle' values of Wood (1979). These projections facilitate comparisons of elements that display similar degrees of 'incompatibility' relative to common phenocryst mineral assemblages. Most basaltic lavas from MSH, MA, and SIM, and low-K IH basalts have relatively smooth convex-upward trace element profiles characteristic of oceanic island basalts (**OIB**s). Only a few IH lavas (e.g. DS23B-81, DS3B-80; Table 2) display relative depletions in high field strength elements (HFSE; notably Nb and Ta) which are characteristic of many arc magmas (Pearce, 1983; Briqueu et al., 1984; Weaver et al., 1987). Some of these latter lavas have unusually high contents of large-ion lithophile elements (LILE; especially Sr, Ba, Th, U, K, and light REE). These distinctions are further emphasized in **Figure 5** wherein the majority of **SWC** basalts (and several from the Oregon High Cascades; Hughes and Taylor, 1986) have Ta/Yb-Th/Yb ratios that plot along a so-called 'mantle array' defined by mid-ocean ridge (MORB) and oceanic island (OIB) basalts. Only a few mafic lavas and assorted evolved lavas actually plot in the field of volcanic arc magmas. Those **SWC** basalts conforming to the mantle array display other similarities to OIB-like magmas: e.g., low boron contents (1-4 ppm) and Ba/La (<18 for most) compared to basalts from virtually all other modern arcs (Leeman, 1987; Morris and Hart, 1983). None of the **SWC** basalt types analyzed so far have detectable concentrations of ^{10}Be (Morris et al., 1989). In these regards, the modern Cascade arc appears to be unusual. The question arises as to whether these features reflect unusual conditions of magma genesis, and if so, has this been a persistent situation or a relatively recent turn of events.

Another remarkable feature of the **SWC** basalts is their compositional diversity, which is further illustrated in **Figure 6.** Ba and Nb, selected as typical LIL and HFS elements, are plotted vs. SiO_2. This choice of elements was based on the availability of such data in most of our samples, but also serves to emphasize several fundamental points that emerge in considering all the data. First, the ranges in Ba (~20x), Nb (~12x), and Ba/Nb (~9x) are substantial. The SIM alkalic basalts resemble many OIBs in having high Nb (20-60) and low Ba/Nb (10-20). Low-K tholeiitic basalts from IH and MA have the lowest Ba and Nb, but have Ba/Nb ratios which overlap with those in the alkalic basalts. Because Ba and Nb are both strongly partitioned into such basaltic magmas during melting and crystallization processes, it is unlikely that the Ba/Nb ratio can be easily fractionated (cf. Hofmann, 1988). Thus, there may be some form of petrogenetic linkage between all of the aforementioned basalts (e.g., they could represent variable degrees of fusion of common source materials). Secondly, the HFSE-depleted IH lavas have elevated Ba and extremely high Ba/Nb ratios (30-90); these lavas are unlikely to be related to the other basalt types via closed system evolution or by partial melting of similar sources. Some mechanism is required to explain both their Nb-depletion and their Ba-enrichment. Nb-depletion is presumably 'source-related' as it is very difficult to conceive of magma contamination models that can produce this effect while retaining a basaltic bulk composition (cf. Hickey et al., 1986).

It is also useful to consider how these elements are distributed in more evolved lavas to appreciate the efficacy of various petrogenetic processes. **Figure 6** clearly shows that MA and MSH have distinctive evolutionary patterns. The trends for MSH indicate that Ba/Nb increases six-fold in going from basalts to rhyodacites. In magma fractionation models, for example, this trend would suggest that Nb is actually more compatible than Ba, which is apparently the case at MSH given the crystallizing assemblages; Smith and Leeman (1987; Table 7) calculated average bulk D_{Ba} (0.54) < D_{Ta} (0.86) for MSH whole rock-glass pairs. However, the striking decrease in Nb with increasing SiO_2 at MSH is inconsistent with the inferred distribution coefficients, thus ruling out simple fractionation models. As a more attractive hypothesis, Smith and Leeman (1987) proposed that MSH dacites represent crustal melts which have no derivative relationship to the associated basalts. On the other hand, MA evolved lavas do show progressive increases in both Ba and Nb, and a slight *decrease* in Ba/Nb with increasing SiO_2, all of which seem more consistent with crystal fractionation processes; this is not to say that there is an obvious linkage with any of the associated basalts, which are themselves somewhat variable in composition. In passing, the strong Ba-depletion seen in the SIM rhyolite is suggestive of extreme fractionation involving K-feldspar; the high Nb and very low Ba/Nb ratio in this rock do not support significant involvement of crust.

Variation in Ba and Nb contents are displayed directly (**Figure 7a**), and also as normalized to Zr, which is a slightly more compatible trace element (**Figure 7b**). For basaltic magmas, this element ratio plot minimizes scatter related to variations in degree of crystallization or partial melting. In both plots two distinct trends emerge for the **SWC** basaltic lavas. First, a 'mantle array' is again evident, here embellished by data from representative OIB (e.g., Tristan da Cunha; B.L. Weaver et al., 1987) and N-MORB (Le Roex et al., 1983). These comparative samples were chosen simply because they approach extremes in Ba and Nb contents of oceanic basalts, but the light stippled field in **Figure 7b** represents a compilation of several hundred Pacific island basalts (Leeman, unpub. data and literature survey). Ba/Nb for this group of **SWC** basalts is ca. 11.5. Secondly, a small number of HFSE-depleted IH basalts (and a few miscellaneous older basalts from West Crater and the Hood River valley) define a distinct linear array which trends toward a high Ba/Nb component. Strong LILE vs. HFSE correlations in both of these arrays apparently reflect some form of open system mixing between compositionally distinct end members. Either melting of previously mixed sources or contamination of ascending magmas would be reasonable causes for the observed near-linear arrays, whereas simple variations in degree of melting or crystallization are are not plausible.

The **SWC** basalts which conform to the 'mantle array' defined by OIB and MORB analyses could represent melting of hybrid mantle material comprising OIB- and MORB-source components, or possibly magma-wall rock interactions involving such mantle components. The

absence of significant LILE/HFSE fractionations in most young **SWC** basalts is atypical of most volcanic arc magmas. The HFSE-depleted basalts could result from combined fractional crystallization and assimilation of a high Ba/Nb contaminant; rocks similar to estimated average crustal composition would be inadequate contaminants. As an example, an mixing vector is shown that heads toward compositions of pelagic sediments (e.g., 'PAWMS' composition of Hole et al., 1984; also cf. Kay, 1984). The data for **SWC** andesites and more evolved samples are consistent with this possibility because SiO_2, Ba, and Ba/Zr are all positively correlated in these rocks. However, some other explanation seems required for the IH *basaltic* lavas. As pointed out by many authors (e.g., Pearce, 1983; Hole et al., 1984; Tatsumi et al., 1986), high LILE/HFSE ratios could also reflect source metasomatism by LILE-rich 'fluids' released during dehydration of subducted oceanic crust. However, it is difficult to see how such large-scale processes could selectively enrich the sources of only a few magma batches without similarly affecting very large volumes of the mantle wedge.

Isotopic compositions

Sr, Nd, Pb, and O isotopic compositions have been measured for selected samples to test some of the questions posed above. The observed ranges in $\delta^{18}O$ (5.4-7.7 per mil), $^{87}Sr/^{86}Sr$ (0.7028-0.7040), $^{143}Nd/^{144}Nd$ (0.51284-0.51304), $^{206}Pb/^{204}Pb$ (18.68-19.40), $^{207}Pb/^{204}Pb$ (15.53-15.66), and $^{208}Pb/^{204}Pb$ (38.4-39.2) are significant and these ratios display important correlations with other geochemical data. Isotopic ranges for other Cascade volcanoes are comparable (cf. Peterman et al., 1970; Church and Tilton, 1973; Church, 1976; Leeman, 1982; Grove et al., 1982, 1988; Bacon et al., 1988). For comparison, analyses of Eocene terrigenous sediments from the Oregon Coast Range (representative of likely subducted materials or possibly sedimentary sequences in the sub-arc crust) have present-day isotopic ratios as follows (Peterman et al., 1967, 1981; Heller et al., 1985; Leeman, unpub. data): $\delta^{18}O$ (ca. 10 per mil), $^{87}Sr/^{86}Sr$ (0.706-0.711), $^{143}Nd/^{144}Nd$ (0.5122-0.5124); Pb isotopic compositions are shown in Figure 11 (cf. Church, 1976).

The **SWC** data are portrayed as a function of silica content in **Figure 8** to illustrate how they vary with bulk composition. Oxygen compositions of the basalts vary beyond normal analytical precision, but because much of the observed range (5.4-6.4 per mil) corresponds to whole-rock analyses for the older (and possibly slightly altered) SIM lavas, it is not clear how significant these variations may be. Data for IH and MSH whole-rock and plagioclase samples are more restricted, averaging about 5.8 per mil, whereas $\delta^{18}O$ progressively increases for more silicic MSH samples. As is indicated in **Figure 8b**, the rate of increase in $\delta^{18}O$ in MSH rocks exceeds that predicted for fractionation of observed phenocrysts. Radiogenic isotopic ratios display two styles of variation. First, the basalts cover nearly the entire range in Sr, Nd, and Pb isotopic compositions, but show no significant correlations between silica and these ratios. Secondly, isotopic variations in the evolved lavas are more systematic, but differ between volcanoes: (a) in MSH lavas, SiO_2 is positively correlated with $^{87}Sr/^{86}Sr$ and negatively correlated with $^{143}Nd/^{144}Nd$; a weak negative correlation exists between SiO_2 and the Pb isotopic ratios; (b) in MA lavas SiO_2 is poorly (negative?) correlated with all these ratios. It is evident that open system processes must have operated to produce **SWC** magmas, and that petrogeneses of the basaltic and more evolved magmas at each volcanic center are not identical (or perhaps even linked).

Figure 9 shows isotopic compositions plotted vs. Ba/Nb to emphasize the distinctions in trace element variations noted earlier. Unfortunately, there are as yet no Nd isotopic data for the strongly HFSE-depleted IH lavas. For the basaltic rocks, there is little correlation between Ba/Nb, $\delta^{18}O$, or Pb isotopic ratios. With exception of SIM basalts, there is actually little variation in these parameters. $^{87}Sr/^{86}Sr$ correlates positively with Ba/Nb (also Ba/Zr, not shown), but this trend belies considerable complexity when it is recalled that Ba/Nb exhibits *opposite* correlations with silica in MSH (+) and MA (-) evolved lavas. The high Ba/Nb IH basalts have $^{87}Sr/^{86}Sr$ ratios similar to those in the more evolved **SWC** lavas. However, it appears that LILE/HFSE

fractionation (i.e., Ba, Sr enrichment) and elevated $^{87}Sr/^{86}Sr$ in these basaltic magmas result from different processes than those involved in production of **SWC** intermediate and silicic magmas. For example, the basalts differ in that they display positive correlation between Sr content and $^{87}Sr/^{86}Sr$, and Sr contents correlate positively with abundances of the incompatible trace elements (e.g., Nb, La, Ba, Th); both features suggest that their compositional characteristics were established at pressures above the stability of plagioclase (e.g., subcrustal depths; cf., Leeman and Hawkesworth, 1986).

Isotope-isotope correlations provide additional constraints. Sr-Nd variations in **SWC** volcanic rocks (**Figure 10**) mimic the fields of oceanic basalts, with more evolved rocks displaced toward estimated 'bulk Earth' composition. SIM basalts define a distinct trend slightly below the 'mantle array', whereas MSH evolved lavas trend slightly to the right of the array. Pb isotope data define distinctive positive correlations between $^{206}Pb/^{204}Pb$ and both $^{207}Pb/^{204}Pb$ and $^{208}Pb/^{204}Pb$ (**Figure 11**) and lie between fields for oceanic basalts (represented by Pacific MORB [White et al., 1987] and the northern hemisphere regression line [NHRL; Hart, 1983] for oceanic basalts) and that for NE Pacific sediments (Church, 1976). Compositions of Cascade ore leads (Church et al., 1986) overlap with the most radiogenic lavas. Average Juan de Fuca Ridge basalt is indicated for reference (Hegner and Tatsumoto, 1987), along with the model crustal Pb isotope growth curve of Stacey and Kramers (1975). The trend of the Cascade array suggests that the arc magmas contain a component of Pb similar to that in the sediments (or the crust), as was pointed out by Church and Tilton (1973) and Church (1976). However, the new results show that the *basaltic* magmas contain more radiogenic Pb than that in associated silicic magmas. One possible explanation for this trend is that, owing to their low Pb contents, the basalts may be more susceptible to effects of crustal contamination. Accuracy of the available XRF Pb analyses precludes detailed discussion of the systematics. However, production of the high $^{207}Pb/^{204}Pb$ basalts via contamination is possible if average crust resembles the ore lead data. This is an unlikely scenario if Pb compositions of MSH silicic magmas (Figure 11; also cf. Halliday et al., 1983) are more representative of the crust (cf. Figure 8a).

As an alternative explanation, radiogenic Pb signatures in **SWC** basalts could be attributed to inheritance from subduction modified mantle source regions (cf. Morris and Hart, 1983; Hickey et al., 1986). For several reasons this possibility is considered less plausible. **Figure 12** shows little or no correlation between Sr and O isotopic compositions of **SWC** basalts, whereas there is a *negative* correlation between Pb and O compositions. The latter trend does not support involvement of significant quantities of marine sediments which typically have high $\delta^{18}O$ (e.g., Heller et al., 1985). Pb, Sr, and O compositions of MSH intermediate and silicic rocks are correlated and suggest that these magmas contained a significant crustal component in concert with their proposed crustal anatectic origin (Smith and Leeman, 1987). The SIM basalts are notable because, rather than follow the trend of other Cascades data in **Figure 11**, analyses of these rocks approximate the NHRL line; there is little reason suspect that these magmas contain much of a subduction component.

Another line of reasoning against significant contribution of subducted sediment to **SWC** magmas involves the geochemistry of boron. Strong correlation of B with ^{10}Be concentrations in arc magmas (Morris et al., 1989) provides compelling evidence that the observed B enrichments are related to subduction processes. Leeman (1987) demonstrated that volcanic arc magmas are systematically enriched in B relative to within plate magmas, and that OIB lavas have low B/Nb ratios (<0.1) whereas arc magmas have much higher ratios (>0.5, and usually between 1-20). **Figure 13** compares B/Nb ratios with other parameters. All **SWC** basalts contain less than 5 ppm B, and average ca. 2 ppm, essentially overlapping with OIB values. Those which conform to the mantle arrays discussed earlier have high Ta/Sm (0.25-0.5) and low B/Nb ratios (<0.2) similar to those in OIB. The distinctive HFSE-depleted IH basalts display higher B/Nb (up to 0.5) and radiogenic Sr, as well as enrichments in Sr, Ba, and other incompatible elements. Even andesitic **SWC** lavas have B/Nb below 0.5. In contrast, MSH dacites have high B (up to 24 ppm) and B/Nb (1 to 3). Thus, the range in B/Nb in these various MSH magmas is inconsistent with cogenetic relations because magmatic processes are unlikely to fractionate such highly incompatible

elements. Near-linear variation of B/Nb and other parameters in the evolved lavas (Figure 13) more likely result from mixing between high-B crustal melts and low-B mafic magmas. A possible implication of these results is that the mafic magmas were produced with little input from the subducted oceanic slab compared to the situation in other volcanic arcs.

Discussion

The foregoing descriptive information places a number of constraints on the nature of magma generation associated with Cascades subduction processes, but perhaps more importantly illustrates how little we really understand these processes. The modern (ca. <1 Ma) Cascades magmatism, at least in southern Washington, stands out as being unusual compared to most volcanic arcs. Some of the most notable features are summarized here.

Compared to many other continental margin arcs (cf. Leeman, 1983), basaltic volcanism is relatively common in the **SWC**. This is apparently typical of much of the Cascades arc (e.g., Hughes and Taylor, 1986; Hughes, 1989; Guffanti et al., 1989; Taylor, 1989), although true basalts are not everywhere present (cf. Luedke and Smith, 1982; Bacon et al., 1989) and more evolved lavas dominate the major stratovolcanoes. Although Basin and Range style deformation has recently propagated northwestward into the southern Cascades and to the backarc region of central Oregon, it seems unlikely that this development is responsible for the abundance of basaltic lavas in the Cascades. First, basaltic magmatism was volumetrically significant in central Oregon throughout the Neogene (since ca. 40 Ma) when convergence rates were much higher than at present (Rea and Duncan, 1986; Verplanck and Duncan, 1987; Priest, 1989); initiation of Basin and Range style deformation in the Great Basin postdates and could not have influenced this early Cascade volcanism. Also, as emphasized here, orientations of late Neogene structures in the **SWC** are inconsistent with Basin and Range style extension (cf. Zoback and Zoback, 1980). The abundance of basalt in the central Cascades may be enhanced by additional factors such as the presence of thinner or more mafic crust relative to adjacent segments in northern California or north-central Washington (McBirney, 1978), proximity to segmentation boundaries (Hughes et al., 1980; Weaver and Michaelson, 1985; Guffanti and Weaver, 1988), or development of intra-arc extension related to along-strike variations in obliquity of convergence (Rogers, 1985) or decrease in convergence rates with time (Verplanck and Duncan, 1987). At this stage we feel it is premature to critically evaluate these possibilities, much less adopt any single explanation for high basaltic magma production in the Cascades.

Another striking anomaly concerns the prevalence in the **SWC** of basaltic magmas that have strong geochemical similarities to oceanic island basalts (OIB); many of those at SIM are true alkali olivine basalts (some containing sparse spinel lherzolite xenoliths). Alkali basalts also occur in backarc regions of several volcanic arcs (e.g., Japan, Argentina; cf. Gill, 1981; Sakuyama and Nesbitt, 1986; Stern et al., 1986) and it is tempting to draw analogies between the Cascades and backarc settings, especially concerning the SIM basalts. More rarely, such magmas occur within intra-arc extensional zones (e.g., New Hebrides, Fiji; Gill, 1981, 1984). Even more enigmatic shoshonitic variants occur along the volcanic front in the northern seamount province of the Mariana-Volcano arc (Stern et al., 1988). Unlike these exceptional examples, OIB-like basalts are distributed across the entire **SWC** traverse, whereas such rocks are truly scarce in other convergent margin settings.

Relative to OIB magmas, for example, most volcanic arc basaltic lavas are characterized by anomalous enrichments of alkali and alkaline earth metals, by depletions of HFSE, and by high LILE/HFSE ratios such as Ba/Nb (Green, 1980; Perfit et al., 1980; Arculus et al., 1981; Morris and Hart, 1983; Ito and Stern, 1985; Hickey et al., 1986; Sakuyama and Nesbitt, 1986; Tatsumi et al., 1986; Hildreth and Moorbath, 1988). As discussed by these authors, the unique chemical characteristics of *arc* magmas are commonly attributed to the influence of aqueous fluids on phase equilibria and element transport in the subduction zone environment (possibly augmented by crustal contamination of arc magmas). Specifically, most recent arc petrogenetic models propose that dominantly aqueous fluids are released from the downgoing slab of oceanic lithosphere, and that these fluids may promote melting of the slab or, following upward migration, of the mantle

wedge. Under high pressure conditions the fluid phase could preferentially extract from the slab and transport soluble components (e.g., LIL trace elements) into the overlying wedge; melting of such metasomatized wedge mantle could produce arc magmas.

However, there are few **SWC** basalts with arc-like HFSE-depleted compositions regardless of distance from the subduction zone. Those from the IH field are closely associated with essentially contemporaneous OIB-like variants. Although volumetric proportions vary from place to place, basalts having similar compositional diversity to that in the SWC occur elsewhere in the Cascade arc (cf. Hughes and Taylor, 1986; Hughes, 1989; Clynne, 1989; Bullard and Clynne, 1989). Thus, the **SWC** basalts that we have studied do not appear to be anomalous with respect to other contemporaneous Cascades basalts. Whether OIB-like basalts were so common throughout the history of the arc, or are characteristic only of the modern Cascades is an important question that cannot be resolved without further study. Nevertheless, in recent geologic history there appears to have been a variety of basaltic sources simultaneously available within what must be a heterogeneous mantle beneath the Cascades.

Implications of basalt diversity in the SWC

There are perhaps two extreme viewpoints on the origin of basalt diversity in the Cascades. First, the spectrum of basalt compositions may reflect varied degrees of modification (e.g., by wall-rock interaction) of relatively primitive magma produced from a uniform mantle reservoir (cf. Leeman, 1983; Hildreth and Moorbath, 1988). On the other hand, the compositional variations may be source-related and reflect partial melting of heterogeneous mantle beneath the arc, in which case the heterogeneity may result at least partly from subduction processes (cf. Ellam and Hawkesworth, 1988; Plank and Langmuir, 1988). To evaluate these possibilities we consider briefly the compositional constraints provided by lavas of the **SWC** as well as their geologic setting.

The strong similarity to OIB and the absence of significant correlations between isotopic and trace element parameters (Figs. 8, 9, 12) in most **SWC** basalts argue against significant crustal contamination of these magmas (with possible exception of the Pb isotopic data). The rarer HFSE-depleted basalts may in part reflect some form of magma contamination process because isotopic compositions (O, Sr, Pb) display weak correlations with bulk compositions (Figures 8, 9, 12); trends for these basalts are usually distinct from those of more evolved lavas, indicating the need for different contaminants in each case. However, because the **SWC** basalt compositional variants have similar Mg# and transition metal abundances (cf. Table 2), it is unlikely that their differences in incompatible trace element contents can be explained solely by contamination of a common parental magma type. Thus, we conclude that basaltic magmas in this region tapped a heterogeneous mantle source that is in part characterized by high LILE/HFSE enrichments (similar to those in normal arc magma sources) and in part consists of MORB- and OIB-like domains. If the relative volumes of such domains are reflected by extrusive proportions of the respective basalt variants, then the source must be dominated by the MORB and OIB end members. Furthermore, Nb/Zr ratios correlate with magma type, being lowest in the tholeiitic and highest in the alkalic basalts (see Fig. 7). Though speculative, this relationship may signify greater contribution of the MORB-like end member to magmas produced by higher degrees of melting. A heterogeneous distribution of lower melting temperature OIB-source component in a more refractory matrix of MORB-source material could explain such melting behavior. Such a model source is certainly consistent with the geologic and tectonic history of the Pacific Northwest margin.

The Cascade arc is a relatively young edifice built largely upon a basement of amalgamated oceanic and island arc terranes that were laterally translated and accreted to North America at least by latest Cretaceous time. As pointed out by AveLallemant and Oldow (1988), oblique convergence along the Pacific margin resulted in complex jostling and transport of these coastal blocks. Thus, underlying lithospheric mantle (to the extent that such rocks are preserved below the accreted terranes) likely includes scraps and fragments of sub-arc and sub-oceanic mantle domains, perhaps comingled by tectonic mixing. We would expect there to be heterogeneously distributed lithospheric domains having both OIB- and MORB-source affinities. Prior to initiation of

Cascades volcanism, calcalkalic magmatism was concentrated in a broad belt further to the east (east-central Oregon to SW Idaho; Norman et al., 1986; Norman and Leeman, 1988; Hart et al., 1989). This belt was active between about 45 to 20 Ma (Eocene to Oligocene time), and is inferred to be related to an ancestral subduction zone located near the present Cascade axis. Accretion of the Coast Range block (which is interpreted as a oceanic island chain; Duncan, 1982) about 40 Ma presumably led to gradual demise of this older arc and initiated the modern Cascade subduction zone and volcanic arc (Simpson and Cox, 1977; Duncan and Kulm, in press). Timing of this event is constrained by the 43 Ma age of the youngest Coast Range volcanic rocks (Duncan, 1982), and by the 40-35 Ma ages of earliest Cascades volcanic rocks (Lux, 1982; Verplanck and Duncan, 1987). One consequence of a seaward jump in the subduction zone is that the mantle wedge under the present Cascade arc must contain a significant volume of sub-oceanic mantle, presumably with MORB-source affinities, and possibly part of the older mantle wedge. It is in this context that one must evaluate the sources of modern Cascade arc magmas.

The paucity of typical arc basalts argues against the applicability of conventional subduction zone models involving pervasive metasomatism of the mantle wedge by slab-derived fluids. If subduction components (fluids, sediments) were added to the sub-arc mantle in the past, it is difficult to understand why high LILE/HFSE sources have not been tapped more often by young SWC magmas. We therefore conclude that the underlying mantle wedge was not metasomatized or, if so, this effect only produced local heterogeneities (as in relicts of fossil sub-arc mantle associated with some of the accreted terranes). The apparently minor contribution of slab-derived fluids likely relates to the youthfulness (<10Ma at the trench) and warmth of the downgoing slab (Duncan and Kulm, in press). Using conductive thermal models, Abbott and Lyle (1984) concluded that dehyration of such a young slab would likely result in loss of volatiles (H_2O and CO_2) well before reaching a position beneath the volcanic front (roughly 150 km depth; Rasmussen and Humphries, 1988). From petrologic considerations, Wyllie (1984, Figure 9) also concluded that dehydration of hot slab would occur outboard of the volcanic front. Also, despite high sedimentation rates in the Cascadia Basin, input of sediment in the Cascade subduction zone may be retarded significantly due to development of a large accretionary prism (Duncan and Kulm, in press).

However, the above view of the Cascade arc raises important questions about what triggers melting in this case, and whether fluids are necessary in producing arc magmas in general. We feel that the Cascade arc may represent a 'dry' end member in the continuum of volcanic arcs, in which melting is induced by some form of convective mantle flow (e.g., 'corner flow' of Hsui et al., 1983). Our suggestion that the source of most SWC basalts is a mixture of MORB- and OIB-source domains is not really new, as such components have previously been proposed on other grounds (e.g., Kay, 1978; Morris and Hart, 1983; Gill, 1984). However, because the slab contributions so characteristic of most other arcs have been repressed, we are able to discern more clearly the effects of processes operating in the mantle wedge. We speculate that such processes may be overprinted and even masked by slab contributions elsewhere.

Conclusions

The present study documents that the geochemistry and tectonic features of the Cascade arc are unusual if not unique. Basaltic magmatism has been significant throughout the history of the arc, and particularly in the SWC sector where there is a variety of basaltic magma types including tholeiitic, calcalkalic, and alkalic types. The role of crustal contamination in modifying Cascade basaltic magmas is considered to be small, whereas associated andesitic and dacitic magmas clearly have evolved by open system processes. Some dacites (e.g., MSH) are interpreted as crustal anatectic melts formed in response to stagnation of hot basaltic magmas at or just above the crust-mantle boundary (e.g., the MASH zones of Hildreth and Moorbath, 1988). The primitive nature of the erupted basalts and their relatively common occurrence in the SWC sector both imply that such magmas had little residence time in the crust; this view is supported by the occurrence of mantle spinel lherzolite xenoliths in some SIM basalts. The fact that the basaltic magmas either

References

Abbott, D., and M. Lyle, Age of oceanic plates at subduction and volatile recycling, *Geophys. Res. Lett., 11,* 951-954, 1984.

Arculus, R.J., and R.W. Johnson, Island-arc magma sources: a geochemical assessment of the roles of slab-derived components and crustal contamination, *Geochemical J., 15,* 109-133, 1981.

AveLallemant, H.G., and J.S. Oldow, Early Mesozoic southward migration of Cordilleran transpressional terranes, *Tectonics, 7,* 1057-1075, 1988.

Bacon, C.R., Implications of silicic vent patterns for the presence of large crustal magma chambers, *J. Geophys. Res., 90,* 11243-11252, 1985.

Bacon, C.R., M.A. Lanphere, and J.R. O'Neil, Strontium and oxygen isotopes in volcanic rocks near Crater Lake, Oregon, and their bearing on arc magmatism, *this volume,* 1989.

Blackwell, D.D., R.G. Bowen, D.A. Hull, J.F. Riccio, and J.L. Steele, Heat flow, arc volcanism, and subduction in northern Oregon, *J. Geophys. Res., 87,* 8735-8754, 1982.

Briqueu, L., H. Bougault, and J.L. Joron, Quantification of Nb, Ta, Ti, and V anomalies in magmas associated with subduction zones: petrogenetic implications, *Earth Planet. Sci. Lett., 68,* 297-308, 1984.

Bullen, T.D., and M.A. Clynne, Geochemical and isotopic constraints on magmatic evolution at Lassen volcanic center, southernmost Cascade Range, *this volume,* 1989.

Campbell, N.P., and Bentley, R.D., Late Quaternary deformation of the Toppenish Ridge uplift in south central Washington, *Geology, 9,* 519-524, 1981.

Church, S.E., The Cascade Mountains revisited: a re-evaluation in light of new lead isotopic data, *Earth Planet. Sci. Lett., 29,* 175-188, 1976.

Church, S.E., and G.W. Tilton, Lead and strontium isotopic studies in the Cascade Mountains: bearing on andesite genesis, *Geol. Soc. Amer. Bull., 84,* 431-454, 1973.

Church, S.E., A.P. LeHuray, A.R. Grant, M.H. Delevaux, and J.E. Gray, Lead-isotopic data from sulfide minerals from the Cascade Range, Oregon and Washington, *Geochim. Cosmochim. Acta, 50,* 317-328, 1986.

Clynne, M.A., Nature of volcanic centers in the southernmost Cascade Range, California: the Lassen volcanic center, *this volume,* 1989.

Duncan, R.A., A captured island chain in the Coast Range of Oregon and Washington, *J. Geophys. Res., 87,* 10827-10837, 1982.

Duncan, R.A., and L.D. Kulm, Plate tectonic evolution of the Cascades Volcanic Arc and subduction complex, in *Geol. Soc. Amer. DNAG Centennial, East Pacific vol. xxx,* in press.

Ellam, R.M., and C.J. Hawkesworth, Elemental and isotopic variations in subduction related basalts: evidence for a three component model, *Contrib. Mineral. Petrol., 98,* 72-80, 1988.

Evarts, R.C., R.P. Ashley, and J.G. Smith, Geology of the Mount St. Helens area: record of discontinuous volcanic and plutonic activity in the Cascade arc of southern Washington, *J. Geophys. Res., 92,* 10155-10169, 1987.

Farooqui, S.M., J.D. Beaulieu, R.C. Bunker, D.E. Stensland, and R.E. Thoms, Dalles Group: Neogene formations overlying the Columbia River Basalt Group in north-central Oregon, *Oregon Geology, 43,* 131-140, 1981.

Gill, J.B., *Orogenic andesites and plate tectonics*, Springer-Verlag, New York, 390 pp., 1981.

Gill, J.B., Sr-Pb-Nd isotopic evidence that both MORB and OIB sources contribute to oceanic island arc magmas in Fiji, *Earth Planet. Sci. Lett., 68,* 443-458, 1984.

Govindaraju, K., Compilation of working values and sample description for 170 international reference samples of mainly silicate rocks and minerals, *Geostandards Newsletter, 8, Special Issue,* 3-16, 1984.

Green, T.H., Island arc and continent-building magmatism - a review of petrogenetic models based on experimental petrology and geochemistry, *Tectonophys., 63,* 367-385, 1980.

Grove, T.L., D.C. Gerlach, and T.W. Sando, Origin of calc-alkalic series lavas at Medicine Lake volcano by fractionation, assimilation and mixing, *Contrib. Mineral. Petrol., 80,* 160-182, 1982.

show no correlation between isotopic and trace element components, or show trends quite distinct from those of the evolved lavas, suggests that their compositional variability is attributable to sub-crustal processes.

The majority of samples studied are indistinguishable from oceanic island basalts (OIB) in trace element and isotopic compositions. The absence of LILE enrichment and HFSE depletion distinguishes most **SWC** basalts from typical volcanic arc magmas. Because these features are generally attributed to the role of fluids released by dehydration of subducted oceanic lithosphere, and to the effects of sediment subduction, we conclude that these features are not essential in producing the **SWC** basalts. We infer that these basalts formed by variable degree melting of a mixed mantle source consisting mainly of heterogeneously distributed OIB- and MORB-source domains. Minor occurrences of HFSE-depleted (arc-like) basalts in the **SWC** may reflect the presence of a small proportion of slab-metasomatized sub-arc mantle (possibly remnants of older accreted island arc terranes or of the Paleogene arc). The juxtaposition of such different mantle domains within the lithospheric mantle is viewed as a consequence of (1) tectonic mixing associated with accretion of oceanic and island arc terranes along the Pacific margin of North America prior to Neogene time, and (2) a seaward jump in the locus of subduction at about 40 Ma.

Finally, the Cascades arc is unusual in that the subducting oceanic plate is very young and hot. Because dehydration of this slab occurs outboard of the volcanic front, the role of aqueous fluids in generating arc magmas is strongly diminished compared to the situation at most convergent margins, as judged by compositions of the magmas produced. Under low fluid flux conditions basalt generation is presumably triggered by other processes that raise the temperature of the mantle wedge to its solidus (e.g., convective mantle flow, shear heating, etc.). Although fluid-enhanced melting is an attractive feature for models of subduction zone magma production, it may not be an essential one. The Cascades provide a 'dry' perspective on what is surely a wide spectrum of arc models; in this case, reduced slab contributions offer the advantage that we can see in more detail the effects of processes that occur in the mantle wedge.

Acknowledgments

WPL thanks M.A. Menzies for his aid in arranging a sabbatical visit to the Open University where much of this work was accomplished. C.J. Hawkesworth kindly provided access to the isotope facilities there, and the Open University staff provided support in many ways. We are indebted to J.G. Fitton and D. James who provided numerous critical XRF analyses at the University of Edinburgh. M. Dehn, E. Pestana, and several students at Rice University assisted with sample preparation and ICP analyses. Oxygen isotopic data were provided by M. Matsuhisa (Geological Survey of Japan) and R. Harmon (Southern Methodist University), and J.W. Valley (University of Wisconsin) provided **DRS** access to his laboratory for further analyses. A large portion of this research was funded by the National Science Foundation (Grants EAR82-14876 and EAR85-12172). **ZAP** was supported by a NERC post-doctoral fellowship.

Grove, T.L., R.J. Kinzler, M.B. Baker, J.M. Donnelly-Nolan, and C.E. Lesher, Assimilation of granite by basaltic magma at Burnt lava flow, Medicine Lake volcano, northern California: decoupling of heat and mass transfer. *Contrib. Mineral. Petrol., 99,* 320-343, 1988.

Guffanti, M., and Weaver, C.S., Distribution of late Cenozoic volcanic vents in the Cascade Range: volcanic arc segmentation and regional tectonic considerations, *J. Geophys. Res., 93,* 6513-6529, 1988.

Guffanti, M., M.A. Clynne, L.J.P. Muffler, and J.G. Smith, Spatial, temporal, and compositional trends of mafic volcanism in the Lassen region of northeastern California, *this volume,* 1989.

Gust, D.A., and M.R. Perfit, Phase relations of a high-Mg basalt from the Aleutian Island Arc: implications for primary island arc basalts and high-Al basalts, *Contrib. Mineral. Petrol., 97,* 7-18, 1987.

Halliday, A.N., A.E. Fallick, A.P. Dickin, A.B. Mackenzie, W.E. Stephens, and W. Hildreth, The isotopic and chemical evolution of Mount St. Helens, *Earth Planet. Sci. Lett. 63,* 241-256, 1983.

Hammond, P.E., A tectonic model for the evolution of the Cascade Range, in *Pacific Coast Paleogeography Symposium, 3, Cenozoic Paleogeography of the western United States,* edited by J.M. Armentrout, M.R. Cole, and H.J.R. Terbest, pp. 219-237, The Pacific Section Society of Economic Paleontologists and Mineralogists, 1979.

Hammond, P.E., Reconnaissance geologic map and cross sections of southern Washington Cascade Range, Lat. 45°30' - 47°15'N, Long. 120°45' - 122°22.5'W, Portland State Univ., *Publ. Dept. of Earth Sciences,* 1980.

Hammond, P.E., and M.A. Korosec, Geochemical analyses, age dates, and flow-volume estimates for Quaternary volcanic rocks, southern Cascades Mountains, Washington, *Wash. Div. Geol. Earth Resour. Open File Rep., 83-13,* 36 pp., 1983.

Hart, S.R., A large-scale isotopic anomaly in the southern hemispheric mantle, *Nature, 309,* 753-757, 1984.

Hart, W.K., M.D. Norman, R.W. Carlson, and W.P. Leeman, Andesite petrogenesis in the northwestern Basin and Range: implications for the geochemical evolution of subcontinental mantle, *Geol. Soc. Amer. Abst. with Prog., 21,* in press, 1989.

Hegner, E., and M. Tatsumoto, Pb, Sr, and Nd isotopes in basalts and sulfides from the Juan de Fuca Ridge, *J. Geophys. Res., 92,* 11380-11386, 1987.

Heller, P.L., Z.E. Peterman, J.R. O'Neil, and M. Shafiqullah, Isotopic provenance of sandstones from the Eocene Tyee Formation, Oregon Coast Range, *Geol. Soc. Amer. Bull., 96,* 770-780, 1985.

Hickey, R.L., F.A. Frey, D.C. Gerlach, and L. Lopez-Escobar, Multiple sources for basaltic arc rocks from the Southern Volcanic Zone of the Andes (34°-41°S): trace element and isotopic evidence for contributions from subducted oceanic crust, mantle and continental crust, *J. Geophys. Res., 91,* 5963-5983, 1986.Hildreth, W., and S. Moorbath, Crustal contributions to arc magmatism in the Andes of central Chile, *Contrib. Mineral. Petrol., 98,* 455-489, 1988.

Hildreth, W., and J. Fierstein, Mount Adams: Eruptive history of an andesite-dacite stratovolcano at the focus of a fundamentally basaltic volcanic field, *U.S. Geol. Surv. Open File Rep., 85-521,* 44-50, 1985.

Hoblitt, R.P., D.R. Crandall, and D.R. Mullineaux, Mount St. Helens eruptive behavior during the last 1500 years, *Geology, 8,* 555-559, 1980.

Hofmann, A.W., Chemical differentiation of the Earth: the relationship between mantle, continental crust, and oceanic crust, *Earth Planet. Sci. Lett., 90,* 297-314, 1988.

Hole, M.J., A.D. Saunders, G.F. Marriner, and J. Tarney, Subduction of pelagic sediments: implications for the origin of Ce-anomalous basalts from the Mariana Islands, *J. Geol. Soc. Lond., 141,* 453-472, 1984.

Hughes, J.M., R.E. Stoiber, and M.J. Carr, Segmentation of the Cascade volcanic chain, *Geology, 8,* 15-17, 1980.

Hughes, S.S., Mafic magmatism and associated tectonism of the central High Cascade Range, Oregon, *this volume,* 1989.

Hughes, S.S., and E.M. Taylor, Geochemistry, petrogenesis, and tectonic implications of central High Cascade mafic platform lavas, *Geol. Soc. Amer. Bull., 97,* 1024-1036, 1986.
Hsui, A.T., B.D. Marsh, and M.N. Toksoz, On melting of the subducted oceanic crust: effects of subduction induced mantle flow, *Tectonophys., 99,* 207-220, 1983.
Irvine, T.N., and W.R.A. Baragar, A guide to the chemical classification of the common volcanic rocks, *Can. J. Earth Sci., 8,* 523-548, 1971.
Ito, E., and R.J. Stern, Oxygen and strontium isotopic investigations of subduction zone volcanism: the case of the Volcano Arc and the Marianas Island Arc, *Earth Planet. Sci. Lett., 76,* 312-320, 1985.
Kay, R.W., Aleutian magnesian andesites: melts from subducted Pacific Ocean crust, *J. Volcanol. Geotherm. Res., 4,* 117-132, 1978.
Kay, R.W., Elemental abundances relevant to identification of magma sources, *Philos. Trans. Roy. Soc. London, A310,* 535-547, 1984.
Kim, K., S.A. Dischler, J.R. Aggson, and M.P. Hardy, The state of in-situ stresses determined by hydraulic fracturing at the Hanford Site: Richland, Washington, *Rockwell Hanford Operations Rep. RHO-BW-ST-73P,* 172 pp, 1986.
Klein, F.W., Earthquakes in Lassen Volcanic National Park, California, *Seism. Soc. Amer. Bull., 69,* 867-875, 1979.
Leeman, W.P., Tectonic and magmatic significance of strontium isotopic variations in Cenozoic volcanic rocks from the western United States, *Geol. Soc. Am. Bull., 93,* 487-503, 1982.
Leeman, W.P., The influence of crustal structure on compositions of subduction-related magmas, *J. Volcanol. Geotherm. Res., 18,* 561-588, 1983.
Leeman, W.P., Boron geochemistry of volcanic arc magmas: evidence for recycling of subducted oceanic lithosphere, *EOS, 68,* 462, 1987.
Leeman, W.P., and C.J. Hawkesworth, Open magmatic systems - some isotopic and trace element constraints, *J. Geophys. Res., 91,* 5901-5912, 1986.
Le Roex, A.P., H.J.B. Dick, A.J. Erlank, A.M. Reid, F.A. Frey, and S.R. Hart, Geochemistry, mineralogy and petrogenesis of lavas erupted along the southwest Indian Ridge between the Bouvet triple junction and 11 degrees East, *J. Petrol., 24,* 267-318, 1983.
Luedke, R.G., and R.L. Smith, Map showing distribution, composition, and age of late Cenozoic volcanic centers in Oregon and Washington, *U.S. Geol. Surv. Misc. Invest. Map I-1091D,* 1982.
Lux, D.R., K-Ar and ^{40}Ar-^{39}Ar ages of mid-Tertiary volcanic rocks from the western Cascade Range, Oregon, *Isochron West, 33,* 27-32, 1982.
MacDonald, G.A., ant T. Katsura, Chemical composition of Hawaiian lavas, *J. Petrol., 5,* 82-133, 1964.
McBirney, A.R., Volcanic evolution of the Cascade Range, *Ann. Rev. Earth Planet. Sci., 6,* 437-456, 1978.
McBirney, A.R., and C.M. White, The Cascade Province, in *Andesites: Orogenic Andesites and Related Rocks,* edited by R.S. Thorpe, pp. 115-135, John Wiley, New York, 1982.
McKee, E.M., W.A., Duffield, and R.J. Stern, Late Miocene and early Pliocene basaltic rocks and their implications for crustal structure, northeastern California and south-central Oregon, *Geol. Soc. Amer. Bull., 94,* 292-304, 1983.
Michaelson, C.A., and C.S. Weaver, Upper mantle structure from teleseismic P wave arrivals in Washington and northern Oregon, *J. Geophys. Res., 91,* 2077-2094, 1986.
Miyashiro, A., Volcanic rock seriesin island arcs and active continental margins, *Am. J. Sci., 274,* 321-355, 1974.
Morris, J.D., and S.R. Hart, Isotopic and incompatible element constraints on the genesis of island arc volcanics from Cold Bay and Amak Island, Aleutians, and implications for mantle structure, *Geochim. Cosmochim. Acta, 47,* 2015-2030, 1983.
Morris, J.D., Leeman, W.P., and Tera, F., The subduction component in island arc lavas: constraints from Be isotopes and B-Be systematics, *Nature,* submitted, 1989.

Nakamura, K., Volcanoes as possible indicators of tectonic stress orientation, *J. Volcanol. Geotherm. Res., 2,* 1-16, 1977.
Norman, M.D., K.R. McElwee, R.A. Duncan, and W.P. Leeman, K-Ar ages of Oligocene Salmon Creek Volcanics, Owyhee Mountains, SW Idaho, *Isochron West, 46,* 15-19, 1986.
Norman, M.D., and W.P. Leeman, Temporal evolution of Cenozoic through late Cretaceous magma sources and tectonic setting, SW Idaho, *Geol. Soc. Amer. Abst. with Prog., 20,* 460, 1988.
Ort, K.M., R.W. Tabor, and V.A. Frizell, Jr., Chemical analyses of selected Tertiary and Quaternary volcanic rocks, Cascade Range, Washington, *U.S. Geol. Surv. Open File Rep. 83-1,* 1-14, 1983.
Pearce, J.A., Role of subcontinental lithosphere in magma genesis at active continental margins, *In:* C.J. Hawkesworth and M.J. Norry (eds.), *Continental Basalts and Mantle Xenoliths,* Shiva Geology Series, Nantwich, U.K., pp. 230-249, 1983.
Perfit, M.R., D.A. Gust, A.E. Bence, R.J. Arculus, and S.R. Taylor, Chemical characteristics of island-arc basalts: implications for mantle sources, *Chem. Geol., 30,* 227-256, 1980.
Peterman, Z.E., C.E. Hedge, R,G, Coleman, and P.D. Snaveley, Jr., $^{87}Sr/^{86}Sr$ ratios in some eugeosynclinal sedimentary rocks and their bearing on the origin of granitic magma in orogenic belts, *Earth Planet. Sci. Lett., 2,* 433-439, 1967.
Peterman, Z.E., I.S.E. Carmichael, and A.L. Smith, Sr^{87}/Sr^{86} ratios of Quaternary lavas of the Cascade Range, northern California, *Geol. Soc. Amer. Bull., 81,* 311-318, 1970.
Peterman, Z.E., R.G. Coleman, and C.E. Bunker, Provenance of Eocene graywackes of the Flournoy Formation near Agness, Oregon - a geochemical approach, *Geology, 9,* 81-86, 1981.
Phillips, W.M., M.A. Korosec, H.W. Schasse, J.L. Anderson, and R.A. Hagen, K-Ar ages of volcanic rocks in southwest Washington, *Isochron West, 47,* 18-24, 1986.
Plank, T., and C,H, Langmuir, An evaluation of the global variations in the major element chemistry of arc basalts, *Earth Planet. Sci. Lett., 90,* 349-370, 1988.
Priest, G.R., Overview of the geology of the central Oregon Cascade Range, in Priest, G.R., and B.F. Vogt, eds., Geology and geothermal resources of the central Oregon Cascade Range, *Oregon Dept.. Geol. Mineral Indus. Spec. Pap. 15,* 3-28, 1983.
Priest, G.R., Volcanic and tectonic evolution of the Cascade volcanic arc, 44°00' to 44°52.5' N, *this volume,* 1989.
Rasmussen, J., and E. Humphreys, Tomographic image of the Juan de Fuca plate beneath Washington and western Oregon using teleseismic P-wave travel times, *Geophys. Res. Lett., 15,* 1417-1420, 1988.
Rea, D.K., and R.A. Duncan, North Pacific plate convergence: a quantitative record of the past 140 m.y., *Geology, 14,* 373-376, 1986.
Riddihough, R.P., Recent movements of the Juan de Fuca Plate system, *J. Geophys. Res., 89,* 6980-6994, 1984.
Rogers, G.C., Variation in Cascade volcanism with margin orientation, *Geology, 13,* 495-498, 1985.
Sakuyama, M., and R.W. Nesbitt, Geochemistry of the Quaternary volcanic rocks of the northeast Japan arc, *J. Volcanol. Geotherm. Res., 29,* 413-450, 1986.
Sherrod, D.R., and J.G. Smith, Quaternary extrusion rates from the Cascade Range, northwestern United States and British Columbia, *this volume,* 1989.
Sheppard, R.A., Geology of the Simcoe Mountains volcanic area, Washington, *Wash. Div. Mines and Geol. Geol. Map GM-3,* 1967.
Simpson, R.W., and Cox, A.V., Paleomagnetic evidence for tectonic rotation of the Oregon Coast Range, *Geology, 5,* 585-589, 1977.
Smith, D.R., and W.P. Leeman, Petrogenesis of Mount St. Helens dacitic magmas, *J. Geophys. Res., 92,* 10313-10334, 1987.
Smith, G.A., Late Cenozoic structures on the Columbia Plateau: implications for tectonics in the Pacific Northwest, *EOS, 63,* 1116, 1982.

Smith, G.A., L.W. Snee, and E.M. Taylor, Stratigraphic, sedimentologic, and petrologic record of late Miocene subsidence of the central Oregon High Cascades, *Geology, 15,* 389-392, 1987.
Stacey, J.S., and J.D. Kramers, Approximation of terrestrial lead isotope evolution by a two-stage model, *Earth Planet. Sci. Lett., 26,* 207-221, 1975.
Stern, C.R., K. Futa, S. Saul, and M.A. Skewes, Nature and evolution of the subcontinental mantle lithosphere below southern South America and implication for Andean magma genesis, *Revista Geol. Chile, 27,* 41-53, 1986.
Stern, R.J., S.H. Bloomer, P.-N. Lin, E. Ito, and J. Morris, Shoshonitic magmas in nascent arcs: new evidence from submarine volcanoes in the northern Marianas, *Geology, 16,* 426-430, 1988.
Tatsumi, Y., D.L. Hamilton, and R.W. Nesbitt, Chemical characteristics of fluid phase released from a subducted lithosphere and origin of arc magmas: evidence from high-pressure experiments and natural rocks, *J. Volcanol. Geotherm. Res., 29,* 293-309, 1986.
Taylor, E.M., Volcanic history and tectonic development of the central High Cascade Ranhe, Oregon, *this volume,* 1989.
Taylor, S.R., and S.M. McLennan, *The continental crust: its composition and evolution,* Blackwell Scientific Publ., Oxford, England, 312 pp., 1985.
Verplanck, E.P., and R.A. Duncan, Temporal variations in plate convergence and eruption rates in the Western Cascades, Oregon, *Tectonics, 6,* 197-209, 1987.
Walker, J.R., and Naslund, H.R., Tectonic significance of mildly alkaline Pliocene lavas in Klamath River gorge, Cascade Range, Oregon, *Geol. Soc. Am. Bull., 97,* 206-212, 1986.
Weaver, B.L., D.A. Wood, J. Tarney, and J.L. Joron, Geochemistry of ocean island basalts from the South Atlantic: Ascension, Bouvet, St. Helena, Gough, and Tristan da Cunha, *In:* J.G. Fitton and B.J. Upton, *Alkaline Igneous Rocks, Geol. Soc. Lond. Spec. Publ. 30,* pp. 253-267, 1987.
Weaver, C.S., and S.D. Malone, Overview of the tectonic setting and recent studies of eruptions of Mount St. Helens, Washington, *J. Geophys. Res., 92,* 10149-10154, 1987.
Weaver, C.S., W.C. Grant, and J.E. Shemeta, Local crustal extension at Mount St. Helens, Washington, *J. Geophys. Res., 92,* 10170-10178, 1987.
Weaver, C.S., and G.E. Baker, Geometry of the Juan de Fuca plate beneath Washington - evidence from seismicity and the 1949 South Puget Sound earthquake, *Bull. Seismol. Soc. Am., 78,* 264-275, 1988.
Weaver, C.S., and C.A. Michaelson, Seismicity and volcanism in the Pacific Northwest: evidence for the segmentation of the Juan de Fuca plate, *Geophys. Res. Lett., 12,* 215-218, 1985.
White, W.M., A.W. Hofmann, and H. Puchelt, Isotope geochemistry of Pacific mid-ocean ridge basalt, *J. Geophys. Res., 92,* 4881-4893, 1987.
Williams, D.L., D.A. Hull, H.D. Ackerman, and M.H. Beeson, The Mount Hood region: volcanic history, structure, and geothermal energy potential, *J. Geophys. Res., 87,* 2767-2781, 1982.
Wood, D.A., A variably veined sub-oceanic upper mantle - genetic significance for mid-ocean ridge basalts from geochemical evidence. *Geology, 7,* 499-503, 1979.
Zoback, M.L., and M.D. Zoback, States of stress in the conterminous United States, *J. Geophys. Res., 85,* 6113-6156, 1980.

Table 1. Distribution of magma types in major eruptive centers of the SWC

Compositional types	St. Helens	Indian Heaven	Adams	Simcoe
Basalts				
Tholeiitic	-	xx	x	-
Transitional	x	x	x	-
Calcalkalic	x	xx	xx	-
Alkalic	-	-	-	xx
Basaltic Andesites	x	x	x	-
Andesites	xx	x	xx	x?
Dacites, Rhyodacites, Rhyolites	xx	-	x	x?

Key: - = not recognized
x? = present but volume unknown
x = present to common
xx = common to abundant

Table 2. Representative lavas from the Southern Washington Cascades

Sample	DS-27	DS-6	DS-72	DS15A-80	DS3B-80	DS23B-81	DS63	83-49	82-31	82-26	82-24	L83-67	L83-94	L83-97	L84-65	L84-67
Volcano	MSH	MSH	MSH	IH	IH	IH	IH	MA	MA	MA	MA	SIM	SIM	SIM	SIM	SIM
SiO2	48.64	49.96	52.96	49.29	50.53	52.21	59.02	48.95	51.42	52.73	59.41	50.48	49.14	49.98	63.78	74.26
TiO2	1.47	2.04	1.43	1.35	1.40	1.32	0.96	1.52	1.66	1.27	1.24	2.25	2.57	2.26	0.87	0.13
Al2O3	17.50	16.85	18.33	17.91	17.51	16.88	17.86	16.82	17.18	17.48	16.74	16.43	15.50	17.12	16.63	13.59
FeO*	11.69	10.14	8.22	10.59	9.99	7.65	6.50	10.69	10.06	8.79	6.76	10.55	11.99	10.97	5.10	2.13
MnO	0.16	0.15	0.13	0.18	0.15	0.13	0.11	0.17	0.17	0.15	0.12	0.16	0.16	0.16	0.11	0.03
MgO	6.58	6.62	5.46	6.50	5.85	6.02	3.49	7.89	5.78	6.46	3.21	6.06	6.88	5.80	1.37	0.08
CaO	9.60	8.63	7.96	10.44	9.98	8.85	6.45	10.40	8.94	8.79	5.90	7.20	9.39	6.50	3.83	0.22
Na2O	3.66	3.89	4.27	3.36	3.49	4.18	4.31	3.04	3.64	3.38	4.16	4.13	3.22	4.28	4.92	4.71
K2O	0.56	1.31	0.99	0.22	0.86	2.19	1.05	0.33	0.87	0.74	2.15	2.00	0.76	2.17	3.10	4.83
P2O5	0.15	0.41	0.25	0.15	0.23	0.57	0.26	0.17	0.27	0.22	0.31	0.74	0.39	0.76	0.29	0.02
Cs	0.36	0.25	0.31		0.21										2.38	0.75
Ba	118	316	225	57	291	947	314	88	233	306	421	554	194	640	425	18
Rb	11	25	23	5	15	22	16	4.5	16	10	58	34	13	38	76	159
Sr	321	620	528	248	512	1650	685	298	354	501	383	861	497	838	514	4
Y	23.0	24.9	21.3	20.8	21.4	20.5	12.6	25.0	29.5	23.0	28.0	27.0	27.0	25.0	34.0	18.0
Zr	132	203	154	96	151	218	170	111	208	144	311	257	164	262	355	431
Nb	8.7	32.7	12.5	5.5	9.7	12.3	12	8.2	15.0	11.0	25.0	50	22	53	34	76
V	210	212	184	211	224	181	124	178	179	157	114	129	186	106	49	3
Ni	85	97	66	58	41	64	56	103	69	80	29	137	87	85	7	4
Co	41.7	36.3	28.3	41.4	39.1	28.3	20.9					38.1	45.5	36.9	6.7	0.3
Cr	175	196	113	182	141	134	81	252	141	160	32	144	159	125	13	6
Sc	33.3	25.9	19.1	37.9	37.7	20.1	13.8	32	29	27	17	15.8	24.8	15.0	6.6	0.4
Zn	83	74	74	64	67	85	78	65	78	74	73	96	106	98	78	114
La	8.1	21.2	11.3	3.7	17.5	65.9	13.1	13	14	16	31	37.8	17.1	40.5	38.6	21.1
Ce	21.1	45.3	26.8	10.6	40.0	141.0	30.0	16	37	35	67	76.0	37.5	78.4	84.2	40.3
Nd						70.1		11	20	20	29	38.0	23.0	39.0	39.0	16.4
Sm	3.52	5.54	3.42	2.39	5.77	10.90	3.10					7.91	6.13	7.96	7.73	3.61
Eu	1.29	1.79	1.21	1.05	1.87	3.22	1.33					2.67	2.18	2.61	1.85	0.16
Tb	0.69	0.74	0.49	0.57	0.83	1.10	0.39					1.12	1.06	1.01	1.15	0.70
Yb	2.35	2.11	1.61	2.14	2.43	2.02	1.15					2.15	2.16	2.07	3.00	2.50
Lu	0.33	0.33	0.25	0.34	0.39	0.31	0.16					0.34	0.32	0.31	0.48	0.38
Hf	3.03	4.30	3.10	2.30	4.10	5.57	4.00					5.71	4.27	5.91	7.60	12.80
Ta	0.57	2.35	0.67	0.33	0.64	0.80	0.64					3.52	1.58	3.82	2.07	4.45
Th	0.94	2.47	1.36		3.29	9.51	1.33					4.18	1.67	4.22	9.80	18.70
B	3.4	4	5.7	1.1		2.9	5.6	1.7		3.4	12	2.0	2.2	1.5		
U			0.75		0.41	2.00						1.50	0.70	1.50	3.00	4.30
Be	1.0	1.7	1.5													
Pb	5	5	8					1	4	3	7	6.7	4.9	7.5	7.0	12.0
Sr87/86	0.70313	0.70304	0.70318	.70304	.70354	.70358	.70350	0.70291				.70303	.70287	.70302		
Nd143/144	0.512997	0.513012	0.513003	.512997	.512930		.512912	0.512987				.512912	.512997	.512880		
Pb206/204	18.869	18.961	18.812	18.875	18.960	18.934		18.838					19.409	18.680		
Pb207/204	15.573	15.590	15.577	15.577	15.634	15.576		15.565					15.604	15.537		
Pb208/204	38.513	38.569	38.495	38.538	38.790	38.609		38.422					38.773	38.349		
dO-18	5.71	5.79	6.19	5.79	5.53	5.88	6.06					5.78	5.84	6.36		

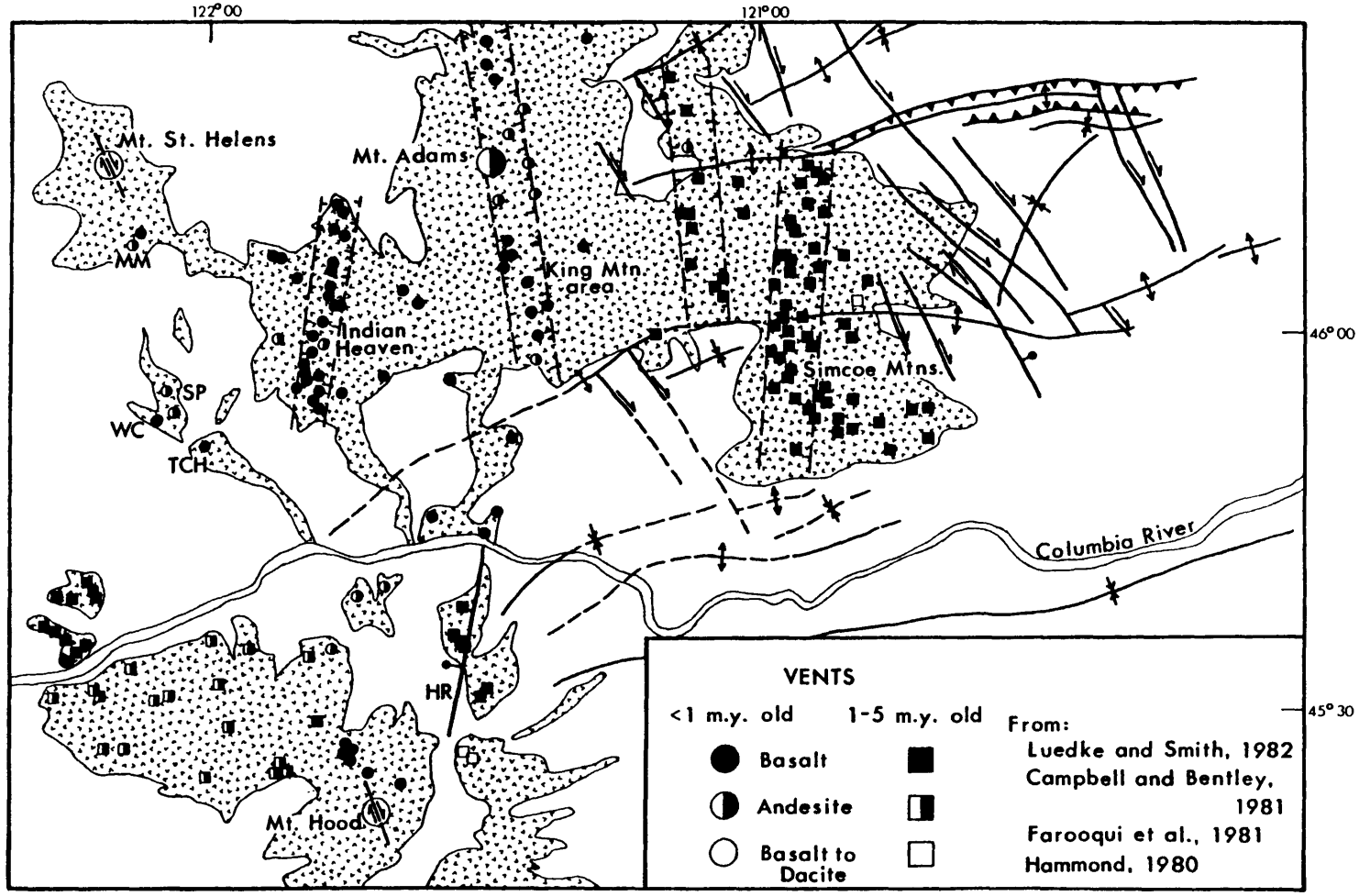

Figure 1. Geologic setting of the SWC traverse showing extent of late Pliocene to Recent volcanic rocks (stippled areas) and locations of major vents (from Luedke and Smith, 1982). Miscellaneous sampling localities indicated by letters include Marble Mtn. (MM), Soda Peak (SP), West Crater (WC), Trout Creek Hill (TCH), and Hood River valley (HR). Conspicuous vent alignments (outlined by dashed lines) are believed to be fault-controlled. Major structures (indicated by conventional symbols) offsetting Miocene to Pliocene age volcanic deposits include ENE-trending folds and thrust faults, NW-trending strike-slip faults, and N-trending normal faults (after Hammond, 1980; Campbell and Bentley, 1981; Farooqui et al., 1981). These structural elements are compatible with N-S regional compression (σ_1 N-S) and are distinct from Neogene structural patterns of the Basin and Range province (σ_1 vertical).

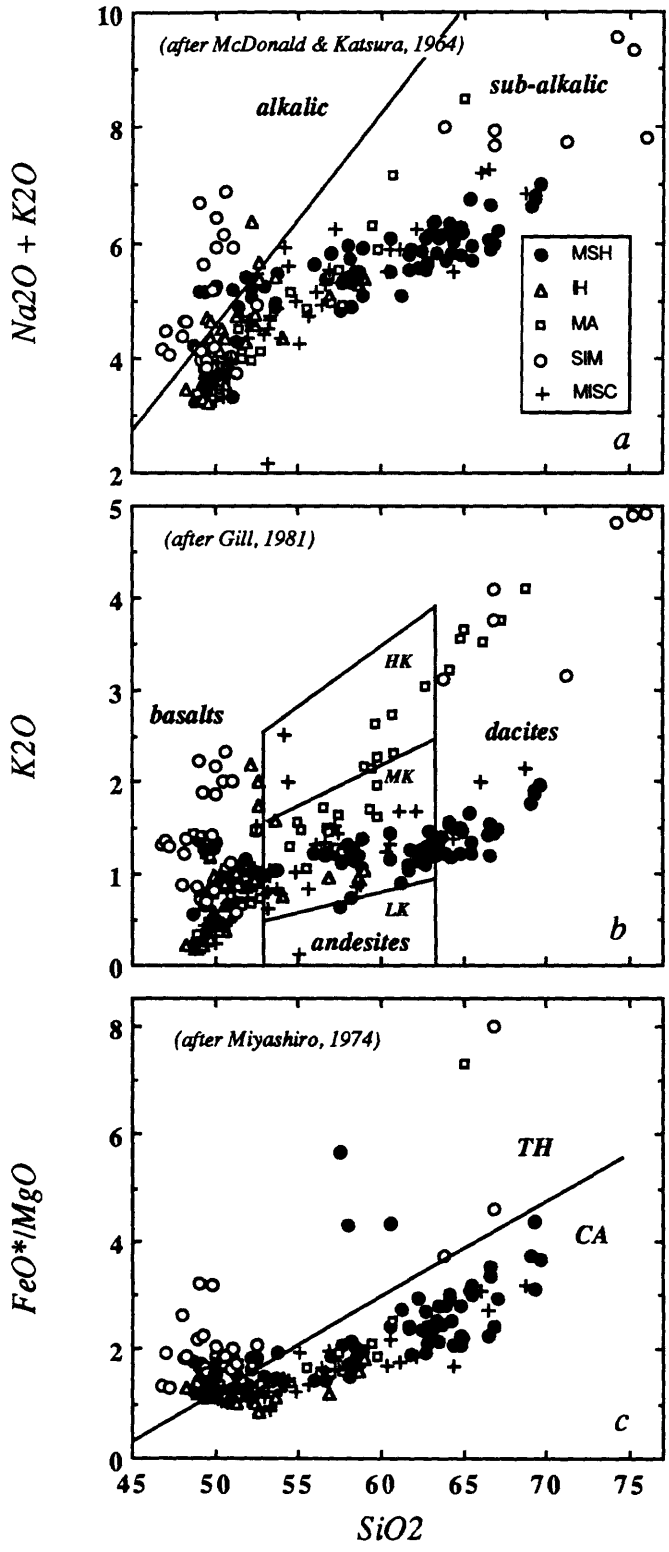

Figure 2. Variation diagrams showing SiO_2 versus total alkalies (a), K_2O (b), and FeO*/MgO (c). Classification criteria are discussed by Gill (1981). This plot compares samples from the four major volcanic complexes (MSH, IH, MA, and SIM) and from miscellaneous minor vents shown by letters in Figure 1. A few silicic lavas with very high FeO*/MgO plot off the field of view.

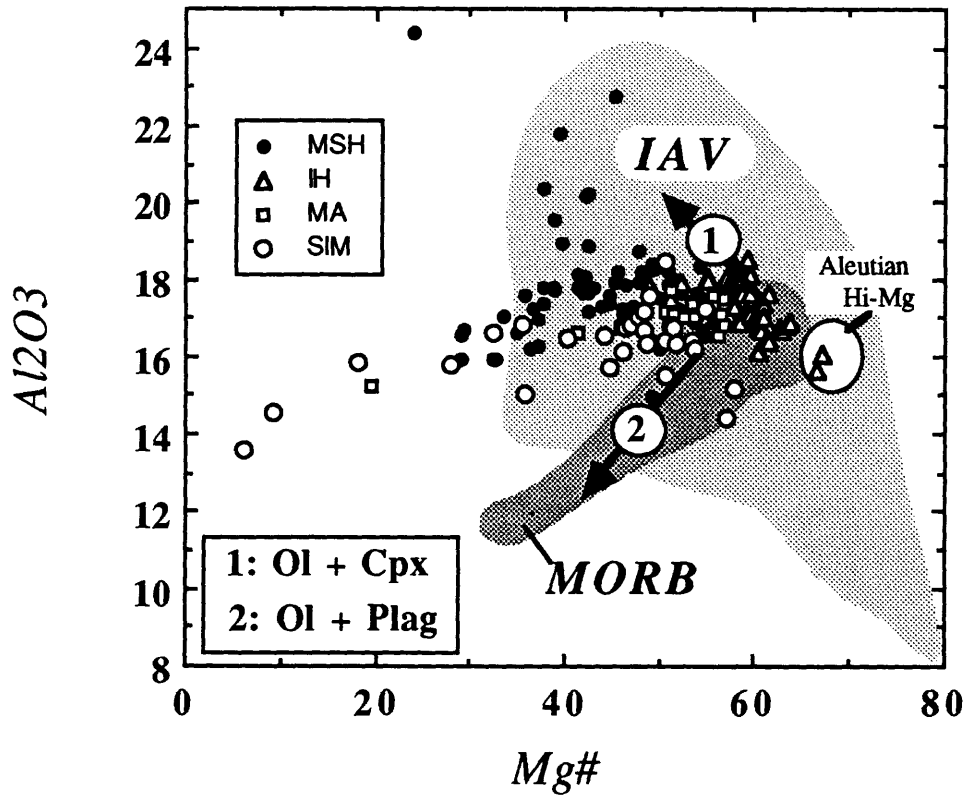

Figure 3. Mg#-Al_2O_3 diagram showing Cascades lavas relative to fields for mid-ocean ridge basalts (MORB), island arc volcanic rocks (IAV), and Aleutian high-magnesian basalts (after Gust and Perfit, 1987). Vectors are shown corresponding to approximate compositional variations resulting from removal of olivine and either clinopyroxene (**1** - high pressure) or plagioclase (**2** - low pressure). All MSH samples with Mg# near or below 40 and high Al_2O_3 (>19%) are dacitic whole pumice clasts from early eruptive periods.

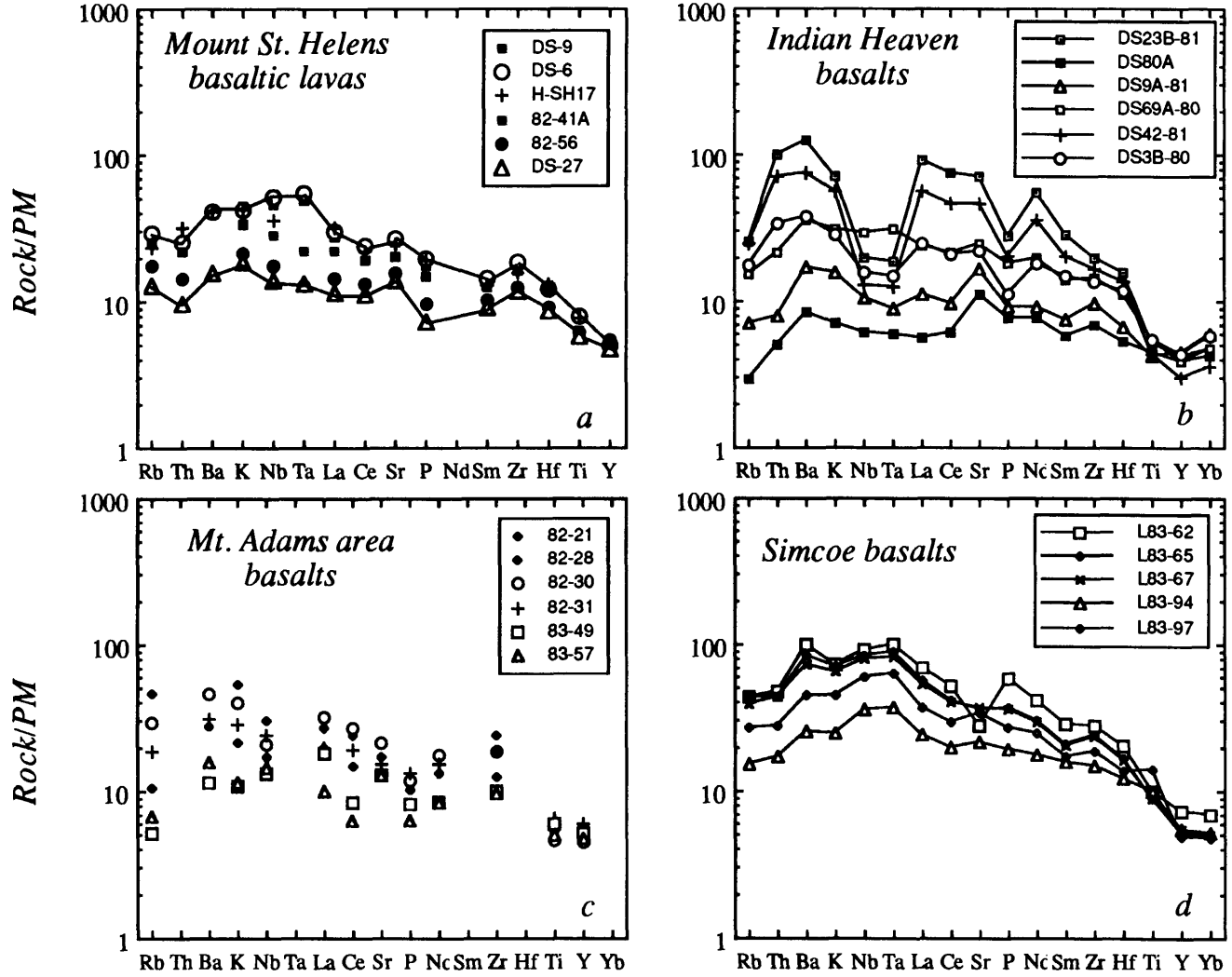

Figure 4. 'Incompatible' trace element abundances in selected SWC *basalts* (all <53% SiO_2) as normalized to Wood's (1979) estimated primitive mantle composition (model MORB source). Representative samples showing the range in basalt compositions are shown for each major volcano as follows: MSH (a), IH (b), MA (c), and SIM (d). Line profiles are omitted for MA samples because analytical data are less complete and La, Ce, and Nd were measured by relatively imprecise XRF methods. Note that few SWC basalts display relative depletions of HFSE (e.g., Nb, Ta) which are characteristic of volcanic arc magmas. Only a few samples from IH (also from some of the miscellaneous vents, not shown) display these features; these samples also exhibit relative depletions of P_2O_5. Profiles for the other three volcanoes are much more internally similar.

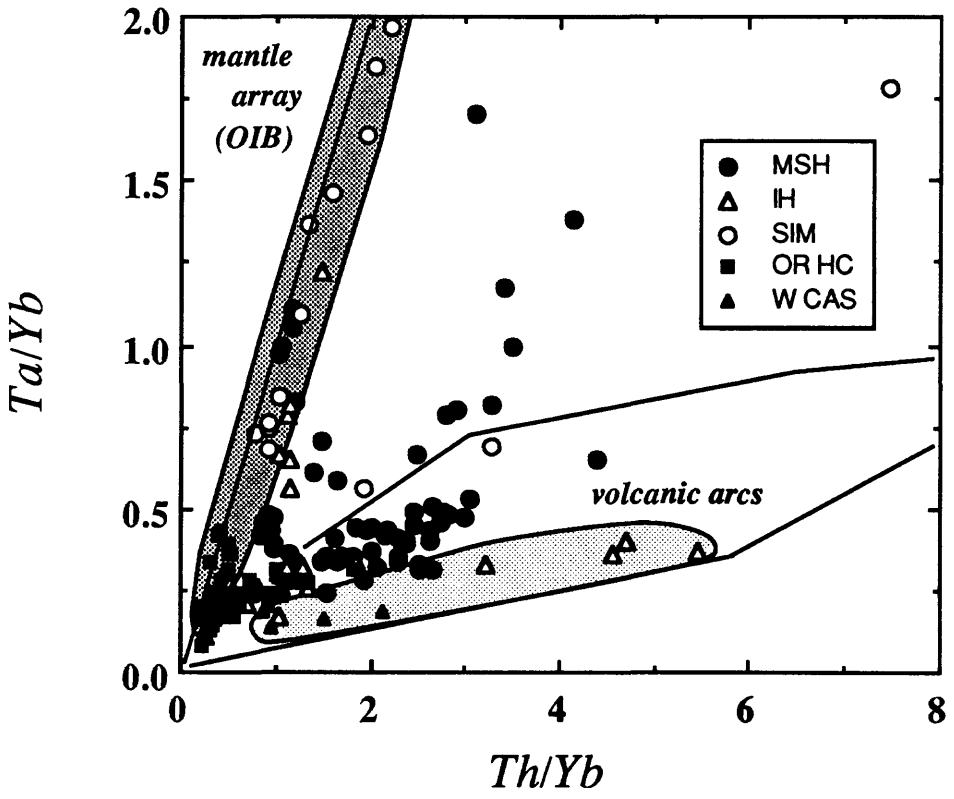

Figure 5. Th/Yb-Ta/Yb diagram showing **SWC** lavas; a few basalts from the Oligocene-Pliocene Western Cascades (**W CAS**; Leeman, unpublished data) and Pleistocene central High Cascades (**OR HC**; Hughes and Taylor, 1986) of Oregon are shown for comparison along with the field for typical volcanic arc magmas (Pearce, 1983). Distinct stippled fields are shown for HFSE-depleted (low Ta/Yb) basalts from the IH field and a 'mantle array' defined by most other **SWC** basalts, and by typical oceanic island basalts (OIB). Samples plotting between these two fields are evolved lavas (>53% SiO_2).

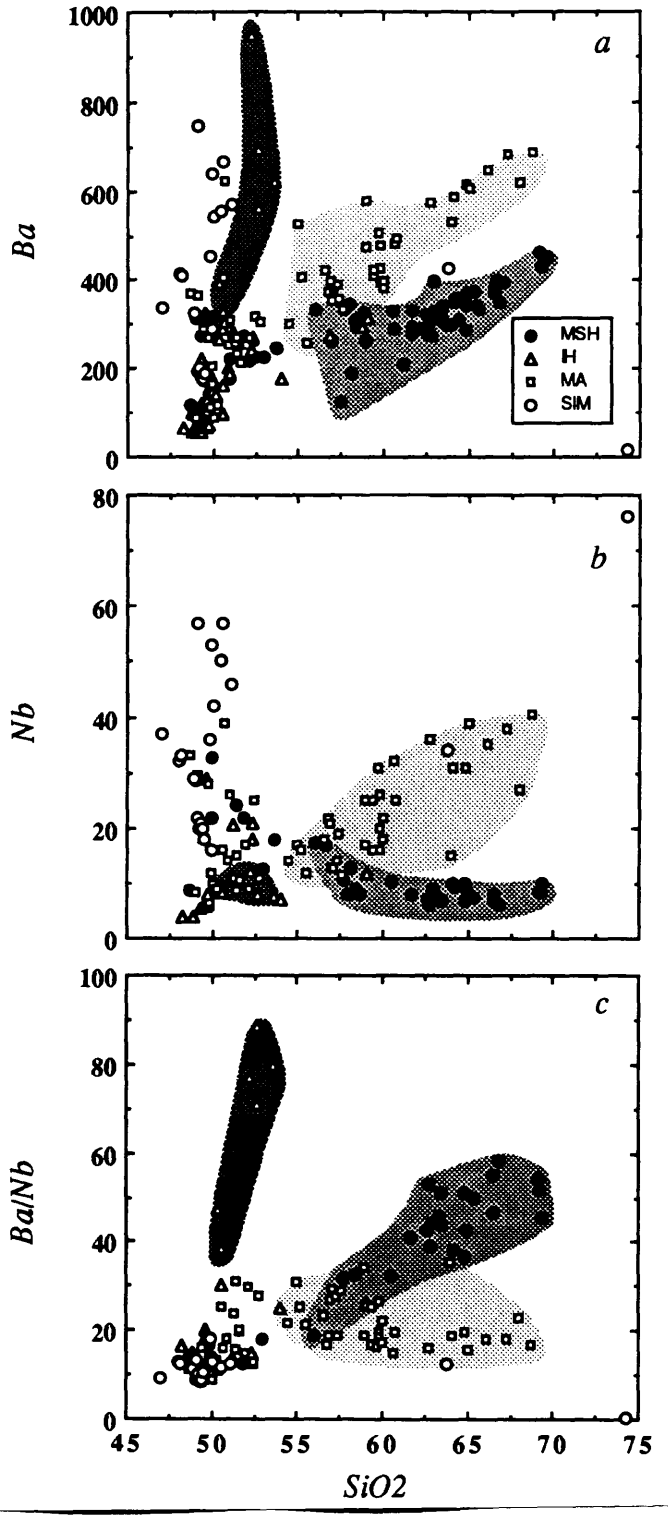

Figure 6. Variations in Ba (a), Nb (b), and Ba/Nb (c) versus SiO_2. *Basaltic lavas* define virtually the entire range in Ba and Nb concentrations. Most of these rocks have low Ba/Nb (<20), typical of OIB; those with higher Ba/Nb are HFSE-depleted IH basalts (dark stippled field). *Evolved lavas* from MA (light stippling) show Ba and Nb enrichments and slight Ba/Nb decrease with increasing SiO_2, consistent with dominantly fractional crystallization differentiation. Those from MSH (medium stippling) display compositional variations inconsistent with simple crystal fractionation (see text).

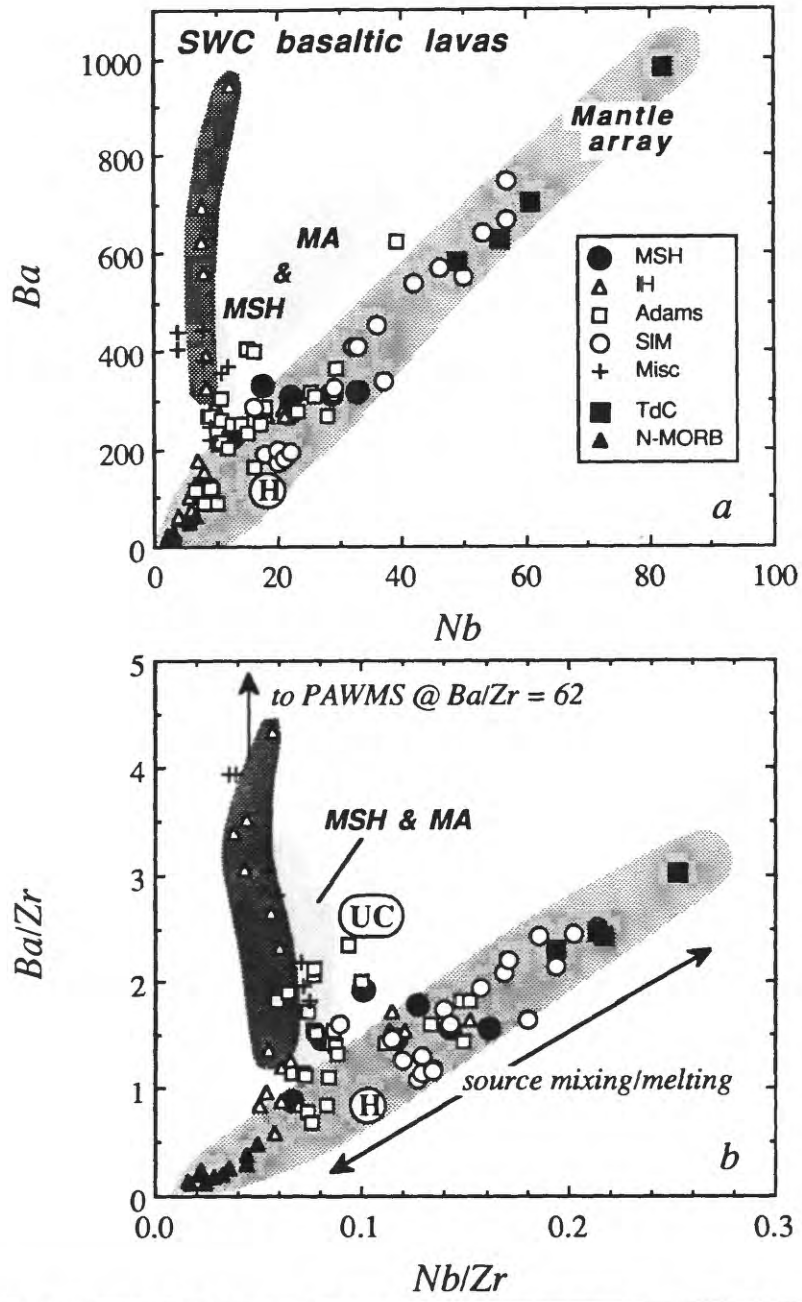

Figure 7. Ba vs. Nb (a) and Ba/Zr vs. Nb/Zr (b) in **SWC** *basaltic* lavas (<53% SiO_2). For clarity, the compositional field for evolved MA and MSH rocks is shown only by light stippling. HFSE-depleted IH basalts (dark stippling) and samples from some of the miscellaneous smaller vents display Ba and Ba/Zr enrichments toward approximate composition of pelagic sediments (as represented by PAWMS average of Hole et al., 1984). Average upper crust (point ***UC***; Taylor and McLennan, 1985) is plotted to show that melting of, or contamination by such material cannot explain the high Ba/Zr and Ba/Nb values observed. Remaining samples display coupled enrichment in Ba and Nb and define a 'mantle array' trend (medium stippling) similar to that for oceanic basalts (represented by Tristan da Cunha [Weaver et al., 1987], BHVO-1 Hawaiian tholeiite [point ***H***; cf. Govindaraju, 1984], N-MORB [Le Roex et al., 1983]; the stippled field covers the range for several hundred OIB analyses [Leeman, unpub. data and literature compilation]). The strong linearity of this array suggests that this group of **SWC** basalts could be derived by melting a mixed reservoir consisting of OIB- and MORB-source mantle components.

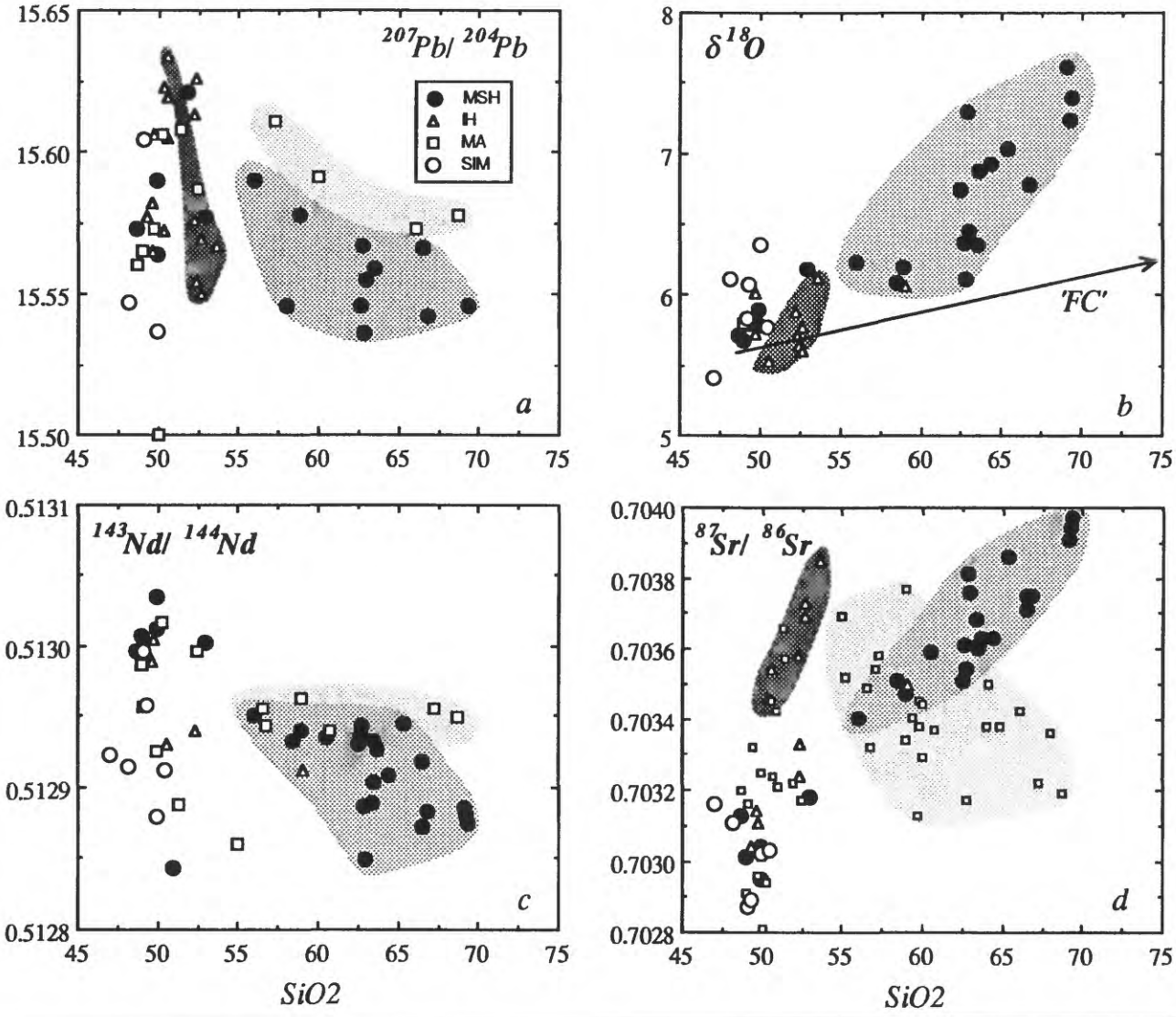

Figure 8. SiO_2 versus Pb, O, Nd, and Sr isotopic compositions for **SWC** volcanic rocks. *Basaltic* rocks define virtually the gamut of radiogenic isotopic compositions, but they are relatively uniform in $\delta^{18}O$. HFSE-depleted IH lavas (dark stippling) display significant correlations between SiO_2 and $^{207}Pb/^{204}Pb$ (a), $\delta^{18}O$ (b), and $^{87}Sr/^{86}Sr$ (d); they have not yet been analyzed for $^{143}Nd/^{144}Nd$. Evolved lavas from MSH (medium stippling) and MA (light stippling) are distinctive (although oxygen isotopic data are not available for the MA samples); this is especially true for $^{87}Sr/^{86}Sr$ trends. Each volcano has experienced open-system evolution, but specific processes must differ in each case. A vector indicating fractional crystallization (FC) effects is shown for $\delta^{18}O$ to illustrate that MSH magmas cannot be related simply by this process; they more likely represent mixtures between silicic crustal melts (i.e., the dacites) and basaltic magmas (cf. Smith and Leeman, 1987). The low $^{143}Nd/^{144}Nd$ (also $^{87}Sr/^{86}Sr = 0.7041$) mafic sample from MSH is a gabbroic xenolith from one of the dacite dome eruptions (Goat Rocks); its relation to other MSH basalts is unclear.

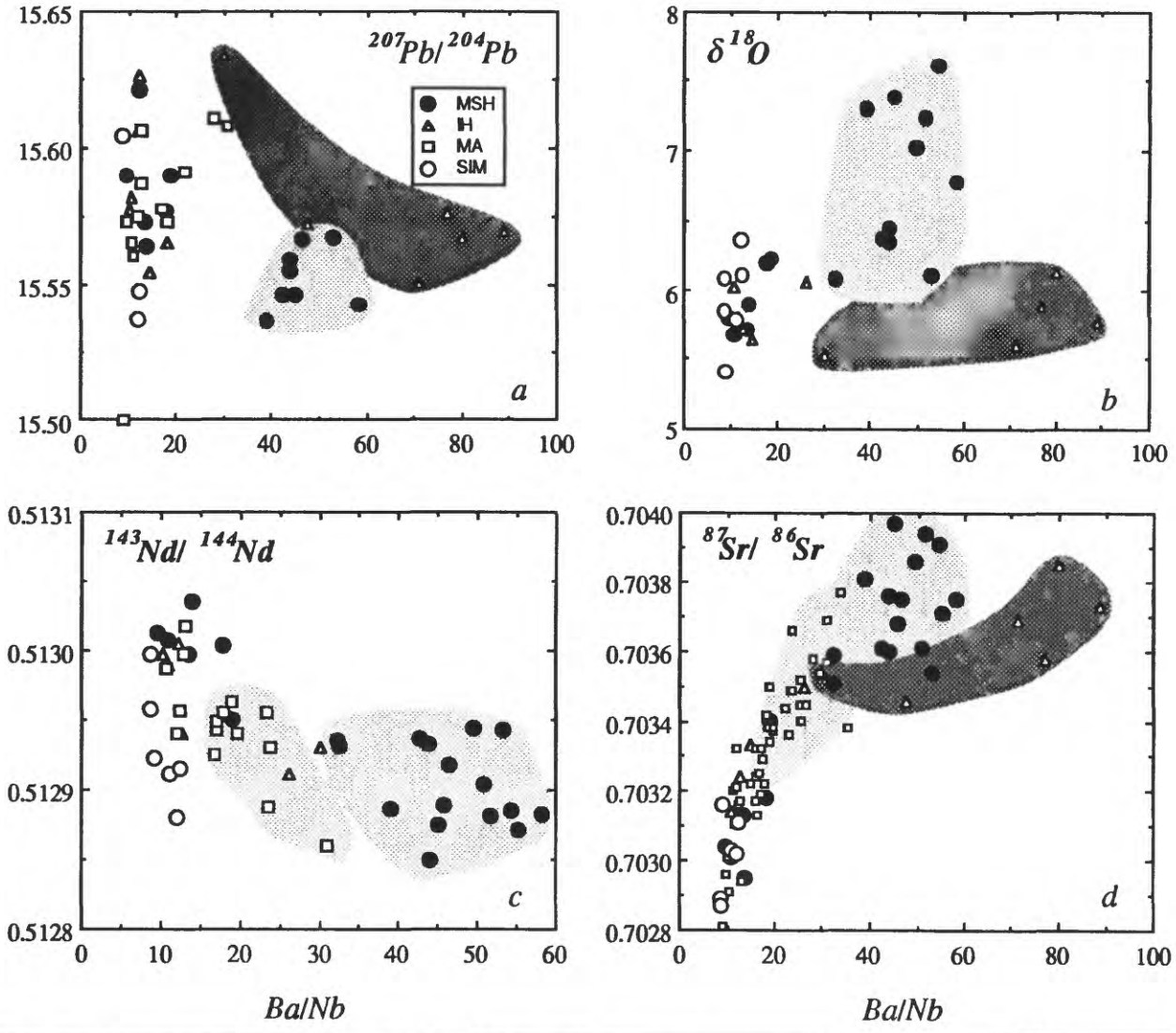

Figure 9. Ba/Nb ratio versus Pb, O, Nd, and Sr isotopic compositions. Excepting the high-Ba IH variants, SWC basalts have Ba/Nb<20 and display poor correlations with all isotopic parameters except $^{87}Sr/^{86}Sr$; they generally resemble typical OIB lavas (cf. Morris and Hart, 1983). Ba/Nb in HFSE-depleted IH basalts (dark stippling) is correlated negatively with $^{207}Pb/^{204}Pb$ and positively with $^{87}Sr/^{86}Sr$, but these rocks are distinctive from more evolved lavas in the transect (e.g., MA and MSH andesites and dacites; light stippling). Ba/Nb enrichment seems to have no significant correlation with O isotopic compositions.

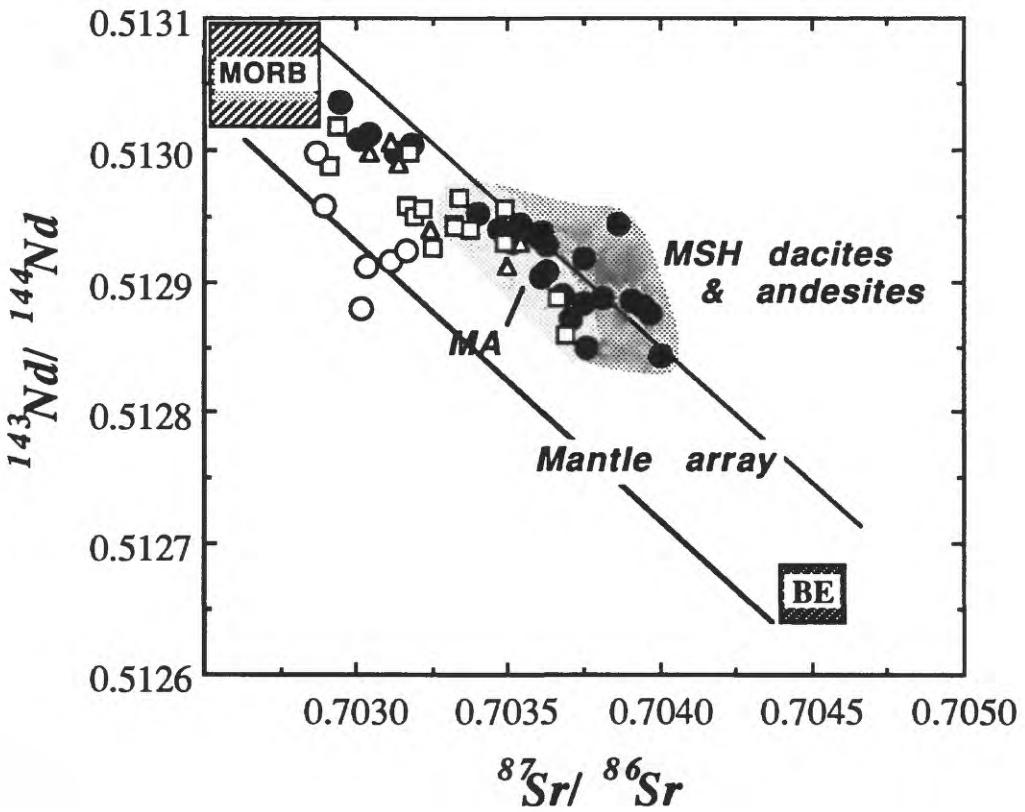

Figure 10. Sr-Nd isotopic compositions of SWC lavas relative to typical MORB, estimated 'bulk Earth', and the 'mantle array' defined by typical oceanic island basalts (cf. Hofmann, 1988). Evolved rocks from MA and MSH (stippled field) are shifted toward bulk earth from the basaltic lavas, which closely resemble many OIBs.

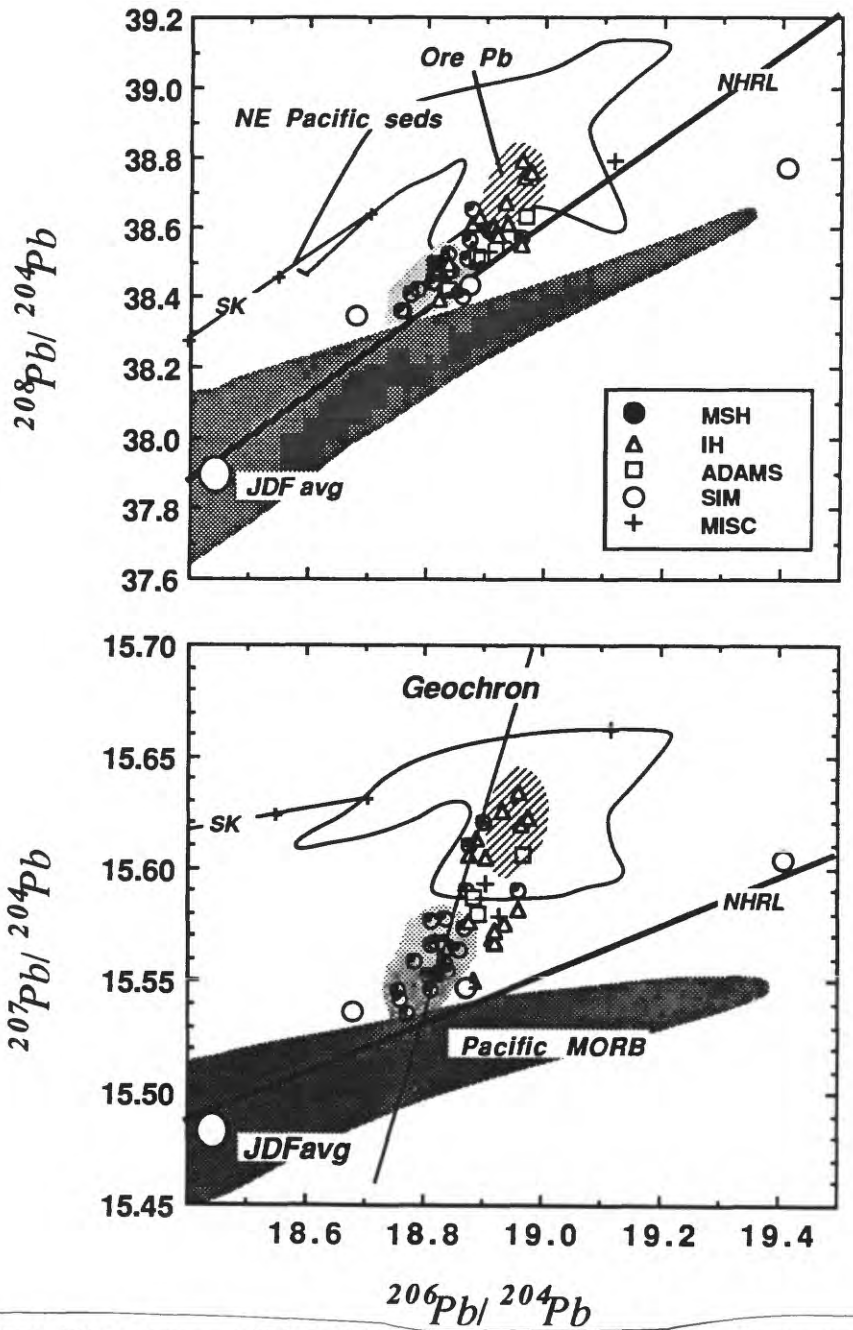

Figure 11. $^{208}Pb/^{204}Pb$ (a) and $^{207}Pb/^{204}Pb$ (b) versus $^{206}Pb/^{204}Pb$ diagram for **SWC** lavas relative to the fields of NE Pacific sediments (outlined field; Church, 1976) and Pacific MORB (dark stippling; White et al., 1987). The regression line for northern hemisphere oceanic basalts (***NHRL***; Hart, 1983), and an average of Juan de Fuca Ridge basalts (Hegner and Tatsumoto, 1987) also provide estimates of oceanic crust composition. The 'geochron' (shown only in [b]) is the locus of model single-stage Pb compositions, and the Stacey-Kramers (1975) growth curve (SK) represents the time-dependent evolution of conformable Pb ores which approximate average crust. Actual Cascades ore leads (Church et al., 1986) plot in the cross-hatched field at the radiogenic end of the volcanic rock array. The highest $^{207}Pb/^{204}Pb$ samples are predominantly basalts (also see Fig. 8a), whereas dacites from MSH (light stippling) plot nearer the NHRL line. SIM basalts are distinctive because the fall near NHRL (in [b]) and exhibit no anomalous enrichment in $^{207}Pb/^{204}Pb$.

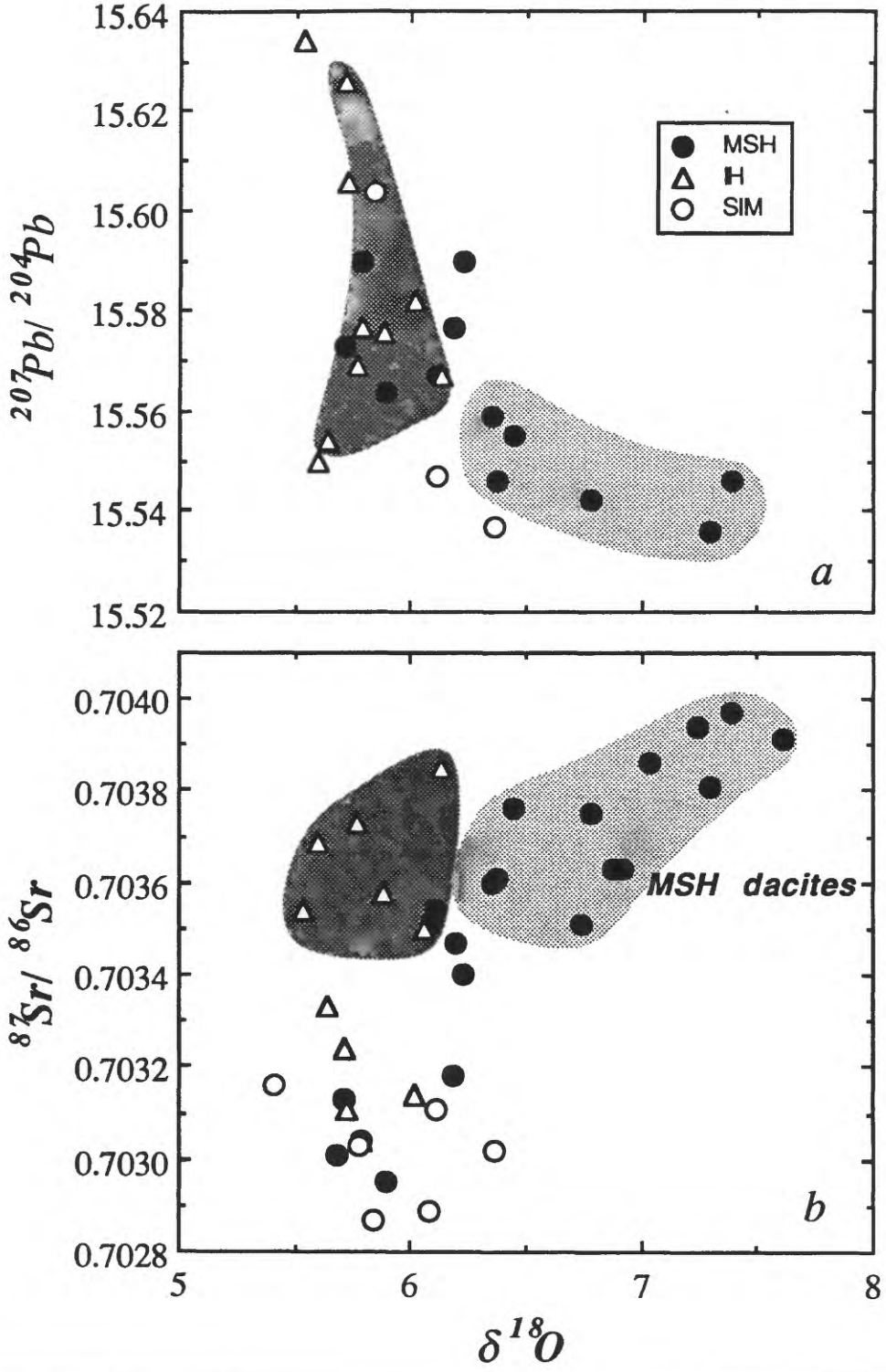

Figure 12. $\delta^{18}O$ versus $^{207}Pb/^{204}Pb$ (a) and $^{87}Sr/^{86}Sr$ (b). MSH dacites (light stippling) and andesites (3 points with $^{87}Sr/^{86}Sr$ between 0.7034-0.7036) display significant correlations between all three isotopic parameters. The basaltic lavas (excluding HFSE-depleted IH lavas; dark stippling) display a weak negative correlation between O and Pb compositions, but neither of these correlate significantly with Sr composition.

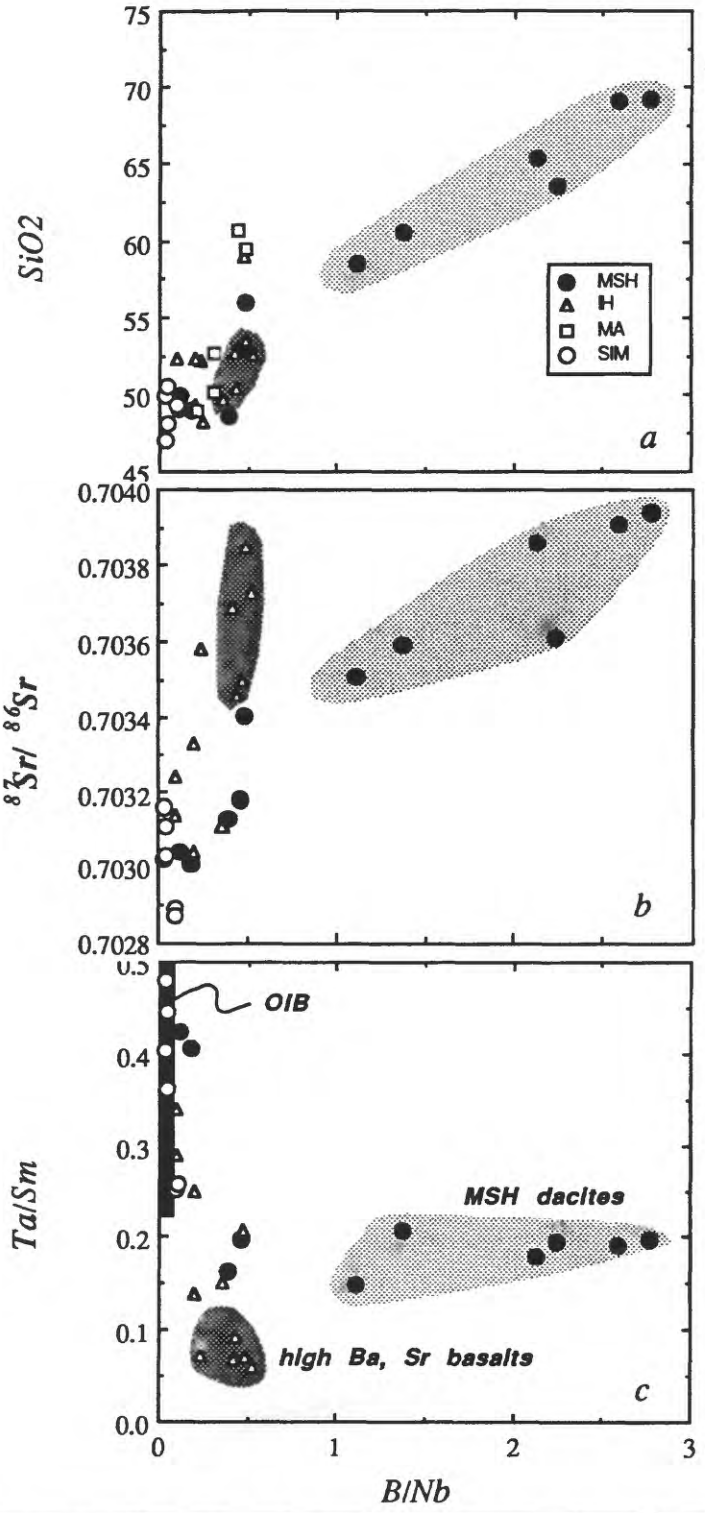

Figure 13. B/Nb vs. SiO_2 (a), $^{87}Sr/^{86}Sr$ (b), and Ta/Sm (c) for **SWC** volcanic rocks. B/Nb ratios in most volcanic arc magmas exceed 0.5, whereas OIBs are characterized by values below 0.1 (Leeman, 1987, in preparation); also, in arc magmas B correlates positively with ^{10}Be, which is a robust indicator of incorporation of subducted oceanic sediments and crust (Morris et al., 1989). The absence of B enrichment in **SWC** basalts suggests that they contain little subducted material.

Some notes on the Neogene structural evolution of the Cascade Range in Oregon

David R. Sherrod and LedaBeth G. Pickthorn
U.S. Geological Survey, Menlo Park, California 94025

INTRODUCTION

Radiometric dating has given us an increasingly precise understanding of the stratigraphic history of the Cascade Range. Few experiments, however, have sought to date particular structural events. The problems are compounded by the paucity of unique, extensive marker beds. Also, luxuriant forest commonly obscures the extent of displacement.

This paper is a preliminary presentation of figures and K-Ar ages useful for interpreting the Neogene (Miocene and younger) structural evolution of the Cascade Range in Oregon. The paper deals mostly with extension in the eastern part of the range, but figure 1 shows the orientation of the stress regime as inferred chiefly from dike orientations, and figures 2, 3, and 4 show some evidence pertinent to the style and timing of middle and late Miocene folding and tilting.

DIKES AND VEINS

Dikes and veins are commonly oriented perpendicular to the extension direction or minimum compressive stress, σ_3 (Anderson, 1951; Nakamura, 1977). Thus, a history of dikes should record the momentary stress field through time (which in the Cascade Range has probably been sequentially rotated; Magill and Cox, 1980). Chiefly steep to vertical dikes and veins are exposed throughout the Western Cascades. Mineralized fracture-filling veins in the Bohemia mining district (fig. 1c; data from Diller, 1900) were emplaced about 22 Ma (Power and others, 1981) and trend WNW-ESE to NW-SE, with σ_3 oriented broadly NNE-SSW. Vein orientations could be misleading if the veins were emplaced by means other than hydraulic fracturing. But the vein orientations are not in conjugate pattern, which might be expected if the veins passively filled preexisting fractures.

Dikes farther east, which are chiefly 17-12 Ma but as young as 4 Ma, trend mainly between WNW-ESE and NNW-SSE (fig. 1b) (Sherrod, 1986). For these dikes, σ_3 was oriented broadly NE-SW. The greater spread of data probably results from the greater age range of rocks sampled.

The contemporary stress regime in the High Cascades has a N-S-oriented σ_1 and an E-W-oriented σ_3 (fig. 1a) (Couch and Lowell, 1971). It is unclear whether the orientation of σ_3 changed abruptly or gradually since Miocene time. Avramenko (1981) showed a strong NW-SE-trend for upper Miocene and lower Pliocene dikes near the boundary of the Western and High Cascades. Therefore, σ_3 was oriented NE-SW as recently as about 4 Ma.

FOLDS

The Columbia River Basalt Group in northern Oregon has been deformed into a series of synclines and asymmetric, locally overturned anticlines, some with reverse faults on their steeper flank (fig. 2). The folding occurred 17-11 Ma, as inferred from the increasingly restricted distribution of the younger parts of the Grande Ronde and Wanapum Basalts to synclinal troughs (Vogt, 1981; Beeson and others, 1985). Presumably the early-erupted lava was folded into synclines and anticlines that funnelled the younger flows along structural lows. Exactly when folding ceased is poorly known. The 12-Ma Pomona member of the Saddle Mountains Basalt is thrust over volcaniclastic rocks in the Columbia River gorge (Anderson, 1980); whereas the 11-9 Ma Last Chance Andesite unit of Priest and others (1982; also dated by Keith and others, 1985) is only slightly faulted and probably not folded. Therefore, the folding of Columbia River Basalt Group and younger rocks in the Cascade Range of northern Oregon had probably culminated by 11 Ma.

Structural relief on the folds is 1 km or less (fig. 2). Folds trend NE-SW on the east side of the range, diminish in amplitude westward, and disappear completely on the west flank of the range, where the Group

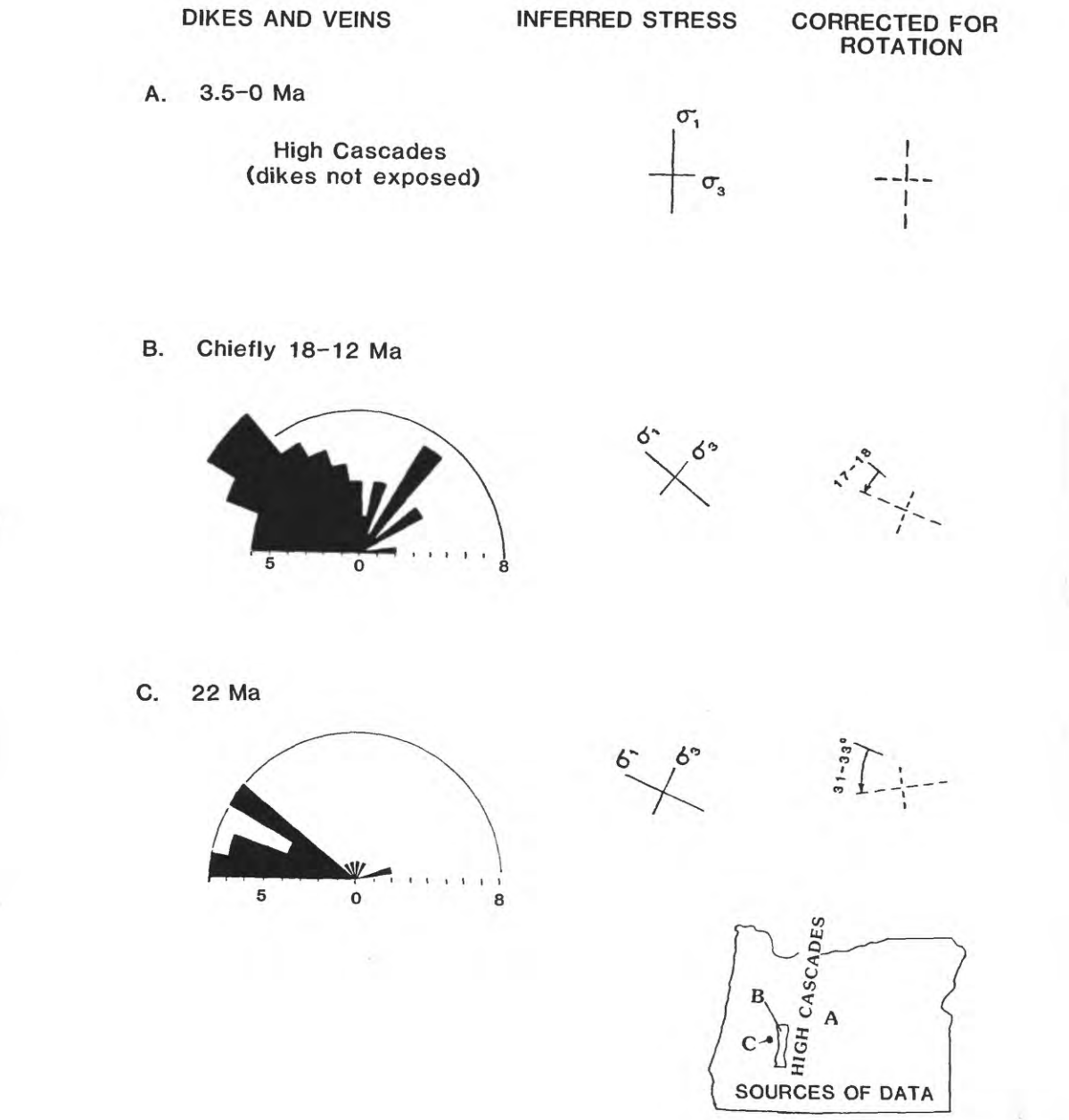

Figure 1. Dike and vein data from Western Cascades, latitudes 43-44°N (after Diller, 1900; Sherrod, 1986). "Inferred stress" shows the orientation of σ_3 and the σ_3-σ_1 plane. "Corrected for rotation" assumes 14-15° clockwise rotation per 10 m.y. There is no paleomagnetic data specific to these particular rocks.

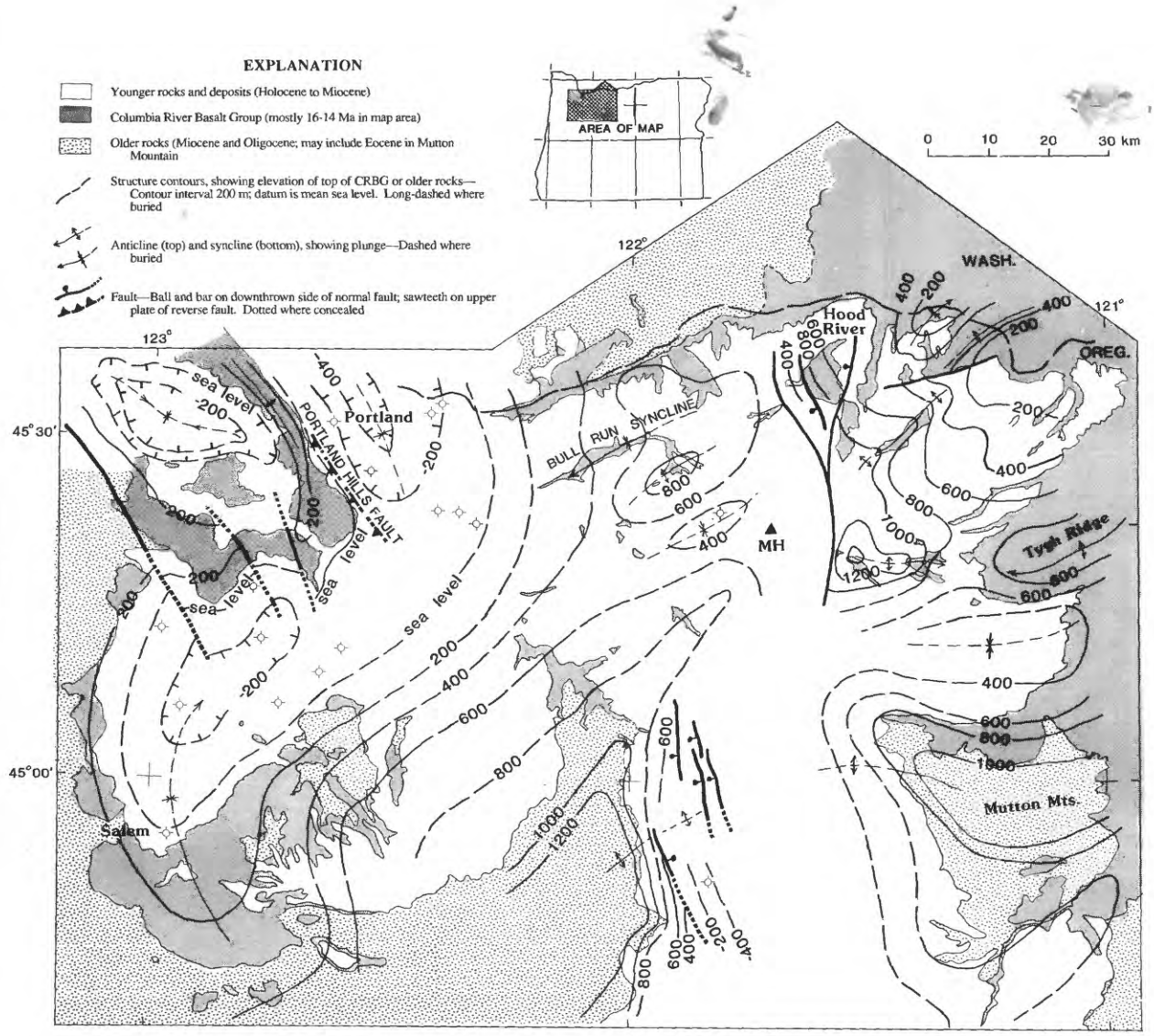

Figure 2. Structure-contour map showing altitude on top of Columbia River Basalt Group or older rocks. Compiled mostly from Sherrod and Smith (1988; see there for sources) but northwest corner unmodified from Hart and Newcomb (1965). "MH" indicates Mount Hood. Structure-contour surface not configured south of there (High Cascades) because information is lacking. Elsewhere, scattered drill holes (circles) and outcrop provide sufficient evidence to infer position of buried surface.

forms a broadly W- or NW-dipping series of flows. The Columbia River Basalt Group dives below sea level in structural downwarps of the Portland basin and central Willamette Valley, which is filled largely by upper Miocene and Pliocene nonmarine silt and coalescing alluvial fans of the Sandy River Mudstone and Troutdale Formation, then re-emerges in NW-trending folds exposed in the northern Coast Range. The area of unfolded, W-dipping basalt on the flank of the Cascade Range probably results from fold interference and warping in a Miocene stress regime that changes orientation across northern Oregon.

The Cascade Range folds in the Columbia River Basalt Group are similar in form and age to folds in the Yakima fold belt of central Washington. Reidel (1984), in calculating fold rates for the Yakima fold belt, showed that 65-70 percent of the 1.4 km of structural relief on the Saddle Mountains uplift was developed between 17 and 13 Ma. The rate of folding in central Washington has diminished dramatically since 13 Ma, but folding probably continues into the Quaternary (Reidel, 1984). This timing fits well with the main growth of folds 17 to 11 Ma in the Cascade Range. However, there is no published evidence that Cascade Range folding in Oregon has continued since 11 Ma. Subsidence in the Portland basin west of the Cascades probably continued during the deposition of the Sandy River Mudstone and Troutdale Formation.

Folding in the Western Cascades dies out by the latitude of Salem, Oreg. South of latitude 44°30'N, strata older than about 7 Ma dip gently eastward, as shown by the map pattern of figure 3. Although a regional series of folds was mapped in the Western Cascades of Oregon by early workers (Thayer, 1936; Peck and others, 1964), only the NNE-trending Breitenbush anticline (about 40 km NW of Mount Jefferson) has been corroborated by subsequent mapping and dating (for example, Hammond and others, 1982; Priest and others, 1987; Walker and Duncan, 1988). The Breitenbush anticline formed between 18 and 12 Ma (Sherrod and Conrey, 1988). Strata in the Western Cascades have been broadly warped throughout the range, however, and the few small local folds (rarely traceable beyond roadcut or outcrop) generally trend northeast (for example, Sherrod, 1986; Priest and others, 1987).

Pi-diagrams for rocks 24-17 and 17-12 Ma (fig. 4) summarize the attitude of strata in the Western Cascades between latitudes 43° and 44° N. Beds are nearly flat-lying; 70-80 percent of the dips range from 0° to 24°. The visual locus of bedding poles suggests that the average tilt of strata is less than 5° east. The scatter on the diagrams results mostly from the initially radial dip of beds around volcanic centers.

The similar pattern for the two age groups of rocks probably indicates that most of the tilt deformation occurred after 12 Ma. This age is not well constrained by K-Ar dating, however. The age of the youngest unit affected by tilting is 12.4 Ma (Verplanck and Duncan, 1987), and unconformably overlying basalt and basaltic andesite lava flows are generally 7-4 Ma (Appendix A in Priest and Vogt, 1983; Verplanck and Duncan, 1987).

The southern Willamette Valley (Salem to Eugene) is not a structural depression but instead is a strike-valley that results from the greater ease of erosion of upper Eocene and Oligocene marine and strandline deposits in the absence of basalt lava and sills that are so abundant near Eugene. There is no stratigraphic evidence for the fault interpreted by Baldwin (1976, his figure 3-1) to bound the east side of the valley. Oil exploration data from several deep wells (Newton, 1969; McKeel, 1985) indicate that Narizian strata (late middle Eocene to late Eocene ages) deepen from about 30 m above sea level near Corvallis (fig. 3) to 820 m below sea level near Lebanon, 20 km east (for example, McKeel's (1985) correlation line 5). Quaternary and any Pliocene(?) deposits are thin.

EXTENSION

Extension-related deformation has formed (1) NW-SE-trending fault zones (younger than 10 Ma) in the Western Cascades, (2) major N-S-trending faults that bound parts of the High Cascades (mostly about 3.5-4.5 Ma), and (3) short to lengthy narrow grabens along the boundary between Basin and Range and Cascade Range (younger than 2 Ma).

NW-SE-trending fault zones

Several pronounced lineaments in the Western Cascades result from stream erosion along NW-SE-trending fault zones. For example, the informally named Clackamas

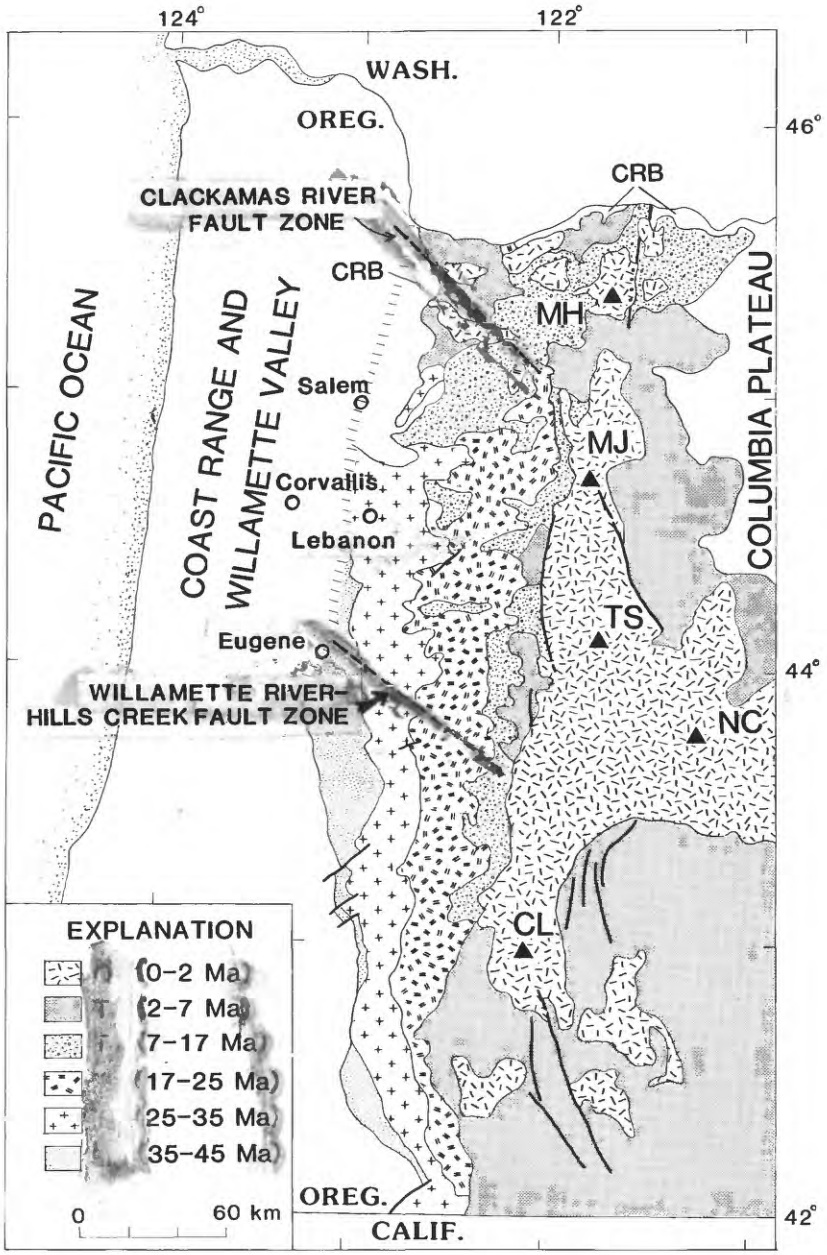

Figure 3. Generalized map showing distribution of Tertiary and Quaternary rocks in Cascade Range (from Sherrod, 1987). Note homoclinal map pattern south of latitude 44°30' N. Unpatterned areas labeled "CRB" within Cascade Range indicate Columbia River Basalt Group. Major faults shown with solid bold lines; Willamette River-Hills Creek and Clackamas River fault zones shown with dashed lines. MH = Mt. Hood; MJ = Mount Jefferson; TS = Three Sisters; NC = Newberry caldera; CL = Crater Lake.

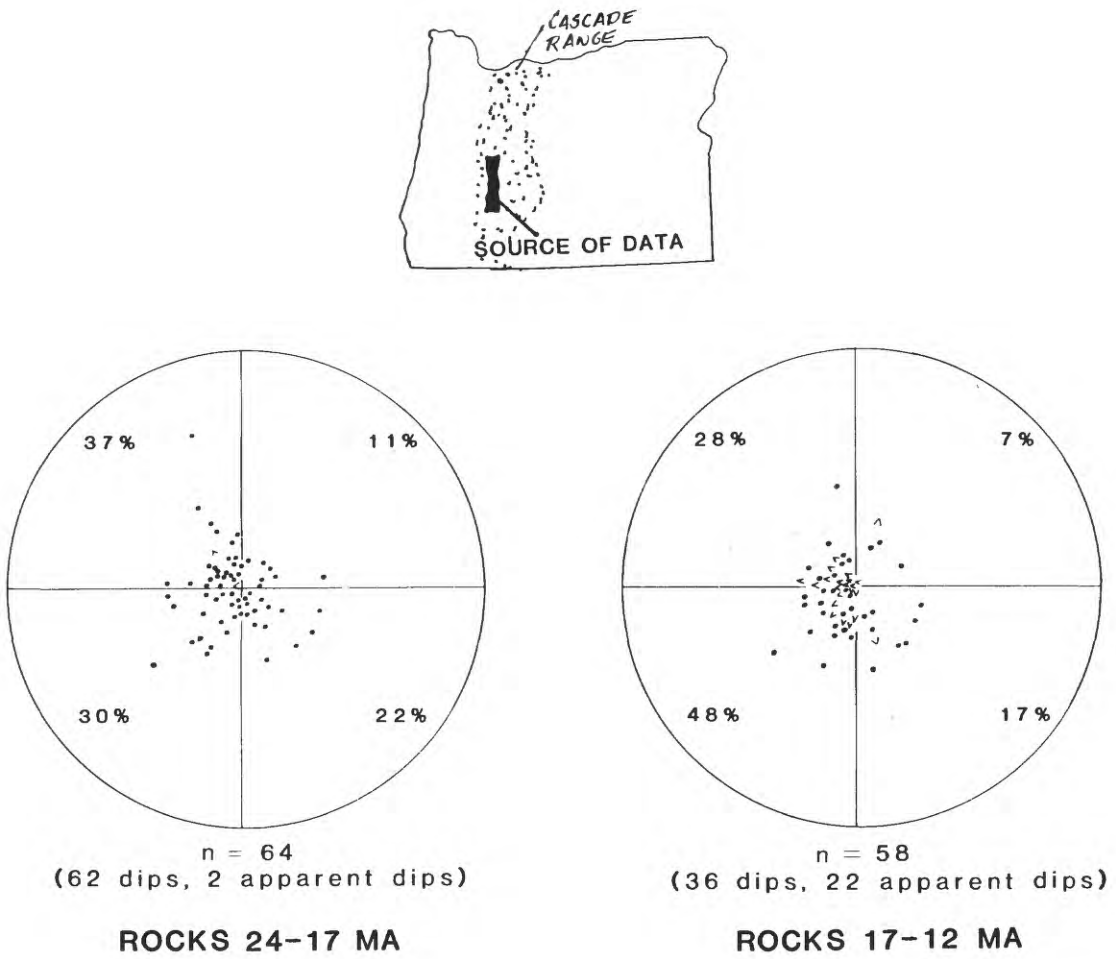

Figure 4. Pi-diagram showing poles to bedding (dots) for rocks 24-17 Ma and 17-12 Ma (Sherrod, 1986). Arrowheads show orientations of lava flow sequences interpreted from apparent-dip data. The similar patterns suggest that the two rock sequences have shared the same overall structural history.

River fault zone (Priest, 1982, his figure 1; see fig. 5) represents several NW-SE-trending vertical or near-vertical faults delineated by Anderson (1978). Those faults have displacements ranging up to 200 m (some chiefly strike-slip and others chiefly dip-slip), on the basis of slickensides and offset strata in the Grande Ronde and Wanapum Basalts of the Columbia River Basalt Group (Anderson, 1978).

The Clackamas River fault zone is younger than the middle Miocene Grande Ronde and Wanapum Basalts and older than Pliocene or lower Pleistocene intracanyon lava. Hammond and others (1982) showed many more faults in this same zone, but they acknowledged that few of their faults juxtapose rock units; many of their "faults" are lineaments along a fracture zone of uncertain origin. To the northwest, the Clackamas River fault zone is aligned with the Portland Hills (fig. 5), a faulted NW-SE-trending asymmetric anticline of Columbia River Basalt Group lava (Beeson and others, 1985); to the southeast (east of Cascade Range), the fault zone aligns with two stream segments and eventually with the Brothers fault zone (fig. 5) (Smith, 1986; Sherrod and Conrey, 1988). The deformation along the Clackamas River fault zone probably occurs along NW-SE-trending shear zone related to Basin-Range extension east of the Cascade Range, as first suggested by Lawrence (1976), although the faults in the Cascade Range have far less strike separation than he suggested.

A similar zone of deformation was postulated by Lawrence (1976) to explain the lineament of the Middle Fork of Willamette River and its tributary Hills Creek (part of his "Eugene-Denio zone"); see figure 3. In the Cascade Range this fault zone (here termed the Willamette River-Hills Creek fault zone) comprises numerous slickensided fracture planes in chiefly Oligocene and Miocene volcanic rocks. There is no discernible offset in units ranging from 22 to 17 Ma (Woller and Priest, 1983; Sherrod, 1986), although as much as 1.5 km of strike-separation could go unrecognized amongst the gentle 5°-eastward dip of Miocene and older strata and thick forest cover of the Western Cascades. There is no displacement of gravity or magnetic anomalies transverse to the fault zone (Pitts and Couch, 1978; Couch and others, 1978). Thus, the Willamette River-Hills Creek fault zone is similar to the Clackamas River fault zone by virtue of its small cumulative offset and NW-SE orientation.

The age of faulting along Willamette River-Hills Creek is poorly constrained but is pre-Quaternary, because Hills Creek was well incised along its present NW-SE trend when 1.98-Ma intracanyon lava filled the drainage (Woller and Black, 1983; Sherrod, 1986). A physiographic lineament may have existed as early as 3.3 Ma, when the now topographically inverted basalt that caps Kitson Ridge was emplaced along a northwest-trending stream course (Sherrod, 1986).

Lawrence (1976) considered the "Eugene-Denio zone" to represent a major fault zone with 10-20 km of right-lateral separation in Quaternary time. That interpretation assumed flexure and offset of the trace of his "High Cascade volcanic trend", which subsequent work has proven to be an arbitrary line connecting normally and reversely polarized Quaternary volcanoes that range widely in age (Sherrod, 1986; N.S. MacLeod and D.R. Sherrod, *in* Sherrod and Smith, 1989).

Major N-S-trending faults

High-angle normal faults with as much as 600 m offset occur sporadically along the west and east sides of the High Cascades in Oregon (fig. 5 for north half of Oregon). Allen (1966) first suggested that (throughout Oregon) these faults bound the High Cascades, which Taylor (1981) described as "Pleistocene fill in a Pliocene graben". Smith and Taylor (1983) summarized the history of the High Cascades graben in the Santiam Pass area of central Oregon (west of Green Ridge on fig. 5), an area where there is good geologic evidence and topographic expression of bounding faults on both sides of the High Cascades. There is no evidence, however, that the High Cascades are fault-bounded throughout the length of Oregon.

Hood River fault. The Hood River fault (Hodge, 1938; see fig. 5) is a NNW-trending narrow fault zone 1 to 3 km wide formed by an *en echelon* succession of normal faults (Swanson and others, 1981; Bela, 1982). The faults have chiefly normal separation (down on west) but some planes show right-lateral slip inferred from slickensides (Timm, 1979). According to Timm (1979), the lower Hood River valley is not a graben. Some would call it a half-graben, as it is bounded on the west by

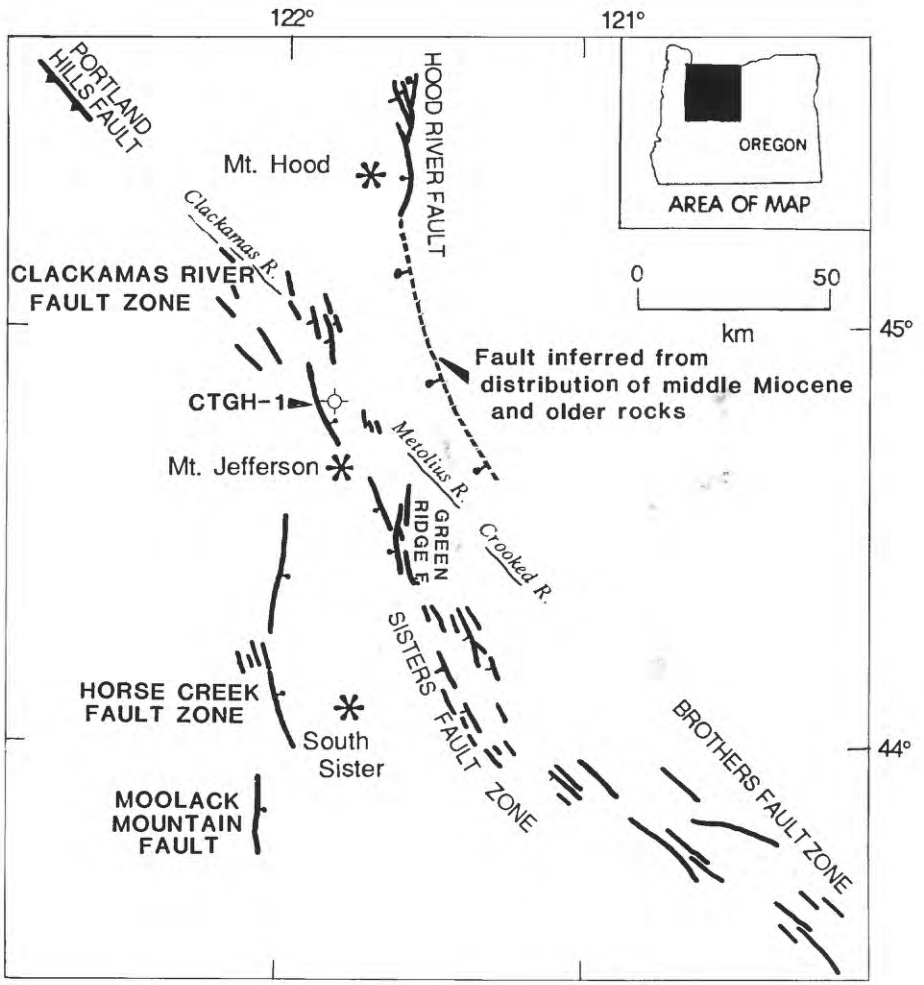

Figure 5. Fault map for Cascade Range in northern Oregon. Ball-and-bar indicates downthrown side and displacement more than 300 m; tick indicates downthrown side and displacement less than 300 m. River lineaments (thin lines) labeled in italics; stars indicate stratovolcanoes; circle is 1.4-km-deep CTGH-1 drill hole. Figure modified from Sherrod and Conrey (1988) and compiled from Sherrod and Smith (1988).

gently east-dipping strata in the lower part of the Columbia River Basalt Group and on the east by the Hood River fault. There is no evidence for thick fill beneath the Hood River valley, however, unlike highly extended half-grabens that may be filled by several kilometers of sediment or volcanic rocks.

Offset on the Hood River fault near Mount Hood is 300 to 600 m on the basis of map units that Wise (1969) correlated across the Hood River valley. Inasmuch as these units are incompletely dated and correlated, offset locally could be in excess of 600 m.

The escarpment produced by the Hood River fault existed by about 2.7 Ma, when andesite (dated by Keith and others, 1985) flowed west down the escarpment and north along the ancestral Hood River drainage (D.R. Sherrod, unpub. mapping, 1985). The only constraint on earliest offset requires the fault to be younger than about 12 Ma, because the Columbia River Basalt Group does not thicken across the fault. The Hood River fault presumably formed between 3 and 5 Ma, during a time when large faults developed elsewhere along the margins of the High Cascades.

The Hood River fault is enigmatic southeast of Mount Hood. It may be buried by upper Miocene and Pliocene volcanic rocks west of the Mutton Mountains, however, as suggested by the distribution of the Columbia River Basalt Group and older rocks (fig. 2 and fig. 5). Alternatively, the apparent structural disruption of Columbia River Basalt Group and older rocks at the eastern margin of the High Cascades in northern Oregon could have occurred before 3-5 Ma.

Extension along the boundary between High Cascades and Basin and Range

Grabens mark a large part of the boundary between High Cascades and Basin and Range. The grabens range from 5 to 20 km wide and have structural relief ranging from less than 0.5 km to more than 1 km. The few K-Ar ages from lava flows suggest the offset is largely of Quaternary age. From north to south they are the La Pine, Chemult, and Klamath grabens. Figure 6 shows the La Pine valley and a line of cross section across the La Pine graben; figure 7 shows the cross section.

La Pine graben. The La Pine graben is situated between Newberry volcano and the axis of the High Cascades in central Oregon (fig. 6). It consists of two buried grabens separated by a NNE-trending horst of Pliocene and Pleistocene lava (fig. 7), including a rhyolite dome at Eaton Butte (K-Ar plagioclase age 3.68±3.3 Ma; Fiebelkorn and others, 1983) and overlying faulted basaltic andesite shield of Gilchrist Butte (K-Ar whole rock age 0.61±0.05; table 1). Structural relief is about 600-800 m, on the basis of water wells that penetrated 400 m of alluvium before hitting bedrock lava flows (Couch and Foote, 1985), and topographic relief that ranges from 200 to 400 m (top of horst to stream floors).

The age of the La Pine graben is difficult to interpret. Some faulting is clearly younger than the 0.61-Ma shield of Gilchrist Butte, but Gilchrist could be surmounting a previously faulted block. Couch and Foote (1985), in concluding that the basin is younger than 0.73 Ma, relied on a shaky conclusion that areas of net negative magnetization on aeromagnetic anomaly maps correspond to reversely polarized volcanic rocks, and therefore that the grabens are floored by reversely polarized lava (older than 0.73 Ma).

Chemult graben. The Chemult graben is named for the town of Chemult, west of the Walker Rim escarpment (fig. 6, 8). The Chemult graben is about 10 km wide and has topographic and structural relief of about 450 m. The floor of the graben is a series of exposed bedrock horsts that have been surrounded and blanketed by Holocene pyroclastic deposits from Mount Mazama (N.S. MacLeod, *in* Sherrod and Smith, 1989). There is no gravity anomaly associated with the graben (Pitts and Couch, 1978). Faulting is younger than lava flows along Walker Rim (K-Ar whole rock age 2.33±0.09 Ma, table 1); rocks on the downthrown side near Chemult range in age from 2.52±0.96 to 0.88±0.03 Ma (table 1).

Extensional strain of about 5-10 percent is indicated for the Chemult and La Pine grabens, on the basis of the cross sections in figures 7 and 8. These estimates assume fault angles of 60°, characteristic of many faults exposed in the Basin and Range east of the Cascade Range (D.R. Sherrod, unpublished mapping, 1985).

Klamath graben. The 20-km-wide Klamath graben, which has 1-2 km of structural relief, is by far the largest of the grabens along the east side of the Cascades in Oregon (fig. 9). It is a composite graben now

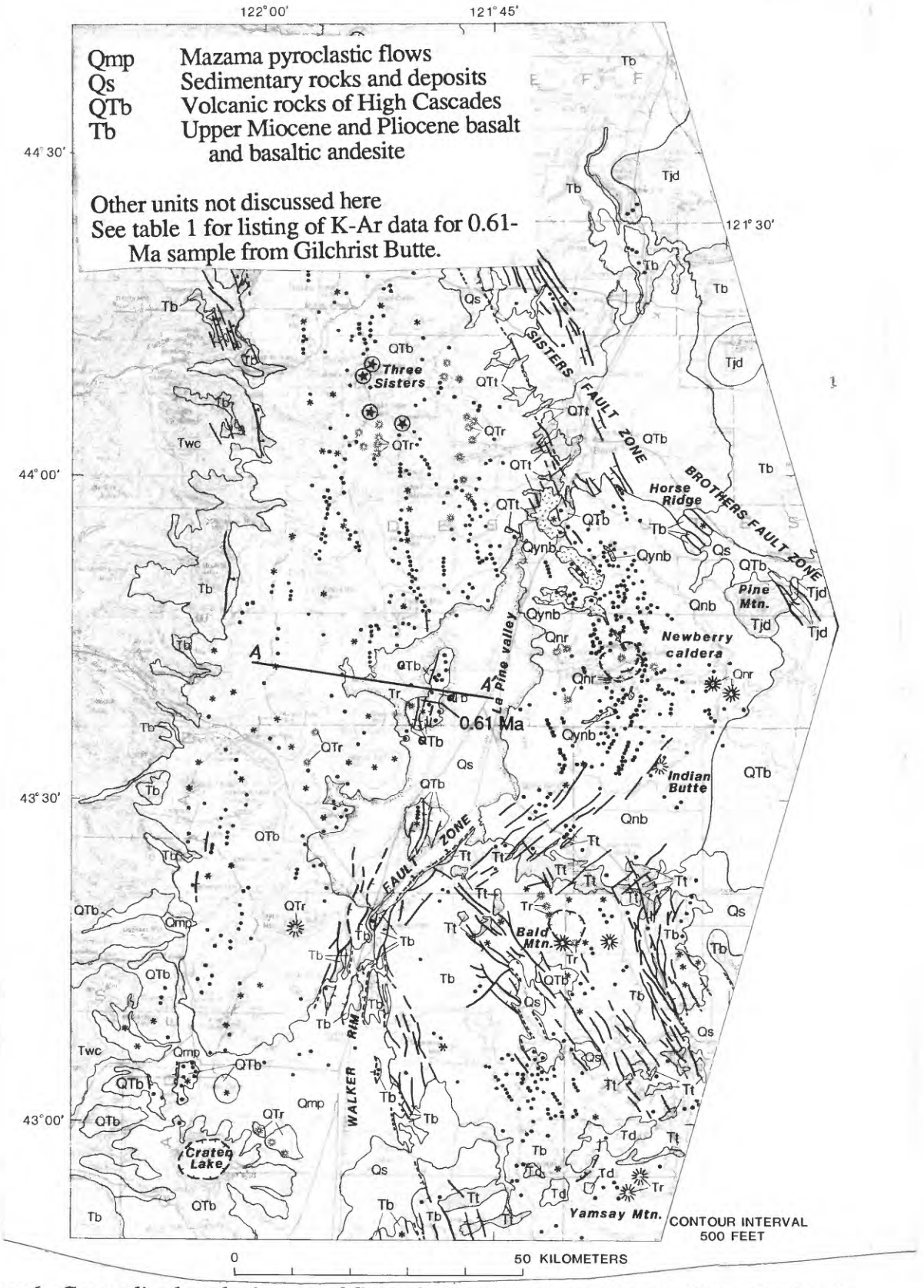

Figure 6. Generalized geologic map of Cascade Range in central Oregon (from MacLeod and Sherrod, 1988; see there for sources). Line A-A' locates cross section of figure 7.

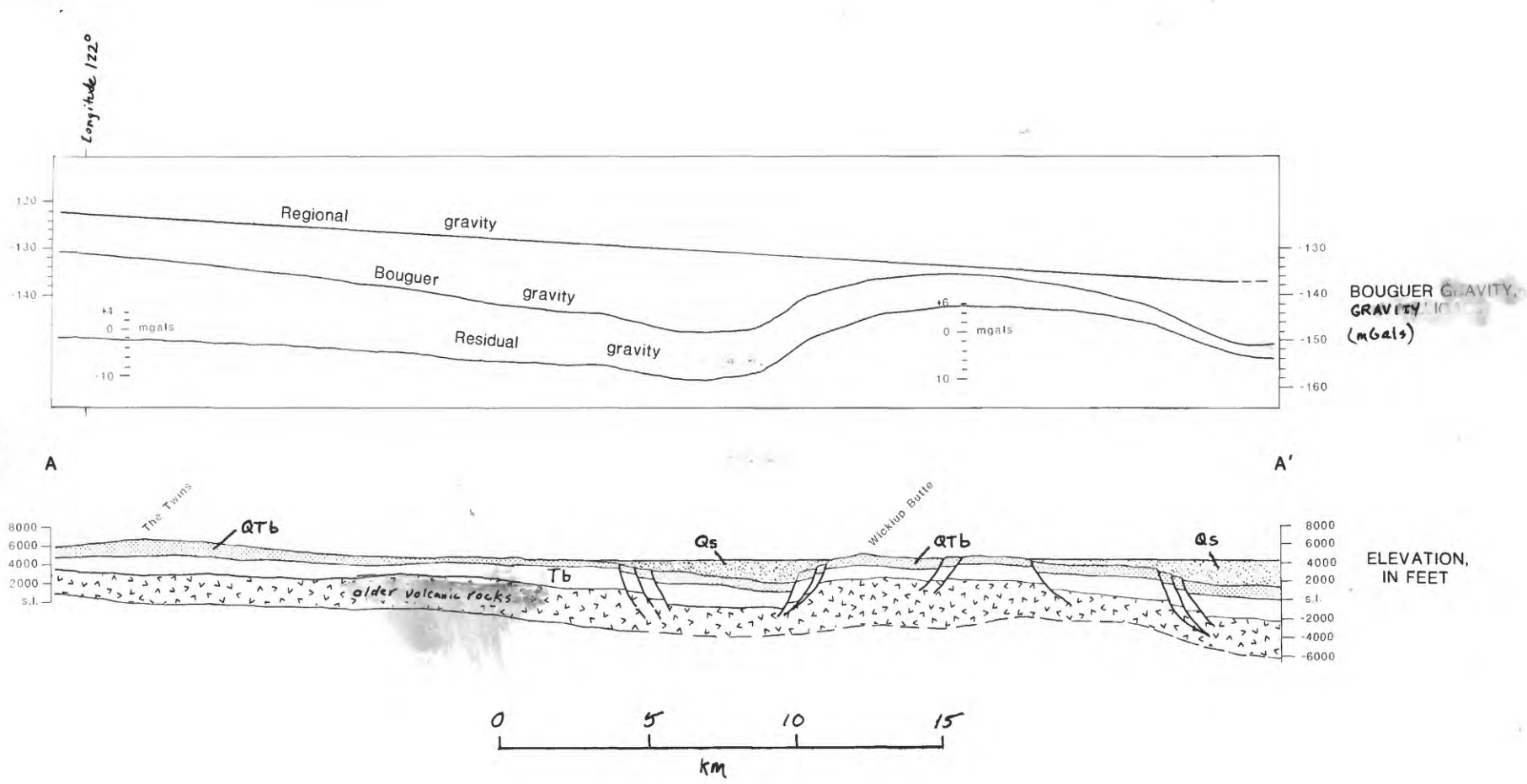

Figure 7. Cross section from La Pine to crest of High Cascades (summit of The Twins), from Sherrod (1986). Regional gravity profile drawn from Thiruvathakal and others (1970); Bouguer gravity profile drawn from Pitts and Couch (1978); residual gravity solved graphically. Geologic units same as figure 6.

Sample number	Location Latitude (N)	Location Longitude (W)	Locality	Rock type	Material dated	K_2O (wt %)[1]	$^{40}Ar_{rad}$ (10^{-11} moles/g)	Percent $^{40}Ar_{rad}$	Calculated age (Ma) [2]	Assigned age (Ma) [2]	Reference
S81-57	43°09.5'	122°04.0'	Mt. Thielsen	Basaltic andesite	Whole rock	(0.926) 0.918 0.933	 0.03824 0.03902	 1.7 1.8	 0.29 0.29	0.29±0.10	Sherrod, 1986
S82-73	43°16.0'	122°01.5'	Mule Mtn.	Dacite	Whole rock	(1.846) 1.839 1.852	0.1695	12		0.64±0.04	Sherrod, 1986
S86-21	43°38.75'	121°39.15'	Gilchrist Butte	Basaltic andesite	Whole rock	(1.045) 1.040 1.031 1.060 1.048	 0.08632 0.09645	 3.77 6.02	 0.574 0.641	0.61±0.05	This paper[3]
S86-22	43°19.35'	121°48.95'	NW of Chemult	Basaltic andesite	Whole rock	(1.737) 1.726 1.723 1.744 1.756	 0.2186 0.2242	 14.9 26.7	 0.874 0.896	0.88±0.03	This paper[3]
S86-23	43°16.20'	121°44.05'	Walker Rim	Andesite	Whole rock	(1.420) 1.404 1.403 1.449 1.423	 0.4912 0.4641	 60.3 50.6	 2.40 2.27	2.33±0.09	This paper[3]
M4-127	43°19.2'	121°53.3'	Burn Butte	Rhyolite	Plagioclase	0.385	0.1395	4.6		2.52±0.96	Fiebelkorn and others, 1983
S5-1	42°23.8'	121°48.6'	Rim east of U. Klamath Lake	Basalt	Whole rock	(2.233) 2.231 2.230 2.244 2.228	 0.8855 0.9133	 40.8 32.8	 2.75 2.84	2.79±0.08	This paper[3]
S5-12	42°12.6'	121°47.2'	Klamath Falls	Basalt	Plagioclase	(0.213) 0.208 0.217	 0.1472 0.1369	 7.14 14.1	 4.8 4.5	4.6±0.3	This paper[3]

Notes:

[1]For multiple determinations, value in parentheses is arithmetic mean used in age calculation.

[2]K-Ar ages were calculated using the constants for the radioactive decay and abundance of ^{40}K recommended by the International Union of Geological Sciences Subcommission on Geochronology (Steiger and Jager, 1977). These constants are: $\lambda_\varepsilon = 0.580 \times 10^{-10} yr^{-1}$, $\lambda_\beta = 4.962 \times 10^{-10} yr^{-1}$, and $^{40}K/K_{total} = 1.167 \times 10^{-4}$ mol/mol.

[3]Sample preparation and analytical work were done at U.S. Geological Survey.

Table 1. K-Ar ages from border of High Cascades with Basin and Range, Oregon.

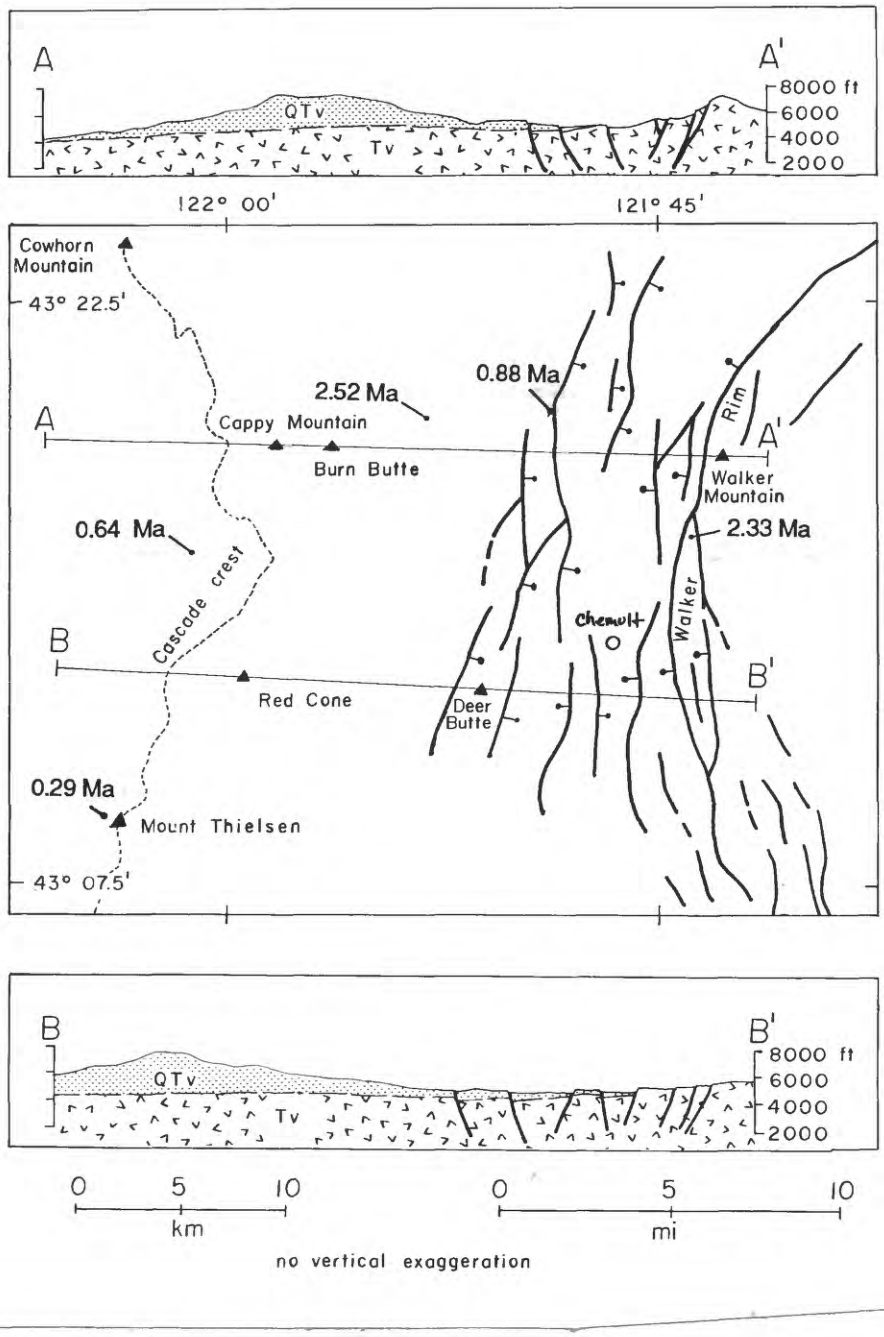

Figure 8. Generalized structure map and cross sections of Chemult graben, from Sherrod (1986). QTv, upper Pliocene to Holocene volcanic rocks; Tv, older rocks. See table 1 for listing of K-Ar ages.

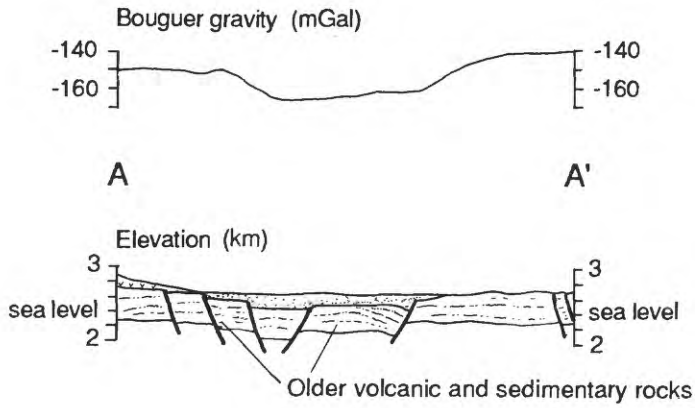

EXPLANATION OF MAP AND CROSS SECTION

- Pyroclastic flows from Mount Mazama (Holocene)
- Younger sedimentary rocks and deposits (Holocene and Pleistocene)
- Younger volcanic rocks (Holocene and Pleistocene)
- Older sedimentary rocks (Pliocene and upper Miocene)
- Older volcanic rocks (Pliocene and upper Miocene)

  Note: older sedimentary and volcanic rocks shown combined on cross section
- Contact
- Fault, dashed where inferred, dotted where concealed. Ball and bar on downthrown side where offset greater than 100 m. Tick on downthrown side where offset less than 100 m
- Caldera margin at Crater Lake
- FK — FK, Fort Klamath; KF, Klamath Falls
- 4.6 Ma — Age of isotopically dated rocks (see table 1)

(Geologic map on next page)

Figure 9. Geologic map and cross section of the Klamath graben, south-central Oregon. Geology generalized from Sherrod and Smith, 1989 (see there for sources); Bouguer gravity on cross section from Couch and others, 1981.

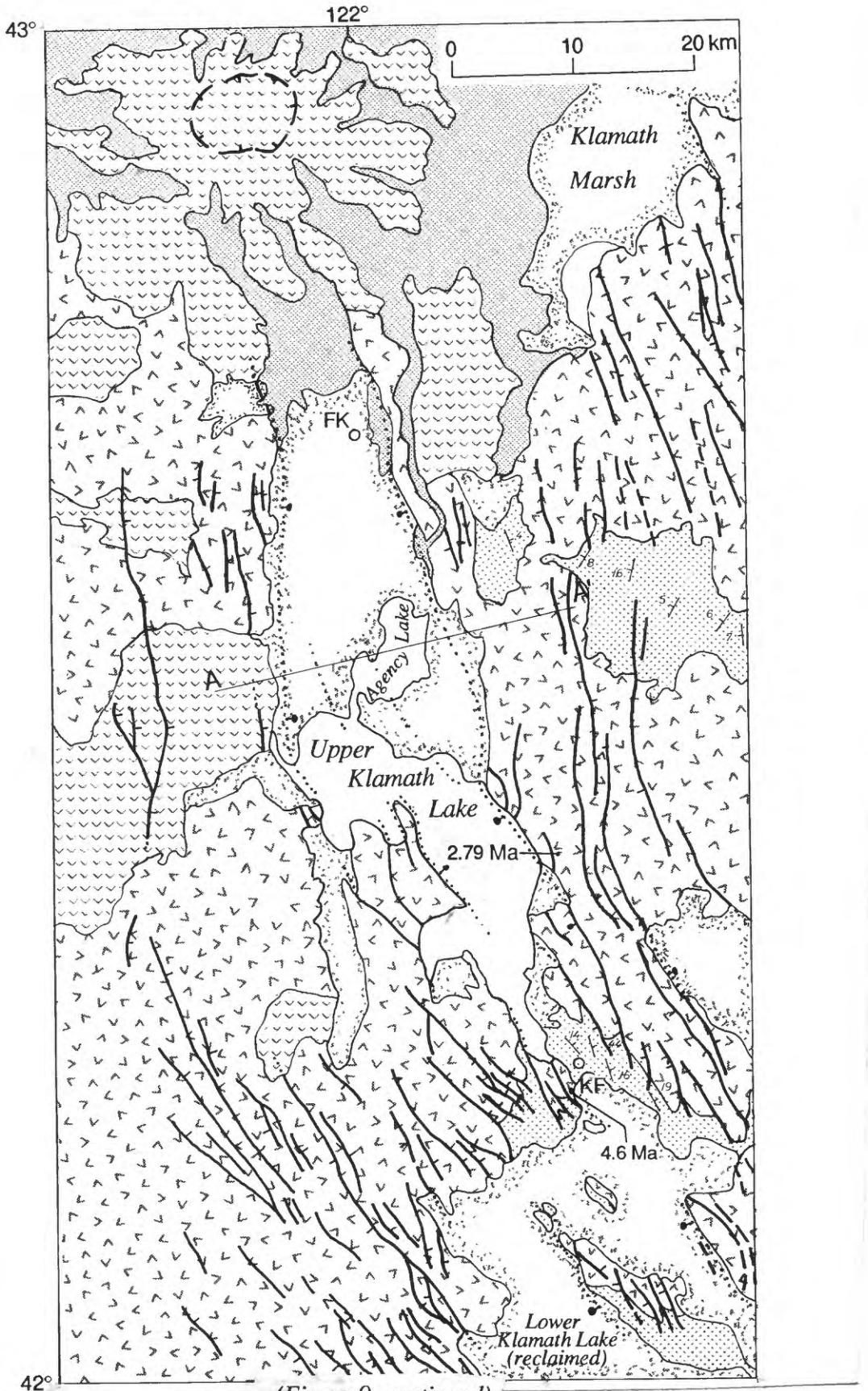

(Figure 9, continued)

largely filled by Quaternary fluvio-lacustrine deposits. At Klamath Falls the depression shoals and the Quaternary fill laps against pre-graben upper Miocene and lower Pliocene bedrock of interbedded lava flows and sedimentary rocks. A dated basalt lava flow in a highway roadcut at Klamath Falls has a K-Ar plagioclase age of 4.6±0.3 Ma (table 1).

South of Klamath Falls, the basin of Lower Klamath Lake (drained for agriculture) coincides with a depression of 20 mGals relief on the Bouguer gravity anomaly map, indicating that the sedimentary fill may be as thick as 2 km (calculated using density contrast of 0.4 gm-cm^{-3} by Sammel and Peterson, 1976). North of Klamath Falls, the basin of Upper Klamath and Agency Lakes extends northward toward Crater Lake in the Cascade Range. The eastern escarpment of the Upper Klamath basin has 450 m of structural and topographic relief. Topographic relief diminishes to the north but the gravity data indicate 0.4-1.2 km of structural relief (density contrast ranging from 1.0 to 0.3 gm-cm^{-3}; Veen, 1982) (cross section on fig. 9). The faulting in the Upper Klamath basin is younger than basalt lava at the top of the eastern escarpment of Upper Klamath Lake that has a K-Ar whole rock age of 2.79±0.08 Ma (table 1). Offset talus deposits in the central and southern Klamath graben (D.R. Sherrod, unpublished mapping, 1985), the absence of alluvial fans adjacent to high, steep escarpments in the Klamath graben, and linear troughs in the bathymetry of 3-4-m deep Upper Klamath Lake indicate that faulting has continued into Holocene time.

ACKNOWLEDGMENTS

We wish to acknowledge Ray E. Wells for his review of this manuscript.

REFERENCES CITED

Allen, J.E., 1966, The Cascade Range volcano-tectonic depression of Oregon, *in* Lunar Geologic Field Conference Transactions: Oregon Department of Geology and Mineral Industries, p. 21-23

Anderson, E.M., 1951, *The dynamics of faulting and dyke formation with application to Britain.* London: Oliver and Boyd, 2nd ed., 206 p.

Anderson, J.L., 1978, The structure and stratigraphy of the Columbia River Basalt in the Clackamas River drainage: Portland, Oreg., Portland State University master's thesis, 136 p.

———1980, Pomona Member of the Columbia River Basalt Group: an intracanyon flow in the Columbia River Gorge, Oregon: Oregon Geology, v. 42, no. 12, p. 195-199.

Avramenko, Walter, 1981, Volcanism and structure in the vicinity of Echo Mountain, central Oregon Cascade Range: Eugene, Oreg., University of Oregon, M.S. thesis, 156 p.

Baldwin, E.M., 1976, *Geology of Oregon*: Dubuque, Iowa, Kendall/Hunt Publishing Co., revised ed., 147 p.

Beeson, M.H., Fecht, K.R., Reidel, S.P., and Tolan, T.L., 1985, Regional correlations within the Frenchman Springs member of the Columbia River Basalt Group: new insights into the middle Miocene tectonics of northwest Oregon: Oregon Geology, v. 47, no. 8, p. 87-96.

Bela, J.L., 1982, Geologic and neotectonic evaluation of north-central Oregon: The Dalles 1°x2° quadrangle: Oregon Department of Geology and Mineral Industries Geological Map Series GMS-27, scale 1:250,000.

Couch, R., and Foote, R., 1985, The Shukash and La Pine basins: Pleistocene depressions in the Cascade Range of central Oregon: Eos (American Geophysical Union, Transactions), v. 66, no. 3, p. 24.

Couch, R.W., Gemperle, M, and Connard, G.G., 1978, Total field aeromagnetic anomaly map, Cascade Mountain Range, central Oregon: Oregon Department of Geology and Mineral Industries Geologic Map Series GMS-9, scale 1:125,000.

Couch, R.W., and Lowell, R.P., 1971, Earthquakes and seismic energy release in Oregon: Ore Bin, v. 33, p. 61-84.

Couch, R.W., Pitts, G.S., Veen, C.A., and Gemperle, M., 1981, Free-air gravity anomaly map and complete Bouguer gravity anomaly map, Cascade Mountain Range, southern Oregon: Oregon Department of Geology and Mineral Industries Geologic Map Series GMS-16, scale 1:250,000.

Diller, J.S., 1900, The Bohemia mining region of western Oregon, with notes on the Blue River mining region and on the structure and age of the Cascade Range: U.S. Geological Survey 20th Annual Report, part 3, p. 1-36.

Fiebelkorn, R.B., Walker, G.W., MacLeod, N.S., McKee, E.H., and Smith, J.G., 1983, Index to K-Ar age determinations for the state of Oregon: Isochron/West, no. 37, p. 3-60.

Hammond, P.E., Geyer, K.M., and Anderson, J.L., 1982, Preliminary geologic map and cross-sections of the upper Clackamas and North Santiam Rivers area, northern Oregon Cascade Range: Portland, Oreg., Portland State University Department of Earth Sciences, scale 1:62,500.

Hart, D.H., and Newcomb, R.C., 1965, Geology and ground water of the Tualatin Valley, Oregon: U.S. Geological Survey Water-Supply Paper 1697, 172 p.

Hodge, E.T. 1938, Geology of the lower Columbia River: Geological Society of America Bulletin, v. 49, no. 6, p. 831-930.

Keith, T.E.C., Donnelly-Nolan, J.M., Markman, J.L., and Beeson, M.H., 1985, K-Ar ages of rocks in the Mount Hood area, Oregon: Isochron/West, no. 42, p. 12-16.

Lawrence, R.D., 1976, Strike-slip faulting terminates the Basin and Range province in Oregon: Geological Society of America Bulletin, v. 87, p. 846-850.

MacLeod, N.S., and Sherrod, D.R., 1988, Geologic evidence for a magma chamber beneath Newberry volcano, Oregon: Journal of Geophysical Research, v. 93, no. B9, p. 10,067-10,079.

Magill, J.R., and Cox, Allan, 1980, Tectonic rotation of the Oregon Western Cascades: Oregon Department of Geology and Mineral Industries Special Paper 10, 67 p.

McKeel, D.R., 1985, Biostratigraphy of exploratory wells, southern Willamette Basin, Oregon: Oregon Department of Geology and Mineral Industries Oil and Gas Investigation 13, 17 p.

Nakamura, K., 1977, Volcanoes as possible indicators of tectonic stress orientations: principles and proposal: Journal of Volcanology and Geothermal Research, v. 2, p. 1-16.

Newton, V.C., Jr., 1969, Subsurface geology of the lower Columbia and Willamette basins: Oregon Department of Geology and Mineral Industries Oil and Gas Investigations, no. 2, 121 p.

Peck, D.L., Griggs, A.B., Schlicker, H.G., Wells, F.G., and Dole, H.M., 1964, Geology of the central and northern parts of the Western Cascade Range in Oregon: U.S. Geological Survey Professional Paper 449, 56 p.

Pitts, G.S., and Couch, R.W., 1978, Complete Bouguer gravity anomaly map, Cascade Mountain Range, central Oregon: Oregon Department of Geology and Mineral Industries Geologic Map Series GMS-8, scale 1:125,000.

Power, S.G., Field, C.W., Armstrong, R.L., Harakal, J.E., 1981, K-Ar ages of plutonism and mineralization, Western Cascades, Oregon and southern Washington: Isochron/West, no. 31, p. 27-29.

Priest, G.R., 1982, Overview of the geology and geothermal resources of the Mount Hood area, Oregon, *in* Priest, G.R., and Vogt, B.F., eds., Geology and geothermal resources of the Mount Hood area, Oregon: Oregon Department of Geology and Mineral Industries Special Paper 14, p. 6-15.

Priest, G.R., Beeson, M.H., Gannett, M.W., and Berri, D.A., 1982, Geology, geochemistry, and geothermal resources of the Old Maid Flat area, Oregon, *in* Priest, G.R. and Vogt, B.F., eds., Geology and geothermal resources of the Mount Hood area, Oregon: Oregon Department of Geology and Mineral Industries Special Paper 14, p. 16-30.

Priest, G.R., and Vogt, B.F., eds., 1983, Geology and geothermal resources of the Mount Hood area, Oregon: Oregon Department of Geology and Mineral Industries Special Paper 14, 100 p.

Priest, G.R., Woller, N.M., and Ferns, M.L., 1987, Geologic map of the Breitenbush River area, Linn and Marion Counties, Oregon: Oregon Department of Geology and Mineral Industries Geological Map Series GMS-46, scale 1:62,500.

Reidel, S.P., 1984, The Saddle Mountains: The evolution of an anticline in the Yakima Fold Belt: American Journal of Science, v. 284, p. 942-978.

Sammel, E.A., and Peterson, D.L., 1976, Hydrologic reconnaissance of the geothermal area near Klamath Falls, Oregon, with a section on preliminary interpretation of geophysical data: U.S. Geological Survey Water Resources Investigation Open-File Report WRI 76-127, 129 p.

Sherrod, D.R., 1986, Geology, petrology, and volcanic history of a portion of the Cascade Range between latitudes 43°-44° N, central Oregon, U.S.A.: Santa Barbara, University of California doctoral dissertation, 320 p.

———1987, New compilation map of the Cascade Range in Oregon: Geothermal Resources Council Transactions, v. 11, p. 305-307.

Sherrod, D.R., and Conrey, R.M., 1988, Geologic setting of the Breitenbush-Austin Hot Springs area, Cascade Range, north-central Oregon, *in* Sherrod, D.R., ed., Geology and geothermal resources of the Breitenbush-Austin Hot Springs area, Clackamas and Marion Counties, Oregon: Oregon Department of Geology and Mineral Industries Open-File Report O-88-5, p. 1-14.

Sherrod, D.R., and Smith, J.G. 1989, Preliminary map of upper Eocene to Holocene volcanic and related rocks of the Cascade Range, Oregon: U.S. Geological Survey Open-File Report 89-14, scale 1:500,000.

Smith, G.A., 1986, Stratigraphy, sedimentology, and petrology of Neogene rocks in the Deschutes basin, central Oregon: A record of continental-margin volcanism and its influence on fluvial sedimentation in an arc-adjacent basin: Richland, Washington, Rockwell Hanford Operations Publication RHO-BW-SA-555 P, variously paged.

Smith, G.A. and Taylor, E.M., 1983, The central Oregon High Cascade graben: What? Where?

When?: Geothermal Resources Council Transactions, v. 7, p. 275-279.
Steiger, R.H., and Jager, E., 1977, Subcommission on geochronology: Convention on the use of decay constants in geo- and cosmochronology: Earth and Planetary Science Letters, v. 36, p. 359-362.
Swanson, D.A., Anderson, J.L., Camp, V.E., Hooper, P.R., Taubeneck, W.H., and Wright, T.L., 1981, Reconnaissance geologic map of the Columbia River Basalt Group, northern Oregon and western Idaho: U.S. Geological Survey Open-File Report 81-797, scale 1:250,000.
Taylor, E.M., 1981, Central High Cascade roadside geology, *in* Johnston, D.A., and Donnelly-Nolan, J.M., eds., Guides to some volcanic terranes in Washington, Idaho, Oregon, and northern California: U.S. Geological Survey Circular 838, p. 55-58.
Thayer, T.P., 1936, Structure of the North Santiam River section of the Cascade Mountains in Oregon: Journal of Geology, v. 44, p. 701-716.
Thiruvathakal, J.V., Berg, J.W., and Heinrichs, D.F., 1970, Regional gravity of Oregon: Geological Society of America Bulletin, v. 81, p. 725-738.
Timm, Susan, 1979, The structure and stratigraphy of Columbia River Basalt in the Hood River valley: Portland, Oreg., Portland State University, M.S. thesis, 56 p.
Veen, C.A., 1982, Gravity anomalies and their structural implications for the southern Oregon Cascade Mountains and adjoining Basin and Range province: Corvallis, Oregon State University, Master's thesis, 86 p.
Verplanck, E.P., and Duncan, R.A., 1987, Temporal variations in plate convergence and eruption rates in the central western Cascades, Oregon: Tectonics, v, 6, no. 2, p. 197-209.
Vogt, B.F., 1981, The stratigraphy and structure of the Columbia River Basalt Group in the Bull Run watershed, Multnomah and Clackamas Counties, Oregon: Portland, Oreg., Portland State University, M.S. thesis, 151 p.
Walker, G.W., and Duncan, R.A., 1988, Geologic map of the Salem 1°x2° sheet, Oregon: U.S. Geological Survey Miscellaneous Investigations Map I-1893, scale 1:250,000.
Wise, W.S., 1969, Geology and petrology of the Mt. Hood area: A study of High Cascade volcanism: Geological Society of America Bulletin, v. 80, no. 6, p. 969-1006.
Woller, N.M., and Black, G.L., 1983, Geology of the Waldo Lake-Swift Creek area, Lane and Klamath Counties, Oregon, *in* Priest, G.R., and Vogt, B.F., eds., Geology and geothermal resources of the central Oregon Cascade Range: Oregon Department of Geology and Mineral Industries Special Paper 15, p. 57-68.
Woller, N.M., and Priest, G.R., 1983, Geology of the Lookout Point area, Lane County, Oregon, *in* Priest, G.R., and Vogt, B.F., eds., Geology and geothermal resources of the central Oregon Cascade Range: Oregon Department of Geology and Mineral Industries Special Paper 15, p. 49-56.

VOLCANIC HISTORY AND TECTONIC DEVELOPMENT OF THE CENTRAL HIGH CASCADE RANGE, OREGON

Edward M. Taylor
Department of Geology, Oregon State University, Corvallis

ABSTRACT

Two distinct volcanic assemblages exist in the central Cascades of Oregon. The earlier, larger, and longer lived of the two is part of a calc-alkaline, continental-margin andesite belt exposed in the Western Cascades. The younger assemblage, conventionally known as the "High Cascades," overlies the eastern part of the older assemblage and extends eastward to the Deschutes Valley. The High Cascades are also calc alkaline, but mafic components of a broad platform surround isolated silicic centers. A short-lived episode of subsidence produced a graben structure within the central High Cascades. Subsequent mafic eruptions have largely filled the graben as the silicic centers have continued to be active.

This two-fold volcanic development followed by extreme localized crustal tension is ascribed to the influence of slow circulating currents in the sub-Cascade mantle, induced by drag against the subducted slab. Circulation of the lithosphere is enhanced by prolonged metasomatism and loss of strength in the mantle wedge, and may be a common or even essential component of volcanism above subduction systems. Rate of convergence and subduction has decreased in the Cascade system to a degree which has permitted conductive heating of the slab and adjacent mantle. Circulation has been restricted, causing a more direct interaction with the crust. The outcome has been development of a new mafic-dominated volcanic assemblage and graben subsidence.

INTRODUCTION

The central Cascade Range of Oregon is here defined as an east-west transect approximately confined by N. latitudes 43.5° and 44.5°, extending from the Willamette Valley eastward to the Deschutes Valley (Figure 1). It has been long recognized that within this region, a Tertiary Western Cascade volcanic province is structurally and physiographically distinct from an eastern, Quaternary High Cascade volcanic province. Recent studies have revealed a more complex framework in which magmatic and tectonic processes have interacted to produce volcanic associations that transgress the boundaries of previously recognized physiographic provinces. The Western Cascades are composed of tholeiitic and calc-alkaline lavas, tephras, and intrusives ranging from basalt to rhyolite. Early dominance of tholeiitic eruptives extended

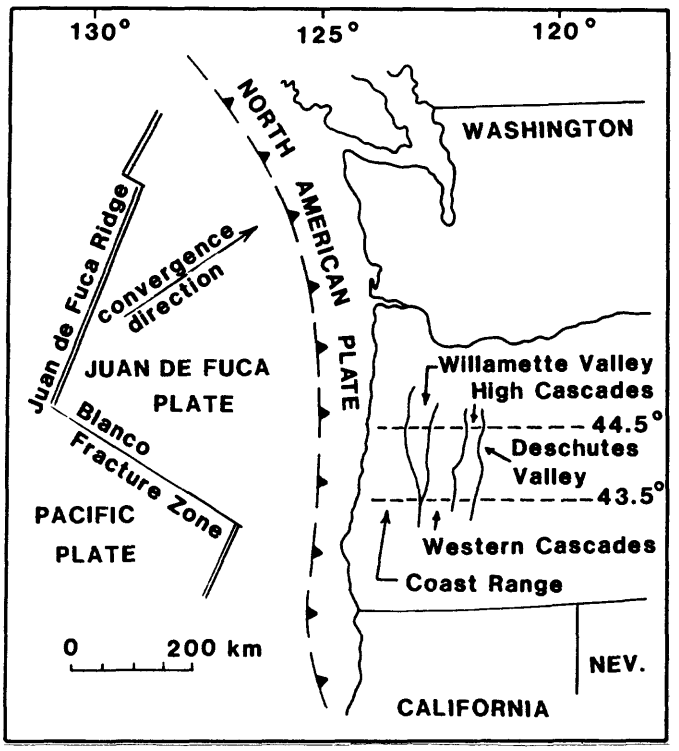

Figure 1. Location of Oregon central Cascade Range and related provinces between N. Latitudes 43.5° and 44.5°, relative to Juan de Fuca subduction system.

westward into the Coast Range. Later dominance of calc-alkaline eruptives merged eastward with alkalic rocks in the Ochoco Mountains. Products of this widespread volcanic activity have been subjected to deformation, alteration, and degradation. In the central Cascades, this material is overlain by similar lavas and tuffs that are well preserved, generally flat-lying, and were deposited on an erosional surface, extending eastward to the Deschutes River. Intense activity along the east side of this volcanic system was followed by extensive subsidence and eruption of mafic lavas to form the modern High Cascades. Consequently, the central Cascades are composed of two principal and independent parts: (1) an older continental-margin andesite belt, whose activity was concentrated in the Western Cascades but whose diverse components appeared over a width of 300 km, and (2) a younger, narrower volcanic field which extended from the Western Cascades to the Deschutes Valley and was subjected to crustal rifting. A model will be presented below in which the dual character of central Cascade volcano-tectonic development will be attributed to mobility of the upper mantle in a subduction system of diminishing convergence rate.

VOLCANIC ACTIVITY

Subduction-related eruptions began in the central Cascades at approximately 42 Ma [Lux, 1982]. In the forearc setting, tholeiitic basalts were dominant until approximately 30 Ma in the form of submarine and subaerial basaltic lavas, mafic volcaniclastics interbedded with near-shore marine sediments, and gabbroic intrusives in Coast Range sedimentary rocks. In the Western Cascades, until approximately 18 Ma, a volcanic belt was constructed in which tholeiitic, intermediate, and highly differentiated silicic magmas produced lavas and tuffs accompanied by widespread ash-flow sheets. It is not known if these rocks extend eastward beneath the younger Cascades; however, tholeiitic lavas and alkali-rhyolite domes and pyroclastic flows of similar age are preserved in the adjacent Ochoco Mountains of central Oregon. The intensity of this episode is reflected in the extensive distal volcanic ash deposits of the 37-to-19 Ma John Day Formation, east of the Cascades [Robinson et al., 1984] and in the abundance of vitric particles in Oligocene tuffaceous marine sediments west of the Cascades [Wells et al., 1984]. During this interval, iron-enriched basalts appeared in the Coast Range [MacLeod and Snavely, 1973], in the Western Cascades [Priest, this issue], and in the Ochoco Mountains [Robinson, 1969]. Consequently, a magmatic series is represented from west to east: tholeiitic basalt, calc-alkaline dacite-rhyolite, and alkali rhyolite, each with associated iron-rich variants. Petrogenetic investigation of these rocks based upon isotopic and trace-element data is incomplete; however, it must be considered that the dominant magmas evolved at successively greater depths eastward, controlled by a subduction system, while some magmas ascended to shallow levels, fractionating to iron-rich varieties.

Eruption of 40-30 Ma western tholeiites is difficult to relate to a Cascade subduction system if the mantle wedge under the Coast Range was as thin then as it now appears to be. By all published estimates of subduction zone thermal structures, tholeiitic magma could not have been produced, even if such a wedge became saturated with volatiles. It has been suggested that these late Eocene - Oligocene tholeiites erupted in the early Cascades, then were displaced to the Coast Range during a clockwise rotation of western Oregon [Wells, et al., this issue]. However, the Coast Range tholeiitic rocks are more common to the north where rotation would have been less effective, and many of them are unlike mafic Cascade rocks, especially with regard to Al_2O_3 content [MacLeod and Snavely, 1973].

Eruption of less explosive two-pyroxene andesite lavas became the predominant mode of volcanic activity in the central Western Cascades at approximately 18 Ma [Priest et al., 1983b]. Occurrence of related tuffs east of the Cascades is limited to

sites that were especially favorable to accumulation and preservation, as represented by the 15 Ma Simtustus Formation in the Deschutes Valley [Smith, 1986a; Smith and Hayman, 1987; Hayman, 1983].

Late Western Cascade eruptive activity apparently migrated eastward across the arc with diminishing intensity until 8-10 Ma. Explanations of this temporal-spacial pattern have ranged from that of a gradual west-to-east shift in the locus of volcanic activity [Peck et al., 1964] to a proposed regional eastward dip of strata which, after erosion, has resulted in exposure of younger rocks to the east [Verplanck and Duncan, 1987]. Evaluation of available age data [Fiebelkorn et al., 1982; Sutter, 1978; Verplanck, 1985] and of regional structure and stratigraphy, suggests an alternate view. Although the oldest accessible rocks are restricted to the west side and young rocks are more common to the east, a long-term reduction in activity occurred across the arc. It was more pronounced to the west than to the east, leading to a gradual eastward migration of a volcanic front, probably because loss of heat was more efficient in the thinner western part of the underlying mantle wedge.

At 8-10 Ma, an independent and intensely active High Cascade volcanic system, dominated by mafic lavas, was established along the east side of the arc and remained active into Holocene time. The original size of this volcanic field is still unknown but the components that have been recognized serve to outline a north-south belt at least 120 km long and 50 km broad, extending from the latitude of Mount Jefferson, south to Willamette Pass (Figure 2). Stratigraphic records of early High Cascade volcanism are preserved only along the east and west sides because late High Cascade volcanoes have buried the central part of this field.

On the west side, early High Cascade lavas are chiefly flat-lying basalts and basaltic andesites which cap ridges between 1300 and 1500 m elevation, although these rocks are up to 1500 m thick in some areas. Among the lavas of this group, from north to south (Figure 2), are flow rocks on the summit of Outerson Mountain (6.3 Ma), Triangulation Peak (6.0 Ma), and Bachelor Mountain (6.3 Ma) [Priest et al., 1987]; Three Pyramids (6.3 Ma), Crescent Mountain, and Echo Mountain (5.8-7.2 Ma) [Black et al., 1987]; Bunchgrass Mountain (5.1 Ma) and Frissell Ridge (6.3 Ma) [Armstrong et al., 1975]; Lookout Ridge (8.3 Ma) [Priest et al., 1983b]; English Mountain (6.5 Ma) [Flaherty, 1981]; Olallie Mountain (4.96 Ma) [Priest et al., 1988]; and "ridge capping basalts" near Oakridge (6.6 Ma) [Sherrod, 1986]. Many of the basalts are open textured (diktytaxitic), which is a very uncommon feature in Western Cascade lavas. High-silica pyroclastic rocks are rare in this group, but mixed andesitic-dacitic ash-flow tuffs occur at Outerson Mountain [Priest et al., 1987], dacitic pyroclastic-flow deposits (6.3-8.7 Ma) have been found at Tipsoo Butte [Priest et al., 1988], and a welded

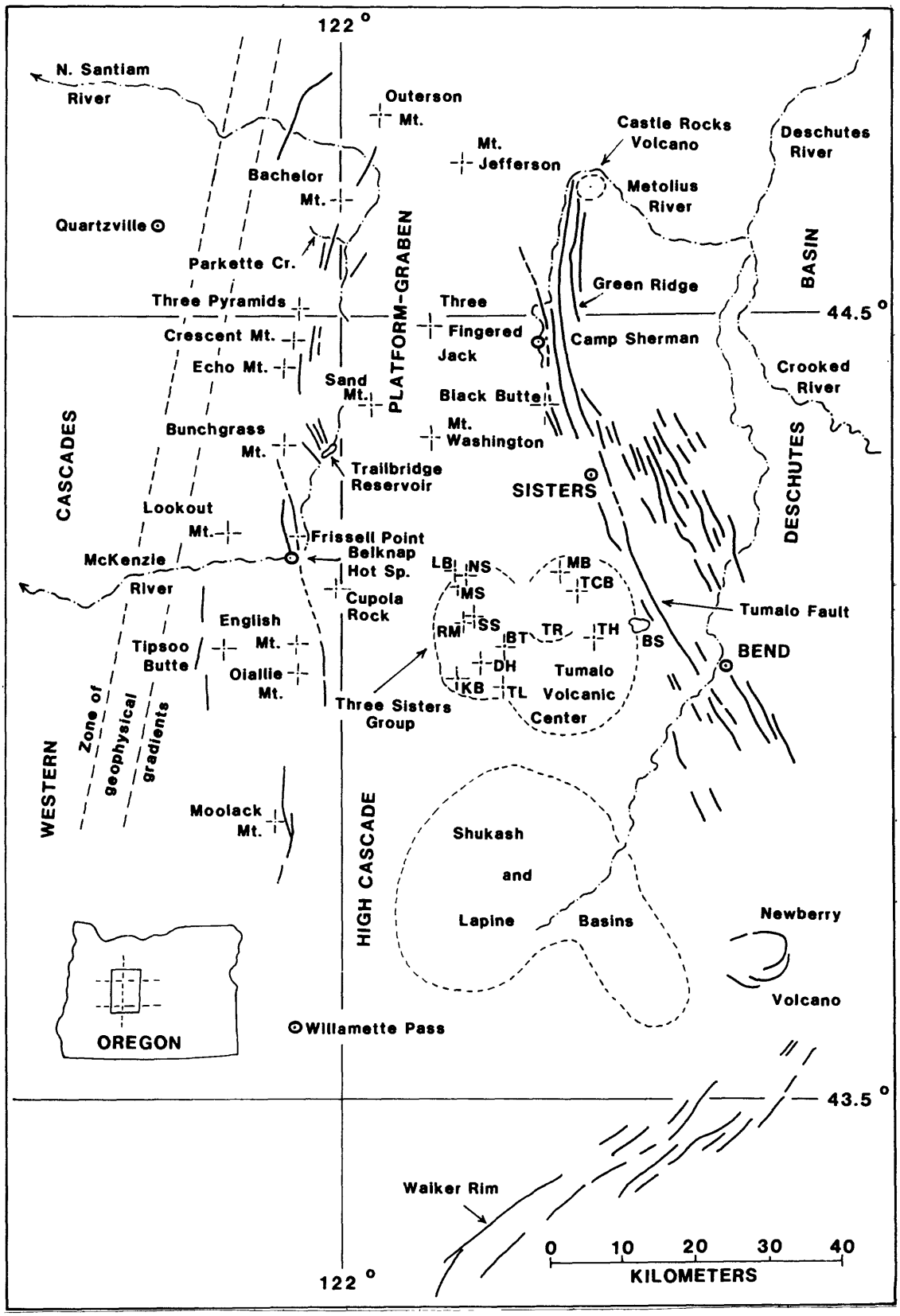
122°
N. Santiam River
Outerson Mt.
Bachelor Mt.
Quartzville
Parkette Cr.
Three Pyramids
Crescent Mt.
Echo Mt.
Sand Mt.
PLATFORM-GRABEN
Mt. Jefferson
Castle Rocks Volcano
Deschutes River
Metolius River
BASIN
Green Ridge
Three Fingered Jack
Camp Sherman
44.5°
Crooked River
Black Butte
Mt. Washington
CASCADES
Bunchgrass Mt.
Trailbridge Reservoir
SISTERS
DESCHUTES
Lookout Mt.
Frissell Point
Belknap Hot Sp.
McKenzie River
Cupola Rock
LB
NS
MS
MB
TCB
Tumalo Fault
English Mt.
Tipsoo Butte
Oiallie Mt.
RM
SS
BT
TR
TH
BS
BEND
DH
KB
TL
Tumalo Volcanic Center
Three Sisters Group
Zone of geophysical gradients
WESTERN
Moolack Mt.
HIGH CASCADE
Shukash and Lapine Basins
Newberry Volcano
OREGON
Willamette Pass
43.5°
Walker Rim
122°
0 10 20 30 40
KILOMETERS

Figure 2. Central High Cascades of Oregon with locations of volcanic groups, structural features, and place names discussed in text. Three Sisters group and Tumalo volcanic center: (BS) Bull Springs, (BT) Broken Top, (DH) Devils Hill, (KB) Kaleetan Butte, (LB) Little Brother, (MB) Melvin Butte, (MS) Middle Sister, (NS) North Sister, (RM) Rock Mesa, (TCB) Three Creek Butte, (TH) Triangle Hill, (TL) Todd Lake, (TR) Tam Rim.

basaltic andesite tuff (5.5 Ma) crops out between Trailbridge Reservoir and Belknap Hot Springs [Taylor, 1981]. Dikes and plugs are exposed near eroded volcanic centers [Avramenko, 1981], but many distinctive lavas appear to have followed topographic channels from eastern source cones.

Equivalent rocks on the east side make up Green Ridge, a north-south, 30-km-long faulted block of Cascade crust, containing the andesitic Castle Rocks composite volcano (7.5-8.3 Ma) [Hales, 1975; Wendland, 1988] and younger lavas (5.3-7.3 Ma) [Conrey, 1985; Smith et al., 1987]. The younger Green Ridge lavas are correlatives of the Deschutes Formation (5.4-7.4 Ma) [Smith et al., 1987] which covers much of the central High Cascade slope east to the Deschutes River. The Deschutes Formation contains the best preserved and most extensively studied record of early central High Cascade volcanism [Smith, 1986b, 1987a, 1987b]. It is more than 700 m thick at Green Ridge, thinning to 250 m near the Deschutes River, and makes up a broad prism of mafic lavas, andesite-dacite ignimbrites, debris-flow deposits, ash layers, and epiclastic beds extending 90 km north from Bend. With few exceptions, these units were derived from volcanic centers to the west and most of them were emplaced after 6 Ma. Thin, extensive sheets of diktytaxitic basalt occur at many different stratigraphic levels. Banded textures and mixed pumices, representing incomplete blending of magmas of distinct compositions and crystal contents, is a common feature of Deschutes Formation silicic lavas and ash-flow tuffs [Jay, 1982; Conrey, 1985; Dill, 1988].

Reconstruction of the early High Cascade volcanic field, based upon west-side and east-side geochronology, paleotransport directions, and distribution of lithologies, must include an extensive cover of mafic diktytaxitic lavas from broadly dispersed cones and shields, accompanied after 6 Ma by large central vent complexes of silicic composite volcanoes. Green Ridge is a preserved eastern segment of a large mafic system in which several overlapping volcanoes were interbedded with channelized ash-flow tuffs [Conrey, 1985]. Another prolific source of ash-flow tuffs was located near the site of modern Three Sisters volcanoes [Cannon, 1984; Smith, 1986b].

Some late Miocene to late Pliocene mafic volcanism which persisted in the Western Cascades could be an extension of early High Cascade activity, in the sense that magmas underplating the High Cascade crust might have spread westward, then found a route to the surface. Possible examples include Snow Peak shield volcano (3 Ma) [Verplanck, 1985] adjacent to the Willamette Valley, lavas at Marks Ridge (4.5 Ma) near Sweet Home, and Pleistocene cinder cones and associated lava flows near Quartzville.

Graben subsidence occurred along the central part of the early High Cascade axis at 5.4 Ma [Smith, et al., 1987]. Cascade-derived lavas, ash-flow tuffs, and debris-flow deposits were structurally isolated and no longer reached the Deschutes basin [Smith, 1986b; Smith et al., this issue]. Subsequent late High Cascade volcanism was a continuation of the previous type of activity except that lavas, hyaloclastites, and ash-flow tuffs were deposited within the graben while airborne ash and lapilli were added to the top of the Deschutes Formation in the Deschutes basin. Most of this graben-fill is no longer exposed; however, parts of the graben floor are preserved on topographic shelves that were isolated between parallel faults along both east and west sides of the graben. One of these remains at the south end of Green Ridge as an inclined ramp which, at 1130 m elevation, was not buried by lavas and has probably lost its cover of ash to erosion. Another shelf, 13 km to the north at 980 m elevation, is capped by the Camp Sherman beds of sideromelane tuff and diatomite [Smith, 1986b]. On the west side, several isolated shelves became sites of interrupted drainage as the adjacent graben filled with lavas. Diatomaceous lacustrine tuffs, palagonitic tuffs, and pillow lavas were formed as part of the Parkette Creek sedimentary rocks (1.8 Ma) southwest of Mount Jefferson [Black et al., 1987] and the Scott Creek beds (2.35 Ma) near Belknap Hot Springs [Priest et al., 1988]. The oldest known graben-fill lava (4.3 Ma) [Yogodzinski, 1985] appears to have been an intracanyon diktytaxitic basalt, marking the site of ancestral Metolius River drainage from the graben. An analogous record is provided by the diktytaxitic basalt of Cupola Rock (2.2 Ma) [Armstrong et al., 1975] and underlying welded tuff (3.64 Ma) Priest et al., 1988] which might have been intracanyon to an ancestral McKenzie River.

A broad platform composed of overlapping shield volcanoes is now the principal component of the central High Cascades. Development of this platform has obscured early High Cascade source volcanoes and has nearly filled the graben. Although repeated outpouring of diktytaxitic basalt from relatively small cinder cones continued throughout Pleistocene time, fine-grained basaltic andesite with pilotaxitic texture became the dominant lava from small cones, shields of intermediate size, and large composite cones such as Three Fingered Jack, Mount Washington, and North Sister. Volcanic centers, often of different age and

lithology, commonly formed north-south alignments of many vents [Taylor et al., 1987]; these vent alignments probably mark the location of north-south intragraben faults, now buried beneath the platform.

Light rare-earth element content of most basaltic andesites of the central High Cascade platform is similar to, or less abundant than, platform basalts. Consequently, the basaltic andesites could not have been derived from platform basaltic magma by crystal fractionation. A more likely model involves melting of a LIL-enriched spinel lehrzolitic source under conditions of variable volatile content and degree of melting in the mantle wedge above the subduction zone [Hughes and Taylor, 1986]. Rare-earth element compositions do not support a significant influence of garnet-bearing source rocks in generation of these magmas; therefore, last equilibration with source rocks probably occurred at depths less than 50 km, near the base of the crust. Most mafic platform lavas appear to be near-primitive melts of a high-level hydrous mantle, having undergone only moderate fractionation. However, a few platform rocks have become so highly evolved through a process of iron enrichment as to resemble icelandites; others have become enriched in silica and are transitional to andesites.

On the east flank of the central High Cascades, eruptions of silicic lavas, domes, and pyroclastic flows produced a highland of rhyolite, rhyodacite, and dacite known as the "Tumalo volcanic center" [Hill, 1988] (Figure 2). Late flows of basaltic andesite lava have covered a large part of this center, but its form is outlined by a broad and steep topographic protrusion of the east Cascade slope west of Bend. At least seven volcaniclastic units were vented from the Tumalo volcanic center. They include Desert Springs ash-flow tuff [Taylor, 1980], Bend Pumice lapilli deposit and associated Tumalo ash-flow tuff [Hill, 1985], and Century Drive and Shevlin Park ash-flow tuffs [Taylor, 1981]. Bend Pumice and Tumalo Tuff appear to be proximal equivalents of the Loleta Ash (0.3 $\pm$ 0.1 Ma) of northern California [Sarna-Wojcicki et al., 1987]. The Shevlin Park Tuff is the youngest and best preserved pyroclastic flow deposit on the east slope of the central Cascades. It becomes thicker, coarser, and more densely welded toward a site in the Tumalo volcanic center which is marked by a circular, 8-mgal negative Bouguer gravity anomaly [Pitts and Couch, 1978], a 3-km ring of cones and domes, and Triangle Hill, an andesitic cinder cone at the center of the ring whose composition is similar to the Shevlin Park Tuff. Many silicic domes were constructed late in the development of the Tumalo volcanic center and remain as distinct landforms. Large rhyolite domes at Three Creek and Melvin Buttes were beyond the reach of Pleistocene glaciers. Extensive glaciation at higher elevations reduced the Todd Lake volcano to a massive plug within a pile of dissected dacite lavas.

Rhyodacite lavas and pumice cones at Tam MacArthur Rim were erupted during early stages of activity at nearby Broken Top volcano. Basaltic andesite lavas and micronorite intrusive rocks are the most abundant constituents in Broken Top; however, magmas of andesitic and dacitic composition erupted to form lavas and pyroclastic deposits at many sites on the flanks of the cone [Taylor, 1978].

The snow-capped Three Sisters volcanoes are the largest and best known Pleistocene stratocones in the central Cascades. North Sister is the oldest of the group; it is stratigraphically above Shevlin Park Tuff and is probably younger than Broken Top. North Sister rests upon the Little Brother basaltic shield volcano but is, itself, chiefly composed of uniform basaltic andesite lavas, dikes, sills, and plugs accompanied by minor, late-stage lavas and dikes displaying an iron-enrichment trend. South Sister is the youngest of the group and is composed of andesite, dacite, and minor rhyodacite lavas [Wozniak, 1982; Clark, 1983]. Latest Pleistocene eruptions produced a summit crater and enveloped the top of the cone in a thin shroud of oxidized basaltic andesite lavas and red cinders. Flank eruptions of rhyodacite domes have been a persistent feature of activity at South Sister. Glaciated remnants include Kaleetan Butte, Devils Hill, and many partly exposed domes extending to the northeast base of South Sister [Taylor, 1978, 1987]. Holocene examples include Rock Mesa, Devils Hill chain, Newberry flow, and Carver Lake chain [Scott, 1987]. Middle Sister is intermediate in both composition and age. Although the principal component of Middle Sister is a diktytaxitic basalt porphyry, a broad compositional range from basaltic andesite through andesite, dacite, and rhyodacite is also represented. Some lavas contain bands and clots of distinct composition and multiple generations of phenocrysts that were not in mutual equilibrium. Early Middle Sister lavas include units similar to the late North Sister iron-enrichment series; late Middle Sister lavas are interbedded with distinctive fountain-fed lavas of early South Sister.

The Tumalo and Three Sisters volcanic centers do not conform to the classical concept of an isolated reservoir of evolving magma beneath each volcano, yielding intermittent contributions to a central conduit during the lifetime of that volcano. Field relationships, modal data, and trace-element compositions support more complex models of partial melting in mantle and crust, selective assimilation, crystal fractionation, and mixing of magmas [Hughes, 1982; Clark, 1983]. It is likely that many different magma types have evolved and reside at various depths in a plexus of reservoirs beneath this region. One volcano may have received increments from several reservoirs and a single reservoir may have contributed to several volcanoes. Specific durations and locations of surface vents may represent little more of significance than "thermal trails" heated by passage of

earlier magmas through zones of structural weakness. Silicic volcanism has been active intermittently at this site for at least 6 Ma; the modern volcanoes are only the latest expression of a long-lived and deep-seated system.

True calc-alkaline andesites with silica content between 57 and 63 weight per cent are very rare in the central High Cascades. The resulting basalt - basaltic andesite and dacite - rhyodacite compositional bimodality might reflect a dominance of partial melting in mantle and crust, respectively, as mechanisms by which most Cascade magmas have been produced.

Many general problems related to High Cascade silicic centers are unresolved. Why are they concentrated in a few large clusters instead of small, widely distributed flows and domes? They appear to have been established in almost random position and time, in the sense that spacing and age are variable; some are displaced from the axis of volcanic activity, some are old, and some are very young. None appears to be totally extinct, which suggests that once begun, they tend to persist. How can they endure for periods that exceed the thermal longevity of even a large crustal reservoir? If the High Cascade crust is underplated by a body of continually replenished mafic magma, cupolas might develop in the base of the crust in response to inhomogeneities in composition or structure. A large cupola could serve as an open convecting system, supplying energy and magma to drive processes of crustal anatexis and crystal fractionation in restricted locations for extended periods.

Under these conditions of locallized, long-lived silicic volcanism, it is reasonable to assume that the High Cascade mafic platform is not continuous beneath the silicic centers. At Mount Jefferson, another long-lived silicic center, this relationship is valid [Conrey, 1988], but at Three Sisters, where glaciation has not cut as deeply into surrounding terrain and where mafic and silicic eruptions were closely associated, discontinuity of the mafic platform is less certain.

TECTONIC DEVELOPMENT

The Cascade volcanic arc is thought to be a product of subduction tectonics because it shares many features that characterize other well defined Pacific-margin subduction systems. Although deep earthquakes associated with Juan de Fuca plate subduction are unknown and trench morphology is currently absent, active seismicity of nearby oceanic spreading ridges, symmetric magnetic anomaly patterns on the sea floor, and compressional deformation of the continental slope reveal a history of late Tertiary convergence with the North American plate. An inclined slab at subcrustal depth beneath the Oregon

Coast Range is suggested by reflection data [Keach, 1986]. The subducted slab is assumed to be relatively elevated in temperature because its age at the zone of convergence has been less than 20 Ma during the last 40 Ma [Engebretson et al., 1985]. Heat flow is minimal in the Coast Range, but in the Western Cascades it increases abruptly from less than 60 to more than 100 mW/m^2 over a west-to-east transition zone only 15 km wide [Blackwell et al., 1982]. Reconstruction of plate motions, based upon Atlantic and Pacific hot-spot reference frames and relative Farallon-Pacific plate spreading rates, supports a model of northeast-southwest oblique convergence of the Juan de Fuca and North American plates [Engebretson et al., 1985]. During the last 40 Ma, the rate of convergence has decreased by a factor of 2.7 and obliquity of subduction has increased [Verplanck and Duncan, 1987]. If late Tertiary clockwise rotation of western Oregon [Simpson and Cox, 1977; Magill and Cox, 1980] is taken into account, the rate of convergence orthogonal to the continental margin has decreased by a factor of 5 [Duncan and Kulm, 1989].

A decrease of Bouguer gravity in excess of 50 mgals occurs from west to east in the central Cascades, 10-15 km west of the High Cascade - Western Cascade province boundary (Figure 2) [Couch, et al., 1981]. Coincident with this Bouguer gradient are a north-south linear trend of negative residual gravity anomalies [Couch et al., 1982b], a heat-flow gradient increasing by more than 40 mW/m^2 from west to east [Blackwell et al., 1982], a west-to-east decrease in estimated depth to a Curie-point isotherm [Connard et al., 1983], and a corresponding decrease in depth to the top of a crustal zone of electrical resistivity [Stanley et al., this issue]. Several interpretations have been advanced to account for this narrow zone of geophysical gradients: 1. Low density volcaniclastic sediments have been displaced 1.5 km down on the east side of a north-south fault, against a higher density section of mafic lavas [Couch et al., 1982a]. 2. Hydrothermal systems associated with heat sources beneath the High Cascades are masked by a shallow groundwater "rain curtain" but cause increased heat flow along marginal zones where thermal waters approach the surface [Ingebritsen et al, this issue]. 3. An upper crustal heat source, probably a complex of magma bodies, underlies the High Cascades at a depth of 10 km and extends westward to the zone of heat flow gradient [Blackwell et al., 1982].

Structural geology of the central Western Cascades is not well documented because distinctive stratigraphic units are not aerially extensive, isotopic dating of altered rocks is difficult, and quality of exposure is poor. It is clear that deformation has occurred because faulted blocks of unknown dimensions, diverse orientations, and indefinite displacements are commonly observed where bedrock is adequately exposed. Many northwest-trending faults display horizontal striations and widely spaced folds of

northeast trend have been described [Peck et al., 1964].

Central Western Cascades have been subject to late-Tertiary uplift [Priest et al., 1983b], but this also is poorly documented. The observable vigorous dissection of high relief topography, characterized by steep, unstable slopes and narrow canyons seems out of place in a volcanic terrain that has been quiescent for 10 Ma in a region of abundant rainfall, unless uplift has occurred. Changes in Miocene and Pliocene paleoflora of central Oregon have been interpreted as a direct result of increasing effectiveness of a Cascade "rainshadow" [Ashwill, 1983].

The east part of the central High Cascade Range has undergone an episode of subsidence leading to abrupt east and west structural discontinuities, outlining the boundaries of a graben (Figure 3). The west side of this graben is an erosional escarpment which rises 800 m above the High Cascade platform and extends from North Santiam Valley, 90 km south to Moolack Mountain [Priest et al., 1987; Black et al., 1987; Priest et al., 1988; Sherrod, 1986]. In the Belknap Hot Springs area, distinctive stratigraphic units have been traced in accumulated offset of 600 m down on the east sides of several north-south

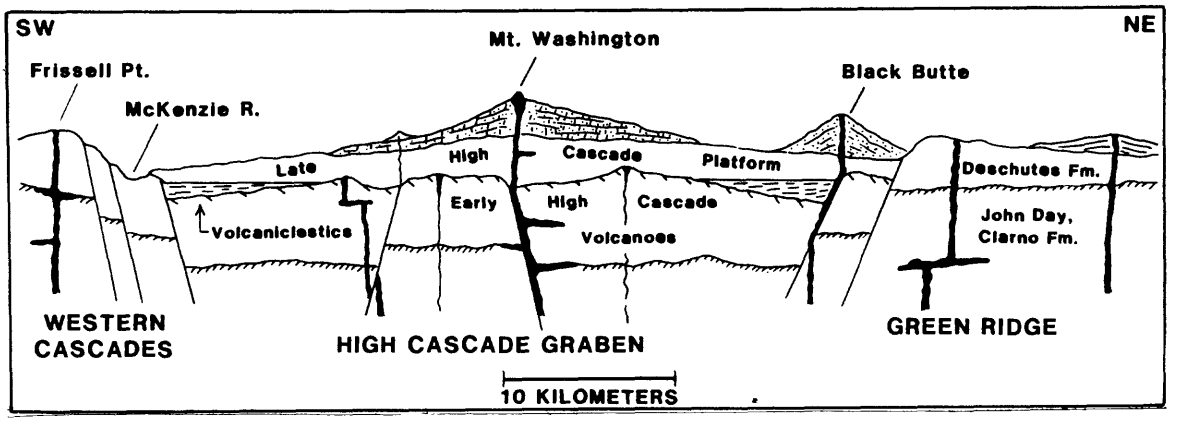

Figure 3. Diagrammatic SW-NE cross section of central High Cascade graben. Three-fold vertical exaggeration.

normal faults. Additional displacement probably occurred on faults which are now buried under the High Cascade platform but are marked by alignments of eruptive vents such as the Sand Mountain group [Taylor, 1981].

The east side of the graben is represented by a fault escarpment at Green Ridge which, by topography alone, has been

offset 700 m, down on the west side. Detailed study of Green Ridge has revealed many parallel north-south faults with net displacement exceeding 600 m, exposed upon the face of the escarpment [Conrey, 1985; Wendland, 1988]. Additional subsidence on faults that may be buried under the adjacent High Cascade platform is suggested by alignments of eruptive vents, especially west of Wizard Falls. The Green Ridge fault merges to the southeast with the Tumalo fault zone, extending from Sisters to Bend [Peterson et al., 1976]. This trend can be followed in a broad 150-km arc of minor faults and vent alignments, southeast to Newberry Volcano, then southwest to Walker Rim [MacLeod and Sherrod, 1988]. West of the Tumalo fault, near Bull Springs, a topographic prominence of Deschutes Formation lavas was not completely inundated by the High Cascade platform. This suggests that faults now obscured by the Tumalo volcanic center are part of the graben boundary. It is presently unclear whether a buried graben extends south from Green Ridge in constant width or is distributed over an east-west breadth of 60 km from Moolack Mountain to Newberry Volcano and is therefore indistinct as a topographic or structural feature.

Although faults are not seen over most of the High Cascade platform, a condition of distributed tension across the graben during the time of its formation is suggested by many north-south vent alignments [Hughes and Taylor, 1986; Taylor et al., 1987], in contrast with their rarity outside of the graben. Because many alignments consist of volcanic centers of different age and lithology, it is likely that magmas have ascended through zones of crustal weakness established by previously active intragraben faults. Some alignments may represent a response to crustal stresses in effect during eruption. Diktytaxitic textures so common in High Cascade basalts are probably produced when mafic magma of moderate volatile content passes through the uppermost crust at such a rate that efficient nucleation and expulsion of gases do not occur prior to eruption. Rapid ascension of magmas should be enhanced by crustal tension. If diktytaxitic basalt is a characteristic of tensional stress within the crust, it must have been operative throughout development of the High Cascade platform.

Minimum graben subsidence as derived from surface features is approximately 700 m. Thickness of low density volcaniclastic graben fill has been estimated to be 3 km, based on gravity data [Foote and Couch, 1983]. Total subsidence will probably remain unknown until information from deep drilling becomes available. However, it should be recognized that a volcanic highland, 25 km wide, with eruptive centers able to supply hundreds of pyroclastic flows and lava units both east and west, during an interval of only 0.6 Ma, has now been engulfed and buried without trace of even one of the source cones.

Estimates of the age of the High Cascade graben have been based upon K-Ar dates of units whose relationship to the subsidence is known. Minimum ages of lavas on the crests of west and east escarpments and maximum ages of platform lavas lie between 4.7 and 4.3 Ma, respectively, but large errors are reported [Fiebelkorn et al., 1982]. A more reliable approach has been that of Smith et al. [1987], in which 40Ar-39Ar ages of lavas within the Deschutes Formation were used to date the stratigraphic level of change from intense arc-derived pyroclastic- and debris-flow deposition to a prolonged development of ashy paleosols. This age is 5.4 Ma.

DISCUSSION

Current models of subduction-related magmatism emphasize the critical importance of volatiles that are carried into the mantle by hydrous minerals within the slab. Pore water is probably expelled at shallow levels as early hydration reactions produce chlorites, zoisites, brucite, and serpentine. Successive dehydration reactions during greenschist-to-amphibolite metamorphism yield amphiboles $\pm$ talc. It is not certain that water is released at this stage because most of the basaltic slab could be converted to amphibole. Amphibole is unstable below 75-80 km because it undergoes pressure-controlled decomposition as amphibolite is converted to quartz eclogite [Allen et al., 1975]; this is regarded as the principal source of volatiles expelled from a descending slab [Fyfe and McBirney, 1975]. However, depth to Benioff zones under most active volcanic arcs is 100-125 km [Gill, 1981]. Recognition of this discrepancy in location of volatile source and volatile-rich magma has stimulated many suggestions, including (1) lateral migration of volatiles through the wedge to a position of elevated temperature beneath the arc [Burnham, 1981], (2) location of Benioff zones within, rather than on top of, subducted slabs [Boettcher, 1977], (3) extended stability of micas in the descending slab [Fyfe and McBirney, 1975] and hydrous reaction products of serpentine in the descending lithosphere [Ringwood 1975], and (4) convective circulation within the mantle wedge as a mechanism by which the hydrous ultramafic solidus can be brought into a region of volatile flux above the slab [Anderson et al., 1980].

The concept of induced circulation within the deep asthenospheric part of a mantle wedge has been introduced by several investigators with reference to back-arc basin tectonics in oceanic systems [Andrews and Sleep, 1974; Hsui and Toksoz, 1979]. Such a mechanism, if it exists, is generally thought to have little influence upon the arc itself. Induced circulation of the lithospheric mantle wedge beneath island arcs has been advanced as an explanation of incompatible element enrichment in arc magmas [Tatsumi et al., 1986]. Previous models have called upon large scale convection involving the deep asthenosphere and an

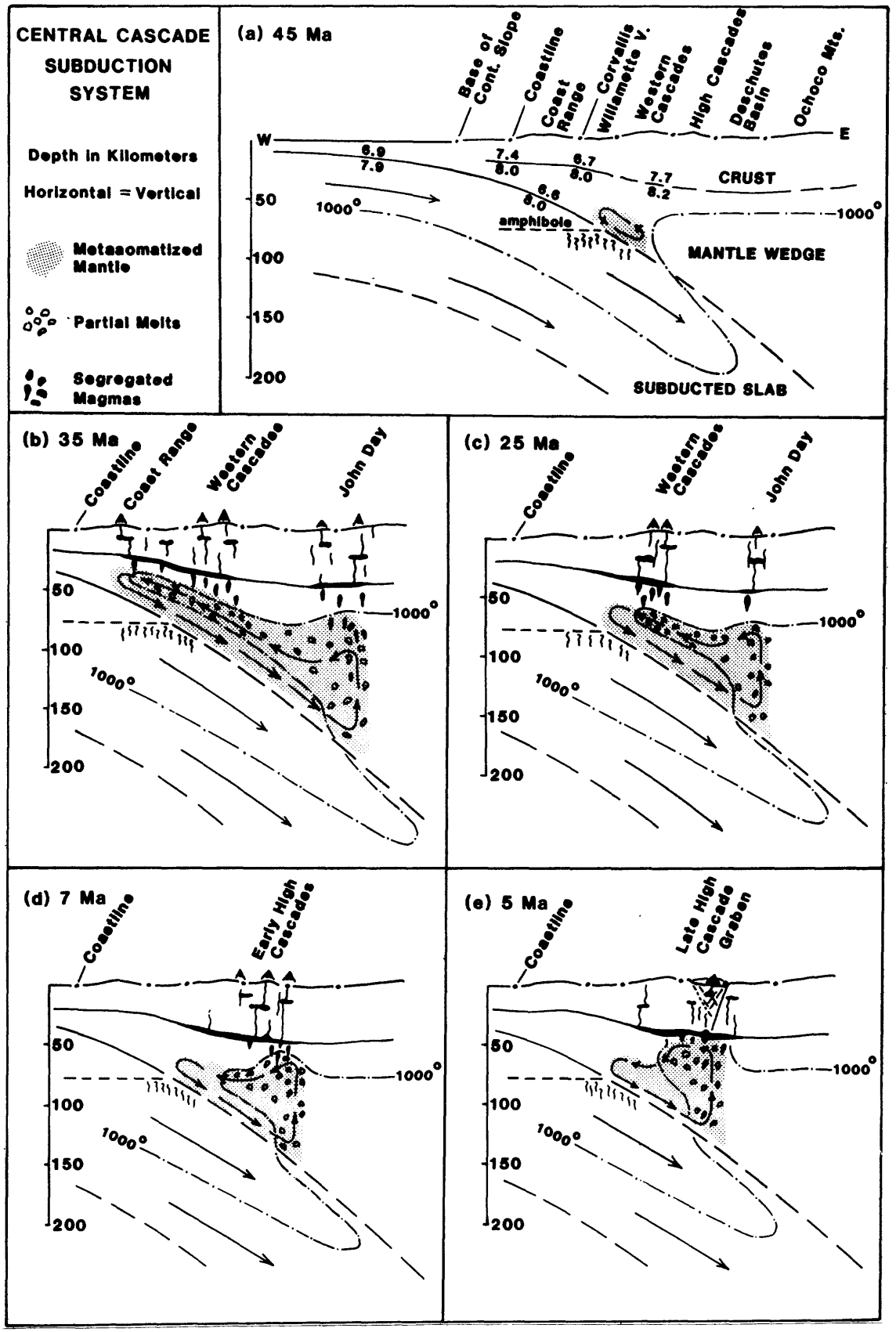
CENTRAL CASCADE SUBDUCTION SYSTEM
Depth in Kilometers
Horizontal = Vertical
Metasomatized Mantle
Partial Melts
Segregated Magmas
(a) 45 Ma
Base of Cont. Slope
Coastline
Coast Range
Corvallis
Willamette V.
Western Cascades
High Cascades
Deschutes Basin
Ochoco Mts.
W
E
6.9
7.9
7.4
8.0
6.7
8.0
7.7
8.2
CRUST
6.6
8.0
amphibole
1000°
MANTLE WEDGE
SUBDUCTED SLAB
50
100
150
200
(b) 35 Ma
Coastline
Coast Range
Western Cascades
John Day
(c) 25 Ma
Coastline
Western Cascades
John Day
(d) 7 Ma
Coastline
Early High Cascades
(e) 5 Ma
Coastline
Late High Cascade Graben

Figure 4. Schematic development of central Cascade subduction system relative to modern physiographic provinces.

(a) Initial conditions of system approximately 45 Ma. Mantle wedge has been metasomatized above amphibole breakdown, circulation has been induced, but melting of mantle wedge has not occurred. Crust and slab boundaries (solid) after Snavely et al., 1980; Couch et al., 1982; Leaver et al., 1984; Keach, 1986. Seismic velocities in km/sec. Isotherm estimates are based on slab 100 km thick, subduction rate 8 cm/a, age 3 Ma, shear-strain heating 6.4 ergs/cm^3 sec [Toksoz et al., 1971, Fig. 6a]. Amphibole stability from Allen et al. [1975].

(b) Approximately 35 Ma. Circulation of mantle wedge has reached maximum extent. Isotherm conforms to 4(a) except subduction age is 13 Ma [Toksoz et al., 1971, Fig. 7] and thermal structure has been perturbed by circulation.

(c) Approximately 25 Ma. Circulation of mantle in wedge corner has been restricted by loss of heat, and Coast Range volcanism has ceased. Convection zone has migrated westward in response to decreased rate of subduction.

(d) Approximately 7 Ma. Circulation is further restricted and Western Cascades have become inactive. Convection zone has migrated westward and has reached shallow levels under early High Cascades.

(e) Approximately 5 Ma. Migration of convection zone has brought circulating mantle in contact with High Cascade crust; tension, subsidence, and mafic volcanism result.

essentially inexhaustible reservoir of thermal energy. I propose that on a smaller scale, circulation is induced in the "corner" of the wedge where it has been weakened by volatile flux and that it develops as an isolated convecting cell whose size, location, and duration are controlled by the rate of subduction and the thermal structure of the system. It is here suggested that the mantle wedge under western Oregon has exhibited this motion and that the above-described features of central Cascade volcanic activity and tectonic development have been influenced by it.

In the Cascade subduction system, amphibole breakdown in the slab probably occurred beneath the Willamette Valley where volatiles enriched in silica and incompatible elements were contributed to the mantle wedge peridotite, resulting in metasomatized veins of pyroxenite containing amphibole, talc, and intergranular fluids (Figure 4a). Initially, low temperature did not permit melting. The wedge, after contamination, was reduced

in strength and yielded to frictional drag exerted by the adjacent slab. The accumulated volatiles were carried to greater depth as an elongate circulating cell developed above the slab and became extended. Amphibole was stable in the ultramafites to somewhat deeper levels than in the slab [Wyllie, 1979], but eventually, hydrous phases in the mobilized wedge began to decompose and as temperatures near 1000° were encountered, a small amount of H_2O-saturated, interstitial melt, enriched in LIL elements, was formed. Some phlogopite might have been produced under these conditions [Wyllie and Sekine, 1982]. Magmatic segregation probably did not occur because the limited supply of volatiles permitted only a small proportion of melt. As the wedge material descended, it was heated by conduction. Partial melting continued, leading to H_2O-undersaturation of interganular magmas. If hydrous silicates or fluids were carried in the slab to such depths, they would contribute to melting of the slab and the addition of magmas to the superadjacent wedge. However, these intermediate slab-derived magmas would probably react with the ultramafic wedge, resulting in hybrid solids and liberated volatiles [Wyllie and Sekine, 1982].

A critical range of temperature and melt fraction was reached in which strength and relative density of the wedge were so reduced that multiple diapirs ascended, coalesced, and bulk convection began into the wedge interior. Melt proportion increased in response to pressure release and elevated temperature. During the height of Oligocene volcanic activity in the Western Cascades, when orthogonal subduction rate was approximately 8 cm/a [Duncan and Kulm, 1989], the zone of convective ascension was probably east of the Cascades, beneath Ochoco Mountains. Limited segregation of magmas near the top of the convective zone might have produced alkaline basalts of the John Day Formation. Return flow was directed westward where it ascended toward the corner of the mantle wedge.

While it carried high-temperature material from the interior of the wedge, the circulating cell probably reached its maximum western extent, beneath the Coast Range (Figure 4b). At relatively shallow levels, the proportion of volatile-undersaturated melt increased until mafic magmas were released and the early Western Cascade - Coast Range tholeiitic assemblage was produced. This condition of extended circulation and forearc volcanism was probably short lived as heat was efficiently extracted from the thin part of the wedge. A more stable and restricted configuration in which heat was transferred into the ascending convection zone by conduction from adjacent, stationary mantle, characterized the circulating cell during all of subsequent Cascade development (Figure 4c). As the rate of subduction decreased, conductive heating of the slab and adjacent mantle wedge permitted more extensive melting and forced a migration of the zone of convective ascension westward to shallower levels. The net surface effect of these

reorganizations was a gradual west-to-east reduction of Coast Range and Western Cascade volcanic activity as well as the extinction of John Day volcanism in the Ochoco Mountains. In contrast, the western extremity of circulation maintained its position above the region of amphibole breakdown. Could this persistent downward flow account, in part, for the low elevation of the Willamette Valley, relative to uplifted Coast Range and Western Cascades?

Continued decrease of subduction rate and loss of heat from the wedge restricted the region of melt production and brought the zone of convective circulation closer to the crust beneath the eastern margin of the Cascades (Figure 4d). At this time (8-10 Ma), activity was initiated in the early High Cascade volcanic field. Dominant in this field were high-alumina tholeiites derived from enriched sources and segregated from the ascending wedge at shallow levels. The descending limb of circulating wedge became the western margin of crustal anatexis, intrusion of silicic magmas, and consequent gradients in heat flow and Bouguer gravity. Evolved volcanic systems, possibly driven by cupolas of convecting magma in the base of the crust, produced abundant pyroclastic deposits, and by 6 Ma, silicic centers were established; a new volcanic range was formed.

At approximately 5.5 Ma, ascending currents of circulating mantle wedge came into effective contact with the base of the crust, imparting a sharply localized east-west tension where the High Cascades were carried westward relative to a more rigid eastern block (Figure 4e). Moderate compression was imposed upon the western block. Western Cascade volcanism was further restrained; faulting and uplift occurred. Silicic magmas were produced by partial melting of gabbroic crust; intrusive bodies penetrated the crust but ascent was hindered in western regions of compression while being enhanced in eastern regions of tension. The early High Cascade Range subsided in a graben and diktytaxitic basalts were permitted to ascend in such volume that the graben was filled and most of the range was buried. Silicic centers continued to be active; consequently, their youngest parts were not completely obscured by a mafic platform and are represented by modern cones of the Three Sisters - Broken Top groups.

The graben has not been traced north of Mount Jefferson or south of the Three Sisters. Also, tensional stresses responsible for the principal episode of High Cascade crustal subsidence must have been of short duration because the mafic platform has not been displaced by graben faults. Presumably, ascending currents within the circulating mantle wedge have not made crustal contact beneath all of the High Cascade Range and the regions of contact might not have been constant in location. Oblique subduction and/or variable coupling between slab and wedge might give rise to separate cells with different configurations and ages. The

central High Cascades might have been underlain by a circulating cell which was in contact with the crust beneath a narrow northern zone, then shifted to a wider zone of contact to the south. In this way, younger fault systems of broad distribution and small displacement, such as the Tumalo fault zone, would develop southward, Newberry Volcano would stand above the ascension zone, and the depressed Shukash and LaPine basins [Couch et al., 1982a] would be part of a broadly extended, but shallow and indistinct graben. Another possible example of an isolated convection cell of limited extent and duration might have developed under the Hood River Valley which is an area of High Cascade north-south subsidence with an eastern boundary fault. Diktytaxitic basalts occur on the valley floor and a volcaniclastic apron of western provenance and Miocene age (the Dalles Formation) extends eastward from the crest of the fault block.

CONCLUSIONS

Induced circulation in the sub-Cascade mantle wedge is an hypothesis whose validity can not be conclusively demonstrated at this time. However, many events and relationships in the volcanic, magmatic, and tectonic development of the central Cascades that have generated diverse, often conflicting interpretations, can now be attributed to a single model. Interaction between Cascade crust and a dynamic mantle may have produced all of the following features:

(1) Extensive and voluminous tholeiitic eruptions in the early forearc.
(2) Sub-alkaline - calc-alkaline - alkaline compositional trends exhibited by volcanic products, west-to-east across the arc.
(3) A broad basaltic-andesitic-rhyolitic volcanic belt gradually replaced by a narrow High Cascade locus of basaltic volcanism.
(4) Compressional tectonics and uplift of the Western Cascades accompanied by tensional tectonics and subsidence of the High Cascades.
(5) Last equilibration of distinct magmas with separate mantle sources at shallow levels beneath the Cascade crust.
(6) Long-lived activity of isolated silicic volcanic centers, some of which persist for several million years.
(7) A narrow zone of geothermal gradients in the Western Cascades.
(8) Maintenance of mafic volcanism for 40 Ma while mantle heat was lost to the slab by conduction and to the crust by transfer of magma.
(9) Absence of deep-focus earthquakes.

Although volcanic activity in the central Cascades has been progressively restricted in distribution and intensity as the rate of subduction has decreased, generation of magma in the mantle, reorganization of stress in limited parts of the crust, and intermittent volcanism should continue as long as circulation is induced and maintained within the mantle wedge.

REFERENCES

Allen, J. C., A. L. Boettcher, and G. Marland, Amphibole in andesite and basalt: I. Stability as a function of T-P-fo_2, Am. Min., 60, 1069-1085, 1975.

Anderson, R. N., S. E. DeLong, and W. M. Schwarz, Dehydration, asthenospheric convection and seismicity in subduction zones, J. Geol., 88, 445-451, 1980.

Andrews, D. J. and N. H. Sleep, Numerical modelling of tectonic flow behind island arcs, Geophys. J. Royal Astr. Soc., 38, 237-251, 1974.

Armstrong, R. L., E. M. Taylor, P. O. Hales, and D. J. Parker, K-Ar dates for volcanic rocks, central Cascade Range of Oregon, Isochron/West, 13, 5-10, 1975.

Ashwill, M., Seven fossil floras in the rain shadow of the Cascade mountains, Oregon, Ore. Geol., 45, 107-111, 1983.

Avramenko, W., Volcanism and structure in the vicinity of Echo Mountain, central Oregon Cascade Range, M.S. thesis, Univ. of Oregon, Eugene, Oregon, 1-156, 1981.

Black, G. L., N. M. Woller, and M. Ferns, Geologic map of the Crescent Mountain area, Linn County, Oregon, Ore. Dept. Geol. Min. Industries Map GMS-47, 1987.

Blackwell, D. D., R. D. Bowen, D. A. Hull, J. Riccio, and J. L. Steele, Heat flow, arc volcanism, and subduction in northern Oregon, J. Geophys. Res., 87, 8735-8754, 1982.

Boettcher, A. L., The role of amphiboles and water in circum-Pacific volcanism, pp. 107-125 in Manghnani, M. H. and S. Akimoto, High pressure research: applications in geophysics, Academic Press, 642 p., 1977.

Burnham, C. W., Convergence and mineralization - is there a relation?, Geol. Soc. Am. Mem. 154, 761-768, 1981.

Cannon, D. M., The stratigraphy, geochemistry, and mineralogy of two ash-flow tuffs in the Deschutes Formation, central Oregon, M.S. thesis, Oregon State Univ., Corvallis, Oregon, 1-142, 1984.

Clark, J. G., Geology and petrology of South Sister volcano, High Cascade Range, Oregon, Ph.D. dissertation, Univ. Oregon, Eugene, Oregon, 1-235, 1983.

Connard, G., R. W. Couch, and M. Gemperle, Analysis of aeromagnetic measurements from the Cascade Range in central Oregon, Geophysics, 48, 376-390, 1983.

Conrey, R. M., Volcanic stratigraphy of the Deschutes Formation, Green Ridge to Fly Creek, north-central Oregon, M.S. thesis, Oregon State Univ., Corvallis, Oregon, 1-349, 1985.

Conrey, R. M., Mt. Jefferson area, Oregon High Cascade Range: A long-lived locus of andesitic and dacitic volcanism and plutonism, Geol. Soc. Am. Abs. with Programs, 20, A196, 1988.

Couch, R. W., G. S. Pitts, D. E. Braman, and M. Gemperle, Free-air gravity anomaly map and complete Bouguer gravity anomaly map, Cascade Mountain Range, northern Oregon, Ore. Dept. Geol. Min. Industries Map GMS-15, 1981.

Couch, R. W., G. S. Pitts, M. Gemperle, D. E. Braman, and C. A. Veen, Gravity anomalies in the Cascade Range in Oregon: Structural and thermal implications, Ore. Dept. Geol. Min. Industries, Open-File Report 0-82-9, 1-66, 1982a.

Couch, R. W., G. S. Pitts, M. Gemperle, C. A. Veen, and D. E. Braman, Residual gravity maps of the northern, central, and southern Cascade Range, Oregon, Ore. Dept. Geol. Min. Industries Map GMS-26, 1982b.

Dill, T. E., Stratigraphy of the Neogene volcanic rocks along the lower Metolius River, Jefferson County, Oregon, M.S. thesis,Oregon State Univ., Corvallis, Oregon, 1-345, 1988.

Duncan, R. A. and L. D. Kulm, Plate tectonic evolution of the Cascades arc-subduction complex, Decade of N. Am. Geology, Geol. Soc. Am., 1989 (in press).

Engebretson, D. C., A. Cox, and R. G. Gordon, Relative motions between oceanic and continental plates in the Pacific Basin, Geol. Soc. Am. Special Paper 206, 1-59, 1985.

Fiebelkorn, R. B., G. W. Walker, N. S. MacLeod, E. H. McKee, and J. G. Smith, Index to K-Ar age determinations for the state of Oregon, Isochron/West, 37, 3-60, 1982.

Flaherty, G. M., The Western Cascade - High Cascade transition in the McKenzie Bridge area, central Oregon Cascade Range, M.S. thesis, Univ. of Oregon, Eugene, Oregon, 1-178, 1981.

Foote, R. W. and R. W. Couch, Graben structure of the Cascade Range in Oregon, EOS, Trans. Am. Geophy. Union, 45, 887, 1983.

Fyfe, W. S. and A. R. McBirney, Subduction and the structure of andesitic volcanic belts, Am. Jour. Sci., 275-A, 285-297, 1975.

Gill, J. G., Orogenic andesites and plate tectonics, Springer-Verlag, New York, 390 pp., 1981.

Hales, P. O., Geology of the Green Ridge area, Whitewater River quadrangle, Oregon, M.S. thesis, Oregon State Univ., Corvallis, Oregon, 1-90, 1975.

Hayman, G. A., Geology of a part of the Eagle Butte and Gateway quadrangles, east of the Deschutes River, Jefferson County, Oregon, M.S. thesis, Oregon State Univ., Corvallis, Oregon, 1-97, 1983.

Hill, B. E., Petrology of the Bend pumice and Tumalo tuff, a Pleistocene Cascade eruption involving magma mixing, M.S. thesis, Oregon State Univ., Corvallis, Oregon, 1-101, 1985.

Hill, B. E., The Tumalo Volcanic Center: a large Pleistocene vent complex on the east flank of the Oregon central High Cascades, Geol. Soc. Am. Abs. with Programs, 20, 389, 1988.

Hughes, S. S., Petrochemical evolution of High Cascade volcanic rocks in the Three Sisters region, Oregon, Ph.D. dissertation, Oregon State Univ., Corvallis, Oregon, 1-199, 1982.

Hughes, S. S., and E. M. Taylor, Geochemistry, petrogenesis, and tectonic implications of central High Cascade mafic platform lavas, Geol. Soc. Am. Bull., 97, 1024-1036, 1986.

Hsui, A. T. and M. N. Toksoz, The evolution of thermal structures beneath a subduction zone, Tectonophysics, 60, 43-60, 1979.

Jay, J. B., The geology and stratigraphy of the Tertiary volcanic and volcaniclastic rocks, with special emphasis on the Deschutes Formation, from Lake Simtustus to Madras in central Oregon, M.S. thesis, Oregon State Univ., Corvallis, Oregon, 1-199, 1982.

Keach, R. W., Cenozoic active margin and shallow Cascades structure: COCORP results from western Oregon, M.S.thesis, Cornell Univ., Ithaca, N.Y., 1-51, 1986.

Leaver, D. S., W. D. Mooney, and W. M. Kohler, A seismic refraction study of the Oregon Cascades, J. Geophys. Res., 89, 3121-3134, 1984.

Lux, D. R., K-Ar and 40Ar-39Ar ages of mid-Tertiary volcanic rocks from the Western Cascade Range, Oregon, Isochron/West, 37, 3-60, 1982.

MacLeod, N. S. and P. D. Snavely, Jr., Volcanic and intrusive rocks of the central part of the Oregon Coast Range, Ore. Dept. Geol. Min. Industries Bull., 77, 47-74, 1973.

MacLeod, N. S. and D. R. Sherrod, Geologic evidence for a magma chamber beneath Newberry Volcano, Oregon, J. Geophys. Res., 93, 10067-10079, 1988.

Magill, J. and A. Cox, Tectonic rotation of the Oregon Western Cascades, Ore. Dept. Geol. Min. Industries Special Paper 10, 1-67, 1980.

Peck, D. L., A. B. Griggs, H. G. Schlicker, F. G. Wells, and H. M. Dole, Geology of the central and northern parts of the Western Cascade Range in Oregon, U.S. Geol. Survey Prof. Paper 499, 1-56, 1964.

Peterson, N. V., E. A. Groh, E. M. Taylor, and D. E. Stensland, Geology and mineral resources of Deschutes County, Oregon, Ore. Dept. Geol. Min. Industries Bull. 89, 1-66, 1976.

Pitts, S. and R. Couch, Complete Bouguer gravity anomaly map, Cascade Mountain Range, central Oregon, Ore. Dept. Geol. Min. Industries Map GMS-8, 1978.

Priest, G. R., G. L. Black, N. M. Woller, and E. M. Taylor, Geologic map of the McKenzie Bridge quadrangle, Lane County, Oregon, Ore. Dept. Geol. Min. Industries Map GMS-48, 1988.

Priest, G. R. and N. M. Woller, Geology of the Cougar Reservoir area, Lane County, Oregon in, Priest, G. R., and B. F. Vogt, eds., Geology and geothermal resources of the central Oregon Cascade Range, Ore. Dept. Geol. Min. Industries Special Paper 15, 39-48, 1983a.

Priest, G. R., N. M. Woller, G. L. Black, and S. H. Evans, Overview of the geology of the central Oregon Cascade Range, in, Priest, G. R. and B. F. Vogt, eds., Geology and geothermal resources of the central Oregon Cascade Range, Ore. Dept. Geol. Min. Industries Special Paper 15, 3-28, 1983b.

Priest, G. R., N. M. Woller, and M. L. Ferns, Geologic map of the Breitenbush River area, Linn and Marion Counties, Oregon, Ore. Dept. Geol. Min. Industries Map GMS-46, 1987.

Ringwood, A. E., Composition and petrology of the Earth's mantle, New York, McGraw-Hill, p. 295-297, 1975.

Robinson, P. T., High titania alkali-olivine basalt of north-central Oregon, U.S.A., Cont. Min. Petrol., 22, 349-360, 1969.

Robinson, P. T., G. M. Brem, and E. H. McKee, John Day Formation of Oregon: a distal record of early Cascade volcanism, Geology, 12, 229-232, 1984.

Sarna-Wojcicki, A. M., S. D. Morrison, C. E. Meyer, and J. W. Hillhouse, Correlation of upper Cenozoic tephra layers between sediments of the western United States and eastern Pacific Ocean and comparison with biostratigaphic and magnetostratigraphic age data, Geol. Soc. Am. Bull., 98, 207-223, 1987.

Scott, W. E., Holocene rhyodacite eruptions on the flanks of South Sister volcano, Oregon, Geol. Soc. Am. Special Paper 212, 35-53, 1987.

Sherrod, D. R., Geology, petrology, and volcanic history of a portion of the Cascade Range between latitudes 43-44 degrees N, central Oregon, U.S.A., Ph.D. dissertation, Univ. Calif., Santa Barbara, 1-320, 1986.

Simpson, R. W. and A. V. Cox, Paleomagnetic evidence for tectonic rotation of the Oregon Coast range, Geology, 5, 585-589, 1977.

Smith, G. A., Simtustus Formation: paleogeographic and stratigraphic significance of a newly defined Miocene unit in the Deschutes basin, central Oregon, Oregon Geology, 48, 63-72, 1986a.

Smith, G. A., Stratigraphy, sedimentology, and petrology of Neogene rocks in the Deschutes Basin, central Oregon: A record of continental-margin volcanism and its influence on fluvial sedimentation in an arc-adjacent basin, Ph.D. dissertation, Oregon State Univ., Corvallis, Oregon, 1-467, 1986b.

Smith, G. A., Geologic map of the Madras West and Madras East quadrangles, Jefferson County, Oregon, Ore. Dept. Geol. Min. Industries Map GMS-45, 1987a.

Smith, G. A., Geologic map of the Seekseequa Junction and a portion of the Metolius Bench quadrangles, Jefferson County, Oregon, Ore. Dept. Geol. Min. Industries Map GMS-44, 1987b.

Smith, G. A. and G. A. Hayman, Geologic map of the Eagle Butte and Gateway quadrangles, Jefferson and Wasco Counties, Oregon, Ore. Dept. Geol. Min. Industries Map GMS-43, 1987.

Smith, G. A., L. W. Snee, and E. M. Taylor, Stratigraphic, sedimentologic, and petrologic record of late Miocene subsidence of the central Oregon Cascades, Geology, 15, 389-392, 1987.

Snavely, P. D., Jr., H. C. Wagner, and D. L. Lander, Geologic cross-section of the central Oregon continental margin, Geol. Soc. Am. Map and Chart Series MC-28J, 1980.

Sutter, J. F., K/Ar ages of Cenozoic volcanic rocks from the Oregon Cascades west of 121 degrees, 30 minutes, Isochron/West, 21, 15-21, 1978.

Tatsumi, Y., D. L. Hamilton, and R. W. Nesbitt, Chemical characteristics of fluid phase released from a subducted lithosphere and origin of arc magmas: evidence from high-pressure experiments and natural rocks, Jour. Volc. Geotherm. Res., 29, 293-309, 1986.

Taylor, E. M., Field geology of the S.W. Broken Top quadrangle, Oregon, Ore. Dept. Geol. Min. Industries Special Paper 2, 1-50, 1978.

Taylor, E. M., High Cascade ash-flow tuffs and pumice deposits in the vicinity of Bend, Oregon, Geol. Soc. Am. Abs. with Programs, 12, 155, 1980.

Taylor, E. M., Central High Cascade roadside geology - Bend, Sisters, McKenzie Pass, and Santiam Pass, Oregon, in, Johnston, D. A. and J. Donnelly-Nolan, eds., Guides to some volcanic terranes in Washington, Idaho, Oregon, and northern California, U.S. Geol. Survey Circ. 838, 55-83, 1981.

Taylor, E. M., Field geology of the northwest quarter of the Broken Top 15-minute quadrangle, Oregon, Ore. Dept. Geol. Min. Industries Special Paper 21, 1-20, 1987.

Taylor, E. M., N. S. MacLeod, D. R. Sherrod, and G. W. Walker, Geologic map of the Three Sisters Wilderness, Deschutes, Lane, and Linn Counties, Oregon, U.S. Geol. Survey Map MF-1952, 1987.

Toksoz, M. N., J. W. Minear, and R. B. Julian, Temperature and geophysical effects of a downgoing slab, J. Geophy. Res., 76, 1113-1138, 1971.

Verplanck, E. P., Temporal variations in volume and geochemistry of volcanism in the Western Cascades, Oregon, M.S. thesis, Oregon State Univ., Corvallis, Oregon, 1-115, 1985.

Verplanck, E. P. and R. A. Duncan, Temporal variations in plate convergence and eruption rates in the Western Cascades, Oregon, Tectonics, 6, 197-209, 1987.

Wells, R. E., D. C. Engebretson, P. D. Snavely, Jr., and R. S. Coe, Cenozoic plate motions and the volcano-tectonic evolution of western Oregon and Washington, Tectonics, 3, 275-294, 1984.

Wendland, D. W., Castle Rocks: a late Miocene eruptive center at the north end of Green Ridge, Jefferson County, Oregon, M.S. thesis, Oregon State Univ., Corvallis, Oregon, 1-196, 1988.

Wozniak, K. C., Geology of the northern part of the southeast Three Sisters quadrangle, Oregon, M.S. thesis, Oregon State Univ., Corvallis, Oregon, 1-98, 1982.

Wyllie, J. P., Magmas and volatile components, Am. Mineral., 64, 469-500, 1979.

Wyllie, J. P. and T. Sekine, The formation of mantle phlogopite in subduction zone hybridization, Cont. Min. Petrol., 70, 375-380, 1982.

Yogodzinski, G. M., The Deschutes Formation - High Cascade transition in the Whitewater River area, Jefferson County, Oregon, M.S. thesis, Oregon State Univ., Corvallis, Oregon, 1-165, 1986.

MAFIC MAGMATISM AND ASSOCIATED TECTONISM OF THE CENTRAL HIGH CASCADE RANGE, OREGON

Scott S. Hughes

Departments of Chemistry and Geology and The Radiation Center, Oregon State University, Corvallis, OR 97331

Abstract. Volcanism in the central High Cascade Range has been dominated since late Miocene time by the construction of a mafic platform of coalescent shield volcanoes within an intra-arc graben that developed in response to extensional plate tectonics. Lithospheric extension along the central Cascade arc is attributed to a decrease in the convergence rate of the Farallon-North American plate system since early Tertiary time. Geochemical variations, compiled from new and existing data, are used to delineate four major categories of mafic magma which bear the chemical signatures of source regions: (1) early High Cascade basalts, (2) normal High Cascade basalts, (3) MW (Mount Washington) type basaltic andesites, and (4) NS (North Sister) type basaltic andesites. Chemical signatures argue strongly for the presence of initially depleted upper mantle beneath the central Cascades that has been subjected to variable enrichment processes. Enrichment of refractory elements is largely due to regional mantle metasomatism whereas increased abundances of volatile and other mobile elements is related to the injection of aqueous subduction-derived fluids. Early basalts, erupted on the east flank of the Cascade arc, retain much of the depleted refractory element signature and exhibit meager enrichment of mobile elements due to subduction processes. The depleted chemistries of these units suggests influence of asthenospheric mantle on source regions, possibly by upwelling into the above-slab region of magma genesis. Normal basalt chemistries indicate magma genesis from lower lithosphere which has been enriched in refractory elements by metasomatic processes although they exhibit little effect due to subduction enrichment. Both types of basaltic andesite exhibit similar enrichments in mobile alkali elements related to subduction zone processes, but NS types have a lower overall refractory element signature that is attributed to a lower degree of mantle metasomatism. The implication of initially depleted sources beneath the central Cascades is consistent with the existence of the Columbia Embayment into which a segment of oceanic lithosphere was compressed and thickened.

INTRODUCTION

Coalescent shield volcanoes and cinder cones comprise a roughly N-S trending mafic platform (Taylor, 1981; Hughes and Taylor, 1986) between ~43° and ~45° north latitude that covers older Cascade volcanics. Volcanism in this region has been volumetrically dominated by the eruption of diktytaxitic high-alumina basalt and pilotaxitic basaltic andesite lavas in a narrow belt along the Cascade crest. High Cascade platform lavas are largely restricted to an intra-arc graben ~30-50 km wide although some early units lie outside of fault boundaries. The occurrence of a mafic province within what is widely regarded as an orogenic calc-alkaline system provides an opportunity to examine an unusual tectono-magmatic episode.

Early stages of magmatic arcs are typically dominated by eruptions of high-alumina basalts that become secondary to andesitic magmatism during arc evolution (Miyashiro, 1974). Intermediate and silicic (dacite to rhyodacite) volcanics of the central High Cascades, being much less voluminous than the mafic lavas, are primarily localized in Quaternary stratovolcanoes or domes built upon the platform. Therefore, Pliocene to Holocene volcanic activity reflects a rejuvenation of primary basaltic magmatism within a magmatic arc that, since Eocene time, had been characterized by eruptions of calc-alkaline andesitic to rhyodacitic lavas and ash-flow tuffs. Multi-element analyses and petrochemical models of representative mafic platform rocks (47-62 wt. % SiO_2) allowed Hughes and Taylor (1986) to discriminate between normal basalts and two types of basaltic andesite. Their models revealed that High Cascade basaltic andesites are not derivatives of parental basalts, but that separate sources of primary magma are required. Moreover, the normal basalts display textural and chemical signatures appropriate to extension-related magmatism; whereas the basaltic andesites have attributes typical of convergent plate magmatism.

A combination of volumetric estimates with analytical data (White and McBirney, 1978) indicate that the ratio of calc-alkaline andesite to tholeiitic basalt is greater in the northern and southern extremities of the High Cascades (Washington and N. California) relative to the central part of the range. The chemical data also show that andesites in the central region are slightly less potassic and exhibit lower overall Rb enrichment. The distinctiveness of central High Cascade magmatism may be attributed to a different tectonic framework relative to that underlying the northern and southern segments. Pre-Tertiary continental crust is exposed in Washington, southern Oregon and northern California; however, the central Oregon Cascades are probably underlain by younger oceanic lithosphere (Hamilton and Myers, 1966).

Compositional variations in central Cascade mafic magmatism ostensibly depend on the nature of the lower lithosphere and the configuration of the subducted Juan de Fuca oceanic plate (e.g. Dickinson, 1979; Lipman, 1980). Chemical signatures of arc volcanics, especially of mafic lavas, depend greatly on the configuration and maturity of underlying crust (e.g. Leeman, 1983). This paper summarizes the development of the mafic platform and addresses its uniqueness in terms of geochemical variations and the tectonic elements required to satisfy constraints implied by petrochemical associations. New chemical data are presented which expand the fields of currently known mafic rock types and provide additional complexities toward understanding the identity of crust and mantle components beneath the central part of the Cascade magmatic arc.

EVOLUTION OF THE MAFIC PLATFORM

Early High Cascade Eruptions:

Extension-related mafic magmatism of the central High Cascades began in late Miocene time prior to graben development along the Cascade crest. Representative lavas of this period include late Miocene and early Pliocene mafic lavas (Armstrong *et al.* 1975; Sutter, 1978; Taylor, 1981) of the Outerson Formation on the west and equivalent age lavas and volcanic sediments of the Deschutes Formation (Smith, 1986; Smith *et al.* 1987) on the east.

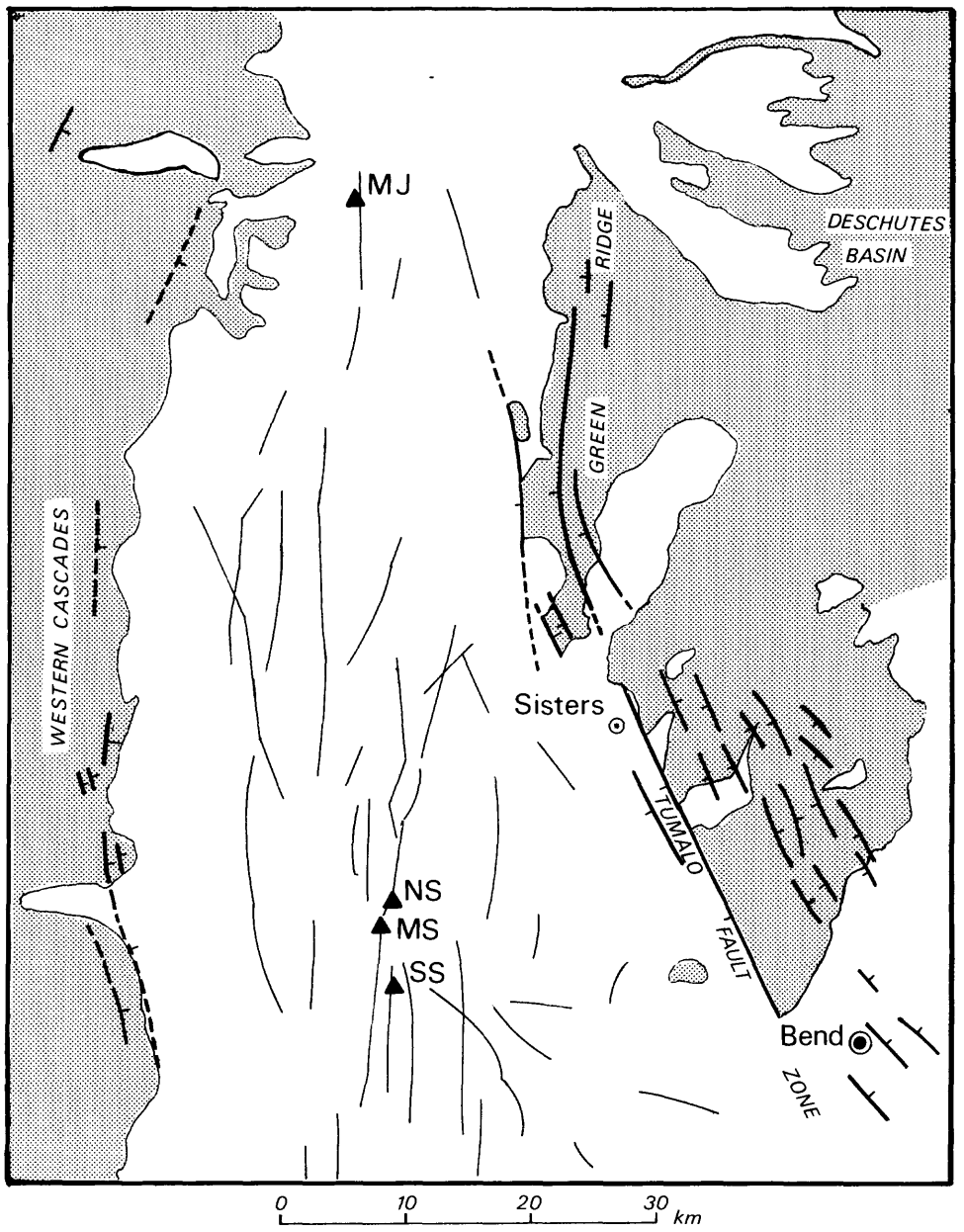

Figure 1. Generalized geologic map of the High Cascade mafic platform, central Cascade Range, Oregon (from Hughes and Taylor, 1986; Smith *et al.* 1987), which is dominated by basalt and basaltic andesite lavas. Shaded regions are mostly pre-Pliocene volcanics of the Outerson Formation (west side) and Deschutes Formation (east side) which bound the Pliocene-Holocene platform. Regions lying just to the east of Green Ridge and the Tumalo Fault Zone are covered by late Miocene to early Pliocene lavas of early High Cascade origin. Dark lines indicate known normal faults; lighter lines within the platform are faults inferred by vent alignments. Major composite volcanoes are: MJ = Mt. Jefferson, NS = North Sister, MS = Middle Sister, and SS = South Sister.

These units cover the latest stages of early Cascade (Western Cascades) arc magmatism, active since Eocene time, which culminated in the development of a substantial range of calc-alkaline volcanoes (Taylor, 1981). Subsidence along the crest of this range began during late Miocene (Smith *et al.* 1987) and caused the sources of Miocene-Pliocene (and older Cascades) volcanics to become buried under the High Cascade mafic platform.

Lavas of the upper Deschutes Formation can be traced to the escarpment of Green Ridge, a segment of the eastern fault boundary of the mafic platform, thereby indicating a High Cascade source for some lavas which flowed east into the Deschutes Basin (Taylor, 1981). K-Ar dates of the uppermost lavas of Green Ridge (Armstrong *et al.* 1975) indicated a maximum 4.5 Ma age of faulting. Correlation of a suite of lavas dated using the $^{40}Ar/^{39}Ar$ technique (Smith *et al.* 1987) suggests that the onset of major Cascade subsidence occurred earlier at 5.4 Ma and that early High Cascade volcanism was active by ~7.3 Ma.

Two flow sequences that erupted in early High Cascade time occur on the east flank of Green Ridge (Fig. 1) and include the Canadian Bench and Fly Lake basalts (e.g. Conrey, 1985; Dill, 1988). Smith (1986) encompasses these flows into the Lower Desert Basalt member of the upper Deschutes Formation which has some petrochemical affinity with mid-ocean ridge basalts (e.g. Smith *et al.* 1987). The Canadian Bench flow has an Ar-Ar date of 5.43 ± 0.05 Ma (Smith *et al.* 1987) and is more extensive than the younger Fly Lake basalt flow. Trace element analyses of samples from different segments of these units (Hughes *et al.* 1988) indicate derivation from a depleted mantle source and are included in this review as representatives of early High Cascade mafic magmatism.

Late High Cascade Eruptions:

Large volumes of late Pliocene high-alumina tholeiitic basalt erupted into the central Cascade graben during the initial stages of mafic platform construction. The dominance of early basalts (<~53 wt. % SiO_2) gradually yielded to basaltic andesites (~53-60 wt. % SiO_2) although both types are important in the growth of High Cascade shield volcanoes. Many eruptive centers were short-lived and produced only a few flows and/or a cinder cone, but several developed into large basaltic andesite composite volcanoes such as North Sister, Mount Washington and Three Fingered Jack (Taylor, 1968, 1981). The actual volume of mafic lavas which fill the central High Cascade depression is unknown; however, Taylor (1981) suggests that the aggregate thickness of overlapping basalts and basaltic andesites exceeds 1200 m in some areas. The earliest radiometric date obtained in the mafic platform is 3.9 Ma and the oldest exposed unit in the vicinity of Green Ridge is 2.5 Ma (Armstrong *et al.* 1975). Assuming that volcanic activity was essentially continuous since early High Cascade eruptions, a significant proportion of the mafic platform including the sources for early High Cascade and Deschutes Formation lavas lies buried beneath presently exposed layers (Taylor, 1981).

Although many early platform basalts are diktytaxitic, textural variations include porphyritic to subphyric units, which contain up to 20 volume percent euhedral olivine and ancillary plagioclase, and some later members that are intergranular, pilotaxitic, or intersertal. Groundmass mineralogies are invariably plagioclase, augite, olivine, titaniferous magnetite, and minor glass. Basaltic andesites have similar phenocryst and

groundmass mineralogies although liquidus plagioclase dominates olivine, and sparse microphenocrysts of hypersthene and augite occur in some units having relatively high SiO_2 contents. Euhedral olivines in basaltic andesites (Hughes and Taylor, 1986) have overall higher Mg/(Mg+Fe) ratios (Fo_{78}-Fo_{85}) relative to those in basalts (Fo_{74}-Fo_{80}). Similarly, the compositions of equilibrated plagioclases in basaltic andesites are more calcic (typically An_{85}) relative to plagioclase phenocrysts in basalts (An_{72}-An_{80}). The primitive mineralogy of many basaltic andesites is consistent with their eruption as near-primary magma derived from sources other than those required to produce the basalts. This disparity is evident in the chemical signatures (e.g. Taylor, 1978, 1987; Hughes and Taylor, 1986) of mafic platform rocks. Specifically, most High Cascade basaltic andesites have relatively low TiO_2 contents that are typical of magmas derived from subduction zones (Green, 1980). Conversely, High Cascade basalts have TiO_2 abundances greater than 1.2 wt.%, which is abnormal for convergent-plate magmatism, but more characteristic of continental rift and some oceanic systems (e.g. Basaltic Volcanism Study Project, 1981).

All major units in the High Cascades display fractionated rare earth elements (REE) and other incompatible element trends that suggest variably enriched source regions. On the basis of multi-element analyses, the basaltic andesites are divided (e.g. Hughes and Taylor, 1986) into two major categories: NS (North Sister) and MW (Mount Washington) types which have distinct ranges in REE. Compared to High Cascade basalts the NS basaltic andesites exhibit lower overall REE patterns; whereas the MW types yield patterns having similar heavy REE (Sm to Lu), but slightly higher light REE (La to Nd). Hughes and Taylor (1986) argue, on the basis of multi-element assessments and modeled source parameters, that at least three separate magmatic sources for basalts, NS basaltic andesites, and MW basaltic andesites are required. Also, some basalts have been analyzed which exhibit divergent chemical characteristics, largely in trace element signatures, which can be attributed to crustal contamination and/or magma mixing.

The trace element patterns of the above types are revised in the present study to include analyses of core samples from holes drilled by Union Oil Co. at two locations within the mafic platform as well as additional surface samples. Twelve samples, analyzed by INAA from a core taken at Abbott Butte (~5 km SE of Mt. Jefferson) in the depth interval 87-531 m (287-1741 ft), fall within the revised realm of normal basalts. Three samples from core taken at Devils Lake (~7 km south of S. Sister) in the interval 554-568 m (1819-1864 ft) were also analyzed; however, their chemical patterns do not allow placement into any of the known categories and are tentatively classified as divergent basalts. Several additional surface samples increased the data base for MW type basaltic andesites and normal basalts, while one additional surface sample increased the number of divergent basalt types to ten. Two samples originally assigned to the MW type (EM-92 and TFJ-436, Hughes and Taylor, 1986) have been reclassified into the normal basalt category. The current data base of major and trace element abundances of mafic rocks is used in this study to develop discriminant diagrams and to present arguments for tectonic arrangement of the central High Cascade Range.

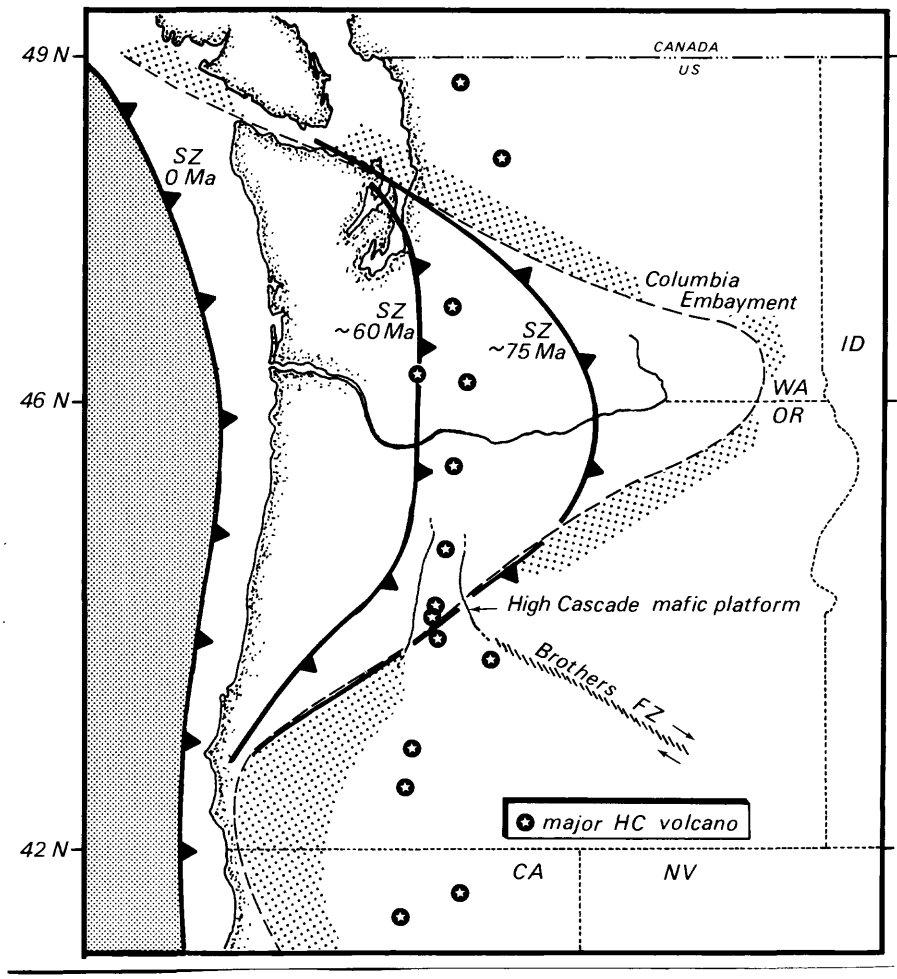

Figure 2. Tectonic map of the Pacific NW continental margin illustrating the position of the High Cascade mafic platform relative to the Columbia Embayment (from Hamilton and Myers, 1966 and Hammond, 1979). Regions inside the embayment are predominantly Tertiary volcanics (probably overlying oceanic crust) while outlying regions are comprised of pre-Tertiary continental crust. Extension in the Cascades is related to decreasing convergent rates and possibly to right-lateral motion along the Brothers Fault Zone. Inferred positions of the Farallon-North American plate convergent margin are adapted from Dickinson (1979) and the present position of the Juan de Fuca (Farallon remnant) plate margin is from Riddihough (1984).

Tectonic Framework and Structural Evolution:

Eruption of large volumes of mafic lava is atypical of mature calc-alkaline activity associated with a convergent plate system (Miyashiro, 1974). An extensional regime is thus evident in the mafic character of the platform, graben formation (Smith and Taylor, 1983), and the presence of numerous north-south vent alignments within the platform (Fig. 1). Transformation to extensional tectonics which is responsible for the abrupt reduction in calc-alkaline volcanism, allowed tapping of deeper, more mafic, source regions that had not experienced significant crustal involvement (Hughes and Taylor, 1986). Rifting along the Cascade crest is therefore considered to be a response by crust which had been thermally weakened during previous calc-alkaline magmatism to a relaxation in the compressional regime. Wells *et al.* (1984) correlate changes in volcanism within the Cascades and adjacent regions with a significant decrease in the convergent rate of the Farallon-North American plate system between 43 and 28 Ma. Their model of Cenozoic plate motions suggests that this decline was responsible for (among other manifestations)

extension in the Cascade arc and voluminous extension-related volcanism over a large back-arc region. A study of magnetic anomalies in the Juan de Fuca plate system (remnant of the Farallon plate) by Riddihough (1984) indicate a more recent overall reduction in the convergence rate from 7 Ma to the present. Riddihough argues that extension is related to a rotational plate system in which slower velocities are attained when younger and more bouyant plate segments are overidden. Correlation by Verplanck and Duncan (1987) of K-Ar age determinations on volcanics from the central Western Cascades with volumetric estimates indicate a five-fold decrease (16.0 to 3.2 cm/a) in the convergence rate and a decreasing angle of convergence since ~35 Ma.

Additional complexities are manifested in the possible intersection of the Brothers Fault Zone (e.g. Lawrence, 1976; Walker and Nolf, 1981) with the mafic platform as expressed in the trends of the Green Ridge and Tumalo Fault systems (Fig. 1). These latter fault zones, defining the eastern boundary of the graben, produce a bend in the eastern edge of the mafic platform away from the N-S Cascade trend. Right-lateral motion along the Brothers Fault Zone (Fig. 2) conceivably contributed in part to the extension along the Cascade crest such that crustal movements were accommodated by the Tumalo and Green Ridge fault systems.

A regional tectonic element which influenced central High Cascade magmatism (Fig. 2) is expressed as the Columbia embayment (e.g. Carey, 1958; Hamilton and Myers, 1966; Hammond, 1979), an area probably representing a segment of crust comprised of young Tertiary volcanics surrounded by known pre-Tertiary continental crust. Existence of younger material within the embayment is consistent with geophysical observations (Cantwell *et al.* 1965; Cantwell and Orange, 1965), and the arrangement of pre-Tertiary and older rock outcrops (Hamilton and Myers, 1966). These observations are supported by the higher proportion of mafic volcanics and low incompatible element abundances of volcanics in the central part of the Cascades relative to the northern and southern extremities (White and McBirney, 1978). Lead isotopic studies of sulfide minerals by Church *et al.* (1986) further suggest that the central Cascades are underlain by Tertiary volcanic crust. However, their assessment supports a considerably smaller region such that the northern margin roughly coincides with the Oregon-Washington border and they suggest that the region be renamed the Oregon embayment.

Westward displacement of the Tertiary subduction margin, depicted in the inferred positions (Fig. 2) of Cretaceous to Holocene plate margins (Dickinson, 1979), is consistent with the position of the Columbia embayment. The tectonic model of Cascade evolution developed by Hammond (1979) suggests that Tertiary oceanic crust, accreted and trapped within the embayment, has been compressed and thickened during regional right-lateral distortion. Oceanward retreat of the subduction margin since Cretaceous time was apparently accelerated by the constriction of oceanic lithosphere within the embayment. These relations argue strongly for the presence, beneath the central Cascade Range, of potential primary magma sources having oceanic chemical signatures. Central High Cascade mafic magmatism is, very likely, the result of primary magma genesis in oceanic lithosphere.

similarities in La/Yb ratios, the segregation of the NSBA field due to lower Yb does not support NSBA source derivation from other High Cascade sources. The overall lower REE signature in NS basaltic andesites and in low-La basalts is, therefore, attributed to less enrichment of refractory elements during regional chemical evolution of the lower lithosphere. Petrochemical similarity between MW basaltic andesites and normal basalts is further evident in variations of a compatible element Sc relative to marginally compatible Yb (Fig. 3E) and Hf (Fig. 3F). Relative abundances of compatible elements will remain nearly constant in liquids derived over a wide range in the amount of partial melting from sources having equivalent initial compositions. The overlap in Sc, Yb and Hf abundances in MWBA and normal basalts illustrates additional evidence that the non-mobile refractory element compositions of the sources for these two groups are roughly equivalent to each other, yet distinct from the sources required to produce the NSBA magmas.

Chemical Signatures of Source Regions:

Enrichment of mobile elements due to fluids derived in the subduction zone have contributed to the petrochemical segregation between basaltic andesites and basalts. Moreover, the occurrence of basaltic magmas such as the Lower Desert members which are relatively depleted in refractory elements (Figs. 3A-3F), indicates the presence of lithospheric mantle that has experienced long-term depletion by previous melting events (Hughes *et al.* 1988). Depleted mantle under the Cascade Range likely has the same chemical characteristics as sources for MORB as evident from the positions of average N-MORB (Wood *et al.* 1979a,b; Sun *et al.* 1979) in Fig. 3. Enrichment of refractory elements in the sources for normal basalts and basaltic andesites (Hughes and Taylor, 1986) requires addition of components during processes of liquid scavenging, zone refining or other mechanisms of mantle metasomatism (Menzies, 1983) which involve magmatic fluids. Such components could also be derived by low degrees of melting from garnet-bearing mantle or an eclogitic subducted slab during calc-alkaline magmatism.

Chemical variations shown in Fig. 3 suggest that magmatic source regions beneath the central Cascades experienced long term depletion as characteristic of oceanic lithosphere, but that many source regions were subsequently enriched during (1) metasomatic evolution of the lower lithosphere and/or (2) input from aqueous fluids derived from the subduction zone. Behavior of an element involved in these two processes depend on ionic potential (Z/r, Z = ionic charge and r = ionic radius) as well as incompatibility (with respect to source mineral phases) in magmatic processes (Pearce, 1983). Besides the enrichment of alkali elements due to mobilization in aqueous solutions, the highly incompatible element Th, and to a lesser extent light REE, will also be enhanced during subduction zone processes. By contrast, Nb and Ta have very high ionic potentials and are excluded from aqueous fluid enrichments, but are commonly enriched during metasomatic processes not involving subduction zone fluids.

Enrichment processes in High Cascade magmas are exemplified (Fig. 4) by variations of Th/Yb vs. Ta/Yb (e.g. Pearce, 1982, 1983) which yield separate trends for basaltic andesites and normal basalts. The positions of Lower Desert basalts on the trend of normal basalts suggests a continuum of lithospheric enrichment due to within-plate processes, such as regional mantle

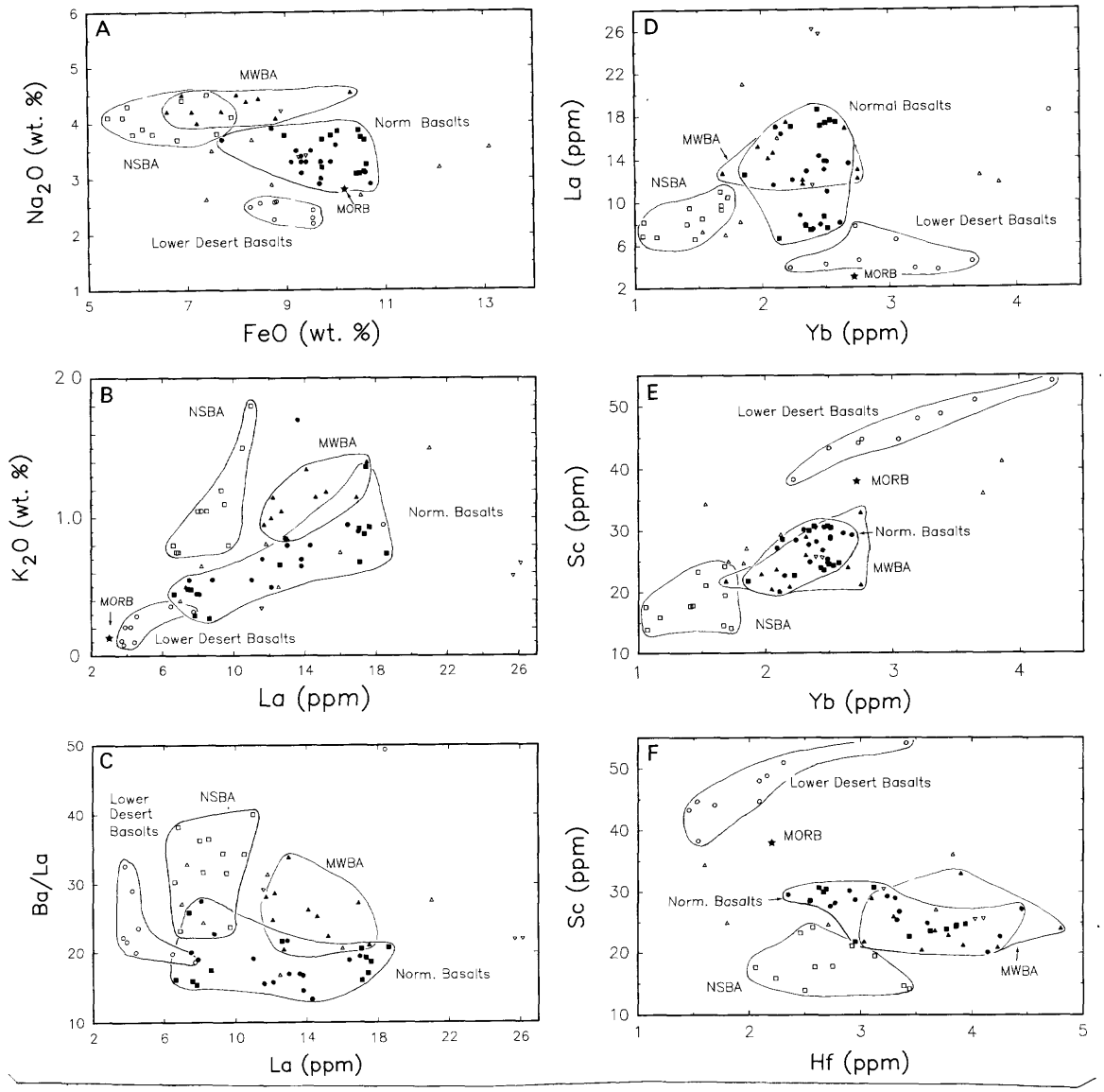

Figure 3. Chemical variation diagrams for Lower Desert basalts (open circles), normal High Cascade basalts (filled circles = surface samples; filled squares = drill core samples from Abbott Butte), MW-type basaltic andesites (filled triangles), NS-type basaltic andesites (open squares), and divergent basalt types (open triangles = surface samples; open inverted triangles = drill core samples from Devils Lake). The outlined fields represent variations in source regions due to (1) regional mantle metasomatism, and (2) influence of subduction-derived aqueous fluids. Normal mid-ocean ridge basalt data are from Wood *et al.* (1979a,b) and Sun *et al.* (1979).

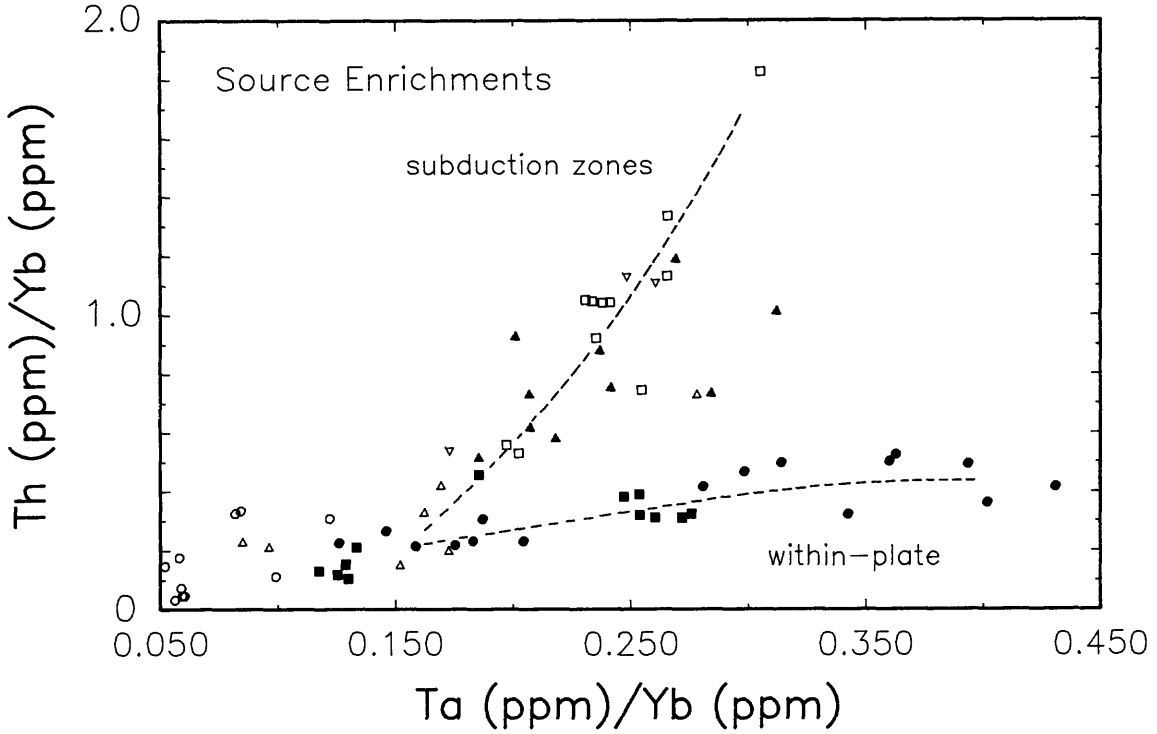

Figure 4. Variations in Th/Yb vs. Ta/Yb (adapted from Pearce, 1982, 1983) illustrate lithospheric enrichment processes due to regional metasomatism exemplified by the within-plate trend and by subduction-derived fluids shown by the trend for basaltic andesites. Symbols are the same as in Fig. 3.

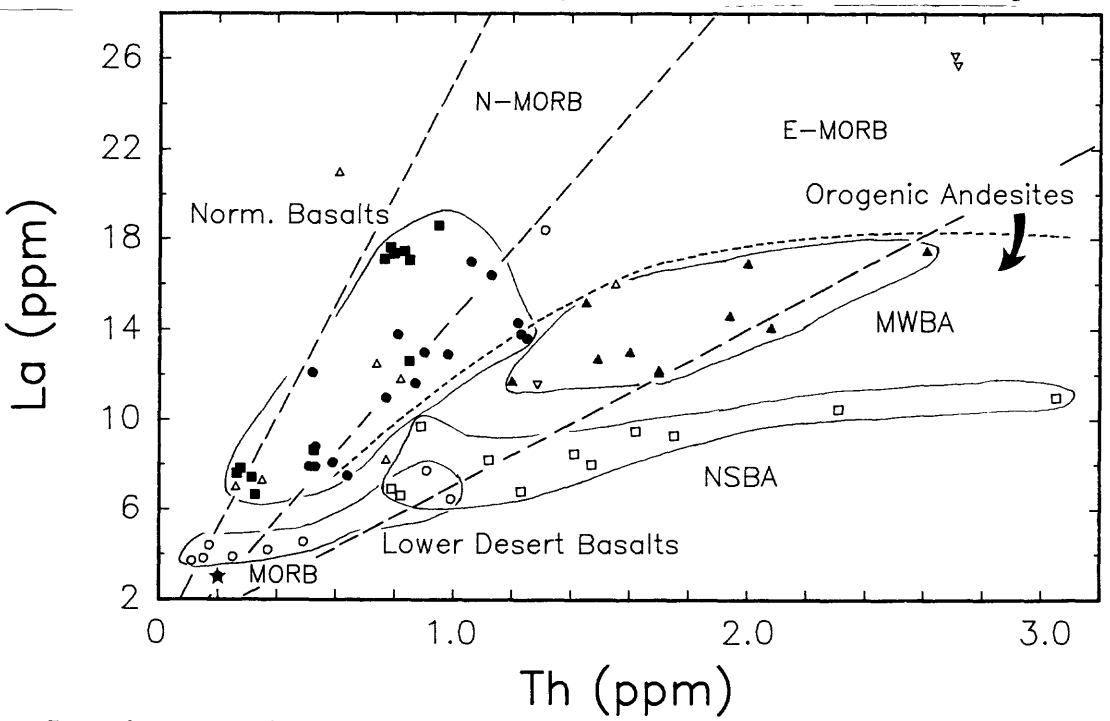

Figure 5. La vs. Th signatures of mantle source regions (boundaries from Gill, 1981) indicate the derivation of early Lower Desert and normal basalts from depleted N-MORB type lithosphere although minor orogenic enrichment is observed in some of these units. Basaltic andesite lie exclusively within the region of calc-alkaline andesites illustrating the imprint of subduction enrichment processes.

GEOCHEMICAL SYSTEMATICS

Discrimination of Chemical Types:

Relative abundances of incompatible trace elements within basaltic suites are important indicators of source composition primarily because overall variations are often too large to be related to simple mineral fractionation or to variable degrees of melting from a common source. This is especially true in provinces where influences due to crustal contamination are believed to be minor. Isotopic Pb and Sr signatures (e.g. Hedge *et al.* 1970; Peterman *et al.* 1970; Church and Tilton, 1973) suggest that most High Cascade magmas are essentially unaffected by contamination due to older evolved crustal components and support the concept that chemical variations are primarily source-derived. Separate magmatic sources for High Cascade basalts, NS and MW basaltic andesites (NSBA and MWBA), and Lower Desert basalts are evident in variation diagrams (Fig. 3); however, the outlined fields are subject to revision as the chemical data base is expanded.

Although basaltic andesites typically have more primitive mineralogies relative to normal basalts, they have higher alkali element abundances as depicted by variations in Na_2O and K_2O (Figs. 3A and 3B). A rough negative correlation between Na_2O and FeO is apparent, yet at equal FeO abundances overlapping NSBA and MWBA fields are clearly higher in Na_2O contents. Similar relations are apparent in K_2O variation with La, but the basaltic andesite fields are separated by notable differences in La. These two diagrams exemplify the tendency for basaltic andesites to be equally enriched in alkali elements regardless of differences in bulk chemistry and refractory trace elements. Moreover, the normal basalt field in Fig. 3B portrays a 3X variation in La contents with the implication of possibly three subsets having La = 6-9, 11-15, and 16-20 ppm. Lower Desert basalts, depleted in alkali elements and refractory incompatible elements, may be derived from sources having close chemical affinities to depleted sources of normal mid-ocean ridge basalts (MORB).

Pearce (1983) argues that, due to low ionic potentials, the elements K, Rb, Ba and Sr will become highly mobile in H_2O-rich liquids. The mobility and incompatible behavior of these elements, especially Ba, causes them to become enriched in magmas generated above subduction zones. Subduction zone enrichment of mobile elements in basaltic andesites relative to basalts is supported by variations in Ba/La ratios compared to La abundances (Fig. 3C). It is apparent from this diagram that basalt magmas were generated from sources which experienced less input from subduction-derived fluids. By contrast, fluid enrichment is portrayed by variable Ba/La ratios in the Lower Desert basalt field, implying that a subduction component has partially overprinted the original chemical character of the source region for these units.

Separation of basalts into low-, intermediate- and high-La groups in Fig. 3C might also justify a scenario in which NSBA and MWBA sources are derived by subduction zone enrichment of separate low-La and intermediate-La basaltic sources. Additional chemical data might support this scenario and lead to the delineation of two MWBA subsets. REE variations (Fig. 3D) indicate that NSBA units are petrochemically distinct from a common field of basalts and MWBA. Although both types of basaltic andesite exhibit

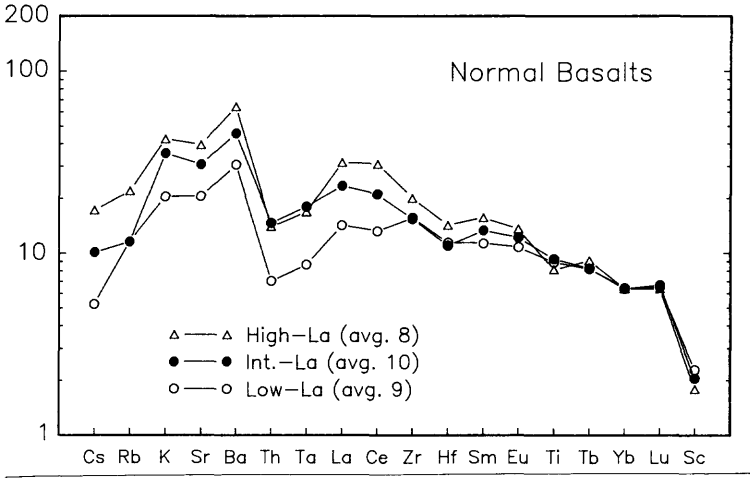

Figure 6. Multi-element diagrams of average low-, intermediate-, and high-La High Cascade normal basalts normalized to primordial mantle abundances (Taylor and McLennan, 1985). The spread in elements Cs to Ce reflect variable source enrichment due to regional mantle metasomatism.

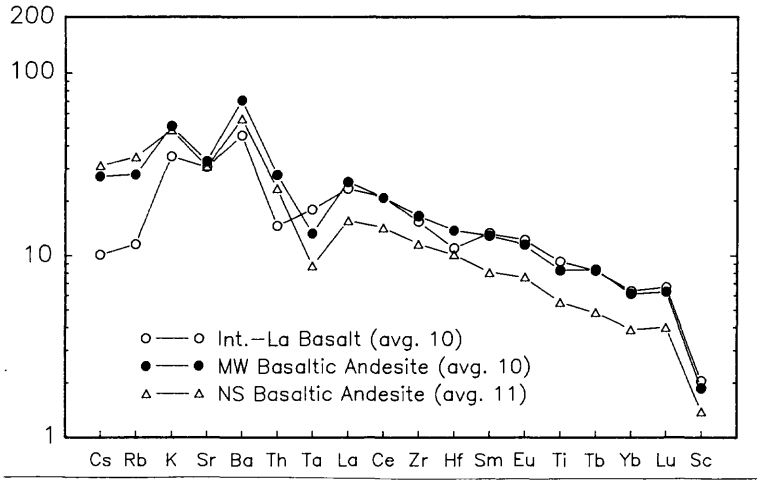

Figure 7. Multi-element diagrams of High Cascade NS and MW type basaltic andesites compared to that of normal basalts (same parameters as Fig. 6). Lower overall refractory elements (Ta to Sc) in NS types reflect less metasomatic source enrichment while the similarities in mobile element patterns (Cs to Th) between NS and MW types reflect subduction-derived processes.

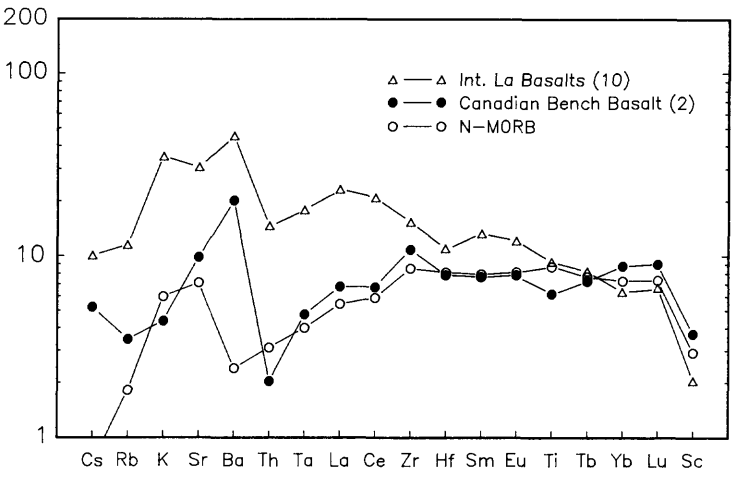

Figure 8. Multi-element of Canadian Bench basalts (average of two low-Th analyses) relative to mid-ocean ridge basalts and High Cascade normal basalts (same parameters as Fig. 6). MORB data are from Wood *et al.* (1979 a,b) and Sun *et al.* (1979). Similarities in refractory element patterns between MORB and the Canadian Bench lavas reflect derivation of early High Cascade mafic magmas from depleted oceanic lithosphere.

metasomatism. Chemical signatures of High Cascade source regions, summarized in Fig. 5 (e.g. Gill, 1981, p. 134), indicate N-MORB-like sources for basalts and typically orogenic sources for basaltic andesites. Minor enrichment due to subduction zone processes is evident for normal basalts and some Lower Desert basalts (Fly Lake member), but the overall signature of all High Cascade basalts is due to the presence of oceanic lithosphere beneath the central High Cascades.

Average multi-element abundances (Figs. 6-8) normalized to primordial mantle abundances (Taylor and McLennan, 1985) illustrate overall variations as well as similarities among central High Cascade mafic rocks. The average patterns for low-, intermediate-, and high-La normal basalts (Fig. 6) indicate a 3-5X variation in incompatible element abundances (Cs to Ce) in contrast to nearly equal heavy REE, Ti and Sc. Although this spread may be partly related to variable degrees of partial melting, the wide range is probably more indicative of variable source modification. Using the intermediate-La basalt pattern for reference, average basaltic andesite patterns (Fig. 7) reiterate the overall similarity in refractory elements between normal basalts and MW basaltic andesites as well as the overall lower signature of NS basaltic andesites. The difference between subduction zone and metasomatic enrichment is evident in (1) nearly identical mobile element patterns (Cs to Th) for basaltic andesites relative to systematic differences in the refractory elements, and (2) a crossover pattern of the Th-Ta signature between basaltic andesites and normal basalts. With the exception of some highly mobile elements, the pattern of the Canadian Bench Basalt member of the Lower Desert basalts (Fig. 8) indicates a stong chemical affinity for N-MORB sources. Refractory element abundances in these units have not been affected by metasomatic enrichments and therefore retain the signature of depleted oceanic lithosphere. Most likely, the relative proportion of unmetasomatized lower lithosphere within the Columbia Embayment has diminished throughout the Tertiary period.

SUMMARY

Mafic magmatism has predominated in the central High Cascade Range since late Miocene time due to a change from compressional to extensional tectonism. Crustal extension allowed tapping of deeper mafic magmas which ascended without significant crustal contamination or differentiation. The change in tectonic style is attributed to a decrease in the rate of Farallon-North American plate convergence since early Tertiary time which allowed a relaxation in the compressional regime. Subsidence of the Cascade crest into an intra-arc graben during late Miocene time was probably facilitated by failure of crust thermally weakened by previous calc-alkaline magmatism. Some of the extension in the central Cascade Range might have been taken up by right-lateral movement along the Brothers Fault Zone. Basalt and basaltic andesite lavas have, since late Pliocene time, constructed a mafic platform of coalescent shield volcanoes and mafic composite cones within the graben. Less voluminous silicic eruptions contributed to the growth of several large stratovolcanoes and smaller rhyodacitic domes.

Geochemical variations in central High Cascade mafic rocks require the presence of at least four separate magmatic source regions. Refractory trace element signatures of basalts (SiO_2 < ~53 wt.%) have close affinities to non-subduction related sources and infer the presence of oceanic lithosphere

beneath the central Cascade Range. Early central High Cascade basalts yield trace element signatures having affinities to N-type MORB sources in oceanic lithosphere, while later basalts were derived from metasomatized oceanic lithosphere. Volatile and other mobile trace element signatures of basaltic andesites (~53 - 60 wt.% SiO_2) are consistent with evolution and enrichment due to subduction zone processes. A weaker imprint of subduction-derived aqueous fluids is also evident in the mobile element signatures of some basalts. Overall chemical variations further suggest that, aside from volatile element enrichments, MW basaltic andesites were generated as primary magma from lithospheric sources similar to that which produced the normal basalts, and that NS basaltic andesites were generated from separate sources that had experienced a lesser amount of metasomatic enrichment.

Geochemical data for High Cascade mafic units argue strongly for the presence of oceanic lithosphere within the Columbia Embayment although this segment has most likely been compressed and thickened. The successive development of mafic magma sources suggests that the original depleted lithosphere trapped within the embayment has experienced a series of variable enrichments due to (1) regional metasomatism and (2) aqueous fluids derived from the subduction zone. These processes and the resultant chemical signatures in mafic volcanics provide implications for the early developmental stages of continental lithosphere.

Acknowledgements

Support for analytical work was provided by grants for reactor time and analytical facilities at the Oregon State University Radiation Center. The author also expresses gratitude to the O.S.U. TRIGA Reactor crew for assistance in neutron activations and to S.K. Vetter, U. of S. Carolina, for providing additional data. Manuscript preparation was supported by NASA Grant NAG9-63 to R. A. Schmitt. Drill core samples were obtained with the assistance of G. R. Priest and G. L. Black through the courtesy of Oregon Department of Geology and Mineral Industries. This paper benefitted from numerous field excursions and lengthy discussions of High Cascade volcanism with E. M. Taylor.

REFERENCES

Armstrong, R.L., E.M. Taylor, P.O. Hales, and D.J. Parker, K-Ar dates for volcanic rocks, central Cascade Range of Oregon, *Isochron/West*, no. 13, 5-10, 1975.

Basaltic Volcanism Study Project, Basaltic volcanism on the terrestrial planets, New York, Pergamon Press, 1286 p., 1981.

Carey, S.W., The tectonic approach to continental drift, in S.W. Carey, ed., *Continental drift--a symposium*, Hobart, Australia, University of Tasmania, 177-355, 1958.

Cantwell, T., P. Nelson, J. Webb, and A.S. Orange, Deep resistivity measurements in the Pacific Northwest, *J. Geophysical Res.*, 70, no. 8, 1931-1937, 1965.

Cantwell, T., and A. Orange, Further deep resistivity measurements in the Pacific Northwest, *J. Geophysical Res.*, 70, no. 16, 4068-4072, 1965.

Church, S.E., and G.R. Tilton, Lead and strontium isotopic studies in the Cascade mountains: bearing on andesite genesis, *Geol. Soc. Am. Bull.*, 84, 431-454, 1973.

Church, S.E., A.P. LeHuray, A.R. Grant, M.H. Delevaux, and J.E. Gray, Lead-isotopic data from sulfide minerals from the Cascade Range, Oregon and Washington, *Geochim. Cosmochim. Acta*, 50, 317-328, 1986.

Conrey, R.M., Volcanic stratigraphy of the Deschutes Formation, Green Ridge to Fly Creek, north-central Oregon (M.S. thesis), Oregon State University, Corvallis, 349 p., 1985.

Dickinson, W.R., Cenozoic plate tectonic setting of the Cordilleran region in the United States, in J.M. Armentrout, M.R. Cole, and H. Terbest, Jr., eds., *Cenozoic Paleogeography of the Western United States*, Pacific Coast Paleogeography Symposium, 3, 1-13, 1979.

Dill, T.E., Stratigraphy of the Neogene volcanic rocks along the lower Metolius River, Jefferson County, Oregon (M.S. thesis), Oregon State University, Corvallis, 345 p., 1988.

Gill, J.B., Orogenic Andesites and Plate Tectonics, New York, Springer-Verlag, 390 p., 1981.

Green, T.H., Island-arc and continent-building magmatism--a review of petrogenic models based on experimental petrology and geochemistry, *Tectonophysics*, 63, 367-385, 1980.

Hamilton, W., and W.B. Myers, Cenozoic tectonics of the western United States, *Reviews of Geophysics*, 4, no. 4, 509-549, 1966.

Hammond, P.E., A Tectonic model for evolution of the Cascade Range, in J.M. Armentrout, M.R. Cole, and H. Terbest, Jr., eds., *Cenozoic Paleogeography of the Western United States*, Pacific Coast Paleogeography Symposium, 3, 219-237, 1979.

Hedge, C.E., R.A. Hildreth, and W.T. Henderson, Strontium isotopes in some Cenozoic lavas from Oregon and Washington, *Earth Planet. Sci. Lett.*, 8, 434-438, 1970.

Hughes S.S. and E.M. Taylor, Geochemistry, petrogenesis, and tectonic implications of central High Cascade mafic plarform lavas, *Geol. Soc. Am. Bull.*, 97, 1024-1036, 1986.

Hughes, S.S., E.M. Taylor, and Y.B. Dong, Geochemistry of early High Cascade basalts indicates depleted mantle signature, *EOS, Transactions of the American Geophysical Union*, 69, no. 44, p. 1494, 1988.

Lawrence, R.D., Strike-slip faulting terminates the Basin and Range province in Oregon, *Geol. Soc. Am. Bull.*, 87, 846-850, 1976.

Leeman, W.P., The influence of crustal structure on composition of subduction-related magma, *Jour. Volc. Geoth. Res.*, 18, 561-588, 1983.

Lipman, P.W., Cenozoic volcanism in the western United States: Implications for continental tectonics, in B.C. Burchfiel, J.E. Oliver, and L.T. Silver, co-Chmn., *Continental Tectonics*, Washington, D.C., National Academy of Sciences, 161-174, 1980.

Menzies, M., Mantle ultramafic xenoliths in alkaline magmas: Evidence for mantle heterogeneity modified by magmatic activity, in C.J. Hawkesworth and M.J. Norrey, eds., *Continental basalts and mantle xenoliths*, Cheshire, U.K., Shiva Publications, Ltd., 92-110, 1983.

Miyashiro, A., Volcanic rock series in island arcs and active continental margins, *Am. Jour. Sci.*, 274, 321-355, 1974.

Pearce, J.A., Trace element characteristics of lavas from destructive plate boundaries, in R.S. Thorpe, ed., *Andesites: orogenic andesites and related rocks*, New York, J. Wiley and Sons, 525-547, 1982.

_____, Role of the sub-continental lithosphere in magma genesis at active continental margins, in C.J. Hawkesworth and M.J. Norrey, eds., *Continental basalts and mantle xenoliths*, Cheshire, U.K., Shiva Publications, Ltd., 230-249, 1983.

Peterman, Z.E., I.S.E. Carmichael, A.L. Smith, $^{87}Sr/^{86}Sr$ ratios of Quaternary lavas of the Cascade Range, Northern California, *Geol. Soc. Am. Bull.*, 81, 311-318, 1970.

Riddihough R., Recent movements of the Juan de Fuca plate system, *J. Geophysical Res.*, 89, no. B8, 6980-6994, 1984.

Smith, G.A. and E.M. Taylor, The central Oregon High Cascade graben: What? Where? When?, Trans. Geotherm. Res. Council, 7, 275-279, 1983.

Smith, G.A., Stratigraphy, sedimentology, and petrology of Neogene rocks in the Deschutes basin, central Oregon: A record of continental-margin volcanism and its influence on fluvial sedimentation in a arc-adjacent basin (Ph.D. thesis), Oregon State University, Corvallis, 467 p., 1986.

Smith, G.A., L.W. Snee, and E.M. Taylor, Stratigraphic sedimentologic, and petrologic record of late Miocene subsidence of the central Oregon High Cascades, *Geology*, 15, no. 5, 389-392, 1987.

Sun, S.-S., R.W. Nesbit, and A.Y. Sharaskin, Geochemical characteristics of mid-ocean ridge basalts, *Earth Planet. Sci. Lett.*, 44, 119-138, 1979.

Sutter, J.F., K-Ar ages of Cenozoic volcanic rocks from the Oregon Cascades west of 121°30′, *Isochron/West*, no. 21, 15-21, 1978.

Taylor E.M., Field geology of S.W. Broken Top Quadrangle, Oregon, *Ore. Dept. Geol. Min. Ind.*, Spec. Paper 2, 50 p., 1978.

_____, Central High Cascade roadside geology: Bend, Sisters, McKenzie Pass, and Santiam Pass, Oregon, in D.A. Johnston and J. Donnelly-Nolan, eds., *Guides to some Volcanic Terranes in Washington, Idaho, Oregon, and Northern California*, U.S. Geol. Surv. Circular 838, 59-83, 1981.

_____, Field geology of the northwest quarter of the Broken Top 15′ Quadrangle, Deschutes County, Oregon, *Ore. Dept. Geol. Min. Ind.*, Spec. Paper 21, 20 p., 1987

Taylor, S.R., and S. McLennan, *The Continental Crust: its composition and evolution*, London, Blackwell Scientific Publications, 312 p., 1985.

Verplanck, E.P., and R.A. Duncan, Temporal variations in plate convergence and eruption rates in the Western Cascades, Oregon, *Tectonics*, 6, no. 2, 197-209, 1987.

Walker, G.W., and B. Nolf, High lava plains, Brothers Fault Zone to Harney Basin, Oregon, in D.A. Johnston and J. Donnelly-Nolan, eds., *Guides to some Volcanic Terranes in Washington, Idaho, Oregon, and Northern California*, U.S. Geol. Surv. Circular 838, 105-118, 1981.

Wells, R.E., D.C. Engebretson, P.D. Snavely, Jr., and R.S. Coe, Cenozoic plate motions and the volcano-tectonic evolution of western Oregon and Washington, *Tectonics*, 3, no. 2, 275-294, 1984.

White, C.M. and A.R. McBirney, Some quantitative aspects of orogenic volcanism in the Oregon Cascades, in R.B. Smith and G.P. Eaton, eds., *Cenozoic tectonics and regional geophysics of the western Cordillera*, Geol. Soc. Am. Memoir 152, 369-388, 1978.

Wood, D.A., J.-L. Joron, M. Treuil, M. Norry, and J. Tarney, Elemental and Sr isotope variations in basic lavas from Iceland and the surrounding ocean floor, *Contrib. Mineral. Petrol.*, 70, 319-339, 1979a.

Wood, D.A., J.-L. Joron, and M. Treuil, A re-appraisal of the use of trace elements to classify and discriminate between magma series erupted in different tectonic settings, *Earth Planet. Sci. Lett.*, 45, 326-336, 1979b.

AN ISOSTATIC MODEL FOR BASIN FORMATION IN AND ADJACENT TO THE CENTRAL OREGON HIGH CASCADE RANGE

Gary A. Smith
Department of Geology
University of New Mexico
Albuquerque, NM 87131

Kirk R. Vincent
Department of Geosciences
University of Arizona
Tucson, AZ 85721

Lawrence W. Snee
U.S. Geological Survey
Box 25046, MS 905
Federal Center
Denver, CO, 80225.

ABSTRACT

The late Miocene subsidence history of the Deschutes basin, adjacent to the Oregon High Cascade Range, implies a coupling of basin development with the volcanic and tectonic history of the Cascade arc. Subsidence was temporally greatest during periods of inferred higher extrusion rates and spatially greatest adjacent to that segment of the arc in which the largest volume of magma was erupted. Basin subsidence ended, and may have been followed by uplift, when the adjacent Cascades collapsed into an intra-arc graben. These relationships suggest that basin subsidence, and subsequent uplift, were caused by flexural loading of elastic lithosphere by the growing, and then collapsing, Cascade arc. Quantitative models, though necessarily generalized and only partly constrained by geologic data, indicate that flexural isostasy can realistically account for the depth and width of the Deschutes basin. This study suggests that flexural deformation associated with growth of the volcanic chain, a long recognized phenomenon for trough-and-arch bathymmetry adjacent to the Hawaiian Islands, is applicable to continental-margin arcs. The scale of the deflection (maximum ~1 km) is small, however, compared to other rapid vertical movements associated with active tectonic margins.

INTRODUCTION

Cenozoic terrestrial volcaniclastic strata derived from the Cascade Range, in the northwestern United States, were deposited in two types of basins. The first type is arc-adjacent basins, located both trenchward and cratonward of the arc, with varying tectonic styles and dimensions (Smith, 1985). The most conspicuous of these basins are shallow (150 to 300 m deep) and were filled with aprons of coarse-grained volcaniclastic and volcanic rocks with wedge-shaped cross-sections that thin away from the Cascades (Smith, 1987c). Thicker (> 1 km) accumulations of volcanic and volcaniclastic material accumulated within subsiding intra-arc basins along the axis of the range (Smith, 1987c; Smith et al., 1987). This paper describes the subsidence history for adjacent basins of each type, the Deschutes basin and central Oregon High Cascade graben, and proposes a model for their development.

GEOLOGIC SETTING

The Deschutes basin lies immediately east of the High Cascade Range in central Oregon (Fig. 1). The outline of the basin is marked by the distribution of the upper Miocene to lower Pliocene Deschutes Formation, a sequence of volcanic and volcaniclastic lithologies that thicken toward the Cascades, thin toward the east and north, and are buried beneath younger lavas to the south. The western margin of the Deschutes Formation is marked, in part, by a north-south trending zone of normal faults. The Green Ridge fault scarp (Fig. 1) faces away from the Deschutes basin and marks the eastern margin of the central Oregon High Cascade graben, an intra-arc basin that formed in the latest Miocene and early Pliocene (Taylor, 1981; Smith and Taylor, 1983; Smith et al., 1987). Ancestral High Cascade volcanoes that were the source for Deschutes Formation volcanics and sediments subsided into this graben and were subsequently buried. Subsidence along the axis of the range appears to diminish northward and well-defined graben-bounding faults are restricted to the latitude where the most voluminous volcanics were erupted both immediately before and subsequent to the initiation of graben subsidence (Smith et al., 1987). Rapid subsidence along the east side of the graben near Green Ridge began at about 5.4 Ma and produced a very abrupt stratigraphic break in the Deschutes basin above which there are virtually no Cascade-derived volcanics or eruption-related sedimentary facies because the basin became structurally isolated from its principal source of volcanic and sedimentary fill (Smith et al., 1987).

Volcanic and volcaniclastic rocks correlative to the Deschutes Formation occur along the western margin of the High Cascade graben (Fig. 1; Priest et al., 1987, 1988; Black et al., 1987). Most of the preserved late Miocene volcanics and virtually all occurrences of late Miocene volcaniclastic sediments in the western Cascades occur south of the latitude of Mount Jefferson. Subsidence along the Horse Creek fault zone (Fig. 1) probably started at about 5.5 Ma (Priest et al., 1988) and is, therefore, close to being synchronous with development of the Green Ridge fault zone. Mapping along both sides of the graben (Conrey, 1985; Priest et al., 1987, 1988; Black et al., 1987) and a COCORP seismic reflection profile (Keach, 1986) suggest that the graben in this region may consist of two asymmetric segments. The Green Ridge faults may represent major subsidence facing an east-sloping ramp and the Horse Creek faults may be the major zone of displacement facing a west-sloping ramp (Fig. 1).

An unknown thickness of Pliocene-Pleistocene sediments and volcanics have accumulated within the High Cascade graben and gravity data (Couch et al., 1982) imply the occurrence of about 1 km of volcaniclastic basin-fill adjacent to the base of the Green Ridge fault scarp. Scattered outcrops of Pliocene volcaniclastic sediments, including lacustrine facies, cap fault blocks on the lower east face of Green Ridge and occur on the adjacent valley floor (Smith, 1986). The 610-m deep UNOCAL Abbott Butte 82-3 hole, drilled 6.5 km west of Green Ridge,

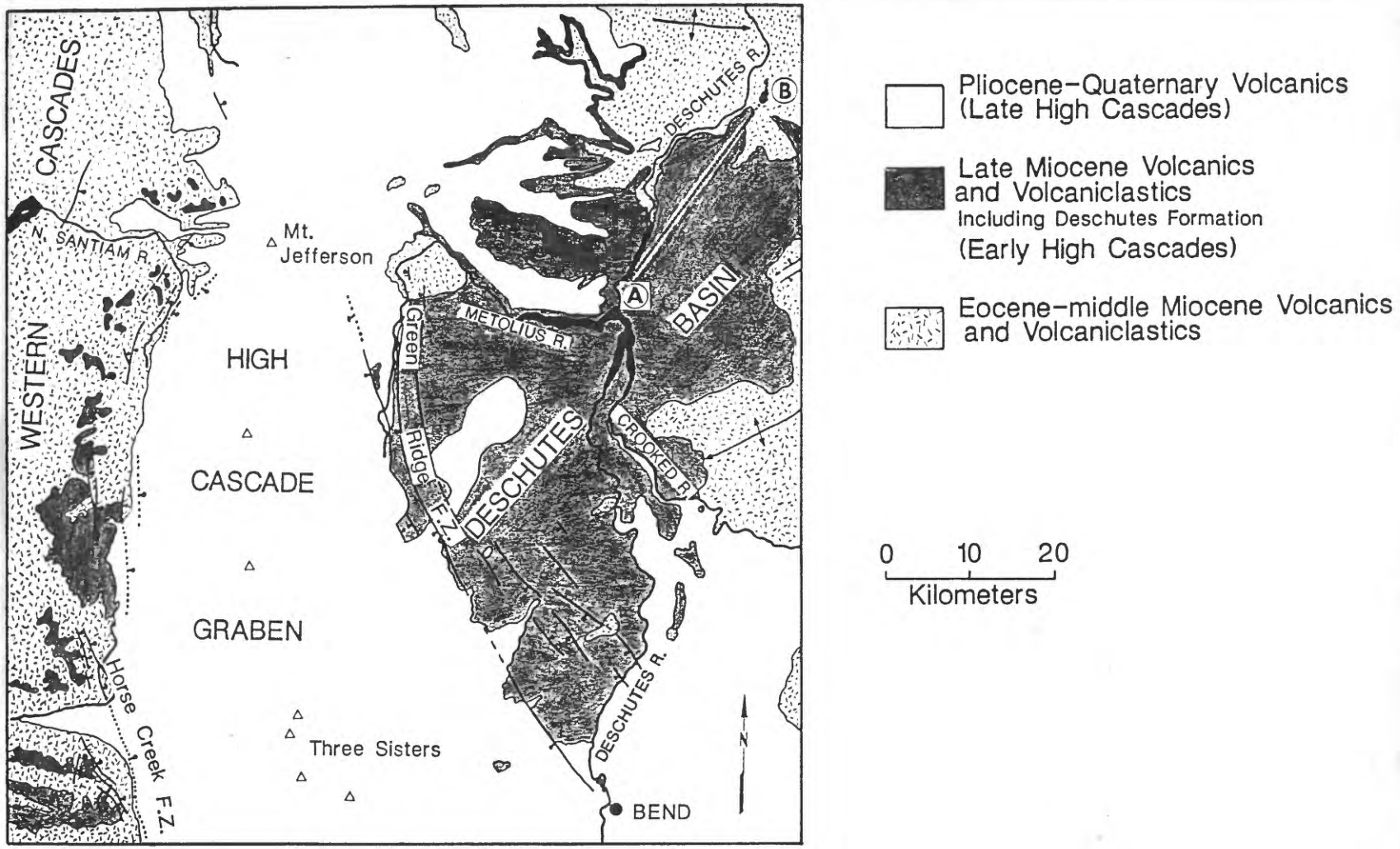

Figure 1. Simplified geologic map of the central Oregon Cascade Range and Deschutes basin (modified from Smith et al., 1987; Priest et al., 1987, 1988; Black et al., 1987; White, 1980).

encountered a total of 210 m of volcaniclastic material, mostly of sedimentary character. Pliocene diatoms occur to a depth of more than 500 m (J.P. Bradbury, person. commun., 1988). Correlative volcaniclastic sediments also crop out at the base of the topographic and structural highlands along the west side of the graben (Black et al., 1987; Priest et al., 1988).

DEPOSITIONAL HISTORY OF THE DESCHUTES FORMATION

The sedimentology of the Deschutes Formation is presented in detail by Smith (1987d), and only those aspects critical to the analysis of this paper are presented here. Near the center of the basin, the Deschutes Formation rests unconformably on middle Miocene strata. To the north and east, the Deschutes Formation onlaps a variety of lower and middle Tertiary units that were previously faulted and folded along primarily east-west and northeast-southwest trends. It is notable that the Deschutes depositional basin is elongated north-south, parallel to the Cascades, and does not appear to be influenced by these other structures. Onset of Deschutes deposition is constrained to be younger than 9 Ma by the occurrence of Hemphillian vertebrates within a few meters of the base of the formation. A 7.42 $\pm$0.22 Ma basalt flow occurs about 30 m above the base.

The bulk of the Deschutes Formation was emplaced on an east-sloping alluvial plain that merged with a north-flowing river, just east of the present Deschutes and Crooked Rivers. Figure 2 illustrates a cumulative stratigraphic accumulation curve composited from measured sections at the toe of the alluvial plain, near the modern confluence of the Deschutes and Crooked Rivers (Fig. 1). Volcanic lithologies comprise about 15 % of this section and are included with the sediments in the accumulation curve. The data points are $^{40}Ar/^{39}Ar$ plateau ages for lava flows within the sediment-dominated sequence (Smith et al., 1987; Snee et al., in prep.).

The accumulation curve consists of three segments. The first segment represents an early period of very low net aggradation rate. The line is not well constrained on the left end, but deposition began before 7.42 $\pm$0.22 Ma. The beginning point of about 8.2 Ma is based on extrapolation of the subsidence curve, to be explained below, with the assumption that the onset of aggradation and subsidence are synchronous. This relatively thin basal interval of the Deschutes Formation contains very few intercalated volcanic units and consists of both eruption-induced flood and debris-flow facies (Smith, 1987d) and normal fluvial conglomerates. The occurrence of both syneruption and inter-eruption facies suggests that subsidence was occurring at a sufficient rate to accomodate the influx of volcaniclastic debris on the aggrading alluvial plain (Smith and Vincent, 1987).

The second, steep segment of the curve is well-constrained by dated basalt flows that enclose a stratigraphic interval of different character. Within this interval there are more than 100 Cascade-derived ignimbrites and countless lava flows exposed within the Deschutes basin, thus recording a period of voluminous volcanism. Nearly all of these volcanic units are

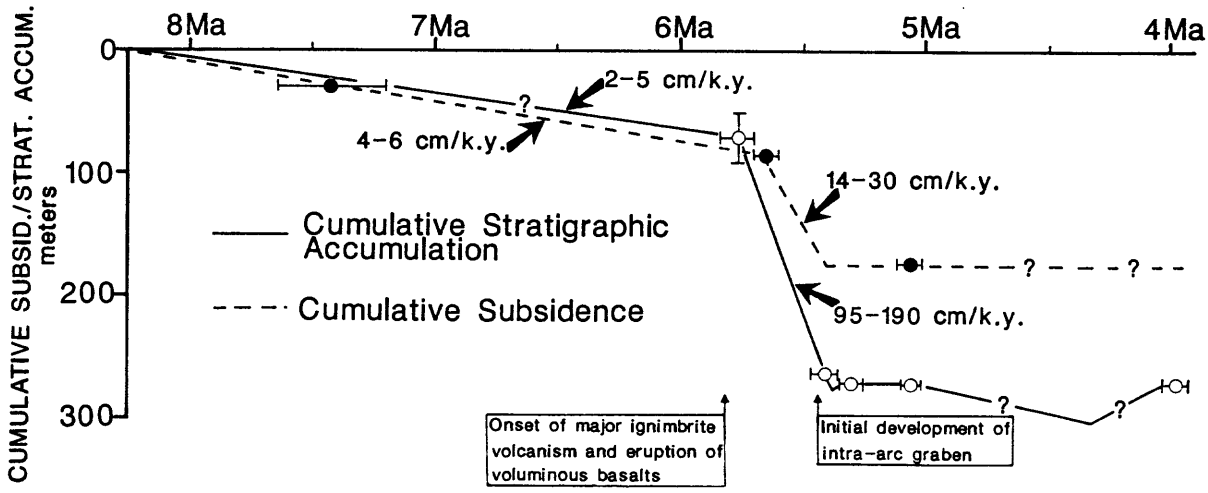

Figure 2. Cumulative stratigraphic accumulation and subsidence curves for the Deschutes basin. Subsidence curve relfects relative subsidence between points A and B on Figure 1. Calculated rates consider all uncertainities in stratigraphic position, age, and alternative intepretations of the relative subsidence curve as constrained by data points.

located at, or south of, the latitude of Green Ridge (Smith, 1986; Smith et al., 1987). Sedimentologically, this interval consists almost entirely of sequences of eruption-related flood and debris-flow deposits, separated by erosion surfaces with as much as 60 m of relief. Normal fluvial facies are very rare and generally restricted to thin units, 1- to 3-m thick, at the bases of paleochannels incised into syneruption sequences. This facies architecture suggests that the basin was aggrading faster than subsidence could provide accomodation space (Smith and Vincent, 1987). Deposition was largely restricted to times when streams were choked with eruption-produced pyroclastic debris, and inter-eruption periods were marked by incision. The change in facies architecture and the increased accumulation rate are responses to the observed increase in large-volume extrusion events in the Cascades.

The third segment of the curve records very minor net sediment accumulation. The change in slope of the curve at about 5.4 Ma occurs at the above noted stratigraphic break that marks the development of the intra-arc graben. The greatly diminished accumulation rate reflects the isolation of the basin from lavas and pyroclastic flows erupted along the Cascade axis and from large sediment influx of pyroclastic material stripped from the steep, proximal slopes of the volcanic chain. Sedimentologically, the diminished accumulation rate is recorded by a sequence of superimposed paleosols (Smith, 1987d; Smith et al., 1987). Dated basalt flows that were erupted from vents within the basin between 5.3 and 4.0 Ma occur at similar elevations, where they fill valleys, but are locally separated by a few tens of meters of sediment. These relationships suggest cut-and-fill episodes with little net change in base level and account for the

opposing slopes of line segments on the accumulation curve (Fig. 2).

In summary, the stratigraphic accumulation curve is consistent with observed sedimentological and stratigraphic relationships. Three distinct depositional intervals are recorded: 1) an early period of slow sedimentation, probably related to continuous base-level rise, 2) an intermediate period of short duration in which most of the Deschutes Formation was deposited in response to voluminous extrusions in the Cascades that provided copius quantities of pyroclastic material to the basin in an episodic fashion, and 3) a final period of essentially no net aggradation, during which there were periods of incision, that reflects structurally induced starvation of the basin.

SUBSIDENCE HISTORY OF THE DESCHUTES BASIN

Also illustrated on Figure 2 is a cumulative relative subsidence curve. Because there is no accurate way to account for changing paleotopography during Deschutes Formation deposition it is not possible to construct a subsidence curve like those resulting from geohistory analysis of primarily marine basins where analogous estimates of changing paleobathymetry can be made. The curve shown on Figure 2 shows relative subsidence between two points (A and B on Figure 1) and is less than total basin subsidence.

The relative subsidence curve was constructed from consideration of back-tilted paleoriver profiles. Points A and B (Fig. 1) locate vertical sections that expose sediments deposited by the axial river in the Deschutes basin. Within these sections are lava flows and ignimbrites that filled and preserved the geometry of this axial paleochannel, which was displaced to a new course following each valley-filling event. Although sediment composition, facies patterns, and paleocurrent data indicate that this drainage flowed northeastward (Smith, 1986, 1987d), elevations of the bases of volcanic channel-filling units obtained from measured sections (Smith, 1986) and during mapping (Smith, 1987a,b; Smith and Hayman, 1987) indicate that the preserved paleochannels are inclined very gently to the southwest with upstream inclinations that diminish upsection (Fig. 3). An extensive 5.31 $\pm$0.05 Ma basalt (Tetherow Butte basalt member) near the top of the section does slope northeastward with an inclination similar to the modern river gradient. Similar observations can be made along the east-flowing Metolius River canyon (Fig. 1) where Cascade-derived lava flows intercalated with boulder conglomerates low in the Deschutes Formation section are horizontal or inclined slightly westward, whereas those higher in the section dip eastward at 1^{o} to 4^{o} (Dill, 1988). These relationships indicate deformation during Deschutes Formation deposition, which can be assumed to represent differential subsidence with absolute subsidence increasing to the southwest and west, the directions in which the formation thickens.

To calculate a relative subsidence curve, it was assumed that the Tetherow Butte basalt, by virtue of its northeastward dip, is essentially undeformed and records the gradient of the

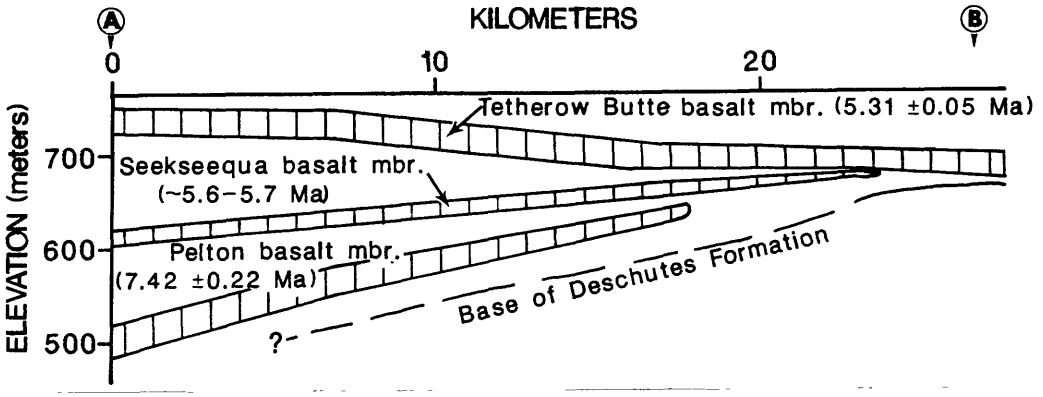

Figure 3. Profile A-B (see Fig. 1) illustrating increasing southwestward dip of lower stratigraphic horizons in the Deschutes Formation. Basalt flows filled an ancestral Deschutes River channel that sloped northeastward.

ancestral Deschutes River. Backtilted profiles were sequentially restored to this gradient to obtain a measure of relative subsidence. Compaction was ignorred because the section is thin (about 280 m), has never been buried beneath younger units, and consists, in part, of essentially uncompactable lava flows and welded ignimbrites. Four profiles were used for the calculations. The first is the base of the basal conglomerate of the Deschutes Formation. The second is the base of the 7.42 $\pm$0.22 Ma Pelton basalt member near the base of the formation. The third datum is the Seekseequa basalt member that has not been directly dated by isotopic methods, but whose age is constrained within the range shown by the error bars in Figure 2 by stratigraphic relationships to dated units and comparison of magnetic polarity (determined in the field by fluxgate magnetometer) with the anomaly timescale of Harrison et al.(1979). The fourth datum is the nontilted Tetherow Butte basalt flow (5.31 $\pm$0.05 Ma) near the top of the section. The first datum, the base of the formation, is not directly dated, but must be defined in order to determine the position of the dated units. The base is plotted at about 8.2 Ma by extrapolating the slope between the data points for the Pelton and Seekseequa basalts to also include the thin (~30 m) of section below the Pelton basalt (Fig. 2), and is consistent with paleontological age constraints.

The cumulative relative subsidence curve, like the sediment accumulation curve, consists of three segments that we assume to represent the late Miocene and earliest Pliocene subsidence history of the Deschutes basin (Fig. 2). The geometric relationships shown in Figure 3 require a three-stage subsidence history. We emphasize, however, that the amount of subsidence shown in each of the first two segments of the subsidence curve in Figure 2 may be in eroor by as much as 30 m because of the assumptions used in reconstructing the backtitlted paleodrainages. The first segment records a period of slow subsidence. The relative subsidence rate is very similar to the sedimentation rate and supports the interpretation, presented above, that the rates of sedimentation and base-level rise (i.e., subsi-

dence) were subequal during this period.

The second, steeper segment is not precisely constrained. Subsidence must, however, have ended prior to 5.31 Ma, the age of the untilted Tetherow Butte basalt flow. This period of more rapid subsidence cannot have begun before extrusion of the Seekseequa basalt because there are no lacustrine facies to indicate a period of subsidence in excess of sediment accumulation. Therefore, this segment of the subsidence curve is roughly synchronous with the steep segment of the sediment accumulation curve and corresponds to the period of voluminous extrusion in the Cascades immediately prior to the climax of intra-arc basin development. The lower slope of the subsidence curve, compared to the the sediment accumulation curve, is consistent with the previous interpretation, based on facies architecture, that sediment was accumulating episodically at a faster rate than subsidence.

The third segment of the curve is shown as flat because of the initial assumption that the Tetherow Butte basalt is untilted, which requires no net subsidence after some time shortly before 5.31 Ma. Periods of incision, indicated by line segments with negative slopes on the stratigraphic accumulation curve, may be associated with uplift.

THE PROBLEM

Quantitative analysis of sedimentation and subsidence utilizing geochronologic data aids and corroborates interpretations based on qualitative sedimentologic and stratigraphic observations in the field. The segmented nature of the sediment accumulation curve (Fig. 2) is consistent with field observations of facies type and architecture and emphasizes the importance of volcanism, to produce large volumes of sediment, and tectonism, to determine the site of deposition, in the overall history of Deschutes Formation deposition.

The segmented nature of the subsidence curve is not as easily explained by field relationships. Although the data do not uniquely constrain the cumulative subsidence curve to the shape shown in Figure 2, the geometric relationships illustrated in Figure 3 do require an increasing rate of subsidence during deposition until abrupt cessation of subsidence at about 5.4 Ma. The increase in subsidence rate appears to correlate to an increase in the extrusion of large-volume volcanic units within the Cascades. The end of basin subsidence appears to correlate with the rapid development of fault scarps along the east side of the intra-arc graben. What caused the subsidence history of the Deschutes basin to be yoked to volcanic and tectonic processes within the adjacent Cascade Range?

THE HYPOTHESIS

We propose that subsidence of the Deschutes basin was caused by loading of the lithosphere, principally by the growing Cascade volcanic chain, and secondarily by the Deschutes Formation, itself. The load was isostatically compensated by the flexural strength of an elastic lithosphere.

The role of flexural loading as a contributor to the subsidence of passive-margin sedimentary prisms and as the principal cause of subsidence in foreland basins is now widely accepted (e.g, Steckler and Watts, 1978; Beaumont, 1981; Jordan, 1981). The response of lithosphere to the load imposed by a growing volcanic arc may be envisioned as similar to the sigmoidal deflection of the lithosphere observed beneath and adjacent to thrust sheets. In a qualitative sense, the hypothetical load-deformation produced by the Cascade Range should resemble the long-recognized (Menard, 1964) deep trough and adjacent low arch that parallel the Hawaiian-Emperor seamount chain and are a reflection of the flexural load placed upon Pacific Basin oceanic lithosphere by the mass of the volcanoes (Watts, 1978).

A flexural-loading origin for the Deschutes basin explains several, otherwise puzzling, field relationships. The structural setting of the Deschutes basin is ambiguous; depositional patterns do not indicate any influence from structures exposed in older rocks at the basin margins and there are no known syn-depositional faults or folds other than the faults that define the adjacent intra-arc graben. The general trend of the basin is north-south, parallel to the load imposed on the lithosphere by the Cascades, and at an angle to other regional structures. Thickness patterns and the southwestward, rather than westard, tilt of units in Figure 3 suggests greater subsidence at, and south of, the latitude of Green Ridge than in the northern part of the basin. This is consistent with field relationships (Smith, 1986; Smith et al., 1987) indicating a much lower volume of late Miocene to Recent extrusive activity, and hence a smaller flexural load, north of the end of Green Ridge than to the south.

The flexural-load hypothesis also explains the shape of the subsidence curve (Fig. 2). Assuming an elastic lithosphere, flexure-induced subsidence rate should be proportional to the extrusion rate of volcanics in the arc; hence subsidence rate in the Deschutes basin increases when a large increase in voluminous ignimbrites and lava flows is recognized in the basin-fill stratigraphy. Basin subsidence is replaced with flexural rebound when the intra-arc graben forms because the Green Ridge fault zone represents a vertical boundary across which the bending moment and vertical shear forces are not transmitted. As long as that vertical boundary exists, the lithospheric load of the arc is isostatically compensated only over the cross-section of the graben.

THE MODEL

To test the hypothesis stated above, a quantitative model of the deflection produced by an infinite line load on a continuous elastic plate was constructed with the aid of a computer program developed by Dr. Clement Chase of the University of Arizona. The formulation follows elastic thin-plate theory of Hetenyi (1946), in which two-dimensional loads are imposed upon a lithosphere of laterally invariant elastic thickness and flexural rigidity. The resulting flexure is calculated along a profile perpendicular to the long axis of the load. The axis of

the line load was placed at the present axis of the High Cascade Range. For the model, the shape and mass distribution of the line load was assumed to be symmetrically distributed on either side of the load axis. On the accompanying diagrams, however, only the east half of the load and the resulting lithospheric deflection is portrayed. This allows for more convenient comparison to observed dimensional parameters in the Deschutes basin. We recognize that the symmetrical mirror image of the load shown in Figure 4 does not adequately describe the geology of the western Cascades. Application of the flexural-load concept to the western Cascades will be discussed at a later point in this paper.

The generalized cross-sectional shape for the eastern half of the lithospheric load is shown in Figure 4. The shape of the load east of Green Ridge is based on the observed morphology of the Deschutes Formation. Farther west the ancestral High Cascades are assumed to have had dimensions similar to the modern volcanic chain. The load was further generalized as blocks of fixed density. The density values were determined with reference to the known distribution of rock types in the Deschutes Formation and the Bouger gravity anomaly models of Couch et al. (1982) and Couch and Foote (1983, and unpub. data). Our model included consideration of a pre-Deschutes Formation load, shown in the unshaded lowere part of Figure 4, which is poorly constrained because the distribution of pre-8.0 Ma rocks over most of this section is essentially unknown. Furthermore, pre-late Miocene volcanism is inferred to have been centered in the western Cascades. The pre-8.0 Ma load cannot, therefore, be considered as symmetrical about a load axis coincident with the High Cascade volcanic axis. The high degreee of uncertainity in modeling the pre-7.5 Ma load does not, however, effect the shape of the flexural-load deflection associated with growth of the ancestral High Cascades.

Additional parameters had to be assumed in order to calculate the shape of the deflection produced by the modeled load. A mantle density of 3300 kg/m^3 and a Poisson's ratio of 0.250 were assumed for all calculations. Selected values of Young's modulus range from 50 to 90 Gpa. Values for elastic thickness, ranging from 10 km to 50 km, resulted in calculated flexural rigidity values between 6.2×10^{22} and 7.8×10^{23} Nm. Figure 5 illustrates the shape of the load-induced deflection for various values of elastic thickness.

Principal weaknesses of the model are related primarily to and a lack of consideration of lateral changes in elastic thickness and flexural rigidity and secondarily to generalizations of the geometry of the load. Also, to meet geologic restrictions the line load cannot have an infinite length as assumed by the model. The stratigraphic record of early High Cascades volcanism preserved within the Deschutes basin suggests less voluminous volcanism north of Mount Jefferson (Smith, 1986; Smith et al,m 1987). Notably, the Deschutes Formation also thins northward in the basin. These observations support the flexural loading hypothesis and the relationship between volume of extrusions in the Cascades and subsidence in the Deschutes basin and would explain why the direction of syndepositional

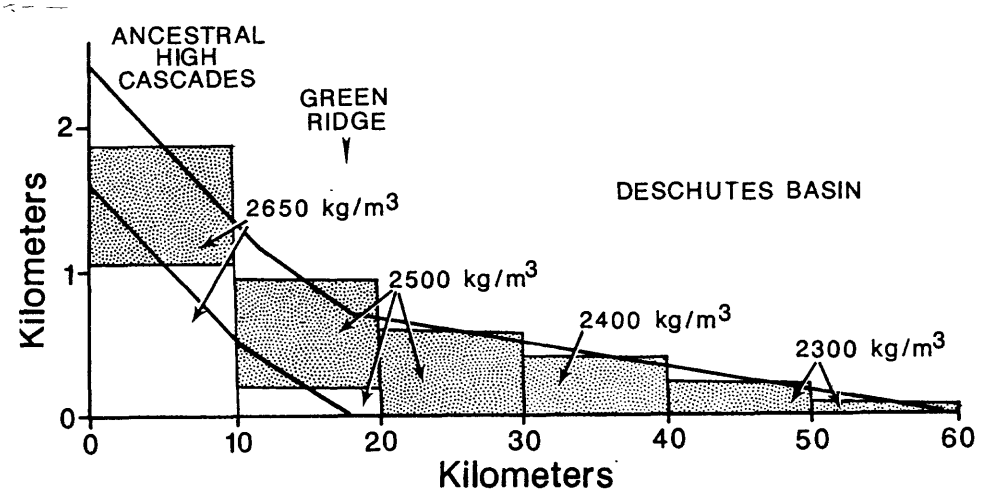

Figure 4. Geometric features of the eastern half of the model load. Heavy lines outline the cross-section of the Deschutes Formation and reconstructed ancestral High Cascade Range west of Green Ridge. The loads are generalized as rectangular boxes of fixed density. The stippled boxes represent the load placed on the lithosphere by the ancestral High Cascades and Deschutes Formation. The eastward decrease in density represents the rapid eastward increase in the ratio of volcaniclastic lithologies to denser lava flows. The unpatterned boxes in the lower left corner of the diagram represent the pre-8.0 Ma load discussed in the text.

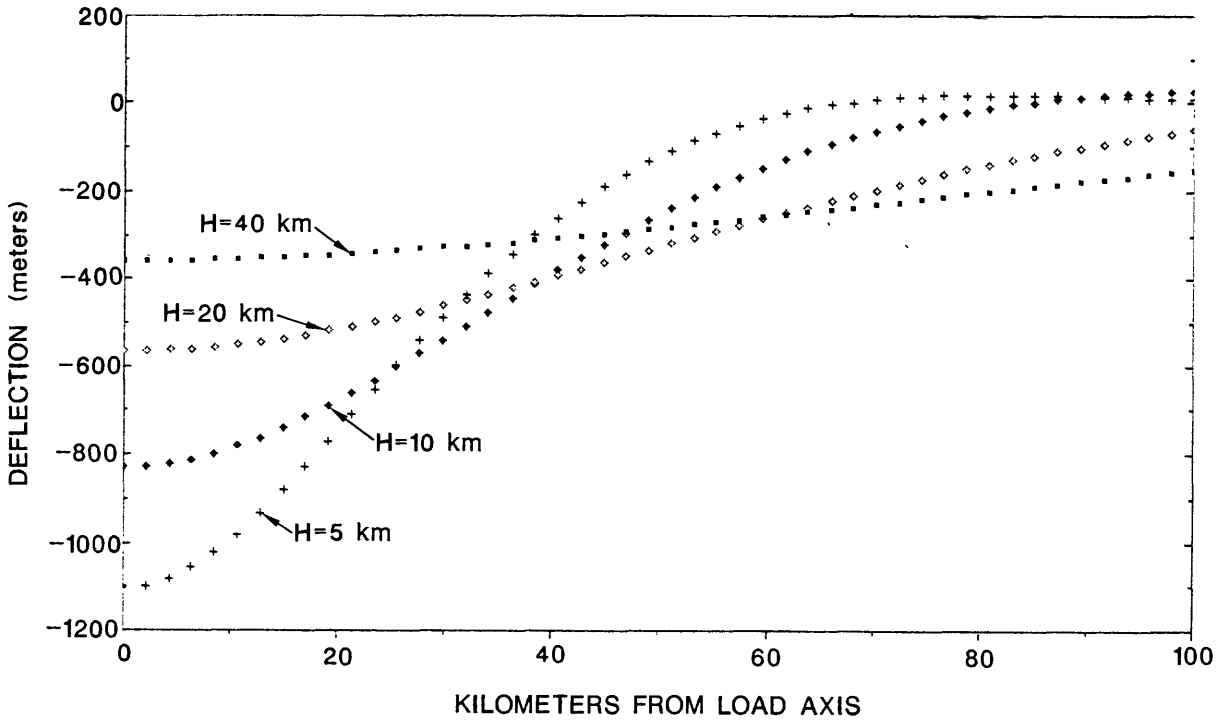

Figure 5. Selected modeled flexural-load deflections for variable elastic thickness and a Young's modulus of 70 Gpa.

tilting between points A and B in Figure 1 is to the southwest rather than west. Therefore, we envision the nature of the load and the resulting lithospheric deflection to be analogous to the well-studied case of the Hawaiian Islands where the line load is not infinite, but ends to the south of the island of Hawaii, as does the extent of the flexurally produced depression (Watts, 1978).

Although elastic lithosphere models work well in some cases (e.g., Watts, 1978), other authors have argued that viscoelastic models are more realistic (Walcott, 1970; Beaumont, 1978, 1981; Schedl and Wiltschko, 1984). For high loading rates (Schedl and Wiltschko, 1984) and characteristic loading times of 10^5 to 10^6 years (Walcott, 1970), as argued for this example, the shape of the deflection is very close to the same for elastic or viscoelastic models regardless of the assumptions that are made in defining the relaxation time constant. We conclude, therefore, that the elastic model is a reasonable assumption for use in this case.

Because of the simplifications and assumptions applied to the geophysical model and construction of the basin subsidence curve, we do not anticipate a precise match between any modeled deflection curve and observed basin depth and width. It is important to note, however, that small values of elastic thickness are required to obtain relative subsidence on the order of 150 to 200 m over the profile length shown in Figure 3, and a basin width on the order of 65 to 70 km, which is the extent of preserved Deschutes Formation east of the High Cascade axis. An elastic lithosphere thickness on the order of 5 to 10 km is defensible, for at least the western part of the profile, given isotherm models based on present-day heat-flow measurements (Blackwell et al., 1982). The thermal characteristics of the lithosphere in the late Miocene are, of course, impossible to determine.

As a basis for further consideration of the flexural loading mechanism for basin development, and with the above cited constraints in mind, we will evaluate the model deflections for an elastic thickness of 10 km and a Young's modulus of 70 Gpa. This model (Fig. 6) predicts 172 m of relative subsidence between points A and B of Figure 1, which compares well with 180 km cumulative subsidence illustrated in Figure 2. A hypothetical initial horizontal datum at the base of the Deschutes Formation would be tilted only 0.35° to the west as a result of the flexural load. Eastward and northeastward sloping depositional surfaces with inclinations of 0.5° to greater than 1.0° would be maintained throughout Deschutes Formation deposition, consistent with field observations. The width of the modeled deflection, from the load axis to the edge of the flexural arch, is 80 km. The Deschutes Formation would, therefore, be entirely contained within the modeled flexural moat.

To complete the modeling exercise, the loaded continuous elastic plate is broken, to simulate development of the High Cascade graben, by nullifying shear stresses and bending moment at faults located 18 km to the east and west of the load axis. Breaking of the plate allows elastic rebound (uplift) to the

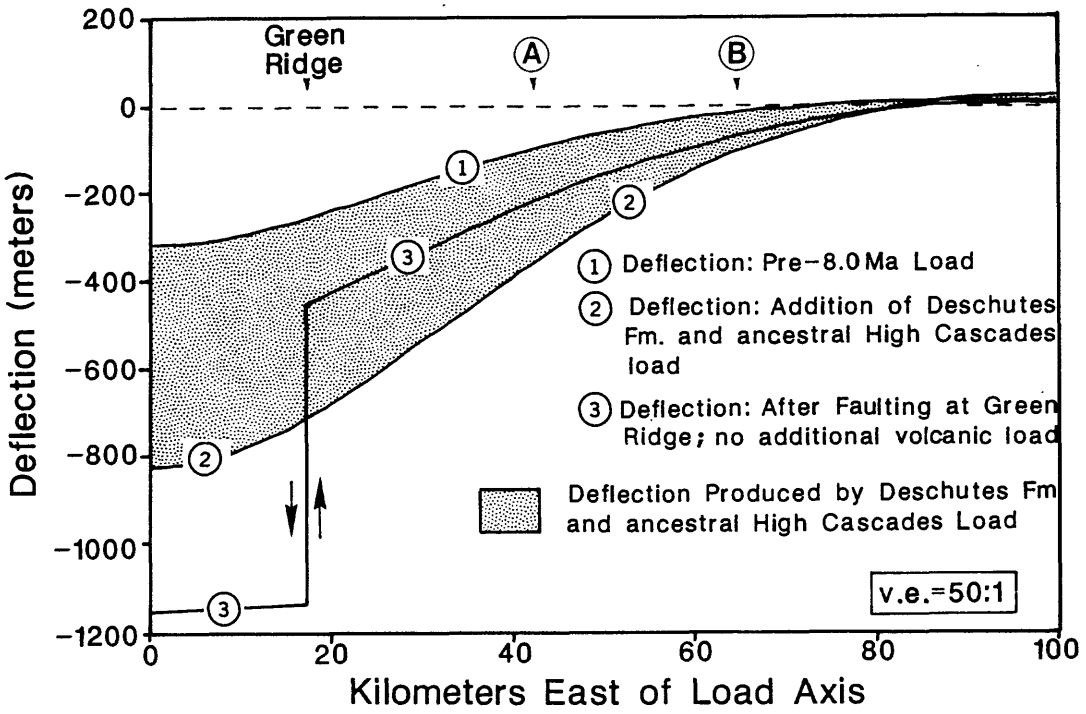

Figure 6. Flexural-load deflections modeled for a Young's modulus of 70 Gpa, flexural rigidity of 6.22×10^{21} Nm, and an elastic thickness of 10 km.

east and west of the breaks, because the elastic lithosphere there is no longer supporting the weight of the High Cascades, and subsidence in the area between the breaks, because the High Cascade load is now being isostatically supported only by the lithosphere directly beneath it (Figure 6, curve 3). The magnitudes of these vertical adjustments produced by breaking the plate are difficult to arrive at because they are dependent not only on the ancestral High Cascade-Deschutes Formation load, but also on the poorly constrained pre-Deschutes Formation load, which is probably underestimated in the model calculation.

With the values shown in Figures 4 and 6, graben development produces about 140 m to 250 m uplift between the center of the Deschutes basin and Green Ridge. Although these are possibly minimum values, they adequately predict a very low (0.25^{o}) eastward tilt associated with rebound. The eastward slope from Green Ridge to the Deschutes basin would, therefore, essentially represent a depositional surface, as argued by Smith (1987d), and would not be exclusively the result of tilting associated with uplift of Green Ridge.

The model predicts a minimum of 700 m of relative subsidence within the High Cascade graben that is a product of changing the nature of the isostatic compensation. Net subsidence along the Green Ridge fault zone could be much greater, not only because this is minimum value from isostatic considerations, but because subsidence was probably not symmetrical about the load axis (mapping and gravity data suggest greater subsidence on the east side of the graben) and additional subsidence of at least 200 m would occur in response to subsequent additional loading of Pliocene and Quaternary mafic platform lavas, assuming that

the graben-bounding faults prohibit transfer of vertical load stresses beyond the boundaries of the graben. The total known subsidence in the High Cascade graben is poorly constrained. A minimum value of 700 m is required to account for the height of the Green Ridge fault scarp. Couch and Foote (1983) suggest, on the basis of gravity models, that subsidence may amount to as much as 3 km. It is difficult, however, to determine which density layers in their model correspond to pre-subsidence and post-subsidence volcanics.

It is not our intention that the model illustrated in Figures 4 and 6 be used to constrain values for crustal parameters, or to imply that the model accurately portrays the effects of isostatic compensation of the Cascade Range. We use the model to show that a flexural loading model is a reasonable solution to the problem of interpreting the subsidence history of the Deschutes basin and the central Oregon High Cascade graben. Because of assumptions and generalizations involved in constructing the model and in reconstructing the subsidence history, we hesitate to emphasize the quantitative aspects of either exercise. It is the geometric relationships of Figures 3, 4, and 6 that are important. Selection of the values used to construct the curves shown in Figure 6 provide the best opportunity for close comparison of the subsidence history and the flexural model to test the hypothesis. Although we emphasize the shape of the deflection, rather than the quantitative parameters, the values selected are realistic and model a basin width that is close to the observed width and a basin depth that is within the limits that can be constrained from field observations.

IMPLICATIONS FOR THE WESTERN CASCADES

The quantitative flexural loading model, using reasonable geophysical parameters, adequately accounts for the shape and subsidence history of the late Miocene Deschutes basin. This suggests that isostatic compensation of the growing High Cascade Range played a role in the development of the Deschutes basin.

This load deflection should have been symmetrical about the load axis and, therefore, also caused subsidence to the west of the High Cascades. There is not, however, a mirror image of the Deschutes basin on the west side of the High Cascades. The principal reason for lack of recognizeable basin development rests in the presence of the western Cascade Range. Mapping by Hammond et al. (1982), Priest et al. (1987, 1988), and Black et al. (1987) indicates that pre-late Miocene volcanic constructional topographic relief in the western Cascade Range exceeded 1000 m. The relatively modest isostatic subsidence that would result from growth of the late Miocene High Cascade volcanoes (Figs. 5 and 6) would not generate a low-relief depositional basin in the western Cascades. At the latitude of the High Cascade graben there are, however, isolated sections of late Miocene volcaniclastic sediments in the western Cascades that are as thick as 200 m (Black et al., 1987; Priest et al., 1988). The distribution of these sediment-dominated packages suggest that they represent valley fills, rather than local volcano-

flank volcaniclastic aprons. Deposition and preservation of this fragmental material may have been in response to subsidence, and hence local base-level rise, of river valleys draining across the high-standing western Cascades. It is notable that similar volcaniclastic sequences have not been mapped in the western Cascades at a latitude north of Mount Jefferson (Priest et al., 1987) where the volume of late Miocene extrusions is much smaller and the expected isostatic deflection would be much less.

Another difficulty in assessing the evidence that bears on the role of isostatic adjustment in the western Cascades is the intense dissection and erosion that has occurred in response to subsequent uplift. Although some uplift would be expected as a rebound effect of graben development, this cannot, alone, account for the spatial and temporal characteristics of western Cascade uplift. For example, dissection along the western side of the High Cascade graben has extended more than 400 m downward into Pliocene-Pleistocene graben-fill volcanics (Priest et al., 1988). This suggests that Pliocene and Quaternary uplift, not related to rebound, has affected the western Cascades and part of the High Cascades.

DISCUSSION AND CONCLUSIONS

The stratigraphy and subsidence history of the Deschutes basin suggest a coupling of the basin development with the growth of the ancestral High Cascades. The most straightforward interpretation of this relationship hypothesizes that basin subsidence was controlled principally by flexural loading of an elastic lithosphere by the growing Cascade Range. Spatially, late Miocene subsidence was greatest at the latitude of the largest volume of contemporary volcanic extrusions. Temporally, subsidence was largest during the period of greatest rate of extrusion in the adjacent Cascades and terminated when development of the High Cascade graben structurally separated the Deschutes basin from the Cascade Range. Quantitative modeling of the flexural-load deflection is necessarily generalized, but indicates that the hypothesis is realistic. The observations of Menard (1964), Walcott (1970), and Watts (1978) in the Hawaiian Islands demonstrated the importance of rising volcanic landforms to produce adjacent subsiding basins. It should not be surprising, therefore, to find evidence of basin development adjacent to continental-margin volcanic arcs that is influenced by isostatic adjustment of the lithosphere to the load represented by the arc.

A general model for basin development in volcanic areas should include the role of isostatic compensation of the volcanic edifices (Fig. 7). This isostatic effect might explain the generally synformal structure of the Cascade Range (Hammond, 1979) and other continental-margin arcs (Hildebrand and Bowring, 1984). Shallow basins can form in the flexural moat of relatively high-standing arcs in the absence of large horizontal compressive stresses in the lithosphere that would prohibit isostatic subsidence. The basin-fill stratigraphy would be largely influenced by the attendent volcanism because subsidence

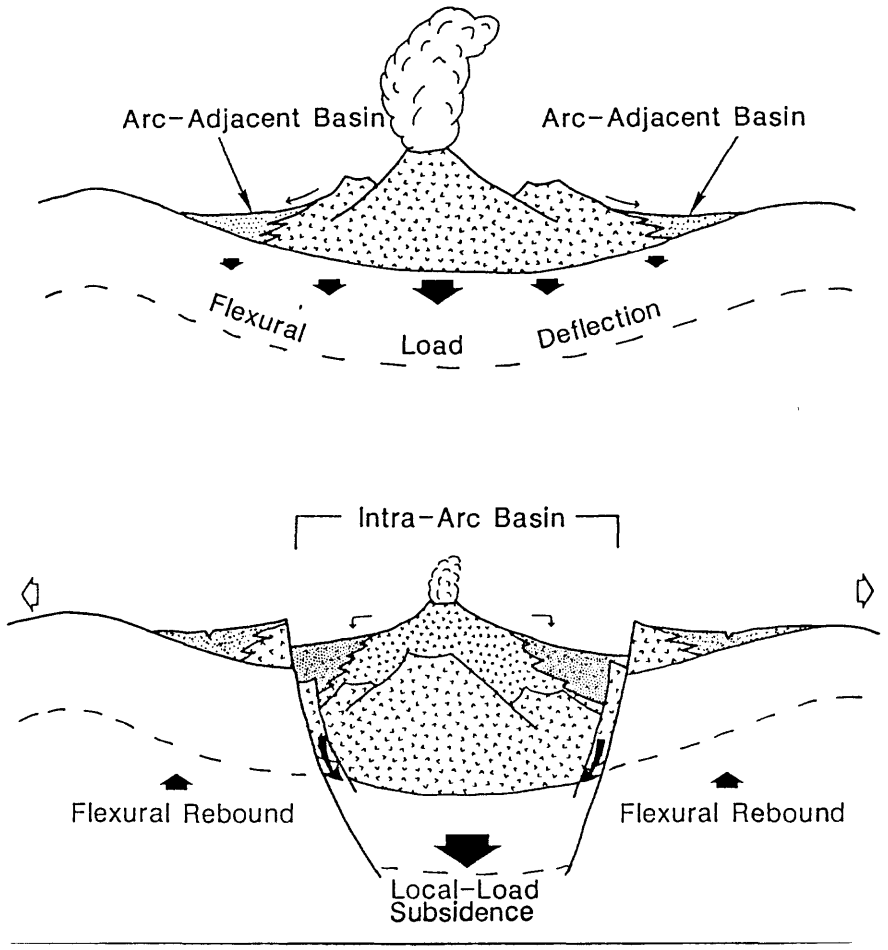

Figure 7. A schematic diagram illustrating the generation of shallow arc-adjacent basins within the flexural moat of symmetrical high-standing arcs with nearly neutral horizontal stress, followed by isostatically enhanced subsidence of intra-arc basins under extensional conditions.

would be tied to arc growth and sedimentation character would be determined by the style, volume, and frequency of eruptive events that episodically produce large volumes of fragmental material (Smith, 1987c).

Under the influence of extension, the thermally weakened arc crust may rupture to form intra-arc basins whose subsidence is determined not only by the extent of crustal thinning associated with extension, but also by the change in isostatic compensation of the volcanic arc. This mechanism alone may produce hundreds of meters of subsidence. Development of intra-arc grabens produces topographic barriers that starve the arc-adjacent basins of sediment. Thick sequences of volcaniclastic material will accumulate within the intra-arc basin that was formerly a high-standing area of sediment bypass. In addition, isostatic rebound will cause uplift and contribute to dissection of the arc-adjacent basin fill.

Based on the stratigraphic observations in the Deschutes basin and the geophysical model for the flexural deflection, the amount of crustal deformation that can be attributed to isostat-

ic loading by the volcanic arc is small. This means that the basin formation model discussed above may not be applicable in all cases because other vertical tectonic movements may be of considerably greater magnitude and mask the isostatic effects. These tectonic complexities may explain, in part, the lack of a preserved late Miocene depositional basin west of the High Cascades. The results of this study, however, suggest that further consideration should be given to the role of isostasy in the structural development of the Cascade Range and adjacent areas, and to the problems of basin development in volcanic terrains more generally.

ACKNOWLEDGEMENTS

We appreciate the guidance of Clem Chase in the use of his FLEX7 software and interpretation of the flexural loading model. We thank R. Couch for sharing with us the unpublished gravity model for the Three Fingered Jack profile that he developed with R. Foote. Reviews of an early version of the manuscript by Clem Chase and Ed Taylor were very helpful. Smith's research is supported by the donors to the Petroleum Research Fund, American Chemical Society.

REFERENCES

Beaumont, C., 1978, The evolution of sedimentary basins on a viscoelastic lithosphere: theory and examples, Geophys. J. R. Astr. Soc., 55,471-497, 1978.

Beaumont, C., Foreland basins, Geophys. J. R. Astr. Soc., 65, 291-329, 1981.

Black, G.L., N.M. Woller, and M.L. Ferns, Geologic map of the Crescent Mountain area, Linn County, Oregon, Oregon Department of Geology and Mineral Industries Geological Map Series GMS-47, scale 1:62,500, 1987.

Blackwell, D.D., R.G. Bowen, D.A. Hull, J.F. Riccio, and J.L. Steele, Heat flow, arc volcanism, and subduction in northern Oregon, J. Geophys. Res., 87, 8735-8754, 1982.

Conrey, R.M., Volcanic stratigraphy of the Deschutes Formation, Green Ridge to Fly Creek, north-central Oregon, M.S. thesis, 349 p., Oregon State University, 1985.

Couch, R.W. and R.W. Foote, Graben structures of the Cascade Range in Oregon, EOS, Transactions of the Amer. Geophys. Union, 45, 887, 1983.

Couch, R.W., G.S. Pitts, M. Gemperle, D.E. Braman, and C.A. Veen, Gravity anomalies in the Cascade Range in Oregon: structural and thermal implications, Oregon Department of Geology and Mineral Industries Open-File Report O-82-9, 43 p., 1982.

Dill, T.E., Stratigraphy of the Neogene volcanic rocks along the lower Metolius River, Jefferson County, central Oregon, M.S. thesis, 345 p., Oregon State University, 1988.

Hammond, P.E., A tectonic model for evolution of the Cascade Range, in Cenozoic paleogeography of the western United States, edited by J.M. Armentrout, M.R. Cole, and H. Terbest, Jr., Soc. of Econ. Paleon. and Mineral., Pacific

Section, p. 219-237, 1979.
Hammond, P.E., K.M. Geyer, and J.L. Anderson, Preliminary geologic map and cross sections of the upper Clackamas and North Santiam Rivers area, northern Oregon Cascade Range, Portland State University Dept. of Earth Sciences, scale 1:62,500, 1982.
Harrison, C.G.A., I. McDougall, and N.D. Watkins, A geomagnetic field reversal time scale back to 13.0 million years before present, Earth Planet. Sci. Lett., 42, 143-152, 1979.
Hetenyi, M., Beams on Elastic Foundations, Univ. of Michigan Press, Ann Arbor, 255 p, 1946.
Hildebrand, R.S. and S.A. Bowring, Continental intra-arc depressions: a nonextensional model for their origin, with a Proterozoic example from the Wopmay Orogen, Geology, 12, 73-77, 1984.
Jordan, T.E., Thrust loads and foreland basin evolution, Cretaceous, western United States, Amer. Assoc. Petrol. Geol. Bull., 65, 2506-2520, 1981.
Keach, R.W., III, Cenozoic active margin and shallow Cascades structure: COCORP results from western Oregon, M.S. thesis, 51 p., Cornell University, 1986.
Menard, H.W., Marine geology of the Pacific, McGraw Hill, 271 p, 1964.
Priest, G.R., N.M. Woller, and M.L. Ferns, Geologic map of the Breitenbush River area, Linn and Marion Counties, Oregon, Oregon Department of Geology and Mineral Industries Geological Map Series GMS-46, scale 1:62,500, 1987.
Priest, G.R., G.L. Black, N.M. Woller, and E.M. Taylor, Geologic map of the McKenzie Bridge quadrangle, Oregon, Oregon Department of Geology and Mineral Industries Geological Map Series GMS-48, scale 1:62,500, 1988.
Schedl, A. and D.V. Wiltschko, Sedimentological effects of a moving terrain, J. Geol., 92, 273-288, 1984
Smith, G.A., Late Cenozoic sedimentation on the east flank of the Cascade Range, Oregon and Washington, Program, 2nd Annual Midyear Meeting, Soc. Econ. Paleon. Mineral., 84, 1985.
Smith, G.A., Stratigraphy, sedimentology, and petrology of Neogene rocks, Deschutes basin, central Oregon: the record of continental-margin volcanism and its influence on fluvial sedimentation in an arc-adjacent basin, Ph.D. thesis, 467 p., 1986.
Smith, G.A., Geologic map of the Madras East and Madras West quadrangles, Jefferson County, central Oregon, Oregon Department of Geology and Mineral Industries Geologic Map Series GMS-45, scale 1:62,500, 1987a.
Smith, G.A., Geologic map of the Seekseequa Junction and part of the Metolius Bench quadrangles, Jefferson County, central Oregon, Oregon Department of Geology and Mineral Industries Geologic Map Series GMS-44, scale 1:24,000, 1987b.
Smith, G.A., Sedimentology of volcanism-induced aggradation in fluvial basins: Examples from the Pacific Northwest, in Recent developments in fluvial sedimentology, edited by F.G. Ethridge, R.M. Flores, and M.A. Harvey, Soc. Econ. Paleon. Mineral. Spec. Pub. 39, 217-229, 1987c.
Smith, G.A., The influence of explosive volcanism on fluvial

sedimentation: the Deschutes Formation (Neogene) in central Oregon, J. Sed. Petrol., 57, 613-629, 1987d.
Smith, G.A. and G.A. Hayman, Geologic map of the Eagle Butte and Gateway quadrangles, Jefferson and Wasco Counties, central Oregon, Oregon Department of Geology and Mineral Industries Geologic Map Series GMS-43, scale 1:24,000, 1987.
Smith, G.A., L.W. Snee, and E.M. Taylor, Stratigraphic, sedimentologic, and petrologic record of late Miocene subsidence of the central Oregon High Cascades, Geology, 15, 389-392, 1987.
Smith, G.A. and E.M. Taylor, The central Oregon High Cascade graben: what? where? when?, Trans. Geotherm. Res. Coun., 7, 275-279, 1983.
Smith, G.A. and K.R. Vincent, Rates of sedimentation, subsidence, and volcanism as controls on facies architecture in terrestrial volcaniclastics, Geol. Soc. Amer. Abstr. Progs., 19, 849, 1987.
Steckler, M.S. and A.B. Watts, Subsidence of the Atlantic-type continental margin off New York, Earth Planet. Sci. Lett., 41, 1-13, 1978.
Taylor, E.M., Central High Cascade roadside geology -Bend, Sisters, McKenzie Pass, and Santiam Pass, Oregon, in Guides to some volcanic terranes in Washington, Idaho, Oregon, and northern California, edited by D.A. Johnston and J. Donnelly-Nolan, U.S. Geological Survey Circ. 838, 55-58.
Walcott, R.I., Flexural rigidity, thickness, and viscosity of the lithosphere, J. Geophys. Res., 75, 3941-3954, 1970.
Watts, A.B., An analysis of isostasy in the worlds oceans, part 1, Hawaiian-Emperor seamount chain, J. Geophys. Res., 83, 5989-6004, 1978.
White, C., Geology of the Breitenbush Hot Springs quaadrangle, Oregon, Oregon Department of Geology and Mineral Industries Spec. Paper 9, 26 p., 1980.

VOLCANIC AND TECTONIC EVOLUTION OF THE CASCADE VOLCANIC ARC, 44° 00" to 44° 52' 30" N

George R. Priest
Oregon Department of Geology and Mineral Industries

ABSTRACT

The geology of the Cascades is examined with the aim of correlating the plate tectonic and geologic history. The rate of volcanic production (R_V) in the Cascades decreased by a factor of 2 from the interval 35-17 Ma to 16.9-7.4 Ma. The decrease may have been caused by decreasing convergence rate (V_c) and decreasing extensional stress. Decreasing extensional stress is inferred from the change from eruption of high-TiO_2 tholeiitic lavas and voluminous silicic tuff at 35-17 Ma to eruption of calc-alkaline andesite and basaltic andesite at 16.9-7.5 Ma. Decreased extension at 16.9-7.5 Ma may have been caused by mild west-northwest compression and/or by decreased thermally induced extension caused by decreased R_V. At 7.4-0 Ma, increased R_V of silicic tuff and high-TiO_2, highly mafic lava implies that extension was again relatively high. The direction of minimum horizontal stress, sigma 3, rotated clockwise at 22-0 Ma from north-northwest or north-south to east-west. This progressive change in extension direction may reflect decreasing influence of northeast compression at the Juan de Fuca plate-North American plate (JDFP-NAP) boundary relative to north-south compression at the Pacific-Plate(PP)-NAP boundary, as V_c and the angle of convergence (A_c) decreased. Increased extension at 7.4-0 Ma may have been caused by (1) the decreased coupling of the JDFP and NAP, and/or (2) focusing of thermally induced extension over a narrowing zone of magma production.

The volcanic front of the central Oregon Cascade arc migrated progressively eastward at 35-0 Ma, as the volcanic belt narrowed. The narrowing was probably caused by progressive steepening of the slab behind the volcanic front, possibly enhanced by decreasing volcanism accompanying decreased V_c. Assuming that the volcanic front was about 100-125 km above the subducted slab at any given time, the eastward velocity of volcanic front migration (V_f) was probably controlled in large part by the rate of change of the shallow (0-100 km) slab dip and by absolute westward velocity (V_o) of the NAP relative to the free roll-back rate (V_r) of the slab. Shallow dip probably decreased as a result of erosion, heating, and extension of the overriding plate, moving the 100-125-km depth-to-slab eastward. V_r of the JDFP increased at 4 Ma due to splitting off of the buoyant Explorer Plate. The arc in British Columbia and Washington moved west at 4-0 Ma, reflecting $V_o<V_r$. Extension in and behind the arc in hot, weak continental lithosphere in the central Oregon High Cascades and Basin and Range Province increased V_o enough to prevent westward arc migration at 4-0 Ma.

The Western Cascades were tilted west in a trap-door uplift that started after about 5.1-4.5 Ma, ending about 3.3 Ma. The uplift may have been caused by increased upper mantle circulation accommodating the increase in V_r of the JDFP at 4 Ma. The largest rivers were rapidly entrenched in the

uplifted Western Cascades, reaching approximately their present grade by 0.5 Ma.

INTRODUCTION

This paper is the result of nine years of field geologic observations and sampling in the Cascades between 44° N and 44° 52' 30" N (Figure 1). The area is an ideal natural laboratory to study volcanism related to subduction of the Juan de Fuca Plate (JDFP), because it is landward of a relatively simple part of the plate boundary free of the complicated motions attributed to segments of the JDFP at its extreme north and south ends (Figure 1; Riddihough, 1984).

Volcanic arcs around the Circum-Pacific are now universally thought to be the product of partial melting events caused by the subduction of oceanic crust. Many of these volcanic arcs have features in common with the Cascade arc, including:

1. Volcanic rocks with calc-alkaline and tholeiitic differentiation trends.

2. An inactive volcanic arc seaward of an active arc.

3. A history punctuated by periods of uplift and deformation.

4. Progressive changes in the relative and absolute eruption rates of mafic, intermediate, and silicic volcanic rocks.

This paper will examine the geologic evolution of the Cascade volcanic arc with the aim of understanding the processes responsible for these features. I will show that most of these phenomena are most likely controlled either directly or indirectly by the absolute and relative motions of the Farallon plate (FAP)-JDFP, Pacific plate (PP), and North American plate (NAP). The tendency to develop an inactive volcanic arc seaward of the active arc is chiefly dependent upon the slab dip at 0-100-km depth and the free roll-back rate of the subducted oceanic plate (V_r) relative to the absolute motion of the overriding plate (V_o). Lowering of the slab dip by thinning of the overriding plate was probably the most important factor for the last 35 Ma, but the V_r-V_o ratio could also have been a factor, as demonstrated by changes in the British Columbia arc position accompanying a change in V_r at 4 Ma (Rogers, 1985). The rate and composition of volcanism seem most directly controlled by the rate of convergence and state of stress in the overriding plate. I will show that the highest rates of volcanic production occur when convergence and extension rate are both high. A major uplift event at about 4 Ma was probably triggered by an increase of V_r that caused increased mantle circulation into the wedge. Uplift is most pronounced where the mantle wedge is overlain by relatively thick, rigid lithosphere.

LITHOLOGIC NOMENCLATURE

Rock names are assigned according to the following system, based on analyses recalculated to 100% totals, volatile-free:

1. Silica $<$ 53% = basalt
2. Silica $\geq$ 53 and $\leq$ 57% = basaltic andesite
3. Silica $>$ 57 and $<$63 = andesite
4. Silica $\geq$ 63 and $<$70 = dacite
5. Silica $\geq$ 70%; $K_2O \leq$ 4% = rhyodacite
6. Silica $\geq$ 70%; $K_2O >$ 4% = rhyolite

The terms "high-silica" and "low-silica" will be used to designate silica contents in the upper and lower half of each range, respectively. Basalt has no lower limit on its range, so "high-silica" will mean silica $\geq$ 50.5%; "low-silica" will mean silica $<$ 50.5 %.

The term "tholeiitic" will be used to designate rocks with high Fe/Mg and high Fe contents, plotting in the tholeiitic fields of Miyashiro's (1974) FeO/MgO versus SiO_2 diagram and Irvine and Baragar's (1971) AFM diagram. The term "calc-alkaline" will refer to rocks that plot in the calc-alkaline fields of the latter two diagrams.

STRATIGRAPHIC NOMENCLATURE

This paper will deal with five time divisions or "episodes" that are marked by rocks and unconformities that can be recognized in the field with minimal support from isotopic age data. The units will henceforth be referred to as episode 1 (43.2-17.0 Ma), 2 (16.9-7.5 Ma), 3 (7.4-4.0 Ma), 4 (3.9-0.731 Ma), and 5 (0.730-0 Ma). Lithologic characteristics and relationships to previous rock-stratigraphic and time-rock units are shown in Figure 2. Note that these episodes, with exception of numbers 4 and 5, are virtually identical to volcanic episodes of Priest and others (1983). Even episodes 4 and 5 are simply subdivisions of the late High Cascade episode of Priest and others (1983). These numbered episodes are utilized here for convenience to shorten the text. However, the nomenclature of Priest and others (1983) will be used interchangeably with the numbered episodes, as appropriate.

In maps and cross sections symbols will be used for rock units formed within these volcanic episodes. The symbol nomenclature is summarized in Figures 4 and 5. Note that for the geologic cross sections (Figure 5) episode 1 is locally split into two time-rock units labeled To(b,a,r)1 and To(b,a,r)2, where sufficient map data allow. This was done to illustrate an angular unconformity that appears to separate 25-18-Ma rocks from older rocks (Figure 5).

ANALYTICAL PROCEDURE

INTRODUCTION

The following is a summary of methods used to infer the geologic history, crustal structure, volcanic production rate ($R\underline{v}$), and changes in the configuration of the volcanic arc and subducted slab.

GEOLOGIC HISTORY AND STRUCTURE

The the geologic history and structure were inferred from geological and geophysical compilation maps and cross sections (Figures 3-6). Geologic data is based on a 1:250,000-scale geologic map produced primarily from geologic maps of the Bend 1^{o} X 2^{o} sheet (Sherrod and Smith, 1988) and Salem 1^{o} X 2^{o} sheet (Walker and Duncan, 1989) with modifications from my reconnaissance mapping in 1988 and from detailed mapping of Priest and others (1987, 1988), Black and others, (1987), and (G.R. Priest and N.S. MacLeod, 1987, unpublished mapping). Cross sections were constructed only where relatively detailed mapping was available.

ISOTOPIC AGE DATA

Isotopic age data (Figure 7) are taken from a compilation by Fiebelkorn and others (1982; 1983), (Hammond and others, 1980), and Walker and Duncan (1989), modified by new data from Priest and others (1987; 1988), Black and others (1987), and an unpublished K-Ar age (see caption of Figure 7). These ages were determined primarily with the K-Ar and ^{40}Ar-^{39}Ar techniques, although one fission track age is also included (Hammond and others, 1980).

Some age data were judged highly inaccurate and were excluded from the compilation. Inaccuracies were generally caused by alteration effects.

The age compilation contrasts strongly with that of McBirney and others (1974), owing to more complete data. The episodic distribution noted by McBirney and others (1974) is not apparent. The distribution is skewed toward younger ages, primarily because of more investigations of younger units, and because younger rocks, being less altered, are more attractive candidates for age determinations than older rocks.

CALCULATION OF VOLCANIC PRODUCTION RATES

Volcanic production rates were calculated as follows:

1. A 1:250,000-scale map was constructed of the pre-erosion distribution of all time-rock units based on geological inference (generalized version shown in Figure 8).

2. The area of each time-rock unit was measured utilizing a planimeter. The areas were tabulated separately for the rectangular areas illustrated in Figure 8.

3. The average thickness of mafic, andesitic, and silicic rocks was estimated for each time-rock unit in each rectangular area. Average thickness was determined from geological cross sections, detailed traverses in representative areas, and measurement of the areal frequency of outcrops of various rock types. In the case of volcaniclastic sequences, the relative amounts of mafic, andesitic, and silicic rocks was estimated from random sampling of clasts and from direct field tabulations of well-exposed, representative sections. These relative amounts were then taken as proportions of the thickness of the volcaniclastic units and added to the other average thickness estimates.

4. Volume (Table 1) was calculated for each rectangular area by multiplication of the average thickness by the area. Total volume was then determined by summing. Density differences between clastic and crystalline rocks were ignored.

5. Volcanic rate (Table 2) was calculated by dividing the total volume of each rock composition by the span of geologic time and length of the volcanic arc between 44° N and 44° 52' 30" N.

Uncertainties in rate estimates are large and not easily quantifiable. Most of the uncertainty arises from two factors. First, the estimate of average thickness of each unit is, by the nature of the calculation, subjective and highly sensitive to the amount of detailed map data. Second, the amount of each unit lost to erosion is not known.

Volcanic tephra was undoubtedly lost from each episode by erosion and by wind dispersal of ash. The large amount of ash lost through wind dispersal is a major factor for episode 1, which is characterized by numerous explosive eruptions. The chemistry of thick air-fall ash deposits of the John Day Formation of eastern Oregon is consistent with an origin in the episode 1 Cascade arc (Robinson and Brem, 1981). Estimation of the volume of Cascade ash in the John Day Formation is beyond the scope of this paper, but it is likely that addition of this rock would increase the episode 1 volcanic rate by a significant amount.

Likewise, it might well be argued that the contemporaneous rocks of the 47-35-Ma Clarno Formation (Enlows and Parker, 1972) and 37-18-Ma John Day Formation (Robinson and Brem, 1981) of eastern Oregon should be included in the episode 1 rate estimates. These rocks were not included because of insufficient detailed map data and because of their complex relationship to the subduction-zone volcanism in the study area. The Clarno rocks may be a rifted arc remnant (Vance, 1982). It may be that the highly alkaline character of the locally erupted John Day basalt (e.g. TiO_2 = 2.8-4.8%, $Na_2O + K_2O$ = 3.4-6.1%; Robinson, 1969; Weidenheim, 1980) is indicative of eruption in a back-arc setting not directly related to the subducted slab. Back-arc rocks of later episodes (e.g. Columbia River Group) were not included for the same reasons. The volcanic volumes and rates listed here, especially for episode 1, must therefore be considered minimum estimates of overall volcanic rate for the listed time periods.

The amount of tephra lost to erosion is heavily dependent on whether a basin of deposition was available to catch sediments. As explained below sediment in the lower part of episode 1 sections was preserved by a subsiding basin, but widespread unconformities between and within the episodes illustrate that such basins did not persist. An example of this phenomenon is the Deschutes Basin where volcaniclastic rock trapped during episode 3 is now eroding away. Likewise, these episode 3 volcaniclastic rocks are almost entirely missing from the west side of the Cascades, because no basin was ever available to trap them. As explained below, the amount lost to erosion was probably quite large for episode 2 rocks, making volume estimates highly uncertain.

There are some notable differences between my calculations (Table 1) and those of previous workers. First of all, I found that one of the lowest rates was in the middle Miocene whereas somewhat higher rates prevailed before and after. I also did not find andesite to be a particularly abundant eruptive product overall, whereas andesite dominates the early history of arc, according to McBirney and others (1974). I did, however, find the same decrease in

Western Cascade eruptive rate noted by Verplanck and Duncan (1988) from the Oligocene to the middle Miocene. I also agree with the finding of McBirney and others (1974) that basaltic rocks (including basaltic andesite) are the dominate rock type in Pliocene and Quaternary sequences.

The differences between my calculations and those of previous workers stem from four factors. First, I have much more detailed map and age data. Second, the area I am considering is smaller than that considered in previous studies. Third, I have lumped iron-rich (tholeiitic) andesites of episode 1 with the mafic rocks, whereas previous workers did not generally recognize the iron-rich nature of these rocks, lumping them with normal calc-alkaline andesites. Finally, I have assumed that a substantial amount of the episode 3 and 4 volcanic rock is buried in a graben under the High Cascades. The reasoning behind the graben offsets is explained below and by Taylor (1981; 1989).

The potential errors in volcanic rate calculations are so large that modest or even substantial differences from one calculation to another should not be given too much emphasis. This observation applies particularly to absolute rates, which are sensitive to the particular methodology used. Relative rates among volcanic episodes are probably more reproducible, because the same methodology was used throughout.

LOCATION OF VOLCANIC FRONTS THROUGH TIME

Volcanic fronts for each time-rock unit (Figure 9) were located by geologic inference based on available map data. Location of volcanic fronts for episodes 3, 4, and 5 was relatively easy, owing to good preservation of western-most vent areas or near-vent volcanic rocks. Location of the volcanic front for episode 2 is highly uncertain owing to extensive erosion (see geologic history section). Figure 9 indicates the probable limits of the uncertainty for the locations of the volcanic front of episode 2.

Location of the episode 1 volcanic front is ostensibly easy, being marked by a line of basaltic intrusions on the east side of the Willamette Valley. Intrusions with isotopic ages at the volcanic front are 35-30 m.y. old (Lux, 1982). However, there were volumetrically significant eruptions of basalt at 44-35 Ma and highly alkaline lava at 35-30 Ma in the Coast Range (MacLeod and Snavely, 1973; Snavely and Wagner, 1963; Wells and others, 1984). There is little evidence in oil well logs or in outcrops in the Willamette Valley that the present forearc basin was a major volcanic vent area at 35-30 Ma. I conclude that there was a gap in the volcanic field at that time between the main arc and the alkaline volcanism in the forearc. This gap may signify fundamentally different controlling processes between volcanism in the arc and forearc. I will therefore assume that the location of the volcanic front in the main arc at 35-0 Ma is not related to forearc volcanism, being controlled instead by the 100-125-km depth-to-slab that is characteristic of volcanic arcs world-wide (Gill, 1981).

It is also apparent that the volcanic front has migrated toward the east (Figure 9). Available map data is not detailed enough to recognize whether the migration was continuous or episodic. Isotopic age data suggests that volcanic rocks at each volcanic front erupted near the beginning of the contemporaneous episode. It is therefore probable that the front locations shown here are most representative of the beginning of each episode. The uncertainty of the age estimates for the volcanic fronts is listed on Figure 9.

REGIONAL CROSS SECTIONS

A generalized cross section across the continental shelf and Cascades in the central part of the study area (Figure 10) was constructed from geophysical and geological data. The location of the upper surface of the subducted Juan de Fuca plate and the crust-mantle boundary in the west half of the cross section were taken from Keach (1986). The crust-mantle boundary in the east half of the cross section was taken from Leaver (1982).

The current location of the upper surface of the subducted slab was inferred by assuming that the current volcanic front is about 100-125 km above the slab (Gill, 1981) and that the narrow width of the volcanic arc is indicative of a slab dip of about 70^{o} (Guffanti and Weaver, 1988). The rest of the subducted slab surface was reconstructed by simply extending the dip from the west half of the cross section to the intersection with the 70^{o} dip. The intersection of these two dips produces a sharp knee bend in the slab at about 70 km depth. This depth is in the range of depth expected for the basalt-eclogite transition in subduction zones world wide (Grow and Bowin, 1975; Ahrens and Schubert,1975). Most subducted slabs that are well defined by seismic data are inferred to have downward curving surfaces rather than sharp bends (e.g. Jarrard, 1986, p. 223). Cartoons showing possible slab configurations in the past are therefore drawn with curving profiles (Figure 11).

Slab positions in the past were inferred based on five factors:

1. Dip increases in the depth range 60-100 km (Jarrard, 1986) as a result of the basalt/eclogite transition (Grow and Bowin, 1975: Ahrens and Schubert, 1975).

2. The slab was 100-125 km below past volcanic fronts (Gill, 1981).

3. The dip of the slab below 100 km has increased through time. This is inferred from progressive decrease in the width of the volcanic arc (Figure 8). Decrease of the width of the arc through time is inferred from the eastward migration of the volcanic front and from local outcrops of near-vent rocks of episode 1, 2, 3, and 4 on the east side of the arc. These local outcrops are: 1) episode 1 calc-alkaline dacite on the east margin of the Deschutes Basin (Smith, 1986; Weidenheim, 1980), 2) a large volcano of episode 2 basaltic andesite and andesite at Green Ridge (Hales, 1975; Conrey, 1985), 3) a mafic vent complex of episode 3 volcanic rocks northeast of Green Ridge (Yogodzinski, 1985), and 4) episode 4 volcanic centers that occur east of episode 5 rocks within the High Cascades and in the vicinity of Green Ridge (Figure 6).

4. Accretion of a sedimentary prism caused oceanward migration of the oceanic trench relative to a fixed point on the NAP. Accretion is assumed to have occurred at a decreasing rate as convergence rate decreased for the last 35 m.y. Total accretion is estimated to be about 20 ± 4 km, based on the crustal section of Couch and Riddihough (1988) at the latitude of Three Fingered Jack.

GEOLOGIC HISTORY OF THE VOLCANIC ARC

43-17 Ma - EARLY WESTERN CASCADE VOLCANISM (EPISODE 1)

Eruptive activity began in the Cascade volcanic arc sometime between about 43 Ma and 35 Ma. These ages were determined for basaltic lavas in the outermost part of the arc. There are only a few samples with ages older than 35 Ma (Figure 7), and some of these rocks are in stratigraphic positions suggestive of a younger age (Walker and Duncan, 1989), however, the available age data leaves little doubt that the arc was active by 35 Ma. The isotopically dated lavas are predominantly of tholeiitic composition and are by far the largest component of lithic fragments found in Oligocene and early Miocene volcaniclastic rocks in the study area. The lavas are interbedded with thick sequences of these volcaniclastic rocks composed of vitric-rich and lithic-rich debris-flow deposits, ash-flow tuff, and volcaniclastic sandstone, mudstone, and minor conglomerate.

The source of most of the volcanic rocks in the lowest part of the episode 1 sequence is unknown owing to burial by younger rocks. Some of the volcanic centers are, however, exposed on the western edge of the arc. The largest of the mafic volcanic centers that dominated much of the outer arc activity in the Oligocene occurred near Sweet Home (SHVC, Figure 6). Immediately southeast of the SHVC numerous silicic intrusions may mark the source of some of the explosive silicic volcanism (Figures 4 and 6).

The arc was apparently skirted by a marine embayment that swept up from what is now the mouth of the Columbia River in the late Oligocene (Snavely and Wagner, 1963). Marine and estuarine rocks of this embayment interfinger with continental volcaniclastic rocks at the volcanic front (Snavely and Wagner, 1963; Orr and Miller, 1984).

The arc must have had low relief in the initial stages of development, because of the wide dispersal of single ash-flow sheets, the excellent preservation of thick sequences of easily erodible volcaniclastic rock, and lack of evidence in fossil flora of any rain shadow effect to the east (e.g. Ashwill, 1983). A hornblende-bearing non-welded ash-flow tuff with an isotopic age of about 32 Ma (Walker and Duncan, 1989) has been traced north-south for a distance of about 28 km in the study area, and a 35-Ma biotite-bearing ash flow at the base of the Cascade section has been traced north-south through Cascade foothills in the southern half of Oregon (Smith and others, 1980). About 2.7 km of volcaniclastic rocks are exposed below rocks with a minimum age of about 26.5 Ma (see next paragraph on the SMVC) in a tilted fault block in the central part of the arc (Figure 5). Surely these rocks would not be present unless the arc was a subsiding basin of low relief. A cross section constructed from available field and drill hole data requires substantial thickening of the volcaniclastic sequence toward the east, supporting the existence of a basin (Cross section A-A', Figure 5).

This basin probably continued to subside when about 2 km of hornblende-pyroxene-phyric andesitic lavas erupted east of the volcanic front at the Sardine Mountain volcanic center (SMVC of Figure 6). All of the rocks of the SMVC are altered, so the age is not known for certain. A sample from near the base of the sequence has $^{40}Ar/^{39}Ar$ ages for various heating increments that range from 32.28 to 23.68 Ma with a total fusion age of 26.46 $\pm$ 0.52 Ma, but this sample has slight alteration and no well-defined plateau age (Priest and others, 1987). The SMVC ceased activity sometime prior to about 25 Ma, the age of tholeiitic lava that unconformably overlies the Sardine rocks (Priest and others, 1987). Rocks similar in composition to those at the SMVC

occur in the southern part of the study area, but they are not well exposed and appear to change in composition toward the south, increasingly dominated by interbedded tuffaceous sedimentary rocks and calc-alkaline basaltic andesite.

A period of uplift ensued after the SMVC during which time the rocks were faulted and sharply flexed upward in a west-tilted block near the SMVC (Figure 5 and 6). Broad uplift apparently occurred in the rest of the study area, creating a widespread unconformity..

Between about 25 Ma and 18 Ma, extensive ash flows and subordinate lavas of both calc-alkaline and tholeiitic composition partially buried the topography developed during the uplift (Priest and others, 1987; Tob2, Toa2, and Tor2, of Figure 5). These rocks could not be shown separately from the rest of the episode 1 sequence on Figure 5, because of scale and insufficient detailed mapping. In the vicinity of the SMVC, where the rocks have been studied in most detail, the flare up of pyroclastic eruptions began with non-welded quartz-bearing rhyodacite ash-flows and proceeded to more mafic dacitic ash flows that are extensively welded (Priest and others, 1987). The tholeiitic lavas are interbedded primarily in the lower part of the sequence immediately above the quartz bearing ash-flows. Calc-alkaline andesite occurs in small amounts throughout the section but is more abundant toward the top. Rhyodacite lava with distinctive embayed quartz phenocrysts occurs near local volcanic centers in the eastern half of the Western Cascades. Thick sequences of tholeiitic lava and subordinate calc-alkaline lava cap many of the ridges in the western half of the study area.

The source of the 25-18-Ma rocks is not well known except in a few areas. Abundant rhyodacite and dacite lava and intrusions in the Quartzville Creek Volcanic Center (QCVC; Figure 6) are in the same stratigraphic position as these rocks and, according to Munts (1978), cauldron subsidence occurred there. The QCVC appears to be one of a series of such concentrations of rhyodacite and dacite intrusions that occur in the Western Cascades mainly east of the line shown in Figures 3 and 4. Most of the propyllitic-grade hydrothermal alteration and exposed hypabyssal intrusions are also concentrated in the core of the Western Cascades east of this line, suggesting that this area was a major volcanic axis during at least the latter part of episode 1. The continental crust also appears to be somewhat thickened in the vicinity of this volcanic axis (Figure 3).

Mafic intrusions of episode 1 are much more widespread than the silicic intrusions at the volcanic axis. These rocks appear to have erupted mainly from widely dispersed fissures and central-vent volcanos throughout the arc.

As previously mentioned, calc-alkaline dacite that may be related to subduction-zone volcanism crops out about 180 km east of the episode 1 volcanic front (Smith, 1986; Weidenheim, 1980). Taking into account intra-arc extension calculated from paleomagnetic rotation data (Wells and Heller, 1988), the main volcanic arc was about 140-120 km wide. The dacite outcrops on the east side of the arc are also inferred to be at or near the source area for contemporaneous volcanic rocks of the John Day Formation (Robinson and Brem, 1981), so this width estimate is probably near the total arc width whether the John Day rocks are included or not.

16.9-7.5 Ma - LATE WESTERN CASCADE VOLCANISM (EPISODE 2)

A period of erosion or non-deposition occurred between about 18 Ma and about 14 Ma. There is a well defined unconformity separating rocks of about

18-20 Ma age from rocks of 13-14 Ma age all along the eastern margin of the Western Cascades. Where I have examined rocks in the study area with K-Ar ages in the interval 15-17 Ma, it is apparent that many of them are andesite that has experienced deep weathering or low-grade zeolite facies alteration. It is likely that the alteration has modified the age by liberating radiogenic argon and/or modifying the potassium content. This hiatus or erosional episode does not persist south of the study area, because extensive sequences of 17-13 Ma calc-alkaline basaltic andesite and andesite occur in the Waldo Lake 15' quadrangle (Woller and Black, 1983; Sherrod, 1986).

Non-welded and minor welded ash-flow tuff of dacitic and, rarely, andesitic composition forms most of the basal part of the rocks of episode 2. This burst of pyroclastic activity occurred at about 14-13 Ma and was accompanied by local eruptions of calc-alkaline basalt, basaltic andesite, and andesite. Andesite and subordinate basaltic andesite eruptions were predominate in the period from 13 Ma to 8.7 Ma.

As previously explained, the extent and volume of the episode 2 volcanos is difficult to reconstruct, because later erosion has removed much of the volcanic material. The arc was strongly emergent at this time, causing efficient removal of tephra. This interpretation is supported by the moderate relief on most of the contacts within the sequence and limited areal extent of ash-flow tuff units. It is quite likely that the andesitic and dacitic volcanos of episode 2 were episodically destroyed by sector collapse, flowing out into streams which quickly removed the fragmental material. The sequence is also near the top of the Western Cascade section, so it has been particularly vulnerable to erosion accompanying uplift of the area during the early Pliocene. Erosion was accelerated by the tendency of basal nonwelded ash-flow and air-fall tuff to act as a slip plane for giant landslides. In fact nearly all of the large (several km^2) landslides that I have mapped were caused by failure of this poorly indurated tuff.

Some volcanic centers are, however, preserved. Andesitic intrusions and thick flows of andesite and dacite occur in the Western Cascades east of the easternmost volcanic front for episode 2 (Figures 4 and 9). There is also a large hornblende andesite volcano exposed on the north end of Green Ridge (Hales, 1975; Tm outcrop east of Mount Jefferson, Figure 4). The minimum width of the volcanic arc was therefore probably about 60 km.

7.4-4 Ma - EARLY HIGH CASCADE VOLCANISM (EPISODE 3)

A major burst of silicic and basaltic volcanism occurred between 7.4 Ma and 4 Ma. Rocks of this age are exposed on both sides of the High Cascades, and an average arc width (after any later extension) of about 45 km can be inferred. The main axis of volcanism is now entirely buried by younger lavas of the High Cascades. Andesite and dacite lava was probably a significant component of episode 3 volcanism near the volcanic axis, but this cannot be proven from available exposures. Mapped exposures show that episode 3 represents a fundamental shift toward eruption of predominantly calc-alkaline basalt and basaltic andesite. This shift toward mafic volcanism characterizes all later volcanic episodes in the study area (Priest and others, 1983).

Rocks of episode 3 are best exposed in the Deschutes Basin, where Smith and others (1987) describe the following record of early High Cascade volcanic activity: 1) deposition of a large quantity of volcanic and volcaniclastic rock at 7.42 Ma-5.4 Ma; 2) development of west-facing fault scarps at Green Ridge, largely isolating the basin from early High Cascade

sources after 5.4 Ma; and 3) continued deposition of mafic lava at a low rate until about 4 Ma .

Volcanic centers of episode 3 occur on the eastern margin of the Western Cascades and form a well-defined volcanic front composed predominantly of basalt and basaltic andesite. The largest of these centers occurs in the Iron Mountain area (IMVC, Figure 6) where much of the mafic lava issued from swarms of N35W-trending dikes (Avramenko, 1981; Black and others, 1987). A similar mafic vent complex occurs on the east flank of the Cascades where numerous dikes trend about N35W (Yogodzinski, 1986).

5.4-4.0 Ma (END OF EPISODE 3)

The amount of volcanism in episode 3 was not evenly distributed north-south along the arc. According to detailed studies of the Deschutes Basin stratigraphy, most of the episode 3 eruptions appear to have come from the latitude of Mount Jefferson to the latitude of the Three Sisters volcanos (Smith, 1986; Figure 6). This part of the arc also became the site of a large arc-parallel graben that started to form at 5.4 Ma, effectively ponding much of the volcanic ejecta that erupted at the end of episode 3 and beginning of episode 4 (Taylor, 1981; Smith and others, 1987; Figures 4 and 6). This structure will henceforth be referred to as the High Cascade graben. A similar but narrower graben also apparently formed north of Mount Jefferson at the close of episode 3 (Sherrod and Conrey, 1988; Figure 6). The configuration of the High Cascade graben is shown on Figures 4 and 5. Constraints on the total offset are explained below in the structural geology section.

The end of episode 3 was also punctuated by a trapdoor uplift of the Western Cascades hinged at the Willamette Valley. As explained below (structural geology section), this uplift was abrupt, starting at about 5.1-4.5 Ma and ending at about 3.3 Ma.

3.9- 0.731 MA - LATE HIGH CASCADE VOLCANISM (EPISODE 4)

The volcanic rock of episode 4 is the platform upon which the modern volcanic arc of episode 5 is built. The distribution of these and younger rocks define the geomorphic area referred to as the High Cascades, a volcanic arc varying in width from about 16 km to 51 km, north to south. The volcanic landforms of this episode are generally not very well preserved, although it is apparent that valleys ancestral to modern valleys have controlled the distribution of the rocks.

Most of the rocks of episode 4 are buried deep within the High Cascade graben. The thickness and composition of these intra-graben rocks is largely a matter of speculation, but, judging from the few exposures available, the composition was little different from the episode 3 rocks. There are local occurrences of andesite, dacite ash-flow tuff, and locally thick accumulations of intra-graben sedimentary rocks, but the majority of the rock appears to be basalt and basaltic andesite. One exception to this generalization is the area in the vicinity of Mount Jefferson, where andesite and subordinate dacite and rhyodacite erupted (G.R. Priest, 1983, unpublished mapping; R.M. Conrey, 1985-1988, unpublished mapping; Sherrod and Conrey, 1988).

Intra-graben rocks in the age range 3.9-2.8 Ma are only exposed in two places on the west side of the High Cascade graben. An east-tilted sequence

in the basal part of Foley Ridge (FR, Figure 6) is characterized by basaltic andesite and subordinate andesite and ash-flow tuff (K-Ar age of 3.64 Ma near the base, Priest, and others, 1988). Compact basalt and basaltic andesite are the predominate rock type in a thick sequence exposed southwest of Mount Jefferson (K-Ar ages of 3.07 and 2.7 Ma at the base (Priest and others, 1987); Figure 6).

Outpourings of diktytaxitic basalt with a low (48-50%) silica content characterized many of the intra-graben eruptions from about 2.7 Ma to the end of episode 4 in the central part of the High Cascade graben (Taylor, 1981; Priest and others, 1988). These rocks are well exposed in the Foley Ridge area (Figure 6).

As previously mentioned, the Western Cascades were strongly uplifted at the end of episode 3. Prior to about 1.7 Ma, this uplifted, generally fault-bounded rock blocked the flow of episode 4 rocks from the High Cascade graben. This 1.7 Ma age is on a High Cascade intracanyon lava flow exposed 17 km west of the graben at an elevation of 730 m (6.5 km west of FR on Figure 6; Priest and others, 1988). Prior to this time, intra-graben sediment and lava of episode 4 accumulated to elevations of 1100-1200 m, banking up against graben-bounding fault scarps (e.g. the sedimentary rocks of Parkett Creek, Black and others, 1987; basalt of Cupola Rock of Priest and others, 1988).

Episode 4 may be viewed as a continuation of episode 3 volcanism in an intra-graben setting. The graben faults and fractures probably offered magmas easy access to the surface, and this factor, plus probable continued eastward migration of the volcanic front, caused nearly all of the eruptions to be confined to the High Cascades. There are, however, some significant exceptions to this generalization. Basaltic volcanos erupted in the Western Cascades at the Battle Ax volcanic center (BAVC), Snow Peak volcanic center (SPVC), and an unnamed volcanic center near the IMVC (Figure 6).

0.730-0 Ma - LATE HIGH CASCADE VOLCANISM (EPISODE 5)

I have separated the late High Cascade episode into episodes 4 and 5 at 0.730 Ma, the beginning of the Brunhes normal magnetic polarity epoch. This division was pursued primarily for use in volcanic rate calculations, taking advantage of mapping by Sherrod and Smith (1989) in the High Cascades. A similar division may prove to be useful for regional correlation of mappable units in the future, since volcanic rocks erupted prior to 0.3-0.7 Ma are generally in poorly preserved volcanic landforms and intra-canyon benches perched on the sides of modern valleys. Volcanic rocks erupted after this time are generally in well preserved volcanic landforms with intra-canyon flows lying at the bottom of modern valleys. For instance, isotopic age data suggest that major High Cascade stratocones in the study area were formed within the last 300,000 years (e.g. Priest and others, 1987; Taylor, 1987), and intracanyon flows at current river levels in the Western Cascades are probably about 0.5 Ma or younger. This latter observation is based on a K-Ar age of 0.540 $\pm$ 0.049 Ma (0.57% K; 0.54 x 10^{-12} moles $^{40}Ar_{rad}$; 91.7% $^{40}Ar_{atm}$; Paul Damon, analyst) on the base of an intra-canyon flow near Pigeon Prairie (PP, Figure 6). The flow is within a few meters of the elevation of the current North Santiam River and may record the time when the largest streams became essentially graded.

Episode 5 volcanism was, again, little different in style or composition from episodes 3 or 4. The dominate volcanic rock erupted was basalt and

basaltic andesite, although voluminous andesite, dacite, and rhyodacite erupted locally. The main locus of dacite and rhyodacite activity was a silicic highland that includes the South Sister and a bench of silicic lava domes and short flows (Taylor, 1978; Figures 4 and 6). Dacite and rhyodacite lava and ash-flow and air-fall tuff erupted from the northern part of the silicic highland at about 0.3 Ma, and younger eruptions of silicic lavas occurred in the southern part of the highland (Taylor, 1978; 1987; Hill, 1985). The main center of andesite activity was, like in episode 4, in the Mount Jefferson area (Conrey, 1988). Most of the rest of the volcanic arc erupted basaltic andesite and subordinate basalt, forming shield volcanos and local composite cones such as the North Sister, Middle Sister, and Three Fingered Jack (Figure 6).

The modern volcanic arc is narrower than the episode 4 arc, ranging in width from 3 km on the north to 38 km on the south, with the volcanic front 7.0-1.4 km east of the episode 4 front (Figure 8). This narrowing may reflect a permanent change in the locus of volcanism, or the fact that episode 5 is a short period of time relative to episode 4. More volcanism would be expected near the volcanic axis at any given time, with decreasing amounts east and west. It may be that if episode 5 were allowed to continue for an additional 2.6 Ma, matching the length of episode 4, increased opportunity for eruptions from low-probability sites would widen the arc until it more closely matched the episode 4 arc.

SUMMARY

The eruptive history of the Cascade volcanic arc consists of three main compositional phases, modified by continuous and discontinuous tectonic events. Continuous landward migration of the volcanic front and narrowing of the arc has changed the locus of volcanism, whereas episodic uplift and faulting events have produced widespread unconformities. These tectonic events are superimposed on changes in the composition of volcanism that led from 1) a 43.2-18-Ma episode characterized by eruption of tholeiitic differentiates and highly differentiated silicic and intermediate rocks to 2) a 14-8.7-Ma episode characterized by eruption of calc-alkaline lavas and subordinate pyroclastic rocks of intermediate composition to 3) a 7.4-0-Ma episode of High Cascade volcanism characterized by eruption of voluminous calc-alkaline basalt and basaltic andesite. The interplay of these compositional and tectonic changes allows 5 volcanic episodes to be recognized and mapped in the field.

Early Western Cascade volcanism of episode 1 may have begun as early as 43.2 Ma, but most of the volcanic rock seems to have erupted at 35-18 Ma. Local andesitic volcanos and voluminous eruptions of tholeiitic differentiates and silicic pyroclastic rock characterized the volcanism. The main volcanic arc was about 180 km wide at this time and was relatively low in elevation, particularly in the early part of the episode, when it was almost certainly a subsiding basin. The strandline of a Pacific embayment was located at or within a few km the volcanic front (Snavely and Wagner, 1963; Orr and Miller, 1984). At present this entire period of Cascade history is combined as episode 1, but more detailed mapping in the future should be able to distinguish at least three major episodes in this interval:

1. An initial episode of chiefly tholeiitic and silicic volcanism ending sometime prior to 26.5 Ma, during which time the arc was a strongly subsiding basin.

2. An intermediate episode characterized by eruption of calc-alkaline andesite, basaltic andesite, and dacite from the central part of the arc. This episode ended prior to 25 Ma. Hornblende-phyric andesite and calc-alkaline basaltic andesite are the most characteristic rocks, although abundant tholeiitic lava continued to erupt near the volcanic front.

3. A final episode of silicic and tholeiitic volcanism that followed a period of uplift and deformation. This episode probably started at about 25 Ma and ended by about 18 Ma. Ash-flow tuff, rhyodacite lava, and subordinate tholeiitic lava are the characteristic rocks. The silicic rocks are locally notable for the occurrence of embayed quartz phenocrysts.

Early Western Cascade volcanism ended with a period of uplift and/or low volcanic activity that lasted from about 18 Ma to about 14 Ma. Eruption of dacitic ash flows and air falls of the late Western Cascade episode began at about 14 Ma, but even more voluminous eruptions of calc-alkaline two-pyroxene andesite and subordinate basaltic andesite and dacite dominated volcanism from about 13 Ma to 8.7 Ma. These events define volcanic episode 2.

High Cascade volcanism is characterized by eruptions of basalt and basaltic andesite that began at about 7.4 Ma centered on a volcanic axis essentially coincident with the current High Cascade axis. High Cascade volcanism is divided into three episodes based primarily on mappable unconformities.

Early High Cascade volcanism, episode 3, was characterized by eruption of voluminous basalt, basaltic andesite, and subordinate silicic ash flows and air falls. This volcanic arc was about 13 km wider than the modern High Cascade arc, and is now largely hidden from view, owing to subsidence into a graben that ended the episode at about 5.4-4 Ma. A trapdoor uplift of the Western Cascades, hinged at the Willamette Valley, also began after about 5.1-4.5 Ma and was probably largely complete by about 3.3 Ma. The uplift left the western margin of the early High Cascade volcanic arc perched at the top of Western Cascade ridge tops.

Late High Cascade volcanism at 3.9-0 Ma was largely confined to the vicinity of the modern High Cascades by the High Cascade graben and the uplifted Western Cascade block. This volcanic episode is compositionally identical to episode 3, although it can be conveniently separated into two episodes at 0.730 Ma, the beginning of the Brunhes normal magnetic polarity epoch. Volcanic rocks erupted prior to this time (episode 4) are generally in poorly preserved volcanic landforms and intra-canyon benches perched on the sides of modern valleys. Volcanic rocks erupted after this time (episode 5) are generally in well preserved volcanic landforms with intra-canyon flows lying at the bottom of modern valleys.

Intra-canyon relationships allow a detailed history of erosion and deposition to be constructed for the period after the beginning of uplift in the Western Cascades and graben faulting in the High Cascades at 5.4-4.5 Ma. Rapidly eroding drainages spilled sediments east and west from the crest of the west-tilted Western Cascades. Sediment and newly erupted volcanic rock was trapped in the graben, causing erosion to decrease progressively as sediment accumulated. Graben fill reached elevations of 1100-1200 m on west-side fault scarps by about 2 Ma. The combination of westward retreat of the west graben scarp and headward erosion of the ancestral McKenzie River allowed lava to escape the graben by about 1.7 Ma. Large trunk streams like the

North Santiam River and McKenzie River continued to cut into the uplifted Western Cascades during episode 4, probably reaching about their current grade and elevation by 0.5 Ma.

STRUCTURAL GEOLOGY

ORIENTATION OF INTRUSIVES

Subvertical plutonic bodies are generally elongated perpendicular to the minimum horizontal stress, sigma 3, and parallel to the maximum and intermediate stress axes, sigma 1 and 2, respectively (Nakamura, 1977). I will use known dike orientations to infer changes in sigma 3.

Statistical analyses of dike orientation in the study area suggest that the dominant direction in the Western Cascades is northwest. Sherrod (1986) showed that about 90% of the measured orientations of vertical dikes in the Western Cascades in the study area varied from north-south to N80W with a strong maximum at N40-50W. His data lumps together dikes of episode 1, 2, and 3. Sherrod (1986) also summarized vertical dike and vein trends from episode 2 and 3 rocks in the south-central Western Cascades. He found that nearly all of the dikes trend about N75W to N15W with about half of them at N70W to N30W. He also pointed out that Diller's (1900) study of the orientation of dikes and veins in the Bohemia Mining district (19 km south of the study area) is indicative of crustal stress at about 22 Ma (age from Power and others, 1981). Diller (1900) found that 90% of the dikes and veins trend N60W to east-west. He included many non-vertical dikes and veins in his data, so the work is not directly comparable to Sherrod's compilations.

Studies of dike swarms at episode 3 volcanic centers on the west side (Avramenko, 1981) and east side (Yogodzinski, 1985) of the High Cascades found a dominant trend of N35^{o}W. This trend is remarkably consistent at both volcanic centers with nearly all of the data between about N20W and N50W.

Numerous workers have noted the obvious north-south alignments of young volcanic vents in the High Cascades (e.g. Figure 6; Taylor, 1981; Bacon, 1985; Sherrod, 1986). These data are consistent with a sigma 3 east-west, essentially parallel to the direction inferred from modern earthquake data for central Oregon (Couch and Lowell, 1971). Sherrod and Pickthorn (1989) conclude that sigma 3 was east-west at 3.5-0 Ma.

The original dike orientation can be inferred by correcting for the tectonic rotation deduced from paleomagnetic data. Assuming that the clockwise rotation of 30^{o} noted in 25-Ma rocks in the study area (Magill and Cox, 1980; modified by Gromme' and others, 1986) occurred at a constant rate through time, the following original dike orientations can be surmised:

1. Episode 1 (22 Ma; 90% of data): N86W-S64W
2. Episode 2 + 3 (17-4 Ma; 50% of dike data): N35W-E-W
3. Episode 3 (7-5 Ma; statistical maximum): N42$\pm$16^{o} W
4. Episode 4-5 (3.5-0 Ma): N-S

I conclude from these observations that horizontal stress in the arc changed progressively from episode 1 to 5 such that sigma 3 changed from north-northwest or north-south to east-west. As explained below (fault and fractures section), sigma 3 was probably oriented east-northeast at the end of episode 3 (5-4 Ma).

FOLDS

There are no obvious large-scale fold belts in the Cascades, although local folds and monoclines can be traced for several km in some areas. The local nature of the folds is consistent with a response to local rather than regional compressive stress fields, although this cannot be proven. Priest and others (1988) argued that the Breitenbush anticline (Figure 6) of Thayer (1939) may be related to local compressive stresses generated in an area of oblique-slip faulting. Sherrod (1986) concluded that the anticline is more likely due to regional crustal contraction oriented northwest-southeast. Sherrod and Conrey (1988) suggest that the folding probably began after 18 Ma, ending by 12 Ma. The limbs of the fold trend from about N20E on the southwest end of the structure (Priest and others, 1987) to about N45E at the northeast end (Sherrod and Conrey, 1988), so crustal contraction would be parallel to N70-45W. Similar northeast orientations have been found in folds in the Coast Range (Wells and Peck, 1961) and areas of the Western Cascades north (Beeson and others, 1982) and south (Sherrod, 1986) of the study area.

I conclude from the above discussions that there is permissive evidence of mild compression in the volcanic arc during episode 2. The direction of crustal shortening, corrected for the clockwise tectonic rotation (i.e. Magill and Cox, 1980; Gromme' and others, 1986), was approximately east-west to west-northwest.

FAULTS AND FRACTURES

General Observations

There are many shear zones in the Western Cascades but few areas have enough detailed stratigraphic control to constrain the extent or sense of movement on these structures. No systematic study of the orientation of shear zones and fractures is available for the study area, although some lineament studies have been done (Venkatakrishnan and others, 1980; Kienle and others, 1981). The predominate lineament directions in the Western Cascades are north-south, northwest, and northeast (Venkatakrishnan and others, 1980; Kienle and others, 1981). In the North Santiam River area many of the small-displacement faults and sheared joints are oriented northwest, producing strong lineaments, whereas the major faults trend northeast (Priest and others, 1987).

Most mapped faults with offsets greater than a few meters have been mapped on the margins and in the interior of contemporaneous volcanic arcs. As previously explained, north-south faults bound graben in the High Cascades at the margins and probably the interior of the episode 4 volcanic arc. These north-south to north-northwest-trending faults at Green Ridge appear to merge southward with a series of young northwest-trending faults (Tumalo fault zone, Figure 6). Episode 4 or 5 faulting is not known to affect the Western Cascades, except at the edge of the episode 4 volcanic front (Priest and others, 1983; Sherrod, 1986). Small-displacement, northwest-trending normal faults of episode 3 occur north of Pigeon Prairie (Figure 6) in the episode 3 volcanic front (Priest and Woller, 1983b). A north-south fault with greater than 152 m of dip slip offset occurs at Cougar Reservoir; the fault is located spatially and temporally between the episode 2 and episode 3 volcanic fronts (CRFZ, Figure 6; Priest and Woller, 1983a). North-northeast-

trending faults with large offsets bound a west-tilted block of episode 1 rock on the east side of the SMVC near the probable volcanic axis during episode 1 and the volcanic front of episode 2 (Hoover fault zone (HFZ) and unnamed fault to the west; Figure 6). The HFZ affects rocks 18 Ma and older, but, as previously explained, the age of tilting of the episode 1 rocks on the west side of the fault appears to be older than about 25 Ma. The HFZ may therefore have had Oligocene and Miocene activity, contemporaneous with both the episode 1 and 2 arcs.

All of the faults discussed above, except the episode 3 faults north of Pigeon Prairie, have northerly strikes approximately parallel to the contemporaneous volcanic arc. Even the northeast trending faults of episode 1 and 2, when corrected for clockwise tectonic rotation (i.e. Magill an Cox, 1980; Gromme' and others, 1986), have essentially north-south trends.

Many of the large-displacement faults older than the High Cascade graben have evidence of oblique slip. The HFZ bounds the east side of the tilted block at the SMVC and appears to have generated a secondary northeast-trending anticline on the downthrown (east) block of the fault (Priest and others, 1987; Figures 5 and 6). This anticline is broken near its axis by small-displacement faults with subhorizontal slickensides, possibly indicating a component of lateral shear along the HFZ (Priest and others, 1987). Some horizontal slickensides on splinter faults related to CRFZ suggest that it may have a significant component of lateral slip (Priest and Woller, 1983a).

Arc-parallel Graben in the High Cascades

As previously explained, the High Cascade graben formed about 5.4 Ma, and faulting may have continued into episode 4. The west side of the graben is well defined, with displaced units indicating offset of at least 600 m (Black and others, 1987; Brown and others, 1980; Priest and others, 1988). The east side of the graben is not as well defined as the west side, except at Green Ridge, where a prominent fault scarp occurs (Figure 6). The east side of the graben may continue south, lying immediately west of a small inlier of episode 3 rock that protrudes through the extensive cover of episode 4 and 5 rocks near Bull Springs (Figure 6; Hill, 1988). Alternatively, the eastern boundary may swing southeastward, parallel to small-displacement normal faults of the Quaternary Tumalo fault zone (Figure 6; Smith, 1986). Keach (1986), utilizing extremely poor quality seismic reflection data, inferred that the southern part of the graben may be a trap door structure with most offset on the west side. The amount of downward offset on the east side of the southern half of the graben could therefore be modest, the amount of the offset on the Tumalo fault zone, or as large as that on the west side. If there is a large east-side offset, it could be localized under the Tumalo fault zone or west of the Bull Springs inlier.

The total dip-slip offset on the High Cascade graben is probably in excess of the 600 m measured on the outermost faults. The contact of 2.7-Ma and younger episode 4 rocks with pre-graben rocks on the western side of the High Cascade graben is an east-dipping unconformity indicative of erosion into the graben. This unconformity cuts across all exposed pre-graben rocks, <u>including</u> rocks on down-dropped blocks <u>within</u> the west margin of the High Cascade graben (contact of the sedimentary rocks of Parkett Creek with pre-graben rocks of Black and others, 1987; Priest and others, 1988). This relationship demands that there be at least one pre-2.7-Ma, large downward offset on the graben east of the mapped faults on the west margin (Priest and

others, 1988). A possible location of the buried faults bounding this structure are well-aligned Holocene basaltic vents that occur at the longitude of Sand Mountain (Figure 6). The offset on this buried structure is inferred in cross section B-B' from three observations: 1) the offset must produce a basin capable of holding material eroded from the westernmost intra-graben fault block; 2) the offset must be sufficient to completely bury the episode 3 volcanic arc; and 3) the buried topographic profile of the episode 3 arc is assumed to be parallel to the episode 5 topographic profile on the west flank, but, on the east flank, it is assumed to be the westward extrapolation of the dip slope of Green Ridge.

An arc-parallel graben has been inferred north of Mount Jefferson (Figure 6). This graben is defined on the west by a north-trending fault with at least 500-600 m of dip-slip displacement (Sherrod and Conrey, 1988) and a similar fault on the east side of the High Cascades (Sherrod and Smith, 1989). The activity on the west-side fault is inferred to be contemporaneous with formation of the High Cascade graben (Sherrod and Conrey, 1988).

Formation of north-south-trending graben implies that sigma 3 shifted to an east-west direction. However, this direction of extension may have been influenced by the northerly trend of the arc, concentrating deformation in thermally weakened, volcanically loaded zones. Indeed the northwesterly trend and en echelon pattern of many graben-bounding faults of the HCFZ (Figure 6) suggests that sigma 3 was oriented east-northeast, about half way between east-west and the northeast direction to the direction deduced from episode 3 dikes. I conclude that sigma 3 rotated from northeast to east-northeast during episode 3.

Conclusions

Major faults were localized at the margins or interior of the contemporaneous active volcanic arc. The best known event of this kind was the formation of arc-parallel graben at about 5.4 Ma in an environment of east-northeast extension and dip-slip faulting. Earlier arc-parallel faults appear to have had both dip slip and strike slip components of displacement.

UPLIFT

As previously explained, the Western Cascades were uplifted at the end of episode 3 in the early Pliocene. The available evidence suggests that the uplift was relatively abrupt, approximately coinciding with formation of arc-parallel graben in the High Cascades.

There is excellent geomorphic evidence for early Pliocene uplift. The largest rivers, the North Santiam and McKenzie River, have about 1 km of relief on the east side of the Western Cascades, varying to essentially no relief at the Willamette Valley. The youngest volcanic rocks at the tops of the uplifted ridges have ages of 4.5 $\pm$ 0.3 Ma at Marks Ridge (Verplanck, 1985) to an average, weighted for error, of 5.13 $\pm$ 0.01 Ma near the Horse Creek Fault Zone (Figure 6; Priest and others, 1988). Younger volcanic rocks occur on intra-canyon benches that are the record of old valleys that were clearly precursors to modern valleys (e.g. lavas of Battle Ax Mountain and basalt of Pigeon Prairie of Priest and others, 1987).

The entrenchment of streams in the Western Cascades cannot be explained by lowering of a base level represented by the sea, because the sea

has been absent from the mouths of Western Cascade streams since the early Miocene (Snavely and Wagner, 1963: Orr and Miller, 1984). Only local base level represented by the Willamette Valley forearc basin has had any significance for the Western Cascades since the retreat of the sea, and there is no evidence that the valley has undergone post-5-Ma changes in elevation sufficient to cause the entrenchment of streams. The easiest explanation for the entrenchment is that there has been a trap door uplift of the volcanic arc hinged at the central part of the Willamette Valley. This hypothesis could be tested if 6-5 Ma stream profiles could be inferred from long east-west flows of 6-5-Ma lava in the Western Cascades. No such flows have been found.

The uplift of the Western Cascades undoubtedly started after about 5.1-4.5 Ma, but was it abrupt or gradual?. Sherrod (1986) presents evidence from immediately south of the study area that suggests that abrupt uplift occurred there after about 5-6 Ma, the age of ridge-capping basalt flows. He showed that stream profiles reconstructed from mapping two long intra-canyon lava flows in the Willamette River drainage rapidly decreased in gradient from about 3.3 Ma to 2 Ma, decreasing much more slowly from 2 Ma to present. He concluded that the evidence is permissive of rapid uplift between 6 and 3.3 Ma (Sherrod, 1986). The similarity of this age to the age of faulting at the High Cascade graben is suggestive that the two events are linked.

There were probably other periods of uplift that were responsible for widespread unconformities at about 18-14 Ma and some time after the eruptions at the SMVC but before the ash-flow flare up at 25 Ma. These unconformities could also be the result of erosion during a period of relative volcanic quiescence.

SUBSIDENCE

Substantial subsidence of the volcanic arc probably occurred during each burst of activity as a result of crustal loading. Gentle (5^{o}) eastward dips, decreasing in angle upward in the section, are common in strata throughout the western half of the episode 1 arc (e.g. Figures 5 and 6). As explained earlier, it is difficult to account for preservation of the thousands of feet of episode 1 volcaniclastic rock without substantial subsidence. Eastward dips in episode 1 rocks appear to steepen to about $6\text{-}10^{o}$ next to the margin of the episode 3 arc in the northern and central part of the study area where episode 2 rocks also dip gently eastward. Gentle eastward dips have also been mapped in strata of episode 4 near the margin of the episode 5 volcanic arc, although some of these dips may be the result of intra-graben faulting (Flaherty, 1981; Priest and others, 1988).

Smith and others (1989) show that strata on the east side of the early High Cascades were tilted westward during episode 3. They argue that formation of the High Cascade graben occurred when the crust failed from loading by the early High Cascade volcanic arc. They also conclude that some rebound of marginal horst blocks occurred when the structural connection with the episode 3 arc was broken. The previously mentioned east-tilting of 3.6-Ma intra-graben rocks at Foley Ridge suggests that post-3.6-Ma subsidence of the High Cascades may have been accommodated by intra-graben faulting (Priest and others, 1988).

CONCLUSIONS

Sigma 3 in the Cascades rotated progressively from approximately north-south in episode 1 to east-west in episode 5. The orientation of the maximum and intermediate stress directions is largely unconstrained by the available data, although the maximum principal stress could have been roughly east-west or west-northwest during mild folding that characterized episode 2.

Faulting and sharp flexures seem to have been concentrated in the active parts of the arc at any given time in the past. The volcanically inactive western margin of the Cascades shows no evidence of post-5.4-Ma deformation, apparently forming a more or less coherent, west-tilted block. This tilting probably occurred abruptly, starting about 5.1-4.5 Ma and ending about 3.3 Ma.

CHANGES IN THE COMPOSITION OF VOLCANISM

INTRODUCTION

I will answer the following questions in this section:

1. Has volcanism shifted toward eruption of less evolved (e.g. high Mgo, Ni) magmas through time?

2. Has K and Rb content decreased through time at a given level of differentiation?

3. Has volcanism changed from tholeiitic to calc-alkaline with time?

4. How do basaltic magmas of the Cascades compare with basalts from other tectonic environments?

OBSERVATIONS

Histograms of MgO and SiO_2 (Figure 12) clearly show that basaltic andesite makes up a high proportion of the analyses of every episode. It is also apparent that low-silica basalt with relatively high MgO has been sampled more frequently in early and late High Cascade episodes (3-5) than in previous times. Finding rocks with undifferentiated compositions (high MgO) is apparently quite difficult in the episode 1 terrane. Nearly all of the episode 1 samples have highly evolved compositions, even though some have relatively low silica contents. This latter observation is consistent with the common occurrence of very highly differentiated tholeiitic lavas in episode 1, as is shown by the high FeO/Mg and low MgO of these rocks (Figure 13; Table 3).

The shift to less evolved compositions with time is also demonstrated in the compilation of most mafic (highest MgO, Ni; lowest SiO2) and average basalt compositions (Table 3). MgO and Ni increase while SiO2 decreases from episode 1 to 3. Rocks of episodes 3-5 seem to have similarly mafic compositions, although there are some subtle variations. Compared to episodes 3 and 4, basalt seems to have been less frequently sampled in episode 5 relative to more evolved (higher SiO2, lower MgO) rocks (Figure 12).

The tholeiitic affinity of the episode 1 rocks shows up clearly in the FeO/MgO versus SiO2 plot, although a separate compositional field of typical

calc-alkaline rocks is also apparent (Figure 13). Tholeiitic differentiates also occur in episodes 3-5, which show a similar two-fold fields of tholeiitic and calc-alkaline compositions (Figure 13). Most of the high FeO/MgO values of episode 3-5 are, however, at higher SiO2 than equivalent values for episode 1, suggesting less tholeiitic affinity. Episode 2 rocks are nearly devoid of samples with high FeO/MgO, being a typical calc-alkaline assemblage.

The plots of Rb and K versus MgO show that the overall content of these elements has been approximately constant with time (Figures 14 and 15; Sherrod, 1986). Average compositions of Cascade basalt show the same pattern (Table 3).

Comparison of the composition of Cascade basalt to basalt of other tectonic provinces can provide useful insights into petrogenesis. Average episode-2 basalt is very similar in composition to average continental-arc basalt (CAB), although K_2O and Rb are closer to the low values typical of island arc tholeiite (IAT; Table 3). TiO_2 and FeO (Table 3) are distinctly higher in average episode 1, 3, 4, and 5 basalt relative to average CAB, IAT, back-arc-basin basalt (BABB; Table 3), and episode-2 basalt (Figure 16). Much of the basalt from episodes 1, 3, 4, and 5 has TiO_2 in excess of 1.5%, similar to Basin and Range basalt (BRB; Figures 16 and 17; Table 3) and basalt from extensional tectonic regimes in general (Gill, 1981). MgO and Ni of average episode-1 basalt is lower than all other episodes, being most similar to average IAT, and very dissimilar to BRB (Table 3). MgO and Ni of episodes 3-5 basalt is most similar to BABB and BRB. However, Cascade basalt generally has lower CaO than BABB and BRB (Table 3).

CONCLUSIONS

I conclude from the above observations that during episode 1 highly MgO-, Ni-rich magma did not reach the surface, but resided for long periods in the crust where it differentiated along calc-alkaline and tholeiitic paths. Many of the tholeiitic rocks have high TiO_2, similar to TiO_2 of middle Miocene and younger Basin and Range rocks, but the episode-1 basalt is much more differentiated (lower MgO and Ni) than BRB. The high TiO_2 is similar to that of volcanic rock erupted in extensional tectonic regimes.

The arc produced abundant calc-alkaline differentiates during all episodes, but episode 2 is unique because it has only calc-alkaline rocks. Episode 2 basalt is very similar to average CAB, albeit somewhat less enriched in Rb and K_2O.

Rocks with SiO_2 in the range of 47-48% and with MgO of 8-9% are virtually unique to episodes 3-5. Basalt of these episodes has many compositional similarities to BABB and Basin and Range basalt, being most similar to BRB, particularly with respect to generally high TiO_2 . I conclude that magma could reach the surface with less modification by differentiation during the early and late High Cascade episodes than during any previous time in the arc. Petrogenetic processes during episodes 3-5 must have been somewhat similar to processes operative in the Middle Miocene to Holocene Basin and Range.

All episodes produced rocks with relatively constant amounts of Rb and K at similar degrees of differentiation. Petrogenetic models for the arc must explain lack of change of these relatively incompatible elements with time.

INTERPRETATIONS

MIGRATION OF THE VOLCANIC FRONT

A number of workers have noted the common occurrence of an extinct volcanic arc outboard from the active arc (e.g. Dickinson 1973; Gill, 1981). Dickinson (1973) argued that the arc-trench gap tends to increase at the rate of about 1 km/m.y., when comparing subduction zones world-wide.

The Cascade volcanic arc has a landward migration of the volcanic front at an average rate (V_f) of about 2.4 km/m.y. over the last 30-35 Ma (Figure 11).

Landward migration of the volcanic front might be achieved by:

1. Progressive increase in the depth of melt generation by cooling the mantle wedge and/or decreasing inflow of volatiles and asthenospheric mantle into the wedge (e.g. James, 1971; Taylor, 1989).

2. Progressive lowering of the dip of the slab in the 0-100-km depth range, perhaps by erosion or heating of the lithosphere of the overriding plate (Jarrard, 1986), or by lithospheric extension.

3. Roll-back velocity (v_r) of the slab slower than v_o..

Figure 18 illustrates these models.

The cool upper part of the subducted slab acts as a heat sink for the overlying mantle wedge. Immediately after the proposed westward jump of the subduction zone in the middle Eocene (Duncan, 1982; Simpson and Cox, 1977), the mantle wedge might have been hotter than at a later time when the heat had migrated from the wedge to the slab (James, 1971). Alternatively, the progressively decreasing V_c could have caused, the addition of volatiles and new hot asthenosphere to decrease, restricting initial partial melting to deeper and more landward locations in the wedge (Taylor, 1989). A hot mantle wedge at depths of less than 100-125 km might also result from extension-induced partial melting of the NAP mantle lithosphere, or by subduction of unusually hot oceanic lithosphere. Some combination of these mechanisms might account for the unusual forearc volcanism at 45-30 Ma (e.g. Wells and others, 1984). However, unique heating and extension events are not satisfying explanations for consistent landward arc migration for the last 35 Ma. They also do not account for the world-wide occurrence in subduction-related arcs of (1) the 100-125-km depth of magma generation at volcanic fronts (Gill, 1981), and (2) landward migration of volcanic fronts (Dickinson, 1973).

Slab roll-back is a function of the tendency for oceanic lithosphere to sink vertically into the mantle (Dewey, 1980). For young (<50 Ma), buoyant oceanic lithosphere like that present beneath the Cascades (Figure 11), the point of roll-back action is the basalt-eclogite transition, which probably causes the knee bend in subducted slabs (Rogers, 1985). If V_o exceeds V_r, the knee bend could move landward causing migration of the volcanic arc.

Relative changes in V_o and V_r in the Cascades are probably mostly due to changes in V_o. V_r is a function of the buoyancy and thus the age of the slab (e.g. Oldenburg, 1975). It is apparent from Figure 11 that for the last 35 Ma slab age at the latitude of the study area has not changed significantly, so V_r has probably not undergone any major changes, with one exception. Rogers (1985) argues that V_r of the JDFP increased at about 4 Ma as a result of separation of the buoyant Explorer plate. The westward component of

absolute motion of the NAP has, however, decreased through time, undergoing about a 20% reduction (-5.6 km/m.y) at about 9 Ma at the Yellowstone hot spot (Pollitz, 1988). Similar decreases occurred at earlier times (Morgan, 1983).

The decreases in absolute NAP motion should have caused decreases in V_f, unless (1) they do not really equal V_o,.or (2) V_r and V_o do not control V_f. The abrupt increase in V_r at 4 Ma offers a partial test of these hypotheses. There is no evidence that the NAP changed velocity abruptly at 4 Ma, so abrupt increase of V_r should have caused either a decrease in landward V_f or oceanward migration of the arc. Oceanward migration of the arc did occur in British Columbia at 4-0 Ma (Rogers, 1985), but the arc remained stationary or moved eastward in Oregon (Figure 11). I conclude from the V_f of the British Columbia arc that the relative magnitude of V_r and V_o are important controls on V_f. The 4-0-Ma V_f in Oregon implies that V_o there adjusted to the increased V_r, possibly by extension in the NAP. Extension of the NAP in Oregon is supported by evidence of Pliocene and younger extensional faulting in the High Cascades (e.g. Taylor, 1981; Sherrod and Pickthorn, 1989), and the adjacent Basin and Range (Donath, 1962; Lawrence, 1976).

Likewise, high amounts of 37-0-Ma arc and back-arc extension (200-250 km at 42° N) inferred from paleomagnetic data (Wells and Heller, 1988) suggest that V_o in Oregon has been accelerated by NAP extension throughout the life of the arc (Figure 21). Pollitz (1988) inferred that a 20 percent decrease in the absolute westward velocity of the NAP at 9 Ma at the Yellowstone hot spot accelerated and altered the direction of Basin and Range spreading. Spreading rate in the western NAP after 9 Ma may therefore actually be dependent upon V_o decreases in the eastern NAP, reducing the decreases at the leading edge of the NAP by significant amounts. I conclude that V_o data from hot spots is not representative of V_o at the volcanic front. V_r is unknown and spreading rate and V_f data have large uncertainties; therefore the effect of the V_o-V_r ratio on V_f is not known, at least from 35 Ma to 4 Ma.

The dip of the buoyant JDF slab is probably controlled by the configuration of the lithosphere of the NAP. Thinning of the NAP lithosphere by extension, erosion, or heating would lower the shallow dip, moving the 100-125-km depth of melting landward (Figure 18). Jarrard (1986) found that (1) there is a strong world-wide correlation between high arc-trench gap and low slab dip at the 0-100-km depth (Dip-I), and (2) low Dip-I correlates strongly with high total age of the volcanic arcs . He concluded that lithospheric thinning is the most likely mechanism controlling landward migration of volcanic arcs. Indeed it is difficult to draw credible pre-7.42--Ma slab positions without increasing Dip-I (Figure 11), so thinning of NAP lithosphere may have been an important factor controlling V_f.

I conclude that progressive thinning of the NAP lithosphere by heating, erosion at the base, or extension probably lowered the dip of the slab at 35-0 Ma, moving the volcanic front landward at an average rate of 2.4 km/m.y. The buoyancy of the slab may have caused efficient erosion of the bottom of the NAP. The V_o-V_r ratio was probably an important control on V_f during the last 4 Ma, but its importance at 35-4 Ma is not known. An unusually hot mantle wedge must have existed in the forearc prior to 35 Ma, possibly owing to the initiation of subduction, subduction of unusually hot lithosphere associated with Kula spreading ridge, and/or high extension of the overriding plate.

NARROWING OF THE ARC

The arc apparently narrowed through time (Figure 8). Narrowing of the arc could be caused by decreasing the down-dip extent of mantle wedge generating magma above the slab (Taylor, 1989), or increasing the dip of the subducted slab behind the volcanic front. Taylor (1989) favors the former process, speculating that progressively decreasing convergence rate would cause less volatiles to be carried to great depth and less back circulation of the mantle material into the wedge. Alkaline volcanism would be expected if melts were segregated at great depth (e.g. Green, 1968). The Taylor (1989) hypothesis therefore accounts for eruption of the alkaline basalt of the John Day Formation behind the arc in episode 1 but not in later episodes. Steepening of the slab is favored by the inferred very high (65-70^{o}) dip of the current subducted slab in the Pacific Northwest (e.g. Guffanti and Weaver, 1988; Rasmussen and Humphreys, 1988). If the slab dip were this high in episode 1, the slab would have been at depths below the landward side of the volcanic arc that are high (400-500 km) relative to slabs in other arcs of similar (140 km) width (e.g. compare to Kuno, 1966). Indeed, the model shown by Taylor (his Figure 4) requires a constant slab dip at 50-200 km depth of only about 30-37^{o} for the last 35-40 m.y. I conclude that steepening of slab dip may have operated in concert with decreasing volcanic production to narrow the arc.

CORRELATIONS BETWEEN THE GEOLOGIC AND PLATE TECTONIC HISTORIES

Introduction

Figures 19, 20 and 21 summarize time correlation between geologic events in the Cascades and major changes in the NAP-JDFP system, especially the angle of convergence (A_c) and orthogonal rate of convergence (V_c). These figures are not offered as proof of a causal relationship between any of the events, but they are useful for the purpose of speculation and discussion.

The interpretations and speculations in this section are based in part on the conclusions drawn from the following discussion of theoretical controls on volcanic production and composition. This discussion is segregated here to avoid needless repetition in the text.

Theoretical Controls on Volcanic Production Rate and Composition

Volcanic production rate (R_v) and composition should be dependent on the amount of partial melting at the source, the ease with which the magmas can get through the lithosphere, and the driving pressure of the magma. Extended lithosphere should allow higher rates of intrusion than compressed lithosphere, all other things being equal. Novak and Bacon (1986) showed that high extensional stress lowers the extrusion/intrusion ratio and allows magma to reside for long periods in the crust where the melt becomes highly differentiated. They inferred that in typical arc environments, the minimum compressive stress, sigma 3, is horizontal and relatively large, producing short to medium crustal residence times and limited opportunity for differentiation. Development of large silicic magma chambers would therefore not be common in a typical arc environment.

The amount of partial melting in the upper mantle is the most important factor governing all other partial melting events at shallower levels, because the mantle is the probable source of basaltic magma. Basaltic magma can differentiate to more evolved magmas and produce anatectic silicic magma in the continental crust. Mantle melting can be initiated by raising the temperature or by lowering the melting temperature of hot mantle. Temperature can be efficiently raised by friction between plates or heating from convecting magma. Decompression or addition of a fluxing agent such as hydrous fluid can lower effective melting temperature. Diapirism of upper mantle in response to subduction of the oceanic plate (e.g. Sakuyama, 1983) or from lithospheric extension in the overriding plate can cause decompression melting. Hydrous fluids from the dehydration of the oceanic slab are probably the main fluxing agents. Subduction can thus produce magma from decompression and fluxing, whereas crustal extension utilizes mainly decompression. All other things being equal, I would expect the V_c to control magma production, with crustal extension as a secondary control.

I conclude that the highest rate of mafic magma production in the Cascades should occur when rates of extension and convergence are high. The rate of eruption of mafic magma should be highest when crustal extension is sufficient to allow intrusion of the magma, but not so high as to allow the magma to reside at shallow crustal levels for long periods. High rates of silicic volcanism would be favored when crustal extension was very high.

Subduction-related volcanic rocks are thought to have relatively low TiO_2 (less 1.3%), whereas volcanic rocks erupted in extensional tectonic environments (with or without subduction) are characterized by high TiO_2, rarely less than 1.0% (Gill, 1981). Assuming that low-TiO_2 calc-alkaline andesite and basaltic andesite are produced primarily by subduction processes (e.g. Gill, 1981; Sakuyama, 1983) rather than crustal extension, eruption of these magmas would be favored during periods of active subduction but low crustal extension.

43-17 Ma - EARLY WESTERN CASCADE VOLCANISM (EPISODE 1)

Early Western Cascade volcanism was characterized by high rates of eruption of highly differentiated magmas that accumulated in subsiding basins. V_c decreased by over 50% from the beginning of episode 1 to about 35 Ma (Figures 19 and 20). However, much of the volcanism in the main volcanic arc during episode 1 probably occurred from about 35-18 Ma, as V_c decreased at a much lower rate (Figure 19).

A_c was nearly perpendicular to the continent at the beginning of episode 1, but became increasingly oblique, particularly during the main period of activity at 35-0 Ma (Figure 19). The convergence direction was close to the strike of 22-Ma dikes (Figure 21). Dikes typically align parallel to the maximum horizontal compressive stress (Nakamura, 1977), so I speculate that horizontal compressive stress at the convergent plate boundary was transmitted into the arc at 22 Ma and probably at earlier times in episode 1. The oblique convergence at 35-0 Ma could have initiated strike-slip faulting and transtension in the arc (e.g. the model of Dewey, 1980).

The highly differentiated nature of both the tholeiitic and calc-alkaline rocks of episode 1 suggests that magmas resided in the crust for extended periods of time. The TiO_2 content of the tholeiitic rocks was also very high. These observations are consistent with crust under a high degree of extension with much partial melting caused directly from crustal extension. Conrey and

others (1983) and Smith (1986) also noted that the high TiO_2 of episode 1 rocks may be indicative of eruption in an extensional regime. The east-west to west-southwest orientation of episode 1 dikes suggests that the probable direction of extension was north-south to north-northwest (Figure 21).

Wells and others (1984) suggested that the extension was caused by oblique convergence, developing a component of dextral shear at the plate margin. Conrey and others (1983) suggest that the extension is a heat-driven phenomenon directly related to the rate of magmatic withdrawal and volcanic loading. The thermal model would predict that the arc was emplaced in a subsiding basin with deformation by dip-slip normal faulting at the margins and interiors of volcanic piles. The transtension model predicts a more complicated pattern of strike-slip faulting and normal faulting. Unfortunately geologic evidence is equivocal, because very little detailed mapping is available to evaluate the models. The previously mentioned oblique-slip faulting and sharp flexures in the episode 1 and 2 arc are permissive of the transtensional mechanism. The evidence of a broad subsiding basin is permissive of the thermal model.

The R_V was higher at this time than in any subsequent episode (Verplanck and Duncan, 1987), primarily because of the high rate of silicic volcanism (Figure 19). I conclude that a high rate of extension probably combined with the high V_C to produce high R_V. The source of the extension may have been from transtension within thermally weakened lithosphere and/or thermally driven extension from the high R_V.

16.9-7.5 Ma - LATE WESTERN CASCADE VOLCANISM (EPISODE 2)

Episode 2 was characterized by eruption of calc-alkaline andesite and basaltic andesite with low-TiO_2 relative to other episodes (e.g. Figures 16 and 20). Eruption rate was also lower than in other episodes (Figure 19).

I speculate that the low rate of volcanism was primarily the result of low magma production caused by lower convergence and extension rates in episode 2 compared to episode 1. The lower TiO_2 content of the episode 2 rocks is indicative of lower crustal extension than in episode 1. The V_C was also significantly lower (Figure 19).

The sigma 3 direction deduced from dike orientations in the episode 2 arc was subparallel to the direction of convergence and at a significant angle to direction of Basin and Range extension (Figure 21). Probable mild east-west to west-northwest crustal contraction (Figure 20) suggests maximum compressive stress (sigma 1) oriented west-northwest, approximately parallel to the trend of the dikes. This direction is similar but not equal to the direction of contemporaneous Basin and Range extension (Figure 21).

What factors could have controlled the stress direction? Two possibilities are the close approach of the JDF ridge (Wells and others, 1984), and NAP-PP interactions at the San Andreas transform fault. The former should have enhanced the influence of the northeast compression from convergence; the latter would produce a component of north-south compression. A third possibility is that active Basin and Range spreading produced a "push" in a S68W direction. The stress field could have been affected by all of these factors.

The lack of correlation of vertical dike azimuth to the convergence direction leads me to conclude that the combination of decreased A_c and V_c decreased the influence of NAP-JDFP interactions of all types relative to other sources of stress. The result was a progressive clockwise rotation of the principal horizontal stresses from episode 1 to 2 (Figure 21).

7.4-4 Ma - EARLY HIGH CASCADE VOLCANISM (EPISODE 3)

Episode 3 was characterized by a sharp increase in the rate of both mafic and silicic volcanism relative to episode 2, although the total rate was still significantly lower than in episode 1 (Figure 19). The eruptive rate increase was caused primarily by increases in the rates of eruption of mafic lavas with a significant amount of relatively undifferentiated high-TiO_2 basalt, tholeiitic differentiates, and silicic tuff (Figure 19 and 20). The total rate increase may not be significant in view of the dependence on previously mentioned speculative estimates of thickness and extent of these rocks in the High Cascade graben. If the rate is real, it is most easily explained by a high rate of magma production from increased convergence rate or upper crustal extension. The high TiO_2 content of many of the mafic magmas and high rate of silicic volcanism favors increased extension. The high extension could result from less coupling at the NAP-JDFP boundary as V_c and A_c decreased (i.e. plate models of Riddihough, 1984; Verplanck and Duncan, 1987; Figure 19). The plate convergence model of Engebretson (1982) shows increased V_c from episode 2 to 3 (Figure 19), so the data is permissive of both high extension and convergence being significant factors.

As in episode 2, the orientation of sigma 3 deduced from dike orientation continued to be subparallel to the northeast convergence direction, suggesting again that decreased V_c and A_c reduced the potency of northeast compression at the plate boundary (Figure 21). Sigma 3 was probably nearly perpendicular to the direction of Basin and Range extension throughout much of episode 3 (Figure 21), becoming east-northeast by the time of formation of the High Cascade graben at 5.4 Ma (see structural geology section). Acceleration of Basin and Range extension postulated to have occurred at about 9 Ma (Stewart, 1978; Pollitz, 1988; Figure 20) could have caused a "push" at the arc from the southeast, causing dikes to be sub-aligned with the spreading direction. The postulated "push" could have been taken up at the NAP-JDFP boundary, producing the increase in convergence rate at 9 Ma shown in the convergence model of Engebretson (1982). The degree of this "push" may have decreased as V_c and A_c decreased and/or Basin and Range spreading slowed, producing the change to more easterly sigma 3 at 5.4 Ma.

Alternatively, utilizing the convergence model of Verplanck and Duncan (1987), continuous decreases in V_c and A_c in episode 3 may have led to increasing influence of north-south compression at the NAP-PP boundary relative to northeast compression at the JDF-NAP boundary. This model seems more easily defended than the former model because (1) the convergence model of Verplanck and Duncan (1987) at 7-0 Ma is similar to that of Riddihough (1984), casting doubt on the model of Engebretson (1982); (2) only passive spreading is required, whereas the other stress model requires an active push from spreading; and (3) there is no known evidence of compressional deformation from the postulated "push.".

I speculate that sigma 3 prior to graben formation at 5.4 Ma was low enough to cause modest crustal extension, but not low enough to cause large-displacement normal faults. Indeed, only a few northwest-trending normal faults of small-displacement have been described for episode 3 (e.g. Priest and Woller, 1983b; Priest and others 1987; Sherrod, 1986). This interpretation is supported by the occurrence of basalt more mafic than at any previous time in the arc. Such mafic magmas must have had relatively low crustal residence times, implying modest but not extreme extension [i.e. the above model of Novak and Bacon (1986)]. The crustal residence time and extension rate were therefore probably less than during episode 1, when very highly differentiated, high-TiO_2 magmas erupted. The source of the extension could have been either or both of the mechanisms discussed for episode 1 [e.g. see discussions by Smith, (1986) and Smith and others (1987)]. Narrowing of the arc, either by narrowing of the zone of mantle circulation (Taylor, 1989) or by increasing slab dip, could have increased the effectiveness of thermally induced extension.

Uplift and Formation of Graben at 5.4-3.3 Ma

Smith and others (1989) show that subsidence of the early High Cascade arc affected a much wider area than the arc. Their isostatic model predicts modest rebound of marginal areas when formation of the High Cascade graben at 5.4 Ma severed the structural connection to the volcanic pile. The predicted uplift is less than the 1 km or so needed to explain entrenchment of streams in the Western Cascades and does not explain uplift in parts of the arc without arc-parallel graben or large bursts of 7.4-5.4-Ma volcanism (e.g. in Washington and British Columbia). Thermal expansion of unfaulted blocks from bursts of volcanic activity can also be discounted as a major cause of uplift for similar reasons.

The increase in V_r at 4 Ma (Rogers, 1985) is the most likely means of causing the uplift of the Western Cascades between 5.1 and 3.3 Ma. Injection of mobile mantle material into the arc from increased roll-back would cause uplift to be concentrated in areas like the Western Cascades and the Cascades of Washington and British Columbia where the mantle wedge underlies thick crustal blocks with little evidence of Pliocene extension.

The increase in V_r at 4 Ma may have caused formation of arc-parallel graben in Oregon (Rogers, 1985), although decreases in V_c (Smith and others, 1987) and A_c (Figure 20) may also have played a roll. The orthogonal convergence in Washington and British Columbia (Riddihough, 1984) probably helped to prevent extension (Rogers, 1985), but this factor does not explain the lack of extension in the Western Cascades of Oregon where convergence was highly oblique. Extension was probably also limited in the Western Cascades and the other areas by lack of thermal weakening of the lithosphere, owing to low rates of volcanism. Arc-parallel graben formed most extensively where the continental lithosphere was weakened and loaded by high rates of late Miocene volcanism, as in central Oregon (Conrey and others, 1983; Smith, 1985; Smith and others, 1987).

3.9- 0.731 MA - LATE HIGH CASCADE VOLCANISM (EPISODE 4)

The rate of volcanism, particularly the rate of eruption of mafic lava, continued to be high in episode 4, although not as high as in episode 3

(Figure 19). The decrease in rate may not, however, be real, owing to uncertainties in the determination of volcanic rock volume. If the decrease in rate is real, it may reflect decreased magma production caused by the decreased V_c or crustal extension rate. The ratio of eruption of mafic and silicic magma was similar to episode 3, so I conclude that the magnitude of sigma 3 was little changed.

The orientation of sigma 3 was probably near east-west (Sherrod and Pickthorn, 1989). The postulated increase in V_c at 4 Ma probably produced extension perpendicular to the north-south JDF-NAP boundary (Rogers, 1985).

0.730-0 Ma - LATE HIGH CASCADE VOLCANISM (EPISODE 5)

High rates of eruption of mafic magma continued in episode 5 from vents aligned north-south (Figure 19 and 21). The high rate of mafic volcanism and the north-south alignment of vents is consistent with east-west extension. This change to east-west extension may be the continuation of the clockwise rotation of sigma 3, reflecting progressive decreases in V_c and A_c and increasing influence of stress fields developed from NAP-PP interactions. The east-west sigma 3 could also be the result of the postulated increase in V_r at 4 Ma postulated by Rogers (1985). However, the only episode-5 normal faults that are known occur on the east side of the High Cascades have a northwest trend (TMFZ, Figure 6). These faults must therefore be affected by some other factor, perhaps the right lateral transform deformation associated with the northwest-trending Brothers fault zone (Lawrence, 1976) or changes in lithospheric strength related to heat flow (Priest and others, 1983).

The sharp increase of volcanic rate in episode 5 relative to episode 4 may be an artifact of the large uncertainty in the rate calculation of episode 4. If it is real, it implies either an increase of convergence rate or extension. No increase of convergence or extension rate is known. I conclude that the change in rate is not statistically significant relative to the potential error.

The relative rates of eruption of various magma compositions was similar to those of episodes 3 and 4 (Figure 19). I conclude that the magnitude of sigma 3 was also similar. There was, however, somewhat less basalt produced relative to more evolved compositions in episode 5 compared to episode 4 (Figure 12). The thickening volcanic pile may allowed more opportunity for differentiation.

K and Rb Variations

K and Rb are relatively incompatible with most mafic minerals that might be present in the melting residuum of the mantle, so they would be expected to decrease with time, unless the source was replenished, or the degree of concentration of these elements in partial melts increased. The latter process could be accomplished by decreased degrees of partial melting or increased "gardening" of incompatible elements from wall rocks by wall-rock reaction and zone refining.

No depletion of K or Rb occurred (Figures 14 and 15), so one or more of the above processes must have operated. The common occurrence of calc-alkaline basalt and basaltic andesite in every episode leads me to conclude that there were probably not continuous changes in the petrogenesis (e.g. depth or degree of melting) that would fortuitously keep K and Rb constant in magmas derived from a continuously depleted source. Continuous enrichment of the

source area by (1) circulation of new mantle material accommodating arc and back-arc spreading, roll-back, and subduction, and/or (2) slab-derived fluids are more logical means of maintaining constant K and Rb content.

SUMMARY AND CONCLUSIONS

The volcanic front of the Cascade arc migrated progressively landward at 35-0 Ma as the volcanic belt narrowed. The narrowing was probably caused by progressive steepening of the dip of the subducted slab, possibly enhanced by decreasing R_V from 35-7.4 Ma. The landward migration was probably caused by lowering of the 0-100-km slab dip which was in turn caused by thinning of the overriding plate by extension, heating, and basal erosion. The ratio of V_O to V_r may also have played a role in arc migration, at least for the last 4 m.y.

The rate of Cascade volcanism was highest at 43.2-17 Ma, when V_C was highest. Highly differentiated high-TiO_2 tholeiitic lavas, silicic tuff, and subordinate andesite were the chief eruptive products at this time. The high convergence angle and rate caused the maximum compressive stress direction in the arc to be nearly aligned with the convergence direction. Sigma 3 was oriented roughly north-south and was probably relatively low, causing large amounts of extension and long crustal residence time for magma. Dextral shear from the oblique A_C (Wells and others, 1984) and/or loading and thermally induced lithospheric thinning (Conrey and others, 1983) may have caused the extension.

The rate of volcanism, particularly high-TiO_2 tholeiitic volcanism, decreased at 16.9-7.5 Ma, probably in response to a decrease in V_C and crustal extension. The decreased extension may have been caused by a slight increase in compression, causing mild folding, or from less thermally driven extension owing to decreased V_C.

The R_V, particularly the rate of eruption of basalt, basaltic andesite, and silicic tuff increased at 7.4-4 Ma. The increased R_V may not be real, because of large uncertainties in the calculation. If the rate is real, it may have been caused by increased extension. Extension is required to explain the eruption of some basalt with lower SiO_2 and higher MgO and Ni than any previous basalt, although the low crustal residence time implied by the primitive compositions does not require extreme extension. The TiO_2-rich nature of some of the basalt also implies eruption from an extensional environment (Gill, 1981) with or without subduction-related magma generation. The increase in silicic volcanism requires relatively long crustal residence time and low sigma 3 during episode 3, although silicic volcanism was apparently subordinate to mafic volcanism (Figure 19). I conclude that the amount of extension may have varied at 7.4-4 Ma but was, on average, larger than at 16.9-7.5 Ma but not as high as at 43.2-17 Ma, when silicic volcanism dominated the arc.

The direction of sigma 3 at 7.4-5.4 Ma was approximately perpendicular to the contemporaneous Basin and Range spreading direction, so Basin and Range extension is not a means of increasing extensional stress. The increased extension may be related to decreased coupling of the NAP to the JDFP as V_C and A_C decreased and/or increased thermally driven extension resulting from focusing of the magma generation zone over a steepening subducting plate.

Rates of mafic and silicic volcanism at 3.9-0 Ma were similar to rates at 7.4-4.0 Ma, so the magnitude of sigma 3 was probably similar. The direction of sigma 3, however, probably shifted to east-west, coincident with an increase

in V_r perpendicular to the JDF-NAP boundary. Earthquake source mechanisms and north-south alignment of modern volcanic vents are consistent with continued east-west extension, approximately parallel to contemporaneous Basin and Range extension.

Approximately 1 km of rapid uplift occurred at the faulted boundary between the Western and High Cascades, starting some time after about 5.1-4.5 Ma, ending at about 3.3 Ma. Uplift decreases westward to a probable "hinge" at the Willamette Valley forearc basin. Streams rapidly cut through the uplifted Western Cascades, the largest trunk streams reaching present grade at 0.5 Ma. The uplift may have been triggered by westward injection of mobile mantle material accommodating increased V_r at 4 Ma.

Mass movements of mantle and/or slab-derived fluids probably continuously enriched the upper mantle wedge in incompatible elements throughout the life of arc. The constant levels of K and Rb in episode 1-5 rocks are indications of this process.

ACKNOWLEDGEMENTS

This investigation was supported by the USDOE in cooperation with the State of Oregon. I am deeply indebted to George W. Walker and David R. Sherrod (USGS) for providing their unpublished 1:250,000-scale geologic maps of the study area. Ray E. Wells (USGS), Edward M. Taylor (Oregon State University), David D. Blackwell (Southern Methodist University), and Gary A. Smith (University of New Mexico) offered many helpful ideas and critical discussions. Gerald L. Black of the Oregon Department of Geology and Mineral Industries (DOGAMI) provided invaluable help with compilation and plotting of the chemical data. He and Neil M. Woller (consulting geologist, formerly of DOGAMI) worked by my side through years of arduous field work, producing the detailed geologic maps that were essential to my understanding of the volcanic stratigraphy. Mark Neuhaus (DOGAMI) drafted three of the figures; my wife, Barbara J. Priest, drafted the others.

REFERENCES

Ahrens, T.J. and Schubert, G., 1975, Gabbro-eclogite reaction rate and its geophysical significance: Reviews of Geophysics and Space Physics, v. 13, p. 383-400.

Ashwill, M., 1983, Seven fossil floras in the rain shadow of the Cascade Mountains, Oregon: Oregon Department of Geology and Mineral Industries, Oregon Geology, v. 45, n. 10, p. 107-111.

Avramenko, W., 1981, Volcanism and structure in the vicinity of Echo Mountain, central Oregon Cascade Range: Eugene, Oreg., University of Oregon master's thesis, 156 p.

Bacon, C.R., 1985, Implications of silicic vent patterns for the presence of large crustal magma chambers: Journal of Geophysical Research v. 90, no. B13, p. 11, 243-11, 252.

Beeson, M.H., Moran, M.R., Anderson, J.L., and Vogt, B.F., 1982, The relationship of the Columbia River Basalt Group to the geothermal potential of the Mount Hood area, Oregon, in Priest, G.R., and Vogt, B.F., eds., Geology and geothermal resources of the Mount Hood area, Oregon: Oregon Department of Geology and Mineral Industries Special Paper 14, p. 43-46.

Black, G.L., Woller, N.M., and Ferns, M.l., 1987, Geologic map of the Crescent Mountain area, Linn County, Oregon: Oregon Department of Geology and Mineral Industries Geological Map Series GMS-47, scale 1:62,500.

Brown, D.E., McLean, G.D., Priest, G.R., Woller, N.M., and Black, G.L., 1980, Preliminary geology and geothermal resource potential of the Belknap-Foley area, Oregon: Oregon Department of Geology and Mineral Industries Open-File Report 0-80-2, 58 p.

Conrey, R.M,, 1985, Volcanic Stratigraphy of the Deschutes Formation, Green Ridge to Fly Creek, north-central Oregon: Corvallis, Oregon, Oregon State University master's thesis, 349 p.

Conrey, R.M., 1988, Mt. Jefferson area, Oregon High Cascade Range: A long-lived locus of andesitic and dacitic volcanism and plutonism: Geological Society of America Abstracts with Programs, v. 20, no. 7, p. A196.

Conrey, R.M., Yogodzinski, G.M., and Taylor, E.M., 1983, Implications of heat driven extension for some Cenozoic structures in Oregon: EOS, v. 65,
p. 329.

Couch, R.W., and Lowell, R.P., 1971, Earthquakes and seismic energy release in Oregon: Oregon Department of Geology and Mineral Industries, Ore Bin, v. 33, no. 4, p. 61-84.

Couch, R.W., and Riddihough, R.P., 1988, The crustal structure of the western continental margin of North America, in Pakiser, L., and Mooney, W., eds., Geophysical framework of the U.S.: Geological Society of America Monograph, in press.

Davie, E.I., II, 1980, The geology and petrology of Three Fingered Jack, a High Cascade volcano in central Oregon: Eugene, Oregon, University of Oregon master's thesis, 138 p.

Dewey, J.F., 1980, Episodicity, sequence, and style at convergent plate boundaries: in Strangway, D.W., ed., The continental crust and its mineral deposits: Geological Association of Canada Special Paper 20, p. 553-573.

Dickinson, W.R., 1973, Widths of modern arc-trench gaps proportional to past duration of igneous activity in associated magmatic arcs: Journal of Geophysical Research, v. 78, no. 17, p. 3376-3389.

Diller, J.S., 1900, The Bohemia mining region of Western Oregon, with notes on the Blue River mining region and on the structure and age of the Cascade Range: U.S. Geological Survey Annual Report pt. 3, p. 1-36.

Donath, R.M., 1962, Analysis of basin-range structure, south-central Oregon: Geological Society of America Bulletin, v. 73, p. 1-16.

Duncan, R.A., 1982, A captured island chain in the Coast Range of Oregon and Washington: Journal of Geophysical Research, v. 87, p. 10827-10837.

Engebretson, D., 1982, Relative motions between oceanic and continental plates in the Pacific Basin: Stanford University Ph.D. dissertation, 211 p.

Engel, A.E.J., Engel, C.G., and Havens, R.G., 1965, Chemical characteristics of oceanic basalts and the upper mantle: Geological Society of America Bulletin, v. 76, p. 719-733.

Enlows, H.E., and Parker, D.J., 1972, Geochronology of the Clarno igneous activity in the Mitchell quadrangle, Wheeler County, Oregon: Ore Bin, v. 34, p. 104-110.

Fiebelkorn, R.B., Walker, G.W., MacLeod, N.S., McKee, E.H., and Smith, J.G., 1982, Index to K-Ar age determinations for the State of Oregon: U.S. Geological Survey Open-File Report 82-596, 40 p. [also 1983, Isochron/West, no. 37, p. 3-60].

Finn, C., Williams, D.L., Couch, R.W., Danes, Z.F., Pitts, G.S., and Phillips, W.M., 1986, Gravity anomaly and terrain maps of the Cascade Range, California, Oregon, Washington, and British Columbia: U.S. Geological Survey Geophysical Investigations Map GP-972, scale 1:2,500,000.

Flaherty, G.M., 1981, The Western Cascade-High Cascade transition in the McKenzie Bridge area, central Oregon Cascade Range: Eugene, Oreg., University of Oregon master's thesis, 178 p.

Gill, J.B., 1981, Orogenic andesites and plate tectonics: New York, Springer Verlag, 390 p.

Green, D.H., 1968, Origin of basaltic magmas, in Hess, H.H., and Poldervaart, A., eds., Basalts -- The Poldervaart treatise on rocks of basaltic composition, Volume 2: New York and London, Interscience Publications, Inc., p. 835-862.

Greene, R.C., 1968, Petrography and petrology of volcanic rocks in the Mount Jefferson area, High Cascade Range, Oregon: U.S. Geological Survey Bulletin 1251-G, 48 p.

Gromme', C.S., Beck, M.E., Jr., Wells, R.E., and Engebretson, D.C., 1986, Paleomagnetism of the Tertiary Clarno Formation of central Oregon and its significance for the tectonic history of the Pacific Northwest: Journal of Geophysical Research, v. 91, no. B14, p. 14,089-14,103.

Grow, J.A., and Bowin, C., 1975, Evidence for high-density crust and mantle beneath the Chile Trench due to the descending lithosphere: Journal of Geophysical Research, v. 80, p. 1449-1458.

Guffanti, M., and Weaver, C.S., 1988, Distribution of late Cenozoic volcanic vents in the Cascade Range: volcanic arc segmentation and regional tectonic considerations: Journal of Geophysical Research, v. 93, no. B6, p.6513-6529.

Gunn, B., and Watkins, N., 1970, Geochemistry of the Steens Mountain basalts, Oregon: Geological Society of America Bulletin, v. 81, p. 1497-1516.

Hales, P.O., 1975, Geology of the Green Ridge area, Whitewater River quadrangle, Oregon: Corvallis, Oreg., Oregon State University master's thesis, 90 p.

Hammond, P.E., Anderson, J.L., and Manning, K.J., 1980, Guide to the geology of the upper Clackamas and North Santiam Rivers area, northern Oregon Cascade Range, in Oles, K.F., Johnson, J.G., Niem, A.R., and Niem, W.A., eds., Geologic field trips in western Oregon and southwestern Washington: Oregon Department of Geology and Mineral Industries Bulletin 101, p. 133-167.

Hart, W.K., 1982, Chemical, geochronologic and isotopic significance of low K, high-alumina olivine tholeiite in the northwestern Great Basin, U.S.A.: Cleveland, Ohio, Case Western Reserve University Ph.D. dissertation, 410 p.

Hayman, G.A., 1984, Geology of a part of the Eagle Butte and Gateway quadrangles east of the Deschutes River, Jefferson County, Oregon: Corvallis, Oreg., Oregon State University Master's thesis, 97 p.

Hill, B.E., 1985, Petrology of the Bend pumice and Tumalo tuff, a Pleistocene Cascade eruption involving magma mixing: Corvallis, Oreg., Oregon State University master's thesis, 101 p.

Hill, B.E., 1988, The Bull Springs inlier and its significance to Oregon central High Cascade tectonics: Proceedings of the Oregon Academy of Science, in press.

Hughes, S.S., 1983, Petrochemical evolution of High Cascade volcanic rocks in the Three Sisters region: Corvallis, Oreg., Oregon State University doctoral dissertation, 199 p.

Irvine, T.N. and Baragar, W.R.A., 1971, A guide to chemical classifications of the common volcanic rocks: Canadian Journal of Transactions, v. 6, p. 31-34.

James, D.E., 1971, Plate tectonic model for the evolution of the central Andes: Geological Society of America Bulletin, v. 82, p. 3325-3346.

Jan, M.Q., 1967, Geology of the McKenzie River valley between the South Santiam Highway and the McKenzie Pass Highway, Oregon: Eugene, Oreg., University of Oregon master's thesis, 70 p.

Jarrard, R.D., 1986, Relations among subduction parameters: Journal of Geophysical Research, v. 24, p. 217-284.

Jay, J.B., 1982, The geology and stratigraphy of the Tertiary volcanic and volcaniclastic rocks, with special emphasis on the Deschutes Formation, from Lake Simtustus to Madras in central Oregon: Corvallis, Oreg., Oregon State University master's thesis, 119 p.

Keach, R.W., II, 1986, Cenozoic active margin and shallow Cascades structure: COCORP results from western Oregon: Ithaca, New York, Cornell University master's thesis, 51 p.

Kienle, C.F., Nelson, C.A., and Lawrence, R.D., 1981, Faults and lineaments of the southern Cascades, Oregon: Oregon Department of Geology and Mineral Industries Special Paper 13, 23 p.

Kuno, H., 1966, Lateral variation of basalt magma type across continental margins and island arcs: Bulletin Volcanologique, v. 29, p. 196-221.

Lawrence, R.D., 1976, Strike-slip fault terminates the basin and range province in Oregon: Geological Society of America Bulletin, v.87, no.6, p 846-850.

Leaver, D.S., 1982, A refraction study of the Oregon Cascades: Seattle, Wash., University of Washington master's thesis, 67 p.

Leaver, D.S., Mooney, W.D., and Kohler, W.M., 1984, A seismic refraction study of the Oregon Cascades: Journal of Geophysical Research, v. 89, no. B5, p. 3121-3134.

Lux, D.R., 1982, K-Ar and ^{40}Ar-^{39}Ar ages of mid-Tertiary volcanic rocks from the Western Cascade Range, Oregon: Isochron/West, no. 33, p. 27-32.

MacLeod, N.S., and Snavely, P.D., Jr., 1973, Volcanic and intrusive rocks of the central part of the Oregon Coast Range: Oregon Department of Geology and Mineral Industries Bulletin 77, p. 47-74.

Magill, J., Cox, A., and Duncan, R., 1981, Tillamook Volcanic Series: Further evidence for tectonic rotation of the Oregon Coast Range: Journal of Geophysical Research, v. 86, no.B4, p. 2953-2970.

McBirney, A. R., 1968, Petrochemistry of Cascade andesite volcanoes, in Dole, H. M., ed., Andesite conference guidebook: Oregon Department of Geology and Mineral Industries Bulletin 62, p. 101-107.

McBirney, A.R., Sutter, J.F., Naslund, H.R., Sutton, K.G., and White, C.M., 1974, Episodic volcanism in the central Oregon Cascade Range: Geology, v. 2 , p. 585-589.

McKee, E.H., Duffield, W.A., and Stern, R.J., 1983, Late Miocene and early Pliocene basaltic rocks and their implications for crustal structure, northeastern California and south central Oregon: Geological Society of America Bulletin, v. 94, p. 292-304.

Miyashiro, A., 1974, Volcanic rock series in island arcs and active continental margins: American Journal of Science, v. 274, no. 4, p. 321-355.

Morgan, W.J., 1983, Hotspot tracks and the early rifting of the Atlantic: Tectonophysics, v. 94, p. 123-139.

Munts, S.R., 1978, Geology and mineral deposits of the Quartzville mining district, Linn County, Oregon: Eugene, Oreg., University of Oregon master's thesis, 213 p.

Nakamura, K., 1977, Volcanos as possible indicators of tectonic stress orientation - principle and proposal: Journal of Volcanology and Geothermal Research, v. 2, p. 1-16.

Novak, S.W., and Bacon, C.R., 1986, Pliocene volcanic rocks of the Coso Range, Inyo County, California: U.S. Geological Survey Professional Paper 1383, 44 p.

Oldenburg, D.W., 1975, A physical model for the creation of the lithosphere: Royal Astronomical Society Geophysical Journal, v. 43, p. 425-451.

Orr, W.N.,and Miller, P.R., 1984, Geologic map of the Stayton NE quadrangle, Oregon: Oregon Department of Geology and Mineral Industries Geological Map Series GMS-34, scale 1:24,000.

Parker, D.J., 1974, Petrology of selected volcanic rocks of the Harney Basin, Oregon: Corvallis, Oreg., Oregon State University doctoral dissertation, 119 p.

Peck, D.L., Griggs, A.B., Schlicker, H.G., Wells, F.G., and Dole, H.M., 1964, Geology of the central and northern parts of the western Cascade Range in Oregon: U.S. Geological Survey Professional Paper 449, 56 p.

Pollitz, F.F., 1988, Episodic North America and Pacific plate motions: Tectonics, v. 7, no. 4, p. 711-726.

Power, S.G., 1984, The "tops" of porphyry copper deposits - mineralization and plutonism in the Western Cascades: Corvallis, Oreg., Oregon State University master's thesis, 243 p.

Power, S.G., Field, C.W., Armstrong, R.L., and Harakal, J.E., 1981, K-Ar ages of plutonism and mineralization, Western Cascades, Oregon and southern Washington: Isochron/West, no. 31, p. 27-29.

Priest, G.R., Black, G.L., Woller, N.M.,and Taylor, E.M., 1988, Geologic map of the McKenzie Bridge quadrangle, Lane County, Oregon: Oregon Department of Geology and Mineral Industries Geological Map Series GMS-48, scale 1:62,500.

Priest, G.R., and Woller, N.M., 1983a, Geology of the Cougar Reservoir area, Lane County, Oregon, in Priest, G.R., and Vogt, B.F., eds., Geology and geothermal resources of central Oregon Cascade Range: Oregon Department of Geology and Mineral Industries Special Paper 15, p. 39-48.

Priest, G.R., and Woller, N.M., 1983b, Geology of the Devils Creek-Outerson Mountain area, Marion County, Oregon, in Priest, G.R., and Vogt, B.F., eds., Geology and geothermal resources of the Cascades of the central Oregon Cascade Range: Oregon Department of Geology and Mineral Industries Special Paper 15, p 29-38.

Priest, G.R., Woller, N.M., Black, G.L., and Evans, S.H., Jr., 1983, Overview of the geology of the central Oregon Cascade Range, in Priest, G.R., and Vogt, B.F., eds., Geology and geothermal resources of the central Oregon Cascade Range: Oregon Department of Geology and Mineral Industries, Special Paper 15, p. 3-28.

Priest, G.R., Woller, N.M., and Ferns, M.L., 1987, Geologic map of the Breitenbush River area, Linn and Marion Counties, Oregon: Oregon Department of Geology and Mineral Industries Geological Map Series, GMS-46, scale 1:62,500.

Rasmussen, J., and Humphreys, E., 1988, Tomographic image of the Juan de Fuca plate beneath Washington and western Oregon using teleseismic P-wave travel times: Geophysical Research Letters, v. 15, no. 12, p. 1417-1420.

Riddihough, R., 1984, Recent movements of the Juan de Fuca plate system: Journal of Geophysical Research, v. 89, no. B8, p. 6980-6994.

Robinson, P.T., 1969, High titania alkali-olivine basalt of north-central Oregon, USA: Contributions to Mineralogy and Petrology, v. 22, p. 349-360.

Robinson, P.T., and Brem, G.F., 1981, Guide to geological field trip between Kimberly and Bend, Oregon, with emphasis on the John Day Formation, in Johnson, D.A., and Donnelly-Nolan, J. eds., Guides to some volcanic terranes in Washington, Idaho, Oregon and northern California: U.S. Geological Survey Circular 838, p. 29-40.

Rogers, G.C., 1985, Variation in Cascade volcanism with margin orientation: Geology, v. 13, no. 7, p. 495-498.

Rogers, J.J.W., 1982, Criteria for recognizing environments of formation of volcanic suites; Application of these criteria to volcanic suites in the Carolina Slate Belt, in Bearce, D.N., Black, W.W., Kish, S.A., and Tull, J.F., eds., Tectonic studies in the Talladoga and Carolina Slate Belts, southern Appalachian orogen: Geological society of America Special Paper 191, p. 99-107.

Rollins, A., 1976, Geology of the Bachelor Mountain area, Linn and Marion Counties, Oregon: Corvallis, Oreg., Oregon State University master's thesis, 83 p.

Sakuyama, M., 1983, Petrology of arc volcanic rocks and their origin by mantle diapirs, Journal of Volcanology and Geothermal Research, v. 18, p. 297-320.

Sherrod, D.R., 1986, Geology, petrology, and volcanic history of a portion of the Cascade Range between latitudes 43° -44°N, central Oregon, U.S.A.: Santa Barbara, California, University of California Santa Barbara doctoral dissertation, 320 p.

Sherrod, D.R., and Conrey, R.M., 1988, Geologic setting of the Breitenbush-Austin Hot Springs area, Cascade Range, North-Central Oregon, in Sherrod, D.R., ed., Geology and geothermal resources of the Breitenbush-Austin Hot Springs area, Clackamas and Marion Counties, Oregon: Oregon Department of Geology and Mineral Industries Open-File Report O-88-5, p. 1-14.

Sherrod, D.R., and Pickthorn, L.B.G., 1989, Some notes on the Neogene structural evolution of the Cascade Range in Oregon, in Muffler, L.J.P., Blackwell, D.D., and Weaver, C.S., eds., Geology, geophysics, and tectonic setting of the Cascade Range: U.S. Geological Survey Open-File Report, in press.

Sherrod, D.R., and Smith, J.G., 1989, Preliminary map showing Upper Eocene to Holocene volcanic and related rocks of the Cascade Range in Oregon: U.S. Geological Survey Open-File Report 89-14, scale 1:500,000.

Simpson, R.W., and Cox, A., 1977, Paleomagnetic evidence for tectonic rotation of the Oregon Coast Range: Geology, v. 5, p. 585-589.

Smith, G.A., 1986, Stratigraphy, sedimentology, and petrology of Neogene rocks in the Deschutes Basin, central Oregon: Corvallis, Oreg., Oregon State University doctoral dissertation, 467 p.

Smith, G.A., Snee, L.W., and Taylor, E.M., 1987, Stratigraphic, sedimentologic, and petrologic record of late Miocene subsidence of the central Oregon High Cascades: Geology, v. 15, no. 5, p. 389-392.

Smith, G.,A., Vincent, K.R.,and Snee, L.W., 1989, An isostatic model for basin formation in and adjacent to the central Oregon High Cascade Range, in Muffler, L.J.P., Blackwell, D.D., and Weaver, C.S., eds., Geology, geophysics, and tectonic setting of the Cascade Range: U.S. Geological Survey Open-File Report, in press.

Smith, J.G., Sawlan, M.S., and Katcher, A.C., 1980, An important lower Oligocene welded-tuff marker bed in the Western Cascade Range of southern Oregon [abs.]: Geological Society of American Abstracts with Programs, v. 12, no. 3, 153 p.

Snavely, P.D., Jr., and Wagner, H.C., 1963, Tertiary geologic history of Western Oregon and Washington: State of Washington Division of Mines and Geology Report of Investigations No. 22, 25 p.

Snavely, P.D., Jr., Wagner, H.C., and Lander, D.L., 1980, Geologic cross-section of the central Oregon continental margin: Geological Society of America Map and Chart Series MC-28J, scale 1:250,000.

Stewart, J.H., 1971, Basin and range structure: a system of horsts and grabens produced by deep-seated extension: Geological Society of America Bulletin, v. 82, p. 1019-1044.

Stewart, J.H., 1978, Basin-Range structure in western North America: a review, in Smith R.B. and Eaton, G.P., eds., Cenozoic tectonics and regional geophysics of the Western Cordillera: Boulder, Colorado, Geological Society of America Memoir 152, p. 1-31.

Sutton, K.G., 1974, The geology of Mt. Jefferson: Eugene, Oreg., University of Oregon master's thesis, 120 p.

Taylor, E.M., 1978, Field geology of S.W. Broken Top quadrangle, Oregon: Oregon Department of Geology and Mineral Industries, Special Paper 2, 50 p.

Taylor, E.M., 1981, Central High Cascade roadside geology--Bend, Sisters, McKenzie Pass, and Santiam Pass, Oregon, in Johnston, D.A., and Donnelly-Nolan, J., eds., Guides to some volcanic terranes in Washington, Idaho, Oregon, and northern California: U.S. Geological Survey Circular 838, p. 55-58.

Taylor, E.M., 1987, Field geology of the northwest quarter of the Broken Top 15' quadrangle, Deschutes County, Oregon: Oregon Department of Geology and Mineral Industries Special Paper 21, 20 p.

Taylor, E.M., 1989, Volcanic history and tectonic development of the central High Cascade Range, Oregon, in Muffler, L.J.P., Blackwell, D.D., and Weaver, C.S., eds., Geology, geophysics, and tectonic setting of the Cascade Range: U.S. Geological Survey Open-File Report, in press.

Thayer, T.P., 1937, Petrology of later Tertiary and Quaternary rocks of the north-central Cascade Mountains in Oregon, with notes on similar rocks in western Nevada: Geological Society of America Bulletin, v. 48, no. 11, p. 1611-1651.

Thayer, T.P., 1939, Geology of the Salem Hills and the North Santiam River basin, Oregon: Oregon Department of Geology and Mineral Industries Bulletin 15, 40 p.

Vance, J.A., 1982, Cenozoic stratigraphy and tectonics of the Washington Cascades [abs.]: Geological Society of America Abstracts with Programs, v. 13, p. 241.

Venkatakrishnan, R., Bond, J.G., and Kauffman, J.D., 1980, Geological linears of the northern part of the Cascade Range, Oregon: Oregon Department of Geology and Mineral Industries Special Paper 12, 25 p.

Verplanck, E.P, 1985, Temporal variations in volume and geochemistry of volcanism in the Western Cascades, Oregon: Corvallis, Oreg., Oregon State University master's thesis, 115 p.

Verplanck, E.P.,and Duncan, R.A., 1987, Temporal variations in plate convergence and eruption rates in the Western Cascades, Oregon: Tectonics, v. 6, no. 2, p. 197-209.

Walker, G.W., and Duncan, R.A., 1988, Geologic Map of the Salem 1° x 2° sheet, Oregon: U.S. Geological Survey, Miscellaneous Investigations Map I-1893, scale 1:250,000.

Weidenheim, J.P., 1980, Petrography, structure, and stratigraphy of Powell Buttes, Crook County, central Oregon: Corvallis, Oreg., Oregon State University masters thesis, 95 p.

Wells, F.G., and Peck, D.L., 1961, Geologic map of Oregon west of the 121st meridian: U.S. Geological Survey Miscellaneous Investigations Series Map I-325, scale 1:500,000.

Wells, R.E., Engebretson, D.C., Snavely, P.D., Jr., and Coe, R.S., 1984, Cenozoic plate motions and the volcano-tectonic evolution of western Oregon and Washington: Tectonics, v. 3, no. 2, p. 275-294.

Wells, R.E., and Heller, P.L., 1988, The relative contribution of accretion, shear, and extension to Cenozoic tectonic rotation in the Pacific Northwest: Geological Society of America Bulletin, v. 100, p. 325-338.

Woller, N.M., and Black, G.L., 1983, Geology of the Waldo Lake-Swift Creek area, Lane and Klamath Counties, Oregon, in Priest, G.R., and Vogt, B.F., Geology and geothermal resources of the central Oregon Cascade Range: Oregon Department of Geology and Mineral Industries Special Paper 15, p. 57-68.

Yogodzinski, G.M., 1986, The Deschutes Formation-High Cascade transition in the Whitewater River area, Jefferson County, Oregon: Corvallis, Oreg., Oregon State University master's thesis, 168 p.

Zoback, M.L., Anderson, R.E., and Thompson, G.A., 1981, Cainozoic evolution of the state of stress and style of tectonism of the Basin and Range province of the western United States: Philosophical Transactions of the Royal Society of London, v. A-300, p. 407-434.

Zoback, M.L., and Thompson, G.A., 1978, Basin and Range rifting in northern Nevada: clues from a mid-Miocene rift and its subsequent offsets: Geology, v. 6, p. 111-116.

TABLE 1. Volcanic Rock Volumes, km^3.

Rock Type	43.2(35)*-17.5 Ma	16.9-7.5 Ma	7.4-4.0 Ma	3.9-0.731 Ma	0.730-0 Ma
Mafic	12,316	1,106	4,046	2,541	980
Andesitic	3,929	4,461	4	316	36
Silicic	20,639	865	935	222	118
Total	35,882	6,432	4,984	3,079	1,134

*Volume probably mostly from 35-17-Ma rocks.

TABLE 2. Volcanic Production Rate (R_v), km^3 $m.y.^{-1}$(km arc length)$^{-1}$.

Rock Type	43.2-17 Ma	35-17* Ma	16.9-7.5 Ma	7.4-4.0 Ma	3.9-0.731 Ma	0.730-0 Ma
Mafic	4.8	7.0	1.2	12.1	8.2	13.7
Andesitic	1.5	2.2	4.8	0	1.0	0.5
Silicic	11.7	8.0	0.9	2.8	0.7	1.6
Total	20.9	14.3	6.9	14.9	9.9	15.8

*Preferred R_v (see Table 1 and text).

TABLE 3. BASALT COMPOSITIONS

Episode				1	1	2	2	2	3	3	3	4 & 5	4	4	5	5
Rock Type*	Ave. Basalt	Ave. Thol.	Ave. Basalt	Low-K HAOT	R.M. Basalt	Ave. Basalt	Ave. Basalt	R.M. Basalt	Ave. Basalt	Ave. Basalt	R.M. Basalt	Ave. Basalt	Ave. Basalt	R.M. Basalt	Ave. Basalt	Ave. Basalt	R.M. Basalt
Province*	Back Arc	Island Arc	Cont. Arc	B & R	Cascades	Cascades	B & R	Cascades	Cascades	B & R	Cascades	Cascades	B & R	Cascades	Cascades	B & R	Cascades
Reference	1	1	2	1	3	4	5	6	7	8	9	10	11	12	13	14	15
No. Analyses**	43	52	?	81	3	52	21	3	26	10	3	183	23	3	111	3	76
SiO_2***	49.32	52.41	51.6	47.82	50.8	51.6	49.2	50.1	51.4	48.9	49.2	51.0	49.37	49.5	50.4	49.2	51.1
TiO_2	1.24	0.85	1.29	1.02	1.7	1.59	1.88	1.31	1.21	1.01	1.21	1.54	1.57	1.24	1.52	1.48	1.4
Al_2O_3	16.45	18.73	18.2	17.02	16.8	17.4	16.73	17.6	17.7	16.92	17.7	17.0	15.63	16.9	16.8	16.4	17.1
FeO	8.68	9.04	8.5	9.74	10.1	9.88	11.15	9.81	9.08	9.74	9.86	10.01	10.43	10.2	10.28	10.16	9.09
MnO	0.18	0.17		0.17	0.2	0.22	0.13	0.15	0.13	0.17	0.16	0.13 (122)	0.07	0.17	0.13 (110)	0.17	0.07
MgO	7.93	4.68	6.1	9.03	6.02	5.05	6.15	7.4	6.61	8.67	8.38	6.8	8.14	8.74	7.27	9.45	7.66
CaO	11.61	9.99	8.9	11.11	9.36	9.64	9.92	9.66	9.36	11.13	9.95	9.35	11.02	9.6	9.46	9.37	9.05
Na_2O	2.77	2.97	3.5	2.73	3.43	3.1	3.20	3.02	3.17	2.62	2.74	3.16	2.98	2.78	3.03	3.21	3.42
K_2O	0.32	0.62	0.85	0.23	0.85	0.68	0.86	0.47	0.58	0.34	0.36	0.61	0.46	0.46	0.54	0.43	0.7
P_2O_5	0.15	0.17		0.12	0.51	0.36	0.35	0.31	0.27	0.17	0.26	0.29 (122)	0.07	0.17	0.22 (110)	0.19	0.18
FeO/MgO	1.09	1.93	1.4	1.08	1.68	2.13	2.04	1.33	1.4	1.15	1.18	1.61	1.33	1.17	1.45	1.06	1.22
Rb	3.0	12.6 (46)	20	2.4	7	17 (33)	15 (14)	15 (2)	10	2 (3)	8 (2)	11 (74)	5 (3)	6	8 (72)	8 (2)	9 (37)
Ba	79 (20)	167 (29)	274	141	340	245 (36)	543 (14)	240 (2)	250	150 (3)	206	332 (65)	183 (3)	154	223 (59)	145 (2)	293 (31)
Sr	214	310 (47)	501	269	556	442 (35)	496 (14)	376 (2)	487	327 (3)	375	517 (76)	272 (3)	387	355 (72)	392 (2)	542 (37)
Ni	135	28 (26)	88	146	80	40 (27)	97 (19)	96 (2)	81	142 (3)	130	93 (65)	120 (3)	122	97 (50)	150 (2)	117 (33)

* Ave. = average; HAOT = high-Al olivine tholeiite; R.M. = representative mafic; Cont. = continental;
B & R = Basin and Range of Oregon west of longitude 118° W.

** Total samples analyzed. If value based on fewer samples, the number of samples is in parentheses next to value.

*** Major oxides in weight %; trace elements in ppm.

1 Hart (1982).
2 Rogers (1982).
3 Lux (1981); Priest and others (1988); G.R. Priest (unpublished data).
4 Lux (1981); Munts (1978); G.R. Priest (unpublished data); Verplanck (1985).
5 Gunn and Watkins (1970); Hart (1982); McKee and others (1983); Parker (1974).
6 Black and others (1987); G.R. Priest (unpublished data); Rollins (1976).
7 Black and others (1987); Priest and others (1988); G.R. Priest (unpublished data); Rollins (1976); Verplanck (1985).
8 Hart (1982); McKee and others (1983).
9 Black and others (1987); Priest and others (1988); G.R. Priest (unpublished data).
10 Avramenko (1981); Black and others (1987); Flaherty (1981); Hayman (1983); Jay (1982); Priest and others (1988); G.R. Priest (unpublished data); Rollins (1976); Smith (1986); Sutton (1974); Thayer (1937).
11 Hart (1982); Parker (1974).
12 Priest and others (1988); G.R. Priest (unpublished data).
13 Avramenko (1981); Black and others (1987); Conrey (1985); Davie (1980); Flaherty (1981); Hales (1975); Hughes (1983); Jan (1967); Priest and others (1988); G.R. Priest (unpublished data); Smith (1986); Verplanck (1985); Yogodinzki (1985).
14 Priest and others (1988); G.R. Priest (unpublished data).
15 Avramenko (1981); Black and others (1987); Conrey (1985); Davie (1980); Flaherty (1981); Greene (1968); Munts (1978); Priest and others (1988); G.R. Priest (unpublished data); Rollins (1976); Hughes (1983); Taylor (1978); Taylor (1987).

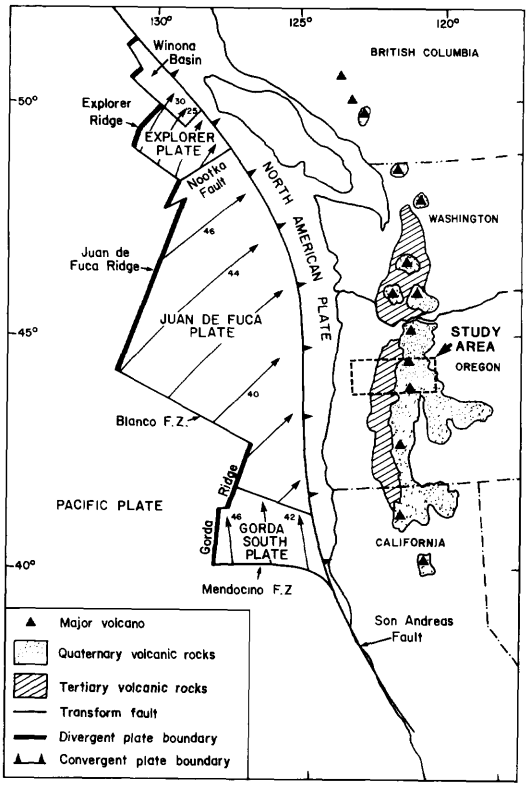

Fig. 1. Plate-tectonic map of the northwestern American continent showing major crustal boundaries, the Cascade volcanic arc, and location of the study area. Arrows show the directions of net convergence in kilometers per million years. Figure modified from Riddihough (1984) and McBirney (1968).

		THIS PAPER EPISODES	PRIEST AND OTHERS (1983) EPISODES	PECK AND OTHERS (1964)
Quaternary		5	Late High Cascades	High Cascade Volcanic Rocks
Tertiary	Pliocene	4		
	Miocene	3	Early High Cascade	
		2	Late Western Cascade	Sardine Fm.
	Oligocene	1	Early Western Cascade	Little Butte Volcanic Series
	Eocene			-?-?-?-?-

Fig. 2. Correlation of volcanic episodes and regional rock units.

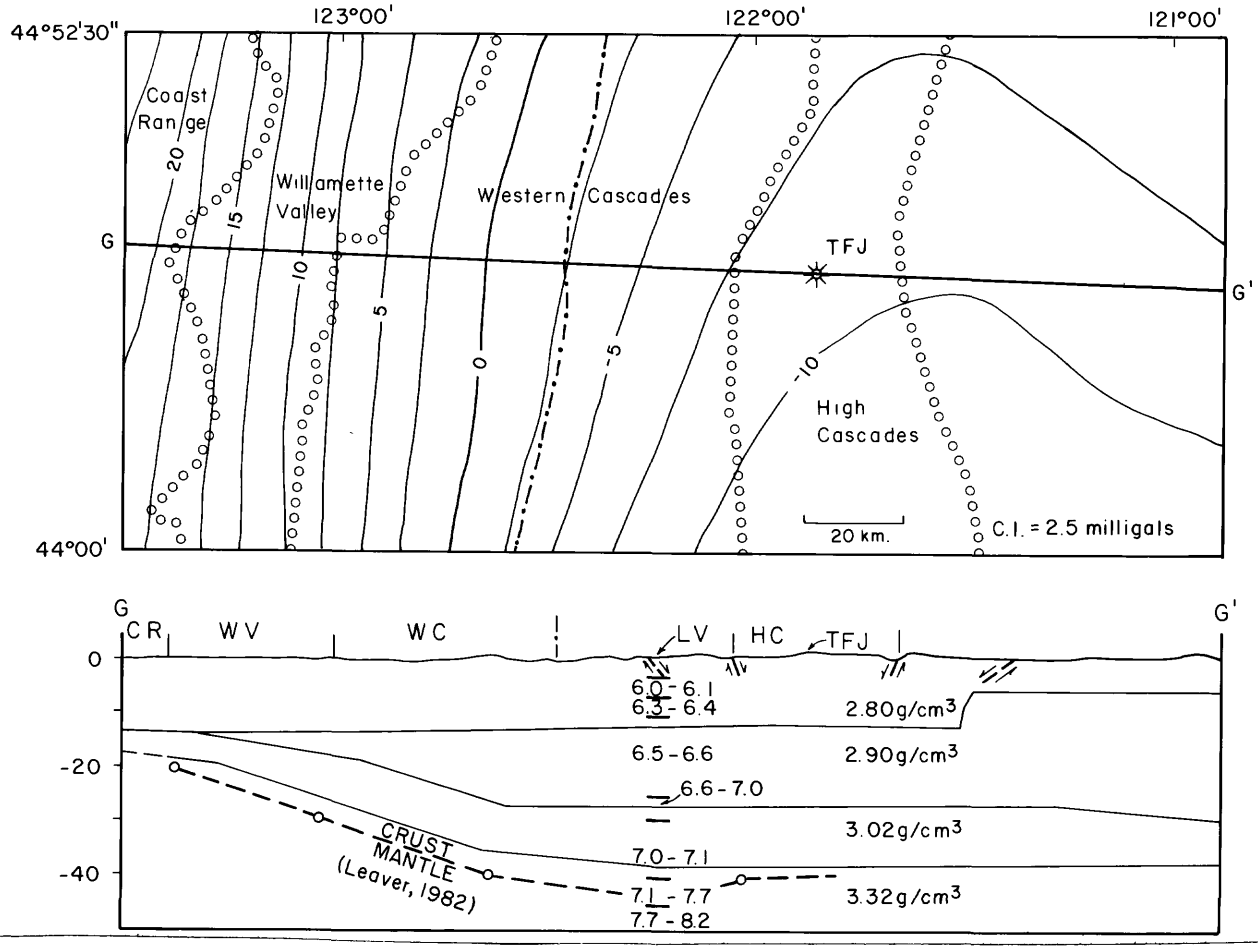

Fig. 3. Regional wavelength-filtered Bouguer gravity map of Finn and others (1986) with crustal section of Couch and Riddihough (1988). The solid lines are the geomorphic province boundaries of, from west to east, the Coast Range (CR), Willamette Valley (WV), Western Cascades (WC), and High Cascades (HC). The solid line with dots represents the western margin of an area of concentrated hypabyssal plutons, silicic dikes and plugs, and pervasive hydrothermal alteration in the core of the Western Cascades. Lines of open circles are geomorphic province boundaries. Estimated crust-mantle boundary of Leaver (1982) is also shown with location a north-south seismic refraction study (LV) of Leaver and others (1984) in the cross section. Numbers between short horizontal lines are the P-wave velocities (km/sec) of the Leaver and others (1984) profile over the indicated vertical distances.

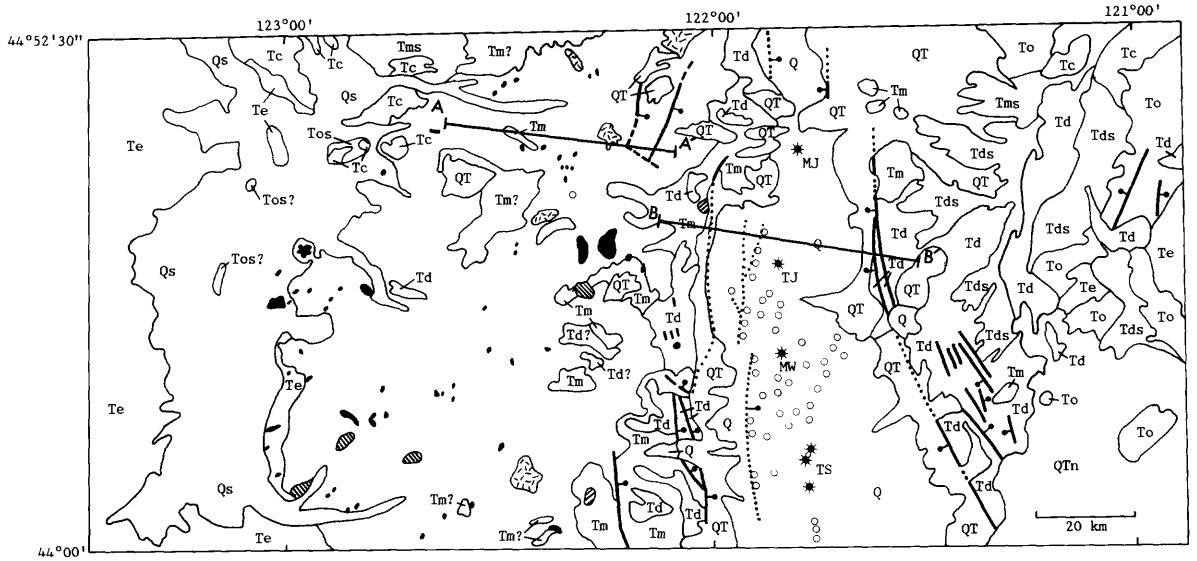

EXPLANATION

Q 0.730 to 0 Ma volcanic rocks
Qs 0.730 to 0 Ma sediments
QT 3.9 to 0.731 Ma volcanic rocks
QTn Volcanic rocks of Newberry Crater
Td 7.4 to 4.0 Ma volcanic rocks
Tds 7.4 to 4.0 Ma sedimentary rocks
Tm 16.9 to 7.5 Ma volcanic rocks
Tms 16.9 to 7.5 Ma sedimentary rocks
Tc Columbia River Basalt Group
To 43.2 to 17.0 Ma volcanic rocks
Tos 43.2 to 17.0 Ma sedimentary rocks
Te Eocene rocks (pre-Cascade and fore-arc rocks)

Diorite to granodiorite intrusive
Basaltic intrusive
Andesitic intrusive
Dacitic intrusive
Contact
Fault--Dashed where inferred; dotted where concealed; bar and ball on downthrown side
0.730 to 0 Ma monogenetic vent
0.730 to 0 Ma composite cone
MJ Mt. Jefferson
TJ Three Fingered Jack
MW Mt. Washington
TS Three Sisters

Fig. 4. Generalized geologic map of the study area modified from Walker and Duncan (1989) and Sherrod and Smith (1989; see text for explanation of modifications). This map is a generalized version of a more detailed 1:250,000-scale map utilized for interpretations of volcanic volume and geologic history.

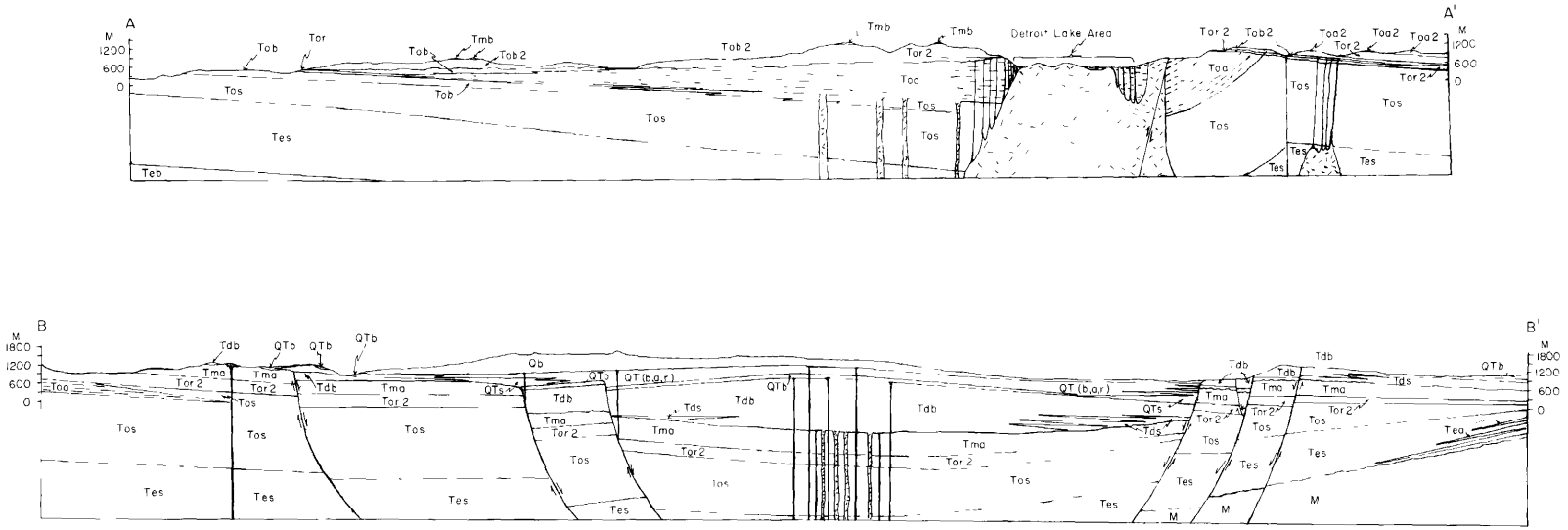

Fig. 5. Cross sections A-A' and B-B' of the geologic map (Figure 4). Note that time-rock units of Figure 4 are broken into more units on the cross sections to show geologic relationships. Unit To is broken into two units: Unit and unit . Units are defined by age (Q = 0.730-0 Ma, QT = 3.9-0.731 Ma, Td = 7.42-4.0 Ma, Tm = 16.9-7.5 Ma, To = 43.2-17 Ma, To_1 = 43.2-25.1 Ma, To_2 = 25.0-17.0 Ma, Te = pre-43.2-Ma Eocene units, and M = Mesozoic rocks), and lithology (b = mafic lava flows, a = andesite, r = dacite and rhyodacite, s = continental volcaniclastic rocks). For example, Tdb is a unit composed mainly of 7.4-4.0-Ma mafic lava flows.

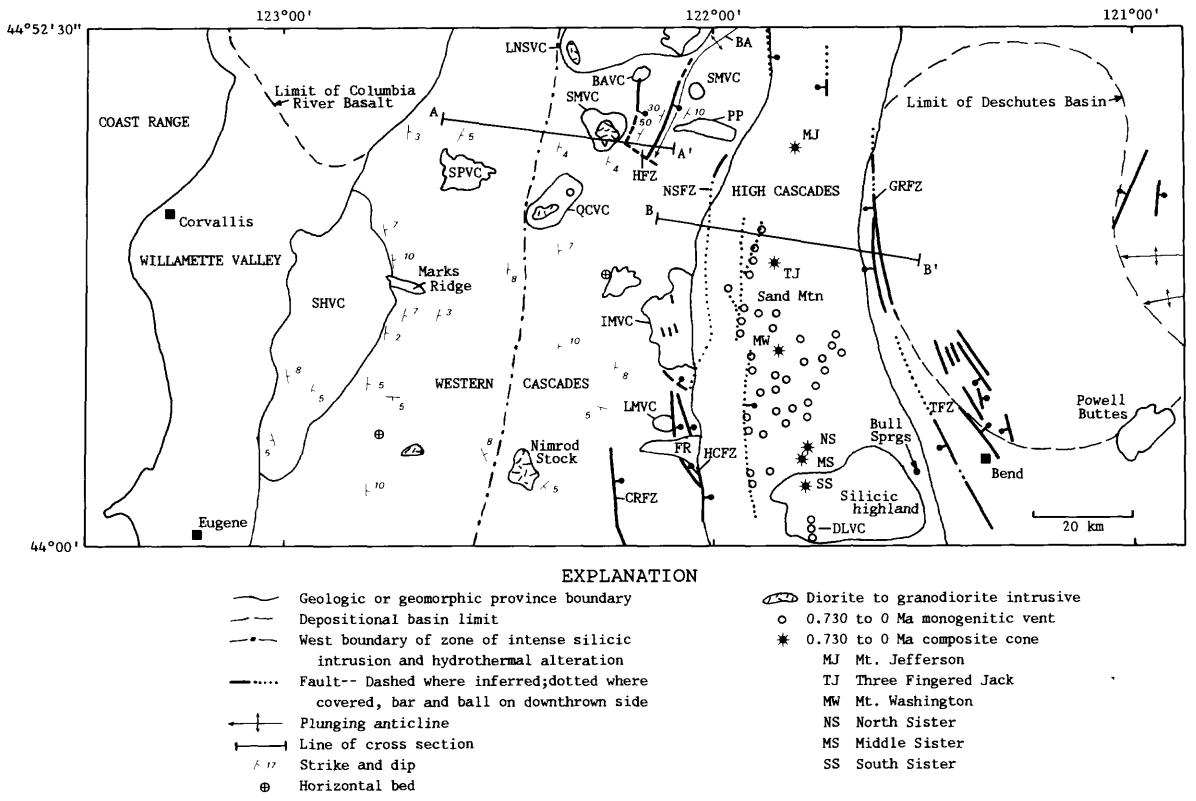

Fig. 6. Tectonic map of the study area with the same geomorphic province boundaries and same dotted solid line as Figure 3. Notable concentrations of volcanic vent rocks are labeled as follows: LNSVC = Little North Santiam volcanic center; SPVC = Snow Peak volcanic center; QCVC = Quartzville Creek volcanic center; SMVC = Sardine Mountain volcanic center; BAVC = Battle Ax volcanic center; SMVC = Scorpion Mountain volcanic center; SHVC = Sweet Home volcanic center; IMVC = Iron Mountain volcanic center; LMVC = Lookout Mountain volcanic center; MJ = Mount Jefferson; TJ = Three Fingered Jack; MW = Mount Washington; NS = North Sister; MS = Middle Sister; SS = South Sister; DLVC = Devils Lake volcanic center. Major structural features are labeled: BA = Breitenbush anticline; HFZ = Hoover fault zone; NSFZ = North Santiam fault zone; HCFZ = Horse Creek fault zone; CRFZ = Cougar Reservoir fault zone; GRFZ = Green Ridge fault zone; TFZ = Tumalo fault zone. Important geographic localities are labeled: PP = Pigeon Prairie; FR = Foley Ridge. The limit of the Deschutes Basin is taken from Smith (1986).

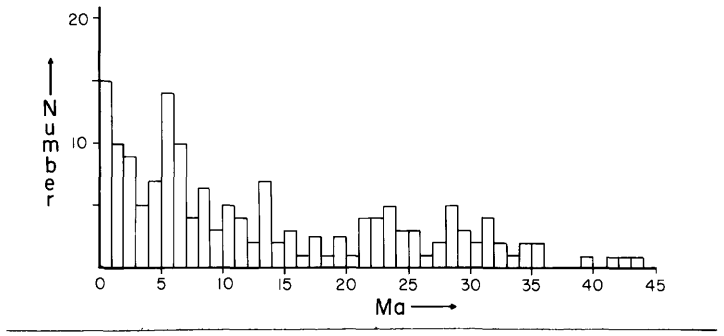

Fig. 7. Histogram of isotopic age data taken from Hammond and others (1980), Fiebelkorn and others (1983), Walker and Duncan (1989), Verplanck (1985), Priest and others (1987; 1988), Black and others (1987), and an unpublished K-Ar age of 0.857 ± 0.060 Ma (Paul Damon, analyst) on the base of the Pigeon Prairie intra-canyon flow sequence (PP, Figure 5). Isotopic ages were eliminated where I resampled the field locality and found excessive rock alteration, or where stratigraphic relationships indicate that the age is grossly in error.

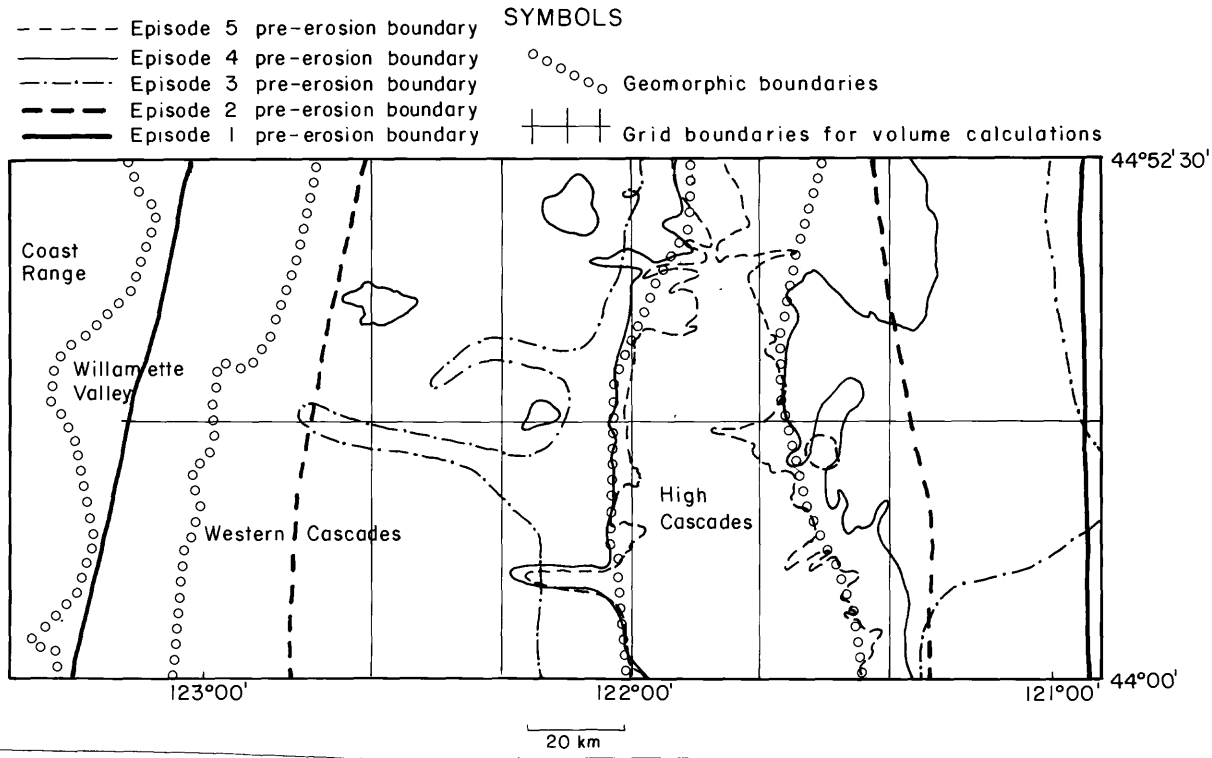

Fig. 8. Shows inferred original extent of rocks of each episode before erosion. Grid lines show areas for which an average thickness of each unit was inferred for volume calculations.

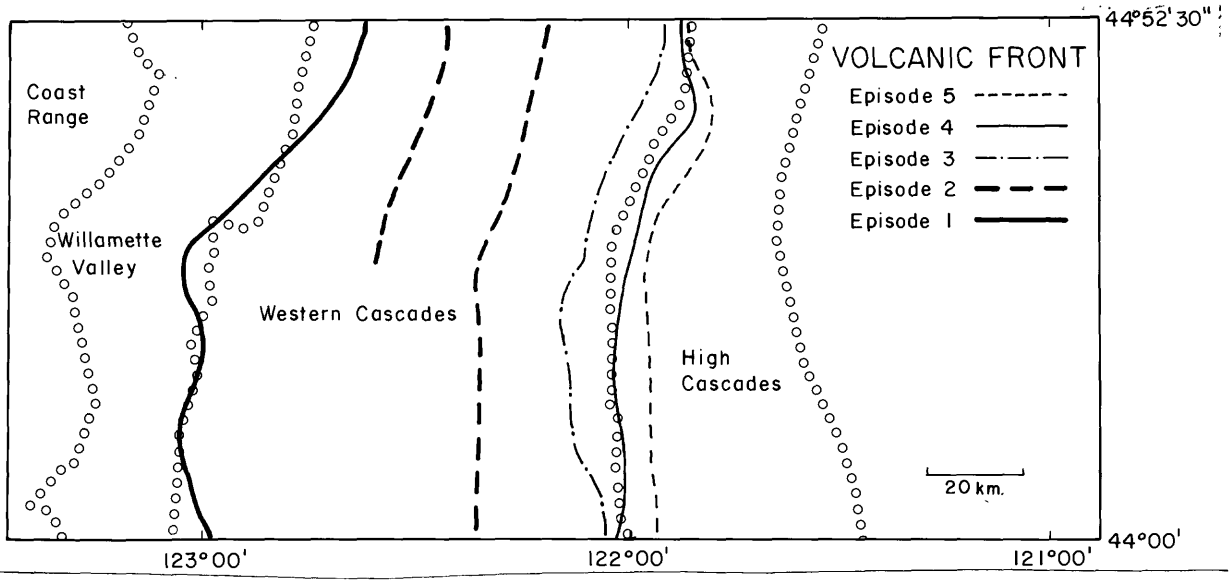

Fig. 9. Map showing inferred volcanic fronts. Symbols as in Figure 8. The two lines shown for episode 3 indicate the limits of uncertainty in the location. Volcanic front locations are probably most valid for the earliest part of each episode. The uncertainty in the age is of this earliest part is: Episode 1 front = 35-30 Ma; episode 2 front = 16.9-13 Ma; episode 3 front = 7.4-6.3 Ma; episode 4 front = 3.9-2.7 Ma; episode 5 front = 0.730-0 Ma.

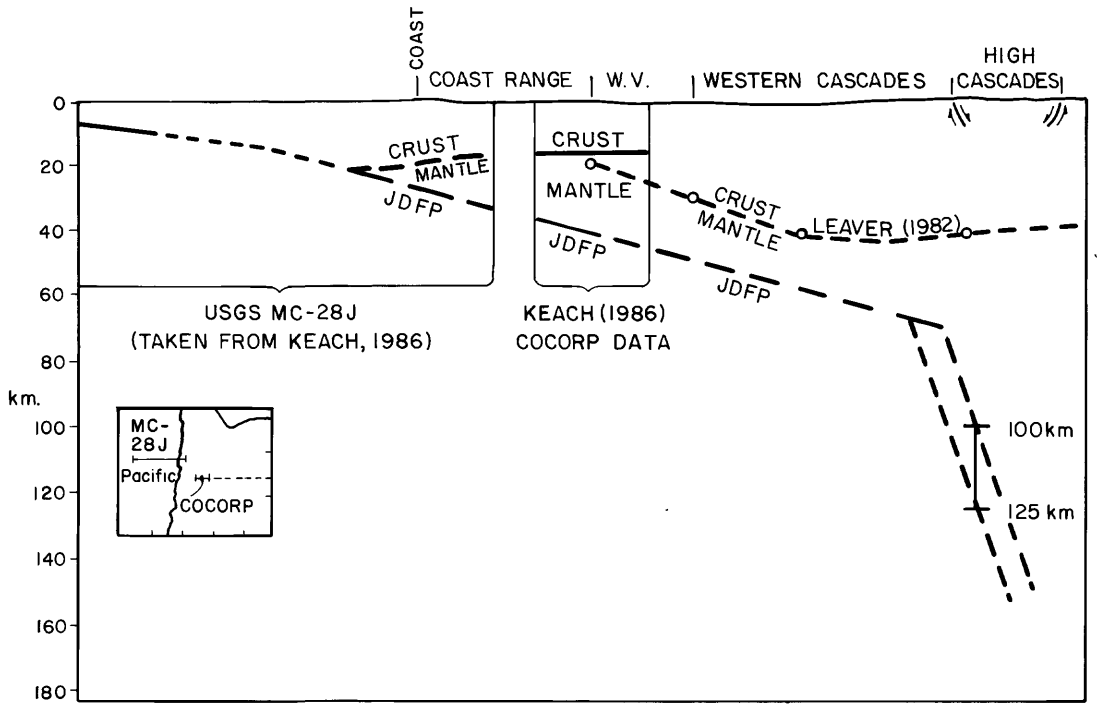

Fig. 10. Regional cross section showing the current crust-mantle-Juan de Fuca plate boundaries. Figure is modified from Keach (1986, Figure 9, p. 41-42) by 1) adding the crust-mantle boundary of Leaver (1982); 2) assuming a 70^{o} dip for the slab under the High Cascades; 3) assuming that the current volcanic front is about 100-125 km above the slab; and 4) extending the known shallow dip of the slab to meet the 70^{o} dip. USGS MC-28J refers to a U.S. Geological Survey continental margin transect (Snavely and others, 1980); W.V. = Willamette Valley; JDFP = upper surface of the Juan de Fuca plate..

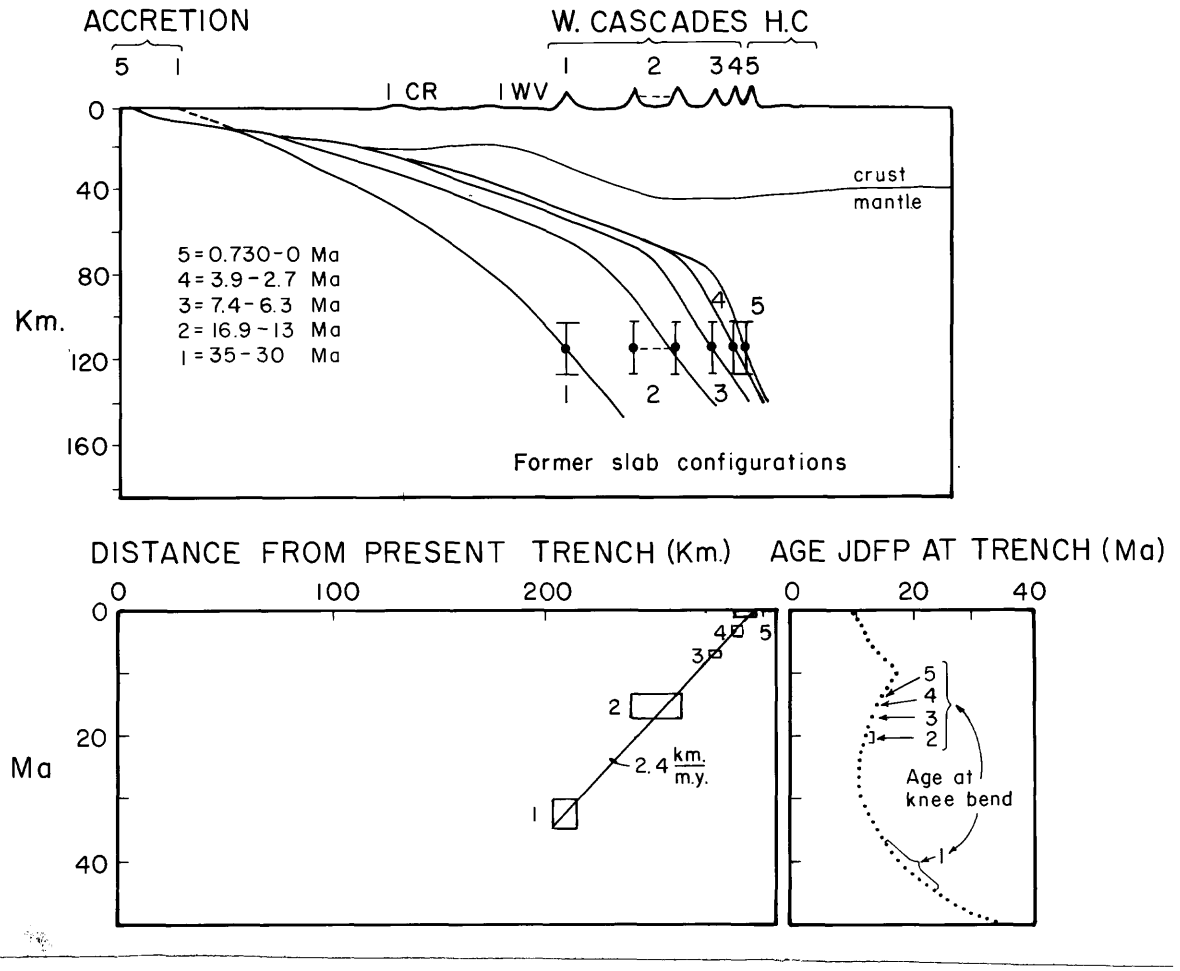

Fig. 11. Regional cross section showing the crust-mantle boundary and the subducted slab. Modified from Figure 10 by adding speculative reconstructions of the slab positions under the volcanic arc during episodes 1-5 (see text), and, in the east half of the section, the crust-mantle boundary of Leaver (1982). Lower figure shows volcanic front migration in time-distance space. The bars and boxes represent the uncertainty of location of the volcanic front in time and space; straight line through the boxes is the average path with slope of 2.4 km/m.y.. Also shown is the age of the JDFP at the trench from Verplanck (1985) with inferred age of the JDFP at the knee bend for each volcanic episode.

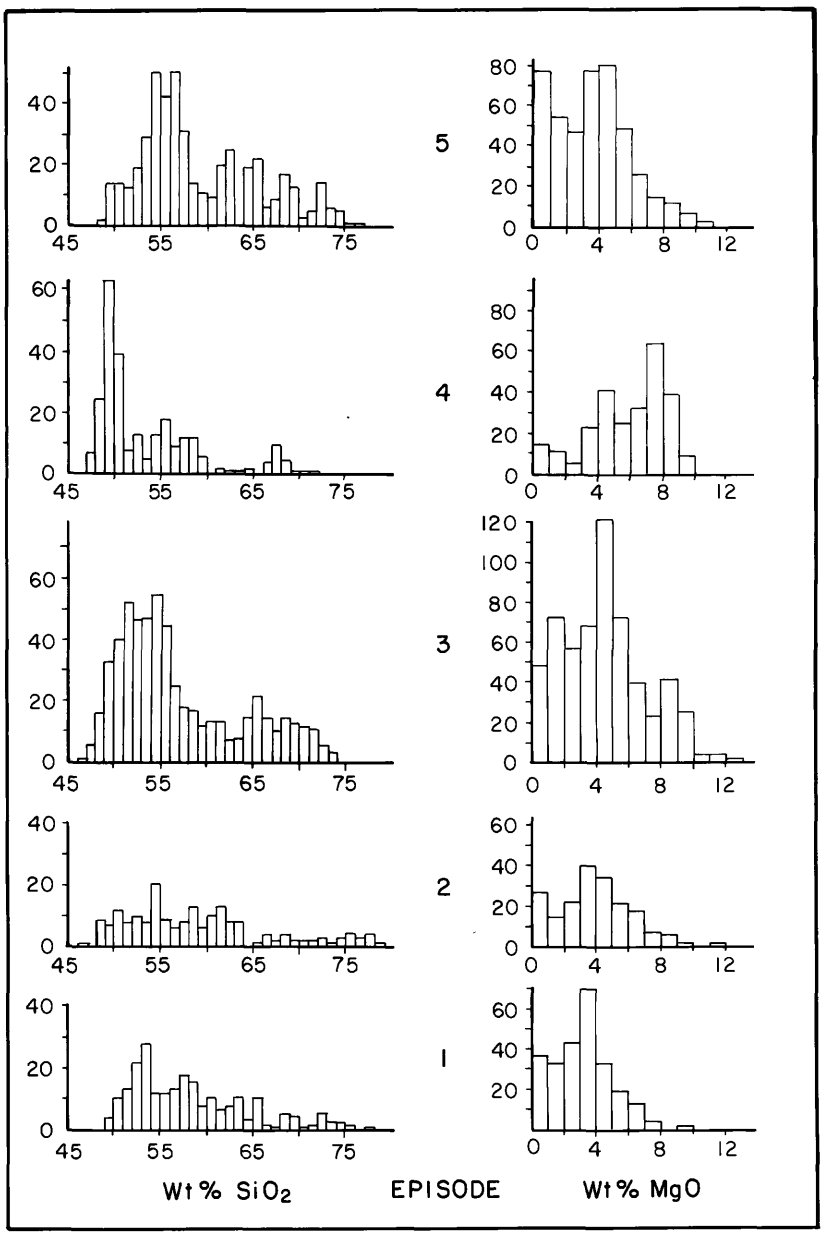

Fig. 12. Histograms of representative chemical data for Cascade volcanic rocks in the study area. Numbers in the center indicate that histograms to the left and right are from that episode. Data sources are the same as those listed for average Cascade basalt compositions in Table 3. Note the larger number of low-silica, high-MgO analyses in episodes 3-5 compared to earlier episodes, particularly episode 1. Also note the predominance of basaltic andesite analyses in all episodes.

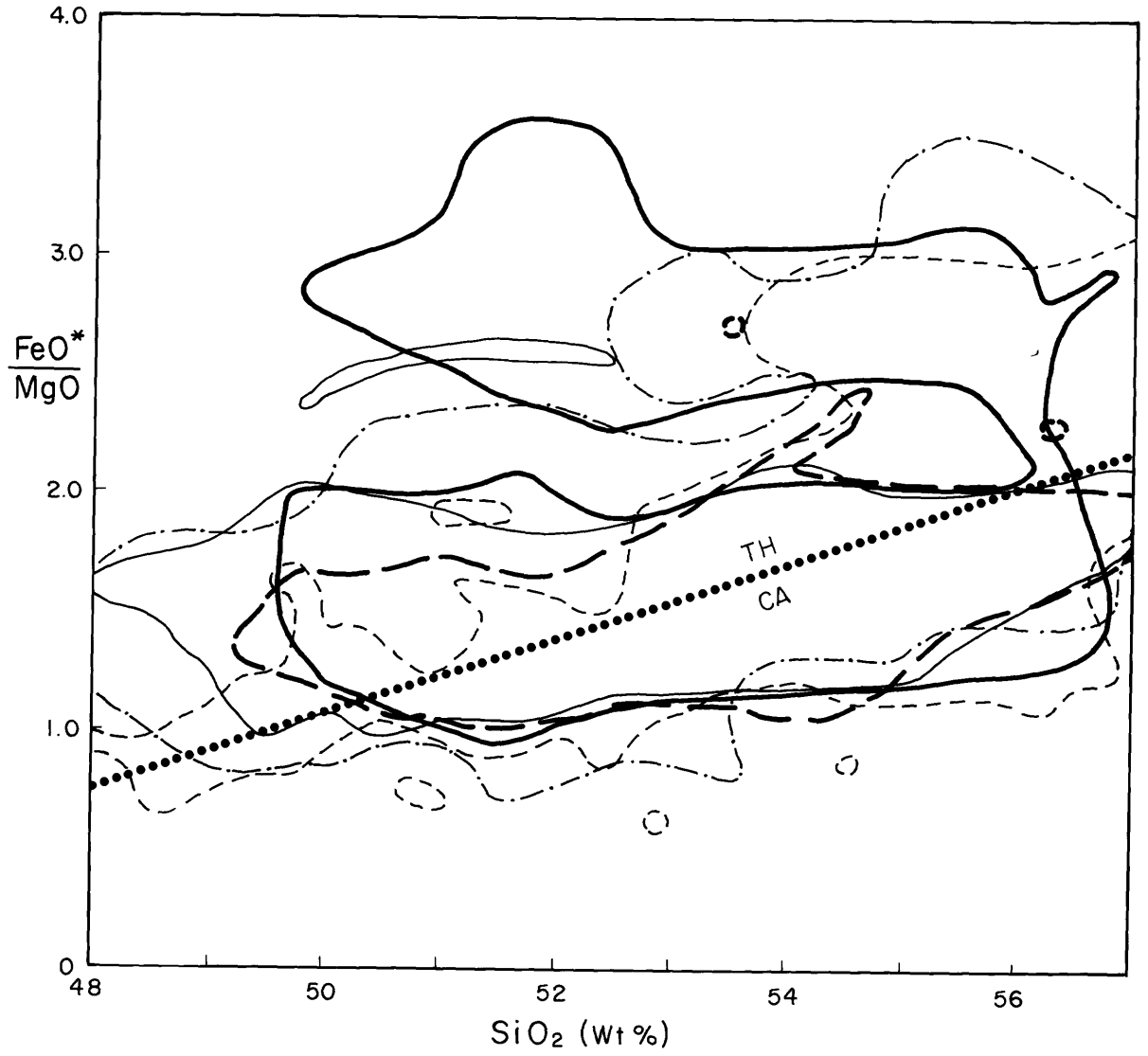

Fig. 13. FeO/MgO versus SiO_2. Analyses normalized to 100% totals, volatile-free with all iron as FeO. Compositional fields are shown with same line symbols used as for the volcanic fronts in Figure 9: Episode 1 = heavy line; episode 2 = heavy dashed line; episode 3 = thin line with dots; episode 4 = thin line; episode 5 = thin dashed line. Data sources are the same as those listed for average Cascade basalts in Table 3. TH = tholeiitic; CA = calc-alkaline; CA-TH boundary from Miyashiro (1974). Note that episode 2 rocks have a much more calc-alkaline composition than the other episodes.

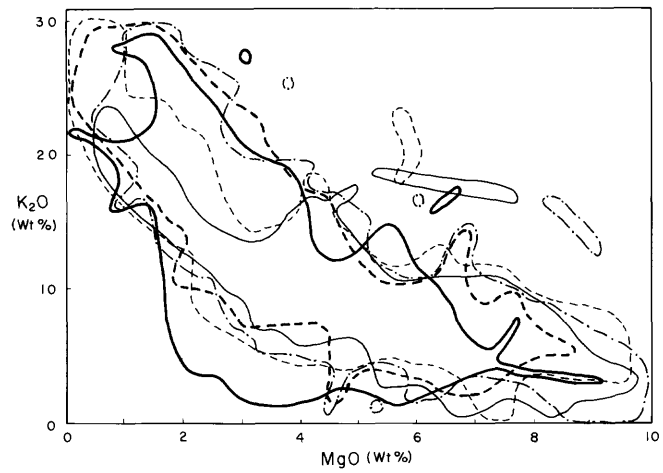

Fig. 14. K_2O versus MgO. Same symbols, data sources, and normalization as in Figure 13. Note how similar the K_2O values are for each episode.

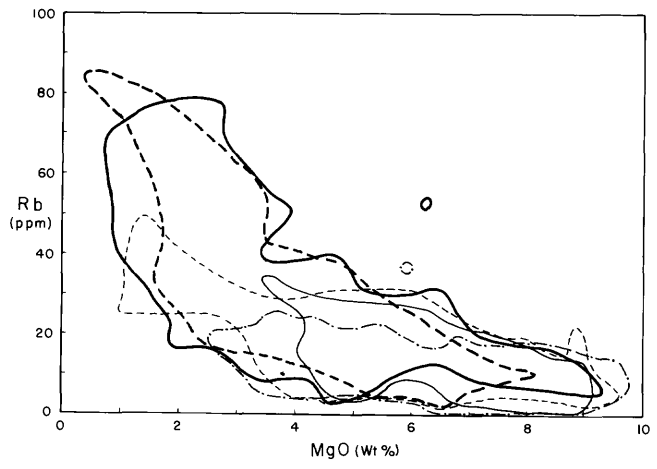

Fig. 15. Rb versus MgO. Same symbols, data sources, and normalization as in Figure 13. Note how similar the Rb values are for each episode.

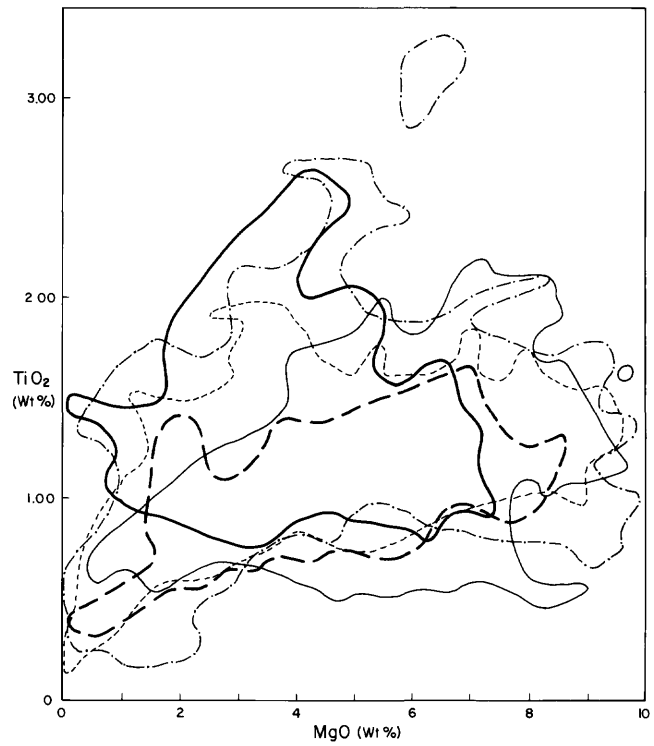

Fig. 16. TiO_2 versus MgO for Cascades rocks. Same symbols, data sources, and normalization as in Figure 13. Note the high values of TiO_2 for episodes 1, 3,4, and 5 compared to episode 2. Also note the similarity of the high-TiO_2 Cascade episodes to Basin and Range rocks of Figure 17.

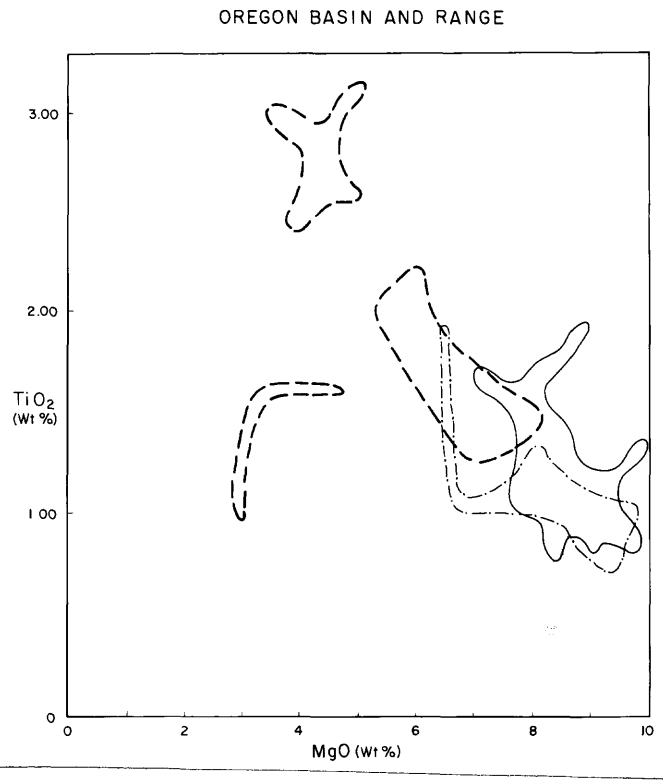

Fig. 17. TiO_2 versus MgO for Basin and Range mafic rocks contemporaneous with Cascade episodes 2-5. Same symbols as in Figure 13, except that the solid line outlines rocks equal in age to episodes 4 and 5 combined. Same data sources as average Basin and Range basalts of Table 3. Note the high TiO_2 of these compositional fields.

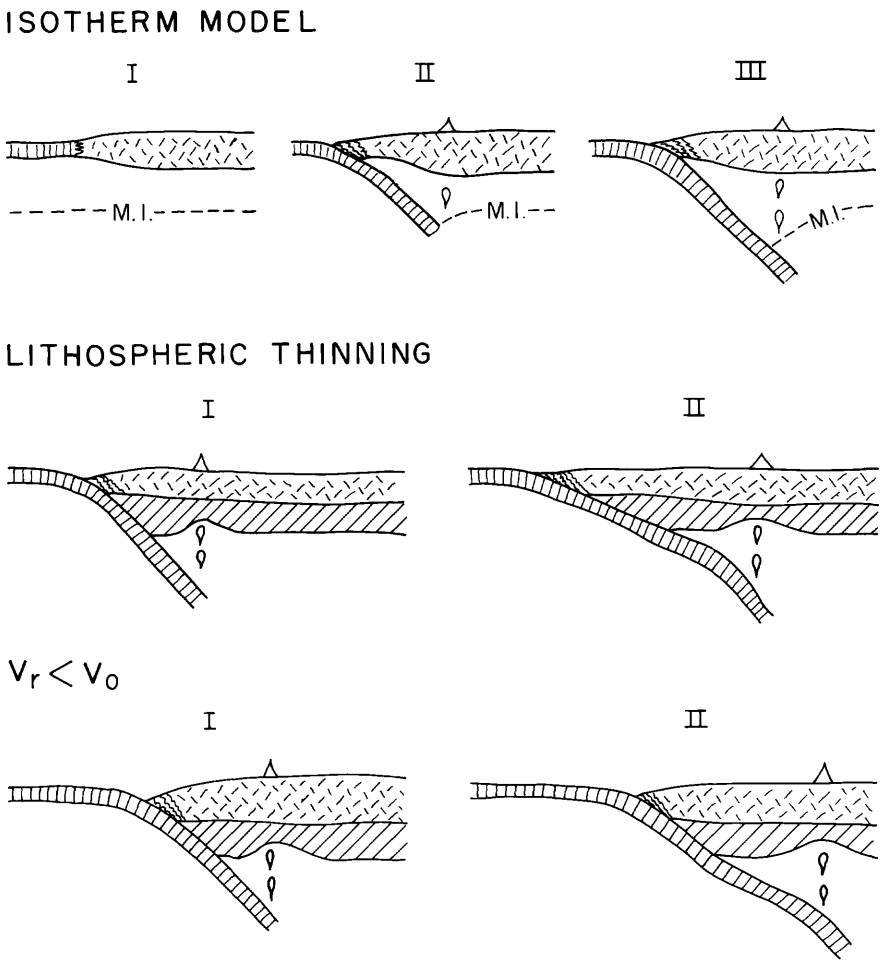

Fig. 18. Cartoons showing three different ways for the volcanic front to migrate landward. Cartoons are not drawn to any real-world scale, being schematic illustrations. Vertical lined pattern indicates basaltic crust; random short-lined pattern indicates continental crust; slanted lines indicate mantle lithosphere. In the top cartoon, M.I. refers to the "magic isotherm" of James (1971), which is the temperature where melt can be generated by the subduction process. See text for further explanation.

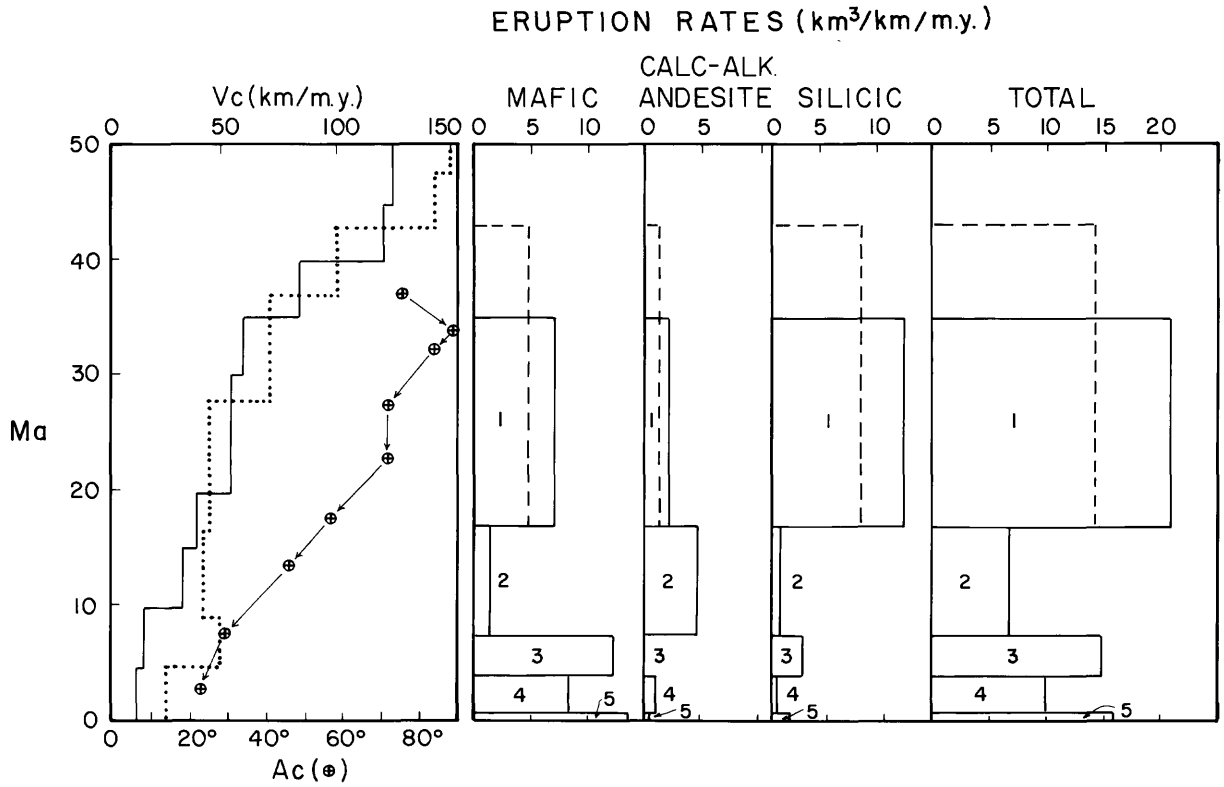

Figure 19. Comparison of convergence rate (V_c), angle of convergence vector to NA plate boundary (A_c), to rates of eruption (volcanic production rate) from Table 2. A_c was taken from Verplanck (1985) and Verplanck and Duncan (1987). Solid line represents convergence model of Verplanck and Duncan (1987); dotted line represents the model of Engebretson (1982). Mafic rocks are basalt, basaltic andesite, and tholeiitic andesite; silicic rocks are dacite, rhyodacite, and rhyolite. Calc-alk. = calc-alkaline. Note correlation of high volcanic production rate and high V_c during episode 1.

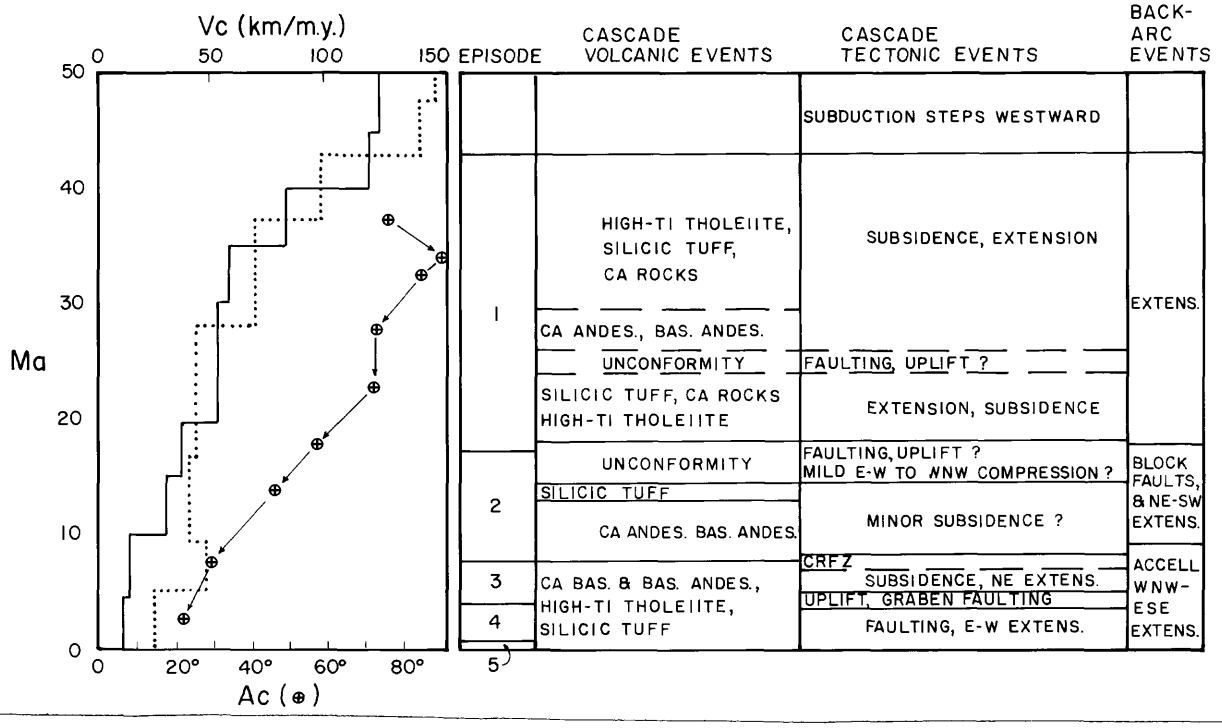

Fig. 20. Comparison of V_c and A_c to geologic events in the Cascade arc and back arc. Back-arc extensional events are inferred from Wells and Heller (1988), Stewart (1978), and Zoback and others (1981). Convergence models as in Figure 19. Accell. = accelerated; andes. = andesite; bas. = basalt or basaltic; CA = calc-alkaline; extens. = extension. Note (1) sharp drop in V_c when uplift occurred in the Western Cascades and arc-parallel graben formed in the High Cascades; (2) occurrence of High-Ti tholeiite at times of both high and low V_c and A_c; and (3) good correlation between changes in back-arc and arc events. See text for discussion.

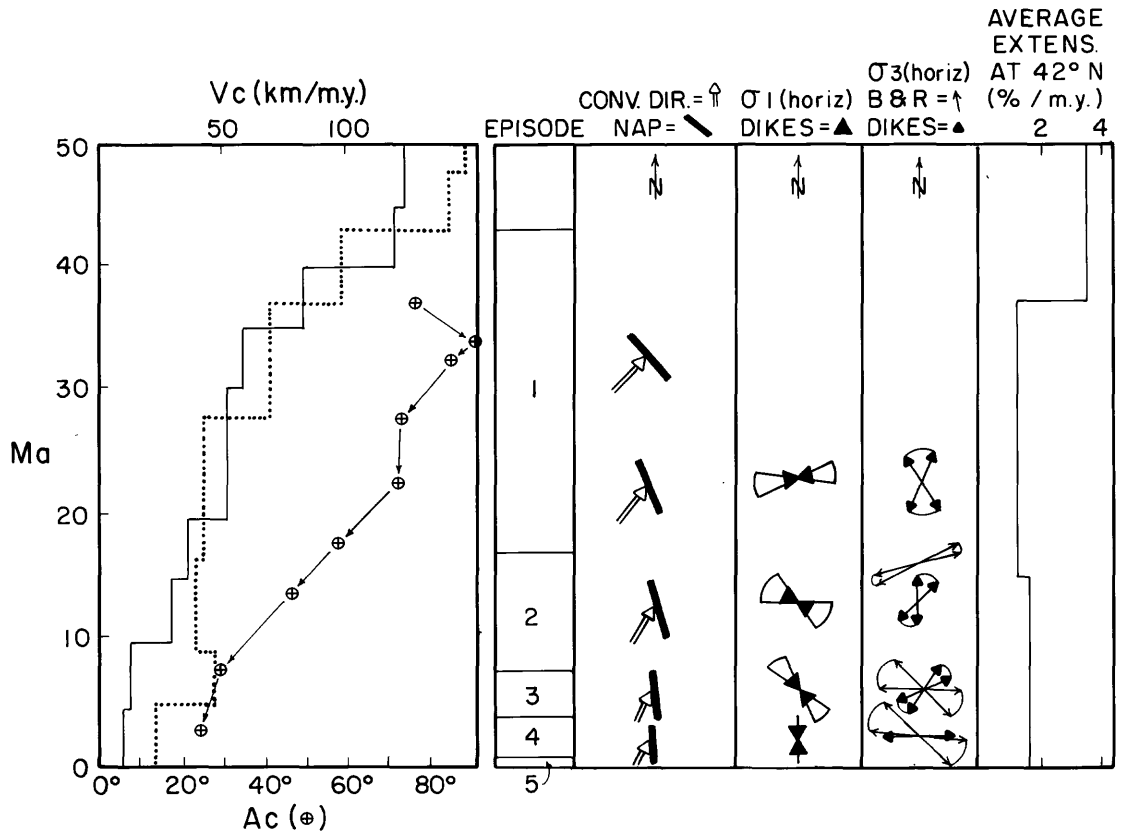

Fig. 21. Comparison of V_c and A_c to contemporaneous Basin and Range (B&R) spreading directions and principal horizontal stress directions inferred from Cascade dike orientations corrected for tectonic rotation inferred from paleomagnetic data of Gromme' and others (1986) and Wells and Heller (1988). Double lines with arrows represent the direction of convergence relative to the continent (solid line with no arrows). Normal arrows represent the directions of Basin and Range extension inferred from Zoback and Thompson (1978) and Zoback and others (1981). Data for dike orientations is from Avramenko (1981), Yogodzinski (1986), and a compilation of Sherrod (1986). See text for further discussion of dike data. Average extension rates refer to total percent of arc and back-arc extension per million years necessary to explain rotation of Western Oregon rocks at latitude 42° N (Wells and Heller, 1988). A_c and orientations of the NAP taken from Verplanck (1985) and Verplanck and Duncan (1985). Convergence models as in Figure 19. Note (1) correspondence of sigma 1 with convergence direction in episode 1 and with Basin and Range spreading directions in episode 3; and (2) correspondence of Basin and Range spreading direction with sigma 3 in episodes 4 and 5.

STRATIGRAPHIC DEVELOPMENT AND HYDROTHERMAL ACTIVITY IN THE CENTRAL WESTERN CASCADES, OREGON

Michael L. Cummings[1], J. Michael Pollock[2], Gordon D. Thompson[1], and Marilyn K. Bull[1]

1 Department of Geology, Portland State University, Portland, Oregon, 97207

2 Reed College Reactor Facility, Reed College, Portland, Oregon, 97202

ABSTRACT

Two volcanic sequences bounded by erosional unconformities compose the stratigraphy of the North Santiam mining area, Western Cascades, Oregon. Diorite, granodiorite, and leucocratic quartz porphyry dikes, stocks, and sills, contact metamorphic aureoles, breccias, and complicated stratigraphic relations characterize a volcanic center of the older Sardine Formation in the center of the mining district. Tourmaline-bearing breccia pipes are associated with porphyritic granodiorite intrusions. An erosional unconformity separates the Sardine Formation from the overlying Elk Lake formation. A volcanic center of the Elk Lake formation is exposed on French Creek Ridge. A hydrothermal system developed in response to the younger volcanic sequence. Circulation of hydrothermal solutions was restricted to faults, fractures and the margins of dikes in the Sardine Formation but was less restricted within the weakly cemented tuffs of the Elk Lake formation. The alteration patterns within the North Santiam mining area suggest two stages of mineralization related to different volcanic cycles and separated by a period of deep erosion of the older volcanic pile. Early formation of porphyry copper-style mineralization occurred within the Sardine Formation and, later, epithermal veins and alteration developed in response to eruption of the Elk Lake formation after deep erosion of the Sardine Formation.

INTRODUCTION

The temporal relations among constructional volcanism, emplacement of intrusions, regional and local structural development, erosion, and hydrothermal activity leading to ore mineralization or exploitable geothermal systems are key to understanding processes that occur within a volcanic arc. The development of hydrothermal mineral deposits and geothermal systems is closely related to the introduction of heat, commonly in the form of shallow-seated intrusions, into the volcanic pile [e.g. *Hedenquist and Henley*, 1985; *Sibbett*, 1988]. The migration of heated aqueous solutions along permeable zones is fundamental in active geothermal systems and within fossil geothermal systems currently being mined for the metals they contain [e.g. *Bonham and Giles*, 1983; *Fournier*, 1983; *Ahmad et al.*, 1987].

The Western Cascade Province in Oregon and Washington contains numerous small metal-mining districts that are related to the development of porphyry copper-type systems. Commonly epithermal vein mineralization occurs within the same districts. The epithermal vein mineralization and the porphyry copper mineralization have been viewed as different stages of a single mineralizing event. In the North Santiam mining area (Figure 1), mineralization and alteration patterns allow reconstruction of the volcanic, structural, and fluid migration history within the volcanic pile. In this district, the epithermal veins developed in response to a younger volcanic

cycle and are not contemporaneous with the porphyry copper-type mineralization in the district.

In this paper, we will examine the stratigraphy, structure, and alteration history of the North Santiam mining area, examine the observed mineralization and alteration patterns in relation to development of regional structure and volcanic stratigraphy, and discuss the implications of these findings to mineralization patterns in the Western Cascade Province in Oregon and Washington.

BACKGROUND

The North Santiam mining area is one of five mining districts within the Western Cascade province of Oregon (Figure 1). Production from these districts has been small [*Oregon Department of Geology and Mineral Industries*, 1951; *Brooks and Ramp*, 1968]. The geology and production histories for similar districts in the Western Cascade Province in Washington have been reviewed by *Grant* [1969] and *Huntting* [1956].

The mining districts occur in Oligocene and Miocene volcanic rocks that compose the Western Cascades of Oregon and Washington. In the central part of the Cascade Range in Oregon, these rocks were uplifted relative to the High Cascade Province at approximately 5 m.y.B.P. [*Priest et al.*, 1983].

The North Santiam mining area was first explored for gold in the 1860's. The Ruth vein was discovered in the early part of this century near the eastern end of the mining district and has been the focus of mining efforts for zinc and lead periodically since its discovery. *Callaghan and Buddington* [1938] presented an overview of the geology and mineralization of the district as part of a study of the five mining districts in the Western Cascades of Oregon. The stratigraphy and alteration were examined and tourmaline-bearing breccia pipes along the Little North Fork of the Santiam River were described by *Olson* [1978]. The district was argued to represent the upper levels of a porphyry copper system [*Olson*, 1978; *Power*, 1984]. A copper-mineralized breccia pipe along Cedar Creek was described by *Winters* [1985]. This breccia pipe is within a claim block maintained by Amoco Minerals Co. The district was included in a lead isotope study of sulfide minerals and associated volcanic rocks in the Cascade Range by *Church et al.* [1986].

In 1982, the first study at Portland State University was initiated to determine the relationships among stratigraphy, hydrothermal alteration, and structure in the district. *Pollock* [1985] and *Pollock and Cummings* [1985, 1986] presented data on the eastern portion of the district in the area of the Ruth vein. *Thompson* [1989] and *Mestrovich* [1989] studied the stratigraphy, alteration, and structure within the central part of the district. These studies were integrated to examine the processes active in the subvolcanic portion of a porphyry copper system [*Pollock et al.*, 1986] and as a model to guide geothermal exploration within the younger High Cascades Province [*Cummings et al.*, 1987].

STRATIGRAPHY

The volcanic stratigraphy (Figure 2) in the North Santiam mining area is characterized by its complexity in both the horizontal and vertical dimensions. All rocks of the district were assigned to the Sardine Formation by *Peck et al.* [1964]. *Olson* [1978] recognized that two distinct sequences were present but assigned both to the Sardine Formation. Southeast of the

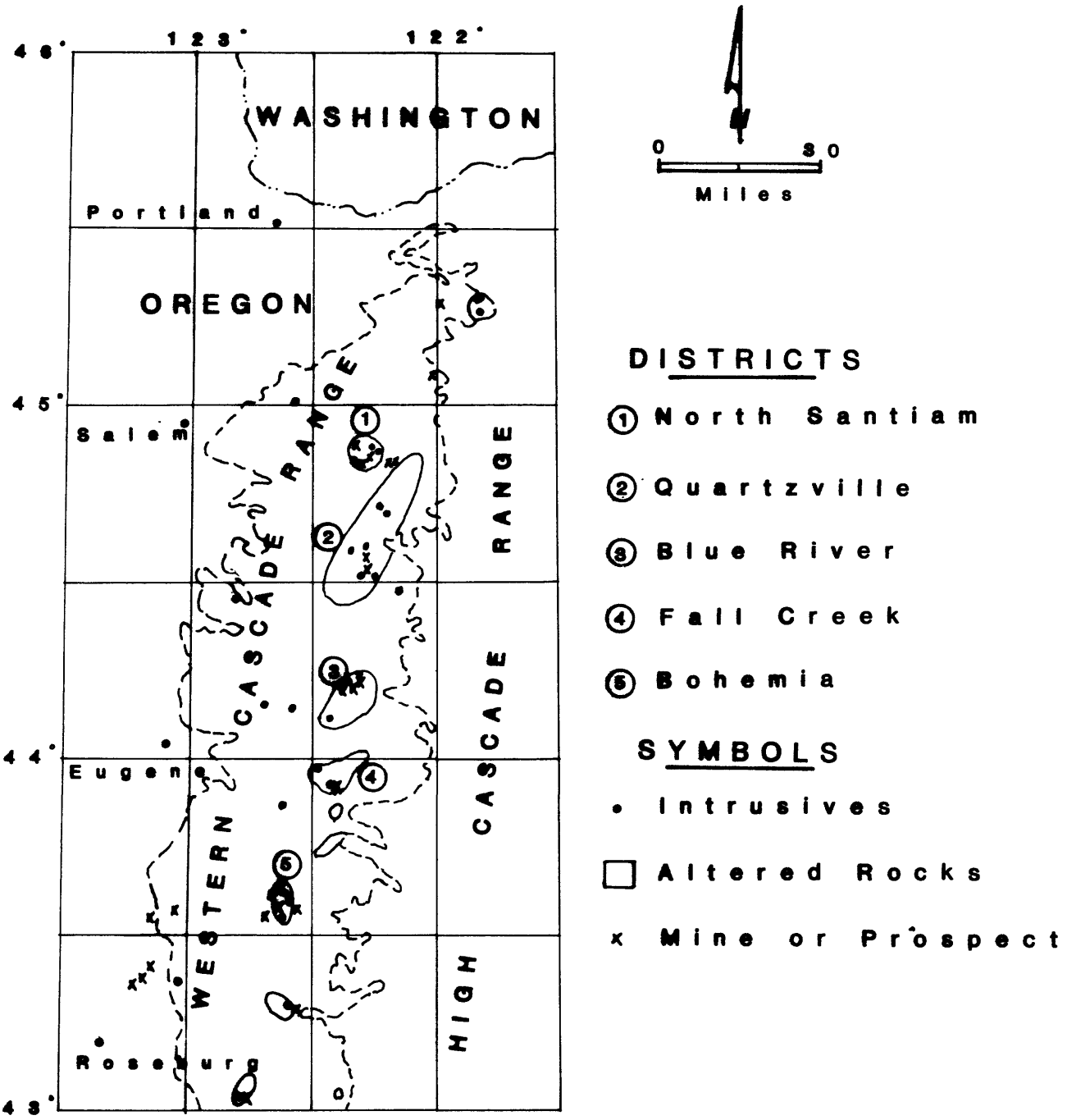

Fig. 1. Distribution of mineralized districts in the Western Cascade Province in Oregon. Modified from Munts, 1978.

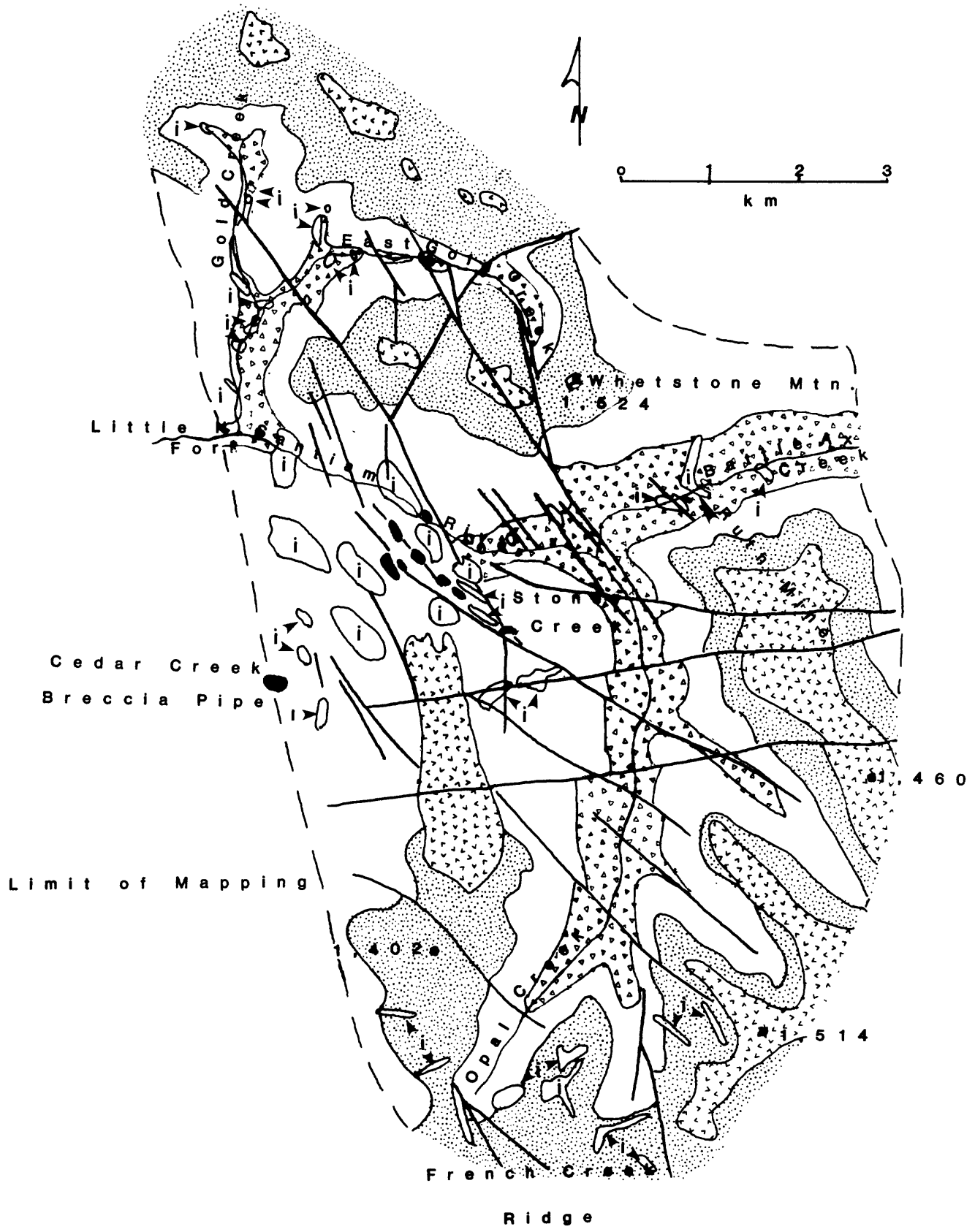

Fig. 2. Generalized geologic map - North Santiam mining area.

KEY

Elk Lake formation and Hugh Creek ignimbrite

 Porphyritic andesite flows

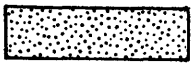 Rhyodacite tuffs, tuff breccias

Sardine Formation

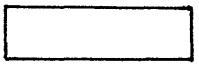 Unit B, andesite flows

 Unit A, andesite tuffs

 Intrusions

 Tourmaline-bearing breccia pipes

Elevations are given in meters.

mining area, *McBirney et al.* [1974] separated the Elk Lake formation from the older Sardine Formation on the basis of exposures in the area of Elk Lake. This formation is composed of rhyodacitic to basaltic tuffs and lavas. They placed the Elk Lake formation as overlying and separated from the Sardine Formation by an angular unconformity.

In this paper, two stratigraphic sequences are recognized in the North Santiam area. Correlations to units defined by other researchers have been made on the basis of lithology, stratigraphic position, and elevation of occurrences. A lower sequence is assigned to the Sardine Formation [*Thayer*, 1936; *Peck et al.*, 1964] and occurs from the bottoms of stream valleys up to an elevation of approximately 1,200 m. The upper sequence overlies the lower sequence across an erosional unconformity. This sequence is at least 400 m thick and underlies the ridge crests of the area. The upper sequence includes the Elk Lake formation [*McBirney et al.*, 1974] and the Hugh Creek ignimbrite [*Dyhrman*, 1975; *Hammond et al.*, 1980]. This sequence was deposited on a moderate relief surface eroded into the Sardine Formation. The rocks are of the Late Western Cascades Eruption - Episode 2 of *Priest* [this volume].

The stratigraphic relations, geometry of units, and the large number of intrusions suggest that the mining area is located within a volcanic center of the Sardine Formation. However, the stratigraphy and alteration patterns indicate that the alteration within rocks of the older volcanic center was

overprinted by a younger alteration system believed to be associated with a volcanic center within the Elk Lake formation in the French Creek Ridge area.

The Sardine Formation includes andesite flows, andesite lapilli and lithic tuffs, sparse sediments, and intrusions. Hydrothermal alteration obscures primary igneous textures and makes lithologic identification and correlation a challenge. In the eastern portion of the district, the stratigraphy is divided into Units A and B (Figure 2) distinguished from each other by the relative proportions of fragmental rocks and flows. Unit A consists of andesitic tuffs and tuff breccias. A block and ash flow is the lowermost flow of unit A. The block and ash flow contains two zones, the lower of which is unsorted, matrix-supported breccia containing rounded to angular clasts ranging in diameter from less than 0.5 cm to 2 m or more in diameter. The lower zone grades upward across a thickness of a few centimeters into the upper zone.

Within the lower zone and extending into the lower 3 to 5 m of the upper zone are parallel-sided, steeply dipping degasing structures that contain predominantly gravel size, rounded clasts. The structures are randomly oriented and from 2 cm to 10 cm wide.

The upper zone is 25 to 30 m thick. The least altered samples display primary textures of an andesitic lithic-crystal lapilli tuff. Clasts larger than 32 mm are uncommon. Lithic fragments are of two lithologies. Both types contain plagioclase and mafic phenocrysts but one alters to a dark reddish gray and the other to a light greenish gray. The matrix consists of ash-size lithic fragments of the same two lithic types, feldspar crystals and altered glass.

Lapilli tuffs, some of which contain flattened lapilli and pumice fragments, form the rest of unit A. The outcrop heights and textures suggest that the thickness of individual cooling units ranges from 10 to 50 m.

Porphyritic andesite flows are interbedded with the lapilli tuffs above an elevation of approximately 850 m south of Battle Ax Creek and 1080 m on the south flank of Whetstone Mountain. This flow-dominated sequence is designated as unit B and is up to 215 m thick south of Battle Ax Creek and 550 m thick along Cedar Creek. In the area of the Morning Star Mine, the lowermost flow is brecciated and has baked the upper part of a sediment layer that is 0.5 to 1 m thick. Plagioclase and pyroxene form phenocrysts and plagioclase, clinopyroxene and orthopyroxene microlites occur in the groundmass. Plagioclase is flow aligned in some flows (Figure 3).

The flows become less abundant to the west towards the valley of East Gold Creek and are supplanted in the section by a thick, well-developed crystal-lithic tuff. The base of this tuff is at an elevation of 800 m.

The upper volcanic sequence overlies the Sardine Formation across an erosional unconformity that locally can be demonstrated to have an angular discordance. The unconformity occurs at different elevations. On Whetstone Mountain, it is at approximately 1,350 m. Although the contact is not exposed, it is located on the basis of a change in lithology and the degree of alteration. Tuffs in the upper sequence are commonly associated with slope instability. Where the tuffs have not been hydrothermally cemented, they are prone to mass movement and the trees that grow on these slopes display wildly variable orientations. The unconformity occurs at 1,125 m south of Battle Ax Creek. The thickness of individual volcanic units in

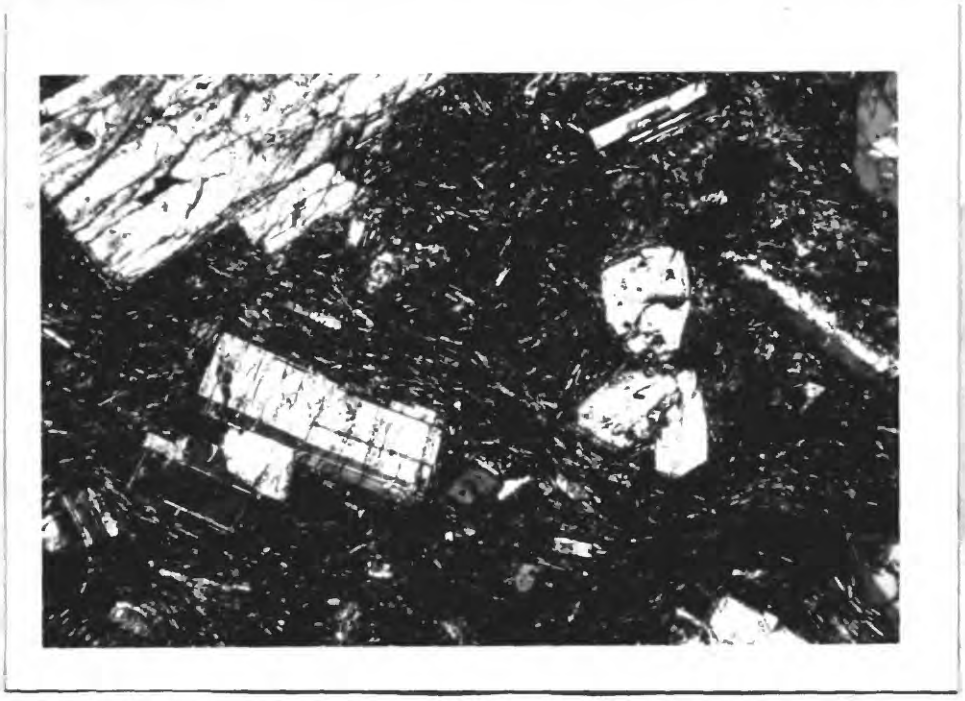

Fig. 3. Porphyrytic andesite flow from Unit B of the Sardine Formation showing flow alignment of plagioclase microlites in the groundmass. Polars crossed. Field of view 4.5 mm.

the tuffs increases to the south.

The unconformity is well exposed on the ridge above Stoney Creek where andesite flows directly overlie rocks of the Sardine Formation at approximately 1,100 m. Along the north flank of French Creek Ridge the unconformity occurs at 1,100 m where rhyodacite tuffs directly overlie the Sardine Formation. In this area, an angular discordance occurs between the two formations. The porphyritic andesite flows of the Sardine Formation dip to the south and southeast, whereas the tuffs of the Elk Lake formation show variations in trend as distributed within a local volcanic vent facies. In the area of Elk Lake, where the formation was informally named by *McBirney et al.* [1974], the unconformity is located between 1,180 to 1,340 m [*White*, 1980].

The Elk Lake formation is composed of two lithologies, rhyodacite-andesite tuffs and andesite flows. *White* [1980] suggested that a rhyodacite dome exposed on French Creek Ridge may be within the vent area for the rhyodacite tuffs mapped in the Elk Lake area to the east. The dome is composed of scoriaceous and partially zeolitized breccia at the base and has been intruded by a dacitic dike [*White*, 1980; *Thompson*, 1989]. In the French Creek Ridge area, crude radial dikes and abundant sills of andesite and chaotic breccia deposits are indicative of a vent facies. Breccias are from 5 to 30 m thick, poorly sorted, unbedded and intruded by andesite dikes and sills. The strike and dip of tuffaceous units around French Creek Ridge indicate deposition on the flanks of a semicircular vent of low topographic relief. The dip of bedding is approximately 20°. Local disconformities are abundant among the tuffs, flows, and tuff breccia units.

A distinctive, 20-25 m thick, rhyodacite tuff is exposed at an elevation of 1,400 m on Whetstone Mountain. This tuff is

finely laminated and contains parallel 1 to 2 mm-thick laminations of alternating light and dark colored clasts. Individual laminae can be traced for tens of meters along strike. Abundant carbonized plant fragments including twigs up to 5 cm long, needles, and seed pods occur on bedding planes. The plant fragments are strongly lineated on bedding planes but the orientation among different layers is not constant.

In the area of French Creek Ridge, these same rhyodacite tuffs are composed of lithic tuff breccia and laminated lapilli tuff. The lithic tuff breccias are poorly sorted and exhibit no size grading of lithic fragments. The clasts range in size from 2 mm to 1.5 m in diameter and are subangular to subrounded; smaller clasts are more rounded than larger clasts. The clasts of rhyodacite tuff, andesite lapilli tuff, massive andesite, and possibly altered tuffaceous fragments occur in a matrix of fine ash and plagioclase crystals. The breccias range from clast supported to matrix supported in relation to distance from the vent area. The thickness of the tuff breccia units ranges from 5 to 25 m and the breccias grade upwards into laminated rhyodacite tuff.

The laminated rhyodacite tuffs consist of alternating layers of coarse- and fine-grained lapilli tuff. The coarse-grained layers range from 30 to 60 cm thick and thin upward in the section. The clasts are subangular to subrounded and 5 to 10 cm in diameter. The lithic fragments include porphyritic andesite, andesite, and lithic crystal tuff in a matrix of plagioclase microlites, quartz, opaque minerals, and ash-sized materials.

The fine-grained layers consist of poorly sorted heterolithic tuff and ash layers. Clasts of porphyritic andesite, andesite, lithic tuff, and pumice range in diameter from 0.5 to 1 mm and are angular. Normal-size grading of lithic fragments is prominent and fragments are well sorted. The ash layers range from 3 to 15 cm thick and are commonly red. The matrix is composed of feldspar fragments and ash. Lineation and rolling of fragments is evident and along the north flank of French Creek Ridge indicate an approximate flow direction to the northwest.

Dark-colored, porphyritic basalt or basaltic-andesite flows occur at various elevations and stratigraphic positions in the tuff sequence. These flows have a somewhat glassy appearance and some contain feldspar and pyroxene phenocrysts while others contain glomerocrysts of plagioclase and/or lath-shaped pyroxene phenocryts to 2 cm long (Figure 4). Two such flows (combined thickness of 30 m) cap Whetstone Mountain (elevation 1500 m) where they were deposited in an intracanyon relation to the rhyodacite tuffs. An intracanyon relation between andesite flows and the rhyodacite tuffs is also indicated on French Creek Ridge. The dikes, sills, and stocks on French Creek Ridge are of similar composition. *White* [1980] described a similar flow series (Tea) capping Marten Butte and overlying rhyodacitic flows and pyroclastic rocks (Ter).

A distinct, partially welded, large-volume hornblende rhyodacite tuff crops out at elevations above 1000 m in the northwestern portion of the map area (Figure 2). The rhyodacite occurs in the valley of East Gold Creek where it overlies rocks of the older Sardine Formation at 900 m. This occurrence is interpreted to be a fill within a paleovalley. The tuff is correlated with the Hugh Creek ignimbrite [*Dyhrman*, 1975; *Hammond et al.*, 1980] and is believed to have a source to the north of the area. The tuff has not been identified south of the Little North Fork of the Santiam River. This tuff is of a similar composition and is tentatively interpreted to interfinger with the tuffs erupted from the French Creek center.

Fig. 4. Porphyritic andesite flow from the Elk Lake formation collected from the capping flows on Whetstone Mountain. Polars crossed. Field of view 4.5 mm.

Intrusions:

Intrusions are common within the Sardine Formation but are sparse within the Elk Lake formation except in the vent area on French Creek Ridge. The different intrusion types and their stratigraphic setting are presented in Table 1.

The intrusions that are confined to the stratigraphic levels of the Sardine Formation include: Equigranular to porphyritic diorite, porphyritic granodiorite, and leucocratic quartz-feldspar porphyry.

The geometry of intrusions changes from sharp-walled dikes whose shapes are strongly controlled by northwest-trending fracture and fault sets in the eastern part of the mining area to irregularly shaped stocks and plugs in the central part of the area. The irregularly shaped intrusions are aligned along northwest-trending structures or are elongate along this trend; however, the overall shapes of the intrusions are not constrained by structures.

The equigranular to porphyritic diorite intrusions (Figure 5) form dikes that are strongly controlled by northwest structural trends throughout the district. These dikes display sharp contacts characterized by minimal alteration of the country rock, narrow chilled margins, hornfelsed aureoles that extend 1-2 m into the country rock, and locally vesiculated margins.

Porphyritic granodiorite intrusions are particularly common near the confluence of Gold Creek and the Little North Fork of the Santiam River. These intrusions occur as dikes and plugs and are spatially associated with tourmaline-bearing breccias.

Fig. 5. Equigranular quartz diorite from near the Ruth Mine. Biotite has been completely altered to chlorite, pyroxenes are partially altered to epidote and chlorite while plagioclase remains relatively fresh. The alteration in this sample is characteristic of the weakly altered intrusions in the district. Polars crossed. Field of view 4.5 mm.

Table 1. Textural and Mineralogical features of intrusions within the Sardine Formation and Elk Lake formation.

	Intrusion type				
	Sardine Formation			Elk Lake formation	
	porphyritic granodiorite	porphyritic and equigranular diorite	quartz-feldspar porphyry	dacite	basaltic andesite
Textures	porphyritic glomeroporphyritic	porphyritic glomeroporphyritic to equigranular	porphyritic	porphyritic	porphyritic
Mineralogy					
Phenocrysts	30% plagioclase	20-30% plagioclase	plagioclase	feldspar	20-30%plagioclase
	10% hornblende	15-20% pyroxene	hornblende	quartz	20% augite
	5-15% quartz		quartz		10% hypersthene
Groundmass	50% plagioclase quartz	55-60% plagioclase microlites, mafics	feldspar quartz	feldspar quartz	50-60% plagioclase pyroxene, opaques
Geometry	Irregular dikes and plugs	Northwest-trending dikes	dikes to sills	dikes	radial dikes in volcanic center
Highest stratigraphic occurrence	Unit B flows	Unit B flows	Unit B flows	Rhyodacite tuffs	All stratigraphic units

The intrusions of this composition were collectively referred to as the Hewlitt Granodiorite by *Olson* [1978]. Xenoliths of the volcanic country rock are common and hornfels zones are wide and well-developed. Dikes commonly range in width from 15 to 20 m. The dikes have brecciated margins and alteration extending into the country rock along the contacts has destroyed primary textures. Irregularly shaped plugs of the granodiorite occur at lower elevations.

Determination of the primary textures of the instrusions is made difficult by pervasive alteration. The determination of the mafic phenocrysts has been largely on the basis of the shapes of pseudomorphs. The texture of the intrusions is porphyritic to glomeroporphyritic. Euhedral to subhedral feldspar crystals form glomerophenocrysts ranging from 5 to 15 mm in diameter. Embayed quartz phenocrysts compose up to 20% of some samples and range in size from 1 to 5 mm in diameter. The distinct crystal outlines of pseudomorphs indicate hornblende phenocryts were the dominant mafic component.

The breccias associated with granodiorite intrusions are varied and due to hydrothermal alteration produce considerable confusion in distinguishing among intrusions, flows, tuffs, and volcanic breccias. The most distinctive breccia type is composed of tabular clasts arranged so that the long dimensions of the clasts are subparallel (Figure 6). The clast alignment ranges from parallel, with clasts separated by open spaces and precipitated minerals, to no distinct orientation within a rock-flour matrix. The matrix contains epidote, chlorite, pyrite and/or chalcopyrite, minor quartz, locally tourmaline, and fine-grained rock flour. The amount of rock flour varies inversely with the amount of secondary minerals and degree of clast alignment, and directly with the volume percentage of matrix in the breccia. The orientation of the breccias is within 30° of vertical or within 25° of horizontal. Breccia pockets are up to 1 m thick and some of the larger pockets have exposed distances of at least 100 m. Similar breccias, referred to as shingle breccias, are described by *Sillitoe* [1976, 1985] in intrusions in porphyry copper-related systems.

The shingle breccias occur in association with porphyritic granodiorite dikes, tourmalinized breccias pipes in the area of Stoney Creek, and in intrusive contact settings along Gold Creek from the confluence with the Little North Fork of the Santiam River to East Gold Creek. All known occurrences of this breccia type are below an elevation of 610 m. Shingle breccias in granodiorite intrusions were also intersected in drill holes into tourmaline-breccia pipes.

A leucocratic quartz-feldspar porphyry (Figure 7) occurs in the workings of the Ruth Mine where it locally forms a host of ore where crackle breccias are present. Outside the mine, the intrusion forms irregular dike- and sill-like masses that range from steeply dipping to nearly horizontal. Relic textures suggest hornblende was a phenocryst phase along with quartz and plagioclase feldspar.

Intrusions within the Elk Lake formation occur within the French Creek volcanic center as fine-grained dacitic and basaltic-andesite dikes and sills. A dacite dike that intrudes vent breccia and scoriaceous spatter deposits is extensively altered; however, the relic primary textures are those of a porphyry. Phenocrysts of feldspar, quartz, hornblende and minor biotite(?) are present. Hornblende ranges from 1 to 2 mm in length and is altered to chlorite.

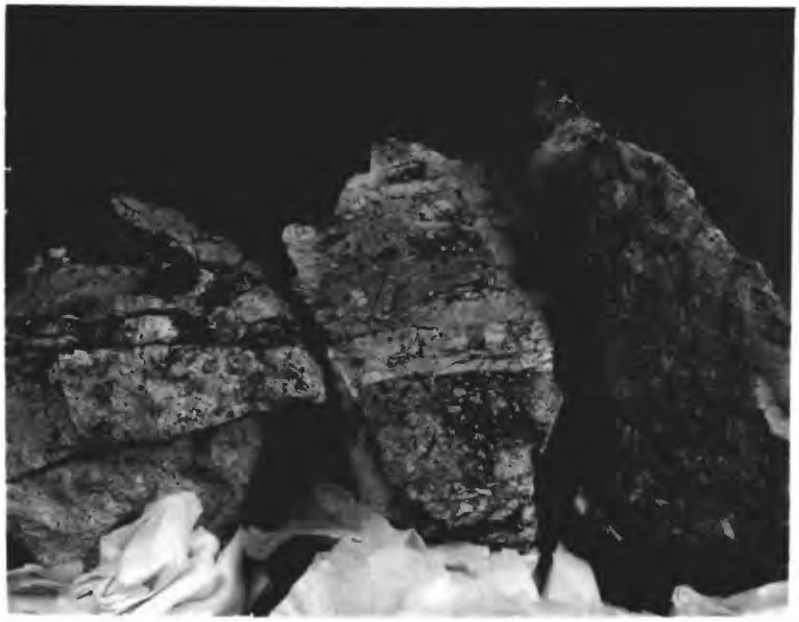

Fig. 6. Three examples of shingle breccias from surface exposures. The sample on the right is 6.4 by 15 cm.

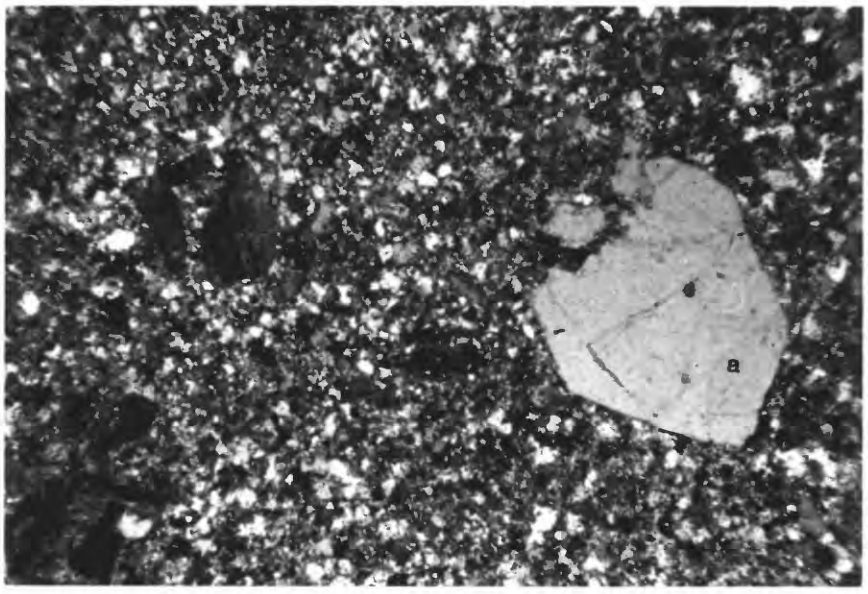

Fig. 7. Quartz (a) and plagioclase (b) phenocrysts in a moderately silicified and sericitized sample of the leucocratic quartz-feldspar porphyry intrusion. Quartz phenocrysts are commonly euhedral in this unit. Fine grained quartz within the groundmass is grown in optical continuity with the grain boundary of the phenocryst. Polars crossed. Field of view 4.5 mm.

The larger of the basaltic-andesite intrusions are up to 20 m wide. The dikes are porphyritic to glomeroporphyritic and have a groundmass of plagioclase microlites, fine-grained pyroxene, and anhedral opaque grains. Flow alignment of plagioclase microlites is locally evident. Plagioclase glomerocrysts are intergrown with clinopyroxene which is more abundant than orthopyroxene.

Basaltic-andesite dikes also occur within the rocks of the Sardine Formation. Four dikes, each 1 to 4 m wide, resemble the porphyritic diorite dikes but are much finer grained. One dike has a N. 40° W. strike and contains up to 5% partially resorbed quartz phenocrysts. A second has a N. 60° E. strike and dips 65° NW. It is located where N. 60° E. fractures are present as a prominent fracture orientation. Two other dikes occur in the adit of the Ruth Mine and are surrounded by strong alteration halos but no base-metal mineralization. These four dikes may be the same age as those that cut the Elk Lake formation.

STRUCTURE

Deposits of the Sardine Formation dip consistantly to the south to southeast. Measured dips range from 5° to 20° and the calculated dip is 11° south for the first occurrence of flows in unit B on the north and south sides of Battle Ax Creek. This dip is in agreement with measured dips of flattened pumice in a tuff of unit A. The dips within the Elk Lake formation vary as a function of relative position in the volcanic center on French Creek Ridge. Dips in the Elk Lake formation are viewed as primary depositional dips that are only slightly, if at all, modified by folding or tilting. The contact between the Sardine Formation and the Elk Lake formation is an angular unconformity as well as an erosional surface.

Faults and fractures are grouped into four trends. The most prominent set is oriented N. 40-60° W. This trend controls the orientation of equigranular and porphyritic diorite dikes, the overall trend of the porphyritic granodiorite intrusions, and the long dimensions and distribution of tourmaline-bearing breccias. Many stream valleys are controlled by faults and fractures along this trend.

A second set is oriented in a generally northerly direction but range from N. 15° E. to N. 20° W. Streams in at least part of their courses are controlled along this trend. A third set is oriented from N. 80° W. to N. 80° E. This trend controls the course of Battle Ax Creek and is prominent along the crest of the ridges above Stoney Creek. The fourth set is oriented N. 30-50° E. This fracture set is most prominent in the French Creek Ridge area.

Displacements across faults are difficult to determine due to the character of exposures, the similarities among lithologies, the intrusions which commonly occupy the faults, and hydrothermal alteration localized along faults and fractures. Slickensides on the N. 40-60° W. faults and east-west faults are all nearly horizontal. In the Ruth Mine, where east-west faults and N. 40-50° W. faults interesect, the east-west faults either offset or bend into alignment with the northwest faults with no apparent offset. The east-west set also displaces the northwest-trending set along the ridge above Stoney Creek. The generally north-south set cuts the northwest and east-west sets. The relative sequence of fault development is consistent with a summary prepared by *Priest et al.* [1983] for the northern and central Cascades. However, the east-west faults that are prominent in the North Santiam mining area are not included in this compilation.

ALTERATION AND MINERALIZATION

The character of the alteration within the rocks of the Sardine Formation is markedly different from that within the Elk Lake formation. We recognize two systems of alteration and mineralization. The oldest occurred within the volcanic center of the Sardine Formation and is believed by the authors to be related to development of copper-mineralized breccia pipes [*Winters*, 1985]. The second system developed in response to the French Creek Ridge volcanic center and overprints the older alteration system. It is related to lead-zinc mineralization at the Ruth Mine. Where the younger system overprints the alteration of the older system, within the rocks of the Sardine Formation, the history is difficult to unravel.

We have established the alteration and mineralization histories by using a combination of techniques including: Petrographic analysis, x-ray diffraction of secondary phases, autoradiography, microthermometric analysis, and mossbauer spectroscopy.

Alteration of the Sardine Formation:

The most prominent pervasive hydrothermal alteration is developed within rocks of the Sardine Formation. The alteration has destroyed all primary porosity and obscured primary mineralogy and rock textures. The mineral assemblages indicate differing water/rock ratios during hydrothermal alteration. Where water/rock ratios were low, the alteration approximates isochemical recrystallization under low-grade metamorphic conditions. Where water/rock ratios were high, the alteration results in total replacement of the primary lithology and changes in mass and bulk composition.

Primary minerals and textures are well-preserved within rocks altered under low water/rock ratios. Weakly altered intrusions and volcanic rocks display partially to completely pseudomorphed primary igneous minerals. Carbonate, epidote, and albite replace plagioclase; chlorite, calcite, and epidote replace primary mafic minerals. This alteration is propylitic alteration.

Within rocks altered under moderate to high water/rock ratios, primary igneous textures are strongly modified or destroyed and significant changes in bulk composition of the rocks are noted. Since these zones are also zones where silicification, tourmalinization, and development of secondary potassium phases has occurred, they are interpreted as zones of fluid up-flow within the hydrothermal system [*Fournier and Rowe*, 1966; *Giggenbach*, 1981].

Five types of alteration are attributed to moderate to high-water/rock ratios. Since there is a distinct difference in the style of alteration between the eastern and central portions of the district, and between these areas and the tourmalinized breccia pipes, the alteration types will be examined in relation to these differences. The alteration types include: Potassic, phyllic, tourmalinization, silicification, and argillic. Potassic, tourmalinization, silicification, and phyllic alteration types are developed in and around breccia pipes. Phyllic, silicification, and argillic are developed throughout the district in settings other than breccia pipes.

Alteration other than in breccia pipes:

In the eastern part of the mining district, the most intense alteration within the Sardine Formation is distributed relative to prominent northwest-trending faults and fractures.

The volcanic and intrusive rocks between these structures are propylitically altered and alteration approximates isochemical recrystallization.

Phyllic alteration: Phyllic alteration is best developed along northwest-trending faults and fractures and along the margins of intrusions that occupy these faults and fractures. Phyllic alteration is characterized by development of sericite, kaolinite, quartz, and pyrite, and destruction of primary rock textures. Zones of bleaching commonly extend outward from the most intensely altered rocks. The phyllic alteration assemblages overprint textures and minerals formed by earlier propylitic alteration. Phyllic alteration is developed around Pb-Zn-bearing quartz veins as in the Ruth Mine.

Phyllic alteration overprints the hornfels textures developed in volcanic rocks along the contacts of the porphyritic granodiorite intrusions in the central area. The alteration assemblage includes fine-grained sericite, clay minerals, and disseminated pyrite. Phyllic alteration in this setting is not associated with noticeable silicification.

Silicification: The base metal veins, such as the Ruth vein, are vuggy, open-textured quartz veins that occur at the center of an envelope of phyllic alteration. The quartz veins are commonly broken and may show recementation. Although the veins represent silicification, it is neither intense nor characterized by silica flooding. Deposition of quartz with calcite occurred late in the vein paragenesis and partially overlaps the deposition of sphalerite and galena.

Argillic: Argillic alteration overprints earlier phyllic alteration and silicification and often obscures earlier developed alteration patterns. Argillic alteration is characterized by replacement of primary minerals as well as alteration minerals by kaolinite. It is best developed along fault-zone breccias and intrusive margins. Well-developed argillic alteration occurs along the ridge crest above Stony Creek and in the eastern end of the district, such as at the Ruth vein.

Alteration associated with breccia pipes:

Potassic alteration: Potassic alteration is characterized by conversion of minerals to secondary sericite, K-feldspar, and biotite and is associated with silicification. It is restricted to areas around tourmaline-bearing breccia pipes and is not present above an elevation of about 850 m.

Phyllic alteration: Phyllic alteration occurs with silicification and tourmalinization in the margins of breccia pipes and within the breccias where sericite, quartz, and pyrite replace breccia clasts and matrix. The phyllic alteration halo extends approximately 5 to 10 m into less altered host rock and is accompanied by a significant decrease in fracture permeability away from the tourmalinized and silicified breccias.

Tourmalinization: Tourmalinization occurs in breccia pipes and the adjacent country rock. Tourmaline-bearing alteration does not occur above an elevation of 730 m.

Silicification: Silicification is the dominant alteration within the margins of tourmaline-bearing breccias and extends into wall rocks. Breccia fragments within the breccia structures are also strongly silicified as are the matrix and cements between clasts.

Tourmaline-bearing breccias: Drill cores of the tourmaline breccia pipes were recovered by Freeport Mining Co. and Amoco Minerals Division. The description of the margins and interiors of the pipes is based on over three thousand meters of drill core. The tourmaline-bearing breccias are elongate along northwest-trending structures, and are 120-200 m long and 25-70 m wide. *Olson* [1978] noted the geometry of the breccia bodies to be circular to elliptical and "pipe-like" in nature. The breccias are developed in granodiorite and porphyritic diorite intrusions and tuffs and flows of the Sardine Formation.

The margins of breccia structures are gradational with the host rock. Silicification and phyllic are the dominant types of alteration. Secondary chlorite and sericite develop after primary plagioclase and mafic phenocrysts, and the primary porphyritic texture of the host rocks is partially destroyed. Tourmaline occurs in microveinlets and as disseminated "starbursts" within the margin, and is partially engulfed in chlorite. Optical properties and color suggest that the tourmaline is of the schorl-dravite solid-solution series. Pyrite is locally abundant and occurs with sericite and tourmaline as disseminated grains and in microveinlets. Quartz-sericite veinlets, disseminated pyrite and chlorite-sericite veinlets overprint a propylitic alteration assemblage dominated by epidote and chlorite. Fracture density and silicification decrease outward through the breccia margin grading to a chlorite-dominated alteration assemblage beyond the quartz-sericite assemblage. This alteration is recognized in the field by the presence of chlorite 'clots' with minor pyrite in a silicified background. Primary textures are more distinct and mafic phenocrysts are pseudomorphed by chlorite and minor epidote; plagiocalse is partially replaced along fracture surfaces by clay minerals.

There are two types of tourmaline-bearing breccias: Granulation breccias that contain rock flour and shatter breccias that lack rock flour.

1) Within the granulation-breccia pipes, the rounded character of clasts and the rock flour matrix may have resulted from milling in the conduit during emplacement. Clasts are irregular in shape, subrounded to subangular, and vary from 5 cm to 5 mm in diameter. Within clasts, relic amphibole phenocrysts are pseudomorphed by epidote, chlorite, magnetite, and minor sphene. Plagioclase phenocrysts are partially to totally replaced by sericite, clay and albite. The groundmass of clasts is altered to fine-grained quartz, albite, sericite, chlorite, and clay. Tourmaline occurs as radiating crystals intergrown with quartz within clasts and in veinlets crosscutting the silicified rock-flour matrix.

The rock-flour matrix is silicified. Very fine-grained quartz occurs in lighter colored zones that merge with quartz-chlorite and chlorite-tourmaline zones within the matrix along clast boundaries. Albite may be interspersed with quartz; however, the fine-grained texture precludes optical identification. Pyrite occurs within the matrix as veinlets mantling and crosscutting clasts and as disseminated subhedral grains in the matrix and clasts.

The intensity of alteration increases with depth as indicated by obliteration of primary textures within the clasts; however, evidence for multistage brecciation and silicification is preserved. The silicified groundmass of the clasts is in sharp contact with the silicified rock-flour matrix of the breccia. Sericite-chlorite and sericite-pyrite-quartz veinlets crosscut the silicified rock-flour matrix but cannot be traced

through clasts. Tourmaline within clasts is surrounded by one or more of the following minerals: Chlorite, sericite, quartz, and carbonate. Precipitated potassium feldspar and quartz in veins cross cut altered breccia fragments composed of tourmaline-sericite-quartz-pyrite within a matrix of quartz-sericite-kaolinite.

Brecciation becomes less prominent with depth where it is supplanted by tourmaline-chlorite-sericite, tourmaline-chlorite, and quartz-feldspar veining. Minor chalcopyrite occurs in quartz-feldspar veins. Potassium feldspar increases in abundance both as a vein-filling mineral and as a component in the breccia matrix. Within the wall rock to the tourmaline-quartz-feldspar veins, subhedral to euhedral biotite grains replace chlorite.

2) Tourmaline-bearing shatter breccias are distinquished by extreme angularity of the clasts, clast-supported framework, and lack of rock flour. Where shatter breccias occur with granulation breccias, they contain fragments of granulation breccia; in other shatter breccias the clasts are volcanic rocks.

The porphyritic diorite and porphyritic andesite clasts are subangular to angular, range in size from 5 to 15 cm. Overall, alteration is similar to alteration in granulation breccias except clasts are cemented by one or more of the following minerals: Tourmaline, chlorite, quartz, potassium feldspar, and sericite.

Sericite and clay mineral pseudomorphs of feldspar phenocryts are associated with tourmaline, chlorite, and silicification of the clast groundmass. In extremely altered samples, primary textures have been obliterated and the rocks are an aggregate of chlorite, tourmaline starbursts, sericite, and quartz. Secondary gash fractures filled by subhedral to euhedral quartz and potassium feldspar transect clasts and silica-rich cement. Open space between large clasts of the breccia are filled with tourmaline, potassium feldspar, and quartz. Sulfide minerals comprise up to 50 percent of the volume of the cement. Throughout, sulfide minerals are associated with potassium feldspar veining and tourmaline-potassium feldspar breccia cement.

With increasing depth, tourmaline-quartz, tourmaline-chlorite, and tourmaline-chlorite-sericite veinlets become prominent. Magnetite occurs with tourmaline in breccia cement and as microveinlets in fault zones. Pyrite is disseminated in the wall rock and occurs with minor chalcopyrite as microveinlets and fracture coatings.

Winters [1985] described the alteration in the Cedar Creek breccia pipe. Two overlapping stages of hydrothermal mineralization occur, both dominated by a phyllic alteration assemblage. Tourmaline rosettes and minor disseminated chalcopyrite accompany the replacement of breccia fragments by fine-grained quartz, sericite, chlorite, and carbonates in the first stage. In the second stage, open-space quartz, sericite, chlorite, tourmaline, apatite, hematite, chalcopyrite, bornite, molybdenite, tetrahedrite, pyrite, galena, and sphalerite were deposited. The sulfides formed late in this stage.

Alteration in the Elk Lake formation:

Alteration within the Elk Lake formation is much less intense than that observed in the Sardine Formation. Significant distinctions are the weak cementation in the tuffs and well-preserved primary porosity. In basaltic-andesite

flows, orthopyroxene phenocrysts are pseudomorphed by uralite and chlorite. Plagioclase phenocrysts are slightly fractured and chlorite occurs along the fractures. Veinlets contain chlorite, calcite and the zeolite minerals, laumontite and stilbite. Vesicles within flows are commonly filled by laumontite followed by calcite and chloritic clay. Along French Creek Ridge, precipitated laumontite, stilbite, and calcite are common in veinlets, vesicles, and vugs. Calcite + chlorite veins and cement occur in tuffs of the Elk Lake formation on Whetstone Mountain.

FLUID COMPOSITION AND TEMPERATURE

Microthermometric analysis of fluid inclusions has been performed on samples from various settings in the district [*Winters*, 1985; *Pollock*, 1985; *Pollock and Cummings*, 1985; *Cummings et al.*, 1987; *Thompson*, 1989).

In the eastern portion of the district homogenization temperatures, T_h, range from 204 to 299 °C. The fluid inclusions are two-phase inclusions within quartz crystals collected from three veins within a phyllic alteration halo. Salinities are low and range from 1 to 6 equivalent weight percent NaCl. No daughter salts or other solid phases were found in the inclusions. In most samples, the T_h for the inclusions is generally within the range of 204 to 256 °C. The highest temperatures are from a base-metal-sulfide-bearing vein where T_h range from 282 to 299 °C. At the same site, a quartz crystal from the core of a vein has a T_h range from 227-236 °C.

Fluid inclusions in quartz crystals from quartz-tourmaline, quartz-sericite-tourmaline, and pyrite-quartz veins were analyzed from drill cores. Indications of boiling were not observed. A histogram of T_h for vein samples is shown in Figure 8. Homogenization temperatures for two-phase inclusions occur in two general ranges, a higher temperature range varies from 270 to 320 °C with a maxima between 285 and 310 °C, and a lower temperature range from approximately 180 to 250 °C. Inclusions with salinity greater than 5 equivalent weight percent NaCl are predominantly in the higher temperature range. The T_h of inclusions in the high temperature group with less than 5 equivalent weight percent NaCl is below 300 °C. The low temperature range contains lower salinity inclusions and salinity decreases to its lowest in inclusions with the lowest T_h.

Three-phase inclusions containing CO_2 were found in drill core samples and in fractured and rehealed quartz phenocrysts in granodiorite collected from the surface. The surface samples, collected from an elevation of 1,025 m near Stoney Creek, contain inclusions in two temperature ranges. The higher range is from 285 to 340 °C; the lower range is from approximately 210 to 260 °C. CO_2-bearing inclusions occur in both temperature ranges. The weight percent CO_2 in these inclusions ranges from 3 to 7 percent. A higher and wider range of salinities occurs in the high temperature grouping where salinities range from 3 to over 20 equivalent weight percent NaCl.

CO_2-bearing inclusions in tourmaline-bearing breccia and inclusions in a quartz-epidote-calcite vein that cuts the breccia were examined in sample NS-2-1589.6. CO_2 was not observed in inclusions from the quartz-calcite-epidote veins. The range in T_h is from 275 to 340 °C and the range in T_h for the CO_2-bearing inclusions in the tourmaline breccia overlaps that of the quartz-epidote-calcite vein. A lower temperature group of inclusions was not detected in this sample.

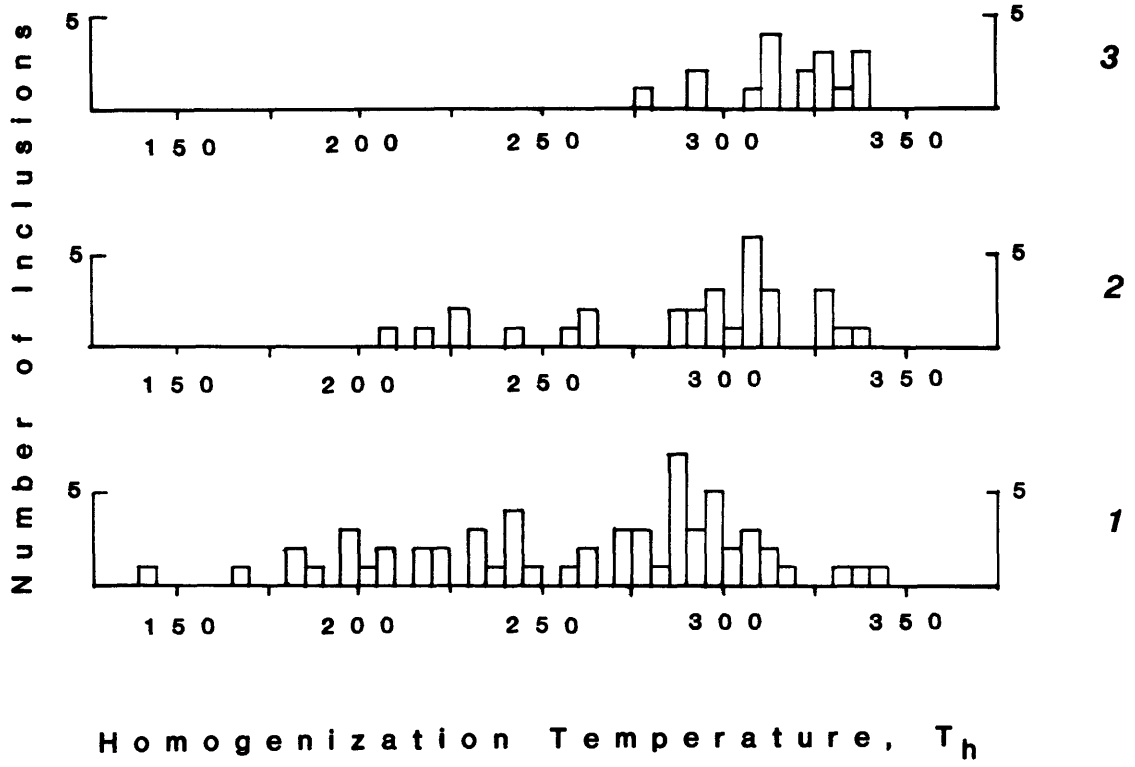

Fig. 8. Temperatures of homogenization for fluid inclusions from the Stoney Creek area of the North Santiam mining area. 1. Inclusions from tourmaline-bearing breccia pipes. This includes inclusions from granulation and shatter breccias. 2. Fluid inclusions containing CO_2, non-CO_2-bearing inclusions from the same sample from breccia pipes and from quartz phenocrysts in porphyritic granodiorite intrusions. 3. CO_2 and non-CO_2 inclusions from tourmaline breccia from sample NS-2-1589.6. Also includes inclusions from associated quartz-epidote-calcite vein cutting tourmaline breccia.

Calculated pressures of trapping for the higher temperature, higher salinity inclusions indicate pressures between 750 and 1100 bars with most between 800 and 900 bars. Such pressures suggest lithostatic pressure controlled the emplacement of the higher temperature part of the system.

In summary, two ranges of T_h are represented in the inclusion data. The higher temperature group ranges from 270 to 340 °C and includes the inclusions of highest salinities. CO_2-bearing inclusions generally populate the high-temperature end of this range and phyllically altered, tourmaline-bearing breccias the lower end of the range. A second group of inclusions forms a lower temperature range. This range is from 265 °C to as low as 141 °C. In general, these inclusions are lower salinity (<5%) and salinity is lowest in low T_h inclusions. The low temperature range from the breccia-pipes and granodiorite overlaps the range in T_h and salinities for samples from the eastern end of the district. A few inclusions that overlap the lower end of T_h in the high temperature group occur within sphalerite/galena mineralization from the eastern part of the district.

Winters [1985] examined the fluid inclusions in the copper-mineralized Cedar Creek breccia pipe. Overall, inclusions from

the Cedar Creek breccia pipe have significantly higher T_h and higher salinities than those from the Stony Creek breccias or veins from the eastern portion of the district. Four types of fluid inclusions are recognized. Type I inclusions consist of vapor and liquid. Those in apatite have T_h from 150 to 300 °C; in quartz 225 to 500 °C. Type II contain vapor, liquid, and halite and T_h is generally between 300 and 425 °C (range is 200 to > 625 °C). Type III inclusions contain vapor, liquid, halite, and sylvite and have T_h from approximately 325 to > 625 °C. Total salinities are from 45 to 80 equivalent weight percent NaCl + KCL. Type IV inclusions consist of vapor, liquid, NaCl, KCl, and one or more other solid phases. Melting, homogenization, and decrepitation phenomena are complex in these inclusions. Liquid-vapor homogenization temperatures are between 383 and 530 °C. CO_2-bearing inclusions were not reported by *Winters* [1985]. Calculated pressures of inclusion trapping for Type I and Type II inclusions range from 220 to 800 and 20 to 875 bars respectively.

Winters [1985] argued for three different hydrothermal episodes on the basis of fluid inclusion data. Type III and IV, the high temperature, high salinity inclusions, were generated first. Type II formed next followed by group I. Types III and IV are genetically related but a relation between types I and II or between these two types and types III and IV was ruled out. *Winters* [1985] was unable to clearly recognize the paragenesis of the different inclusions because of the multiple generations of inclusions in the system.

Two-phase fluid inclusions in quartz crystals from quartz-epidote veins cutting an equigranular diorite intrusion in the area near the Ruth Mine were analyzed in order to determine the homogenization temperature associated with this type of vein and presumably the temperature of propylitic alteration. The T_h range from 250 to 310 °C. These T_h values are somewhat lower than for similar veins in drill core sample NS-2-1589.6 from the Stoney Creek area.

DISCUSSION

The relations among the volcanic, structural, and hydrothermal alteration histories of the Western Cascade Province in Oregon and Washington have been interpreted from the small mining districts that occur along its length. These districts include: In Oregon, the Bohemia [*Lutton*, 1962; *Schaubs*, 1978; *Istas*, 1983; *Katsura*, 1988; *Schieber and Katsura*, 1986], Blackbutte [*Derkey*, 1981], Fall Creek [*Gray and Berri*, 1983], Blue River [*Storch*, 1978], Quartzville [*Gray*, 1977; *Munts*, 1978], North Santiam [*Olson*, 1978; *Pollock*, 1985; *Cummings et al.*, 1987; *Thompson*, 1989; *Mestrovich*, 1989], in Washington, the Wind River [*McGowan*, 1985], Washougal [*Moen*, 1977; *Shepard*, 1979; *Schriener*, 1979; *Schriener and Shepard*, 1981], St. Helens [*Armstrong et al.*, 1976; *Moen*, 1977; *Ashley and Evarts*, 1981], Middle Fork [*Patton et al.*, 1973], and North Fork [*Hollister and Baumann*, 1978]. Summary works have been presented by *Callaghan and Buddington* [1938], *Huntting* [1956], *Mason et al.* [1977], *Hollister* [1978], *Grant* [1969], and *Power* [1984].

The pattern of mineralization over the length of the range has been summarized as a south to north progression from epithermal (Au-Ag), through mesothermal (Zn-Pb-Cu-Ag), to hypothermal (Cu-Mo) environments [*Field and Power*, 1985; *Power*, 1984]. The North Santiam mining area is considered the first district within this north-south progression to exhibit well-developed mineralization and alteration patterns characteristic of the upper levels of a porphyry copper deposit.

Our understanding of the relations among structure, stratigraphy, hydrothermal alteration, and mineralization history in the North Santiam mining area, led us to reevaluate this model and propose a somewhat different picture of the mineralized districts of the Cascade Range. First we will enumerate those salient features of the North Santiam mining area that have led to this conclusion. That will be followed by a brief review of pertinent literature on other districts. Finally, we will suggest an alternative way of looking at the mineralization history of the Cascade Range.

The stratigraphic evolution of the North Santiam mining area has been determined in order to place the hydrothermal alteration and mineralization within the context of the developing volcanic pile. The volcanic section is dominated by flows, tuffs, and intrusions; sedimentary deposits are either sparse or, if present, poorly exposed. The lower sequence, the Sardine Formation, is dominated by andesite flows and tuffs that have been intruded by diorite, granodiorite, and leucocratic quartz-feldspar porphyry intrusions. Some tuff units are partially welded and the block and ash flow at the base of the exposed section indicates proximal source. The upper sequence, including the Elk Lake formation and Hugh Creek ignimbrite, contains rhyodacite and andesite tuffs and andesite flows. At least some of the tuffs were deposited by volcanic surge. Intrusions include irregularly shaped fine-grained andesite and dacite dikes.

The unconformity that marks the boundary between the two formations occurs between 1,100 and 1,350 m; the first elevation is in the French Creek Ridge area, the second from the Whetstone Mountain area. A geomorphic surface at the elevation of the unconformity is particularly well developed in the ridges above Stoney Creek and to the west of Opal Creek. The unconformity marks several changes in the volcanic stratigraphy.

1) The unconformity marks an angular discordance in the French Creek Ridge area between the Sardine Formation and the Elk Lake formation. This is in agreement with observations of *McBirney et al.* [1974] at Elk Lake where the informally named Elk Lake formation was originally defined.

2) The diorite and granodiorite intrusions within the Sardine Formation do not intrude the Elk Lake formation. The intrusions are exposed on the ridge above Stoney Creek where they are immediately overlain by andesite flows of the Elk Lake formation. Intrusions within the Elk Lake formation are aphanitic andesite and dacite. The leucocratic quartz-feldspar porphyry that intrudes the Sardine Formation in the Ruth Mine area is believed to be an intrusion within the Sardine Formation and not to be equivalent to the dacite dikes within the Elk Lake formation. This is based on the rare earth element geochemistry of the porphyry and the dacite dikes and rhyodacite tuffs of the Elk Lake formation. The porphyry uniquely has a distinct negative europium anomaly.

3) The primary porosity throughout the Sardine Formation has been destroyed by hydrothermal recrystallization; whereas the primary porosity in the Elk Lake formation is preserved in most settings. The tuffs within the Elk Lake formation are prone to mass movements reflecting their weakly lithified character. Mass movements do not occur where the Sardine Formation is the bedrock.

4) The alteration assemblages within the Sardine Formation are dominated by propylitic alteration and in the field is most easily recognized by a characteristic yellow green. The

alteration in the Elk Lake formation is dominated by clay minerals, zeolites, and carbonate with locally developed chlorite. The unconformity marks this change in alteration mineralogy and the associated color change.

The hydrothermal alteration in the Sardine and Elk Lake formations indicate that at least two hydrothermal systems of different ages operated within the district. The older system is closely associated with the intrusion of granodiorite stocks and dikes within a volcanic center from which part of the Sardine Formation was erupted. The younger system is believed to be related to the volcanic center developed in the French Creek Ridge area and to have altered rocks within the Sardine Formation and the younger Elk Lake formation. The distinction between these two systems is made on the basis of the following characteristics where the effects of both are present as they are within the Sardine Formation.

The granodiorite intrusions of the Sardine Formation are characterized by wide, well-developed hornfels aureoles, shingle breccias, more plug-like shapes at lower elevations and more dike-like shapes at higher elevations, and close spatial association with tourmaline-breccia pipes. A hydrothermal overprint of the hornfels zones along the margins of the intrusions is common. The hydrothermal alteration within this volcanic center displays characteristics of the upper portions of a porphyry copper system [*Olson*, 1978; *Power*, 1984; *Pollock et al.*, 1986; *Sillitoe*, 1973] and has those characteristics proposed by *Grant* [1982] for similar structures in the Western Cascade Province of Washington.

The tourmaline-bearing breccias were formed in two stages. The earlier stage formed the granulation breccias and the later stage the shatter breccias. Intense silicification, potassic alteration, and tourmalinization accompanied the formation of granulation breccias. The phyllic alteration within the breccia pipes may be of two generations; the most extensive is related to the processes of breccia pipe formation. However, homogenization temperatures of fluid inclusions suggest that there is also a younger phyllic alteration overprint in the breccia pipes.

The T_h of fluid inclusions in the breccia pipes indicate a complex paragenesis. The inclusions with the highest homogenization temperatures and highest salinities are the type III and IV inclusions in the Cedar Creek breccia pipe [*Winters*, 1985]. Other inclusions (Types I and II) display a wide range of homogenization temperatures and low salinities that *Winters* was unable to specifically relate to stages of development in the breccia pipe. *Winters* [1985] argued that temperatures of homogenization and salinities decreased as the alteration system evolved. A pattern consistent with the summary of findings presented by *Beane and Titley* [1981].

In the Stoney Creek area, inclusions with T_h between 270-320 ^{o}C are the CO_2-bearing and CO_2-free inclusions from tourmaline-bearing breccia pipes, secondary inclusions in quartz-phenocrysts in porphyrytic granodiorite, and quartz-epidote veins. Inclusions from the latter two sources populate the upper end of this temperature range and are of higher salinity. Inclusions from the tourmaline-bearing breccias populate the lower end of the temperature range.

The fluid inclusion homogenization temperatures, salinities, and the calculated pressures of inclusion trapping indicate magmatic fluids were involved in formation of the Cedar Creek breccia pipe. The evolution of fluid composition and changes from granulation to shatter breccias follow patterns of

successive stages of second boiling and decompression [*Burnham*, 1985]. These are not the conditions of formation indicated by the textures, fluid inclusion homogenization temperatures and salinities, and alteration patterns of the younger hydrothermal system.

The alteration effects of the younger hydrothermal system within the Sardine Formation are controlled by faults and fractures and the margins of dikes that have intruded along structures. The margins of the dikes and fractures and faults channeled solutions through the Sardine Formation where primary porosity had been destroyed by earlier hydrothermal recrystallization. In the area of the tourmalinized breccia pipes, the structures that earlier had controlled emplacement of intrusions and breccia pipes continued to act as pathways for fluid migration and development of overprinting phyllic alteration.

In the Stoney Creek area, T_h between 180 to 255 ^oC are a distinctly lower temperature range in secondary inclusions and primary inclusions in late-deposited quartz. The range in T_h is the same for samples from the mineralized veins in the eastern part of the district. These inclusions are low salinity and some contain CO_2. The drusy quartz crystals from which the inclusions were examined preceeded and were concurrent with deposition of sphalerite and galena and were followed by deposition of calcite.

Winters [1985] indicates that traces of sphalerite and galena associated with chalcopyrite, pyrite, and tetrahedrite occur in paragenetically late quartz-carbonate veins throughout the Cedar Creek breccia pipe and in quartz veins near the bottom of the pipe. He suggested that deposition of sphalerite and galena postdate the major episode of sulfide mineralization and partially overlaps with a carbonate vein filling stage. We would speculate that inclusions with T_h in the lower range of Type I inclusions are those formed during the late stage, a pattern that is consistent with patterns in the rest of the district.

Inclusions with T_h between 180 and 255 ^oC occur deep within some of the breccia pipes in the Stoney Creek area. Sample NS-1-1832.5 collected 558 m down hole (collar elevation 658 m) has inclusions with T_h in this range as well as in the range from 285 to 340 ^oC. A sample from a depth of 54 m (NS-1-177) in the same hole, also has inclusions that populate both T_h ranges. We interpret these data to indicate that the structure along which the breccia pipes and granodiorite intrusions were emplaced into the Sardine Formation was also a zone of fluid migration during the development of the younger alteration system related to the French Creek Ridge volcanic center in the Elk Lake formation. Other samples, such as NS-2-1589.6 collected 484 m down hole (collar elevation 610 m), only contain inclusions that have T_h in the higher temperature range. We intepret these data to indicate the area of drill hole NS-2 was not in a reactivated structure.

The age of the mineralizing systems, host intrusions, and volcanic rocks in the North Santiam mining area is open to debate. Radiometric age determinations for the North Santiam mining area are sparse and have been determined by K-Ar systematics. The age determinations for the Sardine Formation from the Sardine Mountain area, the type locality as defined by *Thayer* [1939], are 15.9 $\pm$ 0.2, 17.2 $\pm$ 0.2, and 16.4 $\pm$ 0.2 Ma for andesite flows and an andesite dike, respectively [*Sutter*, 1978].

The age of a porphyritic diorite intrusion from the ridge above Stoney Creek in the Sardine Formation was reported as 13.4 ± 0.9 m.y.B.P. [*Power et al.*, 1981a]. The age was determined on a hornblende separate from the intrusion. *Power et al.* [1981b] report a date of 11.0 ± 0.4 m.y. B.P. for sericitic alteration in a quartz diorite collected in the area of the Stony Creek tourmaline-bearing breccias. This age was argued to represent the time of porphyry mineralization in the district.

It is our opinion that the dates for the diorite intrusion and for the tourmaline-bearing breccias are minimum ages representing partial to total resetting of the ages by the younger alteration system. Homogenization temperatures of fluid inclusions indicate fluids with temperatures as high as 340 °C and 255 °C respectively accompanied alteration in these areas. As indicated earlier, we believe that the structure important in controlling the emplacement of the tourmaline-bearing breccia pipes also was a zone of fluid flow and phyllic alteration during the younger alteration system.

The volcanic rocks that we believe were associated with the younger system, the Elk Lake formation, have been dated by *White* [1980]. In the area of French Creek Ridge, the age determinations range from 11.8 to 11.0 m.y.B.P. Age determinations for the Hugh Creek ignimbrite, also located above the unconformity between the Sardine Formation and the upper volcanic sequence, yield ages of 12.0 ± 0.4 and 12.5 ± 0.4 m.y.B.P. [*Hammond et al.*, 1980]. The ages and distribution of units suggest a significant thickness of volcanic rocks erupted from various centers occurred above the unconformity prior to extensive removal by erosion. These volcanic centers were associated with introduction of intrusions and the necessary heat to drive hydrothermal systems. In the Sardine Formation, the fluid migration was largely restricted to pre-existing structures. Above the unconformity, the solutions could spread out in the porous tuffs and produce widespread carbonate, chlorite, clay, and zeolite alteration at lower water/rock ratios.

Erosional surfaces within the Cascade volcanic arc occur at different scales. Localized erosional surfaces are part of the balance between the rate of eruption and erosion within the arc. More widespread erosion surfaces that may be regional in extent reflect fundamental processes within the arc that are related to subduction rate, plate configurations, and the rate of magma generation. As an example, *Gresens* [1981] examined the erosional unconformity at the base of the Wenatchee Formation in central Washington. *Gresens* [1981] argued that this unconformity was equivalent to the Telluride surface in the San Juan Mountains, Colorado. The surface can be traced throughout the western United States and was produced by prolonged erosion during plate reorganization in the Pacific Ocean.

Hammond [1988] described an extensive paleosurface in the Western Cascades that extends from Washington through Oregon and into California. The elevation of the surface varies with locality. West of Three Sisters, Oregon, it is at approximately 1,250 m. The surface formed during a lull in arc activity between about 17 and 12 Ma.

Locally developed unconformities produced by non-deposition or erosion may develop during periods of low rates of volcanic production. *McBirney et al.* [1974] argued for an approximately 5 million-year periodicity of volcanic eruption in the Cascade volcanic arc. Erosional unconformities may be expected to occur between such cycles. However, *Verplanck and Duncan* [1987] argued that volcanism was continuous throughout the evolution of

the Western Cascades. But with some periods of higher magmatic activity occurring between 13-16 Ma, 22-26 Ma and 29-31 Ma.

Priest [this volume] indicates a well-defined unconformity occurs between rocks of 18-20 Ma age and rocks of 13-14 Ma age in the central Western Cascades. The unconformity represents a period of erosion or non-deposition. In the North Santiam mining area located near the northern edge of the area covered by *Priest* [this volume], the unconformity is a distinct erosional unconformity. Extensive calc-alkaline basaltic andesite and andesite in the age span of the unconformity occur south of 44° 00" (Figure 1) suggesting that the unconformity does not extend into areas to the south [*Woller and Black*, 1983]. These patterns and the relations between flows of the Columbia River Basalt and arc volcanics in the area of the Columbia River Gorge [*Beeson and Tolan*, this volume] indicate that unconformities may develop in those parts of the range where erosion or low rates of volcanic production dominate. At the same time volcanic activity may be ongoing elsewhere.

Our findings indicate a significant erosional and angular unconformity developed in the North Santiam mining area between approximately 16 Ma and 12 m.y.B.P. The unconformity developed after the eruption of the Sardine Formation and prior to eruption of the Hugh Creek ignimbrite and Elk Lake formations. The depth of erosion during this period can be estimated from the alteration mineral assemblages. The mineral assemblage of the propylitic assemblage is calcite-epidote-chlorite-albite. In areas of modern geothermal activity, sparse epidote occurs at temperatures from 200 to 250 °C but does not occur in abundance until 260 °C [*Kristmannsdottir*, 1979, 1982]. The depth at which a temperature of 260 °C is attained depends upon the geothermal gradient. At a regional gradient of 50 °C/km, epidote would occur pervasively at a depth of greater than 4 km. The regional gradient for the Cascade Range in southern Washington is 45 $\pm$ 5 °C/km [*Steele et al.*, 1982]. In Iceland, *Kristmannsdottir* [1982] indicates epidote occurring at a depth of 2200 m requiring gradients in the 90 °C/km range.

The thermal structure within a volcanic center is, in part, related to the depth and volume of cooling magma within intrusions. *Sibbett* [1988] formulated a model for hydrothermal systems associated with subvolcanic stocks emplaced at depths of 1 to 4 km beneath stratovolcanoes and shallow magma chambers emplaced at depths of 4 to 9 km. A geothermal system related to subvolcanic intrusions may develop 1 to 2 km beneath the base of a stratovolcano while larger and deeper systems may occur with shallow magma chambers. We believe the alteration patterns, tourmaline-breccia pipes associated with granodiorite intrusions in the Sardine Formation are consistent with a shallow magma chamber rather than subvolcanic intrusions.

In the Mount Hood area, geothermal gradients for two holes drilled at an elevation of 1630 m on the flanks of the mountain have geothermal gradients of 67 and 80 °C/km [*Steele et al.*, 1982]. In the Timberline Lodge holes, temperatures of 42 °C were obtained at a depth of 600 m. If these data are projected to depth, the 250 °C isotherm is at a depth of over 3.5 km below the collar elevation. At Mount Hood, there is no indication of a magma chamber above this depth [*Steele et al.*, 1982].

If the Sardine volcanic center were similar to Mount Hood, at least 3.5 km of erosion has occurred below the flanks of the volcano. If the geothermal gradient is taken as 90 °C/km, the depth of erosion is approximately 2 km. Although these estimates are not well constrained, they are similar to depths of erosion suggested by *Holdaway and Bussey* [1982] based on the greenschist facies alteration assemblages in the Old Maid Flat

drill hole (OMF-7a) drilled to the west of Mount Hood.

The unconformity not only marks significant depths of erosion in the North Santiam mining area but also a change in conditions of hydrothermal mineralization. The link between magmatic and hydrothermal processes is provided by the regional-scale structures along which magmas rise and along which hydrothermal solutions circulate. If regional-scale structures continue to be active through multiple episodes of volcanism, intrusion, and hydrothermal acitivty, a complex overprinting of hydrothermal alteration and ore mineral deposition may occur. Thus ore deposits produced in temporally and physically unrelated mineralizing systems may develop sequentially during multiple cycles of volcanism that are separated by erosion.

The geology of the numerous small mining districts in the Western Cascade province in Oregon and Washington suggests that multiple cycles of hydrothermal alteration and mineralization occurred as the cycles of volcanism and erosion occurred in the range. A common characteristic in several of the districts is the association of quartz diorite to granodiorite intrusions and tourmalinized breccia pipes (e.g., Bohemia, Quartzville, North Santiam, in Oregon; Washougal, Earl in the St Helens district, in Washington). In addition, many districts contain epithermal vein mineralization that is either spatially associated with and cutting tourmalinized breccia pipes (Bohemia, North Santiam, Quartzville, Oregon) or separated from the main area of the tourmalinized breccia pipes-granodiorite intrusions (Washougal, St. Helens, Washington). In still other mining areas, only epithermal mineralization has been identified (Wind River prospect, Washington; Blackbutte, Oregon). In several districts, erosional unconformities within the volcanic pile (Washougal, Washington; Quartzville, North Santiam, Bohemia, Oregon) and at least two different periods of mineralization (St. Helens, Washington, Quartzville, North Santiam, Bohemia, Oregon) have been identified.

Many of the studies in the mining areas have focused on aspects related to porphyry copper-type systems and less attention to the epithermal vein systems. In some settings where the epithermal veins are spatially associated with the tourmalinized breccia pipes, the relative timing has been interpreted differently. In Bohemia, *Schaubs* [1978] placed the epithermal veins prior to tourmalinization. However, *Katsura* [1988] on the basis of mapping at a scale of 1:3200 stated "detailed mapping in the vicinity of the Champion Mine shows that tourmalinization clearly post-dates contact alteration and pre-dates vein mineralization".

Incomplete stratigraphic records and the consequent difficulty in relating alteration systems to the volcanic sequence has obscured the temporal differences of overprinting mineralization and alteration patterns. *Munts* [1978] recognized that different conditions were required for the formation of epithermal vein systems and the tourmaline-bearing breccia pipes in the Quartzville district, but did not relate the differences to evolution of the volcanic pile. The different volcanic cylces and the unconformities that separate them may not always be readily identified because the younger volcanic products that were responsible for the overprinting hydrothermal systems have been eroded. At the Wind River prospect, Washington, gold mineralization occurs within rocks of the Ohanopecosh Formation of Oligocene-Early Miocene age. However, the alteration system and epithermal mineralization developed in a fault zone along which were intruded the feeder dikes for a younger volcanic sequence that has been largely removed by erosion [*McGowan*, 1985].

The North Santiam mining area is one district where volcanic stratigraphy and the development of erosional unconformities can be examined in relation to different ages of alteration and mineralization. The patterns are ultimately related to long-lived regionally-prominent structures that serve as zones of weakness for the rise of magma and the circulation of hydrothermal solutions during volcanic cycles of different ages.

CONCLUSIONS

The contact between the Sardine Formation and the Elk Lake formation in the North Santiam mining area is an erosional unconformity. This unconformity is a topographically mature surface developed to the level of shallow-level intrusions within the volcanic center. The depth of erosion was into the level of propylitic alteration represented by the assemblage epidote + chlorite + calcite + albite in the rocks altered under low water/rock ratios. The estimated depth of erosional stripping is at least 2 km and possibly 3.5 km. The erosion surface was buried by the eruption of the Hugh Creek ignimbrite and of the Elk Lake formation from the French Creek Ridge center.

The alteration and mineralization styles of the older alteration system in the Sardine Formation resemble those expected in the subvolcanic portion of a porphyry copper-type system [*Olson*, 1978; *Power*, 1984; *Pollock*, 1985; *Pollock and Cummings*, 1985; *Pollock et al.*, 1986; *Thompson*, 1989; *Mestrovich*, 1989].

The primary porosity of the Sardine Formation was destroyed by hydrothermal recrystallization. After destruction of the primary porosity, the zones of permeability were those developed along structures and along fractured margins of dikes and intrusions.

The younger hydrothermal system developed in response to a volcanic center on French Creek Ridge. Solutions were forced to flow within the zones of fracture permeability. Where these crossed older mineralization and alteration, an overprinting mineralization and alteration were formed.

Regionally prominent structures within volcanic arcs that remain active through successive volcanic cycles serve as zones of crustal weakness where successive generations of magmas rise and hydrothermal solutions circulate.

ACKNOWLEDGEMENTS

We would like to thank Shiny Rock Mining Corporation and George Atiyeh, President, for support of the projects upon which this paper is based. Access to land, mine workings, and drill core were graciously provided by Shiny Rock Mining Corporation.

REFERENCES CITED

Ahmad, M., M. Solomon, and J. L. Walshe, Mineralogical and geochemical studies of the Emperor gold telluride deposit, Fiji, *Econ. Geol., 82*, 345-370, 1987.

Armstrong, R. L., J. E. Harakol, and V. F. Hollister, Age determination of late Cenozoic porphyry copper deposits of the North American Cordillera, *Trans. Inst. Min. Metall. (London), B85*, 239-244, 1976.

Ashley, R. P., and R. C. Evarts, Geology and ore deposits of the St. Helens mining district, Washington, in *Proceedings of the symposium on mineral deposits of the Pacific Northwest*, edited by M. L. Silberman, C. W. Field, and A. L. Berry, pp. 167, U.S. Geol. Surv. Open File Rept., 81-355, 1981.

Beane, R. E., and S. R. Titley, Porphyry copper deposits Part II. Hydrothermal alteration and Mineralization, in *Seventy-Fifth Anniversary Volume Economic Geology*, edited by B. J. Skinner, p. 235-269, Econ. Geol. Publ. Co., 1981.

Beeson, M. H., and T. L. Tolan, The Columbia River Basalt Group in the Cascade Range: A middle Miocene reference datum for structural analysis, *U.S. Geol. Surv. Open File Rept.*, - this report, 1989.

Bonham, Jr., H. F., and D. L. Giles, Epithermal gold/silver deposits: The geothermal connection, *Geothermal Resource Council Spec. Rept., 13*, 257-262, 1983.

Brooks, H. C., and L. Ramp, Gold and silver in Oregon, *Oregon Dept. Geol. Min. Industr. Bull. 61*, 337 pp., 1968.

Burnham, C. W., Energy release in subvolcanic environments: Implications for breccia formation, *Econ. Geol., 80*, 1515-1522, 1985.

Callaghan, E. and A. F. Buddington, Metalliferous mineral deposits of the Cascade Range in Oregon: *U.S. Geol. Surv. Bull. 893*, 141 pp., 1938.

Church, S. E., A. P. LeHuray, A. R. Grant, M. H. Delevaux, and J. E. Gray, Lead-isotopic data from sulfide minerals from the Cascade Range, Oregon and Washington, *Geochim. Cosmochim. Acta, 50*, 317-328, 1986.

Cummings, M. L., M. K. Mestrovich, J. M. Pollock, and G. D. Thompson, Geothermal systems in the Cascade Range in Oregon: Insights from a fossil system, North Santiam mining area, Western Cascades, *Trans. Geothermal Resource Council, 11*, 235-241, 1987.

Derkey, R. E., Hydrothermal alteration and mineralization at the Blackbutte mercury mine, Lane County, Oregon, in *Proceedings of the symposium on mineral deposits of the Pacific Northwest*, edited by M. L. Silberman, C. W. Field, and A. L. Berry, pp. 167, U.S. Geol. Surv. Open-file Report 81-355, 1981.

Dyhrman, R. F., Geology of the Bagby Hot Springs area, Clackamas and Marion Counties, Oregon, M.S. thesis, 78 pp., Oregon St. Univ., Corvallis, Or., 1975.

Field, C. W., and S. G. Power, Metallization in the Western Cascades, Oregon and southern Washington, *Geol. Soc. of Am. Abstr. with Programs, 17(4)*, 218, 1985.

Fournier, R. O., Active hydrothermal systems as analogues of fossil systems, *Geothermal Resource Council Spec. Rept., 13*, 263-284, 1983.

Fournier, R. O., and J. J. Rowe, Estimation of underground temperature from the silica content of water from hot springs and wet-steam wells, *Am. J. Sci., 264*, 685-697, 1966.

Giggenbach, W. F., Geothermal mineral equilibria, *Geochim. Cosmochim. Acta, 45*, 393-410, 1981.

Grant, A. R., Chemical and physical controls for base metal deposition in the Cascade Range of Washington, *Wash. Dept. Nat. Resources Bull., 58*, 107 pp. 1969.

Grant, A. R., Summary of economic geology data for the Glacier Peak Wilderness, Chelan, Snohomish, and Skagit Counties, Washington, *U. S. Geol. Surv. Open File Rept., 82-0408*, 41 pp., 1982.

Gray, J. J., A geological field trip guide from Sweet Home, Oregon, to the Quartzville Mining District, *Oregon Dept. Geol. Min. Industr., The Ore. Bin, 39(6),* 93-108, 1977.
Gray, J. J. and D. A. Berri, Mineral potential of the Fall Creek mining district: a geological-geochemical survey, *Oregon Dept. Geol. Min. Industr. Open File Rept. O-83-5,* 32 pp., 1983.
Gresens, R. L., Extension of the Telluride erosion surface to Washington state, and its regional and tectonic significance, *Tectonophysics, 79,* 145-164, 1981.
Hammond, P. E., The Cascade paleosurface, Wa, Or and Ca, *Geol. Soc. Am. Abstr. Program, 20(7),* A284, 1988.
Hammond, P. E., J. L. Anderson, and K. J. Manning, Guide to the geology of the upper Clackamas and North Santiam Rivers area, northern Oregon Cascade Range, in *Geological Field Trips in Western Oregon and Southwestern Washington,* edited by K. F. Oles, J. G. Johnson, A. R. Niem, and W. A. Niem, pp. 133-167, Oregon Dept. Geol. Min. Industr. Bull. 101, 1980.
Hedenquist, J. W., and R. W. Henley, Hydrothermal eruptions in the Waiotapu Geothermal System, New Zealand: Their origin, associated breccias, and relation to precious metal mineralization, *Econ. Geol., 80,* 1640-1668, 1985.
Holdaway, M. J., and S. Bussey, Mineralogy of the Old Main Flat geothermal exploratory hole No. 7A, Mount Hood, Oregon, in *Geology and Geothermal Resources of the Mount Hood Area, Oregon,* edited by G. R. Priest and B. F. Vogt, pp. 57-76, Oregon Depart. Geol. Min. Industr. Spec. Pap. 14, 1982.
Hollister, V. F., *Geology of the porphyry copper deposits of the Western Hemisphere,* The American Institute of Mining, Metallurgical and Petroleum Engineers, Inc., New York, New York, 219 pp. 1978.
Hollister, V. F. and F. W. Baumann, The North Fork porphyry copper deposit of the Washington Cascades, *Mineralium Deposita, 13,* 191-199, 1978.
Huntting, M. T., Inventory of Washington Minerals Part II Metallic Minerals, *Wash. Div. Mines Geol. Bull., 37,* 428 pp., 1956.
Istas, L. S., Trace elements in veins of the Bohemia Mining District, Oregon: Ph.D. dissertation, pp., Univ. Wash., Seattle, Wash., 1983.
Katsura, K. T. The geology and epithermal vein mineralization at the Champion Mine, Bohemia Mining District, Oregon, M.S. thesis, 254 pp., Univ. Oregon., Eugene, Or., 1988.
Kristmannsdottir, H., Alteration of basaltic rocks by hydrothermal activity at 100-300 ^{o}C, in *International Clay Conference 1978,* edited by M. M. Mortland, and V. C. Farmer, pp. 359-367, Elsevier, New York, 1979.
Kristmannsdottir, H., Alteration in the IRDP drill hole compared with other drill holes in Iceland, *J. Geophys. Res., 87,* 6525-6531, 1982.
Lutton, R. J., Geology of the Bohemia Mining District, Lane County, Oregon, Ph.D. dissertation, 172 pp., Univ. Ariz., Tucson, AR., 1962.
Mason, R. S., J. J. Gray, and B. F. Vogt, Mineralization in the north-central western Cascades, *Oregon Dept. Geol. Min. Industr., The Ore. Bin, 39,* 185-205, 1977.
McBirney, A. R., J. F. Sutter, H. R. Naslund, K. G. Sutton, and C. M. White, Episodic volcanism in the central Oregon Cascade Range, *Geology, 2,* 585-589, 1974.
McGowan, K. I., Geochemistry of alteration and mineralization of the Wind River gold prospect, Skamania County, Washington, M.S. thesis, 136 pp., Portland St. Univ., Portland, Or., 1985.
Mestrovich, M. K., Breccia formation in the upper levels of a porphyry copper system, North Santiam mining area, Western Cascades of Oregon, M.S. thesis, in progress, Portland St. Univ., Portland, Or, 1989.
Moen, W. S., St. Helens and Washougal mining districts of the southern Cascades of Washington, *Wash. Dept. Nat. Res. Info. Circ., 60,* 71 pp., 1977.

Munts, S. R., Geology and mineral deposits of the Quartzville mining district, Linn County, Oregon, M.S. thesis, 213 pp., Univ. Oregon, Eugene, Or., 1978.
Olson, J. P., Geology and mineralization of the North Santiam Mining District, Marion County, Oregon, M.S. thesis, 135 pp. Oregon St. Univ., Corvallis, Or., 1978.
Oregon Department of Geology and Mineral Industries, Oregon Metal Mines Handbook, *Oregon Dept. Geol. Min. Industr. Bull., 14-D,* pp., 1951.
Patton, T. C., A. R. Grant, and E. S. Cheney, Hydrothermal alteration at the Middle Fork copper prospect, central Cascades, Washington, *Econ. Geol. 68,* 816- 830, 1973.
Peck, D. L., A. B. Griggs, H. G. Schlicker, F. G. Wells, and H. M. Dole, Geology of the central and northern parts of the Western Cascade Range in Oregon, *U.S. Geol. Surv. Prof. Pap., 449,* 56 pp., 1964.
Pollock, J. M., Geology and geochemistry of hydrothermal alteration, eastern portion of the North Santiam mining area, M.S. thesis, 100 pp., Portland St. Univ., Portland, Or., 1985.
Pollock, J. M., and M. L. Cummings, North Santiam mining area, Western Cascades--relations between alteration and volcanic stratigraphy: Discussion and field trip guide: Part I. Discussion, *Oregon Geol., 47,* 139-145, 1985.
Pollock, J. M., and M. L. Cummings, North Santiam mining area, Western Cascades--relations between alteration and volcanic stratigraphy: Discussion and field trip guide: Part II. Field Trip Guide, *Oregon Geol., 48,* 3-9, 1986.
Pollock, J. M., G. D. Thompson, M. L. Mestrovich, M. L. Cummings, and D. G. Howard, Geologic processes in the subvolcanic portion of a porphyry copper deposit, North Santiam mining area, Western Cascades, OR, *Geol. Soc. Am. Abstr. Programs, 18(6),* 720, 1986.
Power, S. G., The "tops" of porphyry copper deposits-mineralization and plutonism in the Western Cascades, Oregon, Ph.D. dissertation, 202 pp., Oregon St. Univ., Corvallis Or., 1984.
Power, S. G., C. W. Field, R. L. Armstrong, and J. E. Harakal, K-Ar ages of plutonism and mineralization, Western Cascades, Oregon and Southern Washington, *Isochron/West,* no. 31, 27-29, 1981a.
Power, S. G., C. W. Field, R. L. Armstrong, and J. E. Harakal, K-Ar ages of plutonism and mineralization, Western Cascades, Oregon and Southern Washington, Additional information, *Isochron/West,* no. 32, 3, 1981b.
Priest, G. R., Volcanic and tectonic evolution of the Cascade volcanic arc, 44° 00" to 44° 52' 30" N, *U.S. Geol. Surv. Open File Rept.*, this report, 1989.
Priest, G. R., N. M. Woller, G. L. Black, and S. H. Evans, Overview of the geology of the central Oregon Cascades Range, in *Geology and Geothermal Resources of the Central Oregon Cascade Range,* edited by G. R. Priest, and B. F. Vogt, p. 3-28, Oregon Dept. Geol. Min. Industr. Spec. Pap. 15, 1983.
Schaubs, M. P., Geology and mineral deposits of the Bohemia mining district, Lane County, Oregon, M.S. thesis, 135 pp., Oregon St. Univ., Corvallis, Or., 1978.
Schieber, J., and K. T. Katsura, Sedimentation in epithermal veins of the Bohemia mining district, Oregon, USA: Interpretations and significance, *Mineralium Deposita, 21,* 322-328, 1986.
Schriener, A., Jr., The geology and mineralization of the north part of the Washougal mining district, Skamania Co., Washington, M.S. thesis, 135 pp., Oregon St. Univ., Corvallis, Or., 1979.
Schriener, A. and Shepard, R. J., Geology and mineralization of the Washougal mining district, Skamania County, Washington, in *Proceedings of the symposium on mineral deposits of the Pacific Northwest,* edited by M. L. Silberman, C. W. Field, and A. L. Berry, pp. 169-175, U.S. Geol. Surv. Open File Rept. 81-355, 1981.

Shepard, R. J., Geology and mineralization of the southern Silver Star stock, Washougal mining district, Skamania County, Washington, M.S. thesis, 113 pp., Oregon St. Univ., Corvallis, Or., 1979.
Sibbett, B. S., Size, depth and related structures of intrusions under stratovolcanoes and associated geothermal systems, *Earth-Science Rev., 25,* 291-309, 1988.
Sillitoe, R. H., The tops and bottoms of porphyry copper deposits, *Econ. Geol., 68,* 799-815, 1973.
Sillitoe, R. H., Andean mineralization: A model for the metallogeny of convergent plate margins, in *Metallogeny and Plate Tectonics,* edited by D. F. Strong, pp. 59-100, Geol. Assoc. Canada Spec. Pap., 14, 1976.
Sillitoe, R. H., Ore-related breccias in volcanoplutonic arcs, *Econ. Geol., 80,* 1467-1514, 1985.
Steele, J. L., D. D. Blackwell, and J. H. Robison, Heat flow in the vicinity of the Mount Hood volcaono, Oregon, in *Geology and Geothermal Resources of the Mount Hood Area, Oregon,* edited by G. R. Priest and B. F. Vogt, pp. 31-42, Oregon Dept. Geol. Min. Industr. Spec. Pap. 14, 1982.
Storch, S. G. P., Geology of the Blue River mining district, Linn and Lane Counties, Oregon, M.S. thesis, 70 pp., Oregon St. Univ., Corvallis, Or., 1978.
Sutter, J. F., K/Ar ages of Cenozoic volcanic rocks from the Oregon Cascades west of 121° 31', *Isochron/West,* no. 21, 15-21, 1978.
Thayer, T. P., Structure of the North Santiam River section of the Cascade Mountains in Oregon: *J. Geol., 44,* 701-716, 1936.
Thayer, T. P., Geology of the Salem Hills and the North Santiam River Basin Oregon, *Oregon Dept. Geol. Min. Industr. Bull., 15,* 40 pp., 1939.
Thompson, G. D., Hydrothermal alteration and volcanic stratigraphy between Opal and Cedar Creeks, North Santiam mining area, Western Cascades Oregon, M.S. thesis, in progress, Portland St. Univ., Portland, Or., 1989.
Verplanck, E. P., and R. A. Duncan, Temporal variations in plate convergence and eruption rates in the Western Cascades, Oregon, *Tectonics, 6,* 197-209, 1987.
White, C. M., Geology and geochemistry of volcanic rocks in the Detroit area, Western Cascade Range, Oregon, Ph.D. dissertation, 178 pp., Univ. Oregon, Eugene, Or., 1980.
Winters, M. B., An investigation of fluid inclusions and geochemistry of ore formation in the Cedar Creek breccia pipe, North Santiam mining district, Oregon, M.S. thesis, 104 pp. West. Wash. Univ., Bellingham, Wa., 1985.
Woller, N. M., and G. L., Black, Geology of the Waldo Lae-Swift Creek area, Lane and Klamath Countie, Oregon, in *Geology and Geothermal Resources of the Central Oregon Cascade Range,* edited by G. R. Priest, and B. F. Vogt, pp. 57-68, Oregon Depart. Geol. Min. Indust. Spec. Pap. 15, 1983

Strontium and Oxygen Isotopes in Volcanic Rocks near Crater Lake, Oregon, and their Bearing on Arc Magmatism

Charles R. Bacon
Marvin A. Lanphere
James R. O'Neil*

U.S. Geological Survey
345 Middlefield Road
Menlo Park, California 94025

ABSTRACT

The isotopic composition of Sr has been measured in representative samples of volcanic rocks from the vicinity of Crater Lake caldera, Oregon. The O isotopic composition of plagioclase, and in some cases quartz or the whole rock, has been determined in many of these samples. Lavas of monogenetic vents are dominantly basaltic andesites, with subordinate andesite, low-K tholeiite, and shoshonitic basaltic andesite. Mount Mazama, the stratovolcano complex in which the caldera occurs, erupted all of these lava types except tholeiite. $^{87}Sr/^{86}Sr$ ranges for the entire data set are: tholeiite, 0.70346-0.70355; basaltic andesite, 0.70349-0.70372; andesite, 0.70324-0.70383; and shoshonitic basaltic andesite, 0.70374-0.70388. Dacites of Mount Mazama have a narrower range (0.70348-0.70373), and rhyodacites focus on 0.7037. Rhyodacite of the climactic eruption is an exception, having lower $^{87}Sr/^{86}Sr$ (0.70355) resulting from an admixed component derived from andesitic magma. Andesitic to mafic cumulate scoriae of the climactic eruption and enclaves in related rhyodacitic lava flows show nearly the range in $^{87}Sr/^{86}Sr$ of the entire data set. Primary $\delta^{18}O$ ranges from lows of +5.7 to +6.0 in tholeiites and basaltic andesites to +7.0 in a dacite. Much of the variability in $^{87}Sr/^{86}Sr$ and the tendency for fractionated rocks to have higher $\delta^{18}O$ may be attributed to interaction with relatively ^{18}O-rich, ^{87}Sr-poor deep crustal rocks, perhaps metamorphosed equivalents of igneous rocks of the Kalamath Mountains. Increased $^{87}Sr/^{86}Sr$ over likely depleted-mantle ratios, at least in primitive tholeiites, may result from addition of a slab-derived component introduced in variable quantity to the mantle wedge.

A particularly noteworthy result is documentation of low $\delta^{18}O$ in partially fused grantoid blocks ejected in the climactic eruption and believed to represent fragments of the magma chamber's walls. These samples have $\delta^{18}O_{pl}$ of +6.7 to +0.8. Three samples for which $\delta^{18}O_{qz}$ was also measured have Δ_{qz-pl} of -0.2 to +0.7, which is correlated with $\delta^{18}O_{qz}$, indicating high-temperature equilibration of O isotopes. The O isotopic composition of plagioclase, and possibly quartz, was lowered by exchange with hydrothermal fluids before reequilibration at high temperature. $\delta^{18}O_{pl} \leq +6.5$ in scoria and pumice of the climactic eruption, and in preclimactic rhyodacites, is consistent with assimilation of low-^{18}O material. The granitoids offer a new kind of evidence for a shallow assimilation origin for low ^{18}O of some silicic magmas.

*Present address: Department of Geological Sciences, Univeristy of Michigan, Ann Arbor, Michigan 48109-1063

INTRODUCTION

Crater Lake caldera is situated within a stratovolcano cluster known as Mount Mazama at approximately latitude 43°N in the southern Oregon Cascade Range (Figure 1). The caldera collapsed ~6840 yr. B.P. during a catastrophic eruption of some 50 km^3 of mostly rhyodacitic magma but also crystal cumulates and partially melted wall rocks. Mazama is the only Quaternary volcano in the Cascades known to have possessed a large shallow silicic magma chamber, as evidenced by a voluminous pyroclastic eruption and associated caldera collapse. Mount Mazama itself is composed of basaltic andesite, andesite, and dacite lava flows and pyroclastic rocks erupted over at least 400 thousand years (ka). Beyond Mazama's limits and on its flanks are basaltic andesite and minor basalt erupted from monogenetic vents and shield volcanoes. With a few notable exceptions, all of these rocks bear the geochemical signature of arc magmatism. Unlike many arcs, the southern Cascades have experienced enough extensional tectonism that primitive magmas have been erupted. Crater Lake is thus particularly interesting in a geochemical and petrologic sense because of the range of magmas whose compositions reflect processes that operated at mantle to upper crustal depths. In this paper we use O and Sr isotopic data in conjunction with geologic and other geochemical information to help define some of these processes.

Problems on which our data bear are: (1) sources of primitive arc magmas; (2) presence of a subduction component in basalts and more evolved magmas; (3) incremental growth of large silicic magma bodies from a variety of parent magmas; (4) cyclic cooling, hydrothermal alteration, and heating of crustal magmatic systems; and (5) nature of the crust beneath the southern Oregon Cascades. The power of isotopic data to uniquely solve these problems is limited by the range of materials available for sampling. Within these constraints that are beyond our ability to change we have attempted to determine the isotopic compositions of all significant materials obtained in a program of detailed geologic mapping and sampling of approximately the area of Crater Lake National Park. Our strategy in studying the Mazama system has benefited from experience gained during this field work and from analysis of other types of data [Bacon, 1983, 1986, 1989; Bacon and Druitt, 1988; Druitt and Bacon, 1986, 1988, 1989]. Temporal control on the volcanic record is critical to interpretation of the geochemical data; ages used in this paper are based on the K-Ar data of M. A. Lanphere [unpublished data, 1988] and the paleomagnetic determinations of D. E. Champion [unpublished data, 1988]. This paper represents an effort to integrate the isotopic data with results of these other studies.

GEOLOGIC BACKGROUND

The following brief summary is taken from Bacon [1983, 1987a] and Bacon and Druitt [1988]. The dominantly andesite and dacite volcano, Mount Mazama, was constructed on a base of Pleistocene basaltic andesite on the W and an extensive rhyodacitic lava field on the E. The oldest dated Mazama lavas are ~400 ka andesites and low-silica dacites that occur to the S, SE, and E of the caldera. The bulk of Mazama consists of andesitic and low-silica dacitic lava; basaltic andesitic and dacitic lavas are locally important. The youngest andesites, which occupy the N caldera rim, may be as young as 40 ka; some dacite may be slightly younger.

The first rhyodacite attributed to the Mazama system formed the flows and related domes and pyroclastic deposits of Grouse Hill, Steel Bay, and Redcloud Cliff between 30 and 25 ka. The rhyodacitic eruption of an extensive pumice fall and the lava flow of Llao Rock is dated at 7015 ± 45 yr. B.P. [Bacon,

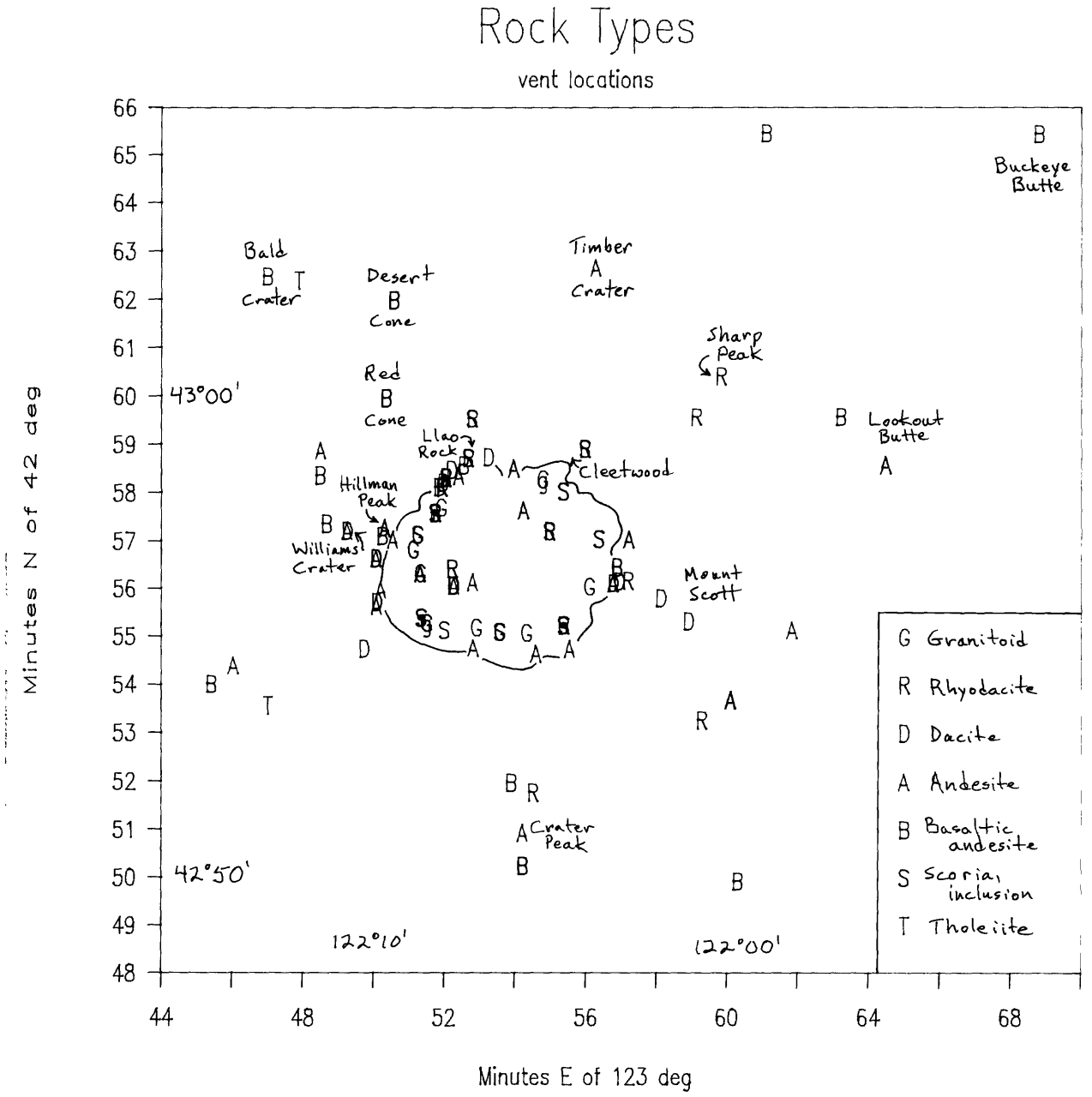

Fig. 1. Map showing analyzed samples plotted by rock type at vent localities. Vents for tholeiites uncertain; may be E of T's. Vents for ring-vent-phase of climactic eruption plotted at base of caldera wall. Crater Lake shoreline shown for reference.

1983]; related dikes are exposed in the caldera wall. All of these rhyodacites are more differentiated than that of the climactic eruption, dated at 6845 ± 50 yr. B.P. [Bacon, 1983]. Rhyodacite of the Cleetwood flow is identical to that of the climactic eruption and was still hot when the climactic event started. Rhyodacite domes of Sharp Peak also are compositionally identical to climactic rhyodacite, but their precise age is uncertain.

The climactic eruption took place in two phases within and between which there is no evidence for any significant pause: (1) a single-vent phase producing a Plinian column that deposited widespread airfall tehpra, followed by valley-hugging welded ignimbrite known as the Wineglass Welded Tuff [Williams, 1942] when the column collapsed to a lower height; and (2) a ring-vent phase of highly-mobile pyroclastic flows generated from relatively high columns as the caldera collapsed. Products of the single-vent phase and much of the ring-vent phase consisted of uniform rhyodacite and very minor silicic andesite. Later ring-vent phase products were dominantly crystal-rich andesitic and basaltic andesitic scoria, followed by mafic cumulate blocks, some of which contain olivine. Partially fused granitoid blocks also were ejected, particularly near the close of the eruption. The climactic ejecta apparently represent the contents of a horizontally stratified magma reservoir erupted in a geologic instant.

Postcaldera volcanism has been confined to the caldera. Andesite was erupted from several vents in the first few hundred years following the climactic eruption. A small rhyodacite dome was extruded at ~4000 B.P. on the E flank of the andesite pile of Wizard Island.

Around Mount Mazama and on its flanks are monogenetic vents and shield volcanoes that have erupted basaltic andesite and lesser volumes of andesite and tholeiitic basalt [Bacon, 1989]. These lavas are thought to include representative parental magmas for Mount Mazama itself. Monogenetic vents commonly form N-S alignments or are associated with normal faults of like trend. These observations are consistent with a mildly extensional tectonic regime, which is manifested S and E of Mazama by the Klamath graben and related Basin and Range structures.

The age and constitution of the crust under the Mazama area are uncertain [Bacon, 1989]. Although S of the projected N limit of Klamath basement [Riddihough et al., 1986], outcrops of pre-Cenozoic rocks are lacking. A reversed N-S seismic refraction profile from Mount Hood to ~30 km WSW of Crater Lake indicates a crustal thickness of 46 km [Leaver et al., 1984] and rather high P velocities. A dominantly mafic crustal composition is implied, perhaps with some metasedimentary rocks also present. Whether this material extends E under Mount Mazama is unknown. If not, the crust could be thinner, lack pre-Cenozoic rocks, and include gabbro underplated during extension.

ANALYTICAL METHODS

Strontium

Samples of rock powder weighing ~100 mg were dissolved in HF and $HClO_4$, and Sr was separated using ion-exchange chromatography. Mass analysis was done on an automated 23-cm-radius, stygmatic-focusing, 90°-sector, double-collector spectrometer utilizing a double filament source. Tabulated $^{87}Sr/^{86}Sr$ ratios (Table 1) are means of 24 ratios collected in a mass spectrometer run; reported errors are standard deviations (1σ) of analytical precision calculated from within-run statistics. Measured $^{86}Sr/^{88}Sr$ ratios were normalized to a value of 0.1194 to correct for mass fractionation. Over a period of several years, measurements of NBS 987 $SrCO_3$ standard have yielded a mean $^{87}Sr/^{86}Sr$ ratio and standard deviation of 0.71023 ± 0.00002.

Oxygen

Plagioclase was analyzed ($\delta^{18}O_{pl}$) where separation was practical. A small number of granitoid samples yielded quartz separates ($\delta^{18}O_{qz}$). Rock powders were analyzed ($\delta^{18}O_{wr}$) when mineral separations were not available, and for comparison with $\delta^{18}O_{pl}$ in a few cases. Extractions

were performed using ClF_3 [Borthwick and Harmon, 1982]. Reported $\delta^{18}O$ (Table 1) are calibrated to a $\delta^{18}O_{qz}$ value of +9.6 for NBS-28 quartz relative to SMOW. Each determination is the mean of two analyses, unless otherwise noted. Precision is estimated to be ± 0.1 (1σ).

VARIATIONS IN ISOTOPIC COMPOSITION

Ranges in Sr and O isotopic compositions for the Crater Lake data set are similar to those for N Pacific intraoceanic island arcs [Stern, 1982] such as the Marianas and Volcano Islands [Ito and Stern, 1985/86]. Variation of isotopic composition can be correlated with composition, time, and vent location.

Variation with Rock Type

Volcanic rocks of the Crater Lake area are classified according to SiO_2 content (recalculated to 100% volatile-free as in Bacon and Druitt [1988]) following LeBas et al. [1986]: basalts have < 52% SiO_2, basaltic andesites 52 to 57%, andesites 57 to 63%, dacites 63 to 68%, and rhyodacites >68%. Sr isotopic data are sufficiently precise and numerous for some correlations with major element compositon to be evident (Figure 2). Only one sample has $^{87}Sr/^{86}Sr$ significantly >0.7038. The greatest range in $^{87}Sr/^{86}Sr$ occurs among andesites (0.70324-0.70383). Most basaltic andesites have $^{87}Sr/^{86}Sr$ between 0.70362 and 0.70374, although Bald Crater and Desert Cone samples have ratios of ~0.7035. The only basalt sample analyzed that has $^{87}Sr/^{86}Sr$ >0.7035 is the basalt of Williams Crater (0.70372, a typical basaltic andesite value) which is, in fact, basaltic andesite contaminated with gabbroic xenoliths [Bacon, 1989]. Tholeiitic basalts have low $\delta^{18}O_{wr}$ (+5.7 to +6.0) and relatively low $^{87}Sr/^{86}Sr$ (0.70346-0.70355), but are more radiogenic than the least radiogenic calc-alkaline rocks. The range in $^{87}Sr/^{86}Sr$ decreases in dacites and rhyodacites in comparison with andesites. Rhyodacites other than those of the Cleetwood flow and climactic eruption have comparatively high $^{87}Sr/^{86}Sr$: 0.70362-0.70378. Scoria of the climactic eruption does not show systematic variation in isotopic composition with major element composition. Scoria $^{87}Sr/^{86}Sr$ fall into different groups that correspond to those defined on the basis of trace element abundances by Bacon and Druitt (1988): samples with low Sr concentrations have more radiogenic $^{87}Sr/^{86}Sr$.

With the exception of shoshonitic samples (435, 753), basaltic andesites have $\delta^{18}O_{wr} \leq +6.5$ and ranging down to +5.8 in magnesian andesite of Red Cone, i.e. similar to tholeiite values; basaltic andesite $\delta^{18}O_{pl}$ is higher by 0.3 to 0.7 per mil in the three samples for which both wholerock and plagioclase were analyzed. Andesites and dacites have similar spread in $\delta^{18}O$ to basaltic andesites, but mean values are higher by ~0.4 per mil. Rhyodacite $\delta^{18}O_{pl}$ are similar to the higher basaltic andesite and lower andesite and dacite values.

Partially melted granitoids have $^{87}Sr/^{86}Sr$ comparable to dacites, to which most are chemically similar. They are isotopically distinct from other samples, however, in their generally low $\delta^{18}O$: all but one (+6.7) are in the range +0.6 to +4.9. Both quartz and plagioclase have been analyzed in three samples; results for both phases agree within analytical precision for two of the three. As will be discussed in detail below, low $\delta^{18}O$ and Δ_{qz-pl} ~0 are due to exchange with hydrothermal fluids prior to reequilibration at high temperature.

TABLE 1. Isotopic and other data for Crater Lake samples

No	Description	Age K-Ar ka	sigma	SiO2 wt%	Rb ppm	Sr ppm	87/86	87/86 sigma	18/16	Material
	Tholeiites									
1143	East of Bald Crater			48.6	3	365	0.70355	3	5.8	WR
894	Rogue River at Bybee Creek			47.8	1	300	0.70346	3	6.0	WR
621	Castle Creek at Little Castle Creek			47.6	1	316	0.70350	1	5.7	WR
	Basaltic andesites									
754	North of hwy 230 13 km west of hwy 97 (M)			53.6	15	555	0.70372	4		
753	Buckeye Butte (M)			54.2	45	1812	0.70374	3	7.8	WR
730	Cinder cone north of Lookout Butte (M)	605	51	53.2	8	508	0.70370	4		
1222	Maklaks Crater (M)	220	67	53.6	9	539	0.70367	6		
825	Caldera wall at Cloudcap Bay	219	14	56.4	17	584	0.70368	4	6.5	WR
825	Caldera wall at Cloudcap Bay								6.8	P
854	Desert Cone (M)	213	26	53.9	11	551	0.70349	3	6.1	WR
854	Desert Cone (M)								6.5	P
1294	Cinder cone north of Crater Peak (M)	207	53	53.4	22	1276	0.70370	6		
1141	Bald Crater bomb (M)	192	20	53.9	14	1142	0.70350	4		
506	Caldera wall at Llao Point, lake level	186	20		25	579	0.70370	4		
1216	Vent south of Crater Peak (M)	118	48	53.7	22	1160	0.70370	4	5.9	WR
1216	Vent south of Crater Peak (M)								6.6	P
845	Caldera wall at Steel Bay (M)	70		52.9	12	589	0.70362	6		
543	Williams Crater "basalt" flow (M)	30		51.5	12	1031	0.70372	4		
353	Red Cone (M)	36			17	1399	0.70369	2		
354	Red Cone bomb (M)	36		53.7	27	1310	0.70372	4	5.8	WR
355	Red Cone (M)	36	12	54.0	25	951	0.70366	3	6.0	WR
435	Hillman Peak hornblende andesite	73	12	56.0	46	2042	0.70388	2	6.8	P*
1241	Cinder cone 2.6 km north-northwest of Williams Crater (M)	30		52.6	13	869	0.70365	4		
814	Cone north of junction of Castle and Little Castle Cks (M)			52.8	21	998	0.70372	16		
	Andesites									
816	Cone north of Little Castle Creek (M)	587	18	58.7	17	606	0.70360	2		
510	Caldera wall near Phantom Ship, lake level	395	16	62.1	27	694	0.70328	2	5.6	P*
L15	Andesite 5 km east of Mount Scott	356	10		46	341	0.70366	3		
218	Caldera wall at Kerr Notch, lake level	346	20	62.6	32	665	0.70331	3		
264	Caldera wall at Cloudcap Bay, inclusion	340		55.5	20	681				
266	Caldera wall at Cloudcap Bay, lake level	340	6	59.2	25	582	0.70371	1		
761	Cinder cone 3.5 km south-southeast of Mount Scott (M)	306	7	62.1	36	589	0.70340	5		
306	Caldera wall south of The Watchman, lake level	276	8	61.4	18	934	0.70327	2		
472	Garfield Peak hornblende andesite	224	9		21	848	0.70339	2	6.6	P
703	Cone southeast of Lookout Butte (M)	155		59.0	26	752	0.70344	10		
705	Cone southeast of Lookout Butte (M)	155	12		23	880	0.70324	3	6.5	P
185	Caldera wall east of Llao Rock, lake level	109	19	58.3	24	557	0.70360	3	6.6	P
533	Crater Peak (M)	95		56.9	28	1024	0.70363	7	6.3	P
1196	Flow 2 km southwest of Red Cone Spring	81	7	60.9	26	712	0.70356	12		
273	Caldera wall below Hillman Peak, pyroxene andesite	75		58.2	27	814	0.70353	4		
274	Caldera wall below Hillman Peak, pyroxene andesite	75		57.4	23	816	0.70366	5	6.6	P

TABLE 1. (continued)

No	Description	Age ka	K-Ar sigma	SiO2 wt%	Rb ppm	Sr ppm	87/86	87/86 sigma	18/16	Material
	Andesites (continued)									
L6	Caldera wall at Grotto Cove, highest flow	68	13		34	543	0.70348	2		
787	Northeast of Grotto Cove	68		61.6	37	565	0.70354	4		
788	Northeast of Grotto Cove, inclusion	68		57.9	27	606	0.70346	2		
433	Hillman Peak	67	12	58.9	34	1214	0.70383	3	6.8	P
312	Caldera wall below Discovery Point	52	4	62.9	43	546	0.70352	4		
379	Inclusion in The Watchman dacite flow	50		61.2	38	637	0.70349	4		
152	East of Pumice Point, highest flow	47	20	59.5	24	594	0.70378	5	6.7	WR
152	East of Pumice Point, highest flow								6.2	P
552	Inclusion in dacite of Munson Valley	36		59.9	28	594	0.70374	4		
539	Flow west of Williams Crater (M)	30		60.5	38	676	0.70371	4		
694	Intracanyon flow, Scott Creek (M)	28		58.8	26	554	0.70362	6		
L18	Intracanyon flow, Scott Creek (M)	28	30		19	555	0.70359	3		
853	Timber Crater (M)	19		58.7	22	761	0.70341	5	6.9	WR
1171	Central Platform, dredge sample	6-7		60.2	30	666	0.70347	3	6.4	P
939	Merriam Cone, dredge sample	6-7		60.4	28	661	0.70370	11		
1172	Merriam Cone, dredge sample	6-7		60.3	27	675	0.70357	4	6.1	P
515	Wizard Island, coarse block flow	6-7		60.0	23	678	0.70354	4		
513	Wizard Island, crater dome	6-7		58.2	16	697	0.70360	2		
669	Wizard Island, north flow	6-7		58.4	19	697	0.70360	3	6.4	P
	Dacites									
L8	Southwest slope of Mount Scott	422	10		45	399	0.70362	5		
262	Caldera wall at Cloudcap Bay, 3rd flow above lake	340		65.3	38	484	0.70365	5		
949	North of Castle Creek	205		65.9	43	387	0.70358	16		
497	Caldera wall at Llao Bay	115	9	64.6	33	524	0.70348	2		
806	Caldera wall at Steel Bay	72	7	65.8	47	470	0.70358	2		
L7	Scott Bluffs	71			62	352	0.70360	3		
166	Caldera wall at Steel Bay, airfall pumice	71		65.8	54	439	0.70359	4		
198	Pumice Castle, airfall pumice	71		66.5	51	406	0.70363	4	6.7	P
310	Caldera wall below Discovery Point, pumice in ignimbrite	50		67.9	55	400	0.70367	8	-2.6	P
378	The Watchman	50		67.4	57	403	0.70360	2		
381	The Watchman	50	6		59	343	0.70356	3	7.0	P
528	Munson Valley	36			37	480	0.70373	4		
529	Munson Valley	36		63.9	36	455	0.70366	4		
530	Munson Valley	36		63.5	36	482	0.70372	4		
550	Munson Valley	36		64.9	44	462	0.70367	3		
553	Munson Valley, pumice	36		67.5	55	399	0.70369	4	6.5	P
538	Flow west of Williams Crater	30		67.1	52	447	0.70369	4		
	Rhyodacites									
768	Hill 4 km south of Mount Scott	724	11	72.9	61	236	0.70368	3		
10	West of Sun Creek	468	9		58	216	0.70362	5		
227	Grouse Hill flow	30		71.2	68	272	0.70372	4		
803	Steel Bay dome	29		71.6	69	286	0.70373	2	6.3	P
161	Redcloud Cliff flow	25		71.1	65	289	0.70369	3		

TABLE 1. (continued)

No	Description	Age ka	K-Ar sigma	SiO2 wt%	Rb ppm	Sr ppm	87/86	87/86 sigma	18/16	Material
	Rhyodacites (continued)									
724	Dome nearest caldera, Sharp Peak group	10		70.6	53	393	0.70369	8		
728	Dome north of Sharp Peak	10		70.5	52	385	0.70378	6	6.5	P
503	Western of two dikes below Llao Rock	7		72.2	54	250				
504	Western of two dikes below Llao Rock	7			56	220	0.70368	3	6.2	P
158	Caldera wall at Llao Rock, basal pumice of Llao pumice fall	7		72.0	60	271	0.70366	3		
153	Llao Rock flow	7		70.8	54	320	0.70367	3	6.3	P
160	Cleetwood flow	7		70.3	53	389	0.70353	3	6.4	P
154	Caldera wall at Llao Rock, base of climactic pumice fall	7		70.7	53	384	0.70354	3	6.5	P
7	Wineglass, Wineglass Welded Tuff vitrophyre	7		70.6	51	381	0.70358	3		
556	Pinnacles, pumice of ring-vent-phase ignimbrite	7		70.8	50	399			6.0	P
631	Rogue River, pumice of ring-vent-phase ignimbrite	7		70.4	50	404	0.70362	8	6.5	P
631G	Rogue River, glass separate of sample 631	7		72.6	56	317	0.70356	4		
673	Postcaldera dome, dredge sample	4		71.7	82	297	0.70372	3	6.5	P
	Scoriae, inclusions in rhyodacites									
226	Inclusion in Grouse Hill dome	25		59.3	31	592	0.70382	4		
811	Inclusion in Steel Bay dome	25		61.1	32	579	0.70370	5	6.8	WR
209	Inclusion in Llao Rock flow	7		59.3	42	1502	0.70358	3		
775	Inclusion in Cleetwood flow	7		61.3	35	1015	0.70339	7	6.4	WR
106	Pumice Point, high-Sr scoria, climactic pumice fall	7		58.8	27	1141	0.70333	4		
572	Pinnacles, high-Sr scoria, ring-vent-phase ignimbrite	7		61.9	35	1061	0.70337	3		
572G	Pinnacles, glass separate from sample 572	7		70.8	50	604	0.70343	4		
574	Pinnacles, high-Sr scoria, ring-vent-phase ignimbrite	7		60.9	38	1064			6.2	P
591	Castle Creek, high-Sr scoria, ring-vent-phase ignimbrite	7		57.8	38	1239	0.70375	3		
591G	Castle Creek, glass separate from sample 591	7		69.8	51	635	0.70372	2		
575	Pinnacles, high-Sr scoria, ring-vent-phase ignimbrite	7		54.0			0.70342	4		
606	Castle Creek, high-Sr scoria, ring-vent-phase ignimbrite	7		53.4	31	1777	0.70344	2	6.5	P
606G	Castle Creek, glass separate from sample 606	7		61.4	38	1344	0.70343	4		
637	Castle Creek, low-Sr scoria, ring-vent-phase ignimbrite	7		59.7	29	628	0.70370	6		
637G	Castle Creek, glass separate from sample 637	7		71.9	60	270	0.70363	4	4.7	P
345	Annie Creek, low-Sr scoria, ring-vent-phase ignimbrite	7		58.9	29	720			6.2	P
582	Pinnacles, low-Sr scoria, ring-vent-phase ignimbrite	7		56.5	23	797	0.70362	2	6.0	P
582G	Pinnacles, glass separate from sample 582	7		68.8	38	387	0.70363	3		
876	Grotto Cove, low-Sr scoria, ring-vent-phase ignimbrite	7		56.2	19	717			6.1	P
862	Llao Rock, low-Sr scoria, ring-vent-phase ignimbrite	7		55.5	18	752			6.5	P
874	Palisade Point, low-Sr scoria, ring-vent-phase ignimbrite	7		55.3	21	791			6.1	P
860	Llao Rock, low-Sr scoria, ring-vent-phase ignimbrite	7		54.9	21	793	0.70365	4		
442	Hillman Peak, low-Sr scoria, ring-vent-phase ignimbrite	7		53.1	18	751	0.70362	5		
885	Grotto Cove, low-Sr scoria, ring-vent-phase ignimbrite	7		51.4	12	648	0.70370	5	6.0	P
870	Palisade Point, olivine scoria, ring-vent-phase ignimbrite	7		53.7	16	581	0.70355	7	6.5	P
866	Llao Rock, olivine scoria, ring-vent-phase ignimbrite	7		52.7	9	378	0.70355	8		
866G	Llao Rock, glass separate from sample 866	7		63.1			0.70360	3		
444	Hillman Peak, olivine scoria, ring-vent-phase ignimbrite	7		51.3	12	591	0.70348	5	5.9	P
1290	Annie Creek, olivine scoria, ring-vent-phase ignimbrite	7		48.2	13	757	0.70373	3	4.8	

TABLE 1. (continued)

No	Description	Age K-Ar ka	sigma	SiO2 wt%	Rb ppm	Sr ppm	87/86	87/86 sigma	18/16	Material
	Granitoids									
195	Caldera rim, Pumice Castle			68.2	50	378	0.70373	3	3.4	P
432	Caldera rim, Hillman Peak			73.4	94	224			0.8	P
432	Caldera rim, Hillman Peak			73.4	94	224	0.70365	8	0.6	Q
452	Caldera rim, Hillman Peak			63.7	48	538	0.70374	6	6.7	P
516	Wizard Island, xenolith in andesite			50.4	4	828	0.70361	2		
799	West of Cleetwood flow			67.4	47	379	0.70372	8	4.3	P
799G	Glass separate from sample 799			75.5	113	52	0.70401	11		
1023	Southeast of Garfield Peak			67.7	41	390			4.9	Q
1023	Southeast of Garfield Peak			67.7	41	390	0.70371	5	4.2	P
1038	Dutton Creek			67.8	37	389	0.70367	4	2.1	P
1038	Dutton Creek			67.8	37	389			2.2	Q*
1092	Caldera rim, Garfield Peak			61.2	32	547	0.70370	8	3.5	P*
1326	South of Dutton Cliff						0.70375	4	2.8	P

Sample numbers from C.R. Bacon except "L" numbers from M.A. Lanphere.
Ages with error estimates are K-Ar data of M.A. Lanphere; ages without error estimates are inferred;
7 ka ages or Llao Rock, Cleetwood, and climactic eruptions rounded from radiocarbon dates in Bacon [1983]
Rb and Sr by energy-dispersive x-ray fluorescence
18/16 material: P = plagioclase, Q = quartz, WR = wholerock; N = number of determinations
(M) = monogenetic vent
*Single 18/16 determination

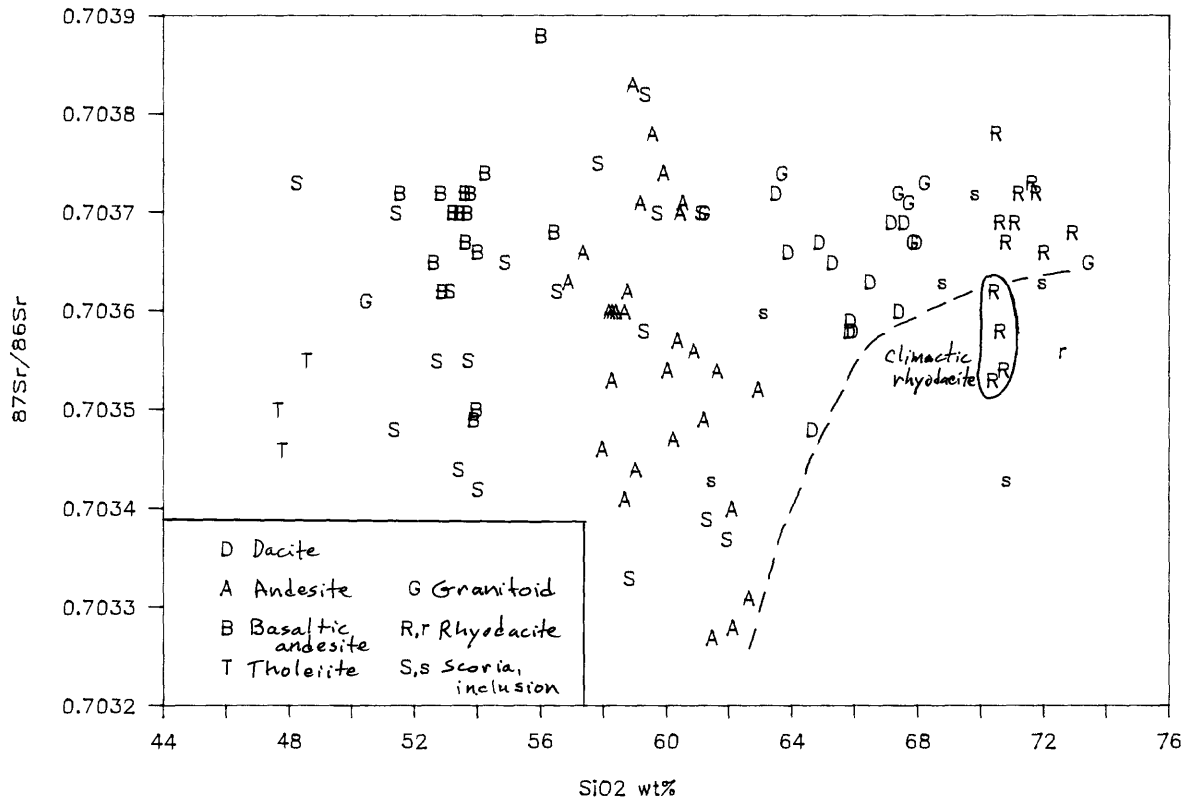

Fig. 2. $^{87}Sr/^{86}Sr$ vs. SiO_2 concentration. Lower case r and s indicate glass separates. Dashed curve defines lower limit of $^{87}Sr/^{86}Sr$ in differentiated rocks.

Trace Element Abundances and Ratios

Most precisely-determined incompatible trace elements (e.g., Ba, Nb, Zr, Ce) are poorly correlated with $^{87}Sr/^{86}Sr$. The overall relation is similar to those for SiO_2 (Figure 2), K_2O, or Mg number, suggesting that variations in isotopic composition with concentration reflect the tendency for dacite and rhyodacite to have higher minimum $^{87}Sr/^{86}Sr$ ratios. These are fairly well correlated with increasing incompatible element content, particularly when climactic rhyodacites are ignored (these being hybrids; see below and Bacon and Druitt [1988]). Moreover, there is a crude positive correlation of the entire data set with incompatible element concentration that is best illustrated by Ba (Figure 3). Not all of this can be attributed to effects associated with increased differentiation because some LILE-rich (and LREE-rich) samples are shoshonitic basaltic andesite and rather primitive andesite. In contrast, HFSE show only the aforementioned increase in minimum $^{87}Sr/^{86}Sr$ with differentiation.

A subtle negative correlation appears to exist between $^{87}Sr/^{86}Sr$ and HREE (Figure 4) within basaltic andesite and andesite arrays: In the most general way, more radiogenic values are associated with more HREE-depleted samples. Consequently, there may be a positive correlation of $^{87}Sr/^{86}Sr$ with Ce/Yb (Figure 5), although this depends heavily on a few extreme samples

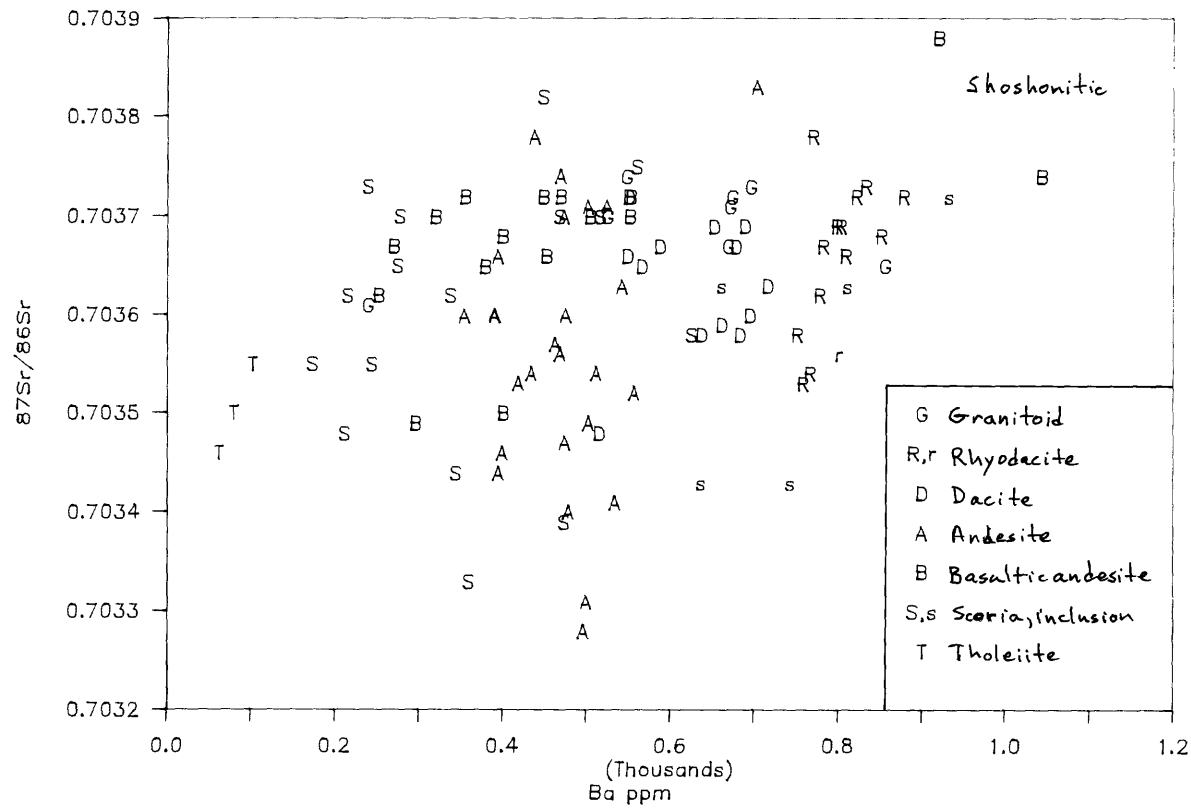

Fig. 3. $^{87}Sr/^{86}Sr$ vs. Ba content. Lower case r and s indicate glass separates.

that are LILE- and LREE-rich and HREE-poor. The effect is not so impressive for La/Sm, which is consistent with the negative correlation with Yb in Figure 4.

Ratios of some other trace elements (Ba/La, Ba/Sr, Rb/Sr) reflect the increase in minimum $^{87}Sr/^{86}Sr$ with differentiation. Ba/Nb, La/Nb, and Zr/Nb, however, do not appear to correlate with $^{87}Sr/^{86}Sr$ either among samples of individual rock types or within the data set as a whole.

Temporal Variation

Overall trends in $^{87}Sr/^{86}Sr$ and clustering of Sr isotopic compositions into contemporaneous and locally erupted groups of limited range are evident in Figure 6. A general decrease in the spread of $^{87}Sr/^{86}Sr$, mainly due to increasing minimum value, with decreasing age is evident among rocks >7 ka old. This effect may be noted in andesites and dacites independently; basaltic andesites do not appear to show this effect. The main temporal trend is broken by the voluminous and rather nonradiogenic andesite of the Timber Crater shield, which is believed to be lastest Pleistocene and is plotted at 20 ka on the basis of degree of glaciation and maximum likely K-Ar age. Low $^{87}Sr/^{86}Sr$ also is characteristic of the high-Sr scoria of the climactic eruption and, relative to other silicic rocks, of the climactic rhyodacite. Scoriae of the climactic eruption (0.70333-0.70375) show almost the complete

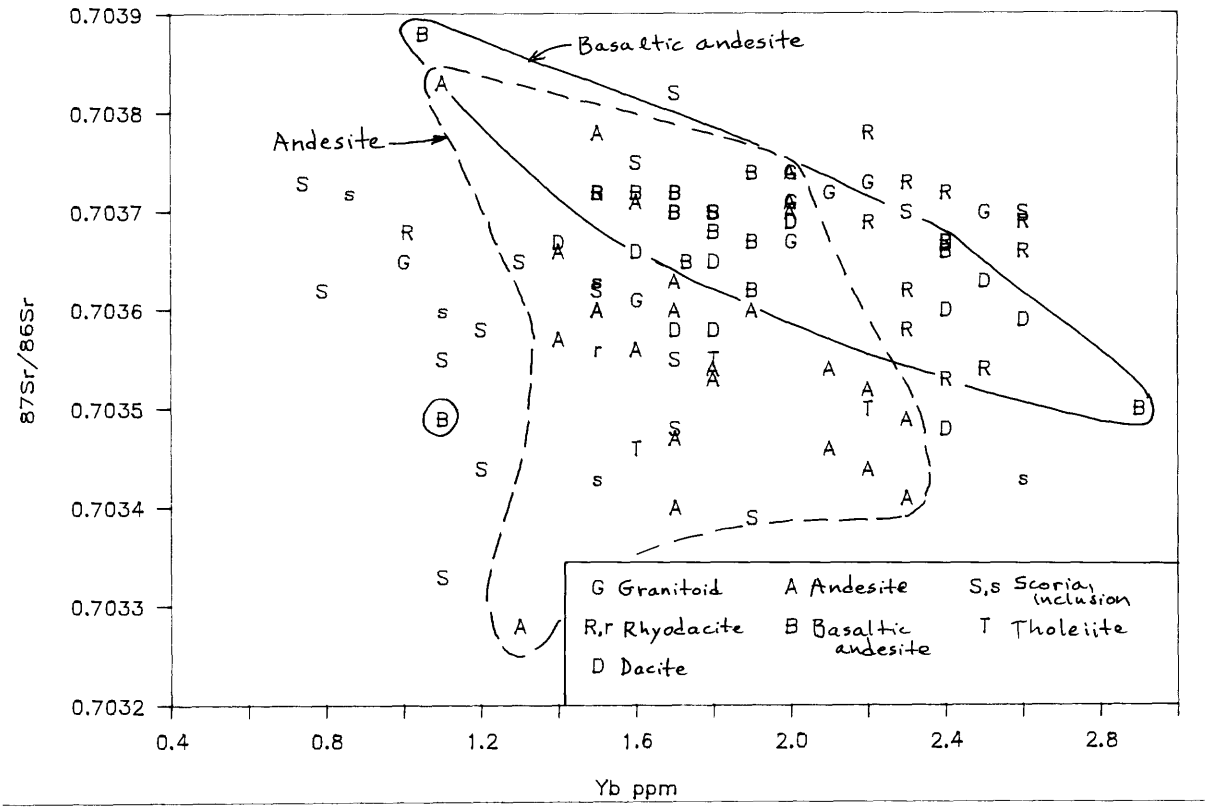

Fig. 4. $^{87}Sr/^{86}Sr$ vs. Yb content. Lower case r and s indicate glass separates. Fields suggest crude negative correlation.

range of $^{87}Sr/^{86}Sr$ of the entire data set. Postcaldera andesites, which do not vary greatly in composition, are heterogeneous in $^{87}Sr/^{86}Sr$: 0.70347-0.70370. The postcaldera rhyodacite dome recovers the slightly >0.70370 value of Pleistocene rhyodacites.

Significant groups of contemporaneous samples, which are also geographically related (see below), are: (1) early andesites of Mount Mazama that form high and low $^{87}Sr/^{86}Sr$ clusters in Figure 6; (2) basaltic andesites of Bald Crater and Desert Cone; (3) four other ~200 ka basaltic andesites; (4) tephra of Pumice Castle, related dacites, and a basaltic andesite on the north wall of the caldera at Steel Bay; (5) the Watchman dacite flow, an andesite inclusion in it, and andesite lava ~1 km S of the Watchman; (6) dacite, andesite, basaltic andesite, and basalt of Williams Crater and Munson Valley ("summit domes"); (7) rhyodacite and andesite inclusions of the evolved Pleistocene rhyodacites of Grouse Hill, Steel Bay, and Redcloud Cliff; (8) rhyodacite domes of Sharp Peak; and (9) stratigraphic units within the climactic ejecta. Although these contemporaneous groups form tight clusters in Figure 6, their intracluster conformity reflects eruption from geographically restricted vent areas because many times are characterized by large isotopic variation between and beyond the clusters. Three clusters, however, are not geographically related. The ~70 ka dacites and the evolved Plesitocene rhyodacites (~25-30 ka) in both cases were erupted from vents

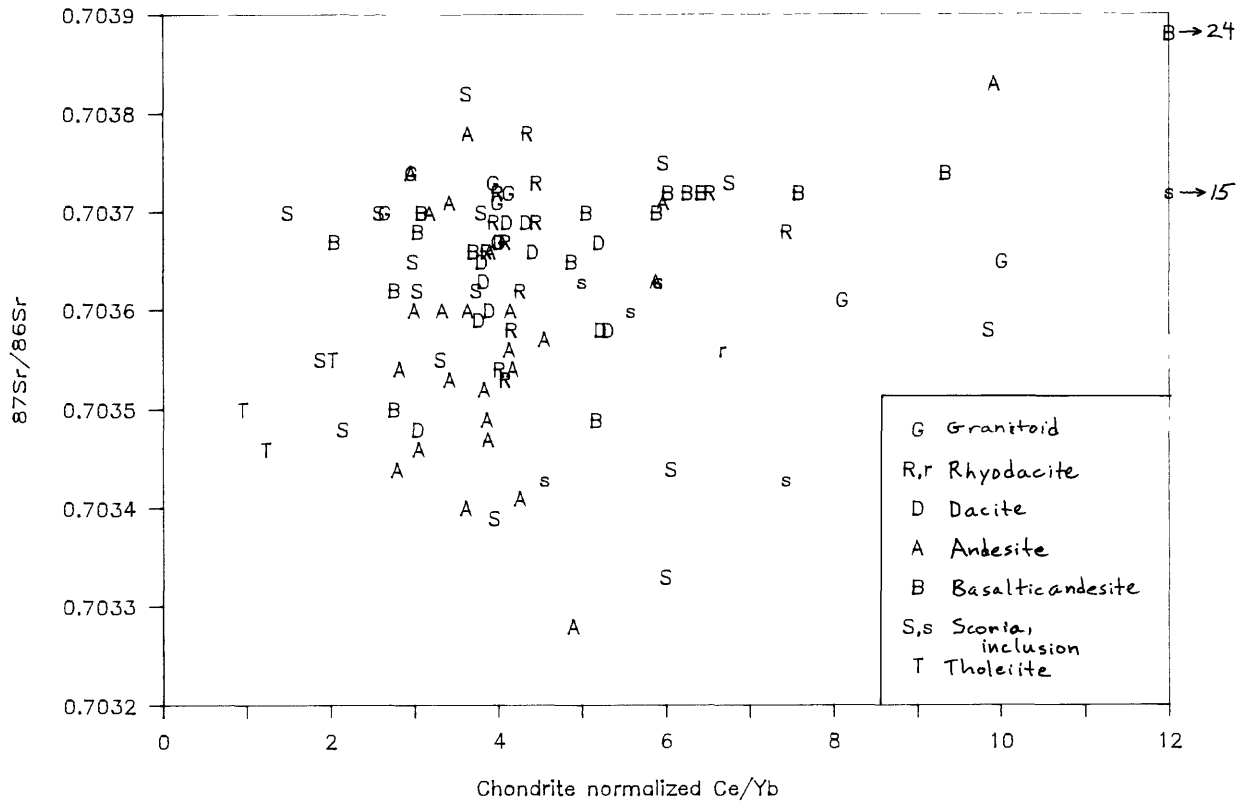

Fig. 5. $^{87}Sr/^{86}Sr$ vs. chondrite-normalized Ce/Yb [Haskin et al., 1968]. Lower case r and s indicate glass separates.

separated by up to 9 km and the apparently consanguinous dacites of Williams Crater and Munson valley from vents separated by some 4 km, implying either substantial areal extent of reservoirs or lateral magma transport. That basaltic andesites through dacites of certain age groups vary little in $^{87}Sr/^{86}Sr$ may indicate consanguinity, or may be coincidence because in some cases the range among andesites and dacites (e.g., The Watchman) is well outside of analytical error or because extreme compositions are known to be unrelated on the basis of geologic and other geochemical data (e.g., Williams Crater).

Oxygen isotope data are inadequate to define temporal trends with certainty. The apparent increase in spread of $\delta^{18}O$ values with decreasing age may only reflect the larger data set for the younger rocks.

Sr Geographic Provinces

Certain regions have erupted magmas characterized by a limited range of $^{87}Sr/^{86}Sr$. As noted above, this applies to many temporally related samples that in some cases represent a wide spread of unrelated compositions. Major features of the areal variation in $^{87}Sr/^{86}Sr$ can be seen in Figure 7. Some of the highest values are characteristic of the second and third sets of basaltic andesites and andesites, respectively, of Hillman Peak [Bacon, 1983], which also have high Sr and other LILE contents and are known to have

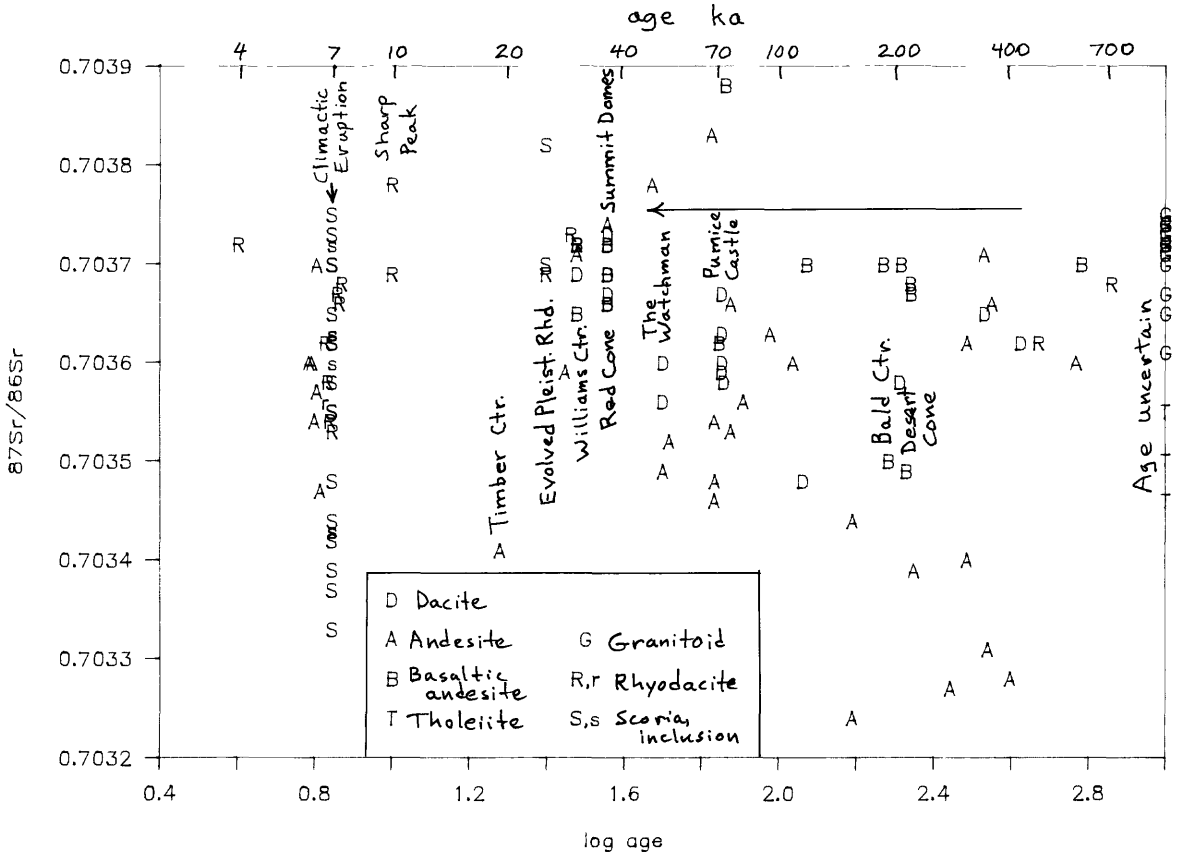

Fig. 6. $^{87}Sr/^{86}Sr$ vs. inferred age of samples. Lower case r and s indicate glass separates. Note log scale.

vented in virtually the same place. The NW part of Figure 7 is characterized by low $^{87}Sr/^{86}Sr$ in the basaltic andesites of Bald Crater and Desert Cone, which have indistinguishable K-Ar ages, and in relatively differentiated low-K tholeiite presumably from an older vent nearby; andesite of Timber Crater also may be considered with this geographic group. The lowest $^{87}Sr/^{86}Sr$ values were measured in andesites from low on the S and W caldera walls, which may have vented from an area more restricted than suggested in Figure 7. Because andesite and dacite of similar age to the S and W wall andesites, but erupted E of the caldera, have $^{87}Sr/^{86}Sr$ more typical of the entire data set we feel that location has a more profound influence on isotopic composition than age of eruption. Most of the rest of the lavas have $^{87}Sr/^{86}Sr$ in the ~0.7036-0.7037 range, so that geographic patterns are difficult to discriminate. It is notable, however, that all samples from the vicinity of Crater Peak fall in the typical range regardless of age or composition and that, in general, the spread in $^{87}Sr/^{86}Sr$ decreases when only nearly contemporaneous lavas from small areas are considered (e.g., Williams Crater). Of course, the most spectacular example of homogeneity independent of vent location is the climactic rhyodacite, which is virtually uniform within precision of all analytical methods [Bacon and Druitt, 1988; Druitt and Bacon, 1989] including isotopic. Variation in $^{87}Sr/^{86}Sr$ among climactic scoriae does not appear to correlate with probable vent location but is tied

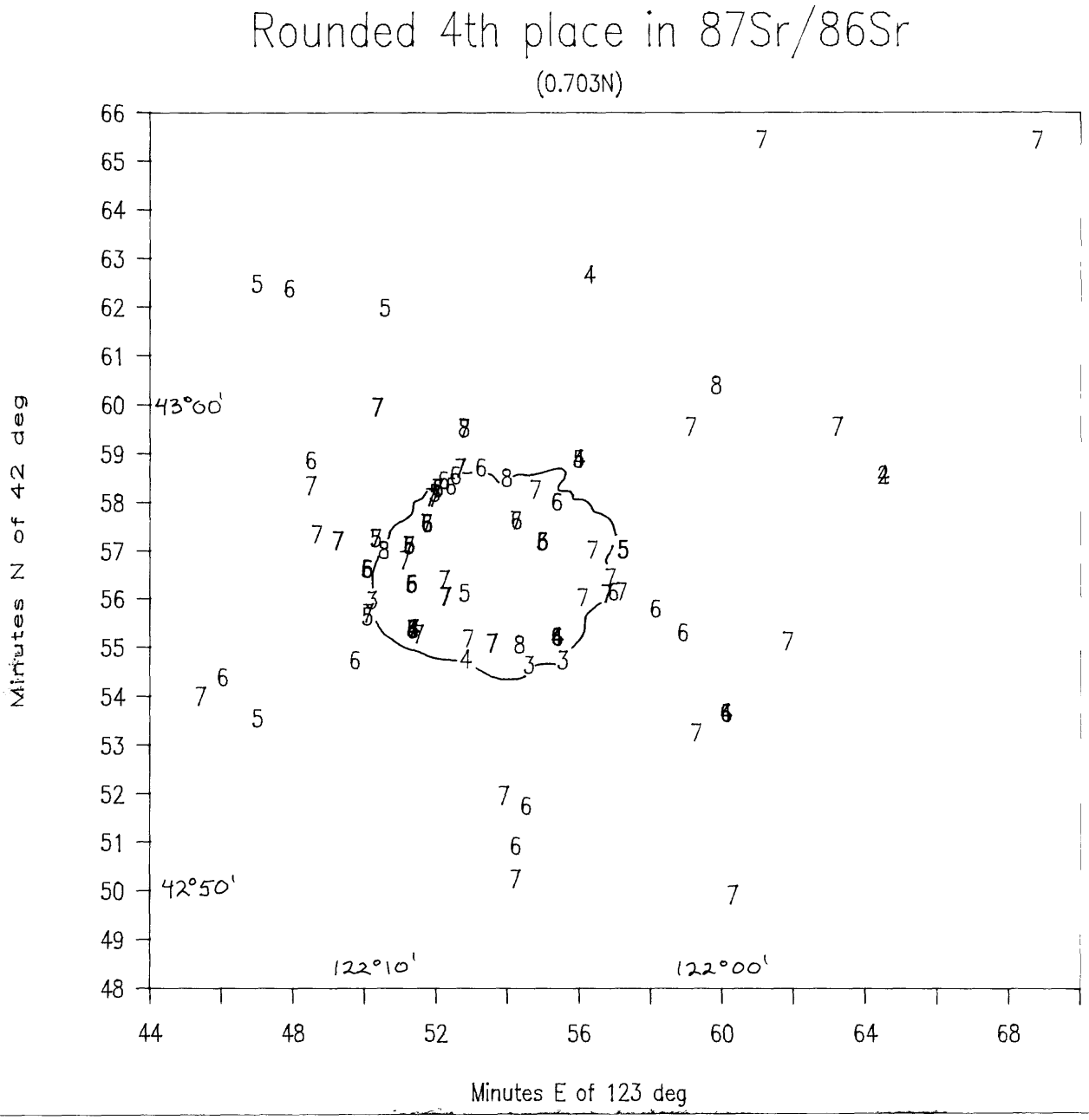

Fig. 7. Map showing rounded fourth place in $^{87}Sr/^{86}Sr$ for samples in Fig. 1. Crater Lake shoreline shown for reference.

to LILE abundances, as noted above. Geographic variability of postcaldera andesite Sr isotopic composition is viewed as highly significant, however, as it may reflect mixing processes associated with foundering of the cauldron block into the disturbed unerupted fraction of the climactic magma chamber (see below).

Sr Concentration

Relations between Sr concentration and isotopic composition are most clearly portrayed on a plot of $^{87}Sr/^{86}Sr$ versus 1/Sr (Figure 8) on which

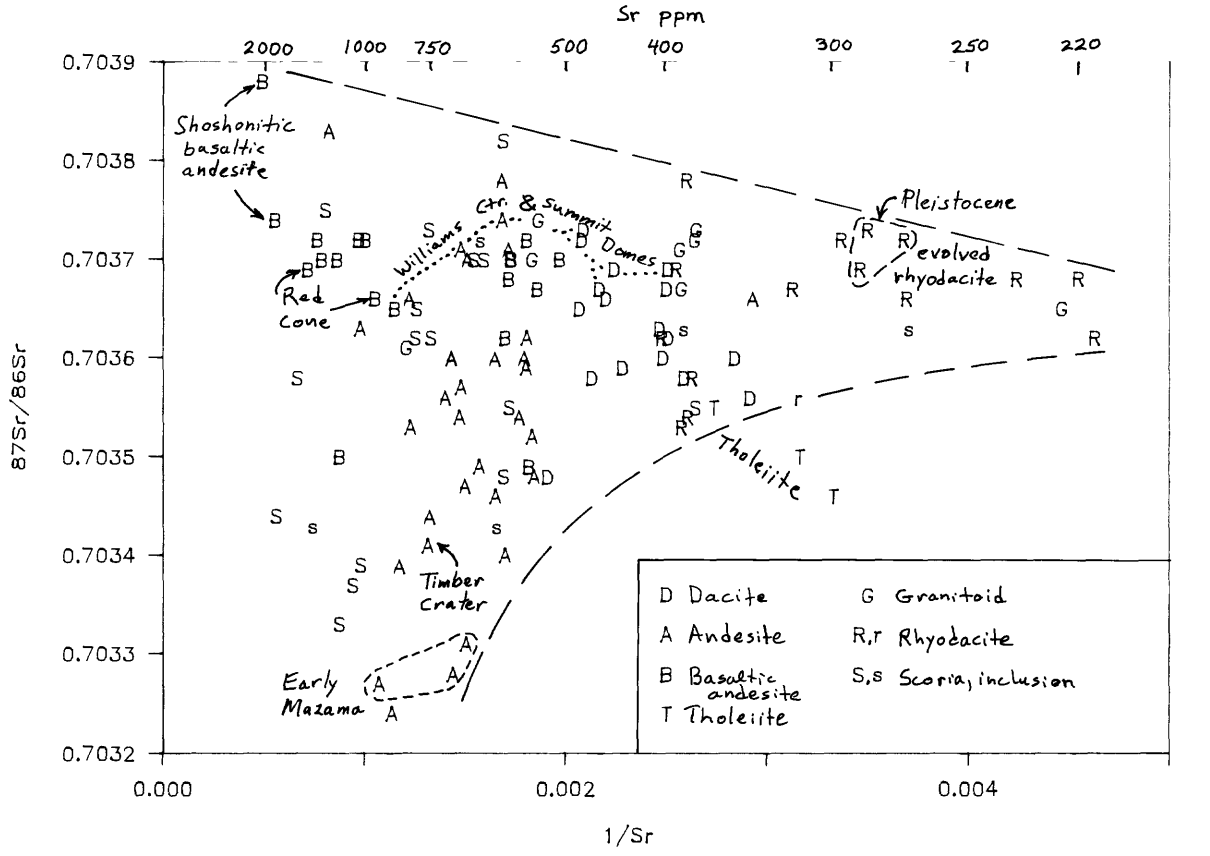

Fig. 8. $^{87}Sr/^{86}Sr$ vs. 1/Sr. Lower case r and s indicate glass separates. Long-dashed curves define $^{87}Sr/^{86}Sr$ envelope for calc-alkaline rocks. Dotted line connects Williams Crater and Munson Valley samples.

mixing relationships are linear. This plot shows the same general trends that reflect the range of LILE contents of andesites and basaltic andesites and differentiation of the more silicic rocks that were evident in other plots. Clustering of samples from the related or nearby eruptive units is apparent (Figure 8): (1) "basalt" of Williams Crater, basaltic andesites of Red Cone, and a vent north of Williams Crater; (2) dacites of Munson Valley and Williams Crater; (3) early andesites of the S and W caldera walls; (4) evolved Pleistocene rhyodacites; and (5) three clusters formed by climactic rhyodacite, low-, and high-Sr climactic scoriae (Figure 11). Glasses from partially fused granitoids and from climactic scoriae plot within precision at the same $^{87}Sr/^{86}Sr$ as their respective wholerocks but at lower Sr concentration.

Mixing relationships known from other information are consistent with Figure 8. These involve the Williams Crater and Munson Valley samples, the rhyodacite of Llao Rock, and the climactic ejecta. Each will be discussed below.

LAVAS OF MONOGENETIC VENTS

These lavas are considered separately from Mount Mazama because their compositions reflect processes that do not require the presence of a large

long-lived volcanic focus.

Tholeiites

Low-K tholeiites occur as lava fields and intracanyon flows west of Crater Lake. Vents are thought to be located at about the longitude of Red Cone but are buried under younger deposits. Some tholeiites may be late Quaternary (e.g., in Castle Creek near Little Castle Creek) but intracanyon tholeiite at Prospect that originated near the latitude of Crater Lake has been dated at 1.25 ± 0.11 Ma [Fiebelkorn et al., 1982]. The tholeiites are characterized by low overall abundances of LILE, REE similar to MORB, and HFSE abundances generally lower than MORB; Sr, Ba, and Th are higher and K and Rb commonly lower than in MORB [Bacon, 1989]. The tholeiites are the only Quaternary basaltic liquids (SiO_2<52%) that have erupted near Crater Lake. Compatible element contents (up to 9.8% MgO, 190 ppm Ni) indicate the that the tholeiites are primitive and may approach primary compositions.

Sr and O isotopic compositions of tholeiites overlap those of the calc-alkaline basaltic andesites and are similar to those suggested by Ito and Stern [1985/86, p. 316] for unfractionated basaltic arc magmas. The isotopic composition of Sr in the tholeiites is surprisingly radiogenic, $^{87}Sr/^{86}Sr$~0.70350, in light of the low Rb/Sr of these lavas (to <0.003). $\delta^{18}O_{wr}$ ranges from +5.7 to +6.0 for three samples, values typical of mantle-derived magmas [Kyser, 1986]. Tholeiite isotopic and chemical compositions are similar to those of high-alumina olivine tholeiites from west of 121° W longitude in California [Hart, 1985] and from the Lassen volcanic center [Bullen and Clynne, this issue]. Trace element abundances require a depleted mantle source, perhaps with minor subduction-related(?) enrichment of Sr, Ba, and Th. Such addition of Sr might account for the observed $^{87}Sr/^{86}Sr$, that is correlated with Sr (Figure 8) and Ba (Figure 3) contents, without altering $\delta^{18}O$ from normal mantle values.

Calc-alkaline lavas

Basaltic andesites of monogenetic vents have $^{87}Sr/^{86}Sr$ of 0.70349 to 0.70372, most being ≥0.70362, and $\delta^{18}O$ of +5.8 to +6.6. Except for HREE (Figure 4), the widely variable incompatible trace element abundances of basaltic andesites [Bacon, 1989] do not correlate with isotopic composition. A single shoshonitic basaltic andesite (1800 ppm Sr) has the most radiogenic Sr of monogenetic vent lavas (0.70374 ± 3) and $\delta^{18}O_{wr}$ = +7.8, the latter probably resulting from intense oxidation of this sample; this rock resembles LILE-rich andesites of Mount Mazama, whose origin is discussed below.

Basaltic andesites of Red Cone, which are chemically similar to magnesian andesite described by Kay [1978], have MgO and Ni contents approximately as high or higher than the low-K tholeiites yet have among the highest LILE concentrations. These samples have $^{87}Sr/^{86}Sr$ ~0.7037, 950-1400 ppm Sr, and $\delta^{18}O_{wr}$ ~+5.9. Trace element variation between a bomb and lavas noted by Bacon [1989] is not accompanied by significant changes in $^{87}Sr/^{86}Sr$. Abundant Ni-rich (≤4300 ppm) $Fo_{<87}$ olivine phenocrysts in the lavas of Red Cone are euhedral and show growth forms that indicate they are not xenocrysts. If these magmas have been contaminated in the crust, contamination must have been selective and could not have involved significant fractionation; radiogenic Sr had to be added to primary liquid without accompanying compatible-element depletion of the liquid. Partial melting of the mantle wedge, previously enriched in LILE by aqueous fluids derived from dehydrating subducted material [Kay, 1980; McCulloch and Perfit, 1981; White and Patchett, 1984; Tatsumi et al., 1986], appears to be consistent with the existing data. In this scenario, increase in $^{87}Sr/^{86}Sr$ occurs in the

mantle because subduction-related Sr reflects seawater alteration of the slab and any sediment that may have been subducted.

Andesites from shields and monogenetic cones have Sr isotopic compositions within the low part of the range (maximum $^{87}Sr/^{86}Sr$ ~0.7036) of data for andesites of Mount Mazama. Andesite from the large, compositionally-uniform late Pleistocene (<19 ka K-Ar age) shield of Timber Crater has $^{87}Sr/^{86}Sr$ = 0.70341 ± 5, lower than any analyzed basaltic andesite, and $\delta^{18}O_{wr}$ = +6.9. The least radiogenic Sr ($^{87}Sr/^{86}Sr$ = 0.70324 ± 3; $\delta^{18}O_{pl}$ = +6.5) was found in andesite from a monogenetic cone (155 ± 12 ka) 10 km ENE of the caldera, although 1σ errors overlap with data for some early Mazama andesites. Both of these phenocryst-poor olivine-bearing andesites have 59% SiO_2 and Sr >700 ppm. Existence of several examples of andesite with $^{87}Sr/^{86}Sr$ <tholeiite or primitive basaltic andesite values suggests that chemically primitive calc-alkaline liquids with similar Sr isotopic composition were present even though not sampled at the surface. Significantly elevated $\delta^{18}O$ relative to analyzed primitive lavas suggests some interaction with crustal rocks during differentiation to andesite [Taylor, 1980; Matsuhisa and Kurasawa, 1984; McBirney et al., 1987] because the increase in $\delta^{18}O$ is beyond that reasonably attributed to crystal fractionation [Taylor and Sheppard, 1986]. The necessary ^{18}O is not likely to have been derived from modern subduction because of the need to keep $^{87}Sr/^{86}Sr$ values lower than sampled primitive lavas.

Combined assimilation-fractional crystallization calculations [AFC; DePaolo, 1981; Taylor, 1980] indicate that ~10% assimilation of low-Sr, low- to moderate-$^{87}Sr/^{86}Sr$, ^{18}O-rich material ($\delta^{18}O$ = +10 to +12) could produce the observed isotopic compositions during ~20% fractionation of a parent with $^{87}Sr/^{86}Sr$ ~0.7030 and $\delta^{18}O$ ~+6.0. These models are sensitive to $\delta^{18}O$ of the assimilant and r, the ratio of mass assimilated to mass crystallized; large values of either improve the fit of a model. The main unknown in the model is the identity of the assimilant. Metaigneous rocks derived from altered MORB and low-Sr metasediments are reasonable ^{18}O-rich candidates. Such materials may be tectonically underplated beneath the arc and thus be important constituents of the deep crust [see Bacon, 1989, for a more detailed discussion of the crust beneath Crater Lake]. Some granitoids of the Klamath Mountains have suitable O and Sr isotopic compositions [Masi et al., 1981; many $\delta^{18}O$ ~+8, a few $\delta^{18}O$ as high as +10; most present day $^{87}Sr/^{86}Sr$ <0.704, all <0.706] and these may reflect deep crust that, if present beneath Crater Lake, might provide suitable assimilants. Similarly, present-day $^{87}Sr/^{86}Sr$ ratios are generally ≤0.704 in Mesozoic granitoid rocks of the Blue Mountains, E of the Cascades [Armstrong et al., 1977]. Assimilation of or interaction with partial melts of deep crustal rocks in which garnet was residual might explain the subtle negative correlation between $^{87}Sr/^{86}Sr$ and Yb content of the lavas [Hildreth and Moorbath, 1988].

BASALTIC ANDESITE TO DACITE OF MOUNT MAZAMA

Because of the large range in LILE contents of andesitic lavas we have chosen to separate the particularly LILE-rich from "normal" samples below.

"Normal" Andesites and Basaltic Andesites

Basaltic andesites of Mount Mazama have isotopic compositions within the range of monogenetic vent lavas. Isotopic compositions of "normal" andesitic lavas of Mount Mazama extend the range defined by monogenetic volcanoes to higher $^{87}Sr/^{86}Sr$ (max. 0.70378 ± 5); most $\delta^{18}O_{pl}$ values are between +6.2 and +6.6. The lowest measured $^{87}Sr/^{86}Sr$ ratios occur in the oldest

exposed lavas (~280 to 400 ka), porphyritic silicic andesites at lake level on the SW, S, and SE caldera walls (0.70327 ± 2 to 0.70331 ± 3). Our only $\delta^{18}O_{pl}$ value for these rocks is +5.6 on plagioclase from Phantom Cone, and probably is lower than magmatic values because of pervasive hydrothermal alteration. At the top of the S caldera wall at Garfield Peak hornblende andesite (224 ± 9 ka) also has low $^{87}Sr/^{86}Sr$ (0.70339 ± 2), and, like some andesites of monogenetic vents, somewhat elevated $\delta^{18}O_{pl}$ (+6.6). High $\delta^{18}O_{pl}$ of this hornblende andesite relative to likely parent magmas must reflect deep-seated AFC: although hydrothermal circulation clearly took place beneath Mount Mazama, interaction with hydrothermal fluids would tend to lower magmatic $\delta^{18}O$, given the -14 value of local meteroic water [Thompson et al., 1987] and the maximum possible ^{18}O shift (~+15) in hydrothermal fluid.

Many andesites have 600-700 ppm Sr, $^{87}Sr/^{86}Sr$ ~0.7037, and $\delta^{18}O_{pl}$ ~+6.6. One young flow (47 ± 20 ka) from the top of the N caldera wall has $^{87}Sr/^{86}Sr$ = 0.70378 ± 5, $\delta^{18}O_{pl}$ = +6.2, $\delta^{18}O_{wr}$ = +6.7. The isotopic compositions of these lavas are readily explained by reasonable degrees of AFC of basaltic andesitic magma where the assimilant(s) have low to moderate $^{87}Sr/^{86}Sr$ and somewhat elevated $\delta^{18}O$. The isotopic data by themselves do not rule out mixing of basaltic andesitic and silicic magmas to form these andesites because Sr and O isotopic compositions can be similar in all three magma types, and this clearly occurred at Williams Crater (see below).

LILE-rich (Shoshonitic) Lavas

A small group of samples, basaltic andesite and andesite from the upper two units of the Hillman Peak center on the W margin of the caldera and basaltic andesite of Buckeye Butte (monogenetic cone 21 km NE of the caldera), have Sr contents of 1100-2000 ppm and generally are rich in LILE. The more LILE-rich rocks fit most definitions of shoshonite and are hornblende phyric. The Hillman Peak lavas have $^{87}Sr/^{86}Sr$ of 0.70383 ± 3 and 0.70388 ± 2, $\delta^{18}O_{pl}$ of +6.8 (both); the oxidized Buckeye Butte sample gives 0.70374 ± 3 and $\delta^{18}O_{wr}$ = +7.8, as noted above. The high Sr contents imply that plagioclase was not a major participant in fractionation of these magmas. We have seen that primitive basaltic andesite can be quite Sr-rich and comparatively radiogenic yet have low $\delta^{18}O$, so that AFC involving relatively Sr- or ^{87}Sr-rich, ^{18}O-rich assimilants can account for the isotopic compositions of the LILE-rich lavas. Again, the critical characteristic of an assimilant is high $\delta^{18}O$.

Dacites

Analyzed dacites fall into three groups on Figures 6 and 8: dacite of Merriam Point at Llao Bay ($^{87}Sr/^{86}Sr$ = 0.70348 ± 2; n=1), other ≥50 ka dacites (~0.7036; n=8), and <50 ka dacites (~0.7037; n=6). Oxygen isotopic analyses are too few (n=4) for meaningful distinctions to be drawn between dacite groups. In general, $\delta^{18}O$ may be inversely correlated with $^{87}Sr/^{86}Sr$ so that the youngest sample (Munson Valley) is isotopically similar to evolved rhyodacites (Figure 9). Pumice in nonwelded ignimbrite in the W caldera wall below Discovery Point has $\delta^{18}O_{pl}$ = -2.6. This low value probably resulted from high-temperature exchange with meteroic water in this unusual deposit, which displays internal structures thought to indicate expolosive interaction with water [Bacon, 1983].

Excluding the Merriam Point sample, the overall range of dacite $^{87}Sr/^{86}Sr$ is equivalent to that of rhyodacites and is much less than that of andesites. The dacite of Merriam Point has $^{87}Sr/^{86}Sr$ similar to

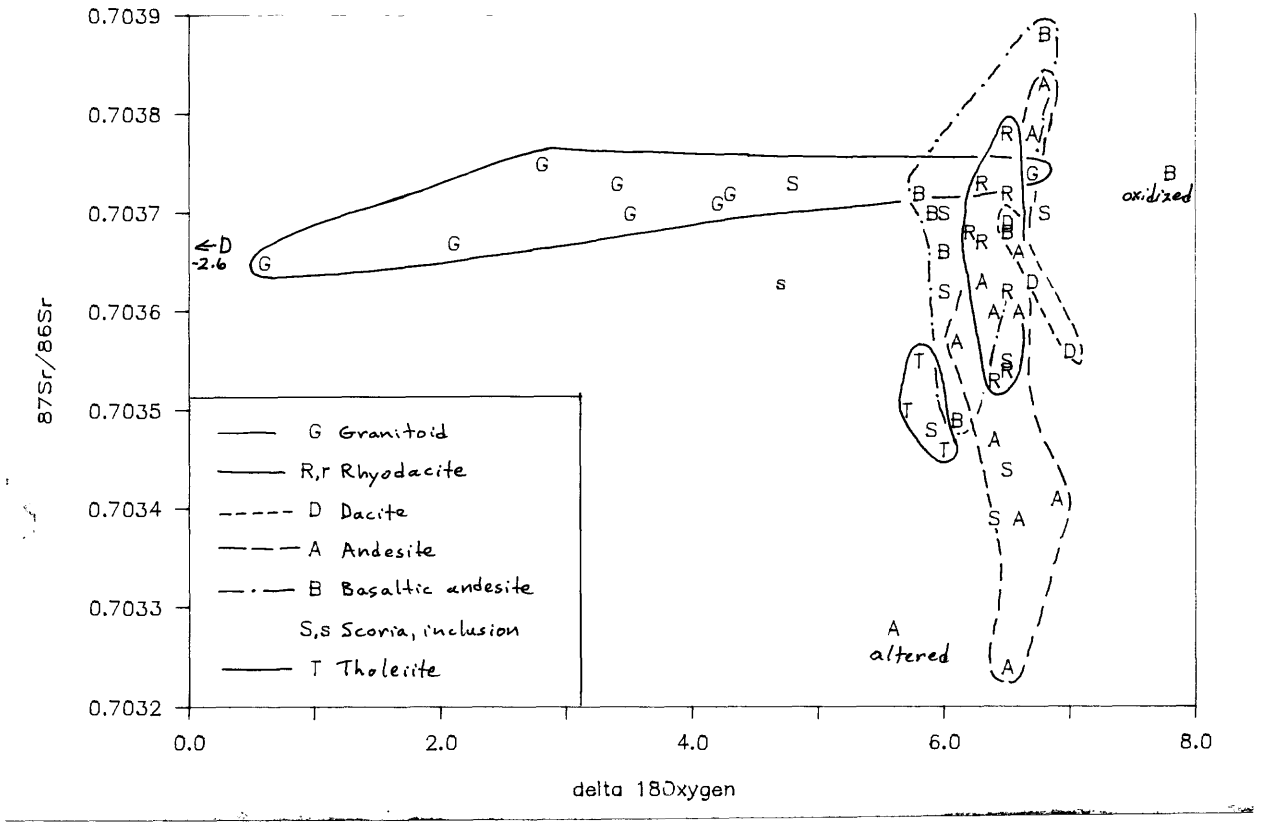

Fig. 9. $^{87}Sr/^{86}Sr$ vs. $\delta^{18}O$. Fields outline rock types. Lower case s is a glass separate. Most data are for plagioclase (see Table 1).

andesites erupted subsequently, probably from other vent areas, and is notable in the present context only in that it has the least radiogenic Sr of the dacites. Dacites ≥50 ka show a narrow range in $^{87}Sr/^{86}Sr$ regardless of vent location or age, although only 2 of the 9 samples are older than ~70 ka (Mount Scott and flow on SW flank of Mount Mazama N of Castle Creek). Dacites <50 ka similarly have restricted $^{87}Sr/^{86}Sr$; these samples are genetically related and evidently were erupted during a short interval.

The dacites <50 ka occur as dominant clasts in the debris-flow and lithic-pyroclastic-flow deposits of Munson Valley and comprise the silicic portion of mingled lava flows of Williams Crater. Bacon [1989] concluded that these dacites were derived from the same magma reservoir at about the same time because: (1) stratigraphic relations indicate the Williams Crater eruptions occurred shortly after those that produced the Munson Valley material; (2) compositions of silicic endmembers in each suite of mixed magmas were similar and unusual; and (3) rare magmatic inclusions in the dacite of Williams Crater are compositionally identical to the abundant inclusions in the dacite of Munson Valley. The Sr isotopic data are consistent with the above observations because the single analyzed dacite of Williams Crater falls in the middle of the small range of values for the five analyzed dacite samples from the Munson Valley deposit (0.70366 ± 4 to 0.70373 ± 4). Perhaps coincidentally, hybrid andesite and gabbro-contaminated basaltic

andesite ("basalt"--see Bacon [1989]) of Williams Crater, a magmatic inclusion in the dacite of Munson Valley, the two basaltic andesite samples from Red Cone (apparently coeval with the Munson Valley material [Bacon, 1983]), and a gabbro-contaminated basaltic andesite from a vent north of Williams Crater all have similar $^{87}Sr/^{86}Sr$ (Figure 6). Moreover, evolved Pleistocene rhyodacites (Grouse Hill, Steel Bay, Redcloud Cliff), that are believed to be somewhat younger than any dacites, and two of three inclusions in these rhyodacites have $^{87}Sr/^{86}Sr$ in the same range (Figure 6). This focusing of Sr isotopic composition following construction of the main edifice of Mount Mazama may reflect limited range in $^{87}Sr/^{86}Sr$ of parent magma(s) at that time or a tendency for differentiated magmas to take on $^{87}Sr/^{86}Sr$ of wallrocks of their shallow reservoirs.

MAGMAS FROM THE CLIMACTIC CHAMBER

Bacon and Druitt [1988] described the preclimactic rhyodacitic lavas and the climactic ejecta of Mount Mazama, and suggested all were vented from the same chamber. Among the climactic ejecta are variably fused granitoid clasts whose isotopic compositions, notably that of oxygen, are important to interpretation of the origin of other samples from the climactic chamber; hence, granitoids are treated first.

Granitoid Blocks in the Climactic Ejecta

Partially fused granitoid blocks occur in deposits of the climactic eruption, particularly near the top of the ring-vent-phase ignimbrite, and as xenoliths in postcaldera andesite [Bacon and Druitt, 1988]. Most have compositions similar to erupted dacites but a few are aplites with ~73% SiO_2. Incipiently-fused fine-grained plagioclase mesocumulates with roughly basaltic compositions form a smaller population. All degrees of melting from 0 to ~35% are represented among the granitoids; rocks with melt fractions >35% may have become disaggregated and assimilated into the magma chamber because their crystallinity would have been insufficient for them to remain coherent under shear [Arzi, 1978; Marsh, 1981]. Sr isotopic compositions of granitoids are $^{87}Sr/^{86}Sr$ = 0.7036-0.7037, within the range of most dacites and rhyodacites. A block with $^{87}Sr/^{86}Sr$ = 0.70372 ± 8 contains Sr-poor (52 ppm) intergranular glass with $^{87}Sr/^{86}Sr$ = 0.70401 ± 11, indicating lack of Sr isotopic homogenization on melting, presumably owing to slow intracrystalline diffusion of Sr in plagioclase. Regardless, $\delta^{18}O$ is the important distinctive isotopic characteristic of the granitoids.

Plagioclase was analyzed in eight samples, quartz also in three of these. $\delta^{18}O_{pl}$ ranged from +6.7 to a low of +0.8. The high value is for a rock that contains a small fraction of intergranular glass but in which hornblende has not broken down, and therefore equilibrated at relatively low temperature. A sample that lacks evidence of melting but contains abundant epidote and chlorite has $\delta^{18}O_{pl}$ = +3.5. For these samples, $\delta^{18}O$ does not correlate precisely with temperature, defined by equilibrated Fe-Ti oxides [Bacon, 1987b], at the time of the climactic eruption. However, silicates in all samples contain fluid inclusions, which are particularly abundant in interstitial alkali feldspar, suggesting they interacted with aqueous fluids at subsolidus temperatures.

Equilibrium fractionation between quartz and plagioclase near solidus temperatures during initial crystallization would have resulted in Δ_{qz-pl} on the order of +2 [Taylor, 1977]. Observed Δ_{qz-pl} are -0.2, +0.1, and +0.7; only the last is outside the range of analytical uncertainty. The three Δ_{qz-pl} values appear to be consistent with equilibration at the >900°C inferred for partial fusion of these samples [Bacon, 1987b]. Equilibrium

exchange with hydrothermal fluid should result in higher Δ_{qz-pl}, probably at least on the order of +4, than exchange at magmatic temperatures. Similarity of $\delta^{18}O_{pl}$ and $\delta^{18}O_{qz}$ must reflect close high-temperature approach to isotopic equilibrium superimposed on low $\delta^{18}O$ granitoids. In light of ubiquitous fluid inclusions and highly variable but generally low $\delta^{18}O$, the simplest explanation for the low $\delta^{18}O$ of these rocks is that of subsolidus exchange with low $\delta^{18}O$ hydrothermal fluids, rather than crystallization from low $\delta^{18}O$ magmas or interaction with fluids at magmatic temperatures. Taking the present $\delta^{18}O_{pl}$ as representative of the whole rock and assuming either open- or closed-system exchange with meteoric water at between 300 and 500°C, fluid/rock ratios [Taylor, 1977] would have been as high as ~0.5 (atomic oxygen units) for the lowest $\delta^{18}O$ sample. Because quartz is known to be substantially more resistant to O-isotopic exchange with hydrothermal fluids than is plagioclase [e.g., Criss and Taylor, 1983] pre-fusion $\delta^{18}O_{pl}$ values probably were lower than those measured on the partially-fused rocks and $\delta^{18}O_{qz}$ values probably did not deviate substantially from those of original crystallization. Hence, the only explanation of low Δ_{qz-pl} is that of high-temperature reequilibration. Mass balance calculations assuming minor decrease in $\delta^{18}O_{qz}$ due to hydrothermal exchange suggest pre-high-T-reequilibration δ^{18}_{pl} values of about -1, +2, and +4 for the three samples for which both quartz and plagioclase were analyzed. Effects of the proposed history of the granitoids are portrayed in Figure 10.

Having established that granitoid rocks beneath Mount Mazama cooled below their solidi and were pervasively hydrothermally altered before reheating associated with the climactic magma chamber, it is natural to look for evidence of assimilation of these low $\delta^{18}O$ materials or their partial melts in juvenile magmas of the climactic chamber.

Preclimactic Rhyodacites

Evolved Pleistocene rhyodacites (Grouse Hill, Steel Bay, Redcloud Cliff) and Holocene rhyodacite of Llao Rock have similar isotopic characteristics: comparatively radiogenic Sr ($^{87}Sr/^{86}Sr$ >0.70366) and light O ($\delta^{18}O_{pl}$ = +6.2 to +6.3). Oxygen in these samples would be expected to be heavier than that of reasonable parents (low-Sr andesite; see below) if fractional crystallization were the only processes operative. Assimilation of a low-^{18}O granitoid component of $^{87}Sr/^{86}Sr$ = 0.7036-0.7037, or its partial melt with more radiogenic Sr but low Sr content, could account for the isotopic composition (Figure 9), as independently inferred on the basis of trace element abundances by Bacon and Druitt [1988]. Evolved rhyodacites cannot have been derived by simple fractionation of climactic rhyodacitic magma because their $^{87}Sr/^{86}Sr$ ratios are different. Interestingly, the dacite of Munson Valley has similar isotopic composition to evolved Pleistocene rhyodacites that probably are only slightly younger.

Rhyodacite of Sharp Peak presents a special case. This minor volume of lava is compositionally and mineralogically identical to climactic rhyodacite, yet apparently is Pleistocene in age. The Sr isotopic compositions of two domes of the Sharp Peak array are significantly more radiogenic than that of climactic rhyodacite; $\delta^{18}O_{pl}$ are similar. The Sr data suggest that either magma of climactic composition was produced more than once or, more likely, some part of the system reached a steady-state composition. Sr in the Sharp Peak domes is isotopically similar to Sr in evolved Pleistocene rhyodacites and their magmatic inclusions. Rhyodacite of Sharp Peak could be a mixture of evolved rhyodacite and residual liquid from partial crystallization of andesite similar to inclusion magma in a manner analogous to formation of

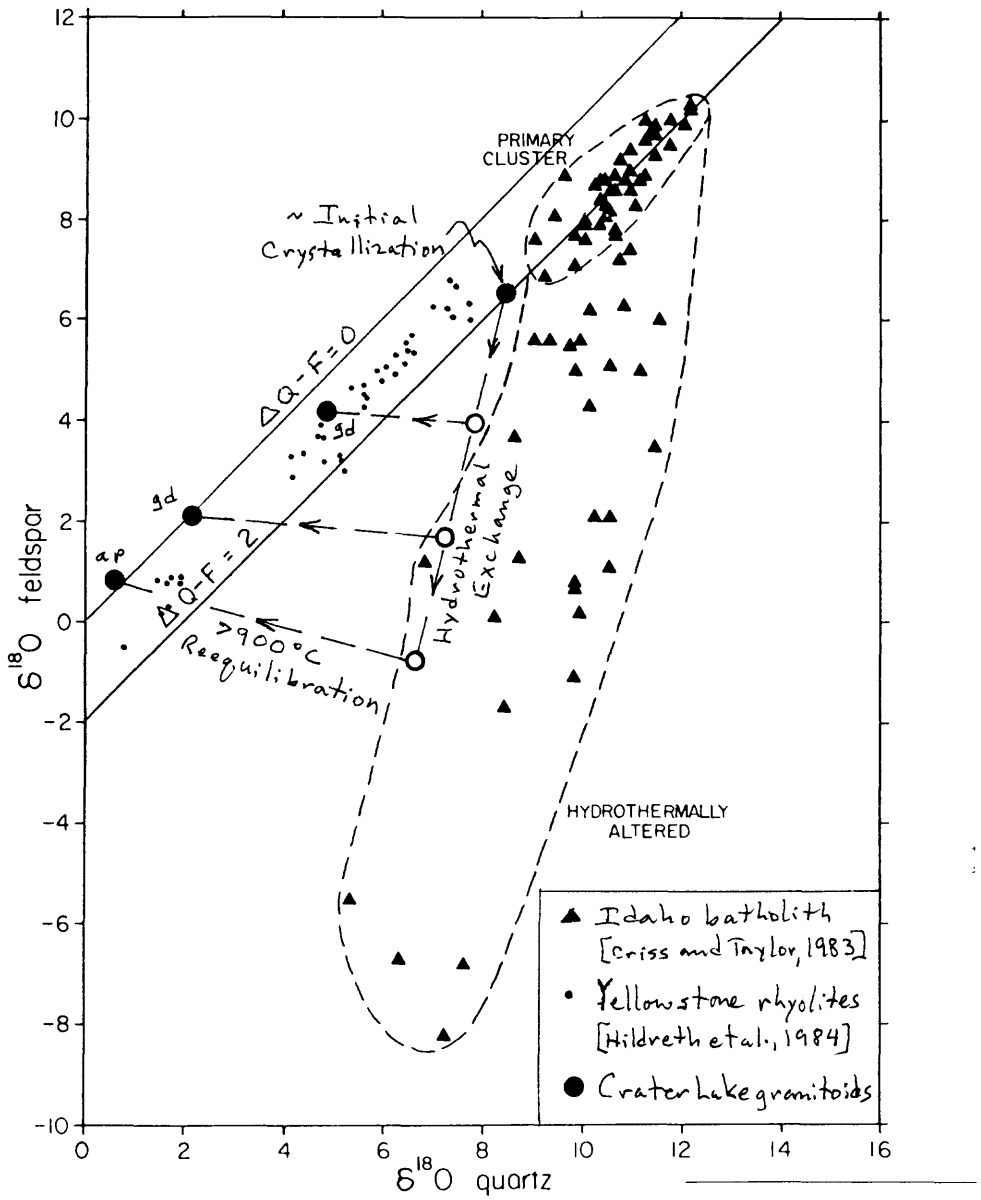

Fig. 10. $\delta^{18}O_{feldspar}$ vs. $\delta^{18}O_{quartz}$ for three partially-fused granitoid blocks from the climactic ejecta (filled circles): ap = aplite, gd = granodiorite. Also shown are data for Atlanta Lobe of Idaho Batholith [Criss and Taylor, 1983, Fig. 3] and for Yellowstone rhyolites [Hildreth et al., 1984]. Initial crystallization point inferred from $\delta^{18}O_{pl}$ of unmelted samples. Open circles are hypothetical pre-melting compositions calculated by mass balance, assuming hydrothermal exchange produced a trend similar to Atlanta Lobe.

climactic rhyodacite (see below). However, Sr abundances require an andesitic parent with higher Sr content than analyzed inclusions in evolved rhyodacites.

The Cleetwood rhyodacite flow was emplaced just before onset of the climactic eruption [Bacon, 1983], and its mineralogy and anhydrous composition are identical to those of climactic rhyodacite [Bacon and Druitt, 1988]. The

isotopic composition of Cleetwood obsidian is identical to that of typical climactic pumice. The origin of climactic rhyodacite magma, discussed below, applies to that of the Cleetwood rhyodacite.

Scoria of the Climactic Eruption

These are described before climactic rhyodacite because discussion of the rhyodacite's origin draws upon knowledge of andesitic to mafic cumulate scoria (collective referred to as "scoria") ejected later in the eruption. Bacon and Druitt [1988] showed that the scoria had at least two compositionally distinct parent magmas that could be distinguished by their LILE contents, and labeled these high-Sr (HSr) and low-Sr (LSr) because that element provided a ready method for distinguishing between them. HSr scoriae were erupted before LSr. A diverse third group characterized by modal olivine was erupted last.

As one might expect, HSr and LSr scoria have different Sr isotopic compositions: weighted means are HSr = 0.70342 ± 1 (n=3) and LSr = 0.70363 ± 1 (n=4). Six wholerock--glass pairs were analyzed, representing all three scoria groups; $^{87}Sr/^{86}Sr$ ratios of glass and wholerock agreed within analytical precision for each pair, and weighted means of pairs are treated as individual data points in the above averages. One HSr sample (106), a hybrid andesite from the Plinian climactic pumice fall, has $^{87}Sr/^{86}Sr$ = 0.70333 ± 4 and one HSr from the ring-vent-phase ignimbrite (591) has $^{87}Sr/^{86}Sr$ = 0.70373 ± 3. An unusual scoria clast from the ring-vent-phase ignimbrite has LSr chemistry but abundant hornblende prisms like HSr scoriae; its $^{87}Sr/^{86}Sr$ = 0.70370 ± 5, which may be significantly more radiogenic than other LSr, and certainly most HSr scoriae.

Oxygen data are somewhat equivocal: $\delta^{18}O_{pl}$ of HSr scoriae average +6.35 ± 0.21 (1σ, n=2), LSr +6.15 ± 0.19 (n=6). However, one LSr sample (637), whose composition was interpreted by Bacon and Druitt [1988] to include assimilated wall rock, has $\delta^{18}O_{pl}$ = +4.7. This result is consistent with assimilation of hydrothermally altered rock, presumably granitoid material (Figure 9). Parent liquids for the scoriae are believed to have been basaltic andesite or andesite. Because $\delta^{18}O_{pl}$ for most scoriae are within the range of basaltic andesitic and andesitic lavas, if in fact lower than many, we cannot discriminate between (1) isotopically rather light parents and (2) small amounts of shallow crustal assimilation of low-^{18}O rock.

Three olivine-bearing scoriae have $^{87}Sr/^{86}Sr$ intermediate between LSr and HSR types, and a fourth (the most magnesian) has a higher value (0.70373 ± 3). $\delta^{18}O_{pl}$ values for the two analyzed samples are virtually within the range of other scoriae; $\delta^{18}O_{wr}$ for the most mafic sample is +4.8, which may suggest assimilation of low-^{18}O material, although hydration of intergranular glass may partially account for the low wholerock value. Varied isotopic composition is not surprising given the complex mineralogy of these samples [Druitt and Bacon, 1989]. The olivine-bearing scoriae are thought to be (1) cumulates from basaltic magma and (2) cumulates from basaltic andesitic or andesitic liquids contaminated with gabbro. Isotopic compositions are similar to those of lavas from monogenetic vents, as should be the case if the lavas indeed represent potential inputs to the climactic chamber.

Magmatic Inclusions (Enclaves) in Preclimactic Rhyodacites

Ellipsoidal inclusions of phenocryst-poor andesite occur in most preclimactic rhyodacite lava flows [Bacon, 1986]. Bacon and Druitt [1988] suggested that these inclusions may represent parent magmas for the climactic chamber at various times during its growth. Inclusions in Pleistocene evolved rhyodacites have trace element abundances that are similar to LSr scoriae; inclusions in Holocene rhyodacites are HSr types, those in the Llao Rock flow

being higher in Sr than those in the Cleetwood flow. $\delta^{18}O_{wr}$ for two inclusions (+6.4, +6.8) are not particularly diagnostic and may have been modified during cooling. Sr isotopic compositions, however, are informative: (1) In evolved Pleistocene rhyodacites, $^{87}Sr/^{86}Sr$ in an inclusion from the rhyodacite of Steel Bay = 0.70370 ± 5, nearly within precision of the weighted mean LSr scoria value. (2) In an inclusion from Grouse Hill, 0.70382 ± 4 is significantly higher than any scoria analysis; this sample extends the LSr trend away from HSr isotopic compositions (Figure 11). It may be significant that this inclusion also has the highest $\delta^{18}O$ (+6.8) of any sample inferred to have come from the climactic chamber. (3) The inclusion from the Cleetwood flow has Sr and O isotopic compositions within error of typical HSr scoriae, in keeping with Bacon and Druitt's [1988] suggestion that Cleetwood inclusions might be representative of HSr parent magma. The inclusion from the Llao Rock flow has $^{87}Sr/^{86}Sr$ significantly higher than most, but not all, HSr scoriae analyzed. The isotopic analyses of inclusions confirm the conclusion of Bacon and Druitt [1988] that several phenocryst-poor andesitic magmas entered the climactic chamber at different times and places.

Climactic Rhyodacite

The ~45 km^3 of rhyodacitic magma erupted in the climactic event is remarkably uniform in composition [Bacon and Druitt, 1988] and mineralogy [Druitt and Bacon, 1989]. Isotopic compositions also show little variation: Three samples from the climactic pumice fall, Wineglass Welded Tuff, and ring-vent-phase ignimbrite, and a fourth from the compositionally identical Cleetwood flow have a weighted mean $^{87}Sr/^{86}Sr$ of 0.70355 ± 2; $\delta^{18}O_{pl}$ of one fall and two ignimbrite pumices are +6.5, +6.0, and +6.5, and obsidian of the Cleetwood flow is +6.4.

Climactic rhyodacite is not a simple differentiate of andesitic parent magma represented by the common HSr scoriae because Sr isotopic compositions of these magmas are significantly different. In order to raise $^{87}Sr/^{86}Sr$ by 0.00013 in such a model, AFC would have to be invoked; however, assimilation of likely wall rocks represented by the granitoids would have lowered $\delta^{18}O_{pl}$, which is not observed in climactic rhyodacite. Without reference to isotopic data Bacon and Druitt [1988] proposed that climactic rhyodacite was formed by mixing of more evolved rhyodacite, that had differentiated from LSr parent magmas and assimilated wall rocks, and residual liquid derived from a HSr andesite parent. Addition of andesitic liquid to a stratified chamber would form an initially hot lens between cooler overlying rhyodacitic magma and cumulate mush; strong undercooling of the added magma would result in rapid partial crystallization, releasing buoyant residual liquid to mix with the growing rhyodacitic volume.

Mixing relations were calculated using the equations of Langmuir et al. [1978]. Mixing of 72% evolved rhyodacite (Llao Rock flow composition) and 28% rhyodacitic residual liquid derived from typical HSr andesite reproduces the Sr concentration and isotopic composition of climactic rhyodacite (model 1, Figure 11), as will a mixture of 89% more highly evolved, early Llao Rock pumice and 11% HSr andesitic liquid (model 2, Figure 11); model 1 is considered more realistic on physical grounds [Sparks and Marshall, 1986]. Such models experience difficulty in reproducing $\delta^{18}O_{pl}$ values, however (Figure 12). Model 2 results predicts $\delta^{18}O_{pl}$ values that are too low, but model 1 results in $\delta^{18}O_{pl}$ within analytical error of measured values. Arguments based on oxygen data are not particularly compelling because the observed variation is near the limits of resolution of the measurements.

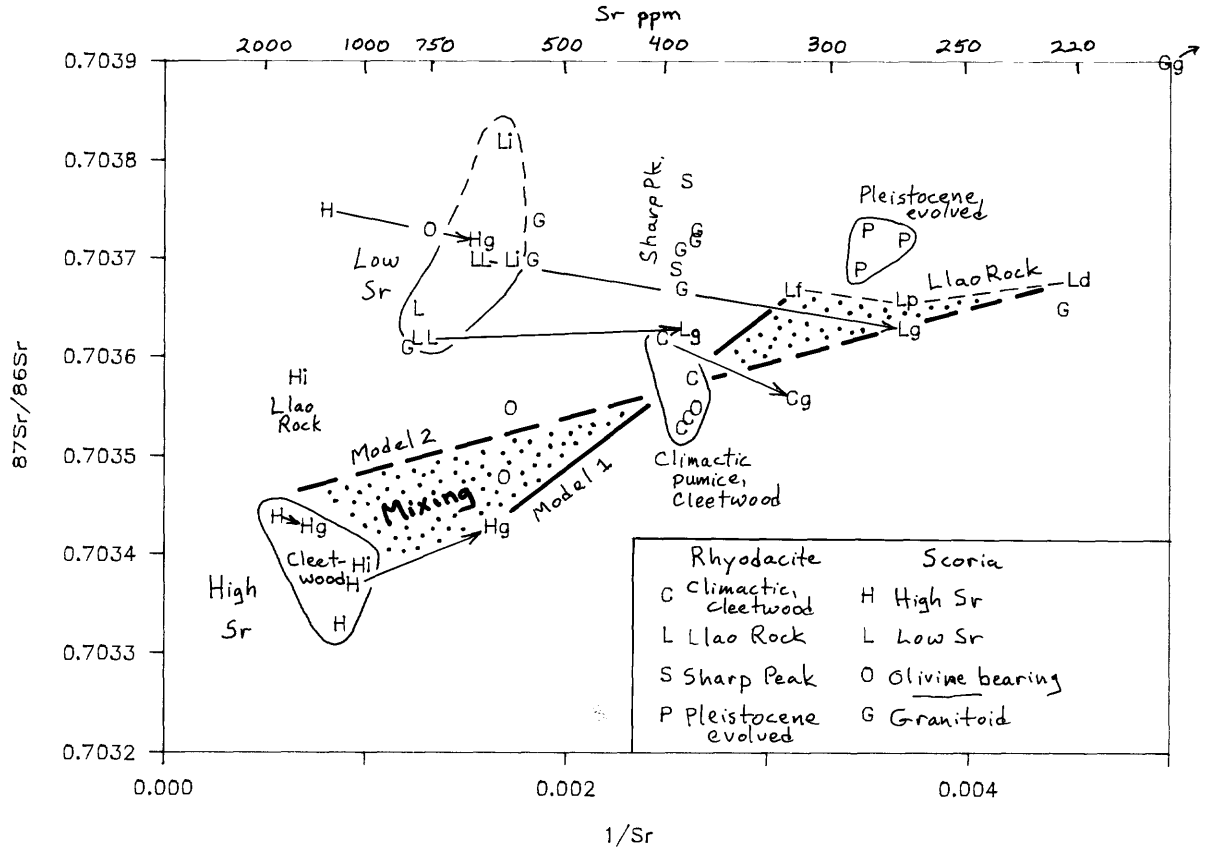

Fig. 11. $^{87}Sr/^{86}Sr$ vs. 1/Sr for preclimactic rhyodacites and climactic ejecta. Arrows connect wholerock values with those of glass separates (suffix "g"). Ld = Llao Rock dike, Lp = early Llao Rock pumice, Lf = Llao Rock flow; suffix "i" indicates inclusion.

POSTCALDERA LAVAS

Postcaldera volcanism produced compositionally restricted andesitic lava that forms cones and domes on the lake floor [Bacon and Druitt, 1988], presumably within a few hundred years following caldera collapse. A sample from the oldest of these andesitic volcanoes, the Central Platform, has $^{87}Sr/^{86}Sr$ = 0.70347 ± 3; two samples from Merriam Cone and three from Wizard Island are virtually within precision of the measurements, with a weighted mean $^{87}Sr/^{86}Sr$ = 0.70359 ± 1. $\delta^{18}O_{pl}$ values are +6.4 for the Central Platform and one Wizard Island sample, +6.1 for one sample from Merriam Cone. The Sr isotopic data are inconsistent with the suggestion of Bacon and Druitt [1988] that postcaldera andesites are mixtures of leftover climactic rhyodacite and LSr mush because: (1) the isotopic composition of Sr in the Central Platform sample is far too low and lies on a mixing line between climactic rhyodacite and typical HSr magma (Figure 13); and (2) other postcaldera andesites have $^{87}Sr/^{86}Sr$ that is too low. Postcaldera andesites either are mixtures of LSr and HSr mush with climactic rhyodacite or at least some of them represent new magma.

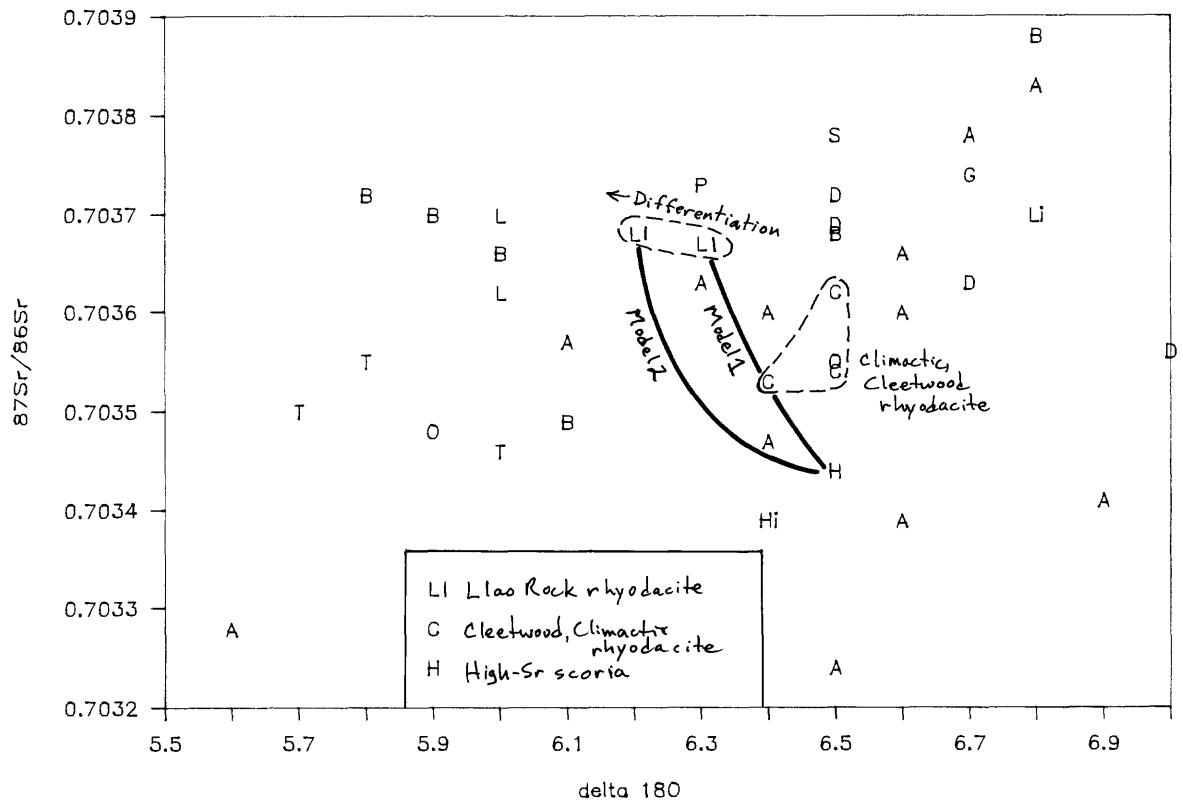

Fig. 12. $^{87}Sr/^{86}Sr$ vs. $\delta^{18}O$. Symbols as in Fig. 1 except as indicated in figure; also, L = low-Sr scoria, Li = low-Sr inclusion, S = Sharp Peak, P = Pleistocene evolved rhyodacite (Steel Bay), R = postcaldera rhyodacite, O = olivine-bearing scoria. Field of Cleetwood and climactic rhyodacite stippled. Llao Rock field (Ll) outlined by dashed curve; arrow shows trend to more differentiated sample.

The small postcaldera rhyodacite dome is substantially younger than postcaldera andesites, having been erupted around 4250 yr. B.P. [S. W. Robinson, unpub. data, 1988]. Bacon and Druitt [1988] suggested that this magma probably formed from postcaldera andesitic magma by AFC but did not identify a specific assimilant. Postcaldera rhyodacite plots with evolved Pleistocene rhyodacites in terms of $^{87}Sr/^{86}Sr$ (0.70372 ± 3) and Sr content (Figure 13) but has $\delta^{18}O_{pl}$ = +6.5 like climactic rhyodacite (R, Figure 12). A successful AFC model starts with postcaldera andesite (660 ppm Sr, $^{87}Sr/^{86}Sr$ = 0.70359, $\delta^{18}O$ = +6.4), uses a Sr-rich (e.g., 700 ppm) assimilant with comparatively high $^{87}Sr/^{86}Sr$ (0.7038) and $\delta^{18}O$ (+6.7), and crystallizes ~45% with r = 0.5 (the ratio of assimilated material to cumulate) and a bulk partition coefficient (D) of 2. Whether this is realistic is debatable, but the model illustrates the general requirements of deriving postcaldera rhyodacite from andesite by AFC: large D and r, and an assimilant with high $^{87}Sr/^{86}Sr$, Sr content, and $\delta^{18}O$. Alternative scenarios for the origin of the rhyodacite that would be consistent with the isotopic data include separation from relatively high-^{18}O LSr cumulate mush

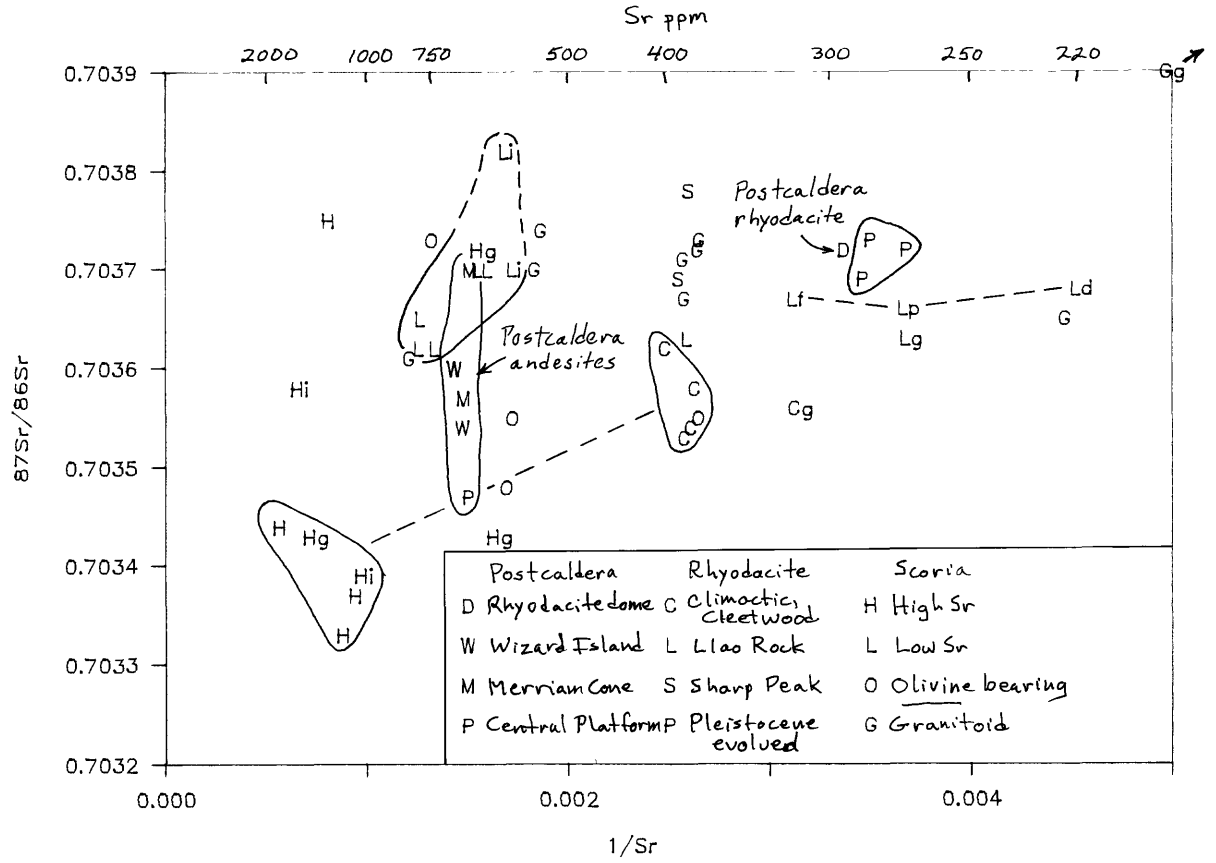

Fig. 13. $^{87}Sr/^{86}Sr$ vs. 1/Sr for preclimactic rhyodacites, climactic ejecta, and postcaldera lavas (Figure 11 with postcaldera lavas added). Ld = Llao Rock dike, Lp = early Llao Rock pumice, Lf = Llao Rock flow; suffix "g" indicates glass separate, "i" inclusion.

or mobilization of evolved preclimactic rhyodacite magma, either of which might have survived reorganization of the system during and following the climactic eruption. Neither of these models is amenable to testing, however, and the origin of the postcaldera rhyodacite remains enigmatic.

DISCUSSION

Results of this study bear on more general problems of arc magmatism and the Cascades in particular.

Isotopic Heterogeneity

Quaternary volcanic rocks of the Crater Lake area, and those of Mount Mazama itself, have variable isotopic compositions. This type of variation has been noted in other volcanic fields of sufficient lifespan and areal extent [e.g., Gerlach et al., 1988].

Sources. The range in $^{87}Sr/^{86}Sr$ among basalts and basaltic andesites may be ascribed to heterogeneity in primary liquid sources only if one accepts that lava isotopic compositions have not been modified in the crust. This may be the case for the primitive tholeiites. If also true for magnesian basaltic andesite (Red Cone), which has near-primary compatible element contents but

relatively radiogenic Sr, then at least two mantle sources were tapped. A possible reason for this postulated mantle heterogeneity might be variations in a slab-derived component added to the mantle wedge. Note, however, that tholeiite $^{87}Sr/^{86}Sr$ values are higher than might be expected for such low-Rb magmas and that $^{87}Sr/^{86}Sr$ is correlated with Ba and Sr, the only mantle-incompatible elements enriched in these magmas beyond MORB levels [Bacon, 1989]. Whether some Sr in primitive tholeiites was added to the mantle source by a subduction-related process [McCulloch and Perfit, 1981; Ewart and Hawkesworth, 1987] or was acquired in the deep crust [Arculus and Johnson, 1981] is equivocal.

It appears likely that basaltic andesites took on some of their isotopic variability during fractionation, presumably in the deep crust. The only compositional parameter that appears to show a (weak negative) correlation with $^{87}Sr/^{86}Sr$ is Yb content (Figure 4). This suggests that exchange of Sr with garnetiferous deep crustal rocks, which would retain HREE, increases $^{87}Sr/^{86}Sr$ in the more HREE-poor basaltic andesites. As noted above, crustal interaction would be consistent with elevated $\delta^{18}O$ in most basaltic andesites relative to the more primitive lavas. The "sources" of basaltic andesites thus probably contain variable fractions of isotopic components from the mantle wedge, subducted slab, and deep crust.

Andesites show the widest range of $^{87}Sr/^{86}Sr$. Logically, this reflects the same processes and "source" heterogeneities of their basaltic andesitic parents, effects of AFC being more pronounced in andesites. That andesites show the lowest $^{87}Sr/^{86}Sr$ can be attributed either to lack of eruption of basaltic andesite with similar isotopic characteristics or to an added nonradiogenic component, such as might be acquired during AFC with a relatively young basaltic assimilant or its partial melt.

Magma Chambers. The climactic eruption and related preclimactic lavas offer an example of isotopic heterogeneity in a crustal chamber: minor variability in silicic magmas, and a large range in andesitic magmas and cumulates. Presumably, heterogeneity, at least in radiogenic isotopes, would have been preserved on solidification if the system had not vented catastrophically. Variability in postcaldera andesite $^{87}Sr/^{86}Sr$ suggests even what remains of the system, which should include a large volume of cumulate and hybrid material [Bacon and Druitt, 1988], would freeze to an isotopically heterogeneous pluton because of the large degree of crystallinity of many scoria samples. Because inputs to the climactic chamber were isotopically diverse at a measurable level it follows that crustal magma chambers, even those located in impressively nonradiogenic crust, may solidify as isotopically heterogenous plutons unless somehow homogenized by late convective motions that are difficult to rationalize in largely-crystalline systems. Indeed, examples of heterogeneous plutons are becoming increasingly well known [Kistler et al., 1987; Hill and Silver, 1988].

Magmatic Inclusions. Lacking catastrophic pyroclastic eruptions, compelling evidence for isotopic heterogeneity in crustal systems resides in magmatic inclusions, or enclaves, in silicic lavas. Sr isotopic contrasts between andesitic inclusions and their andesite, dacite, and rhyodacite hosts at Crater Lake are commonplace and reflect additions of new magma to crustal reservoirs. Because inclusions partially to completely crystallize rapidly on incorporation into more felsic magma, plutonic solidification is unlikely to destroy these contrasts unless intracrystalline diffusion of Sr or recrystallization can homogenize isotopic compositions of host and inclusions. Inclusion and host compositions, however, may be modified by differential motion of intergranular residual liquid or by diffusion between this and liquid remaining in the host.

Low-^{18}O Silicic Magmas

Occurrence of silicic magmas with low primary $\delta^{18}O$ is uncommon but well established. It has been suggested that these erupted magmas owe their O isotopic composition to interaction with large volumes of isotopically light water [Friedman et al., 1974; Lipman et al., 1975; Hildreth et al., 1984] or to assimilation of hydrothermally altered crustal rocks [Taylor, 1977, 1987; Grunder, 1987]. The partially melted granitoids ejected in the climactic eruption of Mount Mazama, which are believed to represent wall rock whose melt fraction was insufficient for plastic flow, support the assimilation hypothesis. Because their chemical compositions are similar to many erupted Mazama dacites (they may be solidified earlier Mazama magmas) assimilation would leave little, if any, detectable chemical signature. Nevertheless, reductions in $\delta^{18}O$ due to exchange with hydrothermal fluids in a subvolcanic environment are profound. Closed-system high-temperature reequilibration of O isotopes in the partially melted rocks indicates that residual crystals, both quartz and feldspar, would not show isotopic fractionation that would indicate a hydrothermally altered source. Only if incorporation into and residence in silicic magma failed to again homogenize O isotopes would a xenocrystic origin of quartz and feldspar be apparent. Thus, the assimilation of hydrothermally altered rock hypothesis is the most reasonable origin of low-^{18}O magmas.

Nature of the Crust in the Southern Oregon Cascades

A mass of literature, exemplified by the recent comprehensive paper by Hildreth and Moorbath [1988], has demonstrated that effects of crustal interaction are evident in arc lavas when the crust is sufficiently distinctive and thick. However, the range of Sr and O isotopic composition in the Crater Lake lavas is virtually the same as in the intraoceanic Volcano and Mariana island arcs [Ito and Stern, 1985/86], which lack continental crust but where interaction with the thickened arc crust cannot be ruled out. Davidson et al. [1987] have shown that consideration of trace element abundances and ratios along with isotopic data can indicate presence of a crustal component where the crust is not isotopically distinctive. Accepting that crustal interaction has affected the Crater Lake area rocks, the isotopic data help to constrain possible crustal composition.

Upper Crust. The upper crust is likely to be composed of <10 km of Cenozoic volcanic and local intrusive rocks [Smith et al., 1982]. Data for products of the shallow climactic chamber do not indicate major O isotopic exchange with either upper crustal sedimentary or weathered igneous rocks. Neither is there Sr isotopic evidence in evolved magmas for assimilation of pre-Cenozoic supercrustal rocks, as might have been detected were such materials present in the environment of the climactic chamber. Evolved magmas apparently did include a component of hydrothermally-altered upper-crustal igneous rocks, as described above.

Lower Crust. Bacon [1989] argued that the elemental abundance patterns were established in andesites and more primitive magmas at depths greater than the upper crustal climactic chamber. Similarly, Hildreth and Moorbath [1988] indicated that crustal modification of Andean lavas takes place near the base of the crust. If we accept that some of the chemical variability among the basaltic andesites and, possibly, andesites came about through AFC in the deep crust, then the isotopic compositions of these lavas can be used to constrain lower crustal composition. Models presented above suggest the increase in $\delta^{18}O$ over primitive lava values reflects assimilation or exchange with mafic rocks that were rich in ^{18}O owing to prior low-temperature alteration or were themselves derived from such a source. Sr isotopic compositions indicate assimilants with low to modest present-day $^{87}Sr/^{86}Sr$. Metaigneous rocks

of the Klamath Mountains province appear to be consistent with these isotopic constraints, and such materials or their underpinnings could be present deep beneath Crater Lake. Alternatively, the deep crust is composed of Cenozoic mafic metaigneous rocks emplaced during extension at the margin of the Basin and Range province. Although consistent with the Sr isotopic data, this model cannot be reconciled with results for O without postulating abnormally high $\delta^{18}O$ primary liquids.

Subduction Component

Trace element abundances of Crater Lake basaltic andesites argue for an added component derived by transfer of aqueous fluid from the subducted slab to the mantle wedge, and thus contributed to parental basaltic liquids [Bacon, 1989]. By analogy with other arcs [e.g., Davidson, 1987; Ewart and Hawkesworth, 1987], at least part of this subduction component is derived via fluid released from subducted sediment and oceanic crust. Mass balance considerations suggest a subduction component would affect O isotopic composition little but Sr, and particularly Pb, compositions significantly. The tendency for the most LILE-rich lavas to have relatively radiogenic Sr may result from a subduction component, as may the rather high $^{87}Sr/^{86}Sr$ of the tholeiites. Because the source of potentially subducted sediment consists of relatively youthful and nonradiogenic materials, isotopic contrast necessary for confirming a sediment-derived component is lacking.

SUMMARY AND CONCLUSIONS

Basaltic to andesitic lavas from the Crater Lake area and from Mount Mazama itself have a range of Sr and O isotopic compositions. The lowest $^{87}Sr/^{86}Sr$ values are found in andesites, with primitive tholeiites having intermediate and shoshonitic basaltic andesites the highest ratios. Geographic variation in $^{87}Sr/^{86}Sr$ among basaltic andesites and andesites suggests discrete vent provinces of low, intermediate, and high ratios. The range in $^{87}Sr/^{86}Sr$ is greatest in andesites (~0.7032-0.7039) and decreases through dacites to a nearly constant value of ~0.7037 in rhyodacites. Climactic rhyodacite, however, has lower $^{87}Sr/^{86}Sr$ (0.70355), apparently reflecting a component derived from Sr-rich low-$^{87}Sr/^{86}Sr$ andesitic magma [Bacon and Druitt, 1988]. Andesitic to mafic cumulate scoriae of the climactic eruption have variable $^{87}Sr/^{86}Sr$ that is generally inversely correlated with Sr content and reflects incremental growth and filling of the climactic chamber with andesitic to basaltic magmas possessing a range of isotopic compositions. Andesitic enclaves in andesitic to rhyodacitic lavas also show a range of isotopic compositions that generally are different from those of their hosts. Postcaldera andesites are chemically similar but have a significant range of $^{87}Sr/^{86}Sr$. Isotopic heterogeneity may be the rule in igneous systems as long as sampling is adequate and protracted cooling or recrystallization have not resulted in homogenization.

Oxygen isotopic compositions suggest that all Crater Lake area magmas except tholeiites and primitive basaltic andesites contain a component derived from metaigneous rocks, presumably acquired in the deep crust. Combined assimilation and fractional crystallization in this environment may be responsible for extending the range of Sr isotopic compositions as well. The isotopic data appear to be consistent with presence in the deep crust beneath Crater Lake of metamorphosed equivalents of nonradiogenic but rather ^{18}O-rich igneous rocks such as exposed in the Klamath Mountains.

Partially-fused granitoid blocks ejected in the climactic eruption have $^{87}Sr/^{86}Sr$ similar to Mazama dacites and rhyodacites but have $\delta^{18}O$ as low

as +0.6. Quartz and plagioclase have similar $\delta^{18}O$ in each of three samples, indicating closed-system high-temperature reequilibration of O isotopes following exchange with hydrothermal fluids. This hydrothermal exchange was responsible for lowering $\delta^{18}O_{pl}$ but not necessarily $\delta^{18}O_{qz}$ before partial fusion. The granitoids are believed to be fragments of the chamber wall that, because of insufficient melt fraction, were not incorporated into the climactic magma. This wall had remained in a steady thermal state for sufficient time for growth of new crystals and O isotopic equilibration of refractory phases before the climactic event. The granitoids are evidence that low ^{18}O magmas can form by assimilation of hydrothermally altered wallrocks in a shallow environment. One scoria sample that was inferred on chemical grounds to contain a significant fraction of assimilated material and contains rhyodacitic interstitial glass has $\delta^{18}O_{pl}$ of +4.7, apparently resulting from this process.

Acknowledgments. We thank S.H. Gunn and A.L. Berry for determining Sr isotopic compositions, L.H. Adami for O isotopic measurements, and M. Hanning and T.H. Druitt for making mineral separations. A review by J.M. Donnelly-Nolan resulted in improvement in the manuscript.

REFERENCES

Arculus, R. J., and R. W. Johnson, Island-arc magma sources: a geochemical assessment of the roles of slab-derived components and crustal contamination, Geochem. Journal, 15, 109-133, 1981.

Armstrong, R. L., W. H. Taubeneck, and P. O. Hales, Rb-Sr and K-Ar geochronometry of Mesozoic granitic rocks and their Sr isotopic composition, Oregon, Washington, and Idaho, Geol. Soc. Am. Bull., 88, 397-411, 1977.

Arzi, A. A., Critical phenomena in the rheology of partially melted rocks, Tectonophysics, 44, 173-184, 1978.

Bacon, C. R., Eruptive history of Mount Mazama and Crater Lake caldera, Cascade Range, USA, J. Volcanol. Geotherm. Res., 18, 57-115, 1983.

Bacon, C. R., Magmatic inclusions in silicic and intermediate volcanic rocks, J. Geophys. Res., 91, 6091-6112, 1986.

Bacon, C. R., Mount Mazama and Crater Lake caldera, Oregon, Geol. Soc. Am. Centennial Field Guide, 1, 301-306, 1987a.

Bacon, C. R., Granitoid blocks in climactic ejecta of Mount Mazama, Oregon: Quenched samples of a magma chamber's partially fused walls, Geol. Soc. Am. Abstr. Prog., 19, no. 7, 577, 1987b.

Bacon, C. R., Calc-alkaline, shoshonitic, and primitive tholeiitic lavas from monogenetic volcanoes near Crater Lake, Oregon, J. Petrol., submitted, 1989?.

Bacon, C.R., and T. H. Druitt, Compositional evolution of the zoned calcalkaline magma chamber of Mount Mazama, Crater Lake, Oregon, Contr. Mineral. Petrol., 98, 224-256, 1988.

Borthwick, J., and R. S. Harmon, A note regarding ClF_3 as an alternative to BrF_5 for oxygen isotope analysis, Geochim. Cosmochim. Acta, 46, 1665-1668, 1982.

Bullen, T. D., and M. A. Clynne, Geochemical and isotopic constraints on magmatic evolution at Lassen volcanic center, California, This Report

Criss, R. E., and H. P. Taylor, Jr., An $^{18}O/^{16}O$ and D/H study of Tertiary hydrothermal systems in the southern half of the Idaho Batholith, Geol. Soc. Am. Bull., 94, 640-663, 1983.

Davidson, J. P., Crustal contamination versus subduction zone enrichment: Examples from the Lesser Antilles and implications for mantle source compositions of island arc volcanic rocks, Geochim. Cosmochim. Acta., 51, 2185-2198, 1987.

Davidson, J. P., M. A. Dungan, K. M. Ferguson, and M. T. Colucci, Crust-magma interactions and the evolution of arc magmas: The San Pedro - Pellado volcanic complex, southern Chilean Andes, Geology, 15, 443-446, 1987.

DePaolo, D. J., Trace element and isotopic effects of combined wallrock assimilation and fractional crystallization, Earth Planet. Sci. Lett., 53, 189-202, 1981.

Druitt, T. H., and C. R. Bacon, Lithic breccia and ignimbrite erupted during the collapse of Crater Lake caldera, Oregon, Jour. Volcanol. Geotherm. Res., 29, 1-32, 1986.

Druitt, T. H., and C. R. Bacon, Summary of compositional zonation and cumulus processes in the Mount Mazama magma chamber, Crater lake, Oregon, Phil. Trans. Roy. Soc. Edinburgh, in press, 1988.

Druitt, T. H., and C. R. Bacon, Petrology of the zoned calcalkaline magma body at Mount Mazama (Crater Lake), Oregon, Contr. Mineral. Petrol., in press, 1989?.

Ewart A., and C. J. Hawkesworth, The Pleistocene-recent Tonga-Kermadec arc lavas: interpretation of new isotopic and rare earth data in terms of a depleted mantle source model, J. Petrology, 28, 495-530, 1987.

Fiebelkorn, R. B., G. W. Walker, N. S. MacLeod, E. H. McKee, and J. G. Smith, Index to K-Ar age determinations for the state of Oregon, U. S. Geol. Survey Open-File Rept. 82-596.

Friedman, I., P. W. Lipman, J. D. Obradovich, J. D. Gleason, and R. L. Christiansen, Metoric water in magmas, Science, 184, 1069-1072, 1974.

Gerlach, D. C., F. A. Frey, H. Moreno-Roa, and L. Lopez-Escobar, Recent volcanism in the Puyehue--Cordon Caulle region, southern Andes, Chile (40.5°S): Petrogenesis of evolved lavas, J. Petrol., 29, 333-382, 1988.

Grunder, A. L., Low $\delta^{18}O$ silicic volcanic rocks at the Calabozos caldera complex, southern Andes, Contrib. Mineral. Petrol., 95, 71-81.

Hart, W. K., Chemical and isotopic evidence for mixing between depleted and enriched mantle, northwestern U.S.A., Geochem. Cosmochim. Acta, 49, 131-144, 1985.

Haskin, L. A., M. A. Haskin, F. A. Frey, and T. R. Wildeman, Relative and absolute terrestrial abundances of the rare earths, in Origin and distribution of the elements, edited by L. H. Ahrens, pp. 889-912, Pergamon Press, 1968.

Hildreth, W., and S. Moorbath, Crustal contributions to arc magmatism in the Andes of Central Chile, Contr. Mineral. Petrol., 98, 455-489, 1988.

Hildreth, W., R. L. Christiansen, and J. R. O'Neil, Catastrophic isotopic modification of rhyolitic magma at times of caldera subsidence, Yellowstone Plateau volcanic field, J. Geophys. Res., 89, 8339-8369, 1984.

Hill, R. I., and L. T. Silver, San Jacinto intrusive complex 3. Constraints on crustal magma chamber processes from strontium isotope heterogeneity, J. Geophys. Res., 93, 10,373-10,388, 1988.

Ito, E., and R. J. Stern, Oxygen- and strontium-isotopic investigations of subduction zone volcanism: the case of the Volcano Arc and the Marianas Island Arc, Earth Planet. Sci. Lett., 76, 312-320, 1985/86.

Kay, R. W., Aleutian magnesian andesites: melts from subducted Pacific Ocean crust, J. Volcanol. Geotherm. Res., 4, 117-132, 1978.

Kay, R. W., Volcanic arc magmas: implications of a melting-mixing model for element recycling in the crust-upper mantle system, J. Geol., 88, 497-522, 1980.

Kistler, R. W., B. W. Chappell, D. L. Peck, and P. C. Bateman, Isotopic variation in the Tuolumne Intrusive Suite, central Sierra Nevada, California, Contrib. Mineral. Petrol., 94, 205-220, 1986.

Kyser, T. K., Stable isotope variations in the mantle, in Stable isotopes in high temperature geological processes edited by J. W. Valley, H. P. Taylor, Jr., and J. R. O'Neil, Reviews in Mineralogy, 16, 141-164, Mineral. Soc. Am., 1986.

Langmuir, C. H., R. D. Vocke, Jr., G. N. Hanson, and S. R. Hart, A general mixing equation with applications to Icelandic basalts, Earth Planet. Sci. Lett., 37, 380-392, 1978.

Leaver, D. S., W. D. Mooney, and W. M. Kohler, A seismic refraction study of the Oregon Cascades, J. Geophys. Res., 89, 3121-3134, 1984.

LeBas, M. J., R. W. LeMaitre, A. Streckeisen, and B. Zanettin, A chemical classification of volcanic rocks based on the total alkali-silica diagram, J. Petrology, 27, 745-750, 1986.

Lipman, P. W., and I. Friedman, Interaction of meteoric water with magma: An oxygen-isotope study of ash-flow sheets from southern Nevada, Geol. Soc. Am. Bull., 86, 695-702, 1975.

Marsh, B. D., On the crystallinity, probability of occurrence, and rheology of lava and magma, Contrib. Mineral. Petrol., 78, 85-98, 1981.

Masi, U., J. R. O'Neil, and R. W. Kistler, Stable isotope systematics in Mesozoic granites of central and northern California and southwestern Oregon, Contrib. Mineral. Petrol., 76, 116-126, 1981.

Matsuhisa, Y., and H. Kurasawa, Oxygen and strontium isotopic characteristics of calc-alkalic volcanic rocks from the central and western Japan arcs: evaluation of contribution of crustal components to the magmas, J. Volcanol. Geotherm. Res., 18, 483-510, 1983.

McBirney, A. R., H. P. Taylor, and R. L. Armstrong, Paricutin re-examined: a classic example of crustal assimilation in calc-alkaline magma, Contr. Mineral. Petrol., 95, 4-20, 1987.

McCulloch, M. T., and M. R. Perfit, $^{143}Nd/^{144}Nd$, $^{87}Sr/^{86}Sr$ and trace element constraints on the petrogenesis of Aleutian island arc magmas, Earth Planet. Sci. Lett., 56, 167-179, 1981.

Riddihough, R., C. Finn, and R. Couch, Klamath-Blue Mountain lineament, Oregon, Geology, 14, 528-531, 1986.

Smith, J. G., N. J. Page, M. G. Johnson, B. C. Moring, and F. Gray, Preliminary geologic map of the Medford 1° x 2° quadrangle, Oregon and California, scale 1:250,000, U. S. Geol. Surv. Open-file Rep., 82-955, 1982.

Sparks, R. S. J., and L. A. Marshall, Thermal and mechanical constraints on mixing between mafic and silicic magmas, J. Volcanol. Geotherm. Res., 29, 99-124, 1986.

Stern, J. R., Strontium isotopes from circum-Pacific intra-oceanic island arcs and marginal basins: Regional variations and implications for magmagenesis, Geol. Soc. Am. Bull., 93, 477-486, 1982.

Tatsumi, Y., D. L. Hamilton, and R. W. Nesbitt, Chemical characteristics of fluid phase released from a subducted lithosphere and origin of arc magmas: Evidence from high-pressure experiments and natural rocks, J. Volcanol. Geotherm. Res., 29, 293-309, 1986.

Taylor, H. P., Jr., Water/rock interactions and the origin of H_2O in granitic batholiths, J. Geol. Soc. Lon., 133, 509-558, 1977.

Taylor, H. P., Jr., The effects of assimilation of country rocks by magmas on $^{18}O/^{16}O$ and $^{87}Sr/^{86}Sr$ systematics in igneous rocks, Earth. Planet. Sci. Lett., 47, 243-254, 1980.

Taylor, H. P., Jr., Comparison of hydrothermal systems in layered gabbros and granites, and the origin of low-^{18}O magmas, in Magmatic Processes: Physicochemical Principles, edited by B. O. Mysen, pp. 337-357, Geochem. Soc. Spec. Pub. 1, 1987.

Taylor, H. P., Jr., and S. M. F. Sheppard, Igneous rocks: I. Processes of isotopic fractionation and isotope systematics, in Stable isotopes in high temperature geological processes edited by J. W. Valley, H. P. Taylor, Jr., and J. R. O'Neil, Reviews in Mineralogy, 16, 227-271, Mineral. Soc. Am., 1986.

Thompson, J. M., L. D. White, and M. Nathenson, Chemical analyses of waters from Crater Lake, Oregon, and nearby springs, U. S. Geol. Survey Open-File Rept. 87-587, 16 p., 1987.

White, W. M., and J. Patchett, Hf-Nd-Sr isotopes and incompatible element abundances in island arcs: implications for magma origins and crust-mantle evolution, Earth Planet. Sci. Lett., 67, 167-185, 1984.

Williams, H., The geology of Crater Lake National Park, Oregon, Carnegie Inst. Washington Publ. 540, 162pp, 1942.

IMPLICATIONS OF POST-11,000-YEAR VOLCANISM AT MEDICINE LAKE VOLCANO, NORTHERN CALIFORNIA CASCADE RANGE

by Julie M. Donnelly-Nolan[1], Duane E. Champion[1], C. Dan Miller[2], and Deborah A. Trimble[1]

[1]U.S. Geological Survey, Menlo Park CA 94025
[2]U.S.G.S. Cascades Volcano Observatory, Vancouver WA 98661

ABSTRACT

Eruptive activity during the past 11,000 years at Medicine Lake volcano has been strongly episodic. Eight eruptions produced about 5.3 km^3 of basaltic lava during a few-hundred-year time interval about 10,500 BP, followed by a hiatus, then one small andesitic eruption at about 4300 BP. Approximately 2.5 km^3 of compositions ranging from basalt to rhyolite was vented in eight eruptions between about 2000 BP and 900 BP. Late Holocene andesitic to rhyolitic lavas were probably derived by fractionation, assimilation, and mixing from high-alumina basalt parental magma, possibly from basalt intruded into the volcano during the early mafic episode. A compositional gap in erupted lavas between 57 and 62% SiO_2 is spanned by chilled magmatic inclusions in late Holocene silicic lavas. The eruptive activity is probably driven by intrusions of basalt that occur during local extensional events in this back-arc setting dominated by regional E-W stretching of the crust. Vents are typically aligned parallel or subparallel to major structural features, most commonly within 30° of north. The nature and timing of future volcanic activity cannot be predicted from the observed pattern, but eruptions high on the edifice could produce high-silica products that might be accompanied by explosive activity, whereas eruptions lower on the flanks are likely to vent mafic lavas.

INTRODUCTION

Medicine Lake volcano is a large Pleistocene and Holocene shield volcano located east of the main Cascade axis in northern California (Figure 1). Most products of the volcano have normal magnetic polarity, suggesting that it erupted mainly during Brunhes time; maximum age is probably about 1 Ma although K-Ar data are insufficient to define the older limit (Mertzman, 1982, 1983; J.M. Donnelly-Nolan and L.B.G. Pickthorn, unpublished K-Ar data, 1980-1988). A broad range of compositions has erupted, from basalt through rhyolite, although dacites are under-represented. Mafic lavas have dominated in terms of volume and number of events.

Post-11,000-yr volcanism at Medicine Lake volcano includes a wide range of chemical compositions arrayed over a large area of the volcano. Figure 2 shows the distribution of these lavas; vent locations are shown on Figure 3. Tectonic control of vent alignments is pronounced in this extensional "back-arc" environment.

Volcanic activity since 11,000 years ago has been strongly episodic. The period began with voluminous basaltic eruptions and culminated in the late Holocene with an episode dominated by silicic volcanism. During the intervening time of about 8,000 years only one small silicic andesite eruption occurred.

PREVIOUS WORK

Previous geologic and petrologic work includes Powers (1932), Anderson (1933), Anderson (1941), Condie and Hayslip (1975), Mertzman (1977a, 1977b), and Mertzman and Williams (1981). More recent papers include petrologic work by Grove and co-workers (Grove et al, 1982; Gerlach et al, 1982; Grove and Baker, 1984; Grove and Donnelly-Nolan; Grove et al, 1988) and a summary of the geology by Donnelly-Nolan (1988). Discussion of the application of paleomagnetic methods to "dating" young lava flows is found in Champion (1980) and Kuntz et al (1986).

DESCRIPTION OF POST-11,000-YR LAVAS

The lavas described here are all unglaciated and very young in appearance. Donnelly-Nolan (1988, Figure 2) included all of these lavas in the Holocene, but radiocarbon ages reported here (Table 1) indicate that some of them erupted in the few hundred years just prior to 10,000 yrs BP and are thus pre-Holocene in age. Seventeen eruptive units have been mapped and are shown on Figure 2. None erupted from only a single vent. The mafic lavas typically erupted from alignments of spatter cones, from pit craters, from cinder cones, or from a combination of vent types. In the largest of the mafic eruptions, the Giant Crater event (No.4 on Figure 2), lava erupted from a complex of vents in three different alignments (N5E, N20W, N55E). Airfall tephra deposits are known to have accompanied several of the late Holocene mafic and silicic eruptions. The silicic lavas erupted from alignments of vents that produced flows and domes, some of which coalesced.

Table 2 lists the seventeen units, their range of silica content, trend of vents, area covered, and estimated volume. Figure 4 displays some of this information in graphical form showing that the distribution of the events in time has been strongly episodic. Each of the units is described below, beginning with the products of the early mafic episode, followed by the mid-Holocene andesite, then the late Holocene episode.

Early mafic episode

The early mafic episode includes 8 units all of which erupted on the flanks of the volcano. Paleomagnetic and radiocarbon data suggest that this eruptive episode lasted about 400 years. The radiocarbon dates alone suggest a longer time span, but all of them were on material collected from large tree molds. Large trees (approximately 1 meter in diameter) at Medicine Lake volcano typically possess 400 or more growth rings. Large tree molds commonly yield fragments of charcoal that cannot be assigned to a particular part of the tree and thus may give an age that is hundreds of years too old. Charcoal from small tree molds would yield more accurate results but small molds are difficult to sample because they are too small to climb into. Radiocarbon dates may be too young if they are contaminated by younger charcoal or organic material, for example from much later forest fires.

A very small basalt flow just south of the Paint Pot Crater flow.is morphologically similar to the units of the early mafic episode. No material for radiocarbon dating has been found under this flow and paleomagnetic data are neither precise nor apparently similar to the directions of the early mafic event. One possible correlation is with units of similar paleomagnetic direction at Mt. Shasta, dated at about 9500 years BP. More likely this unit is somewhat older, post-glacial but pre-11,000 years.

Pre-Giant Crater basalts

The basalt of Giant Crater was produced in one of the largest known events in the history of Medicine Lake volcano. Its estimated 5 km^3 of lava represents nearly $^2/_3$ of the total estimated volume of lavas erupted during the last 11,000 years. On the basis of paleomagnetic and stratigraphic superposition, four units are thought to be precursors:

Spatter vents surrounded by Double Hole flow (Table 2, No. 1)

These small spatter vents are completely surrounded by younger lava from the Double Hole Crater vent of the basalt of Giant Crater. It is unknown whether a lava flow or flows may be associated with them. They are also undated by radiocarbon, but paleomagnetic data (Figure 5) suggest that they immediately preceded the eruption of Giant Crater lavas.

Basalt of the ribbon flows (Table 2, No. 2)

This unit erupted from numerous spatter vents located N of the Burnt Lava flow. The basalt flowed down 2 narrow channels that were probably cut by glacial meltwater. The southernmost extent of this unit is at the south edge of the Burnt Lava flow. Most of the unit is buried by Burnt Lava; thus estimates of its area are highly uncertain. Charcoal from a large tree mold in the eastern flow gives a radiocarbon age of 10,310±60 BP (Table 1, No. 2).

Paleomagnetic data indicate that the eruption occurred immediately prior to the Giant Crater eruption.

Spatter E. of Grasshopper Flat (Table 2, No. 3)

A small amount of basaltic lava was erupted from a N-S alignment of spatter vents less than 4 km NW of Giant Crater proper. A radiocarbon date (10,930±50 BP, Table 1, No. 3) on charcoal collected from a large tree mold places this unit in this time frame. Although the date which suggests that this unit is several hundred years older than Giant Crater basalt may be too old for reasons discussed above, paleomagnetic data (Figure 5a) indicate that it erupted just prior to the Giant Crater eruption.

Basalt of Giant Crater (Table 2, No. 4)

This 45-km-long basalt flow covers more than 15% of the area underlain by Medicine Lake lavas. Two radiocarbon dates on charcoal samples obtained from a single large tree mold in the flow average 10,600 BP (Table 1, No.4). We have arbitrarily chosen this date as the "real" one to which others in this early mafic event are compared (a simple numerical average of the 7 dates for this episode gives 10,549 BP).

The basalt of Giant Crater is compositionally zoned such that the earliest lava is most silicic (52.7% SiO2), the latest is most mafic (47.2% SiO2). Paleomagnetic sampling of early and late phases of the eruption yielded very slight differences in direction suggesting a measurable but very short time duration for this large-volume eruption.

Probable successors to the basalt of Giant Crater

Four additional units are thought to have erupted soon after the basalt of Giant Crater. Three of the four are located on the north side of the volcano (Figure 2).

Basalt of "vent 5" (Table 2, No. 5)

Located at the western edge of the Giant Crater flow, this very small basalt flow clearly overlies the youngest Giant Crater lava. Charcoal from a large tree mold yields a radiocarbon date of 10,355±50 BP (Table 1, No. 5). Paleomagnetic data for this event are not as well constrained as those previously discussed, but the average direction of 2 sites indicates that the event just post-dates the Giant Crater eruption although the relative age with respect to the three other successor eruptions is unknown.

Tree molds flow (Table 2, No. 6)

This very small basalt flow located on the upper north side of the volcano has a radiocarbon date of 10,200±110 BP on charcoal from a large tree mold (Table 1, No. 6). Paleomagnetic data suggest a short time interval of perhaps 50-100 years between the Giant Crater eruption and the eruption of the tree molds flow. The difference in the radiocarbon ages is 400 years, indicating that one or both radiocarbon dates may not be dating the time of eruption accurately.

Basalt of Devils Homestead (Table 2, No. 7)

This undated flow on the far north side of the volcano has a paleomagnetic direction identical to that of the tree molds flow. The Devils Homestead flow is located in a very dry area on the lower flank of the volcano. The downstream, aa portion of the flow has a very youthful appearance. However, the near-vent pahoehoe lava is relatively heavily vegetated and its edges are covered with sediment. Overall, the morphology of the flow is similar to the basalt of Valentine Cave which is situated in a climatically similar area of the volcano.

Basalt of Valentine Cave (Table 2, No. 8)

Also erupted on the north side of the volcano, the basalt of Valentine Cave (Donnelly-Nolan and Champion, 1987) has a radiocarbon date of 10, 850±60 BP (Table 1, No. 8) on charcoal collected from a large tree mold. Paleomagnetic data suggest that this basalt may have erupted about 100 years after the tree molds flow and the basalt of Devils Homestead. If the Giant Crater date of 10,600 BP is correct, then the Valentine Cave flow radiocarbon date is about 400 years too old, which is easily possible if the sampled charcoal represented wood from the center of the tree.

Mid-Holocene episode

Andesite of the pit craters (Table 2, No. 9)

This unit consists of silicic andesite erupted explosively as airfall tephra and spatter from a NE-trending alignment of pit craters located on the poorly-defined SE rim of the caldera. Charcoal collected at two near-vent sites from under the tephra deposit has radiocarbon ages of 4430±70 BP and 4280±40 BP (Table 1, No. 9). The charcoal is thought to have been formed when coarse, hot blocks of airfall scoria scorched forest duff and debris.

Late Holocene episode

Paleomagnetic data indicate a possible time span of about 1100 yrs for the late Holocene episode which produced both mafic and silicic products from numerous vents scattered over much of the volcano, including the caldera.

Medicine dacite flow (Table 2, No. 10)

This viscous, pancake-like flow, located just north of Medicine Lake on the floor of the caldera, is undated but is morphologically very young. Unlike the other Holocene silicic units, it apparently lacks a preceding airfall tephra deposit and presents little opportunity for collecting radiocarbon samples. It is overlain by airfall tephra from the Callahan, Paint Pot, Little Glass Mountain and Glass Mountain eruptions, and thus is older than about 1150 yrs BP. Paleomagnetic data indicate an age of about 2000 yrs BP based on comparison with directions of magnetization from radiocarbon-dated basalt flows at the Craters of the Moon, Idaho, and Mt. St. Helens, Washington (Champion, 1980).

Basalt of Black Crater and Ross Chimneys (Table 2, No. 11)

A small amount of fluid, relatively primitive basalt erupted from en echelon alignments of spatter cones to form tiny overlapping pahoehoe flows on the far north side of the volcano in Lava Beds National Monument (Donnelly-Nolan and Champion, 1987). The lava presents a very youthful appearance although it is overlain by a thin dusting of white pumice from either the Glass Mountain or Little Glass Mountain eruption. Located in a dry, relatively treeless area, this unit is undated by radiocarbon, but paleomagnetic data indicate a possible age of about 1250 yrs based on comparison with the American Southwest archaeomagnetic record (Sternberg, 1982). Comparable paleomagnetic directions occurred at about 3200 BP, 3600 BP, and 4000 BP (Champion, 1980), but we consider the morphologic appearance of this unit to be younger than these alternatives.

Hoffman flows (Table 2, No. 12)

This unit includes the Hoffman flow proper as recognized by Powers (1932) as well as a perlitic rhyolite flow on the NE shoulder of Mt. Hoffman described by Anderson (1941). These 2 flows are identical in appearance and chemical composition, their vents line up on a N30W trend, and we consider them to represent a single eruptive event from the same magma reservoir. A tephra deposit that precedes the flows has been recognized, but no material that dates this event has been found. Some previously published radiocarbon dates (e.g. Chesterman, 1955) may relate to this event rather than the overlying Glass Mountain tephra to which they were ascribed. The flows are overlain by airfall tephra from the Callahan, Little Glass Mountain and Glass Mountain eruptions. By comparison with the archaeomagnetic record from the American Southwest (Sternberg, 1982), paleomagnetic data indicate that these flows are younger than the Black Craters-Ross Chimneys basalt, but older than 1200 BP, perhaps about 1230 BP.

Burnt Lava flow (Table 2, No. 13)

This andesitic unit on the south side of Medicine Lake volcano was considered by Finch (1933) to be about 300 yrs old, although Anderson (1941) estimated it to be older, perhaps 500-1000 yrs. The flow is overlain by a light dusting of white pumice from Little Glass Mountain. Two dates on charcoal collected from a large tree mold are pending. Paleomagnetic data, again by comparison with the archaeomagnetic record, yield an age of about 1200 yrs.

Callahan flow (Table 2, No. 14)

The Callahan flow is broadly similar to the Burnt Lava flow in appearance, composition, and topographic position on the volcano except that it is located on the north side. Radiocarbon

dates of 1110±60 BP (Table 1, No.14; Donnelly-Nolan and Champion, 1987) and 1040±100 BP are both on wood from remnants of trees overrun by the lava flow at two different sites at the eastern edge of the flow. A third date of 1180±35 years was determined on charcoal found immediately underneath the airfall tephra deposit produced by the initial explosive part of the eruption. A weighted average of these 3 dates yields a date of 1130±26 BP for this event. Paleomagnetic data suggest an age of about 1150 BP based on comparison with paleomagnetic directions of well-dated units at Lassen volcanic center (D.E. Champion and M.A. Clynne, unpublished data).

Basalt of Paint Pot Crater (Table 2, No. 15)

Based on paleomagnetic data, the Paint Pot Crater flow is essentially identical in age to the Callahan flow. Paint Pot airfall tephra, which preceded the flow, immediately overlies uneroded Callahan tephra and thus is younger than about 1150 yrs BP. Paint Pot Crater and its flow are overlain by airfall tephra radiocarbon dated at 1065 yrs BP, erupted from nearby Little Glass Mountain. The white tephra on the red cone is responsible for the name of the cinder cone. The age of the flow, by comparison with the Lassen paleomagnetic and radiocarbon records (D.E. Champion and M.A. Clynne, unpublished data) is just slightly younger than the Callahan flow, but more than 1100 BP.

Little Glass Mountain (Table 2, No. 16)

A published radiocarbon age (Heiken, 1978) on a sample collected by one of us (C.D.M.) and dated at a commercial laboratory yielded an age of 1065±90 BP (Table 1, No.16). Tephra from the Little Glass Mountain vent overlies every unit within its areal extent except the tephra from Glass Mountain and the Glass Mountain domes which are younger. With Little Glass Mountain we include as well the chemically and petrographically identical domes to the NE on an approximate N30E trend, some of which are known as the Crater Glass flows. Local tephra deposits are associated with these domes; the deposits underlie the tephra of Glass Mountain. Because paleomagnetic data are less precise on Little Glass Mountain and Glass Mountain than on more easily sampled mafic lavas, the age difference between these two units could be as large as the nearly 200 yrs suggested by the radiocarbon dates in Table 1, or, alternatively, Little Glass Mountain could have immediately preceded Glass Mountain. Comparison of Medicine Lake paleomagnetic data with those on well-dated flows at the Lassen volcanic center (D.E. Champion and M.A. Clynne, unpublished data) suggests that the 1065 date may be slightly too old for the Little Glass Mountain event.

Glass Mountain (Table 2, No. 17)

The age of Glass Mountain, its accompanying small domes to the north and south, and its preceding pumice deposits has a been a matter of discussion for some time (Chesterman, 1955; Ives et al, 1967; Sullivan et al, 1970; Heiken, 1978). A radiocarbon date on a dead cedar tree without limbs or bark that is preserved in the edge of one of the distal tongues of the flow gives 885 BP on a piece of exterior wood containing about 30 annual growth rings. This date may be too old because some of the outside of the tree is missing. The age of the Glass Mountain flow is probably between 850 and 900 BP. The tephra deposits that precede the flow and domes may be somewhat older but are constrained to be less than about 1050 BP from the Little Glass Mountain and Lassen data.

The "1910 event"

Finch (1928) cited a report by a local rancher of earthquakes in 1910 accompanied by flames over Glass Mountain, ground breakage to the north, and "blue mud" on vegetation the same year. No evidence of any such recent deposit nor any likely vent for an eruption has been found by the authors and the "event" is disregarded here.

CHEMICAL COMPOSITION OF POST-11,000-YR UNITS

Variation diagrams of MgO vs. the other major elements for Medicine Lake lavas are shown in Figure 6. Lavas younger than 11,000 years are plotted over the field of older Medicine Lake lavas and have a fairly coherent trend. In general, the older lavas of the volcano tend to show a much more diffuse pattern, especially in the range 1-6% MgO. The younger lavas have higher

SiO2 and K2O contents, while the older lavas are higher in Al2O3, FeO*, CaO, Na2O, TiO2, and P2O5, although three basalts of the early mafic event show elevated FeO*, TiO2, and P2O5 contents as well

Grove and Donnelly-Nolan (1986) and Grove et al (1988) modeled the petrogenetic processes that may have generated the Little Glass Mountain rhyolite and the Burnt Lava flow, both of which were erupted during the late Holocene event. In the case of Little Glass Mountain, the model indicates that fractionation and assimilation produced andesite and then fractionation of the andesite generated rhyolite. Similarly, petrologic modeling of the Burnt lava andesite flow indicates that fractionation along with assimilation of crustal material occurred, together with mixing of magmas. Gerlach and Grove (1982) and Grove et al (1982) had previously discussed the importance of fractionation, assimilation, and mixing at Medicine Lake volcano. These studies by Grove and co-workers indicate that a number of petrogenetic processes were operating during the past 11,000 yrs. The difference between this period of the volcano's history and earlier periods may not be in the kinds of processes operating, but in the extent to which any one process dominated over others.

The inferred parental magma at Medicine Lake volcano is high-alumina basalt (Grove et al, 1982; Grove and Baker, 1984; Donnelly-Nolan, 1988). Fractionation of high-alumina basalt toward andesite would yield higher SiO_2, $FeTO_3$, Na_2O, TiO_2, and P_2O_5, and relatively high CaO. Fractionation would also result in lower Al_2O_3 and MgO, and relatively low but gently increasing K_2O based on model calculations (Grove et al, 1982; Grove and Baker, 1984; Carlson and Hart, 1987) and on chemical analyses of segregation veins which represent in-situ differentiation products at surface conditions. One segregation vein in the basalt of Giant Crater is plotted on Figure 6. This pattern is generally similar to that of many of the earlier lavas of the volcano, with the exception of Al_2O_3. The higher Al_2O_3 shown by earlier lavas in the range 1-6% MgO could be produced by accumulation of plagioclase, and indeed the lavas that show high Al_2O_3 contents contain abundant plagioclase phenocrysts, in contrast to the much more common phenocryst-poor lavas of the volcano. Thus, crystal fractionation and accumulation of plagioclase may be processes that operated much more commonly or extensively during the earlier history of the volcano. Crustal assimilation and (or) mixing of magmas appear to have been relatively important in generating the post-11,000-yr lavas other than high-alumina basalt. Partially-melted granitic inclusions are present in the highest-SiO_2 basalts of Giant Crater and in the basalt of "vent 5", in Medicine dacite, Burnt Lava, Callahan, Paint Pot, Glass Mountain and Little Glass Mountain and provide physical evidence of crustal contamination. In addition, several post-11,000-yr events produced compositionally-zoned lava flows (see Table 2), most notably the basalt of Giant Crater, the Callahan flow, Glass Mountain, and to a more limited extent the Burnt Lava flow. The earliest of the Giant Crater lavas show a tholeiitic trend of iron-enrichment, but as the eruption progressed, higher-silica calc-alkaline lavas erupted (Figure 7a). Burnt Lava and the Callahan flow also show calc-alkaline trends as does the dacitic part of the Glass Mountain eruption which shows clear evidence of magma mixing (Eichelberger, 1975, 1981).

Figure 7 demonstrates that both tholeiitic and calc-alkaline lavas are present at Medicine Lake volcano. Figure 7 shows a well-defined trend in the post-11,000-yr lavas, with the most mafic and most silicic lavas being tholeiitic and compositions in between being calc-alkaline. Petrologic modeling (Grove and Donnelly-Nolan, 1986, and T.L. Grove et al, unpublished data) indicates that fractionation is the dominant process producing the rhyolites and tholeiitic basalts. Experiments conducted by Grove and Baker (1984) identified a fractional crystallization path and conditions that could generate calc-alkaline derivatives from a tholeiitic parent. However, they also discuss the importance of crustal assimilation and mixing of magmas in producing the calc-alkaline trend. The relatively more common iron-enrichment shown of the earlier lavas of the volcano suggests again that fractionation was a relatively important process during this earlier time period.

Inclusions found in post-glacial lavas follow very similar trends to their host lavas with very little iron-enrichment in basaltic and andesitic compositions (Figure 7). Some of the compositional scatter of these inclusions may be caused by interaction with the host magma by diffusion or other processes (Bacon, 1986). Note that all inclusions with more than 70% SiO_2 are

partially-melted crustal inclusions, whereas the more mafic inclusions show crenulate, chilled margins and crystal morphologies indicating that they were liquid and were chilled upon injection into their host magma. For all magmatic inclusions, the host is higher in SiO_2 content and was presumably cooler than its magmatic inclusions. Some of the magmatic inclusions have compositions in the range 56.7-61.8% SiO_2, a range of andesitic compositions not represented by lava flows younger than 11,000 yrs old (Figure 7; Condie and Hayslip, 1975). Most of these andesitic inclusions are present in Little Glass Mountain rhyolite. Petrologic modeling by Grove and Donnelly-Nolan (1986) suggests that these andesites may represent samples generated by the fractionation event that produced the rhyolite. A few inclusions in this composition range are also present in Glass Mountain and in the Medicine dacite flow and the same process that generated Little Glass Mountain rhyolite may also have operated to produce these flows. Thus, andesitic magma was present during late Holocene time but may not have been shallow enough to erupt to the surface.

Magmatic inclusions of basaltic composition are also present in late Holocene lavas, notably in the Burnt Lava flow which contains primitive high-alumina basalt inclusions similar to basalt erupted at Giant Crater. This suggests that an infusion of primitive basalt occurred in late Holocene time on the south flank of the volcano. Very similar basalt reached the surface on the north flank as the basalt of Black Crater and Ross Chimneys shortly before Burnt Lava erupted. Somewhat less primitive basaltic inclusions are present in the Hoffman flows and in Glass Mountain. All four of these late Holocene events took place in an approximately linear N-S array on the east side of the volcano. The existence of open ground cracks that extend to the northeast from the basalt of Black Crater and Ross Chimney in the same N15-25E direction as the trend of these late Holocene vents lends support to the idea that an episode of local crustal extension took place at the time this basalt erupted.

DISCUSSION

Volcanic eruptions have taken place over a broad area of Medicine Lake volcano, approximately 30 km N-S and 15 km E-W, during the past 11,000 yrs. Each of the seventeen units that erupted during this period has more than one vent. Vent alignments are strongly controlled tectonically and are parallel or subparallel to major regional structural features. By contrast, the eruptive activity has not been distributed evenly throughout the time period. Based on radiocarbon and paleomagnetic time control, we known that eruptions have occurred in brief episodes early and late in post-glacial time with only one very small eruption in the mid-Holocene. There is also a strong compositional contrast between the two major episodes: the early mafic episode is characterized entirely by basalt; in late Holocene time, rhyolite exceeds andesitic compositions in volume and only a very small amount of basalt erupted. The next youngest rhyolitic episode occurred in late Pleistocene time, perhaps 20,000 yrs ago or more, when the glaciated rhyolite of Mt. Hoffman erupted on the north rim of the caldera. Lack of age control and the increasing cover by younger lavas as we look back in time for volcanic episodes makes identification of these episodes increasingly difficult and uncertain. The good age control and excellent exposure of Medicine Lake lavas less than 11,000 years old allows for a far better understanding of this period than any previous period in the volcano's history.

We propose here that basalt intruded during the early mafic episode is parental to the rhyolitic and andesitic lavas erupted in late Holocene time. We speculate that a basaltic intrusive event in late Holocene time, represented by the eruption of the basalt of Black Crater and Ross Chimneys about 1250 BP, resulted in eruption of some of the late Holocene lavas. The Hoffman and Burnt Lava flows, which erupted shortly after the Black Crater and Ross Chimneys flows, both contain numerous basaltic inclusions. The Callahan flow is zoned from earliest-erupted andesite to basalt and its vents lie on the extension of ground cracks associated with the major N-S Gillem fault (Donnelly-Nolan and Champion, 1987). Paint Pot Crater and associated spatter vents project directly toward the vents for Little Glass Mountain which erupted shortly after the Paint Pot Crater flow. Little Glass Mountain and several domes to the northeast, some known as the Crater Glass flows, erupted from, and partially buried, a set of northeast-trending ground cracks that

probably resulted from shallow dike intrusion of the rhyolite (Fink and Pollard, 1983). A century or so later on the opposite side of the caldera, the compositionally-zoned rhyolite and dacite of Glass Mountain erupted from at least 13 vents lined up approximately parallel to and less than 2 km east of the chain of vents that erupted the Hoffman flows.

SUMMARY

Tectonic extension and volcanism appear to be linked at Medicine Lake volcano. Episodes of basaltic intrusion may result from extensional episodes that allow deep-seated magmas to reach the surface. Local ground breakage and extension probably occurs in the context of regional stretching of the crust related to plate movements. Some Medicine Lake basalts, including the later-erupted flows of the basalt of Giant Crater, are very primitive and have been compared with mid-ocean ridge basalts (Hart, 1971; Philpotts et al, 1971; McKee et al, 1983; Hart et al, 1984). Extension of the crust may allow some basalt to travel upward rapidly enough to reach the surface essentially uncontaminated.

The episodes of volcanism that we have identified do not aid us in making predictions as to when or where or what kind of lava might erupt next at Medicine Lake volcano. We feel, however, that any strong seismic episode should be carefully monitored; ground breakage might be followed by eruption of lava. The pattern of silicic lavas erupting high on the volcano, and basaltic ones tending to erupt on the flanks (Donnelly-Nolan, 1988 and unpublished mapping) suggests that future extension and ground breakage high on the volcano might result in eruption of silicic lava which could be accompanied by explosive activity such as that which produced the plinian airfall deposits that preceded Little Glass Mountain and Glass Mountain (Heiken, 1978).

The amount of heat available for geothermal energy is unknown but is likely to be a function of the amount of heat stored in cooling magma in the upper crust below the volcano. Drilling of geothermal exploration wells in the caldera is known to have yielded temperature gradients of 88.4, 227.0, and 548.5°C/km in 3 of the drillholes (Mineral Land Classification Board, 1983). Continued interest in drilling exploratory holes, in spite of the paucity of publicly-available drillhole data, suggests that sufficient heat may be available to provide a commerical resource if an adequate fluid supply can be found. Likely sources of heat include a small silicic magma reservoir identified by seismic tomography (Evans and Zucca, 1988) and basalt intruded in late Holocene time.

CONCLUSIONS

Good age control for the last 11,000 years at Medicine Lake volcano has given us an understanding of the episodic nature of volcanism during this time period. The eruptive activity is probably driven by intrusions of basalt during tectonic extensional events. A model of mafic dikes and small derivative magma bodies of more silicic compositions agrees with models proposed by Donnelly-Nolan (1988) and Evans and Zucca (1988), constrained in part by geophysical studies of Finn and Williams (1982), Zucca et al (1986) and Fuis et al (1987). Late Holocene lavas are derived by fractionation, assimilation, and mixing from high-alumina basalt parental magma, possibly from basalt intruded into the volcano during the early mafic episode when 5 km^3 of basalt of Giant Crater erupted. Eruption of late Holocene lavas may have been triggered by a basaltic intrusive episode about 1250 BP. This episode plus stored heat from previous episodes should provide adequate heat for commercial geothermal development if sufficient fluids can be found. The nature and timing of volcanic activity cannot be predicted from present data but crustal extension and seismic swarms should be carefully monitored because they may be followed by eruptive activity.

REFERENCES

Anderson, C. A., Volcanic history of Glass Mountain, northern California, *Am. J. Sci., 26*, 485-506, 1933.

Anderson, C. A., Volcanoes of the Medicine Lake Highland, California, *Univ. Calif. Publ. Bull. Dep. Geol. Sci., 25*, 347-422, 1941.

Bacon, C. R., Magmatic inclusions in silicic and intermediate volcanic rocks, *J. Geophys. Res., 91*, 6091-6112, 1986.

Carlson, R. W., and W. K. Hart, Crustal genesis on the Oregon Plateau, *J. Geophys.Res., 92*, 6191-6206, 1987.

Champion, D. E., Holocene geomagnetic secular variation in the western United States: Implications for the global geomagnetic field, *U.S. Geol. Survey Open-File Report 80-824,* 314 p., 1980.

Chesterman, C. W., Age of the obsidian flow at Glass Mountain, Siskiyou County, California, *Am. J. Sci., 253* 418-424, 1955.

Condie, K. C., and D. L. Hayslip, D.L., Young bimodal volcanism at Medicine Lake volcanic center, northern California, *Geochim. Cosmochim. Acta, 39*, 1165-1178, 1975.

Donnelly-Nolan, J. M., 1988, A magmatic model of Medicine Lake volcano, California, *J. Geophys. Res., 93,* 4412-4420, 1988.

Donnelly-Nolan, J. M., and D. E. Champion, D.E., Geologic map of Lava Beds National Monument, northern California, *U.S.Geol. Survey Map I-1804*, scale 1:24,000, 1987.

Eichelberger, J. C., Origin of andesite and dacite: Evidence of mixing at Glass Mountain in California and at other circum-Pacific volcanoes, *Geol. Soc. Am. Bull., 86*, 1381-1391, 1975.

Eichelberger, J. C., Mechanism of magma mixing at Glass Mountain, Medicine Lake Highland volcano, California, *U.S. Geol. Survey Circ. 838*, 183-189, 1981.

Evans, J. R., and J. J. Zucca, Active high-resolution seismic tomography of compressional wave velocity and attenuation structure at Medicine Lake volcano, northern California Cascade Range, *J. Geophys. Res.*, 93, 1988.

Finch, R. H., Lassen Report No. 14, *The Volcano Letter, no. 161*, 1928.

Finch, R. H., Burnt Lava flow in northern California, *Zeit. Vulkan., 10*, 180-183, 1933.

Fink, J. H., and D. D. Pollard, D.D., Structural evidence for dikes beneath silicic domes, Medicine Lake Highland volcano, California, *Geology, 11*, 458-461, 1983.

Finn, C., and D. L. Williams, Gravity evidence for a shallow intrusion under Medicine Lake volcano, California, *Geology, 10,* 503-507, 1982.

Fuis, G. S., J. J. Zucca, W. D. Mooney, and B. Milkereit, B., A geologic interpretation of seismic-refraction results in northeastern California, *Geol. Soc. Am. Bull., 98*, 53-65, 1987.

Gay, T. E., Jr., and Q. A. Aune, Q.A., Alturas sheet, Geologic map of California, scale 1:250,000, Calif. Div. Mines and Geol., Sacramento, 1958.

Gerlach, D. D., and T. L. Grove, Petrology of Medicine Lake Highland volcanics, characterization of endmembers of magma mixing, *Contrib. Mineral. Petrol., 80,* 147-159, 1982.

Grove, T.L., and M. B. Baker, M.B., Phase equilibrium controls on the tholeiitic versus calc-alkaline differentiation trends, *J. Geophys. Res., 89*, 3253-3274, 1984.

Grove, T. L., and J. M. Donnelly-Nolan, The evolution of young silicic lavas at Medicine Lake Volcano, California: Implications for the origin of compositional gaps in calc-alkaline series lavas, *Contrib. Mineral. Petrol., 92*, 281-302, 1986.

Grove, T. L., D. C. Gerlach, and T. W. Sando, Origin of calc-alkaline series lavas at Medicine Lake volcano by fractionation, assimilation and mixing, *Contrib. Mineral.Petrol., 80*, 160-182, 1982

Grove, T. L., R. J. Kinzler, M. B. Baker, J. M. Donnelly-Nolan, J.M., and C. E. Lesher, C.E., 1988, Assimilation of granite by basaltic magma at Burnt Lava flow, Medicine Lake volcano, northern California: Decoupling of heat and mass transfer: *Contrib.Mineral.Petrol., 99*, 320-343, 1988.

Hart, S. R., K, Rb, Cs, Sr and Ba contents and Sr isotope ratios of ocean floor basalts: *Phil. Trans., R. Soc. London, Ser. A, 268*, 573-587, 1971.

Hart, W. K., J. L. Aronson, and S. A. Mertzman, Areal distribution and age of low-K, high-alumina olivine tholeiite magmatism in the northwestern Great Basin, *Geol. Soc. Am. Bull, 95*, 186-195, 1984.

Heiken, G., Plinian-type eruptions in the Medicine Lake Highland, California, and the nature of the underlying magma, *J. Volc. Geotherm. Res., 4,* 375-402, 1978.

Ives, P.C., B. Levin, C. L. Oman, and M. Rubin, M., U.S. Geological Survey radiocarbon dates IX, *Am. J. Sci., 9,* 513-516, 1967.

McKee, E. H., W. A. Duffield, and R. J. Stern, Late Miocene and early Pliocene basaltic rocks and their implications for crustal structure, northeastern California and south-central Oregon, *Geol. Soc. Am. Bull., 94*, 292-304, 1983.

Mertzman, S. A., Jr., Recent volcanism at Schonchin and Cinder Buttes, northern California, *Contrib. Mineral. Petrol., 61*, 231-243, 1977a.

Mertzman, S. A., Jr., The petrology and geochemistry of the Medicine Lake volcano, California, *Contrib. Mineral. Petrol., 62*, 221-247, 1977b.

Mertzman, S.A., K-Ar results for silicic volcanics from the Medicine Lake Highland, northeastern California--A summary, *Isochron/West, 34,* 3-7, 1982.

Mertzman, S. A., An addendum to "K-Ar results for silicic volcanics from the Medicine Lake Highland, northeastern California--A summary", *Isochron/West, 38*, 3-5, 1983.

Mertzman, S. A., and R. J. Williams, R.J., Genesis of Recent silicic magmatism in the Medicine Lake Highland, California, evidence from cognate inclusions found at Little Glass Mountain, *Geochim. Cosmochim. Acta, 45*, 1463-1478, 1981.

Mineral Land Classification Board, Redefinition by addition to the Glass Mountain Known Geothermal Resources Area, Siskiyou County, California, California Known Geothermal Resources Area Minutes No. 40, 4, 1983.

Miyashiro, A., Volcanic rock series in island arcs and active continental margins, *Am. J. Sci., 274*, 321-355, 1974.

Philpotts, J. A., W. Martin, And C. C. Schnetzler, Geochemical aspects of some Japanese lavas, *Earth Planet. Sci. Lett., 12*, 89-96, 1971.

Powers, H. A., The lavas of the Modoc Lava-Bed quadrangle, California, *Am. Mineral., 17*, 253-294, 1932.

Sternberg, R.S., Archaeomagnetic secular variation of direction and paleointensity in the American Southwest, Ph.D. Dissertation, University of Arizona, 305 p., 1982.

Sullivan, B. M., E. Spiker, and M. Rubin, U.S. Geological Survey radiocarbon dates XI, *Radiocarbon, 12,* 319-334, 1970.

Zucca, J. J., G. S. Fuis, B. Milkereit, W. D. Mooney, and R. D. Catchings, Crustal structure of northeastern California, *J. Geophys. Res., 91*, 7359-7382, 1986.

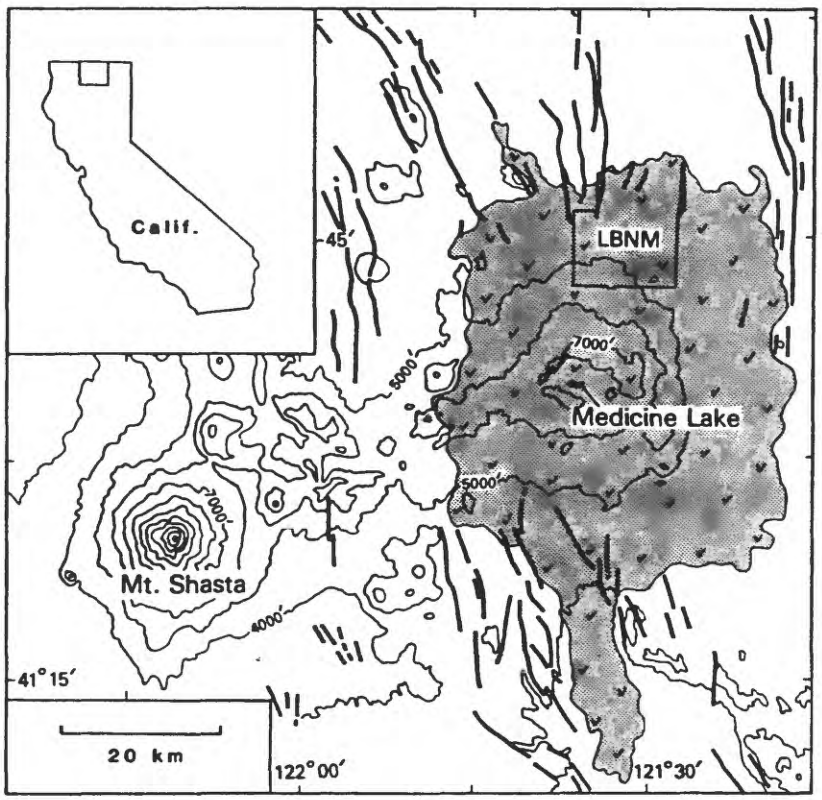

Figure 1. Location map showing extent of lavas of Medicine Lake volcano in pattern. LBNM is Lava Beds National Monument. Contour interval is 1000 feet. Medicine Lake volcano is entirely below 8000 feet and mostly above 4000 feet. Heavy lines are faults (Gay and Aune, 1958). From Donnelly-Nolan (1988).

Figure 2. Map of Medicine Lake volcano showing distribution of post-11,000-yr lavas. Units are numbered 1 to 17 (Table 2) from oldest to youngest. Units 1-8 belong to the early mafic episode; 10-17 are late Holocene. The basalt of Giant Crater extends more than 25 km south of the southern border of the figure. Modified from Donnelly-Nolan (1988).

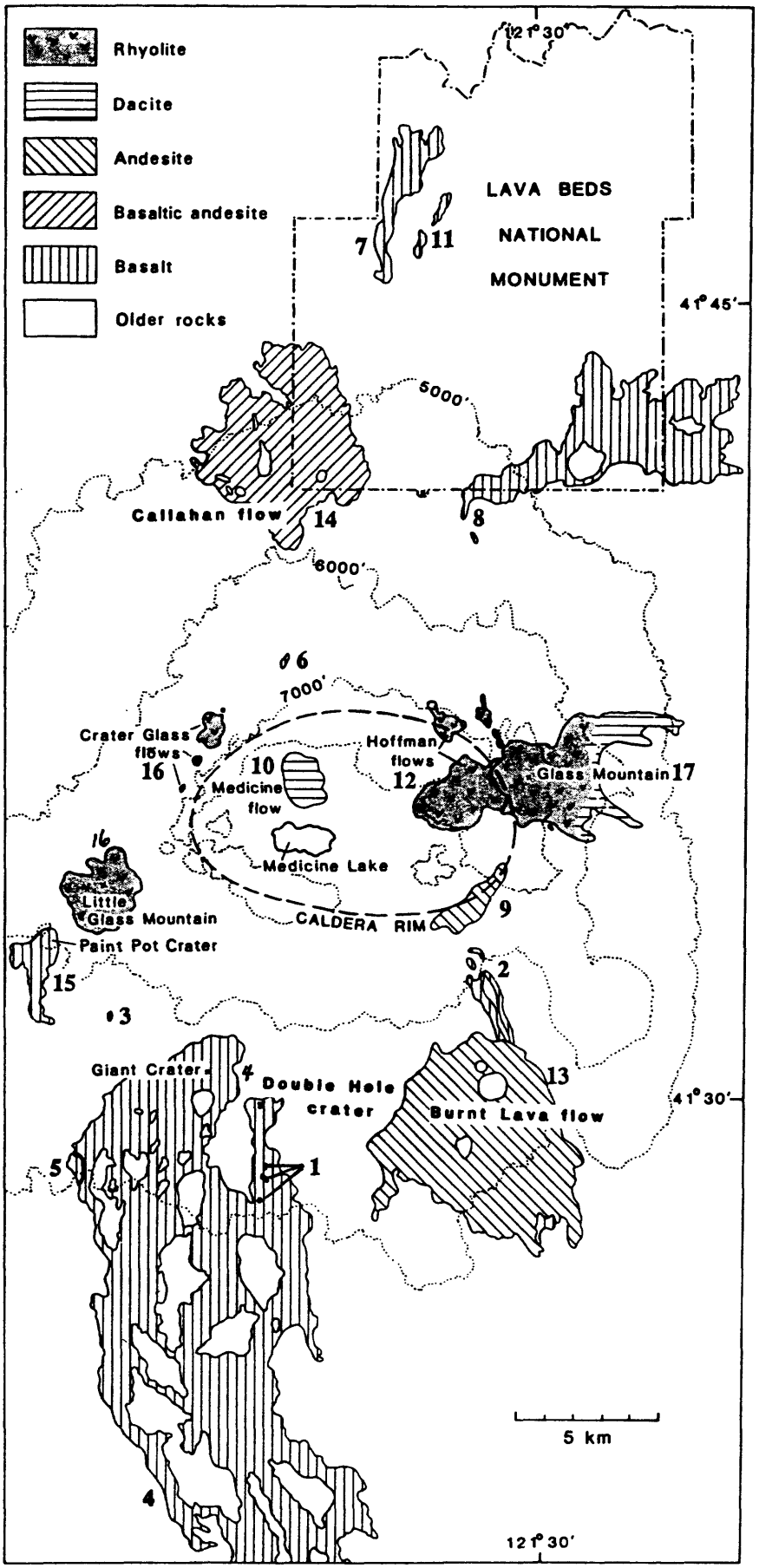
Rhyolite
Dacite
Andesite
Basaltic andesite
Basalt
Older rocks
121°30'
LAVA BEDS
NATIONAL
MONUMENT
41°45'
7
11
5000'
Callahan flow
14
8
6000'
6
7000'
Crater Glass
flows
16
10
Medicine
flow
Hoffman
flows
12
Glass Mountain
17
Medicine Lake
16
Little
Glass Mountain
CALDERA RIM
9
Paint Pot Crater
15
3
2
Giant Crater
4
Double Hole
crater
13
Burnt Lava flow
41°30'
5
1
4
5 km
121°30'

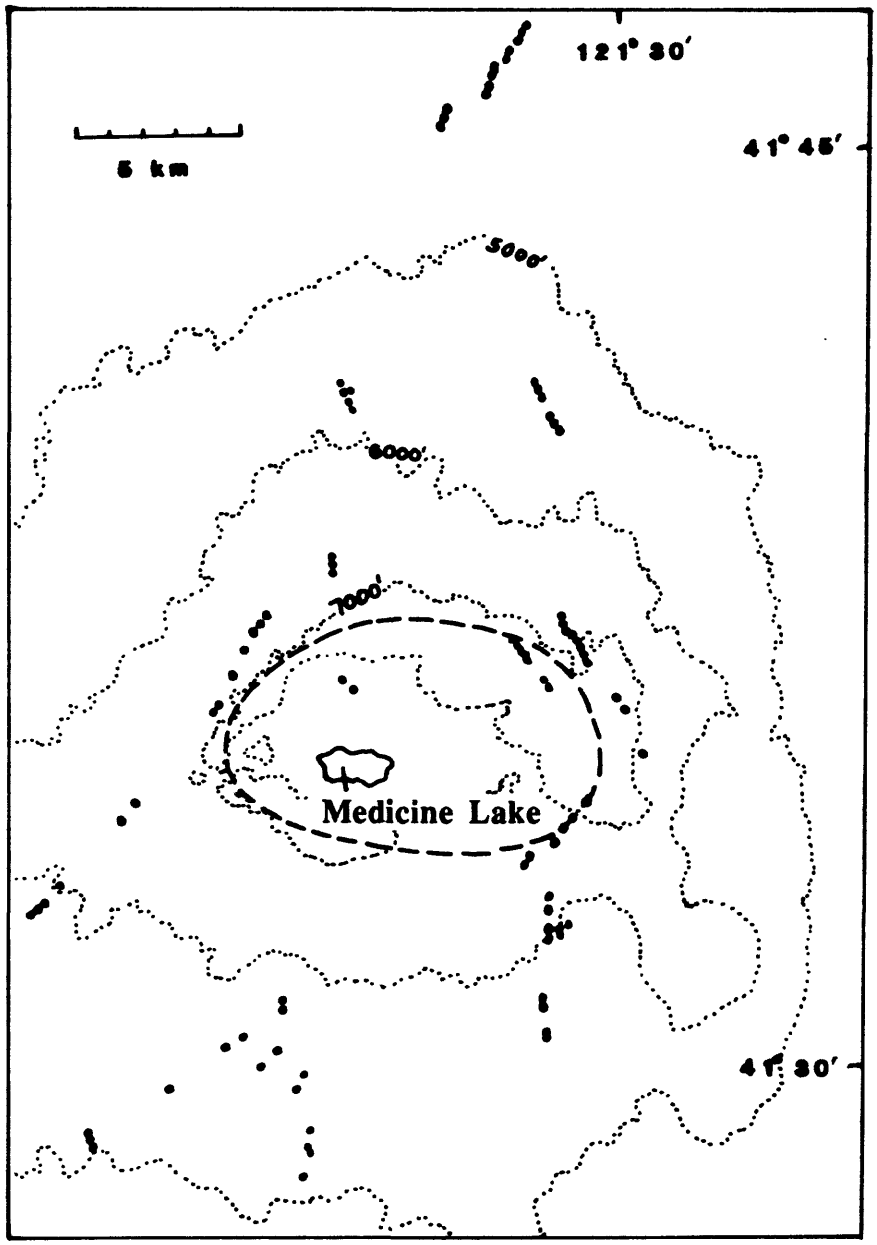

Figure 3. Map showing vent locations of units younger than 11,000 yrs. The approximate location of the caldera rim is shown by the dashed line.

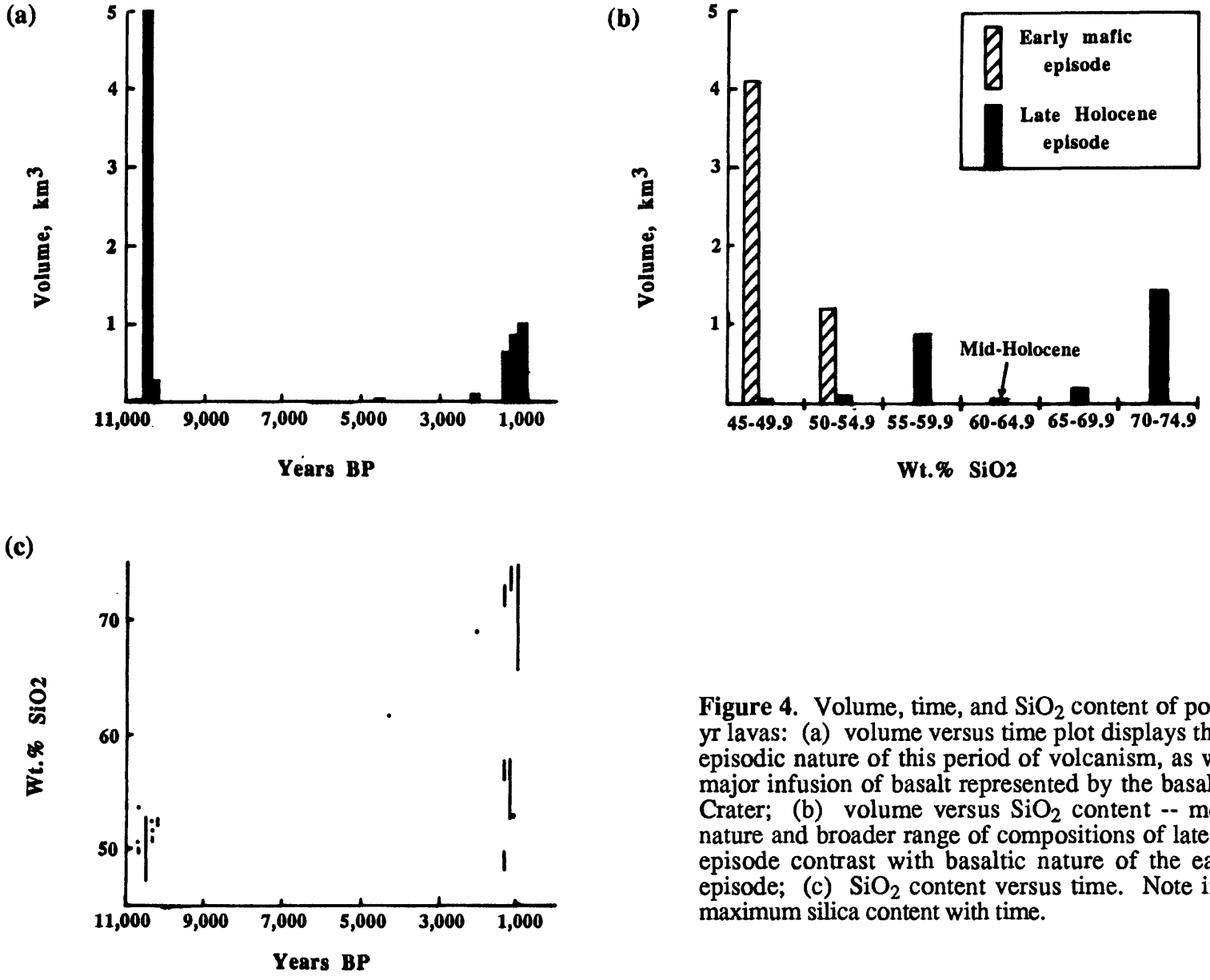

Figure 4. Volume, time, and SiO_2 content of post-11,000-yr lavas: (a) volume versus time plot displays the strongly episodic nature of this period of volcanism, as well as the major infusion of basalt represented by the basalt of Giant Crater; (b) volume versus SiO_2 content -- more silicic nature and broader range of compositions of late Holocene episode contrast with basaltic nature of the early mafic episode; (c) SiO_2 content versus time. Note increase in maximum silica content with time.

Figure 5. Equal-area plots of paleomagnetic directions projected on lower hemisphere for (a) early mafic episode, and (b) late Holocene episode. Circles represent 95% confidence limits of tmean directions. Paths of secular variation are drawn through time. Cross-hatched area in (b) represents paleomagnetic directions from Chaos Crags, Lassen volcanic center (D.E. Champion and M.A Clynne, unpublished paleomagnetic and radiocarbon data).

Figure 5a

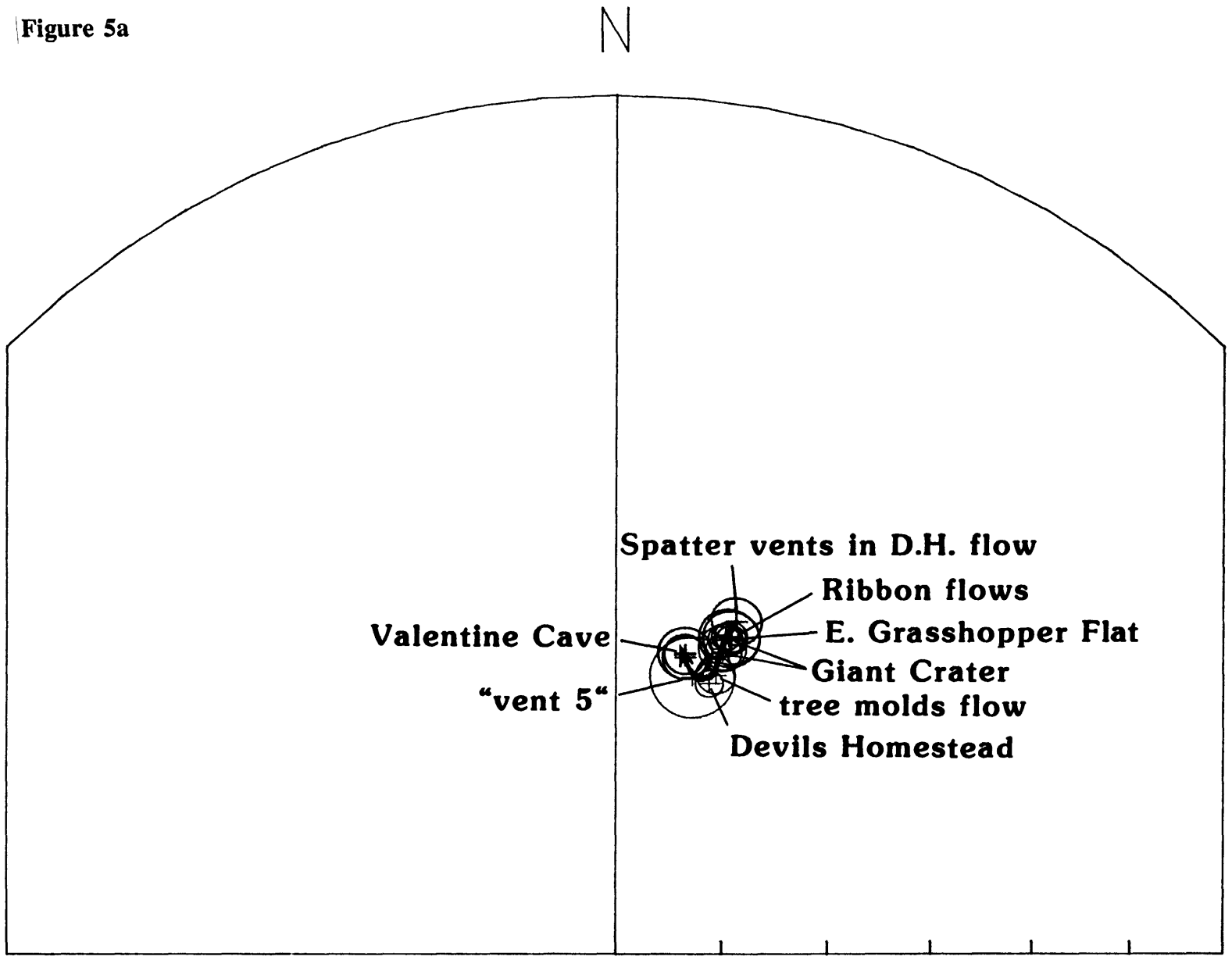
N
Spatter vents in D.H. flow
Ribbon flows
Valentine Cave
E. Grasshopper Flat
Giant Crater
"vent 5"
tree molds flow
Devils Homestead

Figure 5b

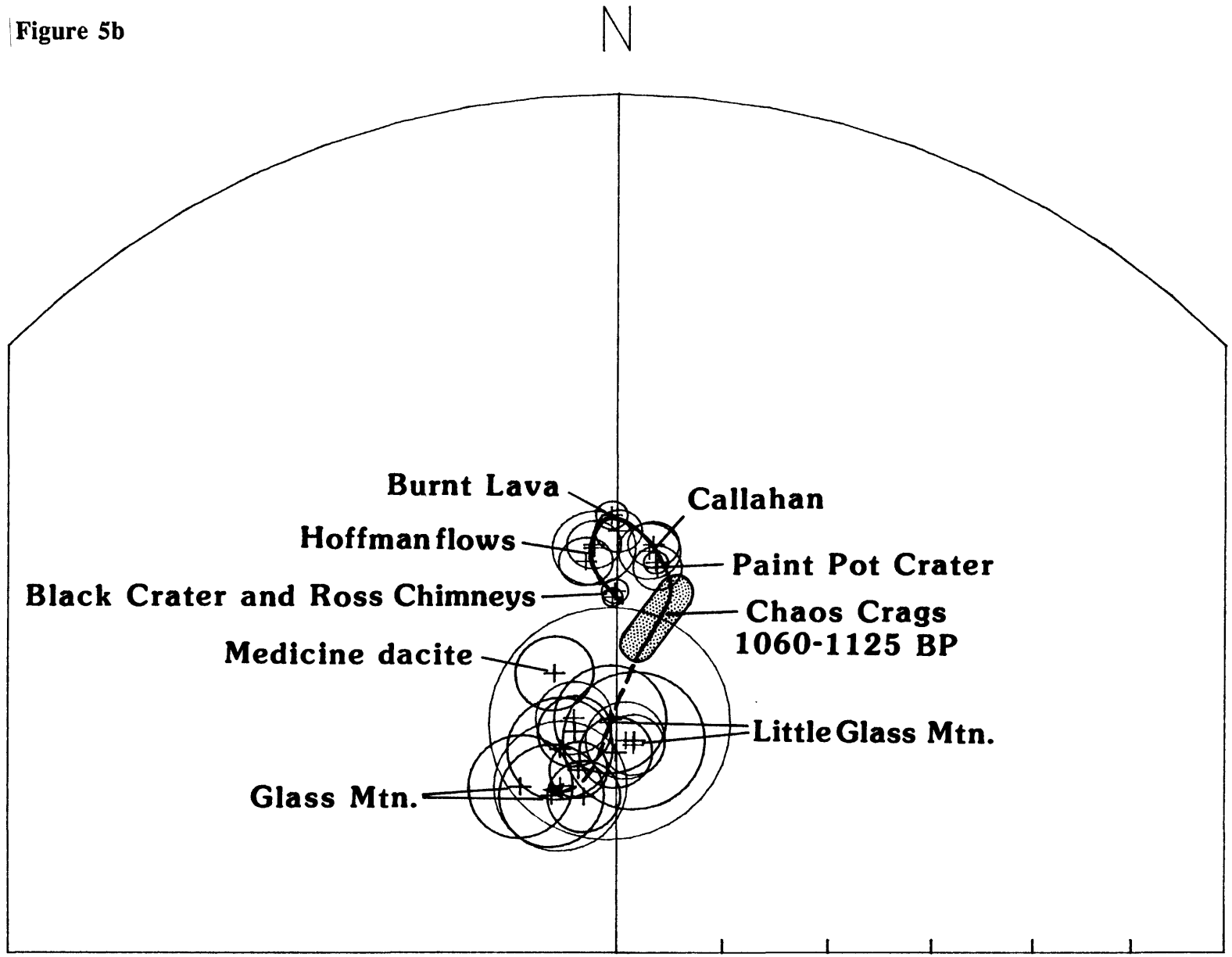
N
Burnt Lava
Callahan
Hoffman flows
Paint Pot Crater
Black Crater and Ross Chimneys
Chaos Crags
1060-1125 BP
Medicine dacite
Little Glass Mtn.
Glass Mtn.

Figure 6. MgO variation diagrams of major elements in Medicine Lake lavas and inclusions; symbols as shown. Outline encompasses the field of pre-11,000-yr Medicine Lake lavas. Segregation vein is in-situ fractionation product of early mafic basalt of Giant Crater under surface conditions; it is lower in MgO than its host. Most of the inclusions are from Glass Mountain and Little Glass Mountain. The gap between about 2.3-4.3% MgO in lavas younger than 11,000 yrs does not exist in the inclusions found in lavas of this time period.

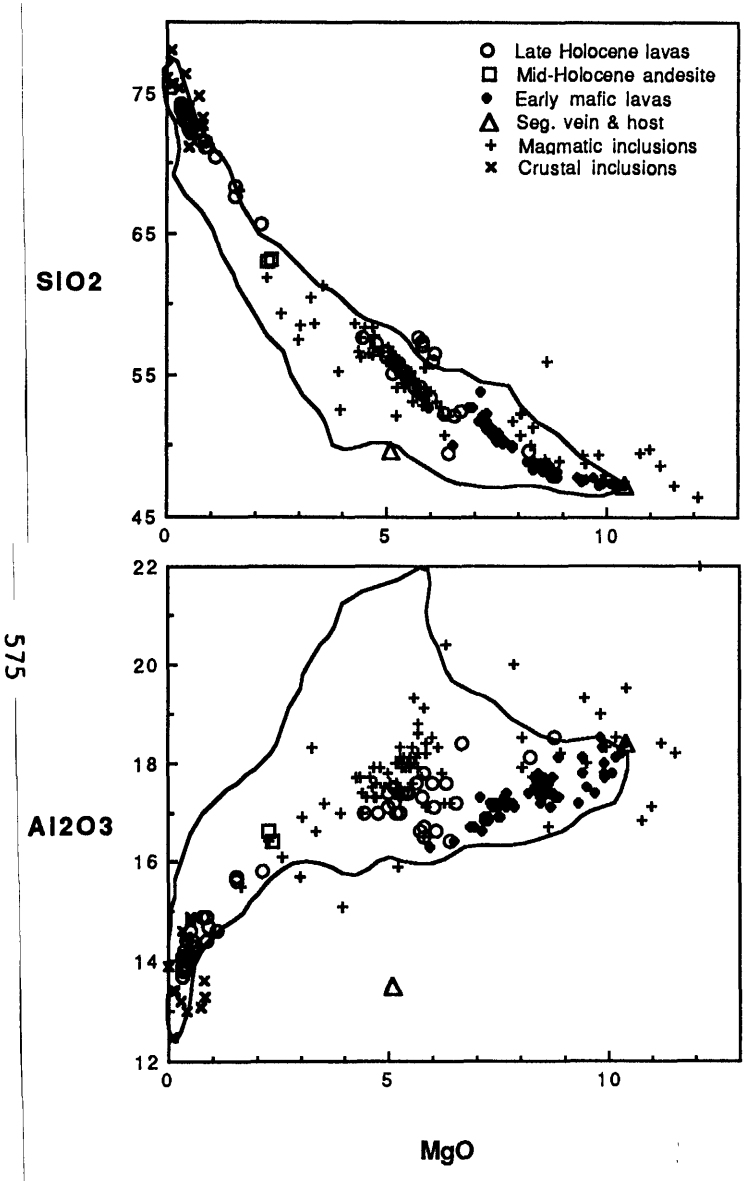
Late Holocene lavas
Mid-Holocene andesite
Early mafic lavas
Seg. vein & host
Magmatic inclusions
Crustal inclusions
SIO2
AI2O3
MgO

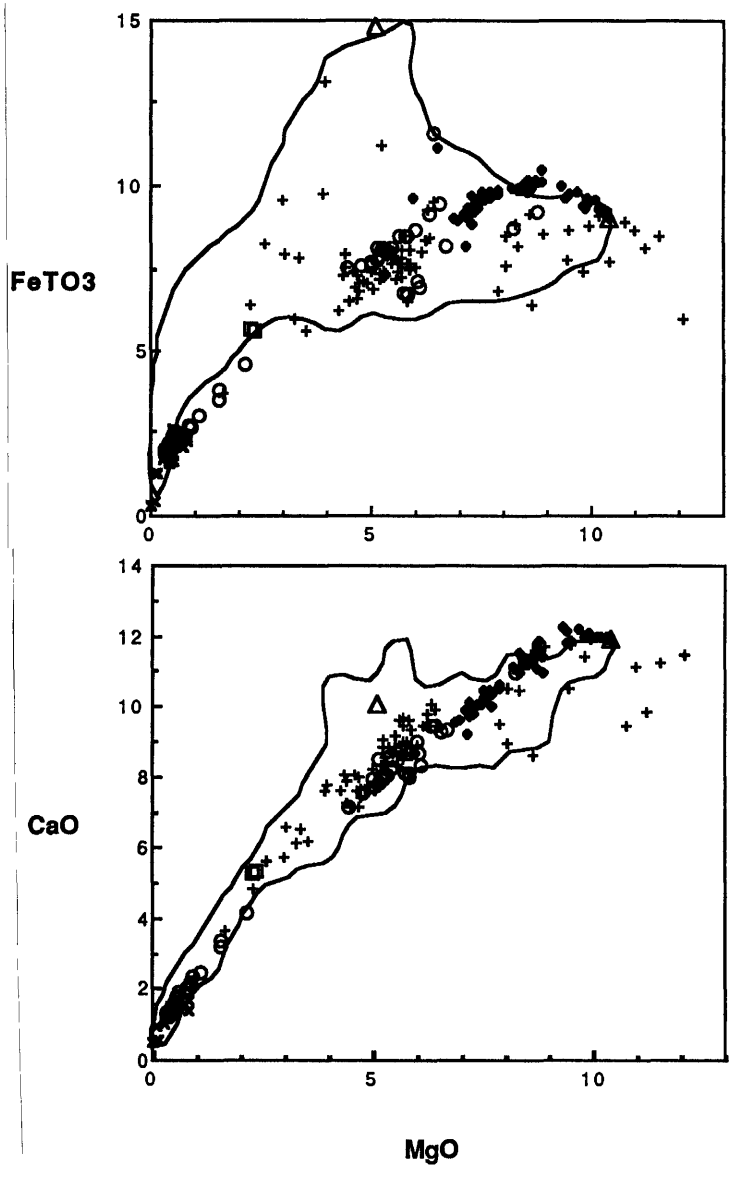
FeTO3
CaO
MgO

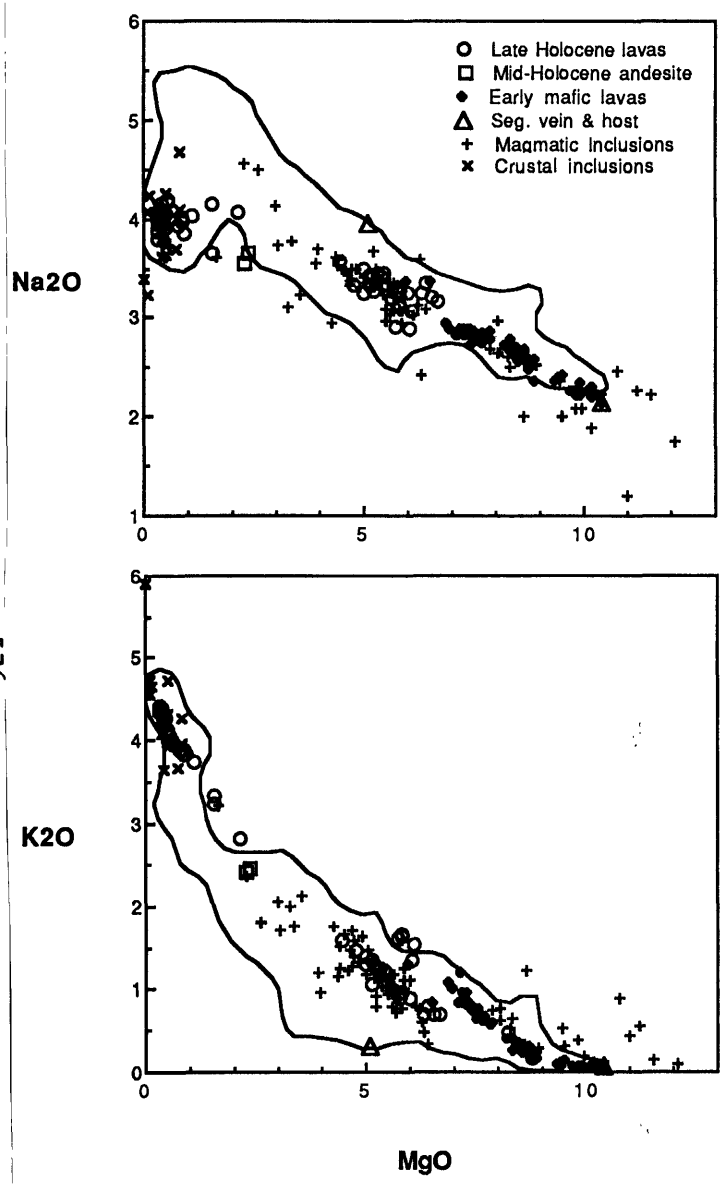
Late Holocene lavas
Mid-Holocene andesite
Early mafic lavas
Seg. vein & host
Magmatic inclusions
Crustal inclusions
Na2O
K2O
MgO

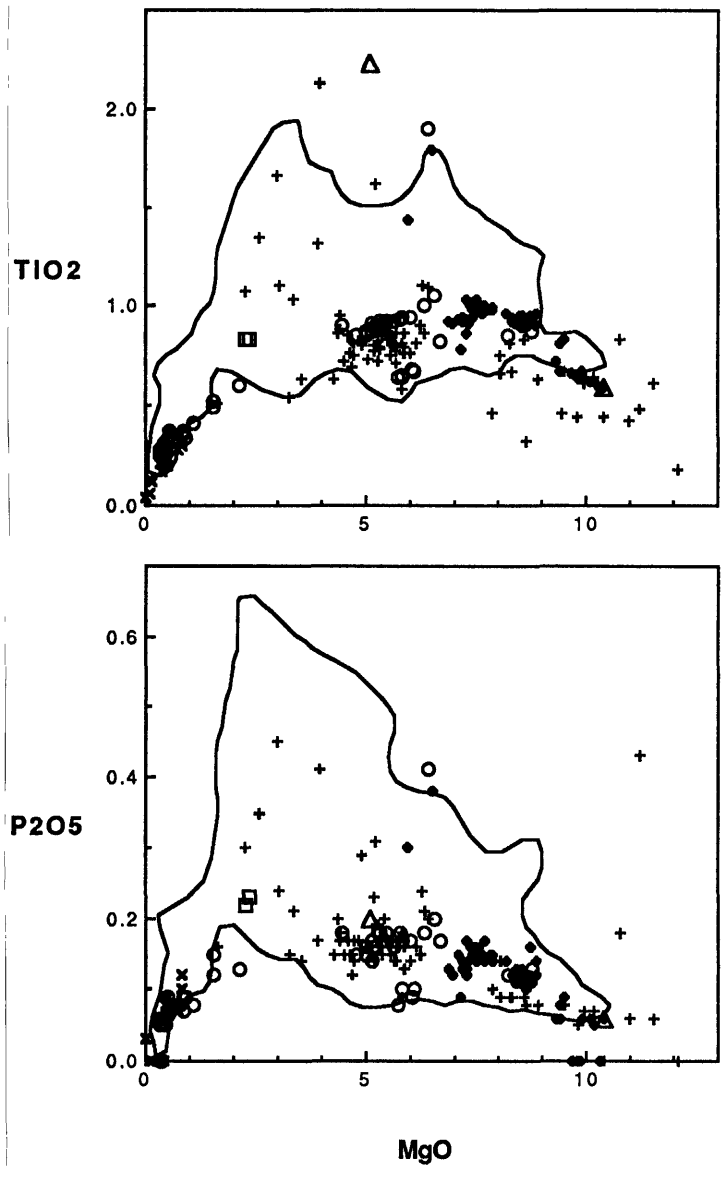
TIO2
P2O5
MgO

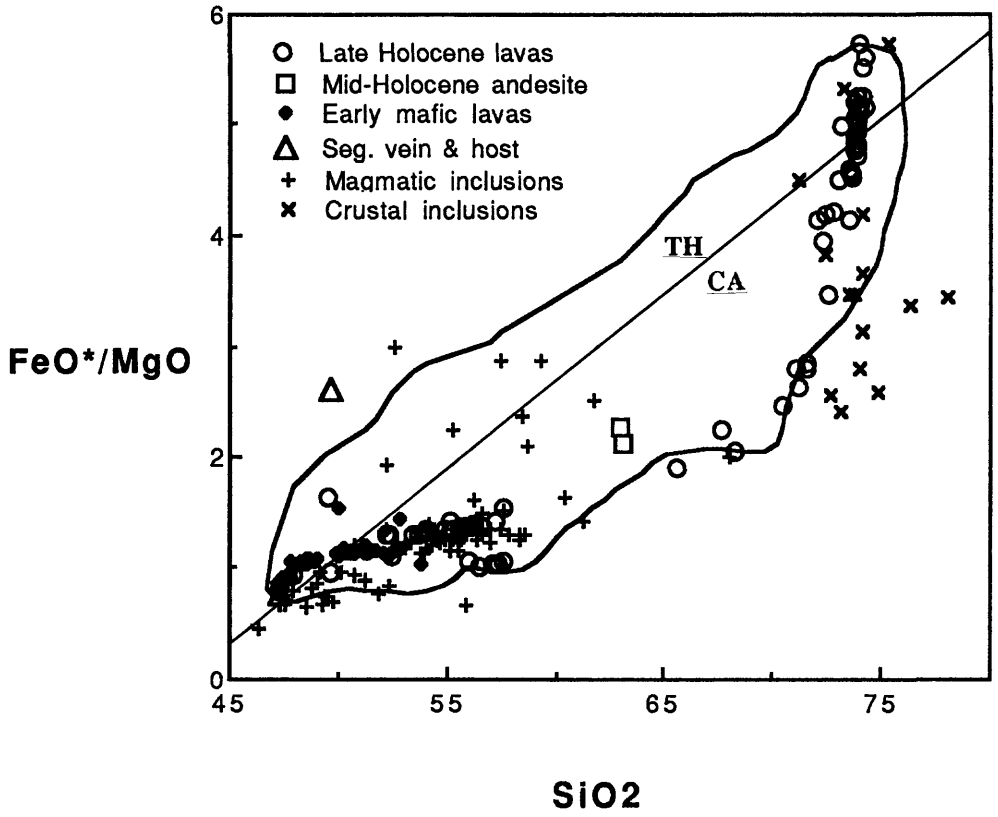

Figure 7. FeO*/MgO versus SiO_2. The field of lavas older than 11,000 yrs is much broader and shows more iron enrichment than younger lavas, although the most mafic Giant Crater lavas and the Glass Mountain and Little Glass Mountain dacite and rhyolites display iron enrichment. The line separating tholeiitic (TH) from calc-alkaline (CA) fields is from Miyashiro (1974).

Table 1. Age Data (all in years BP): Unit numbers correspond to Figure 1, 2, text, and Table 2

Unit No.	Description	Radiocarbon Date	USGS No. or reference	Material	Source	Estimated age from Paleomagnetism
2.	Basalt of the ribbon flows	10,310±60	2700	charred wood & charcoal	Tree mold	≥10,600
3.	Spatter E. of Grasshopper Flat	10,930±50	2650	resinous charred root	"	≥10,600
4.	Basalt of Giant Crater	10,580±80 10,620±80	1904A 1904B	charcoal charcoal	" "	10,600[a]
5.	Basalt of "vent 5"	10,355±50	2701	charcoal & charred wood	"	10,550
6.	Tree molds flow	10,200±110	2053	charcoal	"	10,550
8.	Basalt of Valentine Cave	10,850±60	2651	charred root	"	10,450
9.	Andesite of the pit craters	4430±70 4280±40	2649 2709	charcoal charcoal	In roadcut under tephra	
13.	Burnt Lava flow	pending pending	-- --	charcoal root charcoal root bark	Tree mold "	1200
14.	Callahan flow	1110±60 1040±100 1180±35	858 W-5947[b] 2057	wood " charcoal	Tree remnants in edge of flow In roadcut under tephra	1150
16.	Little Glass Mountain	1065±90	Heiken, 1978	wood, leaves, bark, cones		900-1050
17.	Glass Mountain	885±40	2136	wood	Tree in edge of flow	850-900

[a]10,600 BP was chosen arbitrarily to be the correct radiocarbon age relative to which paleomagnetic ages were estimated.
[b]W-5947 was analyzed by Meyer Rubin in Reston VA.
Radiocarbon ages are reported ± one analytical standard deviation.

Table 2. Post-glacial units: area and volume estimates, vent trends, and range of SiO2 contents

Unit	Description	Estimated	Estimated area (km^3)	Description volume (km^3)	Vent trends of vents	SiO_2 content[c] (wt. %) ( )=No.
1.	Spatter vents in Double Hole flow	<0.01[a]	<0.0001	several spatter vents	N20W, N15E	50.4 (1)
2.	Basalt of the ribbon flows	8[b]	0.02	numerous spatter vents	scattered, N-S	49.5-50.0 (2)
3.	Spatter E of Grasshopper Flat	0.005	<0.0001	several spatter vents	N-S	53.8 (1)
4.	Basalt of Giant Crater	360	5	spatter vents & cones, 2 pit craters	N5E, N55E, N20W	47.2-52.7 (62)
5.	Basalt of "vent 5"	0.01	<0.0001	several spatter vents	N20W	52.3 (1)
6.	Tree molds flow	0.025	0.0001	several spatter vents	N-S	51.4 (1)
7.	Basalt of Devils Homestead	4.3	0.04	several spatter vents	N20E	50.8-50.9 (2)
8.	Basalt of Valentine Cave	21	0.2	numerous spatter vents	N35W	52.3-52.8 (2)
9.	Andesite of pit craters	2.5	0.02	several pit craters	N25E	63.0-63.1 (2)
10.	Medicine dacite flow	2.4	0.08	2 vents	N45W	68.3 (1)
11.	Basalt of Black Crater and Ross Chimneys	0.4	0.001	numerous spatter vents	N15-25E	47.9-49.7 (2)
12.	Hoffman flows	5.1	0.12	≥6 vents	N25W	71.1-72.5 (4)
13.	Burnt Lava flow	33.5	0.5	cinder cone plus spatter vents	N-S	56.0-57.6 (5)

Table 2, Continued

14.	Callahan flow	23	0.4	cinder cone plus spatter vents	N30W	52.3-57.6 (12)
15.	Basalt of Paint Pot Crater	2.5	0.04	cinder cone plus spatter vents	N40E	52.5 (1)
16.	Little Glass Mountain	6.4	0.4	≥10 vents	N30E	72.4-74.2 (6)
17.	Glass Mountain	12.8	1.0	≥13 vents	N25W	65.6-74.2 (31)

[a] Flow, if present, is buried by lava from the Double Hole Crater vent of basalt of Giant Crater.

[b] Much of flow is buried under Burnt Lava flow.

[c] SiO_2 contents calculated by normalizing analyses to 100%, volatile-free, all iron as $FeTO_3$. Major-element analyses performed in USGS laboratories in Lakewood, Colorado and Menlo Park, California.

SPATIAL, TEMPORAL, AND COMPOSITIONAL TRENDS OF VOLCANISM IN THE LASSEN REGION OF NORTHEASTERN CALIFORNIA

Marianne Guffanti, Michael A. Clynne, L. J. P. Muffler, and James G. Smith

U.S. Geological Survey

ABSTRACT

The volcanic record in the Lassen region of northeastern California began in late Miocene time and is substantially shorter than that of most of the Cascade Range to the north. Short-lived, mostly mafic volcanoes of small to moderate volume occur throughout the Lassen region, surrounding a few larger, more silicic, polygenetic volcanic centers. West of 120°30', 521 volcanic vents younger than 7 Ma were identified and classified by age within five time intervals and by composition based on SiO_2 content. Five large-volume polygenetic volcanic centers younger than 3 Ma occur in the western part of the volcanic region where the upper part of the subducting Gorda North plate is estimated to be at a depth of about 85-110 km. During the past 7 Ma, the locus of volcanic activity has shifted westward and contracted, and since 2 Ma volcanic rocks have erupted mostly west of 120°50'. Low-potassium high-alumina olivine tholeiite (HAOT), chemically similar to HAOT found in the northern Basin and Range province, has erupted throughout much of the Lassen region since the late Miocene. Many Quaternary vents in the Lassen area are aligned in NNW-trending groups; the dominantly normal faults in the region also are oriented in the same direction. Thus, the direction of maximum horizontal stress is NNW averaged over the interval 2-0 Ma, and the direction of least principal stress is ENE. In our preliminary volcano-tectonic model, subduction related to interaction of the Gorda North and North American plates and crustal extension related to interaction of the Pacific and North American plates overlap in the southernmost Cascade Range. We suggest that the two primitive magma types in the Lassen region, HAOT and calcalkaline basalt, reflect different tectonic controls on magma generation. Generation of HAOT is thought to be analogous to generation of that magma type in the northwestern Basin and Range province by a process of mantle melting related to extension. Generation of more voluminous calcalkaline basalt is thought to be related to melting of mantle metasomatized by introduction of slab-derived fluids into the mantle wedge.

Introduction

In the Lassen region of the Cascade Range during the late Cenozoic, a few large, long-lived polygenetic volcanic centers characterized by andesitic to rhyolitic volcanism developed within a larger area dominated by small-volume, short-lived, mafic volcanism. The larger area encompasses hundreds of mostly basaltic to intermediate volcanoes, each having erupted over a lifetime of less than about 10,000 years. This volcanism is spatially related to abundant normal faulting and merges eastward with the progressively older volcanism in the adjacent Basin and Range province. Using a data set of 521 identified volcanic vents younger than 7 Ma (Figure 1), we focus on broad spatial, temporal, and compositional trends of the dominantly mafic volcanism in the Lassen region. (In this study, we define the area approximately within the dashed line in Figure 1 as the Lassen region.) Our aim is to better understand the interaction of subduction-related volcanism and extensional tectonics in the southernmost Cascade Range.

Tectonic and Geologic Setting of the Lassen Region

The Lassen volcanic region of northeastern California is associated with subduction of the Gorda North plate beneath the North American plate. Volcanic arcs generally occur where the depth to the Wadati-Benioff zone is 100 km or more (Gill, 1981). For the Gorda North plate, subcrustal earthquake hypocenters along a Wadati-Benioff zone west of the Lassen region define slab dip of 25° between depths of 50-90 km (Walter, 1986; Cockerham, 1984). However, subcrustal earthquakes are not detected at depths greater than 90 km beneath the Lassen portion of the Cascade volcanic arc. Contours of plate depth are shown in Figure 1. The 110 and 130-km contours (dashed lines) are estimated by continued eastward projection of the 25° plate dip; if actual plate dip is steeper than that, the dashed contours would lie closer to the 90-km contour. Most vents of the Lassen region lie in an area beneath which the upper part of the subducting plate is estimated to be 85-130 km deep. The southern edge of the subducting slab is determined by the location of the migrating Mendocino triple junction, and currently the slab beneath the Lassen region does not extend further south than about 40°N (Jachens and Griscom, 1983; Dickinson and Snyder, 1979).

The Lassen volcanic region is bracketed by pre-Tertiary crustal rocks of the Klamath Mountains province on the northwest and of the Sierra Nevada province on the south and southeast (Lydon et al., 1960). Results of a two-dimensional seismic refraction study by Berge and Stauber (1987) suggest that the volcanic cover in the Lassen region is up to 4 km thick and probably overlies basement of the Sierra Nevada batholith. Blakely et al. (1985) suggest that an aeromagnetic anomaly (Figure 1) in the northern part of the Lassen region may represent an isolated fragment of mafic or ultramafic rocks at shallow depth in the crust; this aeromagnetic feature could be part of either the Trinity ophiolite complex of the Klamamth Mountains or an ultramafic body in the Sierra Nevada basement complex. Thus, a transition from Sierran to Klamath basement may occur beneath the Lassen region.

The Great Valley province is west and southwest of the volcanic region

(Figure 1). The contact between the Great Valley and the Quaternary volcanic arc is obscured by the late-Pliocene Tuscan Formation, which is composed predominantly of extensive volcanic mud flows, as well as silicic ash flows, basaltic to andesitic lava flows and rare intrusions, and volcanic sedimentary deposits (Lydon, 1968; Helley et al., 1981). The main source areas of the Tuscan Formation were large volcanic centers to the east within the volcanic arc.

The extensional Basin and Range province lies east of the Lassen region (Figure 1). Since about 16 Ma, the active zone of basaltic volcanism and faulting in the northern Basin and Range province has become progressively concentrated outward along the margins of the province (Wallace, 1984; Christiansen and McKee, 1978). In parts of Oregon and California, volcanism contracted successively westward. Grose and McKee (1982) described an east-to-west decrease in age of volcanism during the late Miocene in the Susanville area, on the eastern edge of the Lassen region.

Guffanti and Weaver (1988) considered the Lassen region as a separate segment of the Cascade arc because: (1) the Lassen region is separated from the Mt. Shasta and Medicine Lake volcanic centers to the north by an area in which there are few recognized late Cenozoic volcanic vents; (2) changes in age and geometry of the subducting slab are inferred between the Gorda North and southern Juan de Fuca plates; (3) more subcrustal seismicity occurs in the Lassen region relative to Oregon and northernmost California.

The Lassen region is geologically distinctive compared with the rest of the Cascade arc to the north in that volcanism older than late Miocene is uncommon in the Lassen region. North of the Lassen region, from west of Mt. Shasta to Mt. Rainier, thick sections of late Eocene or early Oligocene to middle Miocene volcanogenic rocks, the volcanic rocks of the Western Cascade Range, are widely exposed. In contrast, in the Lassen region only a few small areas of middle Miocene rocks are exposed, and late Eocene, Oligocene, and early Miocene rocks are not evident.

Voluminous volcanism with development of intermediate to silicic magmas has occurred in the Lassen region at five centers younger than 3 Ma (Snow Mountain, Yana, Dittmar, Maidu, and Lassen). These are located in the western part of the volcanic region where the upper part of the subducting slab is presumed to be at a depth of approximately 85-110 km (Figure 1). The youngest of the five centers is Lassen volcanic center (<0.6 Ma), which lies largely within Lassen Volcanic National Park (Clynne, this volume). Lassen volcanic center is the largest Quaternary silicic magma system in the Cascades, having produced about 100 km^3 of silicic (>63% SiO_2) rocks, or roughly half of its total eruptive volume.

Another notable feature of the Lassen region is that faults are more abundant than elsewhere in the range except, perhaps, around Medicine Lake volcano. The Lassen region is cut by numerous N- to NW-trending, dominantly normal faults that locally are closely spaced (Figure 2). The Walker Lane, a NW-striking right-lateral strike-slip fault zone that extends from Las Vegas to Susanville (Albers, 1967), occurs in the southeast part of the Lassen region near Honey Lake (Figure 1) and may continue northwest of Honey Lake (Grose, 1985).

Volcanic Trends

We located 521 vents in the Lassen region and assigned them to compositional and age categories. The vent data set was created from published geologic maps (Clynne, 1984; Hazlett, 1984; Helley et al., 1981; Tuppan, 1981; Bean, 1980; Younkin, 1980; MacDonald and Lydon, 1972; MacDonald, 1965, 1964, 1963; Lydon et al., 1960) and unpublished mapping by the authors and T. L. T. Grose. The compositional categories are based on SiO_2 content: basalt, 48-53%; basaltic andesite, 53-57%; andesite, 57-63%; dacite, 63-70%; rhyolite, >70%. The basalt category is further broken down into low-potassium high-alumina olivine tholeiite basalt and calcalkaline basalt. Compositions are determined on the basis of chemical analyses, thin section and hand sample identifications, and some best guesses. The distinction between basalt and basaltic andesite is not always reliable in the absence of chemical analyses. Age categories are slightly modified from those of Smith (1987): 7-2 Ma, 2-0.73 Ma, 730-120 ka, 120-25 ka, and 25-0 ka. Age determinations are based on unpublished K-Ar determinations by G. B. Dalrymple, A. L. Cook, L. B. Pickthorn, and J. G. Smith, 14-C dates by D. A. Trimble and S. W. Robinson, published ages of Grose and McKee (1986), Sarna-Wojcicki et al. (1985), Trimble et al. (1984), Crandell et al. (1974), Crandell (1972), and Ruben and Alaxander (1960), paleomagnetic determinations by D. E. Champion, glacial and volcanic stratigraphy, and geomorphological characterization by the authors.

Both calcalkaline and low-potassium high-alumina olivine tholeiitic basalt occur in the Lassen region. Primitive lavas of each basalt type are found. Following the convention of Hart et al. (1984), we abbreviate low-potassium high-alumina olivine tholeiite as HAOT. M. A. Clynne and T. D. Bullen (in preparation) argue on the basis of geochemical and isotopic data that primitive HAOT and calcalkaline basalt are not related by closed-system fractionation of one from the other. Furthermore, their data indicate that the two basalt types are derived from partial melting of different mantle source material.

Mafic volcanism in the Lassen region is predominately calcalkaline, forming shield volcanoes and cinder cones. Calcalkaline basalts have SiO_2 contents generally 50-53% and FeO/MgO of 0.6-1.9, TiO_2 contents of 0.5-1.9%, K_2O contents of 0.5-1.5%, and high ratios of alkali elements to high-field-strength elements. Calcalkaline basalts and basaltic andesites range from depleted to enriched in abundances and ratios of incompatible large-ion-lithophile elements. Calcalkaline andesite can be derived from calcalkaline basalt through fractionation, assimilation, and mixing processes (Bullen and Clynne, this volume).

HAOT basalt produces fluid, valley-filling lava flows that are widespread but thin, and HAOT lavas are volumetrically minor compared to calcalkaline basalt and basaltic andesite. Lassen HAOT typically is aphyric or sparsely porphyritic with diktytaxitic groundmass and has limited variability of chemical composition: SiO_2 contents generally less than 49%, FeO/MgO of 0.9-1.3, K_2O contents less than 0.4%, TiO_2 contents greater than 0.75%, low ratios of alkali to high-field-strength elements, and flat to slightly LREE-depleted rare-earth-element patterns relative to chondrites. HAOT basalt in the Lassen region is chemically similar in major- and trace-element composition (Table 1) to some basalt

found at Medicine Lake volcano (Mertzman, 1979) and in the northwestern Basin and Range province (Hart et al., 1984).

HAOT lavas have erupted throughout much of the Lassen region since the late Miocene (Figure 3). HAOT vents generally are topographically subdued features easily buried by younger volcanism. Because some HAOT flows do not have locatable vents, the number of vents shown in Figure 3 is a minimum. The oldest HAOT vents are late Miocene and Pliocene and occur east of the Quaternary arc. Among vents <2 Ma, no strong temporal/spatial trend is apparent. In the Quaternary arc, where HAOT vents are best preserved, many HAOT lavas erupted from NNW-trending alignments of vents. HAOT vents do not occur within the aeromagnetic anomaly of Blakely et al. (1985), whereas vents of calcalkaline basalt and basaltic andesite do. HAOT lavas erupt around Lassen volcanic center but not within it. HAOT magma may be generated beneath Lassen volcanic center but its geochemical signature has been swamped by mixing with calcalkaline magma, or HAOT magma is not generated in the area of most intense silicic volcanism.

Map distributions by age of vents of all compositions (including HAOT) show westward shift and contraction of the locus of volcanism during the past 7 Ma in the Lassen region (Figures 4-8). Most vents that formed in the late Miocene from 7-2 Ma (Figure 4) are found east of 121°15'. Late Miocene vents also are found further east of 120°30', beyond the area shown in Figure 4 (Luedke and Smith, 1981). The apparent lack of vents west of 121°15' probably is due in large part to burial of older vents by flows younger than 2 Ma. Compositions are predominantly mafic; basalt and andesite comprise 93% of all vents, and dacite and rhyolite vents comprise 7%. The Yana volcanic center was active around 3 Ma (Lydon, 1968) and the Snow Mountain center (J. G. Smith, unpublished data) and Dittmar center (Clynne, 1984, 1985) about 2 Ma.

During the period from 2 to 0.73 Ma (Figure 5), vents occur only as far east as about 120°50', which indicates that the locus of volcanism contracted westward. In this time interval, 60% of vents occur west of 121°15'. The percentage of andesites is higher (41%) than in the older group (17%), whereas the percentage of silicic vents is about the same (5% and 7%). The Maidu center (Wilson, 1961) became active during this period, and the Dittmar and Snow Mountain centers continued to be active. Linear trends of vents older than 0.73 Ma are not apparent at small scale on Figures 4 and 5.

From 730 to 120 ka (Figure 6), the area of volcanism was smaller than during older time intervals. Basalt and basaltic andesite form 82% of the vents, andesite 9%, and dacite 9%. A few NNW-trending vent alignments are evident. The Lassen volcanic center became active during this time interval (Clynne, 1984, 1985).

From 120-25 ka (Figure 7), the area of the bulk of vents continued to contract, except where vents of the Inskip Hill group (Helley et al., 1981) occur southwest of the Lassen volcanic center and near Eagle Lake. The compositional mix is similar to that of the previous time interval: basalt and basaltic andesite, 82%; andesite, 10%; dacite 8%. Vents are aligned from NNE to NW.

Volcanism younger than 25 Ka (Figure 8) is confined to a narrow, N-trending belt. Nearly all vents younger than 25 ka occur in linear groups having alignments that range from N to NW. A group of HAOT vents

oriented N9°W fed the Hat Creek Basalt flow north of Lassen volcanic center and is closely associated spatially with calcalkaline andesitic and basaltic vents younger than 120 ka. No silicic volcanism occurs outside of Lassen volcanic center during the past 100 ka.

A major volcanic trend of the Lassen region is that nearly all vents younger than 2 Ma occur west of 120°50' (Figure 9). As pointed out by Grose (1985), the Walker Lane appears to be an important structure in the Lassen region; all but two vents younger than 2 Ma are located west of the continuation of the Walker Lane NW from Honey Lake.

Alignments of vents from Figures 4-8 also are shown on Figure 9. This set of alignments is preliminary and is based on visual inspection rather than quantitative methods (e.g., Wadge and Cross, 1988). The criteria used to select alignments are: (a) groups of vents are approximately coeval, (b) vents are in groups of three or more, (c) vents are closely spaced or, if more widely spaced, are thought to be genetically related on the basis of geochemistry or field relations, and (d) only one alignment is obvious for a group of vents.

We assume, following Nakamura (1977), that vent alignments and normal faults trend parallel to the direction of maximum horizontal stress. Azimuths of linear groups of vents in the Lassen region range from N5°E to N55°W; 67% of the azimuths are from N7°W to N30°W. The vent alignments thus indicate that the approximate direction of maximum horizontal stress in the Lassen area west of 120°50', averaged over the past 2 Ma, is NNW. The corresponding direction of least principal stress is horizontal and oriented ENE.

Lassen volcanic center lies along the western edge of the youngest portion of the arc where NNW-trending vent alignments are well-defined. Within Lassen volcanic center, two groups of vents younger than 50 ka also are aligned in a NNW orientation, which indicates the imprint of regional tectonic stress on the silicic center rather than the perturbing effect of a young, large, shallow, magma body (Bacon, 1985; Nakamura, 1977).

N- to NW-striking, dominantly normal faults (Figure 2) indicate a similar NNW direction of maximum horizontal stress as do vent alignments. Faulting and volcanism are spatially related in a general sense in the Lassen region, although not every fault has vents along it, and not all magma rose along faults observable on the surface. Preliminary analysis indicates that the spatial and temporal distribution of faults varies throughout the Lassen region. In some areas, particularly the northern half of the region, normal faulting is concentrated in zones of closely spaced individual faults having separations of about 0.8 km; other areas lack closely spaced faults. Faulting appears to move from zone to zone with time, and the orientation of faults may change with time, becoming more northerly with younger faulting. Older fault scarps have more offset than younger ones.

A NNE-trending volcanic front (defined as the most trenchward extent of vents) delineated on Figure 9 is similar to the volcanic front defined by Guffanti and Weaver (1988) for the Lassen region. The front is roughly parallel to the strike of the Gorda North plate and occurs where the upper portion of the subducting plate is at a depth of approximately 80 km. The observation that vent and fault trends are dominantly NNW suggests that specific eruptive loci are controlled by crustal extension,

whereas the position of the volcanic front demarcates the area beneath which magmas are generated within the mantle wedge over the downgoing slab.

Discussion

A conceptual volcano-tectonic model of the Lassen region should incorporate the following observations: (1) the shorter volcanic history of the Lassen region compared to much of the Cascade Range to the north, (2) widespread, abundant mafic volcanism, (3) NNW trends of vent alignments and normal faults, (4) focusing of intermediate to silicic volcanism at five large-volume centers during the past 3 Ma, (5) concentration of volcanism younger than 2 Ma west of 120°50', and (6) generation of two primitive basalt types. We offer the following comments, recognizing that our model is incomplete.

The pattern of volcanism in northern California is significantly different from the pattern of volcanism in the Oregon Cascade Range. Tertiary arc volcanism of the Western Cascade Range in central and southern Oregon is progressively younger from west to east, and Quaternary arc volcanism is restricted to a belt east of the Tertiary arc (Sherrod, 1987). In contrast, from the Lassen region into Nevada, Tertiary volcanism becomes progressively older from west to east (Grose and McKee, 1986; Smith and Luedke, 1984; Stewart and Carlson, 1978). Accordingly, any tectonic model that ties the volcanic history of the Cascade Range as a whole to plate motions should account for these contrasting temporal/spatial trends.

Although Lassen volcanism is associated with plate subduction, we believe that another aspect of its regional tectonic setting also is pertinent to a volcano-tectonic model. The abundant basaltic volcanism and normal faulting clearly indicate widespread crustal extension in the Lassen region. Convergence of the Juan de Fuca and North American plates at an angle oblique to the convergent margin has been suggested as the cause of extension in the Cascade Range south of Mt. Rainier (Rogers, 1985; Bacon, 1982). However, the faulted Sierra Nevada block, a zone of seismicity in eastern California, the right-lateral Walker Lane, and the northwestern Basin and Range province converge near the Lassen volcanic region (Wallace, 1984, figure 3). This setting suggests to us that the Lassen region lies within the broad zone of distributed crustal extension related to late Cenozoic right-lateral transform displacement between the North American and Pacific plates. In our interpretation, subduction, related to interaction of the Gorda North and North American plates, and crustal extension, related to interaction of the Pacific and North American plates, overlap in the southernmost Cascade Range.

Seismic studies and comparison of regional stress regimes bolster this interpetation. On the basis of seismicity patterns and focal-mechanism solutions, Klein (1979) placed the Lassen region within a NW-trending seismogenic deformation zone of right-lateral shear and roughly E-W crustal extension; that approximate extension direction, based on data from a small seismograph network, is within reasonable agreement to the ENE direction we determine from vent alignments. Klein (1979) noted that the seismogenic deformation zone may be part of the seismic belt along the eastern margin of the Sierra Nevada. Furthermore, the direction of

least principal stress in the Lassen region, determined from vent alignments, is similar to that of the northern Sierra Nevada province, N77E, reported by Zoback and Zoback (1980). The Sierra Nevada province, within which both strike-slip and normal faulting are indicated by focal-mechansim solutions, marks a transition from predominantly strike-slip movement along the San Andreas to extensional deformation of the Basin and Range province (Zoback and Zoback, 1980). In the northern Basin and Range province, basaltic volcanism and faulting have become restricted successively outward into narrower marginal zones of the Great Basin since the mid Miocene (Wallace, 1984; Christiansen and McKee, 1978). This progressive concentration of volcanism and faulting observed in the Great Basin continues westward and impinges upon the Cascade arc in the Lassen region.

The occurrence of HAOT within the subduction-related volcanic arc in the Lassen region is significant because of implications for tectonic control of magma generation. Lassen HAOT is chemically similar in major- and trace-element composition to low-potassium high-alumina olivine tholeiite erupted during the past 10 Ma in the northwestern Basin and Range province (the HAOT of Hart et al., 1984). We presume that the extension-related process of magma generation that has produced HAOT in the Basin and Range province behind the arc, also has produced it within the Lassen volcanic arc. Basalt generation in the northern Basin and Range province is thought to have resulted from asthenospheric upwelling and partial melting beneath lithosphere thinned by extension. Carlson and Hart (1987) reasoned that HAOT, in particular, originated by melting of uppermost mantle at the base of the crust. Lassen calcalkaline basalt, on the other hand, is chemically similar to basalt from continental and mature island arcs and likely is derived from melting of mantle metasomatized by introduction of slab-derived fluids into the mantle wedge.

Thus, different domains of magma generation in the mantle, one related to extension and the other to the presence of a subducting slab, appear to overlap in the Lassen region. This reasoning is supported by the argument of M. A. Clynne and T. D. Bullen (in preparation) that the two primitive basalt types, HAOT and calcalkaline, cannot be related by closed-system fractionation or derived from partial melting of similar mantle source material. The spatial intermingling of calcalkaline and HAOT lavas (Figure 3) defines the zone where magmatism of the Cascade arc and the Great Basin overlap at the surface. Volcanism is primarily calcalkaline, but a lesser volume of HAOT reaches the surface within the subduction-related arc. The greatest flux of calcalkaline magma is generated beneath the large polygenetic centers, where the upper portion of the slab is at depths less than 120 km. Upper-crustal faulting fosters the rise of both calcalkaline and HAOT lavas to the surface.

The cause(s) of the meager early Miocene volcanism and of the westward shift and contraction of the area of volcanism during the late Miocene and Quaternary are not well understood. Our analysis is preliminary at this stage, so we simply outline four possible, not necessarily mutually exclusive, causes: (1) The width of volcanic arcs in various subduction zones has been shown to be related to plate dip (Gill, 1981). During early to mid Miocene time, the dip of the subducting plate beneath the Lassen volcanic arc may have been too shallow for magma generation.

Since then, the subducting slab may have steepened, reaching a sufficient depth for initiation of magmatism. Continued steepening with time would then have caused the area of volcanism to contract westward; (2) Prior to the late Miocene, convergence may have been too oblique for the subducting slab to reach magma-producing depth beneath the Lassen region. The motion of the Juan de Fuca plate system has become less oblique to the convergent margin since the early Miocene (Engebretsen et al., 1985). As the component of motion perpendicular to the strike of the Cascade arc increased with time, the subducting slab may have reached the necessary depth to produce arc volcanism within a shorter distance of the convergent margin; (3) Westward trench migration in response to clockwise propagation of the Juan de Fuca ridge during late Miocene time (Wilson et al., 1984) may have been responsible for concomitant westward volcanic shift in the arc. (4) The process that restricted volcanism and faulting successively westward into marginal zones of the northwestern Basin and Range province appears to have impinged on the Lassen region during the late Miocene and may have initiated widespread volcanism. A compressive crustal stress regime prior to impingement may have inhibited the surface expression of arc magmatism.

Closing Remarks

Our preliminary interpretation of volcanic trends in the Lassen region is based on the interaction of subduction and extension. The Lassen region lies within the broad zone of distributed crustal extension related to transform motion of the North America and Pacific plates. ENE-WSW extension of the upper crust produces NNW-trending vent alignments and normal faults. Within the faulted upper crust, foci of larger magma reservoirs shift over periods of hundreds of thousands of years. Generation of calcalkaline basalt is related to presence of a subducting slab, whereas generation of low-potassium high-alumina olivine tholeiite is associated with extensional tectonism within and behind the arc.

A volcano-tectonic model of northeastern California should explain two important features of the region, the meager volcanic record prior to the late Miocene and the westward shift and contraction of the locus of volcanism during the late Miocene. We give weight to the effect in the Lassen region of extension related to Pacific-North American plate interaction and suggest that the late-Cenozoic volcanic evolution of the southernmost Cascade Range has not been controlled solely by subduction parameters such as convergence angle, spreading rate, or slab dip.

Acknowledgements

We thank Julie Donnelly-Nolan for her helpful review of this paper.

REFERENCES CITED

Albers, J. P., 1967, Belt of sigmoidal bending and right-lateral faulting in the western Great Basin: Geological Society of America Bulletin, v. 78, p. 143-156.

Bacon, C. R., 1982, Geology and geophysics of the Cascade Range: Geophysics, v. 47, p. 423-424.

Bacon, C. R., 1985, Implications of silicic vent patterns for the presence of large crustal magma chambers: Journal of Geophysical Research, v. 90, p. 11243-11252.

Bean, S. M., 1980, Volcanotectonics and geothermal potential in the Big Jack Lake area, Lassen County, California: Golden, Colorado School of Mines, M.S. Thesis, 103 p.

Berge, P. A., and Stauber, D. A., 1987, Seismic refraction study of upper crustal structure in the Lassen Peak area, northern California: Journal of Geophysical Research, v. 92, p. 10,571-10,579.

Blakely, R. J., Jachens, R. C., Simpson, R. W., and Couch, R. W., 1985, Tectonic setting of the southern Cascade Range as interpreted from its magnetic and gravity fields: Geological Society of America Bulletin, v. 96, p. 43-48.

Carlson, R. W., and Hart, W. K., 1987, Crustal genesis on the Oregon Plateau: Journal of Geophysical Research, v. 92, p. 6191-6206.

Christiansen, R. L., and McKee, E. H., 1978, Late Cenozoic volcanic and tectonic evolution of the Great Basin and Columbia Intermontane regions: Geological Society of America Memoir, v. 152, p. 283-311.

Clynne, M. A., 1984, Stratigraphy and major-element geochemistry of the Lassen Volcanic Center, California: U.S. Geological Survey Open-File Report 84-224, 168 p.

Clynne, M. A., 1985, Quaternary volcanism in the southernmost Cascade Range, in Guffanti, M. and Muffler, L. J. P., editors, Proceedings of the Workshop on Geothermal Resources of the Cascade Range, U.S. Geological Survey Open-File Report 85-521, p. 24-30.

Cockerham, R. S., 1984, Evidence for a 180-km-long subducted slab beneath northern California, Bulletin of the Seismological Society of America, v. 74, p. 569-576.

Crandell, D. R., 1972, Glaciation near Lassen Peak, northern California: U.S. Geological Survey Professional Paper 800-C, p. C179-C188.

Crandell, D. R., Mullineaux, D. R., Sigafoos, R. S., and Ruben, M., 1974, Chaos Crags eruptions and rock-fall avalanches, Lassen Volcanic National Park: U.S. Geological Survey Journal of Research, v. 2, no.

1, p. 49-59.

Dickinson, W. R., and Snyder, W. S., 1979, Geometry of subducted slabs related to San Andreas transform: Journal of Geology v. 87, p. 609-627.

Engebretson, D. C., Cox, A., and Gordon, R. G., 1985, Relative motions between oceanic and continental plates in the Pacific Basin: Geological Society of America Special Paper 206, 59 p.

Gill, J. B., 1981, Orogenic Andesites and Plate Tectonics, Springer Verlag, New York, 390 p.

Grose, T. L. T., 1985, Volcanotectonic evidence for stress field changes since late Miocene in Basin and Range-Cascade boundary zone (Walker Lane) of northeastern California (abstract): Eos, Transactions of the American Geophysical Union, v. 66, p. 1091.

Grose, T. L. T., and McKee, E. H., 1982, Late Cenozic westward volcanic progression east of Lassen Peak, northeastern California (abstract): Eos, Transactions of the American Geophysical Union, v. 63, p. 1149.

Grose, T. L. T., and McKee, E. H., 1986, Potassium-argon ages of late Miocene to late Quaternary volcanic rocks in the Susanville-Eagle Lake area, Lassen County, California: Isochron West, v. 45, p. 5-11.

Guffanti, M., and Weaver, C. S., 1988, Distribution of late Cenozoic volcanic vents in the Cascade Range: volcanic arc segmentation and regional tectonic considerations: Journal of Geophysical Research, v. 93, p. 6513-6529.

Hart, W. K., Aronson, J. L., and Mertzman, S. A., 1984, Areal distribution and age of low-K, high-alumina olivine tholeiite magmatism in the northwestern Great Basin: Geological Society of America Bulletin, v. 95, p. 186-195.

Hazlett, D. P., 1984, A volcanotectonic and paleomagnetic investigation in the Hayden Hill area: Golden, Colorado School of Mines, M.S. Thesis, 155 p.

Helley, E. J., Harwood, D. S., Barker, J. A., and Griffin, E. A., 1981, Geologic map of the Battle Creek fault zone and adjacent parts of the northern Sacramento Valley, California: U.S. Geological Survey Map MF-1298, scale 1:62,500.

Jachens, R. C., and Griscom, A., 1983, Three-dimensional geometry of the Gorda Plate beneath northern California: Journal of Geophysical Research, v. 88, p. 9375-9392.

Klein, F. W., 1979, Earthquakes in Lassen Volcanic National Park, California: Bulletin of the Seismological Society of America, v. 69, p. 867-875.

Luedke, R. G., and Smith, R. L., 1981, Map showing distribution, compositon, and age of late Cenozoic volcanic centers in California and Nevada: U.S. Geological Survey Miscellaneous Investigations Series Map 1091-C, scale 1:1,000,000.

Lydon, P. A., 1968, Geology and lahars of the Tuscan Formation, northern California: Geological Society of America Memoir 116, p, 441-475.

Lydon , P. A., Gay, T. E., Jr., and Jennings, C. W., 1960, Geologic Map of California, Westwood (Susanville) sheet: California Division of Mines and Geology, San Francisco, scale 1:250,000.

MacDonald, G. A., 1963, Geology of the Manzanita Lake quadrangle: U.S. Geological Survey Map GQ-248, scale 1:62,500.

MacDonald, G. A., 1964, Geology of the Prospect Peak quadrangle: U.S. Geological Survey Map GQ-345, scale 1:62,500.

Macdonald, G. A., 1965, Geologic map of the Harvey Mountain quadrangle: U.S. Geological Survey Map GQ-443, scale 1:62,500.

MacDonald, G. A., and Lydon, P. A., 1972, Geologic map of the Whitmore quadrangle: U.S. Geological Survey Map GQ-993, scale 1:62,500.

Mertzman, S. A., Jr., 1979, Strontium isotope geochemistry of a low potassium olivine tholeiite and two basalt-pyroxene andesite magma series from Medicine Lake Highland, California: Contributions to Mineralogy and Petrology, v. 70, p. 81-88.

Nakamura, K., 1977, Volcanoes as possible indicators of tectonic stress orientation: Journal of Volcanology and Geothermal Research, v. 2, p. 1-16.

Rogers, G. C., 1985, Variation in Cascade volcanism with margin orientation: Geology, v. 13, p. 495-498.

Ruben, M. and Alaxander, C., 1960, U.S. Geological Survey radiocarbon dates V: American Journal of Science Radiocarbon Supplement, v. 2, no. 2, p. 129-185.

Sarna-Wojcicki, A. M., Meyer, C. E., Bowman, H. R., Hall, N. T., Russell, P. C., Woodward, M. J., and Slate, J. L., 1985, Correlation of the Rockland ash bed, a mid-Pleistocene stratigraphic marker in northern and central California and western Nevada: Quaternary Research Journal, v. 23, p. 236-257.

Sherrod, D. R., 1987, New compilation map of the Cascade Range in Oregon: Geothermal Resources Council Transactions., v. 11, p. 305-307.

Smith, J. G., 1987, New compilation geologic map of the Cascade Range in Washington: Geothermal Resources Council Transactions, v. 11, p. 309-

314.

Smith, R. L., and Luedke, R. G., 1984, Potentially active volcanic lineaments and loci in western conterminous United States, in Explosive Volcanism: Inception, Evolution, Hazards, pp. 47-66, National Academy Press, Washington, D.C.

Stewart, J. H., and Carlson, J. E., 1978, Generalized maps showing distribution, lithology, and age of Cenozoic igneous rocks in the Western United States: Geological Society of America Memoir 152, p. 263-264.

Trimble, D. A., Clynne, M. A., and Robinson, S. W., 1984, The application of uranium-thorium systematics to rocks from the Lassen dome field, California: U.S. Geological Survey Open-File Report 84-371, 100 p.

Tuppan, E. J., 1981, The volcanics and tectonics of the Slate Mountain area, Lassen County, California: Golden, Colorado School of Mines, M.S. Thesis, 130 p.

Wadge, G. and Cross, A., 1988, Quantitative methods for detecting aligned points: an application to the volcanic vents of the Michoacan-Guanajuato volcanic field, Mexico: Geology, v. 16, p. 815-818.

Wallace, R. E., 1984, Patterns and timing of late Quaternary faulting in the Great Basin province and relation to some regional tectonic features: Journal of Geophysical Research, v. 89, p. 5763-5769.

Walter, S. R., 1986, Intermediate-focus earthquakes associated with Gorda plate subduction in northern California: Bulletin of the Seismological Society of America, v. 76, p. 583-588.

Wilson, D. S., Hey, R. N., and Nishimura, N., 1984, Propagation as a mechanism of reorientation of the Juan de Fuca ridge: Journal of Geophysical Research, v. 89, p. 9215-9225.

Wilson, T. A., 1961, The geology near Mineral, California: M.S. Thesis, University of California at Berkeley, 92 p.

Youngkin, M. T., 1980, Upper Cenozoic volcanotectonics of the Eagle Lake in the southeastern Cascade Range, Lassen County, California: Golden, Colorado School of Mines, M.S. Thesis.

Zoback, M. L. and Zoback, M., 1980, State of stress in the conterminous United States: Journal of Geophysical Research, v. 85, p. 6113-6156.

Table 1. Average compositions of low-potassium high-alumina olivine tholeiite (HAOT) from the northwestern Basin and Range province (average of 50 samples as reported in Hart et al., 1984) and from several flows from the Lassen region (35 samples for major-elements, 24 of which have trace-element analyses; M. A. Clynne, unpublished data).

	LASSEN	GREAT BASIN
SiO_2	48.66	47.66
AlO_2	17.75	16.91
CaO	11.10	11.20
Na_2O	2.79	2.53
TiO_2	0.97	1.00
K_2O	0.23	0.23
FeO	9.24	9.88
MgO	8.78	9.06
MgO/FeO	0.94	0.92
Rb	2.16	2.1
Sr	273	255
Rb/Sr	0.0008	0.0008
Ba	121	141
Zr	79	95

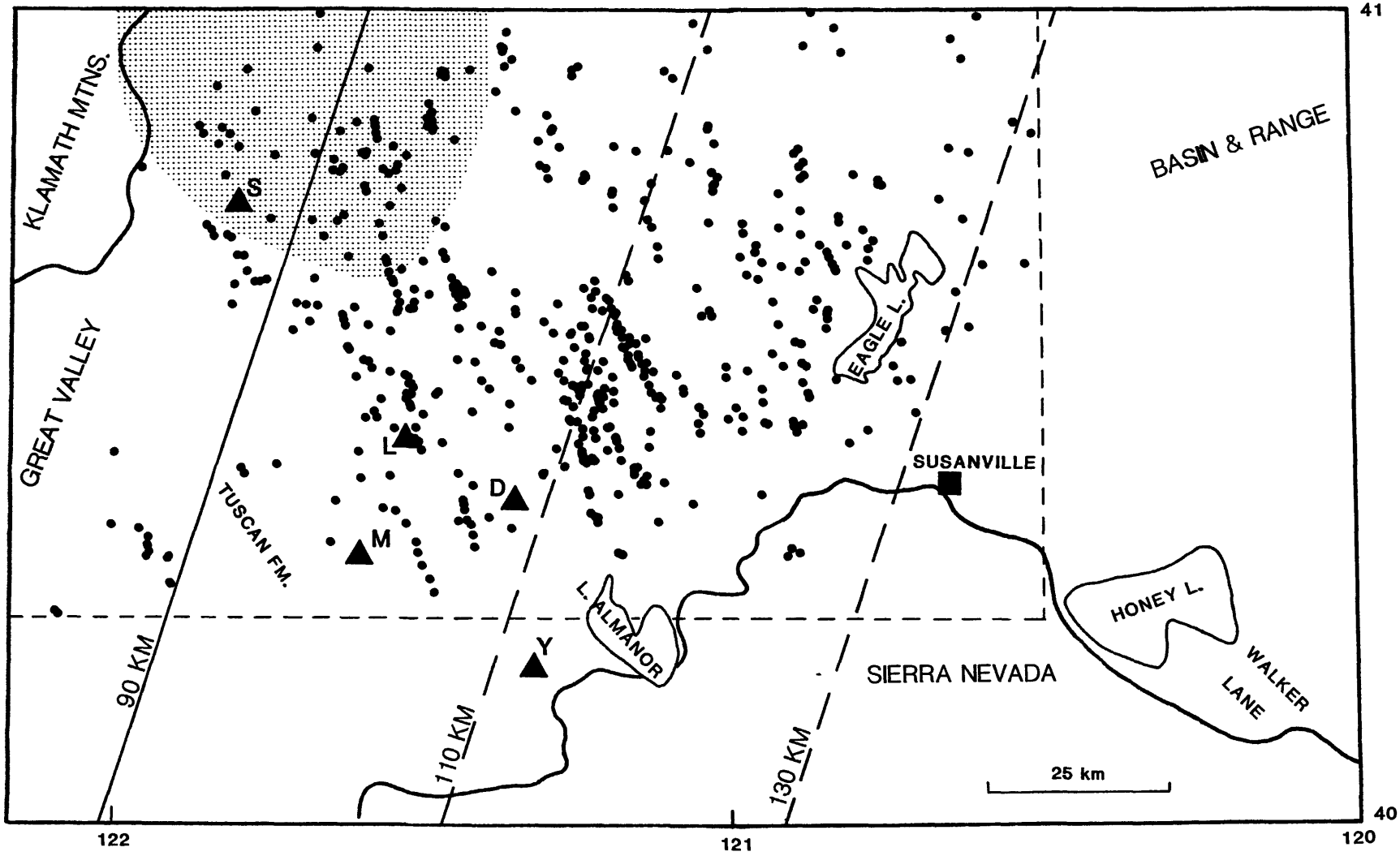

FIGURE 1. Regional geologic and tectonic setting of the Lassen volcanic region. Solid dots depict 521 volcanic vents younger than 7 Ma. Large solid triangles indicate major volcanic centers younger than 3 Ma: Y, Yana; D, Dittmar; M, Maidu; L, Lassen; S, Snow Mountain. Shaded area is aeromagnetic anomaly from Blakely et al. (1985, Figure 7, feature F). Inferred position of subducting plate at depths of 110 km and 130 km shown by NE-trending dashed lines. Rectangle formed by thin dashed line is area in Figures 3-9.

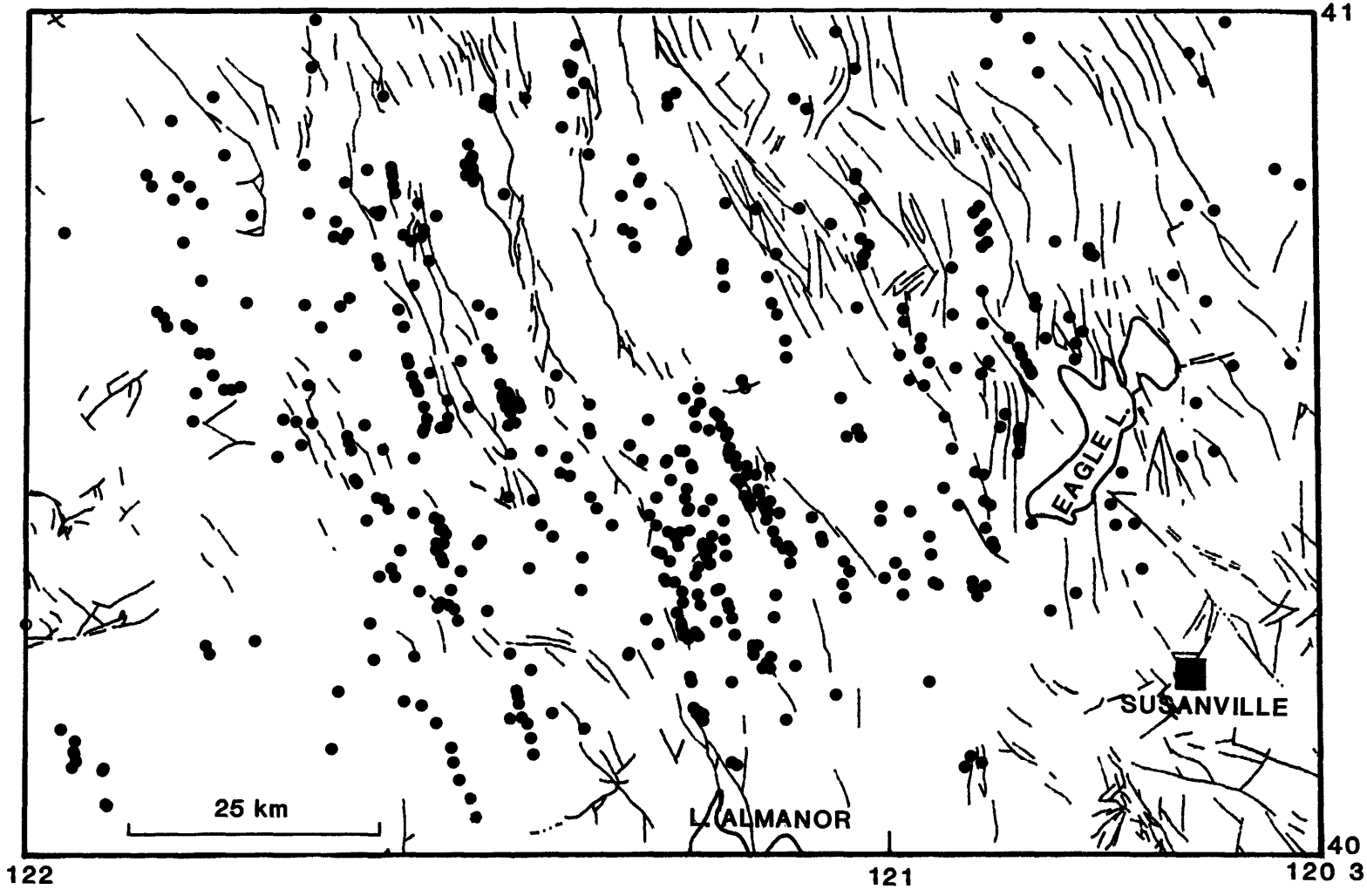

FIGURE 2. Volcanic vents less than 7 Ma (solid dots) and faults (thin lines; from Lydon et al., 1960).

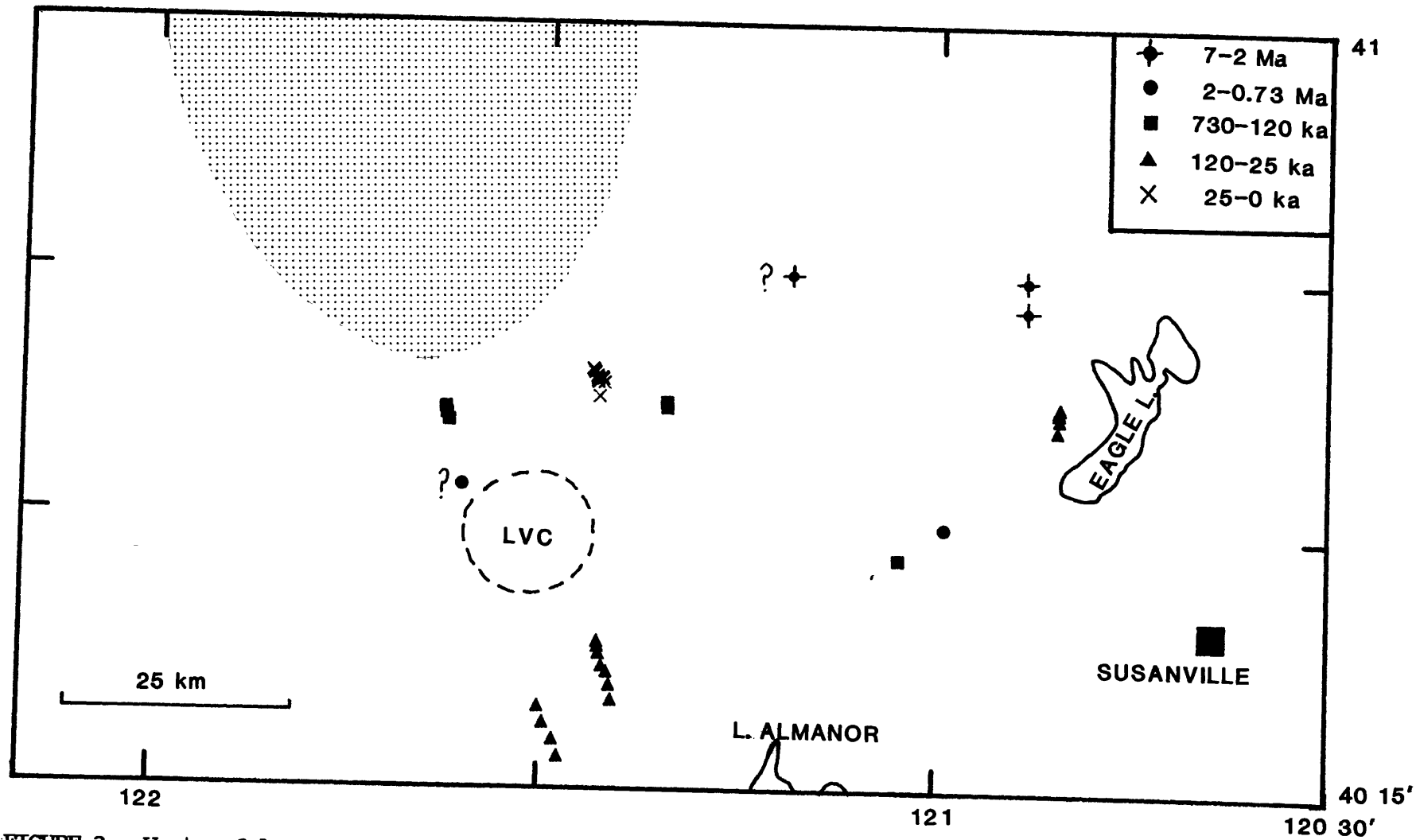

FIGURE 3. Vents of low-potassium high-alumina olivine tholeiite (HAOT). Symbols indicate age categories. Some HAOT flows do not have identifiable vent areas; in 2 cases, inferred vent locations, presumed to be buried by younger flows, are shown by queried symbols. Dashed circle encloses vent area of Lassen volcanic center (LVC). Shaded area is aeromagnetic anomaly from Blakely et al. (1985).

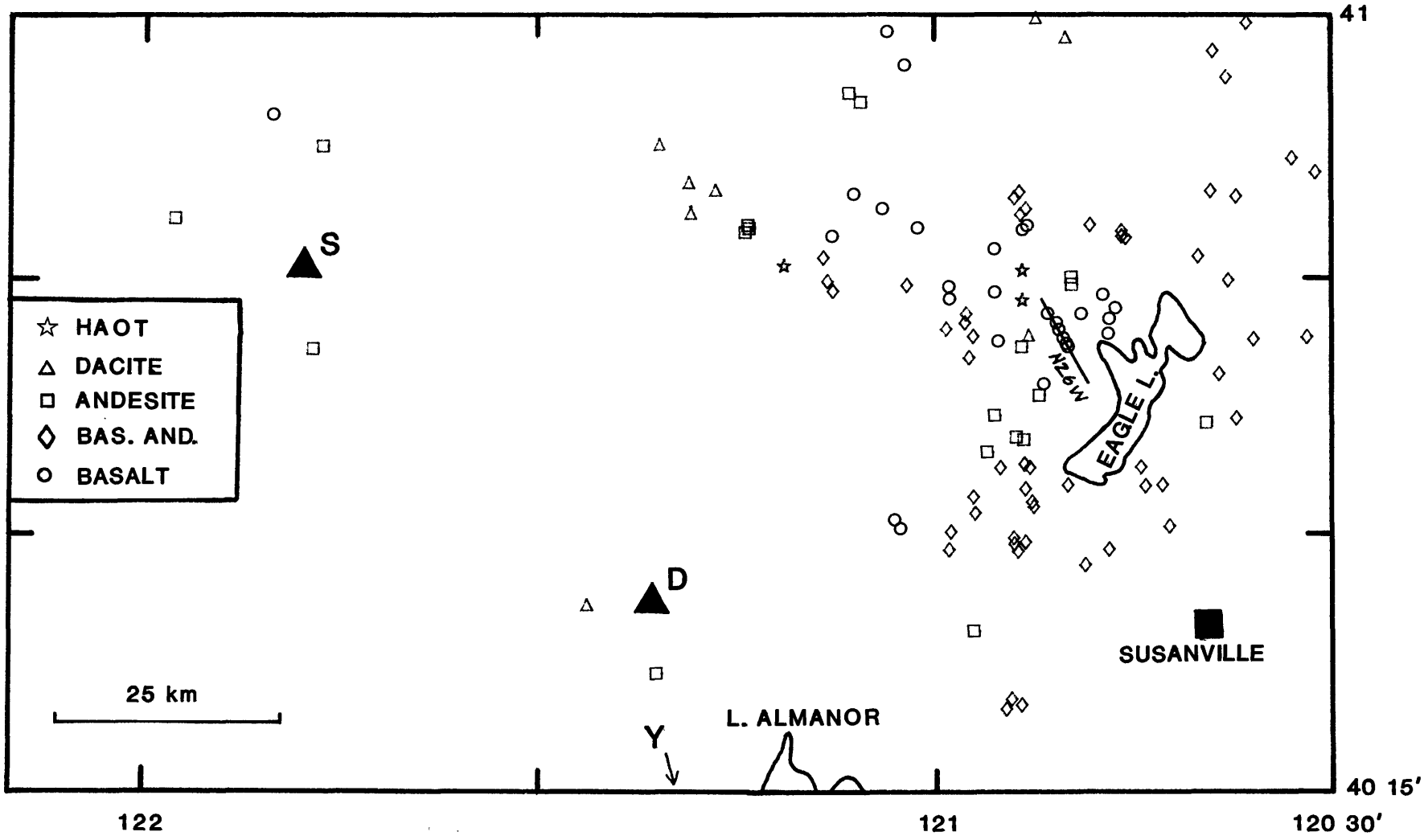

FIGURE 4. 112 volcanic vents formed from 7 to 2 Ma. Symbols indicate compositional categories. Vent alignment shown by oriented line. Volcanic centers: Y, Yana; S, Snow Mountain; D, Dittmar.

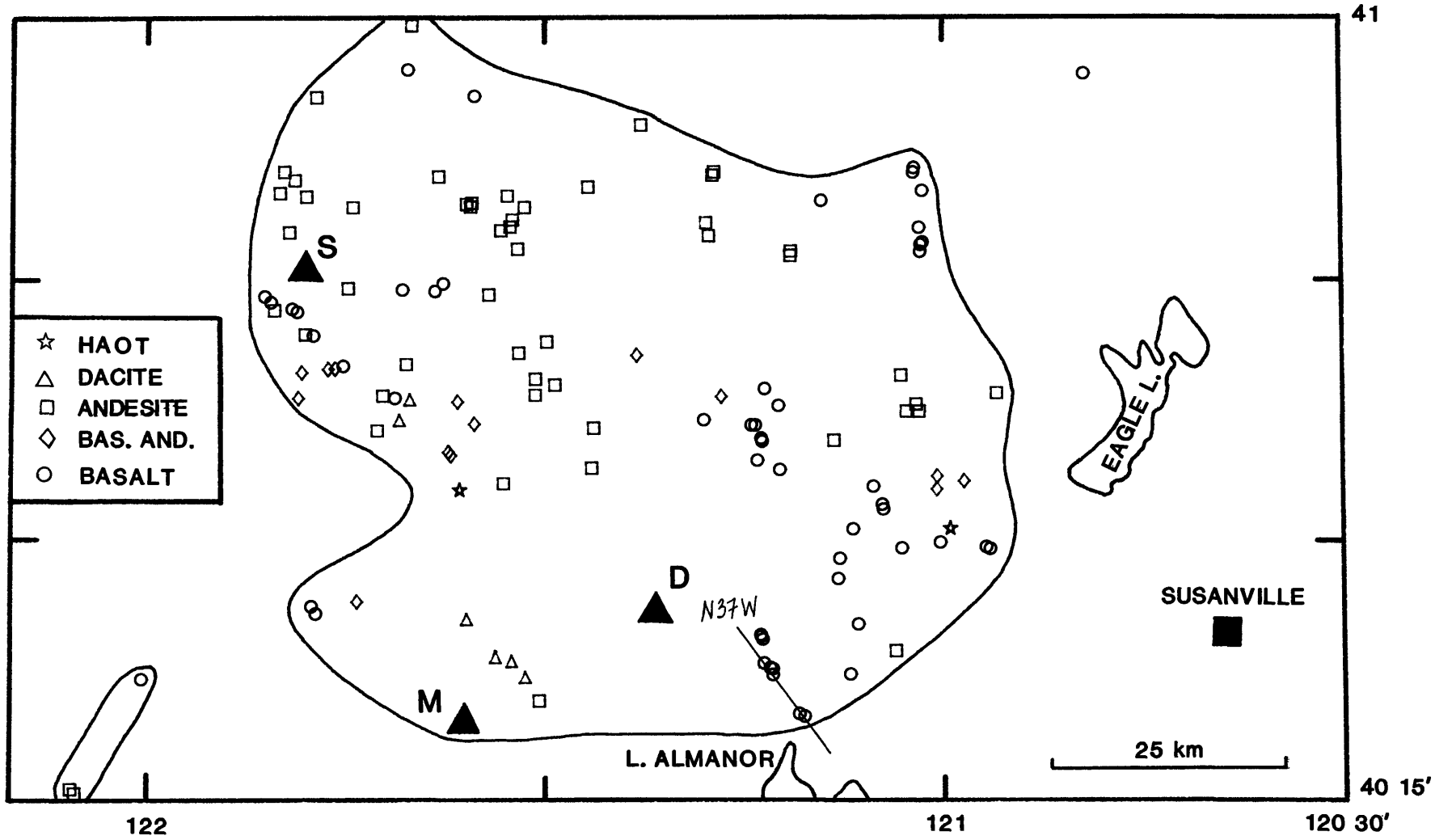

FIGURE 5. 127 vents formed from 2 to 0.73 Ma. Symbols indicate compositional categories. Irregular solid line encloses locus of vents. Vent alignment shown by oriented line. Volcanic centers: S, Snow Mountain; D, Dittmar; M, Maidu.

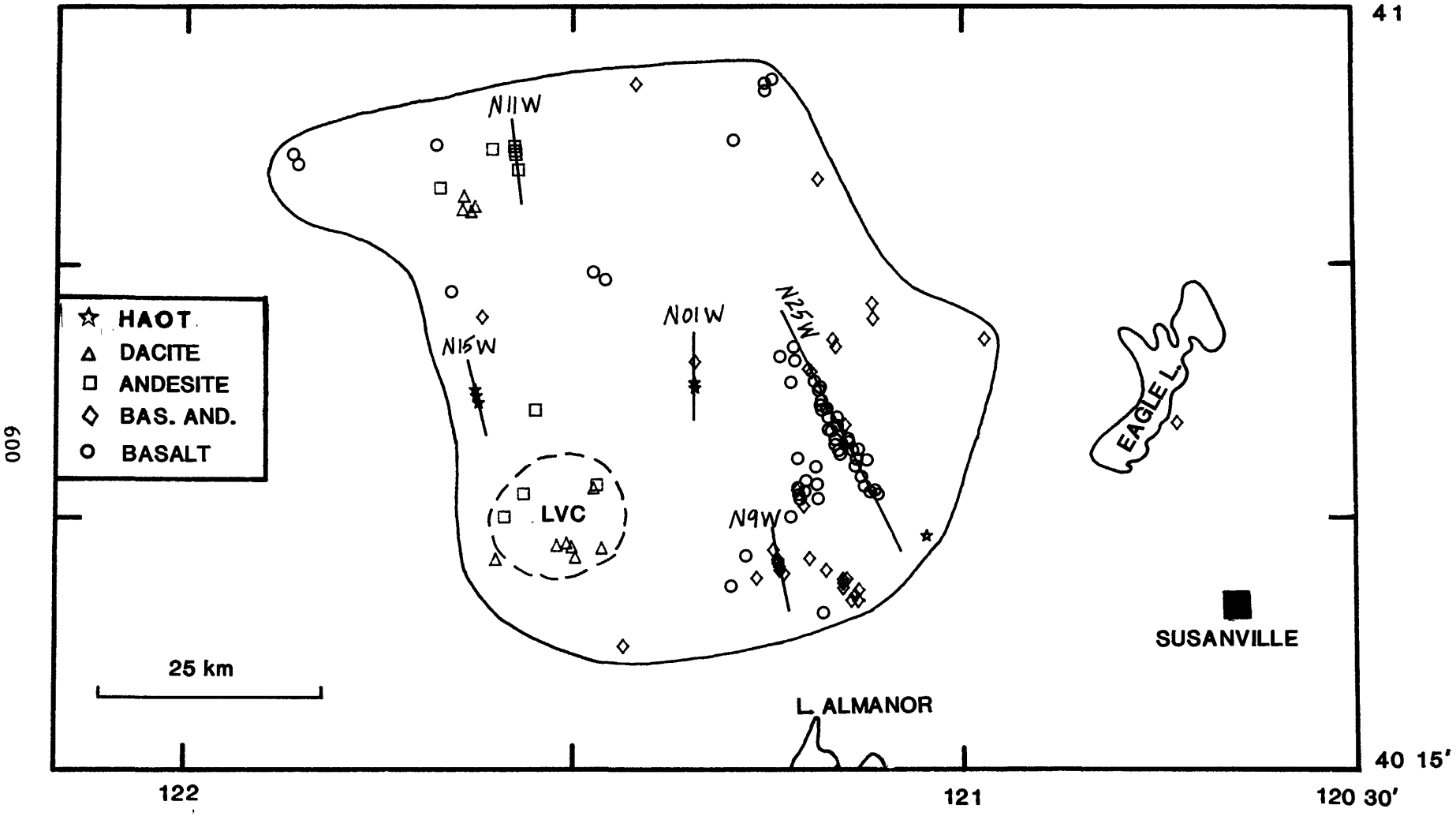

FIGURE 6. 116 vents formed from 730 to 120 ka. Symbols indicate compositional categories. Irregular solid line encloses locus of vents. Vent alignments shown by oriented lines. Dashed circle encloses vents of Lassen volcanic center (LVC).

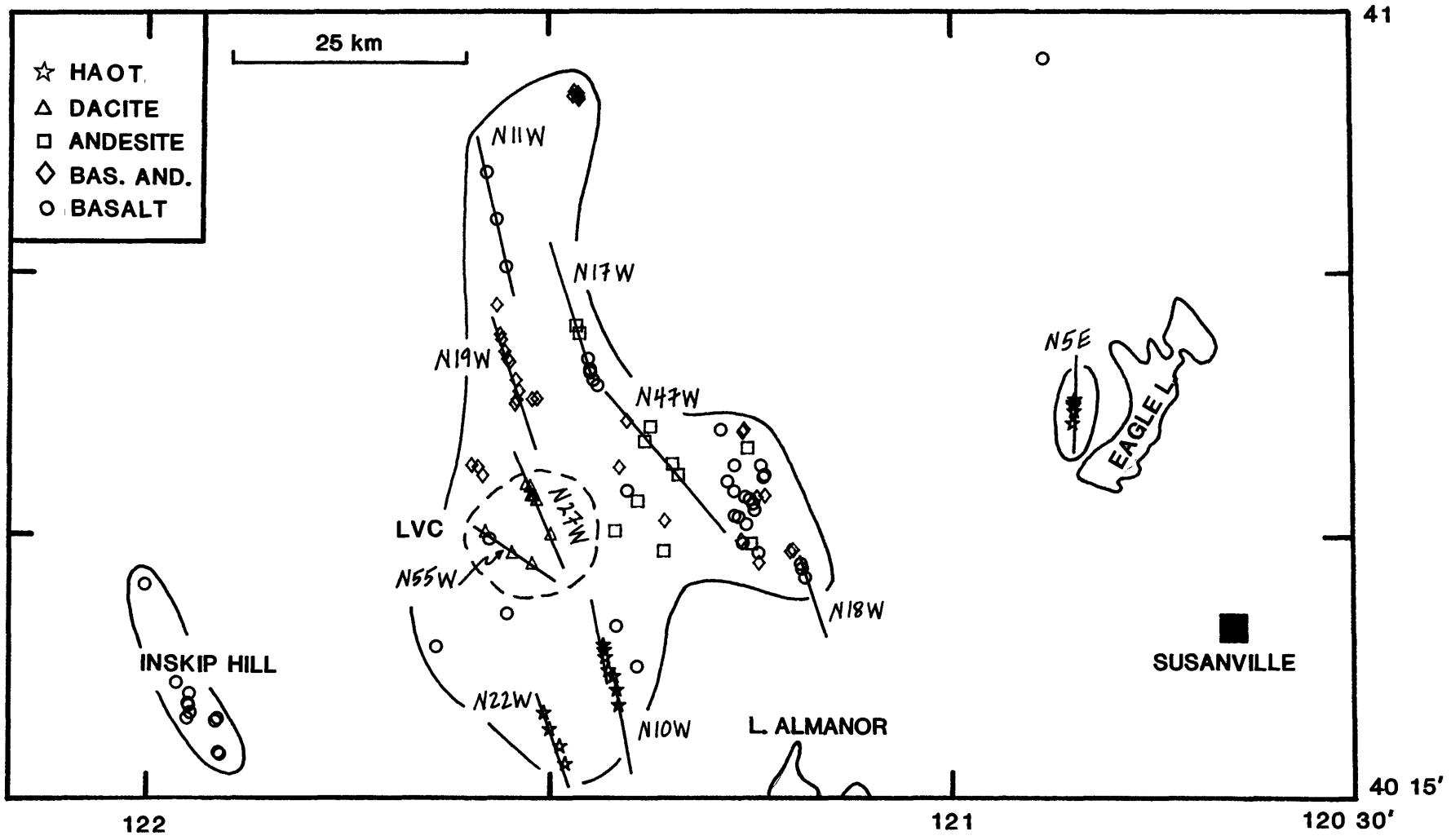

FIGURE 7. 114 vents formed from 120 to 25 ka. Symbols indicate compositional categories. Irregular solid line encloses locus of vents. Vent alignments shown by oriented lines. Dashed circle encloses vents of Lassen volcanic center (LVC).

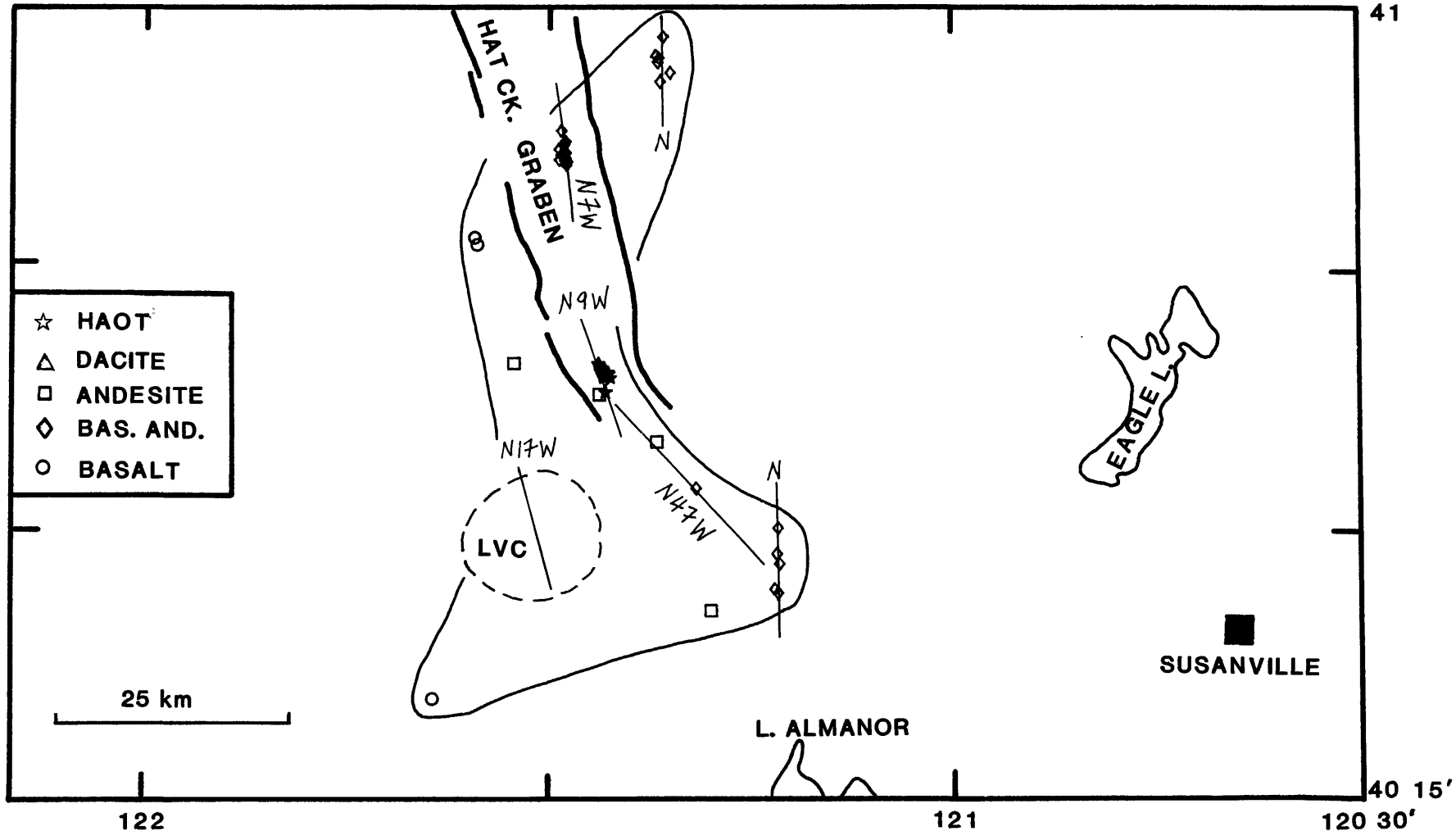

FIGURE 8. 52 vents younger than 25 Ka. Symbols indicate compositional categories. Irregular solid line encloses locus of vents. Vent alignments shown by oriented lines. Dashed circle encloses vents of Lassen volcanic center (LVC). Thick solid lines are faults of Hat Creek graben (generalized from Lydon et al., 1960).

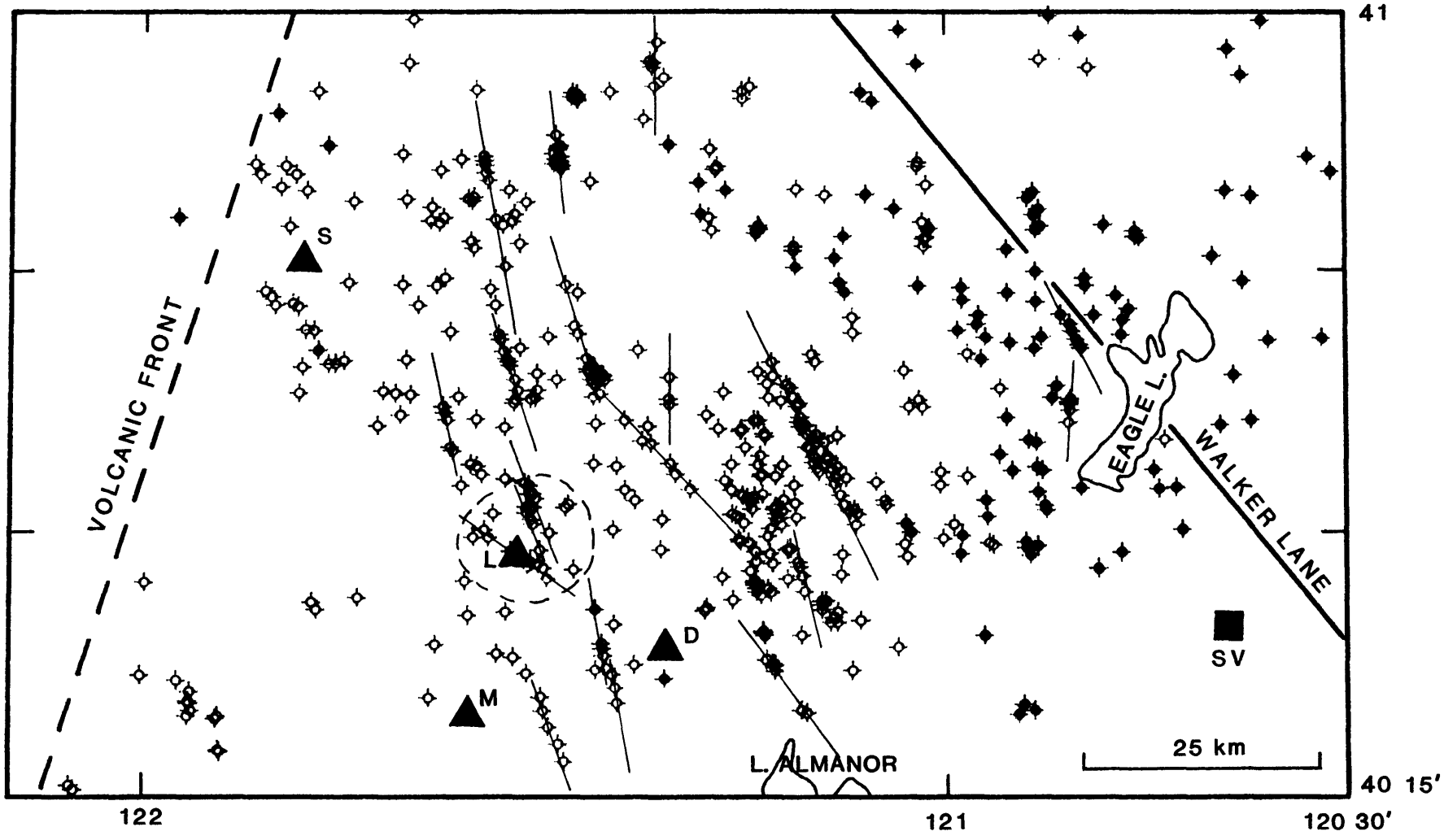

FIGURE 9. 521 volcanic vents younger than 7 Ma. Symbols depict age categories: open symbol, 2-0 Ma; filled symbol, 7-2 Ma. Volcanic centers: L, Lassen; M, Maidu; D, Dittmar; S, Snow Mountain. Short thin lines show vent alignments. Dashed NE-trending line is volcanic front. Solid NW-trending line is continuation of Walker Lane.

Stratigraphic and Lithologic Constraints on the Nature of the Magmatic System at the Lassen Volcanic Center, California

Michael A. Clynne
U. S. Geological Survey
345 Middlefield Road MS 910
Menlo Park, CA 94025

Abstract

The Lassen volcanic center is the most recent of several long-lived centers in the southernmost Cascade Range. These centers have erupted products ranging from basaltic andesite to rhyolite and are superimposed on a background of regional basaltic to andesitic volcanism. The evolution of the Lassen volcanic center is described in three stages. Stages I and II comprise the Brokeoff volcano, an 80 km^3 andesitic stratocone, active from 600 to 400 ka. Stage III comprises a silicic domefield and adjacent area of hybrid andesites, and has a total volume of 120 km^3. Volcanism during Stage III was episodic and is subdivided into four sequences of lithologically and temporally distinct lavas. Stage III began at 400 ka with a rhyolitic, caldera-forming pyroclastic eruption. Additional sequences of dacite and rhyodacite erupted between 250-200 ka and 100-0 ka. Hybrid andesites erupted adjacent to the silicic domefield between 300 and 0 ka.

Porphyritic andesite and dacite with high Al_2O_3, low TiO_2, and medium K_2O contents, and FeO/MgO ratios of 1.5-2.0, are the most abundant rock types in the Lassen volcanic center. The single most voluminous unit is sparsely phyric rhyolite pumice (Rockland tephra). Early basaltic andesite, late rhyodacite, and hybrid andesite are subordinate in abundance. Silica content ranges from 53 to 75 %, and in general the lavas of Lassen volcanic center form a single coherent trend on variation diagrams. In detail, however, the lack of systematic change in silica content and subtly crossing trends indicate a complex origin.

Petrographic and stratigraphic evidence indicate that magma mixing is an important but subtle process in Brokeoff lavas, and that the lavas evolved in small independent batches. Brokeoff volcano is compositionally equivalent to the regional volcanism and is the result of structurally-controlled focussing of the diffuse regional mafic volcanism.

Lavas erupted during Stage III, while predominantly silicic, range from 53-75 % SiO_2. They are not directly derived from andesitic magma related to Brokeoff volcano. Instead, partial melting of young mafic crust is involved in their origin. Mixing with regional basaltic magma and disaggregation of quenched magmatic inclusions play important roles in the compositional diversity of Stage III-lavas.

The long span of activity at LVC and the presence of a vigorous hydrothermal system imply the presence of an evolving magma chamber. Systematic geochemical variation and the mineralogic and geochemical homogeneity of the youngest rocks suggest derivation from a single long-lived magma body. The magmatic system of the Lassen volcanic center is envisaged as an evolving pluton-sized body in the middle crust (10-20 km depth). However, the molten part of the magmatic system is relatively small.

Introduction

Volcanism in the southernmost Cascade Range can be characterized on two scales. On the regional scale, volcanism is predominantly basaltic to andesitic, and hundreds of coalescing volcanoes have small volumes (10^{-3} to 10^{2} km^3) and relatively short lifetimes (10^{0} to 10^{3} years). Individual centers range from monogenetic cinder cones of basalt and basaltic andesite to larger lava cones and shields of basaltic to andesitic composition. Rocks with greater than 60 per cent SiO_2 are sparse. Superimposed on this regional mafic volcanism are a few long-lived, much larger volcanic centers that have erupted products spanning a wide range of composition, from basaltic andesite to rhyodacite or rhyolite.

Each of the larger centers consists of an andesitic composite cone and flanking silicic domes and flows. Four such centers younger than about 3 Ma have been recognized in the Lassen Volcanic National Park area. Each had a similar history, consisting of three stages: (1) an initial cone-building period of basaltic andesite and andesite lava flows and pyroclastic deposits; (2) a later cone-building period of thick andesite and silicic andesite lava flows, and (3) silicic volcanic rocks flanking the main cone. The silicic magma chamber of the third stage provides a heat source for a hydrothermal system that develops within the core of the main cone. Alteration of permeable rocks of the cone facilitates glacial and fluvial erosion of the central part of the volcano. The result is selective preservation of a resistant rim of thick cone-building lava flows and flanking silicic rocks around a central depression, which replaces the altered and eroded core of the composite cone.

The four older volcanic centers in the Lassen area, the Yana, Snow Mountain, Dittmar, and Maidu volcanic centers (Clynne, 1984) have reached this terminal stage and their hydrothermal systems are extinct. The youngest, here called the Lassen volcanic center, however, hosts active silicic volcanism and a well developed hydrothermal system, including the thermal features in Lassen Volcanic National Park and Mill Canyon.

Lassen Volcanic Center

The Lassen volcanic center is located in the western and central parts of Lassen Volcanic National Park and has evolved through the three stages outlined above. The distribution of rock units is shown in figure 1, a generalized geologic map of Lassen Volcanic National Park and vicinity. For more detailed stratigraphy see Clynne (1984). The chemical evolution of the Lassen volcanic center is illustrated schematically in figure 2 and pertinent aspects of the Lassen volcanic center are summarized in table 1.

The evolution of the Lassen volcanic center began with the construction of Brokeoff volcano, an andesitic stratocone. Glaciation, enhanced by hydrothermal alteration of permeable rocks resulted in deep erosion of the volcano. The major remnants are Brokeoff Mtn., Mt. Diller, Mt. Conard, and Diamond Peak. Reconstruction of Brokeoff volcano indicates that its summit was approximately 3,350 m high and that it had a basal diameter of about 12 km. The total volume of Brokeoff volcano was about 80 km^3. The evolution of the Brokeoff volcano can be described in two stages: I and II. Brokeoff volcano was active for about 200 ka: Stage I from 600 to 470 ka, and Stage II from 470 to 400 ka.

The bulk of Brokeoff volcano consists of Stage-I deposits. The core consists of thin, glassy andesite lava flows and abundant, intercalated

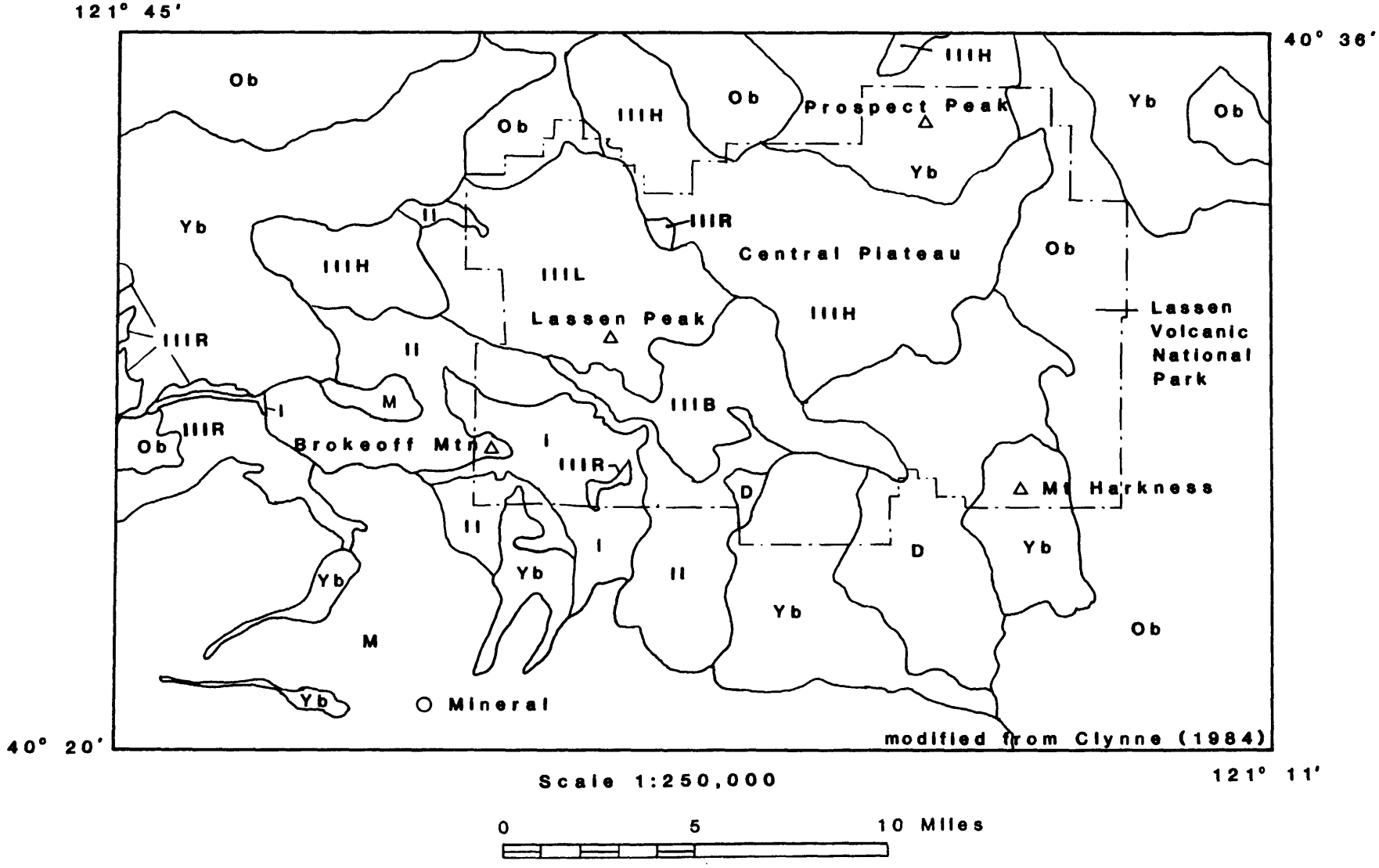

Figure 1. Generalized geologic map of the Lassen volcanic center.

FIGURE 1: LEGEND

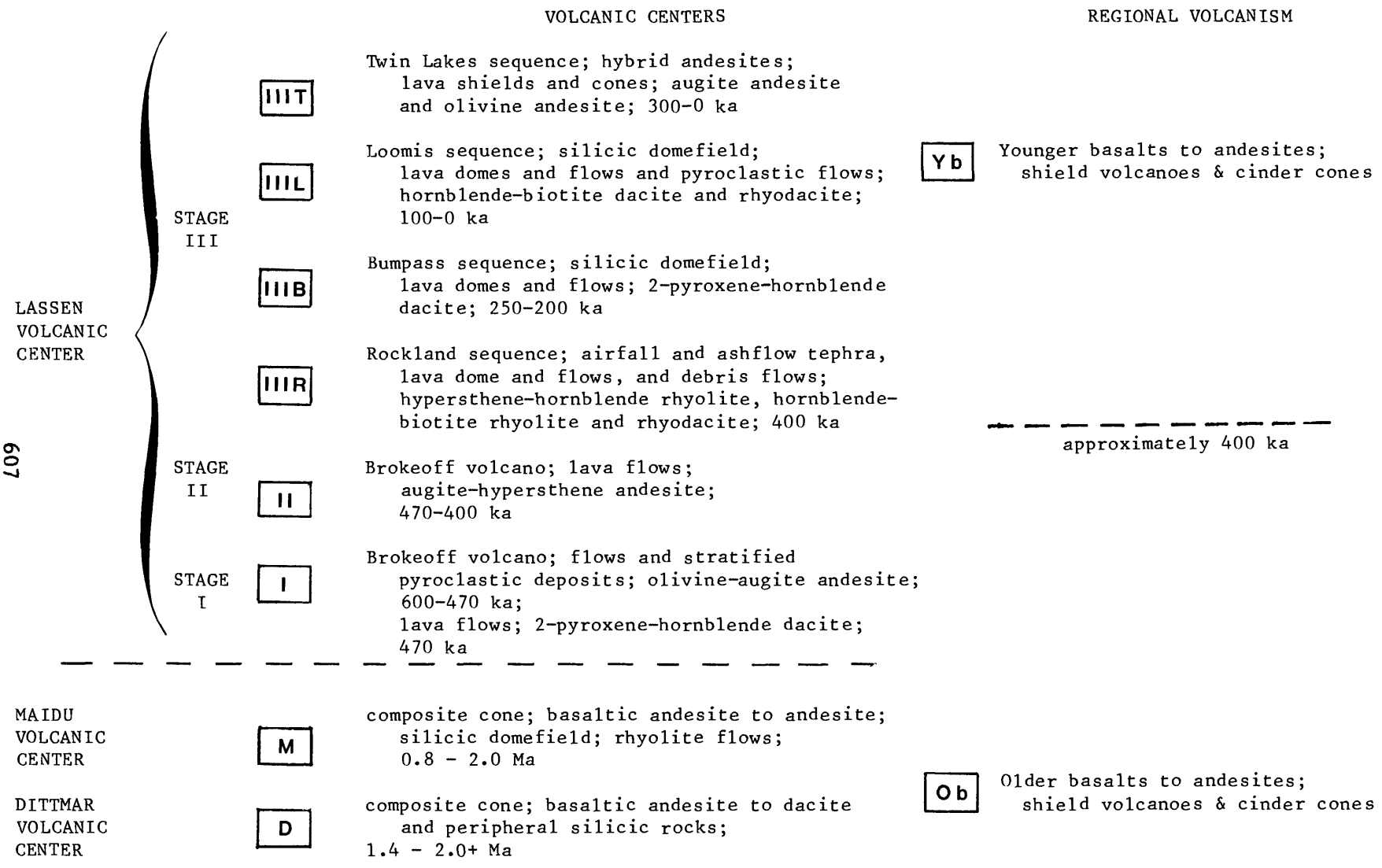

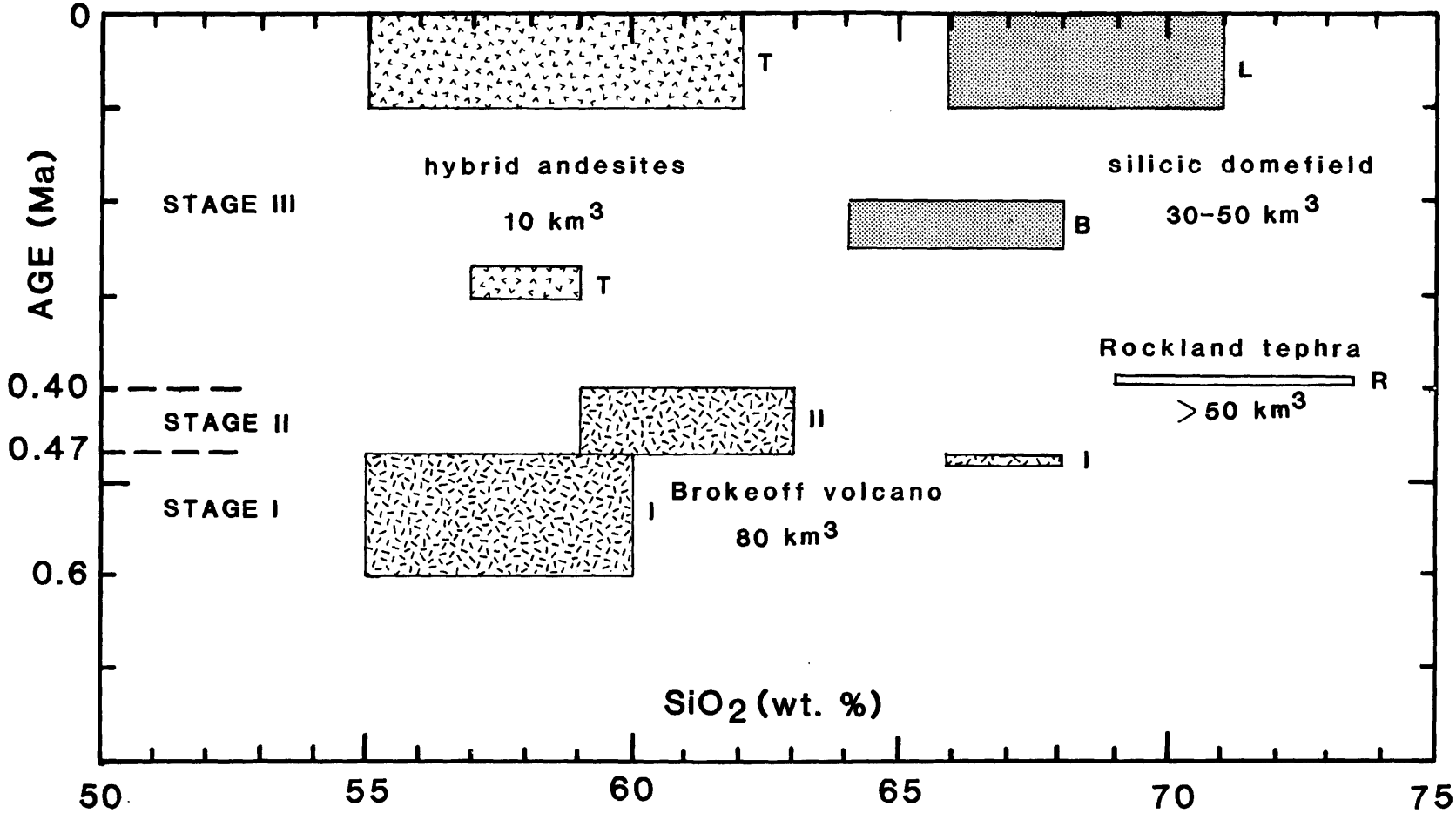

Figure 2. Evolution of the Lassen volcanic center. All volumes are approximate (Rockland tephra not recalculated to dense rock equivalent). Compositional ranges slightly modified to reflect the majority of analyzed samples. Some undated units in the Loomis and Twin Lakes sequences may fall outside the indicated age ranges.

TABLE 1. GENERALIZED PETROGRAPHIC AND PETROLOGIC CHARACTERISTICS OF THE LASSEN VOLCANIC CENTER

	Brokeoff volcano							
	Stage I		Stage II	Stage III				
				Rockland sequence	Bumpass sequence	Loomis sequence	Twin Lakes sequence	quenched inclusions
ROCK TYPE	ol-augite and hyp-aug andesite	2-px-hb dacite	augite-hyp andesite	hyp-hb rhyolite	2-px-hb dacite	hb-bio rhyodacite	ol-aug andesite	andesitic
MINERALOGY								
phenocrysts	10-30%, 2mm	8-15%, 2mm	30-40%, 5mm	10%, 2mm	10%, 5mm	15-40%, 5mm	5-10%, 1-5mm	sparse, 2mm
	plag aug ol hy	plag hb px	plag hyp aug	plag hb hyp	plag hb hyp aug	pl bio hb hyp qtz	pl bio hb hyp qz	ol aug plag hyp hb bio qtz
	disequilibrium	disequilibrium	disequilibrium	equilibrium	equilibrium	disequilibrium	disequilibrium	disequilibrium
groundmass	hyalopilitic, pilotaxitic	hyalopilitic	hyalopilitic	holohyaline	hyalopilitic	holohyaline	holohyaline,	hyalopilitic
glomero-porphyritic clots	sparse	sparse	abundant	absent	sparse	absent	absent	absent
quenched inclusions	absent	abundant	sparse	sparse	sparse to abundant	sparse to abundant	sparse	
CHEMISTRY								
SiO_2	55-64%	66-68%	59-63%	69-74%	64-68%	66-71%	54-65%	53-60%
MgO	2.5-8.0%	1.0-1.5%	3.0-4.0%	0.8-1.2%	1.7-2.8%	0.8-2.8%	2.5-8.5%	2.5-5.0%
K_2O	0.8-2.2%	3.0%	1.5-2.5%	2.7-3.4%	1.8-2.7%	1.8-3.0%	1.1-2.3%	0.7-1.4%
FeO/MgO	0.8-2.0	2.4-3.0	1.3-1.8	2.2-2.9	1.5-2.0	1.5-2.4	0.7-1.2	1.4-1.8
MORPHOLOGY	thin flows, interbedded pyroclastics	thick flows	thick flows	ashflow tuff, dome, flows	domes, thick flows	domes, flows, pyroclastic flows	thick flow complexes	inclusions
AGE (ka)	600-470	470	470-400	400	250-200	100-0	300-0	

fragmental rocks that erupted from central vents. The flanks consist primarily of thicker, more crystalline lava flows with sparse fragmental rocks, probably erupted from vents on the flanks of the volcano.

Stage-I lavas are porphyritic olivine-augite basaltic andesites and olivine-augite, olivine-hypersthene-augite, and hypersthene-augite andesites. Hornblende-pyroxene dacites are present but sparse in Stage I. Phenocryst abundance is variable from 5 to 40 %, and the phenocysts are generally less than a few mm in size. Plagioclase is ubiquitous and usually the dominant phenocryst phase. A conspicuous feature of the lavas of Stage I is their lithologic diversity. Adjacent flows in Stage I often have different textures, radically different phenocryst abundances, and even different phenocryst assemblages. Despite the heterogeneity within Stage I, an evolutionary trend is apparent. Olivine-bearing basaltic andesites and andesites are more common in the lower part of the section, and the average composition of the lower half of the section is more mafic than the upper half by about 2 % SiO_2. Textural (multiple phenocryst populations and resorption) and compositional (reverse zoning and compatible element spikes) evidence for magma mixing is abundant in andesites of Stage I. Stage I culminated in a small-volume but widespread eruption of hornblende-pyroxene dacite lava.

During Stage II, lava flows of porphyritic augite-hypersthene silicic andesite were erupted from flank vents. These flows are 30 m or more thick and lack intercalated fragmental rocks. The lavas of Stage II are preserved all around the volcano on the outer flanks of the major remnants. In contrast to the andesites of Stage I, andesites of Stage II are extremely homogeneous in phenocryst content and mineralogy. Andesites of Stage II contain 30-40 % phenocrysts of plagioclase, hypersthene, augite, and titanomagnetite that are larger (plagioclase usually about 5 mm) than phenocrysts in andesites of Stage I. Hornblende is occasionally present. Andesites of Stage II contain abundant small (5 mm to a few cm) glomeroporphyritic clots of gabbroic to dioritic composition (plagioclase+augite+hypersthene+oxide$\pm$olivine). Cumulate textures, subsolidus recrystallization, and exsolution features suggest that the glomeroporphyritic clots are disrupted cumulates or partly crystallized intrusives. Textural and compositional features of phenocrysts suggestive of magma mixing are common in the lavas of Stage II but less pronounced than in the lavas of Stage I.

Fundamental changes in the character of volcanism at the Lassen volcanic center mark the break between Stages II and III. The locus of volcanism shifted to the northern flank of Brokeoff volcano where the silicic domefield and Central Plateau of Lassen Volcanic National Park were constructed. The lavas of Stage III are generally more silicic than those of Brokeoff volcano and are divided into 4 sequences with stratigraphic and/or lithologic distinction. The Rockland, Bumpass, and Loomis sequences formed the silicic domefield and are dacitic to rhyolitic in composition. The Twin Lakes sequence formed the Central Plateau and is andesitic in composition. The three sequences of silicic volcanism correspond to pulses of volcanism that occurred at 400, 250-200, and 100-0 ka.

Coincident with the extinction of Brokeoff volcano, Stage III began with the eruption of small rhyodacite lava flows and a rhyolite dome of the Rockland sequence. Eruption of at least 50 km^3 (DRE) of rhyolitic magma at 400 ka as the Rockland air-fall tephra and ash flows quickly followed. This eruption is thought to have produced a small caldera on the northern flank of Brokeoff volcano. Subsequent silicic volcanism has obscured topographic and structural expression of the caldera. The Rockland tephra is sparsely phyric

hypersthene-hornblende rhyolite. Domes and flows of the Rockland sequence are sparsely phyric hornblende-biotite rhyolite and porphyritic hornblende-biotite rhyodacite.

Two groups of rocks totaling about 30-50 km^3 comprise the bulk of the lavas of the silicic domefield. During the period from 250 to 200 ka sparsely phyric to porphyritic 2-pyroxene-hornblende dacite magma produced the Bumpass sequence, a group of twelve domes and flows. The vents for the lavas of the Bumpass sequence are concentrated along the contact between the domefield and the Brokeoff volcano, and the lavas form the southern part of the silicic domefield. The lavas contain 5 to 20 % phenocrysts. Plagioclase is the dominant phenocryst, and biotite and quartz occur in small amounts in some rocks, often as resorbed crystals.

The Loomis sequence consists of porphyritic hornblende-biotite dacite and rhyodacite erupted as domes, lava flows, and pyroclastic flows in at least twelve episodes during the past 100 ka. The lavas of the Loomis sequence form the northern and western parts of the silicic domefield. Vents of the youngest domes and flows (30 ka to 1,050 years) form a NNW linear array that suggests regional tectonic control of vent locations rather than the perturbing influence of a large, shallow magma chamber. Lavas of the Loomis sequence are porphyritic, usually containing 20-30 % phenocrysts. Plagioclase often is up to 1 cm in size and is complexly zoned. Quartz is usually present but rarely comprises more than a few % of the rock. Orthopyroxene is usually present in minor amounts.

Evidence of magma mixing is abundant in lavas of the silicic domefield. The lavas of the Bumpass sequence commonly contain resorbed phenocrysts characteristic of more silicic magma, whereas the lavas of the Loomis sequence contain mafic phenocrysts (magnesian olivine and augite and calcic plagioclase). Complex zoning of phenocrysts and multiple phenocryst populations are common in both sequences.

A conspicuous feature of lavas of the silicic domefield is the presence of fine-grained mafic inclusions typically 10-20 mm in diameter, but ranging from a few mm to 1 m in size. These inclusions are ellipsoidal to spheroidal in shape with crenulate margins convex toward the host rock and thought to represent mafic magma injected into and quenched by the silicic magma system (Bacon, 1986). Most silicic rock units contain inclusions, although their abundance varies from negligible to about 20 %, and multiple generations of inclusions are common. In silicic rocks of the Lassen volcanic center the inclusions are basaltic andesite to andesite in composition. Disaggregation of inclusions plays an important role in the origin of multiple and disequilibrium phenocryst populations and enhances compositional diversity at the Lassen volcanic center (Clynne and Christiansen, 1987).

The Twin Lakes sequence consists of about 10 km^3 of hybrid andesite erupted peripheral to the silicic domefield throughout the span of Stage III. The ten lava flows of this diverse group all have strongly disequilibrium phenocryst assemblages characterized by the coexistence of magnesian olivine and quartz. The rocks are porphyritic, black, glassy, olivine or augite andesites and dacites. They also contain strongly resorbed felsic phenocrysts that had compositions and textures similar to those in the dacites and rhyodacites of the silicic domefield. Mafic inclusions are common, but they are small and sparse. Lavas of the Twin Lakes sequence were formed by thorough mixing of subequal amounts of mafic and silicic magma. The mafic component of these lavas was magma similar to that of the regional basaltic volcanism, and the silicic component was dacitic to rhyodacitic magma of the silicic domefield.

Geochemistry

Porphyritic andesite and dacite with high Al_2O_3, low TiO_2, medium K_2O contents, and FeO/MgO ratios of 1.5-2.0 are the most abundant rock types in the Lassen volcanic center. The single most voluminous unit is sparsely phyric rhyolite pumice (Rockland tephra). Early basaltic andesite, late rhyodacite, and hybrid andesite are subordinate in abundance. Rocks of the Lassen volcanic center resemble other medium-K_2O, calc-alkaline volcanic rocks emplaced on continental margins overlying thick crust.

Major-element Harker variation diagrams (figures 3-6) for the LVC show smooth trends from 53-74 per cent SiO_2 (Clynne, 1984). See Clynne (1984) and Bullen and Clynne (this volume) for tables of chemical data. Plots of the MgO and K_2O content of the lavas show coherent variation with SiO_2 and are representative of the other major elements. Variations in trace-element content follow their geochemically similar major elements (Bullen and Clynne, this volume). The overall compositional evolution is from mafic to silicic with time. However, the evolution is not strictly sequential (see figure 2). Compositional variation is restricted in the andesites of Stages I and II but becomes more diverse during Stage III.

The lithologic diversity of the lavas of Stage I of Brokeoff volcano is mimicked by equally diverse chemistry within a limited range of SiO_2. The most mafic compostions have 54-56 % SiO_2 and 8 % MgO. These are separate from the majority of the lavas, which have from 56-60 % SiO_2 and 3.5-5 % MgO. MgO decreases with SiO_2 in this group and converges on the most common composition, which has about 59.5 % SiO_2 and about 4 % MgO. The culminating dacite has 1-1.5 % MgO at 66-68 % SiO_2. The other dacites sparsely fill the gap between the culminating dacite and the andesites. K_2O varies from 0.8-1.6 % at 54 % SiO_2 and from 1.0-2.2 % at 60 % SiO_2. Variation of K_2O with SiO_2 in the lavas of Stage I shows the presence of two parallel trends. One trend has distinctly less K_2O (and other incompatible elements) than the other. The culminating dacite plots on an extension of the high-K_2O trend. The location of the low K_2O lavas does not have stratigraphic significance. They are randomly distributed in both time and space within the section of Stage I.

The andesites of Stage II are remarkably homogeneous chemically. All but a few samples have 61-63 % SiO_2. MgO varies from 3.9 % at 59 % SiO_2 to 2.2 % at 64 % SiO_2. There is little overlap in SiO_2 with lavas of Stage I. K_2O, however, shows a large range of variation (1.5-2.6 %) at 61-62 % SiO_2 and a weak correlation of increasing K_2O with increasing SiO_2. There is a general correlation of increasing SiO_2 with time in the lavas of Stage II.

Rocks of Stage III, while predominantly silicic, span a range from 53 to 74 % SiO_2. There is overlap in composition between silicic sequences but no offset in MgO or K_2O content. There is no consistant variation with stratigraphy. The Rockland sequence is the most silicic composition in the Lassen volcanic center. The dacites of the Bumpass sequence are the least silicic rocks in the silicic domefield, and the Loomis rhyodacites are intermediate in SiO_2. The mixed lavas of the Twin Lakes sequence have diverse compositions at the low-SiO_2 end of the array. The quenched inclusions have less diversity and are also at the mafic end of the array.

The lavas of Stage III form a trend on the MgO versus SiO_2 diagram that crosses the trend of lavas of Brokeoff volcano at a low angle; the two trends cross at about 60-62 wt % SiO_2. At equivalent SiO_2, the silicic lavas of Stage III have a higher MgO content and the inclusions of Stage III a lower

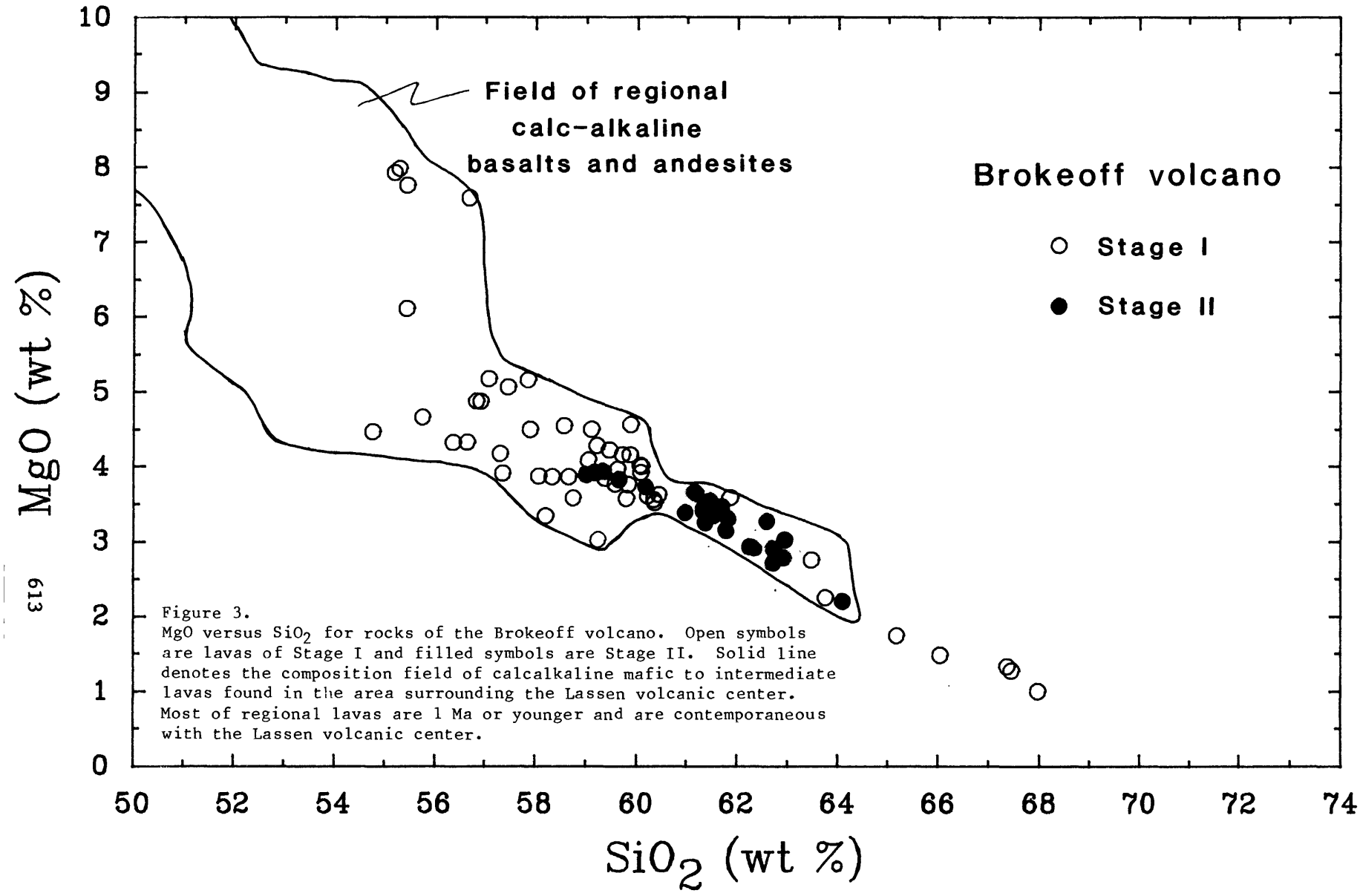

Figure 3.
MgO versus SiO_2 for rocks of the Brokeoff volcano. Open symbols are lavas of Stage I and filled symbols are Stage II. Solid line denotes the composition field of calcalkaline mafic to intermediate lavas found in the area surrounding the Lassen volcanic center. Most of regional lavas are 1 Ma or younger and are contemporaneous with the Lassen volcanic center.

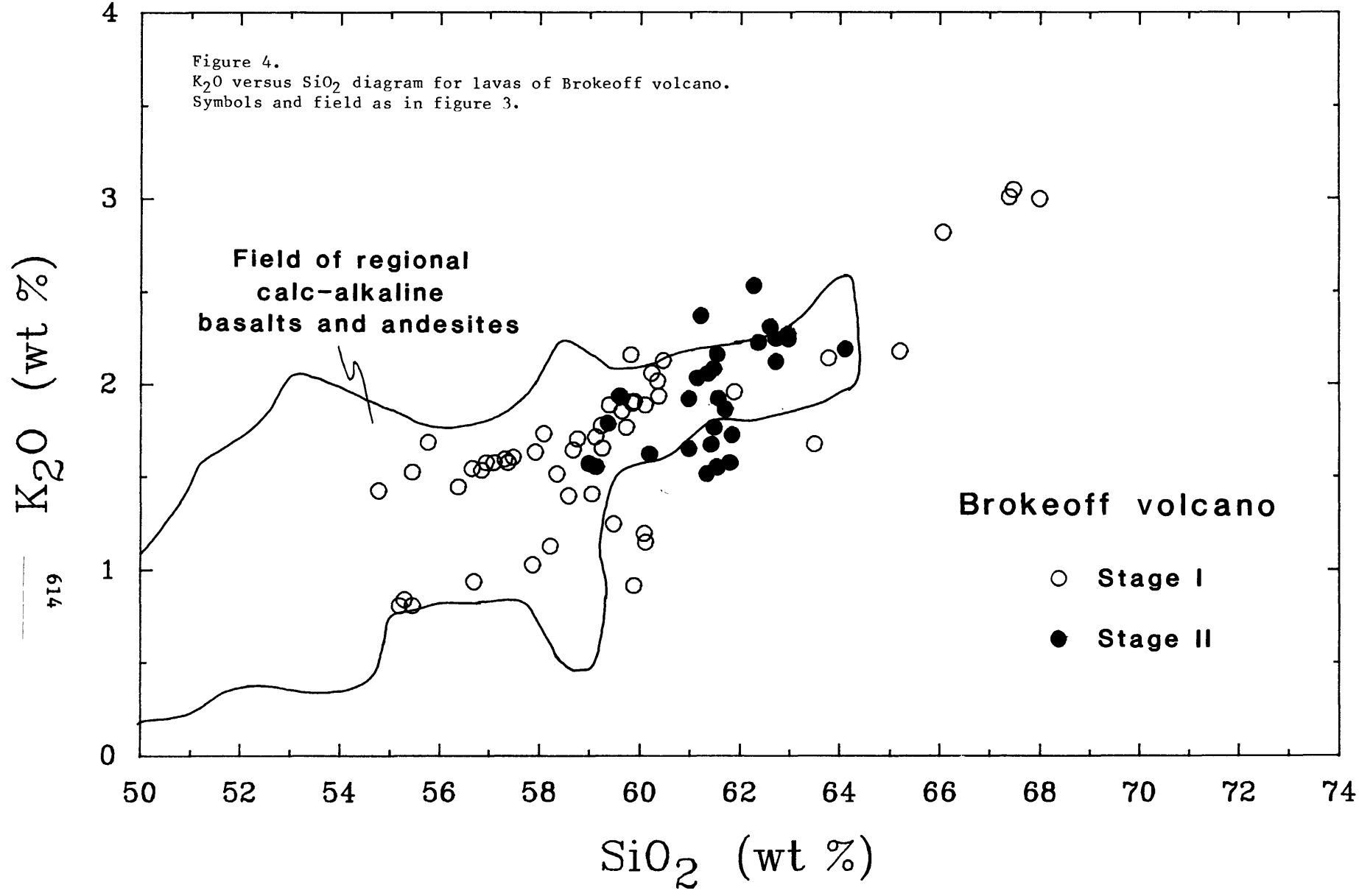

Figure 4.
K_2O versus SiO_2 diagram for lavas of Brokeoff volcano.
Symbols and field as in figure 3.

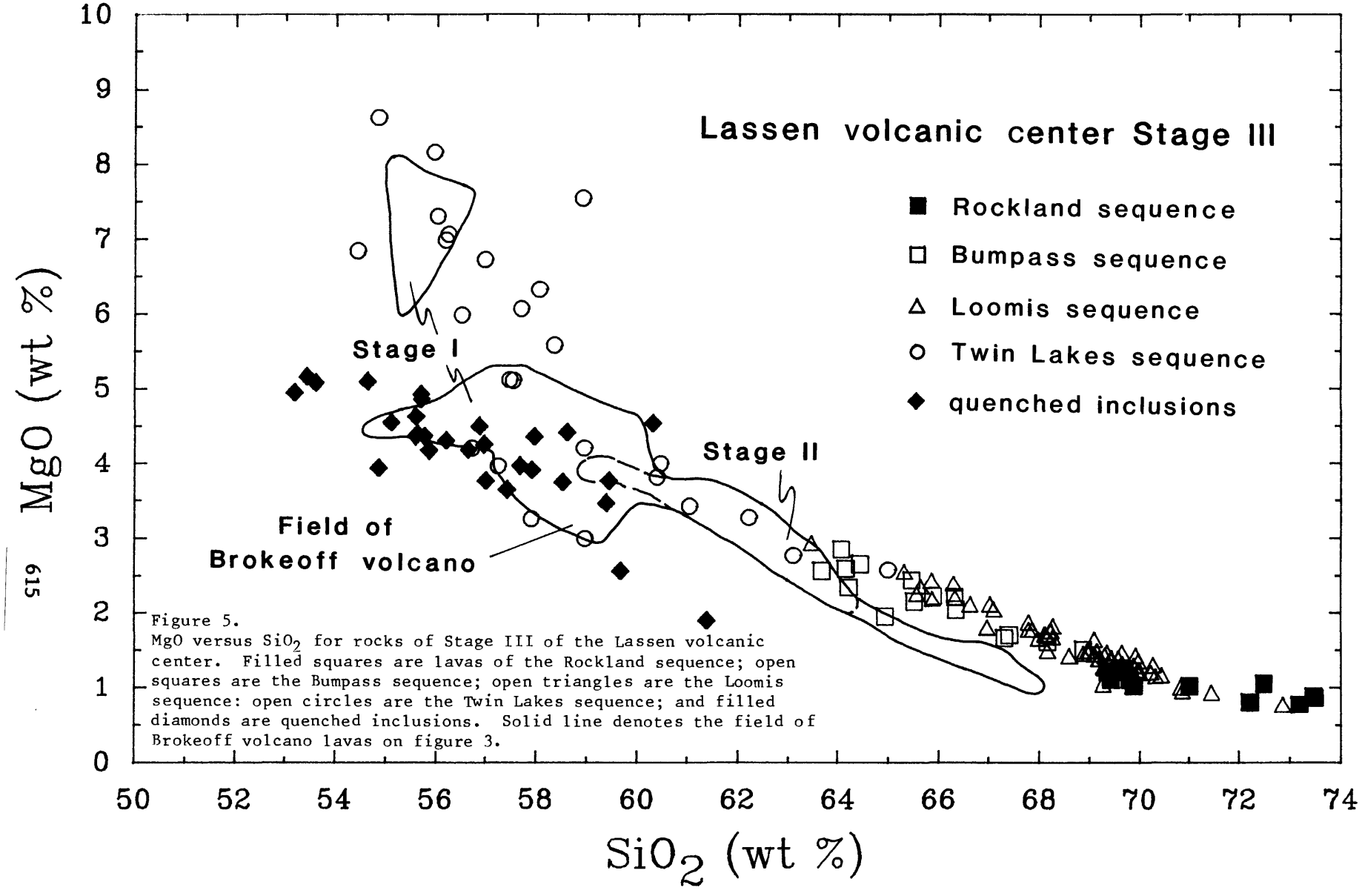

Figure 5.
MgO versus SiO_2 for rocks of Stage III of the Lassen volcanic center. Filled squares are lavas of the Rockland sequence; open squares are the Bumpass sequence; open triangles are the Loomis sequence: open circles are the Twin Lakes sequence; and filled diamonds are quenched inclusions. Solid line denotes the field of Brokeoff volcano lavas on figure 3.

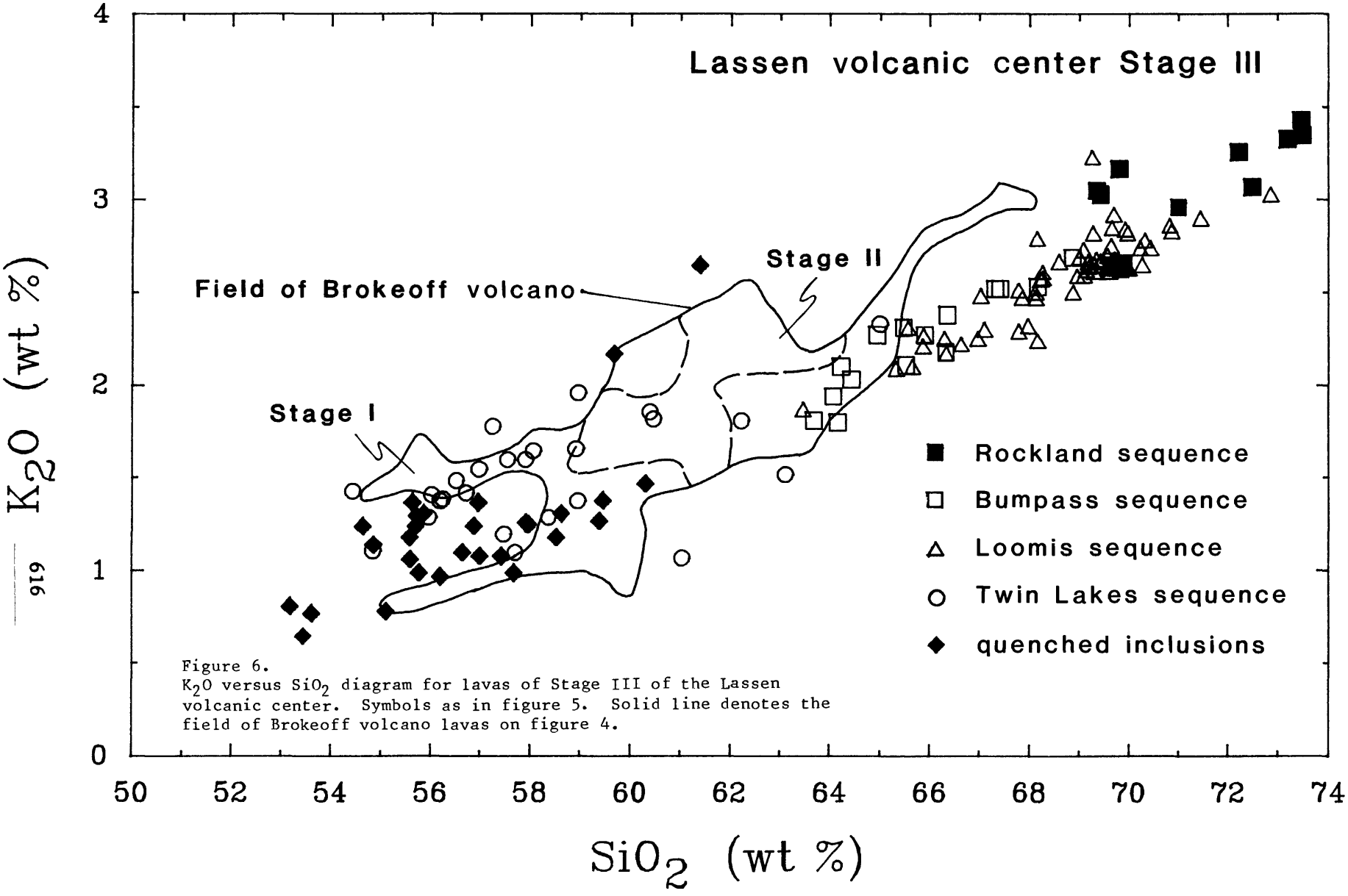

Figure 6.
K_2O versus SiO_2 diagram for lavas of Stage III of the Lassen volcanic center. Symbols as in figure 5. Solid line denotes the field of Brokeoff volcano lavas on figure 4.

MgO content than the lavas of Brokeoff volcano. Most Stage-III compositions have lower K_2O content at equivalent SiO_2 than lavas of the Brokeoff volcano. The lavas of the Twin Lakes sequence have variable compositions.

Discussion

Smooth geochemical trends, increasing silica content with time, spatial relations, and temporal relations of the rocks demand a unified origin for magmas of the Lassen volcanic center.

Brokeoff volcano

Crystal fractionation models, using analyzed compositions of the phenocryst phases present, satisfactorily explain the major-element variation within the high- and low- K_2O groups of Stage I but can not link the groups without addition of another component. Crystal fractionation models fail to predict the range of trace-element compositions observed in Stage-I lavas (Bullen and Clynne, this volume).

The lithologic and geochemical evidence suggest that Stage-I magmas were produced in small independent batches. Magma mixing between the small magma batches was common. It is unlikely that a long-lived magma chamber or an integrated magmatic system existed at this time. Stage-II rocks are very homogeneous in compatible major-elements , but trace-element and isotope data show that these magmas are also formed in independent batches (Bullen and Clynne, this volume).

The lavas of Brokeoff volcano have compositions and trends similar to the more evolved regional mafic lavas, indicating that they have similar sources and evolutionary histories. The difference between Brokeoff volcano and the regional volcanism is the larger-volume and long-lived locus of volcanism at Brokeoff volcano and the lack of basalt at Brokeoff volcano. The similarities suggest that Brokeoff volcano represents a focussing of the regional volcanism, perhaps with increased average residence time in the crust. The differences suggest that the control of focussing is physical and may be related to an increase in the magma supply rate.

The Lassen volcanic center (and the older volcanic centers in the area) are located on the edge of a regional gravity low (Blakely and others, 1985). The gravity low is an expression of near-surface low-density volcanic rocks and the presence of Quaternary plutonic rocks beneath the volcanic field (Pakiser, 1964; LaFehr, 1965). Blakely and Jachens (this volume) suggest that the gravity low also reflects a structural depression and that volcanoes are located around the margins of the depression because boundary faults facilitate ascent of magma to the surface.

Stage III

Crossing geochemical trends and nonsystematic evolution of silica content suggest that the magmas that produced the rocks of Stage III cannot be derived directly from magma producing the Brokeoff volcano. Crystal fractionation and assimilation-fractional crystallization models fail to satisfactorily reproduce the major-element compositions of the silicic rocks from Brokeoff volcano andesites. Partial melting of young mafic crust appears to play a role in the origin of the silicic magmas at the Lassen volcanic center (Clynne, 1984; Bullen and Clynne, this volume).

Mixing and disaggregation of quenched inclusions play an important role in the increased compositional diversity of lavas of Stage III (Clynne and Christiansen, 1987). The quenched andesitic inclusions and the andesites of

the Twin Lakes sequence demonstrate that basaltic to andesitic magma has had access to the silicic magma system at least for the last 300 ka. Intrusion of mafic magma into small reservoirs of silicic magma and mixing between them produces the hybrid andesites. Much of the compositional diversity of the lavas of the Twin Lakes sequence results from mixing with regional mafic magma of diverse composition (Clynne, 1984; Clynne, unpublished data).

Present-Day Magma System

The Cascade Range is the volcanic expression of subduction zone-related magmatism, resulting from interaction of the Juan de Fuca, Explorer, and Gorda plates with the North American plate. Subduction is strongly oblique, and young relatively warm oceanic crust is being subducted. Although a well defined Benioff Zone is lacking, the general character and composition of volcanism is similar to subduction-zone magmatism on continental margins worldwide.

The Lassen volcanic center differs from other Cascade volcanoes by having a larger volume of silicic rocks (100+ km^3 in 400 ka). The stress regime in the southern Cascades is moderate east-west extension. Normal faults with north- to northwest- trends are abundant in the southernmost Cascades and suggest impingement of westward-migrating Basin and Range tectonism on the Lassen area (Guffanti and others, this volume). Relatively primitive mafic magma leaks to the surface, but some mafic magma is retained in the crust by mixing with more differentiated magma (Eichelberger and Gooley, 1977).

The long span of silicic activity at Lassen volcanic center and the presence of a vigorous hydrothermal system imply the presence of an evolving magmatic system. Systematic geochemical variation and the mineralogic and geochemical homogeneity of the youngest rocks suggest derivation from a single long-lived magma body (Clynne, 1984). The pattern of young vents suggests that a magma body 5-8 km in diameter underlies the northwestern corner of Lassen Volcanic National Park. The magma system of the Lassen volcanic center can be envisaged (figure 7) as an evolving pluton-sized body in the middle crust (10-20 km depth). The upper part of the chamber contains crystal-rich rhyodacite, which has varied little in composition over at least the last 50 ka. The system is probably zoned to more mafic compositions at depth. Regional basalt provides heat and material input to maintain the system in its partially molten state. Hybrids and ubiquitous mafic inclusions provide abundant evidence for the interaction of mafic and silicic magma. The molten part of the magmatic system is small enough or its configuration is such that input of mafic magma significantly affects its heat budget and composition. A small volatile-rich cap has periodically developed at the top of the magma chamber, but since eruption of the Rockland tephra 400 ka ago, the cap has vented before increasing to substantial volume. Assuming that the vertical extent of the magmatic system is 10 km results in volume estimates of 200-400 km^3, most of which is at least partially solidified.

Despite the volcanologic and petrologic evidence of a magma system, teleseismic (Berge and Monfort, 1986) and seismic-refraction (Berge and Stauber, 1987) studies have failed to show unambiguously the presence of a magma chamber beneath the Lassen volcanic center. However the resolution of these studies is such that magma chambers smaller than 5 km in diameter could not be detected (Iyer, 1984). New modeling of seismic data suggests the presence of an anomalous body at a mid-crustal level (H.M. Iyer, personal communication).

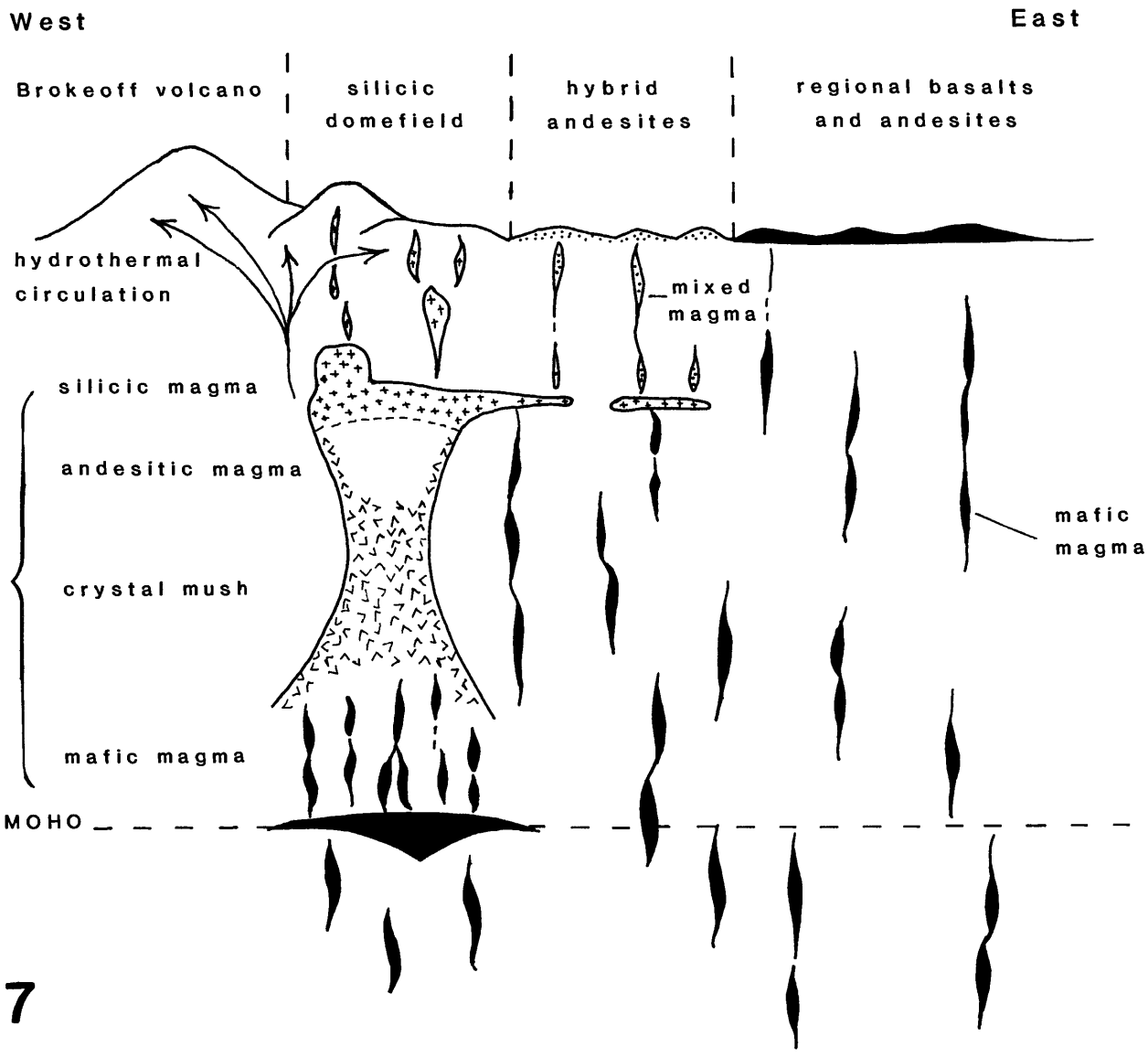

Figure 7

Cartoon of the Magma System of the Lassen Volcanic Center

A compilation of local seismicity shows that most earthquakes are small (magnitude 1-2) and occur at shallow depth (3-8 km) beneath Brokeoff volcano in the upflow zone of the Lassen hydrothermal system (Walter and others, 1984). About 300 of these earthquakes occur per year, with the majority occurring in small swarms. Less frequent earthquakes occur in the shallow crust of the surrounding region. Infrequent long-period seismic events suggestive of magma movement occur below about 15 km (S.R. Walter, personal communication). The area beneath Chaos Crags lacks crustal earthquakes in the depth range from 10-15 km. The juxtaposition of the hydrothermal system and the youngest volcanic vents may indicate the position of the top of the magmatic system.

Conclusions

The data and discussion presented above lead to several conclusions which must be considered in any model of the petrogenesis of the Lassen volcanic center. The stratigraphy, lithology, and chronology of the products of the Lassen volcanic center indicate a single, albeit complex, magmatic system. The Lassen volcanic center is the volcanic expression of a single long-lived magmatic system and is probably related to the generation, rise, evolution, and emplacement of a pluton-sized body in the middle crust.

The voluminous, long-lived edifice of Brokeoff volcano is the result of focussing of diffuse regional mafic volcanism. The location and long lifespan of Brokeoff volcano are probably controlled by structures in the crust. The compositional diversity of Brokeoff volcano is identical to that displayed by regional lavas with similar SiO_2 content. Fractional cystallization models do not satisfactorily reproduce the compositional array of Brokeoff volcano. Petrographic and crystal chemical constraints require Brokeoff magmas to be produced in small independent batches. Mixing between batches was common.

Stage-III lavas are not directly related to Brokeoff volcano lavas by any simple process. Magma mixing is an important process in the origin of compositional diversity of Stage-III lavas; hybrids and ubiquitous mafic inclusions provide abundant evidence for the interaction of mafic and silicic magma. Regional basalt provides the fundamental heat and material input to the magmatic system.

References cited

Bacon, C. R., 1986, Magmatic inclusions in silicic and intermediate volcanic rocks: Journal of Geophysical Research, v. 91, p. 6091-6112.

Berge, P. A. and Monfort, M. E., 1986, Teleseismic residual study of the Lassen Volcanic National Park area, northern California: U. S. Geological Survey Open File Report 86-252, 71 p.

Berge, P. A. and Stauber, D. A., 1987, Seismic refraction study of the upper crustal structure of the Lassen Peak area, northern California: Journal of Geophysical Research, v. 92, p. 10,571-10,579.

Blakely, R. J. and Jachens, R. C., this volume, Volcanism, isostatic residual gravity, and regional tectonic setting of the Cascade volcanic province: U.S. Geological Survey, Proceedings of the Red Book Conference, Geologic, Geophysical, and Tectonic Setting of the Casacade Range.

Blakely, R. J., Jachens, R. C., Simpson, R. W., and Couch, R. W., 1985, Tectonic setting of the southern Cascade Range as interpreted from its magnetic and gravity fields: Geological Society of America Bulletin, v. 96, p. 43-48.

Bullen, T. D. and Clynne, M. A., this volume, Geochemical and isotopic constraints on magmatic evolution at the Lassen volcanic center: U.S. Geological Survey, Proceedings of the Red Book Conference, Geologic, Geophysical, and Tectonic Setting of the Casacade Range.

Clynne, M. A., 1984, Stratigraphy and major-element geochemistry of the Lassen Volcanic Center, California: U. S. Geological Survey Open-File Report 84-224, 168 p.

Clynne, M. A. and Christiansen, R. L., 1987, Magma mixing and the devastating eruptions of May 1915 at Lassen Peak, California (abs.): Abstract Volume, Hawaiian Symposium on How Volcanoes Work, Hilo, Hawaii, Jan. 19-25, 1987, p. 43.

Eichelberger, J. C. and Gooley, R., 1977, Evolution of silicic magma chambers and their relationship to basaltic volcanism: in Heacock, J. G., ed., The Earth's Crust, American Geophysical Union, Geophysical Monograph 20, p. 57-77.

Guffanti, Marianne, Clynne, M. A., Muffler, L. J. P., and Smith, J.G., this volume, Spatial, temporal and compositional trends of mafic volcanism in the Lassen regiion of northeastern California: U.S. Geological Survey, Proceedings of the Red Book Conference, Geologic, Geophysical, and Tectonic Setting of the Casacade Range.

Iyer, H.M., 1984, Geophysical evidence for the locations, shapes and sizes, and internal structures of magma chambers beneath regions of Quaternary volcanism: Philosophical Transactions of the Royal Society of London, Series A, no. 310, p. 473-510.

LaFehr, T.R., 1965, Gravity, isostasy, and crustal structure in the southern Cascade Range: Journal of Geophysical Research, v. 70, p. 5581-5597.

Pakiser, L. C., 1964, Gravity, volcanism, and crustal structure in the southern Cascade Range, California: Geological Survey of America Bulletin, v. 75, p. 611-620.

Walter, S. R., Rojas, Veronica, and Kollman, Auriel, 1984, Seismicity of the Lassen Peak area, California, 1981-1983: Geothermal Resources Council, Transactions, v. 8, p. 523-527.

Geochemical and Isotopic Constraints on Magmatic Evolution at Lassen Volcanic Center, Southernmost Cascade Range

by Thomas D. Bullen and Michael A. Clynne

Abstract

Magmatic evolution at the Lassen Volcanic Center (LVC) is characterized by a transition from predominantly andesitic to predominantly silicic volcanism with time. Magmas of the andesitic, or Brokeoff phase of volcanism range in composition from basaltic andesite to dacite, whereas those of the silicic, or Lassen phase range in composition from basaltic andesite to rhyolite. The chemistries of magmas from each phase define well-organized but distinct variation trends. Compared to magmas of the Brokeoff phase with similar SiO_2-content, the Lassen-phase magmas display a depleted minor and trace element character. Based on the behavior of both incompatible and compatible trace elements, neither the Brokeoff- nor the Lassen-phase geochemical trends can be ascribed to closed-system fractional crystallization processes involving a single mafic parental magma. Moreover, the Lassen-phase magmas cannot be derived from the Brokeoff-phase magmas by fractional crystallization. Rather, the geochemical trends of each volcanic phase define simple mixing arrays between homogeneous silicic and heterogeneous mafic magmas, and manifest the generation and evolution of two physically distinct, but genetically related magma systems.

The LVC magmas have radiogenic isotopic characteristics that approximate two-point mixing arrays. One isotopic end-point is similar in composition to that of N.E. Pacific ridge and seamount basalts (oceanic component), the other to that of ocean-island basalts derived from source regions that have been contaminated by continental material (continental component). Volcanic rocks from both LVC and the Lassen region that range in composition from basalt to rhyolite cluster near the continental end of the isotopic array, whereas rocks at the oceanic end of the array tend to be andesites. The LVC isotopic array is essentially contained by that for the regional mafic lavas, and thus the silicic rocks do not have the most continental isotopic character.

The fact that rocks ranging in composition from basalt to rhyolite share the continental end of the isotopic array seriously limits any model for silicic magma genesis at LVC that relies on assimilation of silicic crust by mafic parental magmas during their ascent to the surface. On the other hand, the isotopic and geochemical uniformity of the most silicic Lassen magmas suggests that they are well-homogenized partial melts. The likely source region for these silicic melts is the heterogeneous lower crust, consisting primarily of underplated mafic rocks that are similar in geochemical and isotopic diversity to the mafic lavas erupted in the Lassen region. The isotopic diversity observed at LVC results primarily from mixing of the silicic melts, that are dominated by the continental component, with mantle-derived mafic magmas that are dominated by the oceanic component.

Magmatic evolution at LVC can be viewed in terms of a series of mantle melting events that subsequently stimulate melting in a progressively increasing volume of the lower crust. Andesites of the Brokeoff phase represent slightly fractionated mixtures of geochemically and isotopically diverse mantle-derived mafic magmas with small volumes of relatively high-

degree silicic melt derived from the lower crust. In contrast, the most silicic magmas of the Lassen phase represent voluminous, chemically and isotopically homogeneous low-degree melts of the lower crust that pooled into sufficient volumes to avoid significant blending and dilution with intruding heterogeneous mafic magmas. Mafic magmatic inclusions in the silicic Lassen-phase magmas record the geochemical and isotopic diversity of the mantle-derived components, and demonstrate the temporal and spatial association of mantle and crustal melting events.

Introduction

The large volcanic centers that typify Quaternary to Recent volcanism in the Cascade Range of the northwestern United States have long been recognized as complex igneous systems that have erupted compositionally diverse magmatic products. However, whereas the number of studies dealing with the general geologic relations of the Cascade volcanoes are legion, relatively little work has been presented detailing geochemical systematics of individual centers. Even scarcer are isotopic studies pertaining to Cascade geology. Perhaps the most significant geochemical studies presented to date include those of Smith and Leeman (1987) for Mount St. Helens, Bacon and Druitt (1988) for Mount Mazama, and the works of Condie and Hayslip (1975), Mertzmann (1977, 1980), and Grove and co-workers (1982, 1984, 1986) for Medicine Lake. The sparse isotopic studies have described both regional systematics (e.g. Smith and Carmichael, 1968; Church and Tilton, 1973; Church, 1976) and local variations (e.g. Halliday et al., 1983, for Mount St. Helens).

Each of the previous geochemical studies has dealt at least in part with the derivation of evolved magmas at each center, with the various data syntheses pointing to clearly disparate conclusions. On one hand, Mertzmann (1977), Grove and co-workers (1982, 1984, 1986) and Bacon and Druitt (1988) point to evidence that fractional crystallization of mafic parental magmas, coupled with assimilation of varying crustal components, is largely responsible for compositional diversity observed at a given volcano. In contrast, Condie and Hayslip (1975) and Smith and Leeman (1987) detail evidence that the silicic magmas at Medicine Lake and Mount. St. Helens, respectively, are generated by partial melting of mafic lower crust. The isotopic studies confirm that a component derived from continental crust is present in the Cascade magmas, and therefore provide important constraint for either interpretation suggested by the geochemical studies. The isotopists consistently point to the tendency for more silicic magmas at any volcano to be more "crust-like" in their isotopic composition compared to spatially and temporally associated mafic magmas.

In this paper, we present new geochemical and isotopic data for magmatic products that span the entire eruptive history of the Lassen volcanic center of the southernmost Cascade Range. Details of the volcanic stratigraphy at this strongly calc-alkaline volcano have been well-documented (Clynne, 1984; 1989), and point to a dramatic temporal evolution of magma composition. Our goal is to reconcile constraints on petrogenetic models imposed by the geochemical and isotopic data with those suggested by the geotectonic setting of magmatism in this region. In doing so, we are able to evaluate the relative roles that various petrogenetic processes have played during the history of the volcano. Our foremost conclusion is that most of the

geochemical and isotopic variability observed can be attributed to corresponding heterogeneity in the mantle-derived magmas that have fed the volcano-plutonic system. Mixing of mafic magmas with silicic melts derived from young mafic lower crust figures prominently in our evolutionary model, whereas fractional crystallization of large magma bodies coupled with assimilation of mid- to upper-level crust is only of secondary importance.

Geologic Overview of the Lassen Volcanic Center

The Lassen volcanic center, the southernmost active Cascade volcano, lies above an easterly-dipping subduction zone along which the south Gorda plate segment, the southernmost in the Juan de Fuca plate system, is thrust beneath the North American plate (Guffanti and Weaver, 1988). The correspondence of the southern termini of both subduction and orogenic volcanism in this region (Figure 1) lends support to models that attempt to relate the two processes. However, whereas plate reconstructions suggest that subduction has occurred throughout much of the Cenozoic in this region (Lipman et al., 1972), the vent distribution and geochronologic compilation of Guffanti et al. (1989) suggest that orogenic magmatism in the southernmost Cascade Range has occurred only within the past 5 Ma. Therefore, a long time interval passed during which the mantle and crust in the Lassen area could have been affected by the subduction process, with no obvious volcanic expression.

Once initiated in the late Miocene or early Pliocene, volcanism in the southernmost Cascade Range can be characterized on two scales. Regional volcanism is predominantly basaltic to andesitic and consists of hundreds of coalescing volcanoes of small volumes (10^{-3} to 10^{2} km^3) and relatively short lifetimes (100 to 10^3 yr). Superposed on this regional mafic volcanism are a few long-lived, much larger volcanic centers that have erupted products ranging from calc-alkaline basaltic andesite to rhyolite. Five such centers, each younger than about 3 m.y., have been recognized in the area of Lassen Volcanic National Park.

Each of the larger centers, of which the Lassen volcanic center (LVC) is typical, consists of an andesitic composite cone and flanking silicic domes and flows. Each center was built in three sequential evolutionary steps referred to herein as "stages" (after Clynne, 1984; 1989):

* Stage I, cone-building basaltic andesite to andesite lava flows and pyroclastics, with or without minor dacite lava flows;
* Stage II, thick cone-building andesite to silicic andesite lava flows;
* Stage III, dacite to rhyolite domes, flows and pyroclastics flanking the main cone.

The four older volcanic centers in the Lassen area, the Dittmar, Maidu, and Yana and Snow Mountain volcanic centers have each progressed through Stage III, and are now extinct. The fifth and youngest center, the Lassen Volcanic Center (LVC), has progressed through Stages I and II, and presently hosts active Stage III-type volcanism.

Taking LVC as a model, the temporal and corresponding compositional evolution of magmatic products at one of these large centers can be envisaged by reference to K_2O-SiO_2 systematics (Figures 2a and 2b). Stages I and II of LVC, referred to herein as the "Brokeoff phase", produced the Brokeoff Volcano, an 80 km^3 andesitic stratocone. The bulk of Brokeoff Volcano

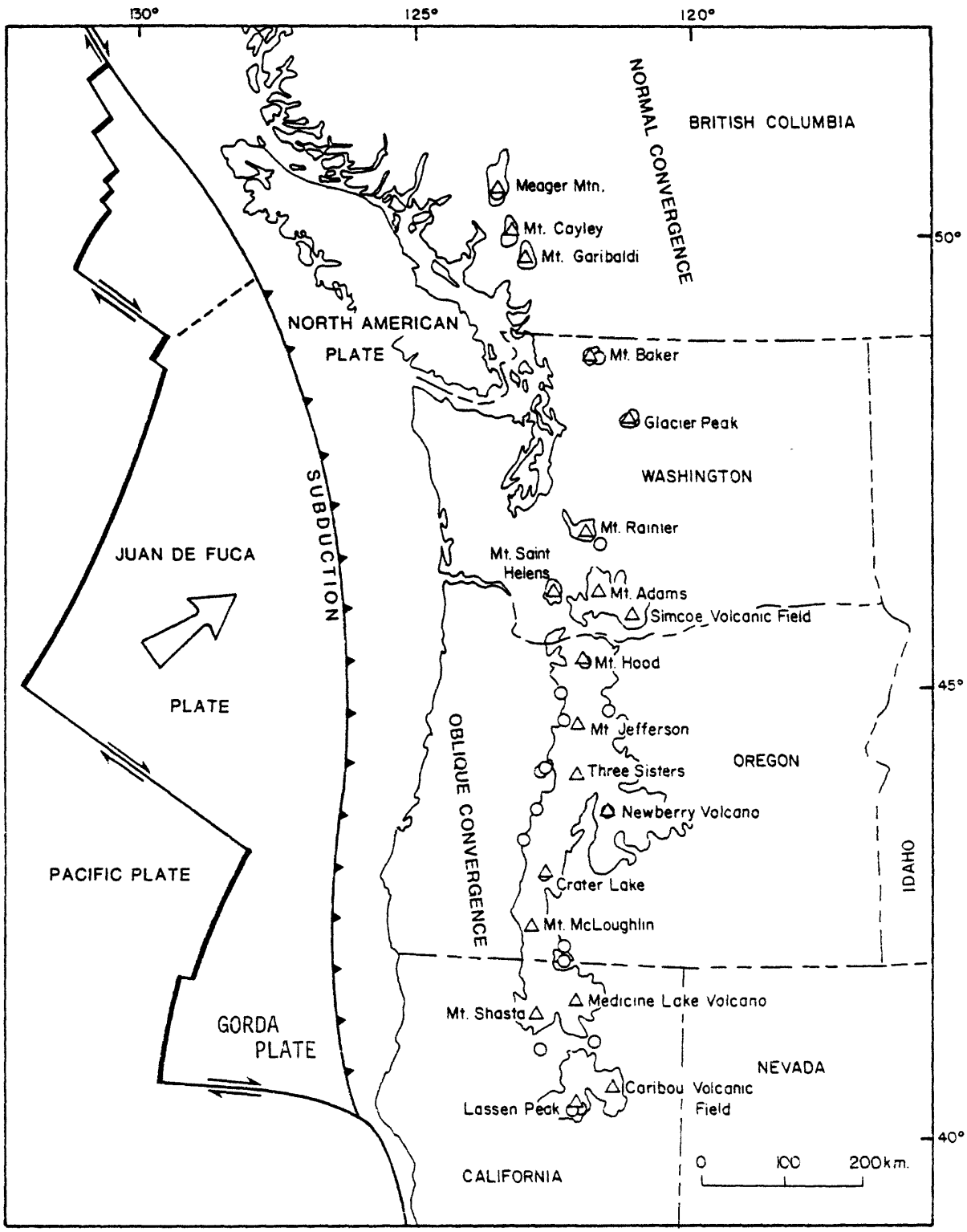

Figure 1. Location and tectonic setting of the Lassen Volcanic Center. Arrow indicates the direction of plate covergence.

SYMBOLS USED IN VARIATION DIAGRAMS

Brokeoff Phase

⧓ Stage I

△ Stage II

Lassen Phase

+ Silicic lavas

■ Hybrid andesites

x Quenched magmatic inclusions

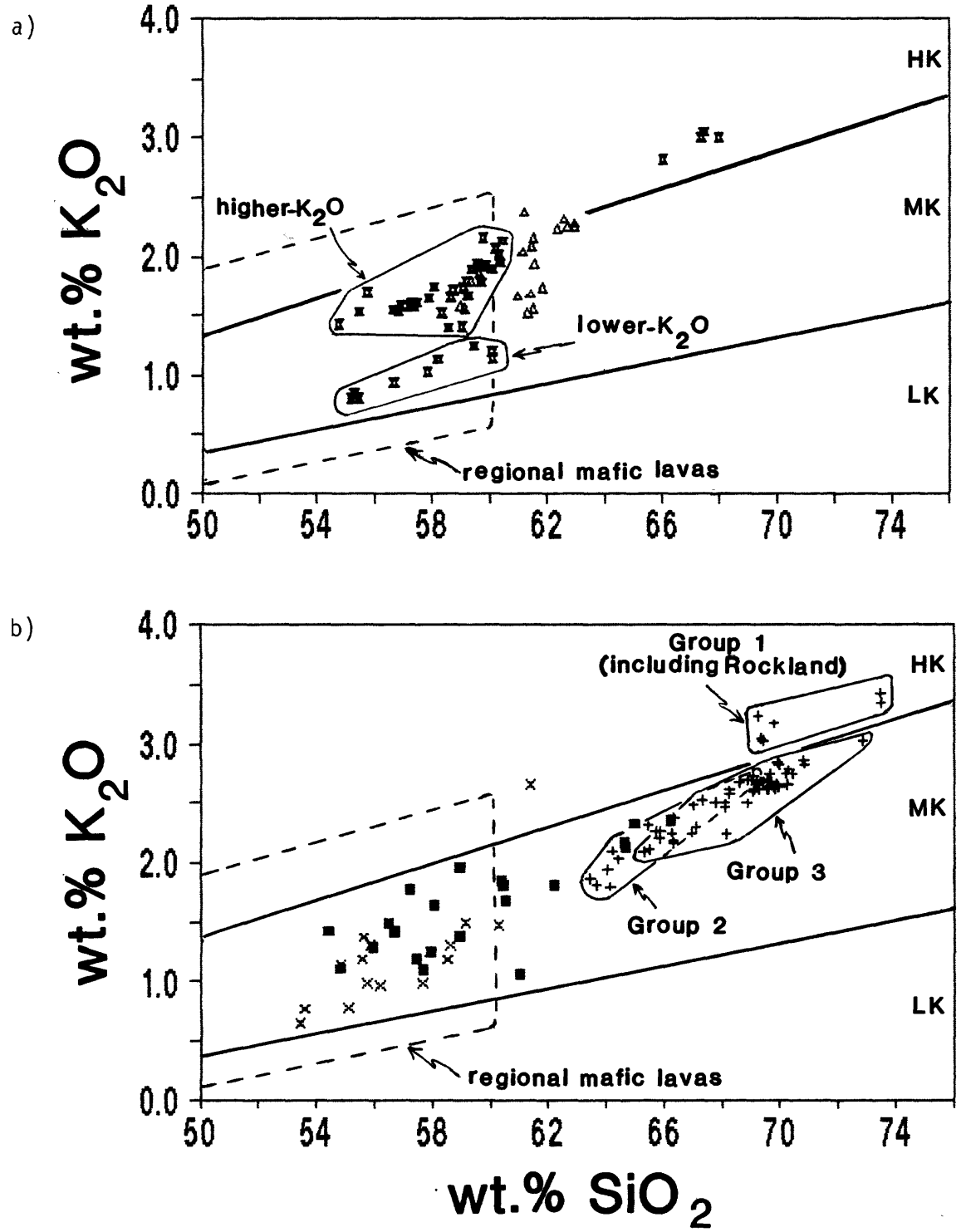

Figure 2. K_2O - SiO_2 variation diagrams for lavas of the Brokeoff phase (a) and Lassen phase (b) of the Lassen Volcanic Center. LK, MK, and HK are the low-, medium-, and high-K_2O fields of Ewart (1979).

consists of medium-K_2O olivine-augite and hypersthene-augite andesite lava flows and stratified pyroclastic deposits that erupted during Stage I from a central vent 0.60-0.47 Ma. Stage I culminated in eruption of a small volume of high-K_2O hornblende-hypersthene-augite dacite lava. During Stage II, which lasted from about 0.47-0.40 m.y., thick flows of medium-K_2O porphyritic augite-hypersthene silicic andesite, generally lacking interbedded pyroclastic material, were erupted.

Stage III, referred to herein as the "Lassen phase", involved a dramatic shift in the locus of volcanism, and was initiated by eruption of a minimum of 50 km^3 of high-K_2O rhyolitic magma (the Rockland air fall and ash flows) from the northeast flank of Brokeoff Volcano at about 0.4 Ma. The sparsely porphyritic Rockland rhyolite pumice is the single most voluminous unit associated with LVC. The eruption of Rockland material is thought to have produced a caldera that is now filled by a dacite domefield, which consists of three groups of rocks totaling about 30-50 km^3 and emplaced in the following order:

*Group 1: high-K_2O, hornblende-biotite rhyodacite lavas related to the Rockland magma at 0.4 Ma;
*Group 2: medium-K_2O, hornblende-hypersthene-augite dacite lavas erupted between 0.25 and 0.2 Ma;
*Group 3: medium-K_2O, hornblende-biotite dacite and rhyodacite erupted as domes, lava flows and pyroclastic flows in at least ten episodes, mostly during the past 100 Ka.

Demonstrably hybrid quenched magmatic inclusions (cf. Bacon, 1986) were incorporated in most of the Lassen-phase units. In addition, throughout the past 0.3 Ma, large flows of hybrid andesite totaling 10 km^3 and consisting of thoroughly mixed mafic and silicic magma were erupted peripherally to the dacite domefield, primarily on the Central Plateau. With rare exception, these inclusions and hybrid lavas are medium-K_2O andesite, similar in most respects to both Brokeoff-phase andesites, and calc-alkaline andesites erupted in the Lassen region away from LVC proper. Importantly, petrographic evidence for mineral disequilibria is present in rocks from all stages of development at LVC, particularly those of the Lassen phase (Clynne, 1984; 1989).

At this point, several important features of the LVC data set should be noted. First, Brokeoff-phase andesites span nearly the entire width of the medium-K_2O field of Ewart (1979), with K_2O-content showing no organized relationship to stratigraphic position (Clynne, 1984). Second, the general evolution of magmatic events at LVC is from mafic to predominantly silicic with time. Third, silicic volcanism at LVC changes with time from high-K_2O to medium-K_2O in character. This is particularly intriguing in that, whereas LVC is compositionally similar to other calc-alkaline volcanoes erupted through thick continental crust (cf. Gill, 1981), it differs from most other Cascade volcanoes by having a larger relative and absolute volume of silicic rocks (Clynne, 1984; 1989). Fourth, mixing appears to have been an important petrogenetic process at least in the Lassen phase, and probably throughout the history of LVC. In consideration of these factors, our purpose here is to utilize various geochemical and isotopic data for magmatic products from each stage of LVC in order to determine the relative importance of various processes that may have controlled the compositional evolution of this calc-alkaline volcanic center. We begin with a demonstration that it is profitable to consider the geochemical systematics of the Brokeoff-phase magmas separately from those of the Lassen-phase magmas.

Sample selection and analytical procedures

Selected major and trace element, as well as isotopic data for samples discussed in this paper are given in Table I. The samples chosen for isotopic analysis were selected from a suite of approximately 200 rocks from LVC that had been analyzed previously for major and trace element composition. The intent of our selection procedure was to choose samples that reflected the geochemical diversity of each stage of magmatic evolution at LVC. The most reliable indices of such diversity are incompatible element (IE)-content relative to Sr-content (IE/Sr), and SiO_2-content. Therefore, samples were chosen to encompass the range of IE/Sr and SiO_2-content observed in each stage.

Major element compositions were determined for whole-rock samples by wavelength-dispersive x-ray fluorescence spectrometric techniques. Analyses listed in Table I are reported on a "dry" basis, recalculated to 100 wt. %. Trace element compositions were determined by a combination of energy-dispersive x-ray spectrometric and instrumental neutron activation techniques. Analytical methods used and pertinent errors for these three techniques are discussed by Bacon and Druitt (1988).

Isotopic compositions of Sr, Nd, and Pb for whole-rock samples were measured using both single- and multi-collector Finnigan MAT 261 mass spectrometers at U.S.G.S. Menlo Park, CA. The isotopic ratios reported in Table I are normalized to correct for mass fractionation as follows: $^{86}Sr/^{88}Sr = 0.1194$; $^{146}Nd/^{144}Nd = 0.7219$. Maximum uncertainty of the reported isotopic ratios at the 95% confidence level (2sdm) is ±0.00003 for $^{87}Sr/^{86}Sr$, and ±0.00002 for $^{143}Nd/^{144}Nd$. Ten measurements of $^{87}Sr/^{86}Sr$ for the NBS-987 Sr-standard over the course of this investigation averaged 0.71025. Eleven measurements of $^{143}Nd/^{144}Nd$ for Ames Nd-metal over the course of this investigation averages 0.512143. In an independent investigation using the same mass spectrometer, Johnson (1986) reported averages of 0.512140 for the Ames Nd-metal, 0.512626 for BCR-1, and 0.511859 for the La Jolla Nd-salt.

Pb-isotope ratios were corrected for 0.12% fractionation per a.m.u. based on replicate analyses of NBS-981 and NBS-982 Pb-standards. In an attempt to standardize the effects of thermal fractionation during the Pb-runs, sufficient whole-rock powder was digested to supply 500 ng. Pb for the filament loading procedure, and each run was performed at 1150°-1200°C. Based on replicate analyses of both NBS Pb-standards and selected Lassen samples during the course of this investigation, the maximum uncertainty of any Pb-isotopic ratio is ±.02% per a.m.u.

Geochemical evolution at LVC

Diagnostic chemical characteristics of Brokeoff-phase magmas

From a volumetric standpoint, the majority of lavas erupted during Stage I are olivine-bearing two-pyroxene andesites with 58-60 wt.% SiO_2, and the bulk of those cluster along the higher-K_2O margin of the data field in Figure 2a. Further, although lavas with less silica and/or lower-K_2O are relatively uncommon, two arbitrary groups of Stage I lavas can be identified. One group is characterized by lower-K_2O, the other by higher-K_2O, and each extends to basaltic andesite compositions. The small-volume, high-K_2O late Stage I dacite lies roughly on the extension of the higher-K_2O andesite array in Figure 2a.

During Stage II, numerous thick flows of two-pyroxene andesite were erupted from the Brokeoff vent system. The majority of these lavas have 61-63 wt.% SiO_2 and, as during Stage I, cluster along the higher-K_2O margin of the data field in Figure 2a. However, as with Stage I, a small number of andesites have lower-K_2O, and a few diverge from the main cluster to lower SiO_2.

At given silica content, the higher-K_2O Brokeoff-phase lavas consistently have elevated contents of all elements generally considered to be incompatible to moderately incompatible, (i.e. high-field strength, large-ion lithophile, and rare-earth elements), similar contents of most compatible elements (i.e. Cr, Co, and Sc), and lower contents of Sr compared to the lower-K_2O lavas. The overall geochemical coherence of the Brokeoff-phase lavas leads to generally smooth arrays on most variation diagrams indexed to an incompatible element. As diagnostic examples, the systematic variations of Sr, Zr, Co and P are shown with respect to K-content in Figures 3a-3d.

The logarithmic nature of Figures 3a-3d is useful for visualizing possible fractionation relationships among the magmas. On these diagrams, vectors representing closed-system parent-daughter crystallization paths have been included for reference. These particular vectors demonstrate the range of intra-sample crystal-glass equilibria determined both by Bacon and Druitt (1988) for andesitic scoria ejected during the climactic eruption of Mt. Mazama, Oregon, and by Luhr and Carmichael (1980) for post-caldera andesitic ejecta from Volcan Colima, Mexico. The residual glasses in these magmatic products range from andesite to rhyolite in composition. Magmas from both Mt. Mazama and Volcan Colima are calc-alkaline in nature, and represent suitable well-documented chemical analogs to LVC magmas.

As shown in Figures 3a-3c, the model fractionation vectors parallel the Brokeoff data array for Sr, are slightly askew to the data array for Zr, and clearly diverge from the data array for Co (as well as for other strongly compatible elements and FeO^*/MgO). These characteristics preclude a simple closed-system fractionation relationship to account for the character of the Brokeoff data array, although in detail the late Stage I dacites do lie along model fractionation vectors projected from the highest-K_2O Stage I andesites.

On the other hand, the data can be interpreted and modeled as a complex mixing array between a silicic component similar to the Stage I dacites and at least two lower-SiO_2 components having diverse contents of K_2O and other incompatible elements. These lower-SiO_2 components may be similar to

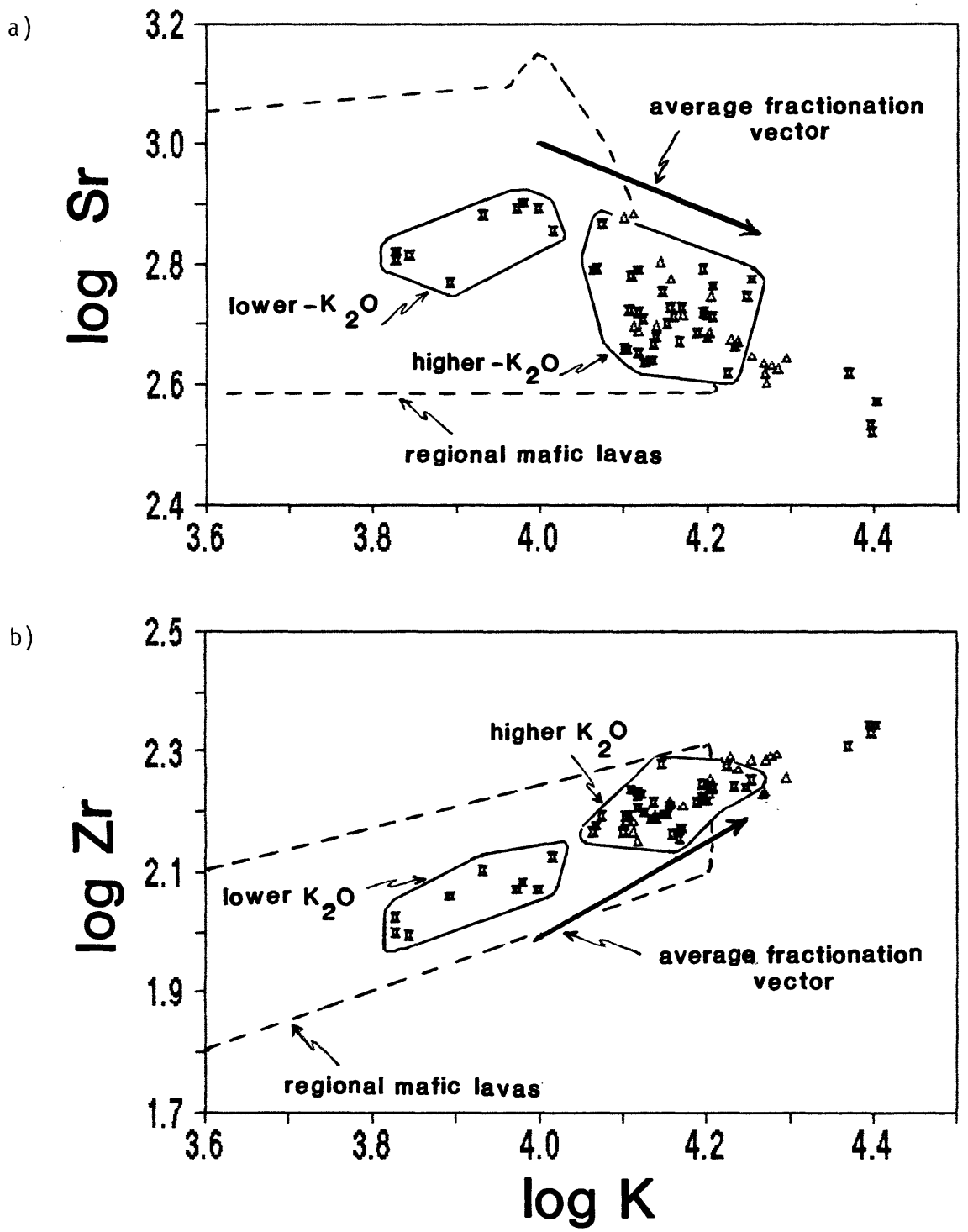

Figure 3. Trace element variation diagrams for lavas of the Brokeoff phase. "Average fractionation vectors" approximate the trends predicted for closed-system fractional crystallization processes.

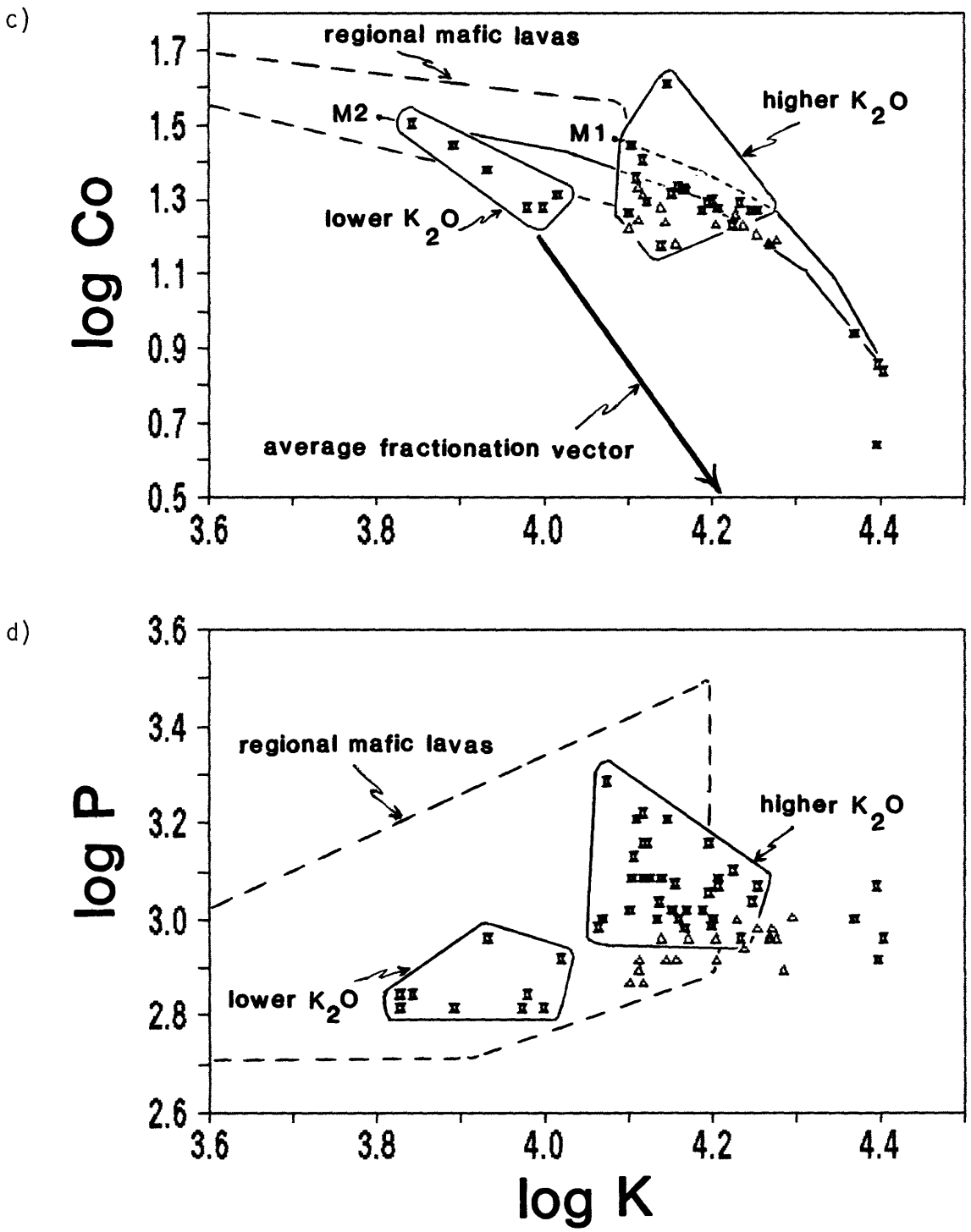

Figure 3. (continued) In c), M1 and M2 are model mixing curves between Stage I dacites and representative high- and low-K_2O mafic lavas.

calc-alkaline mafic lavas erupted in the Lassen region, and away from LVC proper, if it is allowed that a small amount (i.e. a few wt.%) of fractional crystallization accompanies the mixing process, primarily to satisfy the systematics of Co and other strongly compatible elements. Simple model mixing curves are included in Figure 3c in order to demonstrate the validity of this interpretation. We point out that in these and all other variation diagrams, the Stage II magmas are compositionally intermediate between the Stage I andesites and dacites.

The divergent geochemical character of the lower-SiO_2 Brokeoff components is particularly evident in the systematics of phosphorus, as shown in Figure 3d. On this logarithmic plot, the lower-K_2O Stage I andesite group defines an array with a markedly different slope than that of the higher-K_2O Stage I andesite group. The differing slopes of the divergent arrays cannot be attributed to variable modal proportions of apatite in some model fractionation assemblage, because apatite has not been recognized as a phenocryst or microphenocryst phase in any of the Stage I andesites. On the other hand, as shown in Figure 3d, the two andesite arrays do project toward compositions represented by mafic calc-alkaline lavas erupted in the Lassen region and away from LVC proper.

In summary, the overall systematics of the Brokeoff data cannot be explained in terms of simple closed-system fractionation processes involving a single mafic parent. This is not to imply that fractional crystallization does not occur in the Brokeoff magma system, but only that it is not the primary mechanism responsible for the development of compositional diversity. Alternatively, the geochemistry of Stage I magmas can be interpreted in terms of mixing between calc-alkaline mafic magmas and silicic magmas similar to the late Stage I dacites. Moreover, the Stage II magmas can be modeled as mixtures between the Stage I dacites and diverse mafic liquids similar to the andesites erupted during Stage I.

Unfortunately, the origin of the Stage I dacites is problematic. Whereas they can be modeled reasonably well as fractionates of the highest-K_2O andesites, the restricted K_2O-contents of the dacites are troublesome in light of the overall diversity displayed by the Stage I andesites. Alternatively, the dacites may be relatively small-volume, homogeneous partial melts of some mafic source material, as suggested by Smith and Leeman (1987) for Mount St. Helens dacites. Regardless of the mode of origin for the dacites, the generation of silicic magma at LVC appears to be intimately related to petrogenesis of the andesites.

Diagnostic chemical characteristics of Lassen-phase magmas

The onset of the Lassen phase of magmatism with the eruption of the voluminous Rockland tephra represents the sampling of a major body of silicic magma that is markedly different in geochemical character compared to that in the majority of Brokeoff-phase magmas. The key evidence for a dramatic shift in geochemical character, beyond the K_2O-SiO_2 systematics shown in Figure 2b, lies in the fact that Zr in the Rockland and later Stage III silicic magmas is substantially lower (by as much as 40%) than that in both the dacites and the majority of andesites of the Brokeoff phase. The behavior of other high-field strength elements and the middle rare-earth elements mimics that of Zr. The Zr-K systematics of the Stage III magmas are shown in relation to those for the Brokeoff-phase magmas and regional calc-alkaline lavas in Figure 4a.

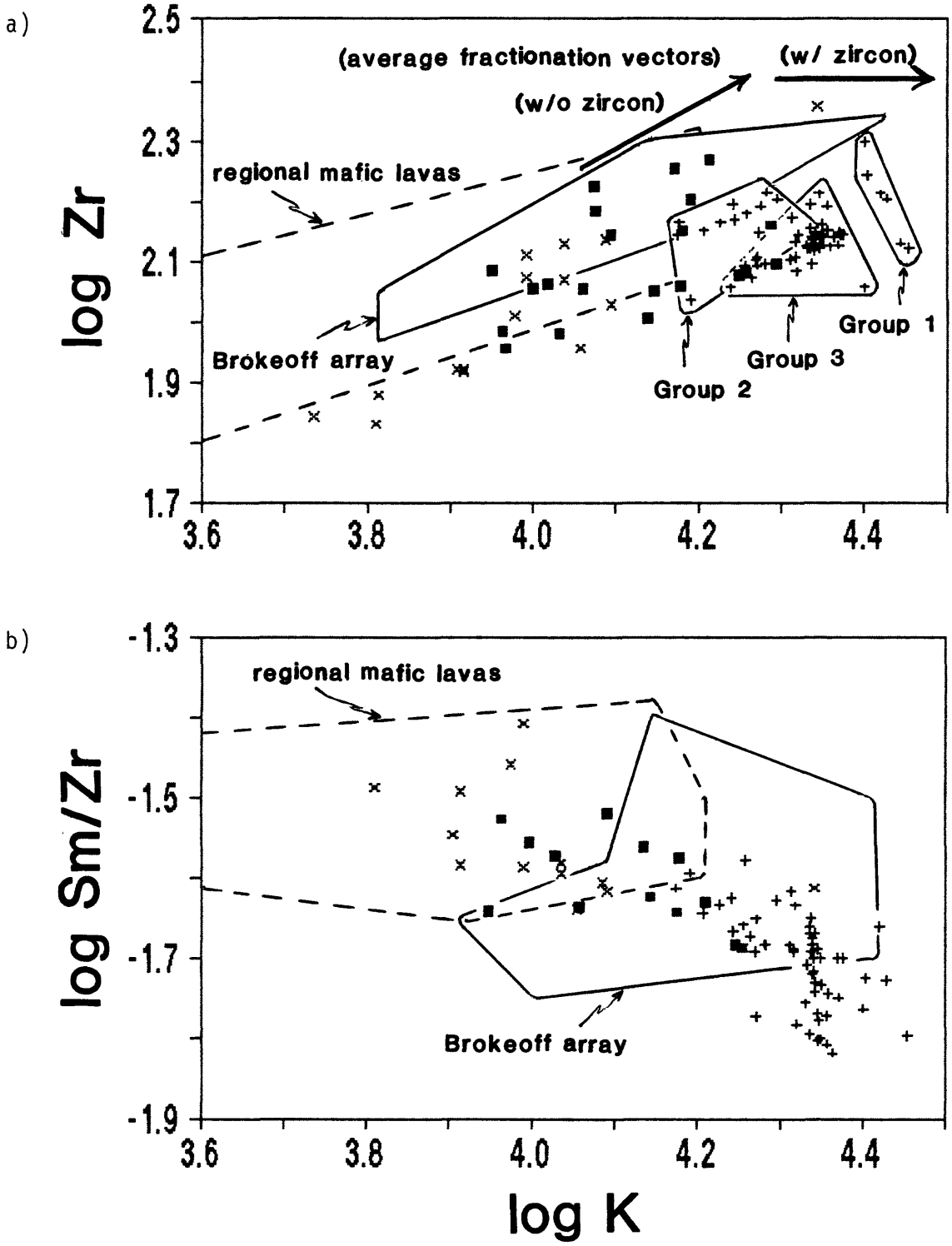

Figure 4. Variation of Zr and Sm/Zr with K-content for lavas of the Lassen phase. In a), "w/zircon" and "w/o zircon" describe trends predicted for zircon-bearing and zircon-free fractionation systems.

We stress that most Stage III magmas are demonstrably hybrid, representing varying mixtures of calc-alkaline mafic and silicic components. Even the mafic magmatic inclusions are mixed to some degree prior to quenching, as they typically contain xenocrysts derived from their silicic hosts (Clynne and Christiansen, 1987; Clynne, 1989). Regardless, the compositions of all Stage III silicic magmas, the majority of mafic magmatic inclusions and many of the hybrid andesites plot below the data array for the Brokeoff-phase magmas in Figure 4a.

In detail, a temporal shift in the Zr-K systematics can be recognized for silicic samples erupted subsequent to the Rockland event. For example, as shown in Figure 4a, the majority of Groups 1 and 2 (early) rhyodacites and dacites plot between the Brokeoff data array at one extreme, and the bulk of Group 3 (late) rhyodacites and Rockland magma at the other. We note, however, that at least some of the hybrid andesite magmas plot on the Brokeoff data array, projecting from the silicic magmas toward elevated Zr-content.

As shown in Figure 4a, the data array for Stage III magmas clearly is not related to that of the Brokeoff magmas by the model fractionation vector derived from the data of Bacon and Druitt (1988) for silicic glass in equilibrium with plagioclase, pyroxenes, hornblende, Fe-Ti oxides and apatite. Moreover, we contend that the generally depressed-Zr nature of Stage III magmas compared to that of Brokeoff magmas cannot result merely from addition of zircon to any hypothetical Brokeoff-type crystallization sequence. According to partition coefficient data summarized by Bacon and Druitt (1988), Zr is moderately incompatible in all the phases listed above except zircon, and always has lower to similar partition coefficients compared to the middle-rare earth element Sm, again except for zircon in which Sm displays extremely low affinity relative to Zr (c.f. Hanson, 1980). These relations suggest that any substantial amount of zircon fractionation will act to reverse the progressive slow decrease in a ratio such as Sm/Zr caused primarily by fractionation of hornblende and pyroxenes. In fact, Sm/Zr in the silicic Stage III magmas is similar to or lower than that in the Brokeoff magmas, as shown in Figure 4b.

We suggest that the geochemical differences between magmas of the Brokeoff and Lassen phases reflect the differing evolutionary histories of two physically distinct, but genetically related magmatic systems. The data indicate that the majority of Brokeoff-phase magmas are derived from parents and/or mixing end-members that are relatively rich in K and Zr (as well as other incompatible elements) compared to those of the Lassen-phase magmas. Of course, the data clearly show that some incompatible element-poor magmas have contributed to the Brokeoff system, whereas some incompatible element-rich magmas have mixed into the Lassen system, particularly in the hybrid andesite suite. Overall, however, the proportion of relatively incompatible element-rich magmas feeding LVC proper has decreased over time. Finally, as shown in Figures 2-4, we note that calc-alkaline mafic magmas erupted in the Lassen region and away from LVC proper display sufficient geochemical diversity to account for the apparent range of both Brokeoff- and Lassen-phase parents and/or mafic mixing end-members.

Isotopic constraints on petrogenetic processes at LVC

We have analyzed the isotopic composition of Sr, Nd, and Pb in a wide variety of samples taken from each stage in the development of LVC. Here we compare these data to our parallel data set for mafic lavas erupted in the Lassen region, to our data for three crustal inclusions incorporated by the Stage III silicic magmas, and to literature data for older rocks of the adjacent Klamath and northern Sierran provinces. Separate discussions of the geochemical and isotopic character of the regional mafic lavas are in preparation.

Our goal in the present discussion of isotopic systematics is two-fold. First, we wish to demonstrate that, although the mafic rocks erupted at LVC display a variable isotopic character, the most silicic rocks are essentially uniform in isotopic composition. Second, we can show that the bulk of isotopic variability observed at LVC is best explained in terms of interaction of the mantle components expressed in the regional mafic lavas, and that little mid- to upper-level crustal isotopic character has been inherited by the LVC magmas during their passage through the crust. We first discuss the isotopic systematics of Sr and Pb which, in LVC magmas, occur in high and low concentrations, respectively. We then discuss the petrogenetic significance of coupled Pb-Sr, Nd-Sr, and Nd-Pb isotopic systematics.

Variability of Sr-isotopic composition

The isotopic composition of Sr is particularly variable at LVC, and serves as the basis for the following discussion. In order to visualize the relationship of isotopic character and geochemical evolution at LVC, $^{87}Sr/^{86}Sr$ is plotted against SiO_2 in Figure 5a. In Figure 5b, $^{87}Sr/^{86}Sr$ is plotted against 1/Sr, a plotting scheme that is useful for demonstrating potential mixing relationships between various compositional extremes. The data field for mafic lavas erupted in the Lassen region is included in these diagrams for purposes of comparison.

Several important observations can be made based on the systematics of Sr-isotopic composition. First, the greatest diversity in $^{87}Sr/^{86}Sr$ at LVC occurs in rocks of andesitic composition. This is particularly true for the demonstrably hybrid Stage III quenched magmatic inclusions, which display greater diversity than the Stage I andesites having similar SiO_2-content. Second, $^{87}Sr/^{86}Sr$ becomes markedly less diverse with increasing SiO_2, converging from extremes of 0.7029 and 0.7042 in the andesitic rocks to 0.7040-0.7041 in the Rockland tephra and related lavas. Magmas of the Brokeoff phase fit within the context of this convergence, as Stage II silicic andesites are intermediate isotopically, as they are geochemically, between the Stage I andesites and dacites.

Third, whereas the more radiogenic samples ($^{87}Sr/^{86}Sr > 0.7037$) display a wide range of whole-rock SiO_2- and Sr-content, the less radiogenic samples ($^{87}Sr/^{86}Sr < 0.7037$) tend to have intermediate SiO_2- (roughly andesitic) and elevated Sr-content (> 1000 ppm). Note, however, that for the spectrum of mafic lavas erupted in the Lassen region, elevated Sr-content is not restricted to less radiogenic Sr-isotopic composition. Fourth, considering that two of the three LVC samples that have $^{87}Sr/^{86}Sr > 0.7042$ are demonstrably hybrid andesites (i.e. are mixtures of mafic and silicic components), the range of Sr-isotopic composition for LVC magmas lies within that for the regional mafic lavas. Importantly, the most silicic magmas are not the most radiogenic, at least in terms of Sr.

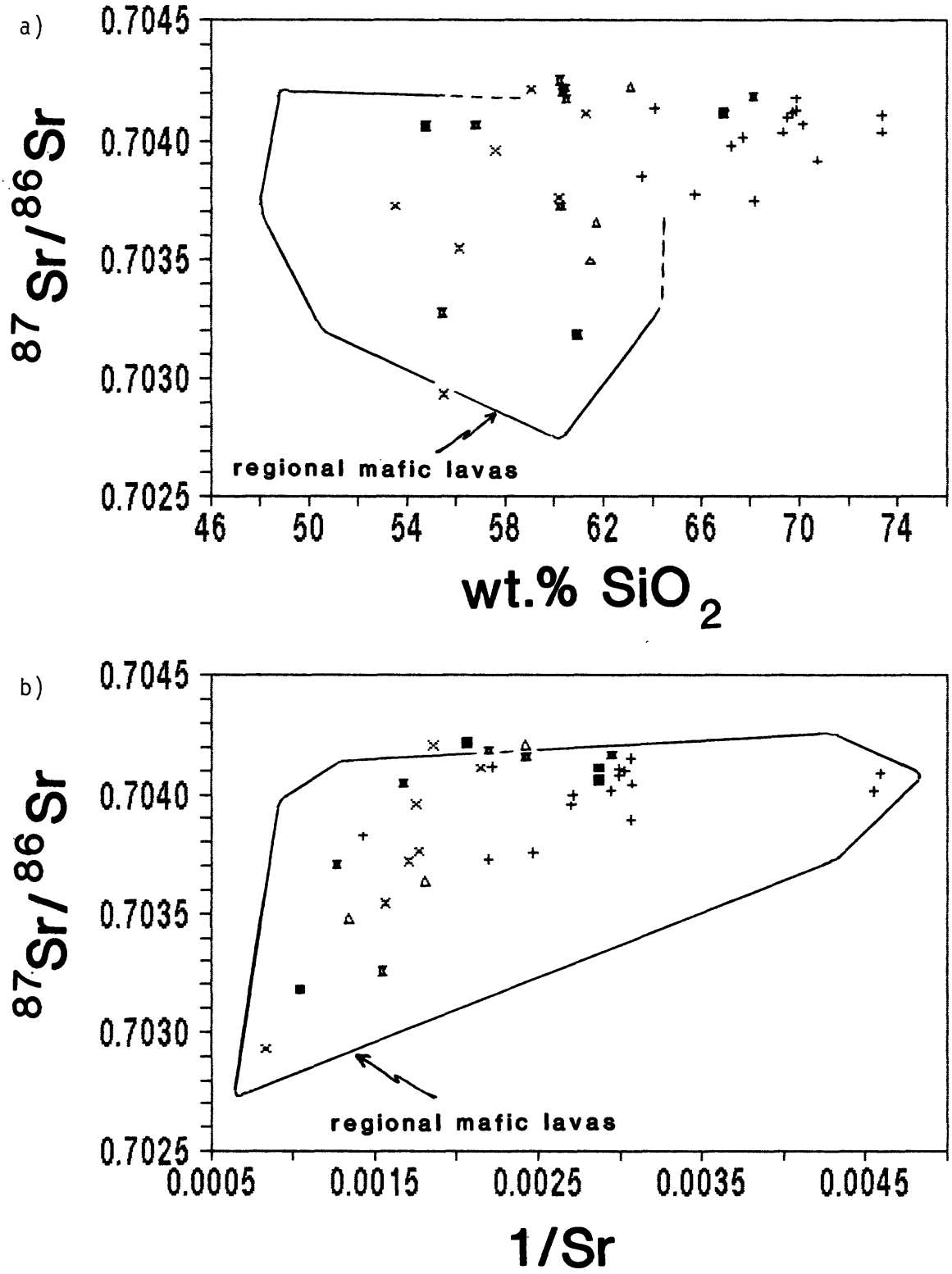

Figure 5. Sr-isotopic systematics for lavas of the Lassen Volcanic Center. In b), simple mixing relationships produce straight-line variations.

Systematics of the Pb-isotopes

Coupled isotopic variations for Pb in the LVC magmas are plotted in Figures 6a and 6b. The essentially linear arrays displayed in these diagrams point to the fact that the Pb-isotopes are well-correlated internally, an observation in accord with Pb-systematics at other Cascade volcanoes (Church and Tilton, 1973; Church, 1976), and at arc volcanoes worldwide (cf. Gill, 1981). Strong correlations of the Pb-isotopes at arc volcanoes are often interpreted in terms of either source- or magma-mixing processes (cf. Gill, 1981; Hawkesworth, 1982). The additional complexity, particularly in Figure 6b, of a subtle kink near the radiogenic end of the LVC data array toward higher $^{207}Pb/^{204}Pb$ is intriguing, but difficult to intrepret in light of analytical uncertaincies.

In detail, features of the Pb-isotopic data mimic those of the Sr-isotopes. For example, the most silicic Stage III magmas are concentrated near the radiogenic end of the data array, but considered together do not represent the most radiogenic samples observed. As with the Sr-isotopes, samples at the extremes of the Pb-data array are andesites, each demonstrably hybrid in character. The significance of this observation is that the Pb-isotopic compositions of the diverse mafic components producing each extreme hybrid andesite would necessarily lie somewhat beyond the ends of the observed data array, directly away from their silicic components.

Figures 7a and 7b demonstrate the relationship of the LVC Pb-data array to the fields defined by both oceanic basalts and regional mafic lavas. Additionally, we include in these diagrams our data for three crustal inclusions sampled by the Stage III magmas, a field outlining N.E. Pacific Ocean sediments as analyzed by Church (1976), and an averaged vector describing initial Pb-isotopic compositions of both Mesozoic granitoids from the Klamath and Sierra Nevada provinces (J. Wooden, A. Robinson, and J. Wright, pers. comm.) and Paleozoic and Mesozoic Pb-ores from the Eastern Klamath Mountains (Doe et al., 1985). Four main points can be made concerning these diagrams.

First, in consideration of analytical uncertainties, the Pb-data array for LVC samples is wholly-contained by that for the regional mafic lavas. The less radiogenic end of the LVC array projects directly toward the Pb-isotopic composition of young ocean-ridge basalts sampled from the Gorda and Juan de Fuca Ridges of the N.E. Pacific Ocean (Church and Tatsumoto, 1975). The more radiogenic end of the LVC array projects toward an elevated $^{207}Pb/^{204}Pb$-composition that lies outside the oceanic array in both Figures 7a and 7b, implying the involvement of some component derived from old continental crust. These relations suggest that petrogenetic models for LVC magmas do not require the involvement of isotopic components beyond those expressed in the regional mafic lavas.

Second, the bulk of presently-analyzed sediments from the N.E. Pacific Ocean are too extreme in their $^{208}Pb/^{207}Pb$-character to qualify as the source of elevated $^{207}Pb/^{204}Pb$ in the more radiogenic LVC magmas. In contrast, the three crustal inclusions do have at least the proper averaged Pb-isotopic compositions to qualify as potential contaminants. If the overall linearity of the LVC Pb-data array results from contamination of relatively non-radiogenic mantle-derived magmas by rocks of crustal affinity, then the three crustal inclusions, rather than the sediments, represent suitable materials with which to test contamination models.

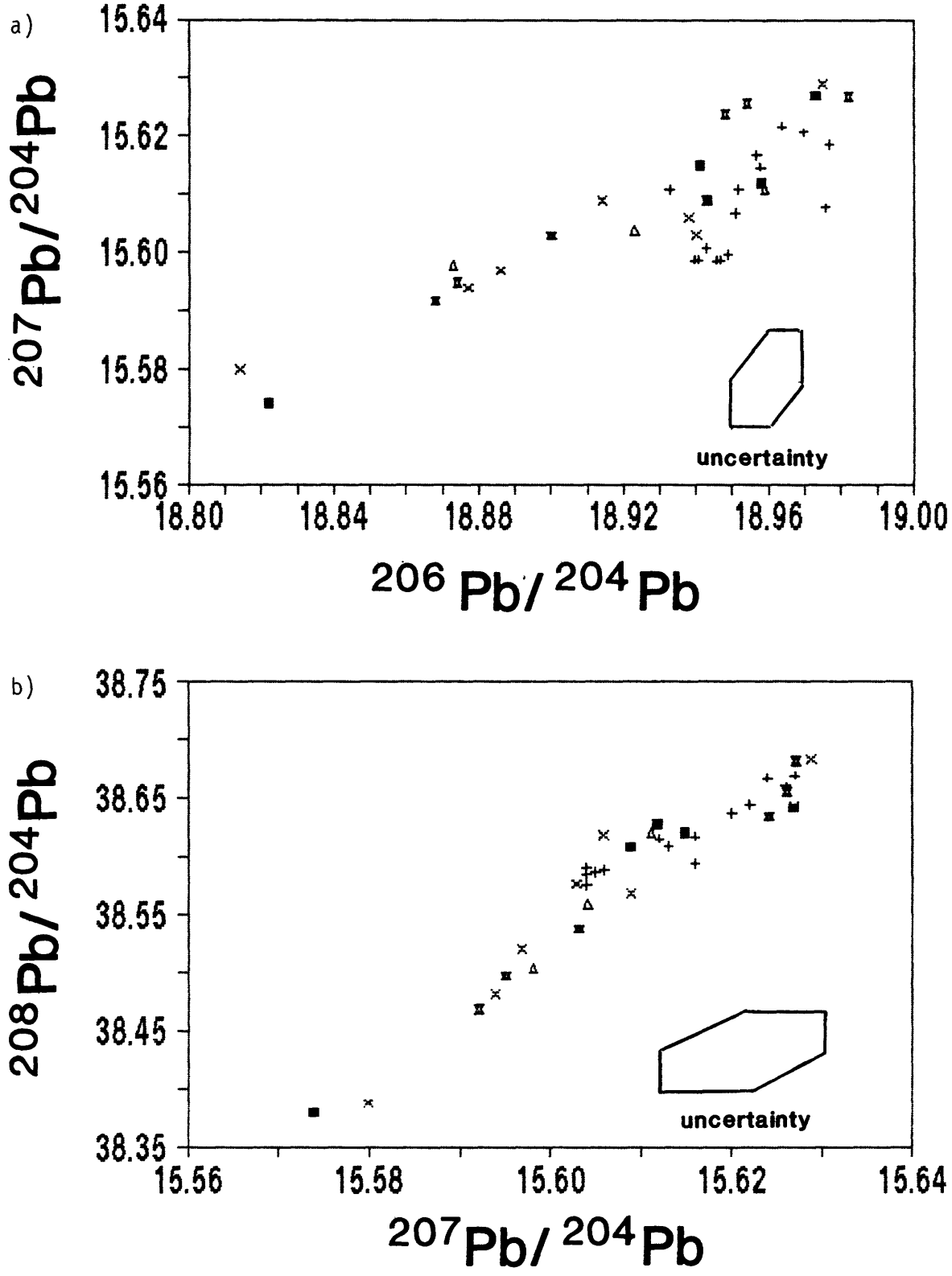

Figure 6. Pb-isotopic systematics for lavas of the Lassen Volcanic Center.

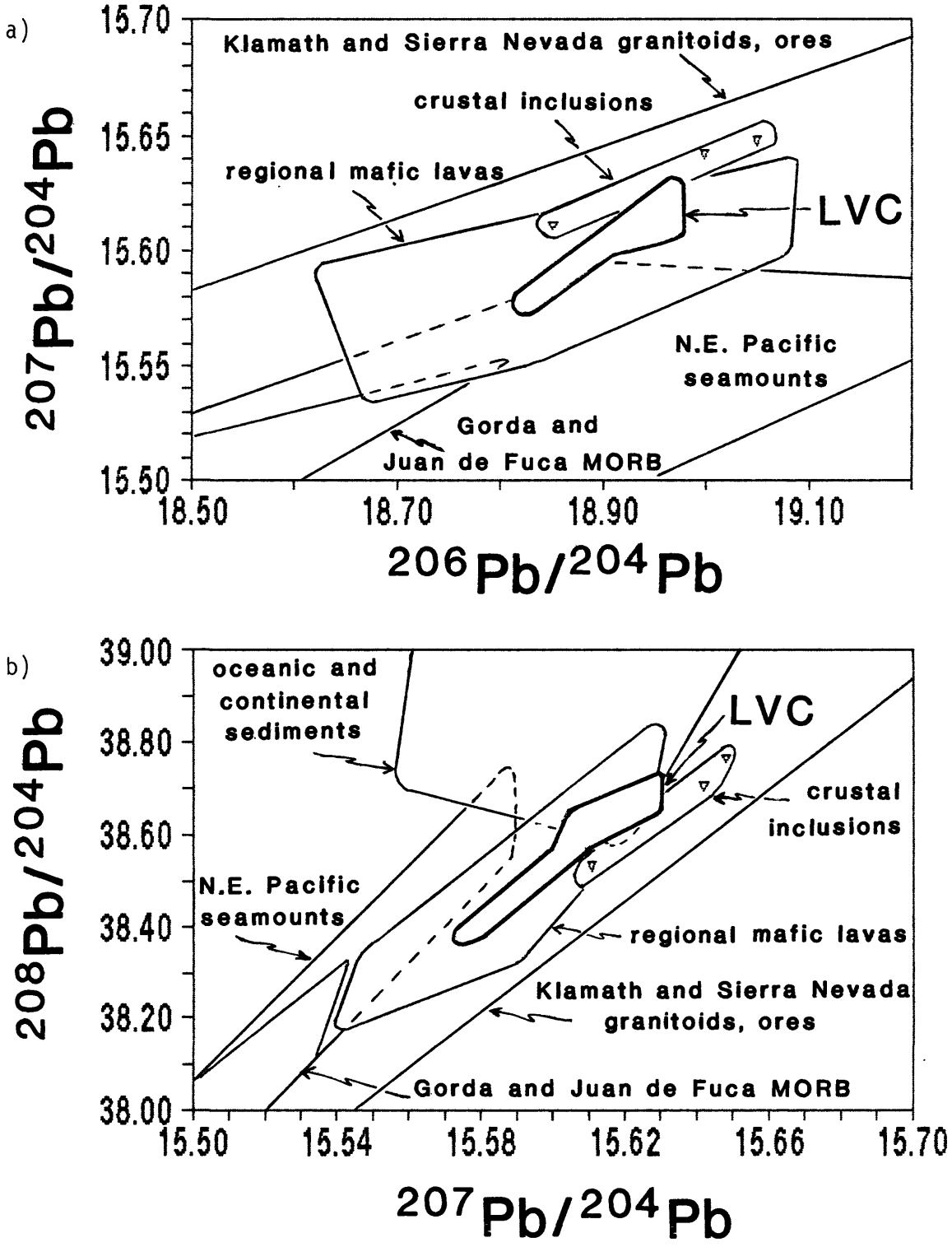

Figure 7. Pb-isotopic systematics for LVC magmas in relation to those for a variety of potential source and contaminant components. The line for the Klamath and Sierra Nevada rocks is a best-fit regression.

Third, considering LVC magmas and regional mafic lavas together, samples ranging in composition from basalt to rhyolite and with variable Pb-contents of from 1 to 15 ppm lie at the upper $^{207}Pb/^{204}Pb$ margin of the data array. This important feature of the isotopic data seriously calls into question the importance of contamination of the LVC magmas during ascent through the crust as a process to account for their apparent crustal isotopic signature. For such a scenario to be valid, the contaminant would have to fortuitously have the same Pb-isotopic composition as the most radiogenic samples in the Lassen data set.

Fourth, the trends of the Pb-data fields for regional mafic lavas are intermediate to and parallel the trends defined by oceanic lavas and by the initial ratios of granitoids and ores from the Klamath and Sierra Nevada provinces. This is a particularly important feature of the Pb-data, as it suggests that the intrinsic nature of source components and/or processes that have governed Pb-isotopic compositions of igneous rocks in this region has not changed appreciably, other than becoming more oceanic, since the Devonian.

Coupled Pb-Sr, Nd-Sr and Nd-Pb isotopic systematics

In order to better constrain the nature of isotopic variability displayed by LVC magmas, we have plotted examples of various coupled isotopic systematics in Figures 8-10. In these diagrams, we have included data fields for the regional mafic lavas, for various oceanic basalts, and for the three crustal inclusions. Our purpose here is two-fold. First, we wish to demonstrate the problems inherent to models that call on contamination of magmas during ascent through the crust to impart the crustal isotopic signature to the LVC magmas. Second, we seek to consider the overall isotopic systematics of LVC in more of a global perspective.

Beyond the fact that the various isotopic systems are remarkably well inter-correlated, several important points can be made concerning the relations shown in Figures 8-10. First, the bulk of the data for LVC magmas in each coupled isotopic system consistently lie within the field defined for the regional mafic lavas. There is the intriguing tendency for a few samples at the high-$^{87}Sr/^{86}Sr$, high-$^{206}Pb/^{204}Pb$ end of the LVC array in each diagram to extend to slightly more extreme values than for the mafic lavas. Considering analytical uncertainties, however, this observation is truly valid only for the Sr-Nd systematics. Regardless, the isotopic compositions for the most silicic Stage III magmas clearly lie within the field defined for the regional mafic lavas.

Second, the majority of lavas sampled from LVC and the surrounding region, with compositions ranging from basalt to rhyolite and with highly variable abundances of Pb, Sr, and Nd, share the more radiogenic Sr- and Pb-end of the overall isotopic array for Lassen region magmas. The three crustal inclusions, on the other hand, clearly lie at elevated $^{87}Sr/^{86}Sr$ relative to that array. Strongly elevated present-day $^{87}Sr/^{86}Sr$ compared to LVC magmas is likewise characteristic of the vast majority of igneous rocks from the adjacent Klamath and Sierra Nevada provinces (Kistler and Peterman, 1973; Brouxel et al., 1988; J. Wright and A. Robinson, pers. comm.). Only the most mafic granitoids from those provinces, by virtue of having low Rb/Sr, have present-day $^{87}Sr/^{86}Sr$ values that overlap those of the LVC magmas (cf. Farmer and DePaolo, 1983).

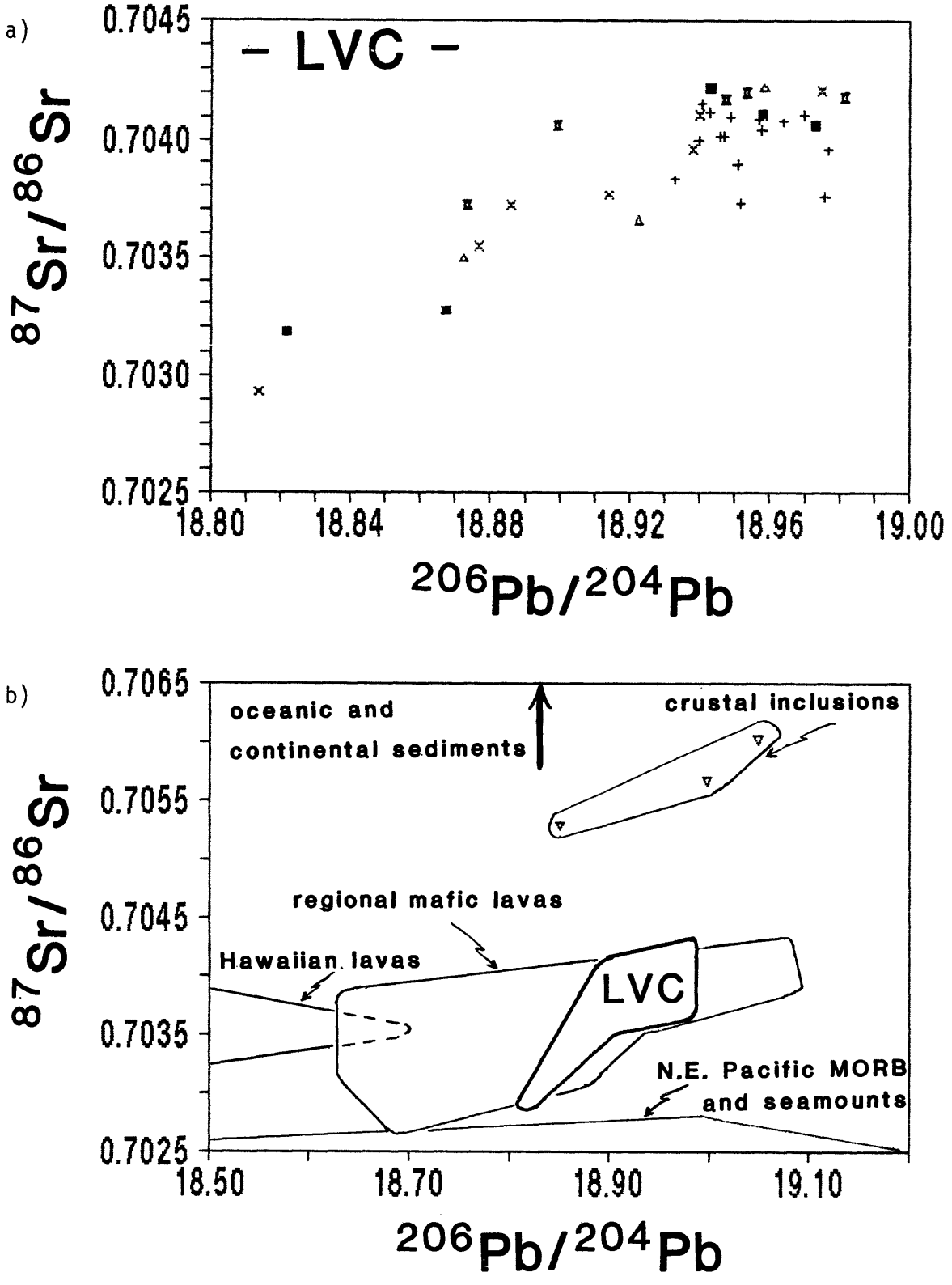

Figure 8. Coupled Sr-Pb isotopic systematics for LVC lavas (a), and for LVC lavas in relation to those for potential source and contaminant components (b).

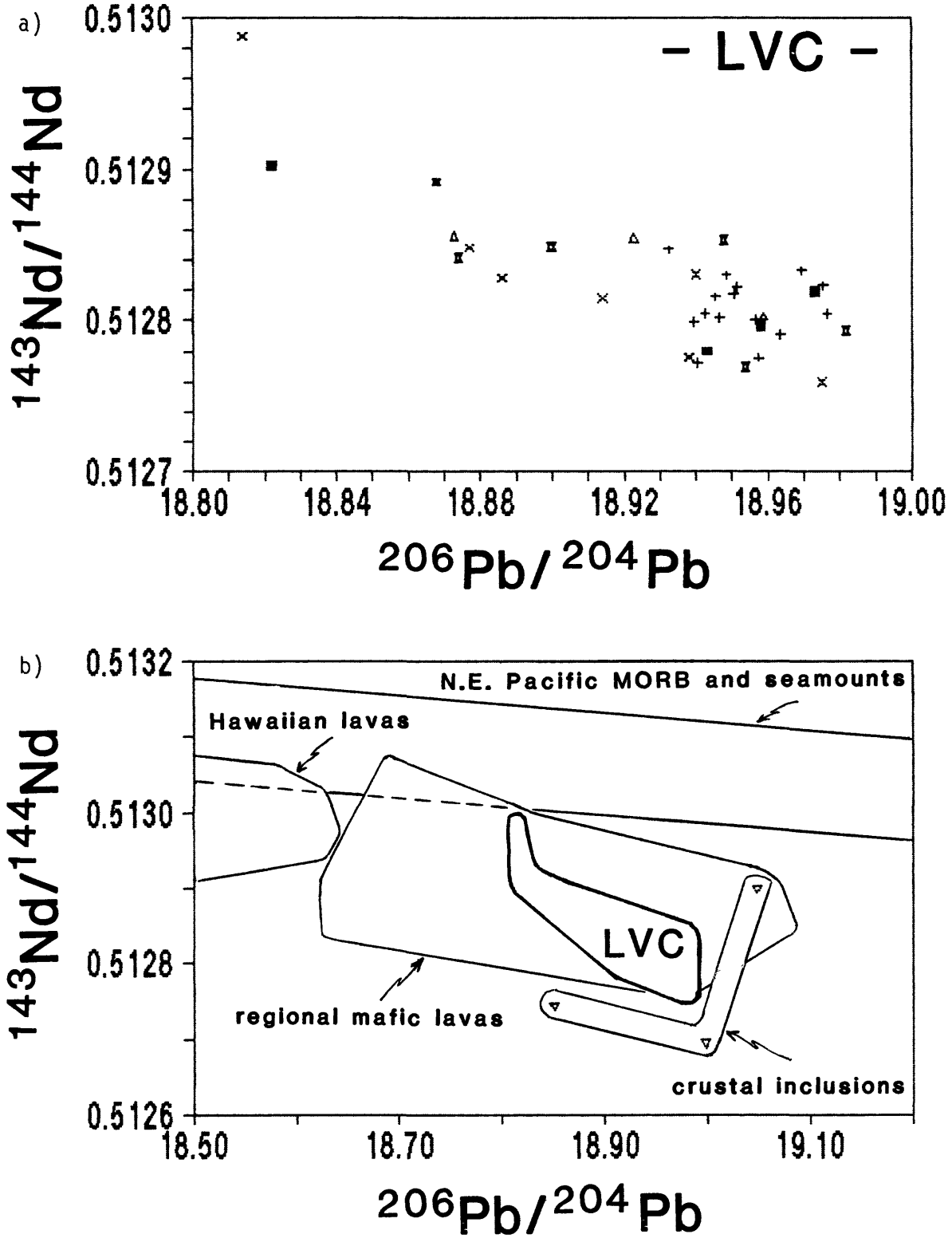

Figure 9. Coupled Nd-Pb isotopic systematics for LVC lavas (a), and for LVC lavas in relation to those for potential source and contaminant components (b).

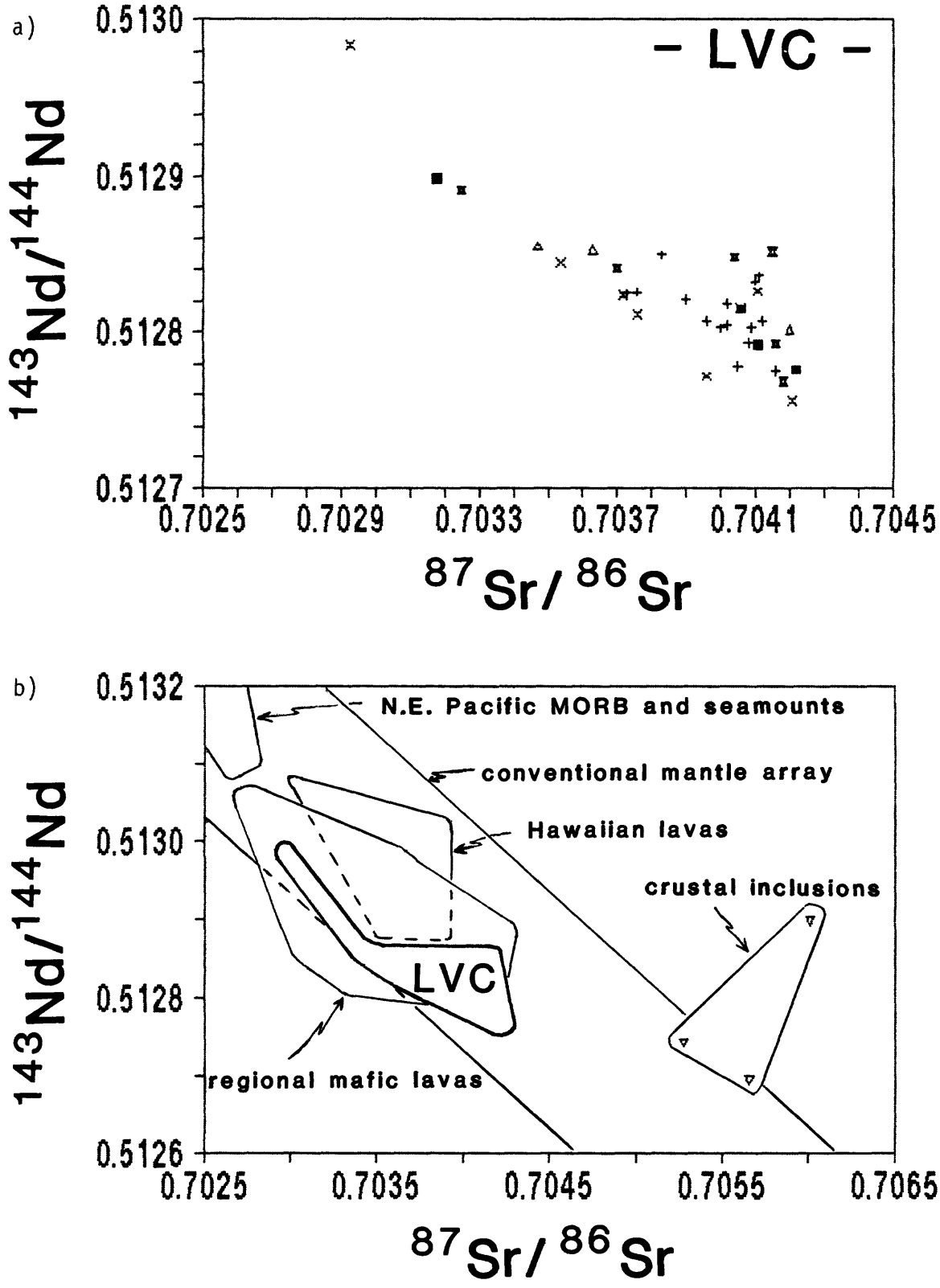

Figure 10. Coupled Nd-Sr isotopic systematics for LVC lavas (a) and for LVC lavas in relation to those for potential source and contamination components (b).

If the mid- to upper-level crust in the Lassen region is similar in isotopic character to that of the three inclusions (i.e. is Klamath- or Sierra Nevada-like in character), and if silicic Stage III magmas have been derived in part by assimilation of that crust by ascending mafic magmas, then the silicic magmas should display elevated $^{87}Sr/^{86}Sr$ relative to the mafic rocks. This is clearly not the case, and thus any model that calls on assimilation of crustal rocks to account for the geochemical character of the silicic magmas must invoke a contaminant that is identical in total isotopic character to that of the presumed mafic parents. While such a scenario is possible, we contend that contamination of presumed Lassen parent magmas by only the most mafic Klamath-type igneous rocks requires a most fortuitous assimilation model.

Third, the low-$^{87}Sr/^{86}Sr$, low-$^{206}Pb/^{204}Pb$ end of the LVC array consistently projects toward the array defined by N.E. Pacific Ocean ridge and seamount basalts. In contrast, the more radiogenic Sr- and Pb-end of the LVC array lies well-displaced from the MORB array in each diagram, but within the conventional oceanic array for the Nd-Sr system. As shown in Figures 8-10, the displacement of the more radiogenic Sr- and Pb-end of the LVC array from the typical MORB array is similar in many respects to that for the array of Hawaiian lavas (Staudigel et al., 1984) and other ocean-island basalts, at least with regard to $^{206}Pb/^{204}Pb$. Moreover, elevated $^{207}Pb/^{204}Pb$ in several ocean-island basalt suites has been attributed by various workers to the transfer of continental material into the source regions of the ocean-island magmas by a variety of complex subduction-related mechanisms (Zindler and Hart, 1986, and references therein). Clearly, sufficient evidence exists that lavas with continental isotopic character can erupt in the ocean basins, away from the influence of continental material during ascent through the crust.

These combined relations suggest to us that the composite isotopic data array for LVC reflects mixing of magmatic components derived from two distinct mantle reservoirs, one similar to the source of N.E. Pacific ocean-ridge and seamount basalts, the other similar to "enriched, continental-like" lithosphere as sampled by certain ocean-island systems. From here, we refer to these two mantle reservoirs as "oceanic" and "continental", respectively, owing to their obvious isotopic affinities. The shape of the LVC array in each of Figures 8-10, then, can be thought of as a bundle of mixing lines between magmatic end-members having variable Sr/Pb, Sr/Nd, and Nd/Pb, as well as variable proportions of the oceanic and continental isotopic components.

Synthesis: a working petrogenetic model for LVC

In this section, we derive a tentative petrogenetic model for the geologic evolution of LVC in light of the geochemical and isotopic constraints presented above. We have developed this model to account for the following: a) the higher-K_2O nature and differing K-Zr systematics of Brokeoff magmas relative to those of the Lassen phase; b) the temporal evolution from dominantly andesitic to dominantly silicic volcanism at LVC; c) the geochemically and isotopically well-averaged nature of the most silicic Lassen magmas; d) the isotopic diversity displayed by both the less silicic Lassen magmas and the Brokeoff magmas; and e) the fact that mixing dominates over fractional crystallization as the mechanism that best explain the geochemical variations for the majority of Brokeoff- and Lassen-phase magmas.

As an essential part of our model, we suggest that the highly-silicic Stage III magmas represent a geochemically and isotopically well-averaged component produced by melting of young, mafic lower crust. This distinct source region for the silicic liquids is formed by underplating of magmas that are similar in geochemical and isotopic composition to mafic lavas erupted in the Lassen region. A young age is required so that isotopic ratios have not had time to evolve to any substantial degree. In effect, the silicic magmas are derived from the mantle, albeit through a two-stage process, rather than through accumulation of residual liquid from mafic magmas that have fractionated and experienced contamination with "continental" isotopic components during ascent through the mid- to upper-level crust.

Production of liquids of dacite to rhyolite composition by melting of mafic rocks at elevated pressure is a process that merits consideration based on both geochemical (i.e. Reid and Cole, 1983; Smith and Leeman, 1987) and experimental studies (Holloway and Burnham, 1972; Helz, 1976). Mixing of these silicic liquids with mafic magmas derived from a heterogeneous mantle will produce hybrids with substantial geochemical, as well as isotopic diversity depending primarily on the relative proportions of oceanic and continental isotopic components in the source regions of the individual mafic magma batches.

Our model follows the progression shown in Figures 11a-11d. Figure 11a depicts the geologic setting prior to the initiation of volcanism in the Lassen region. At this time, the presumably Sierra Nevada- or Klamath-like crust overlay a geochemically and isotopically heterogeneous mantle section. The heterogeneities reflect a complex history of magmatic/metasomatic events probably related to long-term subduction processes. Mafic magmas derived from this mantle section by melting events, at least prior to 5 Ma., were unable to traverse the crust, but rather underplated its base. The newly-emplaced mafic lower crust constituted a site of potential melting in the event of sufficient subsequent heat input from the mantle (cf. Wyllie, 1984).

The Brokeoff stage of magmatism (Figure 11b) was initiated by a melting event in the upper mantle that generated a diverse array of mafic liquids. The mantle melting process may have been continuous in nature (cf. Langmuir et al, 1977), such that a series of progressively higher-degree melt batches were generated and injected into the lower crust. "Underplating units" were formed as early melt batches became trapped in the lower crust, where they may have fractionated slightly, mixed with small volumes of partial melt of

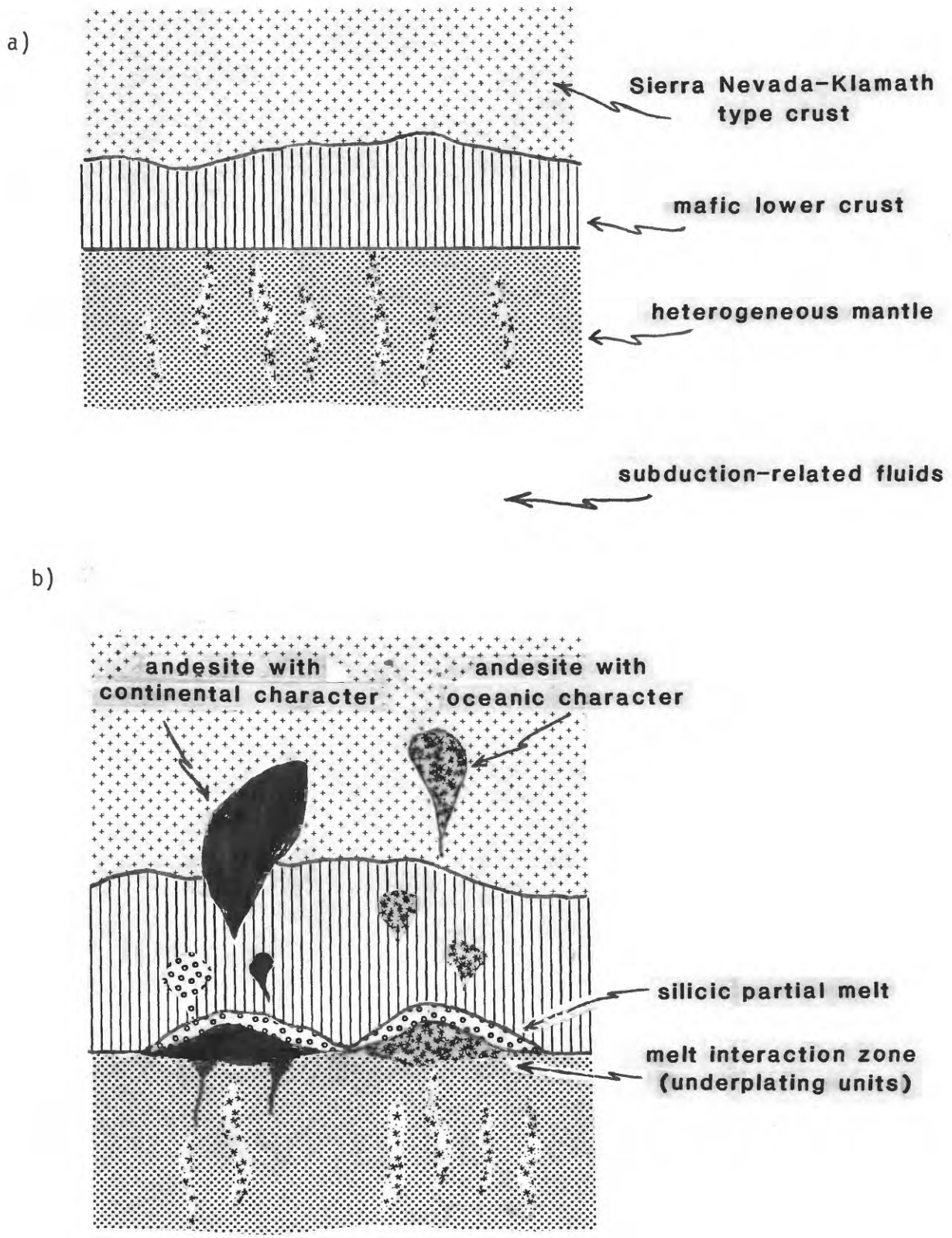

Figure 11. Cartoon depicting evolution of lower crustal melt interaction zone of the Lassen magmatic system.

c)

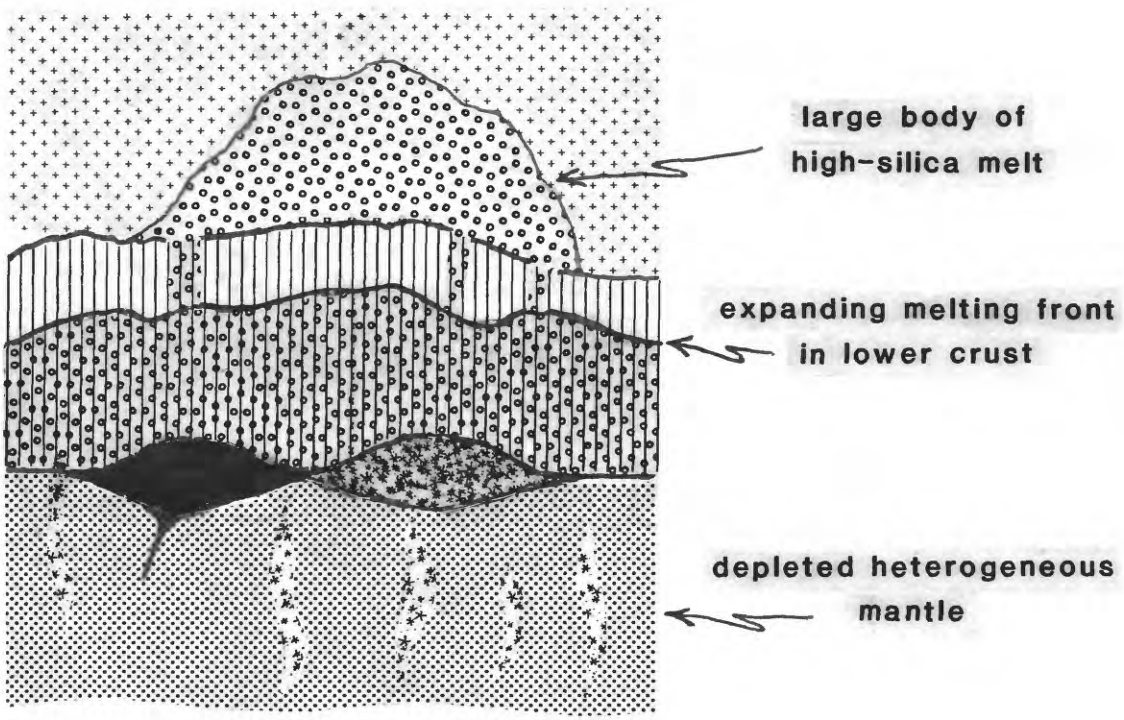

d)

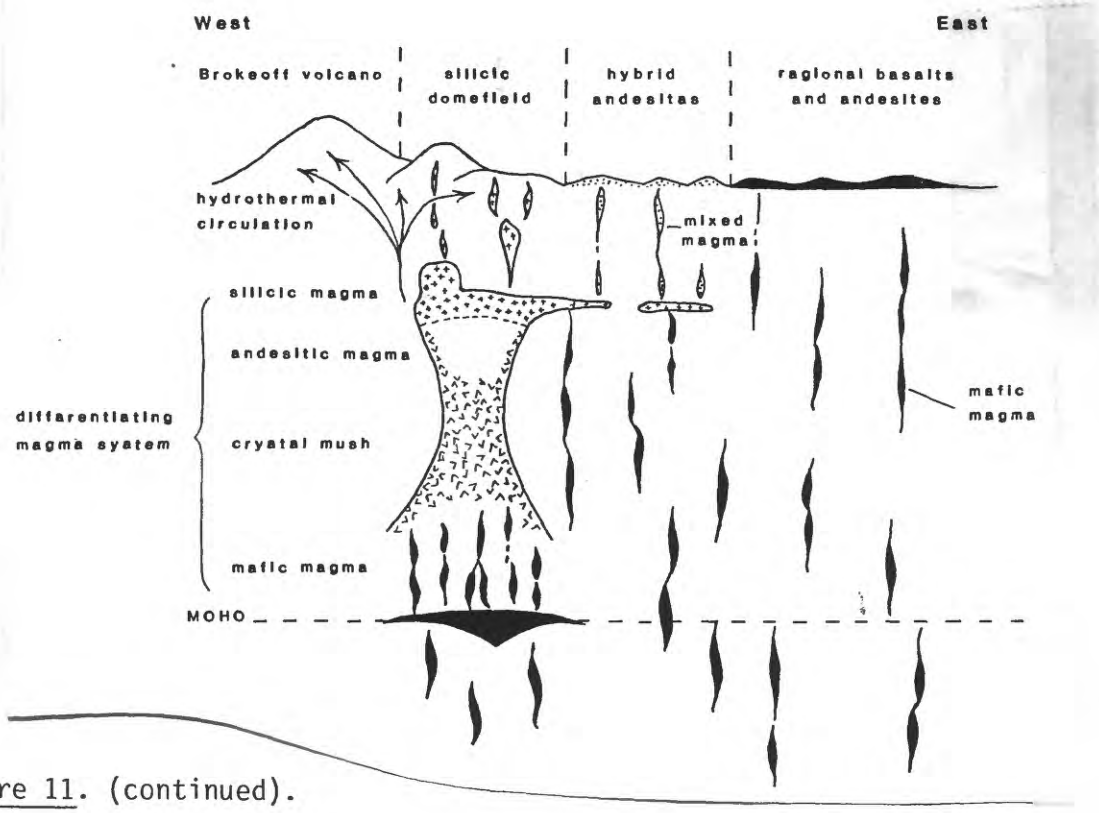

Figure 11. (continued).

the lower crust, and been replenished by subsequent batches of primitive magma. In several respects, this zone of melt processing in the lower crust resembles the MASH zone described by Hildreth (1988).

The fact that two distinct groups of Stage I andesites can be identified (e.g. Figure 2a) suggests that two geochemically and isotopically distinct melting zones and underplating units must have developed during this event. One had higher-K_2O and predominantly continental isotopic character, whereas the other had lower-K_2O and predominantly oceanic isotopic character. Periodic tapping of each underplating unit allowed small batches of basaltic andesite to andesite melt to separate from the zone of melt interaction and feed the Brokeoff plumbing system during the course of Stage I magmatism. The chemistry of each magma batch was determined by the transitory balance between degree of fractional crystallization acheived, amount of crustal partial melt consumed, and rate of recharge with primitive magma.

According to observed eruptive volumes at the Brokeoff Volcano, the amount of high-K_2O andesite produced considerably exceeded that of low-K_2O andesite. Moreover, according to stratigraphic relations at the Brokeoff Volcano, as noted earlier, the eruptive pattern reflects no temporal preference for either low- or high-K_2O magma. Within the stratigraphic section, however, the later erupted flows tend, on average, to be more silicic than earlier flows (Clynne, 1984). This temporal increase in average silica content suggests an increase with time in either the degree of fractional crystallization or the amount of crustal partial melt consumed relative to the amount of replenishment with primitive magma in the melt interaction zone of each underplating unit.

The transition from Stage I to Stage II Brokeoff activity is characterized by eruption of the late Stage I dacites, followed by the instantaneous return to andesite volcanism. Two scenarios for this transition are possible, hinging on the petrogenetic interprtation of the Stage I dacites. If the dacites are merely fractionates of the highest-K_2O Stage I andesites, then the transition could reflect the sampling of dacite from an upper-level, fractionated magma cell. Subsequent Stage II flows would be hybrid andesites sampled from that same upper-level cell that had been invaded from deeper levels by less-fractionated Stage I-type magma batches. This scenario fully accounts for the intermediate nature of Stage II silicic andesites relative to the Stage I andesites and dacites.

Alternatively, the transition from Stage I to Stage II could reflect the sampling of a dacite body that had been generated in the lower crust subsequent to the production of Stage I andesite magmas. In this regard, the dacite may represent a spatially-concentrated and thus fairly high-degree lower crustal partial melt that acheived sufficient volume to avoid blending with mafic magmas in the melt interaction zone. With this scenario, Stage II silicic andesites would be hybrids produced by mixing of residual dacite liquid with either subsequent primitive magma batches or with residual bodies of cooler, more crystalline Stage I andesite magmas.

We favor the second scenario for two reasons. First, the transition from Stage I to Stage II andesitic volcanism was essentially instantaneous.

Therefore, there is no physical justification for a fractionated magma cell to have developed in the upper levels of the Brokeoff plumbing system at this time. Second, the generation of a silicic magma body as a melt of the lower crust at the onset of Stage II is consistent with the progressive volumetric importance of silicic magmatism at LVC. Figure 11b can be used to depict the setting of Stage II magmatism, although we stress that the amount of lower crustal silicic partial melt present in the melt interaction zone has increased considerably over the course of the Brokeoff phase.

The ability of silicic magmas to be generated in and to separate from the lower crust probably reflects the progressive heating of the lower crust due to continued intrusion of mantle-derived magmas. As shown in Figure 11c, we envision the scenario just prior to Stage III volcanism as involving a renewed episode of mantle melting and heating of the lower crust, this time stimulating a spatially less-concentrated, lower-degree, yet more voluminous melting event in the crust than occurred during the Brokeoff event. The silicic partial melt of lower crust thus produced was the primitive Rockland magma that formed the upper portion of the Lassen-phase magma system. Continued development of this system, and its eventual ascent and emplacement into the mid- to upper-crust is probably representative of processes attendant to the evolution of arc-related plutonic systems.

Two points concerning the geochemical characteristics of the Lassen system are worthy of note. First, the highly-silicic nature of the Rockland magma allowed for greatly increased bulk partition coefficients between liquid and source residue minerals for elements like Zr, compared to those for less-silicic magma-residue systems (cf. Mahood and Hildreth, 1983). The lower-Zr nature of the Rockland rhyolite relative to the bulk of Stage I magmas merely reflects the higher partition coefficients operative during Rockland melt generation. Second, the renewed wave of mantle melting tapped a source region that had suffered a previous melt extraction event (i.e. to produce the Brokeoff mafic parents). Melts derived from this previously depleted source displayed the same relative amount of geochemical and isotopic diversity as earlier Brokeoff magmas, but at lower absolute concentrations of incompatible elements. In other words, the bulk of magmas generated in the mantle during Stage III, at least directly beneath the volcano, were lower-K_2O in nature.

Eventual emplacement of the Lassen magma system into the mid- to upper-crust allowed for eruption of the Rockland magma. Continued injection of lower-K_2O mafic liquids into the base of the mamga column resulted in vertical compositional stratification of the Lassen system, as shown in Figure 11d. Early Stage III eruptive units (i.e. Groups 1 and 2 rhyodacites and dacites) have chemistries that reflect lateral interaction of Rockland-type magma with residual Brokeoff magmas, whereas later Group 3 rhyodacites have chemistries that reflect vertical interaction of Rockland-type magma with lower-K_2O mafic liquids. In other words, by the time of eruption of Group 3 units, the lower-K_2O lineage was firmly established in the Lassen system, and the Brokeoff system was essentially extinct.

Most aspects of the geochemical and isotopic variability observed in Stage III magmas can be attributed to mixing between mafic and silicic liquids, and clearly there is abundant petrographic evidence to support this contention

(Clynne, 1984; 1988). Whereas the bulk of mafic magmas that supplied the base of the Lassen system were predominantly lower-K_2O in character, we stress that higher-K_2O magmas were generated in the mantle during the Lassen event. These more Brokeoff-like mafic magmas were injected into the crust primarily away from the volcano proper, in the areas where the majority of hybrid andesites were produced.

This model for the generation of the spectrum of LVC magmas places primary responsibility for the development of magmatic diversity in the realm of mixing processes, with fractional crystallization playing a subordinate role. In this regard, our model lends important support to the concepts stressed by Eichelberger (1975). We note, however, that a limited amount of fractional crystallization must have taken place particularly during Stage III, primarily to account for the overall silicic character of magmas during the entire Lassen-phase. Regardless, our model differs from those of other Cascade researchers, primarily in both the relative importance attributed to mixing/contamination processes and the nature of end-members of those processes.

Specifically, our model is in striking disagreement with models proposed by Grove et al. (1982) and Grove and Baker (1984) for andesite petrogenesis at the Medicine Lake Volcano. These workers contend that fractional crystallization of chemically homogeneous mantle-derived magmas coupled with minor assimilation of silicic crustal materials leads to the bulk of geochemical and isotopic diversity in the magma suite. In contrast, we contend that the opposite is true, that chemically and isotopically heterogeneous mantle-derived melts mix with homogeneous melts of mafic lower crust, thereby producing the magmatic diversity observed. Clearly, the trace element and isotopic systematics of LVC magmas preclude models that place primary responsibility for development of magmatic diversity in the hands of fractional crystallization.

Similarly, our model is in contrast to that proposed for the petrogenesis of silicic magmas by Bacon and Druitt (1988) for Mount Mazama. These workers again stressed the importance of fractional crystallization in generating the liquid line of descent from andesite to rhyolite. At LVC, the key evidence against a fractional crystallization origin for the Rockland magma is that its Zr-content is far less than predicted by model fractionation vectors projected from any andesite sampled at LVC, particularly those of the Brokeoff system. For Mount Mazama, however, the model fractionation vectors projected from andesite do predict the Zr-content of the presumably derivative pre-climactic rhyodacites, supporting the interpretation of Bacon and Druitt (1988) and suggesting that different processes may predominate at any given volcano.

Finally, our observations lead us to consider the nature of the LVC isotopic array, and by inference that for Cascade volcanoes in general, from a different perspective than that of previous workers. Complex isotopic variations identified for Cascade volcanics have been interpreted by Church (1976) and Halliday et al. (1983) in terms of contamination of mantle-derived magmas by crustal rocks, the course of contamination leading to enrichment of $^{207}Pb/^{204}Pb$ in derivative magmas. We propose that on the time-scale of evolution of a Cascade volcano, isotopic contamination occurs in the mafic lower crust and in the reverse direction, such that the fairly-restricted LVC

isotopic array results from the addition of a mantle-derived, well-averaged oceanic component (with low $^{87}Sr/^{86}Sr$ and $^{207}Pb/^{204}Pb$, high $^{143}Nd/^{144}Nd$) to a similarly well-averaged component derived from "enriched" mantle (with high $^{87}Sr/^{86}Sr$ and $^{207}Pb/^{204}Pb$, low $^{143}Nd/^{144}Nd$).

Conclusions

Our analysis of the geochemical and isotopic systematics of LVC leads us to conclude that magmatic diversity observed at the volcano must be attributed primarily to mixing processes. The trace element character of Stages I and II magmas differs markedly from that of the majority of Stage III magmas, suggesting that two physically distinct, but genetically related magma systems were generated during the course of magmatic evolution. We view the tendency for magmatism at LVC to become more silicic with time to reflect the increasing ability of large amounts of silicic magma to be generated in and to segregate from the mafic lower crust.

The similarity in isotopic diversity of Brokeoff- and Lassen-phase magmas suggests that essentially similar source materials were involved in all stages of petrogenesis. The differences between the Brokeoff- and Lassen-phase magmas reflect differences in both the physical conditions of melt generation and the relative contents of certain minor and trace element constituents in the source materials. Finally, we stress that the isotopic diversity observed in LVC magmas does not result from contamination of primitive magmas during their ascent through the mid- to upper-crust. Rather, the isotopic diversity reflects the inherent isotopic heterogeneity of the sub-arc mantle in the Lassen region.

References

Bacon, C.R., Magmatic inclusions in silicic and intermediate volcanic rocks, J. Geophys. Res., 91, 6091-6112, 1986.

Bacon, C.R. and T.H. Druitt, Compositional evolution of the zoned calc-alkaline magma chamber of Mount Mazama, Crater Lake, Oregon, Contrib. Mineral. Petrol., 98, 224-256, 1988.

Brouxel, M. and H. Lapierre, Geochemical study of an early Paleozoic island-arc-back-arc basin system. Part 1: The Trinity Ophiolite (northern California), Geol. Soc. Am. Bull., 100, 1111-1119, 1988.

Brouxel, M., H. Lapierre, A. Michard, F. Albarede, Geochemical study of an early Paleozoic island-arc-back-arc basin system. Part 2: Eastern Klamath, early to middle Paleozoic island-arc volcanic rocks (northern California), Geol. Soc. Am. Bull., 100, 1120-1130, 1988.

Church, S.E., The Cascade Mountains revisited: a re-evaluation in light of new lead isotopic data, Earth. Planet. Sci. Lett., 29, 175-188, 1976.

Church, S.E. and M. Tatsumoto, Lead isotope relations in oceanic ridge basalts from the Juan de Fuca-Gorda Ridge area, N.E. Pacific Ocean, Contrib. Mineral. Petrol., 53, 253-279, 1975.

Church, S.E. and G.R. Tilton, Lead and strontium isotopic studies in the Cascade Mountains: bearing on andesite genesis, Geol. Soc. Am. Bull., 84, 431-454, 1973.

Clynne, M.A., Stratigraphy and major element geochemistry of the Lassen Volcanic Center, California, U.S. Geol. Sur. Open File Rpt. 84-224, 1984.

Clynne, M.A., Nature of volcanic centers in the southernmost Cascade Range, California: the Lassen volcanic center, U.S. Geol. Sur. Open-File Rpt. (this volume), 1989.

Clynne, M.A. and R.L. Christiansen, Magma mixing and the devestating eruptions of May 1915 at Lassen Peak, California, Abstract Volume, Haw aiian Symposium on How Volcanoes Work, Hilo, Hawaii, Jan. 19-25, 1987, p.43.

Condie, K.C. and D.L. Hayslip, Young bimodal volcanism at Medicine Lake volcanic center, northern California, Geochim. Cosmochim. Acta, 39, 1165-1178, 1975.

Doe, B.R., M.H. Delevaux, and J.P. Albers, The plumbotectonics of the West Shasta Mining District, Eastern Klamath Mountains, California, Econ. Geol., 80, 2136-2148, 1985.

Eichelberger, J.C., Origin of andesite and dacite: evidence of mixing at Glass Mountain in California and at other circum-Pacific volcanoes, Geol. Soc. Am. Bull., 86, 1381-1391, 1975.

Ewart, A., A review of the mineralogy and chemistry of Tertiary-Recent dacitic, latitic, rhyolitic, and related salic volcanic rocks, in Trondhjemites, Dacites and Related Rocks, F. Barker, ed., Elsevier Developments in Petrology 6, 659pp, 1979.

Farmer, G.L. and D.J. DePaolo, Origin of Mesozoic and Tertiary Granite in the Western United States and implications for pre-Mesozoic crustal structure,1. Nd and Sr isotopic studies in the geocline of the Northern Great Basin, J. Geophys. Res., 88, B4, 3379-3401, 1983.

Gill, J.B., Orogenic Andesites and Plate Tectonics, Springer-Verlag, 390pp, 1981.

Grove, T.L., D.C. Gerlach, and T.W. Sando, Origin of calc-alkaline series lavas at Medicine Lake Volcano by fractionation, assimilation, and mixing, Contrib. Mineral. Petrol., 80, 160-182, 1982.

Grove, T.L. and M.B. Baker, Phase equilibrium controls on the tholeiitic vs. calc-alkaline differentiation trends, J. Geophys. Res., 89, 3253-3274, 1984.

Grove, T.L. and J.M. Donnelly-Nolan, The evolution of young silicic lavas at Medicine Lake Volcano, California: implications for the origin of compositional gaps in calc-alkaline series lavas, Contrib. Mineral. Petrol., 92, 281-302, 1986.

Guffanti, M. and C.S. Weaver, Distribution of Late Cenozoic volcanic vents in the Cascade Range: volcanic arc segmentation and regional tectonic considerations, J. Geophys. Res., 93, B6, 6513-6529, 1988.

Guffanti, M., M.A. Clynne, L.J.P. Muffler, and J.G. Smith, Spatial, temporal, and compositional trends of mafic volcanism in the Lassen region of northeastern California, U.S. Geol. Sur. Open-File Rpt. (this volume), 1989.

Halliday, A.N., A.E. Fallick, A.P. Dicken, A.B. Mackenzie, W.E. Stephens, and W. Hildreth, The isotopic and chemical evolution of Mount St. Helens, Earth Planet. Sci. Lett., 63, 241-256, 1983.

Hanson, G.N., Rare earth elements in petrogenetic studies of igneous systems, Ann. Rev. Earth Planet. Sci., 8, 371-406, 1980.

Hawkesworth, C.J., Isotope characteristics of magmas erupted along destructive plate margins. In: Andesites (Ed. R.S. Thorpe), John Wiley & Sons, New York, 549-571, 1982.

Hegner, E. and M. Tatsumoto, Pb, Sr and Nd isotopes in basalts and sulfides from the Juan de Fuca Ridge, J. Geophys. Res., 92, B11, 11380-11386, 1987.

Helz, R.T., Phase relations of basalts in their melting ranges at PH2O= 5 kb, II, Melt compositions, J. Petrol., 17, 139-193, 1976.

Hildreth, W. and S. Moorbath, Crustal contributions to arc magmatism in the Andes of Central Chile, Contrib. Mineral. Petrol., 98, 455-489, 1988.

Holloway, J.R. and C.W. Burnham, Melting relations of basalt with equilibrium water pressure less than total pressure, J. Petrol., 13, 1-30, 1972.

Johnson, C.M., The Questa magmatic system: petrologic, chemical, and isotopic variations in cogenetic volcanic and plutonic rocks of the Latir volcanic field and associated intrusives, Northern New Mexico, Ph.D. Dissertation, Stanford University, 1986, 322pp.

Kistler, R.W. and Z.E. Peterman, Variations in Sr, Rb, K, Na and initial $^{87}Sr/^{86}Sr$ in Mesozoic granitic rocks and intruded wall rocks in central California, Geol. Soc. Am. Bull., 84, 3489-3512, 1973.

Langmuir, C.H., J.F. Bender, A.E. Bence, and G.N. Hanson, Petrogenesis of basalts from the FAMOUS area: Mid-Atlantic Ridge, Earth Planet. Sci. Lett., 36, 133-156, 1977.

Lipman, P.W., H.J. Prostka and R.L. Christiansen, Cenozoic volcanism and plate tectonic evolution of western United States, part 1, Early and middle Cenozoic, Phil. Trans. Roy. Soc. London, Ser. A271, 249-284, 1972.

Luhr, J.F. and I.S.E. Carmichael, The Colima volcanic complex, Mexico, I. Post-caldera andesites from Volcan Colima, Contrib. Mineral. Petrol., 71, 343-372, 1980.

Mertzman, S.A., The petrology and geochemistry of Medicine Lake Volcano, Contrib. Mineral. Petrol., 62, 221-247, 1977.

Mahood, G.A. and E.W. Hildreth, Large partition coefficients for trace elements in high silica rhyolites, Geochim. Cosmochim. Acta, 47, 11-30, 1983.

Reid, F.W. and J.W. Cole, Origin of dacites of the Taupo volcanic zone, New Zealand, J. Volcanol. Geotherm. Res., 18, 191-214, 1983.

Smith, A.L. and I.S.E. Carmichael, Quaternary lavas from the southern Cascades, western U.S.A., Contrib. Mineral. Petrol., 19, 212-238.

Smith, D.R. and W.P. Leeman, Petrogenesis of Mount St. Helens dacitic magmas, J. Geophys. Res., 92, B10, 10313-10334, 1987.

Staudigel, H., A. Zindler, S.R. Hart, T. Leslie, C.-Y. Chen, and D. Clague, The isotope systematics of a juvenile intraplate volcano: Pb, Nd, and Sr isotope ratios of basalts from Loihi Seamount, Hawaii, Earth Planet. Sci. Lett., 69, 13-29, 1984.

Wyllie, P.J., Sources of granitoid magmas at convergent plate boundaries, Phys. Earth Planet. Inter., 35, 12-18, 1984.

Zindler, A. and S.R. Hart, Chemical Geodynamics, Ann. Rev. Earth Planet. Sci., 1986.

TABLE 1: Major- and Trace- Element and Isotope Geochemical Data for Rocks of the Lassen Volcanic Center

Sample	LM80-824	LM80-854	LC80-178	LC80-436B	LC85-695	LM80-884	LC84-600	LC80-527	LC80-449
ID	BV1	BV1	BV1	BV1	BV1	BV1	BV1	BV2	BV2
SiO2	60.22	60.10	60.34	55.28	60.09	56.64	67.98	61.32	61.56
Al2O3	17.24	18.05	16.60	15.82	16.72	17.14	15.96	17.52	17.03
Fe2O3	1.24	1.07	1.30	1.50	1.24	1.50	0.69	1.07	1.10
FeO	4.49	3.86	4.70	5.40	4.49	5.41	2.48	3.87	3.98
FeO*	5.61	4.82	5.87	6.76	5.61	6.76	3.10	4.84	4.98
MgO	3.62	4.01	3.57	7.99	3.93	4.34	1.01	3.43	3.49
CaO	6.24	7.27	6.02	9.23	6.77	7.85	3.24	6.39	6.06
Na2O	3.72	3.60	4.06	2.96	3.68	3.98	4.49	3.95	3.80
K2O	2.06	1.15	2.02	0.84	1.89	1.55	3.00	1.52	1.93
TiO2	0.80	0.62	0.96	0.66	0.79	1.07	0.79	0.63	0.73
P2O5	0.21	0.16	0.29	0.16	0.26	0.37	0.27	0.17	0.19
MnO	0.10	0.08	0.10	0.12	0.10	0.11	0.05	0.08	0.08
LOI	0.14	0.26	0.68	0.06	0.92	0.25	0.71	0.25	0.36
FeO*/MgO	1.55	1.20	1.64	0.84	1.42	1.55	3.07	1.41	1.42
Mg#	58.9	64.9	57.5	72.4	60.9	58.8	41.9	61.2	61.0
Rb	51	23	48	16	47	37	81	34	49
Sr	459	799	416	653	526	603	341	754	559
Ba	666	289	622	272	625	641	886	449	576
Y	21	15	25	19	21	23	31	19	22
Zr	175	121	189	99	167	172	221	150	180
Nb	6	2	9	2	6	8	9	6	8
Co	19.6	19.1	17	ND	ND	22.9	4.38	16.7	17.1
Cr	54.9	58	69.6	ND	ND	69.9	3.2	38.4	65
Cs	1.5	0.3	1.1	ND	ND	1	2.17	0.6	1.3
Hf	4.1	2.4	3.3	ND	ND	4	5.75	3.3	4.1
Sb	0.3	0.3	0.6	ND	ND	0.3	0.57	0.2	0.4
Ta	0.65	0.26	0.52	ND	ND	0.64	0.94	0.45	0.57
Th	6	2.1	4.7	ND	ND	4.9	10.9	4.1	6
U	1.9	0.8	1.6	ND	ND	2	3.58	ND	1.9
Zn	64	53	59	ND	ND	78	66.8	64	61
Sc	15.8	15.6	14.9	ND	ND	22.4	11.1	13.3	14.3
La	22	11	19	ND	ND	27	34.4	17	21
Ce	40	21	37	ND	ND	51	58.8	33	40
Nd	21	7	17	ND	ND	26	29.6	16	19
Sm	4.4	2.7	3.7	ND	ND	5.7	6.67	2.8	4.2
Eu	1	0.8	1.11	ND	ND	1.43	1.38	0.87	0.95
Gd	3.6	2.2	4.4	ND	ND	5.2	7	3.2	3.6
Tb	0.55	0.33	0.4	ND	ND	0.64	0.872	0.4	0.54
Tm	ND	0.19	0.27	ND	ND	0.38	0.48	0.26	ND
Yb	2	1.2	1.9	ND	ND	2	3.2	1.5	1.8
Lu	0.32	0.2	0.31	ND	ND	0.3	0.5	0.22	0.28
d18O	7.4	7.0	7.0	6.5	ND	6.7	7.0	6.9	6.7
87Sr/86Sr	0.70418	0.70370	0.70415	0.70325	0.70423	0.70404	0.70416	0.70347	0.70363
206Pb/204Pb	18.954	18.874	18.948	18.868	ND	18.900	18.982	18.873	18.923
207Pb/204Pb	15.626	15.595	15.624	15.592	ND	15.603	15.627	15.598	15.604
208Pb/204Pb	38.657	38.498	38.635	38.469	ND	38.539	38.683	38.505	38.560
143Nd/144Nd	0.512769	0.512841	0.512852	0.512891	ND	0.512848	0.512793	0.512855	0.512853

TABLE 1: continued

Sample	LC82-194	LC81-659	LC84-446	LM80-899	LC81-706	LC84-530	LC84-541	LC83-360	LC84-542A
ID	BV2	3RC	3RC	3RC	3BP	3BP	3BP	3LO	3LO
SiO2	62.96	73.49	73.47	69.42	67.31	63.67	64.21	70.82	68.26
Al2O3	16.80	13.91	13.99	15.78	16.40	17.33	16.93	15.42	15.89
Fe2O3	1.06	0.43	0.44	0.58	0.72	0.90	0.92	0.48	0.66
FeO	3.81	1.56	1.59	2.10	2.60	3.26	3.31	1.75	2.40
FeO*	4.77	1.95	1.99	2.63	3.25	4.07	4.14	2.19	3.00
MgO	2.80	0.87	0.88	1.11	1.66	2.56	2.34	1.00	1.67
CaO	5.41	1.96	2.03	2.88	3.78	5.62	5.15	2.69	3.67
Na2O	3.85	3.98	3.64	4.46	4.37	4.03	4.17	4.43	4.15
K2O	2.24	3.35	3.43	3.03	2.52	1.81	2.10	2.86	2.61
TiO2	0.72	0.28	0.35	0.45	0.44	0.53	0.56	0.33	0.44
P2O5	0.21	0.08	0.10	0.10	0.12	0.17	0.18	0.12	0.14
MnO	0.08	0.05	0.05	0.05	0.06	0.07	0.09	0.05	0.06
LOI	0.66	0.51	2.76	0.66	0.20	0.09	0.34	0.54	1.84
FeO*/MgO	1.70	2.22	2.26	2.36	1.95	1.59	1.76	2.18	1.80
Mg#	56.6	50.0	49.5	48.5	53.2	58.3	55.7	50.5	55.3
Rb	62	88	77	79	67	41	50	76	67
Sr	416	220	218	340	371	704	453	327	457
Ba	715	849	844	888	729	601	672	813	763
Y	21	15	14	20	14	18	17	15	19
Zr	171	135	132	199	139	146	157	139	157
Nb	7	8	6	11	6	5	4	8	9
Co	15.1	ND	3.93	5.1	9.1	13.1	12.9	5.01	8
Cr	45.6	ND	4.5	5.76	9.6	19.8	21	4.8	10.8
Cs	1.8	ND	4.33	4.35	2.6	0.97	0.93	4.09	3.95
Hf	4.1	ND	3.7	4.78	3.6	3.41	4	4.03	4.29
Sb	0.5	ND	0.72	0.721	0.4	0.23	0.37	0.84	0.73
Ta	0.66	ND	0.84	0.801	0.63	0.457	0.61	0.87	0.73
Th	7.6	ND	11.5	10	8.9	7.41	7.3	11.2	9.1
U	2.4	ND	3.86	3.93	2.9	2.22	2.43	3.43	2.87
Zn	56	ND	34	0	52	54.6	59	40.3	46.6
Sc	14	ND	4.6	5.95	8.11	11.5	11.7	5.19	7.49
La	23	ND	23.5	22.9	21	21.5	22.8	24	22.7
Ce	42	ND	37.2	42.4	38	37.6	39.2	40.5	41.2
Nd	20	ND	13.6	17.9	13	18.8	19	15	17.6
Sm	4.2	ND	2.53	3.44	2.3	3.89	3.72	2.77	3.36
Eu	0.95	ND	0.45	0.782	0.68	0.95	0.87	0.641	0.75
Gd	3.1	ND	0.99	2.48	3	3.7	3.8	3.4	3.4
Tb	0.61	ND	0.237	0.454	0.38	0.386	0.45	0.31	0.411
Tm	ND	ND	0.14	0	0.22	0.19	0.28	0	0.25
Yb	1.8	ND	1.27	1.91	1.4	1.48	1.82	1.4	1.6
Lu	0.29	ND	0.214	0.288	0.21	0.232	0.282	0.235	0.26
d18O	7.3	7.4	7.3	6.9	7.1	7.1	7.2	6.9	7.8
87Sr/86Sr	0.70420	0.70402	0.70409	0.70402	0.70396	0.70383	0.70412	0.70390	0.70373
206Pb/204Pb	18.595	18.946	18.957	18.947	18.977	18.933	18.943	18.951	18.952
207Pb/204Pb	15.611	15.604	15.622	15.604	15.624	15.616	15.606	15.612	15.616
208Pb/204Pb	38.621	38.591	38.645	38.591	38.668	38.595	38.589	38.616	38.618
143Nd/144Nd	0.512802	0.512819	0.512804	0.512805	0.512808	0.512850	0.512808	0.512821	0.512825

TABLE 1: continued

Sample	LC84-454	LC81-731	LC84-589	LC84-420	LC84-428	LC84-435	LC84-443	LC81-849	LC84-542C
ID	3LO	3LO	3LO	3LO	3LO	3LO	3LO	3TL	3TL
SiO2	69.97	70.23	65.85	69.95	69.61	67.78	69.81	57.47	61.04
Al2O3	15.47	15.56	16.41	15.41	15.52	15.81	15.60	17.07	18.38
Fe2O3	0.54	0.54	0.83	0.56	0.58	0.74	0.56	1.41	1.03
FeO	1.94	1.94	2.99	2.05	2.11	2.56	2.02	5.07	3.71
FeO*	2.43	2.43	3.74	2.56	2.64	3.33	2.53	6.34	4.64
MgO	1.35	1.20	2.43	1.22	1.28	1.77	1.19	5.12	3.43
CaO	3.12	2.91	4.65	3.29	3.37	4.07	3.31	8.16	6.70
Na2O	4.23	4.32	3.95	4.28	4.32	4.00	4.29	3.38	3.82
K2O	2.82	2.74	2.21	2.64	2.61	2.51	2.64	1.20	1.07
TiO2	0.35	0.35	0.44	0.35	0.34	0.42	0.35	0.82	0.53
P2O5	0.11	0.11	0.12	0.12	0.13	0.12	0.12	0.15	0.15
MnO	0.05	0.05	0.07	0.07	0.06	0.07	0.06	0.11	0.09
LOI	1.53	1.59	0.41	1.09	0.51	0.18	0.76	0.44	1.06
FeO*/MgO	1.80	2.01	1.54	2.09	2.05	1.88	2.12	1.23	1.35
Mg#	55.3	52.5	59.1	51.5	52.0	54.2	51.2	64.2	62.2
Rb	77	69	57	71	73	63	71	32	27
Sr	335	326	406	327	335	370	331	376	955
Ba	744	810	624	795	793	721	804	407	352
Y	14	14	14	13	15	14	13	18	14
Zr	134	141	118	138	132	121	137	114	122
Nb	8	6	6	6	8	8	8	2	4
Co	7	5.4	12.5	6.22	6.83	9.6	6.32	24.3	16.6
Cr	19.7	8.8	26.7	19.9	13.5	14.1	11	117	18
Cs	3.99	3.9	2.01	3.63	3.76	2.97	3.79	1.3	0.95
Hf	3.5	3.2	3.05	3.52	3.77	3.61	3.43	2.6	2.5
Sb	0.68	0.8	0.59	0.84	0.73	0.57	0.68	0.3	0.25
Ta	0.74	0.88	0.645	0.82	0.856	0.79	0.82	0.39	0.276
Th	10.9	10.8	8.41	10.1	10.5	10.1	10.3	4	2.66
U	3.49	3.4	2.59	3.21	3.32	3.18	3.37	0.7	0.9
Zn	41	43	49.5	39	42.9	48.6	38	64	61.2
Sc	5.95	5.12	11.9	6.24	7.48	10.1	6.4	23.3	12.5
La	23	21	18.1	23.1	24.1	22.1	23.6	13	12.6
Ce	36.3	39	31.2	36.4	39.3	35.6	37.4	24	25.3
Nd	12.5	15	10.3	11.4	13.9	13.1	13.5	121	13.3
Sm	2.67	2.2	2.51	2.65	2.88	2.81	2.74	3.18	2.8
Eu	0.569	0.63	0.638	0.601	0.65	0.63	0.64	0.88	0.856
Gd	1.59	2.4	2.48	2.1	2.56	2.7	2.12	3.5	1.7
Tb	0.277	0.27	0.297	0.281	0.347	0.321	0.293	0.46	0.347
Tm	0.127	0.25	0.12	0.146	0.194	0.17	0.103	ND	0.19
Yb	1.12	1.2	1.08	1.24	1.34	1.56	1.24	2	1.17
Lu	0.185	0.2	0.208	0.193	0.213	0.225	0.195	0.32	0.2
d18O	7.6	6.7	ND	4.7	7.9	7.1	7.4	ND	8.4
87Sr/86Sr	0.70411	0.70405	0.70376	0.70416	0.70408	0.70400	0.70410	0.70415	0.70318
206Pb/204Pb	18.970	18.958	18.976	18.941	18.964	18.940	18.949	18.941	18.822
207Pb/204Pb	15.626	15.620	15.613	15.604	15.627	15.604	15.605	15.615	15.574
208Pb/204Pb	38.661	38.638	38.610	38.576	38.670	38.585	38.587	38.622	38.382
143Nd/144Nd	0.512836	0.512779	0.512826	0.512776	0.512794	0.512803	0.512833	ND	0.512902

TABLE 1: continued

Sample	LC83-399	LC81-846	LC86-955A	LC81-707	LC84-634	LC85-715	LC81-844	LC83-362	LC84-540
ID	3TL	3TL	3TL	3BPQB	3LOQB	3LOQB	3LOQB	3LOQB	3LOQB
SiO2	54.85	60.52	66.64	57.67	61.39	53.61	56.20	55.59	60.30
Al2O3	15.83	17.83	16.03	19.49	17.77	18.91	18.66	19.34	17.35
Fe2O3	1.49	1.10	0.77	1.17	1.15	1.70	1.50	1.31	1.14
FeO	5.36	3.98	2.76	4.22	4.17	6.13	5.43	4.72	4.12
FeO*	6.70	4.98	3.45	5.28	5.21	7.67	6.79	5.91	5.15
MgO	8.63	3.64	2.17	3.97	1.90	5.08	4.31	4.37	4.54
CaO	8.73	6.29	4.35	7.92	4.50	10.16	8.79	8.80	6.46
Na2O	3.02	4.06	4.25	3.76	4.93	2.71	3.18	3.56	3.72
K2O	1.11	1.68	2.39	0.99	2.65	0.77	0.97	1.18	1.47
TiO2	0.67	0.62	0.46	0.57	0.90	0.69	0.68	0.80	0.58
P2O5	0.14	0.15	0.13	0.10	0.47	0.08	0.12	0.19	0.17
MnO	0.12	0.09	0.06	0.09	0.12	0.14	0.11	0.09	0.10
LOI	0.08	0.06	0.57	0.04	0.19	0.15	0.10	0.83	0.79
FeO*/MgO	0.77	1.36	1.59	1.32	2.73	1.51	1.57	1.35	1.13
Mg#	74.1	61.9	58.3	62.6	44.9	59.6	58.6	62.2	66.2
Rb	68	47	73	14	57	12	58	34	32
Sr	364	484	348	571	466	585	423	1200	565
Ba	806	489	717	323	868	172	640	236	480
Y	17	15	16	16	25	15	17	15	17
Zr	163	113	133	84	229	68	127	129	137
Nb	8	5	9	2	22	3	6	1	5
Co	35.9	17.9	ND	20.5	9.4	ND	22.6	23.3	22.1
Cr	514	59.1	ND	41.8	2.3	ND	28.4	33.8	152
Cs	1.52	2	ND	0.6	1.61	ND	0.6	0.8	1.34
Hf	2.11	2.4	ND	2	5.6	ND	1.7	2.64	3.34
Sb	ND	0.4	ND	ND	0.3	ND	ND	ND	0.25
Ta	0.377	0.37	ND	0.24	1.69	ND	0.23	0.26	0.407
Th	2.94	5.4	ND	3.9	5.8	ND	1.4	1.76	3.81
U	1.19	1.5	ND	1	1.62	ND	0.5	0.55	1.18
Zn	69.4	59	ND	72	74	ND	72	78.6	63.7
Sc	26.4	14.3	ND	19.2	9.5	ND	25.2	21.3	15.7
La	9.95	14	ND	10	36.6	ND	7	15	15.8
Ce	20.5	27	ND	18	65.6	ND	15	31.5	29.2
Nd	11.8	12	ND	10	26.6	ND	12	20	14.1
Sm	2.72	2.7	ND	2.2	5.62	ND	2.4	3.36	3.42
Eu	0.74	0.79	ND	0.69	1.42	ND	0.78	1.06	0.88
Gd	2.7	2.8	ND	2.3	4.8	ND	0.7	ND	2.9
Tb	0.395	0.34	ND	0.27	0.669	ND	0.28	0.39	0.44
Tm	0.224	0.21	ND	0.17	0.292	ND	0.15	0.17	0.21
Yb	1.61	1.3	ND	1.2	2.79	ND	1.4	1.4	1.63
Lu	0.253	0.2	ND	0.18	0.397	ND	0.21	0.2	0.249
d18O	6.5	ND	ND	6.6	6.7	6.8	7.0	6.9	ND
87Sr/86Sr	0.70406	0.70422	0.70411	0.70396	0.70411	0.70372	0.70354	0.70293	0.70376
206Pb/204Pb	18.973	18.943	18.958	18.938	18.940	18.886	18.877	18.814	18.914
207Pb/204Pb	15.627	15.609	15.612	15.606	15.603	15.597	15.594	15.580	15.609
208Pb/204Pb	38.644	38.610	38.630	38.620	38.578	38.522	38.483	38.389	38.570
143Nd/144Nd	0.512819	0.512780	0.512796	0.512776	0.512830	0.512828	0.512848	0.512988	0.512815

TABLE 1: continued

Sample	LC81-843	LC85-788	LC87-1060	LC87-1229	LC87-1242
ID	3TLQB	INC	INC	INC	INC
SiO2	59.15	46.26	ND	48.13	ND
Al2O3	18.14	17.75	ND	18.53	ND
Fe2O3	1.18	2.67	ND	2.90	ND
FeO	4.25	9.62	ND	10.44	ND
FeO*	5.32	12.02	ND	13.05	ND
MgO	4.16	4.93	ND	5.33	ND
CaO	6.81	16.35	ND	9.60	ND
Na2O	3.91	1.25	ND	3.58	ND
K2O	1.49	0.20	ND	0.33	ND
TiO2	0.63	0.72	ND	0.81	ND
P2O5	0.14	0.11	ND	0.05	ND
MnO	0.09	0.15	ND	0.30	ND
LOI	0.01	0.06	ND	0.03	ND
FeO*/MgO	1.27	2.44	ND	2.45	ND
Mg#	63.5	47.7	ND	47.6	ND
Rb	40	ND	ND	3	7
Sr	539	ND	ND	212	623
Ba	448	ND	ND	100	133
Y	15	ND	ND	16	14
Zr	107	ND	ND	29	57
Nb	4	ND	ND	2	4
Co	21.8	ND	ND	ND	ND
Cr	73.6	ND	ND	ND	ND
Cs	1.9	ND	ND	ND	ND
Hf	2.3	ND	ND	ND	ND
Sb	0.4	ND	ND	ND	ND
Ta	0.32	ND	ND	ND	ND
Th	4.9	ND	ND	ND	ND
U	1.4	ND	ND	ND	ND
Zn	65	ND	ND	ND	ND
Sc	16.3	ND	ND	ND	ND
La	13	ND	ND	ND	ND
Ce	25	ND	ND	ND	ND
Nd	12	ND	ND	ND	ND
Sm	2.6	ND	ND	ND	ND
Eu	0.78	ND	ND	ND	ND
Gd	2.8	ND	ND	ND	ND
Tb	0.29	ND	ND	ND	ND
Tm	0.15	ND	ND	ND	ND
Yb	1.3	ND	ND	ND	ND
Lu	0.18	ND	ND	ND	ND
d18O	7.2	5.4	ND	ND	ND
87Sr/86Sr	0.70421	0.70566	0.70528	0.70601	0.70417
206Pb/204Pb	18.975	18.998	18.851	19.049	ND
207Pb/204Pb	15.629	15.642	15.611	15.648	ND
208Pb/204Pb	38.685	38.705	38.533	38.766	ND
143Nd/144Nd	0.512760	0.512694	0.512743	0.512898	ND

Explanation

BV1 = Brokeoff volcano, Stage I
BV2 = Brokeoff volcano, Stage I
3RC = Lassen volcanic center, Stage III, Rockland sequence
3BP = Lassen volcanic center, Stage III, Bumpass sequence
3LO = Lassen volcanic center, Stage III, Loomis sequence
3TL = Lassen volcanic center, Stage III, Twin Lakes sequence
QB (suffix) = mafic inclusion
INC = crustal inclusion in 3LO

Major element analyses recalculated to 100% anhydrous
Fe_2O_3= 0.2 total Fe as Fe_2O_3
All analyses by Analytical Labs, U.S. Geological Survey
Analysts: major elements: A.J. Bartel, J. Baker, R.V. Mendes, D. Siems, K. Stewart, J. Taggert, and J.S. Wahlberg; trace elements: P.E. Bruggman, L.J. Schwarz, and G.A. Wandless.

Discharge rates of thermal fluids in the Cascade Range of Oregon and Washington and their relationship to the geologic environment

Mariner, R.H., Presser, T.S., Evans, W.C., and Pringle, M.K.W.
U.S. Geological Survey, Menlo Park, California 94025

ABSTRACT

Fluid and heat discharge rates of the thermal springs of the Cascade Range in Oregon and Washington have been determined using the chloride inventory method of Ellis and Wilson (1955). Streams without thermal or mineral springs in their drainage basins were also sampled in hopes of detecting chemical anomalies which might be associated with previously unknown thermal or mineral waters. Discharge rates of thermal spring groups in the Cascade Range of Oregon and Washington range from 1 to 120 L/s. Individual springs with larger flow rates have hotter discharge temperatures, indication that conductive cooling of the thermal water is more important than dilution in determining spring temperatures. The thermal springs of the Cascade Range in Oregon and Washington discharge fluid at a total rate of about 330 L/s and heat at a rate of about 7.8 x 10^4kJ/s. Most of this fluid and heat is discharged from two hot spring groups in northern Oregon.

Only three chemical anomalies not obviously associated with known thermal or mineral springs were identified. A major anomaly occurs southeast of Crater Lake where large discharge cold springs scattered over an area of 130 square kilometers discharge about 58,000 mg/sec more chloride than is typical for volcanic terrains of this part of the Cascades. However, it is not clear that this is a thermal anomaly, nor is it clearly associated with either Mt. Mazama (Crater Lake) or Klamath Falls. A small anomaly (2900 mg-Cl/s) occurs on the south-southeast side of Mt. Baker. Sodium and chloride levels are also high and variable in the streams on and around Mt. Rainier. The general paucity of chloride in the streams and rivers of the Cascade Range which do not contain thermal springs seems to indicate that few undetected high-chloride thermal waters occur at shallow depths.

Introduction

Fluid discharge rates of major thermal areas, world-wide, range from ten to several thousand liters per second. The total thermal water discharge from the Yellowstone Caldera was estimated estimated from chloride flux measurements to be 3200 L/s (Fournier and others, 1976). Pre-exploitation discharge at Wairakei, New Zealand was about 420 L/s (Ellis and Wilson, 1955). The Morgan-Growler Hot Spring area, associated with Lassen Peak at the southern end of the Cascade Range, discharges about 20 L/s (Sorey, 1986). Thermal springs on Meagher Mtn. near the northern end of the Range in British Columbia discharge about 40 L/s (Southier, 1976). Prior to this study, the amount of water discharging from thermal systems in the Cascade Range (Figure 1) was poorly known. Values for some individual springs were available in the literature (Waring,1965; Campbell and others,

1974; and Bowen and others, 1978), but these are generally visual estimates, not measured values.

Discharge measurements for individual thermal springs can establish minimum discharge rates. However, most thermal springs in the Cascade Range discharge from multiple orifices, often on both sides of major streams. Discharge directly into the streams is possible at virtually all thermal spring sites. Leakage from unrecognized geothermal systems should also show up in the streams of the area because most thermal and mineral springs are chloride-rich relative to local streams. This situation is ideal for determining discharge rates of thermal and mineral spring systems using the chloride inventory method of Ellis and Wilson (1955). In this method discharge rates of thermal and mineral springs are determined by sampling the adjacent stream above and below the obvious discharge of thermal or mineral water. The discharge rate of the spring is then calculated from the chloride concentration upstream and downstream from the spring, the chloride concentration of the spring water, and the discharge rate of the stream. A derivation of the equation used to determine the discharge rate of the hot springs was given in Fournier and others (1976). Their derivation, based on mass balance equations is reproduced below:

In the following equations, abbreviations are used for river(r), background(bgd), and spring(spr).

$$(Cl_r)(Flow_r) = (Cl_{bgd})(Flow_{nonhot\ spr}) + (Cl_{hot\ spr})(Flow_{hot\ spr}) \quad (1)$$

$$Flow_r = Flow_{nonhot\ spr} + Flow_{hot\ spr} \quad (2)$$

Solving eq. 2 for $Flow_{nonhot\ spr}$ and substituting into eq. 1,

$$(Cl_r)(Flow_r) = (Cl_{bgd})(Flow_r - Flow_{hot\ spr}) + (Cl_{hot\ spr})(Flow_{hot\ spr}) \quad (3)$$

Rearranging and solving for $Flow_{hot\ spr}$

$$Flow_{hot\ spr} = Flow_r(Cl_r - Cl_{bgd})/(Cl_{hot\ spr} - Cl_{bgd}) \quad (4)$$

Application of equation 4 to groups of thermal or mineral springs is straightforward. However, when streams drain more than one rock type and no thermal or mineral springs are known, there can be uncertainty as to what background chloride concentration to use.

The rate of convective heat discharge was calculated from the discharge rate of the spring group, the enthalpy of the spring water, and a reference temperature of 15°C. (eq. 5):

$$Heat_{convective} = Flow_{hot\ spr}\ (Enthalpy_{hot\ water} - Enthalpy_{15^0C}) \quad (5)$$

Units for heat are kJ/s when flow is in kg/s and enthalpy is in kJ/kg. Discharge rates of springs determined from eq. 4 are in L/s; these values were assumed to equal kg/s for use in eq. 5. This assumption creates an error of 3% or less in the calculated convective heat discharge. A reference temperature for water of 15°C was used so that the convective heat

discharge could be compared to the previous estimates of the high-temperature geothermal resource in this part of the Cascade Range (Brook and others, 1978).

Other conservative constituents that are abundant in the thermal water but of low concentration in the surface water can be substituted for chloride in equation 4. Sodium is not as good as chloride because low-temperature reactions can release some sodium from the rock. However, sodium was used to obtain an independent check on the discharge rates calculated from the chloride concentrations. Sodium and chloride produce similar results in environments such as the Cascade Range because the streams are very low in both chloride and sodium relative to the hot springs. Upstream sample sites were generally within one kilometer of the thermal spring sites, while downstream sample sites were generally several kilometers from the spring. Generally, the discharge rate of the stream was measured downstream from the thermal or mineral spring sites. Some sites were gaged by standard wading techniques using the method described in Carter and Davidian (1968), but many had permanent USGS gaging installations. Where possible, additional samples were collected further downstream (15 to 30 kilometers) to detect discharge of saline fluids away from the obvious spring sites. Streams without thermal or mineral springs were also sampled to detect any previously unidentified discharges of thermal or mineral water. However, a large chloride influx does not necessarily indicate a large geothermal system; it could be associated with a high rate of flow through a shallow block of Cl-rich rock.

The locations of hot springs, major volcanoes, and volcanic fields of the Cascade Range in California, Oregon, and Washington are plotted on Figure 1. In Washington, the area sampled for chloride and sodium analyses included the Nooksack and Baker rivers and some of their major tributaries around Mt.Baker; the Suiattle and White Chuck rivers near Glacier Peak; the Skykomish River below Garland Mineral Spring; the Cowlitz, Nisqually, Carbon, White, and Bumping rivers around Mt. Rainier; and the Wind River below St. Martin's Hot Spring. In Oregon, sampling was carried out on the Clackamas, Breitenbush, Santiam, McKenzie, Willamette, Umpqua and Rogue rivers west of the Cascade Crest, and on the Metolius, Deschutes, and Williamson rivers east of the Crest. In California, only the springs and lakes on Medicine Lake Volcano were sampled.

Data

Chemical analyses of thermal and mineral waters in the drainage areas sampled are listed in Table 1. Two low-chloride soda springs, one near Bachelor Butte and one near the northwest side of Crater Lake National Park, are included for their unusually high Na/Cl ratios. Most other soda springs in the Cascade Range carry much more chloride and have Na/Cl ratios near 1. Three samples from a hydrothermally altered area east of Broken Top in Oregon are also included. Chloride concentrations, sodium concentrations, and calculated discharge rates for the sample sites, are listed in Table 2.

Results and Discussion

A basic characteristic of the thermal waters of the Cascade Range which makes it possible to use the chloride inventory method to determine discharge rates of thermal waters is the high dissolved chloride concentrations. Most thermal waters of the range contain several hundred to several thousand milligrams of chloride per liter. Rock deposited in a marine environment could be the source of the chloride, as could some volcanic rocks. Ash from the May 18, 1980 erruption of Mt. St. Helens was relatively rich in chloride (660 ppm; Fruchter and others, 1980), and dissolution of ash with similar composition could also produce a chloride-rich water. In natural environments most dissolved constituents can change concentration by precipitation as well as dissolution. Two constituents which readily dissolve but do not precipitate easily are chloride and bromide. Based on the data of Goldberg and other (1971), the Br/Cl ratio of sea water is about 3.5×10^{-3}, while the Br/Cl ratio in the ash from Mt. St. Helens is about 1.5×10^{-3} based on the data of Fruchter and others (1980). A plot of Br versus Cl for the thermal waters of the Cascade Range (figure 2) shows that at lower concentrations (<1500 mg-Cl/L) the thermal waters plot on the sea water trend. However, chloride increases more rapidly than bromide at higher concentrations, and Br/Cl for the more saline waters approaches the value of the ash. Perhaps thermal water initially dissolves chloride and bromide from the intergranular spaces in a rock deposited in a marine environment, but as water-rock reaction proceeds, more chloride and bromide are released by rock dissolution until the Br/Cl ratio of the water approaches that of the rock. However, organic material preferentially absorbs bromide (Vinogradov, 1939) so it is also possible that bromide and chloride concentrations are a function of the amount of water-rock reaction plus the amount of organic material which has decomposed. in this case no marine component is required. Gas concentrations in these waters (Mariner and others, manuscript in preparation) indicate that organic material is decomposing at depth.

Sodium and chloride concentrations of stream waters are a function of the amount of sodium and chloride in the local precipitation (wet and dry), the amount released to shallow groundwater by normal weathering of the rock, and the amount from thermal and mineral waters. Sodium and chloride concentrations and Na/Cl ratios of typical local groundwater which do not have a thermal or mineral water component are important in detecting anomalous areas and determining how much chloride and sodium is from fresh water and how much from saline water. In the Washington part of the range, we have a relatively small data set so sodium and chloride concentrations from the upper parts of the streams on the respective volcanoes are used to establish "background" concentrations. Samples collected in areas without known thermal or mineral springs were initially analyzed for sodium because the sodium analytical proceedure is quick and accurate. Samples were analyzed for chloride only when sodium concentrations exceeded about 3 mg/L. This cutoff was used because samples from the Cascade Range in Oregon had background chloride concentrations when sodium concentrations were 3 mg/L or less. In retrospect, a lower cutoff might have been useful in northern Washington where background Na/Cl ratios are lower than in Oregon. In the High Cascades of Oregon, a large data set is available (Ingebritsen and others, 1988) and although sodium and chloride concentrations are variable,

Na/Cl weight ratios are generaly near 5.5 where the waters have no thermal or saline water component (Fig. 3). Streams in the region between Mt. Rainier and Mt. Hood were not sampled because this area received most of the ash from the recent eruption of Mt. St. Helens. The ash contained appreciable chloride (Sarna-Wojcicki and others, 1981) and chloride is readily leached from the ash (Dethier and others, 1981). Individual areas are discussed below in the order they are listed in the tables.

Concentrations of sodium in the streams draining Mt. Baker are generally between 1 and 2 mg/L (Table 1). Exceptions include Baker Creek, below Baker Hot Spring (136 mg/L), Boulder Creek (3.8 mg/L), and Sulphur Creek (17 mg/L). Boulder Creek drains the summit crater of Mt. Baker; changes in the chemical composition of Boulder Creek associated with increased fumarolic activity in the crater during the 1970's are well documented (Bartleson and others, 1977). The water from Boulder Creek is low in chloride so it does not have a saline water component. However, Sulphur Creek, on the south side of Mt. Baker, carries considerable chloride (6.2 mg/L) and sodium (17 mg/L). This anomaly could be associated with a fluid of deep origin. If the fluid is chemically similar to Baker Hot Spring water then 27 L/s of fluid would be entering Sulphur Creek. Warm Spring Creek on the west side of Mt. Baker had no sodium anomaly; the sample from the creek was not analyzed for chloride because of the low sodium concentration.

Discharges from Kennedy and Gamma hot springs on Glacier Peak are not discernible in the White Chuck and Suiattle rivers. Direct discharge measurements of Kennedy Hot Springs indicate a discharge rate of about 0.35 L/s. Chloride and sodium load determinations on Gamma Creek indicate that 2.4 L/s of thermal water is being discharged from Gamma Hot Springs. Discharge from Sulphur Hot Spring, a dilute thermal water at the north-northwest side of Gamma Peak, was not detected in Sulphur Creek.

Sodium and chloride concentrations are variable in the streams draining Mt. Rainier, and no consistant "background" sodium concentration, chloride concentration, or Na/Cl ratio could be determined. This may indicate that small amounts of thermal fluid escape at various places on the mountain. Frank (1985) reported springs with possible thermal components at high elevations on Mt. Rainier. Alternately, some of the high chloride and sodium concentrations, but low Na/Cl ratios (<5.5) may be due to waters circulating through the Ohanapecosh Formation which crops out over most of the area surrounding the volcano. The Ohanapecosh Formation was deposited, at least in part, in brackish water (Fiske and others, 1963) and may therefore contain more chloride than formations deposited under sub-aerial conditions. Mt. Rainier has Ohanapecosh Hot Springs, as well as Longmire Springs, a soda spring, and several unnamed soda springs near or on the mountain. If the chemical composition of the Ohanapecosh River upstream from Ohanapecosh Hot Springs represents "background" chloride and sodium concentrations, then Ohanapecosh Hot Springs discharge about 14 L/s, Longmire Springs about 12 L/s, and the small soda spring on Summit Creek southeast of Mount Rainier about 2 L/s. Longmire Springs probably discharge less than the 12 L/s attributed to them; mineral water that seeps into the river from other sites in the 8 km reach are included in our sampling. If the chloride and sodium concentrations in the upper part of the Ohanapecosh

River are typical of background chloride and sodium concentrations for the area then the Ohanapecosh-Cowlitz rivers do not show any increase in chloride in the next lower 15 km reach, although the discharge rate increases by a factor of three. A soda spring on the upper part of the Puyallup River near the west side of the Park does not generate any anomaly in the Puyallup River. The West Fork of the White River, which drains the north side of Mt. Rainier, has more chloride and sodium than normal, 3.1 and 8.1 mg/L respectively, but a Na/Cl ratio of 2.6, higher than normal on the south side of Mt. Rainier. Since we cannot establish a baseline value for local "background" concentrations or a "background" Na/Cl ratio at Mt. Rainier, we cannot quantify the anomaly with any confidence. However, if the background Na/Cl ratio is 5.5 (the value determined for the High Cascades in Oregon) then as much as 110 L/s of saline and thermal water may discharge into the streams draining Mt. Rainier.

The Warm Springs River below Kah-Nee-Tah Hot Springs on the Warm Springs Indian Reservation in northern Oregon, carries about 12,700 mg-Cl/sec above background. Of this total, 5500 mg-Cl/sec are added in the section extending from just below Kah-Nee-Tah Hot Springs to the highway bridge 1.4 kilometers upstream. Most of the chloride is discharged in the two kilometer reach upstream from the highway bridge where the hotter springs discharge. The springs at Kah-nee-tah are unusual in that they occur for about three kilometers along the Warm Spring River. Hot springs in the Cascade Range typically occur in small groups encompassing small areas. A total of about 69 L/s of thermal water is entering the stream in the reach containing the hot springs. This is the second largest flow-rate determined for any hot spring system in the Cascade Range.

In the Clackamas River System, the major saline fluid inflow is from Austin Hot Springs where 42,000 mg-Cl/s (120 L/s) is discharged. The Collawash River adds about 3,000 mg-Cl/s above background, while the Oak Grove Fork of the Clackamas adds about 2,000 mg-Cl/s above background. No additional chloride of thermal or mineral origin is added to the Clackamas between the confluence of the Clackamas and Collawash rivers and the gage at Three Lynx 10 kilometers to the north.

About 14,400 mg-Cl/s (12 L/s) is being discharged to the Breitenbush River by Breitenbush Hot Springs. No significant additions occur downstream for at least 65 kilometers. Soda springs at Upper Soda and Cascadia contribute about 1.1 L/s to the South Santiam River.

Almost all samples from the Metolius and Deschutes rivers, east of the Cascade Crest, have Na/Cl ratios near the local background value of 5.5. Thus although some samples contain up to 1.7 mg/L chloride (Table 1), they do not have a saline water component by the definition used here. Two slightly anomalous waters occur in the area. The soda spring which discharges 6.7 km north of Bachelor Butte has a higher Na/Cl ratio (9.3) than typical of cold or soda spring waters. Perhaps carbon dioxide from depth has dissolved in the local groundwater and accelerated the rate at which the water reacted with the rock. The unusually large Na/Cl ratio would then be due to the increased dissolution of plagioclase. The only chloride anomaly detected in the upper Deschutes System is at the headwaters of the Spring River (Table 1). The Spring River emerges as a large

discharge cold spring (1270 L/sec) and carries about 500 mg-Cl/sec more than expected. This small influx of chloride is undectectable in the larger Deschutes River (35,700 L/sec at Benham Falls). No anomalies associated with the geothermal activity at Newberry Volcano occur in the Deschutes River above Bend. Although no high-chloride waters have been identified at Newberry, most high temperature geothermal systems have chloride-rich waters at depth. Sammel (1983) clearly demonstrated the presence of a high-temperature geothermal system at Newberry. Another anomalous site which goes undetected in our stream sampling is the hydrothermally altered area along the upper part of Tumalo Creek about 4 kilometers east-southeast of Broken Top. This area contains several dilute neutral to slightly acid Ca-SO_4 waters (Table 2). These weak springs contain insufficient chloride to create an anomaly.

The McKenzie River has four thermal springs associated with it, Belknap, Bigelow, Foley, and Rider Creek (also known as Terwilliger) hot springs. Total chloride discharge from identified hot springs in this river system is about 40,000 mg-Cl/s. At the Vida gage on the McKenzie River, 24 km downstream from the last hot spring, the chloride-load above background is 60,000 mg-Cl/s. However, the large flow rate (98,000 L/s) and low chloride concentration (1.3 mg/L) combine to make the magnitude of the apparent increase in chloride load uncertain. The error bar on the chloride concentration is large enough that the true thermal chloride load at Vida could be anywhere between 40,000 and 80,000 mg-Cl/sec. This implies either no addition of thermal water below the known hot springs or an amount equal to that discharged by known hot springs.

The Willamette River system has Kitson Hot Springs, McCredie Hot Springs, an unnamed warm spring on Warm Spring Creek, and the mineral water at Oakridge as possible sources of saline fluid. Kitson Hot Springs contributes about 4200 mg-Cl/s to Hills Creek, McCredie Hot Springs contributes about 11,000 mg-Cl/s to Salt Creek, and the unnamed warm spring contributes about 2700 mg-Cl/s to Salmon Creek. Surprisingly, mineral water entering the North Fork of the Willamette at Westfir apparently contributes as much as 17,600 mg-Cl/s to the Willamette system. This equals the amount of chloride discharged by all three thermal springs. However, this anomaly disappears during periods of very low stream discharge. Either the fluid ceases to discharge during the driest part of the year or evaporation is high enough to prevent the saline water from reaching the stream. Thus, the surprisingly large apparent chloride load observed during periods of moderate flow may contain some chloride stored near the mineral "spring" during the dry season. Amounts of fluid associated with various thermal and mineral springs, based on the chloride load of the streams, range from 1.1 L/s at Kitson to perhaps as much as 6.3 L/s for the mineral water of unknown source near Westfir.

The North Fork of the Umpqua River at Eagle Rock carries about 37,500 mg-Cl/sec more than expected. This originates from two sources, Umpqua Hot Springs and Toketee Soda Spring. If the chloride concentration of water from Umpqua Hot Springs is taken as typical, then 10.7 L/s of thermal and mineral (soda) water is discharging into the Umpqua River in the 20 km reach starting just above Umpqua Hot Springs. Other chloride inflow to the upper part of the Umpqua River is trivial.

The Rogue River on the west side of Crater Lake National Park carries no anomalous chloride. However, a soda spring of unusual composition (Table 2) discharges into a small tributary of the Rogue near the northwest corner of the Park. Chemically, this water is similar to the soda spring north of Mt. Bachelor (Table 2) and somewhat similar to Paulina and East Lake hot springs in Newberry Caldera. Changes in sodium load of Minnehaha Creek in the reach containing the soda spring indicate a discharge rate of about 1 L/sec. The low chloride concentration indicates that the water does not circulate to great depth. The upper part of the Williamson River east of Crater Lake National Park has a normal Na/Cl ratio of about 5.5. A large chloride anomaly occurs in the Wood River where a 35,000 mg-Cl/sec excess exists. Springs in the area between the Wood River and the Williamson River discharge about 58,000 mg-Cl/sec more than expected. Although a chloride anomaly of major proportions exists in the area, we cannot state that it is associated with either a thermal or mineral fluid. It could equally well be associated with a block of chloride-rich rock. Isotopic data and an independent set of chemical data for these springs are available in Thompson and others (1987).

Samples from springs and lakes in the Medicine Lake Highlands of northern California had no indication of chloride anomalies, sodium anomalies, or an unusual amount of carbon dioxide.

Discharge rates of the thermal springs, summarized in Table 3, are low in northern Washington, increase to a maximum in northern Oregon, then decrease again to the south. Although discharge rates range from <1 to 120 L/s, two-thirds of the sites have discharge rates between 2 and 20 L/s and only two sites have discharge rates of more than 20 L/s. The observation that high discharge rate corresponds to high discharge temperature indicates that conductive cooling rather than mixing is the dominant process controlling spring temperatures in the Cascade Range. Total thermal fluid discharged from the springs of the range is only about 330 L/s; this fluid carries about 7.8×10^4 kJ/s of heat to the surface. Two spring groups in northern Oregon, Austin and Kah-nee-tah, discharge approximately 60 percent of the water and 75 percent of the heat.

The rates of fluid and heat discharge noted above are small compared with the natural rates of discharge in other parts of the country and other nations of the Circum-Pacific Rim. Thermal springs in the Idaho batholith described in Young (1985) discharge more water (1050 L/s) but less heat (1.2×10^4 kJ/s) from an area 1/2 to 1/3 as large as the part of the Cascade Range in Washington and Oregon. For the Long Valley Caldera, thermal fluid discharging at 250 L/s carries with it 1.2×10^5kJ/s of heat to the surface (Sorey and Lewis, 1976; Sorey and others, 1978). Relative to other parts of the Circum-Pacific Rim, the comparison is even less impressive. Horii (1985) gives the natural discharge of thermal fluid in Japan as about 27,000 L/s. Bolton (1976) lists the natural heat discharge of all thermal systems in New Zealand at 2×10^7kJ/s, about 250 times the natural convective heat discharge of the Cascade Range. Brook and others (1978) estimated that geothermal development could produce about 10^{16} kJ from this part of the Cascade Range for 30 years. White (1970) reported that drilling and development can increase fluid discharge rates by factors of 3 to 5 relative to the natural discharge rates. However, experience in Japan (K. Bada in

Suyama and others, 1975) seems to indicate that geothermal areas can be exploited at 10 to 100 times the natural discharge. If development could increase the discharge rates by a factor of 5 and if the aquifer temperatures are 2.5 times the spring temperatures, about 10^{15} kJ would be available over a 30 year period. However, temperatures at depth probably average less than 2.5 times the spring temperatures and the multiplication factor for the mass flow component are very poorly known.

Relationship of thermal waters to the geologic and tectonic setting

In a general sense, the convective discharge of thermal water in the Cascade Range correlates with both the geology and regional tectonic setting. Guffanti and Weaver (1988) divided the Cascade Range into five segments based on the distribution of volcanic vents formed during the last 5 million years. They correlated these segments with the structural elements of the Juan de Fuca and Gorda plates. Only three of their segments are relevant to our study. Segment 1, the most northerly, contains isolated stratovolcanoes such as Glacier Peak and Mt. Baker, and extends northwest into the Coast Ranges of British Columbia. Segment 2 extends from Mt. Rainier to Mt. Hood and consists of primarily basaltic vents, scattered over a wide east-west zone. The few stratocones in this segment are part of a poorly defined andesitic arc. Segment 3 extends from Mt. Hood to the California-Oregon line and consists of a dense concentration of predominately andesitic vents in a well defined arc.

Thermal springs in segment 1 are few in number, low in discharge rate, and have moderate spring temperatures. Thermal springs in the unclassified area between segments 1 and 2 (a region of granitic batholiths) are very low in discharge rate and low in temperature. Thermal springs in segment 2 discharge about an order of magnitude more water than the springs in segment 1. The thermal springs in segment 3 (Mt. Hood to the California-Oregon line) discharge the most fluid, although the distribution of thermal springs and discharged heat is not uniform throughout the segment. Most of the thermal springs occur in the northern part of the segment in an area extending from slightly north of Mt. Jefferson to about the latitude of Newberry Volcano. This region has a high concentration of vents less than one million years old (Guffanti and Weaver, 1988; Smith and Shaw, 1975). Clusters of young (<100,000 year old) dacitic and rhyolitic vents occur in the Cascade Range at Newberry, Crater Lake, Mt. Shasta, Medicine Lake Volcano, Lassen Peak, and Three Sisters (Guffanti and Weaver, 1988). Curiously, no surfical evidence of large high-temperature geothermal systems exist near Crater Lake, Medicine Lake Volcano, or Mt. Shasta. Thermal springs associated with Newberry, The Three Sisters, and Lassen Peak range from weak to moderately strong.

The discharge of heat by thermal springs in the segments defined by Guffanti and Weaver (1988), shown in Table 4, have a positive correlation with the extrusion rates determined for the segments by Sherrod and Smith (this volume). However, the relationship between heat discharged by the hot springs and extrusion rate for the segments is not well constrained; only three data pairs are available, the extrusion rate for one segment has a fairly broad range (3 to 6 $km^3/km/m.y.$), and the amount of heat actually

discharged in Segment 2 may be larger than shown in the table because of leakage of thermal fluid from the flanks of Mt. Rainier.

Summary

The total discharge rate for the hot springs of the Cascade Range in Oregon and Washington is not large (only about 330 L/s); nor is the total convective heat discharge large (only about 7.8 x 10^4 kJ/s). Roughly 75% of the convective heat discharge in the Cascade Range occurs in the central and northern Oregon Cascades. This area also has the greatest concentration of young volcanic systems (Smith and Shaw, 1975) and a high temperature geothermal system (265°C in Newberry Caldera; Sammel, 1983). Temperatures and convective discharge rates of the thermal springs correlate with the amount and style of volcanism in the Cascade Range during the past 5 million years. Thermal springs with the highest discharge rates and temperatures may derive heat from silicic rock younger than 1 m.y. years old.

Sampling streams in the Cascade Range for chloride and sodium did not detect many chemical anomalies which could be associated with undiscovered thermal systems. Sodium and/or chloride anomalies that may reflect thermal water discharge were detected only at Sulphur Creek on Mt. Baker, the area southeast of Crater Lake, and possibly the streams draining Mt. Rainier and the lower part of the McKenzie River.

References cited

Bartleson, G.C., Wilson, R.T., and Foxworthy, B.L., 1977, Water-quality effects on Baker Lake of recent volcanic activity at Mt. Baker, Washington: U.S. Geological Survey Professional Paper 1022-B, 30 pages, 1 plate.

Bolton, R.S., 1976, Recent developments and future prospects for geothermal energy in New Zealand, in Proceedings of the Second United Nations Symposium on the Development and Use of Geothermal Resources, San Francisco California, 20-29 May, 1975, p.37-42.

Bowen, R.G., Peterson, N.V., and Riccio, J.F., 1978, Low- to intermediate-temperature thermal springs anmd wells in Oregon: Oregon Department of Geology and Mineral Industries Geological Map Series GMS-10, scale 1:1,000,000.

Brook, C.A., Mariner, R.H., Mabey, D.R., Swanson, J.R., Guffanti, Marianne, and Muffler, L.J.P., 1979, Hydrothermal convection systems with reservoir temperatures ≥90°C, in Muffler, L.J.P., ed., Assessment of Geothermal Resources of the United States--1978: U.S. Geological Survey Circular 790, p. 18-85.

Campbell, K.V., Miers, J.H., Nichols, B.M., Oliphant, Jerrelyn, Pytlak, Shirley, Race, R.W., Shaw, G.H., and Gresens, R.L., 1974, A survey of thermal springs in Washington State: Northwest Science, v. 44, p. 1-11.

Carter, R.W., and Davidian, Jacob, 1968, General procedure for gaging streams: U.S. Geological Survey Techniques of Water Resource Investigations, Book 3, Chapter A6, 13p.

Dethier, D.P., Pevear, D.R., and Frank, David, 1981, Alteration of new volcanic deposits, in The 1980 Eruptions of Mount St. Helens, Washington, P.W. Lipman, and D.R. Mullineaux, eds., U.S. Geological Survey Professional Paper 1250, p. 649 - 665.

Ellis, A.J., and Wilson, S.H., 1955, The heat from Wairakei-Taupo thermal region calculated from the chloride output: New Zealand Journal of Science and Technology, sec. B, v.36, p. 622-631.
Fiske, R.S., Hopson, C.A., and Waters, A.C., 1963, Geology of Mount Rainier National Park, Washington: U.S. Geological Survey Professional Paper 444, 93p.
Fournier, R.O., White, D.E., and Truesdell, A.H., 1976, Convective heat flow in Yellowstone National Park, in Proceedings of the Second United Nations Symposium on the Development and Use of Geothermal Resources, May 20-29, 1975, San Francisco, California, p. 731-739.
Frank, D.G., 1985, Hydrothermal processes at Mount Rainier, Washington: Doctoral Dissertation, University of Washington, Seattle, Washington, 214p.
Fruchter, J.S., Robertson, D.E., Evans, J.C., Olsen, K.B., Lepel, E.A., Laul, J.C., Abel, K.H., Sanders, R.W., Jackson, P.O., Wagman, N.S., Perkins, R.W., Van Tuyl, H.H., Beauchamp, R.H., Shade, J.W., Daniel, D.L., Erikson, R.L., Sehmel, G.A., Lee, R.N., Robinson, A.V., Moss, O.R., Briant, J.K., Cannon, W.C., 1980, Mount St. Helens ash from the 18 May 1980 Erruption - Chemical, physical, mineralogical, and biological properties: Science, v. 209, no. 4461, p. 1116-1125.
Guffanti, Marianne, and Weaver, C.S., 1988, Distribution of Late Cenozoic volcanic vents in the Cascade Range: Volcanic arc segmentation and regional tectonic considerations: Journal of Geophysical Research, v. 93, no. B6, p. 6513-6529.
Horii, Shozo, 1985, Direct heat update of Japan, in International Symposium Volume on Geothermal Energy, 1985 Geothermal Resources Council Annual Meeting, August 26-30, 1985, Kailua-Kona, Hawaii, Claudia Stone, ed., p. 113-117.
Ingebritsen, S.E., Mariner, R.H., Cassiday, D.E., Shepherd, L.D., Presser, T.S., Pringle, M.K.W., and White, L.D., 1988, Heat-flow and water-chemistry data from the Cascade Range and adjacent areas in north-central Oregon: U.S. Geological Survey Open-File Report 88-702, 205 p.
Sammel, E.A., and Craig, R.W., 1983, Hydrolgoy of the Newberry Volcano Caldera, Oregon: U.S. Geological Survey Water Resources Investigation Report 83-4091, 52p.
Sammel, E.A., 1983, The shallow hydrothermal system at Newberry Volcano, Oregon: A conceptual model: Transactions of the 1983 Annual Meeting of the Geothermal Resources Council, 24-27 October 1983, Portland, Oregon, v. 7, p. 325 - 330.
Sarna-Wojcicki, A.M., Meyer, C.E., Woodward, M.J., and Lamonte, P.J., 1981, Composition of air-fall ash erupted on May 18, May 25, June 12, July 22, and August 7, in The 1980 eruptions of Mount St. Helens, Washington, P.W. Lipman and D.R. Mullineaux, eds, U.S. Geological Survey Professional Paper 1250, p.667 - 681.
Smith, R.L., and Shaw, H.R., 1975, Igneous-related geothermal systems, in Assessment of Geothermal Resources of the United States - 1975, D.E White, and D.L. Williams, eds., p. 58-83.
Sorey, M.L., 1986, Hot spring monitoring at Lasen Volcanic National Park, California 1983-1985: Proceedings of the Eleventh Morkshop on Geothermal Reservoir Engineering, Stanford University, Stanford, California, January 21-23, 1986, p. 141-147.

Sorey, M.L., Lewis, R.E., and Olmstead, F.H., 1978, The hydrothermal system of Long Valley Caldera, California: U.S. Geological Survey Professional Paper 1044-A, 60p.

Sorey, M.L., and Lewis, R.E., 1976, Convective heat flow from hot springs in the Long Valley caldera, Mono County, California: Journal of Geophysical Research, v. 81, no. 5, p. 785-791.

Southier, J.G., 1976, Geothermal potential of Western Canada, in Proceeding of the Second United Nations Symposium on the Development and Use of Geothermal Resources, May 20-29, 1975, San Francisco, California, USA, p. 259-267.

Suyama, J., Sumi,K., Bada, K., Takashima, I., and Yuhara, K., 1975, Assessment of geothermal resources of Japan: Proceedings United States-Japan Geological Surveys Panel Discussion on the Assessment of Geothermal Resources, Tokyo, Japan, Oct. 27, 1975, Geological Survey of Japan, p. 63-119.

Thompson, J.M., 1985, Chemistry of thermal and nonthermal springs in the vicinity of Lassen Volcanic National Park: Journal of Volcanology and Geothermal Research, v. 25, p. 81-104.

Thompson, J.M, White, L.D., and Nathenson, Manuel, 1987, Chemical analyses of waters from Crater Lake, Oregon, and nearby springs: U.S. Geological Survey Open-File Report 87-587, 22p.

Vinogradov, A.P., 1939, Iodine in marine muds: to the problems of the origin of iodine-bromine waters in petroliferous regions (in Russian): Tr. Biogeokhim Lab. Akad. Nauk SSSR v.5, 19-22 (English pp. 33-46).

Waring, G.A., 1965, Thermal springs of the United States and other Countries of the World - A Summary: U.S. Geological Survey Professional Paper 492, 383 p.

White, D.E., 1970, Geochemistry applied to the discovery, evaluation, and exploitation of geothermal resources, in U.N. Symposium on the Development and Utilization of Geothermal Resources, Pisa, 22 Sept.-1 Oct., 1970, E. Barbier, ed., Special Issue 2, v.1, p. 58-80.

Young, H.W., 1985, Geochemistry and hydrology of thermal springs in the Idaho batholith and adjacent areas, central Idaho: U.S. Geological Survey Water-Resources Investigations Report 86-4172, 44p.

Table 1. Chloride concentrations, sodium concentrations, and discharge rates of streams and hot springs in the Cascade Range, Oregon and Washington

Site	Stream Na (mg/L)	Stream Cl (mg/L)	Measured Discharge (L/s)	Hot Spring Na (mg/L)	Hot Spring Cl (mg/L)	Calculated Discharge (L/s)
Mt. Baker area, Washington						
Baker Cr. below Baker HS 44°45.8′ 121°40.1′	136	85	1.75	170	110	1.4 Baker HS
Swift Cr. 48°44.2′ 121°39.5′	1.1	-	-			
Park Cr. 48°44.0′ 121°39.7′	1.2	-	-			
Sandy Cr. 48°41.1′ 121°42.4′	2.0	-	-			
Boulder Cr. 48°43.0′ 121°41.6′	3.8	.6	2700			
Sulphur Cr.(Komokulsan) 48°39.6′ 121°42.8′	10.1	3.3	837			
Sulphur Cr.(trailhead) 48°42.4′ 121°49.1′	17	6.2	506	170?	110?	27 Baker HS eq.
Milk Cr.(trailhead) 48°42.3′ 121°49.2′	1.6	.4	154			
Nooksak R., S. Fork 48°36.0 121°1.0′	1.1	-	-			
Nooksak R., Mid. Fork 48°46.1′ 122°2.3′	1.7	-	-			
Warm Spring Cr. 48°45.4′ 121°58.5′	1.3	-	-			
Nooksak R., N. Fork 48°54.5′ 121°50.6	1.0	-	-			
Glacier Cr. 48°53.5′ 121°56.4′	1.8	-	-			
Wells Cr. 48°54.2′ 121°48.3′	1.5	-	-			

Table 1. Chloride concentrations, sodium concentrations, and discharge rates of streams and hot springs in the Cascade Range, Oregon and Washington----- continued

Site	Stream Na (mg/L)	Stream Cl (mg/L)	Measured Discharge (L/s)	Hot Spring Na (mg/L)	Hot Spring Cl (mg/L)	Calculated Discharge (L/s)
Glacier Peak area, Washington						
Sulphur Cr. at trail br. 48°15.4′ 121°10.3′	s	-	-			
Sulphur Cr. at Suiattle R. 48°14.8′ 121°11.4′	s	-	6485	100	51	<1 Sulphur HS
Suiattle R. at Wilderness 48°14.1′ 121°10.6′	s	-	14,700			
Gamma Cr. below Gamma HS 48°10.6′ 121°2.1′	48	74	25	510	755	2.5 Gamma HS
White Chuck R. at Sauk R. 48°10.3′ 121°28.1′	s	-	19,100			-
Sauk R. 48°10.1′ 121°28.2′	s	-	-			
Kennedy HS 48°7.1′ 121°11.5′	-	-	1 meas.	670	625	1 Kennedy HS
Garland Cr. ab. Garland Sp 47°53.8′ 121°20.3′	7.0	3.5	-			
Garland Cr. bl. Garland 47°53.2′ 121°21.0′	45.	56.	286	2500	3600	4.3 Garland Sp
Skykomish R. bl. Garland 47°53.7′ 121°24.0′	s	-	8210			
Stevens and Snoqualmie Passes, Washington						
Suprise Cr. nr. Scenic HS 47°42.4′ 121°9.3′	1.0	.4	-			
Scenic Cr. bl. Scenic HS 47°42.5′ 121°9.2′	1.4	.6	39.4	49	22	.3 Scenic HS

Table 1. Chloride concentrations, sodium concentrations, and discharge rates of streams and hot springs in the Cascade Range, Oregon and Washington----- continued

Site	Stream Na (mg/L)	Stream Cl (mg/L)	Measured Discharge (L/s)	Hot Spring Na (mg/L)	Hot Spring Cl (mg/L)	Calculated Discharge (L/s)
Rock Cr. nr. Goldmeyer HS 47°29.4′ 121°26.2′	1.2	.6	-			
Burnt Boot Cr bl Goldmeyer 47°29.2′ 121°23.4′	2.2	1.7	338	125	130	2.8 Goldmeyer
Green River ab. Lester HS 47°12.4′ 121°33.1′	3.7	1.0	-			
Green River bl. Lester HS 47°12.7′ 121°28.4′	4.5	1.8	1470	105	115	11 Lester HS
Mt. Rainier area, Washington						
Greenwater R. at Greenwater 47°8.4′ 121°36.1′	4.9	1.3				
White R. nr. Greenwater 47°8.2′ 121°37.8′	4.5	1.7				
West Fk. White River 47°7.4′ 121°37.3′	8.1	3.1				
Ohanapecosh R. ab. HS 46°44.9′ 121°33.4′	1.9	1.1	-			
Ohanapecosh R, bl. HS 46°42.6′ 121°34.5′	4.5	3.6	5000	920	880	14 Ohanapecosh
Summit Cr. ab. soda spr. 46°42.2′ 121°28.9′	32	25	-			
Summit Cr. at campground 46°42.6′ 121°32.1′	32	22	130	1750	1450	2 Summit Cr. SS
Muddy Fk. nr. Packwood 46°39.9′ 121°36.7′	3.1	1.6	6600			
Cowlitz R. at Packwood 46°36.8′ 121°40.7′	4.5	2.9	14,300			24 Ohanapec. eq.

Table 1. Chloride concentrations, sodium concentrations, and discharge rates of streams and hot springs in the Cascade Range, Oregon and Washington----- continued

Site	Stream Na (mg/L)	Stream Cl (mg/L)	Measured Discharge (L/s)	Hot Spring Na (mg/L)	Hot Spring Cl (mg/L)	Calculated Discharge (L/s)
Nisqually R. ab. Longmire 46°45.3′ 121°48.2′	1.8	-	-			
Nisqually R. bl. Longmire 46°43.8′ 121°51.8′	4.6	3.9	2500?	580	810	12?Longmire Sprs
unn. cr. with iron stain 46°43.8′ 121°51.9′	11.5	13	-			
Tahona Cr. 46°44.5′ 121°53.7′	2.7	-	-			
Nisqually R. at National 46°45.1′ 122°5.0′	3.1	2.2	15,000	580	810	18 Longmire eq
Puyallup R. 47°2.3′ 122°12.3′	2.1	-	-			
Carbon R. 47°5.9′ 122°9.1′	2.6	-	-			
Columbia Gorge area, Washington						
Wind R. ab. St.Martins HS 45°44.2′ 121°48.2′	3.7	1.5	-			
Wind R. bl. St.Martins HS 45°43.6′ 121°47.7′	5.3	3.8	3500	360	690	12 St. Martins
Mt. Hood area, Oregon						
Still Cr. ab. Swim WS 45°18.1′ 121°44.1′	8.8	7.1	-			
Still Cr. bl. Swim WS 45°17.7′ 121°44.3′	27	25	58	136	161	6.4 Swim WS

Table 1. Chloride concentrations, sodium concentrations, and discharge rates of streams and hot springs in the Cascade Range, Oregon and Washington----- continued

Site	Stream Na (mg/L)	Stream Cl (mg/L)	Measured Discharge (L/s)	Hot Spring Na (mg/L)	Hot Spring Cl (mg/L)	Calculated Discharge (L/s)	
Clackamas River System, Oregon							
Clackamas R. ab. Austin HS 45°1.0′ 121°55.2′	3.5	.7	9800				
Clackamas R. bl. Austin HS 45°1.9′ 122°3.5′	7.4	5.5	9400	305	390	120	Austin HS
Bagby HS 44°56.1′ 122°10.3′W	53	14	1 meas.				
Collawash R. 44°59.3′ 122°3.9′	2.7	1.2	4200			9	Austin eq.
Qak Grove Fk. Clackamas R. 45°4.3′ 121°57.0′	3.2	.7	10600				
Clackamas R. (Three Lynx) 45°7.5′ 122°4.3′	4.1	2.2	30,600	305	390	120	Austin HS
Santaim River System, Oregon							
N.F. Breitenbush R. ab. HS 44°46.8′ 122°57.8′	2.7	.4					
S.F. Breitenbush R. ab. HS 44°46.7′ 122°57.8′	-	.5					
Breitenbush R. bl. HS 44°45.1′ 122°7.8′	4.3	2.9	6200	745	1200	12	Breitenbush
N. Santiam R. ab. Detroit L. 44°42.5′ 122°6.1′	-	.5					
Little N. Santiam R. 44°47.5′ 122°34.7′	2.9	1.1	977				
N. Santiam R. at Mehama 44°47.3′ 122°37.0′	2.5	<.5	36200				

Table 1. Chloride concentrations, sodium concentrations, and discharge rates of streams and hot springs in the Cascade Range, Oregon and Washington----- continued

Site	Stream Na (mg/L)	Stream Cl (mg/L)	Measured Discharge (L/s)	Hot Spring Na (mg/L)	Hot Spring Cl (mg/L)	Calculated Discharge (L/s)
S. Santiam R. ab. Soda F. 44°24.3′ 122°2.1′	3.6	-	1410			
Soda Fk. 44°24.4′ 122°17.1′	3.2	-	855			
S. Santiam R. bl. Soda Fk. 44°24.2′ 122°18.0′	3.5	1.1	2266	2200	3500	.3 Soda Sp
S. Santiam River 44°23.6′ 122°30.6′	4.3	2.3	2350			1.2 Soda Sp
McKenzie River System, Oregon						
McKenzie R.(Trail Br. Dam) 44°16.1′ 122°2.9′	4.3	.7	20700			
McKenzie R. ab. Belknap Spr 44°12.4′ 122°2.4′	4.3	.9				
Lost Cr. 44°9.7′ 122°1.2′	5.0	1.8				
McKenzie R. bl. Belknap Spr 44°10.8′ 122°7.8′	4.6	1.4	35,100	660	1200	18 Belknap Spr.
Horse Cr. ab. Foley Spr. 44°7.3′ 122°2.1′	3.0	.8				
Horse Cr. bl. Foley Spr. 44°9.8′ 122°9.1′	5.3	1.9	11300	555	1350	9 Foley Spr.
Rider Cr. bl. HS 44°5.0′ 122°14.0′	380	700	5.1	405	790	4.5 unn. HS
S. Fk. McKenzie R. 44°8.2′ 122°14.8′	3.1	.8	27400			
Quartz Cr. 44°6.7′ 122°21.3′	2.9	.8	710			

Table 1. Chloride concentrations, sodium concentrations, and discharge rates of streams and hot springs in the Cascade Range, Oregon and Washington----- continued

Site	Stream Na (mg/L)	Stream Cl (mg/L)	Measured Discharge (L/s)	Hot Spring Na (mg/L)	Hot Spring Cl (mg/L)	Calculated Discharge (L/s)
Blue R. 44°9.3′ 122°20.4′	-	.9				
McKenzie R. (Vida) 44°7.5′ 122°28.2′	3.8	1.3	98000			49 Belknap eq.
Willamette River System, Oregon						
Hills Cr. ab. Kitson Spr. 43°39.7′ 122°20.2′	3.1	.7				
Hills Cr. ab. Kitson Spr. 43°40.8′ 122°22.2′	3.0	1.0				
Hills Cr. bl. Kitson Spr. 43°41.8′ 122°22.7′	5.5	6.2	736	1500	3350	1.2 Kitson Spr.
M. Fk. Willamette ab. res. 43°35.3′ 122°27.3′	3.5	.5	11200			
M. Fk. Willamette bl. res. 43°43.2′ 122°11.2′	3.2	.8	44700			
Salt Cr. ab. McCredie Spr. 43°42.0′ 122°16.9′	3.2	.5				
Salt Ct. bl. McCredie Spr. 43°43.6′ 122°11.2′	4.0	2.5	5470	1000	2150	5.1 McCredie Spr
Salmon Cr. 43°45.8′ 122°17.3′	3.4	1.0	5380	350	610	4.4 unn. WS
N.Fk.William. ab. Westfir 43°47.5′ 122°27.5′	-	.7				
N.Fk.William. bl. Westfir 43°43.4′ 122°30.5′	4.1	2.9	7330	1250	2800	5.8 salt seep

Table 1. Chloride concentrations, sodium concentrations, and discharge rates of streams and hot springs in the Cascade Range, Oregon and Washington----- continued

Site	Stream Na (mg/L)	Stream Cl (mg/L)	Measured Discharge (L/s)	Hot Spring Na (mg/L)	Hot Spring Cl (mg/L)	Calculated Discharge (L/s)
Deschutes River System, Oregon						
Cultus R. 43°50.1′ 121°47.7′	4.5	<.5				
Quinn R. 43°47.1′ 121°50.1′	3.2	<.5	1400			
Deschutes R. ab. Wickieup 43°44.7′ 121°46.7′	3.6	.5				
Falls R. 43°47.8′ 121°34.3′	5.6	<.5				
Deschutes R. bl. L. Des.R. 43°51.8′ 121°27.1′	4.7	.6				
Spring River 43°51.8′ 122°28.6′	9.9	2.5	1270			950 mg-Cl/s
Deschutes R. ab. Bend 43°55.8′ 121°24.6′	6.1	1.0	35700			
Deschutes R. in Bend 44°5.0′ 121°18.4′	6.0	1.1	34000			
Tumalo Cr. 44°5.3′ 121°22.3′	3.7	<.5				
Soda Cr. 44°1.5′ 121°42.5′	2.4	<.5				
Squaw Cr. 44°14.0′ 121°34.0′	3.0	<.5				
Deschutes R. ab. L.Billy 44°29.9′ 121°19.2′	7.3	1.2				
Metolius R. (headwaters) 44°27.0′ 121°38.4′	8.7	1.7	3600			

Table 1. Chloride concentrations, sodium concentrations, and discharge rates of streams and hot springs in the Cascade Range, Oregon and Washington----- continued

Site	Stream Na (mg/L)	Stream Cl (mg/L)	Measured Discharge (L/s)	Hot Spring Na (mg/L)	Hot Spring Cl (mg/L)	Calculated Discharge (L/s)	
Lake Cr. 44°25.7′ 121°43.5′	3.5	.6					
Lake Cr. at Metolius R. 44°27.4′ 121°38.6′	7.4	.8	4600				
Metolius R. at l. bridge 44°33.4′ 121°37.2′	6.9	1.4	33,400				
Jefferson Cr. 44°33.4′ 121°38.4′	2.9	<.5					
Warm Spr. R. ab. Kahneetah 44°52.0′ 121°13.1′	6.8	1.9					
Warm Spr. R. bl. Kahneetah 44°51.6′ 121°12.3′	8.1	2.6	7873	400	240	69	Kahneetah HS
Umpqua River System, Oregon							
Warm Springs Cr. 43°21.8′ 122°14.2′	2.3	.3	637				
Clearwater R. 43°14.7′ 122°17.0′	6.2	1.0					
Fish Cr. 43°13.8′ 122°26.8′	3.0	<.5					
Steamboat Cr. 43°20.9′ 122°43.6′	4.1	1.7	1700			1800	mg-Cl/s
N. Umpqua R. ab. Umpqua HS 43°15.5′ 122°19.3′	3.6	.9				700	mg-Cl/s
N. Umpqua R. bl. Umpqua HS 43°15.0′ 122°20.5′	7.7	8.2	2810	2400	3500	6.2	Umpqua HS
N. Umpqua R. 43°17.8′ 122°32.5′	5.0	1.7	31,200			8.0	Umpqua eq

Table 1. Chloride concentrations, sodium concentrations, and discharge rates of streams and hot springs in the Cascade Range, Oregon and Washington----- continued

Site	Stream Na (mg/L)	Stream Cl (mg/L)	Measured Discharge (L/s)	Hot Spring Na (mg/L)	Hot Spring Cl (mg/L)	Calculated Discharge (L/s)
Crater Lake area, Oregon						
Minnehaha Cr. ab. ss 43°3.9′ 122°13.8′	1.8	.3	-			
Minnehaha Cr. bl. ss 43°3.9′ 122°14.8′	3.2	.5	80			
Muir Cr. 43°2.9′ 122°21.0′	3.4	.4	2090			
Red Blanket Cr. 42°46.7′ 122°25.6′	3.9	-	-			
Rogue River at Prospect 42°46.0′ 122°29.9′	4.9	<1	13,700			
Williamson R.(Military C.) 42°57.2′ 121°40.3′	8.9	1.4	479			
Williamson R.(Kirk) 42°44.2′ 121°50.1′	13	1.5	140			
Big Spr. Cr. 42°57.5′ 121°45.5′	6.4	1.3	1480			
Artesian well 42°57.9′ 121°46.2′	6.4	1.4	.4			
Williamson R. at Chiloquin 42°35.7′ 121°51.6′	7.9	2.0	11,000			7000 mg-Cl/s
Spraque R. at Chiloquin 42°34.0′ 121°51.8′	9.1	1.6	8200			
Spring Cr. 42°38.9′ 121°52.9′	8.2	1.7	7800			2000 mg-Cl/s
unn. spr. 42°41.4′ 121°57.8′	9.9	3.7	700			400 mg-Cl/s

Table 1. Chloride concentrations, sodium concentrations, and discharge rates of streams and hot springs in the Cascade Range, Oregon and Washington----- continued

Site	Stream Na (mg/L)	Stream Cl (mg/L)	Measured Discharge (L/s)	Hot Spring Na (mg/L)	Hot Spring Cl (mg/L)	Calculated Discharge (L/s)
unn. spr. 42°38.9′ 121°52.9′	7.9	2.3	155			150 mg-Cl/s
unn. cr. at Williamson R. 42°39.1′ 121°51.5′	11	2.7	178			140 mg-Cl/s
Crooked R. 42°38.7′ 121°56.7′	14	7.3	1000			5400 mg-CL/s
Reservation Spr. 42°42.2′ 121°57.7′	12	7.1	1600			9000 mg-Cl/s
Wood R.(headwaters) 42°44.4′ 121°58.7′	15	11	-			
Wood R. at Ft. Klamath 42°44.3′ 121°59.5′	8.1	5.0	9010			36,000 mg-Cl/s
Mares Egg Spr. 42°42.2′ 121°57.7′	4.6	.2	-		total	60,000 mg-Cl/s
Medicine Lake area, California						
Medicine Lake 41°34.9′ 121°35.2′	.9	.2				
Blanche Lake 41°33.4′ 121°34.2′	.8	.2				
Bullseye Lake 41°33.3′ 121°34.4′	1.2	.2				
Crystal Spring 41°34.4′ 121°36.5′	2.7	.1				
Payne Spring 41°33.7′ 121°33.6′	3.9	.2				

---

s - samples analyzed only on a preliminary scan basis; values are low and not considered important in this study.

Table 2. Chemical data for selected thermal and mineral springs of Cascade Range. (concentrations are in milligrams per liter)

Name Location	t(°C)	pH	SiO_2	Ca	Mg	Na	K	Cl	SO_4	HCO_3	F	B	Br
Ca-Cl component waters													
St. Martin's H.S. 45°43.7'N 121°47.7'W	48	8.54	48	76	.3	360	6.4	690	16	19	.7	2.9	-
Belknap Sprs. 44°11.6'N 122° 2.9'W	73	7.64	91	210	.3	660	15	1200	150	20	1.1	6.2	5.4
Bigelow H.S. 44°14.3'N 122° 3.5'W	59	7.70	73	195	.5	675	15	1250	140	22	1.5	5.6	8.7
Breitenbush H.S. 44°46.9'N 121°58.5'W	84	7.02	163	95	1.1	745	31	1200	140	137	3.7	4.0	5.0
Foley Sprs. 44° 9.2'N 122° 5.8'W	79	7.99	63	410	.1	555	8.7	1350	510	20	.8	8.6	-
Kitson H.S. 43°41.4'N 122°22.5'W	44	7.32	44	725	1.5	1500	24	3350	185	25	1.8	24	6.9
McCredie Sprs. 43°42.2'N 122°17.2'W	74	7.29	72	485	.9	1000	21	2150	235	23	2.5	18	6.3
Rider Creek H.S. 44° 5.0'N 122°14.0'W	46	8.52	47	215	.1	405	6.1	790	240	21	.9	5.7	2.4
Wall Creek H.S. 43°48.4'N 122°18.6'W	40	7.71	65	115	.2	350	8.4	610	140	44	4.2	6.5	-
Salt spring 43°44.4'N 122°27.6'W	18	8.75	29	490	51	1250	46	2800	83	-	3.7	-	-
Na-Cl thermal water													
Goldmeyer H.S. 47°29.0'N 121°23.1'W	50	8.48	56	6.3	.04	125	3.0	130	40	61	.9	<1	-
Lester H.S. 47°12.5'N 121°32.2'W	46.5	9.19	61	5.3	.03	105	2.0	115	19	61	1.6	<1	-
Austin H.S. 45° 1.3'N 122° 0.5'W	86	7.42	81	35	.1	305	6.4	390	130	36	1.4	2.6	1.4

Table 2. Chemical data for selected thermal and mineral springs of Cascade Range. --continued
(concentrations are in milligrams per liter)

Name Location	t(°C)	pH	SiO_2	Ca	Mg	Na	K	Cl	SO_4	HCO_3	F	B	Br
CO_2-charged Na-Cl waters													
Gamma H.S. 48° 9.1'N 121° 3.7'W	65	6.13	141	71	2.8	510	80	755	30	398	1.4	9	4.2
Garland M.S. 47°54.2'N 121° 0.2'W	29	6.46	105	390	87	2500	200	3600	160	2600	1.6	64	7.5
Kennedy H.S. 48° 7.1'N 121°11.5'W	35	6.27	175	190	48	670	72	625	2	1660	1.2	7.5	-
Ohanapecosh H.S. 46°44.5'N 121°33.5'W	48	6.80	100	60	4.9	920	52	880	170	1060	5.2	12	2.2
Umpqua H.S. 43°42.4'N 122°17.2'W	46	6.37	90	340	41	2400	63	3500	190	1380	1.5	41	7.4
Dilute Na-HCO_3 waters													
Baker H.S. 48°45.8'N 121°40.2'W	44	8.56	103	5.5	.2	170	9.6	110	87	165	3.2	2.7	-
Scenic H.S. 47° 2.4'N 121° 8.5'W	47	9.14	44	2.1	.02	49	.6	22	13	75	.7	<1	-
Pucci well 45°19.3'N 121°42.8'W	20	7.60	20	3	.5	290	7.6	170	<1	380	<.1	<1	-
Swim W.S. 45°17.8'N 121°44.3'W	26	7.22	83	53	41	105	9.9	120	200	175	.3	<1	-
Bagby H.S. 44°56.1'N 122°10.3'W	56	9.37	74	3.3	<1	53	.7	14	42	69	.7	<1	-
Kahneeta area 44°52.0'N 121°13.6'W	83.5	8.1	78	13	.3	400	11	240	31	603	21	5.6	-
East Lake H.S. 43°43.2'N 121°11.9'W	57	6.10	197	73	33	56	9.7	1	120	413	.1	1	-
Paulina H.S. 43°43.6'N 121°15.0'W	52	7.26	184	50	42	110	13	5	2	689	.5	1	-

Table 2. Chemical data for selected thermal and mineral springs of Cascade Range. -- continued
(concentrations are in milligrams per liter)

Name Location	t(°C)	pH	SiO_2	Ca	Mg	Na	K	Cl	SO_4	HCO_3	F	B	Br
CO_2-charged mineral springs													
Soda s.-Wenatchee Ford 47°55.1'N 121° 5.2'W	9	6.48	105	400	73	2120	230	2000	265	3935	.8	45	-
Summit Creek Soda Spr. 46°42.8'N 121°29.0'W	11	6.24	100	240	93	1750	85	1450	<1	3610	.2	50	5.4
Longmire Sprs. 46°45.1'N 121°48.8'W	19	6.35	125	540	170	580	46	810	41	2700	.5	3.7	2.8
Puyallup River Spr. 46°49.8'N 121°55.1'W	10	6.47	54	240	86	320	11	325	2	1490	<.5	3.7	-
Upper Soda Spr. 44°24.3'N 122°17.3'W	11	5.90		510	40	2200	61	3500	310	1600	.7	26	-
Cascadia Soda Spr. 44°23.9'N 122°28.8'W	11	6.05	-	370	120	2200	37	3300	63	2200	.3	53	-
Soda spr. on Soda Cr. 44° 2.4'N 121°41.7'W	10	5.64	92	51	38	50	4.1	5.4	17	506	1.5	<1	-
Toketee Soda Spr. 43°18.5'N 122°29.8'W	16	6.05	85	880	57	1750	50	3500	190	1590	1.5	44	-
Soda spr. Minnehaha Cr. 43° 3.7'N 122°16.6'W	10	-	68	240	210	99	21	19	23	1600	-	-	-
McCallister Soda Spr. 42°23.3'N 122°27.5'W	12	6.13	87	320	235	705	16	1050	135	2120	<.5	41	-
Springs discharging in mineralized area east of Broken Top													
unn. spr. 44° 4.5'N 121°39.6'W	3	6.04	44	13	4.0	4.3	.5	.3	49	25	.1	<.01	-
unn. spr. 44° 4.6'N 121°39.9'W	6	6.34	47	16	5.7	4.1	.6	.4	53	10	.1	<.01	-
unn. spr. 44° 4.5'N 121°39.8'W	3	4.47	48	8.1	2.4	2.8	.8	.3	59	-	.1	<.01	-

Table 2. Chemical data for selected thermal and mineral springs of Cascade Range. -- continued
(concentrations are in milligrams per liter)

Name Location	t(°C)	pH	SiO_2	Ca	Mg	Na	K	Cl	SO_4	HCO_3	F	B	Br
Anomalous area southeast of Crater Lake National Park													
Wood River 42°44.4' 121°58.7'	11	8.20	40	5.3	2.4	15	2.0	11	7.5	42	.2	.23	-
Reservation Spr. 42°42.2' 121°57.7'	6.5	7.69	39	4.5	2.3	12	1.7	7.1	5.7	39	.2	.17	-
Mares Egg Spr. 42°39.6' 121°59.5'	3.5	7.11	35	8.3	3.1	4.6	1.3	.2	.4	53	.1	.01	-
Unn. cr. 42°39.1' 121°51.1'	-	-	35	4.6	3.0	11	1.3	2.7	4.5	-	.2	.05	-
Spring River 42°38.9' 121°52.9'	6	7.83	39	4.0	2.6	8.8	1.4	2.1	3.1	39	.2	.07	-
Unn. spr. 42°41.4' 121°57.8'	-	-	43	4.7	2.7	9.9	1.3	3.7	4.1	-	.2	.11	-
Unn. spr. 42°38.9' 121°52.9'	-	-	46	5.1	3.3	7.9	1.3	2.3	2.8	-	.1	.07	-
Crooked River 42°38.7' 121°56.7'	-	-	38	4.3	2.9	14	1.5	7.3	6.3	-	.2	.18	-
Tecumseh Spr. 42°38.6' 121°56.5'	-	-	38	4.5	2.7	11	1.2	4.0	4.0	-	.2	.12	-
Mt. Shasta													
Acid-sulfate spr. 41°24.5' 122°11.7'	80	2	-	47	36	43	11	<2	2000	-	.4	-	-

Table 3. Convective heat discharge associated with thermal springs of the Cascade Range, Oregon and Washington

Source	Temperature (^{o}C)	Discharge (L/s)	Convective heat[α] kJ/s
WASHINGTON			
Baker H.S.	44	1.4	170
Gamma H.S.	65	2.5	520
Kennedy H.S.	35	1	84
Sulphur H.S.	37	<1	-
Garland Spr.	29	4.3	250
Scenic H.S.	47	.3	40
Goldmeyer H.S.	50	2.8	410
Lester H.S.	46.5	11	1400
Longmire Sprs.	19	12	200
Ohanapecosh H.S.	48	14	1900
St. Martin's H.S.	48	12	1700
OREGON			
Swim W.S.	26	6.4	290
Kahneetah H.S.	84	69	20,000
Bagby H.S.	58	1	180
Austin H.S.	86	120	36,000
Breitenbush H.S.	84	12	3500
Bigelow H.S.[β] & Belknap Spr.	73	18	4400
Foley Sprs.	78	9	2400
unn. spr. on Rider Cr.	44	4.5	550
unn. spr. on Wall Cr.	40	4.4	520
McCredie Sprs.	73	5	1200
Kitson Sprs.	43	1	120
Umpqua H.S.	46.5	6	790
East Lake & Paulina H.S.	57	12[ψ]	2000
	Totals:	330 L/s	7.8×10^{4} kJ/s

α Assuming reference temperature of 15 ^{o}C.
β Name of spring in Berry, Grimm, and Ikelman (1980)
ψ Sammel (1983) and Sammel and Craig (1983) identified 12 L/s but stated that the total thermal discharge could be as high as 20 L/s.

Table 4. Quaternary extrusion rates of volcanic rock and convective discharge rates of thermal waters, Cascade Range northwestern United States

Region	Rock extrusion rate[α] for the Quaternary (km^3/km arc length/m.y.)	Convective heat discharge rate for hot springs (kJ/km arc length/s)
Northern Washington (Segment 1)	0.4	10
Central and southern Washington (Segment 2)	1.9	34
Oregon (Segment 3)	3 to 6	270

α Extrusion rates from Sherrod and Smith, this volume.

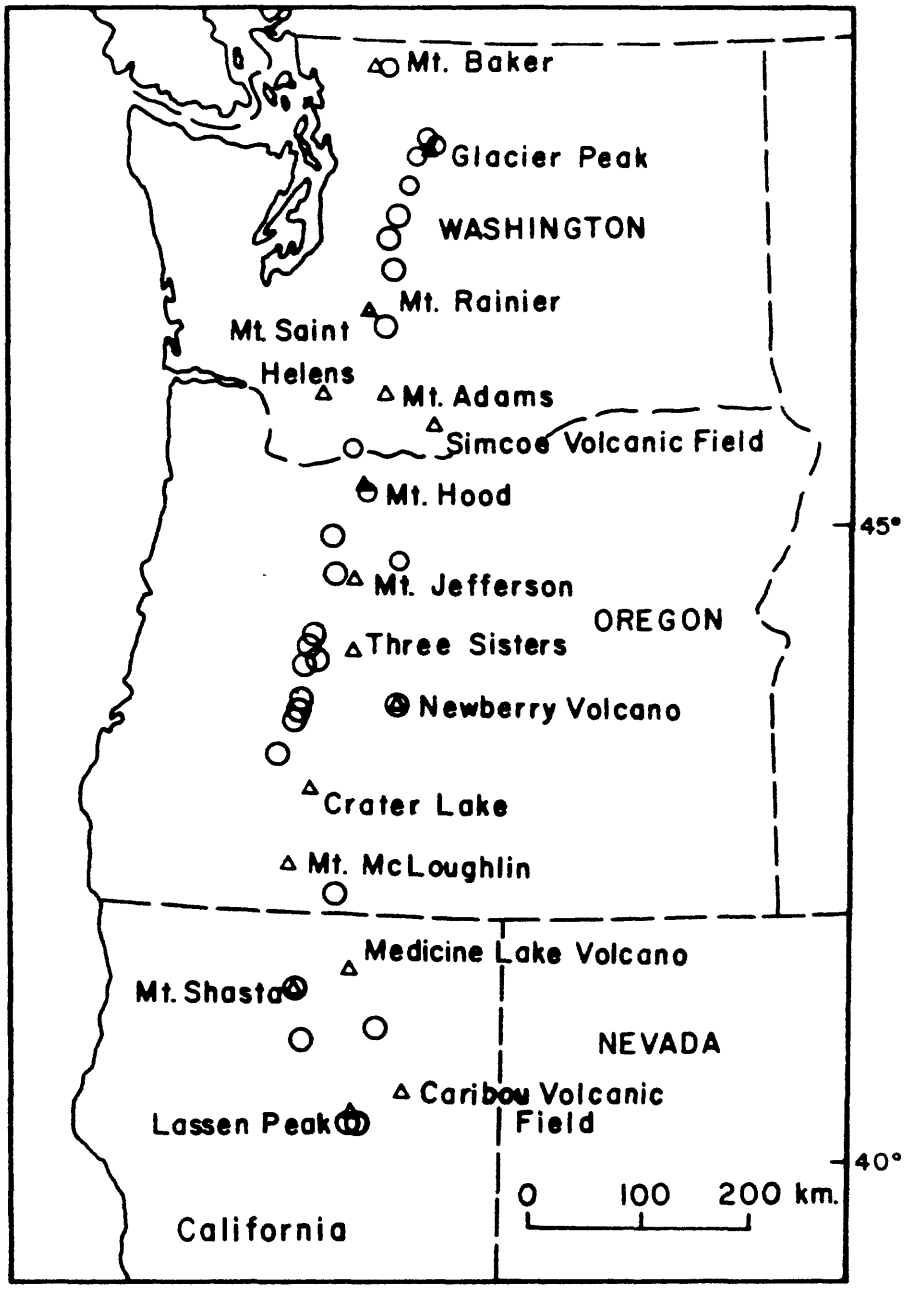

Figure 1. Location of thermal springs and major volcanoes of the Cascade Range. Circles indicate thermal springs. Triangles indicate major volcanoes or volcanic fields.

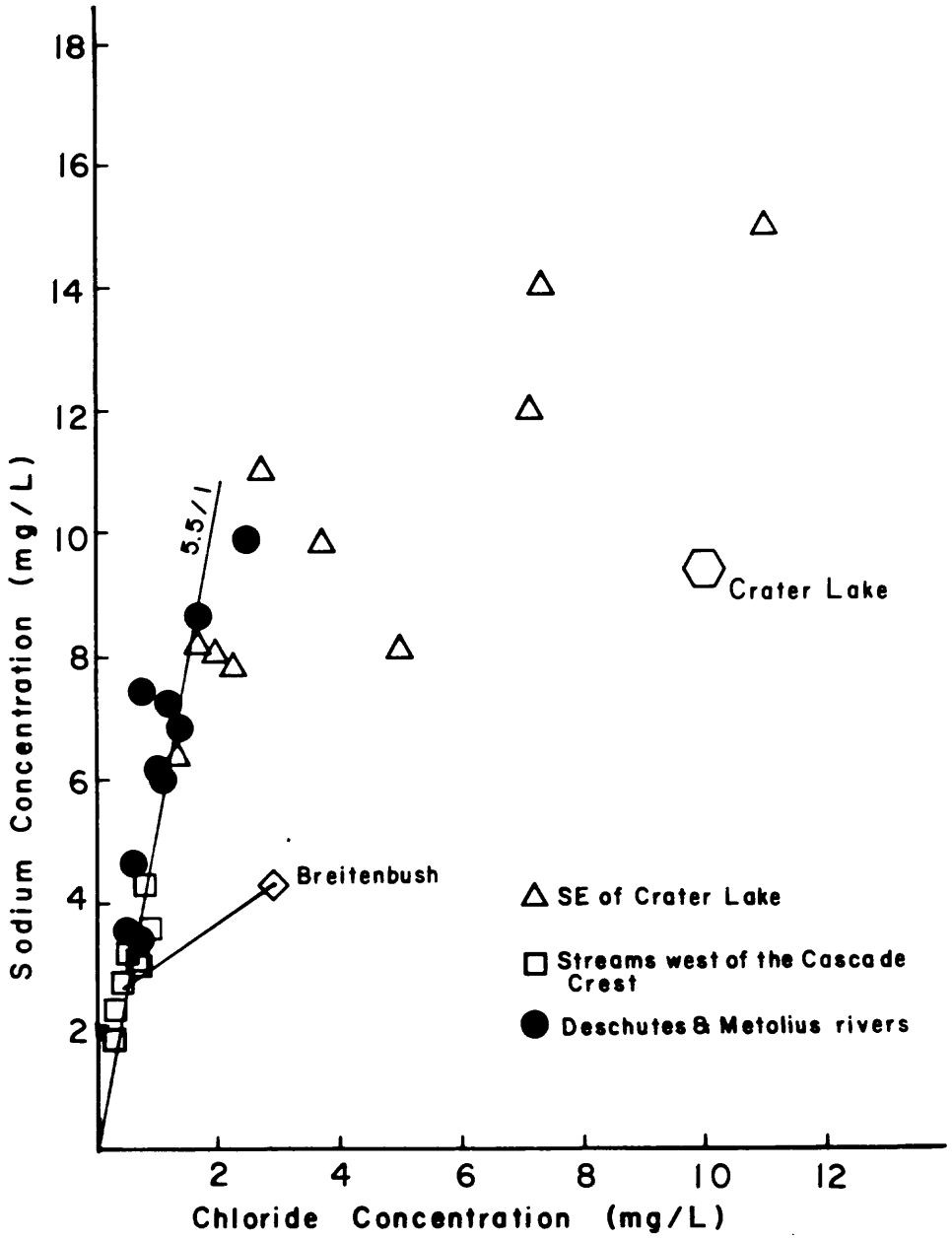

Figure 2. Plot of sodium versus chloride for selected streams, springs, and lakes of the Cascade Range, Oregon. Samples from the west side of the Cascade Range, the Deschutes River, and the Metolius River all have "background" Na/Cl ratios near 5.5. This value apparently represents normal Na/Cl ratios in pristine streams of the Cascade Range in Oregon. The symbol marked Breitenbush is an example from the Breitenbush River, the tie line connects samples from the river above and below Breitenbush Hot Springs

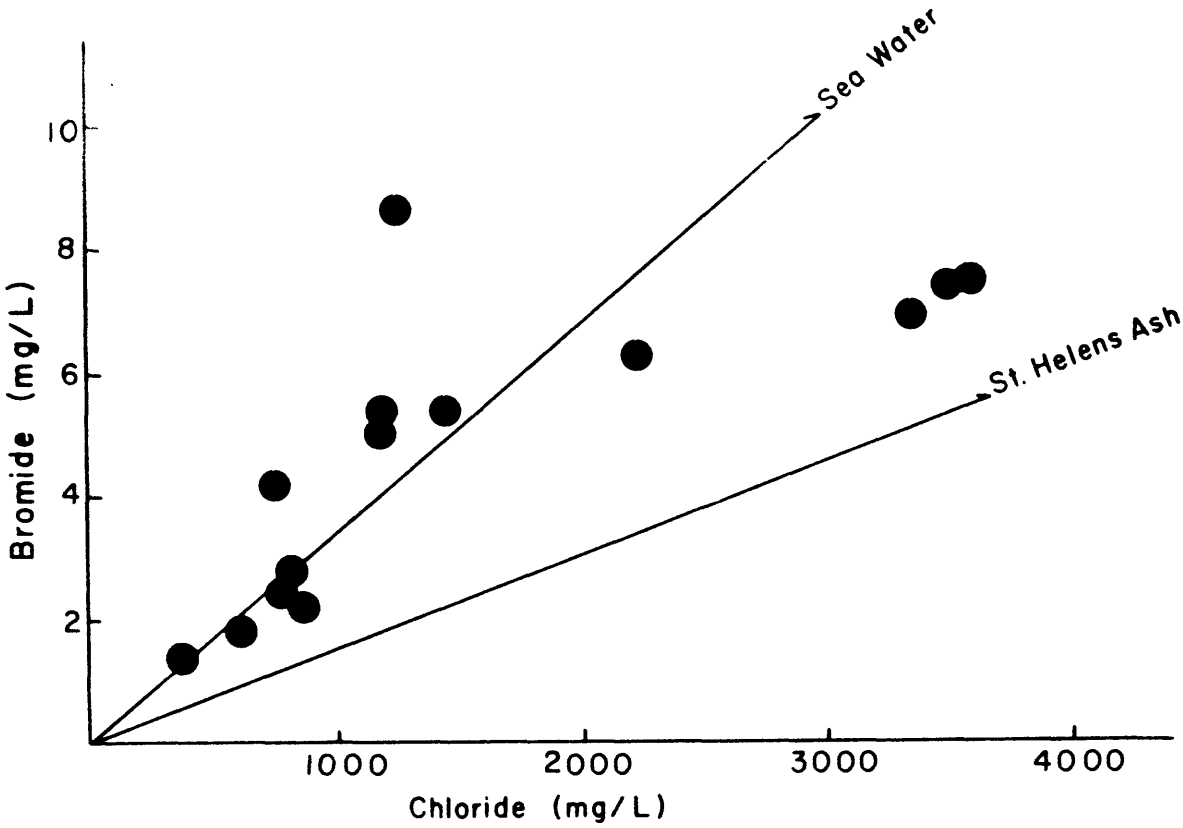

Figure 3. Plot of bromide versus chloride for thermal waters of the Cascade Range, Oregon and Washington. As chloride concentrations increase, bromide increases along the sea water trend until about 1500 mg/L chloride. At higher chloride concentrations, water-rock reaction may drive the water Br/Cl ratio toward the composition of the rock. Data for thermal springs at Lassen Peak (Thompson, 1985) plot on the sea water trend at about 2200 mg-Cl/L.

INTEGRATION OF EARTH-SCIENCE DATA SETS TO ESTIMATE UNDISCOVERED GEOTHERMAL RESOURCES OF THE CASCADE RANGE

L.J.P. Muffler and Marianne Guffanti
U.S. Geological Survey

Abstract

The young volcanism and high regional heat flow of the Cascade Range suggest the presence of substantial geothermal energy, yet the accessible geothermal resource base defined to date is modest (84×10^{18} J). Estimates of the geothermal resource base yet to be discovered at depths less than 3 km range from 105×10^{18} J to $17{,}620 \times 10^{18}$ J. Resolution of these disparate estimates can be addressed in part by the integrated interpretation of regional earth-science data. Intermediate-depth drilling is required, however, to calibrate geophysical interpretations, delineate deep geological units, and determine the temperature, thermal conductivity, porosity, permeability, and fracture patterns at depth.

Geothermal setting

The Cascade Range is a Tertiary and Quaternary volcanic arc that extends north from northeastern California through Oregon and Washington into British Columbia (Canada). The arc lies above an easterly dipping active subduction zone along which the Juan de Fuca, Gorda, and Explorer microplates are thrust beneath the North American plate (Riddihough, 1984). The volcanic arc is active, with historic eruptions at Lassen Peak (1914-17) and Mount St. Helens (mid 1800's; 1980-86), and possibly at Mt. Shasta (1786), Mt. Hood (mid 1800's), Mt. Rainier (mid 1800's), Mt. Baker (mid 1800's), and Cinder Cone (east of Lassen Peak; 1851?). In addition to the major composite volcanoes that have erupted andesite, dacite, and even rhyolite, there are a myriad of smaller, discrete volcanoes that erupted only once, or at most a few times, producing primarily calc-alkaline basalt and basaltic andesite (Guffanti and Weaver, 1988; Luedke and Smith, 1981, 1982; McBirney, 1978).

Geothermal potential in the Cascade Range is indicated not only by the young volcanism, but also by a regional, positive, conductive heat-flow anomaly (Blackwell and others, 1982; Blackwell and Steele, 1983, 1985). For example, the regional conductive heat flow of 100 mW/m^2 of the Cascade Range in Oregon is more than twice that of the Willamette Valley, immediately adjacent to the west (Black and others, 1983). In young, porous rocks of the High Cascades, however, conductive heat flow in holes up to several hundred m deep is generally near zero, owing to hydrologic disturbances (Blackwell and others, 1982; Mase and others, 1982).

The elevated regional heat flow is also expressed by sporadic thermal springs along the Cascade Range. Sorey (1985) has classified these thermal springs into three groups: (1) summit-crater systems, (2) caldera systems, and (3) lateral-flow systems.

Identified geothermal resource base of the Cascade Range

The accessible geothermal resource base (Muffler and Cataldi, 1978) identified to date in hydrothermal convection systems of the Cascade Range is modest (Guffanti, 1985). Fourteen hydrothermal systems in the Cascades were estimated by Brook and others (1979) to contain 84×10^{18} J, with most of this energy in two major systems (Lassen at 42×10^{18} J and Newberry at 27×10^{18} J). Since 1979, exploratory drilling at Medicine Lake volcano in northeastern California apparently has identified a substantial resource, but the data are still held proprietary by the private companies exploring the area. In addition, exploratory drilling at Breitenbush in Oregon has confirmed temperatures of >141°C at 2500 m (Priest, 1985; Blackwell and Baker, 1988), and drilling east of Crater Lake, Oregon, reached temperatures of 107°C at 405 m (Priest and others, 1986; Blackwell and Steele, 1987).

The identified geothermal resource (identified thermal energy that can be extracted legally and used at some future time under reasonable economics) is restricted by laws and government regulations that prohibit geothermal development in National Parks or in Wilderness Areas (where some of the most attractive targets exist); Lassen Volcanic National Park is the most conspicuous example. Furthermore, recent Federal legislation requires that geothermal development adjacent to National Parks be evaluated in terms of possible adverse effects on parks having significant thermal features.

Undiscovered geothermal resources of the Cascade Range

The geothermal dichotomy in the Cascade Range is thus the existence of Quaternary volcanism and high regional heat flow opposed to the sparsity of hot springs and identified hydrothermal reservoirs of geothermal energy (Muffler, 1987). The young volcanism and high regional heat flow suggest the presence of substantial geothermal energy, yet the geothermal resource defined to date is modest. The fundamental geothermal question is what geothermal resources yet remain to be discovered in the Cascade Range. Many workers have suggested that substantial quantities of geothermal energy are masked by cool, near-surface groundwater. This interpretation was supported by the discovery of temperatures of 265°C at 930 m depth beneath Newberry volcano (Sammel, 1981), effectively masked by a surficial zone more than 300 m thick at less than 100°C (Swanberg and others, 1988).

The range of estimates of undiscovered geothermal resources in the Cascade Range is great. Brook and others (1979), based on the favorable volcano-tectonic setting, multiplied the identified reservoir energy of the Cascade Range (excluding Newberry and Medicine Lake, but including National Parks and Wilderness Areas) by a subjective factor of 20 to give an estimate of 1140×10^{18} J for the undiscovered accessible resource base to a depth of 3 km. Newberry volcano was considered with the Oregon Plateaus geologic province, and Klamath Falls (30×10^{18} J) with the northwestern Basin and Range province; in both these provinces, the undiscovered accessible resource base was estimated to be 5 times the identified.

These educated guesses of Brook and others (1979) were influenced indirectly by the model calculations made by Smith and Shaw (1975, 1979) for thermal energy remaining today in igneous-related systems (coupled magma-hydrothermal systems in the upper 10 km of the crust). Smith and Shaw used simple cooling models constrained by available size and age data on

volcanic systems to calculate that roughly 3,900 x 10^{18} J remain today to depths of 10 km in eleven igneous-related systems in the Cascade Range (including Medicine Lake and Newberry volcanoes) for which available data allow calculations. Furthermore, Smith and Shaw (1979) noted that additional igneous-related energy resides in systems not evaluated because of insufficient data. They gave no estimate specific to the Cascade Range, but for the entire United States they estimated that the unevaluated geothermal energy in igneous-related geothermal systems is perhaps 10 times that which could be evaluated in 1978.

Black and others (1983) calculated an accessible resource base for the Oregon Cascade Range of 105 x 10^{18} to 16,965 x 10^{18} J. The low figure assumes permeability only in 100-m-wide fracture zones between 1.75 and 3.0 km depth, whereas the high figure assumes that most of the range is underlain at 1.75-3.0 km by a hydrothermal reservoir at 195°C.

Another large estimate of undiscovered geothermal resources in the Cascade Range was given by Bloomquist and others (1985) for the part of the Cascade Range in Oregon and Washington. Basing their calculations on the temperature-depth model of Blackwell and others (1982), Bloomquist and others (1985) inferred a geothermal reservoir 40 to 60 km wide with a reservoir thickness of 1.25 km in the southern part and 0.5 km in the northern part. Mean reservoir temperature in the southern part was estimated to be 190°C, and in the northern part, 165°C. Bloomquist and others (1985) used these volumes in the accepted volumetric heat equation (Brook and others, 1979, equation 1) to give a stored reservoir thermal energy between the 150°C isotherm and a depth of 3 km of 11,750 to 17,620 x 10^{18} J.

The large estimates of Black and others (1983) and Bloomquist and others (1985) are critically dependent upon the interpretation of the regional heat-flow data of Blackwell and others (1982). These heat-flow data are converted by Blackwell and others (1982) to a set of isotherms in the crust using the method of continuation of thermal data (Brott and others, 1981). Any one of the isotherms shown on the cross section of Figure 8 of Blackwell and others (1982) can explain the heat-flow data. Their choice among the isotherms was based on comparison with regional Bouguer gravity data, under the fundamental assumption that the change in Bouguer gravity along this cross section "is directly associated with the same phenomenon that causes the change in heat flow" (Blackwell and others, 1982, p. 8749). They noted that the observed gravity anomaly is much too great to be explained by simple thermal expansion of rock at any of the subsolidus temperatures of their Figure 8. Accordingly, they concluded that partial melting is required, with partial melting at a depth of 6 to 10 km giving the best correspondence to the observed gravity data. Although Blackwell and others (1982, Figure 10) presented several other models to explain the heat flow data, they prefered "the model that relates the gravity and heat flow data to a (large) zone of hot, low-density (partially molten) material in the upper part of the crust (10 $\pm$ 2 km) beneath the High Cascade Range and extending about 10 km west of the High Cascade Range boundary" (see Blackwell and Steele, 1985, Figure 3).

The thermal and gravity cross sections of Blackwell and others (1982) are in central Oregon between 43°45' and 45°05', and the results were projected to the north and to the south based upon the uniformity of the heat-flow and Bouguer gravity transition zones from north to south. Bloomquist and others (1985) thus applied the conclusions of Blackwell and

others (1982) for central Oregon to the entire Cascade Range in Oregon and Washington, albeit with a less intense heat source in the northern part. The temperature and size of the thermal source preferred by Blackwell and others (1982) were thus the critical input parameters to the thermal energy calculations of Bloomquist and others (1985).

Bloomquist and others (1985, p. 493-496) also calculated thermal energies for individual geothermal systems in the Cascade Range. The total of these estimates (2415×10^{18} J) is heavily weighted by two areas: Mt. McLoughlin and Crater Lake (504×10^{18} and 1630×10^{18} J respectively). Reservoir thicknesses and temperatures for these regions were based on the modeled crustal temperatures of Blackwell and others (1982), and the areas were taken from associated Curie Point isotherm anomalies. However, Bloomquist and others (1985) present neither the isotherm maps nor the assumptions involved in their preparation, and they cite a reference only for central Oregon (Connard and others, 1983).

The thermal energies calculated by Black and others (1983) and by Bloomquist and others (1985) for the shallow crust (<3 km) represent innovative attempts to integrate regional geophysical data to determine the thermal structure of a major geological province. Although the thermal structure, if valid, implies a very large amount of thermal energy in the upper crust, it does not necessarily imply a large amount of recoverable geothermal energy. Much of the calculated thermal energy may be tied up in rock of low porosity and permeability ("hot dry rock") and thus be unavailable for conventional recovery, as from a hydrothermal reservoir. Specifically, the recovery factor of 25%, used for hydrothermal convection systems by Brook and others (1979), is far too high, perhaps by several orders of magnitude, for use throughout a geological province. Accordingly, the figure of 184,948 to 277,420 MW_e for 30 years given by Bloomquist and others (1985, p. 75) is probably two orders of magnitude too high, even if the thermal structure inferred from the geophysical models is correct.

Use of data from regional earth-science investigations

Resolution of the wide ranging resource estimates as well as the fundamental geothermal dichotomy of the Cascade Range can be addressed in two ways: (1) drilling, and (b) integrated interpretation of regional earth-science data sets. Drilling, the ultimate test for any earth-science model, is essential in the Cascade Range. In the ideal world, speculation about the thermal or geologic structure at drillable depths would quickly be tested by drilling. In the Cascade Range, however, economic, institutional, and other pressures have precluded such a direct approach. Commercial geothermal drilling has been limited, primarily because of the short-term energy glut in the United States and the resultant absence of economic incentive to explore for alternative energy sources. Commercial drilling, however, has been supplemented to a small degree by support from the Department of Energy (Blackwell and Steele, 1987; Swanberg and others, 1988). Efforts to implement a program of dedicated scientific drilling in the Cascade Range (Priest, 1986) have yet to bear fruit.

A complement to drilling, however, is the integrated interpretation of regional earth-science data sets. This approach was used by Cataldi and others (1978) in assessing the geothermal resources of central and southern Tuscany, Italy, an area of 8,661 km^2. Using compilations at 1:200,000 of all available drill-hole, geological, gravity, and thermal-gradient data,

the region was divided into 31 zones, each of reasonably homogeneous geology and thermal regime. The upper 3 km of each area was then divided by horizontal surfaces into three volumes. For each of the resultant 93 volumes, temperature, porosity, and recovery factor (for both resources and reserves) were estimated using all available data. Resultant calculations gave resources and reserves in joules and electrical energy in 10^9 watt-years of electricity.

An approach similar to that used by Cataldi and others (1978) in theory could be applied to the Cascade Range, particularly since a number of comprehensive geophysical and geological data sets have been acquired over the past decade. Several of these data sets indicate that the Cascade Range can not be considered as a uniform province either thermally or structurally from California to British Columbia (Weaver, 1985; Weaver and Michaelson, 1985). Recent analyses of seismicity and the distribution of volcanic vents in space and time (Guffanti and Weaver, 1988) have emphasized this segmentation of the Cascade Range and suggest that each major segment should be considered separately in the estimation of geothermal resources. Other geophysical data sets relevant to segmentation of the Cascade Range and subsequent estimation of geothermal resources for the individual segments include gravity (Finn and Williams, 1982; Williams and others, 1988), magnetic (Blakely and others, 1985), magnetotelluric (Stanley and others, 1987), electrical (Fitterman and others, 1988), electromagnetic sounding (EMSLAB Group, 1988), and seismic (Achauer and others, 1988; Catchings and Mooney, 1988; Stauber and others, 1988; Evans and Zucca, 1988).

The past few years also have seen a systematic compilation of the geology of the Cascade Range (Smith, 1987; Sherrod, 1987). This compilation is not only important for subdividing the Cascade Range into reasonably uniform areas, but gives in addition a refined estimate of the rate of volcanic production per unit of arc length (e.g., $km^3/Ma/km$). Comparison of volcanic production between the Cascade Range and other volcanic arcs with identified geothermal resources provides a potentially powerful tool in estimating the geothermal potential of the Cascade Range.

Hydrology clearly plays an important role in evaluating the three-dimensional thermal budget of the Cascade Range. In the early 1970's, R.L. Smith and H.R. Shaw (oral communication, 1973) recognized that many of the thermal springs of the Western Cascades cluster to the west of young silicic volcanic areas on the Cascade crest. They proposed that heat sources under the silicic centers of the High Cascades generate large hydrothermal plumes that move west and emerge at the boundary between the High Cascades and the Western Cascade Range. Based on a heat budget approach, Ingebritsen and others (1988) show that enough heat could be swept out of the High Cascades by groundwater circulation to account for the anomalous convective and conductive heat discharge in adjacent pre-Pliocene volcanic rocks. This model implies that the anomalous heat flow measured in the Western Cascade Range is a shallow-rooted phenomenon and casts serious question upon the concept of a partially molten zone 40 to 60 km wide extending the length of the Cascade Range.

Drilling?

Unfortunately, however, even the best and the most comprehensive geophysical, geological, and hydrological data sets are of restricted use in estimating geothermal resources unless they are calibrated by hard,

subsurface information acquired by the drill bit. A regional seismic reflector or a regional magnetotelluric unit of low resistivity may be exciting science, but are difficult to translate into lithology, porosity, and recoverability without direct sampling of the units concerned. Downward extrapolation of thermal-gradient or heat-flow data will always be fraught with uncertainty and controversy unless temperatures and heat flow are measured in key deep holes.

Given the present abundance and low price of petroleum, the incentive for private industry to complete the costly and difficult drill holes that are needed is simply not there. Certainly the economic incentive will return if the supply of mid-East oil to Europe, the United States, and Japan is cut off, but the resultant drilling is likely to be hasty and directed by short-term economics, with little concern for careful acquisition of the scientific data needed to calibrate the geophysics and to estimate undiscovered geothermal resources. Far preferable to a crash program of drilling in the Cascade Range in response to the next energy crisis would be a pre-crisis program of systematic deep drilling, aimed at calibrating the geophysical interpretations, delineating geological units at depth, and determining the temperature, thermal conductivity, porosity, permeability, and fracture patterns at depth. Such drilling would not only be exciting science, but would have a direct economic and social payoff in the reliable evaluation of an indigenous energy resource. It would be an investment in the energy future, and truly science in the public interest.

In this regard, a comparison between the United States and Japan is in order. The Japanese government is spending approximately $150,000,000 per year in a systematic effort to evaluate geothermal resources throughout the country. This effort is coordinated among national agencies, universities, and private industry with the goal of confirming the amount of geothermal energy that might be available to the country. Japanese geothermal potential is great, but development has been slow. Like the United States, Japan benefits from the current low price and ready availability of petroleum; why should Japan build geothermal plants, when it can purchase cheap oil and conserve its geothermal energy for the future? But unlike the United States, Japan is acting upon the realization that the current situation someday will change for the worse, probably precipitously, and accordingly is making the necessary investment to evaluate its major indigenous resource, geothermal energy.

Although geothermal energy is not the only or even the major energy resource in the United States, it would seem only prudent that the United States also evaluate its long-term geothermal potential, particularly in a region like the Cascades where the available resource estimates are so disparate. Perhaps the time has come for a program of deep scientific drilling to evaluate the geothermal resources of the Cascade Range.

Acknowledgments

We thank S.E. Ingebritsen, C.S. Weaver, R. J. Blakely, and T.E.C. Keith for constructive reviews at various stages in the preparation of this contribution.

References cited

Achauer, Ulrich, J.R. Evans, and D.A. Stauber, 1988, High-resolution seismic tomography of compressional-wave velocity structure at Newberry volcano, Oregon Cascade Range: Journal of Geophysical Research, v. 93, no. B9, p. 10,135-10,147.

Black, G.L., D.D. Blackwell, and J.L. Steele, 1983, Heat flow in the Oregon Cascades, in Priest, G.R., and B.F. Vogt, eds., Geology and geothermal resources of the central Oregon Cascade Range: Oregon Department of Geology and Mineral Industries Special Paper 15, p. 69-76.

Blackwell, D.D., and S.L. Baker, 1988, Thermal analysis of the Breitenbush geothermal system: Geothermal Resources Council Transactions, v. 12, p. 221-227

Blackwell, D.D., R.G. Bowen, D.A. Hull, Joseph Riccio, and J.L. Steele, 1982, Heat flow, arc volcanism, and subduction in northern Oregon: Journal of Geophysical Research, v. 87, no. B10, p. 8735-8754.

Blackwell, D.D., and J.L. Steele, 1983, A summary of heat flow studies in the Cascade Range: Geothermal Resources Council Transactions, v. 7, p. 233-236.

Blackwell, D.D., and J.L. Steele, 1985, Heat flow of the Cascade Range, in Guffanti, Marianne, and L.J.P. Muffler, eds., Proceedings of the Workshop on Geothermal Resources of the Cascade Range, May 22-23, 1985, Menlo Park, California: U.S. Geological Survey Open-File Report 85-521, p. 20-23.

Blackwell, D.D., and J.L. Steele, 1987, Geothermal data from deep holes in the Oregon Cascade Range: Geothermal Resources Council Transactions, v. 11, p. 317-322.

Blakely, R.J., R.C. Jachens, R.W. Simpson, and R.W. Couch, 1985, Tectonic setting of the southern Cascade Range as interpreted from its magnetic and gravity fields: Geological Society of America Bulletin, v. 96, p. 43-48.

Bloomquist, R.G., G.L. Black, D.S. Parker, A. Sifford, S.J. Simpson, and L.V. Street, 1985, Evaluation and ranking of geothermal resources for electrical generation or electrical offset in Idaho, Montana, Oregon and Washington: Bonneville Power Administration, DOE/BP-13609-1, v. 1, 504 p.

Brook, C.A., R.H. Mariner, D.R. Mabey, J.R. Swanson, Marianne Guffanti, and L.J.P. Muffler, 1979, Hydrothermal convection systems with reservoir temperatures $\geq$90°C, in Muffler, L.J.P., ed., Assessment of Geothermal Resources of the United States--1978: U.S. Geological Survey Circular 790, p. 18-85.

Brott, C.A., D.D. Blackwell, and P. Morgan, 1981, Continuation of heat flow data: a method to construct isotherms in geothermal areas: Geophysics, v. 46, p. 1732-1744.

Cataldi, R., A. Lazzarotto, P. Muffler, P. Squarci, and G. Stefani, 1978, Assessment of geothermal potential of central and southern Tuscany: Geothermics, v. 7, no. 2-4, p. 91-131.

Catchings, R.D., and W.D. Mooney, 1988, Crustal structure of east central Oregon: relations between Newberry volcano and regional crustal structure: Journal of Geophysical Research, v. 93, p. B9, p. 10.081-10,094.

Connard, G.G., R.W. Couch, and M. Gemperle, 1983, Analysis of aeromagnetic measurements from the Cascade Range in central Oregon: Geophysics, v. 48, no. 3, p. 376-390.

EMSLAB Group, 1988, The EMSLAB electromagnetic sounding experiment: Eos (Transactions of the American Geophysical Union), v. 69, no. 7, p. 89, 98-99.

Evans, J.R., and J.J. Zucca, 1988, Active high-resolution seismic tomography of compressional wave velocity and attenuation structure at Medicine Lake volcano, northern California Cascade Range: Journal of Geophysical Research, v. 93, no. B12, p. 15,016-15,036.

Finn, Carol, and D.L. Williams, 1982, Gravity evidence for a shallow intrusion under Medicine Lake Volcano, California: Geology, v. 10, p. 503-507.

Fitterman, D.V., W.D. Stanley, and R.J. Bisdorf, 1988, Electrical structure of Newberry volcano, Oregon: Journal of Geophysical Research, v. 93, no. B9, p. 10,119-10,134

Guffanti, Marianne, 1985, Previous estimates by the U.S. Geological Survey of geothermal resources of the Cascade Range, in Guffanti, Marianne, and L.J.P. Muffler, eds., Proceedings of the Workshop on Geothermal Resources of the Cascade Range, May 22-23, 1985, Menlo Park, California: U.S. Geological Survey Open-File Report 85-521, p. 10-13.

Guffanti, Marianne, and C.S. Weaver, 1988, Distribution of late Cenozoic volcanic vents in the Cascade Range: volcanic arc segmentation and regional tectonic considerations: Journal of Geophysical Research, v. 93, no. B6, p. 6513-6529.

Ingebritsen, S.E., R.H. Mariner, and D.R. Sherrod, 1988, Heat flow and hydrothermal circulation in the Cascade Range, north-central Oregon (abs.): Eos (Transactions of the American Geophysical Union), v. 69, no. 16, p. 471.

Luedke, R.G., and R.L. Smith, 1981, Map showing distribution, composition, and age of late Cenozoic volcanic centers in California and Nevada, scale 1:1,000,000: U.S. Geological Survey Miscellaneous Investigations Series, Map I-1091-C.

Luedke, R.G., and R.L. Smith, 1982, Map showing distribution, composition, and age of late Cenozoic volcanic centers in Oregon and Washington, scale 1:1,000,000: U.S. Geological Survey Miscellaneous Investigations Series, Map I-1091-D.

Mase, C.W., J.H. Sass, A.H. Lachenbruch, and R.J. Munroe, 1982, Preliminary heat-flow investigations of the California Cascades: U.S. Geological Survey Open-File Report 82-150, 240 p.

McBirney, A.R., 1978, Volcanic evolution of the Cascade Range: Annual Review of Earth and Planetary Sciences, v. 6, p. 437-456.

Muffler, L.J.P., 1987, Geothermal studies of the U.S. Geological Survey in the Cascade Range: Geothermal Resources Council Transactions, v. 11, p. 281-283.

Muffler, L.J.P., and Cataldi, Raffaele, 1978, Methods for regional assessment of geothermal resources: Geothermics, v. 7, no. 2-4, p. 53-89.

Priest, G.R., 1985, Geothermal exploration in Oregon, 1984: Oregon Geology, v. 47, p. 63-66.

Priest, G.R., 1986, A program for scientific drilling in the Cascades, northern California, Oregon, and Washington: Oregon Department of Geology and Mineral Industries, 15 p.

Priest, G.R., N.M. Woller, D.D. Blackwell, and M.W. Gannett, 1986, Geothermal exploration in Oregon, 1986: Oregon Geology, v. 49, no. 6, p. 67-73.
Riddihough, R.P., 1984, Recent movements of the Juan de Fuca plate system: Journal of Geophysical Research, v. 89, p. 6980-6994.
Sammel, E.A., 1981, Results of test drilling at Newberry volcano, Oregon -- and some implications for geothermal prospects in the Cascades: Geothermal Resources Council Bulletin, v. 10, no. 11, p. 3-8.
Sherrod, D.R., 1987, New compilation map of the Cascade Range in Oregon: Geothermal Resources Council Transactions, v. 11, p. 305-307.
Smith, J.G., 1987, New compilation map of the Cascade Range in Washington: Geothermal Resources Council Transactions, v. 11, p. 309-314.
Smith, R.L., and H.R. Shaw, 1975, Igneous-related geothermal systems, in White, D.E., and D.L. Williams, eds., Assessment of geothermal resources of the United States--1975: U.S. Geological Survey Circular 726, p. 58-83.
Smith, R.L., and H.R. Shaw, 1979, Igneous-related geothermal systems, in Muffler, L.J.P., ed., Assessment of geothermal resources of the United States--1978: U.S. Geological Survey Circular 790, p. 12-17.
Sorey, M.L., 1985, Types of hydrothermal convection systems in the Cascade Range of California and Oregon, in Guffanti, Marianne, and L.J.P. Muffler, eds., Proceedings of the Workshop on Geothermal Resources of the Cascade Range, May 22-23, 1985, Menlo Park, California: U.S. Geological Survey Open-File Report 85-521, p. 63-67.
Stanley, W.D., Carol Finn, and J.L. Plesha, 1987, Tectonics and conductivity structures in the southern Washington Cascades: Journal of Geophysical Research, v. 92, no. B10, p. 10,179-10,193.
Stauber, D.A., S.M. Green, and H.M. Iyer, 1988, Three-dimensional P velocity structure of the crust below Newberry volcano, Oregon: Journal of Geophysical Research, v. 93, no. B9, p. 10,095-10,107.
Swanberg, C.A., W.C. Walkey, and Jim Combs, 1988, Core hole drilling and the "rain curtain" phenomenon at Newberry volcano, Oregon: Journal of Geophysical Research, v. 93, no. B9, p. 10,163-10,173.
Weaver, C.S., 1985, Combined regional seismotectonics and the extent of Cenozoic volcanism: an improved first-order geothermal assessment of the Cascade Range, in Guffanti, Marianne, and L.J.P. Muffler, eds., Proceedings of the Workshop on Geothermal Resources of the Cascade Range, May 22-23, 1985, Menlo Park, California: U.S. Geological Survey Open-File Report 85-521, p. 14-17.
Weaver, C.S., and C.A. Michaelson, 1985, Seismicity and volcanism in the Pacific Northwest: evidence for the segmentation of the Juan de Fuca plate: Geophysical Research Letters, v. 12, p. 215-218.
Williams, D.L., Carol Finn, R.W. Couch, Z.F. Daneš, G.S. Pitts, W.M. Phillips, and R.P. Riddihough, 1988, Residual Bouguer gravity anomaly map of the Cascade Range, California, Oregon, Washington, and British Columbia: U.S. Geological Survey Geophysical Investigations Map GP-973, scale 1:500,000.

CONFERENCES TO DATE

Conference I	Abnormal Animal Behavior Prior to Earthquakes, I Not Open-Filed
Conference II	Experimental Studies of Rock Friction with Application to Earthquake Prediction Not Open-Filed
Conference III	Fault Mechanics and Its Relation to Earthquake Prediction Open-File No. 78-380
Conference IV	Use of Volunteers in the Earthquake Hazards Reduction Program Open-File No. 78-336
Conference V	Communicating Earthquake Hazard Reduction Information Open-File No. 78-933
Conference VI	Methodology for Identifying Seismic Gaps and Soon-to-Break Gaps Open-File No. 78-943
Conference VII	Stress and Strain Measurements Related to Earthquake Prediction Open-File No. 79-370
Conference VIII	Analysis of Actual Fault Zones in Bedrock Open-File No. 79-1239
Conference IX	Magnitude of Deviatoric Stresses in the Earth's Crust and Upper Mantle Open-File No. 80-625
Conference X	Earthquake Hazards Along the Wasatch and Sierra-Nevada Frontal Fault Zones Open-File No. 80-801
Conference XI	Abnormal Animal Behavior Prior to Earthquakes, II Open-File No. 80-453
Conference XII	Earthquake Prediction Information Open-File No. 80-843
Conference XIII	Evaluation of Regional Seismic Hazards and Risk Open-File No. 81-437
Conference XIV	Earthquake Hazards of the Puget Sound Region, Washington Open-File No. 82-19
Conference XV	A Workshop on "Preparing for and Responding to a Damaging Earthquake in the Eastern United States" Open-File No. 82-220
Conference XVI	The Dynamic Characteristics of Faulting Inferred from Recording of Strong Ground Motion Open-File No. 82-591
Conference XVII	Hydraulic Fracturing Stress Measurements Open-File No. 82-1075
Conference XVIII	A Workshop on "Continuing Actions to Reduce Losses from Earthquakes in the Mississippi Valley Area Open-File No. 83-157
Conference XIX	Active Tectonic and Magmatic Processes Beneath Long Valley Open-File No. 84-939
Conference XX	A Workshop on "The 1886 Charleston, South Carolina, Earthquake and its Implications for Today" Open-File No. 83-843

Conference XXXIX	Directions in Paleoseismology Open File 87-673
Conference XL	A Workshop on "The U.S. Geological Survey's Role in Hazards Warnings" Open-File Report 87-269
Conference XLI	A Review of the Earthquake Research Applications in the National Earthquake Hazard Reduction Program: 1977-1987 Open-File 88-13-A
Conference XLII	A Workshop on "Evaluation of Earthquake Hazards and Risk in the Puget Sound and Portland Areas" Open-File Report 88-541
Conference XLIII	A Workshop on "Earthquake Risk: Information Needs of the Insurance Industry" Open-File Report 88-669
Confernece XLIV	Geological, Geophysical, and Tectonic Settings of the Cascade Range Open-File Report 89-[in press]

For information on ordering the above publications, please contact:

U.S. Geological Survey
Books and Open-File Reports Service Section
Building 41, Box 25425
Federal Center
Denver, Colorado 80225